Dissertation zur Erlangung des Doktorgrades
der Fakultät für Chemie und Pharmazie
der Ludwig-Maximilians-Universität München

Synthesis and Characterization of New Energetic Materials Based on Polyfunctionalized Tetrazoles and Covalent Azides

Maximilian Benz

aus

Mainburg, Deutschland

2022

Erklärung

Diese Dissertation wurde im Sinne von § 7 der Promotionsordnung vom 28. November 2011 von Herrn Prof. Dr. Thomas M. Klapötke betreut.

Eidesstattliche Versicherung

Diese Dissertation wurde eigenständig und ohne unerlaubte Hilfsmittel erarbeitet.

München, den 21.08.2022

_____

Maximilian Benz

Dissertation eingereicht am:	22.08.2022
1. Gutachter:	Prof. Dr. Thomas M. Klapötke
2. Gutachter:	Prof. Dr. Konstantin Karaghiosoff
Mündliche Prüfung am:	24.11.2022

Ein Gelehrter in seinem Laboratorium ist nicht nur
ein Techniker, er steht auch vor den Naturgesetzen
wie ein Kind vor der Märchenwelt

Marie Curie (1867–1934)

DANKSAGUNG

Zuerst möchte ich mich bei meinem Doktorvater, Herrn Prof. Thomas Klapötke für das entgegengebrachte Vertrauen bedanken, mich in den Arbeitskreis aufzunehmen und mich direkt auf das Industrieprojekt anzusetzen. Besonders ihre unkomplizierte und nahbare Art konnte ich sehr schätzen. Bei ihnen hatte man immer das Gefühl, sich auch bei kritischen Themen ernstgenommen und verstanden zu fühlen. Zudem danke ich ihnen für die wissenschaftliche Freiheit, die sie mir, während meiner vielen verschiedenen Projekte gewährt haben.

Herrn Prof. Karaghiosoff danke ich für die Übernahme des Zweitgutachtens, aber vielmehr für die vielen Stunden, in denen er für mich unzählige NMR und Kristallmessungen, zu teils unmenschlichen Tages- und Nachtzeiten, vorgenommen hat. Außerdem für die vielen anregenden und lustigen Diskussionen über sämtliche Themen des Lebens und sein stets offenes Ohr für Probleme aller Art.

Daneben danke ich Frau Prof. Dr. Silvija Markic, Herrn Prof. Dr. Andreas Kornath, Herrn Prof. Dr. Hans-Christian Böttcher und Frau Prof. Dr. Lena Daumann für die Bereitschaft an der Prüfungskommission teilzunehmen.

Dr. Jörg Stierstorfer, meinem fachlichen Betreuer, danke ich für ganze viele Dinge wie das Fertigstellen aller Kristallstrukturen, das Korrekturlesen aller Manuskripte und Präsentationen, die Anregung zur Synthese neuer Verbindungen oder die ausgiebigen Trashtalks über alles und jeden. Auch wenn er mich mit seinen just-in-time Korrekturvorschlägen zu fertigen Papern oder utopischen Anforderungen für grafische Illustrationen regelmäßig zur Weißglut gebracht hat, konnte man sich immer auf ihn verlassen und auf ihn zählen. Vielen Dank auch für das von dir entgegengebrachte Vertrauen, den entspannten, freundschaftlichen Umgang und die geteilte Begeisterung für Moleküle, die eigentlich nicht existieren wollen.

Ich danke Frau Scheckenbach für ihre positive, immerzu freundliche und sympathische Art und für das unkonventionelle Lösen sämtlicher administrativer Probleme. Sie behalten auch bei totaler Verwirrung immer den Durchblick im Bürokratiedschungel der Uni und können dabei sogar noch lächeln.

Unserem Techniker Stefan Huber danke ich für seine lustige Art und seinen Humor. Gespräche mit dir dauerten gefühlt nur Minuten, aber in Wirklichkeit verlor man dadurch regelmäßig Stunden. Vor allem aber sei dir für die Zeit, die du trotz deines vollen Terminkalenders immer wieder für die äußerst gewissenhafte und selbstständige Messung der Empfindlichkeiten aufbringen konntest, gedankt.

Ich möchte mich zudem noch bei zwei wichtigen Mitgliedern unseres AKs bedanken, nämlich Sabrina Wahler und Dr. Burkhard Krumm. Beide haben durch unzählige Zurschaustellungen ihres enormen Fachwissens und den leichten persönlichen Umgang, durch ihre zugängliche Persönlichkeit, mir und der gesamten Gruppe das Arbeiten ausgesprochen erleichtert. Danke dafür!

Ich danke dem gesamten Team der zentralen Analytik für den regulären Betrieb, aber auch für manche Extramessungen. Vor allem sei hier Frau Breitenstein für das Messen, vor allem zu Stoßzeiten, unzähliger NMR Proben gedankt. Herrn Dr. Peter Mayer danke ich für seine Hilfe bei problematischen Kristallstrukturen und allgemein für die Messung zumindest jeder vierten abgegeben Struktur. Daneben natürlich unserem X-Ray Team für die Zeit und den Elan, den ihr in das Messen meiner Strukturen gesteckt habt.

Meinen Praktikumsbetreuern während des Studiums Dr. Ferdinand Lutter, Dr. Marc Bölter und Dr. Ivan Gospodinov danke ich für das Wecken des Interesses an synthetischer Chemie.

Ein großes Dankeschön ist auch an meine Bacheloranden und F-Praktikanten Florian Kris, Cedric Pignot, Lukas Bauer, Nina Krüger, Jonas Grandtke und Andreas Selmeier zu richten. Ohne euren Einsatz und die geleistete Synthesearbeit wären niemals derart gute und viele Ergebnisse zustande gekommen. Ein besonderer Dank richtet sich an Lukas für die mittlerweile vielen gemeinsamen und erfolgreichen Projekte. Danke auch für die ruhigen politischen Diskussionen und deine lustige und auffrischende Art. Ich hoffe, du hältst die Liquidität des Arbeitskreises aufrecht.

Ein Riesendank richtet sich an den gesamten AK Klapötke. Das geschaffene Arbeitsklima in unseren Laboren hat stets zu einem reibungslosen Umgang

beigetragen. Trotz der vielen Einschränkungen, die wir wegen Corona mitmachen mussten, hatten wir trotzdem eine wunderbare Zeit. Unvergessen sind einige Ausflüge und Veranstaltungen, die wir gemeinsam erlebt haben wie Saalfeste, Biergartenbesuche, Karten und Pokerspielabende, Skiausflüge, das Pragwochenende, Oktoberfestbesuche, Fußballabende oder die regelmäßigen feuchtfröhlichen Events im Zusammenhang mit Bierpong, Saugern, Flunkyball oder der Hopfendolde. Es ist nicht selbstverständlich, dass sich eine große Gruppe aus verschiedensten Charakteren so gut versteht und schätzt, wie es bei uns der Fall ist. Vielen Dank an Lukas Bauer, Markus Rösch, Simon Endrass, Alex Harter, Vroni Fuchs, Jelena Reinhart, Marcus Lommel, Willi Cremers, Tobi Lenz, Moritz Kofen, Chris Riedelsheimer, Jasmin Lechner, Alex Schweiger, Jonathan Tietze, Alexander Gisnapp, Maurus Völkl und Andi Neuer für die großartigen Erlebnisse und lustige Zeit mit euch. In diesem Zusammenhang möchte ich mich auch besonders bei meinem Labor D3.107 für das unkomplizierte, harmonische, einheitliche und relaxte Miteinander bedanken. Ich werde die Uni-Zeit definitiv vermissen!

Für das Gelingen dieser Arbeit sind jedoch zwei Kollegen besonders hervorzuheben
Zum einen Tobi, mit dem ich mir die meiste Zeit eine Box geteilt habe und den ich schon seit dem ersten Unitag kenne. Für ihn könnte der Absatz nicht lange genug sein. Danke für so viele, teils sinnlose Chemiediskussionen, gegenseitiges Pushen aber auch Unterstützen, dein handwerkliches Geschick und deine Fähigkeit dich für jeden erdenklichen Schmarn begeistern zu können. Bleib so wie du bist! Zum anderen Marcus Lommel für seinen ungemein hohen Stellenwert für den Arbeitskreis und sein bemerkenswertes Fachwissen über Primaries und halblegal zugängliche Literatur. Danke für deine akribische und genaue Arbeitsweise und dafür, dass du dir für keine Tätigkeit oder Messung zu schade bist und immer geholfen hast, wenn es dir möglich war.

Natürlich sei auch einigen ehemaligen Mitgliedern des AKs, nämlich Dr. Teresa Bölter (geb. Küblböck), Dr. Cornelia Unger, Dr. Marco Reichel, Dr. Greta Bikelyte, Dr. Michael Voggenreiter, Vanessa Braun und Dr. Maximilian Wurzenberger gedankt. Letzterem danke ich besonders für die reibungslose Aufnahme und Einführung in die Gruppe und für die ein oder andere SmackDown-Einlage im Biergarten. In diesem Zusammenhang ist auch noch Michael Gruhne zu erwähnen, der sich leider für eine Karriere als

Bakterienzüchter in Kalifornien entschieden hat und sich nun der bösen Seite der Chemie zuwendet. Dir danke ich für die gute Stimmung, die du immer durch deinen unerschütterlichen Kindskopf und dein schier unermüdliches Repertoire an dummen Ideen und schwachsinnigen Aktionen in den Laboralltag eingebracht hast.

Abseits der Uni möchte ich meinem Freundeskreis aus Vohburg und Umgebung für das „auf den Boden bringen“ und die mentalen Resets während der Wochenenden und der Urlaubszeit bedanken.

Größter Dank richtet sich an meine Familie, an meine Eltern Jürgen und Simone, meine Großeltern Heinz, Elfriede, Manfred und Erika und meine Schwester Lina für das gute Zureden und die seelische und finanzielle Unterstützung während der Promotion, aber auch schon während des gesamten Studiums. Ohne euch wäre ich jetzt nicht da, wo ich jetzt stehe! Abschließend möchte ich mich noch besonders bei meiner Jasmin bedanken. Durch deine Art und deine Geduld mit mir machst du mich zu einem besseren Menschen.

CONTENT

1. Introduction

1.1 Definition and Classification

The term "energetic materials" covers a huge class of materials that are used in a variety of different applications. Due to the great interest in energetic materials, ongoing research leads to the steady development of new research properties and the status quo.[1-5] Although, in order to be able to deal with the investigation of this field in more detail, several definitions and a classification into different categories are required first. However, it is difficult to find a uniform definition, as energetic materials are perceived differently depending on the area of implementation and the focus of specific scientific research.[6-7] Based on the chemical background of explosives in this thesis, the definition of Meyer and Köhler is suitable.[8]

Explosives are solid, liquid, or gelatinous substances, alone or mixed with one another, which are in a metastable state and are capable, for this reason, of undergoing a rapid chemical reaction without the participation of external reactants such as atmospheric oxygen. The reaction can be initiated by mechanical means, by the action of heat or by detonating shock. The reaction products are predominantly gaseous. The propagation rate from the initiation site outwards through the explosive material may be much slower than the velocity of sound (deflagration) or may be supersonic (detonation).[8]

One common way for proper categorization of energetic materials is into three major categories, Pyrotechnics, Explosives and Propellants (Figure 1), whereby each category can be further subdivided into many subcategories depending on the application or area of requirement.[9-11] This classification is mainly based on the respective use of the substances and neglects the chemical nature of composition.[6] The chemical building blocks are often not connected to their ultimate use. However, the following only deals with the more precise classification of explosives, since nearly all the substances included in this work are assigned to this category.

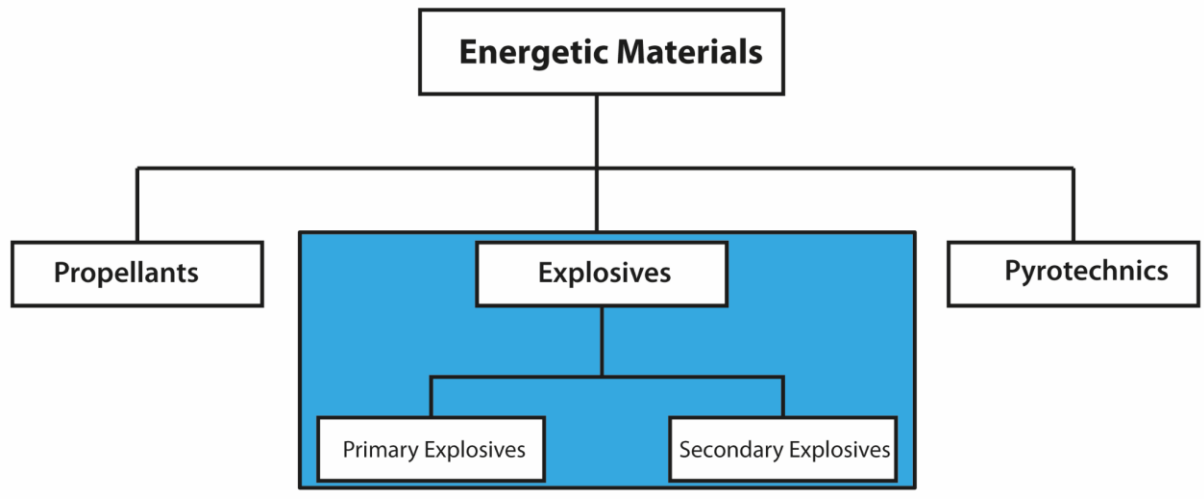

Figure 1. Schematic classification of energetic materials into three main categories as well as subcategorization of explosives into primary and secondary explosives.

Propellants:

Propellants are substances, which can form a large amount of gas within a small period of time. This directly results in the generation of increased pressure, which makes it possible to move objects such as projectiles or flying objects, but without the formation of a shock wave. The best-known representative is black powder, which was already used more than 2200 years ago.[9] Propellants are generally composed of a fuel and an oxidizer and can be ignited by flame or spark. The main derivation within the class is into rocket propellants and gun propellants. The latter can be subclassified into single-, double- and triple-based propellants. Single-base propellants contain exclusively nitrocellulose (NC) as energy source and are used in a wide range of pistols and artillery ammunition. Next to NC, double-base propellants consist of nitroglycerine (NG) as a performance-enhancing additive. Triple-base propellants include mainly NC, NG and nitroguanidine (NQ).[9] Especially for double- and triple-base propellants among others, energetic but insensitive plasticizers (EGDN, DEGDN) are commonly added in order to prevent the mixture from turning out too sensitive and adjust the mixtures to the respective scope of use. Each of the named substances (NC, NG, NQ) can be regarded as an intramolecular redox system, since it contains a carbon backbone as its fuel source as well as an oxidizing part in form of nitrato or nitro groups.[12] Modern research approaches focus on the integration of less corrosive ingredients, as

nitrogen-rich components to lower the corrosion within the gun system. Rocket propellants are available in the form of liquid non-hypergolic mixtures like H_2/O_2 or liquid hypergolic mixtures like H_2O_2/MMH or HNO_3/N_2H_4 or as solid rocket propellant based on mixtures of several metals and ammonium perchlorate (AP) or ammonium nitrate (AN) as oxidizers (Figure 2).[13]

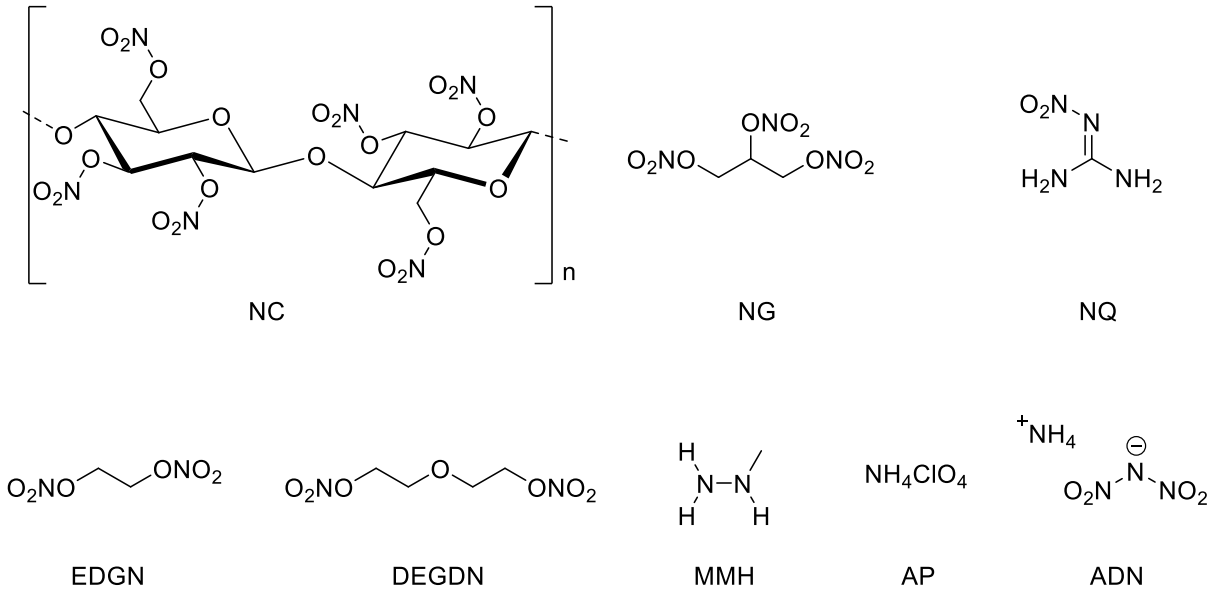

Figure 2. Prominent representatives within the substance class of propellants: nitrocellulose (NC), nitroglycerine (NG), nitroguanidine (NG), ethylene glycol dinitrate (EGDN), diethylene glycol dinitrate (DEGDN), monomethylhydrazine (MMH), ammonium perchlorate (AP) and ammonium dinitramide (ADN).

Since ammonium perchlorate is poisonous to the human body and harmful to the environment due to the chlorine containing decomposition products, great efforts are employed to find a suitable green replacement candidate for AP.[14-16] Up to now, AP cannot be adequately replaced because of its outstanding properties as propellant ingredient. One of the most promising substances, which has been traded for quite some time, is ammonium dinitramide (ADN), since it combines a good oxygen balance with a high nitrogen content and heat of formation.

Pyrotechnics:

Pyrotechnics or pyrotechnical mixtures are always compositions of at least two or more components. The two main parts are a fuel and an oxidizer, to which other additives are added depending on their field of application.[9] Currently applied

mixtures often use potassium perchlorate (PP) or ammonium perchlorate (AP) as oxidizer.[17] After initiation, they can produce special effects such as heat, different colored light, gas or smoke, and a wide variety of sounds.[18-21] The chemical energy is often accumulated in a very compact space and can be released extremely proven by deflagration or prior detonation. The most obvious use of pyrotechnics is in fireworks and light shows, but besides that, the major utilization is for special applications in safety equipment and services or precisely timed-release sequences.

Both, propellants, and pyrotechnics can be classified as substances with slower reaction time then explosives since their prime objective is to show deflagration instead of detonation. Therefore, it is not required for both substance classes to cause a deflagration to detonation transition (DDT).

Primary Explosives:

In principle, primary explosives are compounds that can be initiated by non-explosive impulses such as heat, flame, friction, impact, spark or light, and undergo a fairly rapid deflagration to detonation transition (DDT).[22] Therefore, a deflagration shows an expanding velocity of the reaction front, which is below the speed of sound in the combusting medium whereas the expanding velocity is supersonic for a detonation. In addition, the resulting shock wave should be suitable for igniting less sensitive components such as explosive charges or propellants. The resulting detonation velocity of the primaries plays only a minor role here since the major energy is released by the more powerful secondary explosives or propelling charges.[9] By default, an amplifier or booster is placed after a primary charge, which is easy to initiate and continues the detonation wave and dominates its strength. Typical values for the respective heat of explosion are in the range of 1000–2000 kJ kg^{-1}.[9] In order to react appropriately to the applied impulses, primary explosives are generally the most sensitive explosive class with sensitivity values of ≤ 4 J toward impact, ≤ 10 N toward friction and ≤ 20 mJ toward electrical discharge.[4] However, a balance must be struck here, since high sensitivities improve the responsiveness of the substance, but make it difficult and dangerous to handle the substance, especially in larger quantities. Besides mercury fulminate (MF), which is considered as the first primary explosive[23] but is

hardly used today, lead azide (LA) and lead styphnate (LS) are still of great importance and are applied as standard until today (Figure 3).[24] Since there are harmful effects on the environment and to living organisms, all kind of heavy metal containing substances (mainly mercury, lead or even cadmium), are under investigation to be replaces by suitable substituents.[25-26]

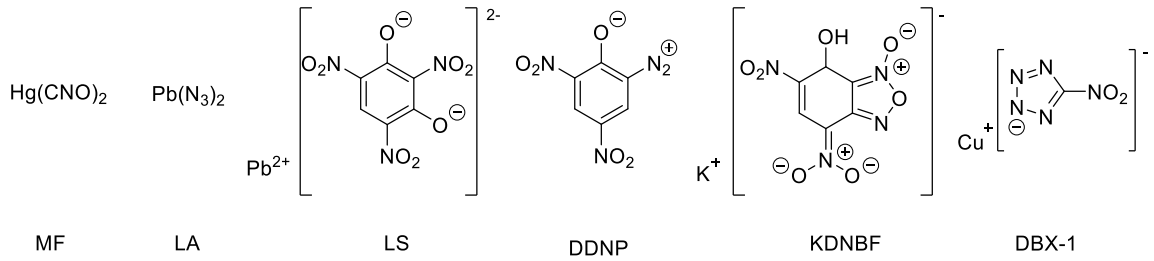

Figure 3. Historically and commonly used primary explosives: mercury fulminate (MF), lead azide (LA), lead styphnate (LS), 2-diazonium-4,6-dinitrophenolate (DDNP), potassium dinitrobenzofuroxan (KDNBF) and copper 5-nitrotetrazolate (DBX-1).

Despite their toxicity, both substances used today (LA and LS) have decisive advantages over other substances, which is mainly due to the low production cost and the simple synthesis. Furthermore, both substances are considered to be extremely reliable and durable. Therefore, current research is moving towards heavy metal-free, more environmentally friendly primary explosives, compounds such as KDNBF or DBX-1.[27-28] Even metal free CHNO based compounds, as 2-diazonium-4,6-dinitrophenolate (DDNP) are in current use.[22] However, DDNP is predicted to have several problems concerning its long-term stability. In addition to the traditional primary explosives, promising innovations have emerged in the field of energetic coordination compounds (ECCs), consisting of transition metal cations (e.g. Cu^{2+}, Zn^{2+}, Mn^{2+}), oxygen or energy-rich anions (e.g. NO_3^-, N_3^-, ClO_4^-) and nitrogen-rich ligands such as substituted tetrazoles, some of which can even be ignited by laser radiation due to their color.[29-32]

Secondary Explosives:

For the initiation of a secondary explosive, a primary explosive is inevitably and unavoidably required since secondary explosives usually cannot be initiated by non-explosive impulses.[22] Therefore, in an explosive charge, a primary explosive initiator is always installed before the main charge, which consists mainly of

secondary explosives. In addition to increased thermodynamic stability, the latter are also generally less sensitive toward friction and impact.[9]

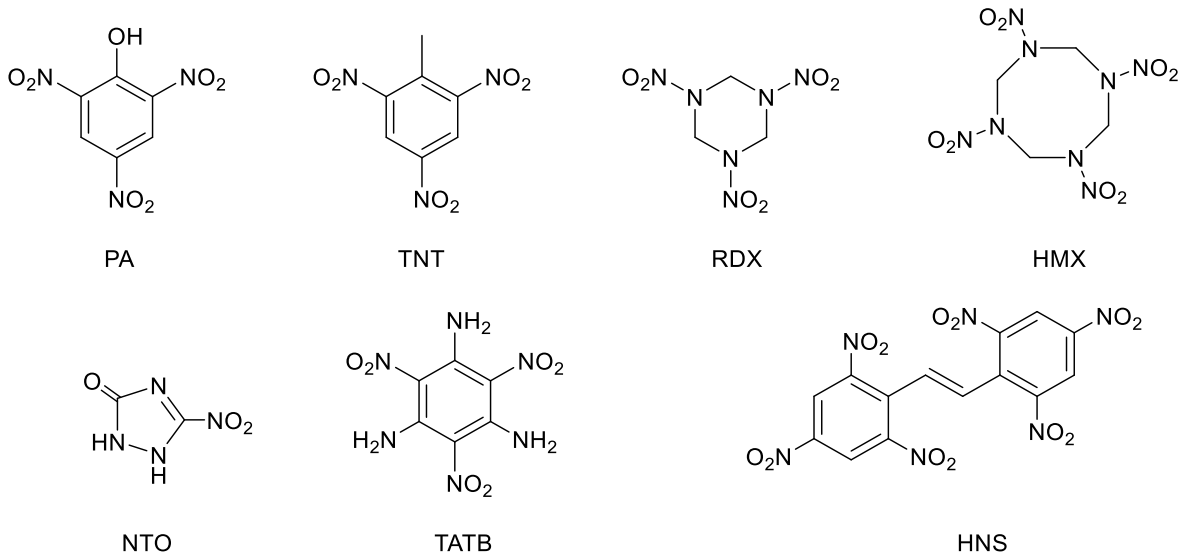

Figure 4. Historically relevant secondary explosives, most of which are still in use: picric acid (PA), 2,4,6-trinitrotoluene (TNT), hexogen (RDX), octogen (HMX), 5-nitro-triazolone (NTO), 2,4,6-trinitrobenzene-1,3,5-triamine (TATB), hexanitrostilbene (HNS).

The limit of sensitivity for secondary explosives is classified to be at 4 J toward impact and 80 N friction, but in no case below that. This is mainly due to safety aspects in large-scale production, since secondary explosives account for the majority of the mass of an explosive charge and are therefore produced in large quantities.[9] In addition to the sensitivities, detonation velocity (V_{det}), detonation pressure ($P_{C\text{-}J}$) and detonation energy ($\Delta_E U$) are the most important parameters of secondary explosives, whereby these performance data largely depend on the respective density, heat of formation and oxygen balance (OB)[9]. The sheer number of secondary explosives used today is relatively small, but by using certain mixtures or admixtures and additives such as plasticizers, binders or polymers, various properties can be achieved. The development of these substances often dates back to more than 100 years and most of them suffer from a bad reputation concerning their environmental impact.[33-35] Many "traditional" explosives are still used exclusively because they offer some advantages over new developments that have not yet been adjusted or surpassed. Trinitrotoluene (TNT) is easy to produce by nitration of toluene and offers ideal properties for use as a melt-castable explosive. Melt-cast secondary explosives are important for the ideal packing of an

explosive charge and should therefore melt at below 100 °C if possible (T_{melt}(TNT) = 80 °C), as this is an interesting aspect for the industry, since it enables the use of a water bath as a heat source. Next to TNT, nitroaromatic based hexanitrostilben (HNS) is used as heat resisting explosive due to its high thermal decomposition (320 °C) in high temperature applications.[36] The main reason for the continued use of TNT and HNS are the above-mentioned parameters, which have not yet been adequately replaced by any explosive that is equally cheap to produce. However, this is countered by the low detonation properties of both compounds compared to other high explosives like hexogen (RDX) or octogen (HMX), which are primarily used for the military sector (Figure 4).[9] The main distinction between explosives for civilian and military uses consists in the different requirements they must meet. Military applicated explosives require high explosive power and reliability of the substances, while for civilian purposes the main issue deals with the production price. Therefore, mixtures of nitrocellulose or ammonium nitrate combined with various oils or plasticizers and fuel oils (ANFO) and other added substances such as aluminum or nitromethane are popular civil explosive mixtures.[9] One of the biggest developments in this field in recent years are emulsion explosives, which, in addition to the explosive, are mainly composed of binders and oils.[8] They are easy to manage because they are insensitive due to their state and are mainly used in mining. For military purposes, TKX-50 (bishydroxylammonium-5,5′-bistetrazolyl-1,1′-diolate) is a prominent replacement candidate, which is free of nitro and nitrato units and shines with outstanding detonative performance.[37-38]

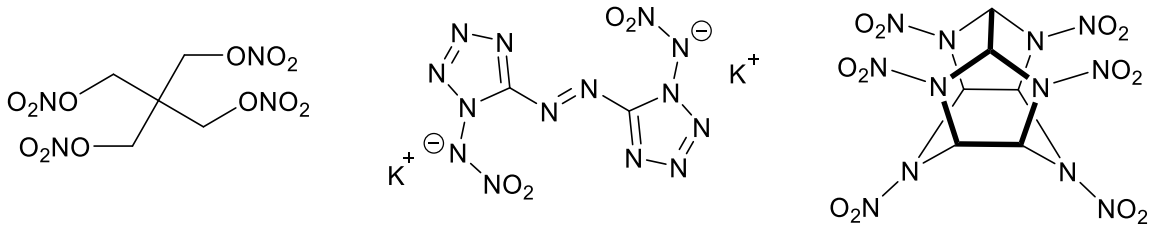

PETN K_2DNAAzT CL-20

Figure 5. Selected explosives falling beyond the scope of the established classification: pentaerytritol tetranitrate (PETN), dipotassium 1,1'-dinitramino-5,5'-azotetrazolate (K_2DNAAzT) and hexanitrohexaazaisowurtzitane (CL-20).

There are several prominent examples that cannot be clearly classified to the class of primary or secondary explosives and therefore must be submitted some kind of between these two categories (Figure 5). Among others, nitropenta (PETN) is assigned to the class of booster explosives, which is even literally between primary and secondary explosives. Booster explosives are inserted in explosive charges behind the primary explosive and are easy to initiate.[22] The main benefit is the propagation and amplification of the detonation wave. Thus, PETN is easier to initiate than most other secondary explosives, yet simple ignition is not sufficient. The sensitivities (IS = 3.5 J, FS = 54 N) are actually in the range for primary explosives.[39] Thus, no clear assignment to primary or secondary explosives is possible for PETN.

K_2DNAAzT was developed as a next generation primary explosive and possible replacement for lead azide.[40] As expected, the substance is extremely sensitive to any kind of external stimuli and detonates at the slightest mechanical impulse and upon contact with flame. Its thermal stability of 180 °C and poor solubility in water would also suggest its possible use as a primary explosive. However, K_2DNAAzT has a detonation velocity of almost 9000 m s^{-1}, which is clearly in the range of a secondary explosive. This value combined with the extremely high sensitivities prevent its current use, as safe handling is rendered extremely difficult. A similar problem arises with CL-20. The cage structure, which stores its energy in the form of nitramine units and ring strain, is regarded as one of the most powerful explosives. However, it is currently not used to any significant extent due to its high sensitivities (IS = 4 J, FS = 48 N) and expensive and inefficient synthesis.[41-42]

1.2 Motivation and Requirements for Synthesis of New Explosives

“Greener, Better, Safer” are the basic buzzwords that best describe the drive to develop new explosives. Especially in the current era, in which sustainability and green awareness are important in every area of life, greater focus on the suitability of the substances used is important in the field of chemistry, and particularly in the field of explosives chemistry.

Many explosives currently in use have shown to have a poor impact on the environment or health, as they have been developed primarily for operational purposes without taking these factors into account. For primary explosives, which mainly contain heavy metals such as lead (previously even cadmium or mercury), the toxicity in particular is a serious problem. They are not only toxic to living organisms but also harmful to the environment. This has been proven, for instance, by studies of the soil and groundwater of highly frequented shooting ranges and military grounds.[26] All compounds belonging to the class of nitroaromatics, with TNT, HNS, TATB or LS as the most prominent representatives, are also associated with a poor environmental factor. For some of them, acute carcinogenicity has even been proven or is at least suspected.[44-46] For substitutes, these components or structural motifs should be omitted. All nitrogen-rich azoles have therefore proved particularly successful since their main decomposition product is gaseous and harmless nitrogen.[9] Potassium, copper, and silver are often traded as possible substitute metals for heavy metal containing compounds. Nonetheless, possible toxicity cannot be ruled out for copper.[47] With silver compounds, unaffordable prices are always a problem for any silver-containing composite.

The search for new compounds, especially secondary explosives with higher performance than the current ones, are in demand especially for military applications. For civilian applications, the prices of these high-performing compounds are often too high and not necessarily required for the purpose. In military usage, explosive performance and precision are paramount. Since nominal performance is not the key parameter for primary explosives, possible innovations should be convincing in terms of their ignition reliability.

Safety, or more specifically safe production and handling, naturally takes priority for all new developments. Especially for the production of large quantities, it is important that safety is always ensured. However, it is inevitable that explosives have a certain sensitivity.[3] Because of the definition as metastable compounds, most explosives have some sensitivity to external stimuli, apart from some recordings. Furthermore, an increase in the resulting performance tends to be observed with an increase in the respective sensitivity.[9] The safety aspect is particularly important for primary explosives since the latter generally have high sensitivities. However, the sensitivities of the final compounds as well as those of any synthetic intermediates must not be too sensitive to be handled safely.

Accordingly, some basic requirements or benchmarks arise for the development, which must be fulfilled in any case to be regarded as a promising replacement candidate. These main principle requirements are stated in Figure 6. The most important ones are discussed below. These values are generally valid and refer to both primary and secondary explosives. Depending on the type of application, additional requirements may also be necessary (e.g., suitable melting temperature for melt-cast explosives).

Figure 6. Key requirements for the development of new explosives.

Toxicity: In addition to the above-mentioned problematic properties with lead and other heavy metals, even more environmental hazards arise with the decomposition products of the organic components. (Figure 6) This involves the formation of NH_3, HCN or nitrogen oxides. The latter are pollutants that have recently gained notoriety from the diesel scandal in the automotive industry.[48] It would be desirable to have a decomposition to only environmentally friendly products such as N_2, water and carbon. In addition to the substances and their decomposition products, it is also important to pay attention to the toxicity of the reactants and solvents required for the production. In the EU, this is already drastically controlled by the REACH regulation (Regulation, Evaluation, Authorization and Restriction of Chemicals).[49]

Performance: This characteristic results in a clear difference between the requirements for primary and secondary explosives. For primaries, the detonation velocity is only of minor importance. Lead azide has a detonation velocity of about 6000 m s^{-1}, while most CHNO-based compounds have similar or higher values. However, it is most important that a primary explosive generates a shock wave induced by an external impulse, which is strong enough to initiate the secondary charge. Therefore, a fast deflagration to detonation transition (DDT) is essential. For secondary explosives, the most important performance parameters are detonation velocity (V_{det}), detonation pressure ($P_{C\text{-}J}$) and detonation energy ($-\Delta_E U$). For new developments, these values have to be at least in the same range or outperform the current standards (RDX: $V_{det} \approx 8800$ m s^{-1}, $P_{C\text{-}J} \approx 380$ kbar, $-\Delta_E U \approx 6100$ kJ kg^{-1}; TNT: $V_{det} \approx 6900$ m s^{-1}, $P_{C\text{-}J} \approx 220$ kbar, $-\Delta_E U \approx 5100$ kJ kg^{-1}).[9] The values can be either measured or calculated using software like “Cheetah” or “EXPLO5”. For most new compounds, theoretical calculations are initially preferred because they give a quick first insight and provide reliable results, whereas accurate practical measurements require significant quantity of the substance and knowhow about the methods. In addition to the chemical formula, the heat of formation and density are required for the computations.[50] The latter is particularly important, as it is included squared in the calculation. Maximizing these two variables becomes fundamental to the design of new explosives and will be discussed in more detail in the next section.

Longevity: During development, it is usually not known where the resulting materials will be used, so their tolerance to temperature fluctuations and moisture must be extremely high. Excluding the extreme weather zones of the earth, the global temperature range covers at least 80 °C. Since explosives are designed to last for several years, they must be able to withstand these conditions without losing performance or reliability. In addition, it should be ensured that the shape remains intact and that no cracks or deformation of the material occurs. A high vapor pressure or low decomposition temperature is particularly critical here. Long-term stability can either be calculated using kinetic models or evaluated by practical experience values or the vacuum stability test.

Compatibility: Explosive charges usually consist of several components. To prevent an unintended reaction, these ingredients must be compatible, as they may be in direct touch with each other. This means that they must not interact or react for any reason and under any conditions. This is verified in the first step by thermal and sensitivity measurements, whereby no noticeable change in the values compared with the pure substances should occur.

Sensitivity: In principle, interest is shown in materials that are as insensitive as possible, to prevent possible accidents during handling or production. Generally, the sensitivity to impact, friction and electrical discharge is considered using the BAM protocol (for friction and impact).[51] Based on the grain size or their habitus, different materials can have varying sensitivities. Materials that are too sensitive can be phlegmatized in certain cases by adding inert substances such as Teflon, wax or water. Conversely, materials or mixtures that are not sensitive enough can be sensitized by the addition of certain components such as tetrazene. The values are usually classified by the “UN Recommendations on the transport of dangerous goods” into not sensitive (IS > 40 J, FS > 360 N), less sensitive (IS ≥ 35 J, FS = 360 N), sensitive (IS ≥ 4 J, 360 N ≥ FS ≥ 80 N), very sensitive (IS ≤ 3 J, FS < 80 N) and extremely sensitive (FS ≤ 10 N).[52]

Solubility: Solubility is important mainly for toxicity but also for synthesis. Water-soluble substances have the property of being well absorbed through the skin. Therefore, special care is required when handling substances whose toxicity is not yet known. For the synthetic properties, it is advantageous if the final substance is

obtained by a precipitation reaction. In this way, particularly high purities are obtained and purification is possible by simple washing. For the reasons given above, water-insoluble substances are particularly in demand.

Stability: Naturally, new developed materials should be stable at least up to a certain temperature. These values depend on the intended use and the requirements of the manufacturing companies. A rough guideline should be at least 150 °C for primary explosives and at least 180 °C for secondary explosives. In addition to thermal stability, chemical stability matters, especially with respect to water and oxygen, which is ubiquitous. Likewise, advantageous is at least a reasonably high stability to alkaline and acidic media. In addition, it is essential that the materials are stable to light and do not change or decompose under slight exposure.

Price: The lower the better. The industry demands low production costs for the materials. The key factor here is the good availability of starting materials and reagents. Particularly the synthesis of TNT starting from industrially available toluene, sulfuric acid and nitric acid is almost unbeatable in this point.

Synthesis/Yield: The synthesis should have good yields not only because of the costs, but also to preserve the green idea. Particularly interesting are synthesis that offer good atom economy and that work with recovery through renewed purification of reagents (e.g., HNO_3). The process should not exceed a few synthesis steps and should not involve any steps, resulting in the formation of isomers that require extensive purification. When selecting reagents, attention must also be paid to their suitability for use. For example, REACH prohibits the use of hydrazine as such. Moreover, the formation of unstable or even explosive intermediates should not occur. The ideal case would be a drop-in replacement, where the synthesis plant does not have to be modified and the new substance can be produced in a comparable way to the old one without major adjustments.

Due to this large number of requirements for new substances, many newly synthesized compounds can already be excluded after first tests, as it is extremely difficult to meet all the prerequisites. Particularly for parameters such as performance, compatibility, sensitivity or density, initial estimations can already be

made on the basis of the chemical structure with a profound knowledge about explosives. However, the exact value can only be determined through tests with the real compound and not certainly through theoretic methods. The initial focus here is on the chemical synthesis of new compounds which, from a performance perspective, would have potential for later application.

1.3 Chemical Design of New Explosives

Accordingly, some basic chemical methods have been established which increase the possible performance of explosives. One strategy involves the introduction of oxygen-rich explosophoric groups like $–ONO_2$, $–NO_2$, $–N(H)NO_2$ or N-oxides to oxidize the molecules' backbone. Some representants are given in Figure 7. As a result, fuel and oxidant are combined in the same molecule. The increased oxygen balance also favors the formation of predominantly gaseous products.[9] Additionally, the introduction of oxygen-containing structural elements typically increases the density of the compounds, which, as mentioned above, has a significant effect on the resulting detonation properties.[53]

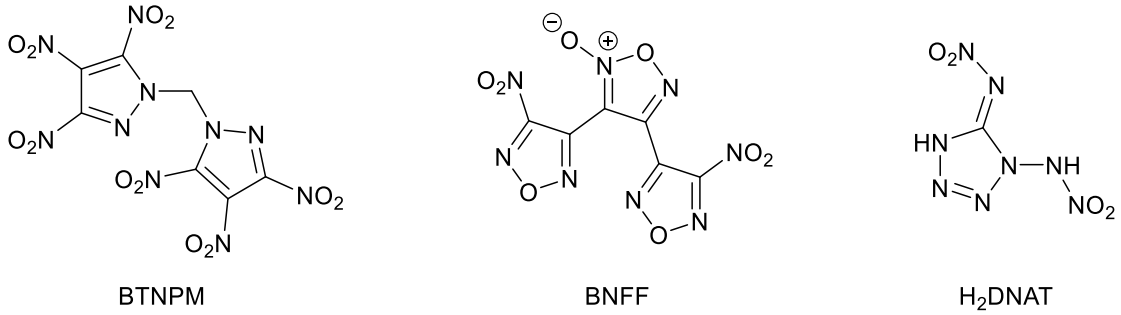

Figure 7. Recently developed explosives with an oxidized backbone: bis-1,1'-(3,4,5-trinitropyrazolyl)-methane (BTNPM), bis-(nitrofurazanyl)furoxane (BNFF) and 1,5-dinitraminotetrazole (H_2DNAT).

A second strategy covers compounds with a high nitrogen content. Enhanced nitrogen concentration provides several benefits. Unlike C–C bonds, which tend to form single bonds, the nitrogen triple bond (BE(N≡N) = 954 kJ mol^{-1}) is thermodynamically clearly preferred over the single (BE(N–N) = 160 kJ mol^{-1}) and double bond (BE(N=N) = 418 kJ mol^{-1}).[9, 54] Therefore, the decomposition of nitrogen-rich, mostly endothermic compounds releases an extremely large amount of energy through the generation of N_2. In addition to the high driving force due to

dinitrogen gas development, the high N-content has environmentally favorable benefits as well. The substance classes of azoles (e.g. pyrazoles, triazoles or tetrazoles) or azines (e.g. triazines or tetrazines) are especially suitable for this purpose (Figure 8).[4, 55-60] Due to the composition of exclusively nitrogen, the addition of azides can be useful in this context. Because of their endothermic character, azides contribute additional energy to the system. The synthesis of new fused or anilated systems consisting of several N-heterocycles, which often feature excellent densities and stability, has been a major focus of research in previous years.[61-62]

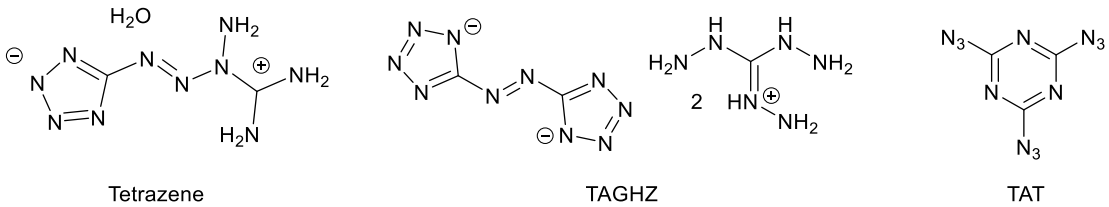

Figure 8. Explosive representatives with high nitrogen content formed by the use of tetrazoles, triazines and azides: tetrazene, bis-(triaminoguanidinium) 5,5'-azotetrazolate (TAGHZ) and 2,4,6-triazido-1,3,5-triazine (TAT).

Equally effective but more cumbersome is the use of additional energy input through the use of motifs with ring or cage strain (Figure 9). The reason for this is the complex synthesis of these representatives. The principle is based on a deviation of the C–C tetrahedral angle (109.5 °) to approx. 90 °. During decomposition, this energy, which is stored in the system due to the unfavorable angles, is released.

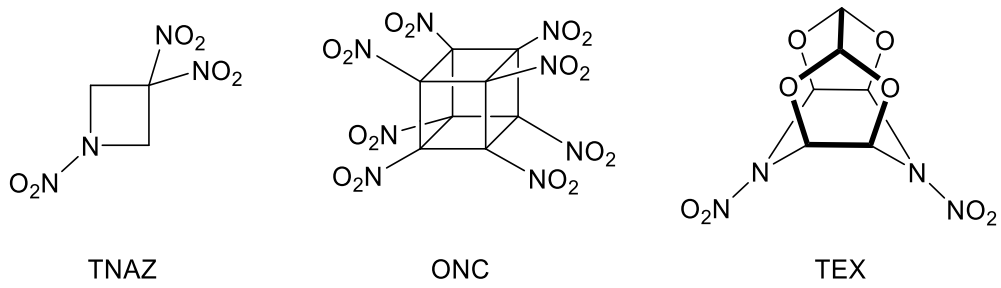

Figure 9. Explosives containing ring or cage strain: 1,3,3-trinitroazetidine (TNAZ), octanitrocubane (ONC) and 4,10-dinitro-2,6,8,12-tetraoxa-4,10-diazatetracylododecane (TEX).

The best-known representative is octanitrocubane (ONC). As the name suggests, its basic structure is in the form of a cube, which is completely nitrated. ONC not only has a balanced oxygen balance towards CO_2 but also calculated detonation properties that are superior to most other explosives (V_{det} > 10.000 m s^{-1}).[63-64] Unfortunately, the synthesis is extremely complex and thus the price for use outside academic interests is utopian.

Using these three strategies (oxidation of the backbone, nitrogen content, and intramolecular strain), it is often possible to add enough energy to a system to make it useful as an explosive. However, one must consider the properties, especially in terms of mechanical and thermal stability. Of course, it would be possible to reduce the sensitivities considerably by introducing bulky rests or substitutes, but this would again compromise the energetic performance. Consequently, three established strategies are available for adjusting these properties and still maintaining or even improving the energetic characteristics.

Especially carbon-substituted, sp^2 hybridized amines, which are located next to an electron-withdrawing group such as $–NO_2$, are suitable for increasing the stability through the generation of intramolecular hydrogen bonds. Likewise, the sensitivities can be reduced by these structural motifs (Figure 10). Unlike C-linked amines, N-NH_2 functions are attractive in terms of energetic purposes. The hydrazine function increases the enthalpy of the system.[9] As can be observed in 1,1'-DABT or 1,5-DAT, N-NH_2 groups are sp^3 hybridized.[65-66] Often, no intramolecular stabilizing effects can be observed with N-amines, but rather increased sensitivity and performance parameters.

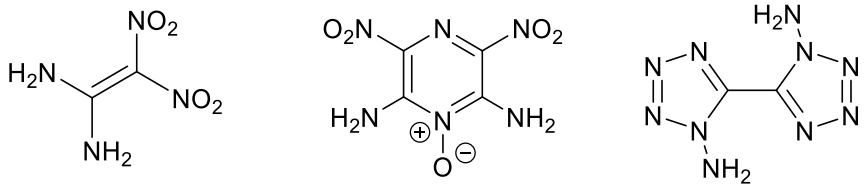

FOX-7 LLM-105 1,1'-DABT

Figure 10. Representatives consisting of an amine function: 1,1-diamino-2,2-dinitroethene (FOX-7), 2,6-diamino-3,5-dinitropyrazine-1-oxide (LLM-105) and 1,1'-diamino-5,5'-bistetrazole (1,1'-DABT).

Forming salts is an effective tool for further tuning the sensitivity and properties of energetic compounds. Most examples for ionic energetic materials are found for

systems containing energetic heterocyclic anions and metal or nitrogen-rich cations.[67-68] The resulting lattice energy lowers the enthalpy of the system, but the properties can be adjusted by selecting the appropriate bases.[9] The deprotonation of the heterocyclic backbone leads to a reduction of the acidity, which reduces the vapor pressure and increases the thermal stability. Salination with hydroxylamine usually increases the density compared to free acid and at the same time reduces the sensitivity (TKX-50 or MAD-X1)(Figure 11).[37, 69] Through its composition, the hydroxylammonium cation has a positive effect on the oxygen balance and enthalpy of formation, which often leads to increased performance. Metal salts (especially potassium or silver) are often used for the formation of primary explosives. Besides increasing densities and decomposition temperatures, they contribute to a clear increase in sensitivities (K_2DNABT).[70-71]

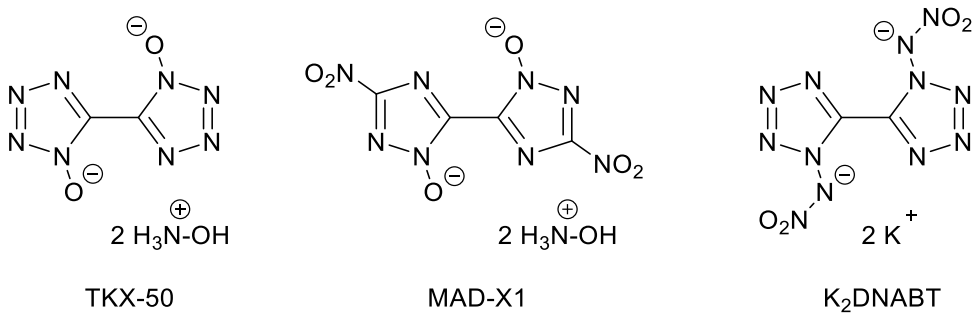

Figure 11. Recently developed ionic energetic compounds: bis-(hydroxylammonium) 5,5'-bistetrazole-1,1'-diolate (TKX-50), bis-(hydroxylammonium) 3,3'-dinitro-5,5'-bis-(1,2,4-triazole)-1,1'-diolate (MAD-X1) and dipotassium 1,1'dinitramino-5,5'bistetrazolate (K_2DNABT).

Similarly, an extended, through-conjugated π-system brings additional stability to the structure. In the simplest case, several heterocyclic rings can be strung together for this purpose. In order to additionally enlarge the chromophore, substituents such as nitro groups, which themselves participate in the delocalization, are useful. The best-known representative is hexanitrostilbene (HNS), which is widely used as a temperature-resistant explosive (Figure 4). New developments involve heterocyclic moieties to the well-established trinitrotoluene units. Worth mentioning are TKX-55 and PYX (Figure 12), which both show lower sensitivities but higher performances at similar decomposition temperatures compared to HNS.[72-73]

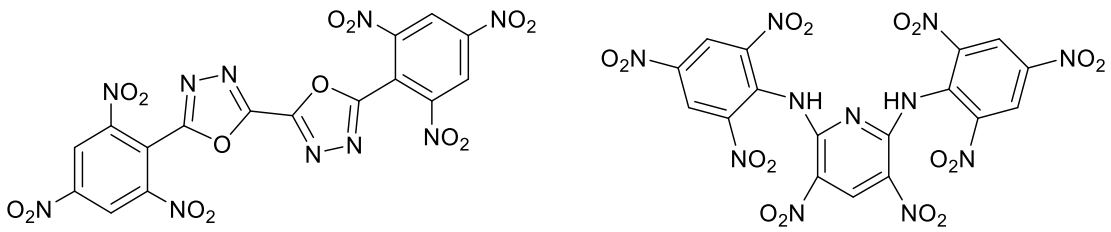

Figure 12. Thermally stable explosives: 5,5'-bis(2,4,6-trinitrophenyl)-2,2'-bi(1,3,4-oxadiazole) (TKX-55) and 2,6-bis(pikrylamino)-3,5-dinitropyridine (PYX).

For most newly developed explosives, it is common to utilize multiple strategies to increase performance and adjust properties. Here, a fine line between sufficient performance, suitable sensitivity and satisfactory stability has to be bridged, which can often only be achieved by trial and error.

1.4 Objectives

In this work, special attention was put on new compounds containing tetrazoles and covalent azides or combinations of these as neutral or ionic compounds. The obtained substances cover the field of new high performing secondary explosives, melt-castable materials, plasticizers, heavy metal-free primary explosives. These substances should fulfill all previously mentioned criteria for a possible use as replacement candidates. A second focus was set to molecules, which are interesting from an academic point of view. This includes substances with particularly low stability, which are on the verge of mere existence (mostly high nitrogen content) as well as particularly unstable molecular motifs, which are difficult to handle and analyze, such as carbonyl azides. Therefore, selected mono-, bis- or tri-heterocyclic systems were modified with specific energetic functional groups to adjust and tune their properties. Figure 13 highlights all utilized heterocyclic motifs, which were used as backbone for synthesis of new energetic materials in this thesis and their respective heats of formation in the gas phase. Except hardly synthetically available pentazole, tetrazole is the heterocycle often favored, as it combines sufficiently high enthalpy of formation, stability and performance with good availability and synthetical accessibility.

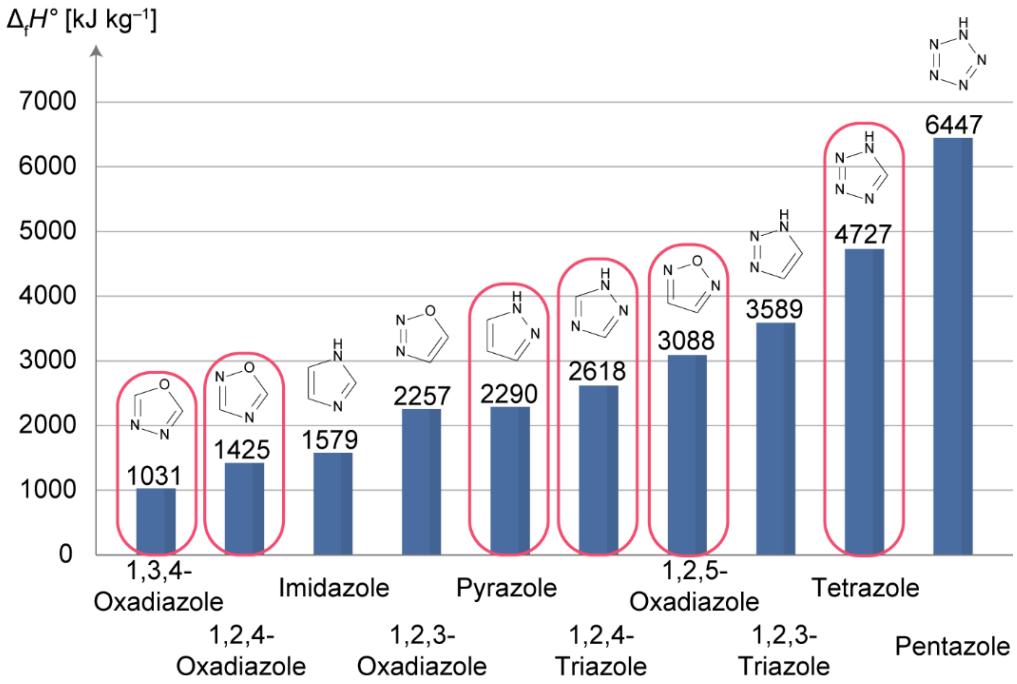

Figure 13. Comparison of frequently utilized azoles' gas phase enthalpy of formation. The values were calculated using the Gaussian09 CBS-4M electronic enthalpies obtained from the atomization method ($\Delta_f H°_{(g,M)} = H_{(M)} - \sum H°_{(A)} + \sum \Delta_f H°_{(A)}$). All heterocycles applicated in this thesis are highlighted in red.

Both predominant motifs, azides and tetrazoles, can be easily introduced. In principle, it is only possible to introduce azide functions in a carbon-bonded form. There are no examples in the literature for N-linked azides on heterocycles, since these are not stable according to calculations and decay similarly to other N-functions. In general, it should be noted that although the enthalpy of formation is drastically increased when azides are introduced, the density of the compounds usually decreases, since azides do not form a good interface for attractive hydrogen bridges due to their hydrophobic character. Azides are mainly obtained through halogen azide exchange reactions or diazotization of hydrazines or hydrazides (Figure 14).

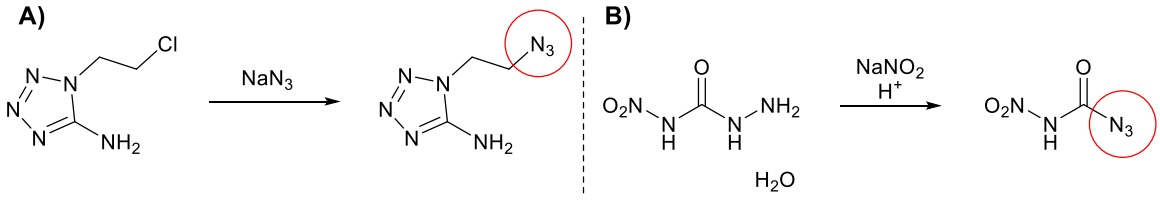

Figure 14. Methods of introducing azides, with selected examples from this work. A) chloro-azide exchange of 1-chloroethyl-5-aminotetrazole with sodium azide; B) diazotization of nitrosemicarbazide with nitrous acid.

Tetrazoles are accessible via click-reactions [3+2 cycloaddition] starting from nitriles and azides. But for the application of tetrazole-containing compounds, multi-substituted compounds are particularly interesting, as they offer several advantages. Apart from a few exceptions (trisubstitution), only monosubstituted (C or N-substitution) or di-substituted (C and N-substitution) tetrazoles are essentially under consideration. In this context, hetero-substitutions are particularly important, since these functions can be used to tune the energetic properties. In addition to the classical energetic substituents such as azido, nitro, nitramino or cyano groups at the C-position, N-oxides and N-amines have proved particularly useful for functionalizing the N-position of a C and N-substituted tetrazole. These units increase the density, lower the acidity and introduce an additional reaction site for further functionalities. Moreover, energetic N-alkyl functions, such as azidoethyl, are also capable of refining the respective moieties into more practical explosives.

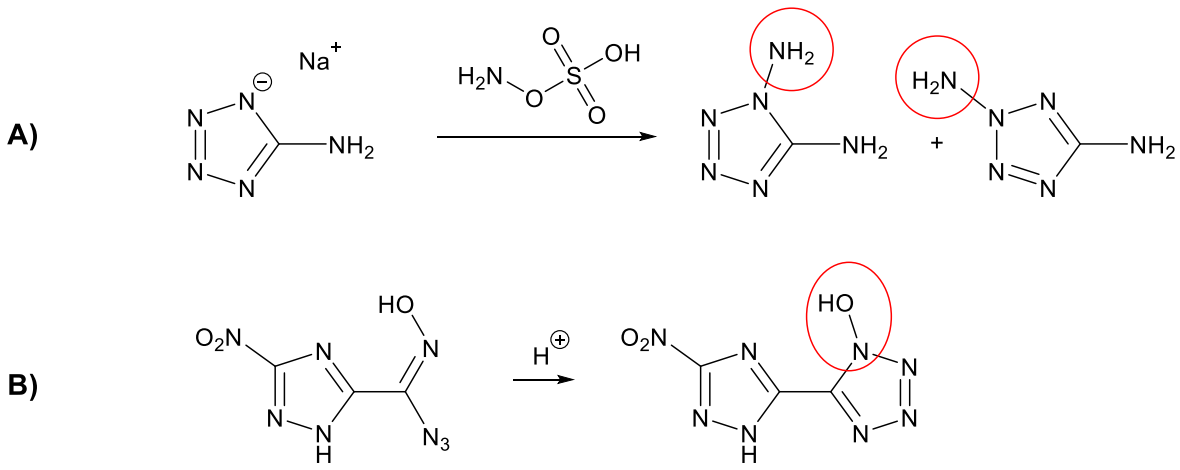

Figure 15. Possible pathways for the synthesis of N-substituted tetrazoles: A) electrophilic substitution of 5-aminotetrazolate using HOSA; B) selective mechanism via azidoxime and acidic produced ring closing reaction.

The introduction of these moieties can basically be achieved through two pathways. Firstly, via an electrophilic substitution reaction of the respective tetrazolate. Here, the formation of isomers can occur dependent on the C-substitution (Figure 15A)). Secondly, via substituted imino azides motifs (e.g. azidoximes, azidohydrazones) which selectively form 1-substituted tetrazoles (Figure 15B)). Both methods were applied extensively to synthesize various new N-substituted tetrazole derivatives.

In addition to the listed main compound components, tetrazoles and azides, almost the entire scope of energetic materials chemistry has been used to create new explosives. This includes the use of numerous endothermic heterocycles, as shown in Figure 13 as well as various energetic functionalization through suitable groups as amino, nitro, nitramino or cyano functions. In addition, compounds with tendentially acidic or basic characteristics were salinized with suitable, energetically useful counterions.

References

[1] E.-C. Koch, *High Explosives, Propellants, Pyrotechnics,* 1st edition, de Gruyter, Berlin/Boston, **2021**.

[2] T. Brinck, *Green Energetic Materials*, 1st edition, John Wiley & Sons, Chichester, **2014**.

[3] J. Akhavan, *The Chemistry of Explosives*, 4th edition, Royal Society of Chemistry, Cambridge, **2022**.

[4] H. Gao, J. M. Shreeve, *Chem. Rev.* **2011**, *111*, 7377–7436.

[5] J. Yount, D. G. Piercey, *Chem. Rev.* **2022**, *122*, 8809–8840.

[6] J. P. Agrawal, *High Energy Materials: Propellants, Explosives and Pryotechnics*, Wiley-VCH, Weinheim, **2010**.

[7] P. A. Politzer, J. S. Murray (Eds.), *Energetic Materials Part1. Decomposition, Crystal and Molecular Properties*, 1st edition, Elsevier, Amsterdam, **2003**, 1–3

[8] R. Meyer, J. Köhler, A. Homburg, *Explosivstoffe*, 10th edition., Wiley-VCH, Weinheim, **2008**, 125–129.

[9] T. M. Klapötke, *Chemistry of High Energy Materials*, 4th edition, de Gruyter, Berlin/Boston, **2017**.

[10] T. L. Davis, *The chemistry of Powder and Explosives*, Volume 3, Parker Publishing Company, West Nyack, **1972**.

[11] F. Zapata, C. Garcia-Ruiz, *Crit. Rev. Anal. Chem.* **2020**, 1–18.

[12] T. Urbanski, *Chemistry and technology of explosives*, Pergamon Press, England, **1985**.

[13] N. Kubota, *Propellants and Explosives: Thermochemical Aspects of Combustion*, 1st edition, Wiley-VCH, Weinheim, **2002**.

[14] B. Sellers, K. Weeks, W. R. Alsop, *Perchlorates Environmental Problems and Solutions,* CRC, Boca Raton FL (USA), **2007**.

[15] H. Bircher, *Chimia*, **2004**, *58*, 355–362.

[16] A. K. Mandal, G. M. Kunjir, J. Singh, S. S. Adhav, S. K. Singh, R. K. Pandey, B. Bhattacharya, M. L. Kantam, *Cent. Eur. J. Energ. Mater.* **2014**, *58*, 83–97.

[17] G. Steinhauser, T. M. Klapötke, *Angew. Chem. Int. Ed.* **2008**, *47*, 3330–3347.

[18] J. Glück, T. M. Klapötke, M. Rusan, J. J. Sabatini, *Angew. Chem. Int. Ed.* **2017**, *56*, 16507–16509.

[19] S. M. Danali, R. S. Palaiah, K. C. Raha, *Def. Sci. J.* **2010**, *60*, 152.

[20] Thomas M. Klapötke, M. Rusan, J. J. Sabatini, *Angew. Chem. Int. Ed.* **2014**, *53*, 9665–9668.

[21] J. J. Sabatini, E.-C. Koch, J. C. Poret, J. D. Moretti, S. M. Harbol, *Angew. Chem. Int Ed.* **2015***, 54,* 10968–10970.

[22] R. Matyas, J. Pachman, *Primary Explosives*, 1st edition, Springer, Heidelberg/New York/Dordrecht/London, **2013**.

[23] W. Beck, J. Evers, M. Göbel, G. Oehlinger, T. M. Klapötke, *Z. Anorg. Allg. Chem.* **2007**, *633*, 1417–1422.

[24] U. Brede, R. Hagel, K. H. Redecker, W. Weuter, *Propellants, Explos. Pyrotech.* **1996**, *21*, 113–117.

[25] D. Gidlow, *Occup. Med.* **2015**, *65*, 348.

[26] M. E. Barsan, A. Müller, *Lead Health Hazard Evaluation* **1996**, HETA Report (Natl. Inst. For Occupational Safety and Health, Cincinnati), No. 91-0346-2572.

[27] J.-S. Li, F.-J. Chen, H.-W. Yang, K.-T. Lu, *Propellants Explo. Pyrotech.* **2020**, *45*, 1313–1325.

[28] R. H. Muir, J. Bragg, A. Pearsall, M. Jorgensen, B. Sims, K. Yonoski, N. Mehta, J. S. Sala, *Org. Process Res. Dev.* **2021**, *25,* 8, 1882–1888.

[29] E. I. Aleksandrov, V. P. Tsipilev, *Combust. Explos. Shock Waves* **1984**, *20*, 690–694.

[30] N. Fischer, M. Joas, T. M. Klapötke, J. Stierstorfer, *Inorg. Chem.* **2013**, *52*, 13791–13802.

[31] M. H. H. Wurzenberger, M. Lommel, M. S. Gruhne, N. Szimhardt, J. Stierstorfer, *Angew. Chem. Int. Ed.* **2020**, *59*, 12367–12370.

[32] T. W. Myers, J. A. Bjorgaard, K. E. Brown, D. E. Chavez, S. K. Hanson, R. J. Scharff, S. Tretiak, J. M. Veauthier, *J. Am. Chem. Soc.* **2016**, *138*, 4685–4692.

[33] G. R. Lotufo, W. Blackburn, S. J. Marlborough, J. W. Fleeger, *Ecotox. Environ. Safe* **2010**, *73*, 1720.

[34] C. A. McFarland, M. J. Quinn Jr., M. A. Bazar, L.G Talent, M. S. Johnson, *Environ. Toxicol. Chem.* **2009**, *28*, 1043–1050.

[35] H. Ek, G. Dave, G. Birgersson, L. Foerlin, *Aquat. Ecosyst. Health Manage.* **2003**, *6*, 415–421.

[36] B. T. Neyer, L. Cox, T. Stoutenborough, R. Tomasoski, *HNS-IV Explosive Properties and Characterization Tests*, Proceedings of 39th Joint Polution Conference, Huntsville, AL (USA), **2003**.

[37] N. Fischer, D. Fischer, T. M. Klapötke, D. G. Piercey, J. Stierstorfer, *J. Mater. Chem.* **2012**, *22*, 20418–20422.

[38] T. M. Klapötke, S. Cudzilo, W. A. Trzcinski, *Propellants, Explos. Pyrotech.* **2022**, *47*, e202100358.

[39] T. Lenz, T. M. Klapötke, M. Mühlemann, J. Stierstorfer, *Propellants Explos. Pyrotech.* **2021**, *46*, 723–731.

[40] D. Fischer, T. M. Klapötke, J. Stierstorfer, N. Szimhardt, *Chem. Eur. J.* **2016**, *22*, 4966–4970.

[41] A. T. Nielsen, R. A. Nissan, A. P. Chafin, R. D. Gilardi, C. F. George, *J. Org. Chem.* **1992**, *57*, 25, 6756–6759.

[42] U. R. Nair, R. Sivabalan, G. M. Gore, M. Geetha, S. N. Asthana, H. Singh, *Combust., Explos. Shock Waves* 2005, *41*, 2, 121–132.

[43] N. C. Johnson, *CL-20 sensitivity round robin*, Naval Surface Warfare Center 2003.

[44] P. Leffler, E. Brännäs, D. Ragnvaldsson, H. Wingfors, R. Berglind, *Toxicol. Environ. Health A.* **2014**, *77*, 19, 1183–1191.

[45] L. A. Smock, D. L. Stoneburner, J. R. Clark, *Water Res.* **1976**, *10*, 6, 537–543.

[46] R. E. Card Jr., R. Autenrieth, *Treatment of HMX and RDX Contamination*, Amarillo National Resource Center for Plutonium, **1998**.

[47] S. Shaligram, A. Campbell, *Toxicol. In Vitro*, **2013**, *27*, 2, 844–851.

[48] D. Carrington, *Wide range of cars emit more pollution in realistic driving tests, data shows,* The Guardian, 30 September **2015**.

[49] R. Cihan, *Interdiscip. Toxicol.* **2009**, *2*, 2, 42–44.

[50] M. Suceska, *EXPLO5-Computer program for calculation of detonation parameters*, **2001**.

[51] *Test methods according to the UN Recommendations on the Transport of Dangerous Goods, Manual of Tests and Criteria*, 4th edition, United Nations Publication, New York/Geneva, **2003**.

[52] Impact: insensitive > 40 J, less sensitive ≥ 35 J, sensitive ≥ 4 J, very sensitive ≤ 3 J; friction: insensitive > 360 N, less sensitive = 360 N, sensitive < 360 N a. > 80 N, very sensitive ≤ 80 N, extreme sensitive ≤ 10 N; According to the UN Recommendations on the Transport of Dangerous Goods.

[53] D. Fischer, J. L. Gottfried, T. M. Klapötke, K. Karaghiosoff, J. Stierstorfer, T. G. Witkowski, *Angew. Chem. Int. Ed.* **2016**, *55*, 16132–16135.

[54] L. E. Fried, M. R. Manaa, P. F Pagoria, R. L. Simpson, *Annu: Rev. Mater. Res.* **2001**, *31*, 9219–9228.

[55] P. Yin, D. A. Parrish, J. M. Shreeve, *J. Am. Chem. Soc.* **2015**, *137*, 4778–4786.

[56] R. A. Wiscons, M. K. Bellas, J. C. Bennion, A. J. Matzger, *Cryst. Growth Des.* **2018**, *18*, 7701–7007.

[57] D. Fischer, T. M. Klapötke, D. G. Piercey, J. Stierstorfer, *Chem. Eur. J.* **2013**, *19*, 4602–4613.

[58] R. Yang, Z. Dong, Z. Ye, *ChemistrySelect,* **2019**, *4*, 14208–14213.

[59] S. E. Creegan, M. Zeller, E. F. C. Byrd, D. G. Piercey, *Cryst. Growth Des.* **2021**, *21*, 3922–3927.

[60] S. Zhang, G. Cheng, H. Yang, *Dalton Trans.* **2020**, *49*, 5590–5596.

[61] D. G. Piercey, D. E. Chavez, B. L. Scott, G. H. Imler, D. A. Parrish, *Angew. Chem. Int. Ed.*, **2016**, *55*, 15315–15318.

[62] M. Deng, Y. Feng, W. Zhang, X. Qi, Q. Zhang, *Nat. Comm.* **2019**, *10*, 1339–1346.

[63] M.-Xi. Zhang, P. E. Eaton, R. Gilardi, *Angew. Chem. Int. Ed.* **2000**, *39*, 2, 401–404.

[64] P. E. Eaton, M.-Xi. Zhang, R. Gilardi, N. Gelber, S. Iyer, R. Surapaneni, *Propellants, Explos. Pyrotech.* **2002**, *27*, 1–6.

[65] A. S. Lyakhov, P. N. Gaponik, S. V. Voitekhovich, *Acta Crystallogr. Sect. C: Cryst. Struct. Commun.* **2001**, *57*, 185–186.

[66] T. M. Klapötke, D. G. Piercey, J. Stierstorfer, *Dalton Trans.* **2012**, *41*, 9451–9459.

[67] N. Fischer, T. M. Klapötke, M. Reymann, J. Stierstorfer, *Eur. J. Inorg. Chem.* **2013**, 2167–2180.

[68] N. Fischer, T. M. Klapötke, S. Marchner, M. Rusan, S. Scheutzow, J. Stierstorfer, *Propellants Explos. Pyrotech.* **2013**, *38*, 448–459.

[69] A. A. Dippold, T. M. Klapötke, *J. Am. Chem. Soc.* **2013**, *135*, 9931–9938.

[70] D. Fischer, T. M. Klapötke, J. Stierstorfer, *Angew. Chem. Int. Ed.* **2014**, *53*, 8172–8175.

[71] C. He, J. M. Shreeve, *Angew. Chem. Int. Ed.* **2016**, *55*, 772–775.

[72] T. M. Klapötke, T. G. Witkowski, *ChemPlusChem* **2016**, *81*, 357–360.

[73] T. M. Klapötke, J. Stierstorfer, M. Weyrauther, T. G. Witkowski, *Chem. Eur. J.* **2016**, *22*, 8619–8626.

2. Nitro carbamoyl Azide $O_2NN(H)C(O)N_3$: A Stable but Highly Energetic Member of the Carbonyl Azide Family

Maximilian Benz, Thomas M. Klapötke, Burkhard Krumm, Marcus Lommel and Jörg Stierstorfer

as published in *Journal of the American Chemical Society* **2021**, *143*, *3*, 1323–1327

DOI: 10.1021/jacs.0c12507

Keywords: acyl azides, diazotization, energetic material, sensitivities, structure elucidation

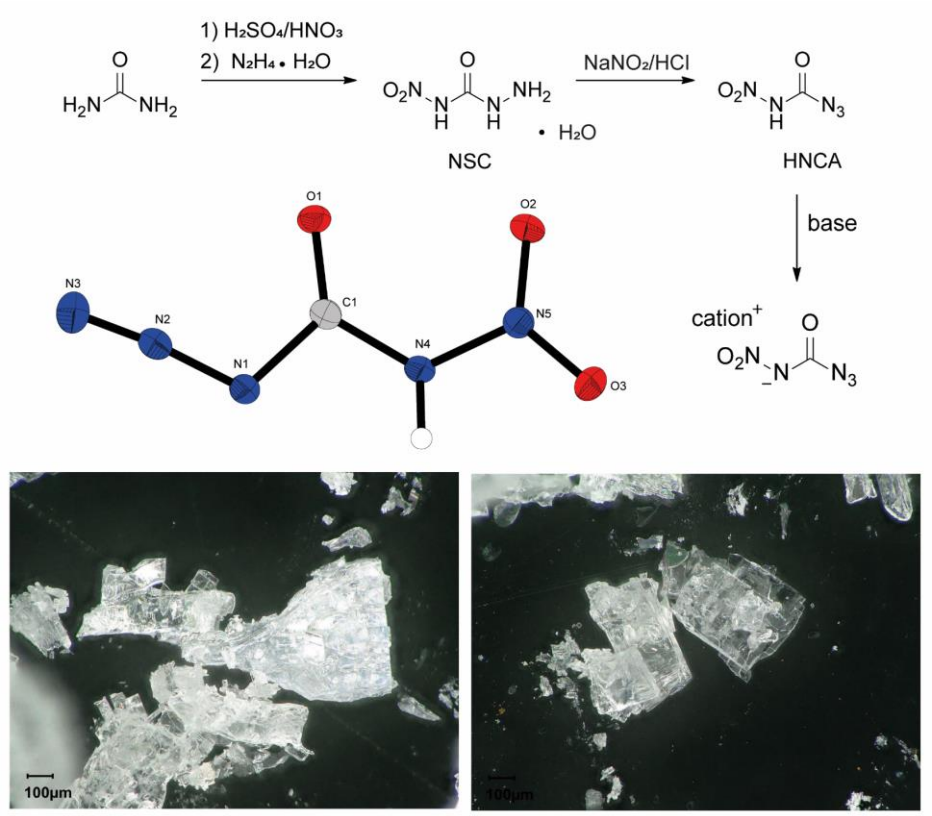

A combined nitrogen and oxygen content of over 90%! By combining azide and nitramine functionality, a unique, low-molecular weight compound was synthesized, which is of great interest not only for its energetic character, but also for its unique molecular chemical properties and decomposition mechanism.

Abstract: The diazotization of nitrosemicarbazide (**1**) resulted in the formation and isolation of nitrocarbamoyl azide (**2**), which was thoroughly characterized by spectroscopic and structural methods. This compound shows surprising stability but also high reactivity and sensitivity, with a melting point of 72 °C and a detonative decomposition point at 83 °C. In addition, five selected salts were synthesized by careful deprotonation. The decomposition mechanism of **2** in solution was investigated and could be clarified by performing experiments using methanol and hydrazine as trapping reagents. The energetic and physicochemical properties of all these compounds were investigated and classified.

2.1 Introduction

Although in most cases they are short-lived, carbonyl azides ($RC(O)N_3$) have been known for more than a century.[1-2] Especially their decomposition to form isocyanates, named after Curtius, makes them interesting and indispensable from a synthetic point of view.[3-5] Nevertheless, there are only a small number of well-characterized low-molecular-weight representatives. Synthesis and proper analysis are complicated by the low stability and often by the explosive nature of acyl azides.[6] Nevertheless, over the past few years it has been possible to completely analyze some simple carbonyl azides such as formyl azide and carbonyl diazide.[7-9] Other simple carbonyl azides such as carbamoyl azide or oxalyl diazide have been described in the literature, but their structures and properties are not yet fully understood (Figure 1).[10-14] Nitrocarbamoyl azide (HNCA, **2**) is another representative of this substance class that is interesting from many perspectives. Above all, this compound is characterized by the fact that with azide and nitramine functions it should have good energetic potential. This was also recognized by Bottaro et al., who attempted to synthesize NCA^- salts by nitration of carbamoyl azides.[15] However, the claimed ionic materials were examined only by IR spectroscopy.[15] In addition, several questions regarding the molecule arise from an academic point of view. On one hand, the acidic proton of the nitramine unit offers many possibilities for functionalization of this site, but on the other hand, it is also uncertain to what extent the decomposition mechanism is affected. By following the Curtius rearrangement for the decomposition of carbonyl

azides, HNCA would provide a platform for further chemistry with various nucleophiles. Furthermore, reactions with energetic building blocks could generate an innovative access to future energetic materials. In this contribution, the synthesis, properties, and crystal structures of pure nitrocarbamoyl azide and several of its salts and decomposition products are reported.

2.2 Results and Discussion

HNCA (**2**) can be synthesized by diazotization of nitrosemicarbazide (**1**)[16-17] with a slight excess of sodium nitrite in 2 M HCl at 0 °C.

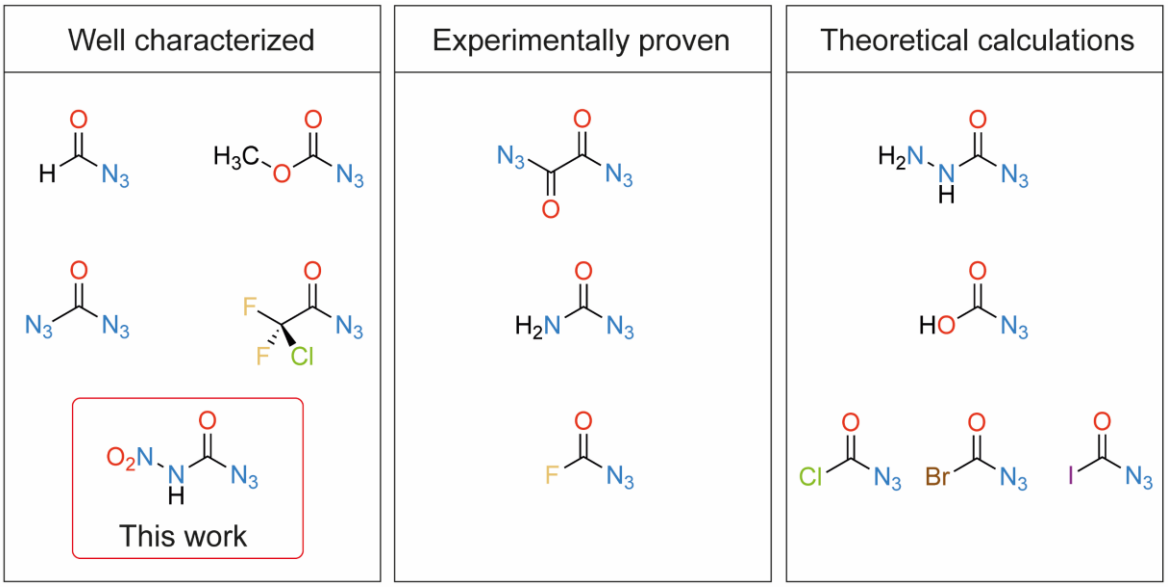

Figure 1. Smallest representatives of the carbonyl azide family.

Yields of up to 76% can be achieved by rapid extraction of the reaction solution with diethyl ether and quick removal of the solvent under a nitrogen stream. These conditions proved to be particularly practicable and favorable, as direct access to neutral **2** was gained (*Caution:* it is strongly recommended that full body protection be worn during work with any compound discussed here). HNCA crystallizes in the form of colorless needle-shaped crystals and is stable under ambient conditions for several weeks. Salts were obtained by dissolving **2** in cold methanol and then adding 1 equiv of the respective bases (Scheme 1).

In order to obtain insight into the structure and bonding of HNCA, the molecular orbital (MO) energies were calculated for three different potential tautomers using the G09W code and various resonance structures using the VB2000 code (version 2.8) (further details and results are provided in the Supporting Information).

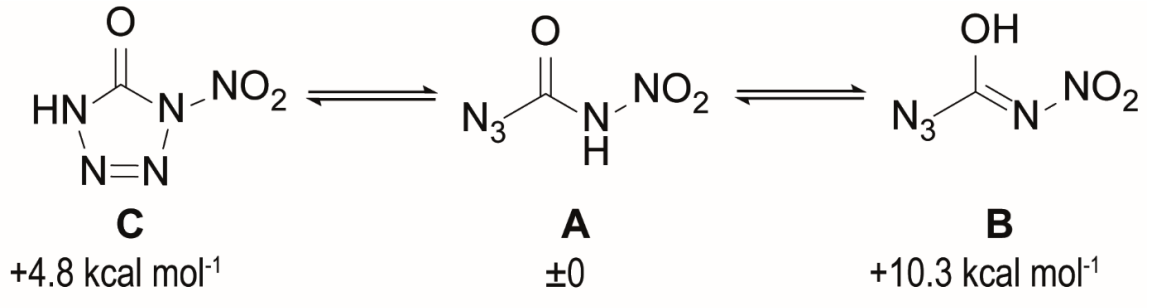

Figure 2. Tautomers of HNCA (**2**): **A**, amide form; **B**, iminol form; **C**, 1-nitrotetrazolone form. Energies relative to **A** are shown.

Of particular interest were the proton location as well as whether there was some indication supporting the presence of the closed tetrazole tautomer. The MO energies of the three tautomers in Figure 2 were calculated at the B3LYP/cc-pVDZ level. The energies of conformations **B** and **C** relative to the amide form **A** are 10.3 and 4.8 kcal mol^{-1}, respectively. The equilibrium is therefore strongly in favor of tautomer **A**. To confirm the theoretical findings, the focus was set on low-temperature single-crystal X-ray diffraction measurements.

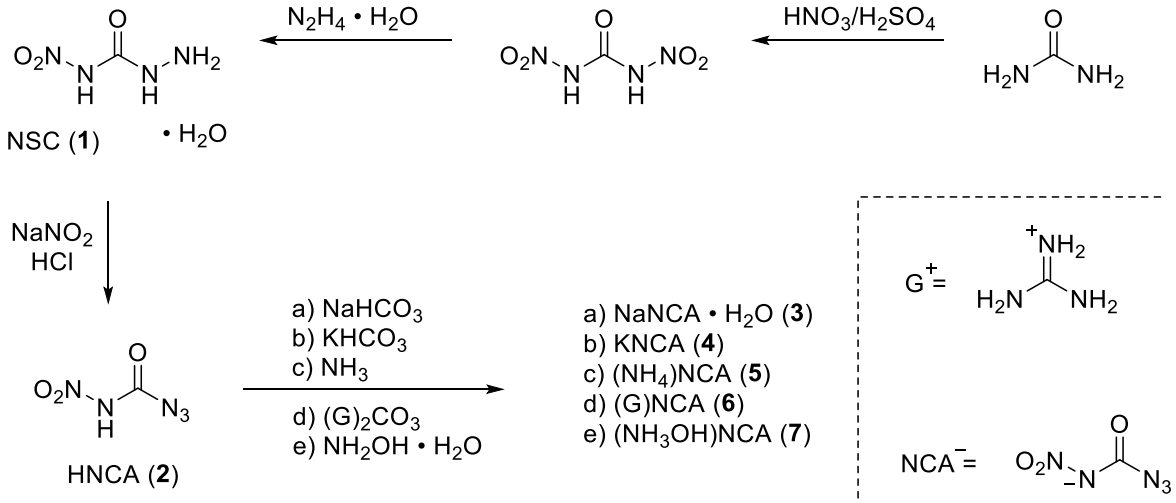

Scheme 1. Synthetic pathway toward HNCA (**2**) and its salts **3**–**7**.

The crystal structures of compounds **1**−**8** were successfully determined. All of the data and structures are shown in the Supporting Information. Despite their high sensitivity toward external stimuli, crystalline **2** is fine to handle, and crystals suitable for X-ray measurements were obtained directly from the crude product. HNCA crystallizes in the monoclinic space group $P2_1/c$ with four molecular units per unit cell (Figure 3). Similar to other comparable carbonyl azides, the azide group is syn to the carbonyl function with respect to the C−N_α bond.[8, 18-19] The molecule itself is nearly planar. Although the azide group is almost in a plane with respect to C=O (N3−N2−N1−C1, 2.1(15)°; N2−N1−C1−O1, 178.62(15)°), the nitro group of the nitramine is twisted out of this plane (O1−C1−N1) by about 10 °. As expected, the azide functionality shows an angle of 174.03(13)° due to negative hyperconjugation and long bonding effects. This is in accordance with the angle in $HC(O)N_3$ (174.49(17)°) and only slightly larger than those in $OC(N_3)_2$ (172.1(5)°, 172.6(6)°). The N1−N2 (1.2685(18) Å) and N2−N3 (1.233(5) Å) bond lengths show no divergence toward other members of the carbonyl azide family (Figure 1).[8-9]

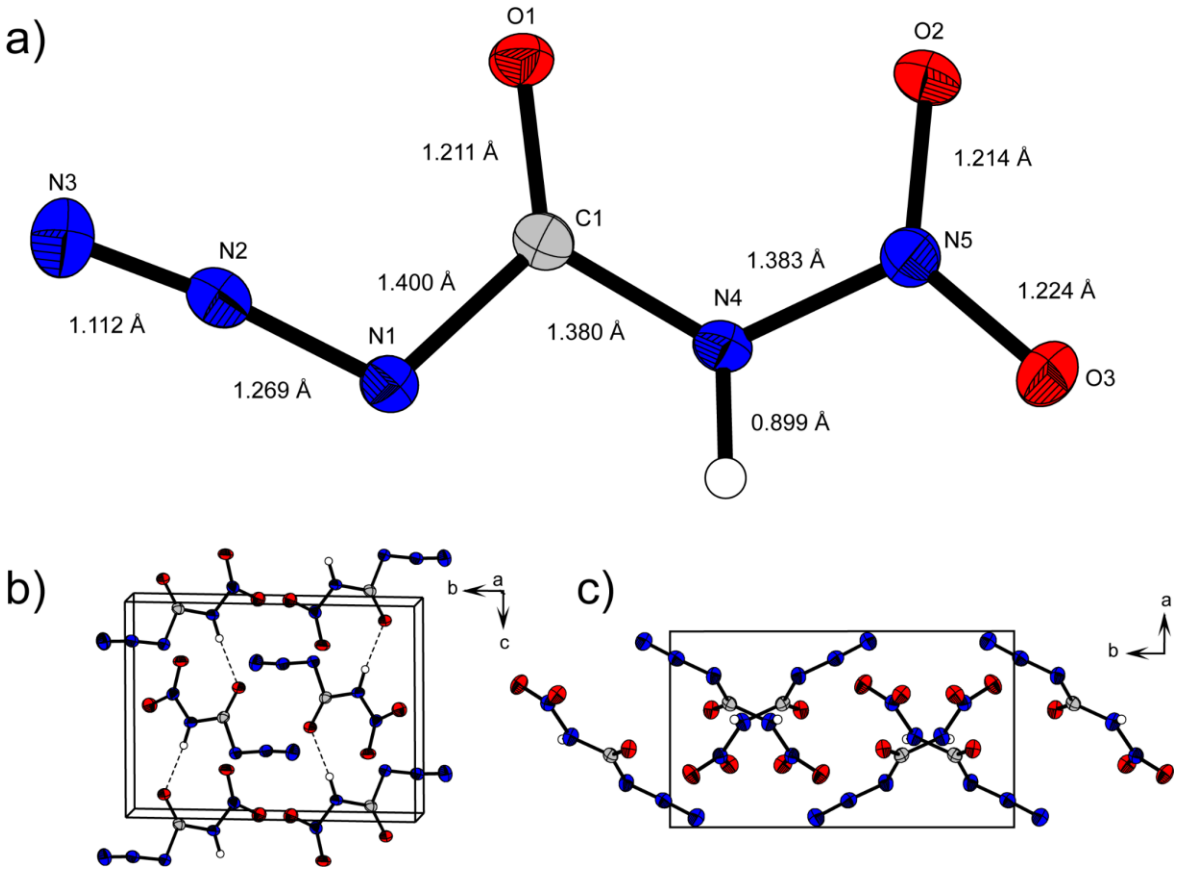

Figure 3. (a) Molecular structure and bond lengths of **2** as determined by low-temperature X-ray diffraction with thermal ellipsoids drawn at the 50% probability level. (b, c) Views of the packing of **2** (b) slightly twisted along the *a* axis and (c) along the *c* axis. Intramolecular H···O interactions are shown as dotted lines.

The sufficient stability and solubility of the parent molecule **2** allowed characterization not only by ^{13}C NMR spectroscopy (δ = 152.1 ppm, ^{1}H resonance not observed) but also by ^{15}N NMR spectroscopy. Since significant decomposition was observed at room temperature, the ^{15}N spectrum was recorded at 0 °C in methanol-d_4. All five resonances were observed, with assignments as displayed in Figure 4 (δ = −45.6, −140.0, −147.2, −184.6, and −262.7 ppm). The resonance of the α-nitrogen atom (N-1) of the azido moiety is significantly shifted to lower field compared with those of organic azides, which is typical for carbonyl azides.[20] In a similar fashion, the resonance of the γ-nitrogen atom (N-3) is also shifted to lower field and detected "left" of that of the β-nitrogen atom (N-2). The assignments of N_β ($\Delta\nu_{1/2}$ = 50 Hz) and N_γ ($\Delta\nu_{1/2}$ = 140 Hz) were based on the line widths of the resonances in the corresponding ^{14}N NMR spectrum. The resonances of the nitramine moiety are found in the typical regions, with the nitro group at −45.6 ppm and the amine resonance at −184.6 ppm.[19, 21] Because of the low solubility and quick decomposition even in cold methanol, only ^{14}N NMR data for the NCA^- anion are available. With ammonium salt **5** as a representative example, in addition to the ammonium signal (−367 ppm, $\Delta\nu_{1/2}$ = 6 Hz), four further resonances are detectable for the NCA^- anion. The signals for the azide nitrogen atoms at −135 ppm ($\Delta\nu_{1/2}$ = 45 Hz), −143 ppm ($\Delta\nu_{1/2}$ = 112 Hz), and −267 ppm ($\Delta\nu_{1/2}$= 162 Hz) are similar to those of the neutral compound. However, the signal of the nitro group is significantly downfield-shifted to −10 ppm ($\Delta\nu_{1/2}$ = 42 Hz) upon deprotonation (the nitramide nitrogen resonance was not observed in the ^{14}N NMR spectrum because of the extremely large line width).

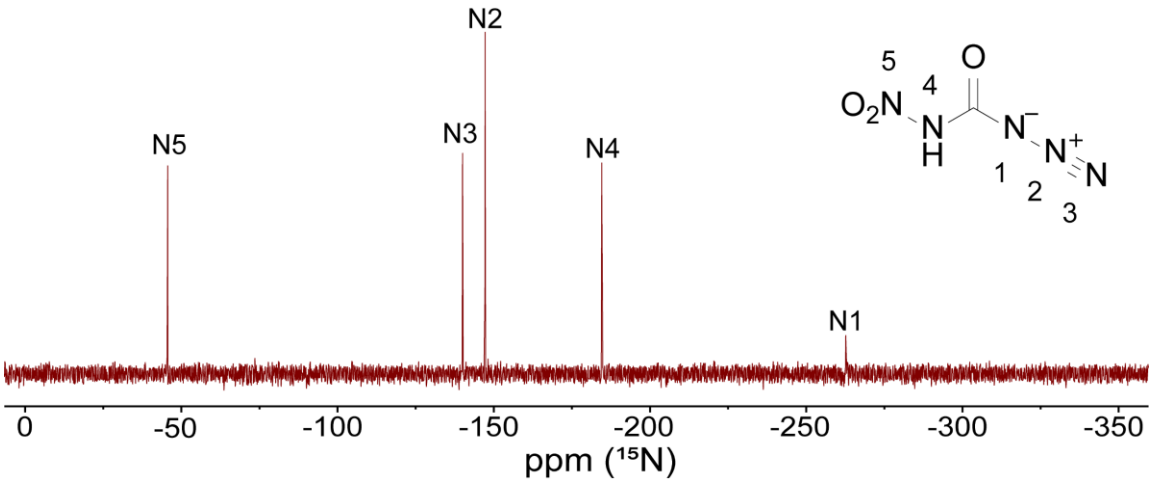

Figure 4. ^{15}N NMR spectrum of **2** in CD_3OD at 0 °C.

As already mentioned above, **2** is bench-stable but decomposes rapidly in solution at ambient temperature, especially in protic solvents. The decomposition of **2** probably does not proceed via a Curtius rearrangement to the isocyanate, as usually occurs for carbonyl azides.[22-24] However, neither isocyanatonitramine nor derivatives thereof were observed as decomposition products. In our opinion, elimination of HN_3 to form an intermediate nitroisocyanate in solution seems likely. The latter has already been reported and analyzed.[25] This hypothesis is supported by trapping reactions with hydrazine hydrate and methanol as nucleophiles, yielding compounds **1** and **8**. In an attempt to form a hydrazinium salt of **2**, the precursor molecule **1** was obtained and isolated in almost quantitative yield. Furthermore, treatment of **2** in methanol at 60 °C furnished methyl nitrocarbamate (**8**) (Scheme 2).

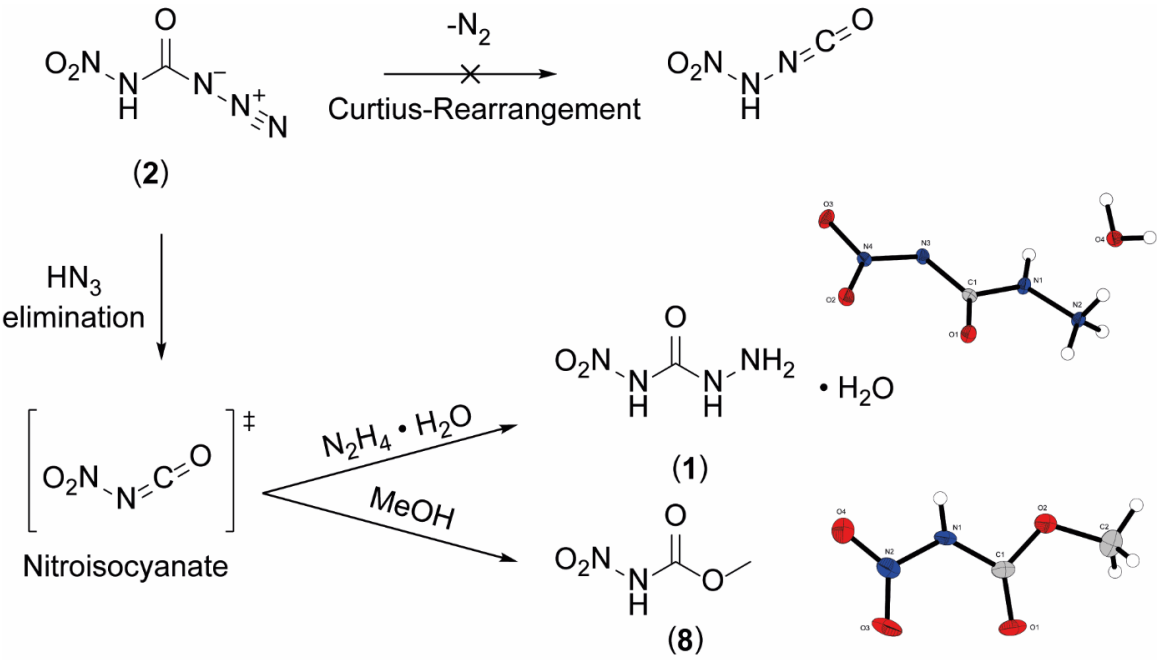

Scheme 2. Proposed decomposition mechanism of **2** and trapping reactions of the intermediate nitroisocyanate with methanol and hydrazine hydrate as nucleophiles.

Besides the guanidinium salt **6** (115 °C), the most temperature-stable compound is the potassium salt, which decomposes by detonation at 120 °C (Table 1). Therefore, KNCA (**4**) was investigated in a classic initiation capability test using pressed pentaerythritol tetranitrate (PETN) as the main charge.

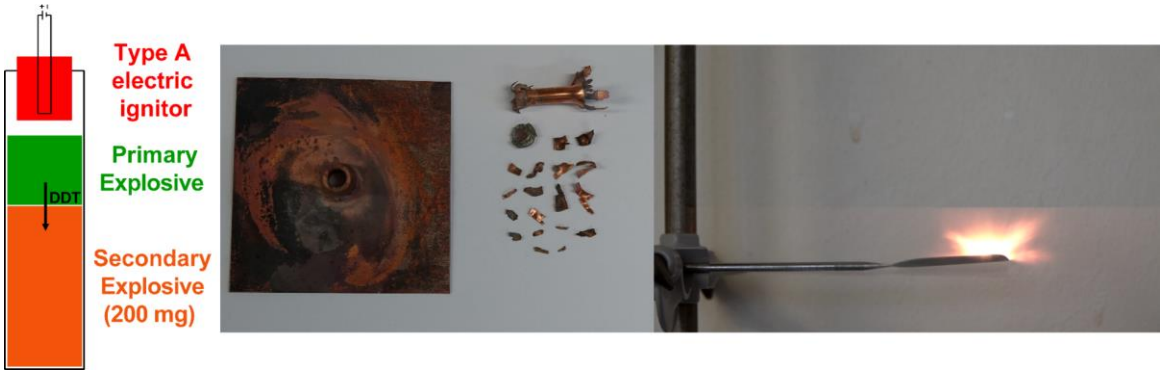

Figure 5. Schematic initiation test setup (left), result of the initiation test of potassium salt **4** toward PETN (center), and flame test of 5 mg of **4** with the moment of detonation (right).

Salt **4** (30 mg) was loosely filled on top of the secondary explosive and ignited using an electrical ignitor, and it was able to cause a positive deflagration-to-detonation transition (DDT) toward the PETN loading (Figure 5). This was indicated by a hole in the copper plate and fragmentation of the shell.

Table 1. Energetic properties and detonation parameters of **1**–**7**.

	1	**2**	**3**	**4**	**5**	**6**	**7**
Formula	$CH_4N_4O_3{\cdot}H_2O$	CHN_5O_3	$NaCN_5O_3{\cdot}H_2O$	KCN_5O_3	$CH_4N_6O_3$	$C_2H_6N_8O_3$	$CH_4N_6O_4$
IS [J][a]	5	<1	<1	<1	6	40	≤3
FS [N][b]	48	0.5	0.4	<0.1	20	324	≤40
ESD [J][c]	0.1	n.d.	0.065	<0.01	0.16	0.27	n.d.
ρ [g cm^{-3}][d]	1.814	1.708	1.891	1.986	1.683	1.648	1.803
N+O [%][e]	87.0	90.0	78.4	69.8	89.2	84.2	90.2
Ω [%][f]	−11.6	6.1	0	4.7[j]	−10.8	−33.7	0
T_{dec} [°C][g]	156	83	81	120	79	115	93
$\Delta_f H^\circ$ [kJ/mol;kJ/g][h]	−88.5; −0.65	147.5; 1.13	−445.8; −2.61	−44.4; −0.26	104.6; 0.71	79.0; 0.42	156.6; 0.95
			EXPLO5 V6.05.02				
$-\Delta_{Ex} U^0$ [kJ kg^{-1}][i]	-	5066	-	4227	4924	3853	6233
P_{CJ} [kbar][j]	-	270	-	223	293	222	367
V_{det} [ms^{-1}][k]	-	8333		7441	8620	7879	9460

[a] Impact sensitivity. [b] Friction sensitivity. [c] Electrostatic discharge. [d] From X-ray diffraction analysis recalculated to 298 K. [e] Combined Nitrogen and Oxygen content. [f] Oxygen balance with respect to CO formation. [g] Decomposition temperature (onset values; β = 5 °C min^{-1}). [h] Calculated enthalpy of formation. [i] Calculated energy of formation. [j] Detonation pressure. [k] Detonation velocity.

The sensitivities cover almost the entire spectrum and range from the insensitive guanidinium salt **6** (impact sensitivity (IS) = 40 J; friction sensitivity (FS) = 324 N) to the extremely sensitive potassium salt **4** (IS < 1 J; FS < 0.1 N). Neutral HNCA has sensitivities of <1 J toward impact and 0.5 N toward friction, which are in the ranges for a primary explosive. The electrostatic discharge (ESD) sensitivities follow the general sensitivity trend. No ESD sensitivity values are given for **3** and **7** because those salts melted under the electrical load.

For all of the water-free compounds, the detonation parameters were calculated using the EXPLO5 code (further details and results are provided in the Supporting Information). All of the metal-free compounds (**2** and **5**–**7**) show positive enthalpies of formation.[26] The calculated detonation velocity (V_{det}) values range from 7441 m s^{-1} for the potassium salt **4** to a remarkable value of 9460 m s^{-1} for the hydroxylammonium salt **7** (Table 1). Thus, **7** outperforms HMX (V_{det} = 9193 m s^{-1}) in terms of detonation velocity and has a value close to that of CL-20 (V_{det} = 9772 m s^{-1}). The neutral compound **2** has V_{det} = 8333 m s^{-1} and a detonation pressure (P_{CJ}) of 270 kbar, which are similar to those of PETN (V_{det} = 8429 m s^{-1}; P_{CJ} = 308 kbar).

2.3 Conclusion

In summary, the synthesis and thorough characterization of nitrocarbamoyl azide (HNCA, **2**) and several salts are reported. HNCA is solid at room temperature (because of the strong hydrogen bridge with a length of d(D–H···A = 2.808(2) Å), melts at 72 °C, and decomposes at 83 °C. The predominantly sensitive compounds show interesting results in the calculation of the detonation parameters, especially the hydroxylammonium salt **7** with V_{det} = 9460 m/s. The potassium salt **4** is a high-performing primary explosive that showed a positive result in an initiation test on 200 mg of PETN. A mechanism for the decomposition of **2** was proposed and verified by two trapping experiments. The mechanism does not follow the Curtius rearrangement as is usual for carbonyl azides, but instead, elimination of hydrazoic acid to form an intermediate nitroisocyanate occurs.

2.4 Acknowledgments

This work is dedicated to the memory of Professor Klaus Banert. Financial support of this work by Ludwig-Maximilian University (LMU), the Office of Naval Research (ONR) under Grant ONR N00014-19-1-2078, and the Strategic Environmental Research and Development Program (SERDP) under Contract W912HQ19C0033 is gratefully acknowledged. We thank Dr. Jiabo Li for providing us with VB2000 version 2.8 and for his help with the CAS calculation. We also thank Dr. Constantin Hoch for taking the photos of HNCA.

2.5 References

[1] T. Curtius, *Ber. Dtsch. Chem. Ges.* **1894**, *27*, 778–781.

[2] T. Curtius, *Ber. Dtsch. Chem. Ges.* **1890**, *23*, 3023–3033.

[3] J. Lee, J. Lee, H. Jung, D. Kim, J. Park, S. Chang, *J. Am. Chem. Soc.* **2020**, *142*, 12324–12332.

[4] Q. Wang, J. A. May, *Org. Lett.* **2020**, *22*, 3039–3044.

[5] M. Balci, *Synthesis* **2018**, *50*, 1373–1401.

[6] S. Bräse, C. Gil, K. Knepper, V. Zimmermann, *Angew. Chem. Int. Ed.* **2005**, *44*, 5188–5240.

[7] K. Banert, C. Berndt, M. Hagedorn, H. Liu, T. Anacker, J. Friedrich, G. Rauhut, *Angew. Chem. Int. Ed.* **2012**, *51*, 4718–4721.

[8] X. Zeng, M. Gerken, H. Beckers, H. Willner, *Inorg. Chem.* **2010**, *49*, 9694–9699.

[9] X. Zeng, E. Bernhardt, H. Beckers, K. Banert, M. Hagedorn, H. Liu, *Angew. Chem. Int. Ed.* **2013**, *52*, 3503–3506.

[10] J. Thiele, O. Stange, *Liebigs Ann.* **1894**, *283*, 1–46.

[11] S. Mohan, K. S. P. Durairaj, S. P. Jose, *Spectrochim. Acta, Part A* **2003**, *59*, 1697–1704.

[12] H. W. Roesky, O. Glemser, *Chem. Ber.* **1964**, *97*, 1710–1712.

[13] L. Fengyi, Z. Xiaoqing, S. Qiao, M. Lingpeng, Z. Shijun, A. Xicheng, Z. Jianping, G. Maofa, W. Dianxun, *Bull. Chem. Soc. Jpn.* **2005**, *78*, 1246–1250.

[14] K. Banert, C. Berndt, S. Firdous, M. Hagedorn, Y.-H. Joo, T. Rüffer, H. Lang, *Angew. Chem. Int. Ed.* **2010**, *49*, 10206–10209.

[15] J. C. Bottaro, M. A. Petrie, P. E. Penwell, A. L. Dodge, R. Malhotra, NANO/HEDM Technology: Late Stage Exploratory Effort; Report No. A466714; SRI International: Menlo Park, CA, 2003; DARPA/AFOSR funded, contract no. F49620-02-C-0030.

[16] V. S. Glukhacheva, S. G. Il'yasov, G. V. Sakovich, T. G. Tolstikova, A. O. Bryzgalov, N. V. Pleshkova, *Russ. Chem. Bull.* **2016**, *65*, 550–560.

[17] S. G. Il'yasov, A. A. Lobanova, N. I. Popov, R. R. Sataev, *Russ. J. Org. Chem.* **2002**, *38*, 1731–1738.

[18] L. A. Ramos, X. Zeng, S. E. Ulic, H. Beckers, H. Willner, C. O. Della Védova, *J. Org. Chem.* **2012**, *77*, 6456–6462.

[19] A. Baumann, A. Erbacher, C. Evangelisti, T. M. Klapötke, B. Krumm, S. F. Rest, M. Reynders, V. Sproll, *Chem. Eur. J.* **2013**, *19*, 15627–15638.

[20] K. Banert, Y.-H. Joo, T. Rüffer, B. Walfort, H. Lang, *Angew. Chem. Int. Ed.* **2007**, *46*, 1168–1171.

[21] T. S. Hermann, T. M. Klapötke, B. Krumm, J. Stierstorfer, *J. Heterocycl. Chem.* **2018**, *55*, 852–862.

[22] T. Curtius, *J. Prakt. Chem.* **1895**, *52*, 243–271.

[23] H. M. Singleton, W. R. Edwards, *J. Am. Chem. Soc.* **1938**, *60*, 540–544.

[24] M. Okaniwa, K. Takeuchi, M. Asai, M. Ueda, *Macromolecules* **2002**, *35*, 6224–6231.

[25] T. M. Klapötke, A. Schulz, *Inorg. Chem.* **1996**, *35*, 7897–7904.

[26] M. Rahm, G. Belanger-Chabot, R. Haiges, K. O. Christe, *Angew. Chem., Int. Ed.* **2014**, *53*, 6893–6897.

2.6 Supporting Information

2.6.1 Experimental and General Procedure

^{1}H, ^{13}C, ^{14}N and ^{15}N NMR spectra were recorded on *BRUKER AMX 400* instruments. Chemical shifts are referenced with respect to tetramethylsilane ($^{1}H/^{13}C$) and nitromethane ($^{14}N/^{15}N$). Infrared spectra (IR) were recorded in the region 4000-400 cm^{-1} on a *PERKIN ELMER Spectrum BX-59343* instrument with

a *SMITHS DETECTION DuraSamplIR II Diamond ATR* sensor. Raman spectra were recorded with a Bruker MultiRAM FT-Raman instrument fitted with a liquid-nitrogen cooled germanium detector and a Nd:YAG laser (λ = 1064 nm) The absorption bands are reported in wavenumbers (cm^{-1}). Decomposition temperatures were measured via differential thermal analysis (DTA) with an *OZM Research DTA 552-Ex* instrument at a heating rate of 5 °C/min and in a range of room temperature to 400 °C. All sensitivities toward impact (IS) and friction (FS) were determined according to BAM (Bundesanstalt für Materialforschung und Prüfung) standards using a BAM drop hammer and a BAM friction apparatus by applying the 1 of 6 method.[S1] All energetic compounds were tested for sensitivity towards electrical discharge using an *Electric Spark Tester ESD 2010 EN* from OZM. Energetic properties have been calculated with the EXPLO5 6.02 computer [S2] code using the RT converted X-ray density and calculated solid state heats of formation.

CAUTION! *All investigated compounds are potentially explosive materials. In particular the potassium salt, KNCA, is extremely sensitive and tends to explode in dry state. Safety precautions and equipment (such as wearing leather coat, face shield, Kevlar sleeves, Kevlar gloves, earthed equipment and ear plugs) must be used during all manipulations.*

Nitrosemicarbazide (**1**)[S3, S4]

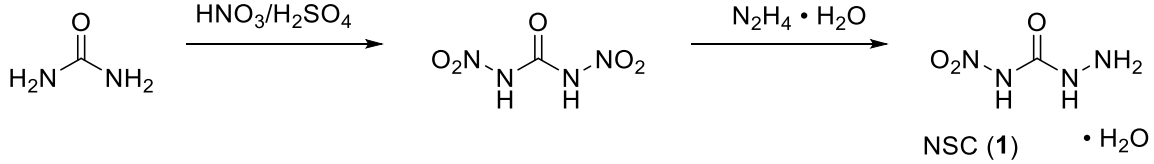

Urea (3.00 g, 50 mmol, 1.0 eq) was carefully added to a mixture of sulfuric acid (6.0 mL, 96%) and nitric acid (8.0 mL, 100%) at 0 °C. The mixture was stirred below 5 °C for one hour during which time a white precipitate was formed. The solid was filtered and washed with trifluoroacetic acid (3 x 20 mL) to remove the remaining nitration mixture to yield dinitrourea (4.90 g, 32.7 mmol, 65%) as white powder, which was subsequently solved in water (4.0 mL). The mixture was cooled with an ice bath and hydrazine monohydrate (1.60 mL, 33.0 mmol, 1.0 eq) was

added dropwise. After the addition was complete, the mixture was allowed to stir at 30 °C for 1 h, during which time a white precipitate was formed. The solid was filtered and washed with little amounts of ice water to obtain nitrosemicarbazide monohydrate (**1**) (1.30 g, 29%). The total yield is 19%.

DTA (5 °C min^{-1}):105 °C (H_2O), 156 °C (dec); Sensitivities: BAM drop hammer: 5 J, friction tester: 48 N, ESD: 0.1 J (at grain size 100–500 µm). IR (ATR) $\tilde{\nu}$ (cm^{-1}) = 3400(m), 3122(m), 2991(m), 1657(s), 1623(m), 1573(m), 1539(s), 1498(s), 1391(s), 1329(s), 1291(m), 1237(s), 1192(s), 1155(s), 1085(s), 1047(m), 1032(s), 971(m), 816(m), 784(s), 747(m), 722(m), 596(s), 532(s), 469(vs), 439(vs), 418(vs); Elem. Anal. ($C_4H_6N_4O_4$, 138.08 g mol^{-1}) calcd.: C 8.70, H 4.38, N 40.58%. Found: C 8.58, H 4.33, N 40.64%; ^{1}H NMR (DMSO-D_6, 400 MHz, ppm) δ = 11.25 (s, 3H), 8.20 (br s, 1H), 3.36 (s, 2H); ^{13}C NMR (DMSO-D_6, 101 MHz, ppm) δ = 153.9.

Nitrocarbamoyl azide (**2**)

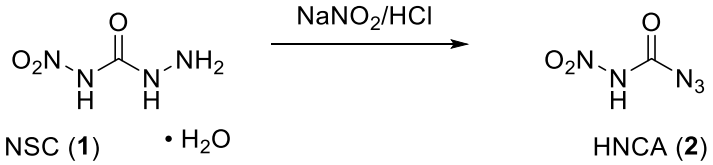

Nitrosemicarbazide monohydrate (**1**) (0.25 g, 1.81 mmol, 1.0 eq) was solved in hydrochloric acid (5.0 mL, 2M) and cooled to 0 °C. At this temperature sodium nitrite (0.14 g, 2.03 mmol, 1.1 eq) solved in water (15 mL) was added dropwise while the temperature was kept below 0 °C. After the addition was complete, the mixture was subsequently extracted with diethyl ether (4 x 20 mL). The organic phase was dried with sodium sulfate and the solvent was reduced under nitrogen stream. Nitrocarbamoyl azide (**2**) precipitates as colorless crystalline needles (0.18 g, 76%).

DTA (5 °C min^{-1}): 72 °C (endo), 83 °C (dec); Sensitivities: BAM drop hammer: <1 J, friction tester: 0.5 N (at grain size 100–500 µm); IR (ATR) $\tilde{\nu}$ (cm^{-1}) = 3250(w), 3125(m), 3023(m), 2882(w), 2775(w), 2401(vw), 2214(m), 2153(s), 1725(m), 1702(s), 1619(s), 1520(w), 1462(s), 1439(m), 1357(m), 1320(m), 1197(vs), 1125(vs), 1098(vs), 1007(s), 984(vs), 831(s), 747(s), 747(s), 727(s), 672(vs), 547(s), 530(s), 455(m), 416(m), 404(m); Raman (1064 nm, 200 mW, 25 °C) $\tilde{\nu}$

(cm^{-1}) = 3123(vw), 3021(vw), 2217(w), 2157(m), 1706(m), 1634(w), 1621(w), 1463(w), 1441(vw), 1357(vw), 1318(s), 1212(w), 1198(m), 1154(w), 1006(vs), 990(w), 751(w), 533(m), 456(w); Elem. Anal. (CHN_5O_3, 131.05 g mol^{-1}) calcd.: C 9.17, H 0.77, N 53.44%. Found: C 9.54 H 0.94, N 52.95%; ^{13}C NMR (CD_3OD, 101 MHz, ppm) δ = 152.1; ^{15}N NMR (CD_3OD, 41 MHz, ppm) δ = −45.6, −140.0, −147.2, −184.6, −262.7.

General procedure for the preparation of ionic derivatives containing the NCA^- anion

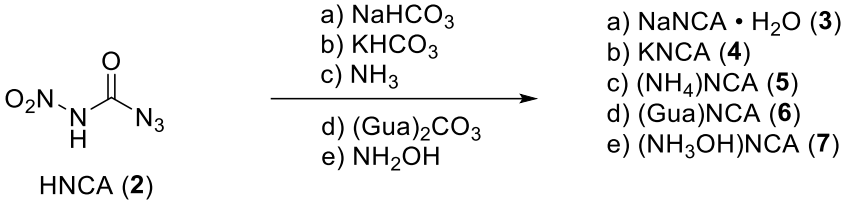

HNCA (**2**) (0.25 g, 1.91 mmol, 1.0 eq) was dissolved in methanol (10 mL) at 0 °C and one equivalent of the respective base (**3**: 161 mg, 1.91 mmol ($NaHCO_3$ in 2 mL water); **4**: 191 mg, 1.91 mmol ($KHCO_3$ in 2 mL water); **5** 965 µL, 1.91 mmol (2M NH_3 solution in MeOH); **6**: 172 mg, 1.91 mmol ($(Gua)_2CO_3$ in 2 mL water); **7**: 117 µL, 1.91 mmol ($NH_2OH \cdot H_2O$ solution)) was added in one portion and the mixture was stirred for 5 min at 0 °C. The salts started crystallizing while standing under nitrogen stream within few minutes to one hour. The compounds were filtered before complete evaporation of the solvent and were washed with little amounts of cold MeOH.

$NaNCA \cdot H_2O$ (**3**)

Compound **3** was obtained subsequently after the addition of the base as colorless powdery solid (275 mg, 84%).

DTA (5 °C min^{-1}): 67 °C (endo), 81 °C (dec); IR (ATR) $\tilde{\nu}$ (cm^{-1}) = 3276(m), 3187(w), 2173(m), 2162(m), 2136(s), 1678(s), 1620(m), 1447(m), 1418(m), 1310(m), 1300(m), 1242(s), 1179(vs), 1124(s), 1083(s), 993(m), 983(s), 827(m), 792(s), 751(s), 731(s), 668(s), 668(s), 639(s), 627(s), 561(s), 541(s), 482(s), 469(s), 459(s), 439(s), 416(s), 405(s); EA ($CN_5O_3Na \cdot H_2O$, 171.07 g mol^{-1}) calcd.:

C 7.02, H 1.18, N 40.94%; found: C 7.22, H 1.41, N 40.38%; Sensitivities: BAM drophammer: <1 J; friction tester: 0.4 N; ESD: 65 mJ (at grain size 100–500 µm).

KNCA (**4**)

Compound **4** precipitates immediately as colorless crystalline needles (246 mg, 76%).
DTA (5 °C min^{-1}): 120 °C (dec); IR (ATR) $\tilde{\nu}$ (cm^{-1}) = 2167(m), 2032(m), 1704(m), 1660(m), 1616(m), 1433(m), 1407(s), 1300(s), 1229(vs), 1206(s), 1184(vs), 1159(vs), 1099(vs), 988(s), 961(s), 830(m), 802(m), 783(s), 763(m), 749(s), 725(m), 663(m), 649(m), 649(m), 642(m), 636(s), 630(s), 583(m), 559(m), 541(m), 501(m), 481(m), 459(m), 448(m), 420(s); EA (CN_5O_3K, 169.14 g mol^{-1}) calcd.: C 7.10, H 0.00, N 41.41%; found: C 7.64, H 0.28, N 40.72%; Sensitivities: BAM drophammer: <1 J; friction tester: <0.1 N; ESD: <10 mJ (at grain size 100–500 µm).

(NH_4)NCA (**5**)

Compound **5** was received as colorless crystals (230 mg, 81%).
DTA (5 °C min^{-1}): 79 °C (dec); IR (ATR) $\tilde{\nu}$ (cm^{-1}) = 3189(s), 3182(s), 3082(m), 2167(m), 2138(s), 1625(s), 1619(s), 1420(vs), 1413(vs), 1288(m), 1233(s), 1160(vs), 1117(s), 1083(s), 991(s), 955(s), 824(s), 781(s), 755(s), 731(vs), 560(s), 545(s), 524(m), 524(m), 518(m), 491(m), 480(s), 461(m), 440(m), 432(m), 424(m), 418(m), 408(m); EA ($CH_4N_6O_3$, 148.08 g mol^{-1}) calcd.: C 8.11, H 2.72, N 56.75%; found: C 8.23, H 2.62, N 56.48%; Sensitivities: BAM drophammer: <6 J; friction tester: 20 N; ESD: 65 mJ (at grain size 100–500 µm); ^{1}H NMR (CD_3OD, 400 MHz, ppm) δ = 7.20 (br s, 4H); ^{13}C NMR (CD_3OD, 101 MHz, ppm) δ = 159.8; ^{14}N NMR (CD_3OD, 29 MHz, ppm) δ = −10 (42 Hz), −135 (45 Hz), −143 (112 Hz), −267 (162 Hz), −367 (6 Hz).
(G)NCA (**6**)

Compound **6** precipitates as yellowish crystalline needles (316 mg, 87%).
DTA (5 °C min^{-1}): 115 °C (dec); IR (ATR) $\tilde{\nu}$ (cm^{-1}) = 3428(m), 3376(m), 3255(m), 3125(m), 2167(m), 2138(m), 2039(w), 1655(s), 1635(s), 1558(m), 1428(m),

1386(m), 1280(m), 1236(s), 1174(s), 1135(s), 992(s), 968(s), 881(m), 788(s), 743(m), 729(s), 597(s), 597(s), 549(vs), 540(vs), 535(vs), 523(vs), 452(s), 418(vs); EA ($C_2H_4N_6O_3$, 190.12 g mol^{-1}) calcd.: C 12.63, H 3.18, N 58.94%; found: C 13.27, H 3.04, N 57.98%; Sensitivities: BAM drophammer: 40 J; friction tester: 324 N; ESD: 270 mJ (at grain size 100–500 µm); ^{1}H NMR (CD_3OD, 400 MHz, ppm) δ = 7.03 (s, 6H); ^{13}C NMR (CD_3OD, 101 MHz, ppm) δ = 164.1, 160.0; ^{14}N NMR (CD_3OD, 29 MHz, ppm) δ = −10 (43 Hz), −135 (38 Hz), −143 (99 Hz), −268 (155 Hz).

(Hx)NCA (**7**)

Compound **7** starts to crystallize in the form of very hygroscopic colorless needles when the solvent had almost completely evaporated (210 mg, 67%).
DTA (5 °C min^{-1}): 93 °C (dec); IR (ATR) $\tilde{\nu}$ (cm^{-1}) = 3124(w), 2983(w), 2740(w), 2204(w), 2142(m), 1740(m), 1614(s), 1451(m), 1318(m), 1139(vs), 993(s), 881(m), 822(m), 785(m), 740(s), 715(s), 550(s), 426(s); Sensitivities: BAM drophammer: ≤3 J; friction tester: ≤40 N.

Trapping reactions

Reaction of HNCA (**1**) with hydrazine hydrate

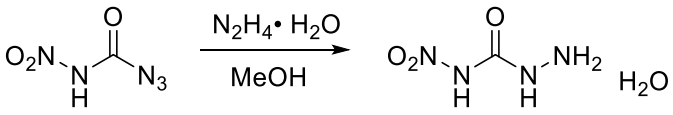

HNCA (**2**) (**1**)

HNCA (**2**) (0.25 g, 1.91 mmol, 1.0 eq) was dissolved in methanol (10 mL) at 0 °C and one equivalent of hydrazinium hydroxide (91 µL, 1.91 mmol) was added in one portion and the mixture was stirred for 5 min at 0 °C. The formed precipitate was filtered and washed with little amounts of cold MeOH. The product could be identified as **1** (0.19 g, 73%).

Methyl nitrocarbamate (**8**)

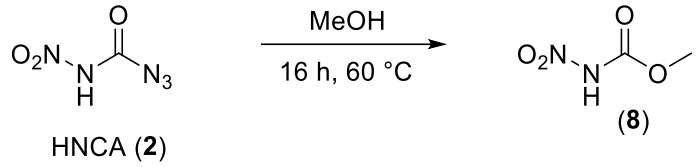

HNCA (**2**) (**8**)

HNCA (**2**) (150 mg, 1.15 mmol) was dissolved in methanol (20 mL) and the mixture was heated to 60 °C for 16 h. Afterwards, the solvent was evaporated and methyl nitrocarbamate (**8**) was obtained as colorless crystalline platelets (126 mg, 91%). IR (ATR) $\tilde{\nu}$ (cm^{-1}) = 3241(m), 3200(m), 3036(w), 1741(s), 1610(vs), 1581(m), 1432(s), 1338(m), 1298(m), 1225(s), 1151(s), 1112(m), 1072(s), 1016(m), 948(s), 913(s), 749(s), 709(s), 610(vs), 489(m), 453(m); EA ($C_2H_4N_2O_4$, 120.07 g mol^{-1}) calcd.: C 20.01, H 3.36, N 23.33%; found: C 19.52, H 3.41, N 22.59%; ^{1}H NMR (CD_3CN, 400 MHz, ppm) δ = 3.81 (s, 3H); ^{13}C NMR (CD_3CN, 101 MHz, ppm) δ = 150.0, 54.1; ^{14}N NMR (CD_3CN, 29 MHz, ppm) δ = −44 (14 Hz).

2.6.2 Vibrational Spectroscopy

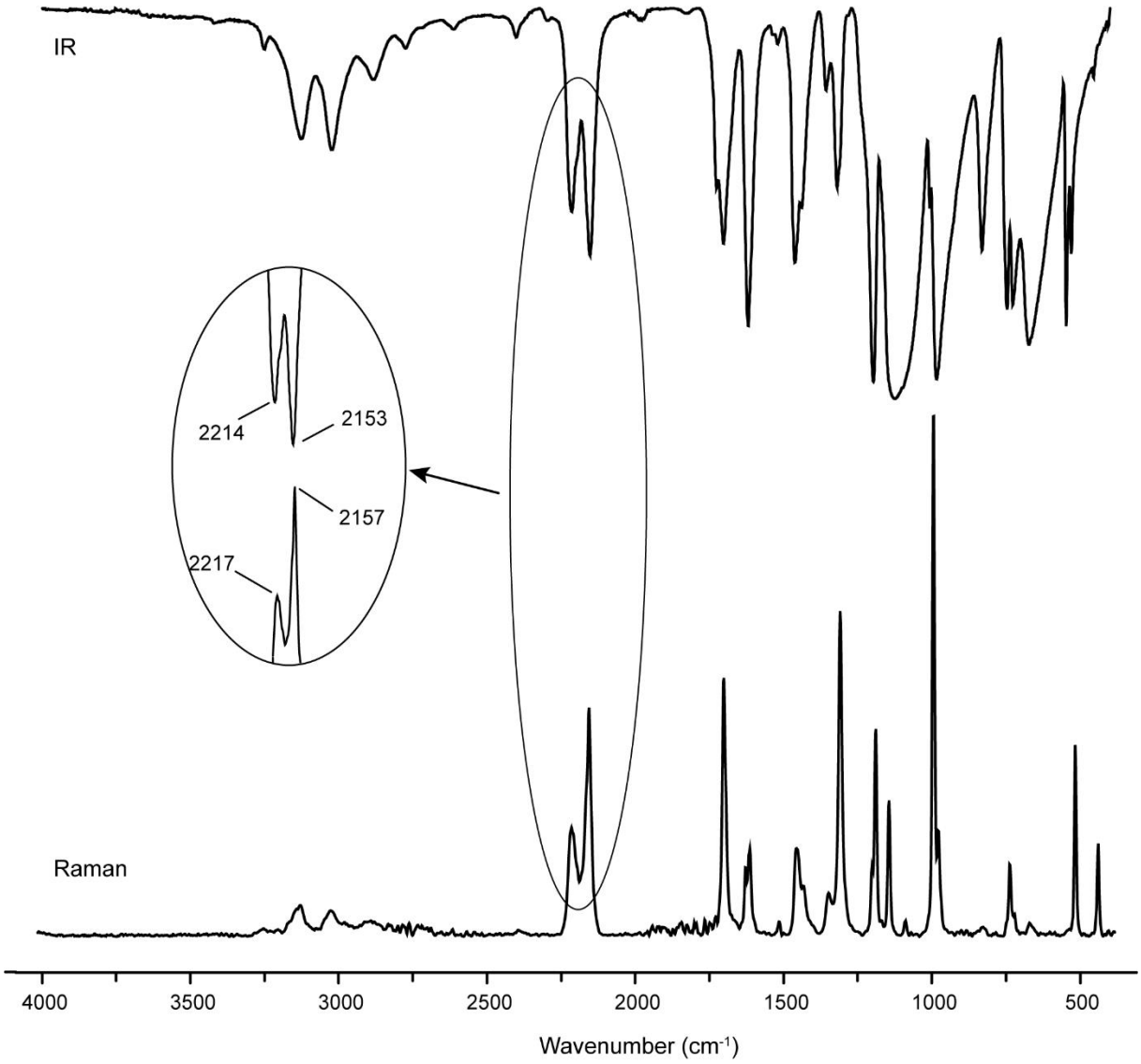

Figure S1. IR (top) and Raman (bottom) spectrum of HNCA. The azide bands are split because of the two different types of azide (in phase and out of phase) moieties in the stacking shown in the crystal structure.

2.6.3 Thermal Analysis

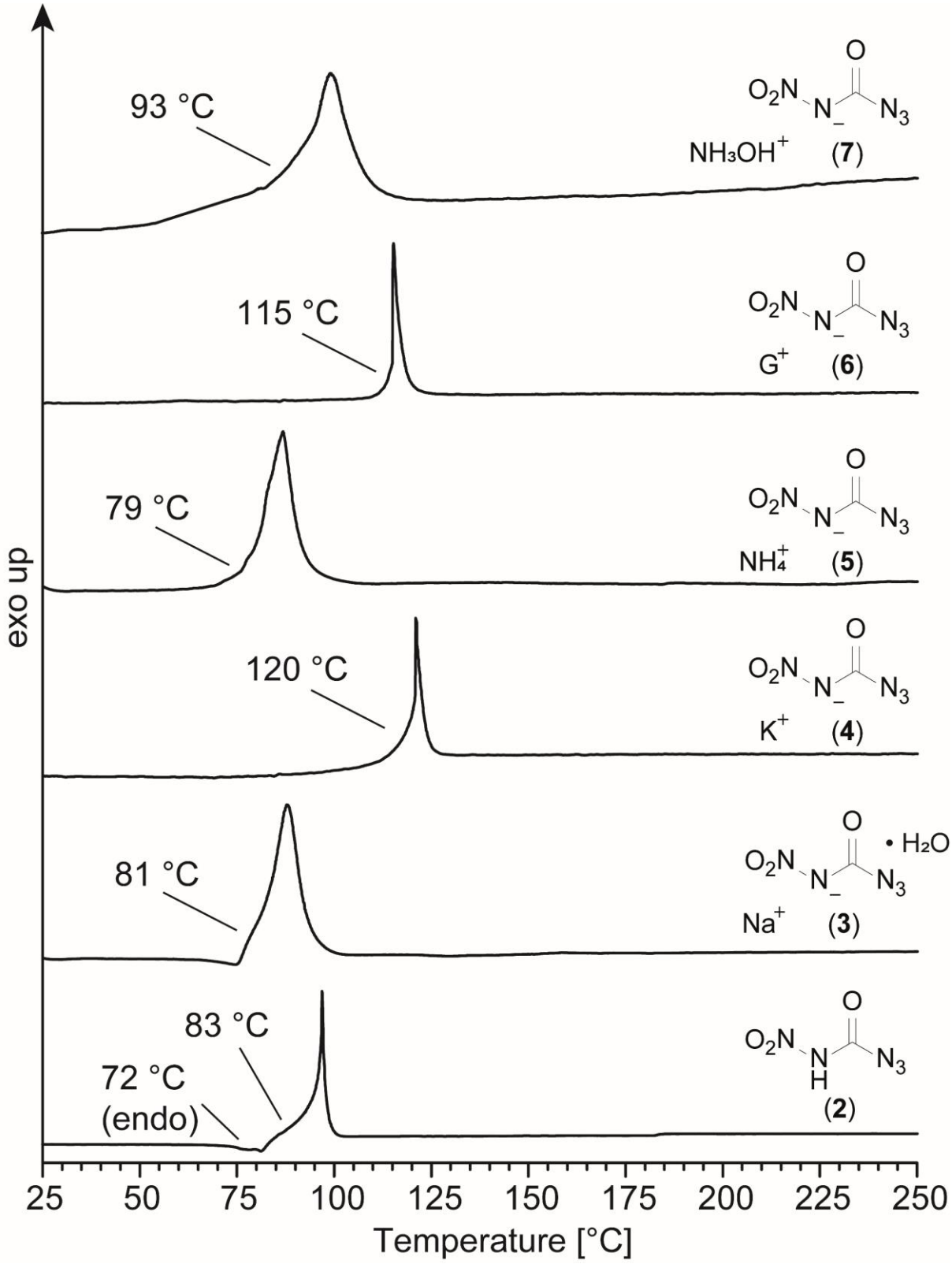

Figure S2. DTA curves of **2** and salts **3**-**7**; the plots were recorded with a heating rate of 5 °C min^{-1} and decomposition points are given as onset temperatures.

In general, all compounds have relatively low decomposition points. Pure HNCA starts to melt at 72 °C and undergoes a detonation-like decomposition with an onset temperature of 83 °C in DTA measurement. The salts **5** and **7** decompose at 79 °C and 93 °C, respectively. Both salts do not show a clear sharp decomposition but a slightly broadened curve. Besides the guanidinium salt **6** (115 °C), the most temperature stable compound is the potassium salt, which decomposes by detonation at 120 °C.

2.6.4 Crystallography

Crystal structure data were obtained from an Oxford Xcalibur3 diffractometer with a Spellman generator (voltage 50 kV, current 40 mA) and a Kappa CCD area for data collection using Mo-*Kα* radiation (*λ* = 0.71073 Å) or a Bruker D8 Venture TXS diffractometer equipped with a multilayer monochromator, a Photon 2 detector and a rotation-anode generator (Mo-K_α radiation). The data collection was performed using the CRYSTALIS RED software.[S5] The solution of the structure was performed by direct methods and refined by full-matrix least-squares on F2 (SHELXT)[S6] implemented in the OLEX2[S7] software suite. The non-hydrogen atoms were refined anisotropically and the hydrogen atoms were located and freely refined. The absorption correction was carried out by a SCALE3 ABSPACK multiscan method.[S8]

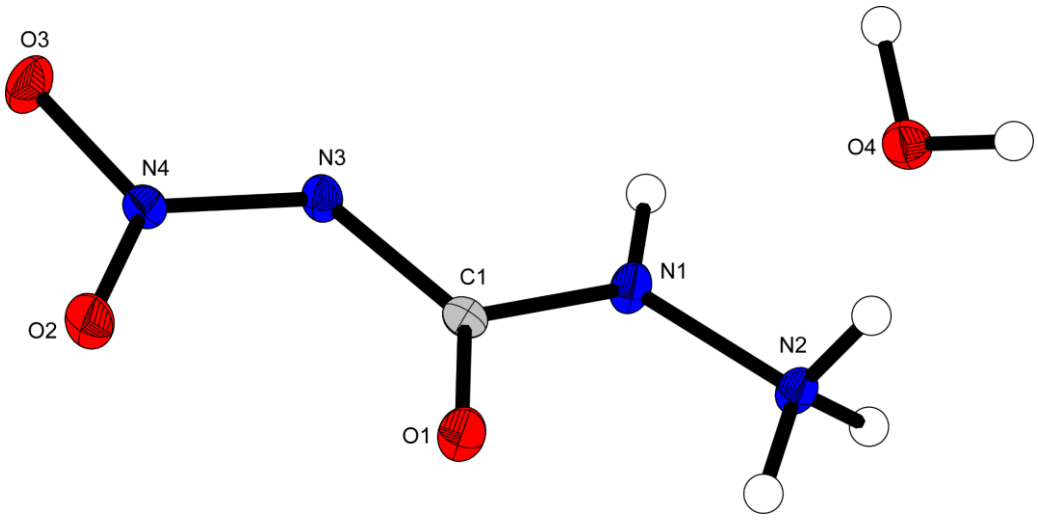

Figure S3. Representation of the molecular unit of **1**, showing the atom-labeling scheme. Thermal ellipsoids represent the 50% probability level and hydrogen atoms are shown as small spheres of arbitrary radius.

The DIAMOND2 plots shown with thermal ellipsoids at the 50% probability level and hydrogen atoms are shown as small spheres of arbitrary radius. The SADABS program embedded in the Bruker APEX3 software was used for multi-scan absorption corrections in all structures.[S9]

Nitrosemicarbazide hydrate (**1**) crystallizes with a density of 1.848 g cm^{-3} at 173 K in the orthorhombic space group *Pbca* with eight molecular units per cell. The molecular unit is shown in Figure S3. The molecule is a zwitterion, where the nitramine function has protonated the hydrazine function on N2. Due to the angles O2-N4-N3-C1 (4.48(15)°), N4-N3-C1-N1 (178.39(9)°) and N2-N1-C1-N3 (177.47(9)°) an approximate planarity can be assumed. The water molecule forms with a length of O4···H2A_c-N2 (2.027(17) Å) and O4···H2B-N2 (1.891(19) Å) hydrogen bonds to the protons of N2.

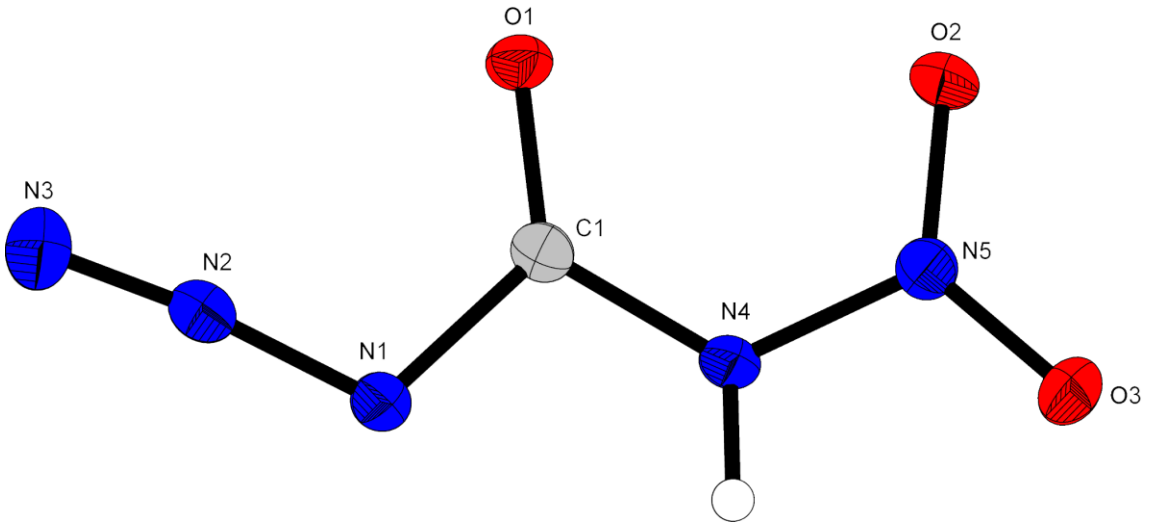

Figure S4. Representation of the molecular unit of **2**, showing the atom-labeling scheme. Thermal ellipsoids represent the 50% probability level and hydrogen atoms are shown as small spheres of arbitrary radius.

HNCA (**2**) crystallizes as colorless platelets with a density of 1.757 g cm^{-3} at 107 K in the monoclinic space group $P2_1c$ with four molecular units per cell and a cell volume of 495.45(12) $Å^3$. The cell parameters are a = 6.1997(9) Å, b = 10.2689(13) Å and c = 8.2547(11) Å. The molecular unit is shown in Figure S4. The bond angle O1-C1-N4 (127.24(11)°) is identical to that of OC(N3)2 (127.2(5)°). With 126.03(13)°, O1-C1-N1 is slightly smaller but still larger than that in $HC(O)N_3$ (125.21(16)°), which is due to the higher steric demand of the functional group. By looking at the bond angles, it is also obvious that the nitramine function takes up

marginally more space than the azide function. The C-O bond length is 1.2105(17) Å and thus slightly longer compared to HC(O)N3 (C-O 1.204(2) Å and $OC(N_3)_2$ (1.200(6) Å). The C–O bond length is 1.2105(17) Å and thus slightly longer compared to $HC(O)N_3$ (C–O 1.204(2) Å and $OC(N_3)_2$ 1.200(6) Å) which is due to the electron withdrawing effect of the nitramine function. Compared with other C(O)NH functionalities the amide bond length is shortened (1.3803(19) Å). The shorter C–N4 and longer C–O bond indicate an amide-iminol rearrangement in the molecule. This is also indicated by the extremely short N4–H1···O1 interaction (d(D–H···A = 2.808(2) Å).

The defining characteristic of the crystal structure is the strong hydrogen bridge N4–H1···O1, which leads to the formation of one-dimensional chains along *c*. The D–H···A is close to 180° (173.0(18)°) and the respective D···A (2.8078(16) Å) length is significantly shorter than the sum of the van der Waals radii (r_w(O) + r_w(N) = 3.07 Å). Each chain considered independently, does not show any interactions with each other and both the azido and the nitro moieties within a chain are oriented in the same direction with respect to *a*.

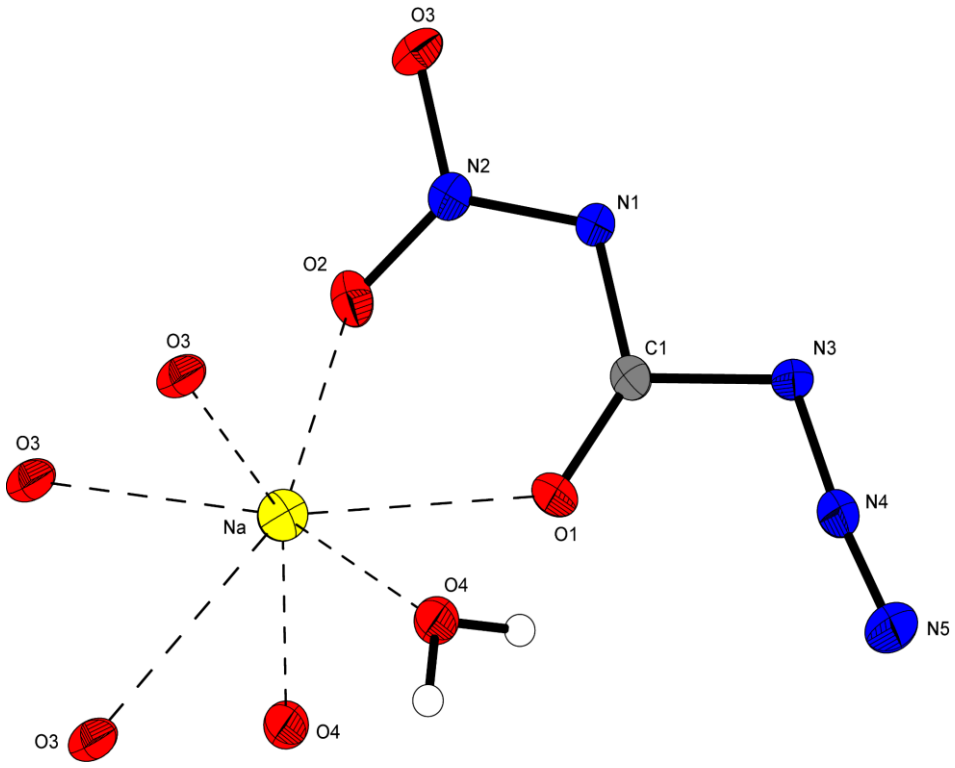

Figure S5. Representation of the molecular unit of **3**, showing the atom-labeling scheme. Thermal ellipsoids represent the 50% probability level and hydrogen atoms are shown as small spheres of arbitrary radius.

The sodium salt **3** crystallizes with a density of 1.926 g cm^{-3} at 173 K in the monoclinic space group $P2_1c$ with four molecular units per cell. The molecular unit is shown in Figure S5. The cation is coordinated by seven oxygen. These are the oxygen of water, the carbonyl group and the nitro group of the own molecular unit as well as of neighboring molecules. The anion points through the angles N2-N1-C1-N3 (176.14(12) Å), N4-N3-C1-N1 (177.15(13) Å) and C1-N1-N2-O3 (172.07(12) Å) an almost planar structure.

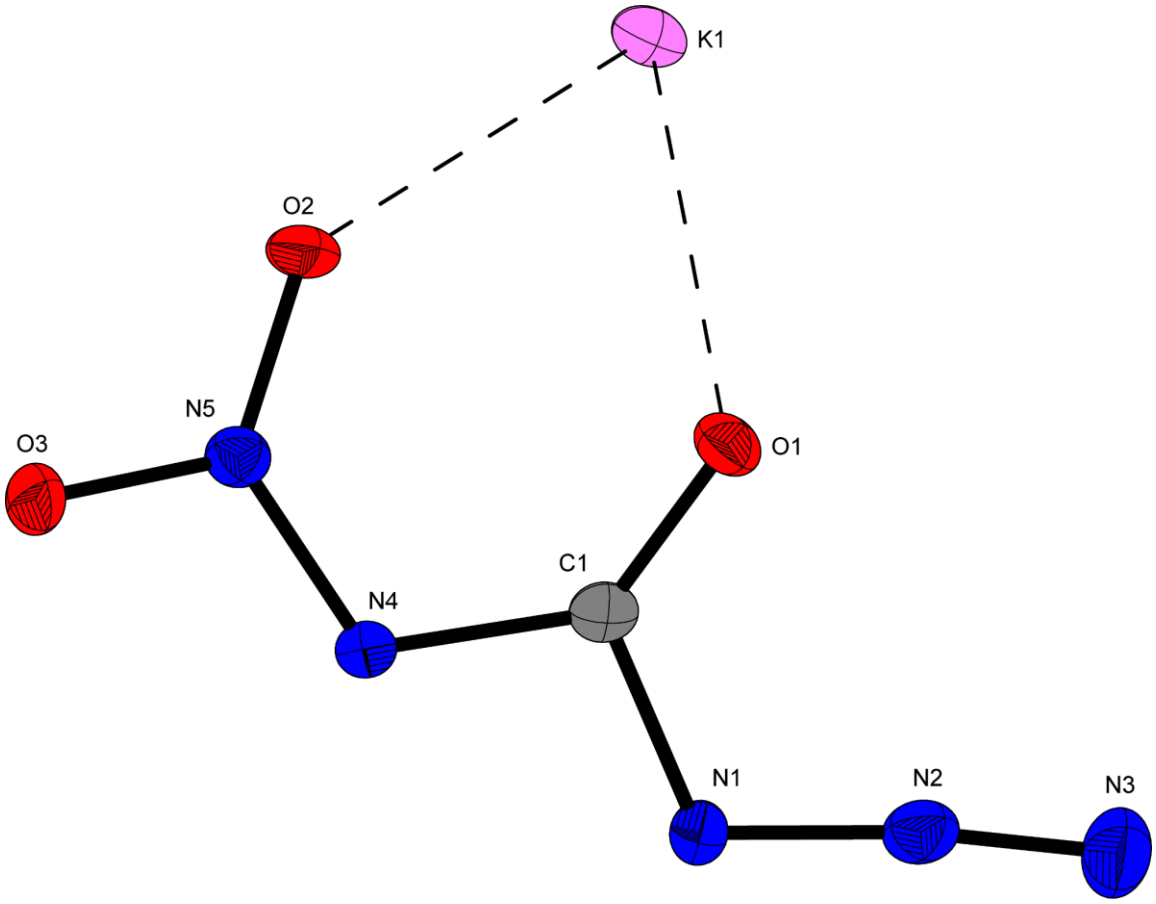

Figure S6. Representation of the molecular unit of 4, showing the atom-labeling scheme. Thermal ellipsoids represent the 50% probability.

The potassium salt **4** crystallizes in the monoclinic space group $P2_1/n$ with four molecular units per cell, a volume of 555.37(5) Å^3 and a density of 2.023 g cm^{-3}, common for alkali metal salts. Each cation is coordinated by five NCA$^-$ anions. The distances of the potassium cation to the respective oxygen atoms are all in the range of 2.787-3.032 Å. Due to interactions with the metal cation, the nitro group is rotated by 21.1(2)°(O2-N5-N4-C1) toward the plane formed by the carbonyl functionality.

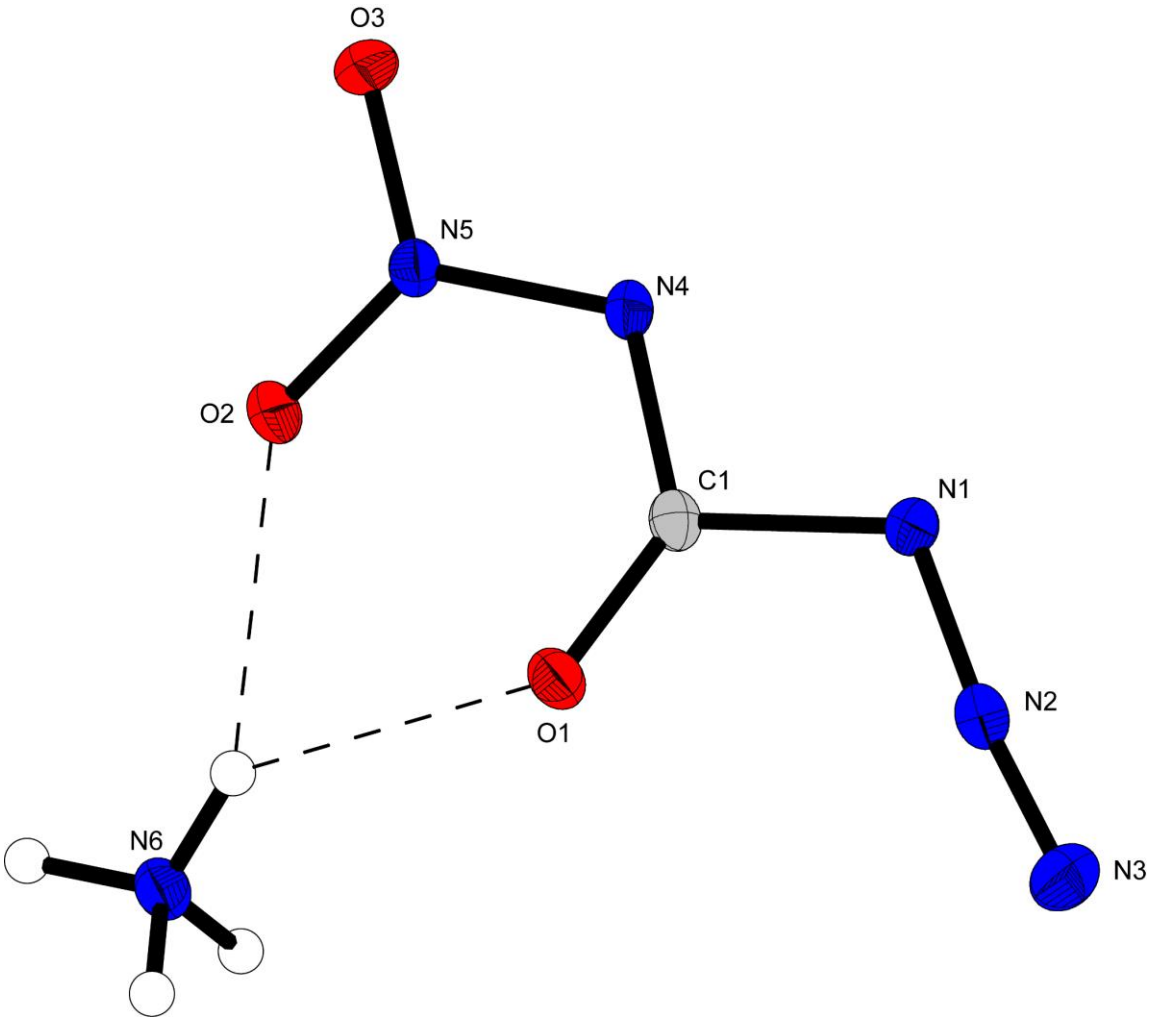

Figure S7. Representation of the molecular unit of **5**, showing the atom-labeling scheme. Thermal ellipsoids represent the 50% probability level and hydrogen atoms are shown as small spheres of arbitrary radius.

The ammonium salt **5** crystallizes with a density of 1.730 g cm^{-3} at 112 K in the triclinic space group *P*−1 with two molecular units per cell. The molecular unit is shown in Figure S7. The ammonium cation is embedded by four anion molecules and thus forms strong to medium strong hydrogen bridges (A···H-D = 2,01(2) Å - 2.228(17) Å). As the other ionic derivatives, the nitro moiety is twisted out of the plane by 15.7(2)° (C1-N4-N5-O3).

The guanidinium salt **6** crystallizes with a density of 1.649 g cm^{-3} at 113 K in the monoclinic space group $P2_1c$ with four molecular units per cell. The molecular unit is shown in Figure S8. Every guanidinium cation is surrounded by three anion moieties and shows strong hydrogen bonds (A···H-D = 2.12(2) Å – 2.21(2) Å). **6** forms a slightly wavy layer-like structure along *b*, which also indicates the low impact and friction sensitivity.

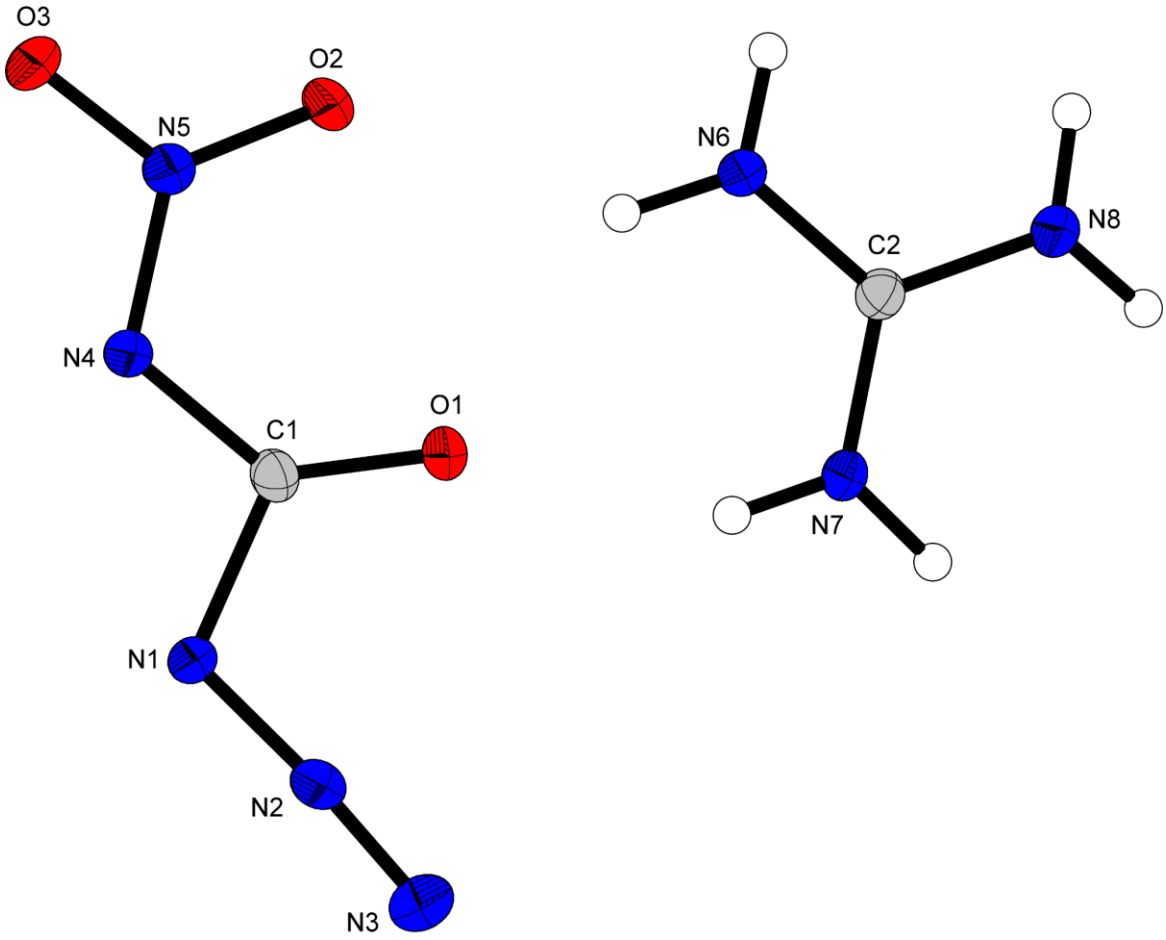

Figure S8. Representation of the molecular unit of **6**, showing the atom-labeling scheme. Thermal ellipsoids represent the 50% probability level and hydrogen atoms are shown as small spheres of arbitrary radius.

(Hx)NCA (**7**) crystallizes as colorless needles with a density of 1.856 g cm^{-3} at 105 K in the orthorhombic space group *Fdd*2 with sixteen molecular units per cell and a cell volume of 2348.9(10) Å^3. The cell parameters are *a* = 14.498(3) Å, *b* = 44.396(12) Å and *c* = 3.6494(9) Å. The molecular unit is shown in Figure S9. Intramolecular interactions are formed by N4, O1 and O2 to the appropriate protons of the cation. The shortest hydrogen bridge is O4–H4···N4 with 1.64(6) Å, the other two are 2.10(8) Å and 2.13(6) Å, respectively. As observed with all other ionic derivatives, the deprotonation of HNCA causes a slight twist within the molecule. Regarding **7**, the nitro group is clearly twisted out of the main molecular plane (C1-N4-N5-O2 19.8(7)°). The intramolecular bond lengths compared to the neutral compound are almost unchanged.

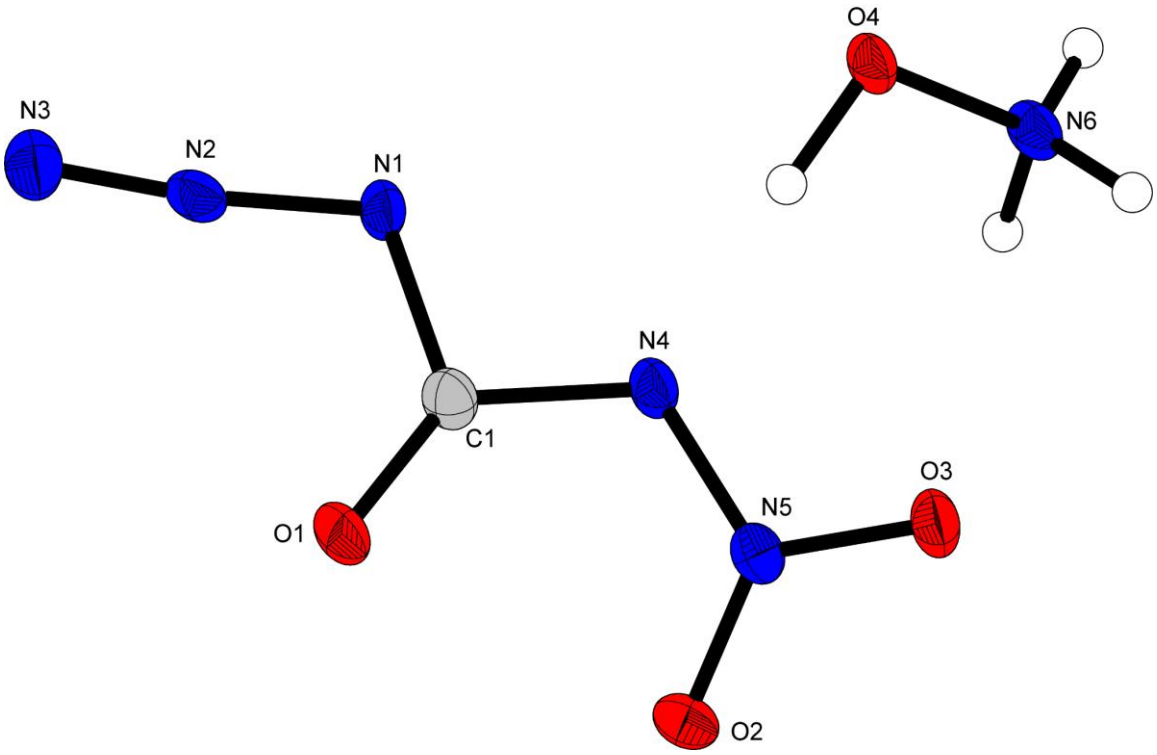

Figure S9. Representation of the molecular unit of **7**, showing the atom-labeling scheme. Thermal ellipsoids represent the 50% probability level and hydrogen atoms are shown as small spheres of arbitrary radius. Selected bond distances [Å] and angles [°]: C1-N1 1.406(6), C1-O1 1.207(5), C1-N4 1.379(6), O4-H4···N4 1.64(6), N1-N2-N3 173.0(5), O1-C1-N1 124.0(4), O1-C1-N4 130.7(4), N2-N1-C1-O1 4.1(4), C1-N4-N5-O2 19.8(7).

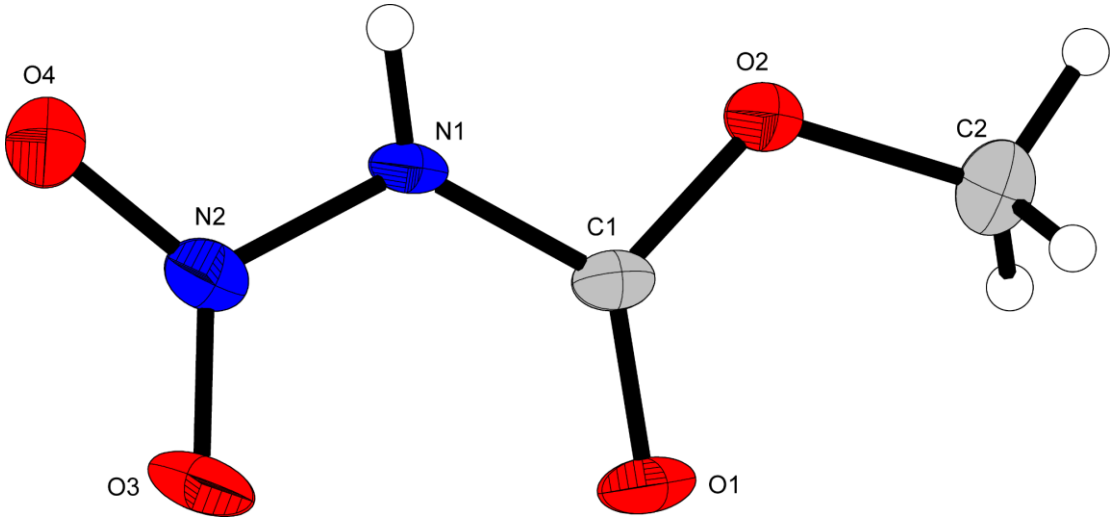

Figure S10. Representation of the molecular unit of **8**, showing the atom-labeling scheme. Thermal ellipsoids represent the 50% probability level and hydrogen atoms are shown as small spheres of arbitrary radius.

The methyl ester **8** crystallizes with a density of 1.676 g cm^{-3} at 110 K in the triclinic space group *P*−1 with four molecular units per cell. The molecular unit is shown in Figure S10. The molecule is almost completely planar ((O3-N2-N1-C1 = 0.9(3)°, N2-N1-C1-O1 = 1.1(3)°, C2-O2-C1-O1 = 0.2(2)° and C2-O2-C1-N1 = −179.9(2)°.

Table S1. Crystallographic data and structure refinement details for the prepared compounds **1**-**3**.

	1	**2**	**3**
Formula	$CH_4N_4O_3 \cdot H_2O$	CHN_5O_3	$CN_5O_3Na \cdot H_2O$
FW [g mol^{-1}]	138.10	131.07	171.07
Crystal system	orthorhombic	monoclinic	monoclinic
Space group	*Pbca* (No. 61)	$P2_1/c$ (No. 14)	$P2_1/c$ (No. 14)
Color / Habit	colorless block	colorless platelet	colorless rod
Size [mm]	0.05 x 0.15 x 0.20	0.02 x 0.06 x 0.07	0.02 x 0.15 x 0.40
a [Å]	9.5532(3)	6.1997(9)	11.9484(9)
b [Å]	6.3625(2)	10.2689(13)	3.6295(2)
c [Å]	16.3333(5)	8.2547(11)	14.0899(10)
α [°]	90	90	90
β [°]	90	109.477(5)	105.130(8)
γ [°]	90	90	90
V [Å^3]	992.77(5)	495.46(12)	589.85(7)
Z	8	4	4
$\rho_{calc.}$ [g cm^{-3}]	1.848	1.757	1.926
μ [mm^{-1}]	0.180	0.168	0.242
F(000)	576	264	344
$\lambda_{MoK\alpha}$ [Å]	0.71073	0.71073	0.71073
T [K]	173	107	173
θ Min-Max [°]	4.3, 28.3	3.3, 26.4	5.2, 26.0
Dataset	-10: 12 ; -8: 7 ; -21: 21	-7: 7 ; -12: 12 ; -10: 10	-14: 9 ; -4: 4 ; -17: 17
Reflections collected	5643	9036	4048
Independent refl.	1238	1015	1157
R_{int}	0.026	0.035	0.027
Observed reflections	1088	914	948
Parameters	107	86	108
R_1 (obs)[a]	0.0281	0.0290	0.0297
wR_2 (all data)[b]	0.0752	0.0822	0.0761
S [c]	1.06	1.12	1.08
Resd. dens [e Å^{-3}]	-0.27, 0.25	-0.23, 0.15	-0.27, 0.22
Device type	Xcalibur Sapphire3	Bruker D8 Venture	Xcalibur Sapphire3
Solution	SIR-92	SIR-92	SIR-92
Refinement	SHELXL-2013	SHELXL-2013	SHELXL-2013
Absorption correction	multi-scan	multi-scan	multi-scan
CCDC	2046599	2046597	2046595

[a] $R_1 = \Sigma||F_0|-|F_c||/\Sigma|F_0|$; [b] $wR_2 = [\Sigma[w(F_0^2-F_c^2)^2]/\Sigma[w(F_0)^2]]^{1/2}$; $w = [\sigma c^2(F_0^2)+(xP)^2+yP]^{-1}$ and $P=(F_0^2+2F_c^2)/3$; [c] $S = (\Sigma[w(F_0^2-F_c^2)^2]/(n-p))^{1/2}$ (n = number of reflections; p = total number of parameters).

Table S2. Crystallographic data and structure refinement details for the prepared compounds **4**-**6**.

	4	**5**	**6**
Formula	CN_5O_3K	CN_5O_3, H_4N	CN_5O_3, CH_6N_3
FW [g mol^{-1}]	169.16	148.10	190.15
Crystal system	monoclinic	triclinic	monoclinic
Space group	$P2_1/n$ (No. 14)	P-1 (No. 2)	$P2_1/c$ (No. 14)
Color / Habit	colorless block	colorless block	colorless block
Size [mm]	0.10 x 0.19 x 0.29	0.14 x 0.24 x 0.30	0.18 x 0.28 x 0.59
a [Å]	6.8957(4)	6.6353(3)	7.4975(9)
b [Å]	11.5328(5)	6.8575(4)	15.4884(16)
c [Å]	7.0382(3)	7.0924(5)	6.6145(8)
α [°]	90	67.848(6)	90
β [°]	97.155(5)	72.382(5)	94.328(9)
γ [°]	90	80.022(5)	90
V [Å^3]	555.37(5)	284.24(3)	765.91(15)
Z	4	2	4
$\rho_{calc.}$ [g cm^{-3}]	2.023	1.730	1.649
μ [mm^{-1}]	0.905	0.161	0.147
F(000)	336	152	392
$\lambda_{MoK\alpha}$ [Å]	0.71069	0.71073	0.71073
T [K]	173	112	113
θ Min-Max [°]	4.3, 26.0	3.2, 26.4	2.6, 26.4
Dataset	-8: 8 ; -14: 14 ; -7: 8	-8: 8 ; -8: 8 ; -8: 8	-7: 9 ; -17: 19 ; -8: 8
Reflections collected	4095	3026	6154
Independent refl.	1092	1162	1564
R_{int}	0.029	0.029	0.040
Observed reflections	956	1000	1234
Parameters	91	107	142
R_1 (obs)[a]	0.0255	0.0299	0.0379
wR_2 (all data)[b]	0.0623	0.0808	0.0923
S [c]	1.06	1.08	1.04
Resd. dens [e Å^{-3}]	-0.34, 0.23	-0.19, 0.21	-0.21, 0.18
Device type	Xcalibur Sapphire3	Xcalibur Sapphire3	Xcalibur Sapphire3
Solution	SIR-92	SIR-92	SIR-92
Refinement	SHELXL-2013	SHELXL-2013	SHELXL-2013
Absorption correction	multi-scan	multi-scan	multi-scan
CCDC	2046598	2046601	2046600

[a] $R_1 = \Sigma||F_o|-|F_c||/\Sigma|F_o|$; [b] $wR_2 = [\Sigma[w(F_o^2-F_c^2)^2]/\Sigma[w(F_o)^2]]^{1/2}$; $w = [\sigma c^2(F_o^2)+(xP)^2+yP]^{-1}$ and $P=(F_o^2+2F_c^2)/3$; [c] $S = (\Sigma[w(F_o^2-F_c^2)^2]/(n-p))^{1/2}$ (n = number of reflections; p = total number of parameters).

Table S3. Crystallographic data and structure refinement details for the prepared compounds **7** and **8**.

	7	**8**
Formula	CN_5O_3, H_4NO	$C_2H_4N_2O_4$
FW [g mol^{-1}]	164.10	120.07
Crystal system	orthorhombic	triclinic
Space group	*Fdd*2 (No. 43)	*P*-1 (No. 2)
Color / Habit	colorless needle	colorless plate
Size [mm]	0.10 x 0.15 x 0.80	0.05 x 0.50 x 0.50
a [Å]	14.498(3)	7.6411(10)
b [Å]	44.396(12)	7.7969(11)
c [Å]	3.6494(9)	8.3332(13)
α [°]	90	99.142(12)
β [°]	90	90.045(12)
γ [°]	90	103.622(12)
V [Å^3]	2349.0(10)	475.99(12)
Z	16	4
$\rho_{calc.}$ [g cm^{-3}]	1.856	1.676
μ [mm^{-1}]	0.178	0.164
F(000)	1344	248
$\lambda_{MoK\alpha}$ [Å]	0.71073	0.71073
T [K]	105	110
θ Min-Max [°]	3.0, 26.4	2.7, 26.4
Dataset	-14: 18 ; -54: 54 ; -4: 3	-9: 9 ; -6: 9 ; -10: 8
Reflections collected	3821	3157
Independent refl.	1136	1947
R_{int}	0.095	0.017
Observed reflections	913	1449
Parameters	116	177
R_1 (obs)[a]	0.0549	0.0489
wR_2 (all data)[b]	0.1274	0.1484
S [c]	0.98	1.04
Resd. dens [e Å^{-3}]	-0.34, 0.28	-0.34, 0.31
Device type	Xcalibur Sapphire3	Xcalibur Sapphire3
Solution	SIR-92	SIR-92
Refinement	SHELXL-2013	SHELXL-2013
Absorption correction	multi-scan	multi-scan
CCDC	2046594	2046596

[a] $R_1 = \Sigma||F_0|-|F_c||/\Sigma|F_0|$; [b] $wR_2 = [\Sigma[w(F_0^2-F_c^2)^2]/\Sigma[w(F_0)^2]]^{1/2}$; $w = [\sigma c^2(F_0^2)+(xP)^2+yP]^{-1}$ and $P=(F_0^2+2F_c^2)/3$; [c] $S = (\Sigma[w(F_0^2-F_c^2)^2]/(n-p))^{1/2}$ (n = number of reflections; p = total number of parameters).

2.6.5 Computation

2.6.5.1 Heat of Formation

All quantum chemical calculations were carried out using the Gaussian G09 program package.[S10] The enthalpies (H) and free energies (G) were calculated using the complete basis set (CBS) method of Petersson and co-workers in order to obtain very accurate energies. The CBS models are using the known asymptotic convergence of pair natural orbital expressions to extrapolate from calculations using a finite basis set to the estimated CBS limit. CBS-4 starts with an HF/3-21G(d) geometry optimization; the zero-point energy is computed at the same level. It then uses a large basis set SCF calculation as a base energy, and an MP2/6- 31+G calculation with a CBS extrapolation to correct the energy through second order. A MP4(SDQ)/6-31+ (d,p) calculation is used to approximate higher order contributions. In this study, we applied the modified CBS-4M.

Heats of formation of the synthesized ionic compounds were calculated using the atomization method (equation E1) using room temperature CBS-4M enthalpies, which are summarized in Table S4.[S11, S12]

$$\Delta_f H^\circ_{(g,\,M,\,298)} = H_{(Molecule,\,298)} - \sum H^\circ_{(Atoms,\,298)} + \sum \Delta_f H^\circ_{(Atoms,\,298)} \qquad (E1)$$

Table S4. CBS-4M electronic enthalpies for atoms C, H, N and O and their literature values for atomic $\Delta H^\circ_f{}^{298}$ / kJ/mol

	$-H^{298}$ [a.u.]	NIST[S13]
H	0.500991	218.2
C	37.786156	717.2
N	54.522462	473.1
O	74.991202	249.5

For neutral compounds the sublimation enthalpy, which is needed to convert the gas phase enthalpy of formation to the solid state one, was calculated by the *Trouton* rule.[S14] For ionic compounds, the lattice energy (U_L) and lattice enthalpy (ΔH_L) were calculated from the corresponding X-ray molecular volumes according to the equations provided by *Jenkins* and *Glasser*.[S15] With the calculated lattice enthalpy the gas-phase enthalpy of formation was converted into the solid state

(standard conditions) enthalpy of formation. These molar standard enthalpies of formation (ΔH_m) were used to calculate the molar solid state energies of formation (ΔU_m) according to equation E2.

$$\Delta U_m = \Delta H_m - \Delta n\, RT \qquad \text{(E2)}$$

(Δn being the change of moles of gaseous components)
The calculation results are summarized in Table S5.

Table S5. Calculation results.

	$-H^{298}$ [a] [a.u.]	$\Delta_f H°$(g,M) [kJ mol^{-1}] [b]	V_M [Å^3] [c]	ΔU_L; ΔH_L [d] [kJ mol^{-1}]	$\Delta_f H°$(s) [e] [kJ mol^{-1}]	Δn [f]	$\Delta_f U$(s) [g] [kJ kg^{-1}]
2	537.332264	214.5	509.7	-	147.5	−4.5	1210.9
4	1135.856939	510.9	565.8	554.1; 555.3	−44.4	−4.0	−264.8
5	593.617580	658.8	292.2	549.2; 554.2	104.6	−6.5	815.5
6	742.274164	594.7	766.5	510.7; 515.7	79.0	−8.5	526.6
7	668.684221	709.9	2416.9	544.3; 549.3	160.7	−7.0	1085.1

[a] CBS-4M electronic enthalpy; [b] gas phase enthalpy of formation; [c] molecular volumes of unit cell taken from X-ray structures and corrected 298K; [d] lattice energy and enthalpy (calculated using Jenkins and Glasser equations); [e] standard solid state enthalpy of formation; [f] Δn being the change of moles of gaseous components when formed; [g] solid state energy of formation.

2.6.5.2 Valence Bond (VB) Calculation

In order to obtain an insight into the structure and bonding of nitramino carbonyl azide (HNCA) we calculated various resonance structures using the VB2000 code (Version 2.8).[S17]

Initially, we performed a CASVB(12,9)/STO-3G calculation obtaining 2520 resonance structures and a total energy of −528.058782 a.u. In the next step we performed a VB(12)/STO-3G calculation on the 12 most relevant resonance structures, including Kekulé-type and Dewar-type (long-bond) structures.[S18] This VB(12) calculation resulted in a total energy of −528.053254 a.u. (ΔE[VB(12) – CAS) = 3.5 kcal mol^{-1}) indicating that we did not miss any relevant resonance structure. The 12 resonance structures are shown in Figure S11 and the Hiberty weights are given in Table S7. Moreover, the VB(12) calculation showed that only

nine out of the 12 resonance structures have significant weight whereas the three structures (X, XI and XII) with a double bond between N3 and N5 are negligible due to two adjacent positive charges. The most important structures are the long-bond (Dewar-type) structures I and II with I being the main contributor to the resonance scheme due to the absence of any formal charges.

Table S7. Hiberty weights for the 12 resonance structures shown in Figure S11.

Structure		**I**	**II**	**III**	**IV**	**V**	**VI**
Hiberty weight		0.31	0.20	0.13	0.11	0.09	0.06
Structure		**VII**	**VIII**	**IX**	**X**	**XI**	**XII**
Hiberty weight		0.04	0.04	0.02	0.0	0.0	0.0

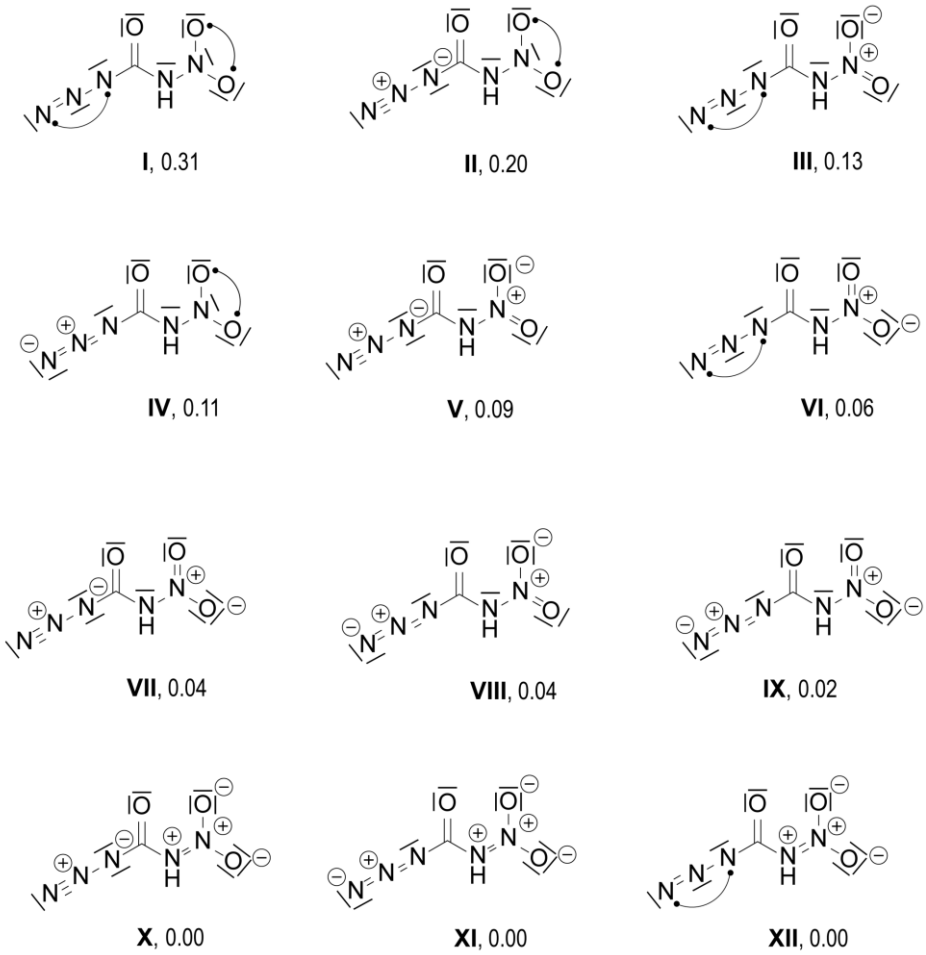

Figure S11. The 12 most relevant resonance structures of the HNCA molecule.

2.6.5.3 MO calculations

In order to access the equilibrium between the amide, iminol and tetrazolone form of HNCA, all three tautomers were computed using the G09W code.[S10] Table S8 summarizes the results.

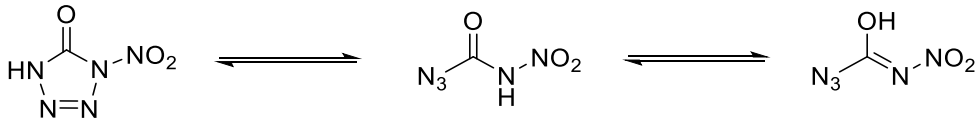

Table S8. Energy differences for the amide, iminol and tetrazolone form of HNCA.

	amide (**A**)	iminol (**B**)	tetrazolone (**C**)
	C_s	C_s	C_s
B3LYP/cc-pVDZ			
-*E* / a.u.	538.002605	537.994943	537.992172
Δ*E* / kcal mol^{-1}	0.0	+4.8	+6.6
B3LYP/cc-pVDZ solvent = water (PCM model)			
-*E* / a.u.	−538.013320	−538.0040445	−538.005085
Δ*E* / kcal mol^{-1}	0.0	+5.8	+5.2m
CBS-4M			
-CBS-4 Enthalpy	−537.332449	−537.315994	−537.324733
Δ*E* / kcal mol^{-1}	0.0	+10.3	+4.8
Δ$H°_f$(g) / kcal mol^{-1} [S19]	+52.0	+62.4	+56.8
Δ$H°_f$(s) / kcal mol^{-1} [S19]	+36.5	+46.7	+41.2

2.6.5.4 Physico-chemical Properties

Table S9. Energetic properties and detonation parameters of anhydrous compounds.

	1	**2**	**3**	**4**	**5**	**6**	**7**	**NC-NO_2** [S19]
Formula	$CH_4N_4O_3 \cdot H_2O$	CHN_5O_3	$NaCN_5O_3 \cdot H_2O$	KCN_5O_3	$CH_4N_6O_3$	$C_2H_6N_8O_3$	$CH_4N_6O_4$	CN_2O_2
M [g mol^{-1}]	138.08	131.05	171.05	169.14	148.08	190.12	164.08	72.02
IS [J][a]	5	<1	<1	<1	6	40	≤3	n.d.
FS [N][b]	48	0.5	0.4	<0.1	20	324	≤40	n.d.
ESD [J][c]	0.1	n.d.	0.065	<0.01	0.16	0.27	n.d.	n.d.
P [g cm^{-3}][d]	1.814	1.708	1.891	1.986	1.683	1.648	1.803	1.24 @ -79°C
N [%][e]	40.6	53.4	40.9	41.4	56.8	58.9	51.2	38.9
Ω [%][f]	−11.6	6.1	0	4.7	−10.8	−33.7	0	0
T_{dec} [°C][g]	156	83	81	120	79	115	93	n.d.
$\Delta_f H^0$ [kJ mol^{-1}][h]	−88.5	147.5	−445.8	−44.4	104.6	79.0	156.6	183.8 (liquid phase)
EXPLO5 V6.05.02								
$-\Delta_{Ex} U^0$ [kJ kg^{-1}][i]	-	5066	-	4338	5045	3942	6256	6574
T_{det} [K][k]	-	4054	-	3292	3521	2862	4131	5941
V_0 [L kg^{-1}][l]	-	794	-	470	894	891	891	740
P_{CJ} [kbar][m]	-	270	-	227	296	239	368	146
V_{det} [m s^{-1}][n]	-	8333	-	7472	8662	8088	9466	6697
I_{sp} [s] [o]		248			255	214	270	273

[a] Impact sensitivity (BAM drophammer (1 of 6)). [b] Friction sensitivity (BAM friction tester (1 of 6)). [c] Electrostatic discharge device (OZM research). [d] From X-ray diffraction analysis recalculated to 298 K. [e] Combined Nitrogen and Oxygen content. [f] Oxygen balance with respect to CO formation. [g] Decomposition temperature (onset temperatures; β = 5 °C min^{-1}). [h] Calculated enthalpy of formation. [i] Calculated energy of formation. [j] Energy of explosion. [k] Detonation temperature. [l] Volume of detonation products (assuming only gaseous products). [m] Detonation pressure at Chapman-Jouguet point. [n] Detonation velocity. [o] Specific impulse, isobaric combustion@chamber pressure 6 MPa.

2.6.6 References

[S1] a) Reichel & Partner GmbH, http://www.reichelt-partner.de; b) Test methods according to the UN Recommendations on the Transport of Dangerous Goods, *Manual of Test and Criteria*, fourth revised edition, United Nations

Publication, New York and Geneva, **2003**, ISBN 92–1-139087–7, Sales No. E.03.VIII.2; 13.4.2 Test 3 a (ii) BAM Fallhammer.

[S2] M. Sućeska, EXPLO5 V6.02 program, Brodarski Institute, Zagreb, Croatia, **2014**.

[S3] P. Goede, N. Wingborg, H. Bergman, N. V. Latypov, *Propellants, Explos., Pyrotech.*, **2001**, *26*, 17–20.

[S4] S. G. Il'yasov, A. A. Lobanova, N. I. Popov, R. R. Sataev, *Russ. J. Org. Chem*., **2002**, *38*, 1731–1738.

[S5] *CrysAlisPro*, Oxford Diffraction Ltd. *version 171.33.41*, **2009**.

[S6] G. M. Sheldrick, *Acta Cryst.* **2015**, *A71*, 3–8.

[S7] O. V. Dolomanov, L. J Bourhis, R. J. Gildea, J. A. K. Howard, H. Puschmann, *J. Appl. Cryst.* **2009**, *42*, 339–341.

[S8] *SCALE3 ABSPACK – An Oxford Diffraction program* (1.0.4, gui: 1.0.3), Oxford Diffraction Ltd., **2005**.

[S9] *APEX3*. Bruker AXS Inc., Madison, Wisconsin, USA.

[S10] M. J. Frisch, G. W. Trucks, H. B. Schlegel, G. E. Scuseria, M. A. Robb, J. R. Cheeseman, G. Scalmani, V. Barone, B. Mennucci, G. A. Petersson, H. Nakatsuji, M. Caricato, X. Li, H.P. Hratchian, A. F. Izmaylov, J. Bloino, G. Zheng, J. L. Sonnenberg, M. Hada, M. Ehara, K. Toyota, R. Fukuda, J. Hasegawa, M. Ishida, T. Nakajima, Y. Honda, O. Kitao, H. Nakai, T. Vreven, J. A. Montgomery, Jr., J. E. Peralta, F. Ogliaro, M. Bearpark, J. J. Heyd, E. Brothers, K. N. Kudin, V. N. Staroverov, R. Kobayashi, J. Normand, K. Raghavachari, A. Rendell, J. C. Burant, S. S. Iyengar, J. Tomasi, M. Cossi, N. Rega, J. M. Millam, M. Klene, J. E. Knox, J. B. Cross, V. Bakken, C. Adamo, J. Jaramillo, R. Gomperts, R. E. Stratmann, O. Yazyev, A. J. Austin, R. Cammi, C. Pomelli, J. W. Ochterski, R. L. Martin, K. Morokuma, V. G. Zakrzewski, G. A. Voth, P. Salvador, J. J. Dannenberg, S. Dapprich, A. D. Daniels, O. Farkas, J.B. Foresman, J. V. Ortiz, J. Cioslowski, D. J. Fox, Gaussian 09 A.02, Gaussian, Inc., Wallingford, CT, USA, **2009**.

[S11] a) J. W. Ochterski, G. A. Petersson, and J. A. Montgomery Jr., *J. Chem. Phys.* **1996**, *104*, 2598–2619; b) J. A. Montgomery Jr., M. J. Frisch, J. W. Ochterski G. A. Petersson, *J. Chem. Phys.* **2000**, *112*, 6532–6542.

[S12] a) L. A. Curtiss, K. Raghavachari, P. C. Redfern, J. A. Pople, *J. Chem. Phys.* **1997**, *106*, 1063–1079; b) E. F. C. Byrd, B. M. Rice, *J. Phys. Chem*. A **2006**,

110, 1005–1013; c) B. M. Rice, S. V. Pai, J. Hare, *Comb. Flame* **1999**, *118*, 445–458.

[S13] P. J. Lindstrom, W. G. Mallard (Editors), NIST Standard Reference Database Number 69, http://webbook.nist.gov/chemistry/ (accessed June **2020**).

[S14] M. S. Westwell, M. S. Searle, D. J. Wales, D. H. Williams, *J. Am. Chem. Soc*. **1995**, *117*, 5013–5015; b) F. Trouton, *Philos. Mag*. **1884**, *18*, 54–57.

[S15] a) H. D. B. Jenkins, H. K. Roobottom, J. Passmore, L. Glasser, *Inorg. Chem.* **1999,** *38,* 3609–3620; b) H. D. B. Jenkins, D. Tudela, L. Glasser, *Inorg. Chem.* **2002**, *41*, 2364–2367.

[S16] J Li, B. Duke, R. McWeeny, VB2000 Version 2.8, SciNet Technologies, San Diego, CA, **2017**.

[S17] Pauling Three-Electron Bonds and Increased Valence Structures as Components of the“Intellectual Heritage” of Qualitative Valence Bond Theory, R. D. Harcourt, T. M. Klapötke, *Research Trends.Inorg. Chem.* **2006**, *9*, 11–22.

[S18] Chemistry of High Energy Materials, 5th edn., T. M. Klapötke, Walter de Gruyter, Berlin/Boston, **2019**, Chapter 4.2.1, pp 143–146.

[S19] M. Rahm, G. Belanger-Chabot, R. Haiges, K. O. Christe, *Angew. Chem., Int. Ed.* **2014**, *53*, 6893–6897.

3. Hybridization of Dinitramide and Dicyanamide: Evaluation of Nitrocyanamide in Energetic Salts and Coordination Compounds

Michael S. Gruhne‡, Maximilian Benz‡, Tizian Lorenzen, Tobias Lenz, Thomas M. Klapötke, Jörg Stierstorfer

As published in *Crystal Growth and Design* **2022**, *22, 1*, 200–212

DOI: 10.1021/acs.cgd.1c00858

Keywords: structure elucidation, ECC, coordination chemistry, energetic materials, nitrocyanamide

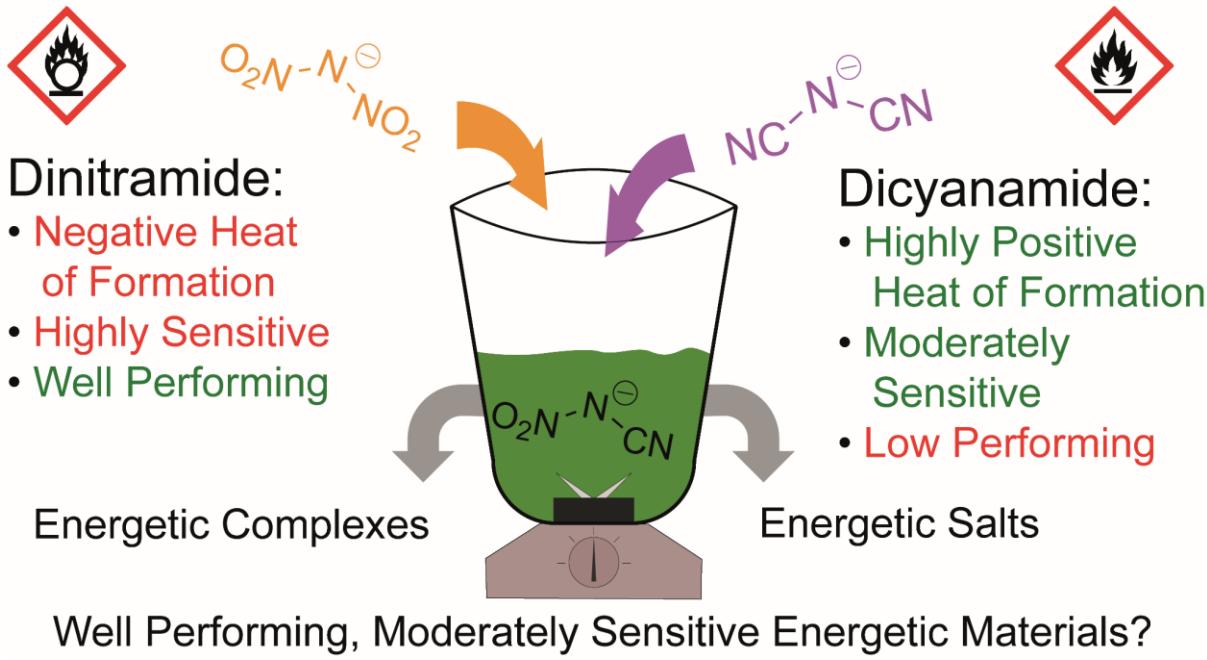

The nitrocyanamide anion which is synthesized from commercially available nitroguanidine, was investigated as a building block in energetic materials. This is of interest, as it combines the high heat of formation of the nitrile moiety as well as the performance resulting from the nitro group.

Abstract: In this work, the anion nitrocyanamide (NCA^-), as a cross between the dinitramide and the dicyanamide anion, was investigated as a building block in various energetic materials. Apart from nonenergetic complexes, only the use in ionic liquids has been investigated so far. Consequently, the focus in this work was on the synthesis of energetic coordination compounds (ECC) involving tetrazole ligands as well on nitrogen-rich salts, which includes not only ammonium but also hydrazinium, hydroxylammonium, and triaminoguanidinium. During the formation of the salts, particular focus was also put on the possible formation of adducts with nitrogen bases. This was proven with the help of IR and NMR spectroscopy. The complexation resulted in two silver(I) and nine copper(II) complexes, which were studied not only in terms of their coordination geometries but also in terms of their energetic properties. Each compound was checked on purity using CHNO elemental analysis. In some cases, X-ray diffraction experiments were carried out to become clear about their final composition. Thermal stability measurements were carried out using differential thermal analysis (DTA) and, for selected substances, thermogravimetric analysis (TGA). The sensitivities toward impact and friction were determined according to BAM (Bundesanstalt für Materialforschung and -prüfung) standard methods, together with measurements regarding sensitivity toward electrostatic discharge. Hot plate and hot needle tests were conducted for every metal salt and complex, whereas the detonation parameters of every nitrogen-rich salt were calculated using the EXPLO5 code.

3.1 Introduction

The nitrocyanamide anion (NCA^-) was discovered rather accidentally in 1950 by McKay.[1] During the preparation of diazomethane from *N*-methyl-*N′*-nitro-*N*-nitrosoguanidine under alkaline conditions, he isolated the corresponding potassium salt as a byproduct. To date, further pathways for accessing the anion have already been examinated. Thus, the reaction of various *N*-alkyl-*N′*-nitro-*N*-nitrosoguanidine derivatives results in the formation of nitrocyanamide salts.[2-3] Furthermore, syntheses starting from 1-alkyl-1,3-dinitroguanidines and *S*-methyl-*N*-nitroisothiourea are described.[4-5] The first energetic investigations of salts based on the nitrocyanamide anion were already carried out by Harris in 1957, i.e.

shortly after its discovery.[6] At that time, he already emphasized the initiation capacity of silver and barium salts.[6]

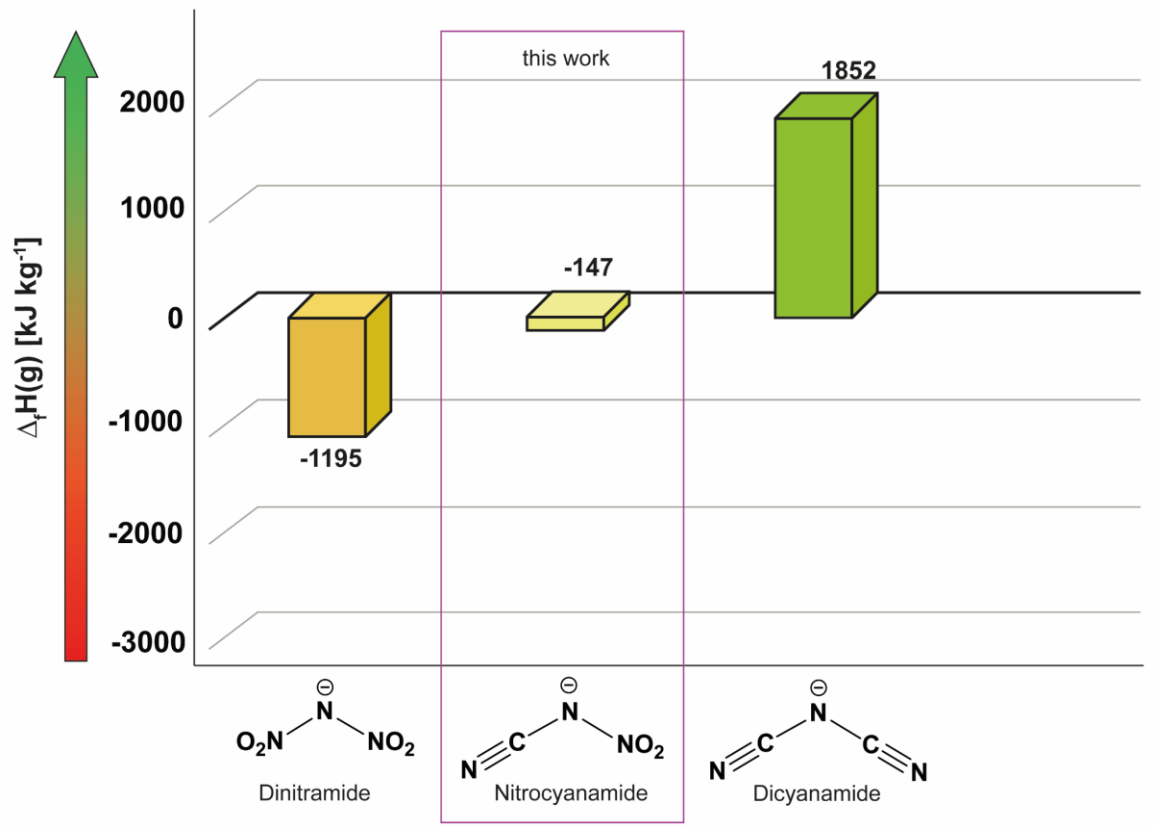

Figure 1. Calculated gas phase heats of formation for the scope of related anions dinitramide (DN^-), nitrocyanamide (NCA^-), and dicyanamide (DCA^-).

The main research on this anion, however, focused on the reaction of nitrocyanamide as a nucleophile,[7-9] resulting in isocyanates, and later the implementation of the anion into transition metal complexes.[10-24] These were mainly based on pyrazole[10-12] and imidazole[10, 13-17] ligands and were largely part of spectroscopic studies. Further energetic investigations were carried out rather recently, focusing on nitrocyanamide as part of ionic liquids used in hypergolic mixtures.[25-32] In this area, the group of Shreeve has been leading the way, whereas mostly dialkylated imidazolium cations [25, 27, 32] or other alkylammonium salts[25, 28-32] were used. However, some energetic salts, such as aminoguanidnium or triaminoguanidinium, which are solids at ambient temperature, have also been investigated.[27]

In this work, the focus is again on the energetic properties of the anion. In general, the previous investigations are to be supplemented in terms of its use in nitrogen-

rich salts. Furthermore, the anion is to be examined as a building block in energetic coordination compounds (ECC). The latter point is particularly interesting with respect to the earlier work of our group about energetic complexes. Thus, the dicyanamide (DCA^-) and more recently the dinitramide anion (DN^-) have already been studied excessively in copper complexes.[33-34] The nitrocyanamide anion is therefore of particular interest in this context because of its structure. Since half of it consists of the oxidizing dinitramide anion due to its nitro group and the other half of the endothermic dicyanamide anion due to the nitrile unit. Accordingly, the heat of formation for the centerpiece is between that of the two anions (Figure 1).

In the preceding studies, the dicyanamide complexes in particular showed only weak performance with sufficient thermal stabilities. The sensitivity of the compounds examined, however, was in rather low. Improved performances were observed for the dinitramide complexes. Nevertheless, the complexes were very sensitive and showed, with exceptions, too low thermal stabilities. However, since the centerpiece consists in part of the two anions, it was expected that the good performance of the complexes could be maintained. The sensitivity, on the other hand, should be within an acceptable range.

Thermal stability of DCA complexes is also partly based on the bridging character of the anion. This behavior is not to be expected especially in copper NCA complexes according to complexes described in the literature, the thermal stability must be influenced in other ways. In contrast to energetic salts, for which only the cation can be varied (*e.g.*, hydrazinium, hydroxylammonium), the concept of energetic coordination compounds offers further possibilities for adjusting the properties. In several studies, for example in copper dinitramide complexes, the thermal stability of the compounds has already been significantly increased by the introduction of bridging ligands.[34]

3.2 Results and Discussion

3.2.1 Synthesis

As already mentioned earlier, the nitrocyanamide anion was discovered rather accidentally as a side product during the preparation of diazomethane from *N*-methyl-*N′*-nitro-*N*-nitrosoguanidine (**1**, MNNG).[2] The reaction equation for the

formation of silver nitrocyanamide is displayed in Scheme 1. Compound **1** can easily be prepared in a two-step synthesis starting from commercially available nitroguanidine.[1] The silver salt of nitrocyanamide (**6a**) was then obtained directly through alkali promoted cleavage of MMNG (**1**) and subsequent precipitation by silver nitrate under nitric acid conditions in 86% yield.[6]

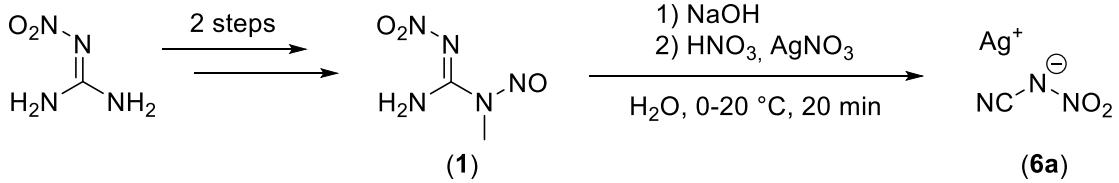

Scheme 1. Preparation of silver nitrocyanamide (**6a**).

A suggested mechanism is displayed in Scheme 2.[35] The reaction is basic catalyzed and involves the intermediate formation of methyldiazotate. Proton rearrangement and the cleavage of water leads to the generation of diazomethane and nitrocyaniamide, which is precipitated as its silver salt **6a**.

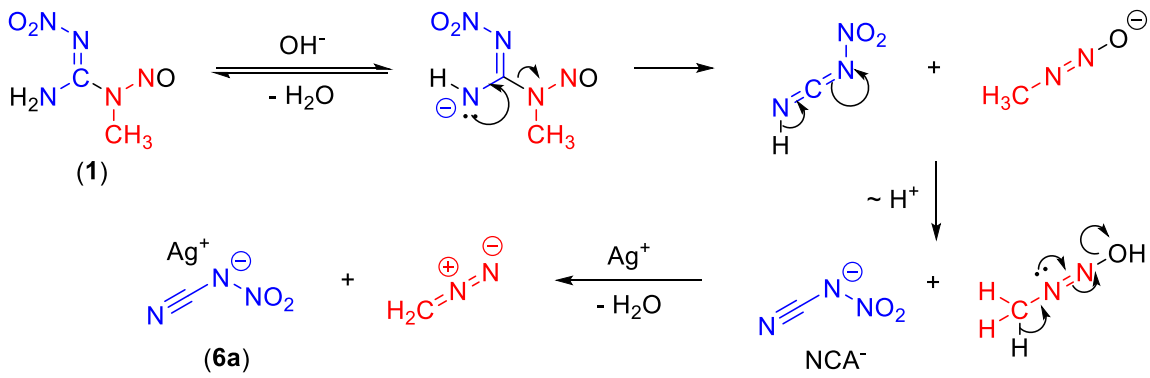

Scheme 2. Proposed mechanism of the formation of silver nitrocyanamide (**6a**) and diazomethane from MNNG (**1**)[35].

Several salts of nitrocyanamide including alkaline, alkaline earth, and transition metal salts are already known in the literature,[6] as well as nitrogen-rich derivatives including ammonium, and the already mentioned guanidinium, aminoguanidinium, and triaminoguanidium (TAG^+) salts,[6, 27] as well as several ionic liquids.[25-32] Since the series of nitrogen-rich derivatives of NCA anions has not been fully investigated, we have focused on the synthesis and investigation thereof, as they tend to be promising compounds, which emerges from the structural hybridization

of DCA and DN. Moreover, there are no energetic calculations or crystallographic studies on the known structures of nitrogen-rich NCA salts.[27] Therefore, compound **6a** was used as a basis for the preparation of the nitrogen-rich salts **2**, **3a**, **4a**, **5a**, and **5b**.[6] A metathesis reaction using the respective chloride or hydrochloride salts of nitrogen-rich cations, yielding silver chloride and the respective salt was performed enabling the convenient preparation of the desired salts in good yields of 74–90% (Scheme 3).[6] As green solvents, a mixture of methanol and acetonitrile (**3a**, **4a**, **5a**, and **5b**) or acetonitrile (**2**) and water was used, affording single crystals of each salt except compound **4a**, which is a liquid at room temperature. Applying an excess of the silver salt **6a** to triaminoguanidinium hydrochloride led to the formation of single crystals of compound **5b** (Scheme 3). Unfortunately, an elemental analysis pure isolation of the triaminoguanidinium nitrocyanamide argentat(I) complex was not possible.

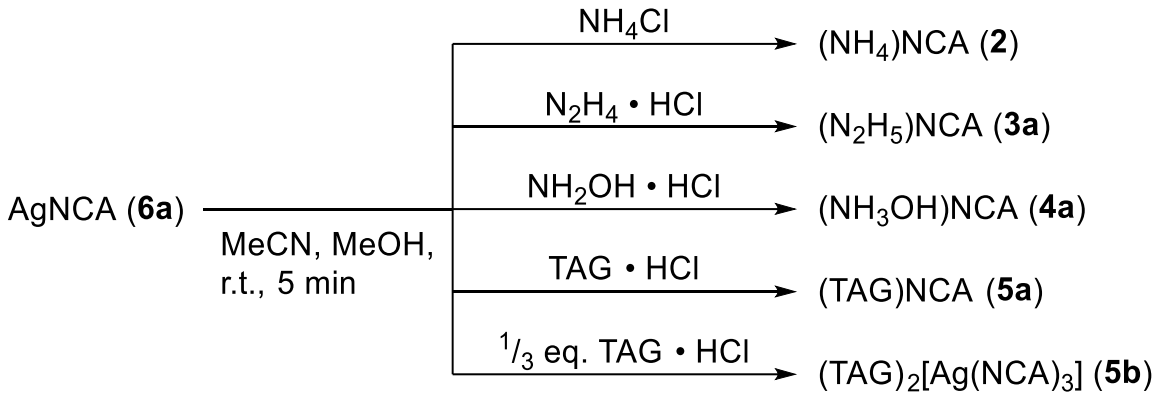

Scheme 3. Formation of the nitrogen-rich salts **2**–**5** of nitrocyanamide from silver nitrocyanamide (**6a**).

Further reactions of nitrocyanamide anions as nucleophiles with alkyl halides, e.g., forming isocyanates and nitrous oxide, are already known in the literature.[7-9] In this work, however, reaction sequences of NCA^- anions, acting as electrophiles, were also investigated. Addition reaction of nitrocyanamine (HNCA) with hydroxylamine or hydrazine at elevated temperatures (100 °C) leads to the formation of the guanidine derivative products displayed in Scheme 4.

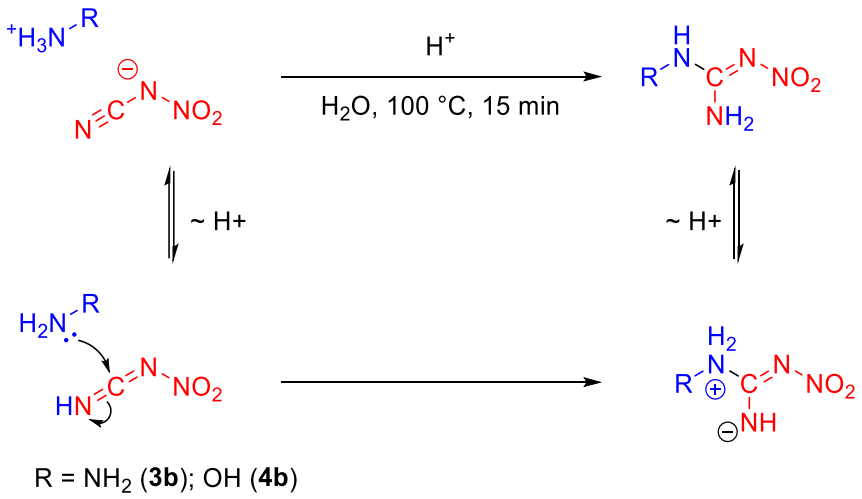

Scheme 4. Formation of the guanidine derivatives of the hydrazinium (**3a**) and hydroxylammonium salts (**4a**) under acidic conditions.

Both compounds, 1-amino-3-nitroguanidine (**3b**) and 1-hydroxy-3-nitroguanidine (**4b**), are already known in the literature but only the hydrazinium adduct is sufficiently characterized.[36-37] A proposed mechanism for the formation of these adducts is shown in Scheme 4.

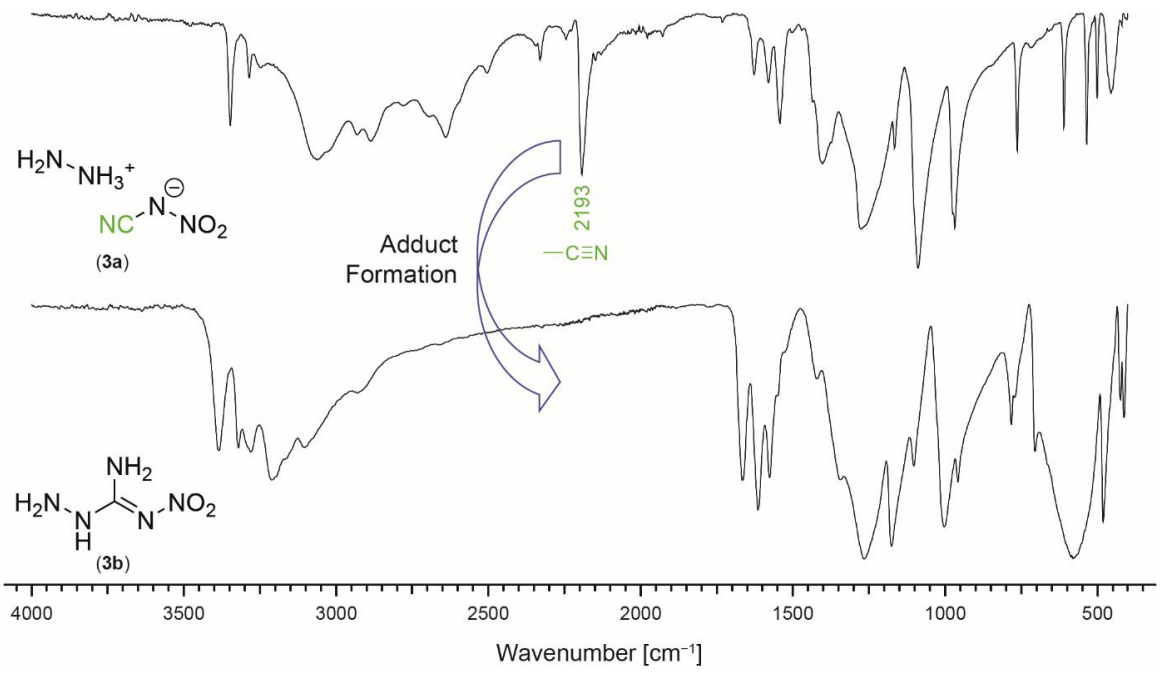

Figure 2. Comparison of the IR spectra of the hydrazinium salt (**3a**) and its respective addition product (**3b**).

The examination whether an addition reaction or a salt formation has been taken place was analyzed according to the characteristic CN oscillation in the IR spectrum. As shown in Figure 2, the nitrile band at 2193 cm^{-1} clearly indicates

whether the investigated substance is a cyanamide salt or guanidium derivative. Further IR spectra of the remaining compounds can be found in the Supporting Information (Figures S1–S4). The shift of the carbon signal in the respective ^{13}C NMR spectrum is also a possible marker of addition product formation. Addition reactions of cyanamide derivatives with nucleophiles under higher temperature are intensively described in the literature. For example, the reaction of guanidinium dicyanamide salts leads to the formation of melamine,[38-39] or the reaction of nitrocyanamide and strong acid to nitrourea.[3]

Besides the formation of energetic salts, the investigation of nitrocyanamide as an anion in energetic coordination compounds (ECCs) is a main aim of this work. Since the NCA^- anion is the center piece between the dinitramide (DN^-) and the dicyanamide anions (DCA^-), it is expected that the complexes properties lie in between those of the two anions. In the best case, the poor solubility as well as the good sensitivity data of the DCA complexes are thus achieved together with the performance of the DN complexes.[33-34]

Some transition metal complexes, mainly based on pyrazoles[10-12] and imidazoles[10, 13-17] and other nitrogen-containing hetrocycles are already known in the literature.[18-19] Nearly all of them were not investigated toward a potential use as energetic material, however, they leave an indication how the complexes most likely built up. With the exception of some triphenylphosphine complexes,[20-22] as well as a trimethyltin complex,[23] only two complexes are known possessing a formula differing from the general $[M(L)_4(A)_2]$ pattern (M = central metal; L = ligand; A = anion).[13,24]

The complexes presented in this work were prepared by first reacting an aqueous solution of copper(II) chloride dihydrate with two equivalents of silver nitrocyanamide (**6a**) in acetonitrile (Scheme 5). Evaporation of the solvent gave the tetraaqua copper(II) nitrocyanamide complex (**7a**), which was already described by Harris.[6] Unfortunately, no single crystals could be obtained of the compound. Instead, a reaction with an aqueous solution of ammonia afforded single crystals of the similarly structured tetraammine complex **7b**. Dissolving the silver salt **6a** in aqueous ammonia afforded single crystals of the second silver complex **6b** obtained in this work (Scheme 5). Applying nitrogen-rich tetrazole ligands to the solution of copper nitrocyanamide instead of aqueous ammonia results in the formation of several ECCs (**8**–**12**) displayed in Scheme 5 (yields: 63–92%). The

nitrogen-rich tetrazole ligands used in this work are shown in Chart 1. Some ligands were excluded (e.g., 1-amino-5*H*-tetrazoles) due to failed reactions.

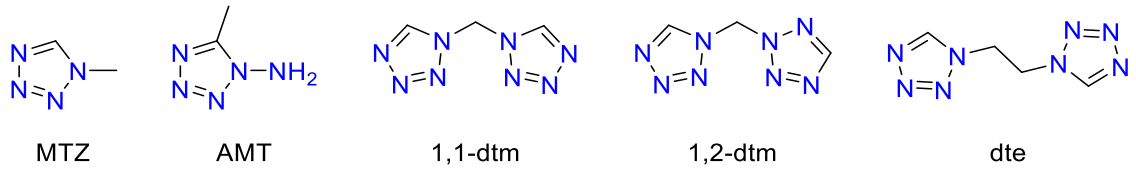

Chart 1. Overview on the nitrogen-rich ligands used for the formation of the ECCs **8**–**12**.

Each ligand used for the preparation of energetic coordination compounds is known in the literature and can easily be prepared either through a substitution reaction of 1,5*H*-tetrazole and an alkyl halide,[40] the amination of 5-methyl-1*H*-tetrazole,[41] or a ring closure reaction of an alkyl amine or diamine with sodium azide and triethyl orthoformate.[42] The nitrogen-rich monotetrazole ligands 1-methyl-5*H*-tetrazole (MTZ) and 1-amino-5-methyltetazole (AMT) were chosen as both ligands are known to form powerful coordination compounds.[41, 43] The ditetrazoles 1,1-ditetrazolylmethane (1,1-dtm) and 1,2-ditetrazolylmethane (1,2-dtm) and 1,1-ditetrazolylethane (dte) were selected because these ligands are showing a bridging behavior, known to increase a coordination compounds' thermal stability.[24, 40]

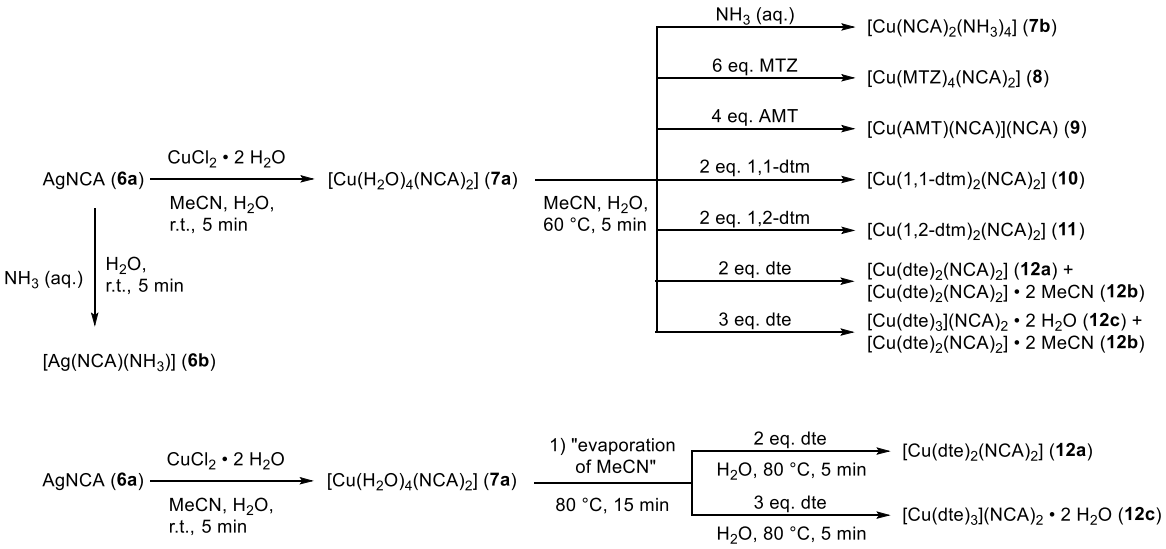

Scheme 5. Overview of the energetic coordination compounds based on the nitrocyanamide anion prepared in this work.

The direct addition of the ditetrazolylethane ligand to copper NCA solution results in a mixture of complexes **12a**–**c**, depending on the amount of ligand used. However, if the acetonitrile is evaporated, or copper(II) NCA (**7a**) is isolated beforehand, it is possible to obtain the complexes **12b** and **12c** in pure form (yield: 76–77%). Both complexes were already described by Joas et al. but were prepared using a different protocol.[44] The side species **12a** could not be obtained elemental analysis pure. The complex **12c** obtained here and the ECC **9** are also the only coordination compounds that exhibit a composition that rejects from $[M(L)_2(A)_2]$.
As already mentioned, it was unfortunately not possible to obtained further coordination compounds with a silver central metal. Furthermore, the use of 1-aminotetrazole, or 1,5-diaminotetrazole, which are known to form some of the best performing ECCs only resulted in decomposition. This behavior was already observed during the investigation of copper(II) dinitramide ECCs and therefore most likely caused by an unwanted interaction with the nitramide moiety of the anion.[34]

3.2.2 X-Ray Diffraction

Low temperature single crystal X-ray diffraction experiments were carried out for every solid compound except for **1**, **3b**, **4a**, and **6a** because the respective structures are already described in the literature,[45] and **7a**, of which unfortunately no single crystals could be obtained. In case of compound **12c** the measurement indicates the compounds' structure, but a finalization of the data set was not possible due to a strong disordered nitrocyanamide moiety. The complexes' composition was finally proved through CHNO elemental analysis. Details on the measurement and refinement data for every crystallographically investigated compound are listed in the Supporting Information (Tables S1–S4). The crystal data sets were uploaded to the CSD database with the CCDC numbers 2099366 (**2**), 2099365 (**3a**), 2099362 (**5a**), 2099357 (**5b**), 2099360 (**6b**), 2099356 (**7b**), 2099361 (**8**), 2099363 (**9**), 2099364 (10), 2099355 (**11**), 2099359 (**12a**), and 2099358 (**12b**) and can be accessed free of charge.[46]
When it comes to the nitrogen-rich salts **2**, **3a**, and **4a**, the ammonium as well as the triaminoguanidinium salt have already been prepared but not structurally

investigated yet.[6, 27] Therefore, their structures were determined together with that of the hydrazinium salt (Figure 3). Every of the three salts crystallize in the monoclinic space group $P2_1/c$ with four formula units per unit cell. Hydrazinium salt **3a** possesses the highest density (1.606 g cm^{-3} at 123 K), followed by ammonium salt **2** (1.561 g cm^{-3} at 173 K), and finally by the triaminoguanidinium salt **5a** with density of 1.457 g cm^{-3} at 102 K. When it comes to the formation of a network of hydrogen bonds compound **5a** shows the strongest network. Intermolecular bonds are formed by each hydrogen atom of the cation. The NCA anion is participating with both of its oxygen atoms of the nitro group as well as with the nitramide and the nitrile nitrogen atoms. In case of the ammonium salt **2**, the cation is again forming hydrogen bonds with every of its hydrogen atoms. The anion, however, is only interacting throughout its amide and nitrile nitrogen atoms. For the hydrazinium salt **3a**, only the NH_3 group of the cation is forming bonds through their hydrogen atoms. The NH_2 group is only participating via its electron pair with a NH_3 group of another nearby hydrazinium cation. The anion is also solely interacting over one of its oxygen and its nitramide nitrogen atom.

The structurally investigated coordination compounds showed various coordination geometries including two- and trifold for both silver(I) complexes, as well as 5- and 6-fold for the copper(II) complexes. The hexacoordinated copper complexes show a classic Jahn–Teller distortion along the axial positions. Except for the silver complexes **5b** and **6b** and the copper complexes **9** and **12c**, in every case the anion is solely coordinating over its nitrile moiety. Of the coordination modes shown in Figure 4, **C** is the only mode known to date, with two other modes described in the literature not observed as part of this work.[19] For the structurally similar dinitramido ligand, a binding behavior via one of the oxygens is mainly known in copper complexes.[47-48]

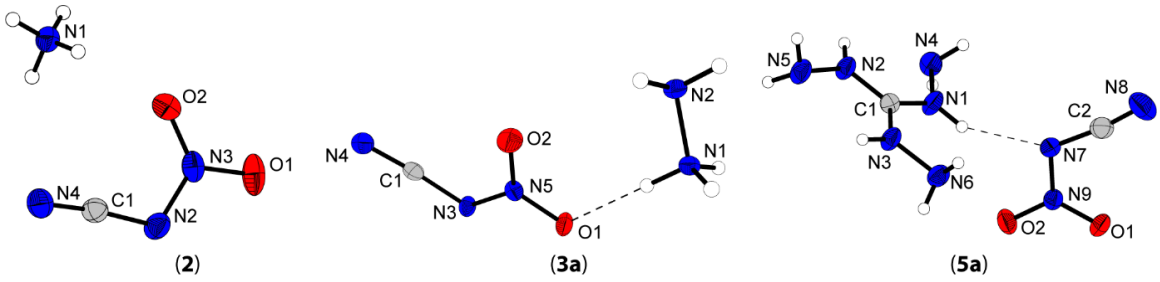

Figure 3. Crystal structures of the ammonium (**2**), hydrazinium (**3a**), and triaminoguanidinium (**5a**) salts of nitrocyanamide.

Recently, however, coordination via the nitramide nitrogen has also been observed by our group.[34] For the equally similar dicyanamide anion, a wide variety of coordination modes have been discovered in copper complexes.[33] Because of the nitrile moiety, one or more bonds originate from this unit in each case, with additional bonds via the amide nitrogen is also possible. In any case, it is interesting to note that the dinitramide anion does not coordinate in most cases, but DCA always does in the complexes described in the literature. Based on this information, it can be concluded that noncoordinating dicyanamide anions are probably not stable.

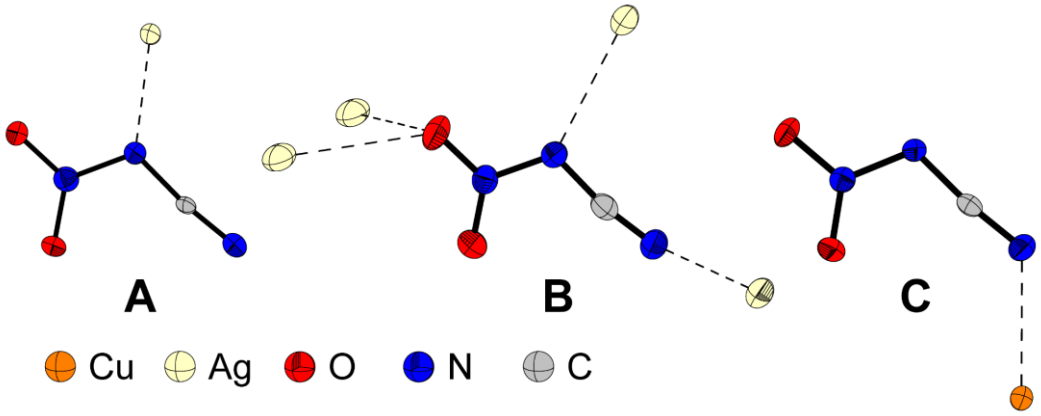

Figure 4. Overview on the interactions of the NCA^- anion with the central metals in the coordination compounds. mode **A**: **5b**. mode **B**: **6b**. mode **C**: **7b**–**12b**.

The tetrazole ligands, except for complex **10**, coordinate in the usual way via the N4 nitrogen. Since the bond lengths and angles in the nonbinding ligands are like those, found in the complexes, they are not part of the discussion.[40-41, 49-50]

The argentat(I) complex **5b** crystallizes in the trigonal space group $P3_1c$ with six formula units per unit cell. The molecular unit consists of one silver, two triaminoguanidinium cations and three nitrocyanamide anions (Figure 5). The density of 1.933 g cm^{-3} (at 123 K) is higher than the ones of the other structurally investigated nitrogen-rich salts but significantly lower than the density published for the neat silver salt **6a** (3.251 g cm^{-3} at 293 K).[45] Hydrogen bonds are, as already observed in the TAG salt **5a**, formed by every hydrogen atom of the cation. The anion, however, is interacting with hydrogen atoms solely via both of its oxygen atoms and the nitrile moiety. The nitramide nitrogen atom is coordinating the silver atoms, leading to slightly distorted trigonal planar coordinated metal cations (Figure

4, mode A). The angles are close to the perfect 120° (N16–Ag3–N16 = 118.98(6)°), but the silver atom is displaced about 0.226(6) Å out of the plane.

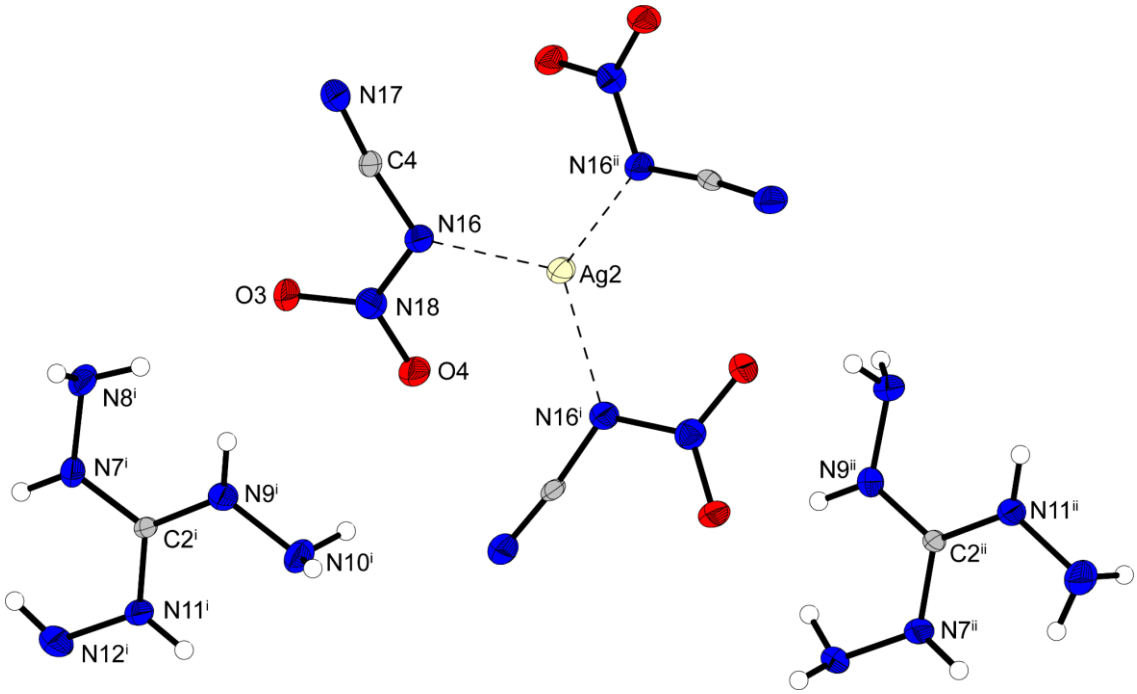

Figure 5. Molecular unit of compound **5b**. Selected bond length (Å): Ag1–N16 2.213(5). Symmetry codes: (i) $1-y, x-y, z$; (ii) $1-x+y, 1-x, z$.

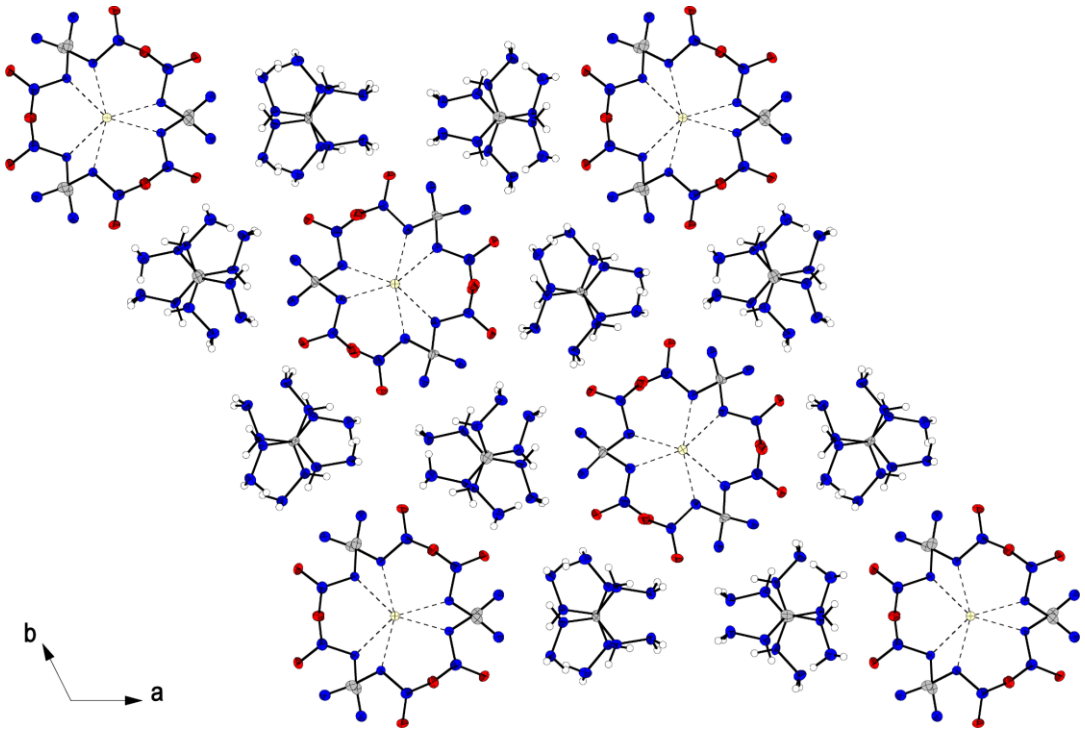

Figure 6. Packing of compound **5b** displayed along the *c* axis.

Furthermore, a one-dimensional network is built up through argentophilic interactions of the silver cations (Ag2–Ag3 = 3.3083(10) Å). The NCA^- anions are arranged here in an alternating order. The TAG^+ cations arrange themselves between the strands and stabilize them by hydrogen bonds (Figure 6).

Both ammine complexes crystallize in the monoclinic space groups $P2_1/c$ (**6b**) and $C2/c$ (**7b**) with four formula units per unit cell, respectively. The silver(I) complex consists of one ammine and one nitrocyanamide ligand (Figure 7). The ligands are arranged almost perfectly linear (N1–Ag1–N4 = 174.77(10)°), whereas the anion is solely coordinating over its nitrile moiety. In addition to that, several stabilizing ionic interactions are formed between the silver center and nearby NCA^- anions as displayed in Figure 4 (mode **B**). The copper center in the ECC **7b** is coordinated by four ammine ligands in equatorial positions and two NCA^- anions (Figure 4, mode **C**) in the axial positions. A structural comparison with ammine complexes based on the dinitramide anion indicates a similar coordination geometry for the copper(II) complex, whereby the anion is coordinating via an oxygen atom.[47] The respective silver(I) complex was not crystallographically investigated, but the composition indicates a 2-fold coordinated diammine complex.[51] This is to be expected, since in this case the dinitramide anion has no coordination possibility via a nitrile group. The copper(II) ECC **8**, based on the MTZ ligand, crystallizes in the form of blue platelets in the monoclinic space group $P2_1/c$ with four formula units per unit cell and a calculated density of 1.715 g cm^{-3} at 100 K. The central metal is coordinated very similar to the copper(II) ammine complex **7b**. Four ligands are arranged in the equatorial sites and anions in the remaining axial spots (Figure 8). The Jahn–Teller distortion (Cu1–N22 = 2.380(2) Å; Cu1–N19 = 2.390(2) Å) is not as distinct as in complex **7b** (Cu1–N3 = 2.610(3) Å).

The copper complex **9** crystallizes in the orthorhombic space group *Pbca*. The unit cell consists of eight formula units and possesses a calculated density of 1.635 g cm^{-3} (at 173 K). The compound is the only copper(II) complex of this work not showing a 6-fold geometry around its central metal (Figure 9). Instead, a slightly distorted square planar pyramidal conformation is observed (N4–N19–N14–N9 = 4.98(8)°). The AMT ligands are forming the basis, with one nitrocyanamido ligand at its tip (Figure 4, mode **C**).

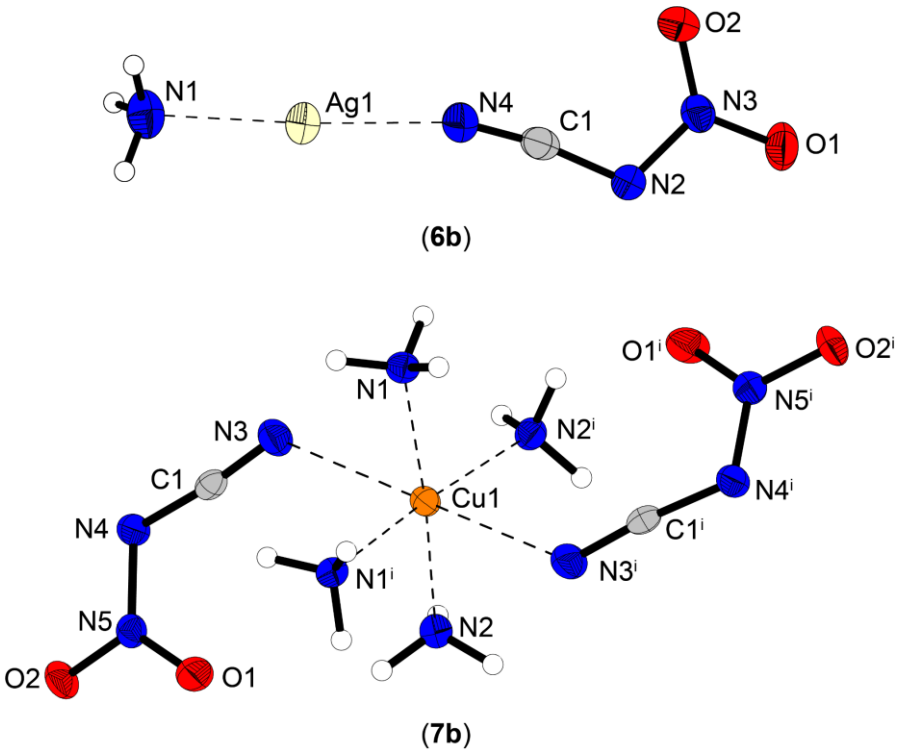

Figure 7. Molecular units of the ammine complexes $[Ag(NCA)(NH_3)]$ (**6b**) and $[Cu(NCA)_2(NH_3)_4]$ (**7b**). Selected bond lengths (Å) of **6b**: Ag1–N1 2.153(3); Ag1–N4 2.135(3). Selected bond lengths (Å) of **7b**: Cu1–N1 2.013(2); Cu1–N3 2.610(3). Selected bond angles (deg) of **7b**: N3–Cu1–N2 90.44(9); N1–Cu1–$N2^i$ 90.08(8). Symmetry code of **7b**: $1-x, y, 0.75-z$.

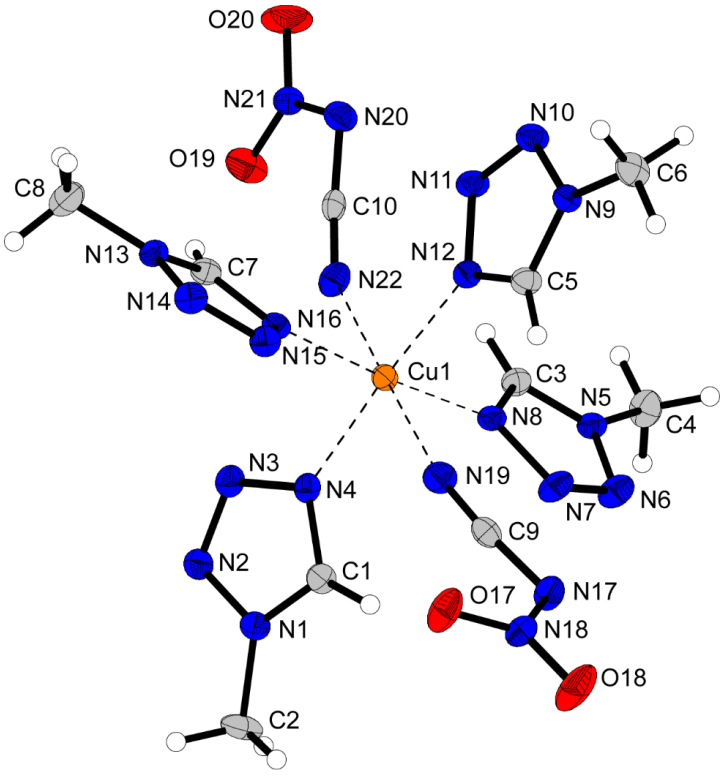

Figure 8. Molecular unit of $[Cu(MTZ)_4(NCA)_2]$ (**8**). Selected bond lengths (Å): Cu1–N4 2.024(2); Cu1–N8 2.030(2). Selected bond angles (deg): N12–Cu1–N16 89.18(8); N16–Cu1–N22 87.31(8); N12–Cu1–N22 91.33(8).

The remaining NCA^- anion is located on the bottom of the pyramid, whereby the distance between nitrile moiety and copper center is too long to be considered as any kind of interaction (Cu1–N26 = 5.375(3) Å). This is most likely caused by the sterically demanding disubstituted monotetrazole ligands and was therefore already observed in earlier studies.[34]

The copper(II) complexes **10** and **11** based on the isomeric dtm ligands crystallize with similar sum formulas in the monoclinic space groups $P2_1/n$ (**10**) and $P2_1/c$ (**11**). Both compounds' unit cells consist of two formula units with slightly differing calculated densities of 1.880 g cm^{-3} (**10**, at 103 K) and 1.932 g cm^{-3} (**11**, at 102 K). In both cases, the complexes' equatorial coordination sites are occupied by dtm ligands of which each links to a different metal center (Figures 10 and 11).

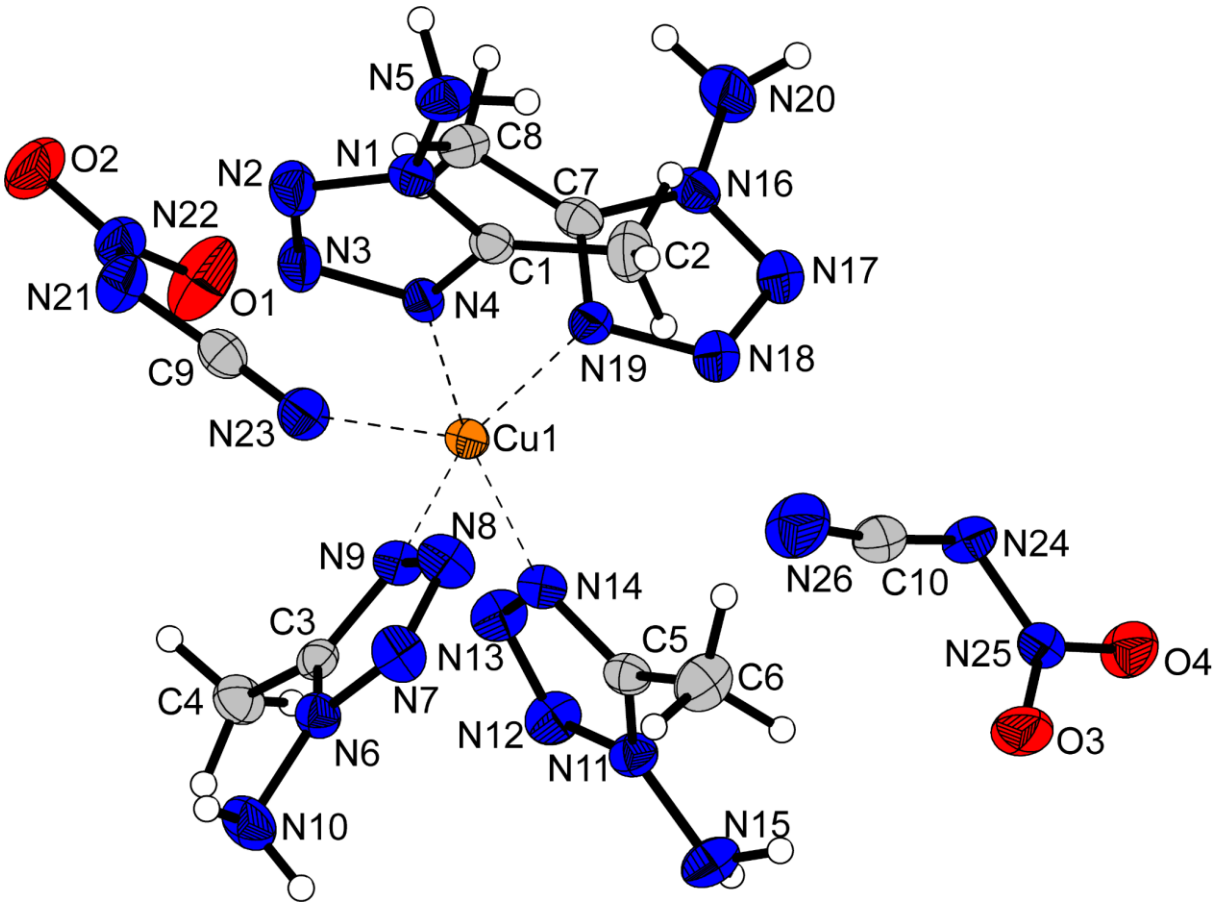

Figure 9. Molecular unit of $[Cu(AMT)_4(NCA)](NCA)$ (**9**). Selected bond lengths (Å): Cu1–N4 2.017(2); Cu1–N23 2.156(2). Selected bond angles (deg): N23–Cu1–N9 100.48(8); N23–Cu1–N4 96.61(8); N9–Cu1–N14 88.35(8); N9–Cu1–N19 159.84(8).

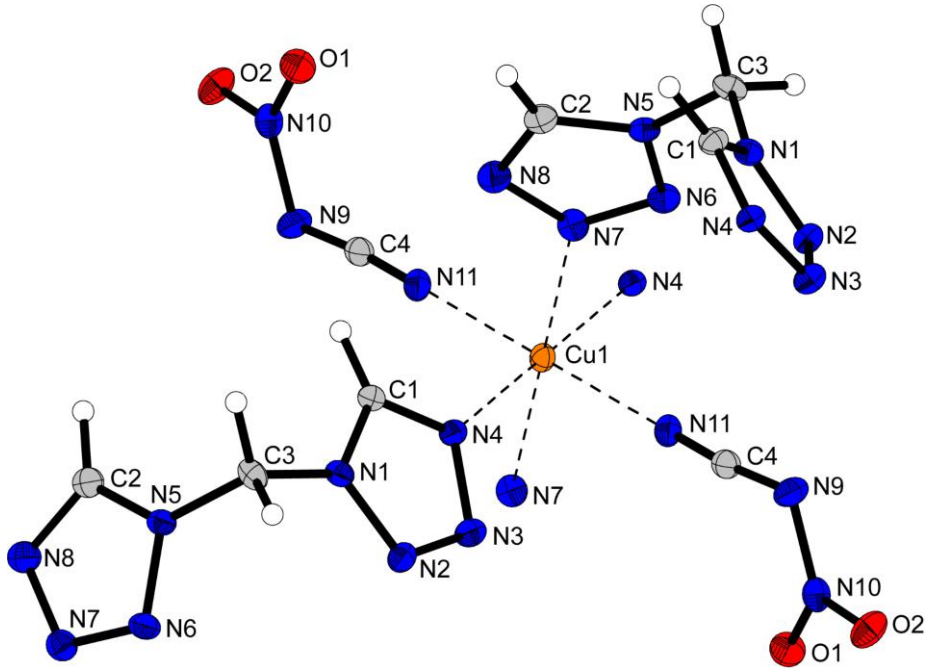

Figure 10. Molecular unit of $[Cu(1,1\text{-dtm})_2(NCA)_2]$ (**10**). Selected bond lengths (Å): Cu1–N4 2.005(2); Cu1–N7 2.414(2); Cu1–N11 1.982(2). Selected bond angles (deg): N4–Cu1–N11 89.44(9); N4–Cu1–$N7^{ii}$ 88.41(8); $N7^{ii}$–Cu1–N11 92.18(8). Symmetry codes: (i) $2-x, 1-y, 1-z$; (ii) $0.5+x, 1.5-y, -0.5+z$; (iii) $1.5-x, -0.5+y, 1.5-z$.

This leads to the formation of two-dimensional polymeric layers. The nitrocyanamido ligands are located in the axial positions and are coordinating via the coordination mode **C** displayed in Figure 4.

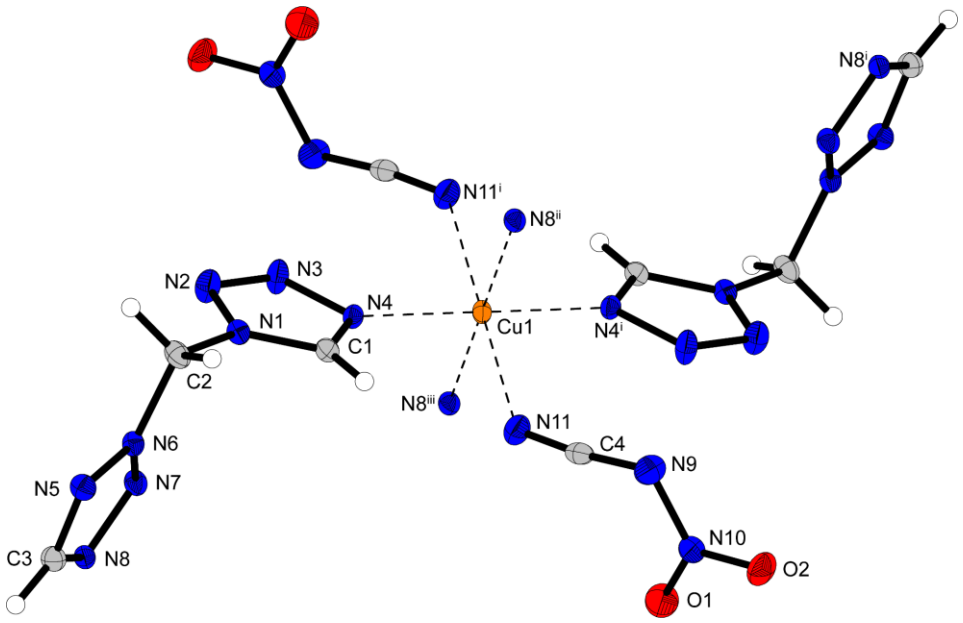

Figure 11. Extended molecular $[Cu(1,2\text{-dtm})_2(NCA)_2]$ (**11**). Selected bond lengths (Å): Cu1–N4 2.0217(18); Cu1–N8 2.0307(17); Cu1–N11 2.3216(19). Selected bond angles (deg): N8–Cu1–N11 91.29(7); N4–Cu1–N8 88.47(7); N4–Cu1–N11 93.23(7). Symmetry codes: (i) $2-x, 1-y, 1-z$; (ii) $x, 0.5-y, -0.5+z$; (iii) $2-x, 0.5+y, 1.5-z$.

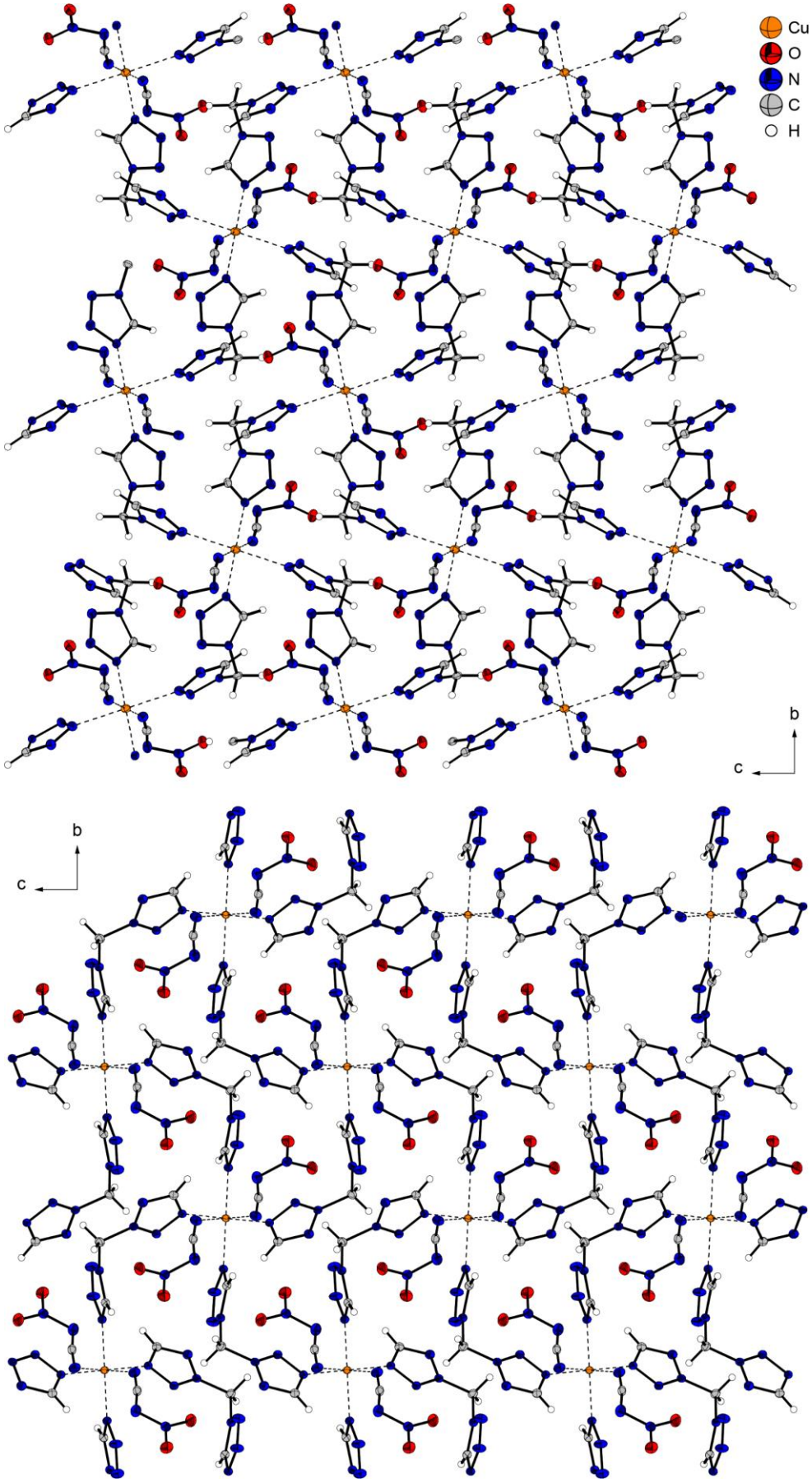

Figure 12. Detail of the packing of complexes **10** (top) and **11** (bottom) displayed along the *a* axis.

Despite the similar built-up nature of both complexes, differently arranged polymeric layers are formed by each ligand (Figure 12). This is not only caused by the different substituted tetrazoles in the different ligands. As already mentioned earlier, complex **10** is the only compound possessing ligands which are not solely coordinating via its N4/N8 nitrogen atoms but also via the N3/N7 nitrogen.

The complexes **12a** and **12b**, both consisting of 2 equiv of the dte ligand, crystallize in the triclinic space group $P\bar{1}$ with only one formula unit per unit cell. The measurement data of **12b** is consistent with the data obtained by Joas et al.[24] The crystallographic density of complex **12b** (1.824 g cm^{-3} at 102 K) is significantly higher than the one calculated for **12a** (1.666 g cm^{-3} at 102 K). The general formula $[M(L)_2(A)_2]$ derived from the coordination sphere of each complex is like the ones of the complexes **10** an **11**.

This is because all the complexes are based on ditetrazole ligands in equatorial positions, which exhibit a linking behavior (Figure 13). In complexes **12a** and **12b**, however, the complexes do not bridge to different metal centers, but instead bridge in pairs to the same metal center. Therefore, instead of a two-dimensional network, 1D polymeric chains are formed. The remaining axial positions are again occupied by NCA$^-$ anions coordination via their nitrile moiety (Figure 4, mode **C**).

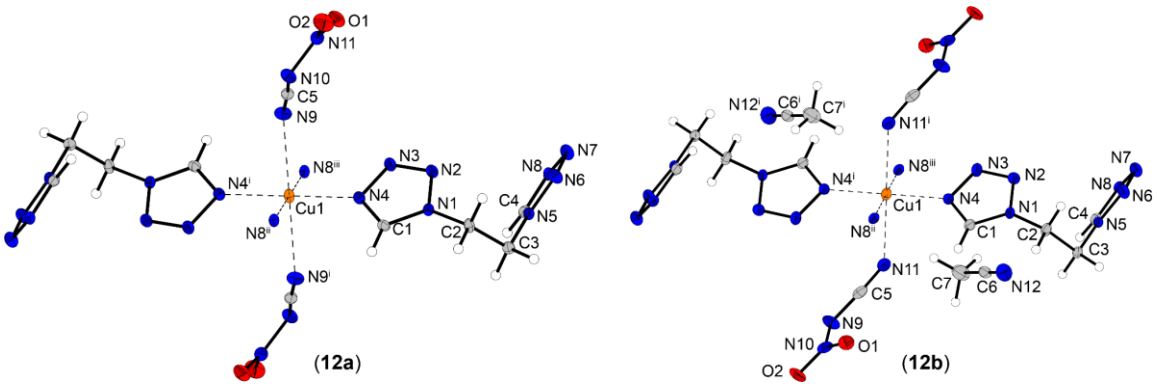

Figure 13. Extended Molecular Units of $[Cu(dte)_2(NCA)_2]\cdot 2$ MeCN (**12a**) and $[Cu(dte)_2(NCA)_2]$ (**12b**). Selected bond lengths (Å) of **12a**: Cu1–N4 2.0217(18), Cu1–N8 2.047(3), Cu1–N11 2.401(3). Selected bond lengths (Å) of **12b**: Cu1–N4 2.019(2), Cu1–N8 2.0308(15), Cu1–N9 2.4139(18). Selected bond angles (deg) of **12a**: N8–Cu1–N11 87.91(10), N4–Cu1–N8 91.19(10), N4–Cu1–N11 88.33(10). Selected bond angles (deg) of **12b**: N8–Cu1–N9 87.45(6), N4–Cu1–N8 90.21(6), N4–Cu1–N9 91.82(6). Symmetry codes of **12a**: (i) $2-x$, $1-y$, $1-z$; (ii) $1+x$, y, z; (iii) $1-x$, $1-y$, $1-z$. Symmetry codes of **12b**: (i) $-x$, $-y$, $1-z$; (ii) x, $-1+y$, z; (iii) $-x$, $1-y$, $1-y$.

However, since complex **12a**, unlike **12b**, has two cocrystallizing acetonitrile molecules, the polymer network formed is slightly different (Figure 14). Caused by

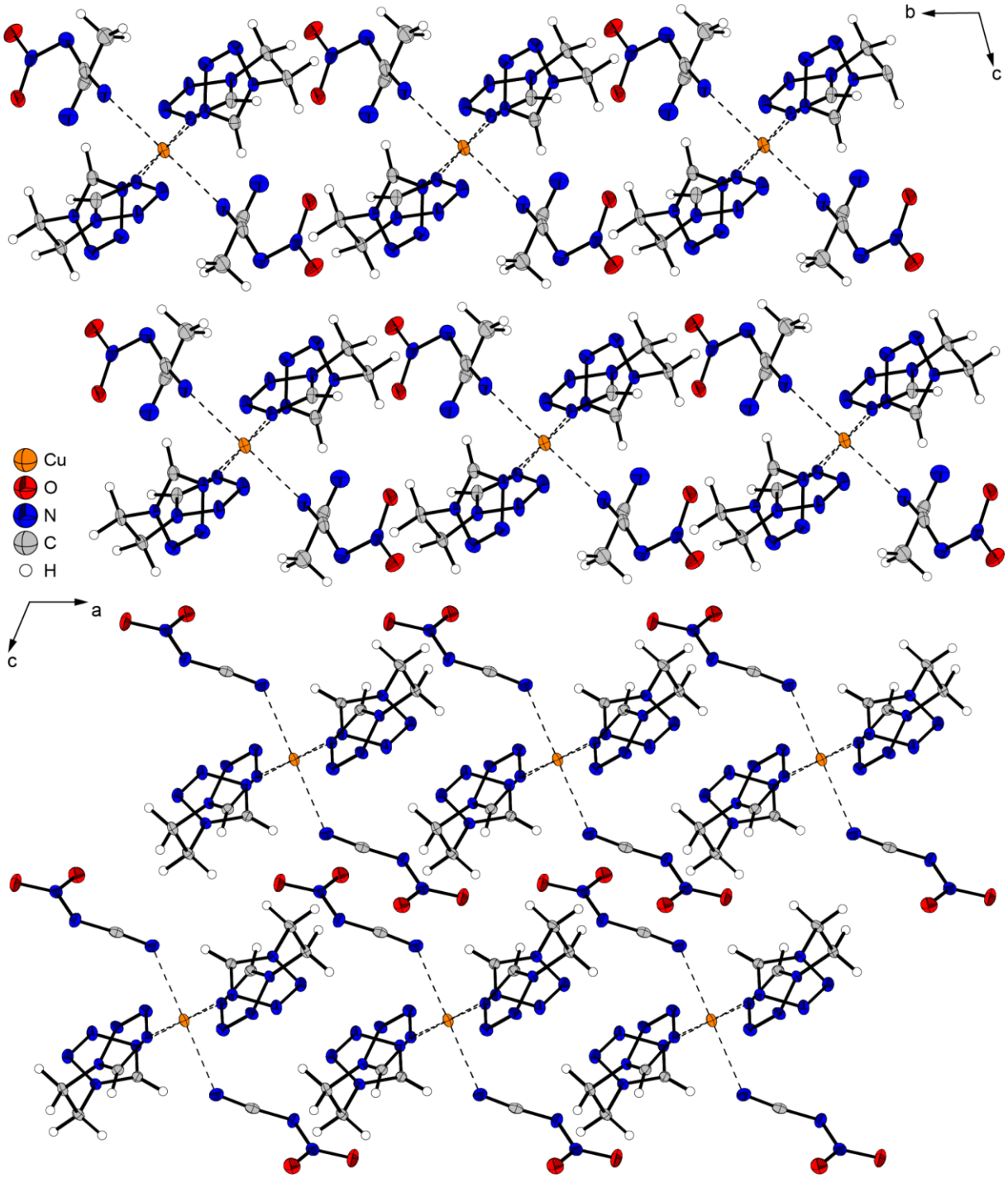

Figure 14. Detail of the packing of complexes **12a** (top) displayed along the *b* axis and **12b** (bottom) shown along the *a* axis.

the interaction with the solvent molecules, the anion is slightly differently arranged in the coordination sphere. This can be represented best by the N8–Cu1–N11–C5 torsion angle in **12a**. This, with a value of 113.43° is considerably different from the respective angle in complex **12b** (N4–Cu1–N9–C5 = 69.25°). In addition to the packing shown in Figure 14, this also results in a lower density for **12a**.

As mentioned earlier, the structure of ECC **12c**, initially described by Joas et al.,[24] could not be finalized due to a heavily disordered anion. However, it is evident from the data obtained that each copper center is coordinated by three bridging dte ligands. This results in a three-dimensional network in which two crystal waters are intercalated. Furthermore, since all coordination sites are occupied, to the best of our knowledge this is the first NCA complex with two noncoordinating anions.

3.2.3 Evaluation of Physicochemical Properties

Besides the cost-efficient synthesis and processing, the physicochemical properties are key factors for the development of new energetic materials.[52] These include the thermal stability, the sensitivity toward various mechanical stimuli and electrostatic discharge as well as detonation parameters and an evaluation of the compounds' performance. The compounds **2**, **3a**, **3b**, **4a**, **5a**, **6a**, **7a**, **8**–**11**, **12a**, and **12c** were selected for further characterization since these substances were obtained elemental analysis pure and are expected to be the most promising materials regarding their energetic properties in this work.

Table 1. Overview on the compounds' (**6a**, **7a**, **8**–**11**, **12b**, **12c)** thermal stability,[a] sensitivities toward various external stimuli and results of hot plate (HP) and hot needle (HN) tests.

Compound	No.	T_{endo} [°C][b]	T_{exo} [°C][c]	*IS* [J][d]	*FS* [N][e]	*ESD* [mJ][f]	HP[g]	HN[g]
AgNCA	**6a**	–	158	3	10	51	defl.	defl.
$[Cu(H_2O)_4(NCA)_2]$	**7a**	89	108	> 40	> 360	1500	dec.	dec.
$[Cu(MTZ)_4(NCA)_2]$	**8**	110	159	40	240	750	dec.	dec.
[Cu(AMT)$_4$(NCA)](NCA)	**9**	124*	124*	≤ 1	20	250	defl.	defl.
$[Cu(1,1\text{-dtm})_2(NCA)_2]$	**10**	–	191	7	112	750	defl.	dec.
$[Cu(1,2\text{-dtm})_2(NCA)_2]$	**11**	–	157	2	80	480	defl.	dec.
$[Cu(dte)_2(NCA)_2]$	**12b**	–	174	6	180	> 1500	dec.	dec.
$[Cu(dte)_3](NCA)_2 \cdot 2\,H_2O$	**12c**	103, 119	168	≤ 1	160	> 1500	dec.	dec.

[a] Onset temperature at a heating rate of 5 °C min^{-1} measured by DTA. [b] Endothermic peak, which indicates melting, or dehydration; [c] Exothermic peak, which indicates decomposition. [d] Impact sensitivity according to the BAM drophammer (method 1 of 6). [e] Friction sensitivity according to the BAM friction tester (method 1 of 6). [f] Electrostatic discharge sensitivity (OZM Electric Spark XSpark10, method 1 of 6). [g] –: Not tested; def.: deflagration; dec.: decomposition. * endothermic closely followed by exothermic event.

Thermal stability measurements were carried out using differential thermal analysis (DTA) at a heating rate of 5 °C min^{-1} in the range 25–400 °C. The outcomes are listed in Tables 1 and 2. The endothermic events observed either indicate a melting (**2**, **3a**, **4a**, **5a**, and **8**), or, if present, a loss of hydrate water (**12c**) or aqua ligands (**7a**). Exothermic events usually indicate a decomposition of the material. In addition to DTA measurements, both aqua molecules containing complexes **7a** and **12c** were further investigated using thermogravimetry (TG) in the range of 30 to 400 °C at a heating rate of 5 °C min^{-1}.

Table 2. Summary on the compounds' (**2**, **3a**, **4a**, **4b** and **5a**) thermal stability,[a] sensitivities toward various external stimuli and detonation parameters (compared with $(NH_4)DCA$ and ADN).

	(NH_4) NCA (**2**)	(N_2H_5) NCA (**3a**)	(NH_3OH) NCA (**4a**)	**4b**	(TAG)N CA (**5a**)	$(NH_4)DCA$[53]	AND[54]
Formula	$CH_4N_4O_2$	$CH_5N_5O_2$	$CH_4N_4O_3$	$CH_4N_4O_3$	$CH_9N_9O_2$	$C_2H_4N_4$	$N_4H_4O_4$
M [g mol^{-1}]	104.07	119.09	120.07	120.07	191.16	84.08	124.06
IS [J][b]	> 40	> 40	> 40	10	6	> 40	4
FS [N][c]	> 360	80	> 360	240	360	> 360	72
ESD [J][d]	> 1500	750	–	750	> 1500	–	0.45
ρ [g cm^{-3}][e]	1.532	1.565	1.68*	1.752	1.415	1.284	1.812
N [%][f]	53.8	58.8	46.7	46.7	66.0	66.6	45.2
Ω [%][g]	−15.4/ −30.7	−20.2/ −33.6	0/ −13.3	0/ −13.3	−31.3/ −40.2	114.2/ −76.1	25.8/ 25.8
T_{endo} [°C][h]	88	101	–	–	73	–	92
T_{exo} [°C][i]	177	129	94	144	173	127	135
$\Delta_f H°$ [kJ mol^{-1}][j]	30.0	186.1	112.1	−25.0	367.1	264.7	−125.3
$\Delta_f U°$ [kJ mol^{-1}][k]	42.4	201.0	125.7	−94.6	391.9	274.61	–
EXPLO5 V6.05.02							
$-\Delta_{Ex}U°$ [kJ kg^{-1}][l]	4606	5509	6216	5161	4673	3572	2784
T_{det} [K][m]	3159	3469	3961	3414	3009	2502	2319
V_0 [L kg^{-1}][n]	937	965	891	877	972	824	984
P_{CJ} [kbar][o]	229	273	329	332	213	161	270
V_{det} [m s^{-1}][p]	7956	8620	8915	8878	7956	6823	8502

[a] Onset temperature at a heating rate of 5 °C min^{-1} measured by DTA. [b] Impact sensitivity according to the BAM drophammer (method 1 of 6). [c] Friction sensitivity according to the BAM friction tester (method 1 of 6). [d] Electrostatic discharge sensitivity (OZM Electric Spark XSpark10, method 1 of 6). [e] Crystallographic density recalculated to 298 K. [f] Nitrogen content. [g] Oxygen balance with respect to CO/CO_2. [h] Endothermic peak, which indicates melting. [i] Exothermic peak, which indicates decomposition. [j] Calculated enthalpy of formation. [k] Calculated energy of formation. [l] Energy of explosion. [m] Detonation temperature. [n] Volume of detonation products (assuming only gaseous products). [o] Detonation pressure at Chapman Jouguet point. [p] Detonation velocity.

The TG plots are displayed in Figure 15. Plots of the DTA spectra together with full size versions of the TG plots can be found in the Supporting Information (Figures S4–S7).

The most significant properties due to their safety relevance are the sensitivities toward external mechanical stimuli. Therefore, the substances were examined regarding their impact sensitivity (IS) and friction sensitivity (FS) according to BAM (Bundesanstalt für Materialforschung and -prüfung) standard measure methods. In addition, measurements evaluating the compounds' stability toward electrostatic discharge (ESD) were performed.

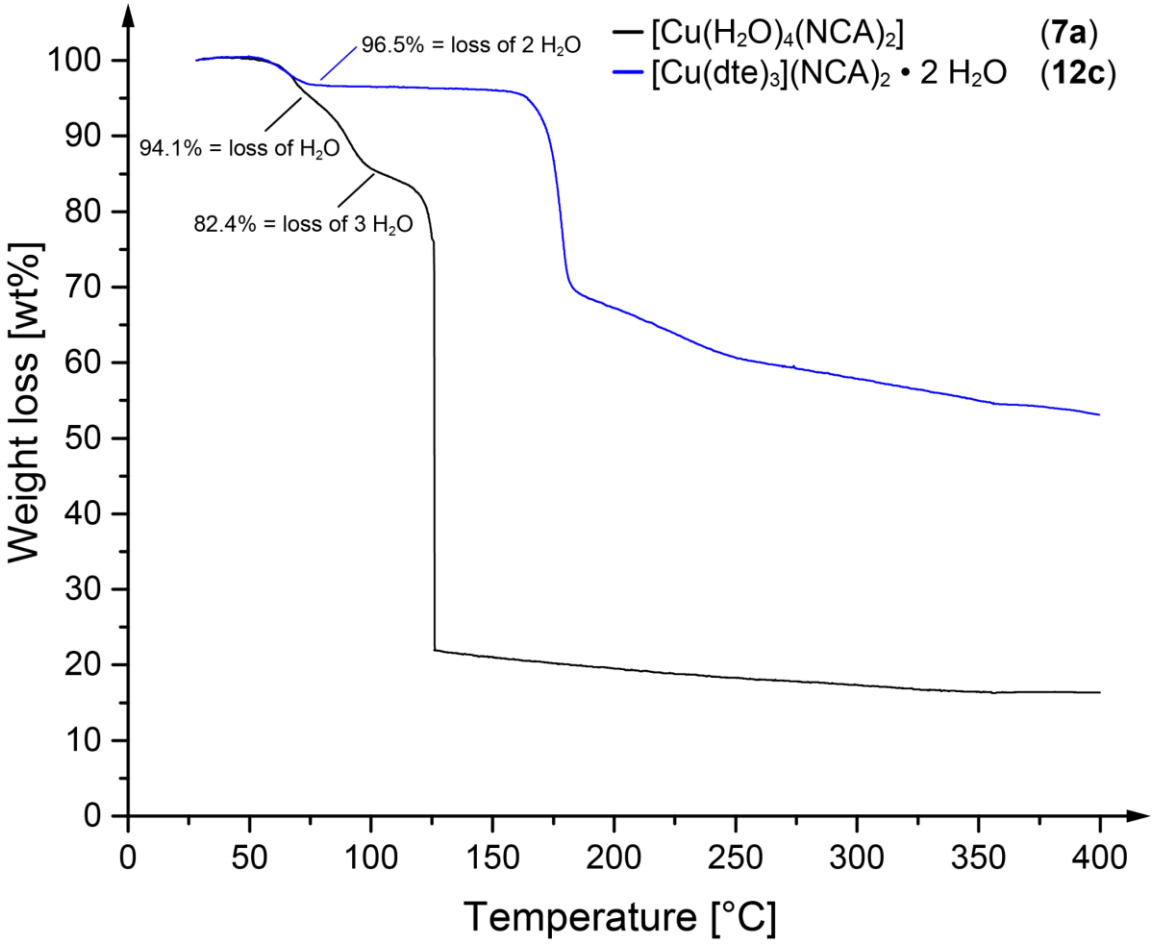

Figure 15. TG plots of $[Cu(H_2O)_4(NCA)_2]$ (**7a**) and $[Cu(dte)_3](NCA)_2 \cdot 2\,H_2O$ (**12c**).

The results are summarized in Tables 1 and 2. Since it is rather difficult to compare energetic salts with complexes with respect to their stability or the stability trends occurring, the nitrogen-rich salts together with the poorly characterized compound **4b** were discussed first followed by the ECCs. First, the ammonium and

hydroxylamine salts **2** and **4a** are classified as insensitive toward friction (FS > 360 N). All other derivatives are friction sensitive in the range of 360 N (for **5a**) to 80 N (for **3a**). The triaminoguanidinium derivative **5a** has the highest impact sensitivity (IS = 6 J), followed by **4b** with an impact sensitivity of 10 J. All other compounds (**2**–**4**) are insensitive toward impact (IS > 40 J). The compounds **4a** and **4b** mainly differ in their sensitivity toward impact, which is reasonable due to the different aggregate state. The ammonium and TAG salt **2** and **5a** show the highest decomposition temperature with 177 and 173 °C, respectively. The thermally most instable compound is ionic liquid **4a**, which sharply decomposes at 94 °C. Explosive properties of the ionic derivatives **2**–**5a** and the hydroxylamine adduct **4b** were calculated using the EXPLO5 code.

The resulting parameters were then compared to those of ammonium dinitramide (ADN). Therefore, the heats of formation were calculated based on the CBS-4 M basis set, and the respective densities from crystallographic measurements were used. In case of compound **4a**, which is a room temperature ionic liquid, the density was estimated according to related molecular structures. The highest densities of the compounds investigated also result in the highest calculated detonation parameters for the hydroxylamine-containing compounds **4a** and **4b**. The detonation velocity and the detonation pressure are approximately equal (**4a**, V_{det} = 8915 m s^{-1}, P_{CJ} = 329 kbar; **4b**, V_{det} = 8878 m s^{-1}, P_{CJ} = 332 kbar) which is in the range of hexogen, and easily outperform ADN (V_{det} = 8502 m s^{-1}, P_{CJ} = 270 kbar), which is also the case for the hydrazinium derivative **3a**. The ammonium and triaminoguanidinium derivatives **2** and **5a** feature a detonation velocity of around 8000 m s^{-1} (V_{det}(**2**, **5**) = 7956 m s^{-1}). For the ammonium derivative **2**, a clear trend is observed by comparing it with the respective ammonium salt of dicyanamide ((NH$_4$)DCA) and dinitramide (AND). The density increases by about 0.25 g cm^{-3} for the replacement of each cyano group by a nitro group from the dicyaniamide anion to the dinitramide anion. A similar trend is observed for the resulting detonation velocity. This increases proportionally from the DCA$^-$ via the NCA$^-$ to the DN$^-$ derivative. The sensitivities, on the other hand, increase in the same order from the insensitive (NH$_4$)DCA and (NH$_4$)NCA to the moderately sensitive AND.

The thermal stability data determined for the ammonium salt (**2**) are consistent with the literature data.[6] Higher values were measured for the TAG salt (**5a**), but a

higher heating rate of 10 °C min^{-1}, as used in this case, is known to result in higher decomposition temperatures of the products.[27] The sensitivity data for **5a** are consistent with the values reported in the literature.[27]

Comparing the ammonium salts of NCA^- and dinitramide, the enthalpy of formation is significantly increased by the exchange of a nitro group of the ADN on the anion to a cyano group on the NCA ($\Delta_f H^0$ (**2**) = 30.0 kJ mol^{-1}; $\Delta_f H^0$(ADN) = −125.3 kJ mol^{-1}). On the other hand, this also significantly reduces the crystallographic density, which generally leads to a significant loss of performance. ADN is clearly superior in all detonation parameters. However, the relatively sensitive ADN (IS = 4 J, FS = 72 N) is opposed by the completely insensitive $(NH_4)NCA$ (**2**).

The endothermic events of the complexes **8** and **9** indicate a melting of the compound, whereby in case of **9** the endothermic signal is directly followed by an exothermic signal. In case of compounds **7a** and **12c**, the endothermic signals represent a loss of hydrate water or aqua ligands (Figure 15).

A comparison of the thermal stabilities of the ECCs shows that the majority of the complexes exceed 150 °C (**6a**, **8**, **9**, **11**, and **12c**) with complex **10** even exceeding 190 °C. Furthermore, the effect of bridging ligands on temperature stability becomes clear. The most stable complex **10** in this context possesses bridging 1,1-dtm ligands. Complexes **11** and **12c** follow closely, but their composition causes a slight reduction in stability. Thus, on the one hand, the thermal stability of the ligands and the resulting complexes reduces when, in the case of dtm, the substitution pattern is changed from 1,1- (**10**) to 1,2- (**11**). On the other hand, it is assumed that complex **12c** loses significant stability after the loss of its hydrate water and therefore decomposes earlier. The same is expected as a reason for the decomposition temperature of the tetraaquacopper(II) complex **7a** after loss of its aqua ligands.

The metal salts and ECCs investigated in this work are almost all significantly more sensitive than the nitrogen-rich salts. The most sensitive compounds are neat silver nitrocyanamide (**5a**, IS = 3 J, FS = 10 N) together with the copper(II) complexes $[Cu(AMT)_4(NCA)](NCA)$ (**9**, IS ≤ 1 J, FS = 20 N) and $[Cu(dte)_3](NCA)_2 \cdot 2H_2O$ (**12c**, IS ≤ 1 J, FS = 160 N). In the case of pure silver nitrocyanamide (**5a**), these results are not surprising, as the compound is described as sensitive, but no BAM sensitivities were reported.[6] Similar findings apply to complexes based on the AMT ligand.[34, 55] For example, $[Cu(AMT)_4(H_2O)](DN)_2$, which also has a pyramidal

structure and has an aqua ligand instead of coordinating anions, is extremely sensitive to IS and FS (IS = 2 J, FS = 3 N).[34] In this context, the low impact sensitivity of **12c** is no longer surprising. Generally, it is assumed that aqua ligands or hydrated water led to less sensitive compounds. However, the measurements indicate that powerful ligands can compensate this influence. Both the AMT ligand used in complexes **9** and $[Cu(AMT)_4(H_2O)](DN)_2$ and the ditetrazolyl ligand showed very high gas phase enthalpies of formation. However, since the respective FS with a value of 160 N is in a completely different dimension, effects influencing the result, like ignition through hot spot formation, should also be considered.[56] Furthermore, based on previous observations of our group, it would be expected that complex **12b** would have to be significantly more sensitive than **12c**, since coordinating anions have led to extremely sensitive complexes in previous work.[24] However, in this study, opposite values were measured. An analysis of the tetraaqua copper(II) complex (**7a**), for example, shows a clear desensitization due to the water ligands. Other trends already known include, for example, the higher sensitivity of 1,2-dtm (**11**, IS = 2 J, FS = 80 N) complexes compared to 1,1-dtm (**10**, IS = 7 J, FS = 112 N), and AMT (**9**, IS ≤ 1 J, FS = 20 N) compared to MTZ (**8**, IS = 40 J, FS = 240 N). Only the assumption that dtm complexes (**10**, **11**), because of their lower carbon content, are more sensitive than similar structured dte complexes (**12b**, IS = 6 J, FS = 180 N) could not be confirmed in this case. The sensitivity data for **12b** and **12c** are only roughly consistent with the values reported in the literature which is most likely due to a difference in the grain size of the investigated samples.

For a proper examination of the substances, a classification according to the UN Recommendation for the Transport of Dangerous Goods was carried out for every material. Accordingly, the earlier mentioned compounds **6a**, **9**, and **12c** are ranked as very sensitive, with pure silver nitrocyanamide (**6a**) being even extremely sensitive. Because of its friction sensitivity of 80 N, coordination compound **11** is also evaluated as a very sensitive material. The remaining compounds were less sensitive (**4b**, **5a**, **8**, **10**, **12b**) and therefore classified as sensitive only or even insensitive et all (**2**, **4a**, **7a**). It must also be added that silver nitrocyanamide exhibits a considerable sensitivity toward electrostatic discharge (ESD = 51 mJ).

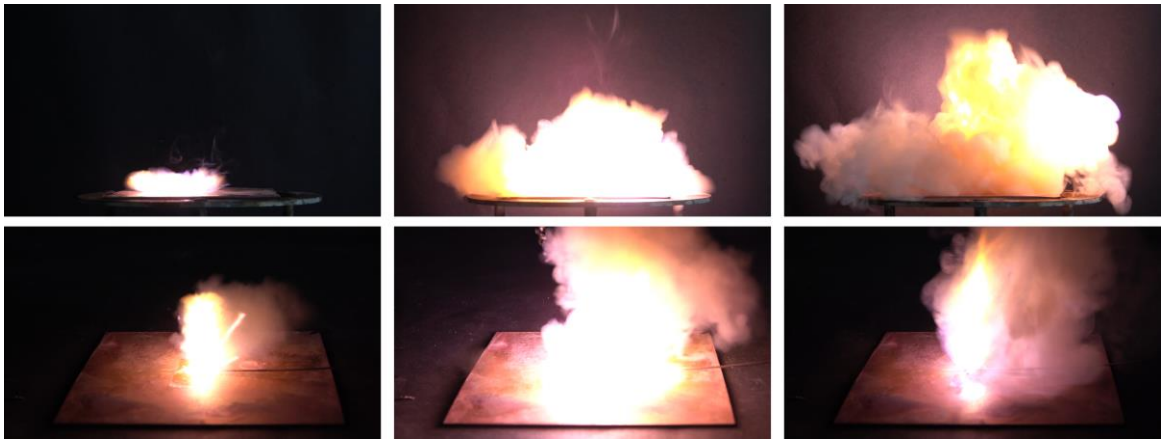

Figure 16. Deflagration of silver nitrocyanamide (**5a**) during hot plate (top) and hot needle tests (bottom).

Performance evaluations were examined for the metal salts and complexes **6a**, **7a**, **8**–**11**, **12b**, and **12c** through hot plate (HP) and hot needle (HN) tests. To perform a hot plate test, the investigated sample is placed on a copper plate and subsequently heated with a Bunsen burner. During a hot needle test, the sample is fixed on a copper plate using adhesive tape. Subsequently, the substance is penetrated with a red heated needle. The experiments are intended to provide insights into the behavior of the substances, respectively, under rapid heating or under light confinement. The outcomes of each investigation were recorded with a high-speed camera and the outcome of each test is displayed in Table 1. The reactions of silver NCA during these experiments are shown in Figure 16. Further high-speed images can be found in the Supporting Information (Figures S8–S11). These experiments are of particular interest for perspective primary explosives. The outcome, in the best case is a detonation, is assumed to give insights into the compounds deflagration to detonation transition (DDT). A fast DDT is required for the initiation of PETN through primary explosives like lead azide. During the investigation of the metal salts and complexes in this work, the main outcomes were deflagrations for the hot plate tests and decompositions reactions during hot needle tests. Since most of the substances were investigated to be less or insensitive, this outcome was expected. Thus, the more sensitive compounds **6a**, **9**, **10**, and **11** showed deflagrations during at least one of both tests. At this point, laser ignition experiments would be discussed, but these tests were not performed due to the results of the HP and HN tests.

3.3 Conclusion

The main objective of this work was to investigate the nitrocyanamide anion (NCA^-)as a building block combining the properties of the dicyanamide and dinitramide anions. This was accomplished through the preparation of the insensitive ammonium, hydrazinium and hydroxylammonium salts. Both the hydrazinium and the hydroxylammonium salts showed impressive detonation parameters. Furthermore, the reactivity of the nitrocyanamide moiety toward hydroxylamine and hydrazine was investigated, which revealed a further method for accessing nitroguanidine derivatives.

As a further application, the anion was incorporated into various transition metal ECCs. Especially here, the aim was to combine the good properties of copper dinitramide and dicyanamide complexes. However, the comparisons proved difficult because the structure was strongly influenced by the coordination behavior of the anions. Regardless of structure and composition, it is apparent that the copper dinitramide complexes are in any case the most sensitive, followed by nitrocyanamide complexes and finally dicyanamide complexes, whereby the majority of complexes are still insensitive or less sensitive only. The thermal stability of the complexes was also greatly increased, especially by the introduction of bridging ditetrazoles up to 191 °C, outperforming the dicyanamide and dinitramide complexes based on such ligands. When it comes to performance, it also becomes clear that the complexes studied in this work could not surpass dinitramide-based copper complexes but are eventually more powerful than copper dicyanamide complexes. Consequently, the nitrocyanamide anion with regard to the energetically relevant properties of its copper complexes is in many aspects between the dinitramide and the dicyanamide anion.

3.4 Acknowledgement

The financial support of this work by Ludwig-Maximilian University (LMU) is acknowledged. The Office of Naval Research (ONR) under Grant No. ONR N00014-19-1-2078 and the Strategic Environmental Research and Development

Program (SERDP) under Contract No. W912HQ19C0033 are gratefully acknowledged. Jasmin Lechner is thanked for several TG measurements.

3.5 References

[1] A. F. McKay, G. F. Wright, *J. Am. Chem. Soc.* **1947,** *69* (12), 3028–3030.

[2] A. F. McKay, W. L. Ott, G. W. Taylor, M. N. Buchanan, J. F. Crooker, *Can. J. Res., Sect. B* **1950,** *28B*, 683–688.

[3] A. A. Astrat'ev, L. L. Kuznetsov, *Russ. J. Org. Chem.* **2002,** *38* (9), 1252–1259.

[4] R. H. Meen, G. F. Wright, *J. Am. Chem. Soc.* **1952,** *74*, 2077–2079.

[5] A. M. Astachov, L. A. Kruglyakova, I. V. Gelemurzina, A. D. Vasiliev, Simple method of synthesis and characterization of some nitrocyanamide salts, University of Pardubice: **2003**; 36.

[6] S. R. Harris, *J. Am. Chem. Soc.* **1958,** *80*, 2302–2305.

[7] J. H. Boyer, T. Manimaran, *Synthesis* **1987,** *1987*, 907.

[8] J. H. Boyer, T. Manimaran, L. T. Wolford, *J. Chem. Soc., Perkin Trans. 1* **1988,** 2137–2140.

[9] T. Manimaran, L. T. Wolford, E. D. Stevens, J. H. Boyer, C. Klein, *J. Chem. Res., Synop.* **1989,** (11), 330.

[10] M. Hvastijová, R. Boča, J. Kohout, L. Jäger, I. Císařová, J. Kožíšek, *Inorg. Chim. Acta* **2003,** *343*, 217–223.

[11] M. Hvastijová, J. Kohout, J. G. Díaz, J. Kožíšek, J. W. Buchler, *Transition Met. Chem.* **2001,** *26* (4), 430–434.

[12] J. G. Diaz, J. Kozisek, V. Langer, *Acta Cryst. E* **2003,** *59* (5), 241–243.

[13] J. Kozisek, J. Garcia Diaz, M. Hvastijova, L. Jager, *Acta Cryst. C* **1997,** *53* (6), 703–705.

[14] M. Hvastijová, J. Kohout, J. Kožíšek, L. Jäger, J Garcia Dıiaz, *Polyhedron* **2000,** *19* (8), 1021–1027.

[15] J. Kohout, M. Hvastijová, J. Kožíšek, J. Garcia Díaz, M. Valko, L. Jäger, I. Svoboda, *Inorg. Chim. Acta* **1999,** *287* (2), 186–192.

[16] J. Garcia Diaz, J. Kozisek, M. Fronc, A. Gatial, I. Svoboda, V. Langer, *Acta Crystallographica Section C* **2005,** *61* (4), 180–182.

[17] R. Boča, M. Hvastijová, J. Kožíšek, M. Valko, H. Ehrenberg, H. Fuess, W. Haase, I. Svoboda, R. Werner, *Inorg. Chem. Commun.* **2005,** *8* (6), 548–551.

[18] L. Vahovska, S. Vitushkina, I. Potocnak, Z. Travnicek, R. Herchel, *Dalton Trans.* **2018,** *47* (5), 1498–1512.

[19] A. M. Kutasi, D. R. Turner, P. Jensen, B. Moubaraki, S. R. Batten, K. S. Murray, *CrystEngComm* **2009,** *11* (10), 2089–2095.

[20] L. Jäger, C. Tretner, H. Hartung, M. Biedermann, *Chem. Ber.* **1997,** *130* (7), 1007–1012.

[21] L. Jäger, C. Tretner, H. Hartung, M. Biedermann, *Z. Anorg. Allg. Chem.* **1997,** *623* (8), 1299–1305.

[22] L. Jäger, C. Tretner, H. Hartung, M. Biedermann, *Chem. Ber.* **1997,** *130* (7), 1007–1012.

[23] L. Jäger, C. Tretner, M. Biedermann, H. Hartung, *J. Organomet. Chem.* **1997,** *530* (1), 13–17.

[24] M. B. Joas, Ph.D. Thesis, Ludwig-Maximilian University Munich, **2014**.

[25] Y. Zhang, H. Gao, Y.-H. Joo, J. M. Shreeve, *Angew. Chem., Int. Ed.* **2011,** *50* (41), 9554–9562.

[26] G. W. Drake, T. Hawkins, US7745635, 16th July, **2010**.

[27] L. He, G.-H. Tao, D. Parrish, J. M. Shreeve, *Chem. Eur. J.* **2010,** *16* (19), 5736–5743.

[28] Y.-H. Joo, H. Gao, Y. Zhang, J. M. Shreeve, *Inorg. Chem.* **2010,** *49* (7), 3282–3288.

[29] Y. Zhang, H. Gao, Y. Guo, Y.-H. Joo, J. M. Shreeve, *Chem. Eur. J.* **2010,** *16* (10), 3114–3120.

[30] Z. Wang, G. Pan, B. Wang, L. Zhang, W. Zhao, X. Ma, J. Zhang, J. Zhang, *Chem. Asian J.* **2019,** *14* (12), 2122–2128.

[31] S. Schneider, T. Hawkins, Y. Ahmed, S. Deplazes, J. Mills, *ACS Symp. Ser.* **2012,** *1117*, 1–25.

[32] P. D. McCrary, G. Chatel, S. A. Alaniz, O. A. Cojocaru, P. A. Beasley, L. A. Flores, S. P. Kelley, P. S. Barber, R. D. Rogers, *Energ Fuel* **2014,** *28* (5), 3460–3473.

[33] M. H. H. Wurzenberger, J. T. Lechner, J. Stierstorfer, *ChemPlusChem* **2020,** *85* (4), 769–775.

[34] M. S. Gruhne, M. H. H. Wurzenberger, M. Lommel, J. Stierstorfer, *Chem. Eur. J.* **2021**, *27* (35), 9112–9123.

[35] C. L. Galtress, P. R. Morrow, S. Nag, T. L. Smalley, M. F. Tschantz, J. S. Vaughn, D. N. Wichems, S. K. Ziglar, J. C. Fishbein, *J. Am. Chem. Soc.* **1992,** *114* (4), 1406–1411.

[36] N. Fischer, T. M. Klapötke, J. Stierstorfer, *Z. Naturforsch. B* **2012,** *67* (6), 573–588.

[37] M. A. Petrie, J. C. Bottaro, P. E. Penwell, A. L. Dodge, US20090139618A1, 6th August, **2002**.

[38] B. V. Lotsch, W. Schnick, *Chem. Mater.* **2005,** *17* (15), 3976–3982.

[39] B. V. Lotsch, W. Schnick, *New J. Chem.* **2004,** *28* (9), 1129–1136.

[40] M. H. H. Wurzenberger, V. Braun, M. Lommel, T. M. Klapötke, J. Stierstorfer, *Inorg. Chem.* **2020,** *59* (15), 10938–10952.

[41] M. H. H. Wurzenberger, B. R. G. Bissinger, M. Lommel, M. S. Gruhne, N. Szimhardt, J. Stierstorfer, *New J. Chem.* **2019,** *43* (46), 18193–18202.

[42] P. N. Gaponik, V. P. Karavai, Y. V. Grigor'ev, *Chem. Heterocycl. Compd.* **1985,** *21* (11), 1255–1258.

[43] N. Szimhardt, M. H. H. Wurzenberger, A. Beringer, L. J. Daumann, J. Stierstorfer, *J. Mater. Chem. A* **2017,** *5* (45), 23753–23765.

[44] M. Joas, T. M. Klapötke, N. Szimhardt, *Eur. J. Inorg. Chem.* **2014,** *2014* (3), 493–498.

[45] L. Jäger, C. Tretner, H. Hartung, M. Biedermann, C. Wagner, *Z. Anorg. Allg. Chem.* **1998,** *624* (9), 1558–1562.

[46] Crystallographic data for the structures have been deposited with the Cambridge Crystallographic Data Centre. Copies of the data can be obtained free of charge on application to The Director, CCDC, 12 Union Road, Cambridge CB2 1EZ, UK (Fax: int.code_(1223)336-033; e-mail for inquiry: fileserv@ccdc.cam.ac.uk; e-mail for deposition: (depos-it@ccdc.cam.ac.uk).

[47] H.-G. Ang, W. Fraenk, K- Karaghiosoff, T. M. Klapötke, P. Mayer, H. Nöth, J. Sprott, M. Warchhold, *Anorg. Allg. Chem.* **2002,** *628* (13), 2894–2900.

[48] M Joas, T. M. Klapötke, J. Stierstorfer, N. Szimhardt, *Chem. Eur. J.* **2013,** *19* (30), 9995–10003.

[49] J. Schweifer, P. Weinberger, K. Mereiter, M. Boca, C. Reichl, G. Wiesinger, G. Hilscher, P. J. van Koningsbruggen, H. Kooijman, M. Grunert, W. Linert, *Inorg. Chim. Acta* **2002,** *339*, 297–306.

[50] M. H. Palmer, S. Parsons, *Acta Cryst. C* **1996,** *52* (11), 2818–2822.

[51] O. A. Luk'yanov, O. V. Anikin, V. P. Gorelik, V. A. Tartakovsky, *Russ. Chem. Bull.* **1994,** *43* (9), 1457–1461.

[52] T. M. Klapötke, *Chemistry of High-Energy Materials*. 5th ed.; De Gruyter: Berlin, Boston, **2019**.

[53] B. V. Lotsch, J. Senker, W. Schnick, *Inorg. Chem.* **2004,** *43*, 895–904.

[54] T. M. Klapötke, *Energetic materials Encyclopedia*. 2nd ed.; DeGruyter: Berlin, Boston, **2021**.

[55] M. H. H. Wurzenberger, M. S. Gruhne, M. Lommel, J. Stierstorfer, *Propellants Explo. Pyrotech.* **2021,** *46* (2), 207–213.

[56] J. G. Reynolds, P. C. Hsu, G. A. Hust, S. A. Strout, H. K. Springer, *Propellants Explo. Pyrotech.* **2017,** *42* (11), 1303–1308.

3.6 Supporting Information

3.6.1 Compound Overview

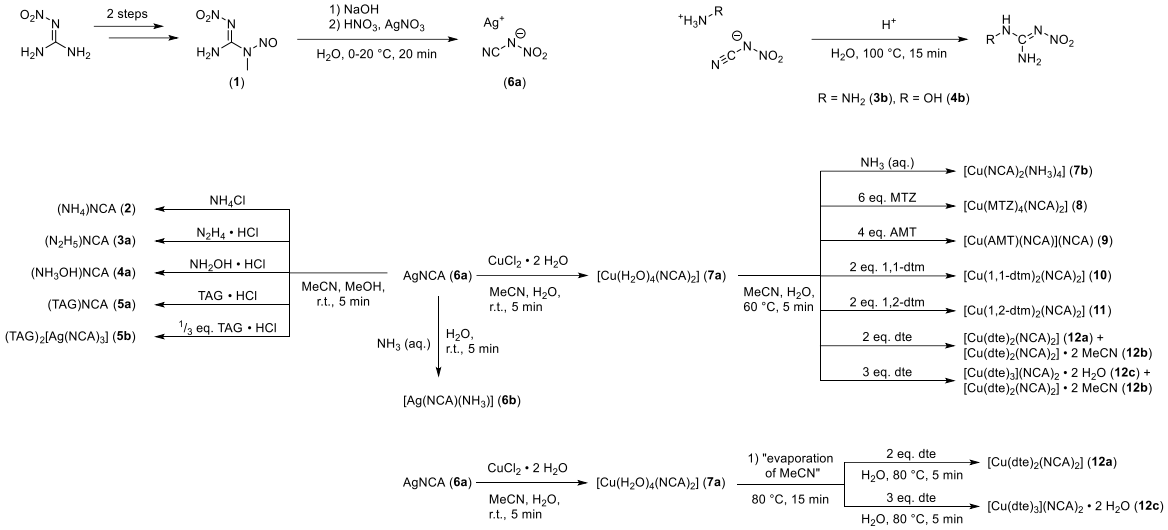

3.6.2 Crystallography

For all crystalline compounds, an Oxford Xcalibur3 diffractometer with a CCD area detector or Bruker D8 Venture TXS diffractometer equipped with a multilayer monochromator, a Photon 2 detector and a rotating-anode generator were employed for data collection using Mo-K_α radiation (λ = 0.7107 Å). On the Oxford device, data collection and reduction were carried out using the CRYSALISPRO software.[S1] On the Bruker diffractometer, the data were collected with the Bruker Instrument Service v3.0.21, the data reduction was performed using the SAINT V8.18C software (Bruker AXS Inc., 2011). The structures were solved by direct methods (SIR-92, [S2] SIR-97, [S3] SHELXS-97[S4] or SHELXT[S5]) and refined by full-matrix least-squares on *F*2 (SHELXL[S4]) and finally checked using the PLATON software[S6] integrated in the WinGX[S7] or Olex2[S8] software suite. The non-hydrogen atoms were refined anisotropically and the hydrogen atoms were located and freely refined. The absorptions were corrected by a SCALE3 ABSPACK or SADABS Bruker APEX3 multiscan method. [S9-S10] All DIAMOND2 plots are shown with thermal ellipsoids at the 50% probability level and hydrogen atoms are shown as small spheres of arbitrary radius.

Table S1. Crystallographic data of **2**, **3a**, and **5a**.

	2	**3a**	**5a**
Formula	$CH_4N_4O_2$	$CH_5N_5O_2$	$C_2H_9N_9O_2$
FW [g mol^{-1}]	104.08	119.10	191.18
Crystal system	Monoclinic	Monoclinic	Monoclinic
Space Group	$P2_1/c$	$P2_1/c$	$P2_1/c$
Color / Habit		Colorless needle	Colorless plate
Size [mm]	0.09 x 0.13 x 0.16	0.15 x 0.20 x 0.50	0.10 x 0.15 x 0.25
a [Å]	7.1131(3)	3.6689(4)	8.5179(9)
b [Å]	7.6039(4)	12.4163(13)	12.3745(11)
c [Å]	8.6741(4)	10.8834(14)	8.3497(9)
α [°]	90	90	90
β [°]	109.218(1)	96.557(9)	97.881(10)
γ [°]	90	90	90
V [Å^3]	443.01(4)	492.54(10)	871.79(15)
Z	4	4	4
$\rho_{calc.}$ [g cm^{-3}]	1.561	1.606	1.457
μ [mm^{-1}]	0.142	0.144	0.124
F[000]	216	248	400
$\lambda_{MoK\alpha}$ [Å]	0.71073	0.71073	0.71073
T [K]	173	123	102
θ Min–Max [°]	3.0, 28.3	3.3, 32.5	2.4, 26.4
Dataset	−9:9; −10:10; –11:11	−5:5; −18:18; −14:15	−10:10; −15:15; −10:9
Reflections collected	10031	4601	5676
Independent refl.	1102	1637	1786
R_{int}	0.046	0.035	0.039
Observed reflections	1006	1185	1261
Parameters	80	93	142
R_1 [obs][a]	0.0371	0.0448	0.0426
wR_2 [all data][b]	0.1068	0.1119	0.0893
GooF[c]	1.10	1.04	1.02
Resd. Dens. [e Å^{-3}]	−0.18, 0.33	−0.28, 0.27	−0.29, 0.21
Absorption correction	Multi-scan	Multi-scan	Multi-scan
Device type	Bruker D8 Venture TXS	Oxford Xcalibur3	Oxford Xcalibur3
CCDC	2099366	2099365	2099362

[a] $R_1 = \Sigma||F_0|-|F_c||/\Sigma|F_0|$; [b] $wR_2 = [\Sigma[w(F_0^2-F_c^2)^2]/\Sigma[w(F_0)^2]]^{1/2}$; $w = [\sigma c^2(F_0^2)+(xP)^2+yP]^{-1}$ and $P = (F_0^2+2F_c^2)/3$; c) GooF = $\{\Sigma[w(F_o^2-F_c^2)^2]/(n-p)\}^{1/2}$ (n = number of reflections; p = total number of parameters).

Table S2. Crystallographic data of **5b**, **6b** and **7b**.

	5b	**6b**	**7b**
Formula	$C_5H_{18}AgN_{21}O_6$	$C_2H_{12}CuN_{10}O_4$	$CH_3AgN_4O_2$
FW [g mol^{-1}]	576.27	303.76	210.94
Crystal system	Trigonal	Monoclinic	Monoclinic
Space Group	*P*31*c*	*C*2/*c*	$P2_1/c$
Color / Habit	Colorless plate	Blue needle	Colorless platelet
Size [mm]	0.15 x 0.40 x 0.40	0.09 x 0.17 x 0.59	0.02 x 0.07 x 0.10
a [Å]	22.7426(4)	11.3361(10)	3.5540(1)
b [Å]	22.7426(4)	6.8501(4)	10.5281(4)
c [Å]	6.6298(2)	15.4436(14)	13.3426(5)
α [°]	90	90	90
β [°]	90	109.949(10)	90.256(1)
γ [°]	120	90	90
V [Å^3]	2969.69(16)	1127.29(17)	499.23(3)
Z	6	4	4
$\rho_{calc.}$ [g cm^{-3}]	1.933	1.790	2.807
μ [mm^{-1}]	1.098	1.965	3.939
F[000]	1740	620	400
$\lambda_{MoK\alpha}$ [Å]	0.71073	0.71073	0.71073
T [K]	123	100	173
θ Min–Max [°]	2.1, 26.4	2.8, 26.4	1.9, 26.4
Dataset	−28:28; −28:28; −8:8	–14:13; –7:8; –16:19	–4: 4 ; –13: 13 ; –16: 16
Reflections collected	43625	3691	10187
Independent refl.	4047	1162	1021
R_{int}	0.034	0.031	0.028
Observed reflections	3483	1006	965
Parameters	305	80	75
R_1 [obs][a]	0.0297	0.0319	0.0211
wR_2 [all data][b]	0.0779	0.0758	0.0489
GooF[c]	1.04	1.07	1.13
Resd. Dens. [e Å^{-3}]	–0.38, 0.47	–0.34, 0.79	–0.35, 0.91
Absorption correction	Multi-scan	Multi-scan	Multi-scan
Device type	Oxford Xcalibur3	Oxford Xcalibur3	Bruker D8 Venture TXS
CCDC	2099357	2099360	2099356

[a] $R_1 = \Sigma||F_o|-|F_c||/\Sigma|F_o|$; [b] $wR_2 = [\Sigma[w(F_o^2-F_c^2)^2]/\Sigma[w(F_o)^2]]^{1/2}$; $w = [\sigma c^2(F_o^2)+(xP)^2+yP]^{-1}$ and $P = (F_o^2+2F_c^2)/3$; c) GooF = $\{\Sigma[w(F_o^2-F_c^2)^2]/(n-p)\}^{1/2}$ (n = number of reflections; p = total number of parameters).

Table S3. Crystallographic data of **8**–**10**.

	8	**9**	**10**
Formula	$C_{10}H_{16}CuN_{22}O_4$	$C_{10}H_{20}CuN_{26}O_4$	$C_8H_8CuN_{22}O_4$
FW [g mol^{-1}]	571.99	632.06	539.90
Crystal system	Monoclinic	Orthorhombic	Monoclinic
Space Group	$P2_1/c$	$Pbca$	$P2_1/n$
Color / Habit	Blue plate	Blue block	Blue block
Size [mm]	0.07 x 0.23 x 0.32	0.03 x 0.04 x 0.08	0.06 x 0.19 x 0.33
a [Å]	10.1734(4)	17.8808(14)	8.3580(6)
b [Å]	21.1681(7)	14.6694(11)	12.8526(7)
c [Å]	10.2868(3)	19.5764(15)	9.1567(6)
α [°]	90	90	90
β [°]	90.652(3)	90	104.174(7)
γ [°]	90	90	90
V [Å^3]	2215.14(13)	5134.9(7)	953.69(11)
Z	4	8	2
$\rho_{calc.}$ [g cm^{-3}]	1.715	1.635	1.880
μ [mm^{-1}]	1.059	0.927	1.224
F[000]	1164	2584	542
$\lambda_{MoK\alpha}$ [Å]	0.71073	0.71073	0.71073
T [K]	100	173	103
θ Min–Max [°]	1.9, 26.4	2.1, 26.4	2.8, 26.4
Dataset	–12:12; –26:26; –12:12	−22:22; −18:18; −24:24	−10:9; −15:16; −10:11
Reflections collected	19424	106003	6195
Independent refl.	4531	5246	1950
R_{int}	0.045	0.073	0.037
Observed reflections	3592	4413	1592
Parameters	338	378	160
R_1 [obs][a]	0.0374	0.0362	0.0352
wR_2 [all data][b]	0.0877	0.0995	0.0818
GooF[c]	1.08	1.05	1.03
Resd. Dens. [e Å^{-3}]	–0.37, 0.55	−0.59, 0.60	−0.43, 0.46
Absorption correction	Multi-scan	Multi-scan	Multi-scan
Device type	Oxford Xcalibur3	Bruker D8 Venture TXS	Oxford Xcalibur3
CCDC	2099361	2099363	2099364

[a] $R_1 = \Sigma||F_0|-|F_c||/\Sigma|F_0|$; [b] $wR_2 = [\Sigma[w(F_0^2-F_c^2)^2]/\Sigma[w(F_0)^2]]^{1/2}$; $w = [\sigma c^2(F_0^2)+(xP)^2+yP]^{-1}$ and $P = (F_0^2+2F_c^2)/3$; c) GooF = $\{\Sigma[w(F_o^2-F_c^2)^2]/(n-p)\}^{1/2}$ (n = number of reflections; p = total number of parameters).

Table S4. Crystallographic data of **11**, **12a** and **12b**.

	11	**12a**	**12b**
Formula	$C_8H_8CuN_{22}O_4$	$C_{14}H_{18}CuN_{24}O_4$	$C_{10}H_{12}CuN_{22}O_4$
FW [g mol^{-1}]	539.90	650.06	567.96
Crystal system	Monoclinic	Triclinic	Triclinic
Space Group	$P2_1/c$	$P\bar{1}$	$P\bar{1}$
Color / Habit	Blue platelet	Blue needle	Blue block
Size [mm]	0.11 x 0.16 x 0.30	0.05 x 0.09 x 0.50	0.25 x 0.50 x 0.50
a [Å]	8.0840(5)	8.5636(9)	7.8539(5)
b [Å]	11.9923(7)	9.0561(7)	8.4594(6)
c [Å]	9.5949(6)	9.5626(9)	9.1422(7)
α [°]	90	98.035(7)	112.562(7)
β [°]	93.891(6)	110.779(9)	110.913(6)
γ [°]	90	104.896(8)	90.123(5)
V [Å^3]	928.04(10)	647.80(12)	517.11(8)
Z	2	1	1
$\rho_{calc.}$ [g cm^{-3}]	1.932	1.666	1.824
μ [mm^{-1}]	1.258	0.919	1.134
F[000]	542	331	287
$\lambda_{MoK\alpha}$ [Å]	0.71073	0.71073	0.71073
T [K]	102	102	102
θ Min–Max [°]	2.5, 26.4	2.4, 26.4	2.6, 26.4
Dataset	−9:10; −14:14; −11:11	−10:10; −11:11; −11:11	−9:9; −10:10; −11:11
Reflections collected	5779	5168	7540
Independent refl.	1883	2657	2125
R_{int}	0.031	0.059	0.038
Observed reflections	1648	2114	1913
Parameters	160	197	169
R_1 [obs][a]	0.0299	0.0508	0.0282
wR_2 [all data][b]	0.0755	0.1126	0.0663
GooF[c]	1.07	1.04	1.09
Resd. Dens. [e Å^{-3}]	−0.30, 0.54	−0.67, 0.72	−0.34, 0.38
Absorption correction	Multi-scan	Multi-scan	Multi-scan
Device type	Oxford Xcalibur3	Oxford Xcalibur3	Oxford Xcalibur3
CCDC	2099355	2099359	2099358

[a] $R_1 = \Sigma||F_o|-|F_c||/\Sigma|F_o|$; [b] $wR_2 = [\Sigma[w(F_o^2-F_c^2)^2]/\Sigma[w(F_o)^2]]^{1/2}$; $w = [\sigma c^2(F_o^2)+(xP)^2+yP]^{-1}$ and $P = (F_o^2+2F_c^2)/3$; c) GooF = $\{\Sigma[w(F_o^2-F_c^2)^2]/(n-p)\}^{1/2}$ (n = number of reflections; p = total number of parameters).

3.6.3 Computation

All quantum chemical calculations were carried out using the Gaussian G09 program package.[S11] The enthalpies (H) and free energies (G) were calculated using the complete basis set (CBS) method of Petersson and co-workers in order to obtain very accurate energies. The CBS models are using the known asymptotic convergence of pair natural orbital expressions to extrapolate from calculations using a finite basis set to the estimated CBS limit. CBS-4 starts with an HF/3-21G(d) geometry optimization; the zero-point energy is computed at the same level. It then uses a large basis set SCF calculation as a base energy, and an MP2/6- 31+G calculation with a CBS extrapolation to correct the energy through second order. A MP4(SDQ)/6-31+ (d,p) calculation is used to approximate higher order contributions. In this study, we applied the modified CBS-4M.

Heats of formation of the synthesized ionic compounds were calculated using the atomization method (equation E1) using room temperature CBS-4M enthalpies, which are summarized in Table S5. [S12-S13]

$$\Delta_f H^\circ_{(g,\,M,\,298)} = H_{(Molecule,\,298)} - \sum H^\circ_{(Atoms,\,298)} + \sum \Delta_f H^\circ_{(Atoms,\,298)} \qquad (E1)$$

Table S5. CBS-4M electronic enthalpies for atoms C, H, N and O and their literature values for atomic $\Delta H^\circ_f{}^{298}$ / kJ mol^{-1}

	$-H^{298}$ [a.u.]	NIST[S14]
H	0.500991	218.2
C	37.786156	717.2
N	54.522462	473.1
O	74.991202	249.5

For neutral compounds the sublimation enthalpy, which is needed to convert the gas phase enthalpy of formation to the solid state one, was calculated by the *Trouton* rule.[S14] For ionic compounds, the lattice energy (U_L) and lattice enthalpy (ΔH_L) were calculated from the corresponding X-ray molecular volumes according to the equations provided by *Jenkins* and *Glasser*.[S15] With the calculated lattice enthalpy the gas-phase enthalpy of formation was converted into the solid state (standard conditions) enthalpy of formation. These molar standard enthalpies of

formation (ΔH_m) were used to calculate the molar solid state energies of formation (ΔU_m) according to equation E2.

$$\Delta U_m = \Delta H_m - \Delta n\, RT \qquad (E2)$$

(Δn being the change of moles of gaseous components)

The calculation results are summarized in Table S6.

Table S6. Calculation results.

	$-H^{298}$ [a] [a.u.]	$\Delta_f H°$(g,M) [kJ mol^{-1}] [b]	V_M [Å^3] [c]	ΔU_L; ΔH_L [d] [kJ mol^{-1}]	$\Delta_f H°$(s) [e] [kJ mol^{-1}]	Δn [f]	$\Delta_f U$(s) [g] [kJ kg^{-1}]
DCA-	240.179134	122.4					
NCA-	352.343049	−11.1					
(NH4)NCA		624.2	113	589.3; 594.3	30.0	5.0	407.3
(NH3OH)NCA		762.3	126	571.3;576.3	186.1	6.0	1687.6
(N2H5)NCA		675.3	138	-558.3; 563.3	112.1	5.5	1047.0
(TAG)NCA		862.0	224	489.9; 494.9	367.1	10.0	2050.1
Adduct		53.4	–	–	−25.0	5.5	−94.6
(NH4)DCA		757.7	228	488.1; 493.0	264.7	-4.0	3265.5

[a] CBS-4M electronic enthalpy; [b] gas phase enthalpy of formation; [c] molecular volumes taken from X-ray structures and corrected to room temperature; [d] lattice energy and enthalpy (calculated using Jenkins and Glasser equations); [e] standard solid state enthalpy of formation; [f] Δn being the change of moles of gaseous components when formed; [g] solid state energy of formation.

3.6.4 IR spectroscopy

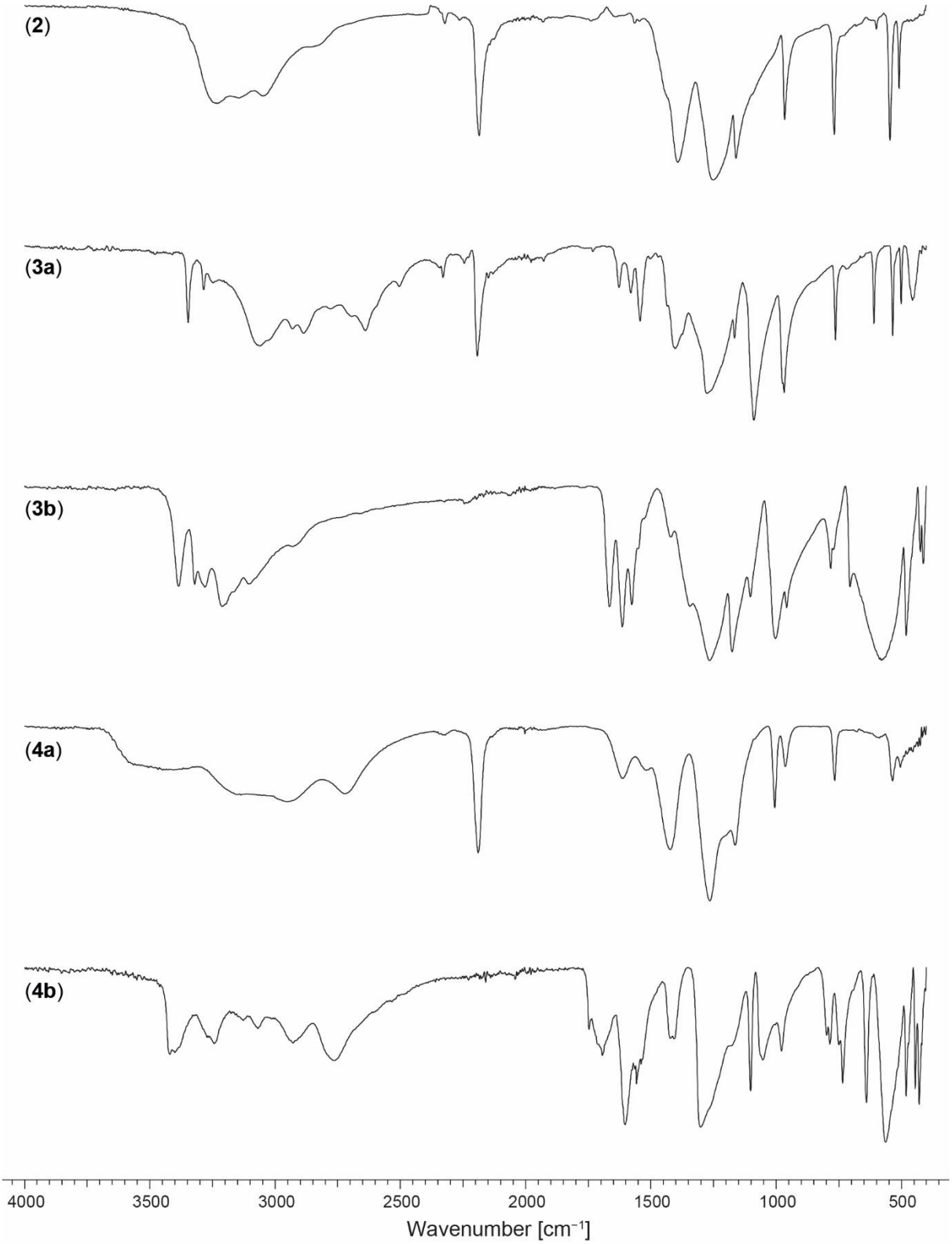

Figure S1. IR spectra of compounds **2**–**4**.

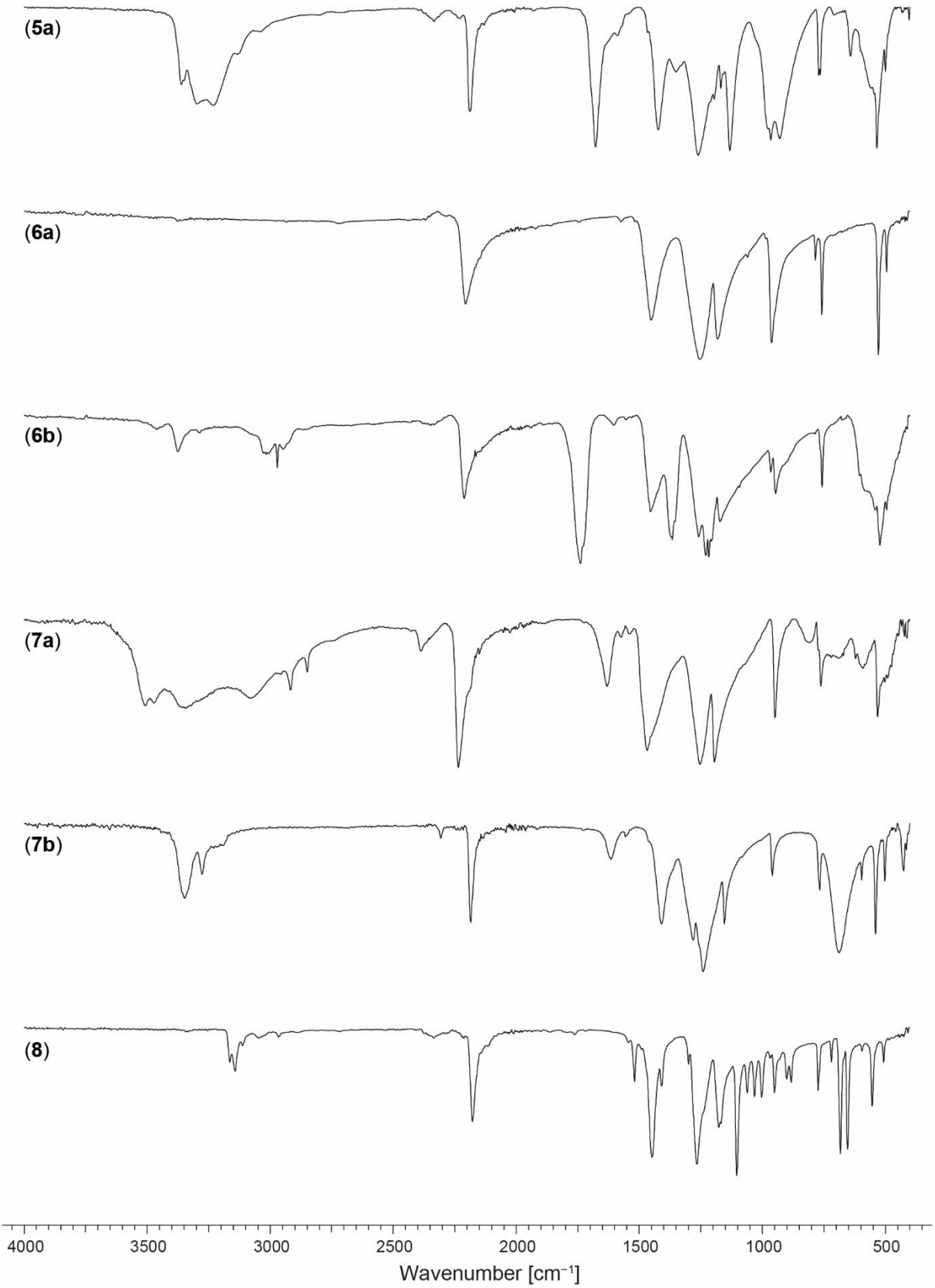

Figure S2. IR spectra of the compounds **5a**, **6**–**8**.

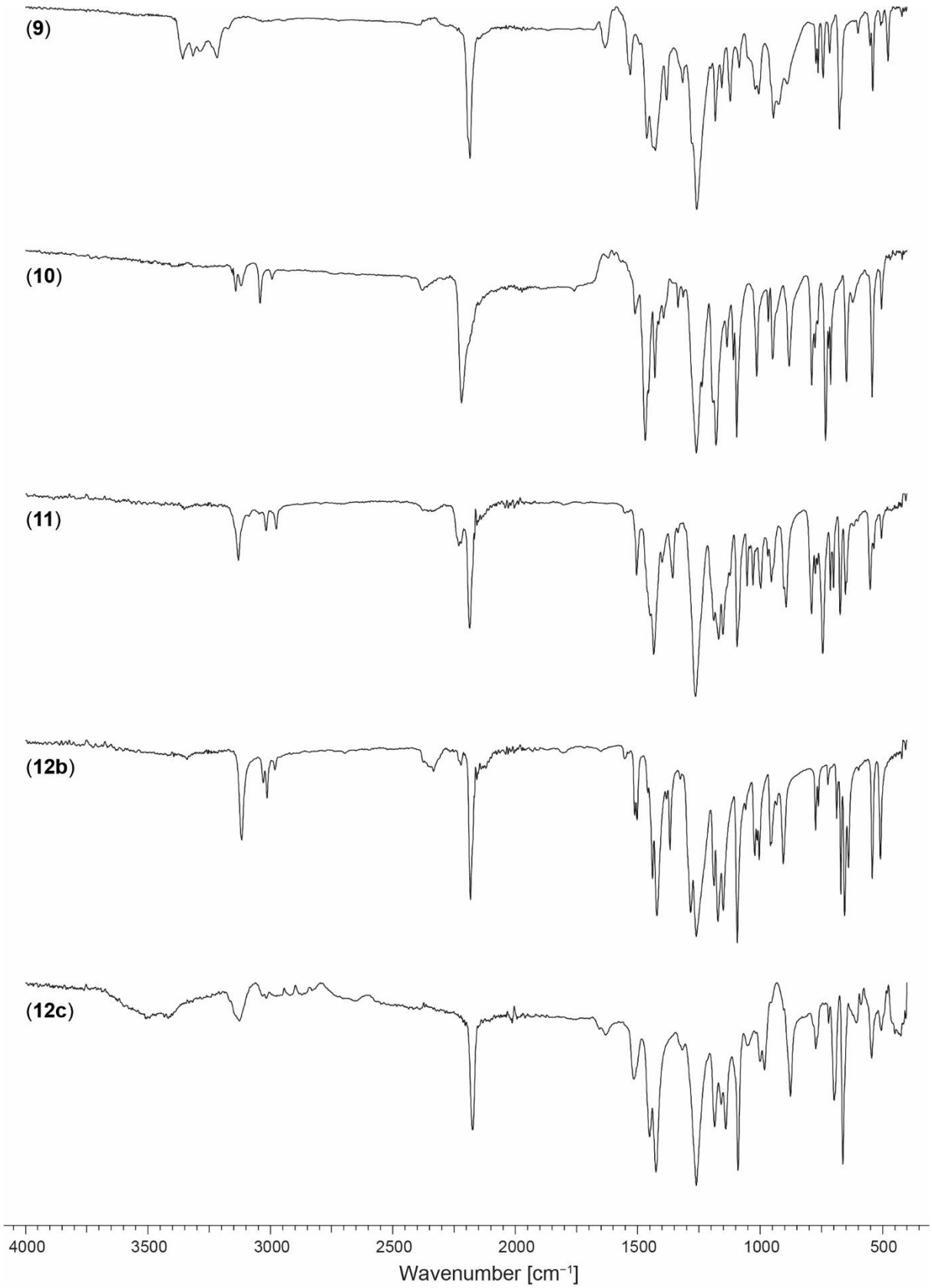

Figure S3. IR spectra of the complexes **9**–**11**, **12a**, and **12c**.

3.6.5 Thermal Analysis

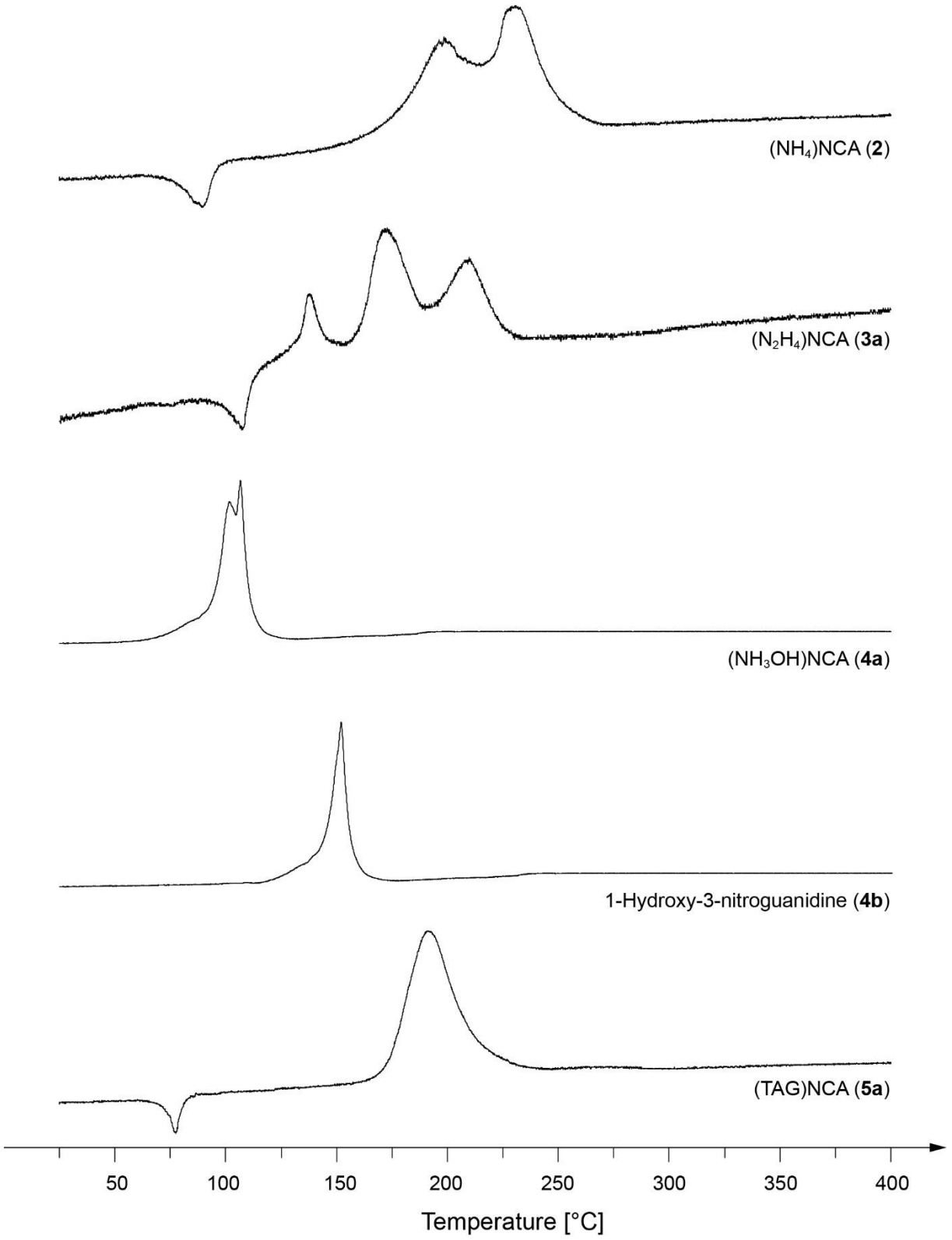

Figure S4. DTA plots of the nitrogen-rich compounds **2**, **3a**, **4a**, **4b**, and **5a**.

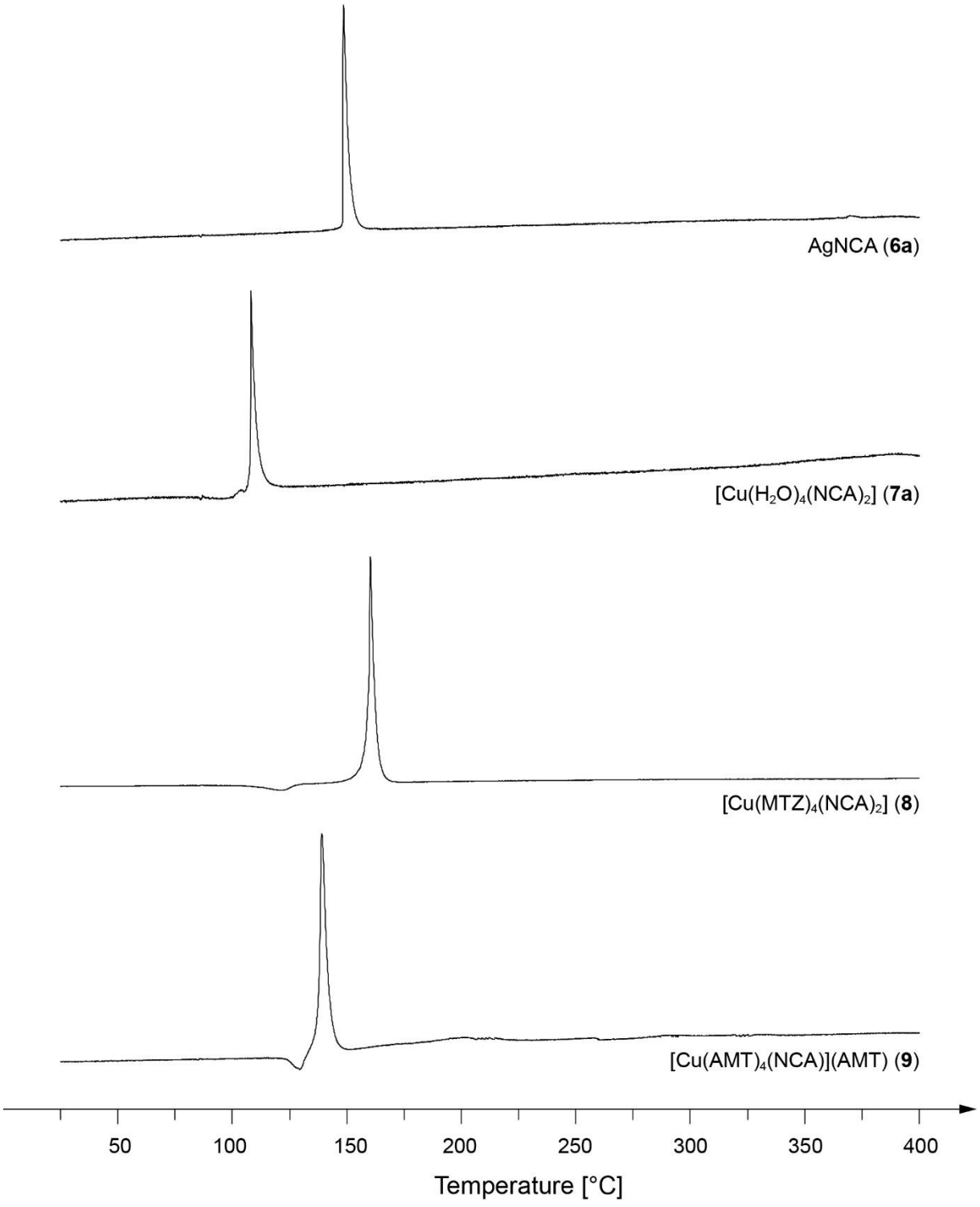

Figure S5. DTA plots of the nitrogen-rich compounds **6a**, **7a**, **8**, and **9**.

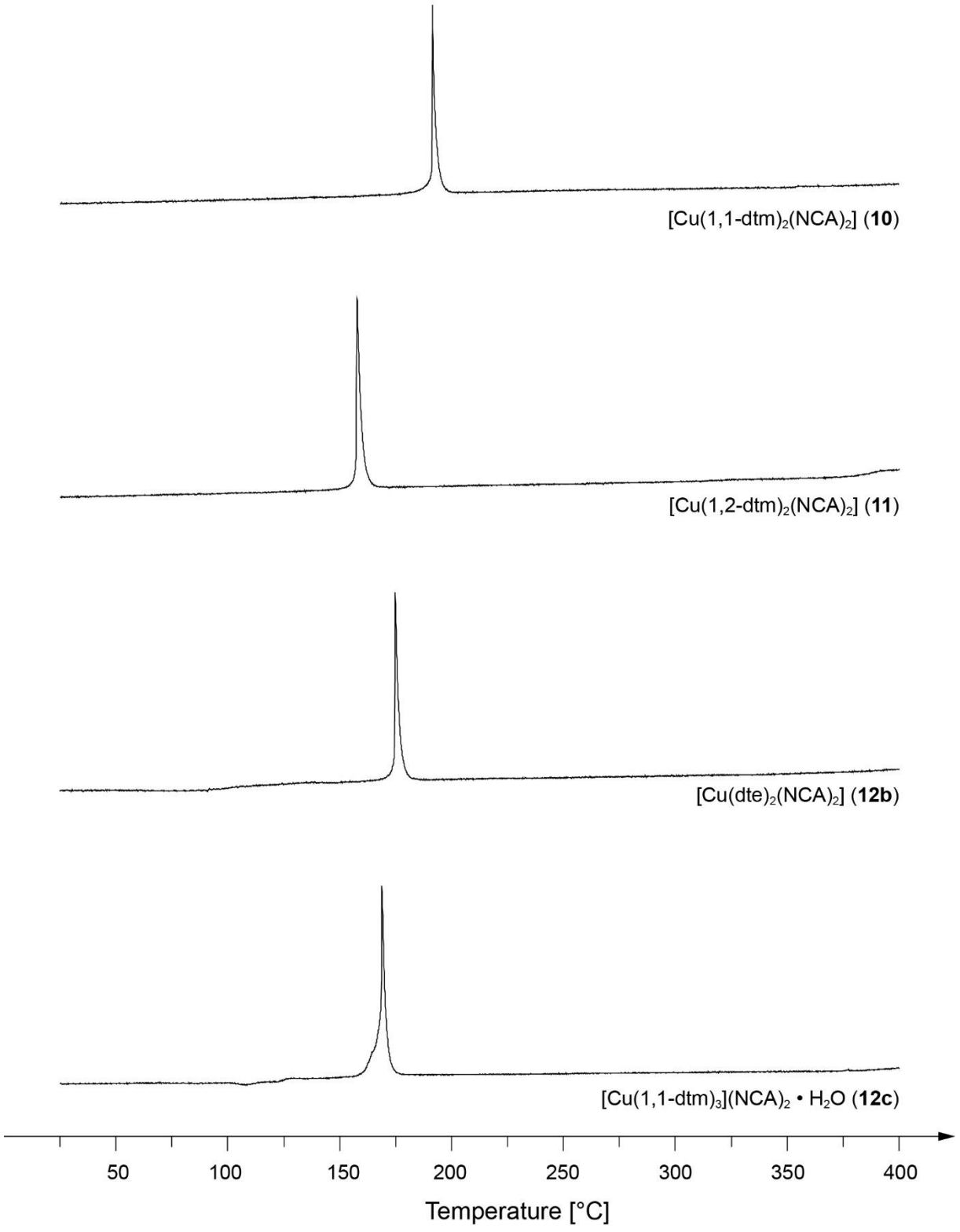

Figure S6. DTA plots of the ECCs **10**, **11**, **12a**, and **12c**.

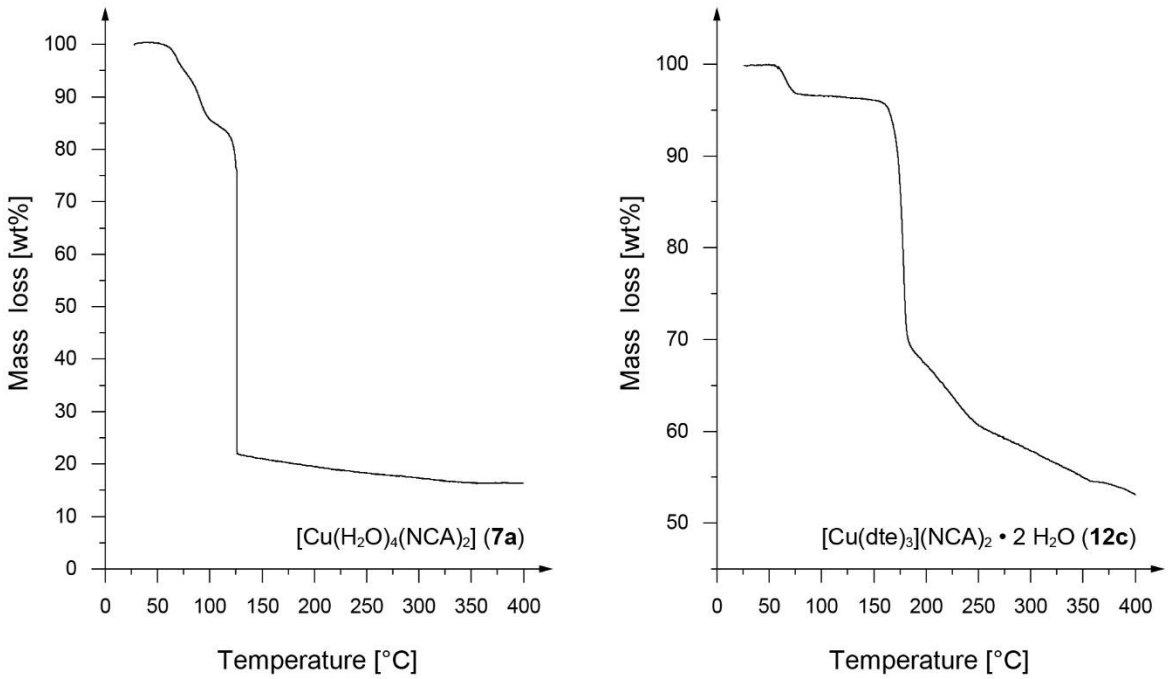

Figure S7. TG plots of $[Cu(H_2O)_4(NCA)_2]$ (**7a**) and $[Cu(dte)_3](NCA)_2 \cdot 2\ H_2O$ (**12c**).

3.6.6 Hot Plate and Hot Needle Test

Figure S8. High-speed images of the deflagration of silver nitrocyanamide (**6a**) during the hot plate test.

Figure S9. Deflagration of silver nitrocyanamide (**6a**) during the hot needle test shown s a sequence.

Figure S10. Reactions of $[Cu(AMT)_4(NCA)](NCA)$ (**9**) during hot plate test (left & middle) and hot needle test (right).

Figure S11. Deflagration of $[Cu(1,1\text{-dtm})_2(NCA)_2]$ (**10**) during hot plate test shown as a sequence.

3.6.7 Experimental Procedure

All chemicals and solvents were employed as received (Sigma-Aldrich, Fluka, Acros, ABCR). ^{1}H, ^{13}C, and ^{14}N NMR spectra were recorded at ambient temperature using a JEOL Bruker 27400, Eclipse 270, JEOL EX 400 or a JEOL Eclipse 400 instrument. The chemical shifts quoted in ppm in the text refer to typical standards such as tetramethylsilane (^{1}H, ^{13}C) nitromethane (^{14}N) in DMSO-d_6 or MeCN-d_3 as the solvent. Endothermic and exothermic events of the described compounds, which indicate melting, loss of crystal water or aqua ligands or decomposition, are given as the extrapolated onset temperatures. The samples were measured in a range of 25–400 °C at a heating rate of 5 °C min^{-1} through differential thermal analysis (DTA) with an OZM Research DTA 552-Ex instrument and in some cases additionally by thermal gravimetric analysis (TGA) with a PerkinElmer TGA4000. Infrared spectra were measured with pure samples on a Perkin-Elmer BXII FT-IR system with a Smith DuraSampler IR II diamond ATR. Determination of the carbon, hydrogen and nitrogen contents was carried out by combustion analysis using an Elementar Vario El (nitrogen values determined are often lower than the calculated ones' due to their explosive behavior). Impact sensitivity tests were carried out according to STANAG 4489[S16] with a modified instruction[S17] using a BAM (Bundesanstalt für Materialforschung) drophammer.

[S18] Friction sensitivity tests were carried out according to STANAG 4487[S19] with a modified instruction[S20] using the BAM friction tester. [S18,S21] The classification of the tested compounds results from the “UN Recommendations on the Transport of Dangerous Goods”. [S22-S23] Additionally, all compounds were tested upon the sensitivity toward electrical discharge using the OZM Electric Spark XSpark10 device. [S21] Hot plate and hot needle tests were performed in order to evaluate the potential initiation capability of selected compounds. The samples were fixed on a copper plate underneath adhesive tape and initiated by a red-hot needle. Strong deflagration or detonation of the compound usually indicates a valuable primary explosive. The safe and straightforward hot plate test only shows the behavior of the unconfined sample toward fast heating on a copper plate. It does not necessarily allow any conclusions on a compound’s capability as a suitable primary explosive. Energetic properties have been calculated with the EXPLO5 6.03 computer code[S24] using the, to RT converted, X-ray density and calculated solid state heats of formation. These were computed by the atomization method as described in recently published papers. Electronic enthalpies were calculated with the Gaussian09 software[S11] suite using the CBS-4M method.
The obtained compounds were washed with cold ethanol when stated, dried overnight in air and used for analytics without further purification.

CAUTION! *All investigated compounds are potentially explosive energetic materials, which show partly increased sensitivities toward various stimuli (e.g. elevated temperatures, impact, friction or electrostatic discharge). Therefore, proper security precautions (safety glass, face shield, earthed equipment and shoes, leather coat, Kevlar gloves, Kevlar sleeves and ear plugs) have to be applied while synthesizing and handling the described compounds.*

N-Methyl-*N*’-Nitro-*N*-nitrosoguanidine (**1**, MNNG)

According to a litreature procedure, [S25] nitroguanidine (10.4 g, 100.0 mmol, 1.0 eq.) was suspended in an aqueous solution (30 mL) of potassium hydroxide (11.8 g, 210.0 mmol, 2.1 eq.). The mixture was heated to 40 °C until the complete dissolution of nitroguanidine. Subsequently, methylamine hyrochloride (13.5 g, 200.0 mmol, 2.0 eq.) was added while stirring. The reaction temperature was

increased to 60 °C over a period of 10 min and kept at that level for another 30 min. In the next step, the solution was cooled with an ice bath and the colorless percipitate was filtrated off. *N*-Methyl-*N*'-nitroguanidine was obtained as a colorless solid and was used without a further purification. Yield : 8.3 g (70.3 mmol, 70%).
^{1}H-NMR (400 MHz, DMSO-d_6, 25 °C) δ (ppm) = 7.97 (s, 2H), 2.75 (s, 3H); ^{13}C-NMR (101 MHz, DMSO- d_6, 25 °C) δ (ppm) = 158.4, 28.2.
Following a procedure by McKay *et al*., [S25] *N*-Methyl-*N*'-nitroguanidine (9.4 g, 80.0 mmol, 1.00 eq.) was supsended in water (100 mL) and concetrated nitric acid (65 wt%, 30 mL) was added to the suspension. The mixture was cooled to 0 °C using an ice salt bath and sodium nitrite (12.4 g, 180.0 mmol, 2.25 eq.) in water (20 mL) was added dropwise over a period of 5 min. The temperature was kept at 0 °C during the whole process and for another 20 min of stirring after the addition was completed. The yellow percipitate was filtrate off an washed with a smal amount of cold water (5 mL) and dreid in air. Compound **1** was obtained as a yellow solid and was used without further purification. Yield: 8.1 g, (55.2 mmol, 69%).
^{1}H-NMR (400 MHz, DMSO-d_6, 25 °C) δ (ppm) = 9.74 (s, 2H), 3.15 (s, 3H); ^{13}C-NMR (101 MHz, DMSO-d_6, 25 °C) δ (ppm) = 158.1, 28.9.

General Procedure for the Preparation of the Nitrogen-Rich salts 2, 3a, 4a, 5a

The following nitrogen-rich salts were prepared based on modified instructions.[S26-S27] Silver nitrocyanamide (**6a**, 194 mg, 1.0 mmol, 1 eq.) was dissolved in acetonitrile (4 mL). Stoichiometric amounts of the respective hydrochloride salt (**2**: NH_4Cl; **3a**: N_2H_4 • HCl; **4a**: NH_2OH • HCl; **5a**: TAG • HCl) dissolved in methanol (4 mL) was added and the suspension was stirred for 10 min. The white precipitate was filtrated off, washed with acetonitrile (2 mL) and the solvent was evaporated.

Ammonium nitrocyanamide (**2**)

The nitrogen-rich salt **2**, was obtained within one day in the form of colorless blocks suitable for X-ray diffraction. Yield: 86 mg (0.83 mmol, 83%)
DTA (5 °C min^{-1}) onset: 88 °C (endothermic), 177 °C (exothermic); IR (ATR, cm^{-1}): $\tilde{\nu}$ = 3232 (m), 3144 (m), 3049 (m), 2322 (w), 2186 (s), 1393 (s), 1252 (vs), 1161 (s), 966 (s), 768 (s), 600 (w), 545 (s), 509 (m); ^{1}H-NMR (400 MHz, DMSO-d_6,

25 °C) δ (ppm) = 7.08 (s, 4H); ^{13}C-NMR (101 MHz, DMSO-d_6, 25 °C) δ (ppm) = 116.6; ^{14}N-NMR (29 MHz, DMSO-d_6, 25 °C) δ (ppm) = −2.4, −160.1, −358.3; EA ($CH_4N_4O_2$, 104.07): calcd: C 11.54, H 3.87, N 53.84%; found: C 11.33, H 3.93, N 53.59%; BAM drophammer: > 40 J; BAM friction tester: > 360 N; ESD: > 1500 mJ (at grain size = 500–1000 µm).

Hydrazinium nitrocyanamide (**3a**)

Compound **3a**, was obtained within five hours in the form of colorless needles suitable for X-ray diffraction. Yield: 107 mg (0.90 mmol, 90%).
DTA (5 °C min^{-1}) onset: 101 °C (endothermic), 129 °C (exothermic); IR (ATR, cm^{-1}): $\tilde{\nu}$ = 3347 (m) 3285 (w), 3247 (w), 3063 (m), 2931 (m), 2887 (m), 2778 (m), 2639 (m), 2505 (w), 2330 (w), 2245 (w), 2193 (s), 2149 (w), 1627 (w), 1580 (w), 1543 (m), 1435 (m), 1403 (m), 1373 (m), 1276 (s), 1166 (m), 1089 (vs), 968 (s), 763 (m), 610 (m), 535 (m), 501 (m), 456 (m); ^{1}H-NMR (400 MHz, DMSO-d_6, 25 °C) δ (ppm) = 8.66 (br s, 5H), ^{13}C-NMR (101 MHz, DMSO-d_6, 25 °C) δ (ppm) = 116.6; ^{14}N-NMR (29 MHz, DMSO-d_6, 25 °C) δ (ppm) = −2.4, −159.4; −358.1. EA ($CH_5N_5O_2$, 119.08): calcd: C 10.09, 4.23, N 58.81%; found: C 9.62, H 4.33, N 55.97%; BAM drophammer: > 40 J; BAM friction tester: 80 N; ESD: 750 mJ (at grain size 500-1000 µm).

Hydroxylammonium nitrocyanamide (**4a**)

After evaporation of the solvent, the hydroxylammonium salt **4a** was obtained as a colorless oil. Yield: 94 mg (0.78 mmol, 78%)
DTA (5 °C min^{-1}) onset: 94 °C (exothermic); IR (ATR, cm^{-1}): $\tilde{\nu}$ = 3449 (w), 3136 (m), 2952 (m), 2722 (m), 2326 (vw), 2189 (s), 1615 (w), 1519 (w), 1424 (s), 1265 (vs), 1164 (s), 1005 (m), 963 (w), 766 (m), 535 (m), 504 (w); ^{1}H-NMR (400 MHz, DMSO-d_6, 25 °C) δ (ppm) = 10.04 (s, 4H); ^{13}C-NMR (101 MHz, DMSO-d_6, 25 °C) δ (ppm) = 116.7; ^{14}N-NMR (29 MHz, DMSO-d_6, 25 °C) δ (ppm) = 3.06, −161.1, −359.0; EA ($CH_4N_4O_4$, 120.07): calcd: C 10.00, H 3.36, N 46.66%; found: C 10.35, H 3.25, N 46.71%; BAM drophammer: > 40 J; BAM friction tester: > 360 N.

Triaminoguanidinium nitrocyanamide (**5a**)

Single crystals of compound **5a**, were obtained within one day in the form of colorless plates. Yield: 141 mg (0.74 mmol, 74%)
DTA (5 °C min^{-1}) onset: 73 °C (endothermic), 173 °C (exothermic); IR (ATR, cm^{-1}): $\tilde{\nu}$ = 3361 (m) 3350 (m), 3298 (s), 3231 (s), 3132 (m), 3040 (w), 2334 (vw), 2228 (vw), 2189 (s), 1678 (vs), 1589 (w), 1423 (s), 1350 (m), 1261 (vs), 1195 (s), 1169 (m), 1158 (m), 1132 (vs), 976 (s), 966 (s), 930 (s), 771 (m), 765 (m), 708 (vw), 642 (m), 545 (m), 535 (vs), 500 (m).; ^{1}H-NMR (400 MHz, DMSO-d_6, 25 °C) δ (ppm) = 8.59 (s, 3H), 4.48 (s, 6H); ^{13}C-NMR (101 MHz, DMSO-d_6, 25 °C) δ (ppm) = 159.0, 116.5; ^{14}N-NMR (29 MHz, DMSO-d_6, 25 °C) δ (ppm) = −2.4, −160.7; EA ($C_2H_9N_9O_2$, 191.16): calcd: C 12.57, H 4.75, N 65.95%; found: C 12.14, H 4.25, N 64.89%; BAM drophammer: 6 J; BAM friction tester: 360 N; ESD: > 1500 mJ (at grain size = 500–1000 µm).

General Procedure for the Preparation of the Compounds 3b and 4b

Silver nitrocyanamide (**6a**, 10.0 mmol, 1.94 g, 1.0 eq.) was dissolved in acetonitrile (20 mL). Concentrated hydrochloric acid (37 wt%, 0.88 mL, 1.1 eq) was added and the suspension was stirred for 5 min. The white percipitate was filtrated off and stoichiometric amounts of an aqueous hyroxylamine (50 wt%) solution or hydrazine hydrate in water (5 mL) were added dropwise to the solution. Subsequently, the mixture was heated to 90 °C for 15 min. After that period, the solvent was evaporated.

1-Amino-3-nitroguanidine (**3b**)

Evaporation of the solvent afforded compound **3b** as a colorless solid. Recrystalization from a mixture of water an methanol afforded single crystals of **3b** within one day. Yield: 953 mg (8.0 mmol, 80%).
IR (ATR, cm^{-1}): $\tilde{\nu}$ = 3385 (m), 3321 (m), 3281 (m), 3211 (s), 3162 (s), 3103 (m), 2929 (m), 1666 (s), 1614 (s), 1576 (s), 1550 (m), 1423 (w), 1344 (s), 1267 (vs), 1176 (vs), 1103 (s), 1002 (s), 958 (s), 782 (m), 772 (m), 705 (m), 588 (vs), 580

(vs), 575 (vs), 481 (s), 424 (m), 412 (m); EA ($CH_4N_4O_2$, 104.07): calcd: C 11.54, H 3.87, N 53.84%; found: C 11.33, H 3.93, N 53.59%.

1-Hydroxy-3-nitroguanidine (**4b**)

Evaporation of the solvent afforded compound **4b** as a colorless solid. Recrystalization from water afforded single crystals of **4b** within one day. Yield: 720 mg (6.0 mmol, 60%).
IR (ATR, cm^{-1}): $\tilde{\nu}$ = 3420(m), 3406 (m), 3400 (m), 3272 (m), 3264 (m), 3243 (m), 3128 (m), 3077 (m), 3069 (m), 2928 (m), 2762 (m), 1747 (m), 1712 (m), 1693 (m), 1683 (m), 1602 (vs), 1575 (m), 1563 (m), 1558 (s), 1539 (m), 1533 (m), 1423 (m), 1408 (m), 1302 (vs), 1102 (s), 1052 (m), 1003 (m), 979 (m), 798 (m), 785 (m), 749 (m), 734 (s), 640 (s), 563 (vs), 481 (s), 445 (s), 429 (s), 419 (m); EA ($CH_4N_4O_3$, 120.07): calcd: C 10.00, H 3.36, N 46.66%; found: C 10.33, H 3.93, N 47.09%; BAM drophammer: 10 J; BAM friction tester: 240 N; ESD: 750 mJ (at grain size = <100 µm).

$(TAG)_2[Ag(NCA)_3]$ (**5b**)

Triaminoguanidine hydrochloride (141 mg, 1.0 mmol) dissolved in acetonitrile (4 mL) was reacted with an excess of silver nitrocyanamide in acetonitrile (4 mL). Single crystals of compound **5b** in the form of colorless blocks were obtained within a week. An elemental analysis pure isolation of the silver complex **5b** was not possible.

Silver nitrocyanamide (**6a**)

Silver salt 6a was prepared based on a modified procedure by Harris.[S27] An aqueous solution (60 mL) of sodium hydroxide (1.6 g, 40 mmol, 1.3 eq.) was cooled with an ice bath. MNNG (**1**, 4.4 g, 30 mmol, 1.0 eq.) was added to the solution over a period of 10 min while stirring. The temperature was kept at 5 °C during the whole addition. The ice bath was removed and stirring was continued for another 20 min. Concentrated nitric acid (65 wt%, 3.6 mL) diluted with water (15 mL) was added, followed by silver nitrate (5.1 g, 30 mmol, 1.0 eq) in water

(5 mL). Subsequently, the colorless percipitate was filtrated off, washed with hot water (10 ml) and dried in air. Silver nitrocyanamide (**6a**) was obained as a colorless solid. Yield: 5.0 g (25.8 mmol , 86%).
DTA (5 °C min^{-1}) onset: 158 °C (exothermic); IR (ATR, cm^{-1}): $\tilde{\nu}$ = 2206 (s), 2166 (m), 1451 (s), 1253 (vs), 1182 (s), 1060 (m), 962 (s), 784 (m), 758 (s), 528 (vs), 495 (m); ^{13}C-NMR (101 MHz, CD_3CN-d_6, 25 °C) δ (ppm) = 235.3; ^{14}N-NMR (29 MHz, CD_3CN-d_6, 25 °C) δ (ppm) = −4.45, −181.6; EA ($CAgN_3O_2$, 193.90): calcd: C 6.19, H 0.00, N 55.643%; found: C 6.30, H 0.00, N 21.41%; BAM drophammer: 3 J; BAM friction tester: 10 N; ESD: 51 mJ (at grain size < 100 µm).

[Ag(NCA)(NH_3)] (**6b**)

The silver salt **6a** (48 mg, 0.25 mmol) was dissolved in aqueous concentrated ammonia (25 wt%, 5.0 mL). Evaporation of the solvent afforded colorless platelets of complex **6b** suitable for X-ray diffraction within three days. Yield: 41 mg (19 mmol, 76%).
IR (ATR, cm^{-1}): $\tilde{\nu}$ = 3457 (vw), 3375 (w), 3028 (w), 3017 (w), 3006 (w), 2971 (m), 2948 (w), 2211 (m), 2164 (w), 2146 (w), 1739 (vs), 1603 (vw), 1455 (s), 1366 (s), 1259 (s), 1230 (vs), 1217 (vs), 1207 (s), 1172 (s), 1093 (m), 965 (m), 946 (m), 757 (m), 605 (m), 541 (s), 522 (s), 495 (s), 456 (m), 443 (w).; EA ($CH_3AgN_4O_2$, 210.93): calcd: C 5.69, H 1.43, N 26.56%; found: C 5.85, H 1.32, N 26.33%.

General Procedure for the Preparation of the ECCs 7–11

According to a modified literature procedure,[S27] an aqueous solution of copper(II) nitrocyanamide was pepared by the reaction of copper(II) chloride dihydrate (170 mg, 1.00 mmol, 1.0 eq.) in water (4 mL) with a solution of silver nitrocyanamide (**6a**, 194 mg, 2.00 mmol, 2.0 eq.) in acetonitrile (4 mL). Both solutions were combined and stirring was continue for 10 min. The formed solid was filtrated off and washed with acetonitrile (2 mL). Evapoation of the solvent gives complex **7a**. The addition of stoichiometric amounts of the respective ligand (**7b**: aq. ammonia; **8**: MTZ, **9**: AMT; **10**: 1,1-dtm; **11**: 1,2-dtm; **12a**: dte) in acetonitrile (4 mL) results in the formation of several copper(II) nitrocyanamide complexes after the evaporation of the solvent.

$[Cu(H_2O)_4(NCA)_2]$ (**7a**)

The copper(II) complex **7a** was obtained as a light blue, non-crystalline solid after one week. Yield: 249 mg (0.81 mmol, 81%).
DTA (5 °C min^{-1}) onset: 89 °C (endothermic), 108 °C (exothermic); IR (ATR, cm^{-1}): $\tilde{\nu}$ = 3506 (m), 3474 (m), 3342 (s), 3076 (m), 2917 (m), 2849 (m), 2388 (w), 2235 (vs), 2191 (m), 1631 (m), 1572 (w), 1468 (s), 1253 (vs), 1195 (vs), 948 (s), 808 (w), 690 (w), 591 (m), 531 (s). EA ($C_2H_8CuN_6O_8$, 307.67): calcd: C 7.81, H 2.62, N 27.32%; found: C 7.47, H 2.52, N 26.53%; BAM drophammer: > 40 J; BAM friction tester: > 360 N; ESD: 1500 mJ (at grain size = 500–1000 µm).

$[Cu(NCA)_2(NH_3)_4]$ (**7b**)

Single crystals of copper(II) ammine complex **7b** were obtained within two days in the form of blue needles. Yield: 279 mg (0.92 mmol, 92%).
IR (ATR, cm^{-1}): $\tilde{\nu}$ = 3348 (m), 3277 (m), 2307 (vw), 2185 (s), 1615 (w), 1557 (vw), 1410 (s), 1281 (s), 1240 (vs), 1154 (s), 1081 (w), 960 (m), 767 (m), 689 (s), 596 (m), 539 (s), 502 (m), 425 (m), 414 (w); EA ($C_2H_{12}CuN_{10}O_4$, 303.73): calcd: C 7.91, H 3.98, N 46.12%; found: C 8.15, H 3.89, N 45.52%.

$[Cu(MTZ)_4(NCA)_2]$ (**8**)

Complex **8** crystallizes in the form of blue platelets suitable for X-ray diffraction within a week. Yield: 504 mg (0.88 mmol, 88%).
DTA (5 °C min^{-1}) onset: 110 °C (endothermic), 159 °C (exothermic); IR (ATR, cm^{-1}): $\tilde{\nu}$ = 3164 (w), 3143 (w), 3112 (w), 3046 (vw), 2965 (vw), 2336 (vw), 2178 (s), 2143 (w), 2115 (w), 1544 (w), 1519 (m), 1491 (w), 1448 (s), 1409 (m), 1300 (w), 1266 (vs), 1177 (s), 1168 (s), 1104 vs), 1062 (m), 1032 (m), 1003 (m), 968 (w), 950 (m), 901 (m), 883 (m), 773 (m), 719 (w), 682 (s), 653 (s), 595 (w), 553 (m), 507 (w); EA ($C_{10}H_{16}CuN_{22}O_4$, 571.93): calcd: C 21.00, H 2.82, N 53.88%; found: C 20.96, H 2.99, N 53.77%; BAM drophammer: 40 J; BAM friction tester: 240 N; ESD: 750 mJ (at grain size = 500–1000 µm).

[Cu(AMT)$_4$(NCA)](NCA) (**9**)

Blue blocks of compound **9** suitable for X-ray diffraction were obtained after 5 days. Yield: 398 mg (0.63 mmol, 63%)
DTA (5 °C min^{-1}) onset: 123 °C (endothermic, followed by exothermic); IR (ATR, cm^{-1}): $\tilde{\nu}$ = 3358 (w), 3316 (w), 3218 (w), 3173 (w), 2185 (s), 1634 (w), 1531 (m), 1492 (w), 1463 (s), 1436 (s), 1428 (s), 1382 (m), 1317 (m), 1279 (s), 1259 (vs), 1202 (m), 1183 (m), 1156 (m), 1122 (m), 1086 (m), 1050 (w), 1020 (m), 1006 (m), 946 (m), 924 (m), 772 (w), 763 (m), 743 (m), 717 (w), 676 (s), 600 (w), 551 (w), 540 (m); EA ($C_{10}H_{20}CuN_{26}O_4$, 631.99): calcd: C 19.00, H 3.19, N 57.62%; found: C 18.93, H 3.09, N 57.80%; BAM drophammer: ≤ 1 J; BAM friction tester: 20 N; ESD: 250 mJ (at grain size = 100–500 µm).
[Cu(1,1-dtm)$_2$(NCA)$_2$] (**10**)

Single crystals in the form of blue plates of compound **10** were obtained within two days. Yield: 445 mg (0.82 mmol, 82%).
DTA (5 °C min^{-1}) onset: 191 °C (exothermic); IR (ATR, cm^{-1}): $\tilde{\nu}$ = 3142(w), 3120 (w), 3042 (w), 2993 (w), 2380 (w), 2219 (s), 2169 (m), 2148 (w), 1759 (w), 1622 (vw), 1511 (m), 1470 (vs), 1456 (s), 1430 (s), 1414 (m), 1394 (m), 1335 (w), 1315 (w), 1261 (vs), 1238 (s), 1192 (s), 1180 (vs), 1135 (m), 1109 (m), 1096 (vs), 1014 (s), 967 (m), 949 (m), 881 (m), 789 (s), 776 (m), 765 (m), 733 (vs), 720 (m), 712 (s), 647 (s), 622 (w), 543 (s), 504 (w); EA ($C_8H_8CuN_{22}O_4$, 539.85): calcd: C 17.80, H 1.49, N 57.08%; found: C 17.73, H 1.56, N 57.00%; BAM drophammer: 7 J; BAM friction tester: 112 N; ESD: 750 mJ (at grain size < 100 µm).

[Cu(1,2-dtm)$_2$(NCA)$_2$] (**11**)

After recrystallization from water, single crystals in the form of blue plates of compound **11** were obtained within two days. Yield: 432 mg (0.80 mmol, 80%).
DTA (5 °C min^{-1}) onset: 157 °C (exothermic); IR (ATR, cm^{-1}): $\tilde{\nu}$ = 3131 (m), 3017 (w), 2976 (w), 2335 (vw), 2231 (w), 2221 (w), 2187 (s), 1552 (vw), 1505 (m), 1449 (s), 1435 (s), 1400 (m), 1357 (m), 1323 (w), 1264 (vs), 1190 (s), 1169 (s), 1152 (s), 1123 (m), 1094 (s), 1053 (m), 1042 (w), 1029 (m), 1019 (w), 998 (m), 968 (m), 954 (m), 904 (m), 894 (m), 790 (m), 775 (m), 766 (m), 744 (s), 713 (m), 700 (m), 673

(m), 652 (m), 618 (w), 551 (m), 536 (w), 504 (w); EA ($C_8H_8CuN_{22}O_4$, 539.85): calcd: C 17.80, H 1.49, N 57.08%; %; found: C 17.85, H 1.73, N 54.58%; BAM drophammer: 2 J; BAM friction tester: 80 N; ESD: 480 mJ (at grain size < 100 µm).

$[Cu(dte)_2(NCA)_2]$ • 2 MeCN (**12a**)

The side species **12a** was obtained within a week in the form of colorless crystals suitable for X-ray diffraction. Depending on whether two or three equivalents of dte were used, complex **12b** or **12c** was obtained as a second species. Consequently, an elemental analysis clean isolation of complex **12a** was not possible.

General Procedure for the Preparation of the ECCs 12b and 12c

According to a modified literature procedure,[S27] an aqueous solution of copper(II) nitrocyanamide was pepared by the reaction of copper(II) chloride dihydrate (170 mg, 1.00 mmol, 1.0 eq.) in water (4 mL) with a solution of silver nitrocyanamide (**6a**, 194 mg, 2.00 mmol, 2.0 eq.) in acetonitrile (4 mL). Both solutions were combined and stirring was continue for 10 min. The formed solid was filtrated off and washed with water (2 mL). Subsequently the solution was heated to 80 °C for 10 min for the complete evaporation of acetonitrile out of the solution. Stoichiometric amounts of dte (**12b**: 2 eq.; **12c**: 3 eq.) dissolved in hot water (4 mL) were added and stirring was continued for 5 min. Finally, the solution was left for crystallization.

$[Cu(dte)_2(NCA)_2]$ (**12b**)

Single crystals in the form of blue blocks of compound **12b** were obtained within two days. Yield: 466 mg (0.82 mmol, 82%).
DTA (5 °C min^{-1}) onset: 174 °C (exothermic); IR (ATR, cm^{-1}): $\tilde{\nu}$ = 3117 (m), 3030 (w), 3014 (w), 2981 (w), 2334 (w), 2222 (w), 2183 (s), 2157 (w), 1553 (vw), 1512 (m), 1502 (m), 1459 (w), 1439 (s), 1421 (s), 1382 (w), 1368 (m), 1326 (w), 1284 (s), 1261 (vs), 1188 (s), 1172 (s), 1151 (s), 1093 (vs), 1059 (m), 1022 (m), 1013 (m), 1004 (m), 958 (m), 953 (m), 933 (m), 906 (s), 773 (m), 762 (m), 723 (w), 688 (m), 670 (s), 655 (s), 639 (s), 598 (w), 542 (s), 509 (m); EA ($C_{10}H_{12}CuN_{22}O_4$,

567.90): calcd: C 21.15, H 2.13, N 54.26%; %; found: C 21.18, H 2.14, N 53.74%; BAM drophammer: 6 J; BAM friction tester: 180 N; ESD: > 1500 mJ (at grain size = 500–1000 µm).

$[Cu(dte)_3](NCA)_2 \cdot 2\ H_2O$ (**12c**)

Blue blocks of compound **12c** suitable for X-ray diffraction were obtained within several ours. Yield: 410 mg (0.76 mmol, 76%).
DTA (5 °C min^{-1}) onset: 103 °C (endothermic), 119 °C (endothermic), 168 °C (exothermic); IR (ATR, cm^{-1}): $\tilde{\nu}$ = 3493 (w), 3417 (w), 3127 (w), 3017 (vw), 2174 (s), 1656 (w), 1631 (w), 1517 (m), 1451 (s), 1425 (vs), 1318 (m), 1261 (vs), 1186 (s), 1159 (m), 1141 (s), 1090 (vs), 1052 (m), 1000 (m), 982 (m), 876 (m), 772 (m), 698 (m), 662 (s), 607 (w), 544 (m), 505 (w), 425 (w); EA ($C_8H_8CuN_{22}O_4$, 539.85): calcd: C 21.84, H 2.88, N 54.57%; %; found: C 21.92, H 2.76, N 54.89%; BAM drophammer: ≤ 1 J; BAM friction tester: 160 N; ESD: > 1500 mJ (at grain size > 1000 µm).

3.6.8 References

[S1] CrysAlisPRO (Version 171.33.41), Oxford Diffraction Ltd., **2009**.

[S2] A. Altomare, G. Cascarano, C. Giacovazzo, A. Guagliardi, *J. Appl. Crystallogr*. **1993**, *26*, 343–350.

[S3] (a) A. Altomare, G. Cascarano, C. Giacovazzo, A. Guagliardi, A. G. G. Moliterni, M. C. Burla, G. Polidori, M. Camalli, R. Spagna, SIR97, **1997**. (b) A. Altomare, M. C. Burla, M. Camalli, G. L. Cascarano, C. Giacovazzo, A. Guagliardi, A. G. G. Moliterni, G. Polidori, R. Spagna, J. Appl. Crystallogr. **1999**, *32*, 115–119.

[S4] (a) G. M. Sheldrick, SHELXL-97, University of Göttingen, Germany, **1997**. (b) G. M. Sheldrick, *Acta Cryst. A* **2008**, *64*, 112–122.

[S5] G. M. Sheldrick, *Acta Cryst. A* **2015**, *71*, 3–8.

[S6] A. L. Spek, PLATON, Utrecht University, The Netherlands, **1999**.

[S7] L. J. Farrugia, L. *J. Appl. Cryst.* **2012**, *45*, 849–854.

[S8] O. V. Dolomanov, L. J. Bourhis, R. J. Gildea, J. A. K. Howard, H. Puschmann, *J. Appl. Cryst.* **2009**, *42*, 339–341.

[S9] Empirical absorption correction using spherical harmonics, implemented in SCALE3 ABSPACK scaling algorithm (CrysAlisPro Oxford Diffraction Ltd., Version 171.33.41, **2009**).

[S10] APEX3, Bruker AXS Inc., Madison, Wisconsin, USA

[S11] M. J. Frisch, G. W. Trucks, H. B. Schlegel, G. E. Scuseria, M. A. Robb, J. R. Cheeseman, G. Scalmani, V. Barone, B. Mennucci, G. A. Petersson, H. Nakatsuji, M. Caricato, X. Li, H.P. Hratchian, A. F. Izmaylov, J. Bloino, G. Zheng, J. L. Sonnenberg, M. Hada, M. Ehara, K. Toyota, R. Fukuda, J. Hasegawa, M. Ishida, T. Nakajima, Y. Honda, O. Kitao, H. Nakai, T. Vreven, J. A. Montgomery, Jr., J. E. Peralta, F. Ogliaro, M. Bearpark, J. J. Heyd, E. Brothers, K. N. Kudin, V. N. Staroverov, R. Kobayashi, J. Normand, K. Raghavachari, A. Rendell, J. C. Burant, S. S. Iyengar, J. Tomasi, M. Cossi, N. Rega, J. M. Millam, M. Klene, J. E. Knox, J. B. Cross, V. Bakken, C. Adamo, J. Jaramillo, R. Gomperts, R. E. Stratmann, O. Yazyev, A. J. Austin, R. Cammi, C. Pomelli, J. W. Ochterski, R. L. Martin, K. Morokuma, V. G. Zakrzewski, G. A. Voth, P. Salvador, J. J. Dannenberg, S. Dapprich, A. D. Daniels, O. Farkas, J.B. Foresman, J. V. Ortiz, J. Cioslowski, D. J. Fox, Gaussian 09 A.02, Gaussian, Inc., Wallingford, CT, USA, **2009**.

[S12] a) J. W. Ochterski, G. A. Petersson, and J. A. Montgomery Jr., *J. Chem. Phys.* **1996**, *104*, 2598–2619; b) J. A. Montgomery Jr., M. J. Frisch, J. W. Ochterski G. A. Petersson, *J. Chem. Phys.* **2000**, *112*, 6532–6542.

[S13] a) L. A. Curtiss, K. Raghavachari, P. C. Redfern, J. A. Pople, *J. Chem. Phys.* **1997**, *106*, 1063–1079; b) E. F. C. Byrd, B. M. Rice, *J. Phys. Chem*. A **2006**, *110*, 1005–1013; c) B. M. Rice, S. V. Pai, J. Hare, *Comb. Flame* **1999**, *118*, 445–458.

[S14] a) P. J. Lindstrom, W. G. Mallard (Editors), NIST Standard Reference Database Number 69, http://webbook.nist.gov/chemistry/ (accessed June **2020**); b) M. S. Westwell, M. S. Searle, D. J. Wales, D. H. Williams, *J. Am. Chem. Soc*. **1995**, *117*, 5013–5015; c) F. Trouton, *Philos. Mag*. **1884**, *18*, 54–57.

[S15] a) H. D. B. Jenkins, H. K. Roobottom, J. Passmore, L. Glasser, *Inorg. Chem.* **1999,** *38,* 3609–3620; b) H. D. B. Jenkins, D. Tudela, L. Glasser, *Inorg. Chem.* **2002**, *41*, 2364–2367.

[S16] NATO standardization agreement (STANAG) on explosives, impact sensitivity tests, no. 4489, 1st ed., Sept. 17, **1999**.

[S17] WIWEB-Standardarbeitsanweisung 4-5.1.02, Ermittlung der Explosionsgefährlichkeit, hier der Schlagempfindlichkeit mit dem Fallhammer, Nov. 8, **2002**.

[S18] BAM, http://www.bam.de, accessed October **2021**.

[S19] NATO standardization agreement (STANAG) on explosive, friction sensitivity tests, no. 4487, 1st ed., Aug. 22, **2002**.

[S20] WIWEB-Standardarbeitsanweisung 4-5.1.03, Ermittlung der Explosionsgefährlichkeit oder der Reibeempfindlichkeit mit dem Reibeapparat, Nov. 8, **2002**.

[S21] OZM, http://www.ozm.cz, accessed October **2021**.

[S22] UN Model Regulation: Recommendations on the Transport of Dangerous Goods – Manual of Tests and Criteria, section 13.4.2.3.3, **2015**.

[S23] Impact: insensitive > 40 J, less sensitive ≥ 35 J, sensitive ≥ 4 J, very sensitive ≤ 3 J; Friction: insensitive > 360 N, less sensitive = 360 N, sensitive < 360 N and > 80 N, very sensitive ≤ 80 N, extremely sensitive ≤ 10 N. According to the UN Recommendations on the Transport of Dangerous Goods, 5th ed., **2009**.

[S24] M. Sućeska, EXPLO5 V6.02 program, Brodarski Institute, Zagreb, Croatia, **2014**.

[S25] A. F. McKay, G. F. Wright, *J. Am. Chem. Soc.* **1947**, *69*, 3028–3030.

[S26] S. R. Harris, *J. Am. Chem. Soc.* **1958**, *80*, 2302–2305.

[S27] L. He, G.-H. Tao, D. Parrish, J. M. Shreeve, *Chem. Eur. J.* **2010**, *16*, 5736–5743.

4. Polyazido-methyl Derivatives of Prominent Oxadiazole and Isoxazole Scaffolds: Synthesis, Explosive Properties, and Evaluation

Lukas Bauer, Maximilian Benz‡, Thomas M. Klapötke, Tobias Lenz, Jörg Stierstorfer

as published in *Journal of Organic Chemistry* **2021**, *86*, *9*, 6371–6380

DOI: 10.1021/acs.joc.1c00216

Keywords: azides, energetic materials, structure eludication, heterocycles, sensitivities

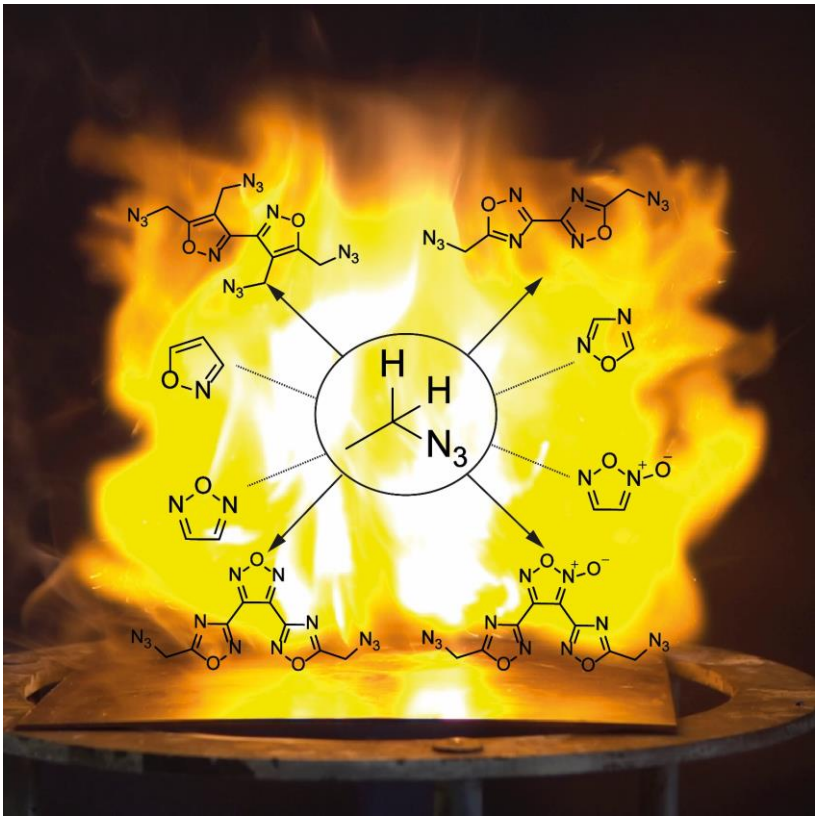

Polyazidomethyl derivatives show promising energetic properties and can be easily introduced to prominent heterocyclic motifs through chlorine-azide exchange. The structural analysis gives interesting insights in the chemistry of this substance class.

Abstract: Recently, different nitrato-methyl-substituted oxadiazoles have been described as potential melt-cast explosives. In this work, corresponding N–O heterocyclic-based compounds with azido-methyl functionalities were synthesized. In each case, the explosophoric azide group is inserted by chlorine–azide exchange during the last synthetic step. All synthesized compounds show interesting characteristics for various applications in the field of energetic materials as energetic plasticizers or as melt-cast explosives. The compounds were extensively analyzed by IR, EA DTA, and multinuclear NMR spectroscopy. Furthermore, the solid compounds 4,4′,5,5′-tetrakis(azidomethyl)-3,3′-bisisoxazole (**2**) and 3,3′-bis(azidomethyl)-5,5′-bis(1,2,4-oxadiazole) (**4**) were characterized using X-ray diffraction. In addition, the sensitivities toward friction and impact were determined with BAM standard techniques, and the energetic performances of all synthesized azido-methyl compounds were calculated using the EXPLO5 code. The properties were compared to recently published, structurally related compounds.

4.1 Introduction

Azide-containing compounds have been indispensable in many areas of chemistry[1] since the discovery of the azide anion by Curtius in 1890.[2] Despite the toxicity of the azide anion,[3] it remains an essential molecular building block and has a great synthetic approach in organic chemistry.[4] Moreover, as an anion or functionality, azides offer unrivaled and unique properties. Traditionally, azides are widely used in addition[5] or substitution[6-7] reactions, as well as in cycloaddition reactions for the production of nitrogen-rich heterocycles, such as 1,2,3-triazoles[8-10] and tetrazoles.[11-12] The azide source for these reactions is mostly NaN_3 or trimethylsilylazide ($TMSN_3$), which are cheap well-manageable chemicals. In addition, there are numerous reactions that benefit from the conversion of azides to isocyanates,[13] nitrenes,[14] or amines.[15] Therefore, azides are included in numerous substances or at least used as intermediates or reagents toward the synthesis. Nevertheless, many chemists are frightened by the compounds themselves or the use thereof in general since organic azides can have explosive properties.[1]

There are various empirical rules, for example, the “Smith rule” or the “rule of six”, which states that “six carbons (or other atoms of approximately equal size) per energetic functional group (azide, diazo, nitro, etc.) should provide sufficient dilution to make the compound relatively safe under appropriate controls and safety procedures”.[4] However, such rules are guidelines, and one must consider the potential hazards associated with newly prepared azides de novo. Properly characterized and handled organic azides in the form of azido-alkyl functions see widespread use and provide a useful platform for their utilization as energetic materials.[16-18]

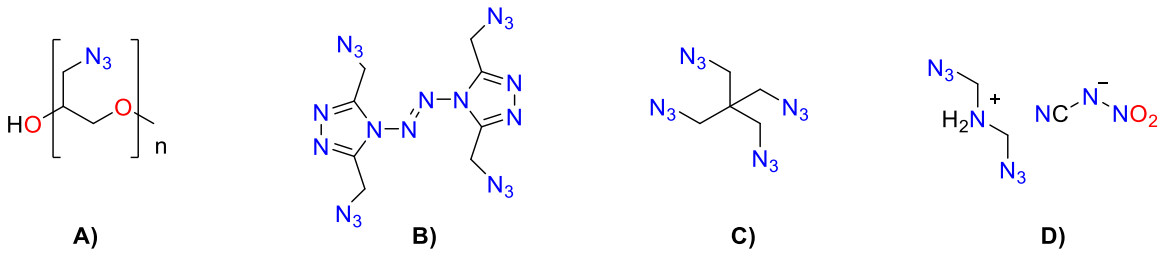

Figure 1. Representative examples for energetic organic compounds containing an alkylazido function: GAP (**A**), 3,3′,5,5′-tetra(azidomethyl)-4,4′-azo-1,2,4-triazole (**B**), tetraazido pentaerythritol (**C**), and bis(2-azidoethyl)dimethylammonium nitrocyanamide (**D**).

For energetic materials, the high heat of formation inserted by azides (about 360 kJ mol^{-1})[19] and the high nitrogen content, that is inherent in the compound, are exploited in particular. In the research for new green explosives, the azide functionality is advantageous since the resulting polyazides often have low solubility in water, and mainly dinitrogen is formed during combustion.[20]

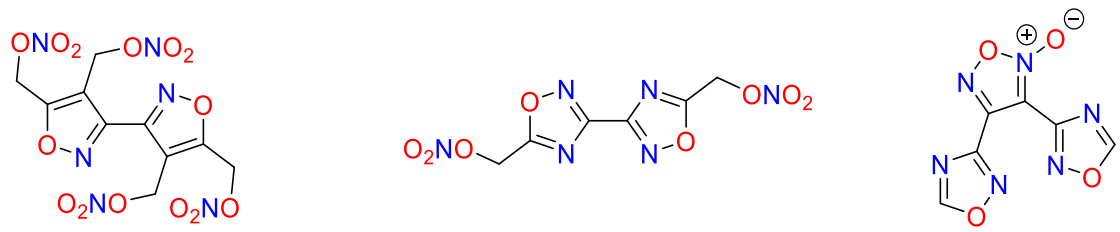

Figure 2. Molecular structures of recently published melt-cast explosives based on isoxazole and oxadiazole scaffolds including tetrakisnitratomethylbisisoxazole (TNMBIO) (**E**), dinitratomethylbisoxadiazole (DNMBO) (**F**), and bisoxadiazolylfuroxan (**G**).

Figure 1 shows some azido-methyl-containing compounds that are widely used in almost all fields of high-energy materials such as energetic polymers (**A**),[21] energetic plasticizers (**B**),[22] initial explosives (**C**),[23] or hypergolic liquids (**D**).[24] Yet, there are few examples of heterocyclic-based molecules that contain azido-alkyl units.[22] However, recently intensively investigated heterocyclic compounds that utilize nitrato-methyl groups, among others as an energy-delivering source, were denoted as promising energetic substances in the field of melt-cast explosives.[25-29] The chemical structures of the mentioned compounds are depicted in Figure 2. These possible TNT replacements are based on isoxazoles and oxadiazoles, which are characterized above all by high thermal stability and easy chemical availability and synthesis. Even so, they contribute to energy performance through their NO content.[30-32]

In this study, we present the combination of an azide functionality with established scaffolds to create a new class of low-melting azido-methyl-based explosives.[33] By the structural similarity toward compounds (**E**)–(**G**), it was assumed that some properties might be identical or even better.

4.2 Results and Discussion

4.2.1 Synthesis

Starting with known literature precursors reported by Wingard et al.,[25] the respective chloromethyl compound **1** was synthesized through classical chlorination reaction with thionyl chloride in pyridine at reflux conditions (Scheme 1). A subsequent chlorine–azide exchange yielded **2** in 77% yield. In order to achieve complete conversion of the product, the reaction was stirred at 90 °C for 12 h in water and was then purified by flash column chromatography. Due to the low melting point of 28 °C, it was obtained as oil and solidified by adding a seed crystal at low temperatures.

Compound **4** was previously discovered through a different synthetic pathway by Zhan et al.[34] but was investigated intensively for the first time in this study. Starting from diaminoglyoxime, a chloroacetyl unit was added under basic conditions to the oxime functionality by the reaction with the corresponding acid chloride (Scheme 2).

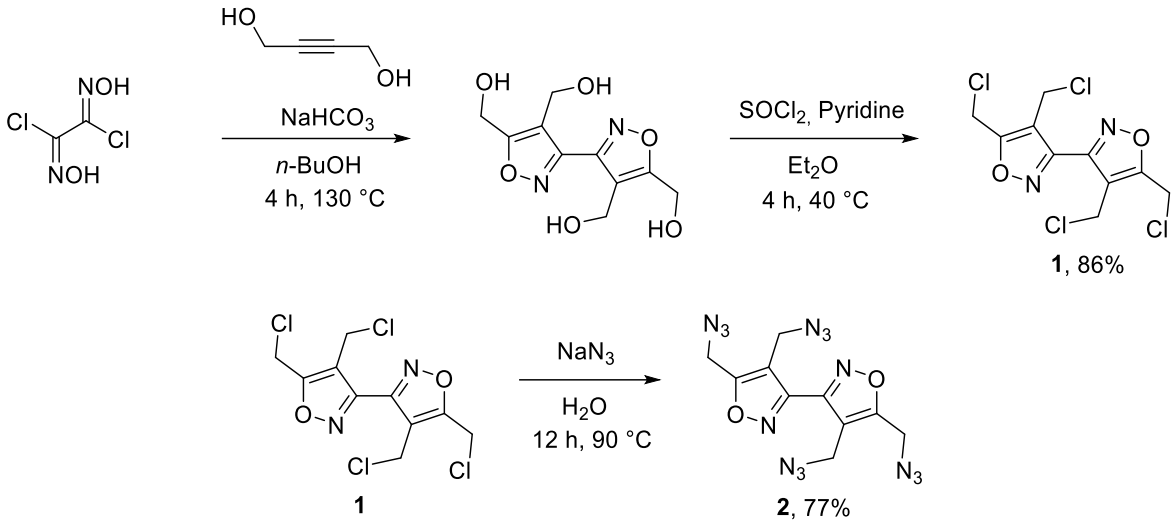

Scheme 1. Synthesis of **2** via chloromethyl derivative **1**.

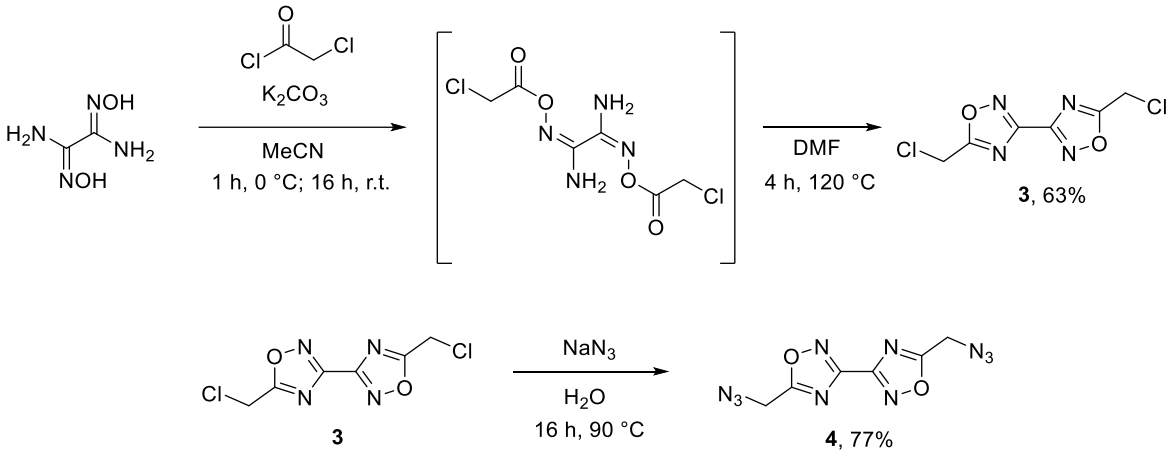

Scheme 2. Synthesis of **4** via chloromethyl derivative **3**.

For the subsequent condensation reaction for the formation of the 1,2,4-oxadiazole units, the solvent was required therefore to be switched from MeCN to DMF since reaction temperatures above 100 °C are required. After chlorine–azide exchange in water, the crude product was recrystallized from hot water to yield pure **4** in 77% yield.

The heterocyclic motif of **6** and **8** is a known scaffold for energetic materials. By combining two oxadiazoles through a furoxane or furazane moiety, a high energy content is stored in a molecule that is nevertheless relatively thermally stable and dense.[30, 35] BNFF and its reduced form BNFFa, which are considered as new-generation melt-cast explosives, have therefore been investigated in detail by many research groups.[36-38] Compounds are synthesized mainly starting from

malononitrile.[39] Here, the 1,2,4-oxadiazole ring closure was performed similarly for **5** by a reaction of chloroacetyl chloride with bisaminohydroximoylfuroxane in toluene.[40] To obtain both the furoxan and furazan-containing derivatives as linkers, a reduction of the furoxan ring was performed in hydrochloric acid and tin(II) chloride as a reducing agent to yield compound **7**. The chlorine–azide exchanges for **6** and **8** were performed in acetonitrile with a reaction time of 120 h for both compounds. Trying to shorten the reaction time by heating led to the decomposition of the compounds. After flash column chromatography, **6** and **8** were obtained as yellowish oils. The synthetic pathway is depicted in Scheme 3.

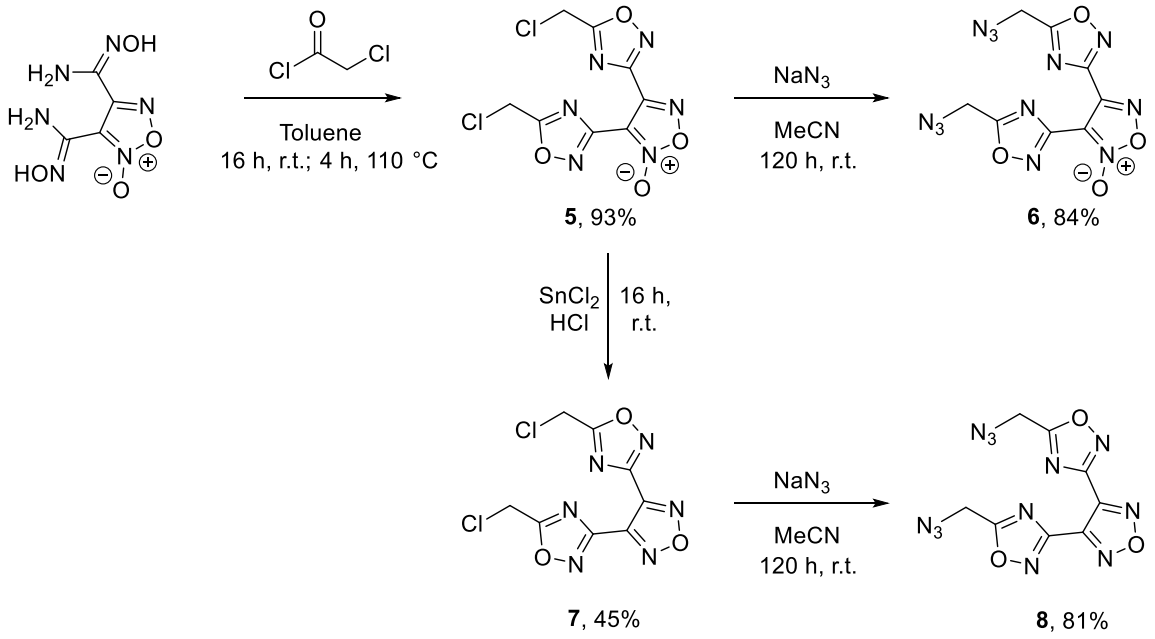

Scheme 3. Synthesis of **6** and **8**.

4.2.2 Spectroscopy

All azido-methyl compounds were characterized with multinuclear NMR, mass spectrometry, and vibrational spectroscopy (IR). Additionally, the thermal behavior was determined by differential thermal analysis (DTA) measurements, and the purity grade was checked by CHN elemental analysis.

The IR spectra of the azido-methyl compounds show strong characteristic azide stretching frequencies in the range between 2200 and 2050 cm^{-1}. For **2**, a broadened band is visible, which indicates an overlap of the two different azide moieties.

Due to the poor solubility or decomposition reactions, different solvents were used for the NMR measurements of the azido-methyl compounds, so no clear continuous trend in the shift of the NMR resonances compared to the chloromethyl precursors can be established.

In the ^{1}H and $^{13}C\{^{1}H\}$ spectra of all chloromethyl precursors, proton signals of the methylene groups are found between 5.27 and 4.82 ppm as sharp singlets, and carbon signals appear in a range of 33.7–32.1 ppm. For the azido-methyl moieties, the CH_2 resonances are found between 5.03 and 4.70 ppm in the proton spectra and between 45.2 and 41.8 ppm for the carbon spectra. The remaining heterocyclic carbon signals appear in a range typical for the respective heterocycles.[25-27]

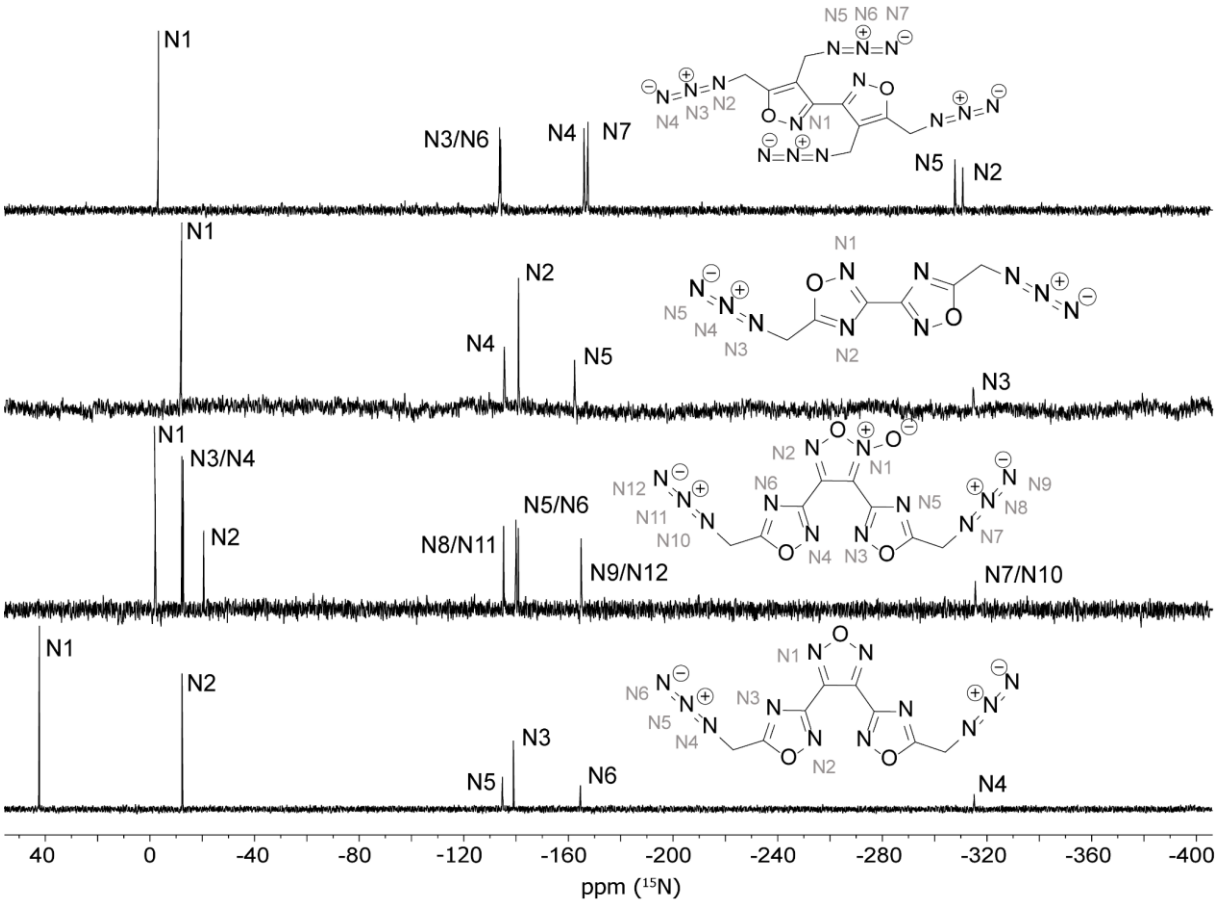

Figure 3. Proton-coupled ^{15}N NMR spectra and assignment of the signals of **2** measured in DMSO-d_6, **4** measured in $CDCl_3$, and **6** and **8** measured in acetone-d_6, respectively.

Proton-coupled ^{15}N measurements were carried out for all azido-methyl compounds and are shown in Figure 3. **2** shows seven sharp signals. The one at −3.2 ppm is assigned to the isoxazole moiety. For the azide resonances, the three

typical signals occur in pairs due to their similar surroundings at −310.8 and −307.7 ppm for N_α, −167.5 and −166.0 ppm for N_γ, and −134.1 and −133.7 ppm for N_β and are therefore in the same range as other azido-methyl compounds.[41] The assignment of N_α and N_γ of the different azido groups was possible by information gained from 2D NMR spectroscopy measurements. These spectra can be found in the Supporting Information.

The spectra, especially those with azido-methyl-1,2,4-oxadiazole units (**4**, **6**, and **8**), show great similarities. The azide signals are located in close ranges from −314.7 to −315.5 ppm for N_α, −162.3 to −164.9 for N_γ, and −134.7 to −135.5 ppm for N_β. Due to the ^3J coupling with the methylene protons, the latter are split into triplets with coupling constants between 4.3 and 4.5 Hz.

Compound **6** is expected to show six azide signals due to the lack of symmetry in the molecule, which, however, are overlapping because of the small difference in their chemical environment. In the oxadiazole units, in contrast to the azide resonances, two different signals for C*N*C (−139.9 and −140.9 ppm) and O*N*C (−12.2 and −12.8 ppm) are still detectable. The remaining heterocyclic signals for 1,2,4-oxadiazole, furoxan, as well as furazan nitrogen atoms show typical shifts.[30, 42]

4.2.3 X-Ray Diffraction

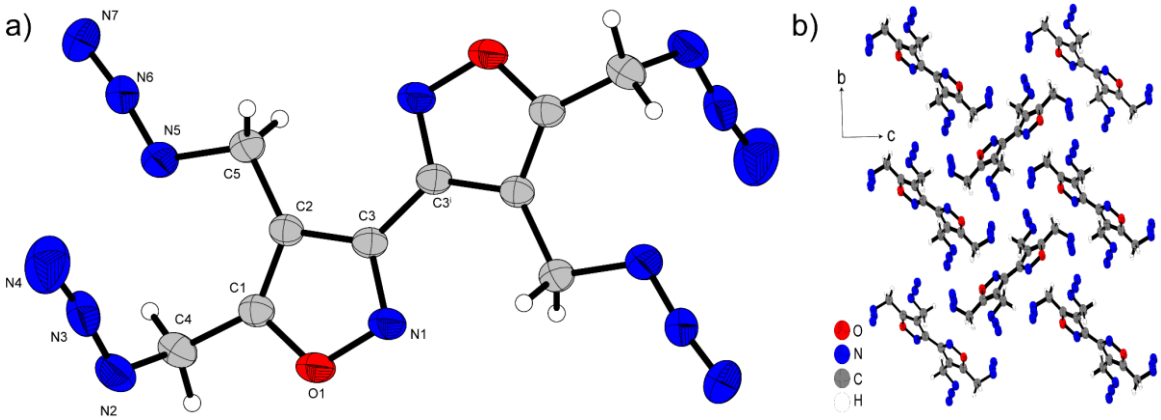

Figure 4. (a) Molecular unit of compound **2**, showing the atom labeling scheme. Symmetry code: (i) −*x*, 1 − *y*, 1 − *z*. (b) Packing of **2**. Thermal ellipsoids represent the 50% probability level, and hydrogen atoms are shown as small spheres of arbitrary radius. Selected bond lengths [Å] and angles [°]: N1–O1 1.3921(17), N1–C3 1.3135(18), O1–C1 1.3594(17), C1–C2 1.3571(19), C1–C4 1.489(2), N3–N2–C4 115.34(13), N2–C4–C1 113.28(13), N5–N6–N7 172.93(16), N2–N3–N4 172.00(19), and O1–C1–C2-C5 179.67(14).

Single crystals suitable for X-ray diffraction experiments for all chloromethyl precursors **1**, **3**, **5**, and **7** (for more information check the Supporting Information) and for azido-methyl derivatives **2** and **4** were obtained by slow evaporation or recrystallization from different common solvents.

Compound **2**, recrystallized from hot methanol, crystallizes in the monoclinic space group $P2_1/n$ with a cell volume of 753.41(5) Å^3 and two formula units per cell. The cell constants are a = 6.9324(3) Å, b = 8.6045(3) Å, and c = 12.6400(5) Å, while the density is 1.571 g cm^{-3} at 298 K. The structure is shown in Figure 4. As expected from structurally similar literature-known compounds, the molecule shows planar assembly of the isoxazole rings. Similarly, the angle of O1–C1–C2–C5 179.67(14)° illustrates that the methylene groups are planar with respect to the ring system. Apart from hydrogen atoms, only the azide groups are twisted out of the plane by 115.34(13)° for N3–N2–C4 and 113.28(13)° for N2–C4–C1. The bond angles of the azides N5–N6–N7 (172.93(16)°) and N2–N3–N4 (172.00(19)°) are also in the range of literature-known azide groups due to negative hyperconjugation. The bond distances in the isoxazole rings are in ranges between single and double bonds with N–O (1.3921(17) Å), N–C (1.3135(18) Å), O–C (1.3594(17) Å), and C–C (1.3571(19) Å) for heterocyclic aromatic compounds.[25]

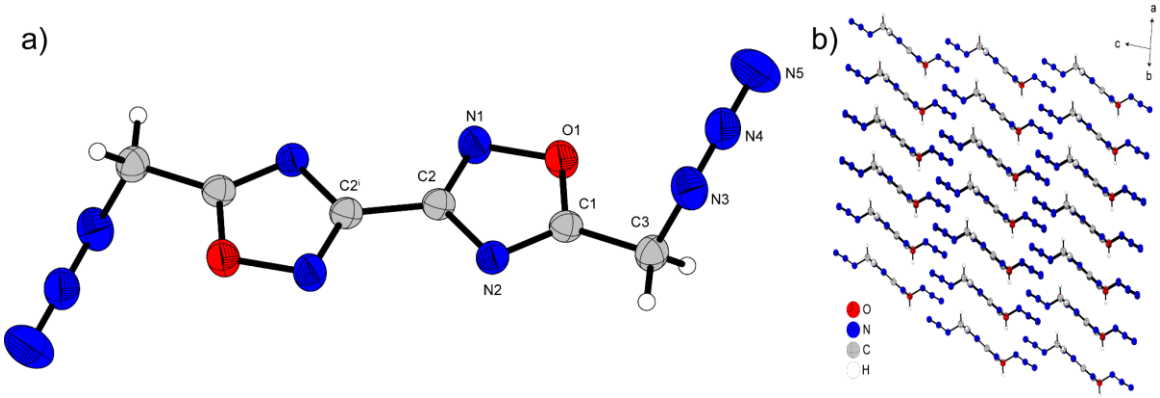

Figure 5. (a) Molecular unit of compound **4**, showing the atom-labeling scheme. Symmetry code: (i) 1 – x 1 – y, −z. (b) Packing of **4**. Thermal ellipsoids represent the 50% probability level, and hydrogen atoms are shown as small spheres of arbitrary radius. Selected bond distances [Å] and angles [°]: N3–N4 1.237(2), N4–N5 1.138(3), C1–N2 1.292(2), N3–N4–N5 173.5(2), C1–C3–N3 110.70 (16), C1–N2–C2 101.84(12), N2–C1–C3–N3 110.88(19), and O1–C1–C3–N3 66.8(2).

Compound **4**, recrystallized from acetone, crystallizes in the triclinic space group P–1 with one formula unit per cell and a density of 1.649 g cm^{-3} at 299 K. The cell constants are a = 3.9473(3) Å, b = 6.7158(4) Å, and c = 10.1067(6) Å, while the

volume is 249.92 Å^3. The structure is depicted in Figure 5. The heterocyclic rings show clear signs of aromaticity, as the respective bond lengths correspond to the range between single and double bonds (N2–C2 1.3713(18) Å, O1–C1 1.3385(16) Å, O1–N1 1.403(2) Å). The two aromatic 1,2,4-oxadiazole rings form a plane from which the azide moieties twist out with a torsion angle of 81.5(2)° (N4–N3–C3–C1). Due to negative hyperconjugation, the azide function shows an angle of 173.5(2)° (N3–N4–N5). **4** forms a layer-like structure in which the azides and the ring systems are superimposed, respectively. The structure results from the medium–strong hydrogen bridges C3–H3A···N1 (2.699(18) Å), C3–H3A···N2 (2.779(18) Å), and C3–H3B···N3 (2.580(19) Å).

4.2.4 Physico-chemical Properties

The results of the computed detonation properties of azides **2**, **4**, **6**, and **8**, together with the calculated energies of formation (details in the Supporting Information) and the corresponding sensitivities, can be found in Table 1.

All synthesized compounds are characterized by very high positive enthalpies of formation (1377.8 kJ mol^{-1} for **2**, 781.5 kJ mol^{-1} for **4**, 1079.9 kJ mol^{-1} for **6**, and 1072.9 kJ mol^{-1} for **8**), which is a typical feature of organic azides. The limit of “the rule of six” mentioned in the introduction is not even remotely reached by any of the synthesized compounds, yet most of them are classified as nonhazardous.

The tetra-functionalized bisisoxazole derivatives show approximately equal values for impact and friction sensitivity, which are comparable to those PETN (IS = 3.5 J, FS = 60 N). For the friction sensitivity of the tetraazido-methyl derivative **2**, a higher sensitivity was expected. However, due to the low melting point, it can be assumed that liquefaction occurs during the performance of the friction test, and thus the sensitivity decreases. The decomposition point of both compounds is slightly above 190 °C, whereas the melting point is lowered by almost 100 °C by the four azide groups compared to the four nitrate groups (Figure 4). **2** shows a calculated detonation velocity that outperforms TNT (V_{det} = 7147 m s^{-1}) but is clearly below the one of TNMBIO (V_{det} = 7847 m s^{-1}).[25] The huge difference compared to the nitrato-methyl derivative mainly results from the distinction of the density of about 0.2 g cm^{-3}.

Table 1. Physicochemical properties and EXPLO5 calculation results of **2**, **4**, **6** and **8** in comparison with nitrato-methyl compounds TNMBIO and DNMBO as well as TNT.

	2	TNMBIO[25]	**4**	DNMBO[26]	**6**	**8**	TNT
Formula	$C_{10}H_8$ $N_{14}O_2$	$C_{10}H_8$ N_6O_{14}	C_6H_4 $N_{10}O_2$	C_6H_4 N_6O_8	C_8H_4 $N_{12}O_4$	C_8H_4 $N_{12}O_3$	C_7H_5 N_3O_6
M [g mol^{-1}]	356.27	436.20	248.17	288.01	332.20	316.20	227.13
IS [J][a]	2	3	>40	8	20	40	15
FS [N][b]	64	60	>360	282	-	-	>360
ESD [J][c]	0.040	0.063	0.060	0.125	-	-	>0.25
ρ (298K)[g cm^{-3}]	1.571[d]	1.786	1.649[d]	1.831	1.80[p]	1.75[p]	1.65
N [%][e]	55.0	19.3	56.4	29.2	50.6	53.2	18.5
Ω [%][f]	−98.8	0	−77.4	0	−67.4	−75.9	−24.7
T_{melt} [°C][g]	28	122	70	85	n.d.	n.d.	80
T_{dec} [°C][g]	192	194	209	183	210	193	295
$\Delta_f H^\circ$ [kJ mol^{-1}][h]	1377.8	−395.0	781.5	−79.4	1079.9	1072.9	−59.3
			EXPLO5 V6.05.02				
$-\Delta_{Ex} U^0$ [kJ kg^{-1}][i]	4655	5086	4256	4884	5127	4759	4426
T_{det} [K][k]	3305	3604	3202	3565	3714	3506	3222
V_0 [L kg^{-1}][l]	688	661	702	675	676	672	633
P_{CJ} [kbar][m]	198	268	192	281	261	227	194
V_{det} [m s^{-1}][n]	7147	7847	7221	8119	8071	7672	6823
I_S [s][o]	222	236	219	236	224	226	-

[a] Impact sensitivity (BAM drophammer (1 of 6)). [b] Friction sensitivity (BAM friction tester (1 of 6)). [c] Electrostatic discharge device (OZM research). [d] From X-ray diffraction analysis recalculated to 298K. [e] Nitrogen content. [f] Oxygen balance with respect to CO. [g] Decomposition temperature; Melting point (DTA; β = 5 °C min^{-1}). [h] Calculated enthalpy of formation. [j] Energy of explosion. [k] Detonation temperature. [l] Volume of detonation products (assuming only gaseous products). [m] Detonation pressure at Chapman-Jouguet point. [n] Detonation velocity. [o] Specific impulse under isobaric (60 bar) conditions. [p] Recalculated from Chloromethyl precursors.

In contrast to DNMBO, which has moderate sensitivities toward impact and friction (IS = 8 J, FS = 282 N), diazidomethyl-bisoxadiazole (**4**) is absolutely insensitive (IS > 40 J, FS > 360 N). Only the sensitivity to electrostatic discharge of **4** is higher (ESD = 60 mJ) compared to the nitrato-methyl derivative (ESD = 125 mJ). Thermal

analysis was carried out using DTA experiments. The related plots for azidomethyl compounds **2**, **4**, **6**, and **8** are shown in Figure 6. The thermochemical properties of the two bisoxadiazole compounds are very similar.

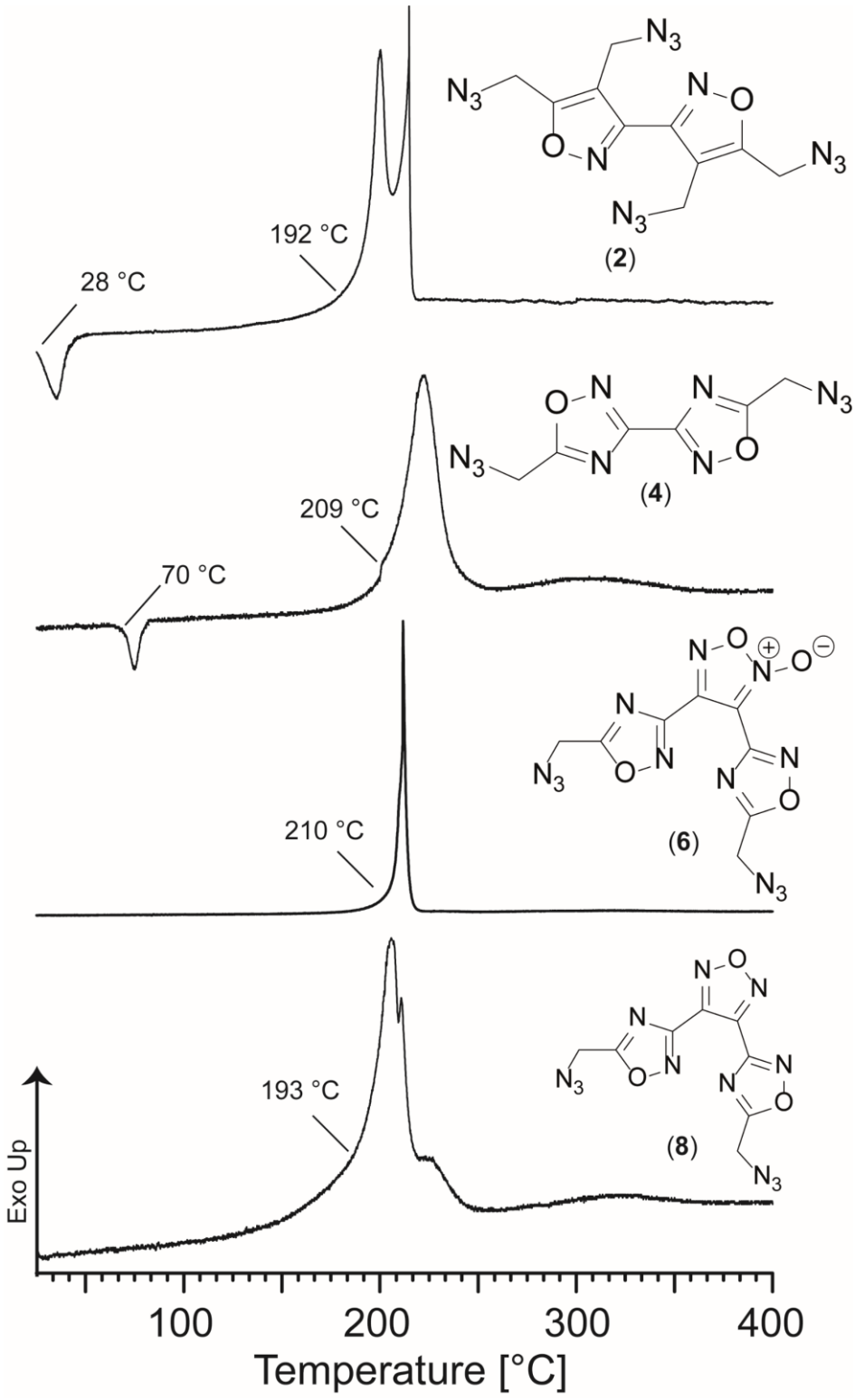

Figure 6. DTA plots of compounds **2**, **4**, **6**, and **8** measured with a heating rate of 5 °C min^{-1}. Melting (endo) and decomposition (exo) points are given as onset temperatures.

Thus, **4** has a melting point in a range similar to the corresponding nitrate ester but with a decomposition point of 209 °C, a significantly higher stability than DNMBO (T_{dec} = 183 °C).[26]

By substitution of the nitrate group through azide, the same effect is observed as with the compound pair **2**/TNMBIO but to a much weaker extent. The same trend can be seen for the density and the strongly associated detonation parameters. Compound **4** has a density of 1.649 g cm^{-3} coupled with a detonation velocity of 7221 m s^{-1}, which exhibits the same trend compared to the corresponding nitrato-methyl derivative (DNMBO), decreasing the density by about 0.2 g cm^{-3} and the detonation velocity by about 900 m s^{-1}. Nevertheless, **4**, like DNMBO, outperforms TNT and shows suitable properties for use as a melt-cast explosive.

Since **6** and **8** are liquids at room temperature, both compounds were only tested toward their impact sensitivity. The impact sensitivity of **6** is 20 J, whereas **8** only shows slight signs of decomposition at a value of 40 J. The decomposition temperature for both compounds is in the range of 200 °C, whereby **6** is marginally more stable and decomposes distinctly more sharply. Despite the flat slope of the curve of **8**, no significant mass loss is observed, which was confirmed by TGA measurements (TGA graphs of **6** and **8** are shown in the Supporting Information). The densities of **6** and **8** were predicted from the crystal structures of the chloromethyl precursors **5** and **7**, respectively. A comparison of the densities obtained by comparing the densities of various chloromethyl to azido-methyl compounds was considered. The detonation velocities calculated from these densities are in the range of 8071 m s^{-1} for **6** and 7672 m s^{-1} for **8**. As expected, the values of furoxan derivative **6** are generally higher than those of the corresponding furazan derivative **8**, which is related to the higher density caused by the *N*-oxide, which additionally delivers more energy to the system. Both substances would be suitable as energetic plasticizers due to their physicochemical properties.

With the crystal structures of **2** and **4** as well as the respective nitrato-methyl compounds TNMBIO and DNMBO in hand, a more in-depth analysis of the different sensitivities, which includes the influence of the functional groups, could be carried out. Hence, Hirshfeld surfaces, based on the respective crystal structures of the compounds, were created. (Figure 7). The thereof generated 2D

fingerprint plots indicate the distance and type of interaction toward the surrounding atoms in the crystal neighborhood with respect to d_i + d_e (d_i: distance from the Hirshfeld surface to the nearest atom interior; d_e: distance from the Hirshfeld surface to the nearest atom exterior).[43] Depending on the type, amount, and strength of the respective interactions, relative conclusions about the different sensitivities of similar compounds can be drawn.[44]

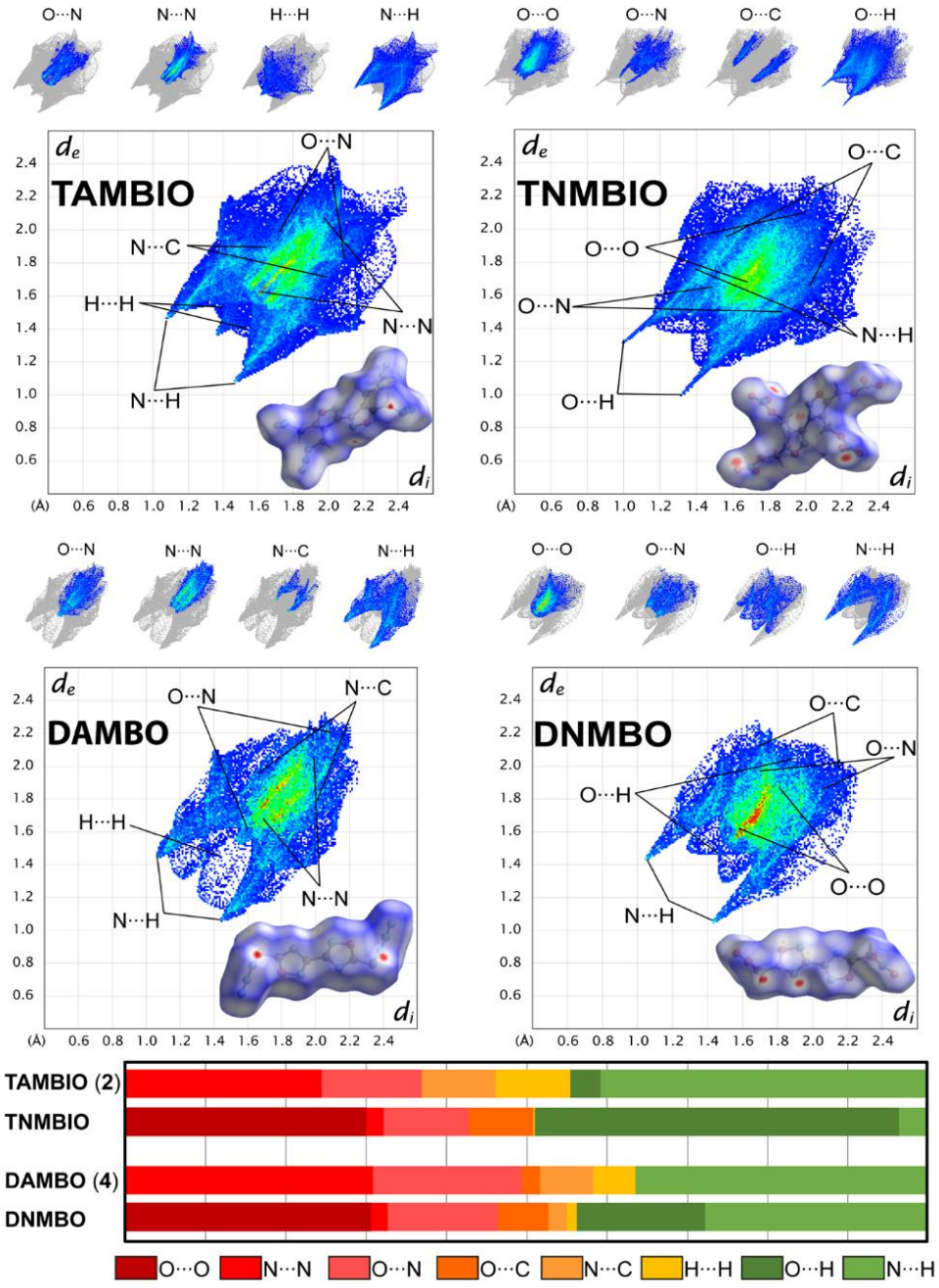

Figure 7. Two-dimensional fingerprint plot in crystal stacking as well as the corresponding Hirshfeld surface of TAMBIO (**2**), TNMBIO, DAMBO (**4**), and DNMBO. Population of close contacts below.

In most cases, a large number of equiatomic interactions indicate an increased sensitivity. Since the homoatomic interactions can be assumed to be caused by the same polarization of the atoms, the size of the atoms also plays a decisive role. Therefore, O···O interactions have a higher destabilizing effect in the crystal lattice than N···N or H···H interactions.[45-46] The same applies to the O···N, C···O, and C···N interactions, whereby these often do not have such a strong influence on the reduced stability toward external mechanical stimuli. The induced destabilization is a result of close contacts within the crystal layering. By shifting the crystal layers against each other, local hotspots are formed by interlayer repulsion. The vulnerable regions for close interactions are marked as red dots in the Hirshfeld plots.

Therefore, it can be concluded that connections with an increased number of red dots or a high frequency of close contacts for repulsive interactions show an increased sensitivity.[47-48]

Intermolecular hydrogen bridges, which result in O···H and N···H interactions, form the majority of the stabilizing interactions and are predominantly found in insensitive compounds. In the case of affecting external stimuli, they hinder the slippage of the crystal layers and thus act preventively against the formation of hotspots. Nevertheless, O···H and N···H contacts create a 3D network and therefore strongly alter the interlayering slide and can sensitize the compounds. However, replacing hard O···O and N···N contacts by hydrogen bridges often leads to better cushioning of external mechanical stimuli.[49]

However, not only the quantity but also the type of interactions within the crystal layers play an important role for estimating the sensitivities. Even more important for evaluation is the relative strength of the individual interactions, which can be estimated from the position in the 2D plot.[45]

As expected, the main source of positive interactions of the nitrate compounds is O···H, whereas the majority of negative ones is due to O···O contacts. For azides **2** and **4**, N···H and N···N contacts form the predominant interactions. For the bisisoxazole derivatives TNMBIO and **2**, the measured sensitivities are in the same range. TNMBIO has the highest number of positive interactions of all compounds analyzed, splitting into 44.5% O···H and 3.5% N···H. The O···H interactions are presented as some strong interactions (d_i + d_e = 2.6 Å); however, the majority occurs at larger distances. The N···H interactions are completely negligible due to

the high distance. TNMBIO has a relatively large number of destabilizing contacts with 29.3% O···O and 10.4% O···N, which occur in the region around $d_i + d_e$ = 3.2 Å. The intermolecular interactions of **2** are mainly dominated by N···N (23.9%), O···N (11.9%), and N···H (39.0%). Despite the low hydrogen content of the compound, large amounts of destabilizing H···H (8.9%) interactions are observed. TNMBIO shows more, albeit weaker, interactions for both attractive and repulsive interactions compared to **2**, so they can be considered as similarly sensitive.

The repulsive interactions (O···O: 30.5%, O···N: 13.7%, N···N: 2.1%) presented in DNMBO are more abundant than the corresponding attractive ones (O···H: 16.0%, N···H: 27.6%). In general, the high content of O···O in association with low O···H, which forms the strongest interactions due to the highest difference in electronegativity, should be noted. Almost half of all interactions occurring in 4 are due to the negative repulsions of N···N (30.0%) and O···N (18.1%). However, they occur in a range of weak intensity, which makes them rather insignificant. In contrast, 35.3% of N···H interactions occur in a distance range in which medium-strong hydrogen bridges are formed. Therefore, O···O in DNMBO has the predominant importance, destabilizing the compound, which must be weighted more heavily than the N···N and O···N interactions occurring mainly in **4**. Unlike in **4**, there are no strong stabilizing interactions to counteract this trend. For this reason, the sensitivity of DNMBO should be higher than that of **4**, which could also be confirmed by the experimental measurement.

4.3 Conclusion

In summary, four new heterocyclic-based polyazido-methyl compounds were synthesized and characterized intensively. **4** shows promising properties for a melt-cast explosive and therefore as a possible replacement for TNT with T_{melt} = 70 °C and T_{dec} = 209 °C, being thermally more stable than its nitrato-methyl derivative DNMBO. Furthermore, it outperforms TNT in terms of detonation velocity. Comparing **4** with its nitrato-methyl derivative DNMBO, the sensitivities toward impact and friction are significantly lower, but DNMBO has a detonation velocity of 8119 m s^{-1}, nearly 900 m s^{-1} higher than that of DAMBO (**4**). Moreover, **2**, **6**, and **8** show promising values for use as energetic plasticizers. **6** and **8** are presented

as liquids, whereas **2** is available as a at room temperature, melting at 28 °C. The most promising of these three compounds is **6**, which was obtained as a moderately impact-sensitive liquid, stable up to 210 °C. Further investigations and mixtures therewith should be carried out to study its compatibility with other energetic materials in formulations.

4.4 Acknowledgement

The financial support of this work by the Ludwig-Maximilian University (LMU), the Office of Naval Research (ONR), under grant no. ONR N00014-19-1-2078, and the Strategic Environmental Research and Development Program (SERDP) under contract no. W912HQ19C0033 is gratefully acknowledged. The authors thank Stefan Huber for his help with the sensitivity measurement. We further thank Dr. Burkhard Krumm and Prof. Konstantin Karaghiosoff for ^{15}N NMR measurements, Dr. Marco Reichel for proofreading of the manuscript, and Jasmin Lechner for providing TGA measurements.

4.5 References

[1] S. Bräse, C. Gil, K. Knepper, V. Zimmermann, *Angew. Chem. Int. Ed.* **2005**, *44*, 5188–5240, .

[2] T. Curtius, *Ber. Dtsch. Chem. Ges.* **1890**, *23*, 3033–3041.

[3] H. Shan, Y. Chu, P. Chang, L. Yang, Y. Wang, S. Zhu, M. Zhang, L. Tao, *Mol Med Rep* **2017**, *16*, 5938–5946.

[4] H. C. Kolb, M. G. Finn, K. B. Sharpless, *Angew. Chem. Int. Ed.* **2001**, *40*, 2004– 2021.

[5] P. P. Goswami, V. P. Suding, A. S. Carlson, J. J. Topczewski, *Eur. J. Org. Chem.* **2016**, *2016*, 4805–4809.

[6] C. Doebelin, M. Schmitt, C. Antheaume, J.-J. Bourguignon, F. Bihel, *J. Org. Chem.* **2013**, *78*, 11335–11341.

[7] M. Miyashita, T. Mizutani, G. Tadano, Y. Iwata, M. Miyazawa, K. Tanino, *Angew. Chem. Int. Ed.* **2005**, *44*, 5094–5097.

[8] J. Miguel-Ávila, M. Tomás-Gamasa, A. Olmos, P. J. Pérez, J. L. Mascareñas, *Chem. Sci.* **2018**, *9*, 1947-1952.

[9] Y. Bai, X. Feng, H. Xing, Y. Xu, B. K. Kim, N. Baig, T. Zhou, A. A. Gewirth, Y. Lu, E. Oldfield, S. C. Zimmerman, *J. Am. Chem. Soc.* **2016**, *138*, 11077–11080.

[10] F.-H. Cui, J. Chen, Z.-Y. Mo, S.-X. Su, Y.-Y. Chen, X.-L. Ma, H.-T. Tang, H.-S. Wang, Y.-M. Pan, Y.-L. Xu, *Org. Lett.* **2018**, *20*, 925–929.

[11] R. Huisgen, *Angew. Chem.* **1963**, *75(13)*, 604–637.

[12] Y. Boland, D. A. Safin, B. Tinant, M. G. Babashkina, J. Marchand-Brynaert, Y. Garcia, *New J. Chem.* **2013**, *37*, 1174–1179.

[13] G. Gody, C. Rossner, J. Moraes, P. Vana, T. Maschmeyer, S. Perrier, *J. Am. Chem. Soc.* **2012**, *134*, 12596–12603.

[14] R. Liu, O. Gutierrez, D. J. Tantillo, J. Aubé, *J. Am. Chem. Soc.* **2012**, *134*, 6528– 6531.

[15] J. T. Markiewicz, O. Wiest, P. Helquist, *J. Org. Chem.* **2010**, *75*, 4887–4890.

[16] M. H. H. Wurzenberger, M. S. Gruhne, M. Lommel, N. Szimhardt, T. M. Klapötke, J. Stierstorfer, *Chem. Asian J.* **2019**, *14*, 2018–2028.

[17] A. L. Shoaf, C. A. Bayse, *New J. Chem.* **2019**, *43*, 15326–15334.

[18] K. A. McDonald, S. Seth, A. J. Matzger, *Cryst. Growth Des.* **2015**, *15*, 5963–5972.

[19] M. A. Petrie, J. A. Sheehy, J. A. Boatz, G. Rasul, G. K. Surya Prakash, G. A. Olah, K. O. Christe, *J. Am. Chem. Soc.* **1997**, *119*, 8802–8808.

[20] T. M. Klapötke, *Chemistry of High-Energy Materials*, De Gruyter, Boston, Berlin, **2017**.

[21] Vandenburg, E. J. Polyethers containing azidomethyl side chains. U.S. Pat. 3,645,917 (**1972**).

[22] Y. Tang, J. M. Shreeve, *Chem. Eur. J.* **2015**, *21*, 7285–7291.

[23] K. A. Lyssenko, Y. V. Nelubina, D. V. Safronov, O. I. Haustova, R. G. Kostyanovsky, D. A. Lenev, M. Y. Antipin, *Mendeleev Commun.* **2005**, *15*, 232–234.

[24] Y.-H. Joo, H. Gao, Y. Zhang, J. M. Shreeve, *Inorg. Chem.* **2010**, *49*, 3282–3288.

[25] L. A. Wingard, E. C. Johnson, P. E. Guzmán, J. J. Sabatini, G. W. Drake, E. F. C. Byrd, R. C. Sausa, *Eur. J. Org. Chem.* **2017**, *13*, 1765–1768.

[26] E. C. Johnson, J. J. Sabatini, D. E. Chavez, R. C. Sausa, E. F. C. Byrd, L. A. Wingard, P. E. Guzmàn, *Org. Process Res. Dev.* **2018**, *22*, 736–740.

[27] E. C. Johnson, E. J. Bukowski, J. J. Sabatini, R. C. Sausa, E. F. C. Byrd, M. A. Garner, D. E. Chavez, *ChemPlusChem* **2019**, *84*, 319–322.

[28] E. C. Johnson, J. J. Sabatini, D. E. Chavez, L. A. Wells, J. E. Banning, R. C. Sausa, E. F. C. Byrd, J. A. Orlicki, *ChemPlusChem* **2020**, *85*, 237–239.

[29] C. Yan, K. Wang, T. Liu, H. Yang, G. Cheng, Q. Zhang, *Dalton Trans.* **2017**, *46*, 14210–14218.

[30] H. Wei, C. He, J. Zhang, J. M. Shreeve, *Angew. Chem. Int. Ed.* **2015**, *54*, 9367–9371.

[31] Y. Cao, H. Huang, X. Lin, J. Yang, X. Gong, *New J. Chem.* **2018**, *42*, 11390–11395.

[32] P. E. Guzmán, R. C. Sausa, L. A. Wingard, R. A. Pesce-Rodriguez, J. J. Sabatini, *Eur. J. Org. Chem.* **2018**, *2018*, 6724–6728.

[33] S. Schneider, T. Hawkins, M. Rosander, J. Mills, A. Brand, L. Hudgens, G. Warmoth, A. Vij, *Inorg. Chem.* **2008**, *47*, 3617–3624.

[34] L. Zhan-Xiong, O. Yu-Xiang, C. Bo-Ren, *J. Beijing Inst. Tech.* **2001**, *10*, 322–325.

[35] D. Fischer, T. M. Klapötke, M. Reymann, J. Stierstorfer, *Chem. Eur. J.* **2014**, *20*, 6401–6411.

[36] R. Tsyshevsky, P. Pagoria, M. Zhang, A. Racoveanu, A. DeHope, D. Parrish, M. M. Kuklja, *J. Phys. Chem. C* **2015**, *119*, 3509–3521.

[37] Y. Zhang, C. Zhou, B. Wang, Y. Zhou, K. Xu, S. Jia, F. Zhao, *Propellants Explo. Pyrotech.* **2014**, *39*, 809–814.

[38] R. Tsyshevsky, P. Pagoria, M. Zhang, A. Racoveanu, D. A. Parrish, A. S. Smirnov, M. M. Kuklja, *J. Phys. Chem. C* **2017**, *121*, 23853–23864.

[39] P. F. Pagoria, M.-X. Zhang, N. B. Zuckerman, A. J. DeHope, D. A. Parrish, *Chem. Heterocycl. Compd.* **2017**, *53*, 760–778.

[40] L. L. Fershtat, I. V. Ananyev, N. N. Makhova, *RSC Adv.* **2015**, *5*, 47248–47260.

[41] Y.-H. Joo, J. M. Shreeve, *Inorg. Chem.* **2009**, *48*, 8431–8438.

[42] C. He, Y. Tang, L. A. Mitchell, D. A. Parrish, J. M. Shreeve, *J. Mater. Chem. A* **2016**, *4*, 8969–8973.

[43] J. J. McKinnon, M. A. Spackman, A. S. Mitchell, *Acta Crystallogr. Sect. B* **2004**, *60*, 627–668.

[44] Y. Ma, A. Zhang, C. Zhang, D. Jiang, Y. Zhu, C. Zhang, *Cryst. Growth Des.* **2014**, *14*, 4703–4713.

[45] C. Zhang, X. Xue, Y. Cao, Y. Zhou, H. Li, J. Zhou, T. Gao, *CrystEngComm* **2013**, *15*, 6837–6844.

[46] M. Reichel, D. Dosch, T. Klapötke, K. Karaghiosoff, *J. Am. Chem. Soc.* **2019**, *141*, 19911–19916.

[47] J. Zhang, Q. Zhang, T. T. Vo, D. A. Parrish, J. n. M. Shreeve, *J. Am. Chem. Soc.* **2015**, *137*, 1697–1704.

[48] D. E. Dosch, M. Reichel, M. Born, T. M. Klapötke, K. Karaghiosoff, *Cryst. Growth Des.* **2021**, *21*, 243–248.

[49] M. A. Spackman, J. J. McKinnon, *CrystEngComm* **2002**, *4*, 378–392.

4.6 Supporting Information

4.6.1 Experimental Procedure

^{1}H, ^{13}C{^{1}H}, and ^{15}N NMR spectra were recorded on BRUKER AMX 400 instruments. Chemical shifts are referenced with respect to tetramethylsilane (^{1}H/^{13}C{^{1}H}) and nitromethane (^{14}N/^{15}N). Infrared spectra (IR) were recorded in the region 4000–400 cm^{-1} on a PERKIN ELMER Spectrum BX-59343 instrument with a SMITHS DETECTION DuraSamplIR II Diamond ATR sensor. Mass spectra and high-resolution mass spectra (HR-MS) were recorded using electroionization (EI). HR-MS was recorded on a Finnigan MAT 95Q with an Ion-Trap MS/MS system or a ThermoFisher Q EXACTIVE GC Orbitrap GC-MS/MS. Decomposition temperatures were measured via differential thermal analysis (DTA) with an OZM Research DTA 552-Ex instrument and partly by thermal gravimetric analysis (TGA) with a PerkinElmer TGA4000 at a heating rate of 5 °C/min and in a range of room temperature to 400 °C. All sensitivities toward impact (IS) and friction (FS) were determined according to BAM (Bundesanstalt für Materialforschung and Prüfung) standards using a BAM drop hammer and a BAM friction apparatus by applying the 1 of 6 method.[S1] All energetic compounds were tested for sensitivity toward electrical discharge using an Electric Spark Tester ESD 2010 EN from OZM.

Energetic properties have been calculated with the EXPLO5 6.02 computer[S2] code using the RT converted and estimated X-ray density and calculated solid-state heats of formation.

CAUTION! *All investigated compounds are potentially explosive materials. Safety precautions and equipment (such as wearing a leather coat, face shield, Kevlar sleeves, Kevlar gloves, earthed equipment, and ear plugs) must be used during all manipulations of energetic materials.*

4,4′,5,5′-Tetrakis(chloromethyl)-3,3′-bisisoxazole (**1**)

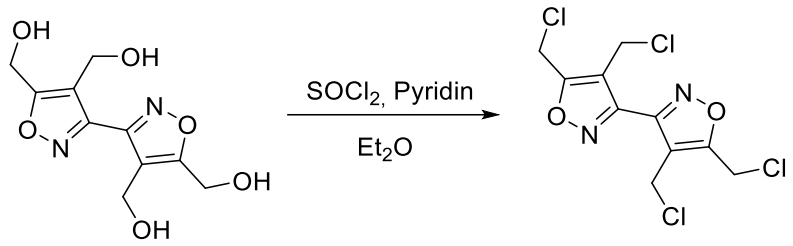

Tetrakis-hydroxymethyl-bisisoxazole (2.00 g, 7.80 mmol, 1.0 equiv) was suspended in Et_2O (40 mL), and $SOCl_2$ (2.10 mL, 34.0 mmol, 4.4 equiv) and pyridine (2.70 mL, 34.0 mmol, 4.4 equiv) were added dropwise. The solution was heated to 40 °C with an oil bath for 4 h, adding more $SOCl_2$ (3.5 g, 2.1 mL, 34 mmol, 4.4 equiv) and pyridine (2.7 g, 2.7 mL, 34 mmol, 4.4 equiv) after 2 h. The brown reaction mixture was filtered and washed with water multiple times. Tetrakis-chloromethyl-bisisoxazole (**1**) was obtained as a brown solid (2.21 g, 6.70 mmol, 86%).

IR (ATR) $\tilde{\nu}$ (cm^{-1}) = 2168(w), 2086(vs), 1620(w), 1438(w), 1418(w), 1337(m), 1265(s), 1221(s), 1179(m), 1139(m), 1067(w), 967(w), 912(m), 879(m), 774(m), 719(m), 654(m), 552(m), 464(m), 438(m), 427(m), 415(m). Elem. Anal. Calcd for $C_{10}H_8N_2O_2Cl_4$: C, 36.40; N, 8.49; H, 2.44. Found: C, 36.60; N, 8.48; H, 2.51. ^{1}H NMR (DMSO-d_6, 400 MHz, ppm): δ = 5.21 (s, 4H), 4.99 (s, 4H). $^{13}C\{^1H\}$ NMR (DMSO-d_6, 100 MHz, ppm): δ = 167.9, 152.9, 114.9, 33.8, 32.6. HR-MS (EI) *m*/*z*: [M] Calcd for $C_{10}H_8N_2O_2Cl_4$ 327.9340. Found: 327.9334.

4,4′,5,5′-Tetrakis(azidomethyl)-3,3′-bisisoxazole (TAMBIO) (**2**)

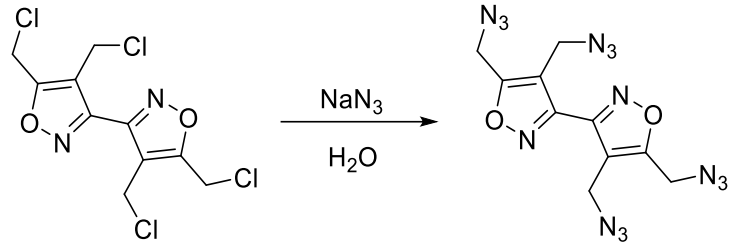

Tetrakis-chloromethyl-bisisoxazole (**1**) (1.00 g, 3.00 mmol, 1.0 equiv) and sodium azide (1.00 g, 15.0 mmol, 5.0 equiv) were solved in water (50 mL) and heated to 90 °C with an oil bath and stirred for 12 h at this temperature. The solution was extracted with EtOAc (3 × 50 mL). The organic phase was dried over anhydrous sodium sulfate, and the product was dried in the air. The crude product was purified by flash column chromatography ($CHCl_3$/NEt_3 99.9%/0.1%). Tetrakis-azidomethyl-bisisoxazole (**2**) was obtained as a slightly brown liquid that crystallized at 4 °C (0.81 g, 2.30 mmol, 77% yield).

DTA (5 °C min^{-1}): 28 °C (melt), 192 °C (dec). Sensitivities: BAM drop hammer: 2 J (<500 µm). Friction tester: 64 N (<500 µm). ESD: 40 mJ (<500 µm). IR (ATR) $\tilde{\nu}$ (cm^{-1}) = 3016(w), 1623(m), 1448(m), 1411(m), 1393(w), 1270(m), 1252(m), 1138(m), 1105(m), 933(s), 898(m), 883(m), 745(s), 706(vs), 683(vs), 638(m), 615(m), 414(w). Elem. Anal. Calcd for $C_{10}H_8N_{14}O_2$: C, 33.71; N, 55.04; H, 2.26. Found: C, 33.66; N, 54.63; H, 2.55. ^{1}H NMR (DMSO-d_6, 400 MHz, ppm): δ = 4.95 (s, 4H), 4.70 (s, 4H). $^{13}C\{^1H\}$ NMR (DMSO-d_6, 100 MHz, ppm): δ = 167.4, 153.0, 111.9, 42.8, 41.6. ^{15}N NMR (DMSO-d_6, 41 MHz, ppm) δ = −3.2, −133.7, −134.1, −166.0, −167.5, −307.7, −310.8. HR-MS (EI) *m*/*z*: [M] Calcd for $C_{10}H_8N_{14}O_2$ 356.0955. Found: 356.0943.

3,3′-Bis(chloromethyl)-5,5′-bis(1,2,4-oxadiazole) (**3**)

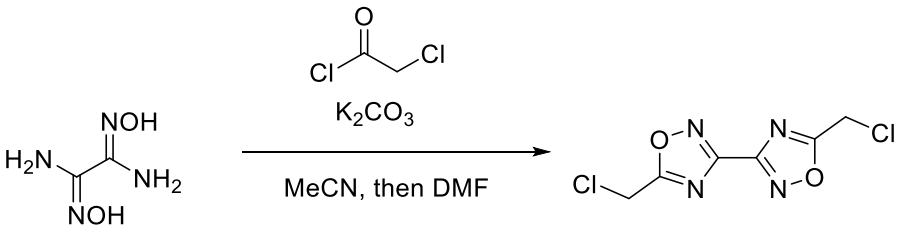

Diaminoglyoxime (2.40 g, 20.3 mmol, 1.0 equiv) was dissolved in acetonitrile (100 mL), and potassium carbonate (5.60 g, 40.6 mmol, 2.0 equiv) was added in one portion. The mixture was cooled to 0 °C with an ice bath, and chloracetyl chloride (6.50 mL, 81.6 mmol, 4.0 equiv) in acetonitrile (20 mL) was added dropwise over 20 min. The mixture was stirred for 1 h at 0 °C and further overnight at room temperature. The solution was quenched on ice water (100 mL), and the white solid was filtered and washed with small amounts of ice water. Afterward, it was solved in DMF (40 mL) and heated with an oil bath for 4 h to 120 °C. After cooling to room temperature, the mixture was quenched on ice water (100 mL) to yield the white powdered crude product. After recrystallization from hot water (60 mL), **3** was yielded as colorless crystalline needles (3.00 g, 12.7 mmol, 63% yield).
IR (ATR) $\tilde{\nu}$ (cm^{-1}) = 3042(w), 2984(w), 1741(w), 1579(s), 1439(m), 1429(m), 1421(m), 1312(m), 1263(m), 1220(vs), 1144(m), 1022(m), 956(m), 933(w), 920(s), 896(m), 778(w), 749(vs), 681(vs), 653(w), 636(m). Elem. Anal. Calcd for $C_6H_4N_4O_2Cl_2$: C, 30.66; N, 23.84; H, 1.72. Found: C, 30.42; N, 23.34; H, 2.02. ^{1}H NMR (DMSO-d_6, 400 MHz, ppm) δ = 5.25 (s, 4H). $^{13}C\{^1H\}$ NMR (DMSO-d_6, 100 MHz, ppm) δ = 177.3, 159.7, 33.7. HRMS (EI) *m*/*z*: [M] Calcd for $C_6H_4N_4O_2Cl_2$ 233.9711. Found: 233.9707.

3,3′-Bis(azidomethyl)-5,5′-bis(1,2,4-oxadiazole) (DAMBO) (**4**)

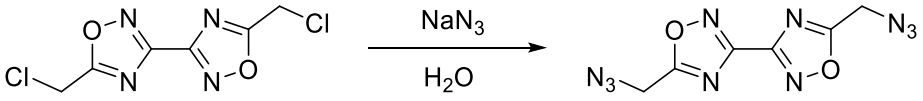

3,3′-Bis(chloromethyl)-5,5′-bis(1,2,4-oxadiazole) (**3**) (500 mg, 2.13 mmol, 1.0 equiv) was dissolved in water (75 mL), and sodium azide (0.43 g, 6.62 mmol, 3.1 equiv) was added. The mixture was heated to 90 °C with an oil bath and stirred overnight. After cooling to room temperature, the solution was extracted with DCM (3 × 50 mL). The organic phase was dried over anhydrous sodium sulfate and evaporated under reduced pressure to yield the crude product, which was recrystallized from hot water (40 mL). 3,3′-Bis(azidomethyl)-5,5′-bi(1,2,4-

oxadiazole) (**4**) was obtained as colorless microcrystals (410 mg, 1.65 mmol, 77% yield).

DTA (5 °C min^{-1}): 70 °C (melt), 209 °C (dec). Sensitivities: BAM drop hammer: >40 J (<500 µm). Friction tester: >360 N (<500 µm). ESD: 60 mJ (<500 µm). IR (ATR) $\tilde{\nu}$ (cm^{-1}) = 3026(w), 2951(w), 2473(vw), 2213(w), 2143(s), 2104(s), 2007(w), 1998(w), 1983(w), 1567(s), 1441(m), 1430(m), 1330(w), 1304(s), 1281(m), 1247(s), 1214(vs), 1196(s), 1196(s), 1054(w), 1038(w), 1024(w), 971(s), 956(m), 915(s), 894(s), 783(s), 688(s), 664(s), 637(s), 555(s), 488(w), 446(w), 430(w), 423(w), 409(m). Elem. Anal. Calcd for $C_6H_4N_{10}O_2$: C, 29.04; N, 56.44; H, 1.62. Found: C, 29.17; N, 55.19; H, 1.86. ^{1}H NMR ($CDCl_3$, 400 MHz, ppm): δ = 4.73 (s, 4H). $^{13}C\{^{1}H\}$ NMR ($CDCl_3$, 100 MHz, ppm): δ = 176.3, 160.0, 45.2. ^{15}N NMR ($CDCl_3$, 41 MHz, ppm): δ = −11.8, −135.5, −140.9, −162.3, −314.7. *m*/*z* (EI+, M = 248.05 g mol^{-1}): 248 (100), 138 (45), 123 (57), 111 (16), 108 (41), 96 (28), 94 (20), 91 (14), 84 (96), 44 (42), 43 (61), 42 (64), 41 (16). HRMS (EI) *m*/*z*: [M] Calcd for $C_6H_4N_{10}O_2$ 248.0519. Found: 248.0516.

3,4-Bis(5-(chloromethyl)-1,2,4-oxadiazol-3-yl)-furoxan (**5**)

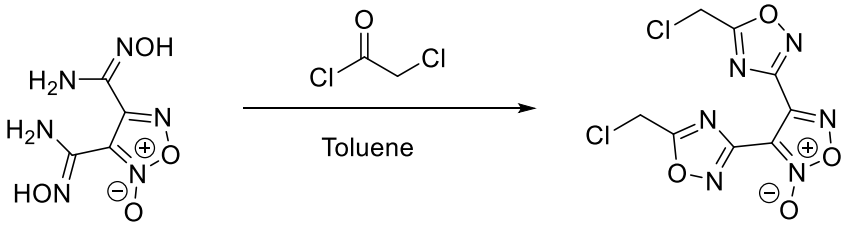

Bisaminohydroximoylfuroxan (2.00 g, 9.90 mmol, 1.0 equiv) was dissolved in toluene (50 mL), and chloracetyl chloride (3.2 mL, 40.2 mmol, 4.1 equiv) in toluene (20 mL) was added dropwise over 20 min. The mixture was stirred at ambient temperature overnight and was subsequently heated to 110 °C with an oil bath and stirred for 4 h at this temperature. After cooling to room temperature, the solvent was evaporated under reduced pressure, and the residue was stirred for 30 min in a mixture of saturated sodium hydrogen carbonate solution (50 mL) and DCM (50 mL). The phases were separated, and the aqueous phase was extracted DCM (2 x 50 ml). The organic phase was dried using sodium sulfate, and the solvent was evaporated under reduced pressure to yield a slightly gray oil, which started to

crystallize after several hours on air, which could be identified as 3,4-bis(5-(chloromethyl)-1,2,4-oxadiazol-3-yl)-furoxan (**5**) (2.94 g, 9.22 mmol, 93%).
IR (ATR) $\tilde{\nu}$ (cm^{-1}) = 3468(w), 3349(w), 3205(w), 3033(w), 2959(w), 2791(w), 1682(w), 1658(m), 1622(vs), 1579(s), 1551(s), 1489(m), 1424(m), 1409(m), 1389(m), 1306(m), 1268(s), 1211(m), 1163(w), 1145(m), 1073(m), 1044(m), 1044(m), 1015(m), 988(m), 972(m), 948(s), 926(s), 902(m), 851(w), 815(s), 788(s), 754(s), 739(s), 690(m), 640(s), 616(m), 571(m), 523(m), 517(m), 496(m), 453(s), 420(s), 412(s), 404(m). Elem. Anal. Calcd for $C_8H_4N_6O_4Cl_2$: C, 30.12; N, 26.34; H, 1.26. Found: C, 29.89; N, 26.01; H, 1.57. ^{1}H NMR (DMSO-d_6, 400 MHz, ppm): δ = 5.27 (s, 2H), 5.23 (s, 2H). $^{13}C\{^1H\}$ NMR (DMSO-d_6, 100 MHz, ppm): δ = 177.0, 176.7, 158.7, 156.7, 145.1, 106.0, 33.5, 33.4. *m*/*z* (EI+, M = 317.97 g mol^{-1}): 290 (22), 288 (24), 193 (14), 183 (12), 183 (11), 108 (35), 77 (17), 61 (14), 58 (26), 58 (22), 51 (14), 51 (10), 49 (48), 43 (100), 43 (79), 42 (20). HRMS (EI) *m*/*z*: [M] Calcd for $C_8H_4N_6O_4Cl_2$ 317.9671. Found: 317.9667.

3,4-Bis(5-(azidomethyl)-1,2,4-oxadiazol-3-yl)-furoxan (DAMBFF) (**6**)

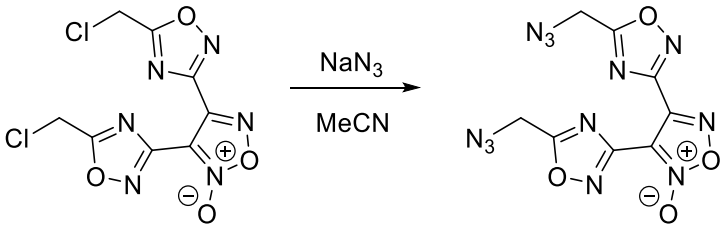

3,4-Bis(5-(chloromethyl)-1,2,4-oxadiazol-3-yl)-furoxan (**5**) (500 mg, 1.57 mmol, 1.0 equiv) was solved in acetonitrile (30 mL), and sodium azide (0.26 g, 4.00 mmol, 2.5 equiv) was added. The mixture was stirred at room temperature for 120 h. Then, the solid was filtered and washed with (2 × 20 mL) of acetonitrile. The filtrate was dried over anhydrous sodium sulfate and reduced at ambient temperature. 3,4-Bis(5-(azidomethyl)-1,2,4-oxadiazol-3-yl)-furoxan (**6**) was yielded as a slightly yellowish oil (440 mg, 1.32 mmol, 84%) after purification by column chromatography using chloroform/ethyl acetate (24:1) and 0.1% NEt_3 as eluent.
DTA (5 °C min^{-1}): 210 °C (dec). Sensitivities: BAM drop hammer: 20 J (liquid). IR (ATR) $\tilde{\nu}$ (cm^{-1}) = 2101(vs), 1624(s), 1577(s), 1557(m), 1430(m), 1391(m), 1330(m), 1271(s), 1208(m), 1073(m), 1045(m), 1011(m), 971(m), 947(m), 910(m), 814(s),

747(m), 665(m), 555(m), 516(m), 469(m), 462(m), 462(m), 433(m), 426(m), 418(m), 402(m). Elem. Anal. Calcd for $C_8H_4N_{12}O_8$: C, 28.92; N, 50.60; H, 1.21. Found: C, 28.38; N, 50.26; H, 1.29. ^{1}H NMR (acetone-d_6, 400 MHz, ppm): δ = 5.02 (s, 2H), 4.97 (s, 2H). ^{13}C{^{1}H} NMR (acetone-d_6, 100 MHz, ppm): δ = 177.1, 176.9, 159.0, 156.9, 145.1, 105.8, 44.8, 44.7. ^{15}N NMR (acetone-d_6, 41 MHz, ppm): δ = −2.1, −12.2, −12.8, −20.6, −135.2, −140.0, −140.9, −164.9, −315.5. *m*/*z* (EI+, M = 332.02 g mol^{-1}): 332 (10), 325 (12), 303 (13), 302 (88), 297 (28), 295 (77), 290 (13), 288 (18), 230 (13), 230 (100), 225 (29), 223 (91), 200 (25), 193 (23), 108 (46), 92 (15), 90 (10), 78 (14), 77 (10), 77 (13), 54 (12), 51 (10), 49 (28), 42 (17). HRMS (EI) *m*/*z*: [M] Calcd for $C_8H_4N_{12}O_4$: 332.0478. Found: 332.0464.

3,4-Bis(5-(chloromethyl)-1,2,4-oxadiazol-3-yl)-furazan (**7**)

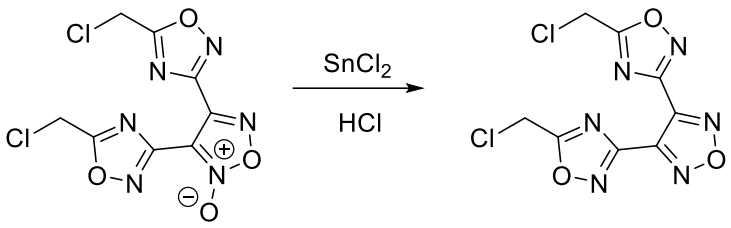

3,4-Bis(5-(chloromethyl)-1,2,4-oxadiazol-3-yl)-furoxan (**5**) (1.00 g, 3.13 mmol, 1.0 equiv) was solved in hydrochloric acid (37%, 20 mL), and tin(II) chloride dihydrate (2.70 g, 12.0 mmol, 3.8 equiv) was added. The mixture was stirred overnight at room temperature, poured on ice water (50 mL), and extracted with DCM (5 × 30 mL). The combined organic phases were dried over anhydrous sodium sulfate and evaporated under reduced pressure to yield 3,4-bis(5-(chloromethyl)-1,2,4-oxadiazol-3-yl)-furazan (**7**) as a white solid (0.43 g, 1.42 mmol, 45%).

IR (ATR) $\tilde{\nu}$ (cm^{-1}) = 3461(m), 3316(m), 3034(m), 2973(m), 1621(s), 1591(s), 1580(s), 1572(s), 1486(m), 1431(m), 1416(m), 1387(s), 1269(m), 1217(m), 1153(m), 1146(m), 1103(vs), 1074(m), 1021(s), 976(s), 953(s), 936(m), 936(m), 924(m), 912(s), 893(m), 873(s), 776(m), 748(s), 726(s), 717(m), 682(m), 652(s), 643(m), 583(m), 569(s), 452(s), 430(s), 407(s). Elem. Anal. Calcd for $C_8H_4N_6O_3Cl_2$: C, 31.71; N, 33.82; H, 1.33. Found: C, 31.43; N, 33.35; H, 1.51. ^{1}H NMR ($CDCl_3$, 400 MHz, ppm): δ = 4.82 (s, 4H). ^{13}C{^{1}H} NMR ($CDCl_3$, 100 MHz, ppm): δ = 176.3,

158.8, 143.7, 33.1. HRMS (EI) *m*/*z*: $[M - H]^-$ Calcd for $C_8H_3N_6O_3Cl_2$ 300.9649. Found: 300.9652.

3,4-Bis(5-(azidomethyl)-1,2,4-oxadiazol-3-yl)-furazan (DAMBFFa) (**8**)

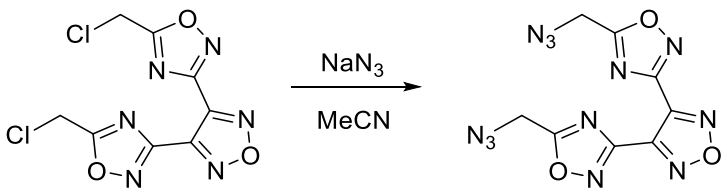

3,4-Bis(5-(chloromethyl)-1,2,4-oxadiazol-3-yl)-furazan (**7**) (0.50 g, 1.65 mmol, 1.0 equiv) was solved in acetonitrile (30 mL), and sodium azide (0.27 g, 4.13 mmol, 2.5 equiv) was added. The mixture was stirred at room temperature for 120 h. The solid was filtered and washed with (2 × 20 mL) of acetonitrile. The filtrate was dried over anhydrous sodium sulfate and reduced at ambient temperature. 3,4-Bis(5-(azidomethyl)-1,2,4-oxadiazol-3-yl)-furazan (**8**) was yielded as a yellowish oil (0.42 g, 1.33 mmol, 81%) after purification by flash column chromatography using ethyl acetate as eluent.

DTA (5 °C min^{-1}): 193 °C (dec). Sensitivities: BAM drop hammer: 40 J (liquid). IR (ATR) $\tilde{\nu}$ (cm^{-1}) = 2933(vw), 2192(w), 2179(w), 2101(vs), 2021(vw), 1723(vw), 1575(m), 1490(w), 1431(m), 1331(m), 1263(s), 1201(m), 1104(s), 1040(w), 1016(m), 979(m), 955(s), 900(s), 767(m), 737(m), 671(m), 622(m), 606(w), 606(w), 554(m), 515(w), 495(w), 482(m), 451(m), 430(m), 423(m), 418(m), 411(m), 405(m). Elem. Anal. Calcd for $C_8H_4N_{12}O_3$: C, 30.39; N, 53.16; H, 1.28. Found: C, 30.55; N, 52.87; H, 1.58. ^{1}H NMR (acetone-d_6, 400 MHz, ppm): δ = 5.03 (s, 4H). $^{13}C\{^1H\}$ NMR (acetone-d_6, 100 MHz, ppm): δ = 178.1, 159.3, 145.2, 45.7. ^{15}N NMR (acetone-d_6, 41 MHz, ppm): δ = 42.1, −12.3, −134.7, −138.9, −164.6, −315.4. HRMS (EI) *m*/*z*: $[M + H]^+$ Calcd for $C_8H_5N_{12}O_3$ 317.0602. Found: 317.0602.

4.6.2 Crystallography

Crystal structure data were obtained from an Oxford Xcalibur3 diffractometer with a Spellman generator (voltage 50 kV, current 40 mA) and a Kappa CCD area for data collection using Mo-*Kα* radiation (*λ* = 0.71073 Å) or a Bruker D8 Venture TXS diffractometer equipped with a multilayer monochromator, a Photon 2 detector and a rotation-anode generator (Mo-K_α radiation). The data collection was performed using the CRYSTALIS RED software.[S3] The solution of the structure was performed by direct methods and refined by full-matrix least-squares on F2 (SHELXT)[S4] implemented in the OLEX2[S5] software suite. The non-hydrogen atoms were refined anisotropically and the hydrogen atoms were located and freely refined. The absorption correction was carried out by a SCALE3 ABSPACK multiscan method.[S6] The DIAMOND2 plots shown with thermal ellipsoids at the 50% probability level and hydrogen atoms are shown as small spheres of arbitrary radius. The SADABS program embedded in the Bruker APEX3 software was used for multi-scan absorption corrections in all structures.[S7]

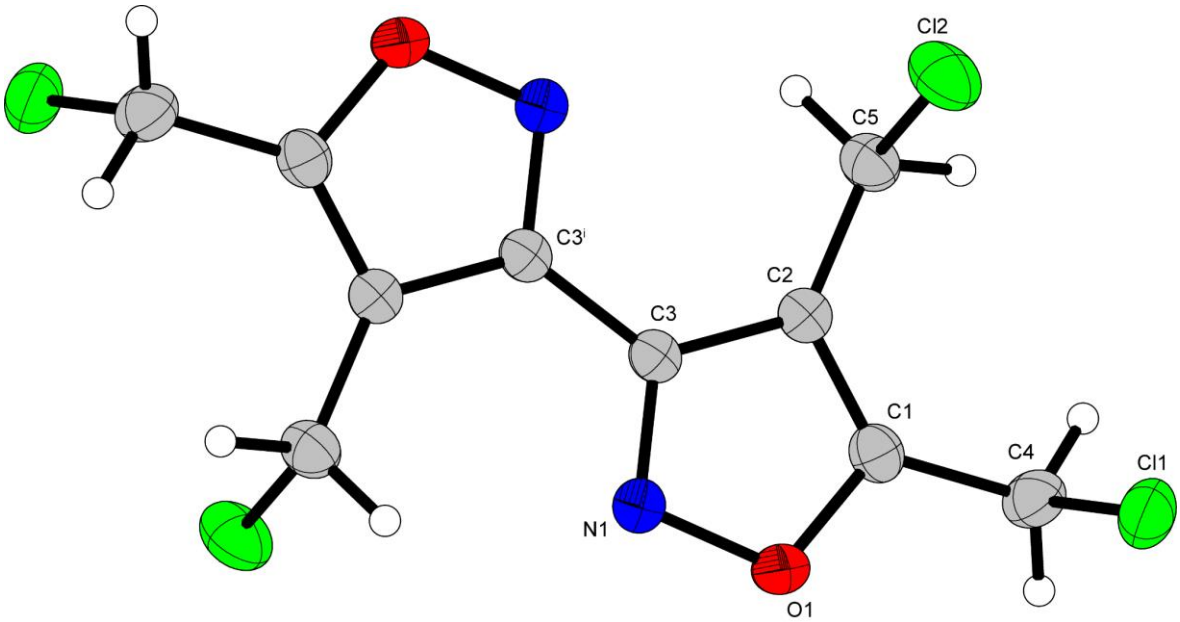

Figure S1. Representation of the molecular unit of **1**, showing the atom-labeling scheme. Thermal ellipsoids represent the 50% probability level and hydrogen atoms are shown as small spheres of arbitrary radius.

1 crystallizes is the monoclinic space group $P2_1/n$ with a cell volume of 651.00(9) Å^3 and two formula units per cell. The cell constants are *a* = 6.8734(5) Å, *b* = 9.3940(7) Å and *c* = 10.3481(8) Å, while the density is 1.683 g cm^{-3} at 123 K.

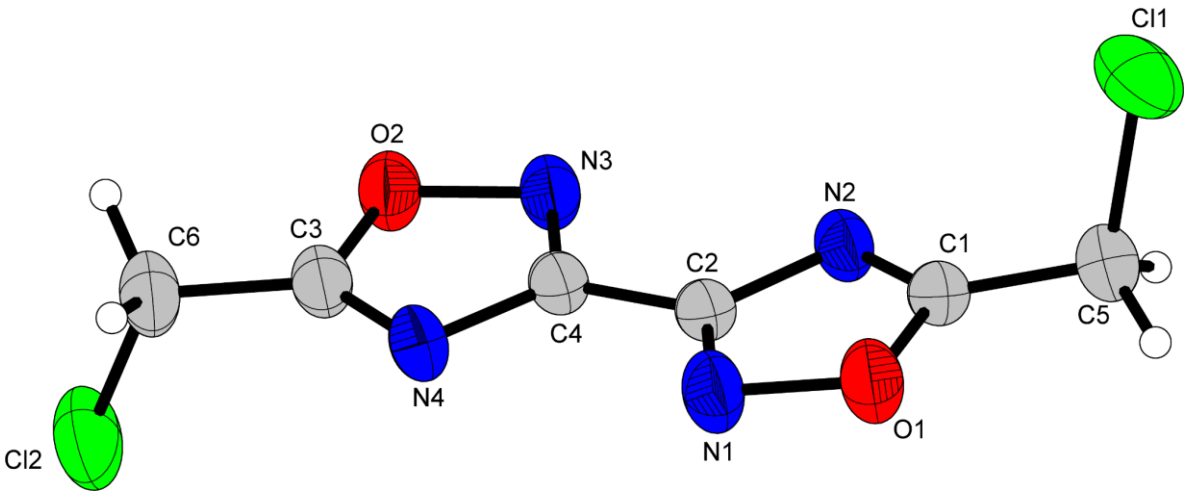

Figure S2. Representation of the molecular unit of **3**, showing the atom-labeling scheme. Thermal ellipsoids represent the 50% probability level and hydrogen atoms are shown as small spheres of arbitrary radius.

3 crystallizes is the monoclinic space group $P2_1/c$ with a cell volume of 1399.84(10) Å^3 and six formula units per cell. The cell constants are a = 8.9213(4) Å, b = 23.4125(9) Å and c = 6.9616(3) Å, while the density is 1.673 g cm^{-3} at 297(2) K. The molecule does not have an intramolecular symmetry like for **1**, **2** and **4**.

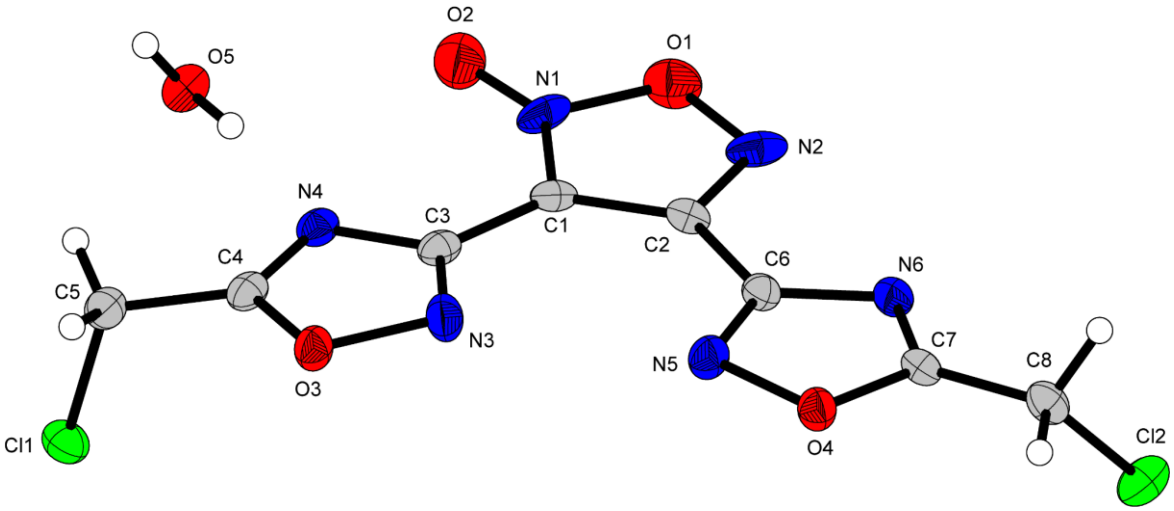

Figure S3. Representation of the molecular unit of **5** · 0.5 H_2O, showing the atom-labeling scheme. Thermal ellipsoids represent the 50% probability level and hydrogen atoms are shown as small spheres of arbitrary radius.

5 crystallizes is the monoclinic space group $C2/c$ with a cell volume of 2369.5(4) Å^3 and four formula units per cell and with the inclusion of 0.5 molecules of water. The

cell constants are a = 30.944(3) Å, b = 4.7670(4) Å and c = 16.2215(16) Å, while the density is 1.839 g cm^{-3} at 103 K.

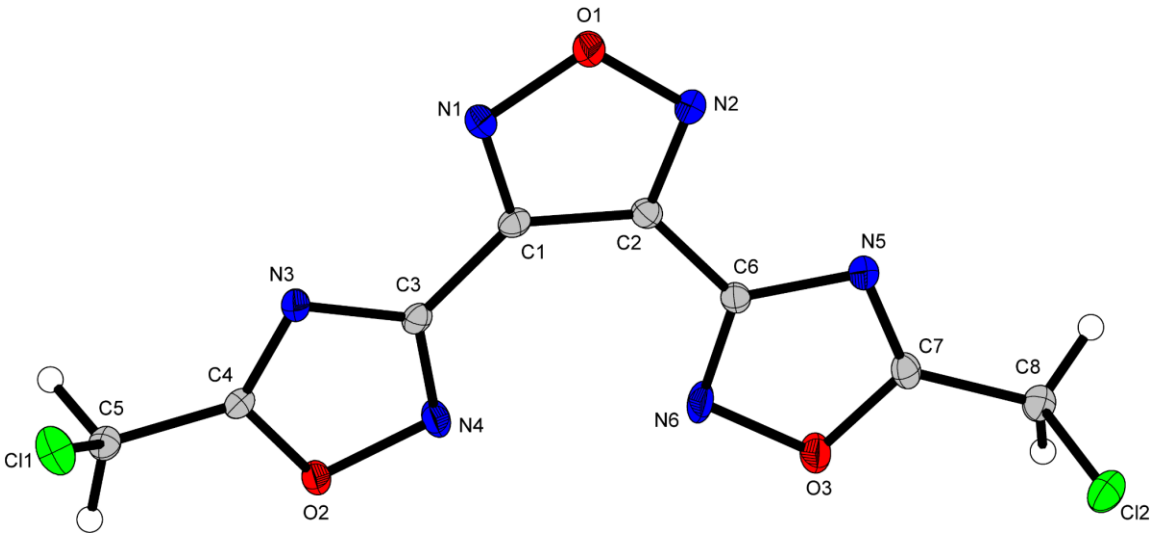

Figure S4. Representation of the molecular unit of **7**, showing the atom-labeling scheme. Thermal ellipsoids represent the 50% probability level and hydrogen atoms are shown as small spheres of arbitrary radius.

Compound **7** crystallizes is the monoclinic space group $P2_1/c$ with a cell volume of 1099.82(9) Å^3 and four formula units per cell. The cell constants are a = 15.6285(8) Å, b = 4.6718(2) Å and c = 16.1306(8) Å, while the density is 1.830 g cm^{-3} at 102 K.

Table S1. Crystallographic data and structure refinement details for the prepared compounds **1**-**3**.

Compound	**1**	**2**	**3**
Formula	$C_{10}H_8Cl_4N_2O_2$	$C_{10}H_8N_{14}O_2$	$C_6H_4Cl_2N_4O_2$
FW [g mol^{-1}]	329.98	356.30	235.03
Crystal system	monoclinic	monoclinic	monoclinic
Space group	$P2_1/n$ (No. 14)	$P2_1/n$ (No. 14)	$P2_1/c$ (No. 14)
Color / Habit	colorless block	colorless block	colorless platelet
Size [mm]	0.05 x 0.20 x 0.40	0.08 x 0.09 x 0.10	0.02 x 0.04 x 0.10
a [Å]	6.8734(5)	6.9324(3)	8.9213(4)
b [Å]	9.3940(7)	8.6045(3)	23.4125(9)
c [Å]	10.3481(8)	12.6400(5)	6.9616(3)
α [°]	90	90	90
β [°]	103.014(8)	92.218(1)	105.697(1)
γ [°]	90	90	90
V [Å^3]	651.00(9)	753.41(5)	1399.84(10)
Z	2	2	6
$\rho_{calc.}$ [g cm^{-3}]	1.683	1.571	1.673
μ [mm^{-1}]	0.902	0.122	0.673
F(000)	332	364	708
$\lambda_{MoK\alpha}$ [Å]	0.71073	0.71073	0.71073
T [K]	123	298	297
θ Min-Max [°]	3.0, 26.4	3.2, 26.4	2.5, 26.4
Dataset	-8: 8 ; -10: 11 ; -10: 12	-8: 8 ; -10: 10 ; -15: 15	-11: 11 ; -29: 29 ; -8: 8
Reflections collected	4730	12801	23236
Independent refl.	1328	1529	2856
R_{int}	0.031	0.027	0.036
Observed reflections	1089	1365	2307
Parameters	98	134	190
R_1 (obs)[a]	0.0396	0.0378	0.0702
wR_2 (all data)[b]	0.1167	0.1013	0.1736
S [c]	1.04	1.09	1.03
Resd. dens [e Å^{-3}]	-0.24, 0.49	-0.19, 0.19	-0.89, 1.09
Device type	Xcalibur Sapphire3	Bruker D8 Venture	Bruker D8 Venture
Solution	SIR-92	SIR-92	SIR-92
Refinement	SHELXL-2013	SHELXL-2013	SHELXL-2013
Absorption correction	multi-scan	multi-scan	multi-scan
CCDC	2058088	2058090	2058086

[a] $R_1 = \Sigma||F_o|-|F_c||/\Sigma|F_o|$; [b] $wR_2 = [\Sigma[w(F_o^2-F_c^2)^2]/\Sigma[w(F_o)^2]]^{1/2}$; $w = [\sigma c^2(F_o^2)+(xP)^2+yP]^{-1}$ and $P=(F_o^2+2F_c^2)/3$; [c] $S = (\Sigma[w(F_o^2-F_c^2)^2]/(n-p))^{1/2}$ (n = number of reflections; p = total number of parameters).

Table S2. Crystallographic data and structure refinement details for the prepared compounds **4**, **5** and **7**.

Compound	**4**	**5**	**7**
Formula	$C_6H_4N_{10}O_2$	$C_8H_4Cl_2N_6O_4 \cdot 0.5\ H_2O$	$C_8H_4Cl_2N_6O_3$
FW [g mol^{-1}]	248.19	328.08	303.07
Crystal system	triclinic	monoclinic	monoclinic
Space group	*P*-1 (No. 2)	*C*2/*c* (No. 15)	$P2_1/c$ (No. 14)
Color / Habit	colorless rod	colorless needle	colorless rod
Size [mm]	0.02 x 0.03 x 0.10	0.06 x 0.07 x 0.62	0.01 x 0.02 x 0.10
a [Å]	3.9473(3)	30.944(3)	15.6285(8)
b [Å]	6.7158(4)	4.7670(4)	4.6718(2)
c [Å]	10.1067(6)	16.2215(16)	16.1306(8)
α [°]	104.873(2)	90	90
β [°]	90.723(2)	98.007(8)	110.960(2)
γ [°]	104.440(2)	90	90
V [Å^3]	249.92(3)	2369.5(4)	1099.82(9)
Z	1	4	4
$\rho_{calc.}$ [g cm^{-3}]	1.649	1.839	1.830
μ [mm^{-1}]	0.133	0.579	0.606
F(000)	126	1320	608
$\lambda_{MoK\alpha}$ [Å]	0.71073	0.71073	0.71073
T [K]	299	103	102
θ Min-Max [°]	3.3, 26.4	2.5, 26.4	3.1, 26.4
Dataset	-4: 4 ; -8: 8 ; -12: 12	-38: 38 ; -5: 5 ; -20: 20	-19: 19 ; -5: 5 ; -20: 20
Reflections collected	4103	13818	17623
Independent refl.	1016	2412	2259
R_{int}	0.022	0.093	0.063
Observed reflections	891	1690	1868
Parameters	90	206	188
R_1 (obs)[a]	0.0396	0.0678	0.0405
wR_2 (all data)[b]	0.1123	0.1770	0.0782
S [c]	1.11	1.03	1.11
Resd. dens [e Å^{-3}]	-0.19, 0.23	-0.41, 1.42	-0.31, 0.28
Device type	Bruker D8 Venture	Xcalibur Sapphire3	Bruker D8 Venture
Solution	SIR-92	SIR-92	SIR-92
Refinement	SHELXL-2013	SHELXL-2013	SHELXL-2013
Absorption correction	multi-scan	multi-scan	multi-scan
CCDC	2058089	2058087	2058091

[a] $R_1 = \Sigma||F_0|-|F_c||/\Sigma|F_0|$; [b] $wR_2 = [\Sigma[w(F_0^2-F_c^2)^2]/\Sigma[w(F_0)^2]]^{1/2}$; $w = [\sigma c^2(F_0^2)+(xP)^2+yP]^{-1}$ and $P=(F_0^2+2F_c^2)/3$; [c] $S = (\Sigma[w(F_0^2-F_c^2)^2]/(n-p))^{1/2}$ (n = number of reflections; p = total number of parameters).

4.6.3 Computation

All quantum chemical calculations were carried out using the Gaussian G09 program package.[S8] The enthalpies (H) and free energies (G) were calculated using the complete basis set (CBS) method of Petersson and co-workers in order to obtain very accurate energies. The CBS models are using the known asymptotic convergence of pair natural orbital expressions to extrapolate from calculations using a finite basis set to the estimated CBS limit. CBS-4 starts with an HF/3-21G(d) geometry optimization; the zero-point energy is computed at the same level. It then uses a large basis set SCF calculation as a base energy, and an MP2/6- 31+G calculation with a CBS extrapolation to correct the energy through second order. A MP4(SDQ)/6-31+ (d,p) calculation is used to approximate higher order contributions. In this study, we applied the modified CBS-4M.

Heats of formation of the synthesized ionic compounds were calculated using the atomization method (equation E1) using room temperature CBS-4M enthalpies, which are summarized in Table S3.[S9, S10]

$$\Delta_f H^\circ_{(g,\,M,\,298)} = H_{(Molecule,\,298)} - \sum H^\circ_{(Atoms,\,298)} + \sum \Delta_f H^\circ_{(Atoms,\,298)} \qquad (E1)$$

Table S3. CBS-4M electronic enthalpies for atoms C, H, N and O and their literature values for atomic $\Delta_f H^{\circ 298}$ / kJ mol^{-1}

	$-H^{298}$ [a.u.]	NIST[S11]
H	0.500991	218.2
C	37.786156	717.2
N	54.522462	473.1
O	74.991202	249.5

For neutral compounds the sublimation enthalpy, which is needed to convert the gas phase enthalpy of formation to the solid state one, was calculated by the *Trouton* rule.[S12] For ionic compounds, the lattice energy (U_L) and lattice enthalpy (ΔH_L) were calculated from the corresponding X-ray molecular volumes according to the equations provided by *Jenkins* and *Glasser*.[S13] With the calculated lattice

enthalpy the gas-phase enthalpy of formation was converted into the solid state (standard conditions) enthalpy of formation. These molar standard enthalpies of formation (ΔH_m) were used to calculate the molar solid state energies of formation (ΔU_m) according to equation E2.

$$\Delta U_m = \Delta H_m - \Delta n\, RT \qquad \text{(E2)}$$

(Δn being the change of moles of gaseous components)
The calculation results are summarized in Table S4.

Table S4. Calculation results.

	$-H^{298}$ [a.u.]	$\Delta_f H°$(g,M) [kJ mol^{-1}]	$\Delta_f H°$(s) [kJ mol^{-1}]	Δn	$\Delta_f U$(s) [kJ kg^{-1}]
2	1300.713532	1462.6	1377.8	−12.0	1407.5
4	927.565799	846.0	781.5	−8.0	801.3
6	1263.155609	1123.4	1079.9	−10.0	3325.4
8	1188.072180	1116.4	1072.9	−9.5	3467.5

4.6.4 Thermal Analysis

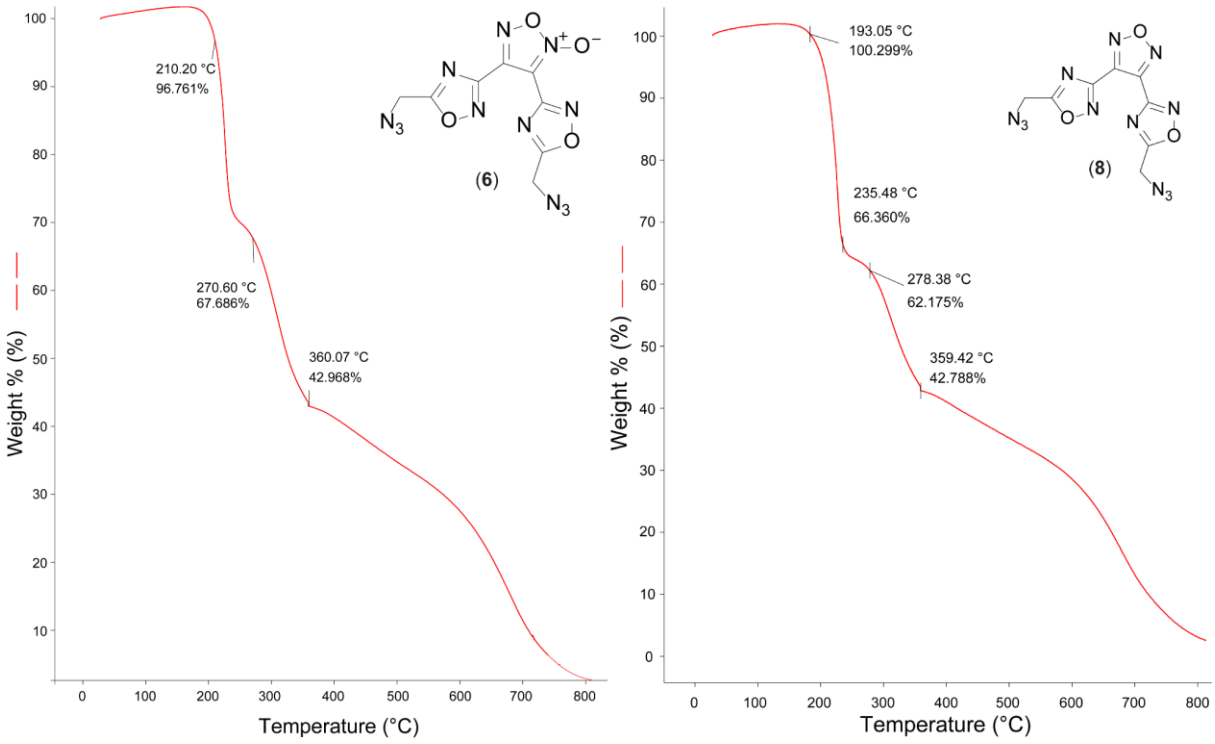

Figure S5. TGA measurements of **6** (left) and **8** (right).

4.6.5 NMR Spectroscopy

^{1}H-NMR (400 MHz, DMSO-D$_6$, ppm)

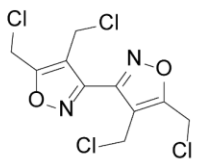

1

^{13}C{^{1}H}-NMR (100 MHz, DMSO-D$_6$, ppm)

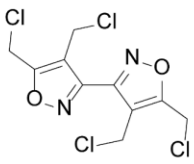

1

¹H-NMR (400 MHz, DMSO-D₆, ppm)

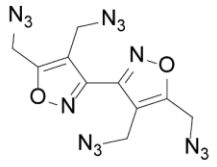

2

¹³C{¹H}-NMR (100 MHz, DMSO-D₆, ppm)

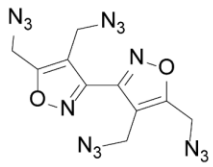

2

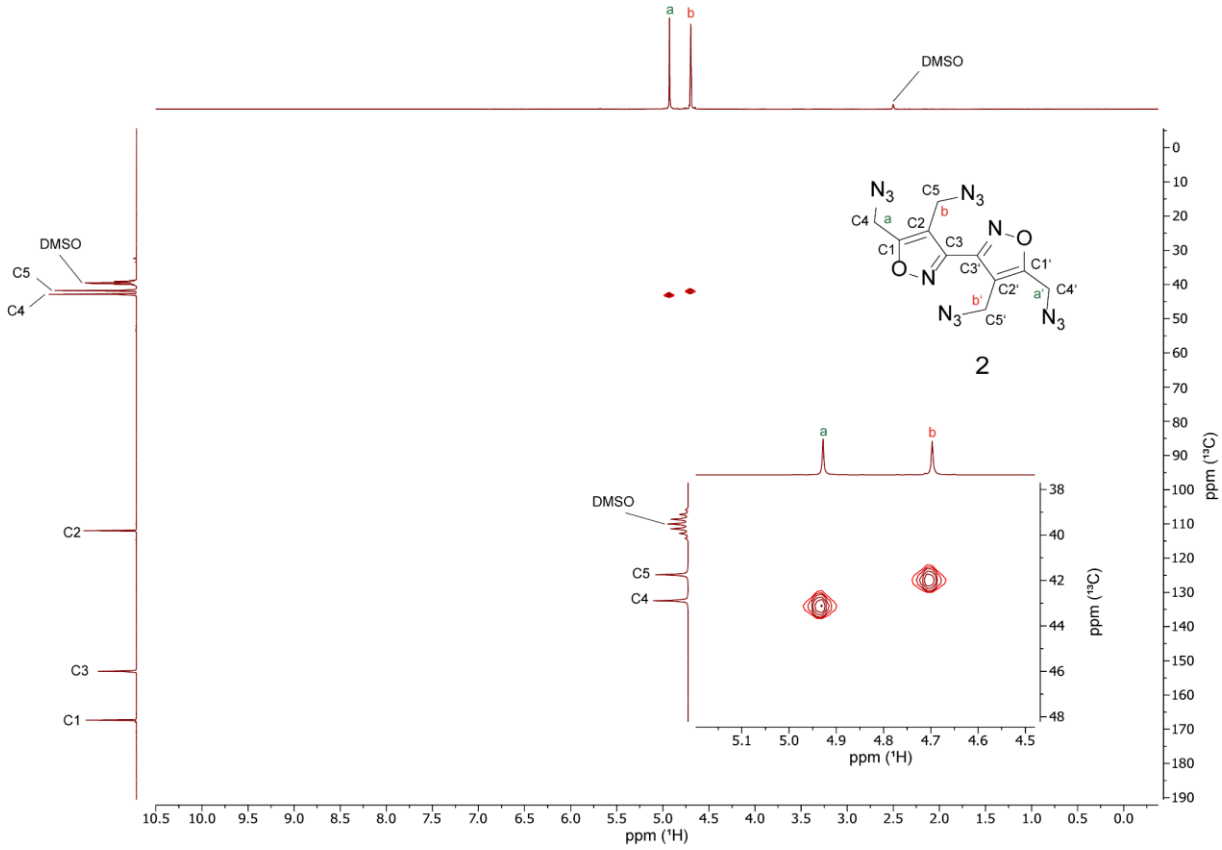
a
b
DMSO
C5
C4
C2
C3
C1
2
ppm (¹H)
ppm (¹³C)

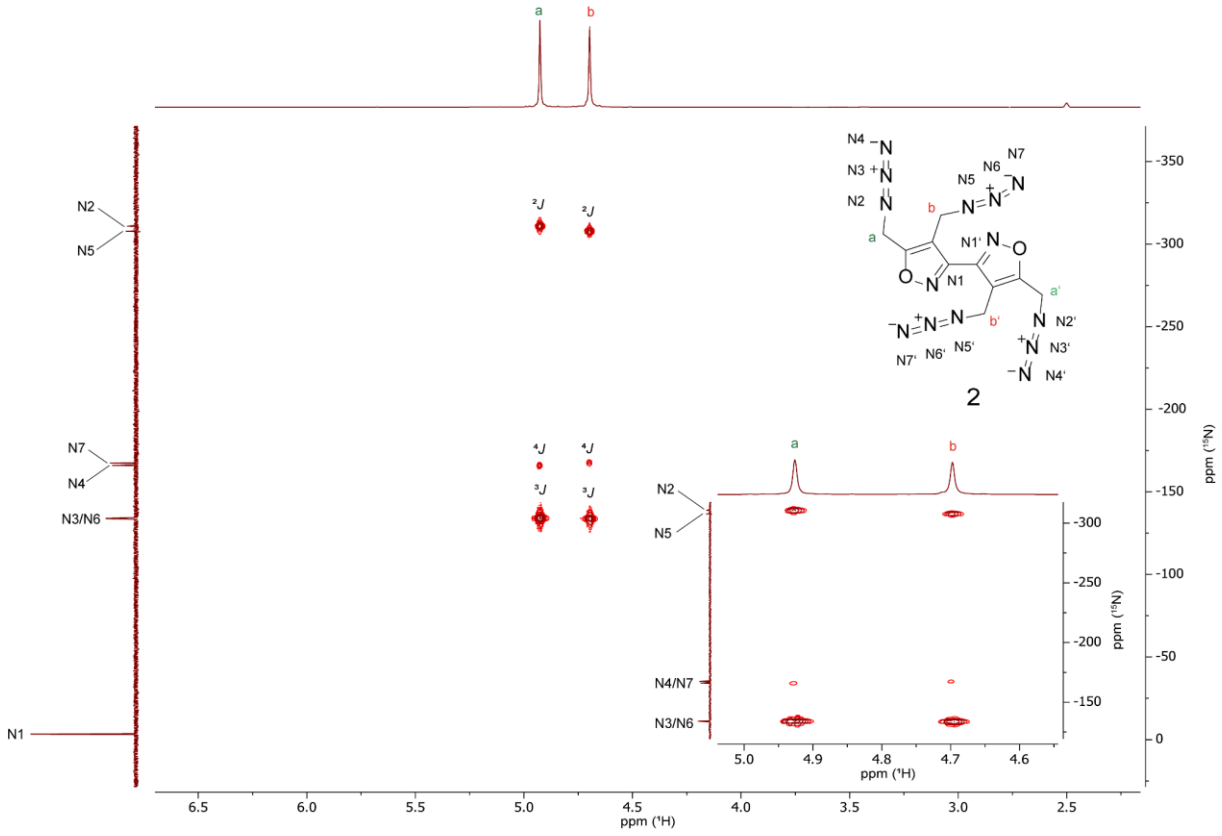
a
b
N2
N5
N7
N4
N3/N6
N1
2
N4/N7
ppm (¹H)
ppm (¹⁵N)

¹H-NMR (400 MHz, DMSO-D₆, ppm)

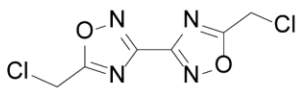

3

¹³C{¹H}-NMR (100 MHz, DMSO-D₆, ppm)

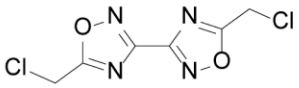

3

¹H-NMR (400 MHz, CDCl₃, ppm)

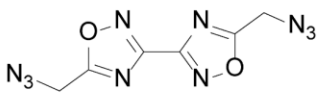

4

¹³C{¹H}-NMR (100 MHz, CDCl₃, ppm)

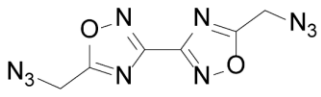

4

^{1}H-NMR (400 MHz, DMSO-D$_6$, ppm)

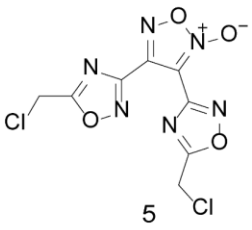

5

^{13}C{^{1}H}-NMR (100 MHz, DMSO-D$_6$, ppm)

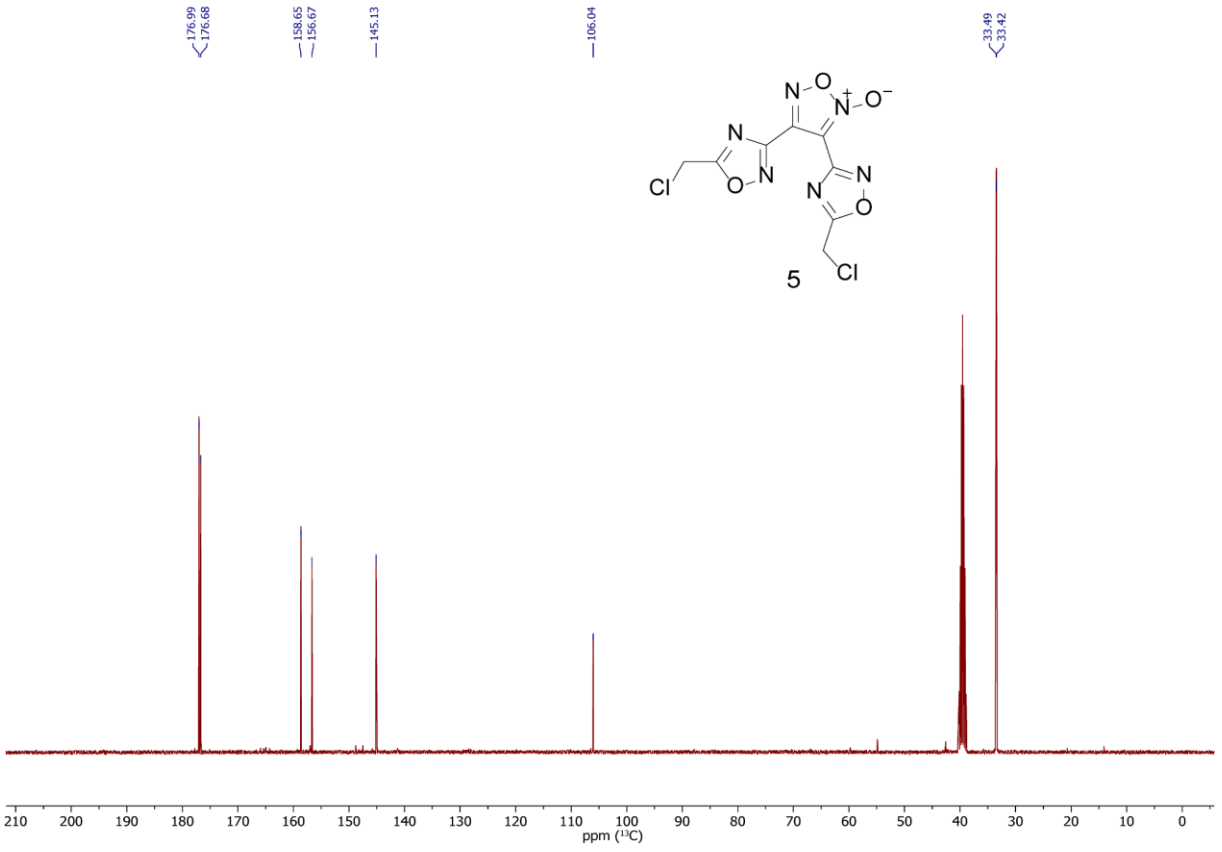

5

^{1}H-NMR (400 MHz, Acetone-D$_6$, ppm)

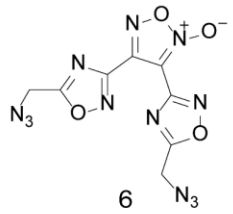

6

^{13}C{^{1}H}-NMR (100 MHz, Acetone-D$_6$, ppm)

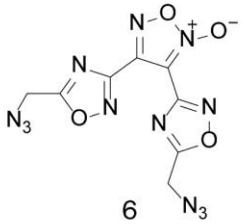

6

¹H-NMR (400 MHz, CDCl₃, ppm)

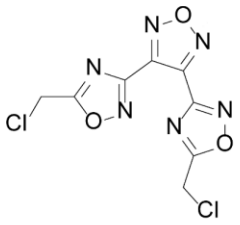

7

$^{13}C\{^{1}H\}$-NMR (100 MHz, $CDCl_3$, ppm)

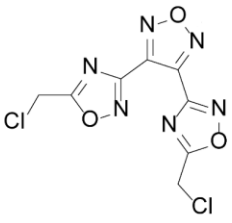

7

¹H-NMR (400 MHz, Acetone-D₆, ppm)

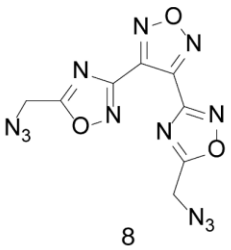

8

$^{13}C\{^{1}H\}$-NMR (100 MHz, Acetone-D₆, ppm)

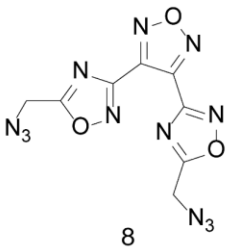

8

4.6.6 References

[S1] a) Test methods according to the UN Recommendations on the Transport of Dangerous Goods, *Manual of Test and Criteria*, ST/SG/AC.10/11/Rev.7, United Nations Publication, New York and Geneva, **2019**, 978-92-1-130394-0; https://unece.org/transport/dangerous-goods/rev7-files; b) Reichel & Partner GmbH, http://www.reichelt-partner.de; c) http://www.ozm.cz

[S2] M. Sućeska, EXPLO5 V6.02 program, Brodarski Institute, Zagreb, Croatia, **2014**.

[S3] *CrysAlisPro*, Oxford Diffraction Ltd. *version 171.33.41*, **2009**.

[S4] G. M. Sheldrick, *Acta Cryst.* **2015**, *A71*, 3–8.

[S5] O. V. Dolomanov, L. J Bourhis, R. J. Gildea, J. A. K. Howard, H. Puschmann, *J. Appl. Cryst.* **2009**, *42*, 339–341.

[S6] *SCALE3 ABSPACK – An Oxford Diffraction program* (1.0.4, gui: 1.0.3), Oxford Diffraction Ltd., **2005**.

[S7] *APEX3*. Bruker AXS Inc., Madison, Wisconsin, USA.

[S8] M. J. Frisch, G. W. Trucks, H. B. Schlegel, G. E. Scuseria, M. A. Robb, J. R. Cheeseman, G. Scalmani, V. Barone, B. Mennucci, G. A. Petersson, H. Nakatsuji, M. Caricato, X. Li, H.P. Hratchian, A. F. Izmaylov, J. Bloino, G. Zheng, J. L. Sonnenberg, M. Hada, M. Ehara, K. Toyota, R. Fukuda, J. Hasegawa, M. Ishida, T. Nakajima, Y. Honda, O. Kitao, H. Nakai, T. Vreven, J. A. Montgomery, Jr., J. E. Peralta, F. Ogliaro, M. Bearpark, J. J. Heyd, E. Brothers, K. N. Kudin, V. N. Staroverov, R. Kobayashi, J. Normand, K. Raghavachari, A. Rendell, J. C. Burant, S. S. Iyengar, J. Tomasi, M. Cossi, N. Rega, J. M. Millam, M. Klene, J. E. Knox, J. B. Cross, V. Bakken, C. Adamo, J. Jaramillo, R. Gomperts, R. E. Stratmann, O. Yazyev, A. J. Austin, R. Cammi, C. Pomelli, J. W. Ochterski, R. L. Martin, K. Morokuma, V. G. Zakrzewski, G. A. Voth, P. Salvador, J. J. Dannenberg, S. Dapprich, A. D. Daniels, O. Farkas, J.B. Foresman, J. V. Ortiz, J. Cioslowski, D. J. Fox, Gaussian 09 A.02, Gaussian, Inc., Wallingford, CT, USA, **2009**.

[S9] a) J. W. Ochterski, G. A. Petersson, and J. A. Montgomery Jr., *J. Chem. Phys.* **1996**, *104*, 2598–2619; b) J. A. Montgomery Jr., M. J. Frisch, J. W. Ochterski G. A. Petersson, *J. Chem. Phys.* **2000**, *112*, 6532–6542.

[S10] a) L. A. Curtiss, K. Raghavachari, P. C. Redfern, J. A. Pople, *J. Chem. Phys.* **1997**, *106*, 1063–1079; b) E. F. C. Byrd, B. M. Rice, *J. Phys. Chem*. A **2006**, *110*, 1005–1013; c) B. M. Rice, S. V. Pai, J. Hare, *Comb. Flame* **1999**, *118*, 445–458.

[S11] P. J. Lindstrom, W. G. Mallard (Editors), NIST Standard Reference Database Number 69, http://webbook.nist.gov/chemistry/ (accessed June **2020**).

[S12] M. S. Westwell, M. S. Searle, D. J. Wales, D. H. Williams, *J. Am. Chem. Soc*. **1995**, *117*, 5013–5015; b) F. Trouton, *Philos. Mag*. **1884**, *18*, 54–57.

[S13] a) H. D. B. Jenkins, H. K. Roobottom, J. Passmore, L. Glasser, *Inorg. Chem.* **1999,** *38,* 3609–3620; b) H. D. B. Jenkins, D. Tudela, L. Glasser, *Inorg. Chem.* **2002**, *41*, 2364–2367.

5. Combining Performance with Thermal Stability: Synthesis and Characterization of 5-(3,5-Dinitro-1*H*-pyrazol-4-yl)-1*H*-tetrazole and its Energetic Derivatives

Maximilian Benz, Thomas M. Klapötke, Jörg Stierstorfer

as published in *Zeitschrift für anorganische und allgemeine Chemie* **2020**, 1380–1388

DOI: 10.1002/zaac.202000123

Keywords: energetic materials, pyrazoles, tetrazoles, polynitro azoles, structure eludication

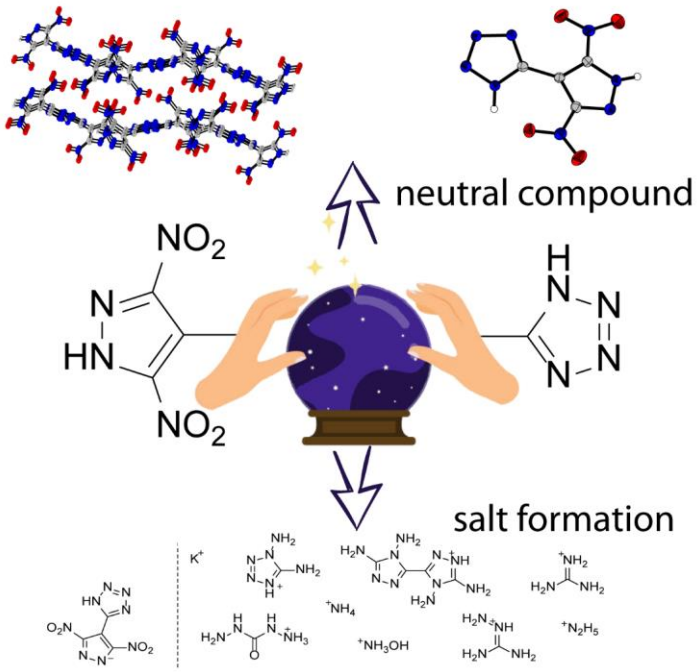

Functionalized azoles are essential in the development of new energetic materials. In this paper we present the synthesis of 5-(3,5-dinitro-1*H*-pyrazol-4-yl)-1*H*-tetrazole and certain energetic derivatives starting from 4-amino-3,5-dinitropyrazole. By using comprehensive analytic methods and theoretical calculations, the new substance class was examined with regard to its suitability for the replacement of RDX.

Abstract: In this study, we present the synthesis of 5-(3,5-dinitro-1*H*-pyrazol-4-yl)-1*H*-tetrazole and its energetic derivatives starting from 4-amino-3,5-dinitropyrazole, which was diazotized and cyanide substituted. A subsequent cycloaddition reaction with sodium azide led to 5-(3,5-dinitro-1*H*-pyrazol-4-yl)-1*H*-tetrazole (**3**). Several alkaline metal and nitrogen-rich salts were prepared and characterized by low-temperature X-ray diffraction. Additionally, all compounds were analyzed by vibrational spectroscopy (IR), ^{1}H, ^{13}C and ^{14}N NMR spectroscopy, elemental analysis and differential thermal analysis (DTA). Additionally, the heats of formation for selected compounds were calculated using the atomization method based on CBS-4M enthalpies as well as important detonation parameters by using the EXPLO5 code (V6.05). Furthermore, the sensitivities of **3** and all synthesized salts toward friction, impact and electrostatic discharge according to BAM (Bundesamt für Materialforschung) were determined and compared to RDX.

5.1 Introduction

The demand for new energetic materials has risen sharply in recent years, as the field of application has been extended not only to the military sector, but also to an increasing number of civilian sectors, such as aerospace technology and the automotive industry.[1-3] Increasingly specialized fields of application also constantly present new challenges in the development of suitable substances.[4-5] Some key characteristics every new HEDM to be developed should meet are a high decomposition temperature, which is especially important for temperature resistant materials. In addition, paired with low sensitivity to external stimuli, this is indispensable for the safety of the persons handling the materials.[6-8] Green chemistry is also becoming an increasingly important point to consider in the development of energetic materials.[3, 9-10] Newly developed materials should therefore be completely free of toxic or environmentally harmful reactants in their synthesis. Of course, the toxicity of the final product is also important and should therefore be as harmless as possible.[11-13] Especially for the military sector, more performance-efficient substances are of interest.[5] In addition, production costs must be regarded as a criterion, as the tendency here is to produce larger

quantities. The latter is particularly easy to achieve if the starting materials are easily available and rapidly accessible.[14-15]

Especially azoles like pyrazoles, triazoles, tetrazoles or oxygen containing five-membered heterocycles like furazan or oxadiazoles have proven to be good building blocks of novel energetic materials.[17-21] Pyrazoles are particularly suitable because they have a relatively high heat of formation (HoF) and still exhibit high thermal stability, which is due to the three linked carbon atoms. In addition, energetic modifications, such as nitration or oxidation, can be carried out rather simply (Figure 1a).[22-23]

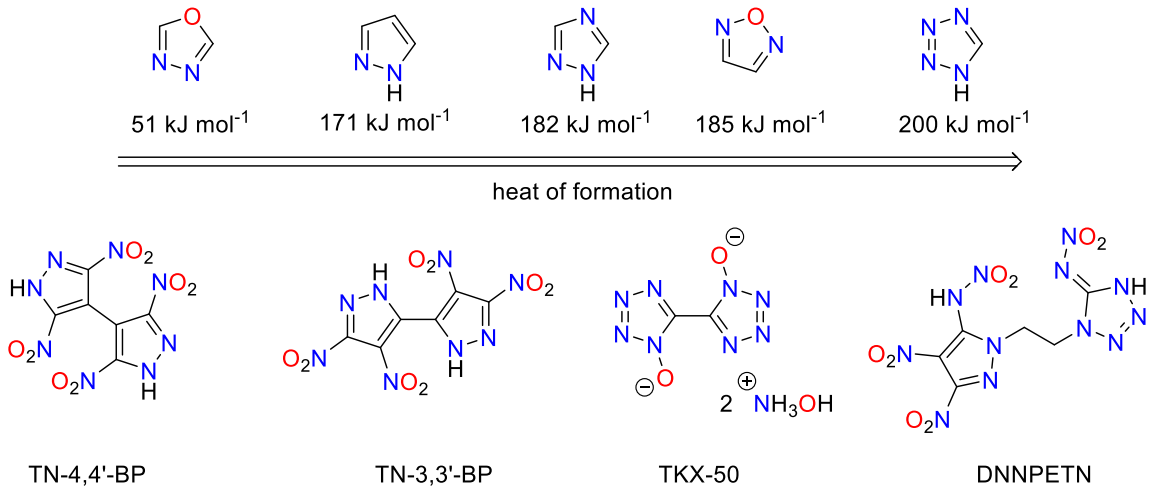

Figure 1. (a) Gas-phase heats of formation for selected azoles and oxadiazoles.[9, 16] (b) Literature known explosives based on linked pyrazoles and tetrazoles: TN-4,4'-BP (tetranitro-4,4'-bipyrazole),[26] TN-3,3'-BP (tetranitro-3,3'-bipyrazole),[27] TKX-50 (dihydroxylammonium 5,5'-bitetrazole-1,1'-dioxide),[14] DNNPENT (*N*-(1-(2-(3,4-dinitro-5-(nitroamino)-pyrazol-1-yl)ethyl)-5*H*-tetrazol-5-ylidene)nitramide).[28]

Tetrazole building blocks are attractive due to their extremely high nitrogen content and by a large heat of formation.[24-25] Although there are many examples of bridged pyrazoles, tetrazoles or combinations thereof (Figure 1b), no C–C linked and fully functionalized pyrazole-tetrazole hybrid, which at best combines the positive properties of the individual building blocks, is yet known.

Energetic materials based on the 5-(pyrazol-4-yl)-tetrazole skeleton have not been mentioned in literature yet. Herein, we report on the synthesis of the first compound combining a dinitropyrazole derivative with a tetrazole via a C–C bond in a five-step reaction. In addition, various mono salts of H_2DNPT (**3**) were synthesized and intensively characterized and compared to each other.

5.2 Results and Discussion

5.2.1 Synthesis

he synthesis of 5-(3,5-dinitro-1*H*-pyrazol-4-yl)-1*H*-tetrazole (H_2DNPT, **3**) starts with the chlorination of 1*H*-pyrazole using in situ generated chlorine (NaOCl/HCl; Scheme 1) to form 4-chloro-pyrazole.[22, 29] A subsequent nitration using a mixture of sulfuric acid and fuming nitric acid formed 4-chloro-3,5-dinitropyrazole.[22, 30-31] The third step was performed in an steel autoclave using aqueous ammonia to yield 4-amino-3,5-dinitropyrazole (ADNP, **1**).[22, 30-31] ADNP was diazotated in diluted sulfuric acid using sodium nitrite.

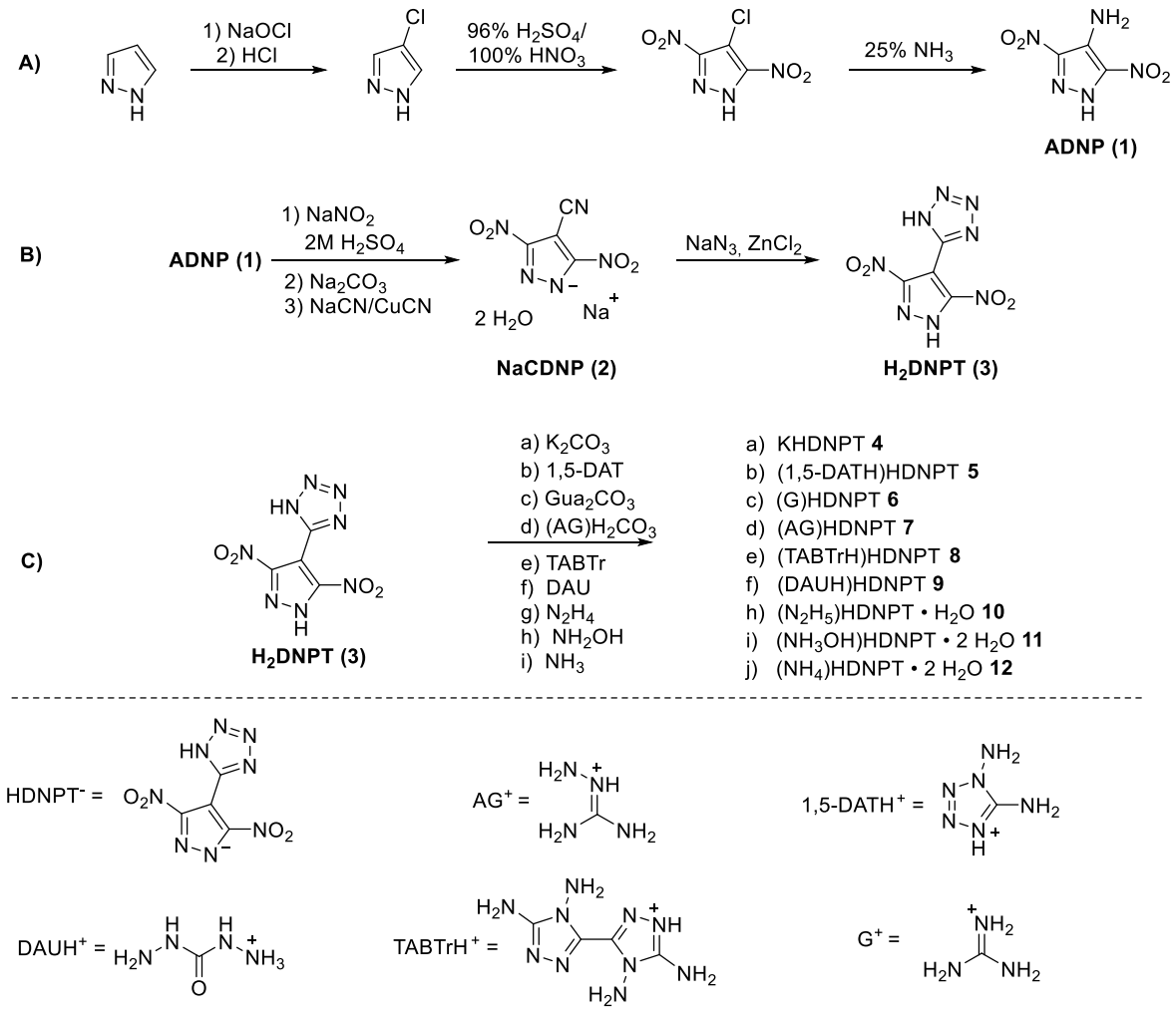

Scheme 1. (A) Literature know synthesis of 4-amino-3,5-dinitropyrazole (ADNP, **1**). (B) Synthesis of 5-(3,5-dinitro-1*H*-pyrazol-4-yl)-1*H*-tetrazole (**3**). (C) Synthesis of new energetic salts of H_2DNPT.

After neutralization with sodium carbonate the in situ generated diazonium group was substituted by cyanide by a reductive elimination reaction to form 4-cyano-3,5-dinitropyrazole (**2**) as sodium salt. H_2DNPT (**3**) was obtained by a reaction using a modified procedure of *Sharpless* and co-workers, which has a broad approach in the synthesis of C–C fused tetrazole azole compounds.[18, 32-34] The [3+2] cycloaddition of NaCDNP (**2**) with sodium azide and zinc chloride as catalyst in water yields **3** in 55 % yield. The corresponding energetic salts of H_2DNPT were produced by diluting the neutral compound in water, alcohol (MeOH, EtOH) or mixtures of those and subsequent addition of one equivalent of the corresponding base (Scheme 1C). The respective salts precipitated immediately or were obtained by evaporation of the solvent in very good yields and high purities. All compounds were fully characterized by IR and multinuclear NMR spectroscopy, mass spectrometry and differential thermal analysis. Further, selected compounds were analyzed using low-temperature single-crystal X-ray measurements.

5.2.2 X-Ray Diffraction

Suitable crystals of compounds **2**–**5**, **7**, **8**, **11** and **12** were obtained by recrystallization of the crude products from methanol or acetonitrile, respectively. Compounds **2**, **11** and **12** crystallize with the inclusion of water molecules. The DAU and hydrazinium derivatives **9** and **10** maintained crystalline morphology, but the solution of the diffraction measurement data could not be completed due to structural disorder. Here, only the low temperature X-ray crystal structures of the neutral compound **3** and anhydrous derivatives **4**, **5**, **7** and **8** are discussed. The other solid-state structures can be found in the Supporting Information.

Compound **3** crystallizes in the orthorhombic space group *Pbca* with a cell volume of 1754.19(12) $Å^3$ and eight formula units per cell. The cell constants are a = 9.5893(3) Å, b = 10.5373(5) Å and c = 17.3604(7) Å, while the density is 1.712 g cm^{-3} at 123 K. Thus, the density is clearly below the value calculated by *Ghule* et al.[35] The nitro groups are almost in one plane with the pyrazole moiety (O2–N3–C3–C2 –3.9°, O3–N4–C1–N2 –2.4°). The pyrazole and tetrazole ring of H_2DNPT each have a planar structure (C3–N1–N2–C1 0.6°, N6–N5–C4–N8 0.2°). However,

both rings in the molecule are not coplanar to each other (C1–C2–C4–N8 129°). The twisting prevents a regular stacking of the molecular units.

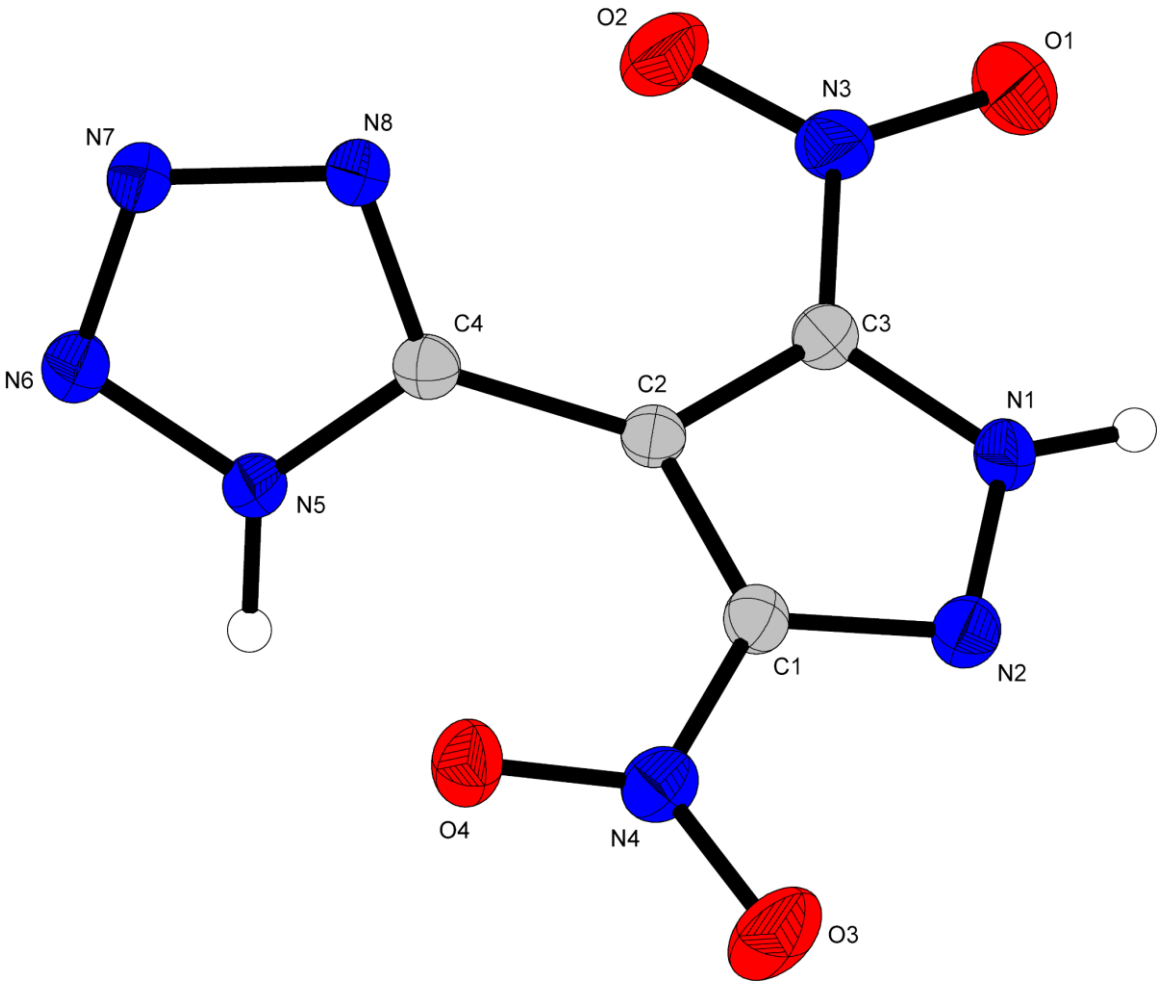

Figure 2. Molecular unit of compound **3**, showing the atom labeling scheme. Thermal ellipsoids represent the 50 % probability level and hydrogen atoms are shown as small spheres of arbitrary radius. Selected bond lengths /Å and angles /°: C2–C4 1.465(2), C1–N4 1.4445(19), C3–N3 1.444(2), O3–N4–C1 116.80(12), O2–N3–C3 117.61(12), O2–N3–C3–C2 –3.9(2), O3–N4–C1–N2 –2.4(2), C1–C2–C4–N8 129.02(17).

This can be assumed to be the main reason for the low density of compound **3** (1.669 g cm^{-3} at 298 K). The bond lengths within the azole rings are between the expected values for C–C, C–N and N–N single and double bonds (C–C:1.47 Å, 1.34 Å, C–N: 1.47 Å, 1.22 Å; N–N: 1.48 Å, 1.20 Å).[36-37] The C–C bond between the two aromatic rings has the classic length of a single bond (C2–C4 1.465 Å)[36, 38] (Figure 2, Figure 3, and Figure 4).

Compound **3** forms a wave-like layering structure along c, with a layer distance of 5.41 Å. The only classical hydrogen bridges are between the acidic protons and the nitrogen atoms of the tetrazole moiety. The nitro groups do not form any

intramolecular interactions in the structure. The tetrazole units form hydrogen bridges in direction of *a* axis N5–H5···N7^{iv} with a length of 1.96 Å and an angle of 166.2°.

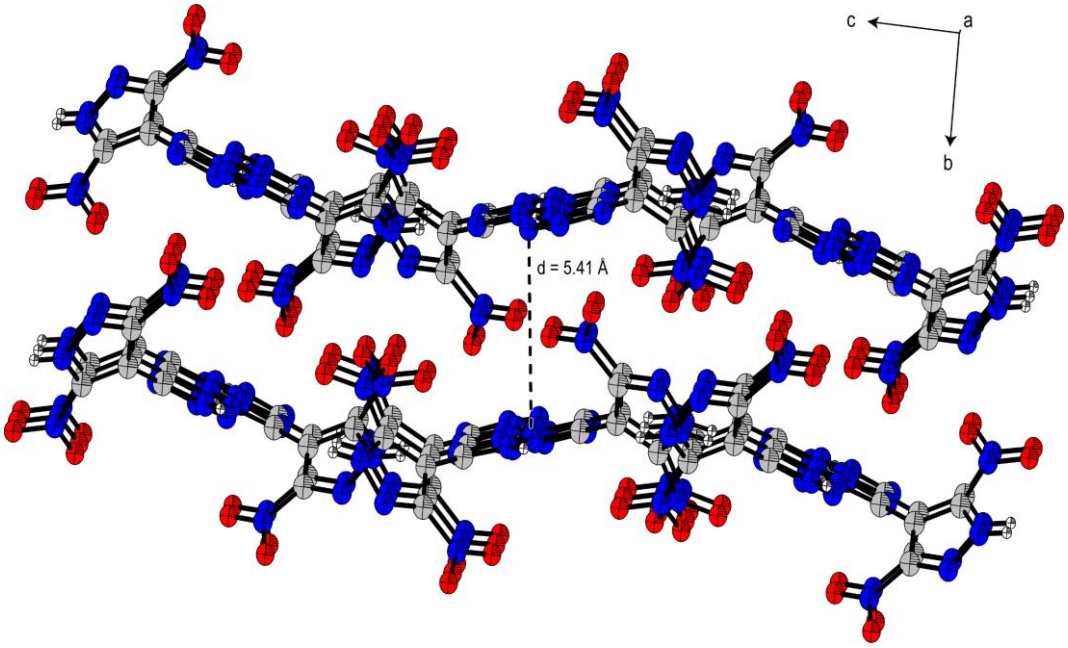

Figure 3. Stacking of layers of compound **3** (layer distance d = 5.41 Å). Thermal ellipsoids are drawn at the 50 % probability level.

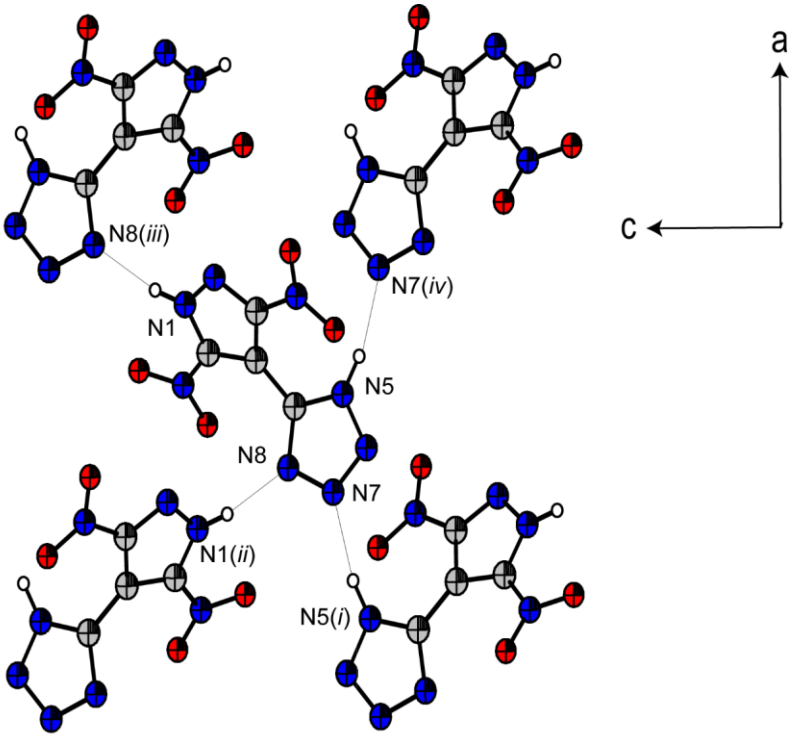

Figure 4. Formation of intramolecular hydrogen bonds of compound **3** along the *ac* plane; Symmetry codes: i) –0.5+x, 0.5–y, –z; ii) –0.5+x, y, 0.5–z; iii) 0.5+x, y, 0.5–z; iv) 0.5+x, 0.5–y, –z; Thermal ellipsoids are drawn at the 50 % probability level.

The molecular moieties in the *ac* plane form a strong intramolecular interaction with N8 at the tetrazole of the adjacent unit through the hydrogen at the pyrazole (N1–H1···N8^{iii}, 1.90 Å). The steric demand of the nitro groups also explains the tilting of the aromatic rings towards each other in the layering.

Compound **4** crystallizes is the monoclinic space group $P2_1$ with a cell volume of 910.47(8) Å^3 and two formula units per cell. The cell constants are a = 9.0333(4) Å, b = 11.3970(6) Å and c = 9.2529(4) Å, while the density is 1.928 g cm^{-3} at 131 K. Deprotonation occurs at the pyrazole ring, which indicates a more acidic character than the tetrazole proton. The pyrazole ring forms an almost flat plane with the two nitro groups (O3–N4–C3–N2 9.2°, O1–N3–C1–C2 176.6°). The ring moieties are not coplanar but around 61° tilted straight to each other. Compared to neutral compound **3**, the twist is more distinctive with about 10 degrees more. All bond lengths in the azole rings are in the range of C–C, C–N or N–N single and double bonds.[36] Compared to the neutral compound **3** the bond lengths do not vary significantly (Figure 5).

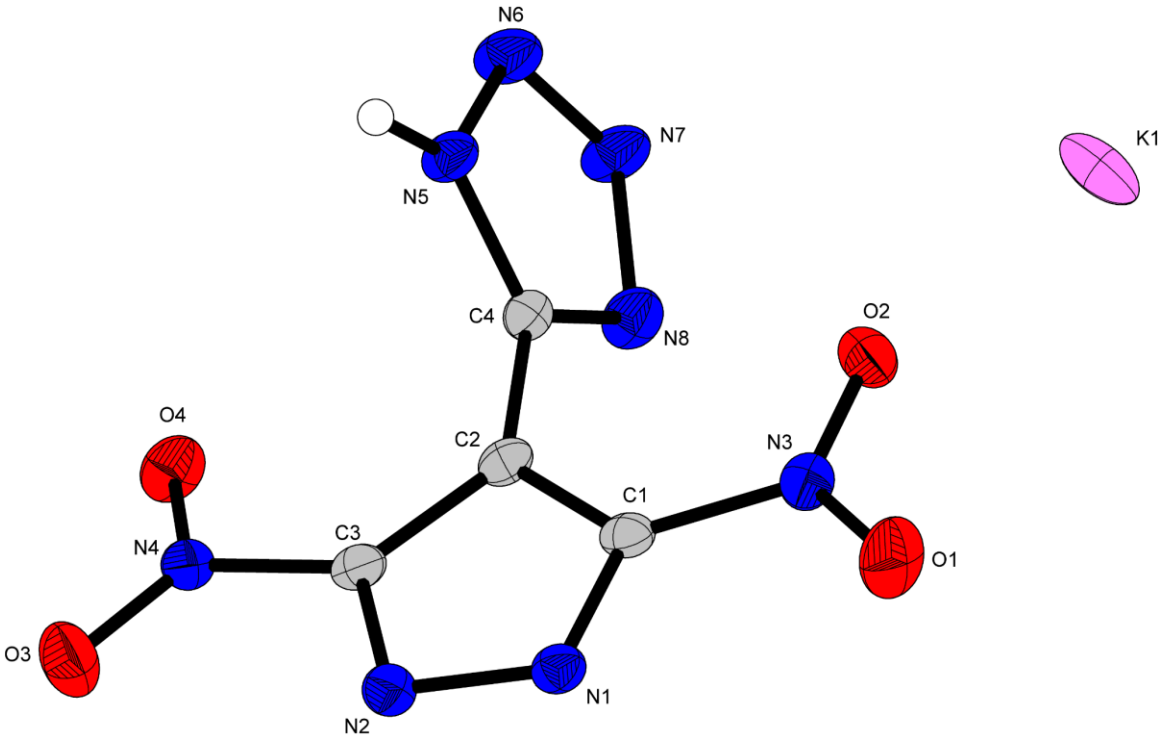

Figure 5. Molecular unit of compound **4**, showing the atom labeling scheme. Thermal ellipsoids represent the 50 % probability level and hydrogen atoms are shown as small spheres of arbitrary radius. Selected bond lengths /Å and angles /°: K1–O2 2.799(3), C2–C4 1.463(6), C3–N4 1.441(6), C1–N3 1.433(5), O2–N3–C1 117.7(3), O3–N4–C3 118.7(3), O3–N4–C3–N2 9.2(6), O1–N3–C1–C2 176.6(4), C3–C2–C4–N8 0.6(6).

1,5-Diamino-tetrazol-4-ium 3,5-dinitro-4-(tetrazol-5-yl)pyrazolate (1,5-DATH)HDNPT (**5**) crystallizes in the monoclinic space group *C*2/*c* with a cell volume of 2395.10(25) Å^3 and eight molecular moieties in the cell unit. The molecular structure of **5** is presented in Figure 6.

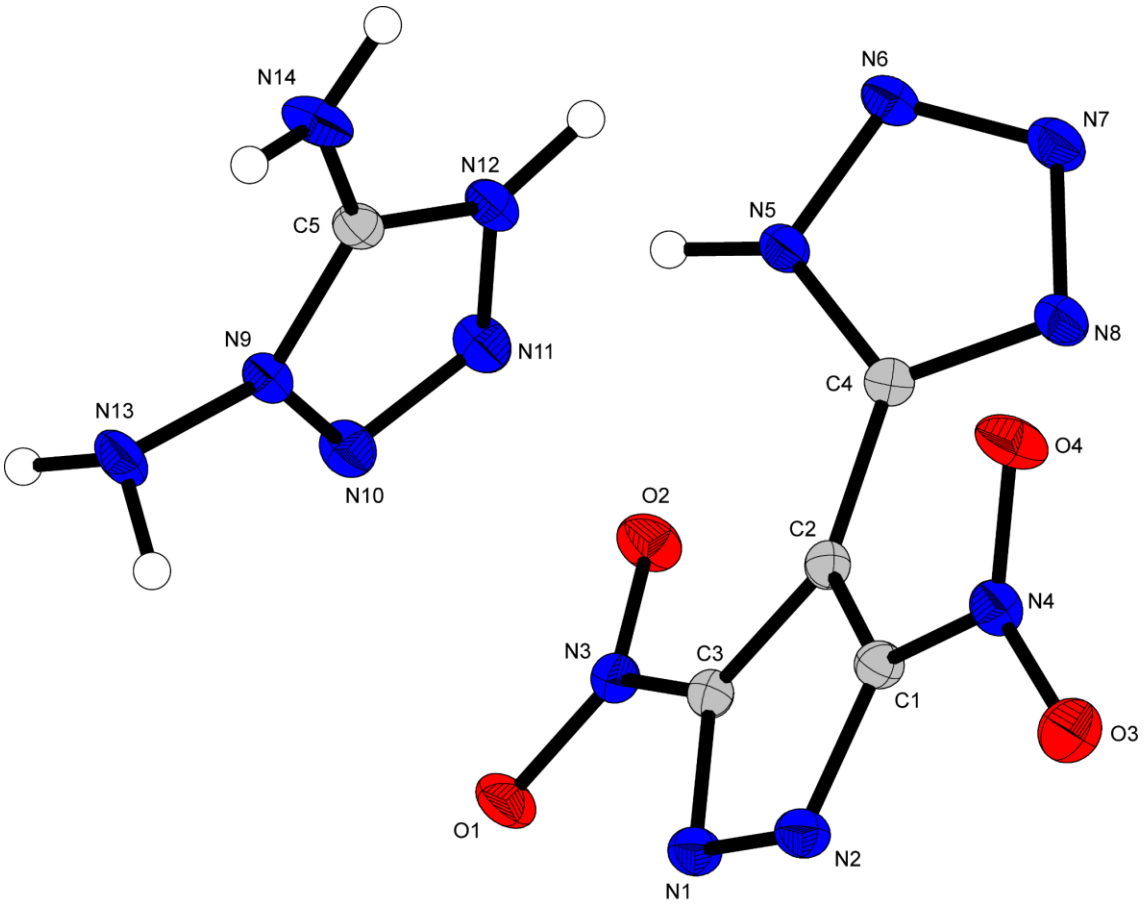

Figure 6. Molecular unit of compound **5**, showing the atom labeling scheme. Thermal ellipsoids represent the 50 % probability level and hydrogen atoms are shown as small spheres of arbitrary radius.

The anions HDNPT$^-$ in **5** form dimers, which build two strong hydrogen bridges via the nitro group and the tetrazolium proton (N5^i–H5···O2, N5–H5···O1^i). Four further nitrogen atoms (i.e., N1, N2, N6 and N8) of the anion are involved as acceptor atoms in further hydrogen bonds (Table 1), thereby resulting strong interactions with surrounding cations. The donors of the hydrogen bridges originate from the amine functionalities N13 and N14 as well as the secondary tetrazole-amine N12.

The anions HDNPT$^-$ in **5** form dimers, which build two strong hydrogen bridges via the nitro group and the tetrazolium proton (N5^i–H5···O2, N5–H5···O1^i).

Table 1. Hydrogen bonds present in the crystal structure of **5**.

D-H···A	d (D-H) [Å]	d (H···A) [Å]	d (D-H···A) [Å]	< (D-H···A)[°]
N5i-H5···O2	0.86(2)	2.58(2)	2.8736(18)	101.4(17)
N5-H5···O1i	0.86(2)	2.14(2)	2.9561(17)	158(2)
N12^{ii}-H12···N2	0.92(2)	1.81(2)	2.7268(18)	174(2)
N13^{iii}-H13A···O4	0.89(2)	2.50(2)	3.1017(18)	126(2)
N13^{iv}-H13B···O2	0.89(2)	2.50(2)	3.1964(17)	132(2)
N13^{v}-H13B···N8	0.89(2)	2.39(2)	3.0859(19)	135(2)
N14^{iv}-H14A···N6	0.83(2)	2.27(2)	2.997(2)	146(2)
N14^{iv}-H14B···N1	0.86(2)	2.17(2)	3.0291(19)	175.2(18)

Symmetry codes: i) 1−x, 1−y, 1−z; ii) 3/2−x, 1/2+y, 3/2−z; iii) x, 1−y, 1/2+z; iv) −1/2+x, 1/2+y, z; v) 3/2−x, −1/2+y, 3/2−z.

Four further nitrogen atoms (i.e., N1, N2, N6 and N8) of the anion are involved as acceptor atoms in further hydrogen bonds (Table 1), thereby resulting strong interactions with surrounding cations. The donors of the hydrogen bridges originate from the amine functionalities N13 and N14 as well as the secondary tetrazole-amine N12.

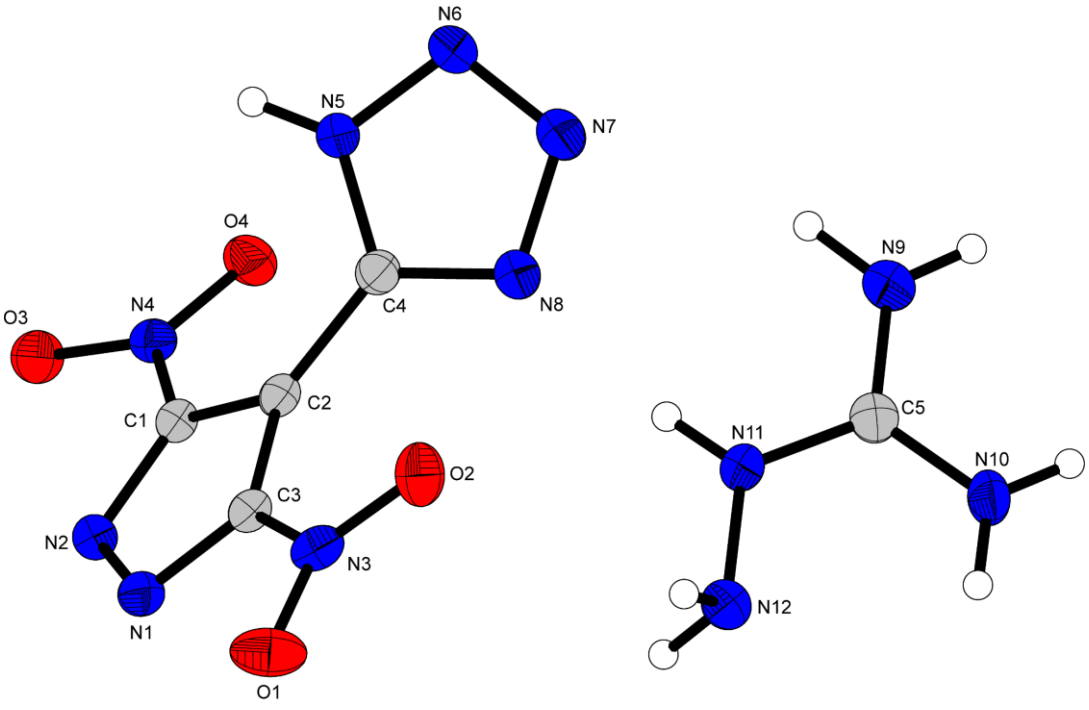

Figure 7. Molecular unit of compound **7**, showing the atom labeling scheme. Thermal ellipsoids represent the 50 % probability level and hydrogen atoms are shown as small spheres of arbitrary radius.

Furthermore, aminoguanidinium 3,5-dinitro-4-(tetrazol-5-yl)pyrazolate (AG)HDNPT (**7**) crystallizes water free in the orthorhombic space group *Pbcn* with eight molecular units per cell and a cell volume of 2263.21(13) Å^3. The molecular structure is shown in Figure 7. The crystal structure shows the formation of layers of cations and anions, respectively, along *c* axis. The anions HDNPT$^-$ create an alternating chain-like structure, whereby one clear interaction N5–H5···N1^i is built. Two aminoguanidinium cations surround the tetrazole ring and interact with the accepting nitrogen atoms N6 and N8. Another cation forms a strong interaction with the deprotonated pyrazole nitrogen (N1 and N2). Surprisingly, only one nitro group with O3 and O4 forms hydrogen bridges with the cation.

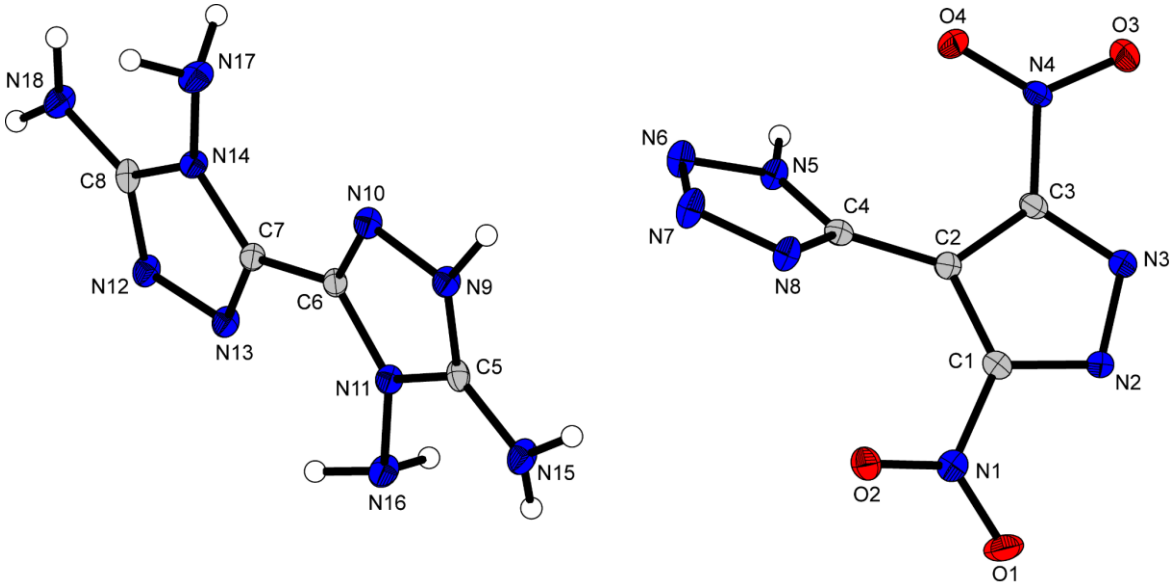

Figure 8. Molecular unit of compound **8**, showing the atom labeling scheme. Thermal ellipsoids represent the 50 % probability level and hydrogen atoms are shown as small spheres of arbitrary radius.

Both, the cations and the anions form linear chains along *c*. In the anion structure strong interactions between the tetrazoles are visible (N5–H5···N8^i). In the TABTrH chains, many interactions between the amines and the nitrogen atoms of the triazoles are detectable. In addition, certain hydrogen bridges between the accepting anion nitrogens N2, N3, N6 and N7 and the amino groups of the cation (N15–H15A, N15–H15B, N17–N17A, N18–H18A, N18–H18B) are formed.

5.2.3 Spectroscopy

All compounds (**3**–**12**) were analyzed by ^{1}H, ^{13}C and ^{14}N spectroscopy with [D_6]DMSO as solvent (Table 2). Additionally, compound **3** was characterized by ^{15}N spectroscopy measurement.

Table 2. NMR resonances for compounds 3–12 measured in [D_6]DMSO.

Compound	δ [ppm]		
	^{13}C	^{14}N	^{1}H
3	153.6, 147.3, 97.5	−24	14.24
4	154.7, 147.6, 96.4	−19	
5	153.9, 153.1, 147.0, 97.1	−22	7.58
6	157.9, 154.7, 147.6, 96.4	−20	6.92
7	158.8, 154.7, 147.5, 96.2	−20	8.55, 7.24, 6.72, 4.68
8	154.7, 153.9, 147.5, 138.6, 96.1	−20	7.40, 5.99
9	159.2, 154.7, 147.4, 96.1	−17	8.68
10 • H_2O	154.8, 147.5, 96.2	−19	7.13, 3.36
11 • 2 H_2O	154.8, 147.5, 96.2	−19, −359	11.33, 10.06, 3.39
12 • 2 H_2O	155.2, 148.6, 98.1	−18, −359	7.24

The highly acidic protons of the pyrazole and tetrazole can only be detected as a broad signal at δ = 14.24 ppm for the neutral compound **3**. The signal only became detectable with an extended measuring time and high substance concentration, since a constant exchange takes place due to the high acidity in DMSO. For all deprotonated compounds (**4**–**12**), the remaining tetrazole proton signal could not be observed in the ^{1}H spectra. While the 1,5-DATH cation proton resonances in **5** are located at δ = 7.58 ppm resulting in a broad signal, the guanidinium compound **6**, representing 6 protons appears as sharp singlet at δ = 6.92 ppm. The aminoguanidinium cation shows four signals, in accordance to the four different types of protons, located at δ = 8.55 (N*H*–NH_2), 7.24 (NH_2), 6.72 (NH_2) and 4.68 ppm (NH–N*H*$_2$). The two different amino groups of the TABTrH cation can be assigned to sharp singlet signals at δ = 7.40 (N–N*H*$_2$) and 5.99 ppm (C–N*H*$_2$). The

protons in the DAU compound **9** result in a broad signal at δ = 8.68 ppm. For the water containing compounds, the water signal can only be observed for the hydrazinium **10** and the hydroxylammonium **11** compound at δ = 3.36 and 3.39 ppm, respectively. Additionally, the cations of the water containing compounds show signals at δ = 7.13 ppm for the hydrazinium **10**, δ = 11.33 and 10.06 ppm for the hydroxylammonium **11** and δ = 7.24 ppm for the ammonium **12** compound.

In all ^{13}C NMR spectra one signal for the tetrazole and according to symmetry two signals for the pyrazole can be observed. The signals are all in the range for C-substituted tetrazoles and 3,5-dinitropyrazoles.[26, 28, 39-40] For the neutral compound **3** C4 can be observed at δ = 153.6 ppm, C1/C3 at δ = 147.3 ppm and C2 at δ = 97.5 ppm. The deprotonation of the pyrazole ring affects a shift of all carbon atoms. For C4 a down field shift can be monitored. The signals for all ionic compounds for C4 are between δ = 153.9 and 155.2 ppm. For C1/C3 the resonances are in the range of δ = 147.0 and 148.6 ppm. Except for the ammonium compound **12** (δ = 98.1 ppm) a trend to high field shift for C2 atoms is identifiable. The signals can be found at δ = 96.1 to 97.1 ppm. The signal for the carbon atom in the cation can be found at δ = 153.1 for **5** which is a usual shift for tetrazolium cations.[41] The guanidinium and aminoguanidinium derivatives show a resonance at δ = 157.9 and 158.8 ppm, respectively. The TABTr derivative has two more signals in the ^{13}C spectrum located at δ = 154.7 and 147.5 ppm. For the DAU salt the urea like carbon resonates at δ = 159.2 ppm.

The ^{14}N spectra of all compounds investigated compounds show the resonance for the nitro groups at the pyrazole. H_2DNPT (**3**) can be observed at δ = –24 ppm. The signals for the ionic species vary within the range of δ = –22 to –17 ppm. Compounds **11** and **12** show an additional signal at –359 ppm for the cation.

Figure 9 shows the ^{15}N NMR spectrum of compound **3**. The assignments were based on comparison with theoretical calculations using Gaussian 09[42] and literature values with similar 3,5-dinitropyrazoles and electron poor 5-substituted tetrazoles.[18, 40, 43] The spectrum shows two sharp signals at δ = –9.5 and –25.4 ppm. Additionally, two broad signals at δ = –93.8 and –98.0 ppm are observed. The sharp signals can be clearly assigned to the nitrogen N4/N4' (–9.5 ppm) of the tetrazole moiety and the nitrogen atoms of the nitro groups N2/N2' (–25.4 ppm). A defined assignment of the two wide signals to N1/N1' and N3/N3' is not possible. Due to the high acidity of the protons, no N–H couplings can be found in the

spectrum. The associated rapid proton exchange in DMSO also explains the width of the signals.

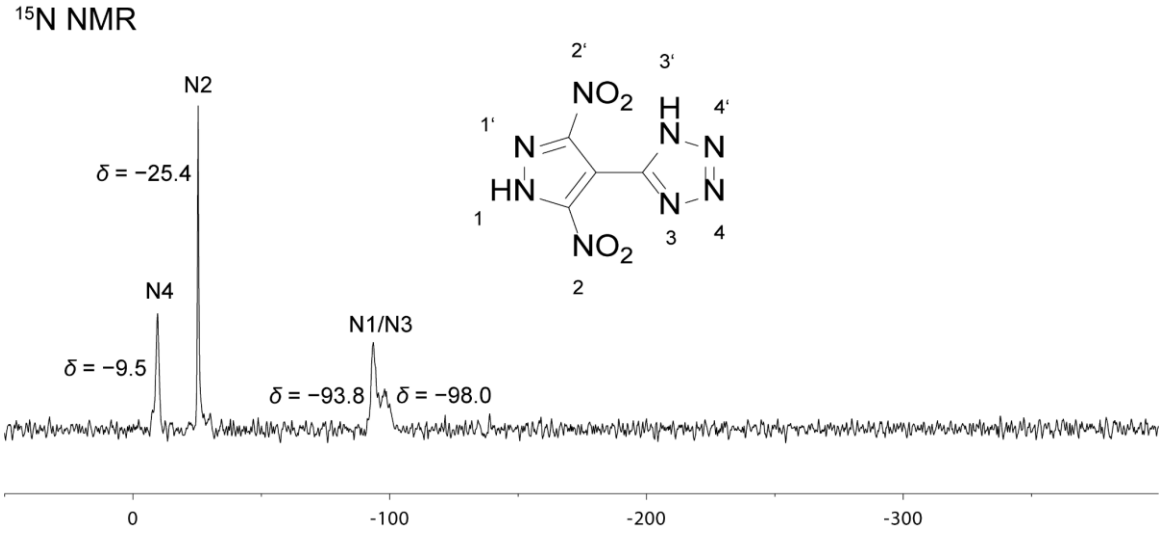

Figure 9. ^{15}N NMR spectra of H_2DNPT (**3**); chemical shifts are given in ppm.

The assignment of the respective oscillations in the IR spectra to the corresponding functional groups was checked with appropriate data.[44] The characteristic bands for the nitro groups (asymmetric and symmetric vibrations) can be found for all compounds investigated. They appear in the range of 1557–1514 cm^{-1} for the asymmetric stretching vibration and 1323–1312 cm^{-1} for the symmetric vibration, respectively. All compounds with an amino group containing cation (**5**–**9**) show significant absorption bands in the range of 3000 cm^{-1} for the NH_2 stretching vibration and in the region of 1600 cm^{-1} for the deformation vibration of the amino group.

5.2.4 Physico-chemical Properties

As all compounds produced can be classified as energetic substances, the energetic properties must be investigated. The theoretically calculated and experimentally determined physicochemical values are shown in Table 3 and compared with the data of RDX. Computed values (detonation velocity, detonation pressure, ect.) are only given for compounds with a preserved crystal structure.
The thermal behavior of all synthesized compounds was determined by differential thermal analysis experiments. The compound with the highest decomposition temperature is the potassium salt **4**, which decomposes at a temperature of 281

°C. H_2DNPT (**3**) shows a clear decomposition at 207 °C (Figure 10). The other decomposition points are in a range of 168 °C for the 1,5-DATH derivative **5** and 240 °C for the tetraaminobitriazole salt (**8**).

Table 3. Physic-chemical properties of compounds **3**–**5**, **7**, **8**, **11**, **12** and RDX.

	3	**4**	**5**	**7**	**8**	**11** • 2 H_2O	**12** • 2 H_2O	RDX
M [g mol^{-1}]	226.11	264.21	326.20	300.20	422.29	295.17	279.17	222.12
IS [J] [a]	2.0	1.0	2.0	20	40	10	5	7.5
FS [N] [b]	120	20	192	360	>360	360	360	120
ESD [J] [c]	0.06	0.12	0.25	0.61	0.54	0.25	0.12	0.2
N [%] [d]	49.56	42.41	60.12	55.99	59.70	42.71	45.16	37.84
Ω [%] [e]	−35.38	−30.28	−44.14	−53.29	−64.41	−29.81	−37.25	−21.61
$T_{dec.}$ [°C] [f]	207	281	168	209	240	197	254	210
Density [g cm^{-3}] [g]	1.669	1.879	1.757	1.713	1.729	1.685	1.667	1.800
$\Delta_f H_m°$ / kJ mol^{-1} [h]	517.1	305.5	820.6	432.7	298.	425.1	348.4	70.3
$\Delta_f U°$ [kJ kg^{-1}] [i]	2369.1	1219.6	2618.2	1557.0	816.4	1564.0	1374.5	433.7
EXPLO5 V6.05								
$-\Delta_E U°$ [kJ kg^{-1}] [j]	5258	4842	4875	4190	2613.1	6240	5682	5740
T_E [K] [k]	4093	3591	3506	2997	2174	4010	3694	3745
p_{CJ} [kbar] [l]	260	236	279	243	188	310	283	336
V_D [m s^{-1}] [m]	8062	7568	8441	8062	7364	8648	8431	8801
Gas vol. [L kg^{-1}] [n]	752	537	786	808	773	833	845	711

a impact sensitivity (BAM drophammer, 1 of 6); b friction sensitivity (BAM friction tester, 1 of 6); c electrostatic discharge device (OZM); d nitrogen content; e oxygen balance; f decomposition temperature from DSC (β = 5°C); g estimated from X-ray diffraction (298 K); h calculated (CBS-4M) heat of formation; i calculated energy of formation; j heat of explosion; k explosion temperature; l detonation pressure; m detonation velocity; n assuming only gaseous products.

For the water containing compounds, the decomposition points for the hydrazinium (**10**·H_2O, 184 °C) and the hydroxylammonium (**11**·2 H_2O, 197 °C) compound are slightly below 200 °C; the ammonium salt (**12**·2 H_2O) reaches a value of 254 °C. The potassium derivative showed detonation-like decomposition in a hot plate test, in which 50 mg of **4** was heated on a copper plate with a Bunsen burner. An

initiation test, in which 50 mg of compound **4** was compressed onto 200 mg of PETN in a copper sleeve and an ignitor, which produced a jet of flame, did not initiate PETN but caused a deflagration.

Additionally, the sensitivity values for external stimuli toward impact, friction and electrostatic discharge were determined following the BAM standards.[45-46]

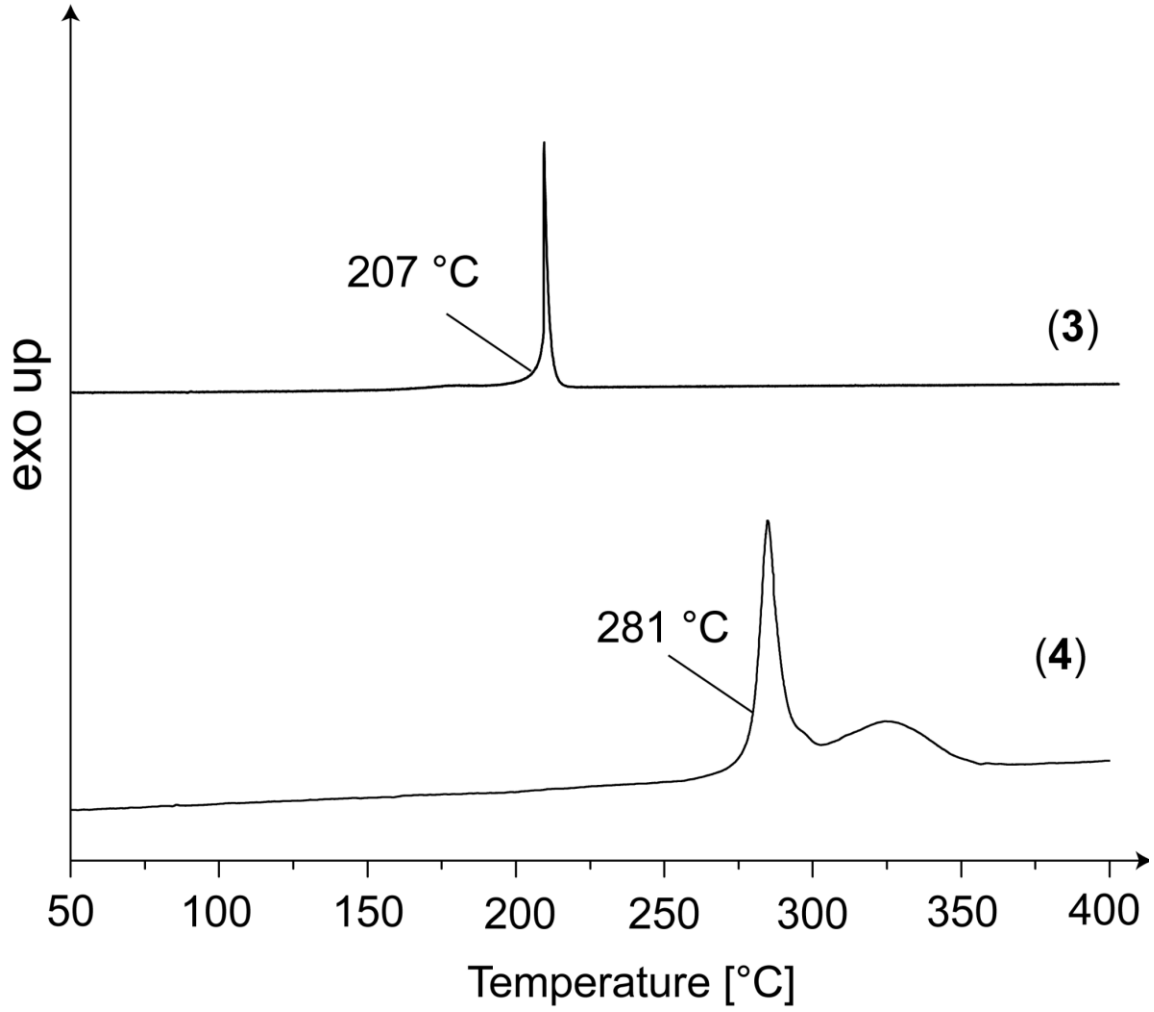

Figure 10. DTA plot of compounds **3** (bottom) and **4** (top) measured with a heating rate of 5 K·min^{-1}. Critical temperatures are given as onset temperature.

The potassium salt (**4**, IS = 1 J, FS = 20 N, ESD = 12 mJ) is the most sensitive compound containing the $HDNPT^-$ anion. The neutral compound **3** shows low values for the sensitivity towards impact of 2 J and electrostatic discharge of 60 mJ. The value for friction sensitivity is moderate with 120 N. Except the 1,5-DAT salt **5** (FS = 192 N), all nitrogen-rich salts are insensitive towards friction (FS = 360 N). Even in terms of impact sensitivity compound **5** (IS = 2 J) has the

lowest value for nitrogen-rich derivatives. The other values vary from 5 J for the hydrazinium **10**·H_2O and ammonium **12**·2 H_2O compound to 40 J for insensitive salts **6**, **8** and **9**. Excluding the ammonium **12**·2 H_2O compound (ESD = 0.12 J), all other values for ESD sensitivity are > 0.25 J.

The detonation velocity V_D and pressure p_{CJ} were calculated using the EXPLO5 code. The densities used in the calculations were determined based on the respective crystal structures. However, these values cannot compete with RDX (V_D = 8801 m·s^{-1}; p_{CJ} = 336 kbar). All compounds listed in Table 3 show a high positive heat of formation from 816.4 kJ·kg^{-1} for **8** to 2618.2 kJ·kg^{-1} for **5**, which clearly exceeds that of RDX (433.7 kJ·kg^{-1}). The water containing hydroxylammonium derivative **11** with V_D = 8648 m·s^{-1} and p_{CJ} = 310 kbar is the only compound that shows values close to those of RDX. The other compounds show calculated values in the range of 7364 m s^{-1} (**8**) to 8441 m s^{-1} (**5**) for the detonation velocity and 188 kbar (**8**) to 283 kbar (**12**·2 H_2O) for the detonation pressure. The neutral compound H_2DNPT (**3**) shows moderate values (V_D = 8062 m·s^{-1}; p_{CJ} = 260 kbar).

5.3 Conclusion

In this study, we report an innovative synthesis leading to a previously unknown C–C connection of a dinitropyrazole moiety with a tetrazole ring. The starting material for the synthesis was 4-amino-3,5-dinitropyrazole (ADNP, **1**), which can be produced from pyrazole in 3 steps via an established synthesis pathway. Subsequently, a diazotization of **1** to the intermediate diazonium compound takes place, which is immediately converted to 4-cyano-3,5-dinitropyrazole (**2**) by cyanide substitution. A final [2+3] cycloaddition reaction with sodium azide and zinc chloride as catalyst yields H_2DNPT (**3**). By reacting H_2DNPT (**3**) with nitrogen-rich organic bases and potassium carbonate, nine ionic derivatives were synthesized. All compounds were fully characterized via vibrational (IR) and NMR spectroscopy as well as sensitivity towards impact, friction and electrostatic discharge. The thermal behavior was investigated using differential thermal analysis (DTA), with the potassium derivative **4** with a T_{dec} = 281 °C being particularly striking. For certain compounds the detonation parameters were calculated with the EXPLO5

code using the corresponding crystal structure data. For the anhydrous compounds, the values range from 7364 m·s^{-1} for TABTrH compound **8** to 8441 m·s^{-1} for 1,5-DATH compound **5**. The neutral compound H_2DNPT (**3**) shows passable values for the detonation velocity and pressure (V_D = 8062 m·s^{-1}, p_{CJ} = 260 kbar). Unfortunately, the apparently most promising cations yield material with included water molecules. Dehydration of these compounds was not possible because water was immediately trapped again when the compounds were dried and then exposed to air again. For the hydroxylammonium salt **11** with two crystal water moieties, the value for V_D is still 8648 m·s^{-1}.

5.4 Acknowledgement

For financial support of this work by the Ludwig-Maximilian University (LMU), the Office of Naval Research (ONR) under grant no. ONR N00014–19–1-2078 and the Strategic Environmental Research and Development Program (SERDP) under contract no. W912HQ19C0033 are gratefully acknowledged. The authors thank Stefan Huber for his help with the sensitivity measurement and Florian Kris for synthetic assistance. Open access funding enabled and organized by Projekt DEAL.

5.5 References

[1] B. Palaszewski, L. S. Ianovski, P. Carrick, *J. Propul. Power* **1998**, *14*, 641–648.

[2] S. B. Kim, K. J. Kim, M. H. Cho, J. H. Kim, K. T. Kim, S. H. Kim, *ACS Appl. Mater & Interfaces* **2016**, *8*, 9405–9412.

[3] H. Gao, J. M. Shreeve, *Chem. Rev.* **2011**, *111*, 7377–7436.

[4] Z. L. Chioato, T. M. Klapötke, F. Mieskes, J. Stierstorfer, M. Weyrauther, *Eur. J. Inorg. Chem.* **2016**, 956–962.

[5] T. M. Klapötke, *Chemistry of High-Energy Materials*, De Gruyter, Boston, Berlin, **2017**.

[6] M. R. Manaa, E. J. Reed, L. E. Fried, N. Goldman, *J. Am. Chem. Soc.* **2009**, *131*, 5483–5487.

[7] E.-C. Koch, *Propellants Explos. Pyrotech.* **2015**, *40*, 374–387.

[8] G. Wang, T. Lu, G. Fan, H. Yin, F.-X. Chen, *New J. Chem.* **2019**, *43*, 1663–1666.

[9] T. Brinck*, Green Energetic Materials*, Wiley, Hoboken, **2014**.

[10] D. Fischer, J. L. Gottfried, T. M. Klapötke, K. Karaghiosoff, J. Stierstorfer, T. G. Witkowski, *Angew. Chem. Int. Ed.* **2016**, *55*, 16132–16135.

[11] C.-J. Lei, H.-W. Yang, H.-L. Xiong, G.-B. Cheng, *Propellants Explos. Pyrotech.* **2019**, *44*, 1–7.

[12] D. Fischer, T. M. Klapötke, M. Reymann, J. Stierstorfer, *Chem. Eur. J.* **2014**, *20*, 6401–6411.

[13] W. Fu, B. Zhao, M. Zhang, C. Li, H. Gao, J. Zhang, Z. Zhou, *J. Mater. Chem A* **2017**, *5*, 5044–5054.

[14] N. Fischer, D. Fischer, T. M. Klapötke, D. G. Piercey, J. Stierstorfer, *J. Mater. Chem.* **2012**, *22*, 20418–20422.

[15] J. Zhang, J. M. Shreeve, *J. Am. Chem. Soc.* **2014**, *136*, 4437–4445.

[16] J. Zhang, P. Yin, G. Pan, Z. Wang, J. Zhang, L. A. Mitchell, D. A. Parrish, J. M. Shreeve, *New J. Chem.* **2019**, *43*, 12684–12689.

[17] M. F. Bölter, T. M. Klapötke, T. Kustermann, T. Lenz, J. Stierstorfer, *Eur. J. Inorg. Chem.* **2018**, *2018*, 4125–4132.

[18] A. A. Dippold, T. M. Klapötke, *Chem. Asian J.* **2013**, *8*, 1463–1471.

[19] A. A. Dippold, D. Izsák, T. M. Klapötke, *Chem. Eur. J.* **2013**, *19*, 12042–12051.

[20] P. F. Pagoria, M.-X. Zhang, N. B. Zuckerman, A. J. DeHope, D. A. Parrish, *Chem. Heterocycl. Compd.* **2017**, *53*, 760–778.

[21] E. C. Johnson, J. J. Sabatini, D. E. Chavez, R. C. Sausa, E. F. C. Byrd, L. A. Wingard, P. E. Guzmàn, *Org. Process Res. Dev.* **2018**, *22*, 736–740.

[22] D. Fischer, J. L. Gottfried, T. M. Klapötke, K. Karaghiosoff, J. Stierstorfer, T. G. Witkowski, *Angew. Chem. Int. Ed.* **2016**, *55*, 16132–16135.

[23] P. Yin, L. A. Mitchell, D. A. Parrish, J. M. Shreeve, *Angew. Chem.* **2016**, *128*, 14621–14623.

[24] R. Yang, Z. Dong, Z. Ye, *ChemistrySelect* **2019**, *4*, 14208-14213.

[25] J. C. Galvez-Ruiz, G. Holl, K. Karaghiosoff, T. M. Klapötke, K. Loehnwitz, P. Mayer, H. Noeth, K. Polborn, C. J. Rohbogner, M. Suter, J. J. Weigand, *Inorg. Chem.* **2005**, *44*, 5192–5192.

[26] K. V. Domasevitch, I. Gospodinov, H. Krautscheid, T. M. Klapötke, J. Stierstorfer, *New J. Chem.* **2019**, *43*, 1305–1312.

[27] T. K. Shkineva, A. V. Kormanov, V. N. Boldinova, I. A. Vatsadze, I. L. Dalinger, *Chem. Heterocycl. Compd.* **2018**, *54*, 703–709.

[28] D. Kumar, G. H. Imler, D. A. Parrish, J. M. Shreeve, *New J. Chem.* **2017**, *41*, 4040–4047.

[29] S. Ek, N. V. Latypov, *J. Heterocycl. Chem.* **2014**, *51*, 1621–1627.

[30] I. L. Dalinger, I. A. Vatsadze, T. K. Shkineva, G. P. Popova, S. A. Shevelev, *Mendeleev Commun.* **2012**, *22*, 43–44.

[31] I. L. Dalinger, I. A. Vatsadze, T. K. Shkineva, G. P. Popova, S. A. Shevelev, *Synthesis* **2012**, *44*, 2058–2064.

[32] Z. P. Demko, K. B. Sharpless, *The Journal of Organic Chemistry* **2001**, *66*, 7945–7950.

[33] H. Huang, Z. Zhou, L. Liang, J. Song, K. Wang, D. Cao, C. Bian, W. Sun, M. Xue, *Z. Anorg. Allg. Chem.* **2012**, *638*, 392–400.

[34] L. Liang, H. Huang, K. Wang, C. Bian, J. Song, L. Ling, F. Zhao, Z. Zhou, *J. Mater. Chem.* **2012**, *22*, 21954–21964.

[35] V. D. Ghule, S. Radhakrishnan, P. M. Jadhav, *Struct. Chem.* **2011**, *22*, 775–782.

[36] A. F. Hollemann, E. Wiberg, N. Wiberg, *Lehrbuch der anorganischen Chemie*, de Gruyter: New York, **2007**.

[37] M. Dachs, A. A. Dippold, J. Gaar, M. Holler, T. M. Klapötke, *Z. Anorg. Allg. Chem.* **2013**, *639*, 2171–2180.

[38] F. H. Allen, O. Kennard, D. G. Watson, L. Brammer, A. G. Orpen, R. Taylor, *J. Chem. Soc.* **1987**, 1–19.

[39] M. Tariq, S. Hameed, I. H. Bechtold, A. J. Bortoluzzi, A. A. Merlo, *J. Mater. Chem. C* **2013**, *1*, 5583–5593.

[40] M. F. Bölter, A. Harter, T. M. Klapötke, J. Stierstorfer, *ChemPlusChem* **2018**, *83*, 804–811.

[41] N. Fischer, T. M. Klapötke, M. Reymann, J. Stierstorfer, *Eur. J. Inorg. Chem.* **2013**, 2167–2180.

[42] M. J. Frisch, G. W. Trucks, H. B. Schlegel, G. E. Scuseria, M. A. Robb, J. R. Cheeseman, G. Scalmani, V. Barone, B. Mennucci, G. A. Petersson, H. Nakatsuji, M. Caricato, X. Li, H. P. Hratchian, A. F. Izmaylov, J. Bloino, G.

Zheng, J. L. Sonnenberg, M. Hada, M. Ehara, K. Toyota, R. Fukuda, J. Hasegawa, M. Ishida, T. Nakajima, Y. Honda, O. Kitao, H. Nakai, T. Vreven, J. A. Montgomery Jr., J. E. Peralta, F. Ogliaro, M. Bearpark, J. J. Heyd, E. Brothers, K. N. Kudin, V. N. Staroverov, T. Keith, R. Kobayashi, J. Normand, K. Raghavachari, A. Rendell, J. C. Burant, S. S. Iyengar, J. Tomasi, M. Cossi, N. Rega, J. M. Millam, M. Klene, J. E. Knox, J. B. Cross, V. Bakken, C. Adamo, J. Jaramillo, R. Gomperts, R. E. Stratmann, O. Yazyev, A. J. Austin, R. Cammi, C. Pomelli, J. W. Ochterski, R. L. Martin, K. Morokuma, V. G. Zakrzewski, G. A. Voth, P. Salvador, J. J. Dannenberg, S. Dapprich, A. D. Daniels, O. Farkas, J. B. Foresman, J. V. Ortiz, J. Cioslowski, and D. J. Fox, *Gaussian 09 Revision C.01*, Gaussian, Inc., Wallingford, CT, USA, **2010**.

[43] J. Stierstorfer, *Dissertation,* Ludwig-Maximilians-Universität München, **2009**.

[44] M. Hesse, H. Meier, B. Zeeh, in: *Spektroskopische Methoden in der organischen Chemie*, Vol. 6, Thieme, Stuttgart, New York, **2002**.

[45] Reichel & Partner GmbH, http://www.reichelt-partner.de.

[46] Test Methods According to the UN Recommendations on the Transport of Dangerous Goods, Manual of Test and Criteria, Fourth Revised Edition, United Nations Publication, New York and Geneva, 2003, ISBN 92-1-139087 7, Sales No. E.03.VIII. 2; 13.4.2 Test 3a (ii)BAM Fallhammer.

5.6 Supporting Information

5.6.1 Experimental Procedure

^{1}H, ^{13}C, ^{14}N and ^{15}N NMR spectra were recorded on *JEOL 270* and *BRUKER AMX 400* instruments. The samples were measured at room temperature in standard NMR tubes (Ø 5 mm). Chemical shifts are reported as d values in ppm relative to the residual solvent peaks of d_6-DMSO (δ_H: 2.50, δ_C: 39.5). Solvent residual signals and chemical shifts for NMR solvents were referenced against tetramethylsilane (TMS, δ = 0 ppm) and nitromethane. Unless stated otherwise, coupling constants were reported in Hertz (Hz) and for the characterization of the observed signal multiplicities the following abbreviations were used: s (singlet), d (doublet),

t (triplet), q (quartet), quint (quintet), sept (septet), m (multiplet) and br (broad). Mass spectra were recorded on a *JEOL MStation JMS700* using the EI or ESI technique. Infrared spectra (IR) were recorded from 4000 cm^{-1} to 400 cm^{-1} on a *PERKIN ELMER Spectrum BX- 59343* instrument with a *SMITHS DETECTION DuraSamplIR II Diamond ATR* sensor. The absorption bands are reported in wavenumbers (cm^{-1}). Decomposition temperatures were measured via differential thermal analysis (DTA) with an *OZM Research DTA 552-Ex* instrument at a heating rate of 5 °Cmin^{-1} and in a range of room temperature to 400 °C. All sensitivities toward impact (IS) and friction (FS) were determined according to BAM (German: Bundesanstalt für Materialforschung und Prüfung) standards using a BAM drop hammer and a BAM friction apparatus by applying the 1 of 6 method. All energetic compounds were tested for sensitivity towards electrical discharge using an *Electric Spark Tester ESD 2010 EN* from OZM.

CAUTION! *All investigated compounds are potentially explosive materials, although no hazards were observed during preparation and handling these compounds. Nevertheless, safety precautions (such as wearing leather coat, face shield, Kevlar sleeves, Kevlar gloves, earthed equipment and ear plugs) should be drawn.*

Sodium 4-cyano-3,5-dinitropyrazolate dihydrate NaCDNP · 2 H_2O (**2**)

4-Amino-3,5-dinitropyrazole (5.00 g, 28.9 mmol, 1.0 eq) was solved in sulfuric acid (100 mL, 1 M) and added to a solution of sodium nitrite (2.5 g, 36.2 mmol, 1.3 eq) in water (50.0 mL) at 5 °C. The mixture was stirred for 20 min at this temperature and further stirred at ambient temperature for 30 min. The mixture was neutralized with sodium hydrogen carbonate to pH = 7. Then, copper-(I)-cyanide (3.20 g, 35.7 mmol, 1.2 eq) was added in one portion and a solution of sodium cyanide (2.50 g, 51.0 mmol, 1.8 eq) in water (50.0 mL) was added dropwise to the mixture. The solution was then stirred for 30 min at room temperature and for 2 h at 70 °C. Afterwards, the mixture was cooled to room temperature and the precipitated solid was filtered and discarded. The solvent was evaporated under reduced pressure and the brown residue was extracted with ethyl acetate (400 mL). The organic layer was dried over anhydrous sodium sulfate and the solvent was evaporated under

reduced pressure to yield sodium 4-cyano-3,5-dinitropyrazolate dehydrate (**2**) (5.80 g, 24.1 mmol, 83%) as brown solid.

DTA (5 °C min^{-1}): 77 °C (endo), 210 °C (dec.); IR (ATR) $\tilde{\nu}$ (cm^{-1}) = 3574(m), 3566(m), 3390(w), 3378(m), 3325(w), 3307(w), 3280(w), 3206(w), 2249(w), 1636(m), 1534(s), 1512(s), 1504(s), 1455(s), 1430(m), 1414(s), 1361(s), 1324(vs), 1239(m), 1185(m), 1145(m), 1130(m), 1044(m), 1044(m), 1024(m), 1016(m), 1003(m), 847(s), 805(m), 767(m), 744(m), 719(m), 693(s), 641(s), 544(s), 500(s), 493(s); Elem. Anal. ($C_4H_4N_5O_6Na$, 241.09 g mol^{-1}) calcd.: C 19.43, N 28.21, H 1.69%. Found: C 19.93, N 29.05, H 1.67%; ^{1}H NMR (d_6-DMSO, 400 MHz, ppm) δ = 3.44 (s, 4H); ^{13}C NMR (d_6-DMSO, 101 MHz, ppm) δ = 156.9, 111.7, 82.5; ^{14}N NMR (d_6-DMSO, 29 MHz, ppm) δ = −22; *m/z* (ESI^-): 182 (anion).

5-(3,5-dinitro-pyrazol-4-yl)-tetrazole H_2DNPT (**3**)

Sodium 4-cyano-3,5-dinitropyrazolate dihydrate (5.80 g, 24.1 mmol, 1.0 eq) was solved in water (400 mL) and sodium azide (4.70 g, 72.3 mmol, 3.0 eq) and zinc chloride (9.85 g, 72.3 mmol, 3.0 eq) were added and the solution was stirred for 72 h at 85 °C. Afterwards, the residue was filtered off, solved in hydrochloric acid (200 mL, 2 M) and extracted with ethyl acetate (4 x 100 mL). The organic phase was dried over anhydrous sodium sulfate and the solvent was evaporated under reduced pressure. The resulting viscous mass was solved in toluene/acetone (1:1, 20 mL) and the solvent was evaporated under reduced pressure. The procedure was repeated twice to yield 5-(3,5-dinitro-1H-pyrazol-4-yl)-1H-tetrazole (**3**) (3.00 g, 13.3 mmol, 55%) as a slightly brown powder.

DTA (5 °C min^{-1}): 207 °C (dec.); Sensitivities: BAM drop hammer: 2 J (500-1000 µm), friction tester: 120 N (500-1000 µm), ESD: 60 mJ (500-1000 µm); IR (ATR) $\tilde{\nu}$ (cm^{-1}) = 3217(w), 2921(m), 2703(m), 2622(m), 1886(w), 1645(w), 1533(s), 1505(s), 1437(m), 1416(s), 1399(s), 1388(s), 1357(s), 1323(vs), 1295(m), 1279(m), 1253(m), 1218(m), 1182(w), 1156(m), 1149(m), 1114(w), 1088(m), 1088(m), 1070(m), 1028(m), 1016(m), 988(s), 854(s), 840(vs), 772(m), 755(m), 715(m), 675(m), 659(m), 637(m), 624(m), 560(m), 514(m), 477(w), 430(m), 416(m), 408(m); Elem. Anal. ($C_4H_2N_8O_4$, 226.11 g mol^{-1}) calcd.: C 21.25, N 49.56, H 0.89%. Found: C 21.13, N 49.21, H 0.87%; ^{1}H NMR (d_6-DMSO, 400 MHz, ppm) δ = 14.24 (br s, 2H); ^{13}C NMR (d_6-DMSO, 101 MHz, ppm) δ = 153.6, 147.3,

97-5; ^{14}N NMR (d_6-DMSO, 29 MHz, ppm) δ = −24; ^{15}N NMR (d_6-DMSO, 41 MHz, ppm) δ = −9.5, −25.4, −93.8, −98.0; *m/z* (ESI$^-$): 225 (anion).

Potassium 3,5-dinitro-4-(1*H*-tetrazol-1-yl)pyrazolate KHDNPT (**4**)

H_2DNPT (0.70 g, 3.10 mmol, 1.0 eq) was solved in a mixture of water and ethanol (1:1, 10 mL) and heated to 80 °C. Potassium carbonate (0.22 g, 1.55 mmol, 0.5 eq) was added and the mixture was stirred until all solid was solved. After cooling to room temperature the formed solid was dried on air and recrystallized from acetone to yield potassium 3,5-dinitro-4-(1*H*-tetrazol-1-yl)pyrazolate (**4**) (0.72 g, 2.73 mmol, 88%) as a brown powder.
DTA (5 °C min^{-1}): 281 °C (dec); Sensitivities: BAM drop hammer: 1 J (500-1000 µm), friction tester: 20 N (500-1000 µm), ESD: 0.12 J (500-1000 µm); IR (ATR) $\tilde{\nu}$ (cm^{-1}) = 2588(w), 2551(w), 1641(w), 1527(s), 1505(s), 1416(m), 1405(m), 1385(s), 1357(s), 1317(vs), 1289(m), 1236(m), 1178(w), 1147(m), 1109(w), 1064(m), 1026(m), 1006(m), 976(m), 850(vs), 823(m), 772(m), 764(m), 764(m), 759(m), 660(s), 649(m), 573(m), 526(m), 494(m), 459(m), 448(m), 442(m), 420(m), 406(m); Elem. Anal. ($C_4HN_8O_4K$, 264.20 g mol^{-1}) calcd.: C 18.18, N 42.41, H 0.38%. Found: C 18.42, N 42.64, H 0.63%; ^{1}H NMR (d_6-DMSO, 400 MHz, ppm) δ = -; ^{13}C NMR (d_6-DMSO, 101 MHz, ppm) δ = 154.7, 147.6, 96.4; ^{14}N NMR (d_6-DMSO, 29 MHz, ppm) δ = −19; *m/z* (ESI$^-$): 225 (anion).

1,5-Diamino-1*H*-tetrazol-4-ium 3,5-dinitro-4-(1*H*-tetrazol-5-yl)pyrazolate (1,5-DATH)HDNPT (**5**)

H_2DNPT (0.78 g, 3.45 mmol, 1.0 eq) was solved in a mixture of water and methanol (1:1, 6 mL) and heated to 40 °C. 1,5-Diamino-1*H*-tetrazole (0.34 g, 3.45 mmol, 1.0 eq) was added and the mixture was stirred for 10 min. After cooling to room temperature, the formed solid was collected by filtration and washed with little amounts of cold methanol to yield 3,5-dinitro-4-(1*H*-tetrazol-5-yl)pyrazolate-1,5-diamino-1*H*-tetrazol-4-ium (**5**) (1.02 g, 3.14 mmol, 91%) as a yellow solid.
DTA (5 °C min^{-1}): 168 °C (dec.); Sensitivities: BAM drop hammer: 2 J (500-1000 µm), friction tester: 192 N (500-1000 µm), ESD: 0.25 J (500-1000µm); IR (ATR) $\tilde{\nu}$ (cm^{-1}) = 3363(m), 3261(m), 3120(m), 1708(s), 1651(m), 1632(s),

1533(s), 1527(s), 1509(m), 1488(m), 1427(m), 1370(s), 1352(s), 1334(s), 1315(s), 1283(s), 1234(m), 1181(m), 1141(m), 1134(m), 1099(m), 1066(s), 1025(m), 1025(m), 998(s), 992(s), 907(s), 842(s), 787(m), 770(m), 754(s), 731(s), 711(s), 685(vs), 647(s), 607(s), 567(s), 516(s), 493(s), 446(vs), 440(vs), 414(vs); Elem. Anal. ($C_5H_6N_{14}O_4$, 326.20 g mol^{-1}) calcd.: C 18.41, N 60.12, H 1.85%. Found: C 18.05, N 59.52, H 1.83%; ^{1}H NMR (d_6-DMSO, 400 MHz, ppm) δ = 7.58 (br s, 4H); ^{13}C NMR (d_6-DMSO, 101 MHz, ppm) δ = 153.9, 153.1, 147.0, 97.1; ^{14}N NMR (d_6-DMSO, 29 MHz, ppm) δ = −22; *m/z* (ESI$^-$): 225 (anion).

Guanidinium 3,5-dinitro-4-(1*H*-tetrazol-5-yl)pyrazolate (G)HDNPT (**6**)

H_2DNPT (0.84 g, 3.73 mmol, 1.0 eq) was solved in a mixture of water and methanol (1:1, 10 mL) and guanidinium carbonate (0.33 g, 1.87 mmol, 0.5 eq) was added and the mixture was heated to 70 °C for 30 min. The solution was cooled to room temperature and the solvent was evaporated under reduced pressure. After recrystallization from hot methanol guanidinium 3,5-dinitro-4-(1*H*-tetrazol-5-yl)pyrazolate (**6**) (0.91 g, 3.21 mmol, 86%) was obtained as a dark red solid.
DTA (5 °C min^{-1}): 231 °C (dec.); Sensitivities: BAM drop hammer: 40 J (500-1000 µm), friction tester: >360 N (500-1000 µm), ESD: 0.54 J (500-1000 µm); IR (ATR) $\tilde{\nu}$ (cm^{-1}) = 3450(m), 3360(m), 3280(m), 3174(m), 1659(s), 1514(s), 1405(m), 1351(s), 1314(s), 1216(m), 1160(m), 1014(m), 848(s), 762(m), 756(m), 673(m), 661(m), 463(vs), 442(vs), 416(vs), 402(vs); Elem. Anal. ($C_5H_7N_{11}O_4$, 285.18 g mol^{-1}) calcd.: C 21.06, N 54.03, H 2.47%. Found: C 21.61, N 53.74, H 2.36%; ^{1}H NMR (d_6-DMSO, 400 MHz, ppm) δ = 6.92 (s, 6H); ^{13}C NMR (d_6-DMSO, 101 MHz, ppm) δ = 157.9, 154.7, 147.6, 96.4; ^{14}N NMR (d_6-DMSO, 29 MHz, ppm) δ = −20 ; *m/z* (ESI$^-$): 225 (anion).

Aminoguanidinium 3,5-dinitro-4-(1*H*-tetrazol-5-yl)pyrazolate (AG)HDNPT (**7**)

H_2DNPT (1.02 g, 4.50 mmol, 1.0 eq) was solved in a mixture of water and methanol (1:1, 10 mL) and aminoguanidine bicarbonate (0.61 g, 4.50 mmol, 1.0 eq) was added and the mixture was heated to 70 °C for 30 min. The solution was cooled to room temperature and the solvent was evaporated under reduced pressure. After recrystallization from hot methanol aminoguanidinium 3,5-dinitro-

4-(1*H*-tetrazol-5-yl)pyrazolate (**7**) (1.26 g, 4.19 mmol, 93%) was obtained as a red solid.

DTA (5 °C min^{-1}): 208 °C (dec.); Sensitivities: BAM drop hammer: 20 J (500-1000 µm), friction tester: 360 N (500-1000 µm), ESD: 0.61 J (500-1000 µm). IR (ATR) $\tilde{\nu}$ (cm^{-1}) = 3446(m), 3360(m), 3329(w), 3270(w), 3175(w), 3033(w), 2971(w), 1682(m), 1666(s), 1628(m), 1548(vs), 1485(m), 1423(m), 1378(s), 1363(s), 1353(vs), 1316(vs), 1288(m), 1229(s), 1218(m), 1147(w), 1084(m), 1074(m), 1074(m), 1010(w), 996(m), 975(m), 956(m), 848(vs), 759(w), 658(m), 530(s), 521(s), 493(s), 464(m), 440(s), 433(s), 411(s); Elem. Anal. ($C_5H_8N_{12}O_4$, 300.20 g mol^{-1}) calcd.: C 20.01, N 55.99, H 2.69%. Found: C 20.56, N 55.04, H 2.64%; ^{1}H NMR (d_6-DMSO, 400 MHz, ppm) δ = 8.55 (s, 1H), 7.24(s, 2H), 6.72 (s, 2H), 4.68 (s, 2H); ^{13}C NMR (d_6-DMSO, 101 MHz, ppm) δ = 158.8, 154.7, 147.5, 96.2; ^{14}N NMR (d_6-DMSO, 29 MHz, ppm) δ = −20 ; *m/z* (ESI^-): 225 (anion).

4,4',5,5'-Tetraamino-[3,3'-bi(1,2,4-triazol)]-1-ium 3,5-dinitro-4-(1*H*-tetrazol-5-yl)pyrazolate (TABTrH)HDNPT (**8**)

H_2DNPT (0.92 g, 4.05 mmol, 1.0 eq) was solved in a mixture of water and ethanol (1:1, 10 mL) and heated to reflux. 3,3'-bi(1,2,4-triazole)-4,4',5,5'-tetraamine (0.79 g, 4.05 mmol, 1.0 eq) was added in one portion and the mixture was refluxed until all precipitate was solved (1 h). The solution was cooled to room temperature and the formed solid was collected by filtration to yield 4,4',5,5'-tetraamino-[3,3'-bi(1,2,4-triazol)]-1-ium-3,5-dinitro-4-(1*H*-tetrazol-5-yl)pyrazolate (**8**) (1.52 g, 3.55 mmol, 88%) as yellowish powder.

DTA (5 °C min^{-1}): 240 °C (dec.); Sensitivities: BAM drop hammer: 40 J (500-1000 µm), friction tester: 360 N (500-1000 µm), ESD: 0.54 J (500-1000 µm); (IR (ATR) $\tilde{\nu}$ (cm^{-1}) = 3400(m), 3338(m), 3329(m), 3320(m), 3280(s), 3271(s), 1629(vs), 1598(s), 1538(vs), 1477(s), 1421(m), 1359(s), 1340(s), 1312(s), 1228(m), 1083(m), 1023(m), 986(vs), 936(s), 842(s), 842(s), 797(m), 722(s), 690(s), 681(s), 628(s), 622(s), 608(s), 524(vs), 516(vs), 506(vs), 494(vs), 452(vs); Elem. Anal. ($C_8H_{10}N_{18}O_4$, 422.29 g mol^{-1}) calcd.: C 22.75, N 59.70. H 2.39%. Found: C 23.07, N 58.79, H 2.29%; ^{1}H NMR (d_6-DMSO, 400 MHz, ppm) δ = 7.40 (br s, 4H) 5.99 (br s, 4H); ^{13}C NMR (d_6-DMSO, 101 MHz, ppm) δ = 154.7, 153.9,

147.5, 138.6, 96.1; ^{14}N NMR (*d*$_6$-DMSO, 29 MHz, ppm) δ = −20; *m/z* (ESI$^-$): 225 (anion).

Carbodihydrazidium 3,5-dinitro-4-(1*H*-tetrazol-5-yl)pyrazolate (DAUH)HDNPT (**9**)

H_2DNPT (1.17 g, 5.18 mmol, 1.0 eq) was solved in methanol (25 mL) and heated to reflux. Carbodihydrazide (0.47 g, 5.18 mmol, 1.0 eq) was added in one portion and the mixture was refluxed until all precipitate was solved (30 min). The solution was cooled to 0 °C and the formed solid was collected by filtration to yield carbodihydrazidium 3,5-dinitro-4-(1*H*-tetrazol-5-yl)pyrazolate (**9**) (1.34 g, 4.25 mmol, 82%) as a slightly brownish powder.
DTA (5 °C min^{-1}): 181 °C (dec.); Sensitivities: BAM drop hammer: 40 J (500-1000 µm), friction tester: 360 N (500-1000 µm), ESD: 0.27 J (500-1000 µm); IR (ATR) $\tilde{\nu}$ (cm^{-1}) = 3339(m), 2922(w), 2851(w), 2664(m), 2563(m), 2483(m), 2439(m), 1704(w), 1689(m), 1642(m), 1600(m), 1538(vs), 1528(vs), 1505(s), 1489(vs), 1420(s), 1409(s), 1390(m), 1357(vs), 1323(vs), 1296(s), 1229(s), 1199(m), 1199(m), 1176(m), 1158(m), 1148(m), 1122(m), 1100(m), 1079(m), 1063(m), 1032(m), 986(s), 849(s), 821(m), 770(m), 756(s), 695(w), 657(s), 577(m), 526(m), 520(m), 504(m), 462(m), 422(m); Elem. Anal. ($C_5H_8N_{12}O_5$, 316.20 g mol^{-1}) calcd.: C 18.99, N 53.16, H 2.55%. Found: C 19.04%, N 52.78%, H 2.68%; ^{1}H NMR (*d*$_6$-DMSO, 400 MHz, ppm) δ = 8.68 (br s, 5H); ^{13}C NMR (*d*$_6$-DMSO, 101 MHz, ppm) δ = 159.2, 154.7, 147.4, 96.1; ^{14}N NMR (*d*$_6$-DMSO, 29 MHz, ppm) δ = −17; *m/z* (ESI$^-$): 225 (anion).

Hydrazinium 3,5-dinitro-4-(1*H*-tetrazol-1-yl)pyrazolate hydrate (N_2H_5)HDNPT·H_2O (**10**)

H_2DNPT (0.91 g, 4.04 mmol, 1.0 eq) was solved in methanol (10 mL) and hydrazinium hydroxide (0.20 mL, 4.04 mmol, 1.0 eq) was added dropwise. The mixture was heated to 70 °C and stirred for 10 min. After cooling to room temperature the solvent was removed under reduced pressure to yield hydrazinium 3,5-dinitro-4-(1*H*-tetrazol-1-yl)pyrazolate hydrate (**10**) (1.03 g, 3.72 mmol, 92%) as a tan powder.

DTA (5 °C min^{-1}): 61 °C (endo), 184 °C (dec.); Sensitivities: BAM drop hammer: 5 J (500-1000 µm), friction tester: 360 N (500-1000 µm), ESD: 0.61 J (500-1000 µm); IR (ATR) $\tilde{\nu}$ (cm^{-1}) = 3601(w), 3339(w), 2921(m), 2591(m), 2449(m), 1910(w), 1741(w), 1635(m), 1596(w), 1525(vs), 1495(s), 1410(s), 1386(m), 1355(vs), 1318(vs), 1287(m), 1245(m), 1177(m), 1146(m), 1085(m), 1064(m), 1027(m), 960(s), 960(s), 851(vs), 822(m), 770(m), 757(m), 658(s), 573(m), 416(s); Elem. Anal. ($C_4H_8N_{10}O_5$, 276.17 g mol^{-1}) calcd.: C 17.40, N 50.72, H 2.92%. Found: C 17.68, N 49.93, H 2.70%; ^{1}H NMR (d_6-DMSO, 400 MHz, ppm) δ = 7.13 (br s, 5H), 3.36 (br s, 2H); ^{13}C NMR (d_6-DMSO, 101 MHz, ppm) δ = 154.8, 147.5, 96.2; ^{14}N NMR (d_6-DMSO, 29 MHz, ppm) δ = −19; *m/z* (ESI^-): 225 (anion).

Hydroxylammonium 3,5-dinitro-4-(1*H*-tetrazol-1-yl)pyrazolate dihydrate (Hx)HDNPT·2 H_2O (**11**)

H_2DNPT (0.84 g, 3.73 mmol, 1.0 eq) was solved in a mixture of water and ethanol (1:1, 10 mL) and heated to 70 °C and hydroxylamine solution (0.22 mL, 3.73 mmol, 1.0 eq, 50 wt% in H_2O) was added dropwise to the solution. The mixture was cooled to room temperature and the solvent was evaporated under reduced pressure. The formed solid was recrystallized from hot acetonitrile (5 mL) to yield hydroxylammonium 3,5-dinitro-4-(1*H*-tetrazol-1-yl)pyrazolate dihydrate (**11**) (1.11 g, 3.28 mmol, 88%) as a brown powder.
DTA (5 °C min^{-1}): 99 °C (endo), 197 °C (dec.); Sensitivities: BAM drop hammer: 10 J (500-1000 µm), friction tester: 360 N (500-1000 µm), ESD: 0.25 J (500-1000 µm); IR (ATR) $\tilde{\nu}$ (cm^{-1}) = 3563(w), 3461(w), 3357(w), 3139(m), 2918(m), 2688(m), 2005(w), 1970(w), 1919(w), 1608(m), 1524(s), 1492(s), 1412(s), 1355(s), 1315(vs), 1248(s), 1179(s), 1146(m), 1069(m), 1029(m), 1000(s), 849(s), 769(m), 769(m), 758(s), 657(s), 646(s), 573(m), 517(s), 458(s), 444(s), 418(s); Elem. Anal. ($C_4H_9N_9O_7$, 295.17 g mol^{-1}) calcd.: C 16.28, N 42.71, H 3.07%. Found: C 16.85, N 43.48, H 2.71%; ^{1}H NMR (d_6-DMSO, 400 MHz, ppm) δ = 11.33 (br s, 3H), 10.06 (br s, 1H), 3.39 (br s, 2H); ^{13}C NMR (d_6-DMSO, 101 MHz, ppm) δ = 154.8, 147.5, 96.2; ^{14}N NMR (d_6-DMSO, 29 MHz, ppm) δ = −19, −359; *m/z* (ESI^-): 225 (anion).

Ammonium 3,5-dinitro-4-(1*H*-tetrazol-1-yl)pyrazolate dihydrate (NH_4)HDNPT·2 H_2O (**12**)

H_2DNPT (**3**) (0.68 g, 3.05 mmol, 1.0 eq) was solved in a mixture of water and ethanol (1:1, 10 mL) and heated to 80 °C. Aqueous ammonia solution (25%, 0.24 mL, 3.05 mmol) was added and the mixture was stirred at this temperature for 10 min. After cooling to room temperature the solution was chilled for crystallization to yield ammonium 3,5-dinitro-4-(1*H*-tetrazol-1-yl)pyrazolate dihydrate (**12**) (0.80 g, 2.87 mmol, 94%) as a yellowish solid.
DTA (5 °C min^{-1}): 103 °C (endo), 254 °C (dec.); Sensitivities: BAM drop hammer: 5 J (500-1000 µm), friction tester: 360 N (500-1000 µm), ESD: 0.12 J (500-1000 µm); (IR (ATR) $\tilde{\nu}$ (cm^{-1}) = 3270(m), 3201(m), 3155(m), 3041(m), 2920(m), 2850(m), 2791(m), 2709(m), 2597(m), 1643(w), 1528(s), 1500(m), 1416(s), 1403(s), 1389(s), 1355(s), 1317(vs), 1290(s), 1238(m), 1178(m), 1146(m), 1104(m), 1066(m), 1066(m), 1028(m), 1005(m), 982(m), 849(vs), 821(m), 771(m), 765(m), 759(m), 718(m), 672(m), 659(s), 574(m), 527(m), 475(m), 457(m), 447(m), 435(m), 421(m); Elem. Anal. ($C_4H_9N_9O_6$, 279.17 g mol^{-1}) calcd.: C 17.21, N 45.16, H 3.25%. Found: C 17.37, N 45.16, H 3.49%; ^{1}H NMR (d_6-DMSO, 400 MHz, ppm) δ = 7.24 (br m, 4H); ^{13}C NMR (d_6-DMSO, 101 MHz, ppm) δ = 155.2, 148.6, 98.1; ^{14}N NMR (d_6-DMSO, 29 MHz, ppm) δ = −18, −359; *m/z* (ESI^-): 225 (anion).

5.6.2 Crystallography

Crystal structure data were obtained by measurements on an Oxford Xcalibur3 diffractometer with a Spellman generator (voltage 50 kV, current 40 mA) and a Kappa CCD area for data collection using Mo-*Kα* radiation (λ = 0.71073 Å) or a Bruker D8 Venture TXS diffractometer equipped with a multilayer monochromator, a Photon 2 detector and a rotation-anode generator (Mo-K_α radiation). The data collection was performed using the CRYSTALIS RED software.[S1] The solution of the structure was performed by direct methods and refined by full-matrix least-squares on F2 (SHELXT)[S2] implemented in the OLEX2[S3] software suite. The non-hydrogen atoms were refined anisotropically and the hydrogen atoms were located

and freely refined. The absorption correction was carried out by a SCALE3 ABSPACK multiscan method.[S4] The DIAMOND2 plots shown with thermal ellipsoids at the 50% probability level and hydrogen atoms are shown as small spheres of arbitrary radius. The SADABS program embedded in the Bruker APEX3 software was used for multi-scan absorption corrections in all structures.[S5]

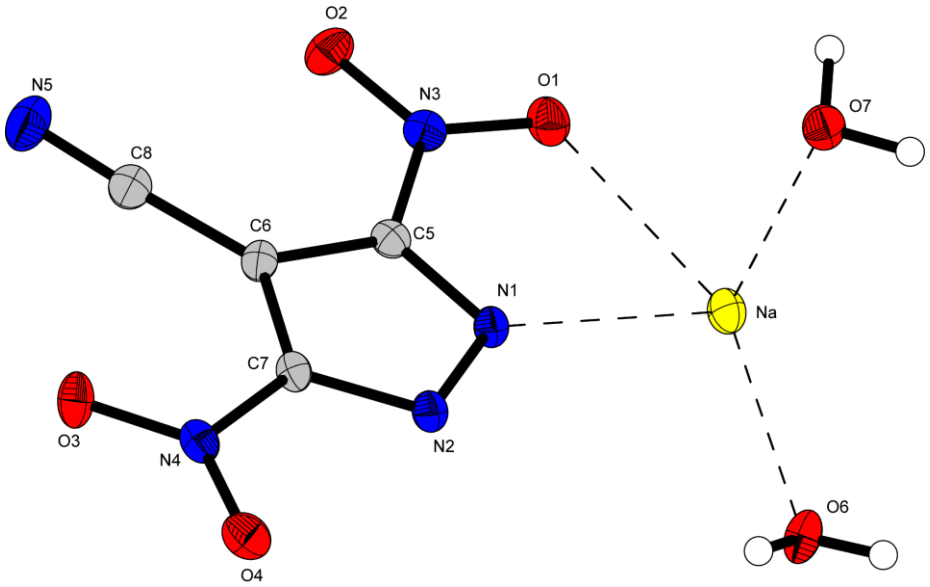

Figure S1. X-ray structure of compound **2**; Thermal ellipsoids are drawn at the 50% probability level and hydrogen atoms are shown as small spheres of arbitrary radius.

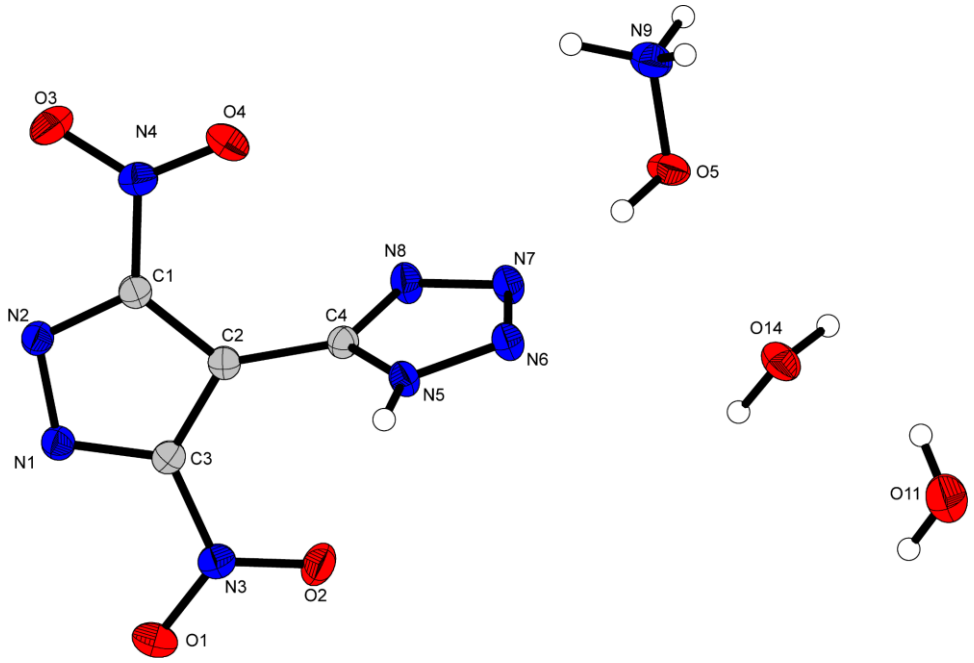

Figure S2. X-ray structure of compound **11** • 2 H_2O; Thermal ellipsoids are drawn at the 50% probability level and hydrogen atoms are shown as small spheres of arbitrary radius.

Compound **2** crystallizes in the triclinic space group *P*−1 with a cell volume of 462.97(7) Å^3 and two formula units per cell. The cell constants are *a* = 6.3499(6) Å, *b* = 8.6737(6) Å and *c* = 9.3553(7) Å, while the density is 1.730 g cm^{-3} at 112 K. Sodium is distorted octahedrally coordinated by the two crystal water by O6 and O7.

Compound **11** • 2 H_2O crystallizes is the monoclinic space group $P2_1/c$ with a cell volume of 2263.77(15) Å^3 and eight formula units per cell. The cell constants are *a* = 9.5937(4) Å, *b* = 11.0673(4) Å and *c* = 21.6905(7) Å, while the density is 1.732 g cm^{-3} at 110 K. The density is rather low due to the inclusion of two water molecules.

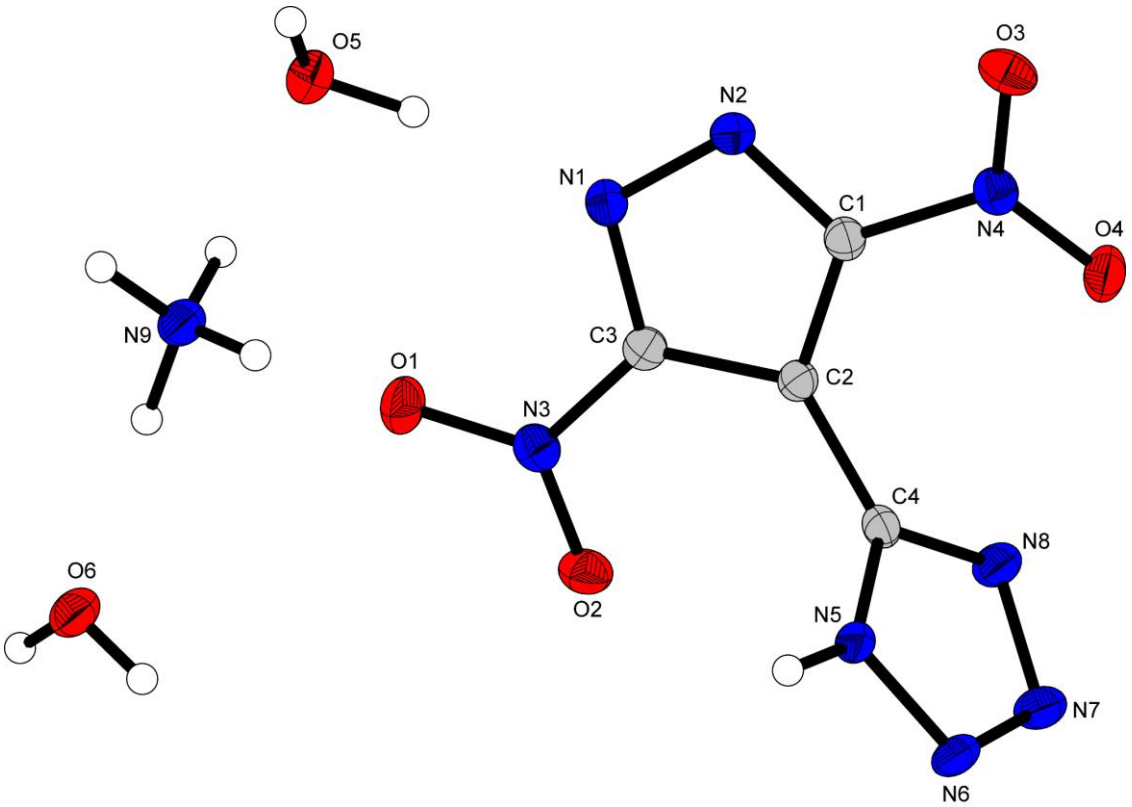

Figure S3. X-ray structure of compound **12** • 2 H_2O; Thermal ellipsoids are drawn at the 50% probability level and hydrogen atoms are shown as small spheres of arbitrary radius.

Compound **12** • 2 H_2O crystallizes is the monoclinic space group $P2_1$ with a cell volume of 541.81(6) Å^3 and two formula units per cell. The cell constants are *a* = 4.5865(3) Å, *b* = 11.3764(7) Å and *c* = 10.3903(6) Å, while the density is 1.711 g cm^{-3} at 121 K. The density is rather low due to the inclusion of two water molecules.

Table S1. Crystallographic data and structure refinement details for the prepared compounds **2**-**4**.

Compound	**2**	**3**	**4**
Formula	$C_4N_5O_4Na$, 2 H_2O	$C_4H_2N_8O_4$	$C_8H_2K_2N_{16}O_8$
FW [g mol^{-1}]	241.11	226.14	528.46
Crystal system	triclinic	orthorhombic	monoclinic
Space group	*P*-1 (No. 2)	*Pbca* (No. 61)	$P2_1$ (No. 4)
Color / Habit	colorless block	yellow block	brown plate
Size [mm]	0.06 x 0.27 x 0.46	0.10 x 0.20 x 0.40	0.11 x 0.21 x 0.49
a [Å]	6.3499(6)	9.5893(3)	9.0333(4)
b [Å]	8.6737(6)	10.5373(5)	11.3970(6)
c [Å]	9.3553(7)	17.3604(7)	9.2529(4)
α [°]	75.299(6)	90	90
β [°]	71.094(8)	90	107.105(4)
γ [°]	75.194(7)	90	90
V [Å^3]	462.97(7)	1754.19(12)	910.47(8)
Z	2	8	2
$\rho_{calc.}$ [g cm^{-3}]	1.730	1.712	1.928
μ [mm^{-1}]	0.198	0.152	0.608
F(000)	244	912	528
$\lambda_{MoK\alpha}$ [Å]	0.71073	0.71073	0.71073
T [K]	112	123	131
θ Min-Max [°]	3.5, 26.4	2.3, 26.4	2.3, 26.4
Dataset	-7: 7 ; -10: 10 ; -11: 11	-11: 11 ; -13: 13 ; -21: 21	-10: 11 ; -14: 9 ; -11: 9
Reflections collected	3610	24946	5275
Independent refl.	1883	1783	2931
R_{int}	0.019	0.052	0.028
Observed reflections	1541	1504	2662
Parameters	161	153	315
R_1 (obs)[a]	0.0329	0.0323	0.0350
wR_2 (all data)[b]	0.0862	0.0797	0.0750
S [c]	1.07	1.05	1.05
Resd. dens [e Å^{-3}]	-0.23, 0.25	-0.20, 0.28	-0.30, 0.38
Device type	Xcalibur Sapphire3	Xcalibur Sapphire3	Xcalibur Sapphire3
Solution	SIR-92	SIR-92	SIR-92
Refinement	SHELXL-2013	SHELXL-2013	SHELXL-2013
Absorption correction	multi-scan	multi-scan	multi-scan
CCDC	1985990	1985991	1985993

[a] $R_1 = \Sigma||F_o|-|F_c||/\Sigma|F_o|$; [b] $wR_2 = [\Sigma[w(F_o^2-F_c^2)^2]/\Sigma[w(F_o)^2]]^{1/2}$; $w = [\sigma c^2(F_o^2)+(xP)^2+yP]^{-1}$ and $P=(F_o^2+2F_c^2)/3$; [c] $S = (\Sigma[w(F_o^2-F_c^2)^2]/(n-p))^{1/2}$ (n = number of reflections; p = total number of parameters).

Table S2. Crystallographic data and structure refinement details for the prepared compounds **5**, **7**-**8**.

Compound	**5**	**7**	**8**
Formula	$C_4HN_8O_4$, CH_5N_6	$C_4HN_8O_4$, CH_7N_4	$C_4HN_8O_4$, $C_4H_9N_{10}$
FW [g mol^{-1}]	326.24	300.23	422.34
Crystal system	monoclinic	orthorhombic	orthorhombic
Space group	*C*2/*c* (No. 15)	*Pbcn* (No. 60)	*Pna*2$_1$ (No. 33)
Color / Habit	yellow block	red block	colorless platelet90
Size [mm]	0.03 x 0.03 x 0.07	0.10 x 0.20 x 0.30	0.02 x 0.04 x 0.07
a [Å]	14.6591(5)	19.1420(5)	11.2322(7)
b [Å]	10.7075(4)	9.1044(3)	28.7679(15)
c [Å]	15.9866(6)	12.9863(5)	4.8768(3)
α [°]	90	90	90
β [°]	107.352(1)	90	90
γ [°]	90	90	90
V [Å^3]	2395.10(15)	2263.21(13)	1575.83(16)
Z	8	8	4
$\rho_{calc.}$ [g cm^{-3}]	1.809	1.762	1.780
μ [mm^{-1}]	0.156	0.151	0.147
F(000)	1328	1232	864
$\lambda_{MoK\alpha}$ [Å]	0.71073	0.71073	0.71073
T [K]	102	108	102
θ Min-Max [°]	2.5, 26.4	2.9, 26.4	2.3, 26.0
Dataset	-18: 18 ; -13: 13 ; -17: 19	-23: 22 ; -11: 11 ; -16: 14	-13: 13 ; -35: 35 ; -5: 6
Reflections collected	17014	17515	25768
Independent refl.	2453	2311	3070
R_{int}	0.038	0.038	0.041
Observed reflections	2135	1912	2918
Parameters	225	222	311
R_1 (obs)[a]	0.0316	0.0338	0.0338
wR_2 (all data)[b]	0.0855	0.0882	0.0809
S [c]	1.07	0.97	1.11
Resd. dens [e Å^{-3}]	-0.27, 0.28	-0.21, 0.27	-0.22, 0.22
Device type	Bruker D8 Venture	Xcalibur Sapphire3	Bruker D8 Venture
Solution	SIR-92	SIR-92	SIR-92
Refinement	SHELXL-2013	SHELXL-2013	SHELXL-2013
Absorption correction	multi-scan	multi-scan	multi-scan
CCDC	1985992	1985996	1985997

[a]$R_1 = \Sigma||F_0|-|F_c||/\Sigma|F_0|$; [b]$wR_2 = [\Sigma[w(F_0^2-F_c^2)^2]/\Sigma[w(F_0)^2]]^{1/2}$; $w = [\sigma c^2(F_0^2)+(xP)^2+yP]^{-1}$ and $P=(F_0^2+2F_c^2)/3$; [c]$S = (\Sigma[w(F_0^2-F_c^2)^2]/(n-p))^{1/2}$ (n = number of reflections; p = total number of parameters).

Table S3. Crystallographic data and structure refinement details for the prepared compounds 11•2 H_2O and 12•2 H_2O.

Compound	**11** • 2 H_2O	**12**• 2 H_2O
Formula	$C_4HN_8O_4$, H_4NO, 2 H_2O	$C_4HN_8O_4$, H_4N, 2 H_2O
FW [g mol^{-1}]	295.20	279.20
Crystal system	monoclinic	monoclinic
Space group	$P2_1/c$ (No. 14)	$P2_1$ (No. 4)
Color / Habit	yellow block	colorless plate
Size [mm]	0.15 x 0.20 x 0.25	0.05 x 0.25 x 0.30
a [Å]	9.5937(4)	4.5865(3)
b [Å]	11.0673(4)	11.3764(7)
c [Å]	21.6905(7)	10.3903(6)
α [°]	90	90
β [°]	100.593(3)	91.998(6)
γ [°]	90	90
V [Å^3]	2263.77(15)	541.81(6)
Z	8	2
$\rho_{calc.}$ [g cm^{-3}]	1.732	1.711
μ [mm^{-1}]	0.161	0.156
F(000)	1216	288
$\lambda_{MoK\alpha}$ [Å]	0.71073	0.71073
T [K]	110	121
θ Min-Max [°]	1.9, 26.4	2.0, 30.4
Dataset	-11: 11 ; -13: 13 ; -27: 24	-6: 5 ; -14: 15 ; -14: 11
Reflections collected	18904	4036
Independent refl.	4624	2733
R_{int}	0.036	0.026
Observed reflections	3710	2303
Parameters	433	208
R_1 (obs)[a]	0.0371	0.0435
wR_2 (all data)[b]	0.0979	0.0821
S [c]	1.04	1.02
Resd. dens [e Å^{-3}]	-0.32, 0.38	-0.21, 0.22
Device type	Xcalibur Sapphire3	Xcalibur Sapphire3
Solution	SIR-92	SIR-92
Refinement	SHELXL-2013	SHELXL-2013
Absorption correction	multi-scan	multi-scan
CCDC	1985994	1985995

[a]$R_1 = \Sigma||F_o|-|F_c||/\Sigma|F_o|$; [b]$wR_2 = [\Sigma[w(F_o^2-F_c^2)^2]/\Sigma[w(F_o)^2]]^{1/2}$; $w = [\sigma c^2(F_o^2)+(xP)^2+yP]^{-1}$ and $P=(F_o^2+2F_c^2)/3$; [c]$S = (\Sigma[w(F_o^2-F_c^2)^2]/(n-p))^{1/2}$ (n = number of reflections; p = total number of parameters).

5.6.3 Computation

All quantum chemical calculations were carried out using the Gaussian G09 program package.[S6] The enthalpies (H) and free energies (G) were calculated using the complete basis set (CBS) method of Petersson and co-workers in order to obtain very accurate energies. The CBS models are using the known asymptotic convergence of pair natural orbital expressions to extrapolate from calculations using a finite basis set to the estimated CBS limit. CBS-4 starts with an HF/3-21G(d) geometry optimization; the zero point energy is computed at the same level. It then uses a large basis set SCF calculation as a base energy, and an MP2/6-31+G calculation with a CBS extrapolation to correct the energy through second order. A MP4(SDQ)/6-31+ (d,p) calculation is used to approximate higher order contributions. In this study, we applied the modified CBS-4M.

Heats of formation of the synthesized ionic compounds were calculated using the atomization method (equation E1) using room temperature CBS-4M enthalpies, which are summarized in Table S4.[S7,S8]

$$\Delta_f H^\circ_{(g,\,M,\,298)} = H_{(Molecule,\,298)} - \sum H^\circ_{(Atoms,\,298)} + \sum \Delta_f H^\circ_{(Atoms,\,298)} \qquad (E1)$$

Table S4. CBS-4M electronic enthalpies for atoms C, H, N and O and their literature values for atomic $\Delta H^\circ_f{}^{298}$ / kJ mol^{-1}.

	$-H^{298}$ [a.u.]	NIST[S9]
H	0.500991	218.2
C	37.786156	717.2
N	54.522462	473.1
O	74.991202	249.5

For neutral compounds the sublimation enthalpy, which is needed to convert the gas phase enthalpy of formation to the solid state one, was calculated by the *Trouton* rule.[S10] For ionic compounds, the lattice energy (U_L) and lattice enthalpy (ΔH_L) were calculated from the corresponding X-ray molecular volumes according to the equations provided by *Jenkins* and *Glasser*.[S11] With the calculated lattice enthalpy the gas-phase enthalpy of formation was converted into the solid state (standard conditions) enthalpy of formation. These molar standard enthalpies of

formation (ΔH_m) were used to calculate the molar solid state energies of formation (ΔU_m) according to equation E2.

$$\Delta U_m = \Delta H_m - \Delta n\, RT \qquad \text{(E2)}$$

(Δn being the change of moles of gaseous components)
The calculation results are summarized in Table S5.

Table S5. Calculation results.

Compound	$-H^{298}$ [a] [a.u.]	$\Delta_f H°$(g,M) [kJ mol^{-1}] [b]	V_M [Å^3] [c]	ΔU_L; ΔH_L [d] [kJ mol^{-1}]	$\Delta_f H°$(s) [e] [kJ mol^{-1}]	Δn [f]	$\Delta_f U$(s) [g] [kJ kg^{-1}]
3	891.171989	517.1	-	-	426.9	7	444.2
HDNPT$^-$	890.698047	228.1	-	-	-	-	-
anion	1489.734017	715.5	142.0	408.8, 410.0	305.5	6.5	1428.8
4	1259.491595	1280.0	142.6	454.5, 459.4	820.6	12	2607.0
5	1151.399849	898.8	142.5	461.2, 466.1	432.7	12	1540.5
7	1595.025435	727.7	142.6	423.8, 428.8	298.9	16	801.8
8	1022.561296	914.5	142.4	-	425.1	9.5	1731.2
11							
12	947.494655	863.4	142.2	-	348.4	9	1524.6

[a] CBS-4M electronic enthalpy; [b] gas phase enthalpy of formation; [c] molecular volumes taken from X-ray structures and corrected to room temperature; [d] lattice energy and enthalpy (calculated using Jenkins and Glasser equations); [e] standard solid state enthalpy of formation; [f] Δn being the change of moles of gaseous components when formed; [g] solid state energy of formation.

5.6.4 References

[S1] *CrysAlisPro*, Oxford Diffraction Ltd. *version 171.33.41*, **2009**.

[S2] G. M. Sheldrick, *Acta Cryst.* **2015**, *A71*, 3–8.

[S3] Dolomanov, O. V., Bourhis, L. J., Gildea, R. J., Howard, J. A. K. & Puschmann, H. *J. Appl. Cryst.* **2009**, *42*, 339–341.

[S4] *SCALE3 ABSPACK – An Oxford Diffraction program* (1.0.4, gui: 1.0.3), Oxford Diffraction Ltd., **2005**.

[S5] *APEX3*. Bruker AXS Inc., Madison, Wisconsin, USA.

[S6] M. J. Frisch, G. W. Trucks, H. B. Schlegel, G. E. Scuseria, M. A. Robb, J. R. Cheeseman, G. Scalmani, V. Barone, B. Mennucci, G. A. Petersson, H.

Nakatsuji, M. Caricato, X. Li, H.P. Hratchian, A. F. Izmaylov, J. Bloino, G. Zheng, J. L. Sonnenberg, M. Hada, M. Ehara, K. Toyota, R. Fukuda, J. Hasegawa, M. Ishida, T. Nakajima, Y. Honda, O. Kitao, H. Nakai, T. Vreven, J. A. Montgomery, Jr., J. E. Peralta, F. Ogliaro, M. Bearpark, J. J. Heyd, E. Brothers, K. N. Kudin, V. N. Staroverov, R. Kobayashi, J. Normand, K. Raghavachari, A. Rendell, J. C. Burant, S. S. Iyengar, J. Tomasi, M. Cossi, N. Rega, J. M. Millam, M. Klene, J. E. Knox, J. B. Cross, V. Bakken, C. Adamo, J. Jaramillo, R. Gomperts, R. E. Stratmann, O. Yazyev, A. J. Austin, R. Cammi, C. Pomelli, J. W. Ochterski, R. L. Martin, K. Morokuma, V. G. Zakrzewski, G. A. Voth, P. Salvador, J. J. Dannenberg, S. Dapprich, A. D. Daniels, O. Farkas, J.B. Foresman, J. V. Ortiz, J. Cioslowski, D. J. Fox, Gaussian 09 A.02, Gaussian, Inc., Wallingford, CT, USA, **2009**.

[S7] a) J. W. Ochterski, G. A. Petersson, and J. A. Montgomery Jr., *J. Chem. Phys.* **1996**, *104*, 2598–2619; b) J. A. Montgomery Jr., M. J. Frisch, J. W. Ochterski G. A. Petersson, *J. Chem. Phys.* **2000**, *112*, 6532–6542.

[S8] a) L. A. Curtiss, K. Raghavachari, P. C. Redfern, J. A. Pople, *J. Chem. Phys.* **1997**, *106*, 1063–1079; b) E. F. C. Byrd, B. M. Rice, *J. Phys. Chem*. A **2006**, *110*, 1005–1013; c) B. M. Rice, S. V. Pai, J. Hare, *Comb. Flame* **1999**, *118*, 445–458.

[S9] P. J. Lindstrom, W. G. Mallard (Editors), NIST Standard Reference Database Number 69, http://webbook.nist.gov/chemistry/ (accessed June **2019**).

[S10] M. S. Westwell, M. S. Searle, D. J. Wales, D. H. Williams, *J. Am. Chem. Soc*. **1995**, *117*, 5013–5015; b) F. Trouton, *Philos. Mag*. **1884**, *18*, 54–57.

[S11] a) H. D. B. Jenkins, H. K. Roobottom, J. Passmore, L. Glasser, *Inorg. Chem.* **1999,** *38,* 3609–3620; b) H. D. B. Jenkins, D. Tudela, L. Glasser, *Inorg. Chem.* **2002**, *41*, 2364–2367.

6. Combining the most suitable energetic tetrazole and triazole moieties: synthesis and characterization of 5-(1-hydroxy-3-nitro-1,2,4-triazol-5-yl)-1-hydroxy-tetrazole and its nitrogen-rich ionic derivatives

Lukas Bauer, Maximilian Benz‡, Thomas M. Klapötke, Cedric Pignot, Jörg Stierstorfer

as published in *Materials Advances* **2022**, *3*, 3945–3951

DOI: 10.1039/D2MA00135G

Keywords: tetrazoles, triazoles, N-oxidation, high explosives, structural elucidation

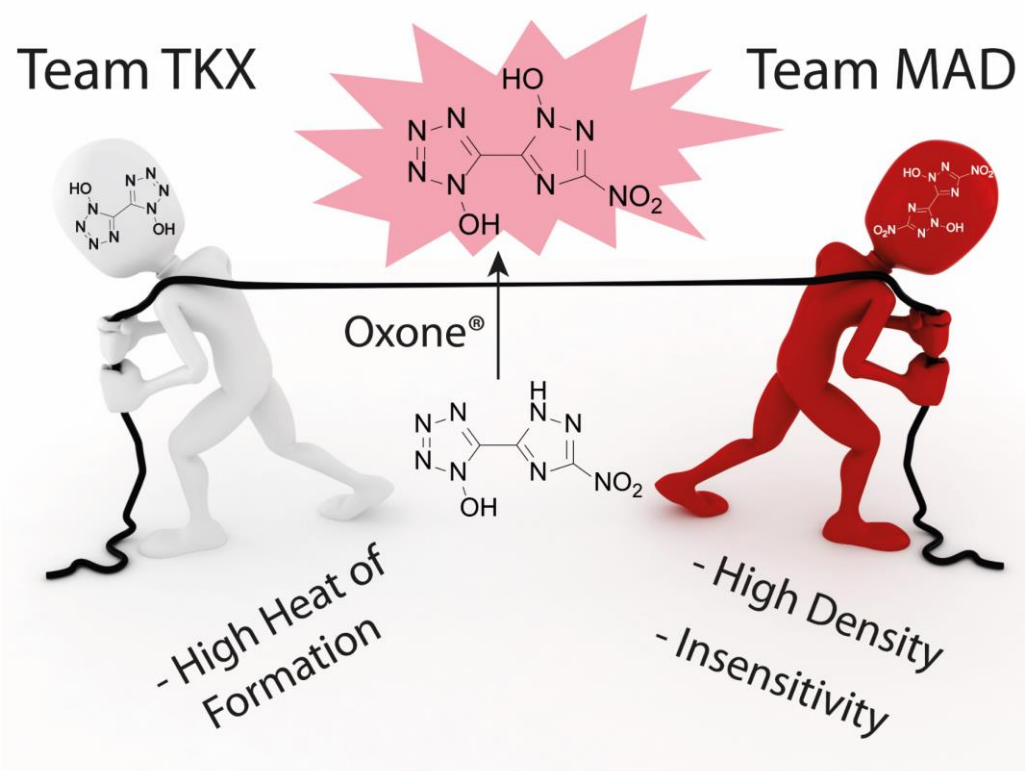

TKX-50 and MAD-X1 are some of the most promising replacement candidates for secondary explosives. The hybrid molecule thereof was accordingly synthesized and characterized especially through the formation of nitrogen-rich salts.

Abstract: With the synthesis of 5-(1-hydroxy-3-nitro-1,2,4-triazol-5-yl)-1-hydroxy-tetrazole (**1**) we can report the first successful production of a combined bis-heterocyclic system composed of 1-hydroxy-tetrazole and 1-hydroxy-1,2,4-triazole. The straightforward synthesis modifies the cyano group of the nitro-triazole starting material within four steps to the tetrazol-1-ol and finally oxidizes the triazole selectively to the 1-hydroxy-triazole, resulting in compound **1**, which is a hybrid molecule of the two in energetic materials chemistry established bis-heterocyclic motifs 1,1′-dihydroxy-3,3′-dinitro-bis-1,2,4-triazole and 1,1′-dihydroxy-5,5′-bistetrazole. In order to tune and improve the performance parameters, several nitrogen rich bases were used to obtain the respective ionic derivatives. All compounds were characterized using multinuclear NMR and IR spectroscopy, differential thermal analysis (DTA) and elemental analysis. Several compounds could be further analyzed using X-ray diffraction measurements. The heats of formation for all investigated compounds were determined and the detonation properties (EXPLO5 V6.05.02) were calculated. These data, as well as the sensitivity values, were compared to related substances.

6.1 Introduction

Since the start of large-scale production of RDX during World War II, the substance, and its eight-membered ring homolog HMX, has been included in almost all energetic military charges as a high explosive (HE) component.[1-3] Despite the good performance data and the simple synthesis, alternative substances are currently being explored, because the main disadvantage of RDX and HMX is their decomposition product's toxicity and environmental incompatibility.[4-6] Therefore, new generation molecules should avoid this drawback and be as environmentally friendly as possible. Another criterion for a possible substitute is, above all, at least comparable performance values to that of RDX or even HMX for the final substance. The best case would be an insensitive compound outperforming RDX/HMX.[7-10]

Of high potential for replacing the currently common secondary explosives are triazole-, tetrazole- and furazan-based compounds, especially in the form of bis-heterocycles. These scaffolds exhibit high densities, highly endothermic heats of

formation and therefore good performance compared to several single ring systems.[7, 11-14]

Since, in addition to a high heat of formation, density plays the major role in the calculation of detonation parameters, some recurring strategies are widely used to increase it, such as nitration of the molecular backbone, formation of a system consisting of π-stacking parts or the synthesis of ionic derivatives to maximize the packing coefficient.[8, 15-16]

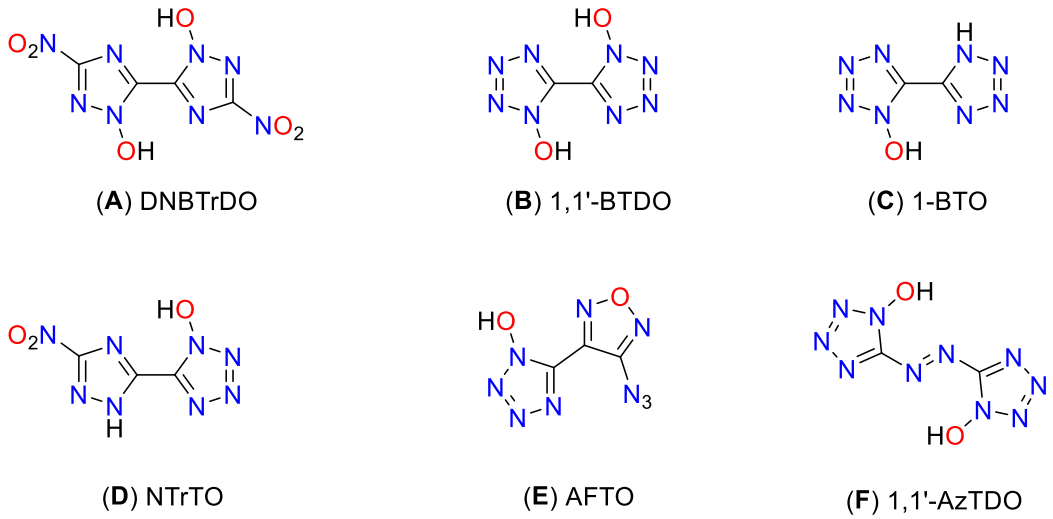

Figure 1. Structures of literature known *N*1-oxidized bicyclic triazole and tetrazole motifs: 1,1′-dihydroxy-5,5′-bistetrazole (A), 1,1′-dihydroxy-3,3′-dinitro-bis-1,2,4-triazole (B), 1-hydroxy-5,5′-bistetrazole (C), 3-nitro-(1,2,4-triazol-5-yl)-1-hydroxy-tetrazole (D), 3-azido-(furazan-4-yl)-1-hydroxy-tetrazole (E), and 1,1′-dihydroxy-5,5′-azotetrazole (F).

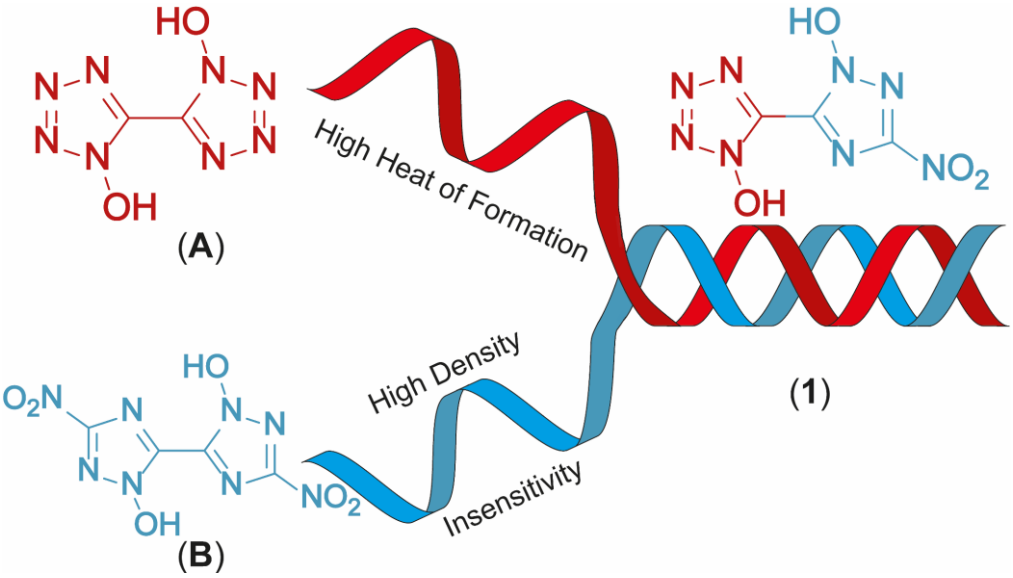

Figure 2. Graphical illustration of the combination of 1,1′-dihydroxy-5,5′-bistetrazole (A) and 1,1′-dihydroxy-3,3′-dinitro-1,2,4-bistriazole (B) resulting in the hybrid molecule 5-(1-hydroxy-3-nitro-1,2,4-triazol-5-yl)-1-hydroxy-tetrazole (**1**).

Another approach is to utilize *N*-oxidation, which not only has the advantage of increasing the oxygen balance but also boosting the density through the addition of a further heteroatom. Figure 1 depicts some prominent molecular moieties containing bis-heterocyclic systems and *N*-oxides at the respective position 1.[17-23]Among the most promising molecules developed with the aim of replacing RDX are the bis-hydroxylammonium derivatives of 3,3′-dinitro-bis-1,2,4-triazol-1,1′-diolate (MAD-X1)[19] and 5,5′-bistetrazol-1,1′-diolate (TKX-50),[18] which are attracting great attention in the international community.[24-30]

Combination of 1-hydroxy-tetrazole and 1-hydroxy-3-nitro-1,2,4-triazole yields the hybrid molecule 1-hydroxy-3-nitro-(1,2,4-triazol-5-yl)-1-hydroxy-tetrazole (**1**) with the aim to combine the positive properties of the fundamental symmetric bis-heterocycles in a new asymmetric molecule: preferable the high heat of formation of 1,1′-dihydroxy-5,5′-bistetrazole (**A**) with the high density and insensitivity toward external stimuli of 1,1′-dihydroxy-3,3′-dinitro-bis-1,2,4-triazole (Figure 2).

6.2 Results and Discussion

6.2.1 Synthesis

The synthesis starts from 3-amino-1,2,4-triazol-5-carbonitrile, which was synthesized according to a literature known procedure starting from oxalic acid and aminoguanidinium hydrogen carbonate.[31]

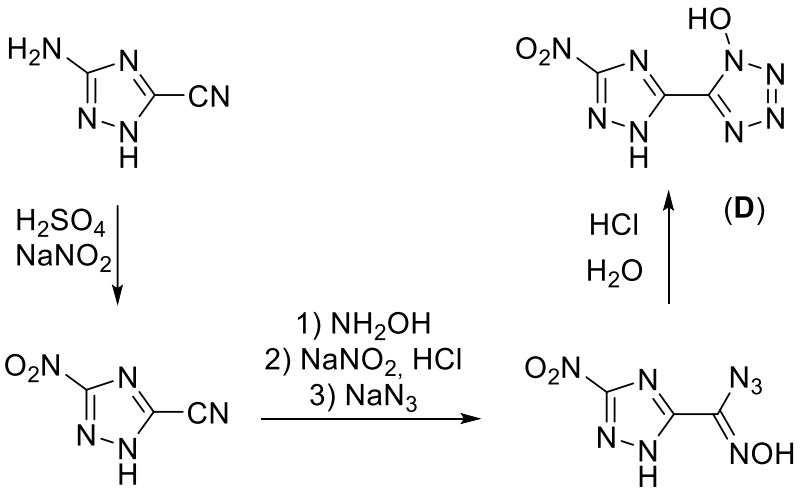

Scheme 1. Literature known synthetic pathway for the precursor compound for the synthesis of **1**.

Diazotization in 1 M sulfuric acid and excess of sodium nitrite led to the nitro-triazole derivative. Therefore, a modified procedure was established, which prevents the long presence of the extremely sensitive diazonium intermediate (for more information see the ESI). Afterwards, the nitrile function was converted into a 1-hydroxy-tetrazole moiety by a proven procedure within four reaction steps (Scheme 1). This reaction sequence includes the addition of hydroxylamine, the diazotization of the aminoxime in hydrochloric acid precipitating the chloroxime, chlorine-azide exchange and finally a proton promoted ring closing reaction to end up with 5-(3-nitro-1,2,4-triazol-5-yl)-1-hydroxy-tetrazole (**D**) in 94% yield.[21] The overall yield of **D** starting from 3-amino-1,2,4-trazole-5-carbonitrile is 61%.

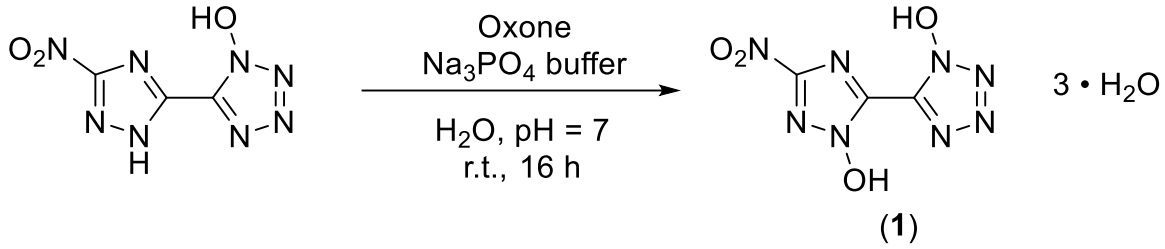

Scheme 2. Synthesis of **1** with Oxone® as an oxidation agent.

Oxidation of 5-(3-nitro-1,2,4-triazol-5-yl)-1-hydroxy-tetrazole at the triazole yielded 5-(1-hydroxy-3-nitro-1,2,4-triazol-5-yl)-1-hydroxy-tetrazole trihydrate (**1**) and was performed with Oxone® as an oxidant (Scheme 2). This has already been established as a suitable reagent in similar reactions.[16, 32-33] The reaction was buffered to pH = 7 in an aqueous medium using tri-sodium phosphate dodecahydrate. Other buffer reagents, such as sodium and potassium acetate and sodium hydrogen carbonate, as well as non-buffered conditions were examined but did not yield **1** at all. Maximal yields of 70% were achieved with a reaction time of 16 h at room temperature (25 °C). Due to the electron withdrawing effect of the nitro group of the triazole, the oxidation occurs selectively at the meta position to the nitro function. All attempts to dehydrate **1** failed, as it kept drawing and absorbing water from the air.

Ionic derivatives **2**–**7** were obtained by dissolving **1** in ethanol or ethanol/water mixtures and adding two equivalents of the respective base to the solution. For the ammonium salt **2**, gaseous ammonia was bubbled through the solution for about 1 minute. Compounds **2**–**5** precipitated immediately as water free salts and were

used for characterization without further purification after washing with a small amount of the respective solvent. For compounds **6** and **7** the solution had to be reduced to precipitate the solid. In the case of compounds **2**–**6**, the double salts were obtained. Despite the use of two equivalents of the base, only the mono triaminoguanidinium derivative **7** could be obtained, which is known to happen from similar systems (Scheme 3).[34]

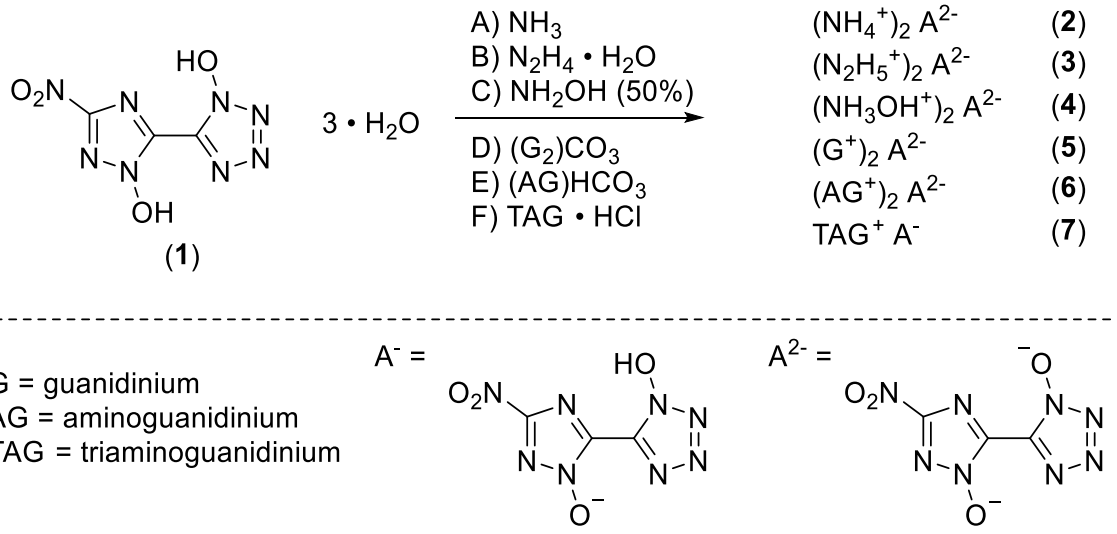

Scheme 3. Synthetic pathway for the formation of ionic derivatives **2**–**7**.

6.2.2 X-Ray Diffraction

Single crystals suitable for X-ray diffraction experiments could be obtained by recrystallizing from common organic solvents for all compounds except **5** due to its bad solubility and crystallization behavior. Even though bis-hydroxylammonium derivative 4 was obtained solvent free, only a crystal structure of the hydrate adduct could be obtained. Details on the measurement and refinement data for every crystallographically investigated compound are listed in the ESI (Tables S1–S3). The crystal data sets were uploaded to the CSD database with the CCDC numbers 2144424–2144432.

Compound **1** crystallizes as a trihydrate in the orthorhombic space group *Cmca* with a cell volume of 1969.5(7) Å^3 and eight molecular units per unit cell. The cell constants are *a* = 6.239(12) Å, *b* = 7.842(16) Å and *c* = 40.259(8) Å while the density is 1.809 g cm^{-3} at 293 K. Compared to the room temperature densities of

1,1′-dihydroxy-5,5′-bistetrazole·2 H_2O (1.778 g cm^{-3}) and 1,1′-dihydroxy-3,3′-dinitro-bis-1,2,4-triazole·2 H_2O (1.829 g cm^{-3}), **1** lies in the middle of the two values as it is a chemical mixture of both of them.[18-19] The crystal structure is depicted in Figure 1. The bond lengths in both azole rings are in the range of N–N (N5–N6, 1.332(3) Å; N2–N3, 1.309(4) Å) and N–C (N1–C1, 1.339(4) Å; N7–C2, 1.341(4) Å) single and double bonds, respectively. The bond lengths for the *N*-oxides are 1.339(3) Å (O1–N1) and 1.337(3) Å (O2–N5) which is a normal value for *N*-bonded hydroxides donating electron density into the aromatic system. The angles N1–O1–H1 (107(3)°) and N5–O2–H2 (102(3)°) are close to the ideal tetrahedral angle, yet deviate slightly from it, which can be explained by the hydrogen bridges that have formed. Due to the orthorhombic symmetry, the molecule itself is completely planar (N1–C1–C2–N5, 180.00°; O3–N8–C3–N7, 180.00°).

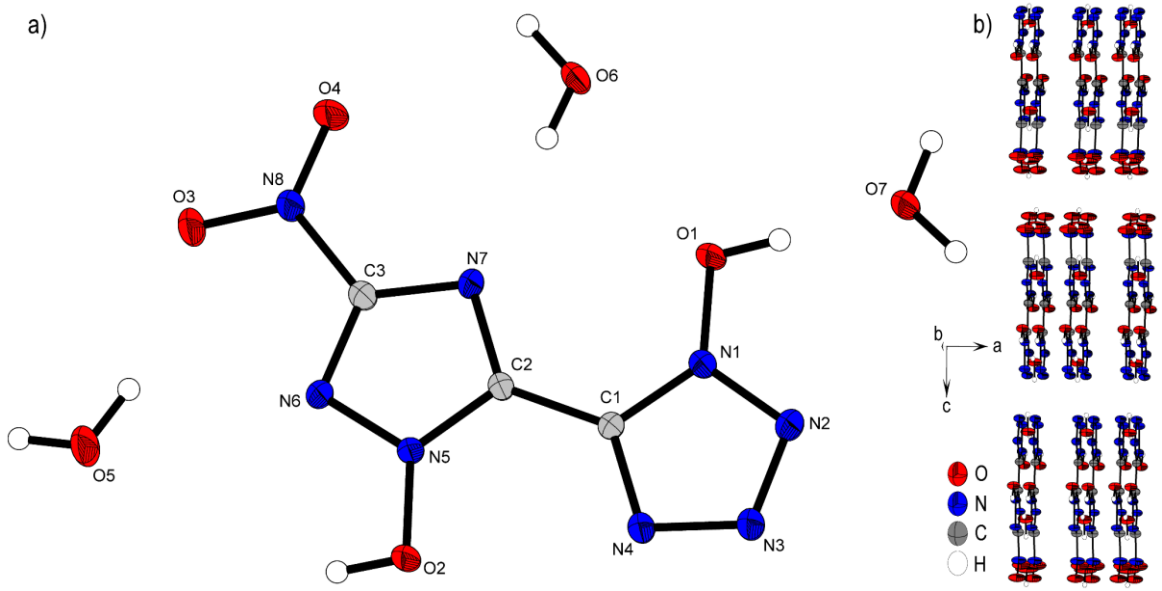

Figure 3. (a) Molecular structure of **1** as determined by X-ray diffraction with thermal ellipsoids drawn at the 50% probability level; (b) 2D layer structure of **1** viewed along the *b* axis.

Each bis-heterocycle is surrounded by eight water molecules. All heteroatoms with the exception of N2 and N8 are involved in the formation of a network consisting of strong to moderately strong hydrogen bonds, which cover a distance range of 1.57(4) Å (O2–H2_a···O6) to 2.63(6) Å (O6–H2_b···O4). This results in the layered stacking of **1** shown in Figure 3b with a layer distance of 3.12 Å.

Bis-ammonium derivate **2** crystallizes in the monoclinic space group $P2_1/n$ with a cell volume of 914.2 $Å^3$ and four molecular units per unit cell. The cell constants

are a = 4.3259(1) Å, b = 26.9849(8) Å and c = 7.9243(2) Å, while the density is 1.803 g cm^{-3} at 106 K.

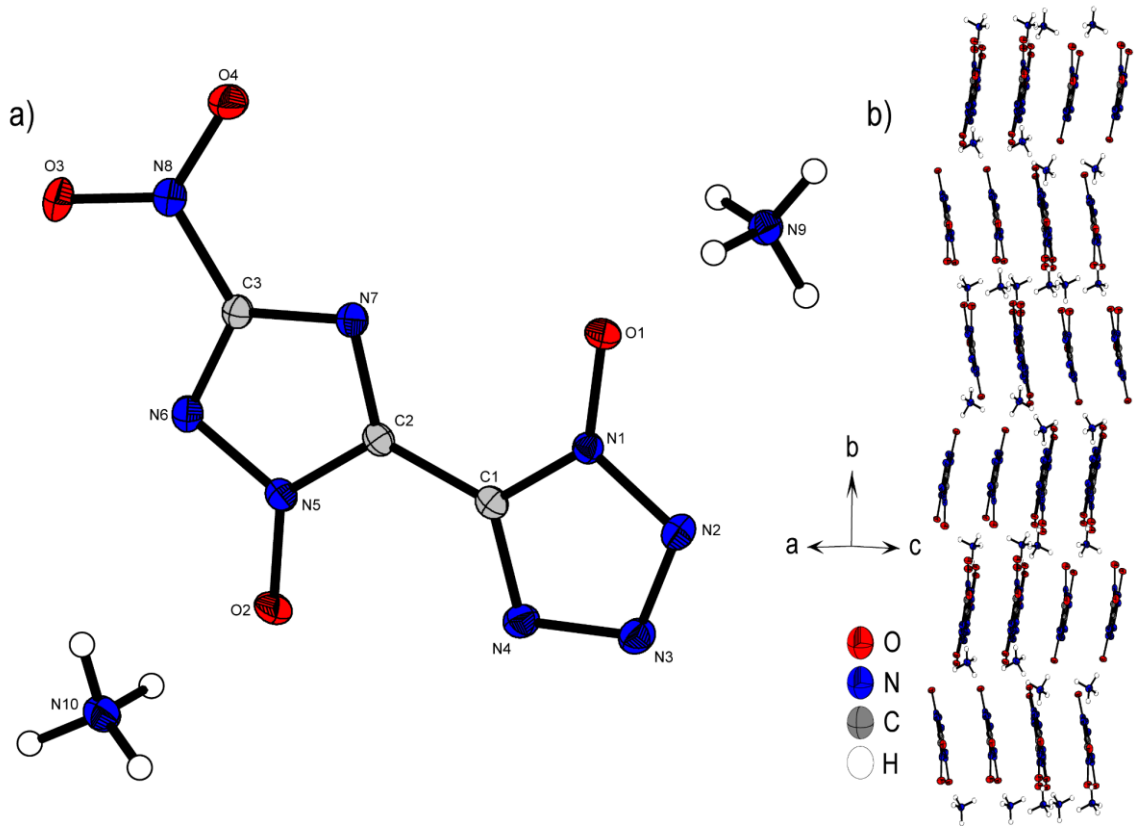

Figure 4. (a) Molecular structure of **2** as determined by low temperature X-ray diffraction with thermal ellipsoids drawn at the 50% probability level; (b) zig-zig pattern of **2** viewed along the *ac* plane.

The two aromatic rings with their *N*-oxides form an almost planar configuration (O1–N1–C1–C2, 0.5(3)°; N4–C1–C2–N7, 170.00(5)°; O2–N5–C2–C1, 175.6(2)°). Only the nitro group of the triazole is twisted out of this plane 13.2(2)°(O3–N8–C3–N6). Every anionic bis-heterocycle is surrounded by nine ammonium cations, forming a large number of hydrogen bonds. **2** forms a wave like structure along the *b* axis (Figure 4b). The change of orientation takes place after two formula units of the anion. The ammonium cations are located between the anion layers.

Compound **3** crystallizes in the triclinic space group $P\bar{1}$ with a cell volume of 528.11(19) Å^3 and two molecular units per cell. The constants are a = 3.6755(4) Å, b = 8.0751(9) Å and c = 17.8693(18) Å while the density is 1.750 g cm^{-3} at 173 K. The nearly planar anion (N5–C2–C1–N1, 175.4(3)°; O4–N8–C3–N6, 173.1(3)°; O1–N1–N2–N3, 179.3(3)°) forms a layer like structure along the *bc* plane, as depicted in Figure 5b. The free spaces between the respective layers are filled by

hydrazinium cations, which form a large number of hydrogen bonds to the double anion.

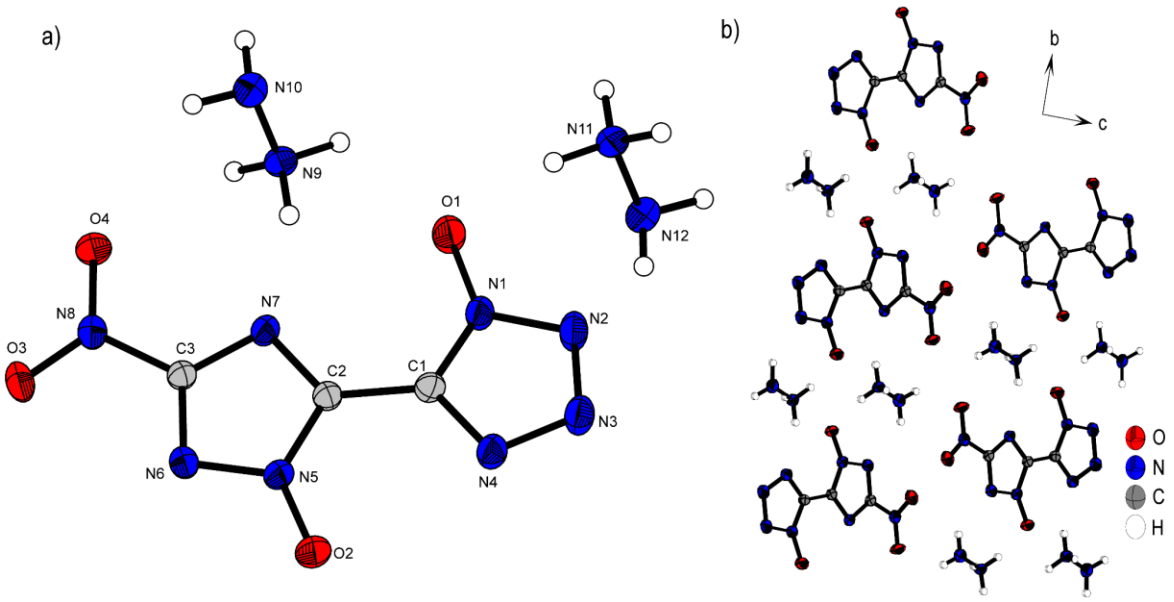

Figure 5. (a) Molecular structure of **3** as determined by low temperature X-ray diffraction with thermal ellipsoids drawn at the 50% probability level; (b) layer structure of **3** viewed along the *a* axis.

Compound **4** crystallizes with the inclusion of one water molecule in the monoclinic space group $P2_1/c$ with a cell volume of 1100.2(3) Å^3 and four molecular units per cell. The cell constants are a = 7.3751(11) Å, b = 15.0961(19) Å and c = 10.4402(14) Å while the density is 1.800 g cm^{-3} at 298 K. The anionic moiety is presented in almost planar conformation (O1–N1–C1–C2, −1.0(4)°; O2–N5–C2–C1, 0.3(4)°; O3–N8–C3–N6, 0.0(4)°).

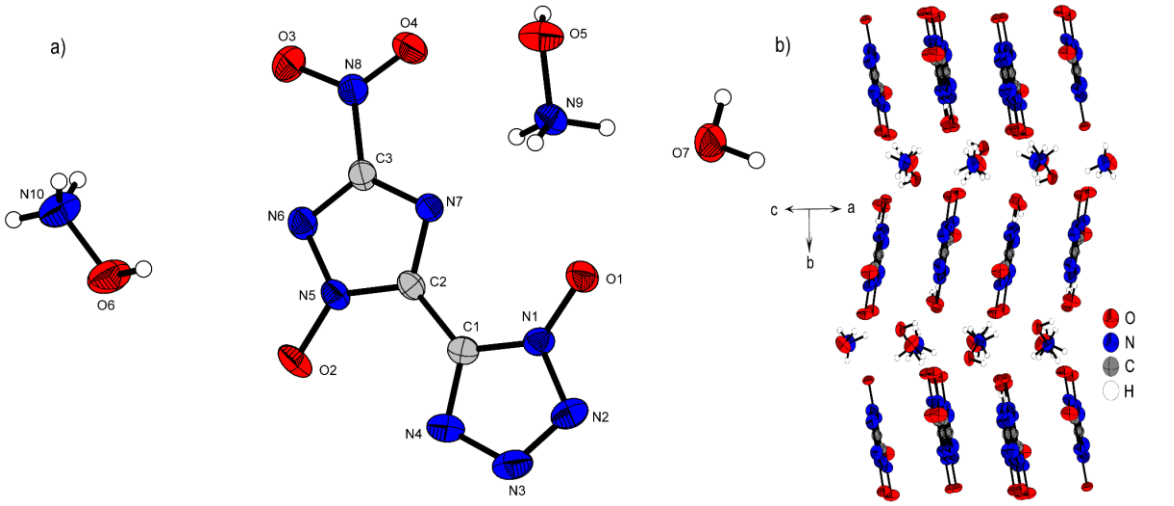

Figure 6. (a) Molecular structure of **4**·H_2O as determined by X-ray diffraction with thermal ellipsoids drawn at the 50% probability level; (b) zig-zag pattern of **4** along the *b* axis.

No other anion structure features this kind of coplanar arrangement of the aromatic rings. Along the *ac* plane, the bis-heterocycle forms a zig-zag-like structure, which is due to the same space group very similar to the three-dimensional structure of **2**. The cations and the crystal water form layers between the respective linear chains of anions (Figure 6b).

Bis-aminoguanidinium derivative **6** crystallizes in the monoclinic space group *I*2/*a* with a cell volume of 2835.0(1) Å^3 and eight molecules per unit cell. The cell constants are *a* = 11.245(2) Å, *b* = 6.7268(15) Å and *c* = 37.486(8) Å while the density is 1.698 g cm^{-3} at 100 K. Compound **6** is the most twisted anion structure for double deprotonated anions compared in this study. The two azole rings are twisted by 148.9(4)°(N4–C1–C2–N7) toward each other. As shown in Figure 7b, the maximum number and strength of hydrogen bonds with the aminoguanidinium cation is achieved by this twist of the anion. Along *b*, the formation of channels of anions and cations occurs. It can also be observed that the aminoguanidinium units are twisted in relation to each other. This also results from the maximization of the intermolecular bonds.

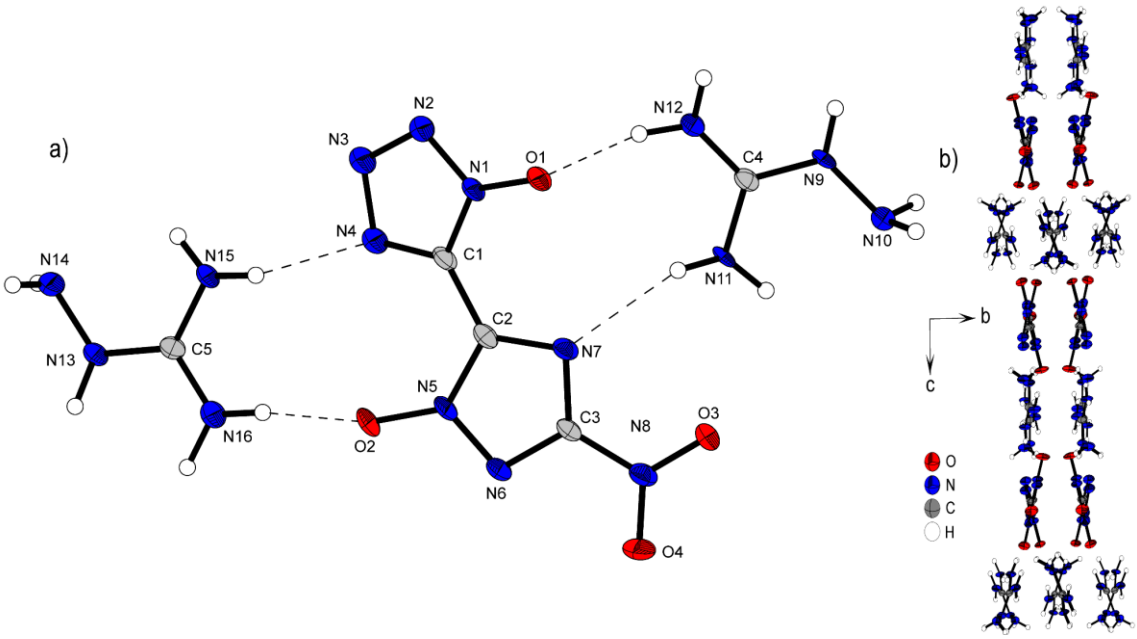

Figure 7. (a) Molecular structure of **6** as determined by low temperature X-ray diffraction with thermal ellipsoids drawn at the 50% probability level; (b) pattern of **6** viewed along the *a* axis.

Compound **7** crystallizes in the triclinic space group *P*−1 with a cell volume of 611.07(13) Å^3 and two molecular units per cell. The constants are *a* = 7.5556(8) Å,

b = 8.1499(8) Å and *c* = 11.4798(12) Å while the density is 1.730 g cm^{-3} at 102 K. It is the only compound that is preserved only as a single salt. Compared to the structures described above, this also results in the unique assembly of **7**. The single deprotonation occurs at the triazole OH group, since the proton there has a lower pK_a value than the proton at the tetrazole as a result of the nitro substituent. This deprotonation also leads to the rotation of the rings relative to each other into a sterically unfavorable position, so that both hydroxy units are on the same side (N7–C2–C1–N4, 15.3(2)°). This ring formation is stabilized by a strong intramolecular interaction formed between the two hydroxy groups and the remaining proton. H1 can be classified as a divided proton, since it is more likely to be bound to O1, but also has a very strong interaction with O2 (O1–H1, 1.05(4) Å; O2–H1, 1.47(4) Å; O1–H1–O2, 171(2)°). Compared to the neutral compound **1**, the bonds O1–H1 and O2–H1 (O1–H1, 0.86(4) Å; O2–H2, 0.85(4) Å) are significantly prolonged. Viewed along the *ab* plane (Figure 8b), the mono-anion forms an oblique cylindrical structure in which the heterocycles are alternately superimposed. This pattern is embedded by triaminoguanidinium cations. Along the space diagonal (Figure 8c), anions and cations are arranged in pairs in a chessboard-like structure, with the respective orientation flipped by 90° toward each other.

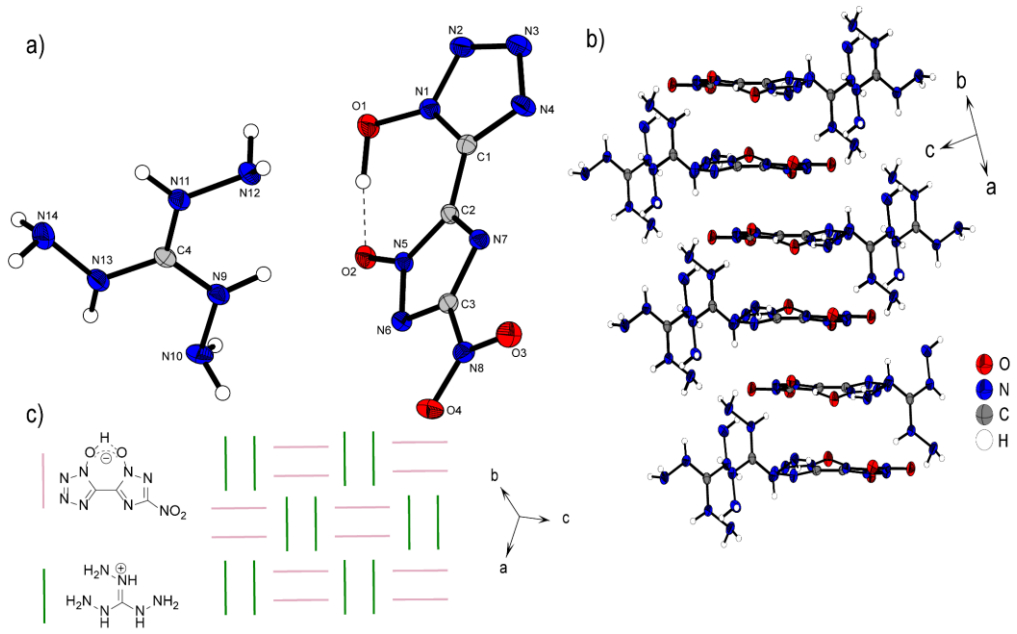

Figure 8. (a) Molecular structure of **7** as determined by low temperature X-ray diffraction with thermal ellipsoids drawn at the 50% probability level; (b) 2D layer structure of **7** viewed along the *ab* plane; (c) schematic arrangement of the anions and cations viewed along the space diagonal.

6.2.3 NMR Spectroscopy

All investigated compounds were characterized using ^{1}H, ^{13}C and ^{14}N NMR spectroscopy. Additionally, compounds **1** and **2** were analyzed using proton coupled ^{15}N NMR spectroscopy. The proton NMR spectrum of **1** shows one broad signal at around 7.80 ppm representing the acidic OH protons. The proton signals for the cations in **2** (7.25 ppm), **3** (7.13 ppm) and **4** (9.66 ppm) can be found as broad singlets in the classical region for the respective cations.[35-36] Derivative **5** shows one singlet resonance at 7.13 ppm for the guanidinium cation. For the aminoguanidinium protons in compound **6** three different signals could be obtained. Broadened singlets at 8.93 ppm (N*H*-NH_2) and 7.21 ppm (C-NH_2) and a sharp resonance at 4.65 ppm (N-NH_2) are characteristic for aminoguanidinium cations.[37] TAG protons for **7** can be assigned to two broad singlets at 8.61 ppm (N*H*-NH_2) and 5.68 ppm (N-NH_2).

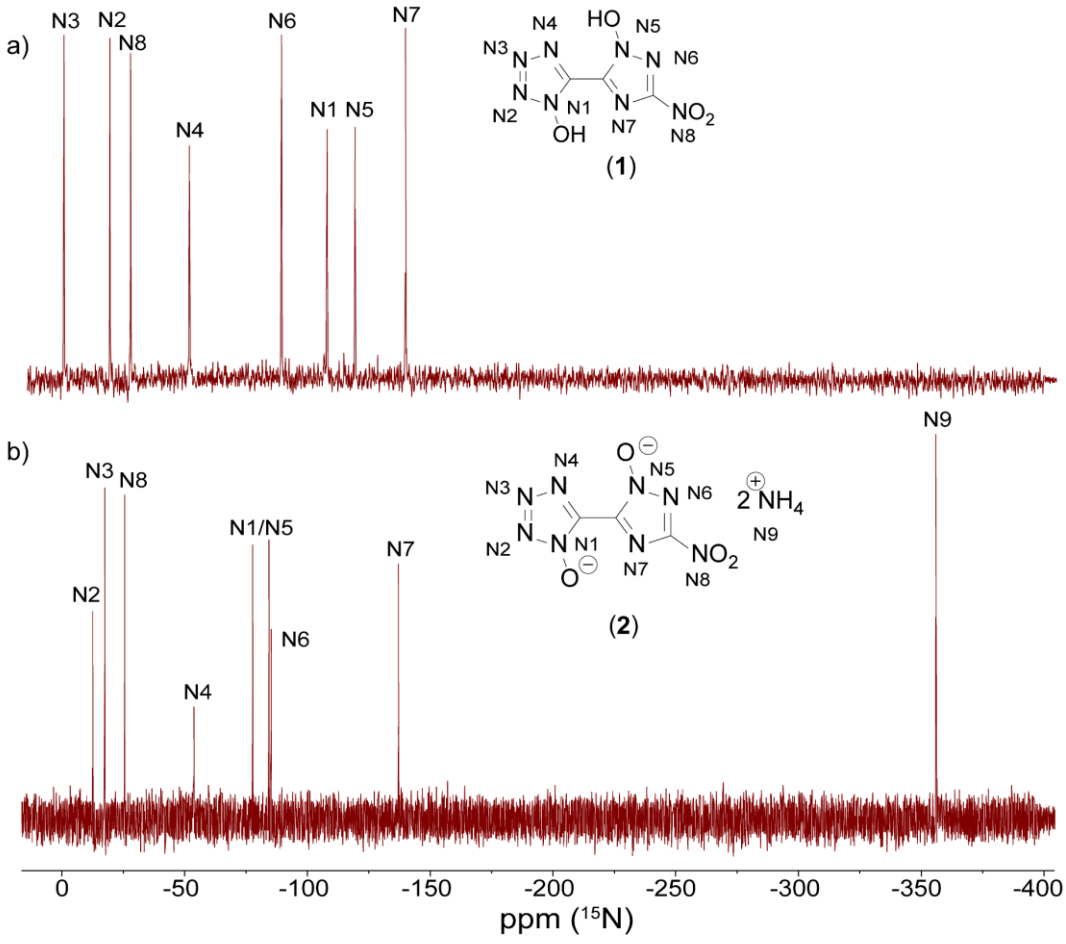

Figure 9. Proton coupled ^{15}N NMR spectra of **1** (top, (a)) and **2** (bottom, (b)) measured in DMSO-D_6. Chemical shifts are given with respect to $MeNO_2$.

All compounds show three signals for the bis-heterocyclic moiety. The resonance, with the greatest shift to lower fields always belongs to the triazole carbon *C*-NO_2 appearing in the range of 155.3 to 151.2 ppm. The two remaining bridging carbon signals emerge in the region of 137.0 to 134.9 ppm for the tetrazole and 133.3 to 132.0 ppm for the triazole. Compounds **5**, **6**, and **7** exhibit one additional signal for the cations at 158.1, 159.0 and 159.0 ppm, respectively. ^{14}N measurements show resonances in the area of around −28 ppm for the nitro groups of the triazole moieties. Additionally, spectra of compounds **2**–**4** show sharp signals for the respective cations at around −360 ppm.

Proton coupled ^{15}N NMR measurements were measured for neutral compound **1** and bis-ammonium salt **2** as a representative for the anion moiety. For the two bis-heterocycles, eight different resonances were obtained. An additional signal is detectable in the spectrum of **2**. This belongs to the resonance of the ammonium cation. By comparison with the spectra of the respective symmetric molecules 1,1-dihydroxy-5,5′-bistetrazole (**A**)[17] and 1,1′-dihydroxy-3,3′-dinitro-bis-1,2,4-triazole (**B**)[19] all signals could be assigned, as shown in Figure 9. The double deprotonation results in a shift of some signals to lower fields. That is the case for the two oxygen-substituted nitrogen atoms N1 and N5 as well as N3. The nitrogen atoms N2, N4, N6, N7 and N8 remain almost unchanged by the deprotonation, with respect to the chemical shift.

6.2.4 Physico-chemical Properties

Experiments for the thermal behavior were determined through DTA measurements with a heating rate of 5 °C min^{-1}. All respective values for compounds **1**–**7** are listed in Table 1. Neutral compound **1** decomposes at 167 °C and starts losing its crystal waters from around 71 °C indicated by an endothermal signal, which was further confirmed by a TGA measurement (for more details see the ESI). Compounds **2**–**4** decompose sharply without any other measurable signal before the exothermic event at 265 °C, 206 °C and 205 °C, respectively. Compounds **5**–**7**, all consisting of a guanidinium-based cation, feature endothermic signals prior to their decomposition points. Guanidinium salt **5** shows a melting

point at 200 °C (T_{dec} = 270 °C) and **6**–**7** melt close to their decomposition (T_{melt} 217 °C (**6**); 165 °C (**7**); T_{dec} = 219 °C (**6**); 204 °C (**7**)).

Table 1. Physicochemical properties of compounds **1–7** as well as for TKX-50, MAD-X1 and β-HMX.

	1	**2**	**3**	**4**	**5**	**6**	**7**	TKX-50	MAD-X1	β-HMX
Formula	$C_3H_8N_8O_7$	$C_3H_8N_{10}O_4$	$C_3H_{10}N_{12}O_4$	$C_3H_8N_{10}O_6$	$C_5H_{12}N_{14}O_4$	$C_5H_{14}N_{16}O_4$	$C_4H_{10}N_{14}O_4$	$C_2H_8N_{10}O_4$	$C_4H_8N_{10}O_8$	$C_4H_8N_8O_8$
M [g mol^{-1}]	268.1	248.1	278.1	280.1	332.2	362.3	318.2	236.2	324.2	296.2
IS [J][a]	>40	>40	10	20	>40	40	7	20	>40	7
FS [N][b]	>360	>360	216	324	>360	>360	192	120	>360	112
ESD [J][c]	0.50	0.37	0.10	0.20	0.25	0.25	0.10	0.10	0.50	0.20
P [g cm^{-3}][d]	1.808	1.753	1.718	1.885*	1.707*	1.649	1.681	1.877	1.90	1.904
N [%][e]	44.8	56.4	60.4	50.0	59.0	61.9	61.6	59.3	43.2	37.84
Ω [%][f]	−19.2	−38.7	−40.3	−22.8	−57.8	−57.4	−45.3	−27.1	−19.7	−21.6
T_{dec} [°C][g]	169	265	206	205	270	219	204	221	217	279
$\Delta_f H^0$ [kJ mol^{-1}][h]	−233.0	200.6	547.3	316.4	261.9	490.6	615.5	447.0	222.3	74.8
$\Delta_f U^0$ [kJ mol^{-1}][i]	-	227.8	579.6	346.2	299.1	532.7	650.2	474.3	254.5	109.5
EXPLO5 V6.05.02										
$-\Delta_{Ex} U^0$ [kJ kg^{-1}][j]	4587	4378	5825	5631	3557	3995	6383	5758	5670	5700
T_{det} [K][k]	3126	2995	3353	3573	2518	2709	3978	3513	3670	3623
V_0 [L kg^{-1}][l]	820	873	907	831	865	889	875	910	778	763
P_{CJ} [kbar][m]	313	284	311	386	244	249	318	401	381	378
V_{det} [m s^{-1}][n]	8666	8650	9052	9490	8271	8358	9058	9940	9270	9193

[a] Impact sensitivity (BAM drophammer (1 of 6)). [b] Friction sensitivity (BAM friction tester (1 of 6)). [c] Electrostatic discharge device (OZM research). [d] From X-Ray diffraction analysis recalculated to 298 K; * Density is based on gas pycnometer measurement at 25 °C. [e] Nitrogen content. [f] Oxygen balance with respect to the formation of CO_2 [g] Decomposition temperature (DTA; β = 5 °C min^{-1}). [h] Calculated enthalpy of formation. [i] Calculated energy of formation. [j] Energy of explosion. [k] Detonation temperature. [l] Volume of detonation products (assuming only gaseous products). [m] Detonation pressure at Chapman-Jouguet point. [n] Detonation velocity.

Derivatives **1**–**2** as well as **5**–**6** are insensitive toward friction and impact, whereas **3**, **4** and **7** are moderately sensitive with values of IS = 7 J and FS = 192 N for **7** and IS = 20 J and FS = 324 N for **4**. The densities recalculated to room temperature are in the range of 1.649 g cm^{-3} (**6**) to 1.885 g cm^{-3} (**4**) for ionic derivatives **2**–**7** and 1.808 g cm^{-3} for neutral compound **1**. The detonation velocities for all synthesized compounds are above 8200 m s^{-1}, and for **3**, **4** and **7** are even over 9000 m s^{-1}. Bis-hydroxylammonium derivative **4**, which is particularly interesting because of its energetic properties, is the overall best compound and has a

calculated detonation velocity of 9490 m s^{-1} and detonation pressure of 386 kbar. These values fit very well with the calculated values for MAD-X1 and TKX-50, since they are approximately in the middle of both and thus support the theory that **4** is also a hybrid molecule in terms of its properties.[18-19]

At least since the synthesis of TKX-50 and MAD-X1 and their establishment as green secondary explosive replacements, the benefit of introducing *N*-oxidation to nitrogen-rich azoles is undeniable.[18, 38-41] The advantages are not only the apparent increase of the oxygen balance, but also the increase of the respective densities as well as higher thermal robustness, since the introduction of an oxygen adds another site for the hydrogen bridge acceptor.

Hydroxylammonium, formally oxidized ammonium, is for several reasons of great interest in energetic materials chemistry. As for the oxidation of the heterocycles, the main advantages are the increased oxidation balance and the elevated density of the resulting salt. With the increasing numbers of *N*-oxides, a clear trend is visible of better performance parameters for a growing number of introduced oxygen atoms. Figure 10 depicts the investigation on the effect of rising numbers of *N*-oxidations based on the heterocyclic motif 5-(3-nitro-1,2,4-triazol-5-yl)-tetrazole.[42] Hydroxylammonium was chosen as the cation for this comparison, but similar trends can be seen for other salts. For the decomposition point, an increase of about 25 °C compared to the minor oxidized compounds **G** and **H** is observed for **4**, even if this trend is not completely unambiguous.

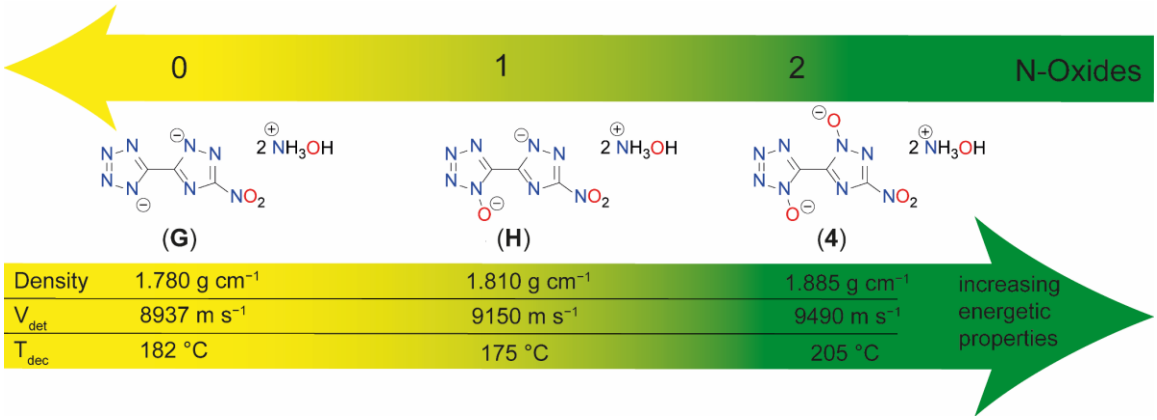

Figure 10. Comparison of the density, detonation velocity and decomposition temperature of bis-hydroxylammonium salts **4** and the respective 5-(3-nitro-1,2,4-triazol-5-yl)-tetrazole homologues without (**G**) and with one (**H**) *N*-oxide.

The densities were all determined through pycnometric measurements and are therefore easily comparable among themselves. The density of **4** is more than 0.1 g cm^{-3} higher than that of **G**, which is due to the double *N*-oxidation. The closely related detonation rate also increases with increasing *N*-oxidation. In general, it can be noted that the rise in density and detonation velocity from **G** to **H** is not as large as from **H** to **4**. However, it can be stated that there is a clear improvement in all energetic parameters with increasing numbers of *N*-oxides.

6.3 Conclusion

The skeleton based on 1-hydroxy-3-nitro-1,2,4-triazole combined with 1-hydroxy-tetrazole has proved to be an interesting platform for new energetic materials. The neutral compound **1** could finally be synthesized through selective oxidation of the triazole moiety using Oxone® under phosphate buffered conditions. The six ionic derivatives **2–7** were obtained by reaction of the respective bases with **1** in an alcoholic medium in good yields and were intensively characterized. While insensitive bis-ammonium and bis-guanidinium derivatives **2** and **5** are the thermally most stable ones (265 °C for **2** and 270 °C for **5**), the bis-hydroxylammonium derivative **4** is, as expected, the best performing compound with a detonation velocity of 9490 m s^{-1} and a moderate sensitivity of IS = 20 J and FS = 324 N. As it is the hybrid-molecule of TKX-50 and MAD-X1, an overlap of some properties and characteristics was expected. **4** exhibits moderate sensitivities, a high density and high heat of formation, which results in high calculated detonation properties and thus confirms the concept under investigation. The method of *N*-oxidation on nitrogen-rich azoles again showed enormous improvement compared to the minor oxidized molecules (**G** and **H**) and an increase in all energetically relevant properties. Generally, all compounds investigated show consistently convincing performance data, even if synthesis is more demanding than for the symmetric 1,1′-dihydroxy-5,5′-bistetrazole (**A**) and 1,1′-dihydroxy-3,3′-dinitro-bis-1,2,4-triazole (**B**).

6.4 Acknowledgement

The financial support of this work by Ludwig-Maximilian University (LMU), the Office of Naval Research (ONR) under grant no. ONR N00014-19-1-2078 and the Strategic Environmental Research and Development Program (SERDP) under contract no. W912HQ19C0033 is gratefully acknowledged. We thank Prof. Konstantin Karaghiosoff for NMR measurements, Jasmin Lechner for TGA measurement, Alexander Harter for pycnometric measurements and Stefan Huber for assistance in sensitivity measurements.

6.5 References

[1] K. B. Landenberger, O. Bolton, A. J. Matzger, *J. Am. Chem. Soc.* **2015**, *137*, 5074–5079.

[2] D. Kumar, Y. Tang, C. He, G. H. Imler, D. A. Parrish, J. M. Shreeve, *Chem. Eur. J.* **2018**, *24*, 17220–17224.

[3] M. C. Schulze, B. L. Scott, D. E. Chavez, *J. Mater. Chem. A* **2015**, *3*, 17963–17965.

[4] H. Gao, Q. Zhang, J. M. Shreeve, *J. Mater. Chem. A* **2020**, *8*, 4193–4216.

[5] M. Deng, Y. Feng, W. Zhang, X. Qi, Q. Zhang, *Nat. Commun.* **2019**, *10*, 1339.

[6] S. Li, Y. Wang, C. Qi, X. Zhao, J. Zhang, S. Zhang, S. Pang, *Angew. Chem. Int. Ed.* **2013**, *52*, 14031–14035.

[7] H. Gao, J. M. Shreeve, *Chem. Rev.* **2011**, *111*, 7377–7436.

[8] Y. Wang, Y. Liu, S. Song, Z. Yang, X. Qi, K. Wang, Y. Liu, Q. Zhang, Y. Tian, *Nat. Commun.* **2018**, *9*, 2444.

[9] J. Zhang, Y. Feng, Y. Bo, R. J. Staples, J. Zhang, J. M. Shreeve, *J. Am. Chem. Soc.* **2021**, *143*, 12665–12674.

[10] A. K. Chinnam, Q. Yu, G. H. Imler, D. A. Parrish, J. M. Shreeve, *Dalton Trans.* **2020**, *49*, 11498–11503.

[11] O. T. O'Sullivan, M. J. Zdilla, *Chem. Rev.* **2020**, *120*, 5682–5744.

[12] A. A. Larin, A. V. Shaferov, M. A. Epishina, I. N. Melnikov, N. V. Muravyev, I. V. Ananyev, L. L. Fershtat, N. N. Makhova, *ACS Appl. Energy Mater.* **2020**, *3*, 7764–7771.

[13] J. R. Yount, M. Zeller, E. F. C. Byrd, D. G. Piercey, *J. Mater. Chem. A* **2020**, *8*, 19337–19347.

[14] M. L. Gettings, M. T. Thoenen, E. F. C. Byrd, J. J. Sabatini, M. Zeller, D. G. Piercey, *Chem. Eur. J.* **2020**, *26*, 14530–14535.

[15] Y. Tang, W. Huang, G. H. Imler, D. A. Parrish, J. M. Shreeve, *J. Am. Chem. Soc.* **2020**, *142*, 7153–7160.

[16] S. E. Creegan, M. Zeller, E. F. C. Byrd, D. G. Piercey, *Cryst. Growth Des.* **2021**, *21*, 3922–3927.

[17] N. Fischer, T. M. Klapötke, M. Reymann, J. Stierstorfer, *Eur. J. Inorg. Chem.* **2013**, 2167–2180.

[18] N. Fischer, D. Fischer, T. M. Klapötke, D. G. Piercey, J. Stierstorfer, *J. Mater. Chem.* **2012**, *22*, 20418–20422.

[19] A. A. Dippold, T. M. Klapötke, *J. Am. Chem. Soc.* **2013**, *135*, 9931–9938.

[20] D. Fischer, T. M. Klapötke, M. Reymann, P. C. Schmid, J. Stierstorfer, M. Sućeska, *Propellants Explo. Pyrotech.* **2014**, *39*, 550–557.

[21] A. A. Dippold, D. Izsák, T. M. Klapötke, *Chem. Eur. J.* **2013**, *19*, 12042–12051.

[22] J. Zhang, P. Yin, G. Pan, Z. Wang, J. Zhang, L. A. Mitchell, D. A. Parrish, J. M. Shreeve, *New J. Chem.* **2019**, *43*, 12684–-12689.

[23] D. Fischer, T. M. Klapötke, D. G. Piercey, J. Stierstorfer, *Chem. Eur. J.* **2013**, *19*, 4602–4613.

[24] B. Yuan, Z. Yu, E. R. Bernstein, *J. Phys. Chem. A* **2015**, *119*, 2965–2981.

[25] J. C. Bennion, J. A. Ciezak-Jenkins, T. A. Jenkins, *Propellants Explo. Pyrotech.* **2019**, *44*, 1263–1269.

[26] M. Herrmann, U. Förter-Barth, *Propellants Explo. Pyrotech.* **2021**, *46*, 262–266.

[27] X. Xu, D. Chen, H. Li, R. Xu, H. Zhao, *ChemistrySelect* **2020**, *5*, 1919–1924.

[28] X. Xu, D. Chen, H. Li, M. Yan, Y. Xiong, H. Zhao, R. Xu, *RSC Adv.* **2020**, *10*, 11939–11944.

[29] Y. Xu, Y. Tan, W. Cao, Y. Zhao, B. Tian, *J. Phys. Chem. C* **2020**, *124*, 5987–5998.

[30] J. L. Gottfried, T. M. Klapötke, T. G. Witkowski, *Propellants Explo. Pyrotech.* **2017**, *42*, 353–359.

[31] L. Kukuljan, K. Kranjc, *Tetrahedron Lett.* **2019**, *60*, 207–209.

[32] M. Göbel, K. Karaghiosoff, T. M. Klapötke, D. G. Piercey, J. Stierstorfer, *J. Am. Chem. Soc.* **2010**, *132*, 17216–17226.

[33] T. M. Klapötke, D. G. Piercey, J. Stierstorfer, *Chem. Eur. J.* **2011**, *17*, 13068–13077.

[34] K. Hafner, T. M. Klapötke, P. C. Schmid, J. Stierstorfer, *Eur. J. Inorg. Chem.* **2015**, *2015*, 2794–2803.

[35] L. Hu, R. J. Staples, J. M. Shreeve, *Chem. Commun.* **2021**, *57*, 603–606.

[36] J. Ma, A. K. Chinnam, G. Cheng, H. Yang, J. Zhang, J. M. Shreeve, *Angew. Chem. Int. Ed.* **2021**, *60*, 5497–5504.

[37] Y. Tang, W. Huang, A. K. Chinnam, J. Singh, R. J. Staples, J. M. Shreeve, *Inorg. Chem.* **2021**, *60*, 8339–8345.

[38] D. G. Piercey, D. E. Chavez, B. L. Scott, G. H. Imler, D. A. Parrish, *Angew. Chem. Int. Ed.* **2016**, *55*, 15315–15318.

[39] D. G. Piercey, D. E. Chavez, S. Heimsch, C. Kirst, T. M. Klapötke, J. Stierstorfer, *Propellants Explo. Pyrotech.* **2015**, *40*, 491–497.

[40] Y. Tang, K. Li, A. K. Chinnam, R. J. Staples, J. M. Shreeve, *Dalton Trans.* **2021**, *50*, 2143–2148.

[41] J. Yuan, X. Long, C. Zhang, *J. Phys. Chem. A* **2016**, *120*, 9446–9457.

[42] M. Dachs, A. A. Dippold, J. Gaar, M. Holler, T. M. Klapötke, *Z. Anorg. Allg. Chem.* **2013**, *639*, 2171–2180.

6.6 Supporting Information

6.6.1 Experimental Procedures

^{1}H, ^{13}C, ^{14}N and ^{15}N NMR spectra were recorded on *BRUKER AMX 400* instruments. Chemical shifts are referenced with respect to tetramethylsilane ($^{1}H/^{13}C$) and nitromethane ($^{14}N/^{15}N$). Infrared spectra (IR) were recorded in the region 4000-400 cm^{-1} on a *PERKIN ELMER Spectrum BX-59343* instrument with a *SMITHS DETECTION DuraSamplIR II Diamond ATR* sensor. Raman spectra were recorded with a Bruker MultiRAM. The absorption bands are reported in

wavenumbers (cm^{-1}). Decomposition temperatures were measured via differential thermal analysis (DTA) with an *OZM Research DTA 552-Ex* instrument at a heating rate of 5 °C/min and in a range of room temperature to 400 °C. Sensitivities toward impact (IS) and friction (FS) were determined according to the UN Recommendations on the Transport of Dangerous Goods (ST/SG/AC.10/11/Rev.7) using a BAM drop hammer and a BAM friction apparatus by applying the 1 of 6 method.[S1] All energetic compounds were tested for sensitivity towards electrical discharge using an *Electric Spark Tester ESD 2010 EN* from OZM. Energetic properties have been calculated with the EXPLO5 6.02 computer [S2] code using the RT converted X-ray density and calculated solid state heats of formation.

CAUTION! *All investigated compounds are potentially explosive materials. Safety precautions and equipment (such as wearing leather coat, face shield, Kevlar sleeves, Kevlar gloves, earthed equipment and ear plugs) must be used during all manipulations.*

A different synthesis procedure was developed for the synthesis of 3-nitro-1,2,4-triazole-5-carbonitrile because of an incident in which a crystallizing shell was destroyed by the detonation of a side compound during the evaporation of the solvent. It was suspected that the highly sensitive intermediate was 3-diazo-1,2,4-triazole-5-carbonitrile. By modifying the reaction procedure, it was possible to prevent the formation of 3-diazo-1,2,4-triazole-5-carbonitrile or to destroy already formed diazonium compound by the appropriate conditions.

Improved synthesis of 3-nitro-1,2,4-triazole-5-carbonitrile

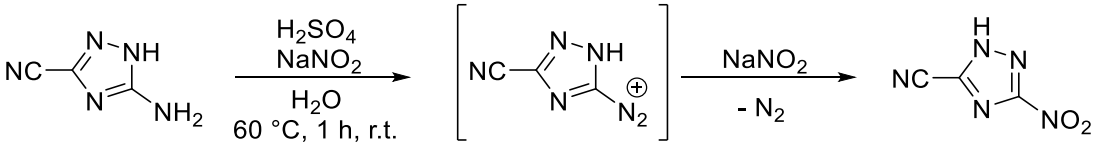

3-Amino-1,2,4-triazole-5-carbonitrile (2.00 g, 18.3 mmol, 1.0 eq.) and sodium nitrite (19.0 g, 275 mmol, 15 eq.) were dissolved in water (40 mL). Sulfuric acid (1 M, 40 mL) was added dropwise to the yellow suspension resulting in a gas evolution (nitrous gases) and clarification to a yellow solution. The solution was heated at 60 °C for one hour, leading to an orange solution. After cooling down to room temperature sulfuric acid (20 %) was added leading to a color change of the solution from orange to yellow to green and the formation of nitrous gases. Just enough sulfuric acid was added until no more visible evolution of nitrous gases could be observed. The aqueous solution was extracted with ethyl acetate (3 x 200 mL) and the organic phase was dried over sodium sulfate. Removing of the solvent led to the formation of orange 3-nitro-1,2,4-triazole-5-carbonitrile (2.16 g, 15.5 mmol, 85%).

All analytic data correspond with the literature values.[S3, S4]

5-(1-Hydroxy-3-nitro-1,2,4-triazol-5-yl)-1-hydroxy-tetrazole trihydrate (**1**)

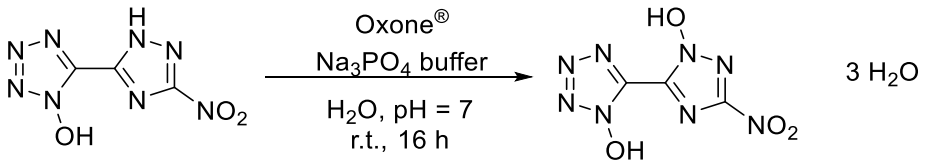

(**1**)

5-(3-Nitro-1,2,4-triazol-5-yl)-1-hydroxy-tetrazole (1.30 g, 6.56 mmol, 1.0 eq)[S4] was dissolved in water (52 mL). The pH value of the solution was adjusted to pH = 7 by adding solid sodium triphosphate. When the desired pH value was reached, Oxone® (24.7 g, 80.4 mmol, 12 eq) and sodium triphosphate dodecahydrate were added equally in that way keeping the pH value at around 7. After complete addition of Oxone®, the yellow suspension was stirred at room temperature for 16 hours. For work up, the suspension was cooled with ice, the formed solid was filtered and washed with small amounts of cold water. The yellow precipitate was dissolved in water (200 mL) and concentrated hydrochloric acid (37%, 65 mL). The mixture was extracted with ethyl acetate (3 x 200 mL). The aqueous phase was further acidified with concentrated hydrochloric acid (25 mL) and extracted with ethyl acetate (2 x 100 mL). This process was repeated two more

times. The combined organic phases were dried over sodium sulfate. Removing of the solvent led to the formation of yellow **1** (1.23 g, 4.59 mmol, 70%).

DTA (5 °C min^{-1}): 103 °C (endo, H_2O), 169 °C (exo, dec.); BAM: drop hammer: >40 J (100–500 µm); friction tester: >360 N (100–500 µm); ESD: 0.50 J (100–500 µm); IR (rel. int.): ν = 3550(s), 3536(s), 3530(s), 3478(s), 3471(s), 3450(s), 3434(s), 3419(s), 3412(s), 3396(s), 3388(s), 3370(s), 3335(s), 3309(s), 3301(s), 3293(s), 3274(s), 1543(vs), 1450(vs), 1361(s), 1315(s), 1267(s), 1144(s), 1144(s), 771(s), 761(s), 725(s), 696(s), 667(s), 625(s), 498(vs), 490(vs), 470(vs), 455(vs), 442(s), 438(s), 410(s) cm^{-1}; ^1H NMR (DMSO-D_6, 400 MHz, ppm) δ = 7.80 (br s, 8H); ^{13}C NMR (DMSO-D_6, 101 MHz, ppm) δ = 155.3, 137.0, 133.3; ^{15}N NMR (DMSO-D_6, 41 MHz, ppm) δ = −0.8, −19.5, −28.0, −51.9 −89.4, −108.0, −119.4, −139.9; Elem. Anal. ($C_3H_8N_8O_7$, 268.15 g mol^{-1}) calcd.: C 13.44, H 3.01, N 41.79 %. Found: C 13.78, H 2.87, N 41.94 %; HRMS (ESI, 70 eV): *m/z*: $[M - H]^-$ Calcd for $C_3HO_4N_8$ 213.0126; Found: 213.0126.

Bis-ammonium 5-(3-nitro-1,2,4-triazol-1-olate-5-yl)-tetrazol-1-olate (**2**)

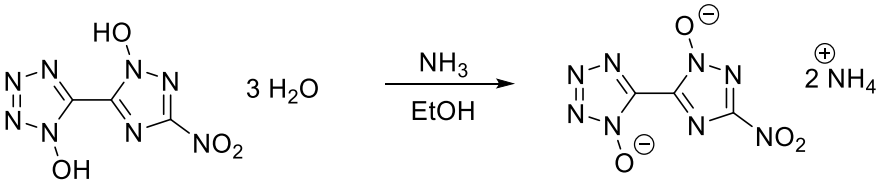

(**1**) (**2**)

5-(1-Hydroxy-3-nitro-1,2,4-triazol-5-yl)-1-hydroxy-tetrazole trihydrate (**1**) (0.52 g, 1.94 mmol, 1.0 eq) was dissolved in ethanol (20 mL). Gaseous ammonia was bubbled through the yellow solution for one minute, resulting in the immediate precipitation of a solid, which was filtered and washed with little amounts of cold ethanol to yield the respective bis-ammonium salt **2** as a yellow-orange solid. (0.41 g, 2.18 mmol, 85%).

DTA (5 °C min^{-1}): 265 °C (exo, dec.); BAM: drop hammer: >40 J (100–500 µm); friction tester: >360 N (100–500 µm); ESD: 0.37 J (100–500 µm); IR (rel. int.): ν = 3235(m), 3216(m), 3163(m), 3115(m), 2989(m), 2801(m), 1538(m), 1458(s), 1441(s), 1419(s), 1372(vs), 1353(s), 1305(vs), 1264(w), 1231(m), 1179(m), 1116(m), 1043(s), 1034(s), 998(m), 852(w), 782(m), 756(w),

756(w), 741(s), 706(w), 681(w), 674(w), 648(m), 563(w), 512(m), 490(w), 478(w), 464(w) cm^{-1}; ^{1}H NMR (DMSO-D_6, 400 MHz, ppm) δ = 7.25 (s, 8H); ^{13}C NMR (DMSO-D_6, 101 MHz, ppm) δ = 151.3, 135.0, 132.0; ^{15}N NMR (DMSO-D_6, 41 MHz, ppm) δ = −12.6, −17.5, −25.7, −54.1, −78.2, −84.9, −85.8, −138.1, −358.7; Elem. Anal. ($C_3H_8N_{10}O_4$, 248.16 g mol^{-1}) calcd.: C 14.52, H 3.52, N 56.44 %. Found: C 14.15, H 3.15, N 55.98 %.

Bis-hydrazinium 5-(3-nitro-1,2,4-triazol-1-olate-5-yl)-tetrazol-1-olate (**3**)

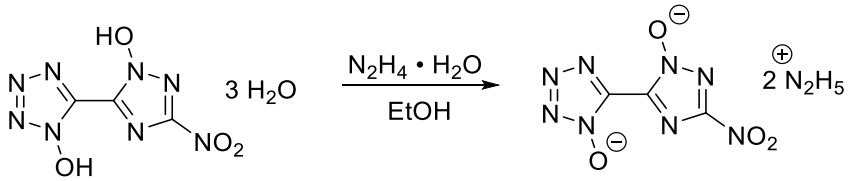

(**1**) (**3**)

5-(1-Hydroxy-3-nitro-1,2,4-triazol-5-yl)-1-hydroxy-tetrazole trihydrate (**1**) (0.50 g, 1.86 mmol, 1.0 eq) was dissolved in ethanol (30 mL). The yellow solution was heated to 50 °C followed by the addition of hydrazine hydrate (0.18 mL, 3.72 mmol, 2.0 eq). The solution was cooled to room temperature and the formed precipitate was filtered off and washed with cold ethanol. The solid was recrystallized from hot methanol, ethanol and acetone to yield the bis-hydrazinium salt **3** as an orange solid (0.47 g, 1.68 mmol, 90%).

DTA (5 °C min^{-1}): 206 °C (exo, dec.); BAM: drop hammer: 10 J (100–500 µm); friction tester: 216 N (100–500 µm); ESD: 0.10 J (100–500 µm); IR (rel. int.): ν = 3351(m), 3324(m), 3291(w), 3257(w), 3244(w), 3072(m), 2971(m), 2939(m), 2804(m), 2725(m), 2633(s), 2362(w), 2343(w), 1644(w), 1619(m), 1591(m), 1516(s), 1467(s), 1371(vs), 1348(s), 1306(vs), 1270(m), 1219(s), 1219(s), 1194(w), 1176(s), 1116(s), 1096(vs), 1045(s), 1033(s), 997(s), 966(s), 852(m), 841(m), 786(s), 746(s), 701(w), 681(w), 674(w), 645(m), 565(w), 511(m) cm^{-1}; ^{1}H NMR (DMSO-D_6, 400 MHz, ppm) δ = 7.13 (br s, 10H); ^{13}C NMR (DMSO-D_6, 101 MHz, ppm) δ = 151.5, 136.0, 133.0; ^{14}N NMR (DMSO-D_6, 29 MHz, ppm) δ = −25, −363; Elem. Anal. ($C_3H_{10}N_{12}O_4$, 278.19 g mol^{-1}) calcd.: C 12.95, H 3.62, N 60.42 %. Found: C 13.21, H 3.68, N 59.58 %.

Bis-hydroxylammonium 5-(3-Nitro-1,2,4-triazol-1-olate-5-yl)-tetrazol-1-olate (**4**)

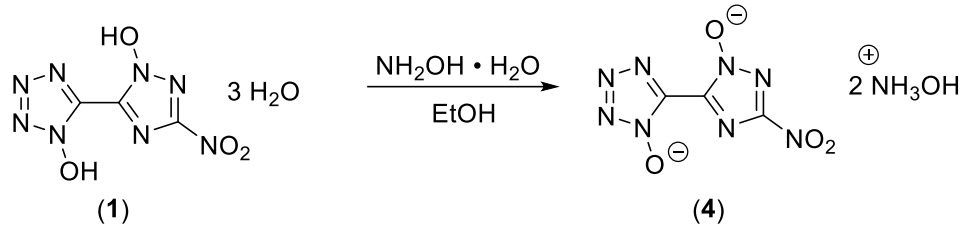

(**1**) (**4**)

5-(1-Hydroxy-3-nitro-1,2,4-triazol-5-yl)-1-hydroxy-tetrazole trihydrate (**1**) (0.20 g, 0.75 mmol, 1.0 eq) was dissolved in ethanol (10 mL). The yellow solution was heated to 50 °C followed by the addition of an aqueous solution of hydroxylamine (50% w/w in H_2O, 0.10 mL, 1.51 mmol, 2.0 eq). The solution was cooled to room temperature and the formed precipitate was filtered off and washed with little cold ethanol to yield the bis-hydroxylammonium salt **4** as a yellow solid (0.17 g, 0.62 mmol, 83%).

DTA (5 °C min^{-1}): 205 °C (exo, dec.); BAM: drop hammer: 20 J (100–500 µm); friction tester: 324 N (100–500 µm); ESD: 0.20 J (100–500 µm); IR (rel. int.): ν = 3222(m), 3202(m), 3188(m), 3151(m), 3137(m), 3116(m), 3090(m), 3056(m), 3049(m), 3034(m), 3020(m), 3008(m), 2962(m), 2928(m), 2841(m), 2678(m), 2514(m), 1530(m), 1523(m), 1513(m), 1465(m), 1450(m), 1376(vs), 1376(vs), 1308(vs), 1233(m), 1224(m), 1183(s), 1147(m), 1119(s), 1046(s), 1033(s), 1008(s), 999(s), 852(m), 781(m), 740(s), 667(m), 646(s), 623(m), 561(m), 505(s) cm^{-1}; ^{1}H NMR (DMSO-D_6, 400 MHz, ppm) δ = 9.66 (br s, 8H); ^{13}C NMR (DMSO-D_6, 101 MHz, ppm) δ = 153.2, 136.5, 133.0; ^{14}N NMR (DMSO-D_6, 29 MHz, ppm) δ = −28, −360; Elem. Anal. ($C_3H_8N_{10}O_6$, 280.16 g mol^{-1}) calcd.: C 12.86, H 2.88, N 50.00 %. Found: C 12.55, H 2.90, N 49.50 %.

Bis-guanidinium 5-(3-Nitro-1,2,4-triazol-1-olate-5-yl)-tetrazol-1-olate (**5**)

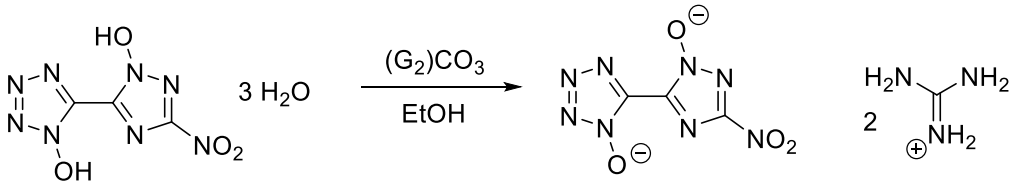

(**1**) (**5**)

5-(1-Hydroxy-3-nitro-1,2,4-triazol-5-yl)-1-hydroxy-tetrazole trihydrate (**1**) (0.64 g, 2.39 mmol, 1.0 eq) was dissolved in ethanol (50 mL). The yellow solution was heated to 50 °C followed by the addition guanidinium carbonate (0.43 g, 2.39 mmol, 1.0 eq). The solution was stirred for 30 min at this temperature and cooled to room temperature. The formed precipitate was filtered off and washed with little cold ethanol to yield the bis-guanidinium salt **5** as a reddish solid (0.71 g, 2.13 mmol, 89%).

DTA (5 °C min^{-1}): 200 °C (endo, melt.), 270 °C (exo, dec.); BAM: drop hammer: >40 J (100–500 µm); friction tester: >360 N (100–500 µm); ESD: 0.25 J (100–500 µm); IR (rel. int.): ν = 3468(m), 3426(m), 3411(m), 3346(m), 3331(m), 3315(m), 3269(m), 3262(m), 3235(m), 3227(m), 3159(s), 3137(s), 2803(w), 1659(s), 1645(s), 1640(s), 1582(m), 1505(m), 1456(s), 1377(vs), 1309(s), 1269(m), 1231(m), 1231(m), 1171(s), 1092(s), 1060(s), 1031(s), 1013(m), 999(s), 850(m), 789(m), 753(s), 671(m), 648(s), 618(s), 546(s), 529(s), 515(s), 505(s), 472(vs), 463(vs), 442(vs), 435(vs) cm^{-1}; ^{1}H NMR (DMSO-D_6, 400 MHz, ppm) δ = 7.13 (s, 12H); ^{13}C NMR (DMSO-D_6, 101 MHz, ppm) δ = 158.1, 151.2, 134.9, 132.1; ^{14}N NMR (DMSO-D_6, 29 MHz, ppm) δ = −28; Elem. Anal. ($C_5H_{12}N_{14}O_4$, 332.24 g mol^{-1}) calcd.: C 18.08, H 3.64, N 59.02 %. Found: C 17.91 H 3.55, N 58.42 %.

Bis-aminoguanidinium 5-(3-Nitro-1,2,4-triazol-1-olate-5-yl)-tetrazol-1-olate (**6**)

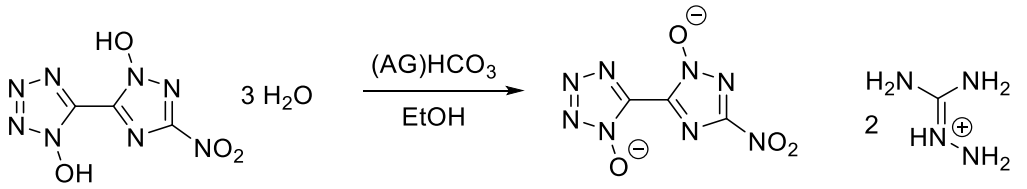

(**1**) (**6**)

5-(1-Hydroxy-3-nitro-1,2,4-triazol-5-yl)-1-hydroxy-tetrazole trihydrate (**1**) (0.78 g, 2.91 mmol, 1.0 eq) was dissolved in a mixture of ethanol (20 mL) and water (10 mL) and heated to 70 °C. Amoniguanidine hydrogen carbonate (0.79 g, 5.82 mmol, 2.0 eq). The solution was stirred for 10 min at this temperature and cooled to room temperature. The solution was reduced under nitrogen stream and the formed precipitate was filtered off and washed with little cold ethanol to yield the bis-aminoguanidinium salt **6** as an orange solid (0.80 g, 2.21 mmol, 76%).

DTA (5 °C min^{-1}): 217 °C (endo, melt.), 219 °C (exo, dec.); BAM: drop hammer: 40 J (100–500 µm); friction tester: >360 N (100–500 µm); ESD: 0.25 J (100–500 µm); IR (rel. int.): ν = 3469(w), 3334(m), 3304(m), 3220(m), 3160(m), 3135(m), 2875(m), 2755(w), 1660(s), 1652(s), 1646(s), 1529(s), 1471(s), 1454(m), 1377(s), 1306(s), 1259(m), 1226(m), 1177(s), 1117(s), 1100(m), 1041(s), 1036(s), 1036(s), 996(s), 966(m), 850(m), 839(m), 785(m), 750(s), 702(m), 681(m), 647(s), 615(s), 547(s), 536(s), 499(vs), 483(vs), 465(vs), 458(vs), 447(vs), 437(vs), 428(s), 420(s) cm^{-1}; ^{1}H NMR (DMSO-D$_6$, 400 MHz, ppm) δ = 8.93 (br s, 2H), 7.21 (br s, 8H), 4.65 (s, 4H); ^{13}C NMR (DMSO-D$_6$, 101 MHz, ppm) δ = 159.0, 151.4, 135.0, 132.2; ^{14}N NMR (DMSO-D$_6$, 29 MHz, ppm) δ = −32; Elem. Anal. ($C_5H_{14}N_{16}O_4$, 362.28 g mol^{-1}) calcd.: C 16.58, H 3.90, N 61.86 %. Found: C 16.58 H 4.12, N 60.72 %.

Triaminoguanidinium 5-(3-Nitro-1,2,4-triazol-1-olate-5-yl)-1-hydroxy-tetrazole (**7**)

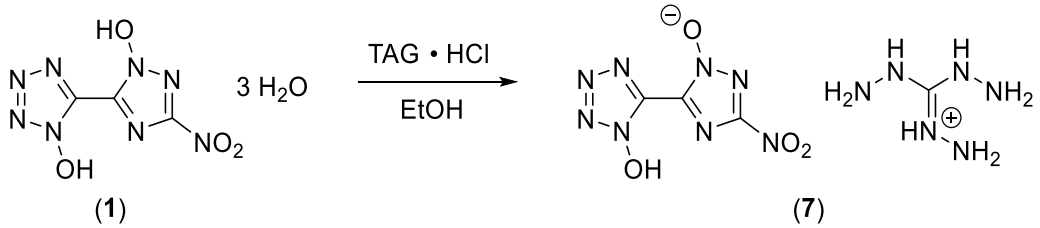

(**1**) (**7**)

5-(1-Hydroxy-3-nitro-1,2,4-triazol-5-yl)-1-hydroxy-tetrazole trihydrate (**1**) (0.58 g, 2.16 mmol, 1.0 eq) was dissolved in a mixture of ethanol (20 mL) and water (10 mL) and heated to 70 °C. Triaminoguanidinium hydrochloride (0.61 g, 4.32 mmol, 2.0 eq). The solution was stirred for 10 min at this temperature and cooled to room temperature. The solution was reduced under nitrogen stream and the formed precipitate was filtered off and washed with little cold ethanol to yield the triaminoguanidinium salt **7** as a yellow/orange solid (0.63 g, 1.98 mmol, 92%). DTA (5 °C min^{-1}): 165 °C (endo, melt), 204 °C (exo, dec.); BAM: drop hammer: 7 J (100–500 µm); friction tester: 192 N (100–500 µm); ESD: 0.10 J (100–500 µm); IR (rel. int.): ν = 3363(m), 3322(m), 3197(s), 1683(s), 1667(s), 1661(s), 1622(m), 1531(s), 1460(s), 1374(vs), 1348(vs), 1309(vs), 1229(m), 1175(s), 1130(s), 1040(s), 1031(s), 1002(s), 961(vs), 851(m), 782(s), 740(s), 702(m), 702(m), 679(s), 667(m), 646(s), 637(s), 612(vs), 533(s), 517(s), 458(s), 436(vs), 412(s) cm^{-1}; ^{1}H NMR (DMSO-D$_6$, 400 MHz, ppm) δ = 8.61 (br s, 3H), 5.68 (br s,

6H); ^{13}C NMR (DMSO-D_6, 101 MHz, ppm) δ = 159.0, 154.9, 136.7, 132.7; ^{14}N NMR (DMSO-D_6, 29 MHz, ppm) δ = −27; Elem. Anal. ($C_4H_{10}N_{14}O_4$, 318.21 g mol^{-1}) calcd.: C 15.10, H 3.17, N 61.62 %. Found: C 14.66 H 3.55, N 60.70 %.

6.6.2 Crystallography

Crystal structure data were obtained from an Oxford Xcalibur3 diffractometer with a Spellman generator (voltage 50 kV, current 40 mA) and a Kappa CCD area for data collection using Mo-*Kα* radiation (λ = 0.71073 Å) or a Bruker D8 Venture TXS diffractometer equipped with a multilayer monochromator, a Photon 2 detector and a rotation-anode generator (Mo-K_α radiation). The data collection was performed using the CRYSTALIS RED software.[S5] The solution of the structure was performed by direct methods and refined by full-matrix least-squares on F2 (SHELXT)[S6] implemented in the OLEX2[S7] software suite. The non-hydrogen atoms were refined anisotropically and the hydrogen atoms were located and freely refined. The absorption correction was carried out by a SCALE3 ABSPACK multiscan method.[S8] The DIAMOND2 plots shown with thermal ellipsoids at the 50% probability level and hydrogen atoms are shown as small spheres of arbitrary radius. The SADABS program embedded in the Bruker APEX3 software was used for multi-scan absorption corrections in all structures.[S9]

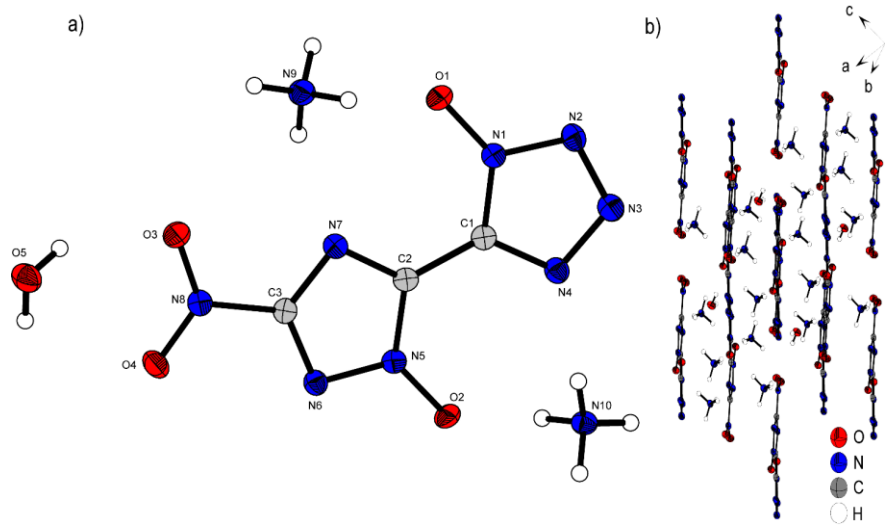

Figure S1. Representation of the molecular unit of bis-ammonium 5-(3-Nitro-1,2,4-triazol-1-olate-5-yl)-tetrazol-1-olate hydrate (**2** • H_2O), showing the atom-labeling scheme. Thermal ellipsoids represent the 50% probability level and hydrogen atoms are shown as small spheres of arbitrary radius. a) Molecular unit of **2** • H_2O, b) packing of **2** • H_2O in the specified direction of view.

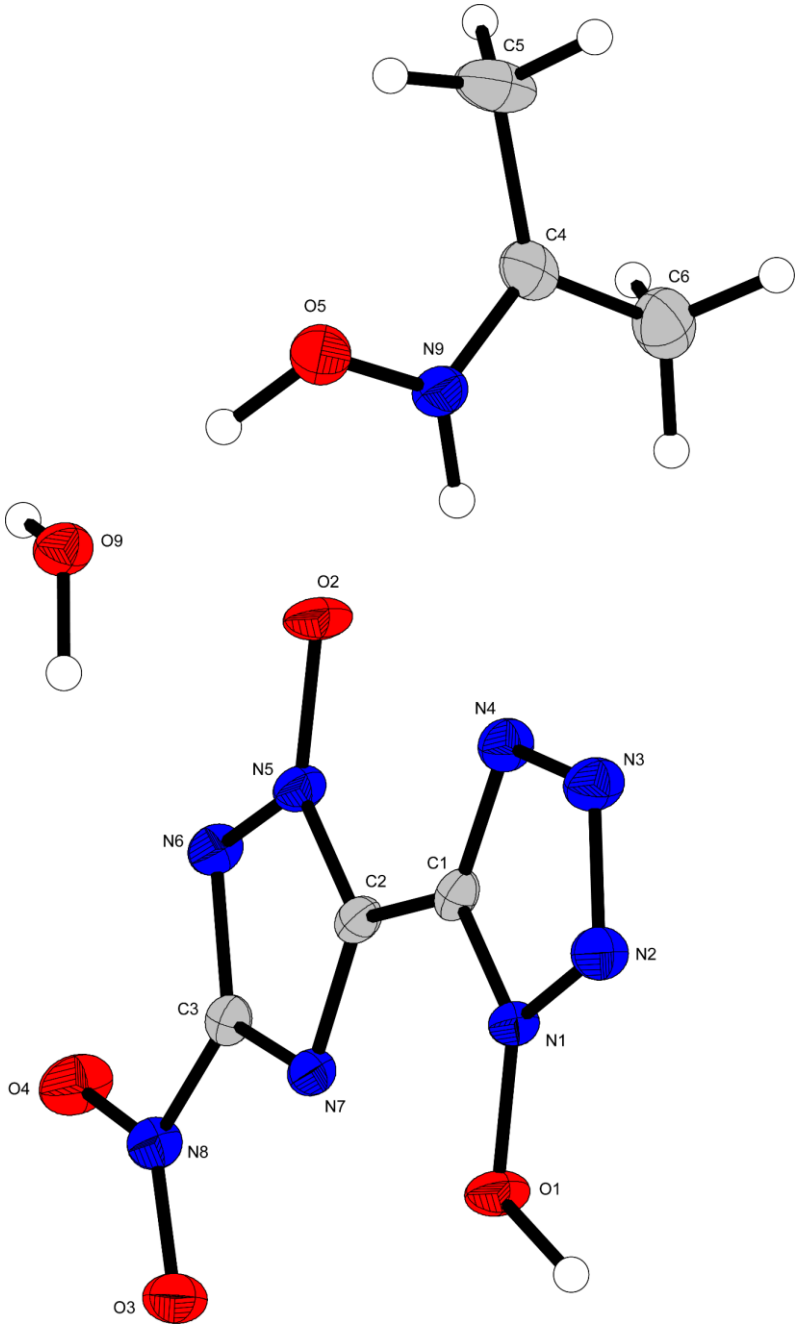

Figure S2. Representation of the molecular unit **4a**, showing the atom-labeling scheme. Thermal ellipsoids represent the 50% probability level and hydrogen atoms are shown as small spheres of arbitrary radius.

Compound **4a** was obtained by recrystallizing **4** from acetone. It can be interpreted as the acetone condensed product of the mono hydroxylammonium salt of **1**. **4a** crystallizes in the triclinic space group *P*−1, with a cell volume of 608.07(9) Å^3 with 2 molecular units per cell. The density is 1.667 g cm^{-3} at 123 K. The proton H1 is bond between O1 and O2^i of the nearby molecular unit (O1–H1, 1.29(2) Å; O2^i···H1, 1.19(1) Å), which is much significantly longer than for the neutral compound **1** (O1–H1; O2–H2, 0.86(4) Å).

Table S1. Crystallographic data of **1**–**3**.

	1	**2**	**3**
Formula	$C_3H_2N_8O_4 \cdot 3\ H_2O$	$C_3N_8O_4\ (NH_4)_2$	$C_3N_8O_4\ (N_2H_5)_2$
FW [g mol^{-1}]	268.17	248.19	278.23
Crystal system	orthorhombic	monoclinic	triclinic
Space group	*Cmca* (No. 64)	$P2_1/n$ (No. 14)	*P*-1 (No. 2)
Color / Habit	colorless rod	colorless rod	yellow rod
Size [mm]	0.02 x 0.02 x 0.05	0.02 x 0.03 x 0.11	0.02 x 0.03 x 0.08
a [Å]	6.2387(12)	4.3259(1)	3.6755(4)
b [Å]	7.8415(16)	26.9849(8)	8.0751(9)
c [Å]	40.259(8)	7.9243(2)	17.8693(18)
α [°]	90	90	87.041(4)
β [°]	90	98.770(1)	88.105(4)
γ [°]	90	90	85.965(4)
V [Å^3]	1969.5(7)	914.22(4)	528.11(10)
Z	8	4	2
$\rho_{calc.}$ [g cm^{-3}]	1.809	1.803	1.750
μ [mm^{-1}]	0.172	0.160	0.154
F(000)	1104	512	288
$\lambda_{MoK\alpha}$ [Å]	0.71073	0.71073	0.71073
T [K]	293	106	173
θ Min-Max [°]	3.0, 25.3	2.7, 26.4	3.3, 25.4
Dataset	-7: 7 ; -9: 9 ; -47: 48	-5: 5 ; -33: 33 ; -9: 9	-4: 4 ; -9: 9 ; -20: 21
Reflections collected	10605	15707	5647
Independent refl.	980	1872	1893
R_{int}	0.035	0.036	0.040
Observed reflections	911	1664	1449
Parameters	133	186	212
R_1 (obs)[a]	0.0468	0.0320	0.0495
wR_2 (all data)[b]	0.1085	0.0781	0.1107
S [c]	1.19	1.15	1.10
Resd. dens [e Å^{-3}]	-0.26, 0.27	-0.25, 0.25	-0.25, 0.24
Device type	Bruker D8 Venture	Bruker D8 Venture	Bruker D8 Venture
Solution	SIR-92	SIR-92	SIR-92
Refinement	SHELXL-2013	SHELXL-2013	SHELXL-2013
Absorption correction	multi-scan	multi-scan	multi-scan
CCDC	2144427	2144428	2144432

[a]$R_1 = \Sigma||F_o|-|F_c||/\Sigma|F_o|$; [b]$wR_2 = [\Sigma[w(F_o^2-F_c^2)^2]/\Sigma[w(F_o)^2]]^{1/2}$; $w = [\sigma c^2(F_o^2)+(xP)^2+yP]^{-1}$ and $P=(F_o^2+2F_c^2)/3$; [c]$S = (\Sigma[w(F_o^2-F_c^2)^2]/(n-p))^{1/2}$ (n = number of reflections; p = total number of parameters).

Table S2. Crystallographic data of **4** • H_2O and **6**–**7**.

	4 • H_2O	**6**	**7**
Formula	$C_3N_8O_4$ $(NH_3OH)_2$ • H_2O	$C_3N_8O_4$ $(CN_4H_7)_2$	$C_3HN_8O_4$ (CH_9N_6)
FW [g mol^{-1}]	298.21	362.32	318.26
Crystal system	monoclinic	monoclinic	triclinic
Space group	*P*2$_1$/*c* (No. 14)	*I*2/*a* (No. 15)	*P*-1 (No. 2)
Color / Habit	colorless rod	yellow platelet	yellow block
Size [mm]	0.02 x 0.02 x 0.10	0.01 x 0.03 x 0.04	0.25 x 0.40 x 0.98
a [Å]	7.3751(11)	11.245(2)	7.5556(8)
b [Å]	15.0961(19)	6.7268(15)	8.1499(8)
c [Å]	10.4402(14)	37.486(8)	11.4798(12)
α [°]	90	90	102.425(8)
β [°]	108.817(5)	91.125(9)	100.781(9)
γ [°]	90	90	112.073(9)
V [Å^3]	1100.2(3)	2835.0(10)	611.07(13)
Z	4	8	2
$\rho_{calc.}$ [g cm^{-3}]	1.800	1.698	1.730
μ [mm^{-1}]	0.169	0.144	0.149
F(000)	616	1504	328
$\lambda_{MoK\alpha}$ [Å]	0.71073	0.71073	0.71073
T [K]	298	100	102
θ Min-Max [°]	3.2, 25.1	3.1, 26.3	1.9, 26.4
Dataset	-8: 8 ; -17: 17 ; -12: 12	-13: 13 ; -8: 8 ; -46: 46	-8: 9 ; -10: 10 ; -14: 13
Reflections collected	17438	21495	4703
Independent refl.	1938	2869	2499
R_{int}	0.039	0.095	0.020
Observed reflections	1634	2110	2121
Parameters	221	282	239
R_1 (obs)[a]	0.0372	0.0723	0.0348
wR_2 (all data)[b]	0.0953	0.1628	0.0937
S [c]	1.12	1.12	1.04
Resd. dens [e Å^{-3}]	-0.26, 0.30	-0.34, 0.39	-0.25, 0.24
Device type	Bruker D8 Venture	Bruker D8 Venture	Xcalibur Sapphire3
Solution	SIR-92	SIR-92	SIR-92
Refinement	SHELXL-2013	SHELXL-2013	SHELXL-2013
Absorption correction	multi-scan	multi-scan	multi-scan
CCDC	2144430	2144425	2144429

[a] $R_1 = \Sigma||F_0|-|F_c||/\Sigma|F_0|$; [b] $wR_2 = [\Sigma[w(F_0^2-F_c^2)^2]/\Sigma[w(F_0)^2]]^{1/2}$; $w = [\sigma c^2(F_0^2)+(xP)^2+yP]^{-1}$ and $P=(F_0^2+2F_c^2)/3$; [c] $S = (\Sigma[w(F_0^2-F_c^2)^2]/(n-p))^{1/2}$ (n = number of reflections; p = total number of parameters).

Table S3. Crystallographic data of **2** • H_2O and **8**.

	2 • H_2O	**4a**
Formula	$C_3N_8O_4$ $(NH_4)_2$ • H_2O	$C_3HN_8O_4$, (C_3H_8NO) • H_2O
FW [g mol^{-1}]	266.21	305.24
Crystal system	triclinic	triclinic
Space group	*P*-1 (No. 2)	*P*-1 (No. 2)
Color / Habit	yellow block	colorless platelet
Size [mm]	0.24 x 0.38 x 0.77	0.04 x 0.10 x 0.30
a [Å]	8.0995(5)	6.7012(5)
b [Å]	8.1851(5)	7.5041(6)
c [Å]	8.7285(4)	13.0554(9)
α [°]	87.370(4)	104.374(7)
β [°]	80.330(5)	102.328(6)
γ [°]	60.399(6)	98.117(7)
V [Å^3]	495.52(6)	608.07(9)
Z	2	2
$\rho_{calc.}$ [g cm^{-3}]	1.784	1.667
μ [mm^{-1}]	0.161	0.147
F(000)	276	316
$\lambda_{MoK\alpha}$ [Å]	0.71073	0.71073
T [K]	103	123
θ Min-Max [°]	2.4, 26.7	2.9, 26.4
Dataset	-7: 10 ; -10: 10 ; -11: 11	-8: 8 ; -9: 9 ; -16: 16
Reflections collected	4782	9231
Independent refl.	2101	2497
R_{int}	0.020	0.042
Observed reflections	1864	1902
Parameters	203	208
R_1 (obs)[a]	0.0356	0.0639
wR_2 (all data)[b]	0.0948	0.1986
S [c]	1.06	1.07
Resd. dens [e Å^{-3}]	-0.20, 1.31	-0.26, 0.62
Device type	Xcalibur Sapphire3	Xcalibur Sapphire3
Solution	SIR-92	SIR-92
Refinement	SHELXL-2013	SHELXL-2013
Absorption correction	multi-scan	multi-scan
CCDC	2144424	2144426

[a] $R_1 = \Sigma||F_o|-|F_c||/\Sigma|F_o|$; [b] $wR_2 = [\Sigma[w(F_o^2-F_c^2)^2]/\Sigma[w(F_o)^2]]^{1/2}$; $w = [\sigma c^2(F_o^2)+(xP)^2+yP]^{-1}$ and $P=(F_o^2+2F_c^2)/3$; [c] $S = (\Sigma[w(F_o^2-F_c^2)^2]/(n-p))^{1/2}$ (n = number of reflections; p = total number of parameters).

6.6.3 Thermal Analysis

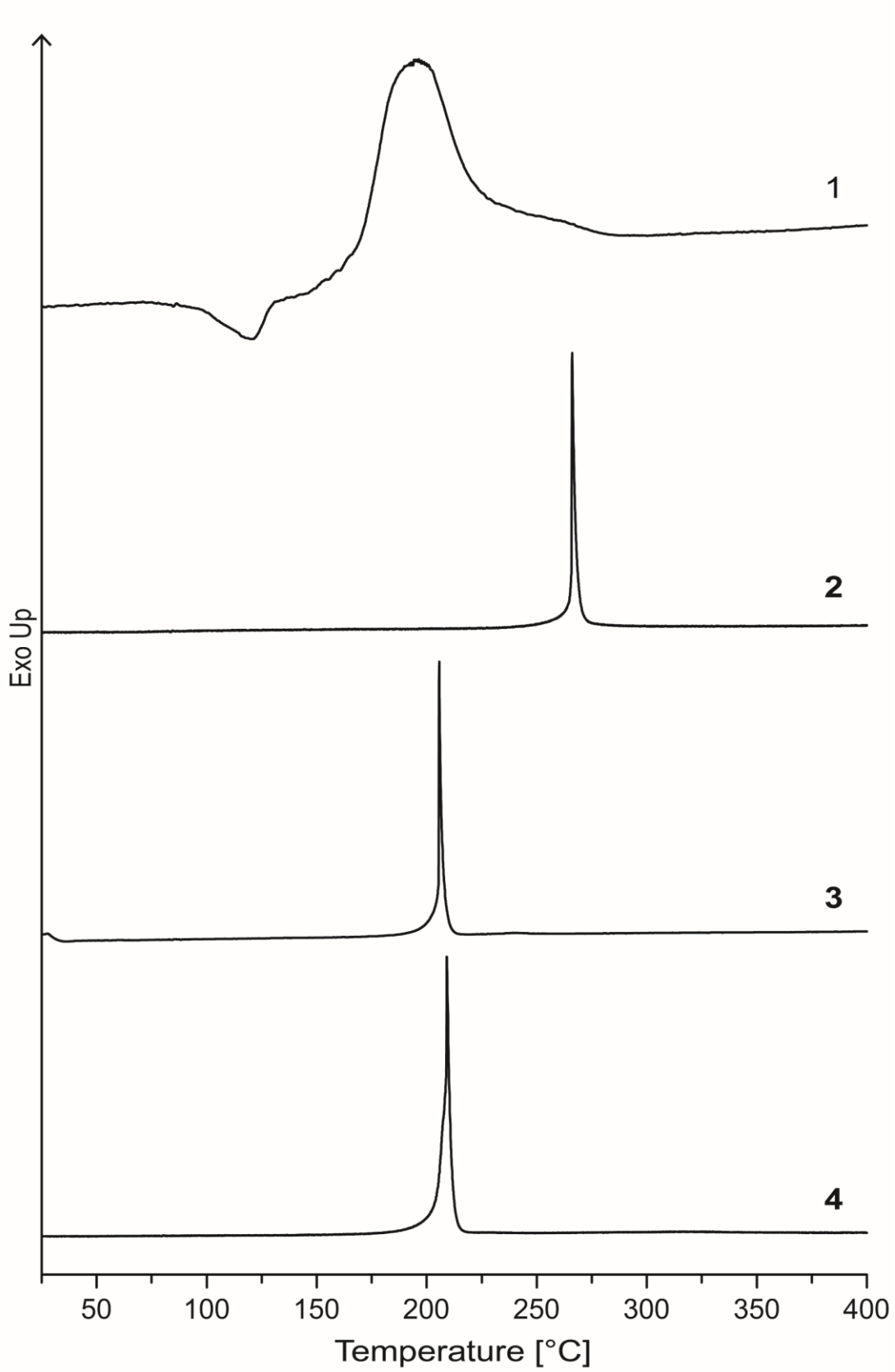

Figure S3. DTA plots of neutral compound **1** and nitrogen-rich derivatives **2-4**.

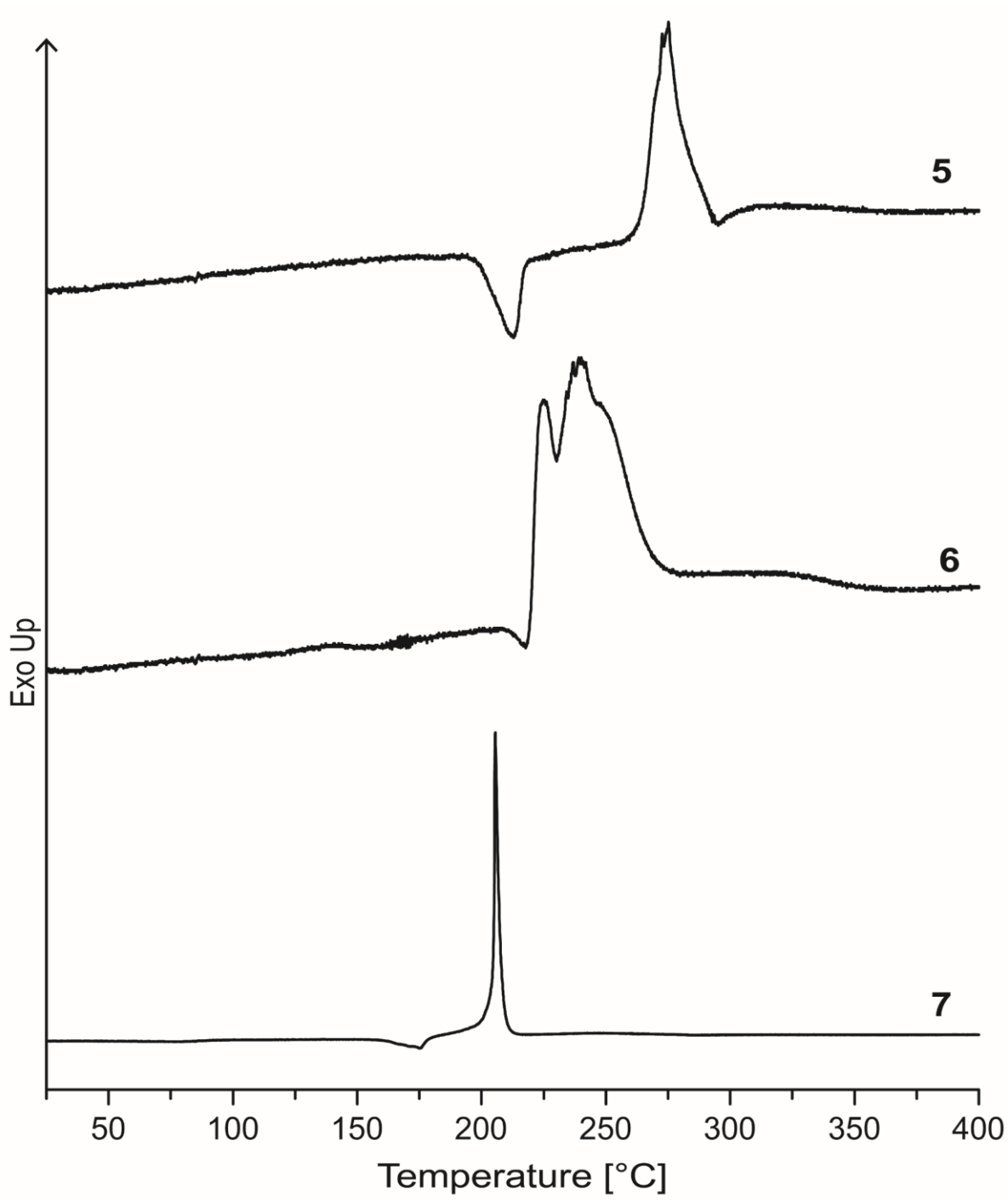

Figure S4. DTA plots of guanidinium derivatives **5**-7.

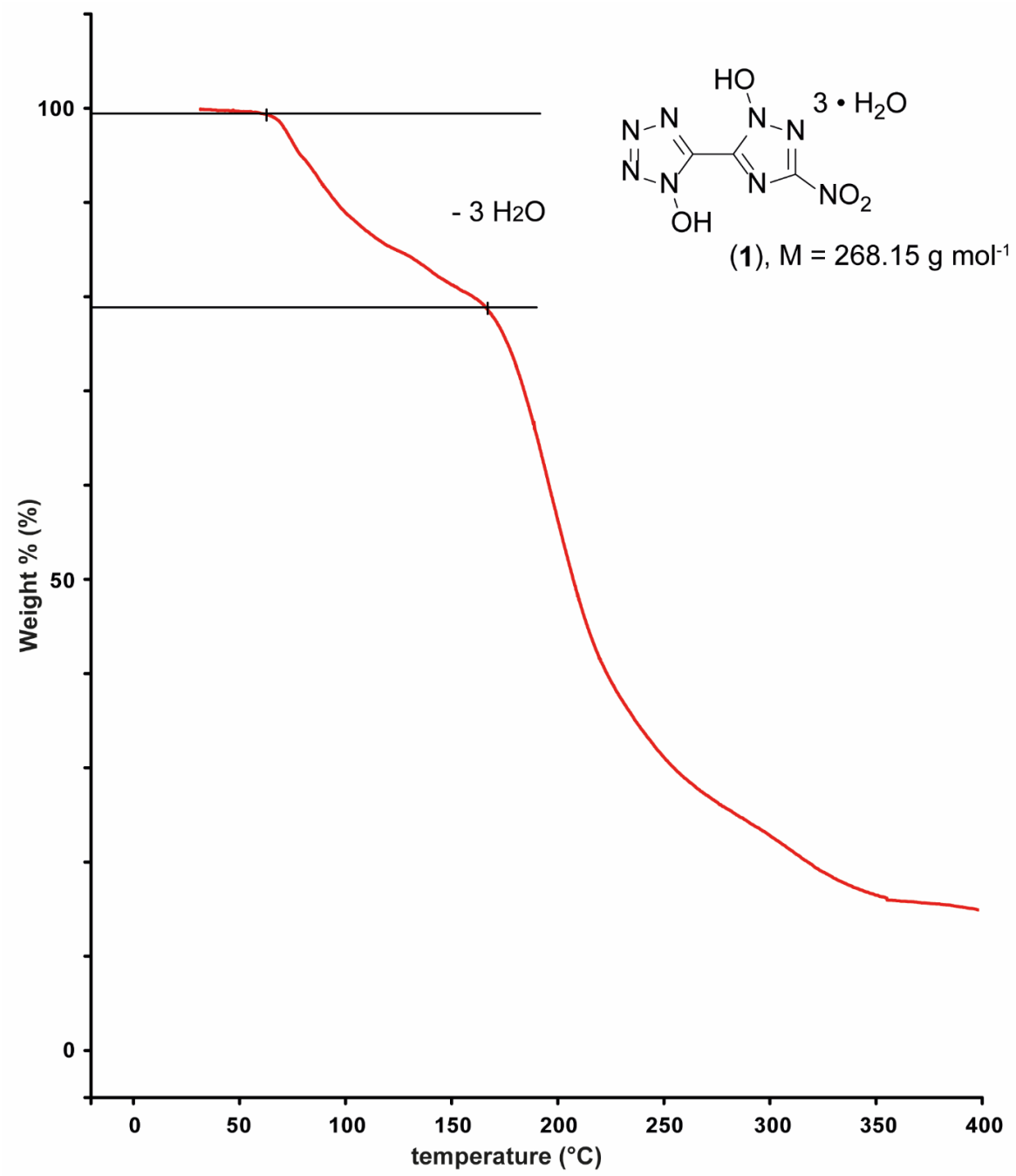

Figure S5. TGA plot of **1** with a heating rate of 5 °C min^{-1}.

6.6.4 Computation

All quantum chemical calculations were carried out using the Gaussian G09 program package.[S10] The enthalpies (H) and free energies (G) were calculated using the complete basis set (CBS) method of Petersson and co-workers in order to obtain very accurate energies. The CBS models are using the known asymptotic convergence of pair natural orbital expressions to extrapolate from calculations

using a finite basis set to the estimated CBS limit. CBS-4 starts with an HF/3-21G(d) geometry optimization; the zero-point energy is computed at the same level. It then uses a large basis set SCF calculation as a base energy, and an MP2/6- 31+G calculation with a CBS extrapolation to correct the energy through second order. A MP4(SDQ)/6-31+ (d,p) calculation is used to approximate higher order contributions. In this study, we applied the modified CBS-4M.

Heats of formation of the synthesized ionic compounds were calculated using the atomization method (equation E1) using room temperature CBS-4M enthalpies, which are summarized in Table S4.[S11, S12]

$$\Delta_f H^\circ_{(g,\,M,\,298)} = H_{(Molecule,\,298)} - \sum H^\circ_{(Atoms,\,298)} + \sum \Delta_f H^\circ_{(Atoms,\,298)} \qquad (E1)$$

Table S4. CBS-4M electronic enthalpies for atoms C, H, N and O and their literature values for atomic $\Delta H^\circ_f{}^{298}$ / kJ mol^{-1}

	$-H^{298}$ [a.u.]	NIST[S13]
H	0.500991	218.2
C	37.786156	717.2
N	54.522462	473.1
O	74.991202	249.5

For neutral compounds the sublimation enthalpy, which is needed to convert the gas phase enthalpy of formation to the solid state one, was calculated by the *Trouton* rule.[S14] For ionic compounds, the lattice energy (U_L) and lattice enthalpy (ΔH_L) were calculated from the corresponding X-ray molecular volumes according to the equations provided by *Jenkins* and *Glasser*.[S15] With the calculated lattice enthalpy the gas-phase enthalpy of formation was converted into the solid state (standard conditions) enthalpy of formation. These molar standard enthalpies of formation (ΔH_m) were used to calculate the molar solid state energies of formation (ΔU_m) according to equation E2.

$$\Delta U_m = \Delta H_m - \Delta n\, RT \qquad (E2)$$

(Δn being the change of moles of gaseous components)

The calculation results are summarized in Table S5.

Table S5. Calculation results.

	$-H^{298}$ [a] [a.u.]	$\Delta_f H°(g,M)$ [kJ mol^{-1}] [b]	V_M [Å^3] [c]	ΔU_L; ΔH_L [d] [kJ mol^{-1}]	$\Delta_f H°(s)$ [e] [kJ mol^{-1}]	Δn [f]	$\Delta_f U(s)$ [g] [kJ kg^{-1}]
A^-	852.651081	196.2					
A^{2-}	852.001852	367.4					
NH_4^+	56.796608	635.3					
$N_2H_5^+$	112.030523	773.4					
NH_3OH^+	131.863229	686.5					
G^+	205.453192	571.2					
AG^+	260.701802	670.7					
TAG^+	371.197775	873.1					
2	-	1638.0	235	1430.0;	200.6	11.0	918.0
3	-	1914.2	269	1437.5	547.3	13.0	2083.4
4	-	1740.4	240	1359.5;	316.4	12.0	1235.6
5	-	1509.8	343	1366.9	261.9	15.0	900.1
6	-	1708.8	365	1416.5;	490.6	17.0	1470.5
7	-	1069.3	315	1423.9	615.5	14.0	2043.3
				1240.5;			
				1247.9			
				1210.8;			
				1218.3			
				448.8; 453.7			

[a] CBS-4M electronic enthalpy; [b] gas phase enthalpy of formation; [c] molecular volumes taken from X-ray structures and corrected to room temperature; [d] lattice energy and enthalpy (calculated using Jenkins and Glasser equations); [e] standard solid state enthalpy of formation; [f] Δn being the change of moles of gaseous components when formed; [g] solid state energy of formation.

6.6.5 References

[S1] a) Test methods according to the UN Recommendations on the Transport of Dangerous Goods, *Manual of Test and Criteria*, ST/SG/AC.10/11/Rev.7, United Nations Publication, New York and Geneva, **2019**, 978-92-1-130394-

0; https://unece.org/transport/dangerous-goods/rev7-files; b) Reichel & Partner GmbH, http://www.reichelt-partner.de; c) http://www.ozm.cz

[S2] M. Sućeska, EXPLO5 V6.02 program, Brodarski Institute, Zagreb, Croatia, **2014**.

[S3] A. A. Dippold, T. M. Klapötke, *Chem. Eur. J.* **2012**, *18*, 16742–16753.

[S4] A. A. Dippold, D. Izsak, T. M. Klapötke, *Chem. Eur. J.* **2013**, *19*, 12042–12051.

[S5] *CrysAlisPro*, Oxford Diffraction Ltd. *version 171.33.41*, **2009**.

[S6] G. M. Sheldrick, *Acta Cryst.* **2015**, *A71*, 3–8.

[S7] O. V. Dolomanov, L. J Bourhis, R. J. Gildea, J. A. K. Howard, H. Puschmann, *J. Appl. Cryst.* **2009**, *42*, 339–341.

[S8] *SCALE3 ABSPACK – An Oxford Diffraction program* (1.0.4, gui: 1.0.3), Oxford Diffraction Ltd., **2005**.

[S9] *APEX3*. Bruker AXS Inc., Madison, Wisconsin, USA.

[S10] M. J. Frisch, G. W. Trucks, H. B. Schlegel, G. E. Scuseria, M. A. Robb, J. R. Cheeseman, G. Scalmani, V. Barone, B. Mennucci, G. A. Petersson, H. Nakatsuji, M. Caricato, X. Li, H.P. Hratchian, A. F. Izmaylov, J. Bloino, G. Zheng, J. L. Sonnenberg, M. Hada, M. Ehara, K. Toyota, R. Fukuda, J. Hasegawa, M. Ishida, T. Nakajima, Y. Honda, O. Kitao, H. Nakai, T. Vreven, J. A. Montgomery, Jr., J. E. Peralta, F. Ogliaro, M. Bearpark, J. J. Heyd, E. Brothers, K. N. Kudin, V. N. Staroverov, R. Kobayashi, J. Normand, K. Raghavachari, A. Rendell, J. C. Burant, S. S. Iyengar, J. Tomasi, M. Cossi, N. Rega, J. M. Millam, M. Klene, J. E. Knox, J. B. Cross, V. Bakken, C. Adamo, J. Jaramillo, R. Gomperts, R. E. Stratmann, O. Yazyev, A. J. Austin, R. Cammi, C. Pomelli, J. W. Ochterski, R. L. Martin, K. Morokuma, V. G. Zakrzewski, G. A. Voth, P. Salvador, J. J. Dannenberg, S. Dapprich, A. D. Daniels, O. Farkas, J.B. Foresman, J. V. Ortiz, J. Cioslowski, D. J. Fox, Gaussian 09 A.02, Gaussian, Inc., Wallingford, CT, USA, **2009**.

[S11] a) J. W. Ochterski, G. A. Petersson, and J. A. Montgomery Jr., *J. Chem. Phys.* **1996**, *104*, 2598–2619; b) J. A. Montgomery Jr., M. J. Frisch, J. W. Ochterski G. A. Petersson, *J. Chem. Phys.* **2000**, *112*, 6532–6542.

[S12] a) L. A. Curtiss, K. Raghavachari, P. C. Redfern, J. A. Pople, *J. Chem. Phys.* **1997**, *106*, 1063–1079; b) E. F. C. Byrd, B. M. Rice, *J. Phys. Chem*. A **2006**,

110, 1005–1013; c) B. M. Rice, S. V. Pai, J. Hare, *Comb. Flame* **1999**, *118*, 445–458.

[S13] P. J. Lindstrom, W. G. Mallard (Editors), NIST Standard Reference Database Number 69, http://webbook.nist.gov/chemistry/ (accessed June **2020**).

[S14] M. S. Westwell, M. S. Searle, D. J. Wales, D. H. Williams, *J. Am. Chem. Soc*. **1995**, *117*, 5013–5015; b) F. Trouton, *Philos. Mag*. **1884**, *18*, 54–57.

[S15] a) H. D. B. Jenkins, H. K. Roobottom, J. Passmore, L. Glasser, *Inorg. Chem.* **1999,** *38,* 3609–3620; b) H. D. B. Jenkins, D. Tudela, L. Glasser, *Inorg. Chem.* **2002**, *41*, 2364–2367.

7. Krapcho Decarboxylation of Ethyl-Carbazate: Synthetic Approach toward 1,1′-Diamino-5,5′-bistetrazole and Its Utilization as a High-Performing Metal-Free Initiator

Maximilian Benz, Thomas M. Klapötke, Jörg Stierstorfer

as published in *Organic Letters* **2022**, *24*, 1747–1751

DOI: 10.1021/acs.orglett.2c00430

Keywords: heterocycles, Krapcho reaction, primary explosives, tetrazoles, X-ray diffraction

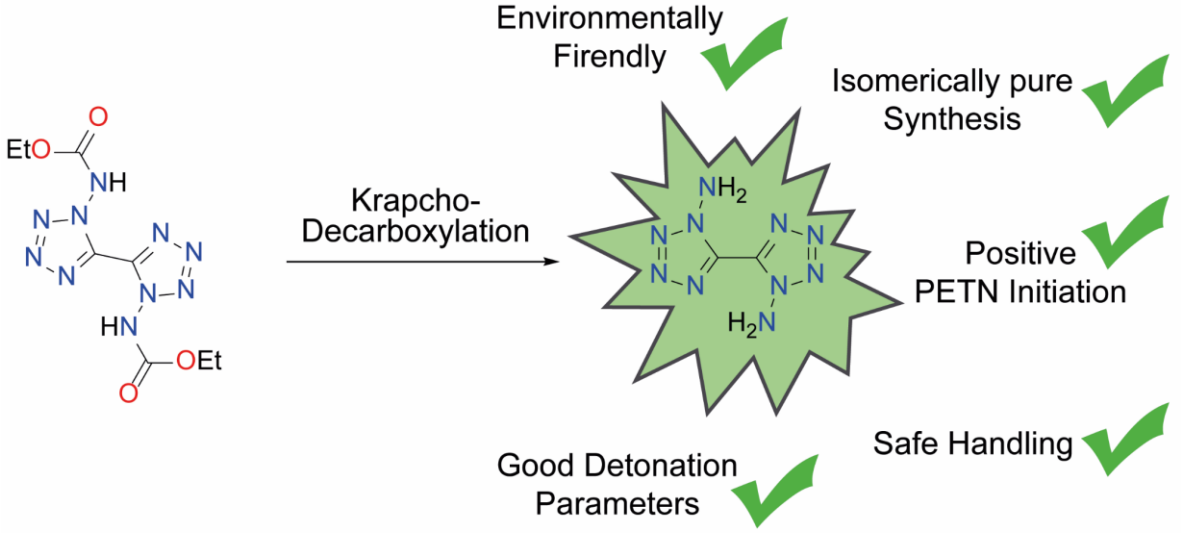

Krapcho Decarboxylation of the ethoxycarbonyl protected diamino-bistetrazole derivative is the first reported carbamate deprotection on a nitrogen-rich azole system. This opens up a new synthetic route toward 1,1'-diamino-5,5'-bistetrazole (1,1'-DABT), providing the opportunity to produce the metal-free primary explosive on a multigram scale.

Abstract: 1,1′-Diamino-5,5′-bistetrazole ($C_2H_4N_{10}$), a highly nitrogen-containing compound with promising energetic characteristics, is available through a classic organic reaction protocol applied on an inorganic azole system. This is the only Krapcho reaction on a carbamate system described in the literature so far. 1,1′-Diamino-5,5′-bistetrazole was extensively characterized through multinuclear spectroscopy, mass spectrometry, thermal analysis, and X-ray diffraction. The sensitivity values were measured, and detonation values were calculated. Its capability to initiate pentaerythritol tetranitrate (PETN) was successfully demonstrated.

7.1 Introduction

In recent years, there has flared up a clear trend in the energetic materials chemistry community toward environmentally friendly high-energy materials.[1-2] This effort began far before the current movement to replace many substitutable everyday items with environmentally friendly ones. Since the problems associated with the world's most widely used high-energy dense materials, including RDX/HMX, TNT, and lead azide (LA), are primarily environmental, there is a particular need for action to find substitutes.[3-4] In particular, LA, which is found in many initiation mixtures, needs to be substituted in the long term. Besides being harmful to the environment, lead is also harmful to many living organisms.[5-6] Accordingly, the focus for the development of new primaries is on heavy-metal-free, mostly C-, N-, H-, and O-based, heterocycles.[7-8] Some representatives that have received attention in recent years are shown in Figure 1. Despite the improvement in their environmental properties, all the compounds presented still have some drawbacks. Similar to TNT, the environmental compatibility of KDNP is a major problem since it is based on a nitroaromatic skeleton.[9] DBX-1, developed by Dynamit Nobel AG in 1960, can reoxidize in solution over a long period of time to form extremely sensitive copper-(II)-bis(5-nitrotetrazolate).[10-12] K_2DNABT is an excellent candidate in many relevant respects. However, its sensitivity is very high, making it difficult to handle, and it can only be produced safely in limited quantities.[13-14] Since the tetrazole backbone with heteroaromatic substituents has turned out to be an interesting moiety, not only as a result of investigation into

K_2DNABT or TKX50,[15-16] our focus here has been placed primarily on aminated bistetrazoles, namely 1,1-diamino-5,5′-bistetrazole. Because aminated bistetrazoles have so far been difficult to access and purify,[17-19] no more detailed investigations have been undertaken with regard to their suitability as initiators despite their promising properties.

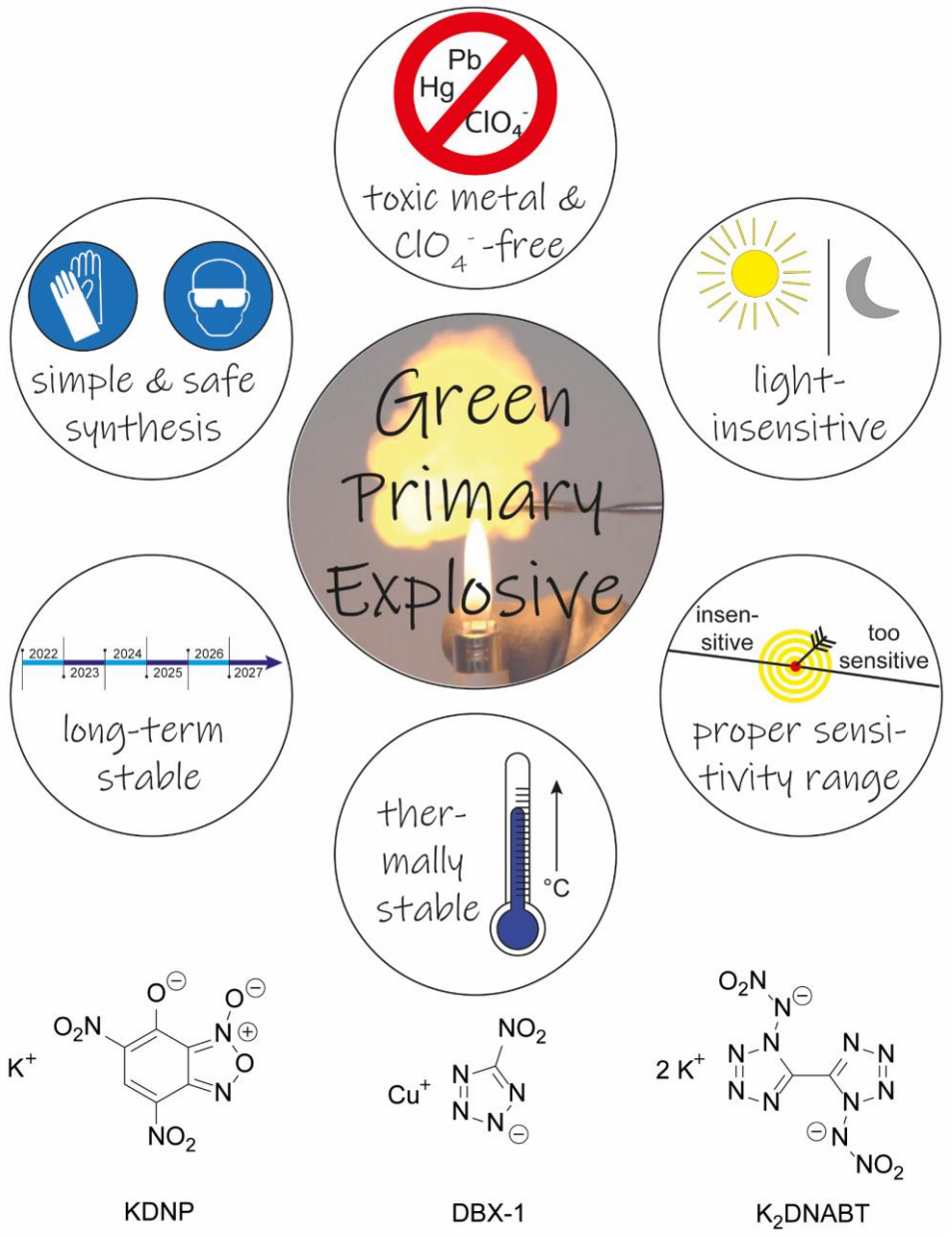

Figure 1. Requirements for the development of new green primaries (top). Recently developed candidates for lead azide substitutes are as follows: KDNP (potassium 5,7-dinitro-[2,1,3]-benzoxadiazol-4-olate-3-oxide), DBX-1 (copper(I) 5-nitrotetrazolate), and K_2DNABT (dipotassium 1,1′-dinitramino-5,5′-bistetrazolate) (bottom).

In this study, we present a new protocol, based on Krapcho decarboxylation, for the synthesis of 1,1′-diamino-5,5′-bistetrazole (1,1′-DABT, **2**) and its applicability as a metal-free initiator.

A classic Krapcho reaction occurs at esters with an electron-withdrawing group in the β-position, like malonic esters or cyanoesters (Figure 2A).[20-22] Since diethoxy-1,1′-diamino-5,5′-bistetrazole (**1**) consists of all the molecular blocks required for Krapcho decaboxylation, as illustrated in Figure 2B (tetrazole as electron-withdrawing group and ethyl carbazate as an ester derivative), we were able to successfully use the Krapcho protocol for our system to perform the decarboxylation of ethyl-carbazate **1**.

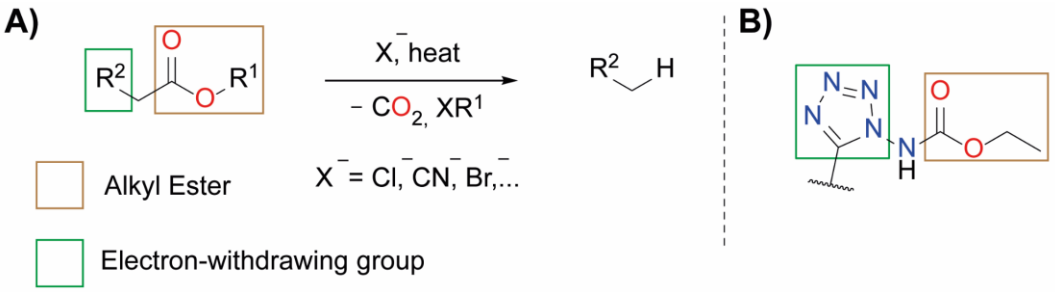

Figure 2. (A) Schematic illustration of the Krapcho reaction. (B) Molecular part of **1** with all requirements for the Krapcho decarboxylation.

7.2 Results and Discussion

1,1′-DABT (**2**) was already described through the amination of 5,5′-bistetrazole with THA (*O*-tosylhydroxylamine), as illustrated in Scheme 1, but the synthesis suffered from the formation of isomers (1,1′ and 1,2′), bad yields (10% for 1,1′ and 6% for 1,2′), expensive chemicals (THA), and complicated purification (column chromatography).[17]

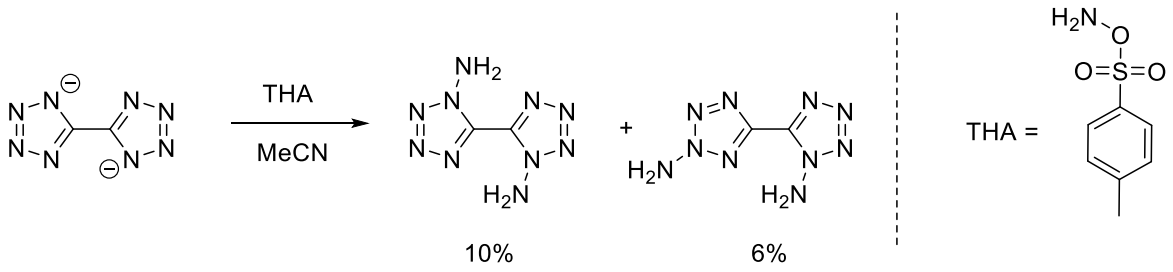

Scheme 1. Previously described synthesis for 1,1′-DABT (**2**) through the amination of 5,5′-bistetrazole applying THA.

Our new method starts with readily available diethoxycarbonyl-1,1′-diamino-5,5′-bistetrazole (**1**), which can be synthesized by an easily scalable four-step procedure starting from aqueous glyoxal.[14] The ethoxy protection group was chosen over the methoxy group due to the higher carbon content and therefore the lower sensitivity of the intermediates.[13-14] With **1** in hand, the appropriate conditions for decarboxylation were examined. Since the classic route for carbamate deprotection using aqueous or alcoholic basic conditions did not yield the product, an alternative strategy had to be pursued. Krapcho decarboxylation with LiCl as an inorganic ingredient and DMSO as high-boiling solvent gave the best results, as described in Scheme 2 (for other tested conditions, see Table 1).

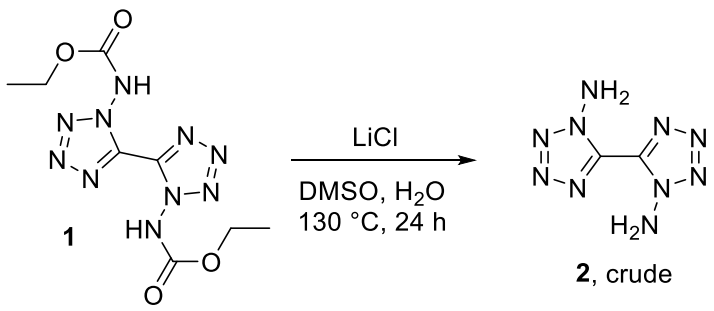

Scheme 2. Krapcho decarboxylation of ethyl-carbazate **1** to crude 1,1′-diamino-5,5′-bistetrazole (**2**).

Table 1. Tested conditions for the Krapcho decarboxylation of 1 to 1,1'-DABT (**2**).

Reaction conditions[a]				
Additive (eq.[b])	Solvent[c]	Time (h)	Temp (°C)	Yield[d] (%)
NaCN (10)	DMF	48	130	0
NaCl (10)	DMSO	48	130	5
LiCl (10)	DMF	48	140	3
LiCl (4)	DMSO	48	130	2
LiCl (12)	DMSO	48	130	15
LiCl (7)	DMSO	48	150	7
LiCl (7)	DMSO	4	130	12
LiCl (7)	DMSO	72	130	21
LiCl (7)	DMSO	24	130	31

[a] Diethoxy-1,1'-diamino-5,5'-bistetrazole (**1**): 1.60 mmol. [b] Equivalents of inorganic additive per reactive site. [c] 10 mL per 1.00 mmol and 0.2 mL water in every entry. [d] Isolated yields after purification.

Since there was not any reference in the literature for our system, we started to use conditions for organic systems. Temperatures of above 120 °C were necessary

to obtain any indication of the product. The reaction of sodium cyanide with DMF as the solvent with a reaction time of 48 h yielded decomposition products only. The switch to chloride as an anion led for the first time to the desired deprotection product, albeit with low yields. By screening the reaction with different amounts of LiCl and various reaction times and temperatures, we finally ended up with a 31% yield. However, we believe that the potential of the reaction has not yet been exhausted with the yield we have achieved.

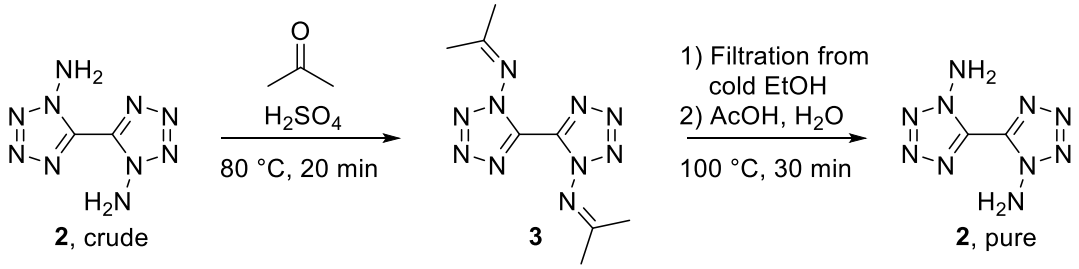

Scheme 3. Work up of crude **2** through protection of the amines with acetone via bishydrazone **3**.

Compound **2** was identified via NMR spectroscopy through the signal of the amino protons at 7.43 (^{1}H NMR) and 141.2 ppm (^{13}C NMR). The additional ^{15}N NMR spectrum of **2** shows five signals.

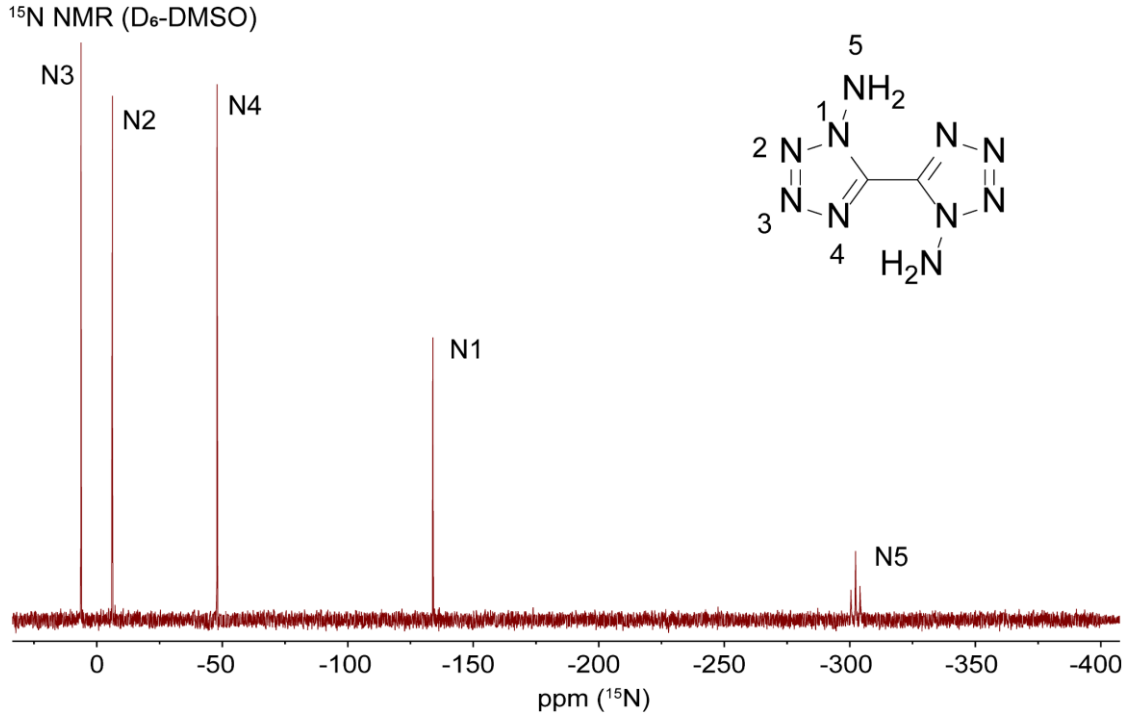

Figure 3. Proton-coupled ^{15}N NMR spectrum of **2**. Chemical shifts are given with respect to $MeNO_2$.

Resonances for tetrazole nitrogen atoms N1–N4 are in accordance with the spectrum of BTDO,[23] which also consists of an electron-pushing substitution at position 1. The amino resonance (N5) occurs at −302.3 ppm and splits into a triplet (^1J = 73.6 Hz) due to the coupling with the respective hydrogen atoms (Figure 3). Crystals of **2** were obtained by the slow evaporation of the acetic acid/water solution. 1,1′-DABT (**2**) crystallizes in the monoclinic space group $P2_1/n$ with a density of 1.757 g cm^{-3} recalculated to room temperature, which is slightly higher than that in the previously reported structure (1.727 g cm^{-3} at 298 K).[17] The structure is depicted in Figure 4. The amino nitrogen atoms are in a plane with the tetrazole rings to which they are attached, whereas the two tetrazole rings are twisted toward each other by 38° (N4–C1–C2–N9 = 37.88(15)°). Weak hydrogen bridges were formed by all amino protons to nitrogen atoms of the tetrazole at positions three and four (N3, N4, N8, and N9).

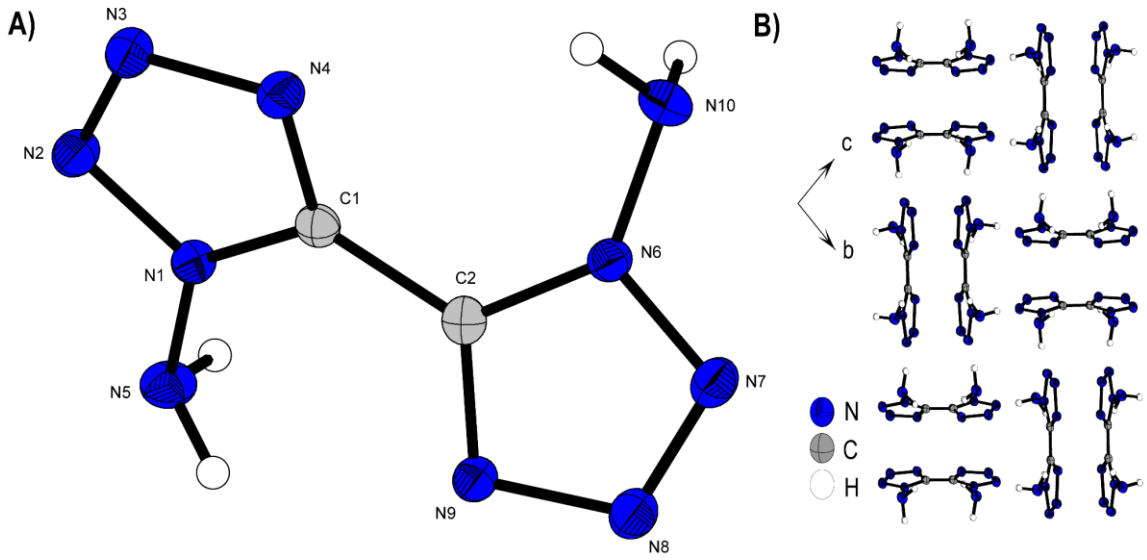

Figure 4. (A) Molecular structure of **2** as determined by low-temperature X-ray diffraction, with thermal ellipsoids drawn at the 50% probability level. (B) 3D layer structure of **2** viewed along the *a*-axis.

Even though 1,1′-DABT is classified as extremely sensitive according to UN guidelines (FS = 3 N and IS < 1 J), the compound is fine to handle, and no incidents occurred during our investigations. In particular, the sensitivity to electrical discharge (ESD = 20 mJ) contributes to this; however, the compound is significantly less sensitive than K_2DNABT or lead azide. **2** melts at 170 °C and then decomposes smoothly starting at 200 °C, as in the case of K_2DNABT. To predict the stability of **2** over a longer period of time, the material was examined for 48 h

at 100 °C using thermogravimetric analysis (TGA). No loss of mass was detected. Additional information regarding the thermal behavior and the corresponding DTA and TGA graphs can be found in the Supporting Information. The high value for the detonation velocity (V_{det} = 9360 m s^{-1}) is mainly due to the very high positive endothermic enthalpy of formation, which clearly outperforms K_2DNABT and lead azide (Table 2). Despite the omission of oxygen, the main decomposition products according to the EXPLO5 calculation are N_2 (74%) and carbon (13%), making **2** environmentally friendly.

Table 2. Physico-chemical properties of **2**, K_2DNABT and lead azide.

	1,1'-DABT (**2**)	K_2DNABT	$Pb(N_3)_2$
Formula	$C_2H_4N_{10}$	$K_2C_2N_{12}O_4$	PbN_6
M [g mol^{-1}]	168.1	334.3	291.3
IS [J][a]	<1	<1	2.5-4
FS [N][b]	3	<0.1	0.1-1.0
ESD [mJ][c]	20	3	7
ρ [g cm^{-3}][d]	1.757	2.11	4.8
N [%][e]	83.3	50.3	28.9
Ω [%][f]	−57.1	−4.8	−11.0
T_{melt}/T_{dec} [°C][g]	170/200	-/200	-/315
$\Delta_f H°$ [kJ mol^{-1}][h]	791.4	326.4	450.1
$\Delta_f U°$ [kJ kg^{-1}][i]	4810.5	1036.1	1574.9
MED [J cm^{-3}][j]	8452.0	2186.0	7559.5
	EXPLO5 V6.05.02		
$-\Delta_{Ex} U°$ [kJ kg^{-1}][k]	4847	4949	1560
T_{det} [K][l]	3128	3514	3372
V_0 [L kg^{-1}][m]	837	486	252
P_{CJ} [kbar][n]	327	310	357
V_{det} [m s^{-1}][o]	9360	8459	6187

[a] Impact sensitivity (BAM drophammer (1 of 6)). [b] Friction sensitivity (BAM friction tester (1 of 6)). [c] Electrostatic discharge device (OZM research). [d] From X-Ray diffraction analysis recalculated to 298 K. [e] Nitrogen content. [f] Oxygen balance with respect to CO_2 [g] Decomposition temperature (DTA; β = 5 °C min^{-1}). [h] Calculated enthalpy of formation. [i] Calculated energy of formation. [j] Maximium energy density: Energy of formation with respect to the volume 1 cm^{-3} assuming the theoretical mayimum density. [k] Energy of explosion. [l] Melting point/Detonation temperature. [m] Volume of detonation products (assuming only gaseous products). [n] Detonation pressure at Chapman-Jouguet point. [o] Detonation velocity.

As the sensitivity data that we remeasured for **2** were far lower those published previously, **2** emerged as a possible initiator candidate. To investigate the behavior of the substance with respect to spot heating, a hot needle test was carried out in

which a glowing needle was held rapidly on 20 mg of taped **2**. This test resulted in detonation. In addition, a hot plate test was performed in which 20 mg of **2** was placed on a copper plate and heated with a Bunsen burner. This test resulted in a sharp deflagration, as depicted in Figure 5. Based on the determined physicochemical properties, **2** was further examined with regard to its ability to initiate the booster material PETN through a classical initiation test.

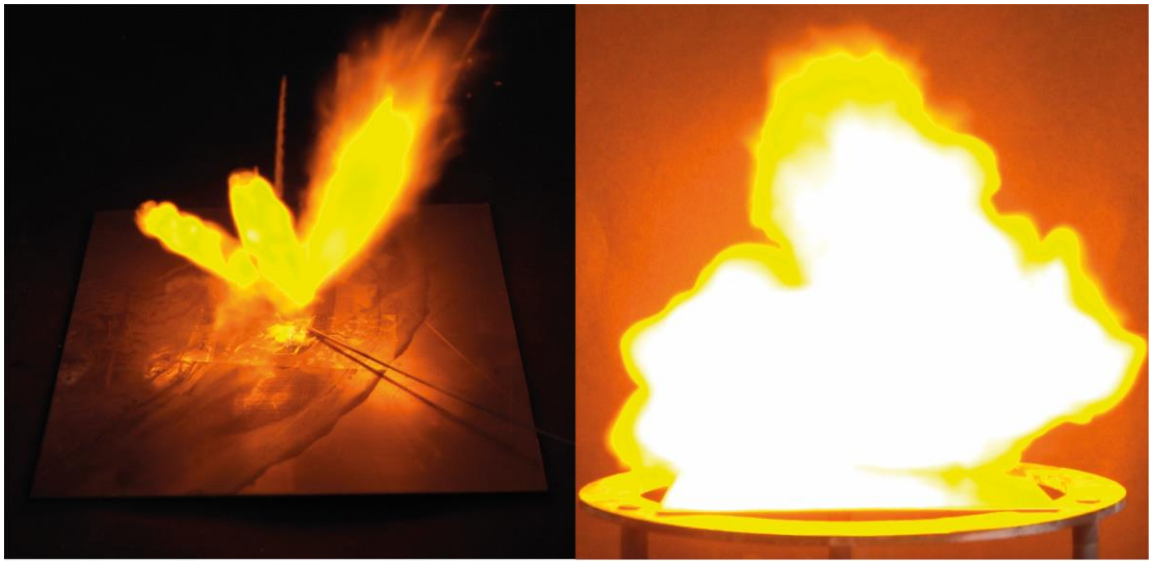

Figure 5. Moment of detonation for 20 mg of 1,1′-DABT (**2**) during the hot needle test (left). Moment of deflagration for 20 mg of 1,1′-DABT (**2**) during the hot plate test (right).

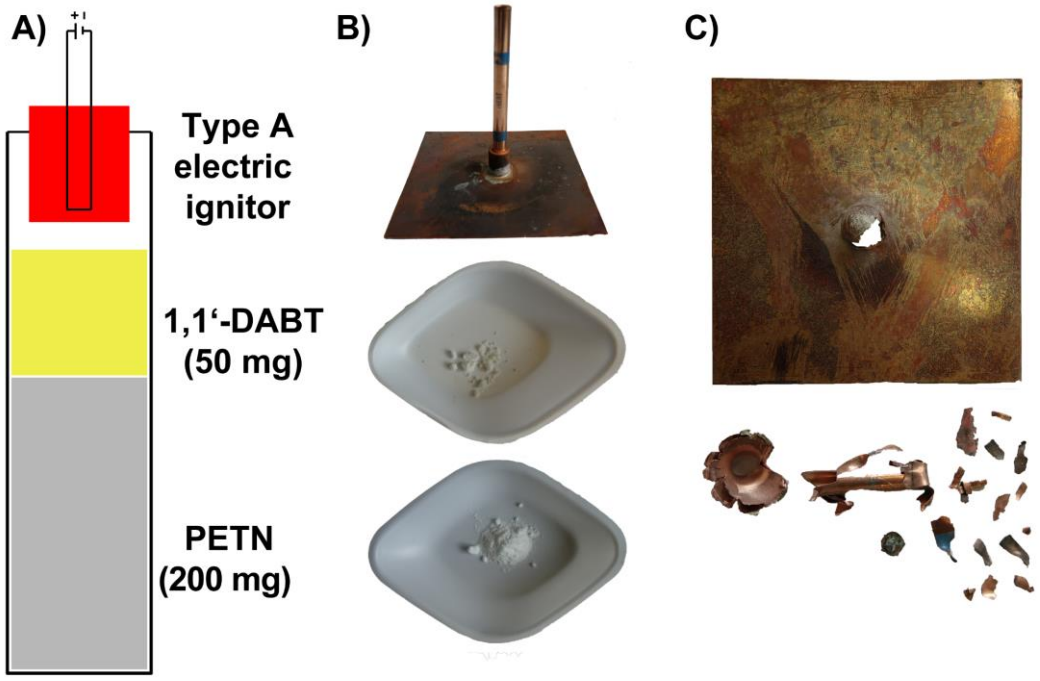

Figure 6. (A) Schematic test setup for the initiation test. (B) Copper plate and sleeve and respective quantities of 1,1′-DABT (≤500 µm) and PETN. (C) Result of the initiation experiment of **2** toward PETN.

Thus, it was tested whether **2** showed a deflagration to detonation transition (DDT) behavior, which is a basic prerequisite for the use as primary initiator (setup depicted in Figure 6). For the test setup, 200 mg of PETN was filled in a copper shell and compressed with 80 N. Then, 50 mg of 1,1′-DABT were filled on top and also compressed with 80 N. The test is considered positive if the copper plate shows a hole and fragmentation of the sleeve occurs. As depicted in Figure 6C, 1,1′-DABT was able to successfully initiate PETN. In case of uncompressed 1,1′-DABT, the test was negative.

7.3 Conclusion

In summary, we developed a new synthetic route for 1,1′-DABT (**2**, 1,1′-diamino-5,5′-bistetrazole) through Krapcho decarboxylation. The method is straightforward, easily scalable, and can be transferred to other *N*-aminated heterocycles. Thus, the preparation of **2** is not dependent on expensive reagents or demanding purification methods, and **2** can be provided in a sufficient quantity. 1,1′-DABT (**2**) has sensitivity values in the range of primary initiators (FS = 3 N, IS < 1 J, and ESD = 20 mJ) and is able to initiate PETN as shown in an initiation capability test but is still good to operate. The density of 1.757 g cm^{-3} and the calculated detonation parameters, including a detonation velocity of 9360 m s^{-1}, are outstanding for an oxygen-free C, N, and H compound. Long-term stability was verified by tempering the substance for 48 h at 100 °C without noticeable decomposition. Therefore, **2** fulfills all requirements for a next-generation green primary initiator as mentioned in the introduction and could work as vulnerable starting material for further derivatizations of *N*-amines.

7.4 Acknowledgement

Financial support of this work by Ludwig-Maximilian University (LMU), the Office of Naval Research (ONR) under Grant ONR N00014-19-1-2078, and the Strategic Environmental Research and Development Program (SERDP) under contract no. W912HQ19C0033 is gratefully acknowledged. We thank Dr. Ferdinand Lutter (Janssen Pharmaceutica) for fruitful discussions about Krapcho reactions, Jasmin

Lechner (LMU Munich) for TGA measurements, and Marcus Lommel (LMU Munich) for performing the initiation test.

7.5 References

[1] T. Brinck*, Green Energetic Materials*, Wiley, Hoboken, **2014**.

[2] G. Zhao, P. Yin, D. Kumar, G. H. Imler, D. A. Parrish, J. M. Shreeve, *J. Am. Chem. Soc.* **2019**, *141*, 19581–19584.

[3] E. C. Johnson, J. J. Sabatini, D. E. Chavez, R. C. Sausa, E. F. C. Byrd, L. A. Wingard, P. E. Guzmàn, *Org. Process Res. Dev.* **2018**, *22*, 736–740.

[4] W. Huang, Y. Tang, G. H. Imler, D. A. Parrish, J. M. Shreeve, *J. Am. Chem. Soc.* **2020**, *142*, 3652–3657.

[5] M. A. S. Laidlaw, G. Filippelli, H. Mielke, B. Gulson, A. S. Ball, *Environ. Health* **2017**, *16*, 34.

[6] T. M. Klapötke, *Chemistry of High-Energy Materials*, De Gruyter, Boston, Berlin, **2019**.

[7] M. Deng, Y. Feng, W. Zhang, X. Qi, Q. Zhang, *Nat. Commun.* **2019**, *10*, 1339.

[8] C. He, J. M. Shreeve, *Angew. Chem. Int. Ed.* **2016**, *55*, 772–775.

[9] J. W. Fronabarger, M. D. Williams, W. B. Sanborn, D. A. Parrish, M. Bichay, *Propellants Explo. Pyrotech.* **2011**, *36*, 459–470.

[10] J. W. Fronabarger, M. D. Williams, W. B. Sanborn, J. G. Bragg, D. A. Parrish, M. Bichay, *Propellants Explo. Pyrotech.* **2011**, *36*, 541–550.

[11] Friedrich, W. Elektrische Zünder und Zündhütchen. DBP 1 088 855, **1960**.

[12] D. D. Ford, S. Lenahan, M. Jörgensen, P. Dubé, M. Delude, P. E. Concannon, S. R. Anderson, K. D. Oyler, G. Cheng, N. Mehta, J. S. Salan, *Org. Process Res. Dev.* **2015**, *19*, 673–680.

[13] D. Fischer, T. M. Klapötke, J. Stierstorfer, *Angew. Chem. Int. Ed.* **2014**, *53*, 8172–8175.

[14] E. L. Müller, T. M. Klapötke, J. Stierstorfer, M. F. Bölter, M. Völkl*, Vol. WO 2018/209366 A2*, **2018**.

[15] N. Fischer, D. Fischer, T. M. Klapötke, D. G. Piercey, J. Stierstorfer, *J. Mater. Chem.* **2012**, *22*, 20418–20422.

[16] Y.-H. Joo, J. M. Shreeve, *Org. Lett.* **2008**, *10*, 4665–4667.
[17] T. M. Klapötke, D. G. Piercey, J. Stierstorfer, *Dalton Trans.* **2012**, *41*, 9451–9459.
[18] R. Raap, *Can. J. Chem.* **1969**, *47*, 3677–3681.
[19] N. Szimhardt, M. H. H. Wurzenberger, L. Zeisel, M. S. Gruhne, M. Lommel, J. Stierstorfer, *J. Mater. Chem. A* **2018**, *6*, 16257–16272.
[20] P. A. Krapcho, *Organic Reactions, Vol. 81*, Wiley-VCH, **2013**.
[21] J. D. Mason, S. S. Murphree, *Synlett* **2013**, *24*, 1391–1394.
[22] P. S. Poon, A. K. Banerjee, M. S. Laya, *J. Chem. Res.* **2011**, *35*, 67–73.
[23] N. Fischer, T. M. Klapötke, M. Reymann, J. Stierstorfer, *Eur. J. Inorg. Chem.* **2013**, 2167–2180.

7.6 Supporting Information

7.6.1 Experimental Procedure

^{1}H, ^{13}C and ^{15}N NMR spectra were recorded on *BRUKER AMX 400* instruments. Chemical shifts are referenced with respect to tetramethylsilane (^{1}H/^{13}C) and nitromethane (^{14}N/^{15}N). Infrared spectra (IR) were recorded in the region 4000-400 cm^{-1} on a *PERKIN ELMER Spectrum BX-59343* instrument with a *SMITHS DETECTION DuraSamplIR II Diamond ATR* sensor. The absorption bands are reported in wavenumbers (cm^{-1}). Decomposition temperatures were measured via differential thermal analysis (DTA) with an *OZM Research DTA 552-Ex* instrument at a heating rate of 5 °C/min and in a range of room temperature to 400 °C. All sensitivities toward impact (IS) and friction (FS) were determined according to BAM (Bundesanstalt für Materialforschung und Prüfung) standards using a BAM drop hammer and a BAM friction apparatus by applying the 1 of 6 method.[S1] All energetic compounds were tested for sensitivity towards electrical discharge using an *Electric Spark Tester ESD 2010 EN* from OZM. Energetic properties have been calculated with the EXPLO5 6.02 computer [S2] code using the RT converted X-ray density and calculated solid state heats of formation. Hot plate and hot needle tests were performed in order to evaluate the potential initiation capability of selected compounds. The samples were fixed on a copper plate underneath adhesive tape and initiated by a red-hot needle. Strong deflagration or detonation of the

compound usually indicates a valuable primary initiator. The safe and straightforward hot plate test only shows the behavior of the unconfined sample toward fast heating on a copper plate. It does not necessarily allow any conclusions on a compound's capability as a suitable primary.

CAUTION! *All investigated compounds are potentially energetic materials. In particular 1,1'-DABT, is a primary initiator and extremely sensitive toward any kind of external stimuli. Safety precautions and equipment (such as wearing leather coat, face shield, Kevlar sleeves, Kevlar gloves, earthed equipment and ear plugs) must be used during all manipulations.*

1,1'-Diamino-5,5'-bistetrazole (1,1'-DABT, **2**)

Diethoxy carbonyl diaminobistetrazole (**1**) (8.00 g, 25.6 mmol, 1.0 eq.) was dissolved in DMSO (50 mL) and water (10 mL) and lithium chloride (15.2 g, 359 mmol, 14 eq.) was added. The reaction mixture was heated to 130 °C using an oil bath and held at this temperature for 24 h. After cooling to room temperature, water (200 mL) was added, the mixture was extracted with ethyl acetate (5 x 100 mL), dried over anhydrous sodium sulfate and the solvent was removed under reduced pressure to obtain crude **2**, with about 20% residual starting material.
For purification, crude **2** was refluxed in acetone (20 mL) and sulfuric acid (0.1 mL, 98%) for 20 min, using an oil bath. The solvent was removed under reduced pressure, cold ethanol (15 mL) was added and the suspension was filtered. The white solid consisting of **3** was subsequently dissolved in acetic acid (100%, 50 mL) and water (5 mL) and stirred at 100 °C for 30 min, using an oil bath. The solvent was removed and **2** already started to crystallize when the solution was cooled to room temperature. After complete removal of the solvent, pure **2** was obtained as colorless micro-crystals (total yield: 1.33 g, 7.94 mmol, 31%).

2:
DTA (5 °C min^{-1}): 170 °C (endo, melt), 200 °C (exo, dec.); Sensitivities: BAM drop hammer: <1 J (<100 µm), friction tester: 3 N (<100 µm), ESD: 20 mJ (<100 µm). IR (ATR) $\tilde{\nu}$ (cm^{-1}) = 3341(s), 3236(m), 3164(s), 1611(s), 1389(m), 1272(m),

1130(s), 1031(vs), 991(s), 921(vs), 754(s), 668(s); Elem. Anal. ($C_2H_4N_{10}$, 168.12 g mol^{-1}) calcd.: C 14.29, H 2.40, N 83.31%. Found: C 14.21, H H2.31, N 81.44%; ^{1}H NMR (d_6-DMSO, 400 MHz, ppm) δ = 7.43 (s, 4H); ^{13}C NMR (d_6-DMSO, 101 MHz, ppm) δ = 141.2; ^{15}N NMR (d_6-DMSO, 41 MHz, ppm) δ = 6.3 (N3), −6.3 (N2), −47.9 (N4), −133.9 (N1), −302.3 (N5, t, ^{1}J = 73.6 Hz) ; HRMS (EI) *m/z*: [M+] Calcd for $C_2H_5N_{10}$ 169.0693, found: 169.0699.

3:

DTA (5 °C min^{-1}):112 °C (endo, melt), 207 °C (exo, dec.); Sensitivities: BAM drop hammer: 1 J (<100 µm), friction tester: 54 N (<100 µm), ESD: 20 mJ (<100 µm). IR (ATR) $\tilde{\nu}$ (cm^{-1}) = 3318(s), 3260(m), 3173(m), 1626(s), 1615(s), 1368(s), 1350(m), 1276(s), 1131(s), 1030(vs), 1004(s), 992(s), 960(s), 925(s), 666(s); Elem. Anal. ($C_8H_{12}N_{10}$, 248.25 g mol^{-1}) calcd.: C 38.71, H 4.87, N 56.42%. Found: C 38.66, H 4.93, N 56.06%; ^{1}H NMR (d_6-DMSO, 400 MHz, ppm) δ = 2.37 (s, 3H), 2.06 (s, 3H); ^{13}C NMR (d_6-DMSO, 101 MHz, ppm) δ = 186.0, 137.7, 25.4, 20.8; HRMS (EI) *m/z*: [M+] Calcd for $C_8H_{13}N_{10}$ 249.1319, found: 249.1326.

7.6.2 Thermal Analysis

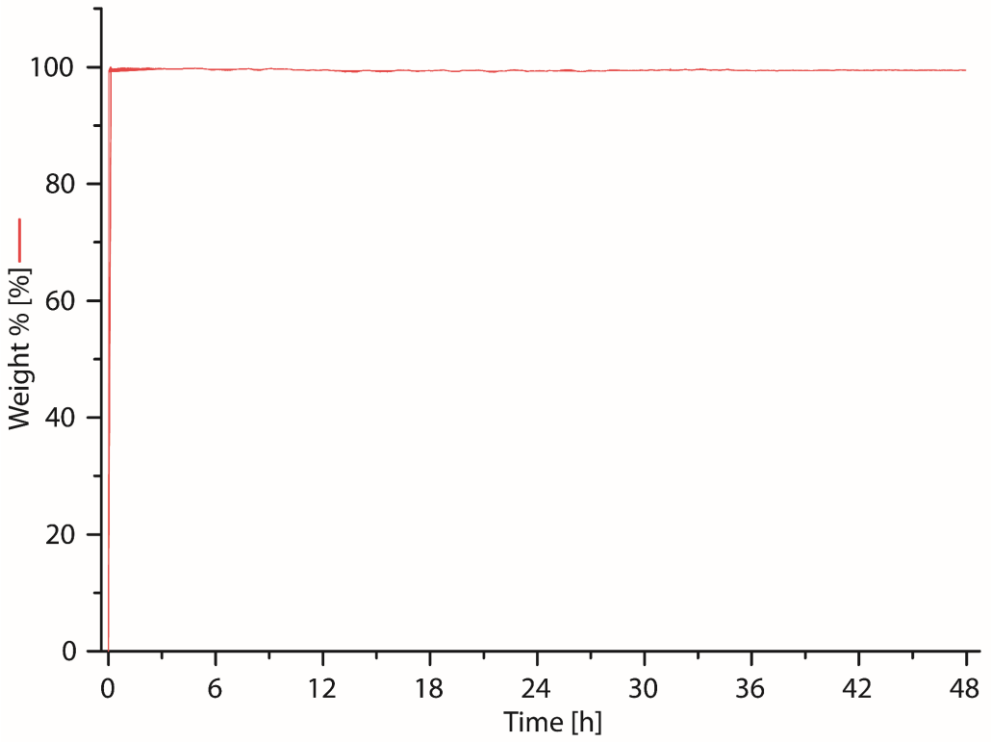

Figure S1. Isothermal TGA measurement of 1,1‘-DABT (**2**) @ 100 °C.

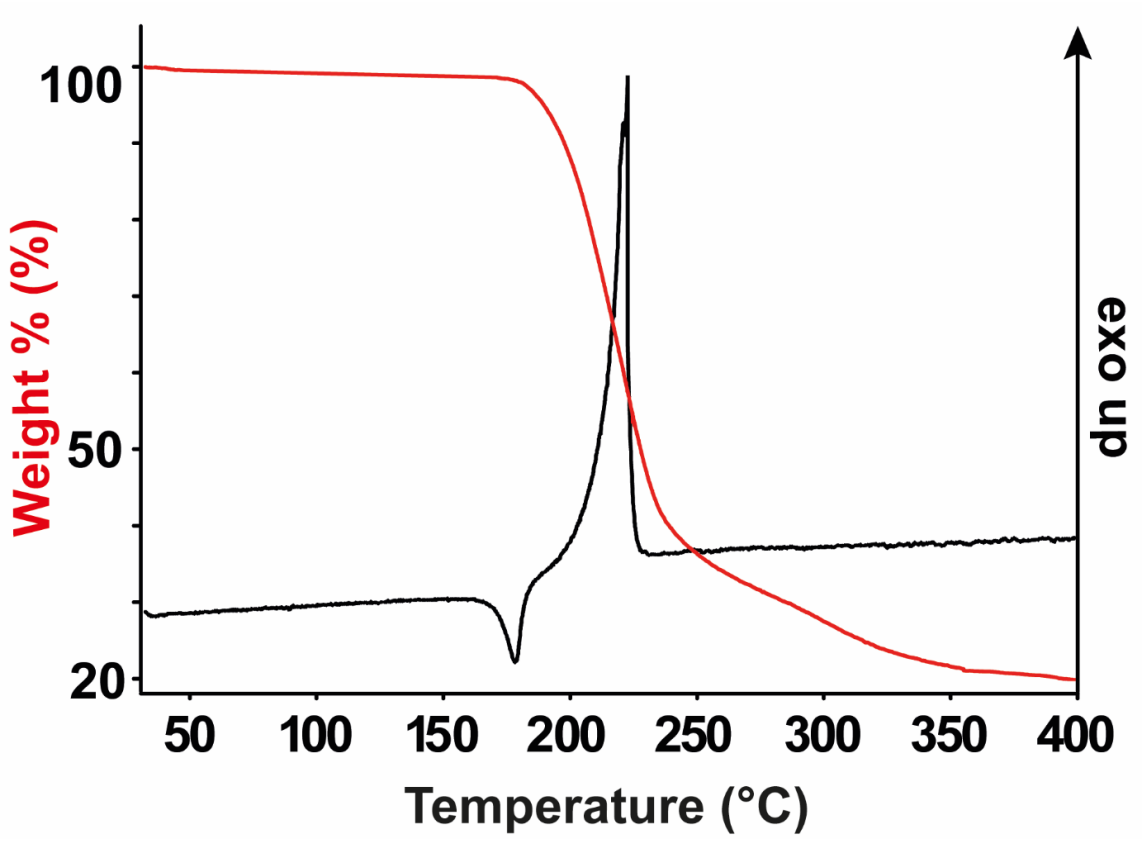

Figure S2. TGA (red) and DTA (black) analysis of 1,1'-DABT (**2**) with a heating rate of 5 °C min^{-1}.

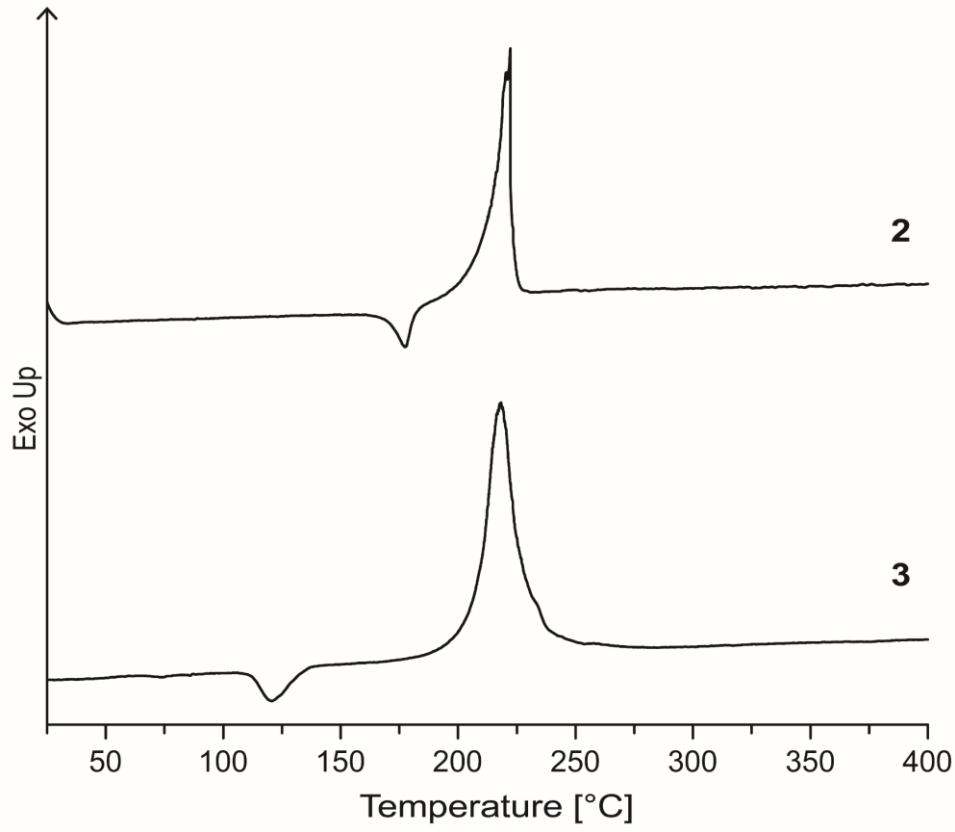

Figure S3. DTA plots of **2** (top) and **3** (bottom) with a heating rate of 5 °C min^{-1}.

7.6.3 Crystallography

Crystal structure data were obtained from an Oxford Xcalibur3 diffractometer with a Spellman generator (voltage 50 kV, current 40 mA) and a Kappa CCD area for data collection using Mo-*Kα* radiation (*λ* = 0.71073 Å) or a Bruker D8 Venture TXS diffractometer equipped with a multilayer monochromator, a Photon 2 detector and a rotation-anode generator (Mo-K_α radiation). The data collection was performed using the CRYSTALIS RED software.[S3] The solution of the structure was performed by direct methods and refined by full-matrix least-squares on F2 (SHELXT)[S4] implemented in the OLEX2[S5] software suite. The non-hydrogen atoms were refined anisotropically and the hydrogen atoms were located and freely refined. The absorption correction was carried out by a SCALE3 ABSPACK multiscan method.[S6] The DIAMOND2 plots shown with thermal ellipsoids at the 50% probability level and hydrogen atoms are shown as small spheres of arbitrary radius. The SADABS program embedded in the Bruker APEX3 software was used for multi-scan absorption corrections in all structures.[S7]

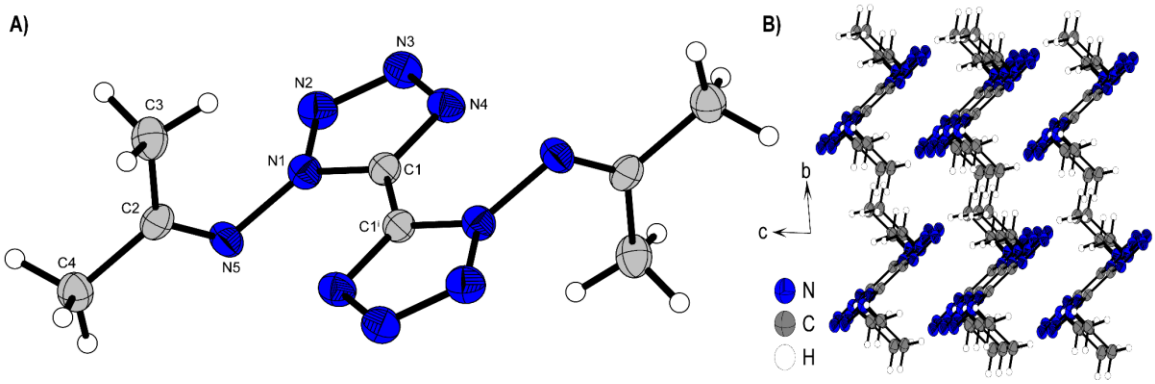

Figure S4. A) Molecular structure of **3** as determined by low temperature X-ray diffraction with thermal ellipsoids drawn at the 50% probability level, Symmetry code: (i) 2−x, 1−y, 1−z; B) 2D layer structure of **3** with view along the *a* axis.

Compound **3** crystallizes in the triclinic space group *P*−1 with a significantly reduced room temperature density of 1.397 g cm^{-3} compared to deprotected form **2**. The diamino-bistetrazole moiety forms a plane and the methyl groups of the isopropyl residues are rotated out of this plane resulting in the formation of a three-dimensional structure along *a*.

Table S1. Crystallographic data and structure refinement details for the prepared compounds **2** and **3**.

	2	**3**
Formula	$C_2H_4N_{10}$	$C_8H_{12}N_{10}$
FW [g mol^{-1}]	168.15	248.28
Crystal system	monoclinic	triclinic
Space group	$P2_1/n$ (No. 14)	P-1 (No. 2)
Color / Habit	colorless rod	colorless rod
Size [mm]	0.20 x 0.20 x 0.50	0.20 x 0.20 x 0.50
a [Å]	6.1708(7)	5.3799(7)
b [Å]	10.0590(11)	6.8654(9)
c [Å]	10.2606(12)	7.9751(10)
α [°]	90	81.857(11)
β [°]	104.156(13)	79.590(11)
γ [°]	90	86.503(11)
V [Å^3]	617.56(13)	286.60(7)
Z	4	1
$\rho_{calc.}$ [g cm^{-3}]	1.809	1.439
μ [mm^{-1}]	0.143	0.103
F(000)	344	130
$\lambda_{MoK\alpha}$ [Å]	0.71073	0.71073
T [K]	100	100
θ Min-Max [°]	2.9, 26.4	2.6, 26.4
Dataset	-7: 7 ; -12: 12 ; -10: 12	-4: 6 ; -8: 6 ; -9: 9
Reflections collected	4617	2109
Independent refl.	1269	1170
R_{int}	0.023	0.029
Observed reflections	1099	770
Parameters	125	106
R_1 (obs)[a]	0.0330	0.0516
wR_2 (all data)[b]	0.0812	0.1008
S [c]	1.06	1.07
Resd. dens [e Å^{-3}]	-0.23, 0.32	-0.23, 0.25
Device type	Xcalibur Sapphire3	Xcalibur Sapphire3
Solution	SIR-92	SIR-92
Refinement	SHELXL-2013	SHELXL-2013
Absorption correction	multi-scan	multi-scan
CCDC	2150464	2150463

[a] $R_1 = \Sigma||F_o|-|F_c||/\Sigma|F_o|$; [b] $wR_2 = [\Sigma[w(F_o^2-F_c^2)^2]/\Sigma[w(F_o)^2]]^{1/2}$; $w = [\sigma c^2(F_o^2)+(xP)^2+yP]^{-1}$ and $P=(F_o^2+2F_c^2)/3$; [c] $S = (\Sigma[w(F_o^2-F_c^2)^2]/(n-p))^{1/2}$ (n = number of reflections; p = total number of parameters).

7.6.4 Computation

All quantum chemical calculations were carried out using the Gaussian G09 program package.[S8] The enthalpies (H) and free energies (G) were calculated using the complete basis set (CBS) method of Petersson and co-workers in order to obtain very accurate energies. The CBS models are using the known asymptotic convergence of pair natural orbital expressions to extrapolate from calculations using a finite basis set to the estimated CBS limit. CBS-4 starts with an HF/3-21G(d) geometry optimization; the zero-point energy is computed at the same level. It then uses a large basis set SCF calculation as a base energy, and an MP2/6- 31+G calculation with a CBS extrapolation to correct the energy through second order. A MP4(SDQ)/6-31+ (d,p) calculation is used to approximate higher order contributions. In this study, we applied the modified CBS-4M.
Heats of formation of the synthesized ionic compounds were calculated using the atomization method (equation E1) using room temperature CBS-4M enthalpies, which are summarized in Table S2.[S9 S10]

$$\Delta_f H^\circ_{(g,\,M,\,298)} = H_{(Molecule,\,298)} - \sum H^\circ_{(Atoms,\,298)} + \sum \Delta_f H^\circ_{(Atoms,\,298)} \qquad (E1)$$

Table S2. CBS-4M electronic enthalpies for atoms C, H, N and O and their literature values for atomic $\Delta H^\circ_f{}^{298}$ / kJ mol^{-1}

	$-H^{298}$ [a.u.]	NIST[S11]
H	0.500991	218.2
C	37.786156	717.2
N	54.522462	473.1

For neutral compounds the sublimation enthalpy, which is needed to convert the gas phase enthalpy of formation to the solid state one, was calculated by the *Trouton* rule.[S12] For ionic compounds, the lattice energy (U_L) and lattice enthalpy (ΔH_L) were calculated from the corresponding X-ray molecular volumes according to the equations provided by *Jenkins* and *Glasser*.[S13] With the calculated lattice enthalpy the gas-phase enthalpy of formation was converted into the solid state (standard conditions) enthalpy of formation. These molar standard enthalpies of

formation (ΔH_m) were used to calculate the molar solid state energies of formation (ΔU_m) according to equation E2.

$$\Delta U_m = \Delta H_m - \Delta n\, RT \qquad \text{(E2)}$$

(Δn being the change of moles of gaseous components)

The calculation results are summarized in Table S3.

Table S3. Calculation results.

	–H^{298} [a] [a.u.]	Δ_fH°(g,M) [kJ mol^{-1}] [b]	Δ_fH°(s) [c] [kJ mol^{-1}]	Δn [d]	Δ_fU(s) [e] [kJ kg^{-1}]
2	625.146147	874.7	791.4	7.0	808.7

[a] CBS-4M electronic enthalpy; [b] gas phase enthalpy of formation; [c] standard solid state enthalpy of formation; [d] Δn being the change of moles of gaseous components when formed; [e] solid state energy of formation.

7.6.5 NMR Spectroscopy

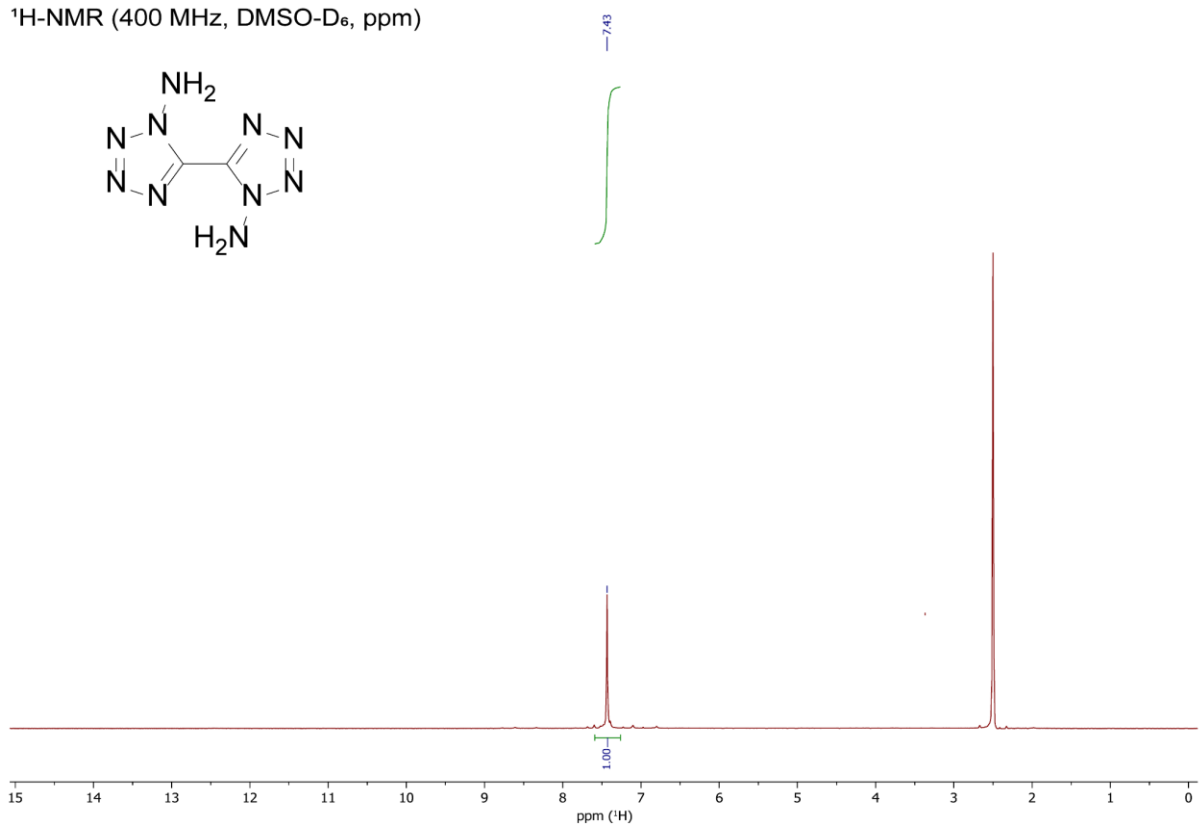

^{13}C-NMR (101 MHz, DMSO-D$_6$, ppm)

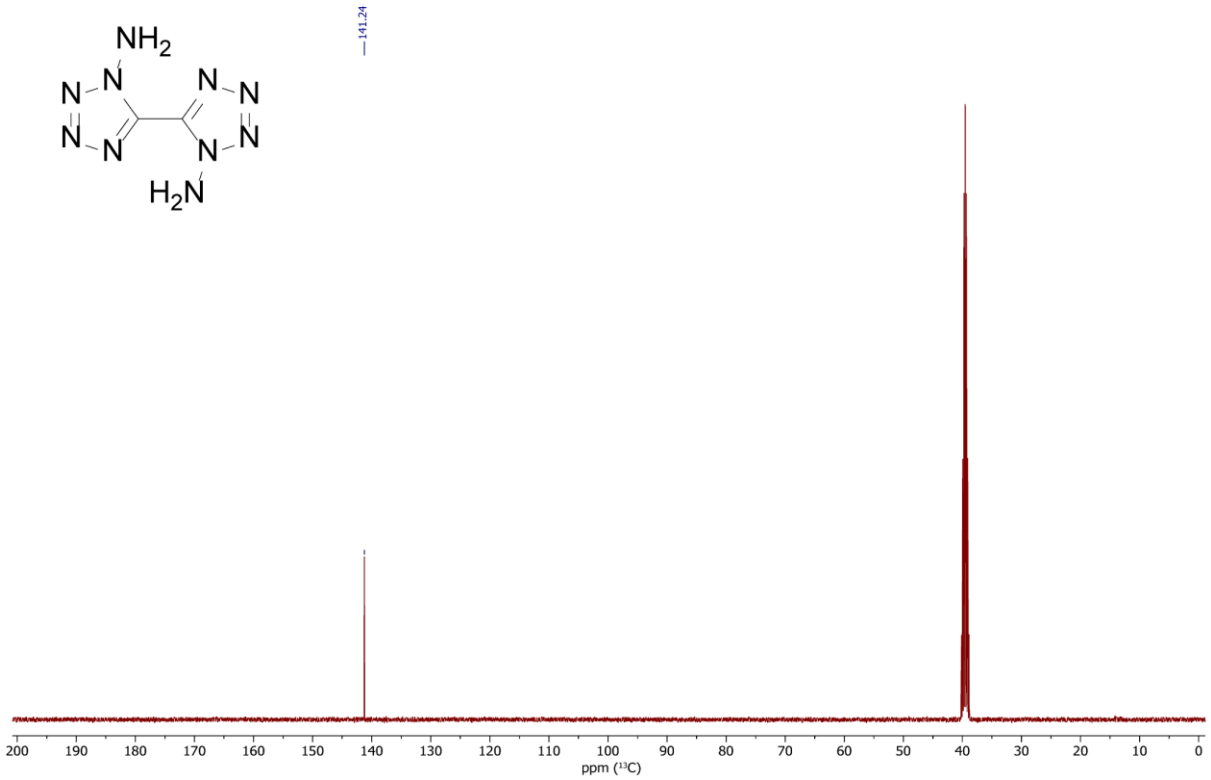

^{1}H-NMR (400 MHz, DMSO-D$_6$, ppm)

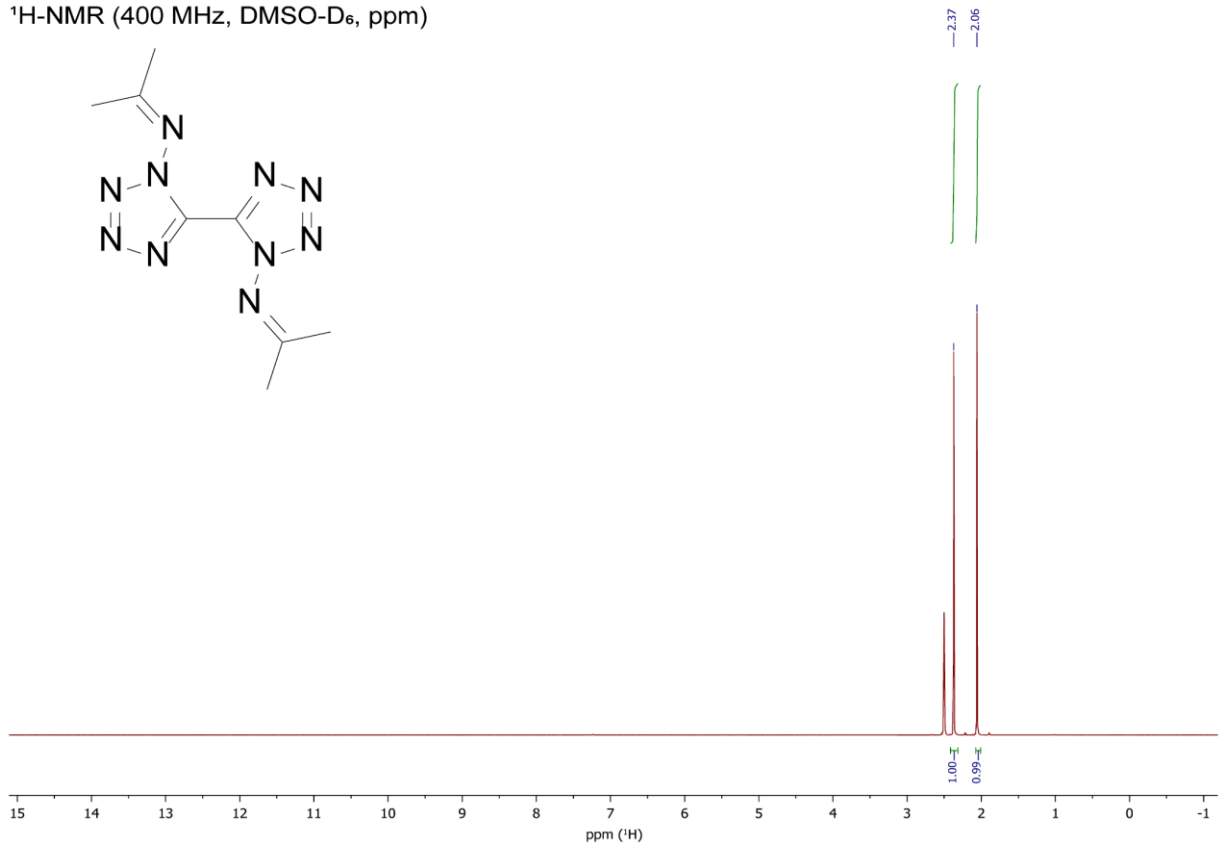

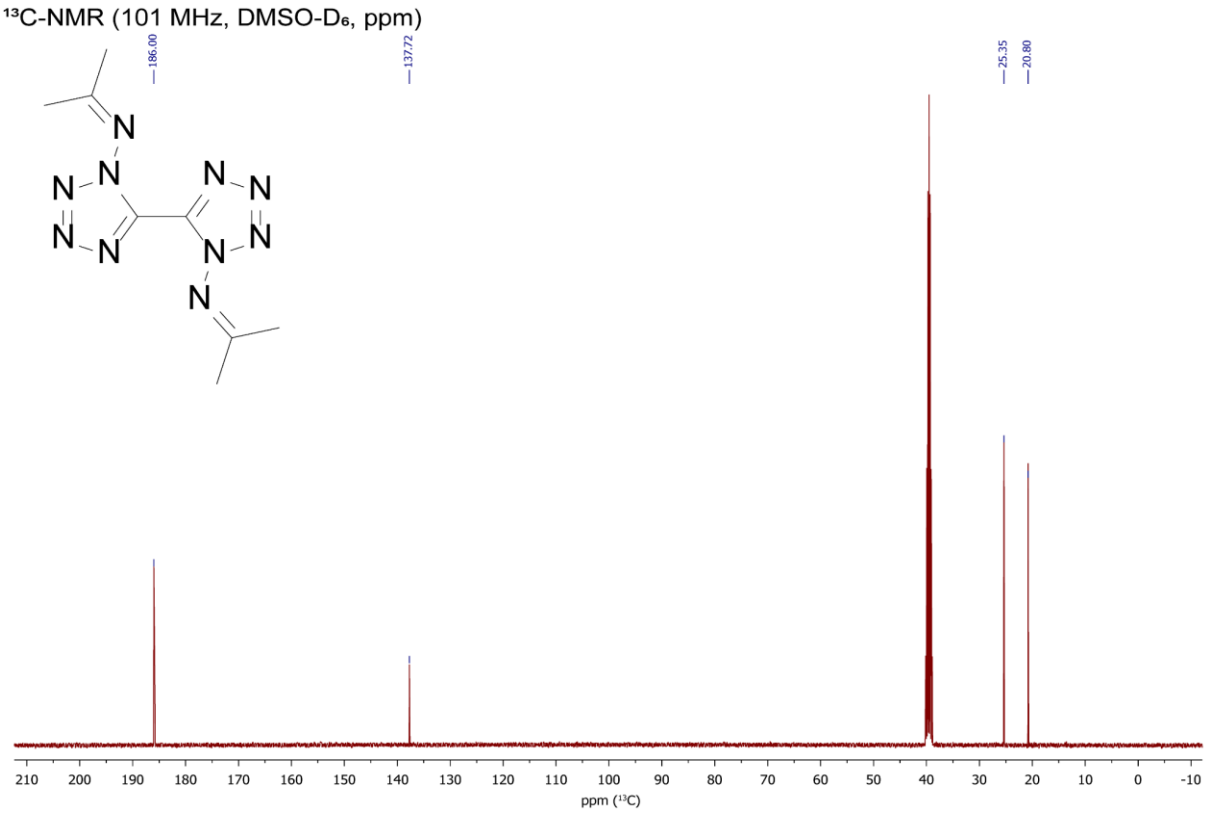

7.6.6 References

[S1] a) Reichel & Partner GmbH, http://www.reichelt-partner.de; b) Test methods according to the UN Recommendations on the Transport of Dangerous Goods, *Manual of Test and Criteria*, fourth revised edition, United Nations Publication, New York and Geneva, **2003**, ISBN 92–1-139087–7, Sales No. E.03.VIII.2; 13.4.2 Test 3 a (ii) BAM Fallhammer.

[S2] M. Sućeska, EXPLO5 V6.02 program, Brodarski Institute, Zagreb, Croatia, **2014**.

[S3] *CrysAlisPro*, Oxford Diffraction Ltd. *version 171.33.41*, **2009**.

[S4] G. M. Sheldrick, *Acta Cryst.* **2015**, *A71*, 3–8.

[S5] O. V. Dolomanov, L. J Bourhis, R. J. Gildea, J. A. K. Howard, H. Puschmann, *J. Appl. Cryst.* **2009**, *42*, 339–341.

[S6] *SCALE3 ABSPACK – An Oxford Diffraction program* (1.0.4, gui: 1.0.3), Oxford Diffraction Ltd., **2005**.

[S7] *APEX3*. Bruker AXS Inc., Madison, Wisconsin, USA.

[S8] M. J. Frisch, G. W. Trucks, H. B. Schlegel, G. E. Scuseria, M. A. Robb, J. R. Cheeseman, G. Scalmani, V. Barone, B. Mennucci, G. A. Petersson, H. Nakatsuji, M. Caricato, X. Li, H.P. Hratchian, A. F. Izmaylov, J. Bloino, G. Zheng, J. L. Sonnenberg, M. Hada, M. Ehara, K. Toyota, R. Fukuda, J. Hasegawa, M. Ishida, T. Nakajima, Y. Honda, O. Kitao, H. Nakai, T. Vreven, J. A. Montgomery, Jr., J. E. Peralta, F. Ogliaro, M. Bearpark, J. J. Heyd, E. Brothers, K. N. Kudin, V. N. Staroverov, R. Kobayashi, J. Normand, K. Raghavachari, A. Rendell, J. C. Burant, S. S. Iyengar, J. Tomasi, M. Cossi, N. Rega, J. M. Millam, M. Klene, J. E. Knox, J. B. Cross, V. Bakken, C. Adamo, J. Jaramillo, R. Gomperts, R. E. Stratmann, O. Yazyev, A. J. Austin, R. Cammi, C. Pomelli, J. W. Ochterski, R. L. Martin, K. Morokuma, V. G. Zakrzewski, G. A. Voth, P. Salvador, J. J. Dannenberg, S. Dapprich, A. D. Daniels, O. Farkas, J.B. Foresman, J. V. Ortiz, J. Cioslowski, D. J. Fox, Gaussian 09 A.02, Gaussian, Inc., Wallingford, CT, USA, **2009**.

[S9] a) J. W. Ochterski, G. A. Petersson, and J. A. Montgomery Jr., *J. Chem. Phys.* **1996**, *104*, 2598–2619; b) J. A. Montgomery Jr., M. J. Frisch, J. W. Ochterski G. A. Petersson, *J. Chem. Phys.* **2000**, *112*, 6532–6542.

[S10] a) L. A. Curtiss, K. Raghavachari, P. C. Redfern, J. A. Pople, *J. Chem. Phys.* **1997**, *106*, 1063–1079; b) E. F. C. Byrd, B. M. Rice, *J. Phys. Chem*. A **2006**, *110*, 1005–1013; c) B. M. Rice, S. V. Pai, J. Hare, *Comb. Flame* **1999**, *118*, 445–458.

[S11] P. J. Lindstrom, W. G. Mallard (Editors), NIST Standard Reference Database Number 69, http://webbook.nist.gov/chemistry/ (accessed March **2022**).

[S12] M. S. Westwell, M. S. Searle, D. J. Wales, D. H. Williams, *J. Am. Chem. Soc*. **1995**, *117*, 5013–5015; b) F. Trouton, *Philos. Mag*. **1884**, *18*, 54–57.

[S13] a) H. D. B. Jenkins, H. K. Roobottom, J. Passmore, L. Glasser, *Inorg. Chem.* **1999,** *38,* 3609–3620; b) H. D. B. Jenkins, D. Tudela, L. Glasser, *Inorg. Chem.* **2002**, *41*, 2364–2367.

8. Chemistry of 2,5-Diaminotetrazole

Josh Bauer, Maximilian Benz‡, Thomas M. Klapötke, Jörg Stierstorfer

as published in *Dalton Transaction* **2022**, *51*, 11806–11813

DOI: 10.1039/d2dt01480g

Keywords: amination, derivatization, tetrazoles, salts, structural eludication

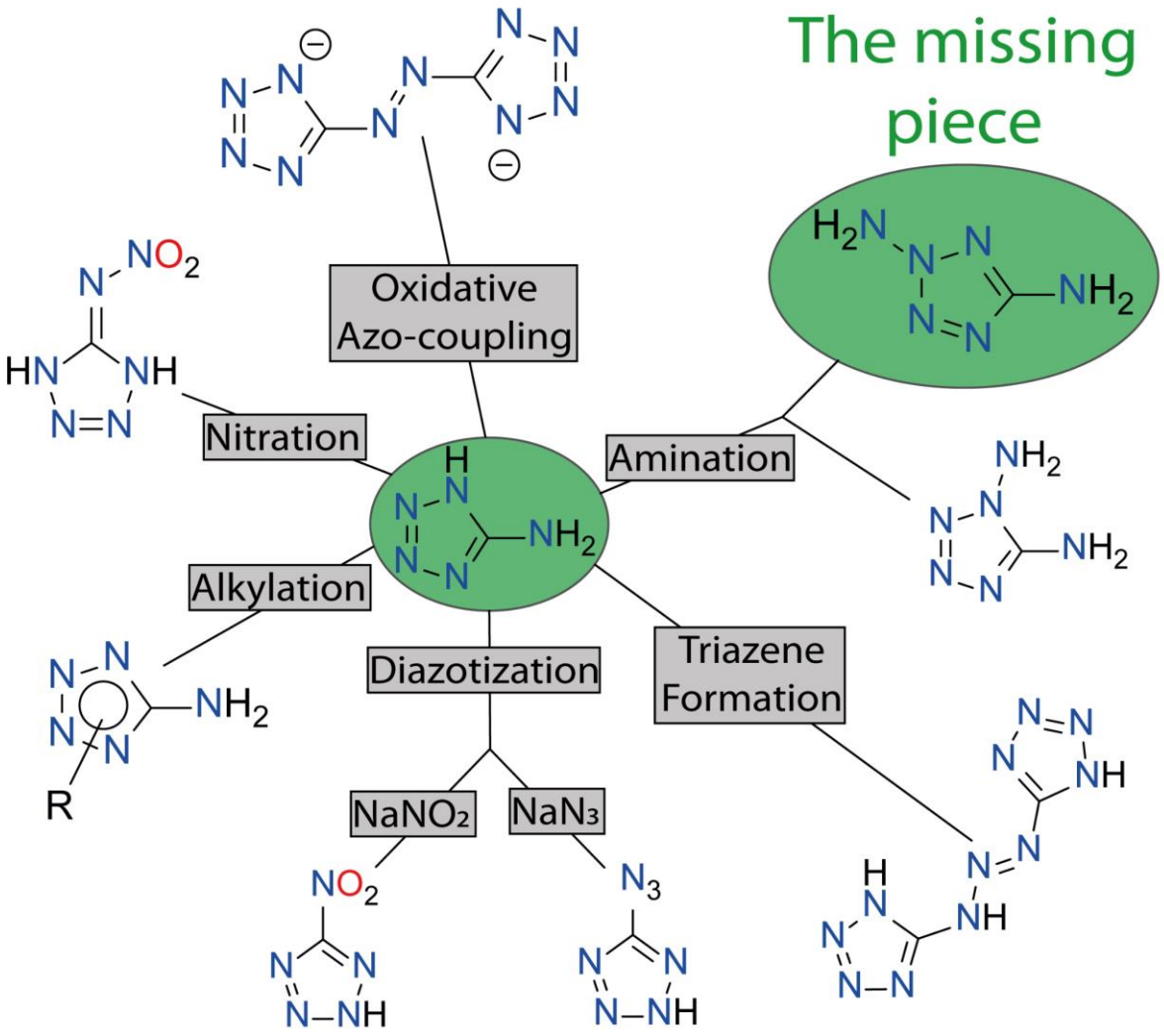

2,5-Diaminotetrazole is one of the easiest double substituted tetrazoles, which is up to now not properly characterized. Similar as for its more prominent isomer, 1,5-diaminotetrazole, many functionalization reactions are possible.

Abstract: 1,5-Diaminotetrazole is one of the most prominent high-nitrogen tetrazole compounds described in the literature. Interestingly the isomer 2,5-diaminotetrazole is nearly undescribed due to its challenging synthetic routes. 2,5-Diaminotetrazol (**1**) was successfully synthesized *via* amination of 5-aminotetrazole followed by various purification steps to separate it from isomeric 1,5-diaminotetrazole. In addition to the extensive characterization of 2,5-DAT further derivates by protonation, methylation and amination of the tetrazole ring were synthesized and characterized. The resulting tri-functionalized, ionic tetrazolium derivatives were combined with energetic anions (nitrate, perchlorate, azide, 5,5′-bistetrazole-1,1′-diolate (BTO^{2-})) to adjust and tune the properties of each compound. All compounds were intensively characterized including IR and multinuclear NMR spectroscopy, thermal analysis through DTA, X-ray diffraction and sensitivity testing. The purity was verified by CHNO elemental analysis and the energetic properties were calculated using the EXPLO5 code and the calculated enthalpy of formation (CBS-4M).

8.1 Introduction

Aminotetrazoles have great influence in the chemical repertoire for explosive materials.[1-2] 5-Aminotetrazole (5-AT), probably the most obvious representative, is produced on a large scale by diazotization of aminoguanidine followed by base-induced cyclization. It is commonly used as a gas generating agent in airbags, since it has some major advantages (non-toxic, chemical robustness, higher nitrogen content) compared to the long-used sodium azide.[3-4] Furthermore, 5-AT provides a great platform for a variety of functionalized tetrazoles, which find wide application in almost all areas of energetic materials. DBX-1[5-8] (copper-(i)-nitrotriazolone, a green primary explosive), produced through diazotization of 5-aminotetrazole with an excess of sodium nitrite and subsequent precipitation of the copper salt and bisguanidinium 5,5′-azobistetrazole[9] (ingredient in halogen-free pyrotechnics) synthesized through oxidative azo-coupling of 5-aminotetrazole are only two examples for energetic materials starting from 5-AT. 1- and 2-Aminotetrazoles and their derivatives are used primarily as powerful primary explosives. For example, the two *N*-substituted aminotetrazoles form a variety of

promising energetic coordination compounds (ECCs),[10] and the potassium salts of the nitriminotetrazoles as heavy metal-free detonants (Figure 1).[11]

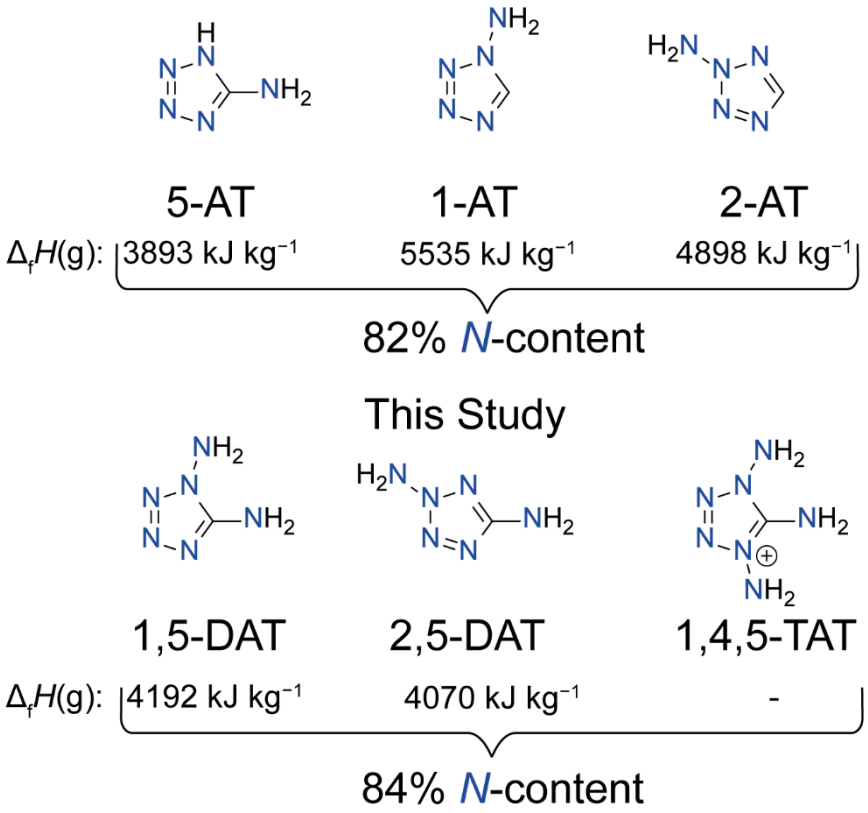

Figure 1. Compounds with exclusively aminotetrazole functionalities, the gas phase heats of formation (calculated on CBS-4M level of theory) and their respective nitrogen content: 5-aminotetrazole, 1-aminotetrazole, 2-aminotetrazole, 1,5-diaminotetrazole, 2,5-diaminotetrazole (**1**) and the 1,4,5-triaminotetrazolium cation.

In addition to the exotic, trisubstituted 1,4,5-triaminotetrazolium cation, which is described as a thermally labile nitrate and nitrotetrazol-2-olate,[12] 1,5-diaminotetrazole is the most versatile aminotetrazole representative and is highly recommended in the energetic materials chemistry community.[13-16] It is synthetically available through at least four different reaction protocols (*e.g.* diazotization of diaminoguanidin, amination of 5-AT, oxidation of semicarbazide and reaction of hydrazine with cyanogen azide).[17-20] The further increased nitrogen content and associated positive environmentally properties make 1,5-DAT an interesting candidate as a next-generation gas generator.

Due to its two differently reactive amino groups and the basicity of the tetrazole ring, a variety of different derivatives can be synthesized using this molecule.[12, 21-24] Many scientific papers in the past years have dealt with the energetic

derivatization of 1,5-DAT, where the parent compound could be extensively functionalized (selected examples are shown inFigure 2).[6, 8-9, 25] Surprisingly, the isomer of 1,5-DAT (2,5-DAT) has not yet been described in detail. The reason for this is the more difficult accessibility of 2-substituted tetrazoles and the need to separate the isomers. It can be expected that the chemistry carried out on the 1,5-isomer can be completely transferred to 2,5-DAT.

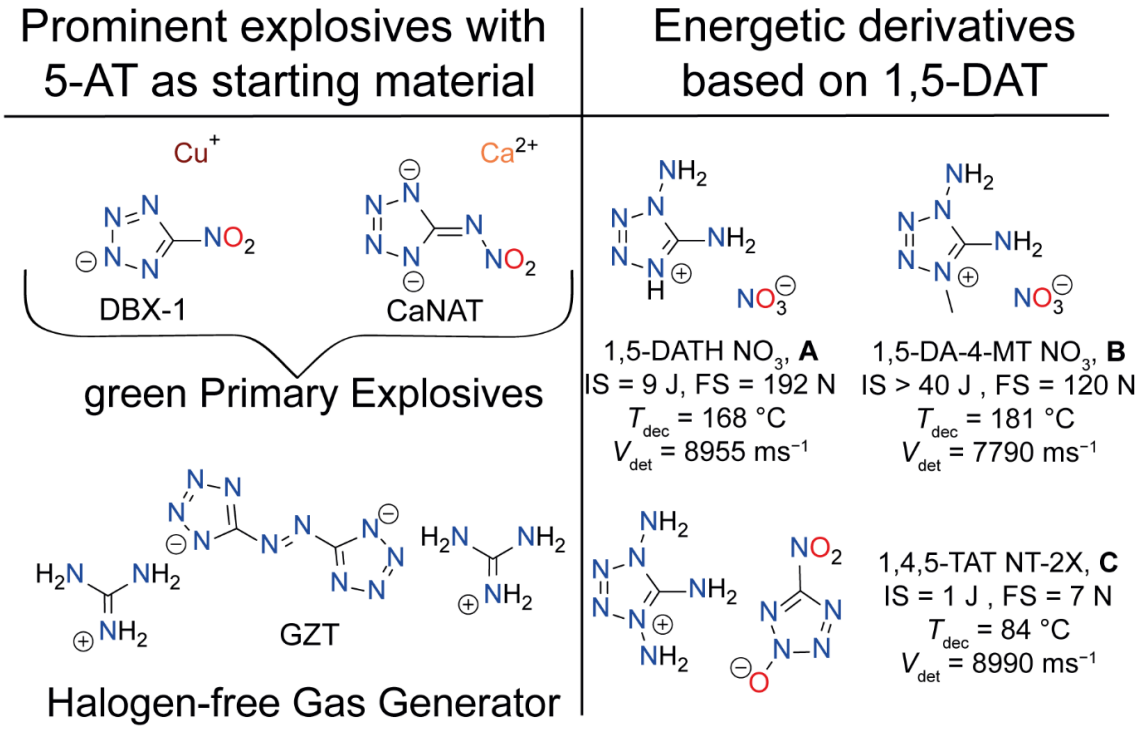

Figure 2. Prominent energetic materials requiring 5-AT as starting materials (left) and energetic derivatives of 1,5-DAT (right).

8.2 Results and Discussion

8.2.1 Synthesis

The synthetic route for the synthesis of diaminotetrazoles was already described 1969 by Raap *et al.*[18] However, the analytical data of 2,5-DAT in this publication do not agree with the values measured within this work. This is mainly due to the fact that the elemental analysis listed in the article gives the same values for both isomers of diaminotetrazole and we therefore suspect that 2,5-diaminotetrazole

was not obtained pure. So probably an isomeric mixture of 1,5 and 2,5-diaminotetrazole was characterized back then.

An isomeric mixture of 1,5-DAT and 2,5-DAT is synthesized through the amination of *in situ* generated sodium 5-aminotetrazolate in a Na_2CO_3 buffered aqueous solution at 100 °C. As amination agent hydroxylamine-*O*-sulfonic acid (HOSA) is used. The main products of the reaction are 1,5-DAT and 2,5-DAT. The majority of the 1,5-DAT can easily be separated by trituration with water. The purification of the remaining isomeric mixture is a time-consuming process including several recrystallization steps as well as column chromatography for the final purification. The reaction results in a yield of 46% 1,5-DAT and 16% 2,5-DAT giving a total yield of 62% (Scheme 1).

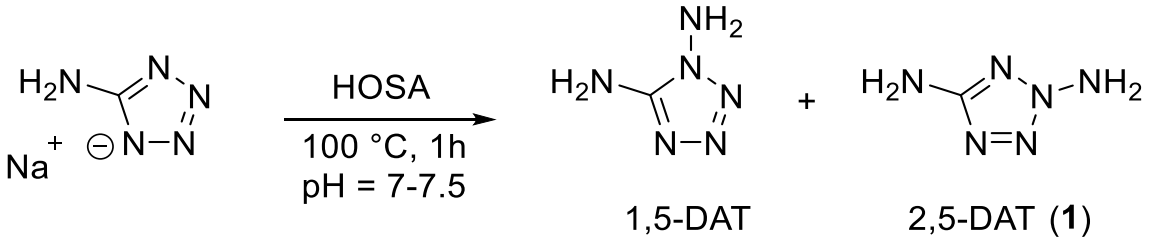

Scheme 1. Amination of sodium 5-aminotetrazolate to yield the isomers 1,5-DAT and 2,5-DAT (**1**).

2,5-DAT (**1**), like 1,5-DAT, is an electron-rich heterocycle due to the electron-pushing effect of the two amino groups and is therefore suitable for reactions with several electrophiles. Therefore, derivatization reactions including the protonation, methylation and amination were investigated.

The synthesis of the energetic salts **2a** and **2b** was performed by dissolving 2,5 diaminotetrazole (**1**) in a minimal amount of the respective acid (65% nitric acid for **2a**; 60% perchloric acid for **2b**) and heating until a clear solution was obtained. Ionic derivatives **2a**–**2b** could be obtained in form of colorless crystalline products after slow evaporation of the solvent (Scheme 2).

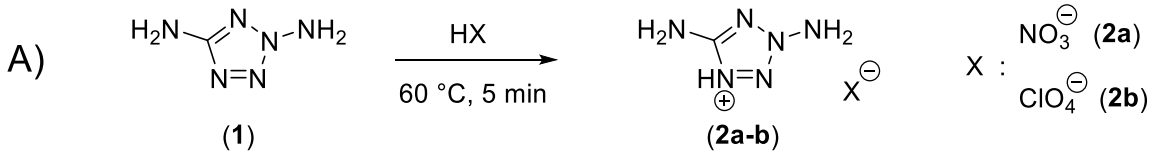

Scheme 2. (A) Preparation of energetic 2,5-diaminotetrazolium salts based on the protonation of 2,5-DAT with respective acids.

The methylation of 2,5-DAT was performed using an excess of methyl iodide as methylation agent. The reaction yields only one isomer (2,5-diamino-4-methyltetrazolium) due to the electronic effects of the two amino groups as its iodide salt (**3**). 2,5-Diamino-4-methyltetrazolium iodide (**3**) could be collected by slow evaporation of the solvent. The subsequent metathesis reactions of the iodide with the respective silver salts yielded 2,5-diamino-4-methyltetrazolium as nitrate (**3a**) and perchlorate (**3b**) and azide (**3c**) derivatives, while silver iodide was precipitated and detached (Scheme 3).

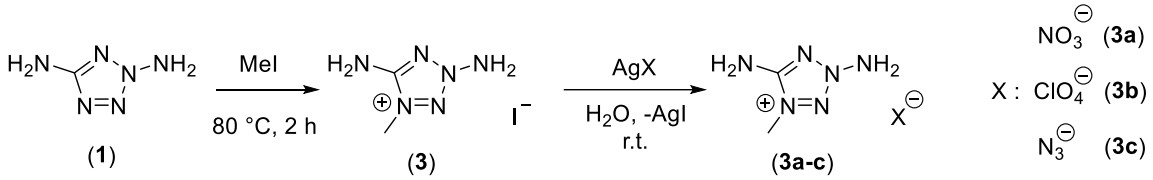

Scheme 3. Methylation of 2,5-DAT (**1**) using methyl iodide in MeCN and metathesis reaction with the respective silver salts.

Similar to the methylation reaction, amination of 2,5-DAT using THA (*O*-tosylhydroxylamine) only yields one product (1,3,5-triaminotetrazolium), which precipitated as its tosylate salt **4**. Next to the 1,4,5-triaminotetrazolium derivative and 1,5-diaminotetrazole-4*N*-oxide, our compounds are only the third scaffold containing a triple heterosubstituted tetrazole.[12, 26]

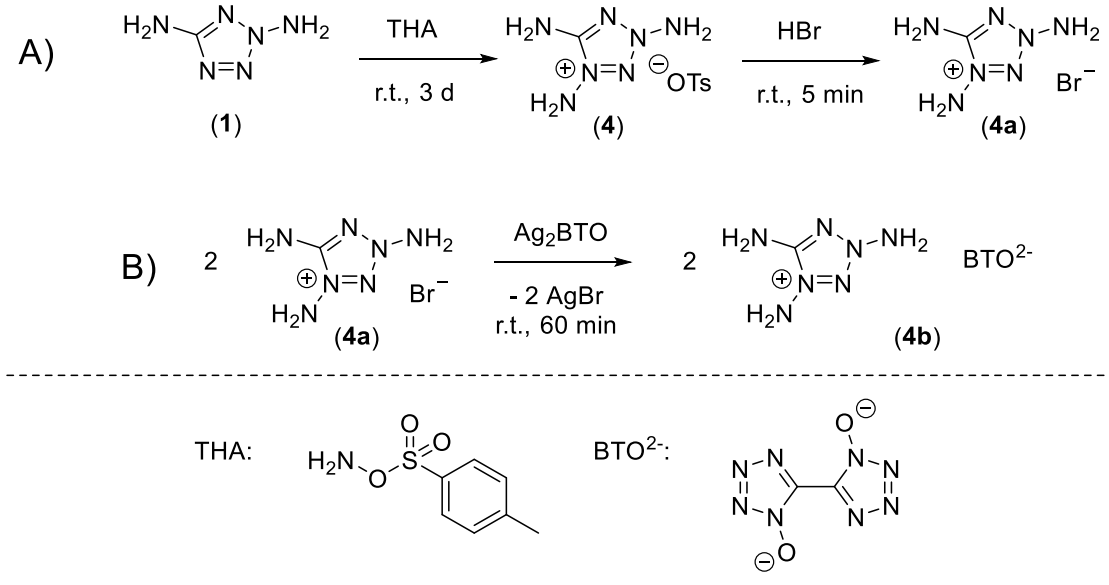

Scheme 4. (A) Amination of 2,5-DAT (**1**), conversion to its bromide salt. (B) Metathesis reaction using $AgNO_3$.

Through the amination at the position next to the C–NH_2 group, the nomenclature changes and therefore a 1,3,5-triaminotetrazolium derivative is obtained. The conversion to the 1,3,5-triaminotetrazolium bromide (**4a**) was necessary to be able to perform metathesis reactions with silver salts and precipitate silver bromide.
The reaction with silver nitrate and silver perchlorate yielded the respective pure and clean 1,3,5-triaminotetrazolium nitrate and perchlorate derivative but unfortunately the products were too hygroscopic for further investigations since they liquified immediately upon exposure to air. Therefore, we pushed for another energetic anionic moiety and chose BTO^{2-} (5,5′-bistetrazole-1,1′-diolate), the anion of TKX-50, since it affords good thermal stability and high heat of formation as well as enough sterically demand so the compound should be easy to mollify and crystallize. As expected the metathesis reaction of **4b** with Ag_2BTO in water yielded compound **4b** in quantitative yields while silver bromide precipitates. Compound **4b** is the BTO derivative with the highest overall nitrogen content (Scheme 4).

8.2.2 X-Ray Diffraction

All compounds presented in this study were intensively studied by low-temperature X-ray diffraction experiments. Herein, we present the crystal structure of 2,5-DAT (**1**) and all energetic derivatives (**2a**, **2b**, **3a–3c** and **4b**).

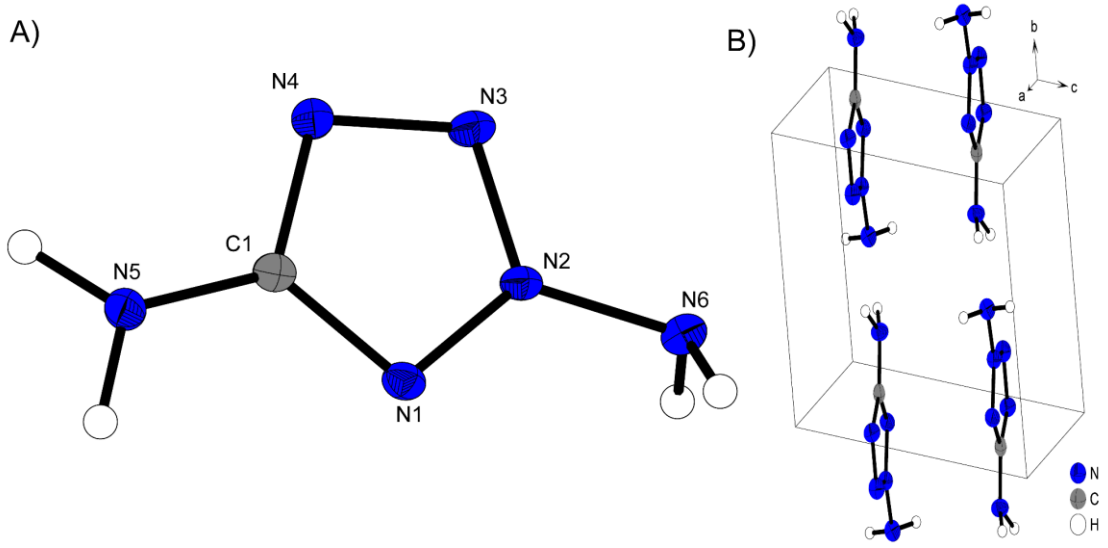

Figure 3. (A) Representation of the molecular unit of 2,5-diaminotetrazole (**1**), showing the atom-labeling scheme. Thermal ellipsoids represent the 50% probability level and hydrogen atoms are shown as small spheres of arbitrary radius. (B) Elemental cell. Selected bond distances [Å] and angles [°]: C1–N5 1.3530(2), N2–N6 1.3877(2), N6–N2–N1 124.81(2), N6–N2–N3 120.31(1), N5–C1–N1 123.93(2).

The crystal structures of the precursor compounds **3**, **4** and **4a** can be found in the ESI. Deposition numbers 2172089 (for **1**), 2172088 (for **2a**), 2172090 (for **2b**), 2172091 (for **3**), 2172087 (for **3a**), 2172093 (for **3b**), 2172084 (for **3c**), 2172092 (for **4**), 2172086 (for **4a**) and 2172085 (for **4b**) contain the supplementary crystallographic data for this paper.

Crystals for the respective compounds were obtained directly by slow evaporation of the respective solvent or by simple recrystallization from popular solvents. All compounds crystallize in common space groups ($P\bar{1}$, $P2_1/c$, $P2_1/n$, $P2_12_12_1$).

2,5-Diaminotetrazole (**1**) crystallizes in the triclinic space group $P\bar{1}$ and comes up with a density of 1.577 g cm^{-3} at 298 K (Figure 3). The density is nearly the same as for 1,5-diaminotetrazole (1.571 g cm^{-3}).[27] **1** contains two amino groups, which show varying reactivities due to their different hybridization. Based on the orientation of the protons, it can be seen that the amino group on the carbon (C–NH_2) is sp^2 hybridized, since the free electron pair is donated into the tetrazole ring. The hydrazine amino group at N2 (N–NH_2) is sp^3 hybridized and accordingly still has its free electron pair located on the amine nitrogen atom and is thus the more reactive amino group. Accordingly, the two amino groups also have different bond lengths, with the carbon-bonded amino group having a shorter bond distance (C1–N5 1.353(3) Å) than the nitrogen-bonded one (N2–N6 1.388(3) Å). 2,5-Diaminotetrazole forms a layered structure along the *b* axis, forming pairs of alternating molecular units that form strong intermolecular interactions between the protons of the C-bonded amino group and N4 (H5B–N4 2.18(2) Å). Additional hydrogen bonds are formed by the protons of the N-amino group and N1 (H6A–N1 2.46(2) Å, H6B–N1 3.14(2) Å).

2,5-Diaminotetrazolium nitrate (**2a**) crystallizes in the monoclinic space group $P2_1/n$ and has a density of 1.737 g cm^{-3} at 298 K. The density is slightly higher than for the 1,5 diaminotetrazolium nitrate isomer **A** (1.726 g cm^{-3}@298 K).[24] **2a** forms a layered structure along the *b*-axis, with both the 2,5-diaminotetrazolium cations and the nitrate anions in the same layer. The distance between the layers is 3.07 Å. A large number of strong interactions are formed between two molecular cation units and between anions and cations. Similar to neutral compound **1**, the interactions of the aminotetrazole units origin from the carbon-bonded amine. In this case, however, the interaction is established with N1, since the most electron-rich site N4 is of the tetrazole system is blocked through the protonation (N1–H5A

2.24(2) Å). The oxygen atoms of the nitrate interact strongly with the protons of both amino groups and with the hydrogen on the aromatic ring.

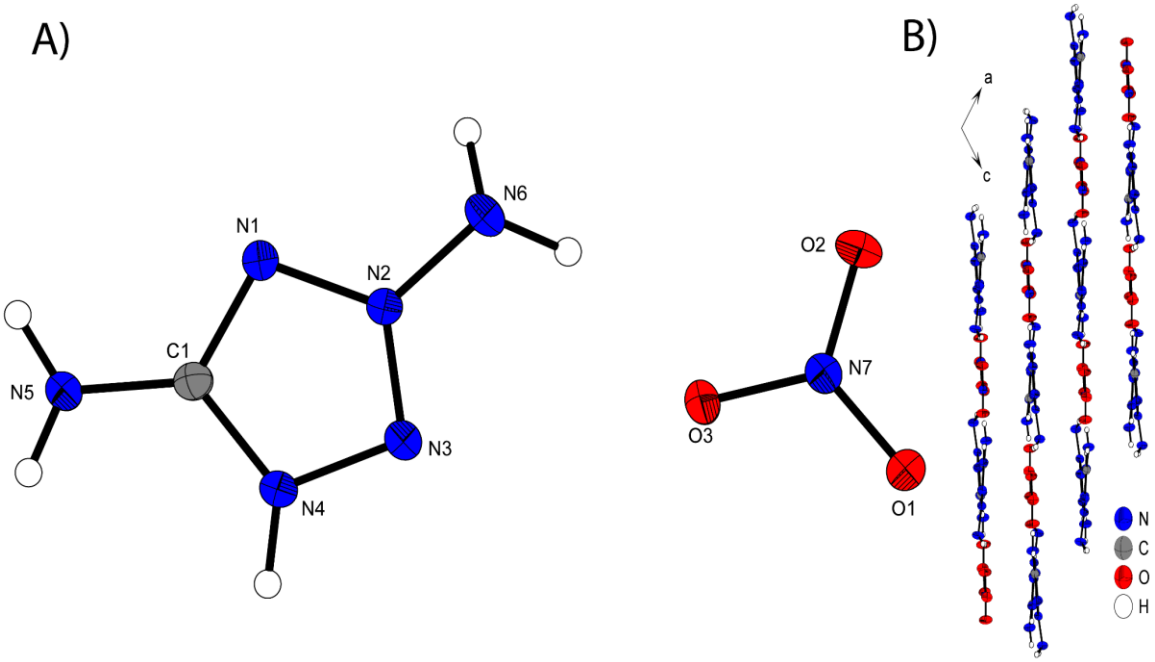

Figure 4. (A) Representation of the molecular unit of 2,5-diaminotetrazolium nitrate (**2a**), showing the atom-labeling scheme. Thermal ellipsoids represent the 50% probability level and hydrogen atoms are shown as small spheres of arbitrary radius. Selected bond distances [Å] and angles [°]: C1–N5 1.328(3), N2–N6 1.365(3), H4–O2^{i} 1.83(3), H5A–N1^{i} 2.26(2), H5B–O3^{i} 2.14(2), H6A–O2^{i} 1.98(2), N6–N2–N3 121.63(2), N5–C1–N1 124.93 (2), N4–H4–O 172(2), O3^{i}–H5B–N5 156(2), N5–H5A–N7 163(2); (B) 3D layer pattern of **2a** along the *b* axis.

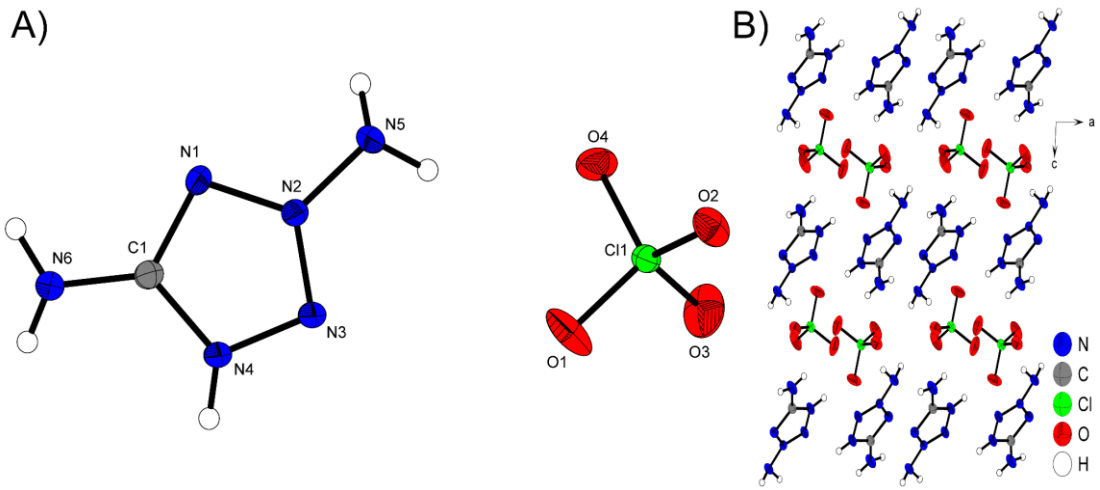

Figure 5. (A) Representation of the molecular unit of 2,5-diaminotetrazolium perchlorate (**2b**), showing the atom-labeling scheme. Thermal ellipsoids represent the 50% probability level and hydrogen atoms are shown as small spheres of arbitrary radius. Selected bond distances [Å] N6–C1 1.316(3), N5–N2 1.372(3), Cl1–O1 1.470(2), N2–N3 1.284(2), H4–O1 2.27(3), H5A–O4 2.25(2), H5B–O4 2.24(2), H6B–O3 2.60(3), H4–N3^{i} 2.52(2), H6A–N1 2.26(3) and angles [°]: N4–H4–O1 134(3), N5–H5A–O4 151(2), N5–H5B–O4 150(2), N6–H6B–O3 160(3), N4–H4–N3 119(2), N6–H6A–N1 163(3); (B) 3D layer pattern of **2b** along the *b* axis.

This results in an arrangement within the plane in which four tetrazolium cations are arranged around one nitrate anion (O3–H6A 1.98(2) Å, O3–H4 1.76(3) Å, O1–H5B 2.13(2) Å) (Figure 4).

2,5-Diaminotetrazolium perchlorate (**2b**) crystallizes in the monoclinic space group $P2_1/c$ and shows a density of 1.870 g cm^{-3} at 298 K. Compared with the isomeric 1,5-diaminotetrazolium perchlorate, hardly any difference in density (ρ(1,5-DATH$^+$ ClO_4^-) = 1.872 g cm^{-3} at 298 K)[24] is observed. Strong interactions are formed between the perchlorate anion and the protons of the amino groups of the cationic unit. These attractive interactions lead to the formation of a layer-like arrangement of anions and cations in the ac plane. In addition, strong interactions are formed between pairs of two cationic units in a plane, favouring the present structure (Figure 5).

2,5-Diamino-4-methyltetrazolium nitrate (**3a**) crystallizes in the monoclinic space group $P2_1/c$ and shows a density of 1.649 g cm^{-3} at 298 K. The density drops about 0.08 g cm^{-3} in comparison to **2a**. Compared with its isomer 1,5-diamino-4-methyltetrazolium nitrate **B** (ρ(1,5-DA-4-MT NO_3) = 1.487 g cm^{-3} at 298 K)[24] the density of **3a** is clearly higher.

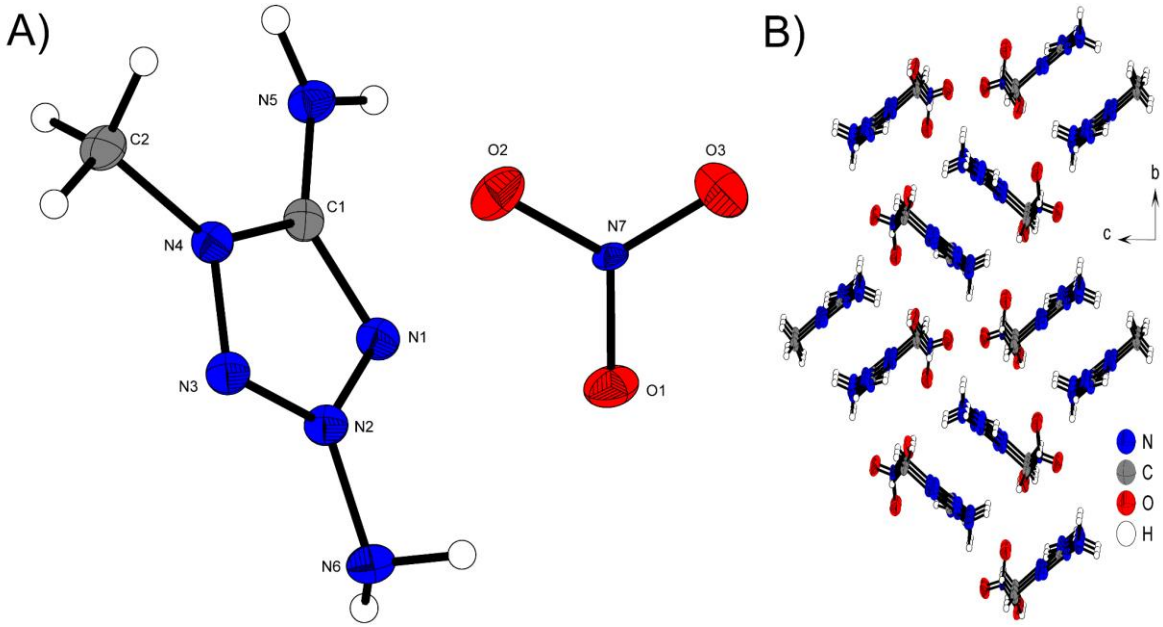

Figure 6. (A) Representation of the molecular unit of 2,5-diamino-4-methyltetrazolium nitrate (**3a**), showing the atom-labeling scheme. Thermal ellipsoids represent the 50% probability level and hydrogen atoms are shown as small spheres of arbitrary radius. Selected bond distances [Å] C1–N5 1.328(2), N2–N6 1.390(2), C2–N4 1.466(3), N7–O2 1.257(2), O1–H6B 2.28(3), O1–H6B^i 2.18(3), O2–H6A 2.11(3), O3–H5A 2.23(3), O3–H5B 2.16(3) and angles [°]: N1–N2–N6 124.5(2), C1–N4–C2 129.1(2), O1–H6B–O1 143(2), O1–H6B^i–N6^i 140(2), O2–H6A–N6 157(2), O3–H5A–N5 164(2), O3–H5B–N5 159(3); (B) 3D layer pattern of **3a** along the *a* axis.

The big difference in density between the two isomers is quite unusual. Various intermolecular interactions are formed between the protons of the amino group and the nitrate anion. The methyl group does not take place in these interactions (Figure 6).

2,5-Diamino-4-methyltetrazolium perchlorate (**3b**) crystallizes in the monoclinic space group $P2_1/n$ and has a room temperature density of 1.770 g cm^{-3}. The methylation results in a decrease of the density by 0.1 g cm^{-3} compared to 2,5-diaminotetrazolium perchlorate (**2b**). This is mainly due to the fact that the 2,5-diaminotetrazolium units interact with the proton on the tetrazolium ring and are therefore more densely packed. The methyl group in **3b** does not form hydrogen bonds. Only three oxygen atoms of the perchlorate are involved in the formation of hydrogen bonds with the cationic moiety. No intermolecular interactions can be observed for O1. Each of the four amino hydrogen atoms form strong interactions with one perchlorate anion (O2–H6B 2.25(2) Å, O4–H6A 2.16(2) Å, O3–H5A 2.15(2) Å, O2–H5B 2.26(3) Å). This results in an environment for each cation structure consisting of four perchlorate anions interacting with the NH_2 protons and one additional anionic unit located with O1 above the centre of the tetrazolium ring (plane of C1–N2–N3) with a distance of 3.023(2) Å.

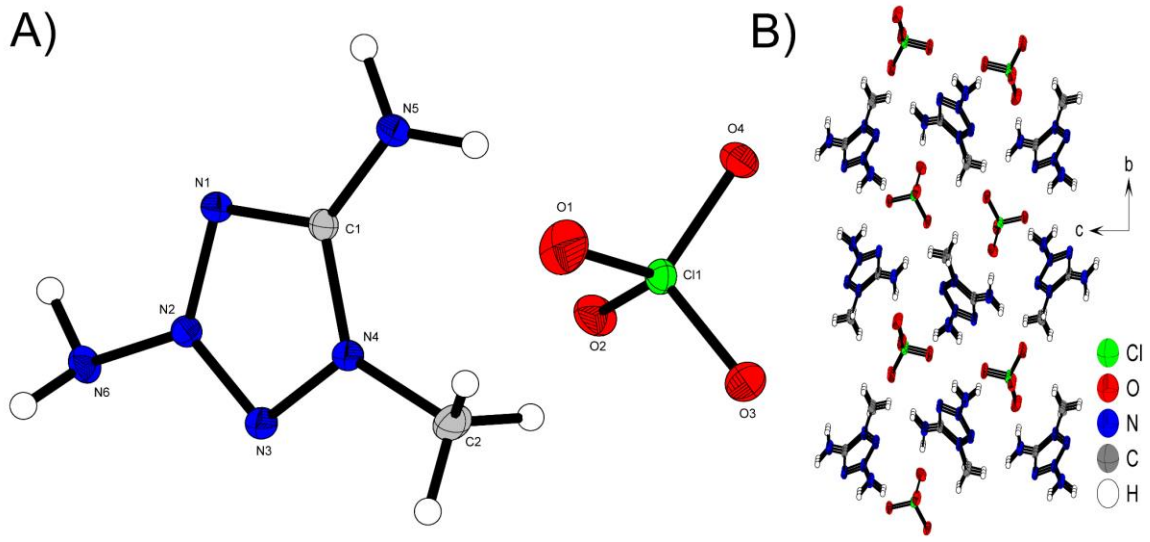

Figure 7. (A) Representation of the molecular unit of 2,5-diamino-4-methyltetrazolium perchlorate (**3b**), showing the atom-labeling scheme. Thermal ellipsoids represent the 50% probability level and hydrogen atoms are shown as small spheres of arbitrary radius. Selected bond distances [Å] and angles [°]: C1–N5 1.337(2), N2–N6 1.379(2), C2–N4 1.454(2), C1–N4–C2 129.2(2), H5A–O3 2.15(2), H5B–O2 2.26(3), H6A–O4 2.16(2) H6B–O2 2.25(2), N5–H5A–O3 163.9(2), N5–H5B–O2 165(2), N6–H6B–O4 168(2), N6–H6B–O2 149(2); (B) 3D layer pattern of **3b** along the *a* axis.

Due to the low polarization of the protons of the methyl group, they do not participate in the formation of intermolecular interactions (Figure 7).

Compound **3c** crystallizes in the orthorhombic space group $P2_12_12_1$ and comes up with a density of 1.447 g cm^{-3} at 298 K. Thus, **3c** is the least dense, energetic compound in the study as a whole. The anionic azide moiety is almost linear (N7–N8–N9 178.1(5)°) and coordinated by four cations, which form strong intramolecular interactions. As in the structures of **3a** and **3b** only the more polarized protons of the amino groups act as action site (Figure 8).

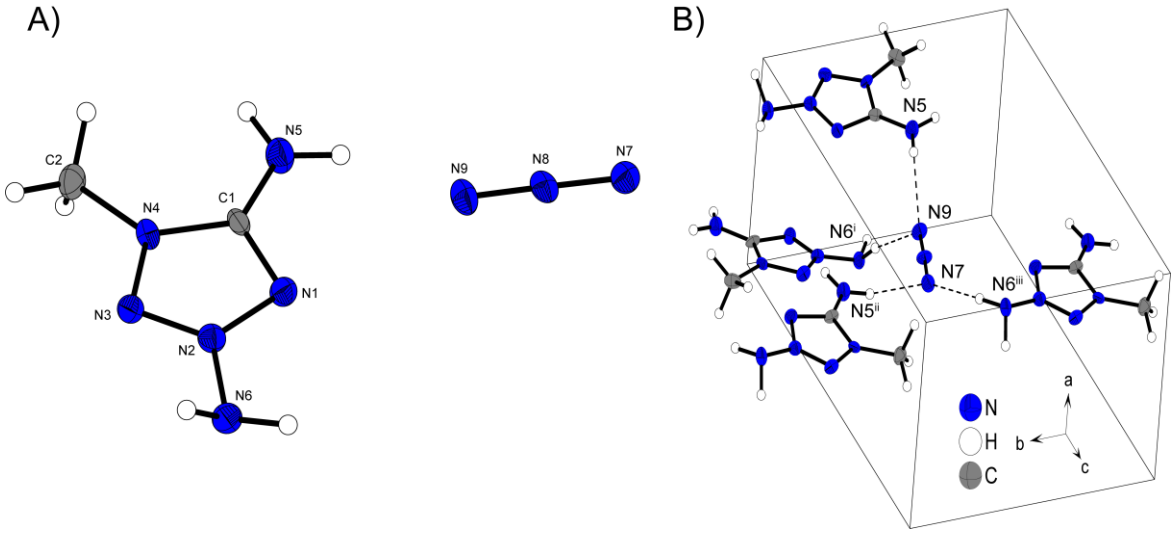

Figure 8. (A) Representation of the molecular unit of 2,5-diamino-4-methyltetrazolium azide (**3c**), showing the atom-labeling scheme. Thermal ellipsoids represent the 50% probability level and hydrogen atoms are shown as small spheres of arbitrary radius. Selected bond distances [Å] and angles [°]: C1–N5 1.310(6), N2–N6 1.366(6), N4–C2 1.468(7), N7–N8 1.181(6), N8–N9 1.168(6), H5B–N9 2.156(4), N5–N9 2.947(6), H6B^{i}–N9 1.97(9), N6^{i}–N9 2.953(7), H5A^{ii}–N7 2.048(4), N5^{ii}–N7 2.912(6), H6A^{iii}–N7 1.96(7), N6^{iii}–N7 2.889(6), N7–N8–N9 178.1(5); (B) embedding of the azide anion and representation of the main amine–azide interactions. Symmetry codes: i: 0.5 + *x*, 0.5 − *y*, 1 − *z*; ii: 1 − *x*, 0.5 + *y*, 0.5 − *z*; iii: 1 − *x*, −0.5 + *y*, 0.5 − *z*.

Compound **4b** crystallizes in the monoclinic space group $P2_1/n$ and has a density of 1.713 g cm^{-3} recalculated to 298 K. The BTO^{2-} di-anion is presented as expected from other ionic derivatives as a planar bis-heterocycle with the two oxygen functions being in the same plane (N11–C2–C2^{i}–N11^{i} 180.0(5)°, O1–N8–C2–N11 179.7(3)°, O1–N8–N9–N10 179.5(3)°).[28-29] The N–NH_2 and C–NH_2 distances are all in the range between single and double bonds with C1–N7 being the shortest one (C1–N7 1.329(4) Å). Compared to the precursor compounds **4** and **4a**, the N-amino group N6 seems to be sp^2 hybridized as N7. Having a closer look at the intermolecular interactions, it becomes clear that the orientation of the protons' origins from the performed interactions to O1 and N4. Therefore, the

direction of the amino protons results from the crystal packing of the compound and not from the different hybridization. A complex network of interactions is formed in which short and thus strong hydrogen bridges occur. Many of these hydrogen bonds have a length D–H···A of less than 2.00 Å (O1–H5A 1.91(4) Å, O1–H5B 1.89(4) Å, O1–H6A 1.92(5) Å, N10–H7B 1.93(6) Å) or slightly more (H6B–N4 2.41(5) Å, N10–H7A 2.39(4) Å) and are formed by all protons of the amino groups to the oxygen atoms of the anion unit as well as to N4 of a neighbouring cation unit and N10 of the BTO anion, which has the highest interaction affinity there (Figure 9).

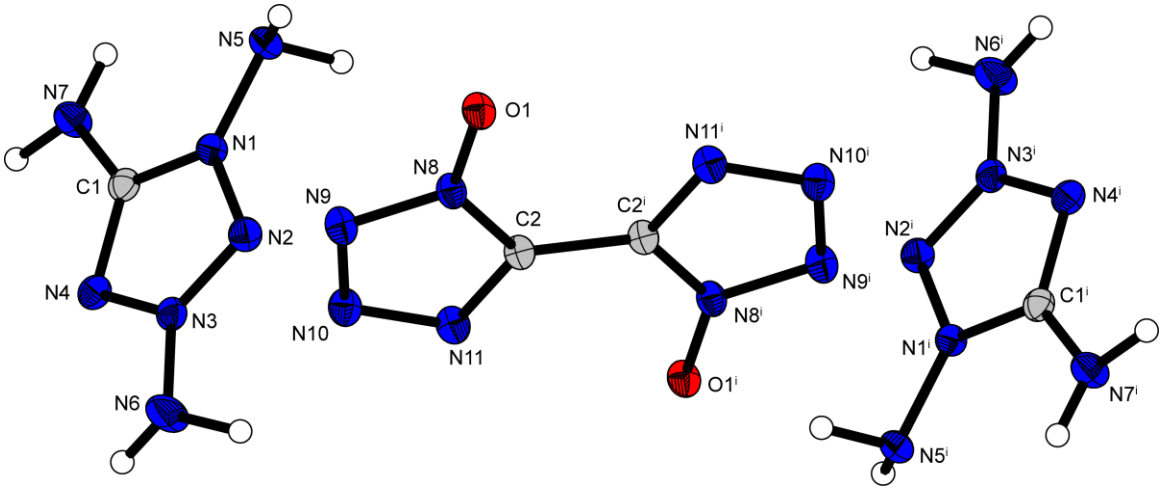

Figure 9. Representation of the molecular unit of di(1,3,5-triaminotetrazolium)-5,5′-bistetrazole-1,1′-diolate (**4b**), showing the atom-labeling scheme. Thermal ellipsoids represent the 50% probability level and hydrogen atoms are shown as small spheres of arbitrary radius. Selected bond distances [Å] N1–N5 1.390(4), N3–N6 1.365(5), C1–N7 1.329(4), O1–N8 1.311(4), O1–H5A 1.91(4), O1–H5B 1.89(4), O1–H6A 1.92(5), N4–H6B 2.41(5), N10–H7B 1.93(6) and angles [°]: N2–N3–N4 117.7(3), C1–N4–N3 101.4(3), O1–H5A–N5 174(3), O1–H5B–N5 162(4), O1–H6A–N6 152(3), N4–H6B–N6 176(3), N7–H7B–N10 173(3). Symmetry codes i: 1 − *x*, −*y*, 2 − *z*.

8.2.3 NMR Spectroscopy

All compounds were intensively studies by multinuclear NMR spectroscopy. The isomeric purity of 2,5-DAT (**1**) could be easily guaranteed by ^{1}H NMR spectroscopy, since two signals at 7.38 ppm and 5.83 ppm are obtained, which are clearly different from those of 1,5-DAT (δ (ppm) = 6.38, 6.36). The signal for the carbon of **1** appears at 165.7 ppm. For protonated compounds **2a** and **2b** the proton signals for all five protons of the tetrazole occur as one broad signal because of the mixing due to the higher acidity. As expected, the methyl signals for

compounds **3**–**3c** show singlet signals in the range of 3.80 ppm in the ^{1}H NMR and 34.5 ppm in the ^{13}C NMR spectrum.[30] The triaminotetrazolium derivatives **4**, **4a** and **4b** show three different resonances for the three different amino groups in the ^{1}H NMR.

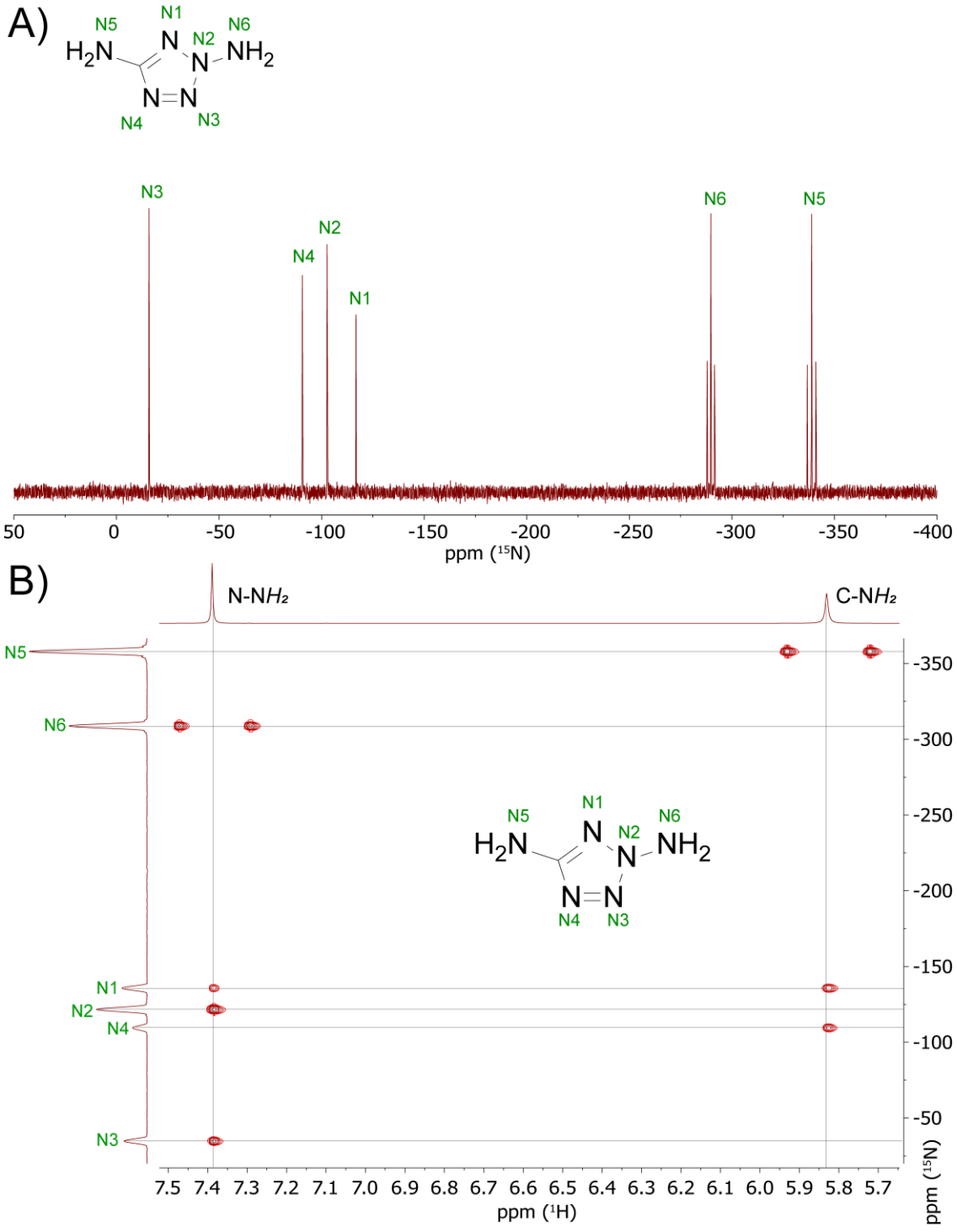

Figure 10. (A) Proton coupled ^{15}N NMR spectrum with signals given in ppm with respect to $MeNO_2$. (B) ^{15}N–^{1}H HMBC spectrum of **1**. Both spectra were measured in DMSO-D_6.

The resonanes for the N–NH_2 are broader then for the C–NH_2, which occurs sharp. For both, the methylated and aminated compounds (**3**–**3c**, **4**–**4b**) the carbon signals of the tetrazoles appear about 10 ppm high-field-shifted compared to 2,5-DAT (**1**).

Compound **1** was further analyzed using proton coupled ^{15}N spectroscopy (Figure 10). The correct assignment could be made by the comparison with the ^{15}N shifts of 2-aminotetrazole, 1,5 diaminotetrazole and by the recording of a ^{15}N–^{1}H-HMBC spectrum.[10] The signals for the tetrazole nitrogen atoms are observed in the range of −15.8 ppm (N3) to −116.7 ppm (N1). The two nitrogen atoms representing the amino groups are detectable as triplets due to their ^{1}J coupling with the respective NH protons. They appear at higher fields at −289.7 (t, N–NH_2, ^{1}J = 72.3 Hz) and −338.8 (t, C–NH_2, ^{1}J = 84.2 Hz).

8.2.4 Physico-chemical Properties

2,5-Diaminotetrazole (**1**) has an onset decomposition temperature of 180 °C, which is in the same range as for its isomer 1,5-DAT (Figure 11). Additionaly, a melting point at 120 °C is observed. Its sensitivity data were measured to be 160 N for friction sensitivity, 5 J for impact sensitivity and 0.2 J for electrical discharge, making it less sensitive than all other compounds within this study. Protonation of **1** with HNO_3 decreases the thermal resistance, with **2a** decomposing already at 112 °C. However, the detonation velocity is significantly increased compared to 2,5 DAT. The EXPLO5 calculations result in a detonation velocity of 9127 m s^{-1} for **2a**, whereas it is calculated to only 8788 m s^{-1} for **1**. For perchlorate derivative **2b**, the same trend is observed as the decomposition decreases to T_{dec} = 115 °C. The detonation velocity is also higher then for the parent compound **1** and reaches a value slightly above 9000 m s^{-1}.

Compared with the protonated nitrate and perchlorate species **2a** and **2b**, the decomposition temperature for the respective methylated salts increases significantly to 203 °C for the 2,5-diamino-4-methyltetrazolium nitrate (**3a**) and 155 °C for the 2,5-diamino-4-methyltetrazolium perchlorate (**3b**).

Table 1. Physic-chemical properties of investigated energetic materials **1**, **2a**–**2b**, **3a**–**3c**, **4b** and 1,5-DAT.

	1	**2a**	**2b**	**3a**	**3b**	**3c**	**4b**	1,5-DAT
M [g mol^{-1}]	100.1	163.1	200.6	177.1	213.6	157.1	400.3	100.1
IS [J][a]	5	3	2	3	2	4	2	40
FS [N][b]	160	60	20	120	10	80	30	360
ESD [J][c]	0.20	0.13	0.10	0.14	0.10	0.07	0.08	>0.5
ρ [g cm^{-3}][d]	1.577	1.737	1.870	1.649	1.770	1.447	1.713	1.569
N [%][e]	84.0	60.1	41.9	55.4	39.2	80.2	77.0	84.0
Ω [%][f]	−48.0/−63.9	−4.9/ −14.7	−4.3/ −13.0	−22.6/ −40.7	−7.5/ −22.5	−56.0/ −76.4	−32.0/ −48.0	−48.0/ −63.9
T_{melt}/T_{dec} [°C][g]	125/180	-/112	-/115	-/203	60/155	125/165	-/170	187
$\Delta_f H°$ [kJ mol^{-1}][h]	345.2	202.1	256.8	264.0	230.0	685.3	1678.1	332.4
$\Delta_f U°$ [kJ mol^{-1}][i]	357.5	220.7	276.6	285.1	252.3	705.1	1722.7	344.8
EXPLO5 V6.05.02								
$-\Delta_{Ex}U°$ [kJ kg^{-1}][j]	3985	5346	5976	5356	5433	4913	5515	3862
T_{det} [K][k]	2628	3542	4289	3376	3800	3005	3492	2580
V_0 [L kg^{-1}][l]	918	918	854	919	847	919919	890	918
P_{CJ} [kbar][m]	265	333	356	284	307	236	333	258
V_{det} [m s^{-1}][n]	8788	9127	9065	8714	8489	8440	9416	8698

a Impact sensitivity (BAM drophammer (1 of 6)). b Friction sensitivity (BAM friction tester (1 of 6)). c Electrostatic discharge device (OZM research). d From X-Ray diffraction analysis recalculated to 298 K. e Nitrogen content. f Oxygen balance with respect to CO/CO_2. g Melting/decomposition temperature (DTA or DSC; β = 5 °C min^{-1}). h Calculated enthalpy of formation. i Calculated energy of formation. j Energy of explosion. k Detonation temperature. l Volume of detonation products (assuming only gaseous products). m Detonation pressure at Chapman–Jouguet point. n Detonation velocity.

However, the explosive properties decrease significantly due to the methylation and is 400 m s^{-1} (for **3a**) and 650 m s^{-1} (for **3b**) less compared to the respective protonated compounds (Table 1).

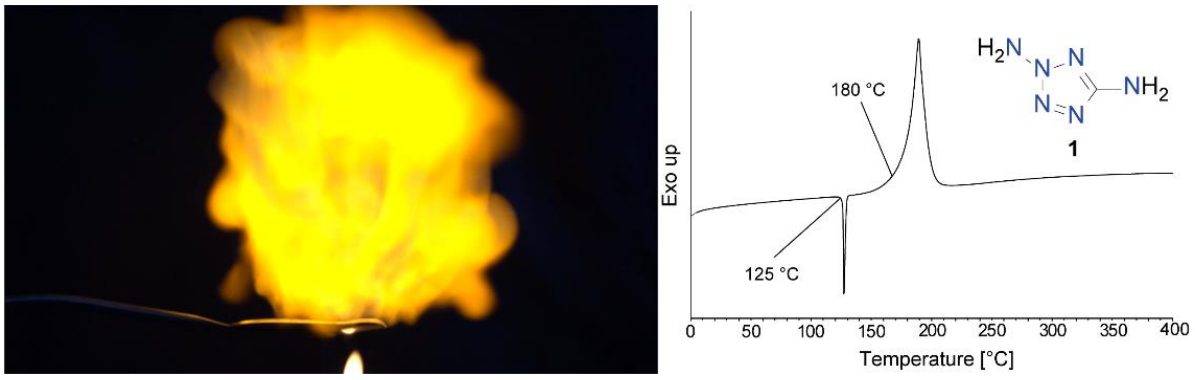

Figure 11. Flame test of approximately 20 mg 2,5-DAT (**1**) (left) and DSC curve of 1 with a heating rate of 5 °C min^{-1} (right).

The impact sensitivity in comparison to **2a** and **2b** with the respective methylated compounds **3a** and **3b** gives the same values (IS (**2a**, **3a**) = 3 J, IS (**2b**, **3b**) = 2 J). The friction sensitivities, however, vary considerably, since the value for the methylated nitrate **3a** decreases significantly to 120 N, but even increases for the methylated perchlorate **3b** to 10 N. Due to the azide moiety included in **3c**, an extremely high heat of formation could be calculated ($\Delta_f H°$ = 685.3 kJ mol^{-1}). However, because of the low density, compound **3c** has the lowest calculated performance data (P_{CJ} = 236 kbar; V_{det} = 8440 m s^{-1}) of all investigated energetic compounds. **3c** has sensitivities in the range of PETN (IS = 4 J, FS = 80 N), decomposes at 165 °C, while melting at 125 °C. 1,3,5-Triaminotetrazolium derivative **4b** shows relatively high sensitivity toward all tested external stimuli (IS = 2 J, FS = 30 N, ESD = 80 mJ). It decomposes sharply at 170 °C and has therefore the same thermal stability then 1,5-diaminotetrazolium 1-hydroxy-5,5′-bistetrazol-1′-olate.[28] The enormously high enthalpy of formation of 1678.1 kJ mol^{-1} with a room temperature density of 1.713 g cm^{-3} results in an extremely high calculated detonation velocity of 9416 m s^{-1}, which is significantly higher than that of RDX. Compared with 1,4,5-triaminotetrazolium nitrotetrazolate-2-olate (**C**), which contains a differently substituted isomer of the 1,3,5-TAT cation, **4b** achieves significantly higher decomposition temperature and explosion parameters, with lower friction and impact sensitivity. The main reason for this, however, seems to be the BTO anion, which, as expected, provided the desired stability and performance properties. Nevertheless, it should be noted that thermally robust explosives can be obtained with triaminotetrazolium cations in combination with suitable energetic anions.

8.3 Conclusion

Summarized, we report 2,5-diaminotetrazole as a missing aminotetrazole scaffold for the design of new energetic materials, with many promising properties. With a nitrogen content of 84%, a stable tetrazole backbone with a good enthalpy of formation coupled with functionalizable amino sites, 2,5-DAT, like its better-studied isomer 1,5-DAT, offers the best conditions for energetic functionalization. By HOSA amination of 5-aminotetrazole and separation of 1,5-DAT from mixture, 2,5-DAT

(**1**) was synthesized for the first time in gram-scale quantities and characterized as a respectable explosive with energetic properties (IS = 5 J, FS = 160 N, V_{det} = 8788 m s^{-1}) in the range of RDX. Through targeted functionalization, we attempted to further tune the energetic properties. In this context, we focused on the protonation, methylation and amination of the tetrazole backbone and further investigated the obtained trisubstituted tetrazolium derivatives with different energetic anions, such as nitrate and perchlorate. The energetic performance could be increased by protonation and the thermal stability by methylation. The amination produces the enormously endothermic 1,3,5-tetrazolium ($\Delta_f H°$ = 1140.3 kJ mol^{-1}) moiety, which has been characterized as 5,5′-bistetrazole-1,1′-diolate salt **4b**. Although the compound has a convincing detonation velocity of over 9400 m s^{-1}, unfortunately the sensitivity toward impact and friction is unacceptable for further applications. Nevertheless, the 2,5 diaminotetrazole derivatives investigated in this study showed they are promising building blocks for energetic materials and that greater research efforts should be devoted to study these compounds. Further, reactions used with 1,5-DAT such as nitration, protection, azo coupling, oxidation or complexation might offer great opportunities for this scaffold and could yield very interesting energetic materials.

8.4 Acknowledgement

For financial support of this work by Ludwig-Maximilian University (LMU), the Office of Naval Research (ONR) under grant no. ONR N00014-19-1-2078 and the Strategic Environmental Research and Development Program (SERDP) under contract no. W912HQ19C0033 are gratefully acknowledged. We thank Prof. Konstantin Karaghiosoff for NMR measurements.

8.5 References

[1] a) O. T. O'Sullivan, M. J. Zdilla, *Chem. Rev.* **2020**, *120*, 5682–5744; b) J.-D. Lin, F. Chen, J.G. Xu, F.-K. Zheng, N. Wen, *ACS Appl. Nano Mater.* **2019**, *2*, 5116–5124; c) Z.-M. Li, Y.-Q. Xu, C. Wang, G.-R. Lei, R. Zhang, L. Zhang,

J.-H. Chen, J.-G. Zhang, T.-L. Zhang, Q.-Y. Wang, *J. Mater. Chem. A* **2022**, *10*, 2795–2799.

[2] Y.-H. Joo, J. M. Shreeve, *Org. Lett.* **2008**, *10*, 4665–4667.

[3] Y. Li, Y. Yang, Z. Yi, D. Song, Y. Cheng, Y. Li, *Chem. Eng. J.* **2021**, *413*, 127442.

[4] S. B. Kim, K. J. Kim, M. H. Cho, J. H. Kim, K. T. Kim, S. H. Kim, *ACS Appl. Mater. & Interfaces* **2016**, *8*, 9405–9412.

[5] D. M. Smith, T. D. Manship, D. G. Piercey, *ChemPlusChem* **2020**, *85*, 2039–2043.

[6] D. D. Ford, S. Lenahan, M. Jörgensen, P. Dubé, M. Delude, P. E. Concannon, S. R. Anderson, K. D. Oyler, G. Cheng, N. Mehta, J. S. Salan, *Org. Process Res. Dev.* **2015**, *1*, 673–680.

[7] T. M. Klapötke, D. G. Piercey, N. Mehta, K. D. Oyler, M. Jorgensen, S. Lenahan, J. S. Salan, J. W. Fronabarger, M. D. Williams, *Z. Anorg. Allg. Chem.* **2013**, *639*, 681–688.

[8] J. W. Fronabarger, M. D. Williams, W. B. Sanborn, J. G. Bragg, D. A. Parrish, M. Bichay, *Propellants Explo. Pyrotech.* **2011**, *36*, 541–550.

[9] T. Küblböck, G. Angé, G. Bikelytė, J. Pokorná, R. Skácel, T. M. Klapötke, *Angew. Chem. Int. Ed.* **2020**, *59*, 12326–12330.

[10] N. Szimhardt, M. H. H. Wurzenberger, L. Zeisel, M. S. Gruhne, M. Lommel, J. Stierstorfer, *J. Mater. Chem. A* **2018**, *6*, 16257–16272.

[11] N. Szimhardt, M. H. H. Wurzenberger, P. Spieß, T. M. Klapötke, J. Stierstorfer, *Propellants Explo. Pyrotech.* **2018**, *43*, 1203–1209.

[12] T. M. Klapötke, D. G. Piercey, J. Stierstorfer, *Eur. J. Inorg. Chem.* **2012**, *2012*, 5694–5700.

[13] Y. Xu, Y. Wang, Y. Zhong, G. Lei, Z. Li, J. Zhang, T. Zhang, *Inorg. Chem.* **2021**, *60*, 5100–5106.

[14] C. Jin, Y. Liu, L. Wang, W. Zhang, T. Zhang, J. Zhu, *RSC Adv.* **2020**, *10*, 30069–30076.

[15] Z. Li, Y. Yuan, Y. Zhang, L. Liu, S. Zhang, *Z. Anorg. Allg. Chem.* **2017**, *643*, 647–652.

[16] Y. Qian, Z. Han, Y. Zhang, Z. Du, Y. Zhao, Y. Yang, J. Zhang, *J. Heterocycl. Chem.* **2016**, *53*, 651–657.

[17] J.-G. Zhang, J.-Y. Li, Y. Zang, Y.-J. Shu, T.-L. Zhang, L. Yang, Philip P. Power, *Z. Anorg. Allg. Chem.* **2010**, *636*, 1147–1151.

[18] R. Raap, *Can. J. Chem.* **1969**, *47*, 3677–3681.

[19] P. N. Gaponik, S. V. Voitekhovich, A. S. Lyakhov, V. E. Matulis, O. A. Ivashkevich, M. Quesada, J. Reedijk, *Inorg. Chim. Acta* **2005**, *358*, 2549–2557.

[20] Y.-H. Joo, B. Twamley, S. Garg, J. M. Shreeve, *Angew. Chem. Int. Ed.* **2008**, *47*, 6236–6239.

[21] T. M. Klapötke, F. A. Martin, J. Stierstorfer, *Chem. Eur. J.* **2012**, *18*, 1487–1501.

[22] L. Liu, C. He, C. Li, Z. Li, *J. Chem. Crystallogr.* **2012**, *42*, 816–823.

[23] F. Li, X. Cong, Z. Du, C. He, L. Zhao, L. Meng, *New J. Chem.* **2012**, *36*, 1953–1956.

[24] J. C. Galvez-Ruiz, G. Holl, K. Karaghiosoff, T. M. Klapötke, K. Loehnwitz, P.Mayer, H. Noeth, K. Polborn, C. J. Rohbogner, M. Suter, J. J. Weigand, *Inorg. Chem.* **2005**, *44*, 5192–5192.

[25] N. Fischer, T. M. Klapötke, J. Stierstorfer, *Journal of Energetic Materials* **2011**, *29*, 61–74.

[26] S. R. Yocca, M. Zeller, E. F. C. Byrd, D. G. Piercey, *J. Mater. Chem. A* **2022**, *10*, 1876–1884.

[27] A. S. Lyakhov, P. N. Gaponik, S. V. Voitekhovich, *Acta Crystallogr. Sect. C: Cryst. Struct. Commun.* **2001**, *57*, 185–186.

[28] N. Fischer, T. M. Klapötke, M. Reymann, J. Stierstorfer, *Eur. J. Inorg. Chem.* **2013**, 2167–2180.

[29] Y. Shang, B. Jin, R. Peng, Z. Guo, Q. Liu, J. Zhao, Q. Zhang, *RSC Adv.* **2016**, *6*, 48590–48598.

[30] N. Szimhardt, M. H. H. Wurzenberger, A. Beringer, L. J. Daumann, J. Stierstorfer, *J. Mater. Chem. A* **2017**, *5*, 23753–23765.

8.6 Supporting Information

8.6.1 Experimental Procedure

All chemicals and solvents were employed as received (Sigma-Aldrich, Fluka, Acros). ^{1}H, ^{13}C, ^{14}N and ^{15}N NMR spectra were recorded using a JEOL Eclipse 270, JEOL EX 400 or a JEOL Eclipse 400 instrument. The chemical shifts quoted in ppm in the text refer to typical standards such as tetramethylsilane (^{1}H, ^{13}C) and nitromethane (^{14}N and ^{15}N). To determine the dehydration, melting and decomposition temperatures of the described compounds an OZM Research DTA 552-Ex instrument (heating rate 5 °C min^{-1} in the range of 25–400 °C) was used. Infrared spectra were measured with pure samples on a Perkin-Elmer BXII FT-IR system with a Smith DuraSampler IR II diamond ATR unit. Determination of the carbon, hydrogen and nitrogen contents were carried out by combustion analysis using an Elementar Vario El (nitrogen values determined are often lower than the calculated ones due to their explosive behavior). Sensitivities toward impact (IS) and friction (FS) were determined according to the UN Recommendations on the Transport of Dangerous Goods (ST/SG/AC.10/11/Rev.7) using a BAM drop hammer and a BAM friction apparatus by applying the 1 of 6 method.[S1] All energetic compounds were tested for sensitivity towards electrical discharge using an Electric Spark Tester ESD 2010 EN from OZM. Energetic properties have been calculated with the EXPLO5 6.02 computer[S2] code using the RT converted X-ray density and calculated solid state heats of formation.

CAUTION! *All compounds described herein are potentially explosive energetic materials, which show partly increased sensitivities toward various stimuli (e.g. elevated temperatures, impact, friction or electrostatic discharge). Therefore, proper security precautions (safety glass, face shield, earthed equipment and shoes, leather coat, Kevlar gloves, Kevlar sleeves and ear plugs) have to be used in the synthesis and handling of the described compounds.*

2,5-Diaminotetrazole (**1**)[S3-S4]

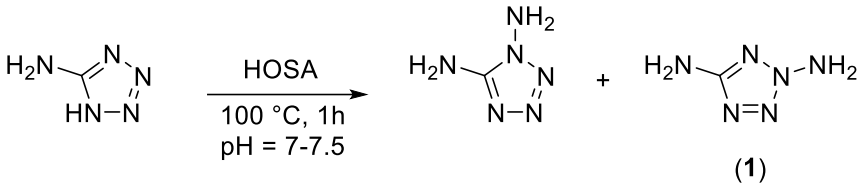

5-Aminotetrazole monohydrate (26.0 g, 252 mmol, 1.0 eq) and trisodium phosphate dodecahydrate (20.0 g, 52.6 mmol, 0.21 eq) were dissolved in water (200 mL). The pH was adjusted to 7 by the addition of sodium carbonate and the solution was brought to a boil. Hydroxylamine-*O*-sulfonic acid (HOSA, 100 g, 0.88 mol, 3.5 eq) dissolved in a minimum amount of ice water (150 mL) was added dropwise over the period of 1 h. The pH was maintained between 7 and 7.5 by the periodic addition of aqueous sodium carbonate. The volume of the reaction mixture was kept at around 400 mL by the addition of water. After the addition the solution was further boiled for 20 min. The solvent was removed under reduced pressure and the solid residue was extracted with hot ethanol (2 x 500 mL). The ethanol was evaporated and the crude product was suspended in water (35 mL) and filtered yielding pure 1,5-diaminotetrazole (9.10 g, 91.0 mmol). The residue obtained from the filtrate was evaporated under reduced pressure and suspended in ethyl acetate (400 mL), heated to reflux and filtered while still hot to remove even more 1,5-diaminotetrazole (2.50 g, 25.0 mmol). The solvent was removed under reduced pressure and the crude product containing an isomeric mixture of mainly diaminotetrazoles was triturated using cold ethanol (15 mL) to remove other byproducts. The obtained solid, containing a pure isomeric mixture of diaminotetrazoles was loaded on silica and purified by column chromatography using Etic/*i*-Hexanes (4:1) as eluent (R_f(1,5-DAT) = 0.10; R_f(2,5-DAT) = 0.40) to yield pure 2,5-diaminotetrazole (**1**) (4.00 g, 40.0 mmol, 16%) as slightly beige powder.

The total yield for the amination of 5-aminotetrazole to diaminotetrazole is 62% (46% of 1,5-diaminotetrazole and 16% of 2,5-diaminotetrazole (**1**)).

DTA (5 °C min^{-1}): 125 °C (endo), 180 °C (exo); Sensitivities: BAM drophammer: 5 J; friction tester: 160 N; ESD: 200 mJ (at grain size 100-500 µm); Elem. Anal. ($C_3H_4N_8$ 100.09 g mol^{-1}) calc.: C 12.00, H 4.03, N 83.97 %; found: C 12.05, H 4.10,

N 83.81 %; IR (ATR) $\tilde{\nu}$ (cm^{-1}) = 3368 (s), 3307 (vs), 3204 (vs), 2730 (w), 2210 (w), 2002 (wnn), 1744 (w), 1615 (vs), 1557 (vs), 1447(s), 1394 (s), 1245 (s), 1201 (s), 1101 (m), 1074 (s), 989.33 (vs), 817 (s), 755 (s), 647(s); ^{1}H NMR (DMSO-D_6, 400 MHz, ppm) δ = 7.38 (s, 2H), 5.83 (s, 2H); ^{13}C NMR (DMSO-D_6, 101 MHz, ppm) δ = 165.7; ^{15}N NMR (DMSO-D_6, 41 MHz, ppm) δ = −15.8 (s, N3), −90.6 (s, N4), −102.7 (s, N2), −116.7 (s, N1), −289.7 (t, N-*N*H_2, *J* = 72.3 Hz), −338.8 (t, C-*N*H_2, *J* = 84.2 Hz); HRMS (EI) m/z: [M+] Calcd for CH_5N_6 101.0570, found: 101.0574.

2,5-Diamino-tetrazolium nitrate (**2a**)

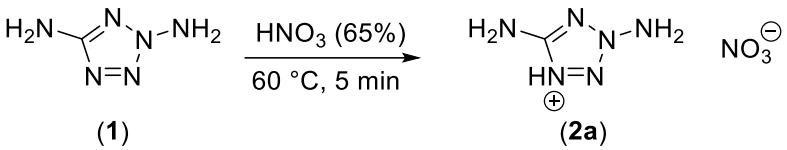

(**1**) (**2a**)

1 (1.00 g, 10.0 mmol, 1.0 eq) and of concentrated HNO_3 (1.5 mL, 65%) were gently heated to give a clear solution. After addition of Et_2O (20 mL) to the solution, a white precipitate was formed. The precipitate was filtered and washed with small quantities of Et_2O to obtain **2a** after recrystallization from EtOH as colorless crystals (1.42 g, 8.71 mmol, 87%).

DTA (5 °C min^{-1}): 112 °C (exo); Sensitivities: BAM drophammer: 3 J; friction tester: 60 N; ESD: 130 mJ (at grain size 100–500 µm); Elem. Anal. ($CH_5N_7O_3$, 163.10 g mol^{-1}): calcd: C 7.36, H 3.09, N 60.12 %; found: C 8.46, H 3.38, N 60.08 %; IR (ATR) $\tilde{\nu}$ (cm^{-1}) = 3424 (s), 3310 (s), 3212 (s), 3115 (s), 2646 (w), 2449 (w), 1667 (s), 1563 (w), 1535 (w), 1385 (vs), 1299 (s), 1249(s), 1223 (w), 1203 (m), 1160 (s), 1127 (m), 1073 (s), 1044 (m), 1026 (m), 993 (vw), 955 (m), 840 (w), 817 (vw), 755 (w), 726 (m), 650 (m), 635 (vw); ^{1}H NMR (DMSO-D_6, 400 MHz, ppm) δ = 7.38 (br s, 5H); ^{13}C NMR (DMSO-D_6, 101 MHz, ppm) δ = 165.7; ^{14}N NMR (DMSO-D_6, 29 MHz, ppm) δ = −9.

2,5-Diamino-tetrazolium perchlorate (**2b**)

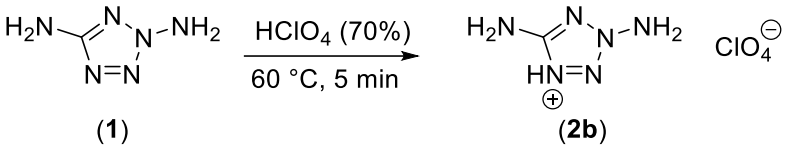

(**1**) (**2b**)

1 (1.00 g, 10.0 mmol, 1.0 eq) and of $HClO_4$ (1.5 mL, 70%) were gently heated to give a clear solution. This solution was washed cold with Et_2O (5 x 10 mL). The resulting aqueous phase was layered with Et_2O (20 mL) and left for crystallization. After 2 weeks, large colorless plates formed, which were filtered and washed with Et_2O to yield **2b** (1.86 g, 9.28 mmol, 93%).

DTA (5 °C min^{-1}): 115 °C (exo); Sensitivities: BAM drophammer: 2 J; friction tester: 20 N; ESD: 100 mJ (at grain size 100–500 µm); Elem. Anal. ($CH_5N_6O_4Cl$, 200.54 g mol^{-1}): calcd: C 5.99, H 2.51, N 41.91 %; found: C 6.23, H 2.51, N 41.65 %; IR (ATR) $\tilde{\nu}$ (cm^{-1}) = 3424 (s), 3310 (s), 3212 (s), 3115 (s), 2646 (m), 2449 (m), 1667 (vs), 1563 (m), 1535 (m), 1385 (vs), 1299 (vs), 1249(w), 1223 (w), 1203 (vw), 1160 (m), 1127 (w), 1074 (m), 1045 (m), 1026 (m), 994 (w), 955 (vw), 840 (s), 755 (m), 650 (s), 635 (w); ^1H NMR (DMSO-D_6, 400 MHz, ppm) δ = 7.30 (br s, 5H); ^{13}C NMR (DMSO-D_6, 101 MHz, ppm) δ = 164.7.

2,5-Diamino-4-methyl-tetrazolium iodide (**3**)

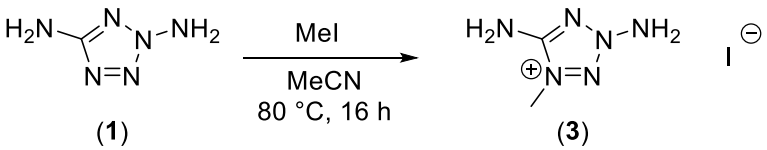

(**1**) (**3**)

To a solution of **1** (1.50 g, 15.0 mmol, 1.0 eq) in of MeCN (50 mL) was added an excess of MeI (6.40 mL, 90.0 mmol, 6.0 eq) and the mixture was refluxed for 16 h. The color of the reaction mixture turned from colorless to deep red. Colorless crystals started to separate from the reduced cold solution after few days and were filtered to yield **3** without further purification (2.54 g, 10.5 mmol, 70%).

DTA (5 °C min^{-1}): 139 °C (endo), 151 °C (exo); Elem. Anal. ($C_2H_7IN_6$, 242.02 g mol^{-1}): calcd: C 9.93, H 2.92, N 34.72 %; found: C 9.65, H 2.99, N

32.57 %; IR (ATR) $\tilde{\nu}$ (cm^{-1}) = 3287 (s), 3173 (s), 3096 (vs), 2710 (m), 1647 (vs), 1579 (m), 1526 (w), 1392 (m), 1368 (w), 1245 (w), 1404 (s), 1283 (s), 1205 (m), 1109 (m), 1031 (m), 926 (s), 887 (m), 710 (m), 676 (m), 630 (m), 551 (w); ^{1}H NMR (DMSO-D_6, 400 MHz, ppm) δ = 9.36 (s, 2H), 8.15 (s, 2H), 3.80 (s, 3H); ^{13}C NMR (DMSO-D_6, 101 MHz, ppm) δ = 157.0, 34.2.

2,5-Diamino-4-methyl-tetrazolium nitrate (**3a**)

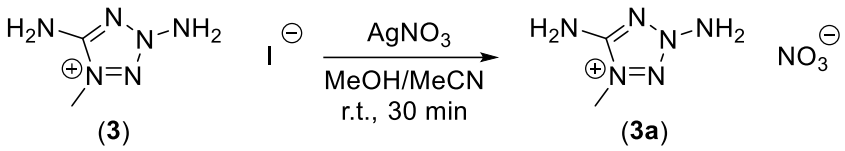

(**3**) (**3a**)

To a solution of **3** (1.00 g, 4.13 mmol, 1.0 eq) in a mixture of MeOH/MeCN (15 mL, 1:1) was added $AgNO_3$ (0.73 g, 4.30 mmol, 1.05 eq) dissolved in water (5 mL) and the resulting mixture was stirred for 30 min in the dark. After the precipitated AgI was removed, the solvent were evaporated *in vacuo* and the residue was recrystallized from MeOH to yield pure **3a** (0.717 g, 4.05 mmol, 98%) as colorless solid.

DTA (5 °C min^{-1}): 203 °C (exo); Sensitivities: BAM drophammer: 3 J; friction tester: 120 N; ESD: 140 mJ (at grain size 100–500 µm); Elem. Anal. ($C_2H_7N_7O_3$, 177.13 g mol^{-1}): calcd: C 13.56, H 3.98, N 55.36 %; found: C 12.74, H 3.93, N 53.67 %; IR (ATR) $\tilde{\nu}$ (cm^{-1}) = 3272(s), 3184(s), 3143 (s), 3000 (vw), 1656 (s), 1493 (s), 1439 (m), 1418 (m), 1335 (vs), 1296 (vs), 1232 (vs), 1106 (m), 1073 (w), 1040 (s), 975 (m), 857 (m), 826 (s), 724 (m), 679 (m), 622 (m), 569 (s), 511 (m); ^{1}H NMR (DMSO-D_6, 400 MHz, ppm) δ = 9.38 (br s, 2H), 8.18 (s, 2H), 3.79 (s, 3H); ^{13}C NMR (DMSO-D_6, 101 MHz, ppm) δ = 157.0, 34.0; ^{14}N NMR (DMSO-D_6, 29 MHz, ppm) δ = −12.

2,5-Diamino-4-methyl-tetrazolium perchlorate (**3b**)

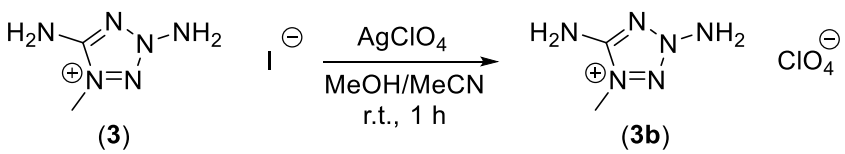

(**3**) (**3b**)

To a solution of **3** (0.29 g, 1.20 mmol, 1.0 eq) in a mixture of MeOH/MeCN (5 mL, 1:1) was added $AgClO_4$ (0.26 g, 1.26 mmol, 1.05 eq) dissolved in water (2 mL) and the resulting mixture was stirred for one hour in the dark. After the precipitated AgI was removed, the solvent was evaporated *in vacuo* and the residue was recrystallized from MeOH to yield pure **3b** (0.20 g, 1.13 mmol, 94%) as colorless crystalline solid.

DTA (5 °C min^{-1}): 60 °C (endo), 155 °C (exo); Sensitivities: BAM drophammer: 2 J; friction tester: 10 N; ESD: 100 mJ (at grain size 100–500 µm); Elem. Anal. ($C_2H_7N_6O_4Cl$, 214.57 g mol^{-1}): calcd: C 11.20, H 3.29, N 39.17 %; found: C 11.01, H 3.42, N 38.87 %; IR (ATR) $\tilde{\nu}$ (cm^{-1}) = 3412(m), 3339(m), 3259(m), 1651(s), 1499(w), 1444(w), 1409(m), 1208(w), 1052(vs), 934(m), 896(m), 817(m), 723(m), 678(m), 620(vs), 527(s), 456(s), 402(m); ^{1}H NMR (DMSO-D_6, 400 MHz, ppm) δ = 9.35 (s, 2H), 8.13 (s, 2H), 3.78 (s, 3H); ^{13}C NMR (DMSO-D_6, 101 MHz, ppm) δ = 156.6, 33.5.

2,5-Diamino-4-methyl-tetrazolium azide (**3c**)

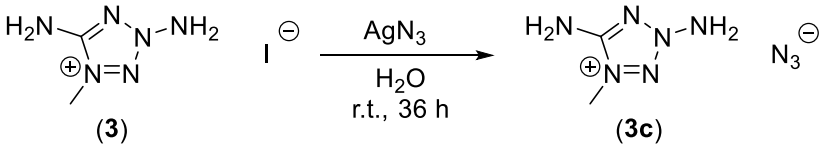

To a solution of **3** (1.00 g, 4.13 mmol, 1.0 eq) in of water (15 mL) was added excess AgN_3 (1.15 g, 7.50 mmol, 1.8 eq) and the resulting mixture was stirred for 36 h in the dark. After the excess AgN_3 and AgI was filtered off, the water was removed and the residue recrystallized from EtOH/Et_2O yielding colorless **3c** (0.62 g, 3.92 mmol, 95%).

DTA (5 °C min^{-1}): 125 °C (endo), 165 °C (exo); Sensitivities: BAM drophammer: 4 J; friction tester: 80 N; ESD: 70 mJ (at grain size 100–500 µm); Elem. Anal. ($C_2H_7N_9$, 157.14 g mol^{-1}): calcd: C 15.29, H 4.49, N 80.22 %; found: C 16.21, H 4.42, N 78.26 %; IR (ATR) $\tilde{\nu}$ (cm^{-1}) = 3286 (s), 2960 (s, br), 2939 (s, br), 2824 (s), 2166 (w), 2026 (vs), 1663 (vs), 1608 (s), 1516 (s), 1458 (m), 1426 (s), 1343 (w), 1285 (m), 1198 (m), 1099 (m), 1058 (w), 1034 (m), 944 (s), 849 (s), 722 (m), 689 (m), 601 (w), 662(w), 631 (s); ^{1}H NMR (DMSO-D_6, 400 MHz, ppm) δ = 9.41 (s, 2H),

8.22 (s, 2H), 3.80 (s, 3H); ^{13}C NMR (DMSO-D_6, 101 MHz, ppm) δ = 157.0, 33.9; ^{14}N NMR (DMSO-D_6, 29 MHz, ppm) δ = −134, −279.

1,3,5-Triaminotetrazolium tosylate (**4**)

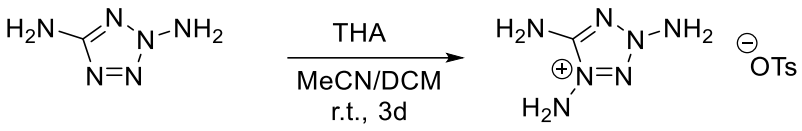

(**1**) (**4**)

Ethyl *O*-*p*-tolylsulfonyl-acetohydroximate (1.54 g, 6.00 mmol, 1.2 eq) was suspended in perchloric acid (60%, 20 mL) and stirred for 2 h. The mixture was poured on ice water (50 mL) and the solution was extracted with dichloromethane (6 x 40 mL) after the ice had melted. The combined DCM solutions were dried over a hydrous sodium sulfate, filtered and added to a solution of 2,5-diaminotetrazole (**1**) (0.50 g, 5.00 mmol, 1.0 eq) in acetonitrile (60 mL). The mixture was stirred for 3 d after which time a turbidity was observed. The solution was evaporated under reduced pressure and recrystallized from methanol (20 mL) to yield triaminotetrazolium tosylate (**4**) (1.32 g, 4.59 mmol, 92%) as slightly orange crystalline blocks.

DTA (5 °C min^{-1}): 198 °C (exo); Elem. Anal. ($C_8H_{13}N_7O_3S$, 287.30 g mol^{-1}): calcd: C 33.45, H 4.56, N 34.13 %; found: C 33.01, H 4.88, N 33.78 %; IR (ATR) $\tilde{\nu}$ (cm^{-1}) = 3174(m), 3024(m), 1682(m), 1602(m), 1551(m), 1497(w), 1424(m), 1159(vs), 1122(vs), 1033(s), 1008(vs), 952(m), 809(s), 681(vs), 657(m), 648(s), 563(vs), 536(s), 490(s), 443(s), 419(s); ^{1}H NMR (DMSO-D_6, 400 MHz, ppm) δ = 9.40 (br s, 2H), 8.10 (s, 2H), 7.48 (d, ^3J = 8.4 Hz, 2H), 7.12 (d, ^3J = 8.5 Hz, 2H), 6.80 (br s, 2H), 2.29 (s, 3H); ^{13}C NMR (DMSO-D_6, 101 MHz, ppm) δ = 155.8, 145.6, 137.7, 128.1, 125.5, 20.8.

1,3,5-Triaminotetrazolium bromide (**4a**)

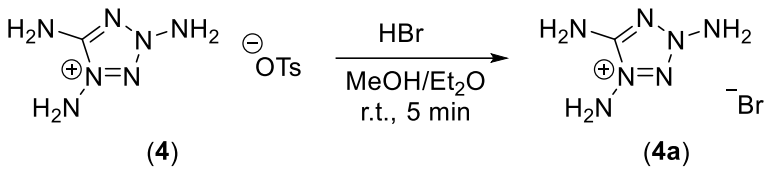

(**4**) (**4a**)

Triaminotetrazolium tosylate (**4**) (1.32 g, 4.59 mmol, 1.0 eq) was dissolved in the minimum amount of methanol (15 mL) and hydrobromic acid (47% in water, 0.54 mL, 4.60 mmol, 1.0 eq) was added. The mixture was stirred for 5 min followed by the addition of diethyl ether (300 mL). The solution clouded and after 10 min of intensive stirring, a slightly yellowish clumpy solid was formed. The liquid phase was discarded and the residue was again dissolved in methanol (10 mL) followed by the addition of diethyl ether (300 mL). After the solid was formed and precipitated, the liquid phase was discarded and the solid was dried on air to yield pure 1,3,5-triaminotetrazolium bromide (**4a**) as slightly beige solid (0.80 g, 4.09 mmol, 89%).

DTA (5 °C min^{-1}): 158 °C (exo); Elem. Anal. (CH_6N_7Br, 196.01 g mol^{-1}): calcd: C 6.13, H 3.09, N 50.02 %; found: C 6.05, H 3.03, N 49.76 %; IR (ATR) $\tilde{\nu}$ (cm^{-1}) = 3273(m), 3073(s), 1677(vs), 1619(s), 1553(m), 1393(s), 1183(s), 1122(m), 1073(m), 1023(s), 941(s), 838(s), 713(s), 686(s), 641(s), 580(s), 500(vs), 452(vs), 436(s); ^{1}H NMR (DMSO-D_6, 400 MHz, ppm) δ = 9.39 (br s, 2H), 8.11 (s, 2H), 6.84 (br s, 2H); ^{13}C NMR (DMSO-D_6, 101 MHz, ppm) δ = 156.3.

Di-(1,3,5-triaminotetrazolium)-5,5’-bistetrazole-1,1’diolate (**4b**)

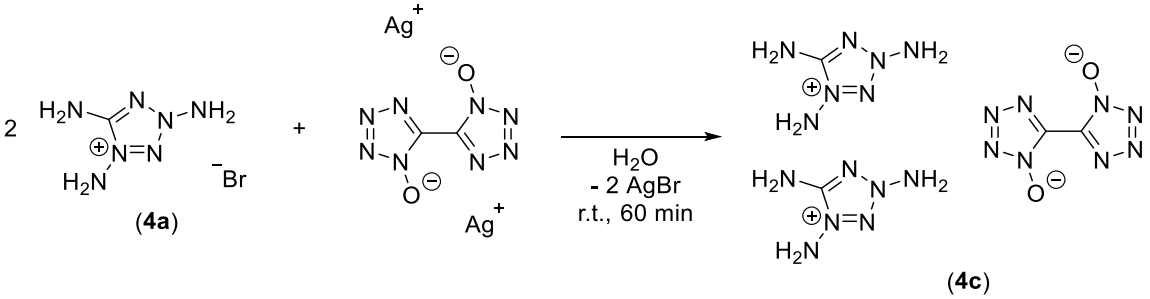

(**4a**) (**4c**)

1,3,5-Triaminotetrazolium bromide (**4a**) (0.41 g, 2.09 mmol, 2.0 eq) was dissolved in water (20 mL) and disilver 5,5'bistetrazole-1,1'-diolate (Ag_2BTDO, 0.40 g, 1.05 mmol, 1.0 eq) was added in one portion and the suspension was stirred for one hour in the dark. The precipitate consisting of AgBr was filtered and washed with small quantities of water to obtain di-(1,3,5-triaminotetrazolium)-5,5'-bistetrazole-1,1'diolate (**4b**) (0.40 g, 1.00 mmol, 95%) as slightly brownish powder. DTA (5 °C min^{-1}): 170 °C (exo); Sensitivities: BAM drophammer: 2 J; friction tester: 30 N; ESD: 80 mJ (at grain size 100–500 µm); Elem. Anal. ($C_4H_{12}N_{22}O_2$, 400.28 g mol^{-1}): calcd: C 12.00, H 3.02, N 76.98 %; found: C 11.82, H 2.90, N 75.91 %; IR (ATR) $\tilde{\nu}$ (cm^{-1}) = 3394(m), 3281(m), 3184(m), 2999(m), 2924(m), 2858(m), 2704(m), 2653(m), 1689(s), 1683(s), 1626(m), 1528(m), 1419(s), 1233(s), 1166(s), 1049(s), 994(s), 923(s), 824(m), 730(s), 716(s), 696(s), 662(s), 566(s), 503(vs), 443(s), 435(s), 423(s), 414(s), 403(s); ^1H NMR (DMSO-D_6, 400 MHz, ppm) δ = 8.89 (br s, 4H), 8.49 (br s, 4H), 6.89 (s, 4H); ^{13}C NMR (DMSO-D_6, 101 MHz, ppm) δ = 156.3, 134.7.

8.6.2 Crystallography

Crystal structure data were obtained from an Oxford Xcalibur3 diffractometer with a Spellman generator (voltage 50 kV, current 40 mA) and a Kappa CCD area for data collection using Mo-*Kα* radiation (*λ* = 0.71073 Å) or a Bruker D8 Venture TXS diffractometer equipped with a multilayer monochromator, a Photon 2 detector and a rotation-anode generator (Mo-K_α radiation). The data collection was performed using the CRYSTALIS RED software.[S5] The solution of the structure was performed by direct methods and refined by full-matrix least-squares on F2 (SHELXT)[S6] implemented in the OLEX2[S7] software suite. The non-hydrogen atoms were refined anisotropically and the hydrogen atoms were located and freely refined. The absorption correction was carried out by a SCALE3 ABSPACK multiscan method.[S8] The DIAMOND2 plots shown with thermal ellipsoids at the 50% probability level and hydrogen atoms are shown as small spheres of arbitrary radius. The SADABS program embedded in the Bruker APEX3 software was used for multi-scan absorption corrections in all structures.[S9]

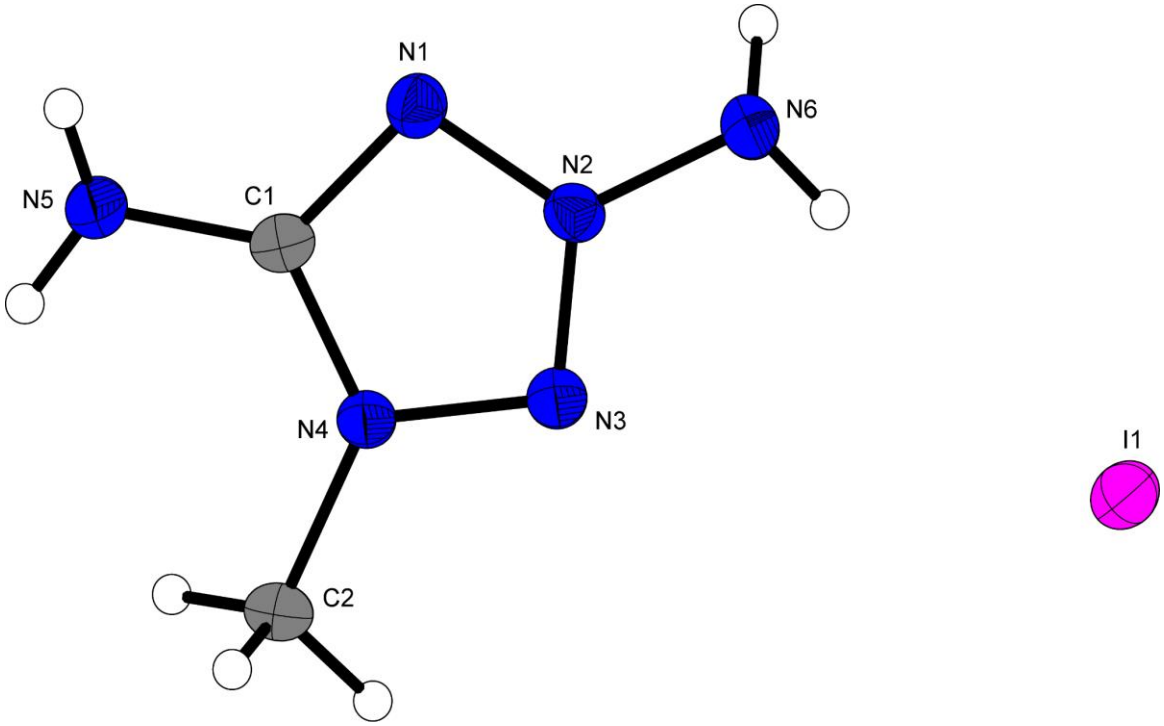

Figure S1. Representation of the molecular unit of 2,5-diamino-4-methyl-tetrazolium iodide (**3**), showing the atom-labeling scheme. Thermal ellipsoids represent the 50% probability level and hydrogen atoms are shown as small spheres of arbitrary radius. Selected bond distances [Å] and angles [°]: C1-N5 1.329(4), C2-N4 1.461(4), N2-N6 1.385(4), H5A-I1 2.84(3), H5B-I1 2.87(4), H6A-I1 2.91(3), H6B-I1 2.86(4), C1-N4-C2 129.1(2), N5-H5A-I1 163(4), N5-H5B-I1 173(3), N6-H6A-I1 153(3), N6-H6B-I1 176(3).

Compound **3** crystallizes in the monoclinic space group $P2_1/c$ and has a density of 2.126 g cm^{-3} at 173 K. The third substitution on the tetrazole ring leads to a compression of the heteroaromatic ring. Actually, angles for a regular pentagon (α = 108 °) should be expected. However, especially the angles N2-N3-N4 (101.6(3) °) N1-N2-N3 (118.2(2) °) deviate strongly from this angle. Each iodide forms strong hydrogen bonds with each hydrogen of the amino groups. This results in a coordination of four cation units around each anion. These result in a hypothetical octahedron in which four of the six corners are occupied.

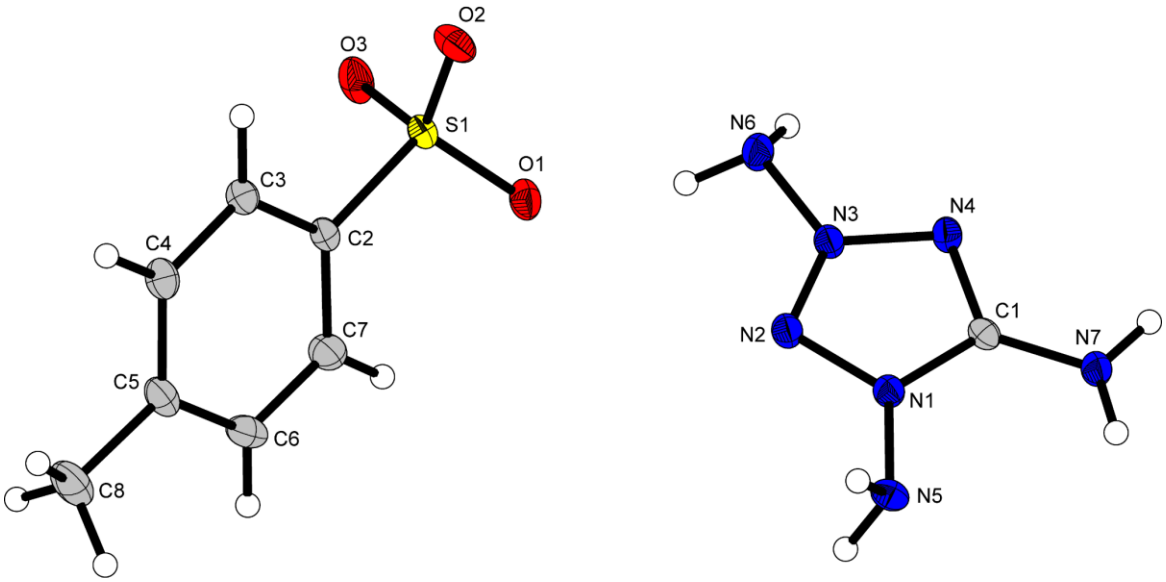

Figure S2. Representation of the molecular unit of 1,3,5-triaminotetrazolium tosylate (**4**), showing the atom-labeling scheme. Thermal ellipsoids represent the 50% probability level and hydrogen atoms are shown as small spheres of arbitrary radius. Selected bond distances [Å] and angles [°]: N1-N5 1.390(2), N3-N6 1.363(2), C2-N7 1.322(2), H5A-O3 2.12(3), H6A-O1 2.01(3), H7B-O1 2.08(3), N5-H5A-O3 179.1(2), N6-H6A-O1 156.2(2), N7-H7B-O1 152(3).

1,3,5-Triaminotetrazolium tosylate (**4**) crystallizes in the monoclinic space group $P2_1/n$ and has a density of 1.494 g cm^{-3} at 101 K. The newly inserted amino group at position 1 is sp^3 hybridized similar to the second N-NH$_2$ function. The triple substitution on the tetrazole ring causes a change in the angles within the tetrazolium ring. It no longer appears smooth but compressed (C1-N4-N3 101.86(13)°, N1-C1-N4 108.69(14)°, N1-N2-N3 101.29(13)°). All protons of the tetrazlium amines are involved in hydrogen bonds with the sulfonic acid moiety (O3-H5A 2.12(3) Å, O2-H5B 2.19(2) Å, O1-H6A 2.01(3) Å, O3-H6B 2.03(2) Å, O1-H7B 2.08(3) Å, 2.12(3) Å). This results in an arrangement in which six OTs$^-$ units are arranged around the cationic unit. The benzene rings are not arranged in layers, since the more attractive effects result from the O···H-N interactions.

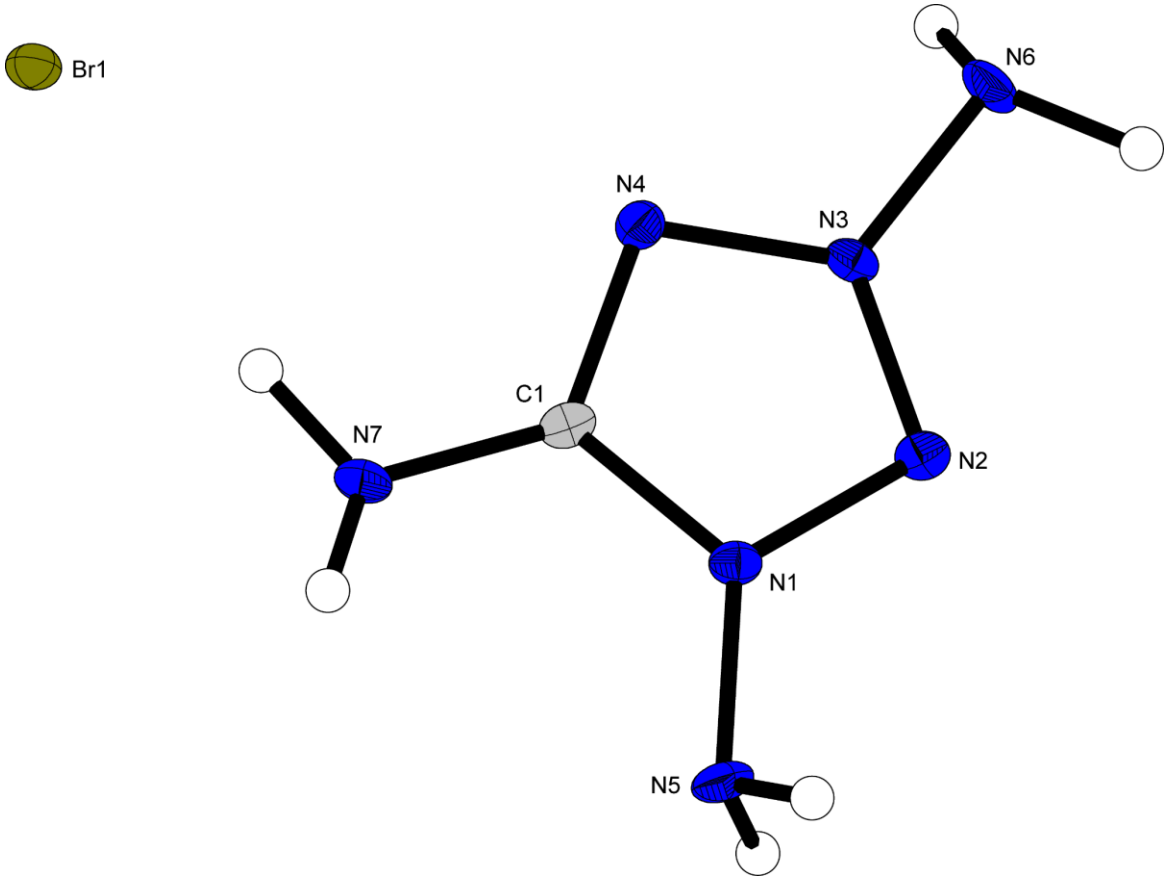

Figure S3. Representation of the molecular unit of 1,3,5-triaminotetrazolium bromide (**4a**), showing the atom-labeling scheme. Thermal ellipsoids represent the 50% probability level and hydrogen atoms are shown as small spheres of arbitrary radius. Selected bond distances [Å] and angles [°]: N1-N5 1.394(6), N3-N6 1.382(5), C1-N7 1.326(7), H5A-Br1 2.69(4), H5B-N4 2.54(5), H6A-Br1 2.48(6), H6B-Br1 2.67(6), H7A-Br1 2.68(4), H7B-Br1 2.49(7), C1-N4-N3 101.3(4), N2-N3-N4 118.4(3), N5-H5A-Br1 160(4), N5-H5B-N4 148(4), N6-H6A-Br1 171(4), N6-H6B-Br1 150(5), N7-H7A-Br1 160(5), N7-H7B-Br1 169(4).

1,3,5-Triaminotetrazolium bromide (**4a**) crystallizes in the monoclinic space group $P2_1/c$ and has a density of 2.009 g cm^{-3} at 101 K. The bromide is involved in strong intermolecular hydrogen bonds with all protons of the amino functions. The bond distances N-H···Br are in a range of 2.48(6) Å for H6A-Br to 2.69(4) Å for H5A-Br1. Each bromide anion is coordinated by five cation units, with only one N-H···Br interaction emanating from each cation. In addition, the cations also interact with each other, forming interactions from the strongly polarized hydrogen H5B to the nitrogen N4 (H5B-N4 2.54(5) Å, N5-H5B-N4 148(4) °). The many interaction possibilities at the cation result in a complicated network, which is filled in its gaps by anions.

Table S1. Crystallographic data of compounds **1**, **2a**, **2b** and **3**.

	1	**2a**	**2b**	**3**
Formula	CH_4N_6	$CH_5N_6\,NO_3$	$CH_5N_6\,ClO_4$	$C_2H_7N_6\,I$
FW [g mol^{-1}]	100.10	163.12	200.56	242.04
Crystal system	triclinic	monoclinic	monoclinic	monoclinic
Space group	*P*−1 (No. 2)	$P2_1/n$ (No. 14)	$P2_1/c$ (No. 14)	$P2_1/c$ (No. 14)
Color / Habit	colorless plate	colorless block	clear white block	colorless block
Size [mm]	0.09 x 0.40 x 0.40	0.10 x 0.20 x 0.35	0.25 x 0.28 x 0.38	0.10 x 0.30 x 0.35
a [Å]	5.2519(10)	10.8782(10)	7.1662(4)	7.0760(3)
b [Å]	6.5141(9)	10.6236(8)	7.1311(4)	11.2519(5)
c [Å]	6.8045(10)	11.5460(11)	13.7130(7)	9.7180(4)
α [°]	105.732(12)	90	90	90
β [°]	107.197(15)	113.414(11)	93.776(5)	102.229(4)
γ [°]	99.007(14)	90	90	90
V [Å^3]	206.84(7)	1224.5(2)	699.25(7)	756.18(6)
Z	2	8	4	4
$\rho_{calc.}$ [g cm^{-3}]	1.607	1.770	1.905	2.126
μ [mm^{-1}]	0.127	0.163	0.538	4.166
F(000)	104	672	408	456
$\lambda_{MoK\alpha}$ [Å]	0.71073	0.71073	0.71069	0.71069
T [K]	173	173	173	173
θ Min-Max [°]	4.2, 26.0	4.2, 26.5	4.1, 26.5	4.2, 26.0
Dataset	-6: 6 ; -8: 8 ; -8: 8	-13: 13 ; -13: 13 ; -14: 13	-8: 5 ; -8: 7 ; -17: 16	-8: 8 ; -13: 13 ; -11: 11
Reflections collected	2037	9899	3629	5437
Independent refl.	801	2534	1431	1482
R_{int}	0.023	0.025	0.024	0.025
Observed reflections	676	1986	1222	1293
Parameters	80	239	129	99
R_1 (obs)[a]	0.0417	0.0398	0.0333	0.0209
wR_2 (all data)[b]	0.1143	0.1157	0.0870	0.0507
S [c]	1.07	1.03	1.06	1.04
Resd. dens [e Å^{-3}]	-0.22, 0.37	-0.28, 0.56	-0.45, 0.37	-0.43, 0.68
Device type	Xcalibur Sapphir3	Xcalibur Sapphir3	Xcalibur Sapphir3	Xcalibur Sapphir3
Solution	SIR-92	SIR-92	SIR-92	SIR-92
Refinement	SHELXL-2013	SHELXL-2013	SHELXL-2013	SHELXL-2013
Absorption correction	multi-scan	multi-scan	multi-scan	multi-scan
CCDC	2172089	2172088	2172090	2172091

[a] $R_1 = \Sigma||F_0|-|F_c||/\Sigma|F_0|$; [b] $wR_2 = [\Sigma[w(F_0^2-F_c^2)^2]/\Sigma[w(F_0)^2]]^{1/2}$; $w = [\sigma c^2(F_0^2)+(xP)^2+yP]^{-1}$ and $P=(F_0^2+2F_c^2)/3$; [c] $S = \{\Sigma[w(F_o^2-F_c^2)^2]/(n-p)\}^{1/2}$ (n = number of reflections; p = total number of parameters).

Table S2. Crystallographic data of compounds **3a**-**3c.**

	3a	**3b**	**3c**
Formula	$C_2H_7N_6NO_3$	$C_2H_7N_6ClO_4$	$C_2H_7N_6N_3$
FW [g mol^{-1}]	177.15	214.59	157.17
Crystal system	monoclinic	monoclinic	orthorhombic
Space group	$P2_1/c$ (No. 14)	$P2_1/n$ (No. 14)	$P2_12_12_1$ (No. 19)
Color / Habit	colorless block	colorless block	colorless block
Size [mm]	0.16 x 0.35 x 0.45	0.30 x 0.50 x 0.50	0.02 x 0.03 x 0.05
a [Å]	7.6448(5)	5.4120(5)	6.2958(3)
b [Å]	8.8744(7)	13.2511(10)	8.4859(4)
c [Å]	10.6105(7)	10.9977(8)	13.1114(6)
α [°]	90	90	90
β [°]	103.315(7)	97.321(7)	90
γ [°]	90	90	90
V [Å^3]	700.50(9)	782.27(11)	700.48(6)
Z	4	4	4
$\rho_{calc.}$ [g cm^{-3}]	1.680	1.822	1.490
μ [mm^{-1}]	0.150	0.487	0.116
F(000)	368	440	328
$\lambda_{MoK\alpha}$ [Å]	0.71073	0.71073	0.71073
T [K]	173	101	100
θ Min-Max [°]	4.3, 26.0	2.4, 32.5	2.9, 25.3
Dataset	-9: 9 ; -9: 10 ; -13: 13	-7: 7 ; -20: 19 ; -16: 16	-7: 7 ; -10: 10 ; -15: 15
Reflections collected	5086	8678	7177
Independent refl.	1371	2622	1274
R_{int}	0.037	0.030	0.046
Observed reflections	1169	2116	1164
Parameters	137	146	109
R_1 (obs)[a]	0.0424	0.0378	0.0831
wR_2 (all data)[b]	0.1156	0.1011	0.2093
S [c]	1.12	1.05	1.10
Resd. dens [e Å^{-3}]	-0.25, 0.30	-0.49, 0.45	-0.33, 1.19
Device type	Xcalibur Sapphire3	Xcalibur Sapphire3	Bruker D8 Venture
Solution	SIR-92	SIR-92	SIR-92
Refinement	SHELXL-2013	SHELXL-2013	SHELXL-2013
Absorption correction	multi-scan	multi-scan	multi-scan
CCDC	2172087	2172093	2172084

[a]$R_1 = \Sigma||F_0|-|F_c||/\Sigma|F_0|$; [b]$wR_2 = [\Sigma[w(F_0^2-F_c^2)^2]/\Sigma[w(F_0)^2]]^{1/2}$; $w = [\sigma c^2(F_0^2)+(xP)^2+yP]^{-1}$ and $P=(F_0^2+2F_c^2)/3$; [c]$S = \{\Sigma[w(F_o^2-F_c^2)^2]/(n-p)\}^{1/2}$ (n = number of reflections; p = total number of parameters).

Table S3. Crystallographic data of compounds **4**, **4a** and **4b.**

	4	**4a**	**4b**
Formula	$C_7H_7O_3S\ CH_6N_7$	$CH_6N_7\ Br$	$C_2N_8O_2\ (CH_6N_7)_2$
FW [g mol^{-1}]	287.31	196.04	400.36
Crystal system	monoclinic	monoclinic	monoclinic
Space group	$P2_1/n$ (No. 14)	$P2_1/c$ (No. 14)	$P2_1/n$ (No. 14)
Color / Habit	colorless block	light orange block	colorless plate
Size [mm]	0.50 x 0.50 x 0.50	0.25 x 0.40 x 0.50	0.02 x 0.30 x 0.40
a [Å]	9.3104(5)	6.2609(7)	10.5454(12)
b [Å]	13.9097(9)	11.5021(13)	5.1159(6)
c [Å]	9.8692(6)	9.3564(12)	14.5922(17)
α [°]	90	90	90
β [°]	91.840(5)	105.817(12)	106.757(10)
γ [°]	90	90	90
V [Å^3]	1277.45(13)	648.28(14)	753.81(16)
Z	4	4	2
$\rho_{calc.}$ [g cm^{-3}]	1.494	2.009	1.764
μ [mm^{-1}]	0.271	6.264	0.146
F(000)	600	384	412
$\lambda_{MoK\alpha}$ [Å]	0.71073	0.71073	0.71073
T [K]	101	101	101
θ Min-Max [°]	2.5, 26.4	2.9, 26.4	2.8, 26.4
Dataset	-11: 7 ; -17: 15 ; -10: 12	-7: 7 ; -14: 12 ; -9: 11	-13: 12 ; -6: 6 ; -18: 18
Reflections collected	5480	2374	5990
Independent refl.	2612	1328	1543
R_{int}	0.020	0.034	0.088
Observed reflections	2254	1045	914
Parameters	224	106	151
R_1 (obs)[a]	0.0352	0.0377	0.0603
wR_2 (all data)[b]	0.0968	0.0890	0.1181
S [c]	1.05	1.03	1.03
Resd. dens [e Å^{-3}]	-0.47, 0.26	-0.83, 1.21	-0.28, 0.29
Device type	Xcalibur Sapphire3	Xcalibur Sapphire3	Xcalibur Sapphire3
Solution	SIR-92	SIR-92	SIR-92
Refinement	SHELXL-2013	SHELXL-2013	SHELXL-2013
Absorption correction	multi-scan	multi-scan	multi-scan
CCDC	2172092	2172086	2172085

[a] $R_1 = \Sigma||F_o|-|F_c||/\Sigma|F_o|$; [b] $wR_2 = [\Sigma[w(F_o^2-F_c^2)^2]/\Sigma[w(F_o)^2]]^{1/2}$; $w = [\sigma c^2(F_o^2)+(xP)^2+yP]^{-1}$ and $P=(F_o^2+2F_c^2)/3$; [c] $S = \{\Sigma[w(F_o^2-F_c^2)^2]/(n-p)\}^{1/2}$ (n = number of reflections; p = total number of parameters).

8.6.3 Computation

All quantum chemical calculations were carried out using the Gaussian G09 program package.[S10] The enthalpies (H) and free energies (G) were calculated using the complete basis set (CBS) method of Petersson and co-workers in order to obtain very accurate energies. The CBS models are using the known asymptotic convergence of pair natural orbital expressions to extrapolate from calculations using a finite basis set to the estimated CBS limit. CBS-4 starts with an HF/3-21G(d) geometry optimization; the zero-point energy is computed at the same level. It then uses a large basis set SCF calculation as a base energy, and an MP2/6- 31+G calculation with a CBS extrapolation to correct the energy through second order. A MP4(SDQ)/6-31+ (d,p) calculation is used to approximate higher order contributions. In this study, we applied the modified CBS-4M.

Heats of formation of the synthesized ionic compounds were calculated using the atomization method (equation E1) using room temperature CBS-4M enthalpies, which are summarized in Table S4.[S11, S12]

$$\Delta_f H^\circ_{(g,\,M,\,298)} = H_{(Molecule,\,298)} - \sum H^\circ_{(Atoms,\,298)} + \sum \Delta_f H^\circ_{(Atoms,\,298)} \qquad (E1)$$

Table S4. CBS-4M electronic enthalpies for atoms C, H, N and O and their literature values for atomic $\Delta H^\circ_f{}^{298}$ / kJ mol^{-1}

	$-H^{298}$ [a.u.]	NIST[S13]
H	0.500991	218.2
C	37.786156	717.2
N	54.522462	473.1
O	74.991202	249.5
Cl	459.674576	121.3

For neutral compounds the sublimation enthalpy, which is needed to convert the gas phase enthalpy of formation to the solid state one, was calculated by the *Trouton* rule.[S14] For ionic compounds, the lattice energy (U_L) and lattice enthalpy (ΔH_L) were calculated from the corresponding X-ray molecular volumes according to the equations provided by *Jenkins* and *Glasser*.[S15] With the calculated lattice

enthalpy the gas-phase enthalpy of formation was converted into the solid state (standard conditions) enthalpy of formation. These molar standard enthalpies of formation (ΔH_m) were used to calculate the molar solid state energies of formation (ΔU_m) according to equation E2.

$$\Delta U_m = \Delta H_m - \Delta n\, RT \qquad \text{(E2)}$$

(Δn being the change of moles of gaseous components)
The calculation results are summarized in Table S5.

Table S5. Calculation results.

	$-H^{298}$ [a] [a.u.]	$\Delta_f H°$(g,M) [kJ mol^{-1}] [b]	V_M [Å^3] [c]	ΔU_L; ΔH_L [d] [kJ mol^{-1}]	$\Delta_f H°$(s) [e] [kJ mol^{-1}]	Δn [f]	$\Delta_f U$(s) [g] [kJ kg^{-1}]
2,5-DATH$^+$	386.790191	1060.8					
2,5-DA-4-MT$^+$	408.033804	1017.6					
1,3,5-TAT$^+$	424.046427	1140.3					
NO_3^-	280.080446	−314.1					
ClO_4^-	760.171182	−278.2					
N_3^-	164.034938	190.5					
BTDO^{2-}	663.687267	585.9					
1	368.453013	412.7			345.2	−5.0	3572.5
2a		746.7	156	539.7; 544.6	202.1	−7.5	1353.0
2b		782.6	178	520.8; 525.7	256.8	−8.0	1379.5
3a		703.5	357	434.6; 439.5	264.0	−8.5	1609.5
3b		739.4	201	504.5; 509.4	230.0	−9.0	1175.7
3c		1208.1	180	519.0; 522.8	685.3	−8.0	4487.4
4a		2312.1	388	1181.0; 1188.4	1678.1	−18.0	4303.7

[a] CBS-4M electronic enthalpy; [b] gas phase enthalpy of formation; [c] molecular volumes taken from X-ray structures and corrected to room temperature; [d] lattice energy and enthalpy (calculated using Jenkins and Glasser equations); [e] standard solid-state enthalpy of formation; [f] Δn being the change of moles of gaseous components when formed; [g] solid state energy of formation.

8.6.4 NMR Spectroscopy

^{1}H-NMR (400 MHz, DMSO-D$_6$, ppm)

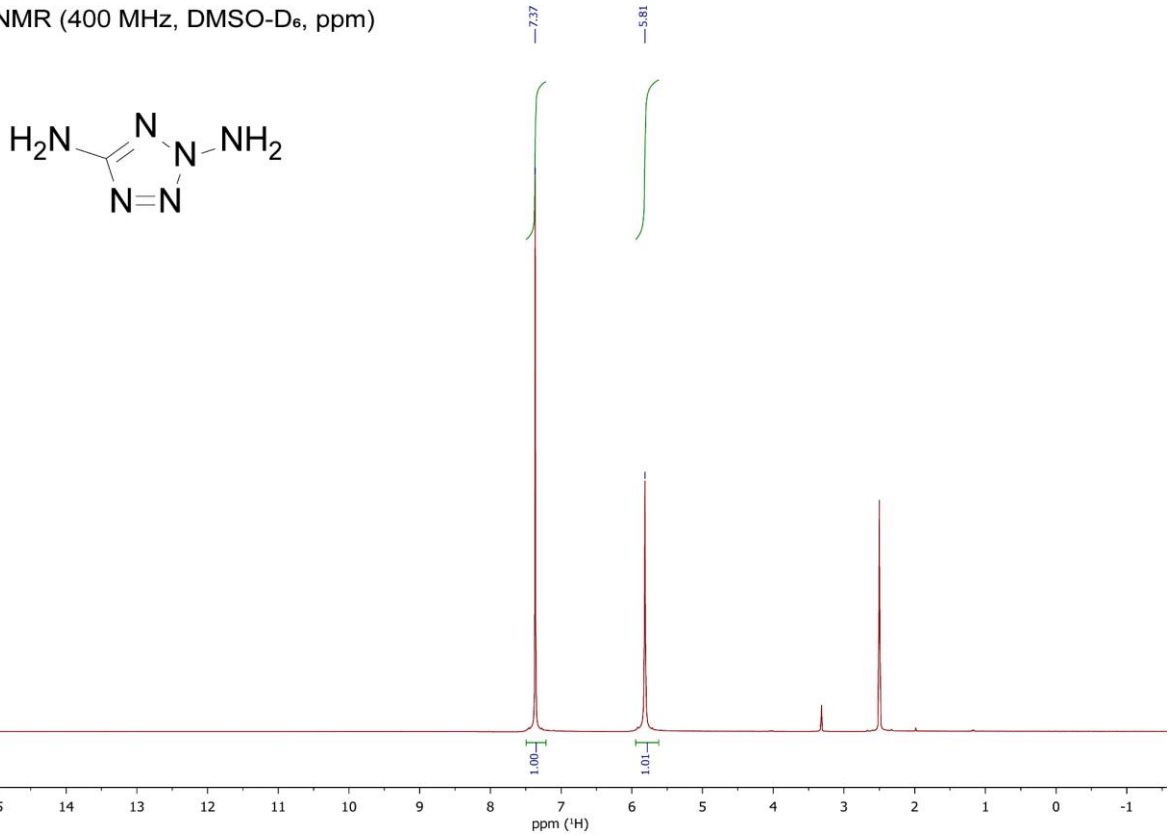

^{13}C-NMR (101 MHz, DMSO-D$_6$, ppm)

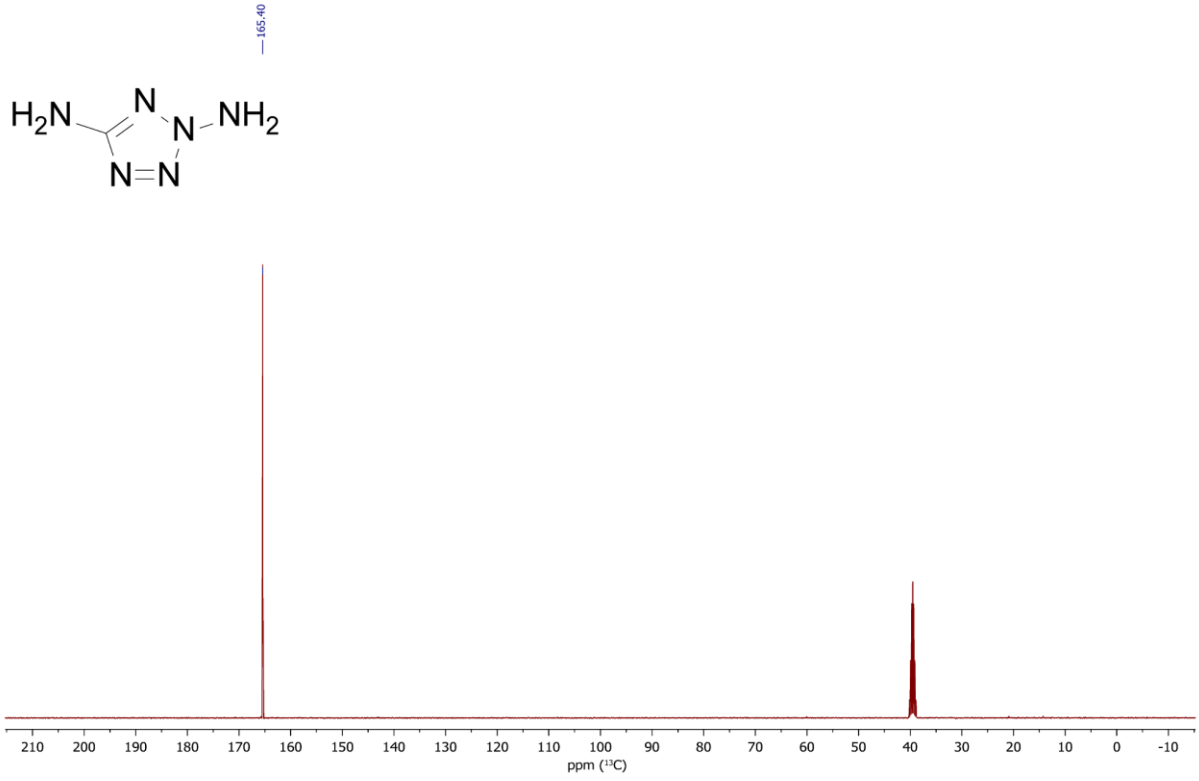

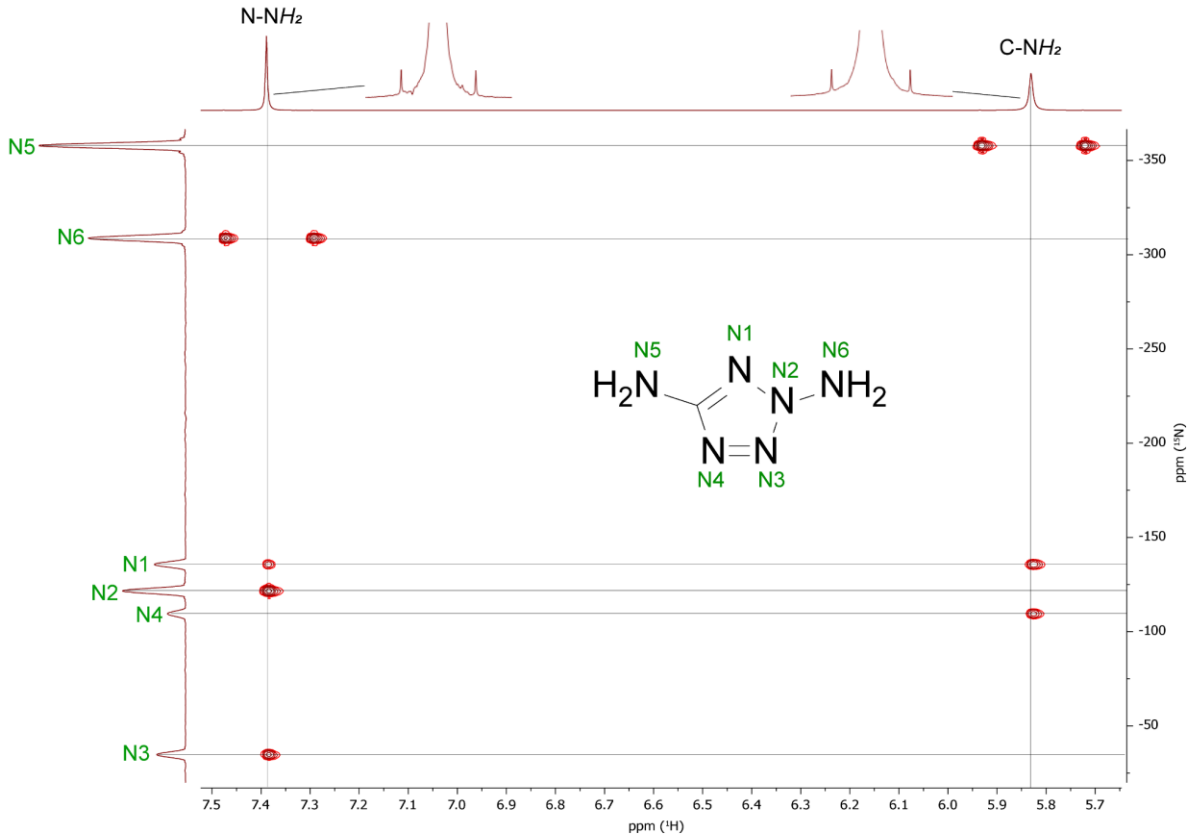

¹H-NMR (400 MHz, DMSO-D₆, ppm)

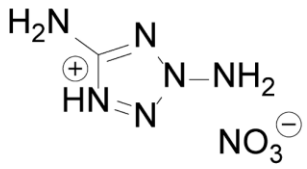

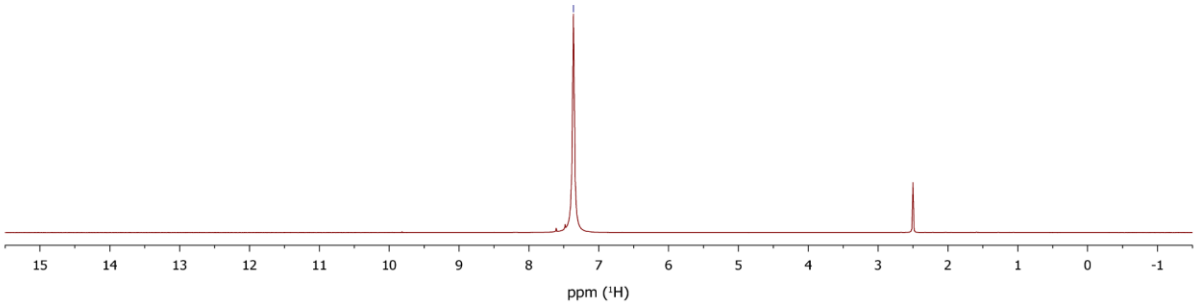

^{13}C-NMR (101 MHz, DMSO-D$_6$, ppm)

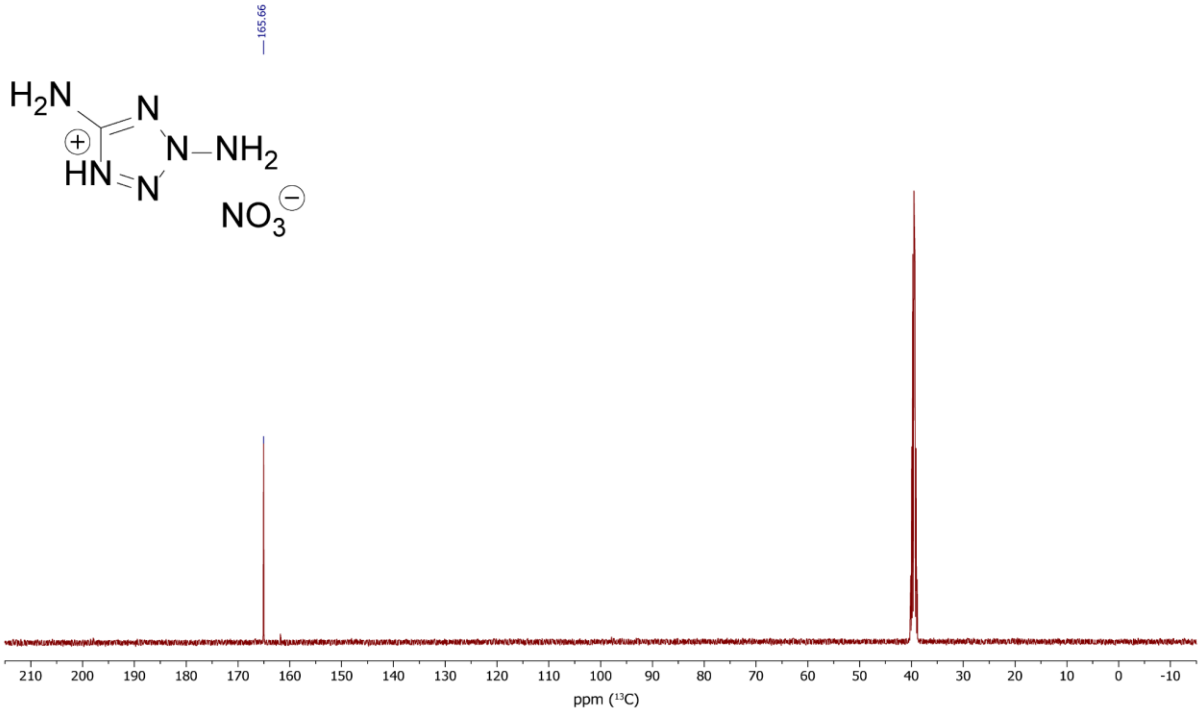

^{1}H-NMR (400 MHz, DMSO-D$_6$, ppm)

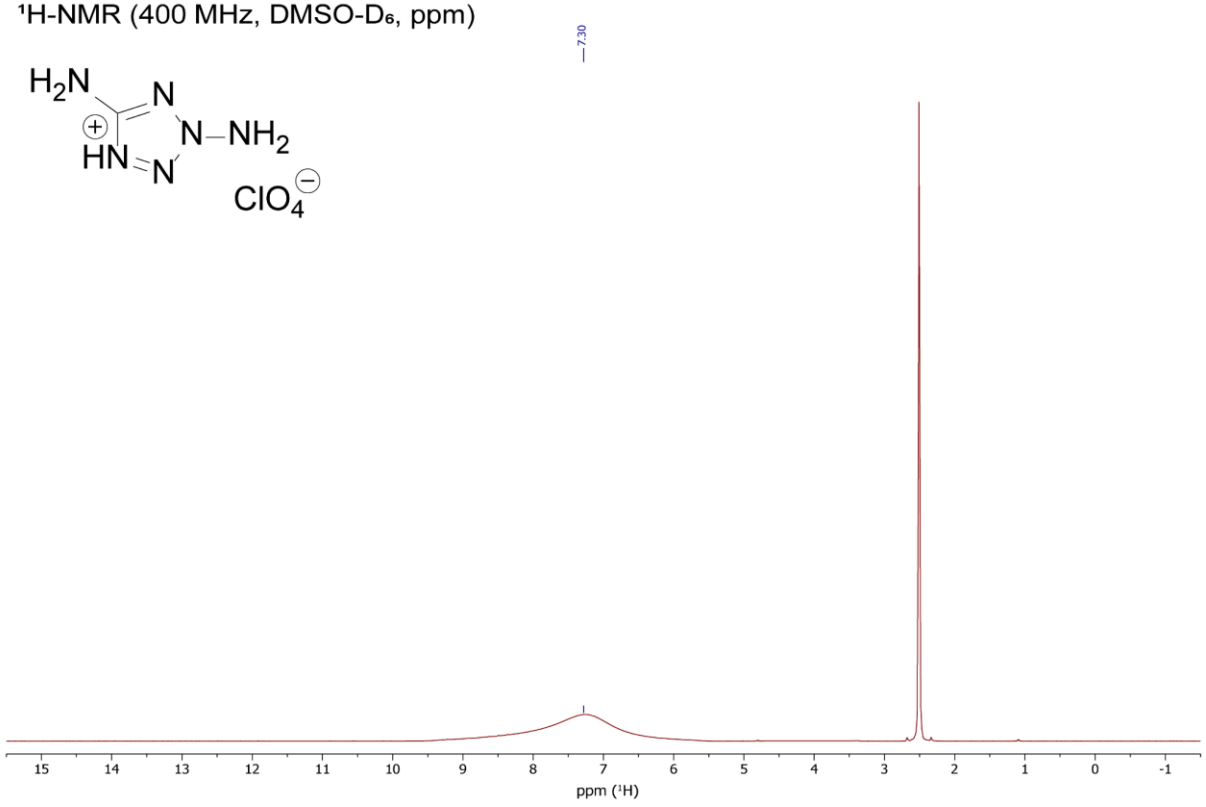

^{13}C-NMR (101 MHz, DMSO-D$_6$, ppm)

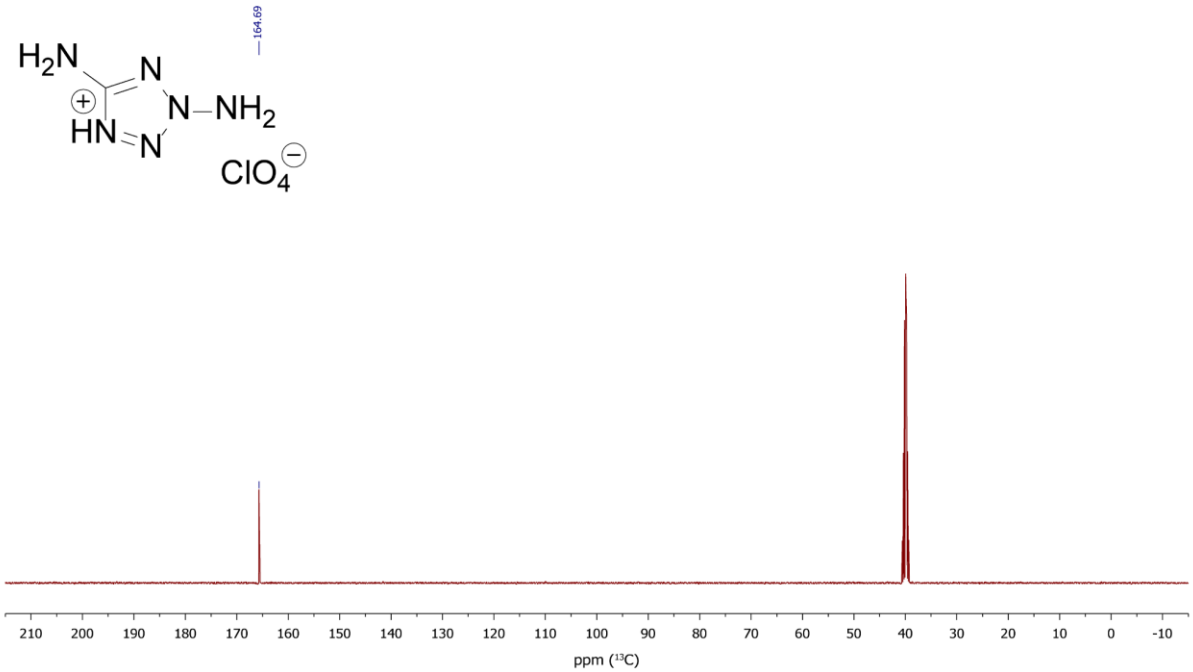

^{1}H-NMR (400 MHz, DMSO-D$_6$, ppm)

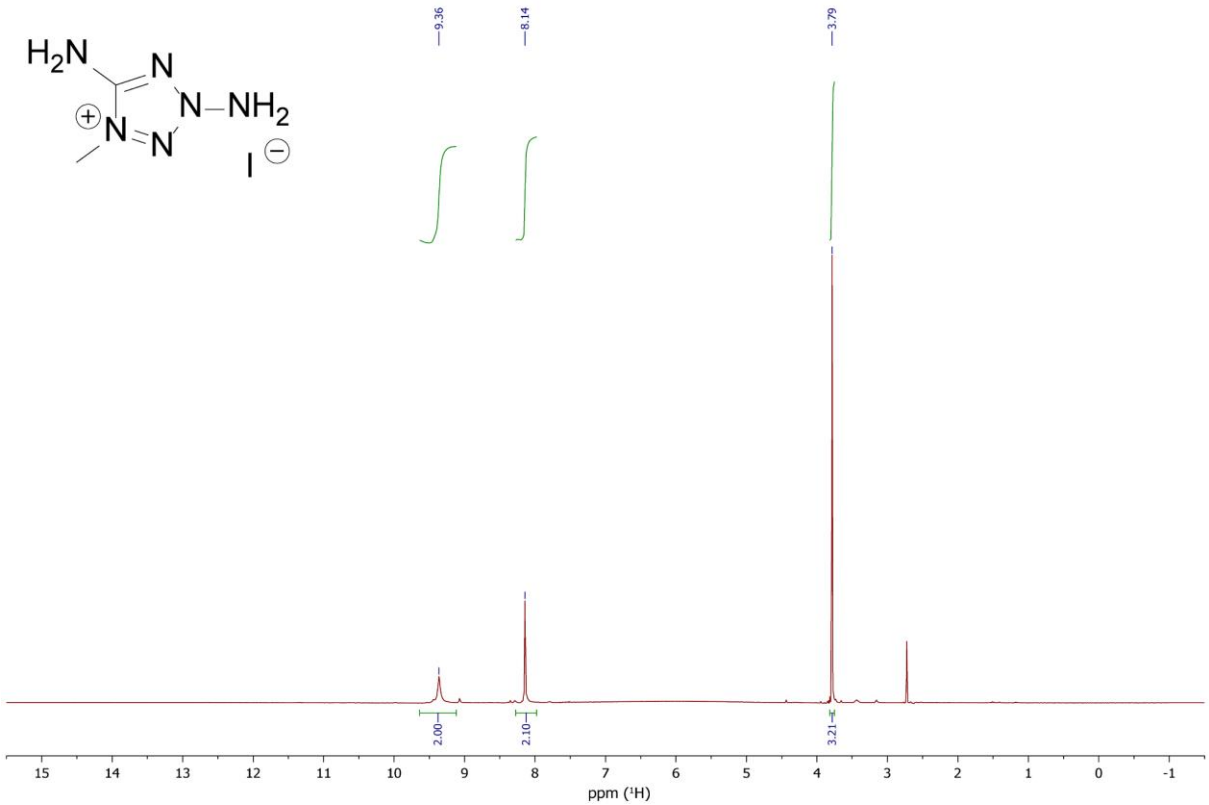

^{13}C-NMR (101 MHz, DMSO-D$_6$, ppm)

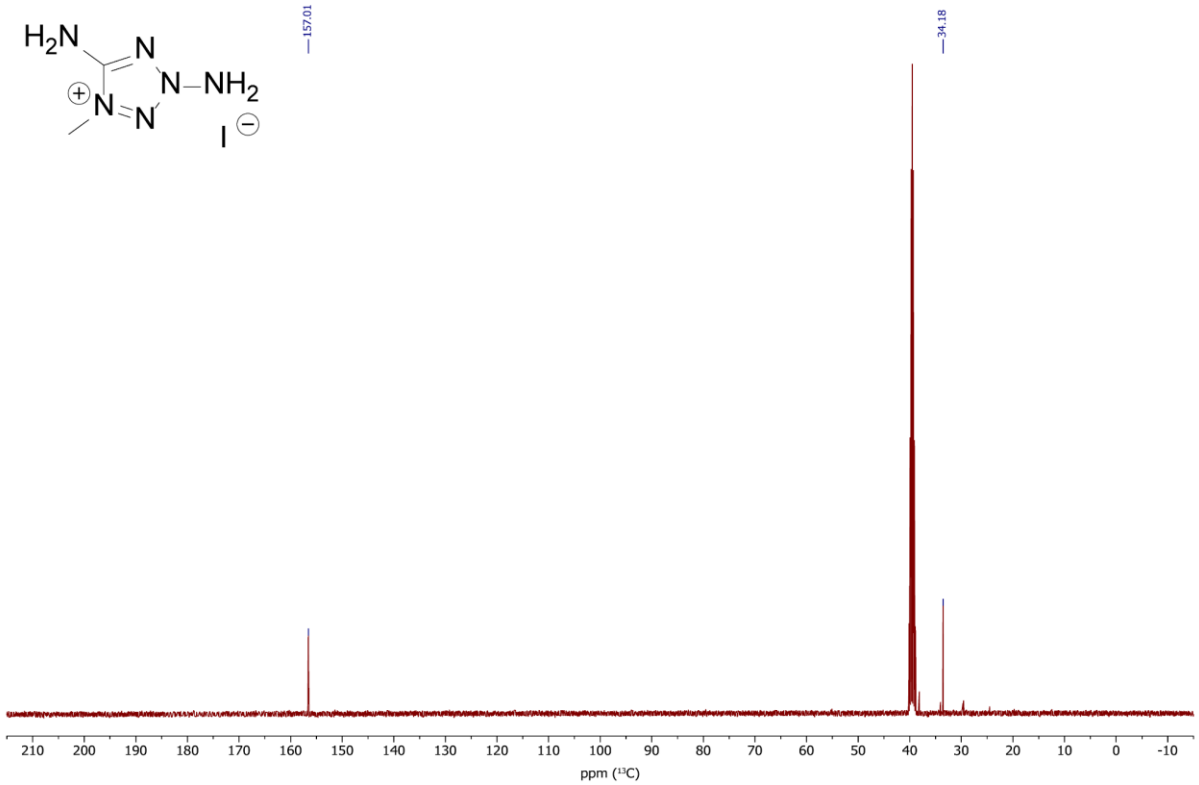

^{1}H-NMR (400 MHz, DMSO-D$_6$, ppm)

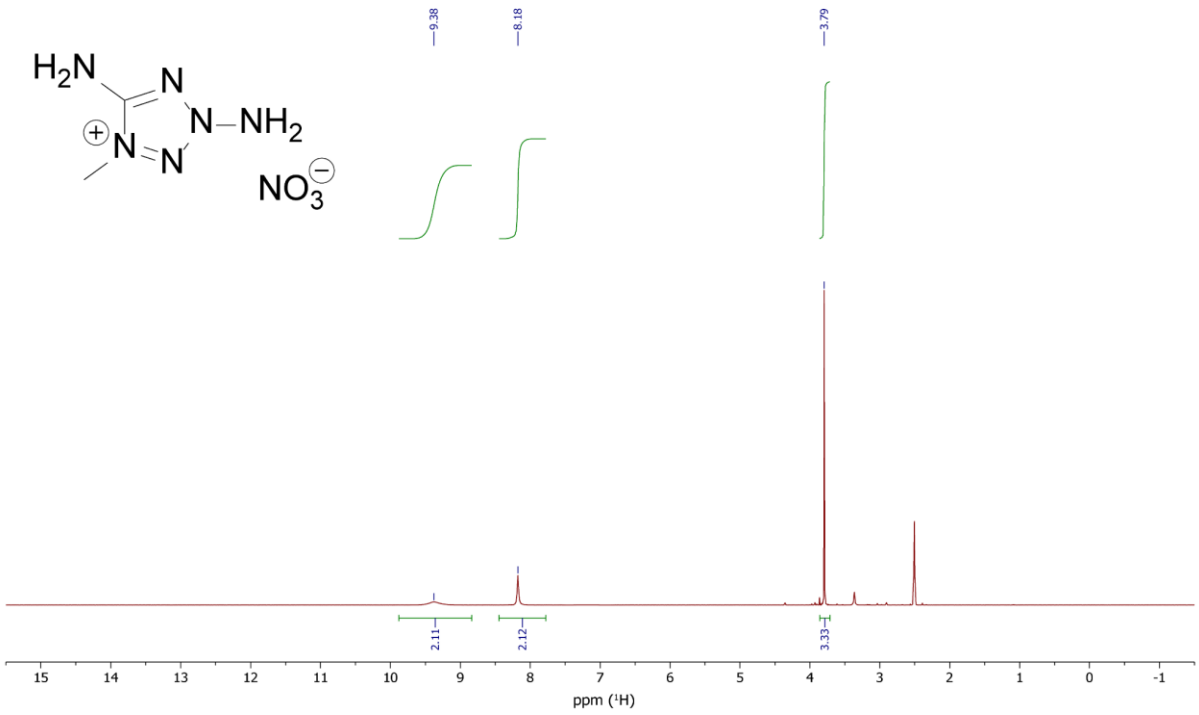

^{13}C-NMR (101 MHz, DMSO-D$_6$, ppm)

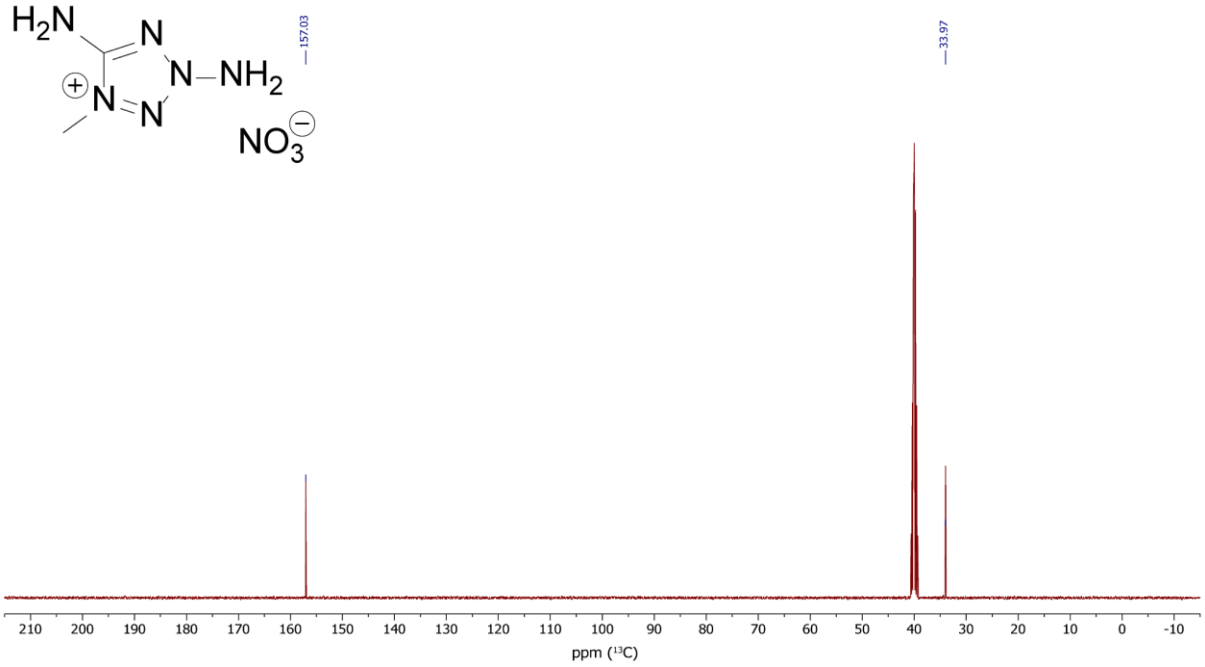

^{1}H-NMR (400 MHz, DMSO-D$_6$, ppm)

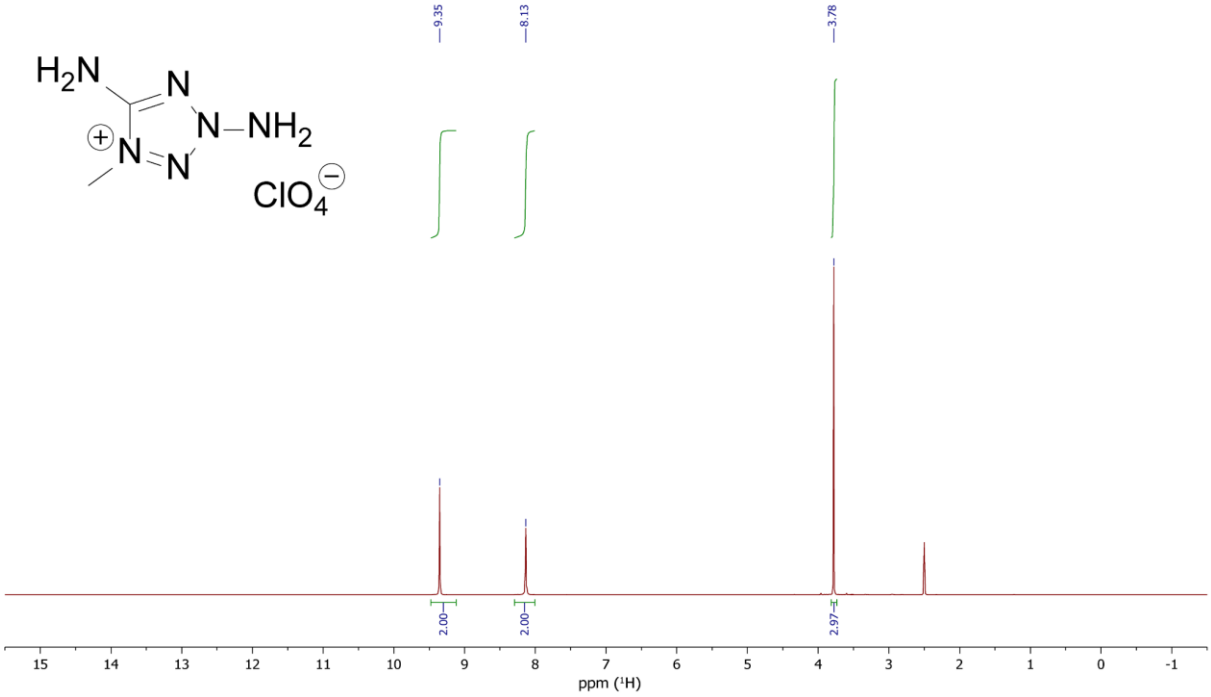

^{13}C-NMR (101 MHz, DMSO-D$_6$, ppm)

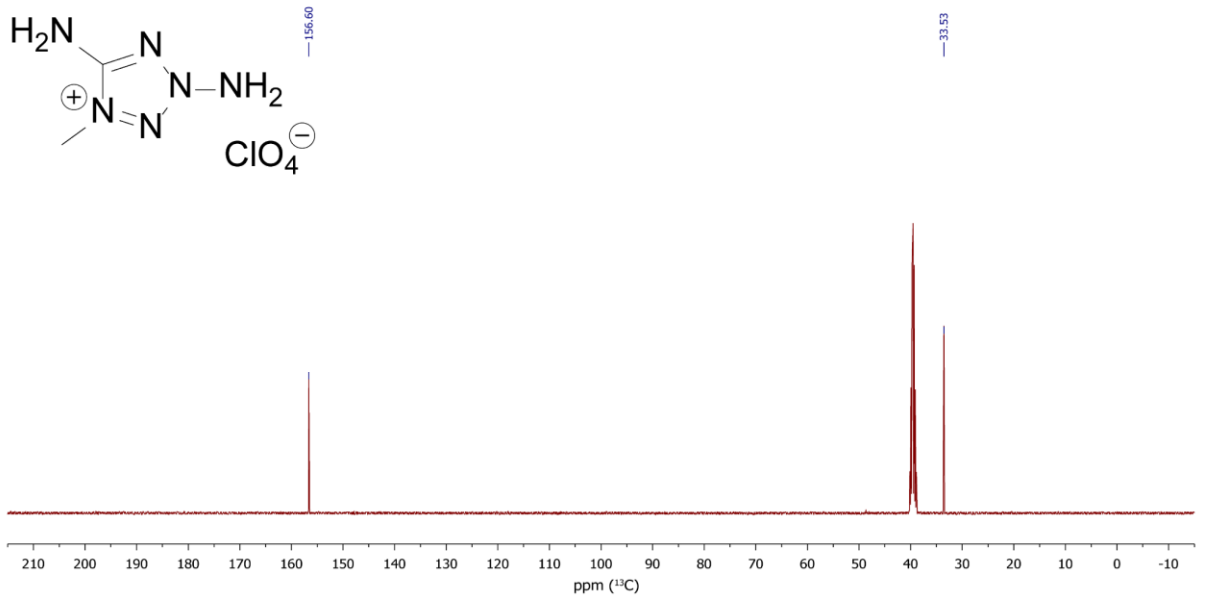

^{1}H-NMR (400 MHz, DMSO-D$_6$, ppm)

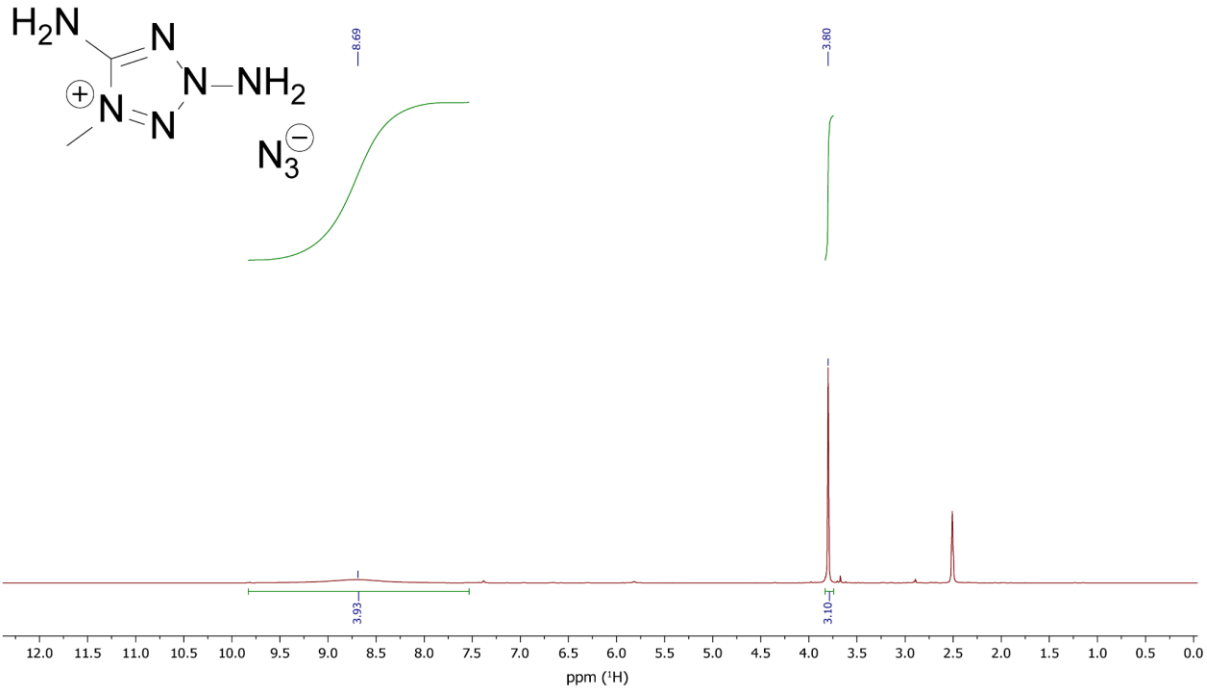

^{13}C-NMR (101 MHz, DMSO-D$_6$, ppm)

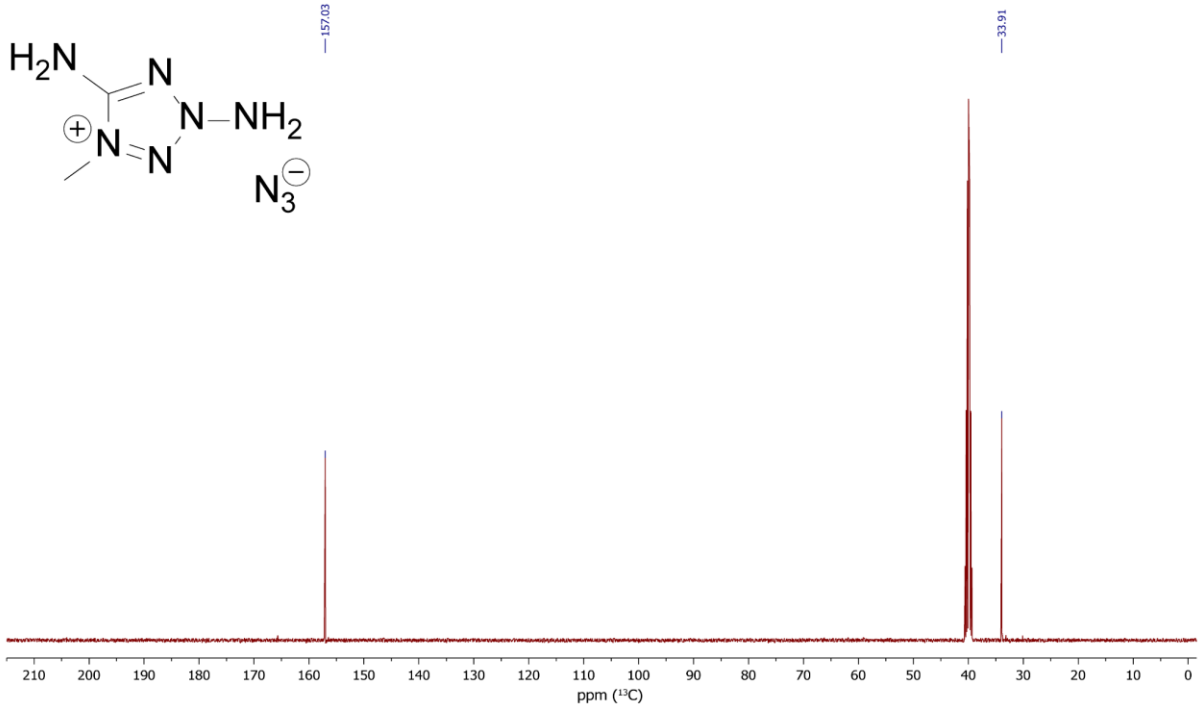

^{1}H-NMR (400 MHz, DMSO-D$_6$, ppm)

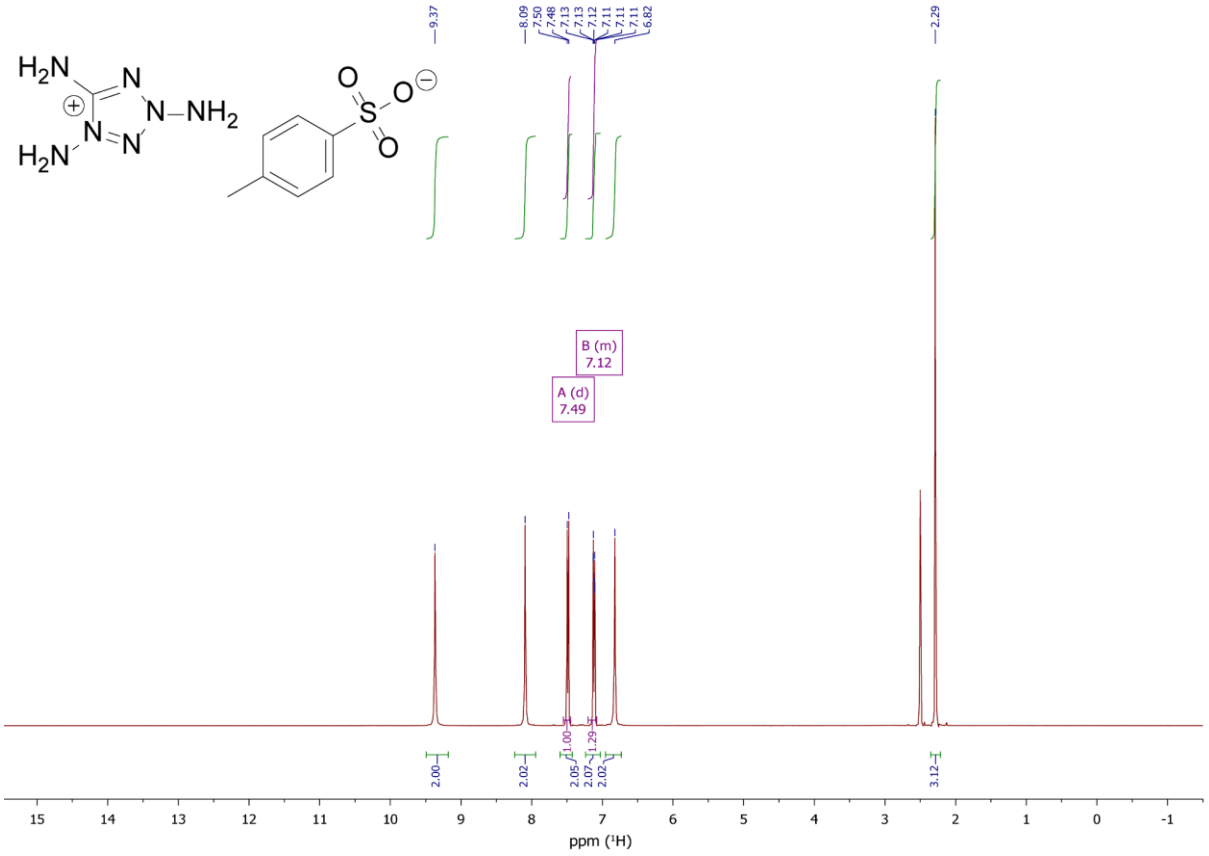

^{13}C-NMR (101 MHz, DMSO-D$_6$, ppm)

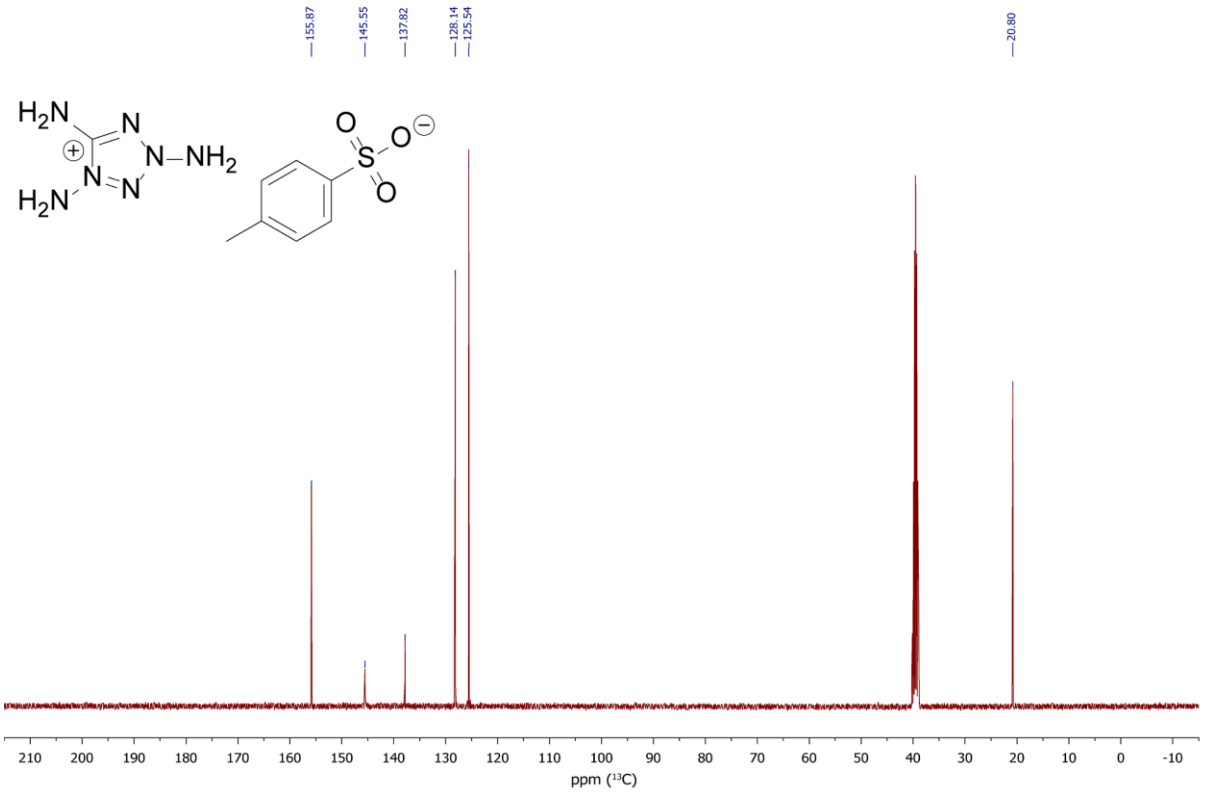

^{1}H-NMR (400 MHz, DMSO-D$_6$, ppm)

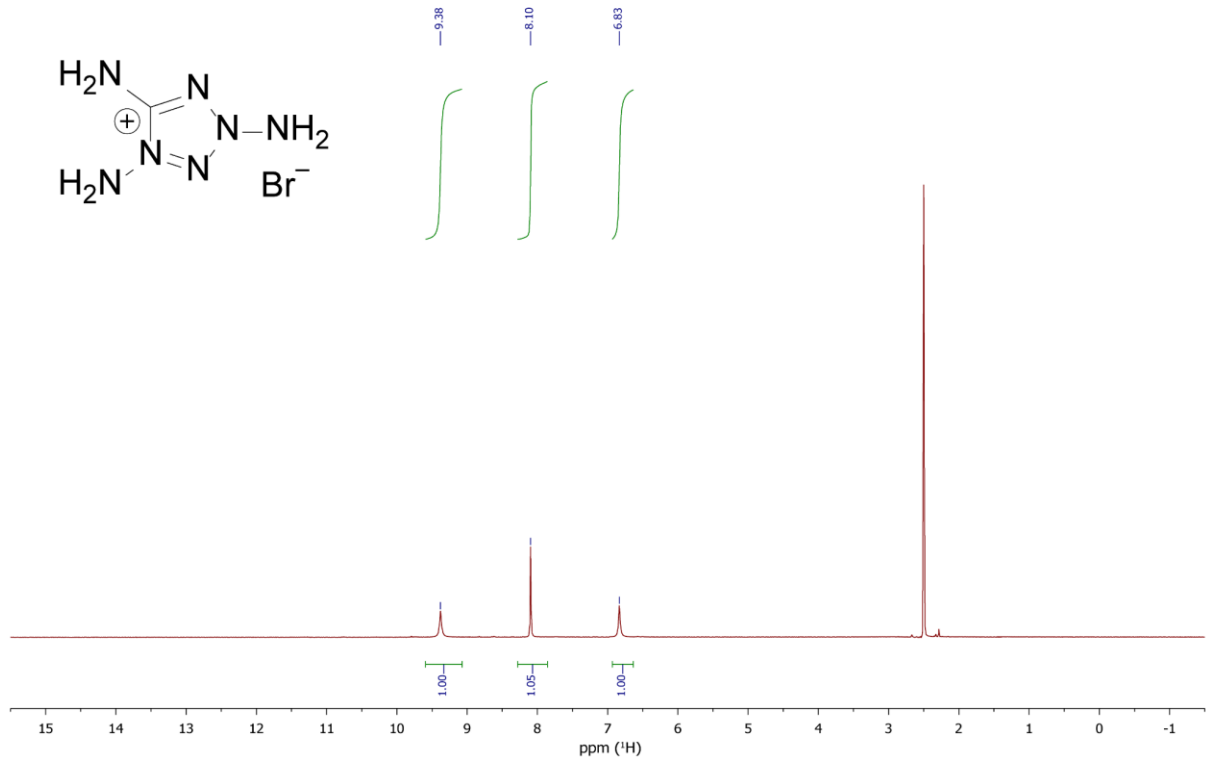

^{13}C-NMR (101 MHz, DMSO-D$_6$, ppm)

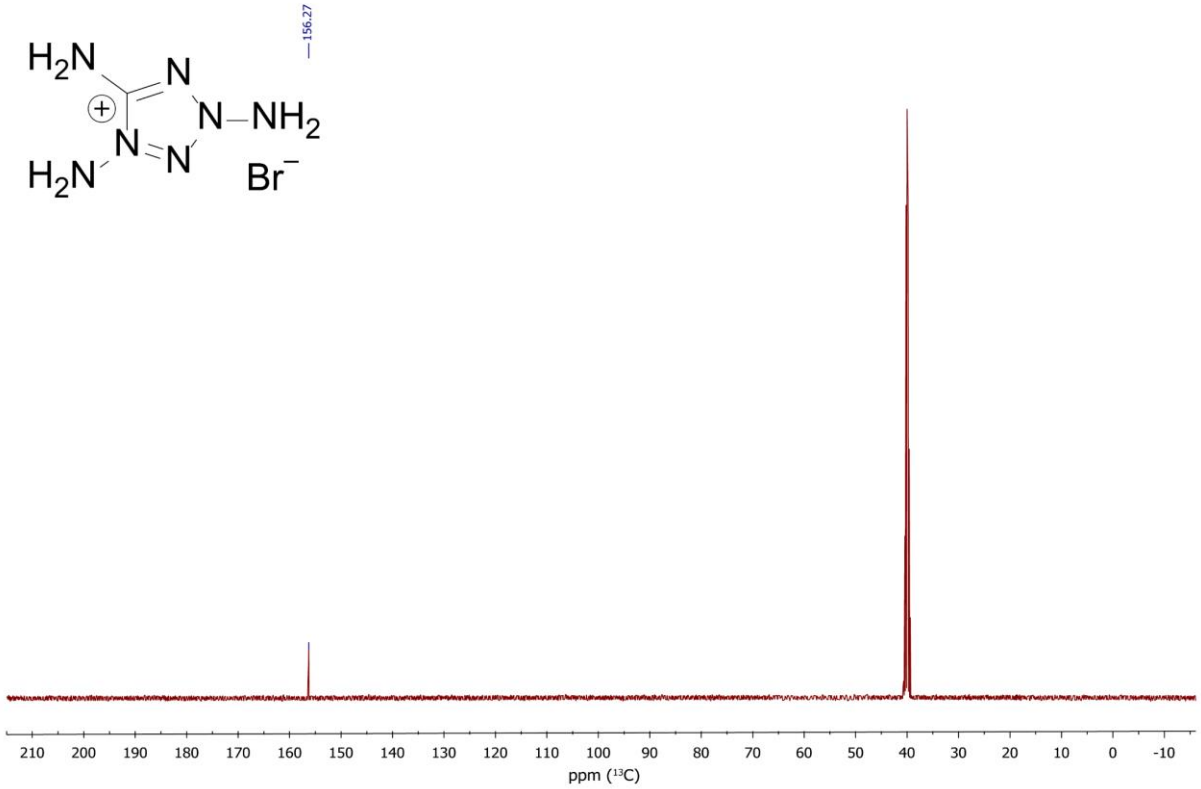

^{1}H-NMR (400 MHz, DMSO-D$_6$, ppm)

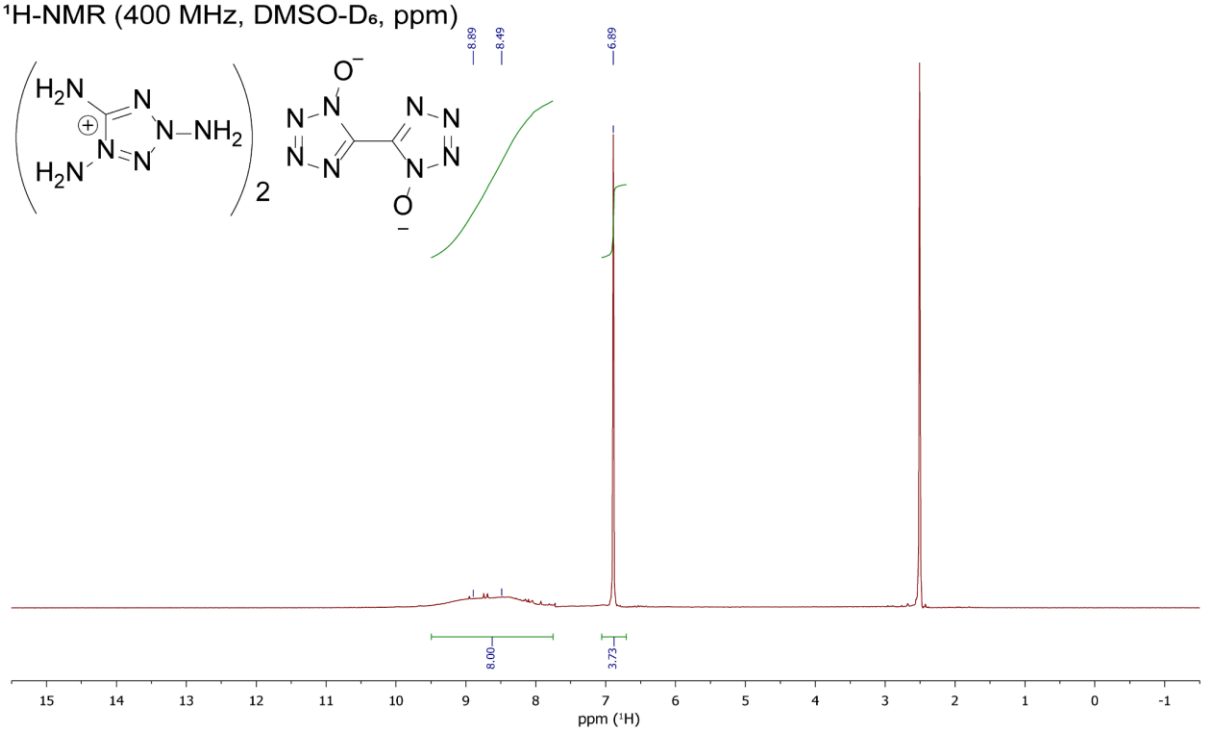

^{13}C-NMR (101 MHz, DMSO-D$_6$, ppm)

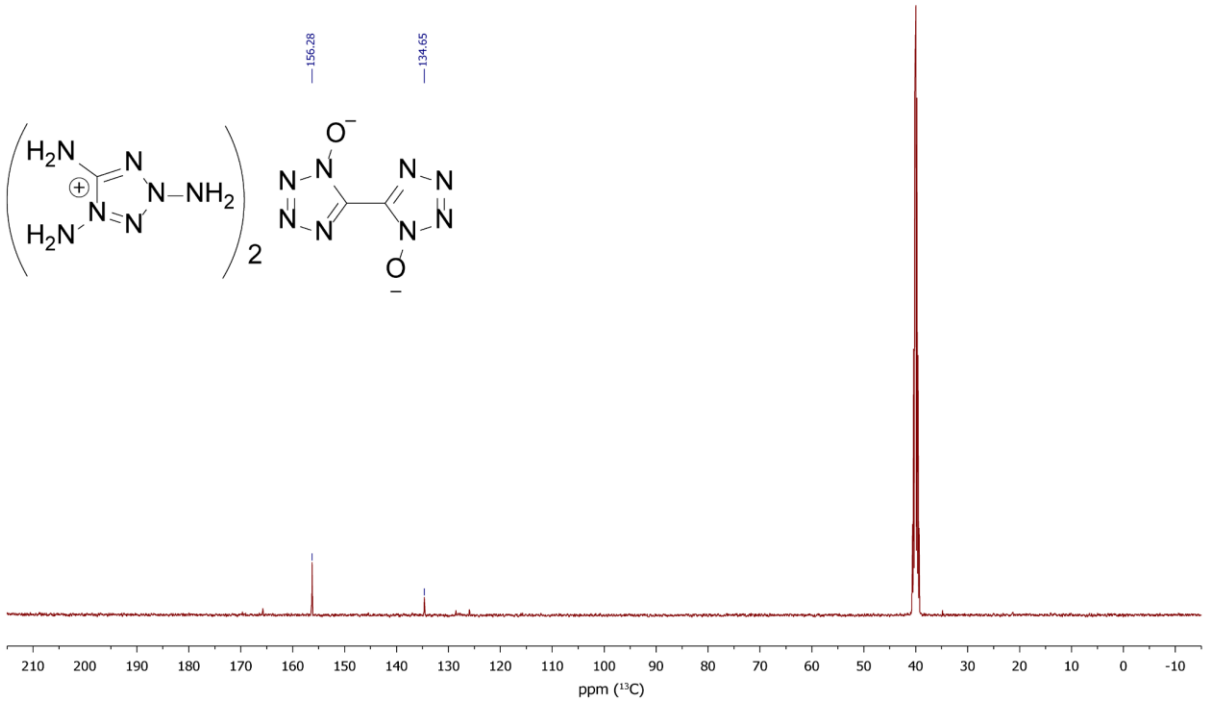

8.6.5 References

[S1] a) Test methods according to the UN Recommendations on the Transport of Dangerous Goods, *Manual of Test and Criteria*, ST/SG/AC.10/11/Rev.7, United Nations Publication, New York and Geneva, **2019**, 978-92-1-130394-0; https://unece.org/transport/dangerous-goods/rev7-files; b) Reichel & Partner GmbH, http://www.reichelt-partner.de; c) http://www.ozm.cz

[S2] M. Sućeska, EXPLO5 V6.02 program, Brodarski Institute, Zagreb, Croatia, **2014**.

[S3] R. Raap, *Can. J. Chem.* **1969**, *47*, 3677-3681.

[S4] A. L. Kovalenko, V. I. Krutikov, I. V. Tselinskii, *Zh. Org. Khim.* **1991**, *27*, 882–884.

[S5] *CrysAlisPro*, Oxford Diffraction Ltd. *version 171.33.41*, **2009**.

[S6] G. M. Sheldrick, *Acta Cryst.* **2015**, *A71*, 3–8.

[S7] O. V. Dolomanov, L. J Bourhis, R. J. Gildea, J. A. K. Howard, H. Puschmann, *J. Appl. Cryst.* **2009**, *42*, 339–341.

[S8] *SCALE3 ABSPACK – An Oxford Diffraction program* (1.0.4, gui: 1.0.3), Oxford Diffraction Ltd., **2005**.

[S9] *APEX3*. Bruker AXS Inc., Madison, Wisconsin, USA.

[S10] M. J. Frisch, G. W. Trucks, H. B. Schlegel, G. E. Scuseria, M. A. Robb, J. R. Cheeseman, G. Scalmani, V. Barone, B. Mennucci, G. A. Petersson, H. Nakatsuji, M. Caricato, X. Li, H.P. Hratchian, A. F. Izmaylov, J. Bloino, G. Zheng, J. L. Sonnenberg, M. Hada, M. Ehara, K. Toyota, R. Fukuda, J. Hasegawa, M. Ishida, T. Nakajima, Y. Honda, O. Kitao, H. Nakai, T. Vreven, J. A. Montgomery, Jr., J. E. Peralta, F. Ogliaro, M. Bearpark, J. J. Heyd, E. Brothers, K. N. Kudin, V. N. Staroverov, R. Kobayashi, J. Normand, K. Raghavachari, A. Rendell, J. C. Burant, S. S. Iyengar, J. Tomasi, M. Cossi, N. Rega, J. M. Millam, M. Klene, J. E. Knox, J. B. Cross, V. Bakken, C. Adamo, J. Jaramillo, R. Gomperts, R. E. Stratmann, O. Yazyev, A. J. Austin, R. Cammi, C. Pomelli, J. W. Ochterski, R. L. Martin, K. Morokuma, V. G. Zakrzewski, G. A. Voth, P. Salvador, J. J. Dannenberg, S. Dapprich, A. D. Daniels, O. Farkas, J.B. Foresman, J. V. Ortiz, J. Cioslowski, D. J. Fox, Gaussian 09 A.02, Gaussian, Inc., Wallingford, CT, USA, **2009**.

[S11] a) J. W. Ochterski, G. A. Petersson, and J. A. Montgomery Jr., *J. Chem. Phys.* **1996**, *104*, 2598–2619; b) J. A. Montgomery Jr., M. J. Frisch, J. W. Ochterski G. A. Petersson, *J. Chem. Phys.* **2000**, *112*, 6532–6542.

[S12] a) L. A. Curtiss, K. Raghavachari, P. C. Redfern, J. A. Pople, *J. Chem. Phys.* **1997**, *106*, 1063–1079; b) E. F. C. Byrd, B. M. Rice, *J. Phys. Chem*. A **2006**, *110*, 1005–1013; c) B. M. Rice, S. V. Pai, J. Hare, *Comb. Flame* **1999**, *118*, 445–458.

[S13] P. J. Lindstrom, W. G. Mallard (Editors), NIST Standard Reference Database Number 69, http://webbook.nist.gov/chemistry/ (accessed March **2022**).

[S14] M. S. Westwell, M. S. Searle, D. J. Wales, D. H. Williams, *J. Am. Chem. Soc*. **1995**, *117*, 5013–5015; b) F. Trouton, *Philos. Mag*. **1884**, *18*, 54–57.

[S15] a) H. D. B. Jenkins, H. K. Roobottom, J. Passmore, L. Glasser, *Inorg. Chem.* **1999,** *38,* 3609–3620; b) H. D. B. Jenkins, D. Tudela, L. Glasser, *Inorg. Chem.* **2002**, *41*, 2364–2367.

9. 1-Amino-5-nitriminotetrazole: Effective Interaction of N-Nitro and N-Amino Functionalities for Outperforming and Applicable Energetic Materials

Maximilian Benz, Thomas M. Klapötke, J. Stierstorfer, Michael Voggenreiter

as published in *ACS Applied Enineering Materials,* **2022**, *Accepted Article*

DOI: 10.1021/acsaenm.2c00031

Keywords: crystal structure, energetic materials, heterocycles, tetrazoles

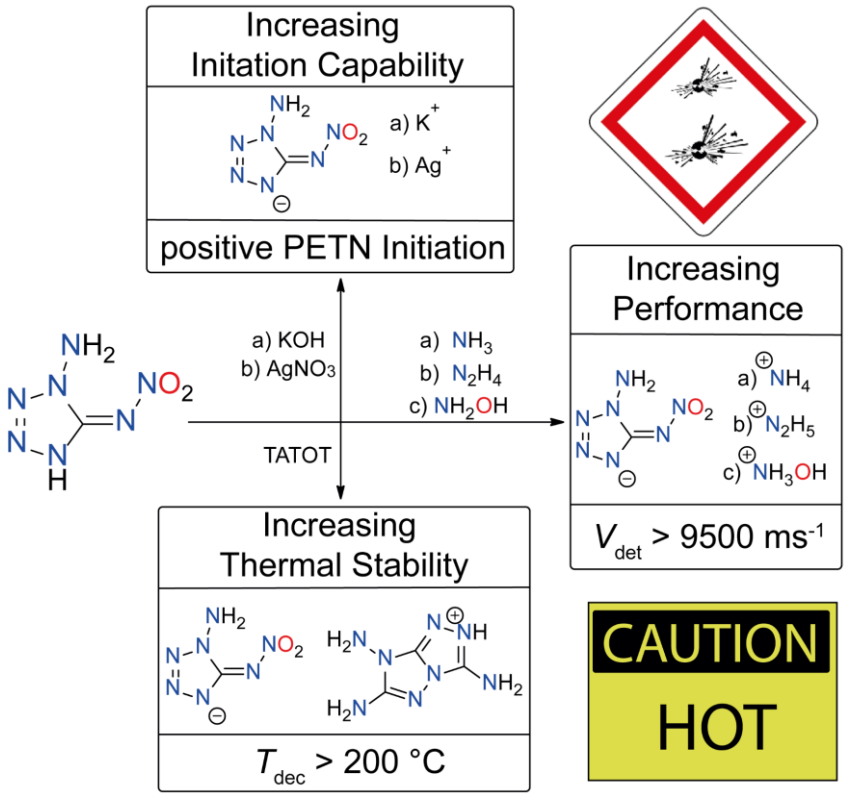

A facile synthesis of 1-amino-5-nitriminotetrazole (HANIT) and the formation of highly energetic salts thereof are reported. The nitrogen-rich salts have detonation velocities close to 10.000 m s^{-1}. The initiation capabilities can be tuned by introducing different metal cations. Further, the energetic performance can be retained but a significant increase in decomposition temperature to above 200 °C can be achieved by the TATOT cation.

Abstact: 1-Amino-5-nitriminotetrazole (HANIT) is synthesized for the first time via acid-catalyzed protection of 1,5-diaminotetrazole (1,5-DAT) with acetone followed by aprotic nitration using N_2O_5 and in situ deprotection. The salts of 1-amino-5-nitriminotetrazolate are synthesized by addition of the corresponding bases. Most of the nitrogen-rich salts show insane explosive properties and compete with the most powerful non-nuclear explosives. The implementation of a fused triazolium cation (TATOT) yields a promising secondary explosive, with high performance but also low sensitivity and high thermal stability. Metal salts (K and Ag) were successfully used to initiate PETN using a classical detonator setup. All compounds were studied by X-ray diffraction, spectroscopic analysis (NMR and IR) and DTA. The sensitivities towards external stimuli were determined and the energetic performances were calculated by the EXPLO5 using the heats of formation obtained by CBS-4M calculation.

9.1 Introduction

Since the beginning of the war in Ukraine in 2022, the defense industry has returned to public interest, and so has research on new energetic environmentally friendly materials. Ideally, these should release energy and environmentally compatible substances (N_2, CO_2 H_2O) in case of detonation.[1] A good starting building block for such energetic materials are tetrazoles, since they exhibit a high nitrogen content itself and a high heat of formation, which can be further enhanced by the introduction of suitable energetic substituents.[1] For example, 5-azidotetrazole and 5-nitrotetrazole feature high heats of formation but various drawbacks as neutral compounds, such as high sensitivity or low thermal stability.[2-5] A good equity is 5-nitriminotetrazole which offers a good combination of heat of formation, stability and energetic performance as neutral compound.[6,7] Over the last decades, 5-nitriminotetrazole was studied and further functionalized at N1 of the tetrazole.[8-9] Some of the representatives can be found in Figure 1. It was possible to obtain alkylated species, in particular the 1-methyl-5-nitriminotetrazole, which has less energetic properties than the parent compound but is also much less sensitive towards impact and friction.[7] The salts of 1-hydroxy-5-nitriminotetrazole feature very good properties but on the other hand,

no values for the neutral compound are available.[10] *Fischer et al.* succeeded in the preparation of 1,5-di(nitramino)tetrazole which has an incredibly detonation velocity of about 10 000 m s^{-1} but at the same time features extreme sensitivities.[11] Another remarkable compound is the 1-nitramino-5-aminotetrazole which is extremely sensitive and less thermally stable but has good detonative properties.[12] The constitutional isomer 1-amino-5-nitriminoterazole has comparable energetic properties with far greater thermal and mechanical stability. This compound was also reported by *Fischer* in a six-step synthesis starting from CS_2.[13]

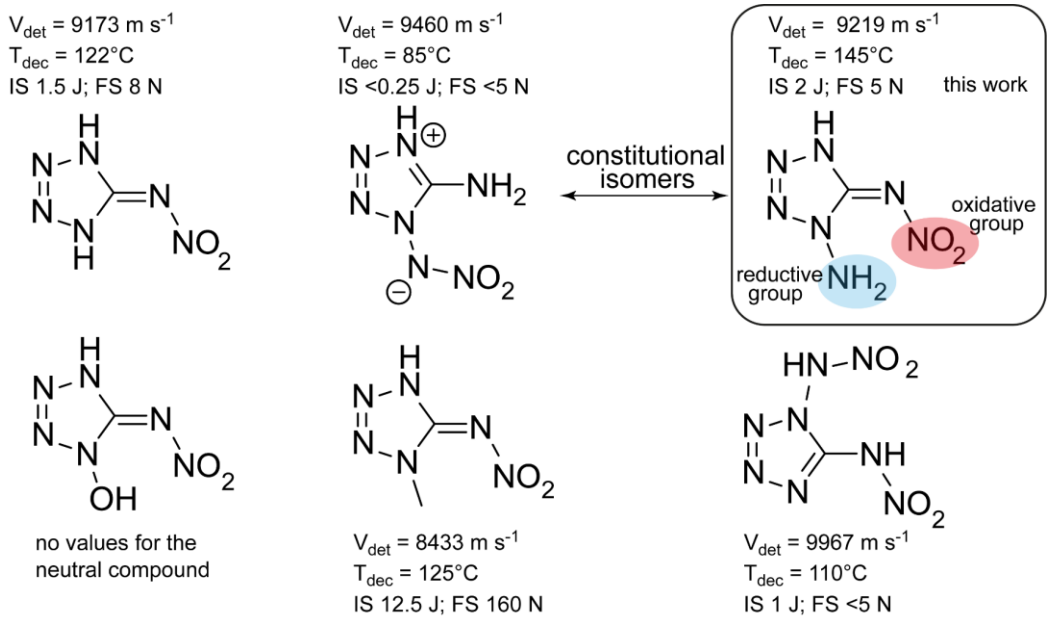

Figure 1. Comparison of different nitriminotetrazoles with emphasis on the constitutional isomers 1-nitramino-5-aminotetrazole and 1-amino-5-nitriminotetrazole, which was synthesized in this work.[7-10]

However, in addition to the high number of synthetic steps and poor yields, the synthesis method also has the disadvantage that in the final step, 3,6-dinitramino-1,2,4,5-tetrazine is formed next to the desired 1-amino-5-nitriminotetrazole. However, we have successfully developed a new and more attractive route with better yields toward this promising target molecule.

In this work, we report on the facile synthesis of 1-amino-5-nitrimino-tetrazole and six different energetic salts, all of which exhibit excellent energetic properties.

9.2 Results and Discussion

1,5-Diaminotetrazole and 1-isopropylideneamino-5-aminotetrazole were synthesized according to literature procedures.[14-16] The main challenge was to reverse the reactivity within the molecule in order to get only a mono-nitration at the more unreactive C-NH_2 position and at the same time to remain the nucleophilic and easy oxidizable N-NH_2 group. It was necessary to use acetone as protecting agent for the hydrazine function at position N1. The hydrazon functionality, which can be easily and selectively introduced on the hydrazine function, can be nitrated under aprotic conditions, since it is already labile under slightly acidic conditions. Therefore, an exact stochiometric amount of dinitrogen pentoxide (obtained through dehydration of HNO_3 using P_4O_{10}) (1.0 eq) was used to obtain 1-isopropylideneamino-5-nitraminotetrazole as intermediate.

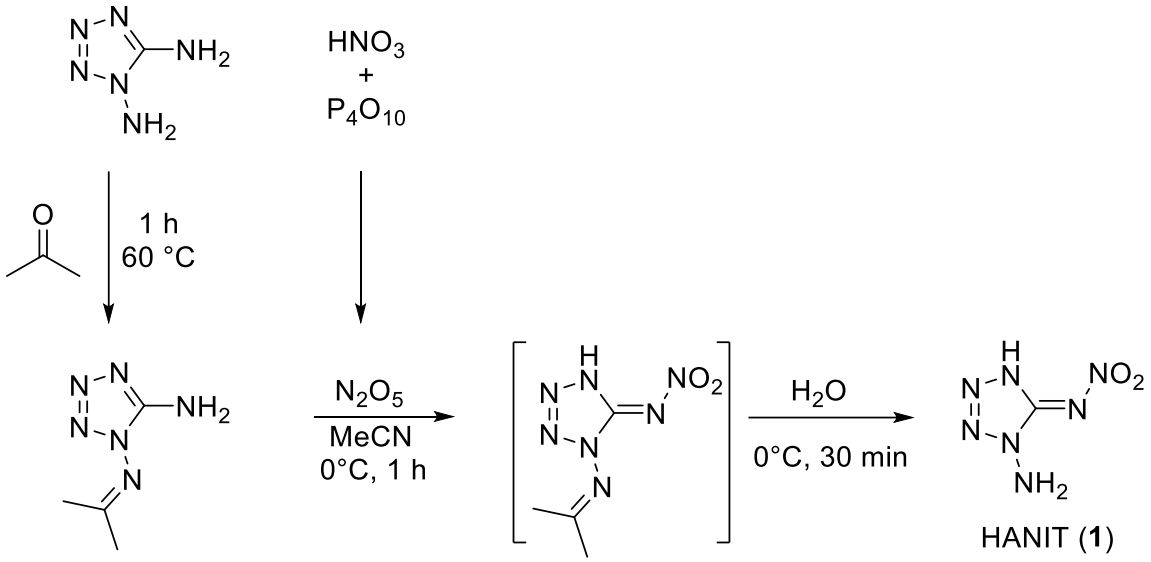

Scheme 1. Direct nitration of 1-isopropylideneamino-tetrazole-5-amine with dinitrogen pentoxide which cleaves the protection group upon quenching with water to yield 1-amino-5-nitriminotetrazole (HANIT, **1**).

Upon quenching with ice-water, the residual nitrate anion of dinitrogen pentoxide forms nitric acid which splits off the protection group of the amine to form the target molecule 1-amino-5-nitriminotetrazole (HANIT, **1**) (Scheme 1).

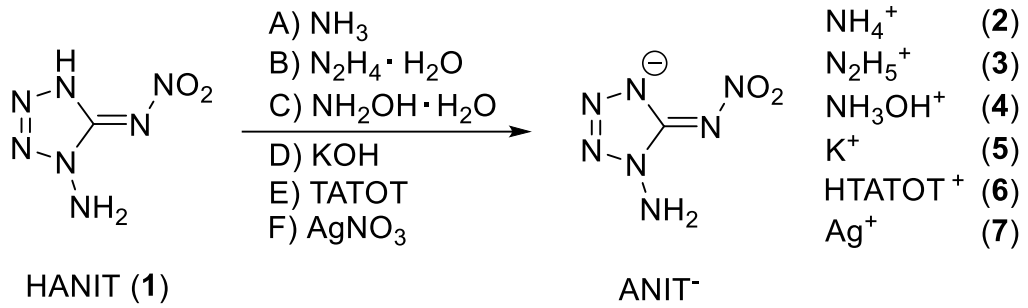

TATOT = 3,6,7-triamino-[1,2,4]triazole[4,3-b][1,2,4]triazole

Scheme 2. Synthetic pathway toward the formation of ionic derivatives **2**–**7**.

HANIT (**1**) had to be extracted with ethyl acetate quickly from the still cold reaction mixture, since the compound has a high solubility in water at room temperature. **1** was then obtained as a yellow crystalline solid in 70% yield. For the formation of the salts, one equivalent of **1** was dissolved in water or ethanol, respectively and one equivalent of the respective base was added. For the precipitation of the silver derivative **7**, an aqueous solution of **1** was treated with silver nitrate solution (Scheme 2).

Single crystals suitable for X-ray diffraction of **1**–**7** were obtained by recrystallization from common organic solvents or water.

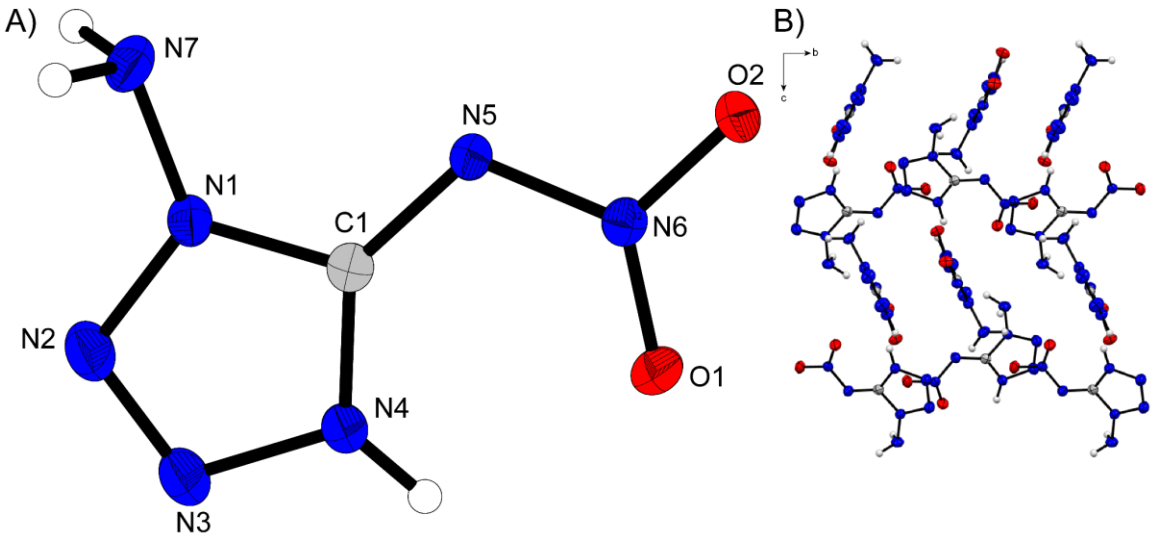

Figure 2. A) Molecular unit of **1** with thermal ellipsoids drawn at the 50% probability level. Selected bond and intermolecular distances (Å) and angles [°]: N4-H4 0.85 (2), N1-N7 1.391(2), C1-N5 1.345(2), O2-H11 1.87(2), O3-H7B 2.16(2), N2-H14A 2.57(2), N5-N6-O1 124.4(1), N6-N5-C1-N4 5.7(2), O2-H11-N11 167.0(2); B) layer structure of **1** with view along the *a*-axis.

Details on the measurement and refinement data for every compound can be found in the Supporting Information. The data were uploaded to the CSD database with the CCDC numbers 2173496-2173502.

HANIT (**1**) crystallizes in the monoclinic space group $P2_1/n$ a density of 1.746 g cm^{-3} at 298 K (Figure 2A). The molecule itself is completely planar. The strongest intermolecular interaction can be found between the oxygen of the nitro group (O2) and the acidic proton of the tetrazole (H11-N11) (d(O2···H11-N11) = 1.87(2) Å). The layer structure of **1** is characterized through a variety of interactions originating from all protons with the oxygens of the nitramino group as well as with N2 of the tetrazole.

Hydroxylammonium 1-amino-5-nitriminotetrazolate (**4**) crystallizes in the triclinic space group $P-1$ and a density of 1.841 g cm^{-3} at 173 K with two molecular units per cell. The density is therefore in the same range as for bis hydroxylammonium 1,5-dinitriminotetrazolate (ρ(173 K) = 1.847 g cm^{-3})[11].

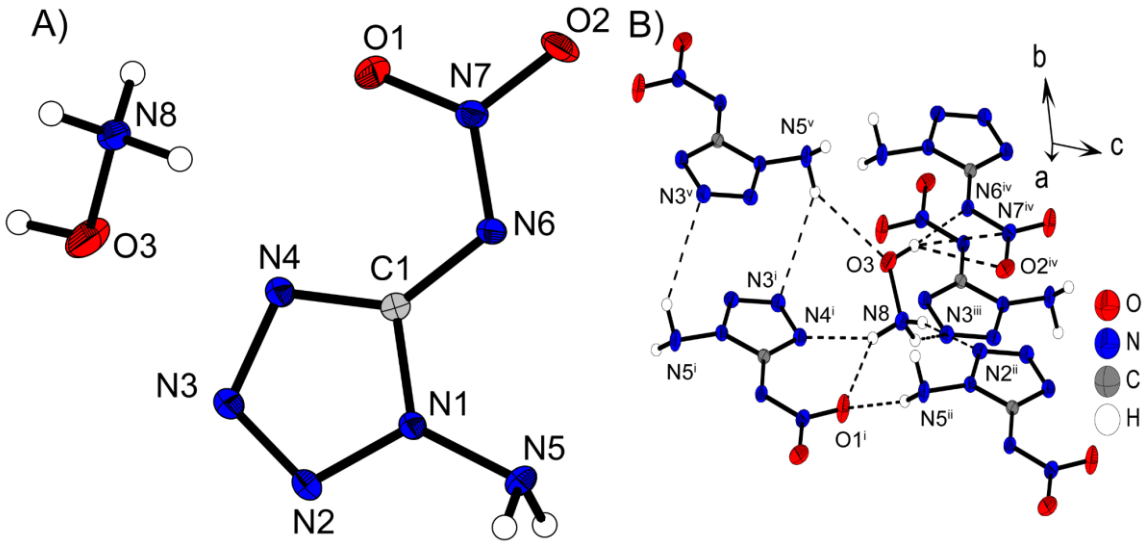

Figure 3. A) Molecular unit of **4** with thermal ellipsoids drawn at the 50% probability level. Selected bond and intermolecular distances (Å) and angles [°]: N1-N5 1.3907 (17), C1-N6 1.366(2), O3-N8 1.403(2), N4-H8A 1.99(2), N6-H3 1.85(2), N5-N1-C1 126.51(11), N7-N6-C1 117.13(10), N4-H8A-N8 149(2), N6-H3-O3 177(3), O1-N7-N6-C1 1.2(3); B) coordination sphere of one hydroxylammonium cation, symmetry codes: (i) 1−x, −y, −z; (ii) 1−x, −y, 1−z, (iii) 1+x, y, z, (iv) 2−x, 1−y, 1−z, (v) x, y, z−1.

The structure is mainly characterized through the interactions between the protons of the hydroxylammonium cation and the 1-amino-5-nitriminotetrazolate anion. The coordination sphere of one hydroxylammonium unit is depicted in Figure 3B). The shortest ones have a bond distance of below 2 Å (N6-H3 1.85(2) Å, N6-H3-O3

177(3)°; N4-H8A 1.99(2) Å, N4-H8A-N8 149(2)°) Additional to the hydrogen bridges between the anions and cations, some minor strong ones are formed originated from the protons of the N5 protons of the amino group of the anion. This results in pairwise interactions between two $ANIT^-$ units (N3-H5B 2.66(3) Å, N3-H5B-N5 136.2(2)°).

Differential thermal analysis (DTA) for ammonium **2** and hydroxylammonium **4** salts showed melting points at 170 °C and 155 °C followed by decomposition at 185 °C and 170 °C, respectively. Compounds **5**, **6** and **7** have decomposition temperatures above 200 °C with the potassium derivative (T_{dec} = 244 °C) being thermally most stable one followed by the silver (**7**, 218 °C) and HTATOT (**6**, 215 °C) derivatives. In relation to the parent compound **1** (145 °C), the thermal stability increases for all synthesized ionic derivatives. All compounds were analyzed regarding their sensitivity according to BAM standards. HANIT has an impact sensitivity of 2 J and a friction sensitivity of 5 N, which is in the range of primary explosives, but the neutral compound can be handled safely if all precautions such as plastic and grounded equipment are obeyed. All tested salts are sensitive towards impact with sensitivities of 1–2 J except **6** which is rather insensitive towards external stimuli (IS = 20 J, FS = 240 N). The potassium salt **5** is just as sensitive to friction as the neutral compound **1** with detonative decomposition at 5 N and the silver salts **7** is extremely sensitive with values below our measuring limit. The other salts can be classified as friction sensitive with a detonation occurring at forces of 15–20 N. The heat of formation of the respective compounds were calculated on the CBS-4M level of theory using the atomization method. All compounds have highly positive calculated enthalpies of formation (**1**: +416.1 kJ mol^{-1}; **6**: +898.1 kJ mol^{-1}). Combined with the crystallographic densities recalculated to room temperature, the energetic performances were calculated with EXPLO5 code.[17] (Table 1) All synthesized compounds have detonation velocities of over 9000 m s^{-1}, the hydrazinium (**3**) and hydroxylammonium (**4**) salt even reach almost 10 000 m s^{-1}. Calculated detonation velocities easily outperform RDX and especially **3** and **4** even compete with TKX–50. The detonation pressure of **4** is 402 kbar, which is slightly higher than for RDX (380 kbar) and in the same range as the value for TKX–50 (401 kbar).

Table 1. Comparison of compounds **1**–**7** with TKX-50[18] and RDX[18].

	1	**2**	**3**	**4**	**5**	**6**	**7**	**TKX-50**	**RDX**
Formula	$CH_3N_7O_2$	$CH_6N_8O_2$	$CH_7N_9O_2$	$CH_6N_8O_3$	$CH_2N_7O_2K$	$C_4H_{11}N_{15}O_2$	$CH_2N_7O_2Ag$	$C_2H_8N_{10}O_4$	$C_3H_6N_6O_6$
IS [J][a]	2	1	2	2	<1	20	<1	20	7.5
FS [N][b]	5	20	15	20	5	240	<0.1	120	120
ρ_{298K} [g cm^{-3}][c]	1.746	1.731	1.725	1.807	1.98[j]	1.803	2.988	1.877	1.806
N+O [%][d]	89.64	71.00	89.23	89.86	71.00	80.37	51.62	86.41	81.06
T_{melt} / T_{dec} [°C][e]	–/145	170/185	–/175	155/170	–/244	–/215	–/218	–/221	205/210
$\Delta_f H°$ [kJ mol^{-1}][f]	416.1	377.6	528.9	436.1	−165.5	898.1	-	446.6	86.3
$-\Delta_E U°$ [kJ kg^{-1}][g]	5793	5400	5899	6343	2966	4595	-	5758	5740
				EXPLO5 V6.05.02					
V_{det} [m s^{-1}][h]	9219	9557	9849	9915	7789	9312	-	9940	8801
$p_{C\text{-}J}$ [kbar][i]	343	347	370	402	235	324	-	401	336

[a] Impact sensitivity (BAM drophammer, 1 of 6). [b] Friction sensitivity (BAM friction tester, 1 of 6). [c] Density from X-ray diffraction analysis recalculated to 298 K: $\rho_{298K} = \rho_T/[1 + \alpha_V(298\ K - T)]$ where $\alpha_V = 1.6 \times 10^{-4}\ K^{-1}$.[1] [d] Combined nitrogen and oxygen content. [e] Melting/decomposition temperature (DTA, β = 5 °C min^{-1}). [f] Calculated enthalpy of formation, CBS-4M. [g] Energy of explosion (EXPLO5, ver. 6.05.02).[17] [h] Detonation velocity (EXPLO5, ver. 6.05.02).[17] [i] Detonation pressure at the Chapman−Jouguet point (EXPLO5, ver. 6.05.02).[17] [j] Gas pycnometer at 298 K.

To get a better insight into the high sensitivities of the neutral compound 1 despite the stabilizing amino-nitro push-pull system, a natural bond orbital (NBO) calculation was performed (Figure 4A). The most positively polarized atoms to central N6 atom of the nitrimine function and the carbon atom of the tetrazole. The strongest negatively charged atoms are N7, followed by N5 and the two oxygen atoms. Due to the clear charge distribution in the molecule, it can be assumed that intermolecular interactions can form here, which is also shown by the crystal structure analysis.

Potassium and silver salt **5** and **7**, unlike the other compounds, showed detonation when heated, therefore we performed an initiation test to investigate whether **5** is suitable as a primary explosive. The setup consists of 200 mg pressed PETN (80 N) in a copper tube and 50 mg of unpressed **5** filled on top.

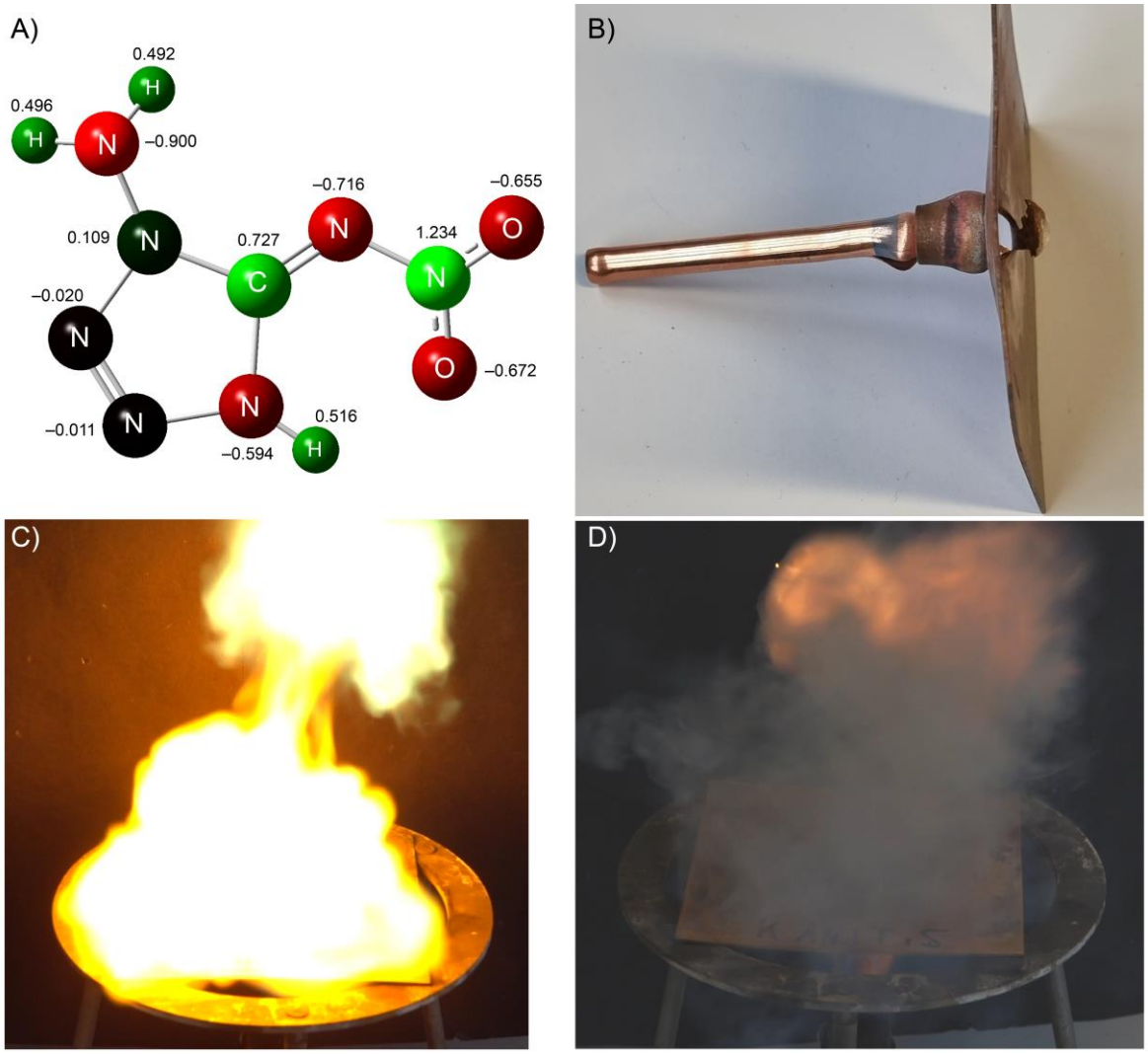

Figure 4. A) Charge distribution as NBO calculation result of the neutral compound **1**. B) Result of the positive initiation test of the potassium derivative **5**. C) Deflagration of HANIT (**1**) on the hot plate test. D) Detonation of KANIT (**5**) on the hot plate test.

The charge is ignited by a commercial igniter. A hole or dent in the copper base plate suggests a positive initiation test. Potassium salt **5** is capable of detonating PETN. (Figure 4B) The same result could be obtained for the silver derivative **7**. To visualize the different thermal behavior upon rapid heating, a hot plate test was performed for compounds **1** and **5**. As depicted in Figure 4C–D, the neutral compound 1 only deflagrates violently, whereas KANIT (**5**) detonates with a dull bang and a smoke cloud.

9.3 Conclusion

We conclude that 1-amino-5-nitriminotetrazole and its salts are very powerful energetic materials. All offer higher thermal stability, higher energetic performance at comparable sensitivities with respect to other 5-nitriminotetrazole derivatives. Hydroxylammonium 1-amino-5-nitriminotetrazolate (**4**), with a detonation velocity of 9915 m s^{-1}, competes with the most powerful non-nuclear explosives but is rather sensitive. The TATOT salt **6** is the most promising derivative, yet, for use as secondary explosive due to low sensitivity (IS 20 J, FS 240 N) combined with a high detonation velocity of higher than 9300 m s^{-1} and a thermal stability of 215 °C. Potassium and silver ANIT derivatives **5** and **7** show promising properties for the use as primary explosives, since they resist decomposition temperatures higher than 200 °C (244 °C for **5** and 218 °C for **7**). Both derivatives are also capable of initiating PETN in a classical initiation test. With this rather simple synthesis, which features a three-step synthesis to the respective ionic derivatives starting from 1,5-diaminotetrazole, we fill a gap in the synthetic world of high-performing energetic tetrazoles and open an important door to future derivatization towards new materials.

9.4 Acknowledgement

Financial support of this work by Ludwig Maximilian University (LMU), the Office of Naval Research (ONR) under Grant ONR N00014-19-1-2078, and the Strategic Environmental Research and Development Program (SERDP) under Contract W912HQ19C0033 is gratefully acknowledged.

9.5 References

[1] T. M. Klapötke, *Chemistry of High-Energy Materials* **2019**, Berlin, Boston: de Gruyter.

[2] T. M. Klapötke, J. Stierstorfer, *J. Am. Chem. Soc.* **2009**, *131*, 1122–1134.

[3] J. Stierstorfer, T. M. Klapötke, A. Hammerl, R. D. Chapman, *Z. Anorg. Allg. Chem.* **2008**, *634*, 1051–1057.

[4] T. M. Klapötke, D. G. Piercey, N. Mehta, K. D. Oyler, M. Jorgensen, S. Lenahan, J. S. Salan, J. W. Fronaberger, M. D. Williams, *Z. anorg. allg. Chem.* **2013**, *639*, 681–688.

[5] T. M. Klapötke, C. M. Sabaté, J. Stierstorfer, *New J. Chem.* **2009**, *33*, 136–147.

[6] J. A. Garrison, R. M. Herbst, *J. Org. Chem.* **1957**, *22(3)*, 278–283.

[7] T. M. Klapötke, J. Stierstorfer, *Helv. Chim. Acta* **2007**, *90*, 2132–2150.

[8] Y.-H. Joo, J. M. Shreeve, *Angew. Chem. Int. Ed.* **2010**, *49*, 7320–7323; *Angew. Chem* **2010**, *122*, 7478–7481.

[9] Y.-H. Joo, J. M. Shreeve, *Angew. Chem. Int. Ed.* **2009**, *48*, 564–567; *Angew. Chem* **2009**, *121*, 572–575.

[10] D. Fischer, T. M. Klapötke, J. Stierstorfer, *Eur. J. Inorg. Chem.* **2015**, 4628–4632.

[11] D. Fischer, T. M. Klapötke, J. Stierstorfer, *Angew. Chem. Int. Ed.* **2015**, *54*, 10299–10302; *Angew. Chem.* **2015**, *127*, 10438–10441.

[12] a) T. M. Klapötke, F. A. Martin, J. Stierstorfer, *Chem. Eur. J*. **2012**, *18*, 1487–1501; b) L. Lui, C. He, C. Li, Z. Li *J. Chem. Crystallogr.* **2012**, *42*, 816–823.

[13] D. Fischer, T. M. Klapötke, J. Stierstorfer, 15*th New Trends in Research of Energetic Materials Seminar, Pardubice, Czech*, **2012**, 115–127.

[14] Y.-H. Joo, B. Twamley, S. Garg, J. M. Shreeve, *Angew. Chem. Int. Ed.* **2008**, *47*, 6236–6239; *Angew. Chem.* **2008**, *120*, 6332–6335.

[15] P. N. Gaponik, V. P. Karavai, *Chem. Heterocycl. Compd.* **1984**, *20*, 1388–1391.

[16] F. Li, Y. Cong, Z. Du, C. He, L. Zhao, L. Meng, *New J. Chem.* **2012**, *36*, 1953–1956.

[17] M. Suceska, EXPLO5 program, Zagreb, Croatia, **2018**.

9.6 Supporting Information

9.6.1 Experimental Procedure

All chemicals and solvents were employed as received (Sigma-Aldrich, Fluka, Acros). ^{1}H, ^{13}C, ^{14}N and ^{15}N NMR spectra were recorded using a JEOL Eclipse 270, JEOL EX 400 or a JEOL Eclipse 400 instrument. The chemical shifts quoted

in ppm in the text refer to typical standards such as tetramethylsilane (^{1}H, ^{13}C) and nitromethane (^{14}N and ^{15}N). To determine the dehydration, melting and decomposition temperatures of the described compounds an OZM Research DTA 552-Ex instrument (heating rate 5 °C min^{-1} in the range of 25–400 °C) was used. Infrared spectra were measured with pure samples on a Perkin-Elmer BXII FT-IR system with a Smith DuraSampler IR II diamond ATR unit. Determination of the carbon, hydrogen and nitrogen contents were carried out by combustion analysis using an Elementar Vario El (nitrogen values determined are often lower than the calculated ones due to their explosive behavior). Sensitivities toward impact (IS) and friction (FS) were determined according to the UN Recommendations on the Transport of Dangerous Goods (ST/SG/AC.10/11/Rev.7) using a BAM drop hammer and a BAM friction apparatus by applying the 1 of 6 method.[S1] All energetic compounds were tested for sensitivity towards electrical discharge using an Electric Spark Tester ESD 2010 EN from OZM. Energetic properties have been calculated with the EXPLO5 6.02 computer [S2] code using the RT converted X-ray density and calculated solid state heats of formation.

CAUTION! *All described compounds are powerful energetic materials with high sensitivities towards shock and friction. Therefore, proper security precautions (safety glass, face shield, earthened equipment and shoes, Kevlar gloves and ear plugs) have to be applied all time while synthesizing and handling the described compounds. Especially KANIT (**5**) and AgANIT (**7**) are extremely sensitive.*

1-Amino-5-nitriminotetrazole (**1**)

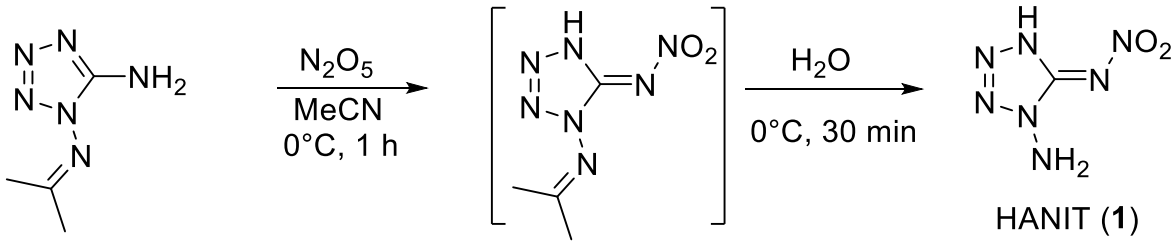

HANIT (**1**)

1-(Propan-2-ylideneamino)-1*H*-tetrazol-5-amine (1.00 g, 7.14 mmol, 1.0 eq.) was suspended in MeCN (5 mL), cooled to 0°C and then dinitrogen pentoxide (0.77 g, 7.14 mmol, 1.0 eq.) in MeCN (15 mL) was added at 0°C. The mixture dissolved

while turning yellow and was stirred for 45 minutes. The solution was poured onto ice (70 g) and extracted with cold ethyl acetate (3 x 25 mL). The combined organic layers were washed with cold brine solution (1 x 25 mL) prior to drying. The solvent was removed to yield 0.72 g (4.96 mmol, 70%) of 1-amino-5-nitriminotetrazole as yellow crystals.

DTA (5 °C min^{-1}): 145 °C (exo, dec.); Sensitivities (≤500 µm): BAM drop hammer: 2 J, friction tester: 5 N, ESD: 40 mJ; IR (ATR) $\tilde{\nu}$ (cm^{-1}) = 3320(m), 3250(m), 3204(m), 3142(m), 1710(m), 1579(s), 1480(m), 1435(s), 1300(s), 1238(vs), 1034(s), 991(s), 950(s), 872(s), 776(s), 753(s), 712(s), 699(s), 643(s), 570(s), 522(s), 463(s), 433(s), 424(s), 409(s); Elem. Anal. ($CH_3N_7O_2$, 145.08 g mol^{-1}) calcd.: C 8.28, H 2.08, N 67.58 %. Found: C 7.83, H 2.54, N 66.74 %; ^{1}H NMR (DMSO-d_6, 400 MHz, ppm) δ = 8.86 (br s, 3H); ^{13}C NMR (DMSO-d_6, 101 MHz, ppm) δ = 149.0; ^{14}N NMR (DMSO-d_6, 29 MHz, ppm) δ = −8.

Ammonium 1-amino-5-nitriminotetrazolate (**2**)

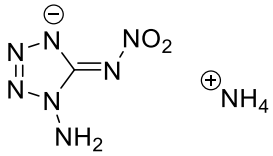

1-Amino-5-nitriminotetrazole (0.30 g, 2.07 mmol, 1.0 eq.) was dissolved in ethanol (10 mL) and ammonia solution (2 M in EtOH, 1.04 mL, 2.07 mmol, 1.0 eq) was added. The solution was stirred for 10 min at 50 °C and the solvent was evaporated. Ammonium 1-amino-5-nitriminotetrazolate (0.29 g, 1.80 mmol, 87%) was obtained after recrystallization from EtOAc/EtOH as orange crystalline powder.

DTA (5 °C min^{-1}): 170 °C (endo, melt.) followed by 185 °C (exo, dec.); Sensitivities (≤500 µm): BAM drop hammer: 1 J, friction tester: 20 N; IR (ATR) $\tilde{\nu}$ (cm^{-1}) = 3324(m), 3304(w), 3254(m), 3192(s), 3034(m), 2845(m), 1611(w), 1507(s), 1440(s), 1385(m), 1362(s), 1282(vs), 1188(s), 1101(s), 1029(s), 991(m), 933(s), 892(s), 775(m), 758(m), 736(m), 709(m), 684(m), 668(w), 532(m), 469(m), 455(m), 448(m), 440(m), 422(w), 415(w), 403(m); Elem. Anal. ($CH_6N_8O_2$, 162.11 g mol^{-1}) calcd.: C 7.41, H 3.73, N 69.12 %. Found: C 7.21, H 3.63, N 68.09 %; ^{1}H NMR

(DMSO-d_6, 400 MHz, ppm) δ = 7.14 (m, 4H), 6.20 (s, 2H); ^{13}C NMR (DMSO-d_6, 101 MHz, ppm) δ = 155.0; ^{14}N NMR (DMSO-d_6, 29 MHz, ppm) δ = −14, −358.

Hydrazinium 1-amino-5-nitriminotetrazolate (**3**)

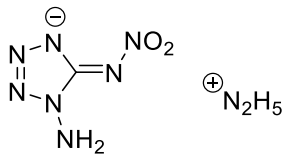

1-Amino-5-nitriminotetrazole (0.25 g, 1.72 mmol, 1.0 eq.) was dissolved in ethanol (10 mL) and hydrazinium hydroxide (83 µL, 1.72 mmol, 1.0 eq) was added. The solution was stirred for 10 min at 50 °C and the solvent was evaporated. Hydrazinium 1-amino-5-nitriminotetrazolate (0.24 g, 1.33 mmol, 77%) was obtained after recrystallization from EtOAc/EtOH as yellowish powder.
DTA (5 °C min^{-1}): 175 °C (exo, dec.); Sensitivities (≤500 µm): BAM drop hammer: 2 J, friction tester: 15 N; IR (ATR) $\tilde{\nu}$ (cm^{-1}) = 3290(s), 3121(s), 2942(m), 2633(m), 1657(m), 1538(m), 1510(s), 1461(m), 1450(m), 1358(s), 1318(vs), 1152(m), 1129(s), 1090(vs), 1020(s), 1007(s), 976(s), 965(s), 880(m), 768(s), 753(s), 735(s), 706(s), 699(s), 686(m), 645(m), 532(s), 475(s), 403(s); Elem. Anal. ($CH_7N_9O_2$, 177.13 g mol^{-1}) calcd.: C 6.78, H 3.98, N 71.17 %. Found: C 7.00, H 4.22, N 69.86 %; ^{1}H NMR (DMSO-d_6, 400 MHz, ppm) δ = 7.10 (s, 5H), 6.19 (s, 2H); ^{13}C NMR (DMSO-d_6, 101 MHz, ppm) δ = 155.5; ^{14}N NMR (DMSO-d_6, 29 MHz, ppm) δ = −15.

Hydroxylammonium 1-amino-5-nitriminotetrazolate (**4**)

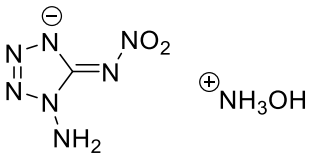

1-Amino-5-nitriminotetrazole (0.24 g, 1.66 mmol, 1.0 eq.) was dissolved in ethanol (10 mL) and aqueous hydroxylamine solution (50 wt%, 0.11 mL, 1.66 mmol, 1.0 eq) was added. The solution was stirred for 10 min at 50 °C. After cooling to room temperature, hydroxylammonium 1-amino-5-nitriminotetrazolate (0.24 g,

1.38 mmol, 81%) was precipitated by the addition of Et2O (100 mL) to the intensively stirring solution as a slightly yellow powder.

DTA (5 °C min^{-1}): 155 °C (endo, melt.) followed by 170 °C (exo, dec.); Sensitivities (≤500 µm): BAM drop hammer: 2 J, friction tester: 20 N; IR (ATR) ṽ (cm^{-1}) = 3325(m), 3213(m), 3063(m), 2852(m), 2772(m), 2674(m), 1633(m), 1516(s), 1464(s), 1419(m), 1352(s), 1307(vs), 1288(vs), 1259(s), 1187(vs), 1168(vs), 1116(s), 1039(s), 998(s), 949(s), 893(s), 776(s), 766(s), 735(vs), 705(vs), 686(s), 667(s), 519(m), 467(m); Elem. Anal. ($CH_6N_8O_3$, 178.11 g mol^{-1}) calcd.: C 6.74, H 3.40, N 62.91 %. Found: C 6.88, H 3.65, N 61.37 %; ^{1}H NMR (DMSO-d_6, 400 MHz, ppm) δ = 9.88 (br s, 4H), 6.19 (s, 2H); ^{13}C NMR (DMSO-d_6, 101 MHz, ppm) δ = 155.6; ^{14}N NMR (DMSO-d_6, 29 MHz, ppm) δ = −15, −359.

Potassium 1-amino-5-nitriminotetrazolate (**5**)

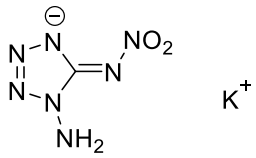

1-Amino-5-nitriminotetrazole (0.42 g, 2.86 mmol, 1.0 eq.) was dissolved in ethanol (10 mL) and potassium hydroxide (0.16 g, 2.86 mmol, 1.0 eq) dissolved in ethanol (5 mL) was added. Potassium 1-amino-5-nitriminotetrazolate precipitated instantly as yellow amorphous powder which was filtered, washed with diethyl ether and dried. Potassium 1-amino-5-nitriminotetrazolate (0.49 g, 2.65 mmol, 93%) was obtained after recrystallization from a methanol/water mixture as dark yellowish to brownish solid.

DTA (5 °C min^{-1}): 244 °C (exo, dec.); Sensitivities (≤500 µm): BAM drop hammer: <1 J, friction tester: 5 N; IR (ATR) ṽ (cm^{-1}) = 3318(m), 3204(m), 1627(m), 1504(s), 1308(vs), 1282(vs), 1101(s), 1030(s), 886(m), 830(m), 777(s), 735(m), 686(m), 419(s); Elem. Anal. ($CH_2N_7O_2K$, 183.17 g mol^{-1}) calcd.: C 6.56, H 1.10, N 53.53 %. Found: too sensitive for measuremen; ^{1}H NMR (DMSO-d_6, 400 MHz, ppm) δ = 6.20 (s, 2H); ^{13}C NMR (DMSO-d_6, 101 MHz, ppm) δ = 155.0; ^{14}N NMR (DMSO-d_6, 29 MHz, ppm) δ = −14.

3,6,7-Triamino-[1,2,4]triazole[4,3-b][1,2,4]triazolium 1-amino-5-nitriminotetrazolate (**6**)

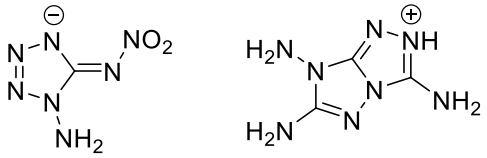

1-Amino-5-nitriminotetrazole (0.12 g, 0.83 mmol, 1.0 eq.) was dissolved in water (10 mL) and 3,6,7-triamino-[1,2,4]triazole[4,3-b][1,2,4]triazole (TATOT) (0.13 g, 0.83 mmol, 1.0 eq) was added. The solution was heated to 60 °C with the aid of an oil bath and stirred for 30 min at this temperature. After filtration, the solution was left for crystallization to yield 3,6,7-triamino-[1,2,4]triazole[4,3-b][1,2,4]triazolium 1-amino-5-nitriminotetrazolate (0.23 g, 0.76 mmol, 92%) as slightly beige crystalline solid.

DTA (5 °C min^{-1}): 215 °C (exo, dec.); Sensitivities (≤500 µm): BAM drop hammer: 20 J, friction tester: 240 N; IR (ATR) $\tilde{\nu}$ (cm^{-1}) = 3290(m), 3114(m), 3006(m), 1683(s), 1669(s), 1651(s), 1645(s), 1509(m), 1464(m), 1399(m), 1305(s), 1257(s), 1167(m), 1107(m), 1077(m), 1046(m), 1028(s), 1014(s), 974(m), 914(s), 837(m), 755(s), 707(s), 694(s), 619(s), 600(s), 521(vs), 460(s), 420(s), 413(s), 404(s); Elem. Anal. ($C_4H_9N_{15}O_2$, 299.22 g mol^{-1}) calcd.: C 16.06, H 3.03, N 70.22 %. Found: C 15.94, H 2.99, N 69.62 %; ^{1}H NMR (DMSO-d_6, 400 MHz, ppm) δ = 13.33 (br s, 1H), 8.10 (s, 2H), 7.20 (s, 2H), 6.17 (br s, 2H), 5.76 (s, 2H); ^{13}C NMR (DMSO-d_6, 101 MHz, ppm) δ = 160.6, 155.6, 148.0, 141.7; ^{14}N NMR (DMSO-d_6, 29 MHz, ppm) δ = −15.

Silver 1-amino-5-nitriminotetrazolate (**7**)

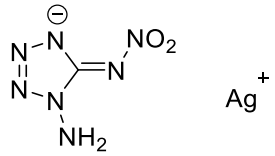

1-Amino-5-nitriminotetrazole (0.30 g, 2.07 mmol, 1.0 eq.) was dissolved in water (5 mL) and silver nitrate (0.351 g, 2.07 mmol, 1.0 eq) dissolved in water (5 mL) was

added. Silver 1-amino-5-nitriminotetrazolate precipitated instantly as dark greyish amorphous powder which was filtered, washed with water and dried. Silver 1-amino-5-nitriminotetrazolate (0.47 g, 1.87 mmol, 90%) was obtained after recrystallization from 2 M ammonia (10 mL) as greyish to colorless crystals.
DTA (5 °C min^{-1}):218 °C (exo, dec.); Sensitivities (≤500 µm): BAM drop hammer: <1 J, friction tester: <1 N; IR (ATR) $\tilde{\nu}$ (cm^{-1}) = 3203 (w), 2154 (w), 2015 (w), 1506 (m), 1465 (m), 1411 (m), 1370 (m), 1330 (s), 1263 (s), 1139 (m), 1090 (m), 1011 (m), 926 (m), 831 (m), 802 (m), 758 (m), 722 (m), 677 (m), 441 (m); Elem. Anal. ($CH_2N_7O_2Ag$, 251.94 g mol^{-1}) calcd.: C 4.77, H 0.80, N 38.92 %. Found: too sensitive for measurement; ^{1}H NMR (DMSO-d_6, 400 MHz, ppm) δ = 6.53 (s, 2H); ^{14}N NMR (DMSO-d_6, 29 MHz, ppm) δ = −4.

9.6.2 Crystallography

Crystal structure data were obtained from an Oxford Xcalibur3 diffractometer with a Spellman generator (voltage 50 kV, current 40 mA) and a Kappa CCD area for data collection using Mo-Kα radiation (λ=0.71073Å) or a Bruker D8 Venture TXS diffractometer equipped with a multilayer monochromator, a Photon 2 detector and a rotation-anode generator (Mo-Kαradiation). The data collection was performed using the CRYSTALIS RED software.[S3] The solution of the structure was performed by direct methods and refined by fullmatrix least-squares on F2 (SHELXT)[S4] implemented in the OLEX2[S5] software suite. The non-hydrogen atoms were refined anisotropically and the hydrogen atoms were located and freely refined. The absorption correction was carried out by a SCALE3 ABSPACK multiscan method.[S6] The DIAMOND2 plots shown with thermal ellipsoids at the 50% probability level and hydrogen atoms are shown as small spheres of arbitrary radius. The SADABS program embedded in the Bruker APEX3 software was used for multi-scan absorption corrections in all structures.[S7]

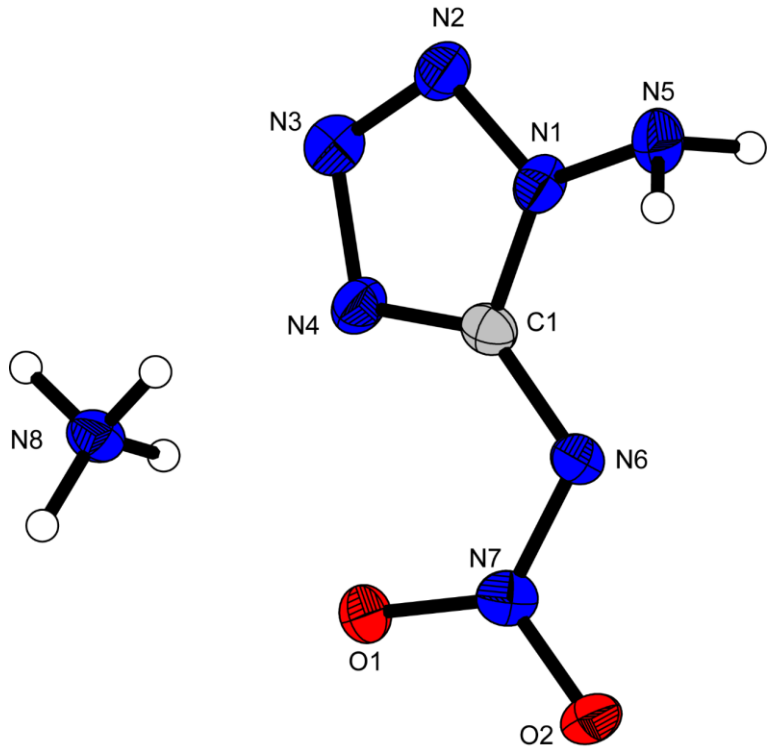

Figure S1. Molecular unit of **2** with thermal ellipsoids drawn at the 50% probability level.

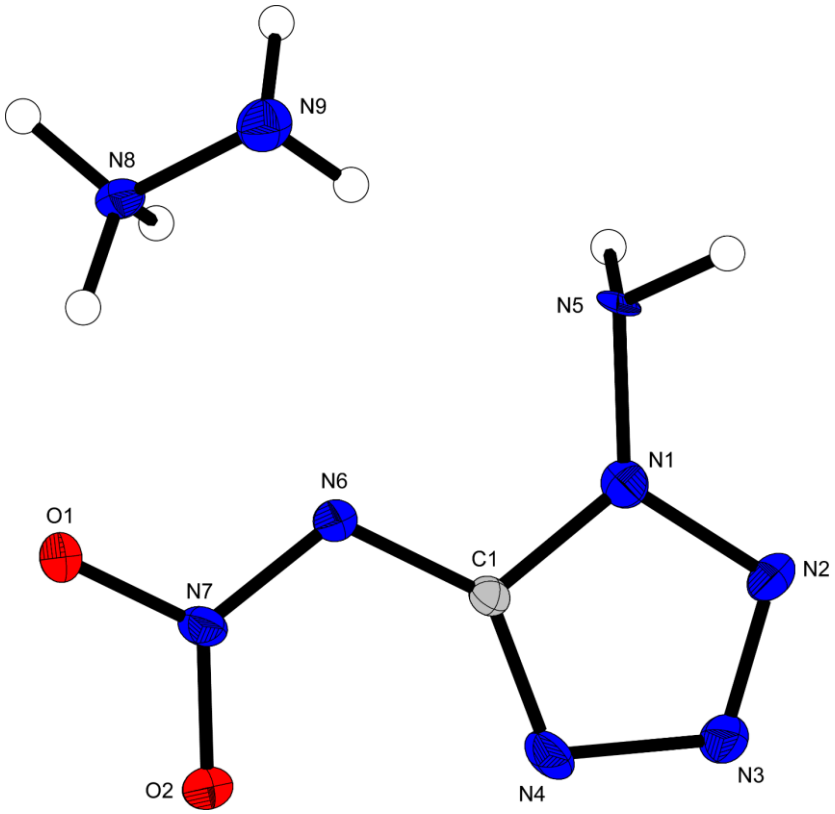

Figure S2. Molecular unit of **3** with thermal ellipsoids drawn at the 50% probability level.

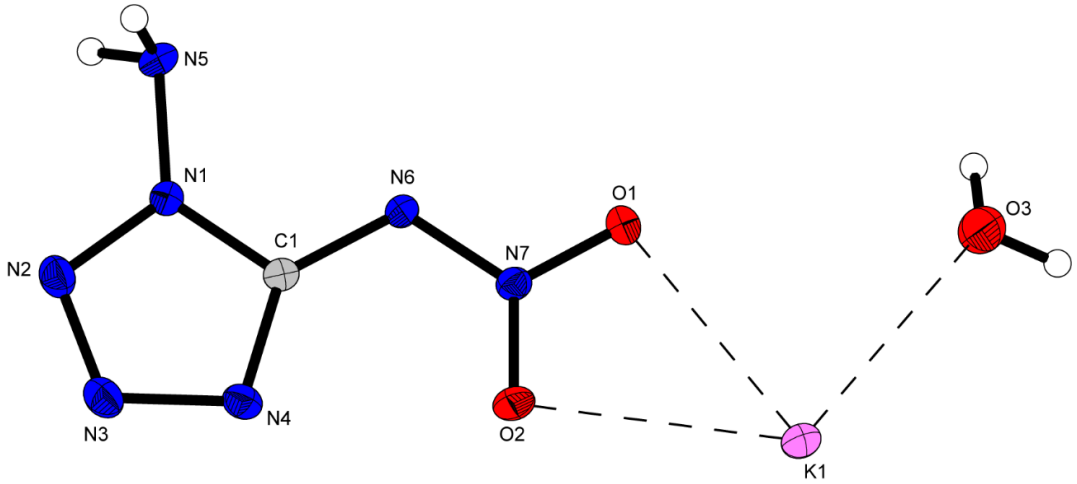

Figure S3. Molecular unit of **5** as monohydrate with thermal ellipsoids drawn at the 50% probability level.

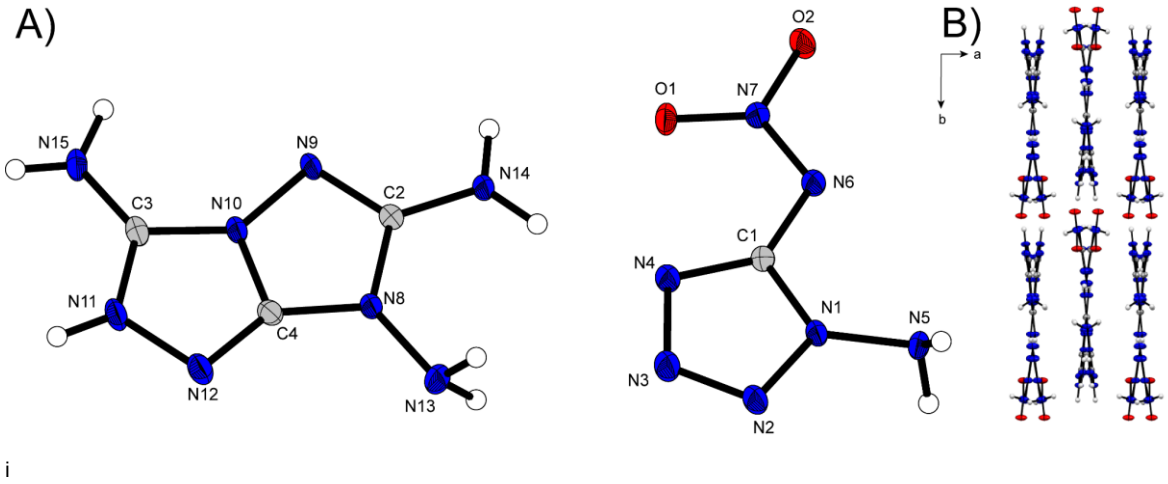

i

Figure S4. A) Molecular unit of **6** with thermal ellipsoids drawn at the 50% probability level. Selected bond and intermolecular distances (Å) and angles [°]: N1-N5 1.398(2), C1-N5 1.370(2), C2-N14 1.330(2), C3-N15 1.322(2), N8-N13 1.399(2), N4-H14B 1.97(2), O2-H15A 1.95(2), N12-H5B 2.31(3), C1-N1-N5 125.9(1), N7-N6-C1-N4 6.8(2), C2-N9-N10-C3 178.9(2);B) layer structure of **6** with view along the *c*-axis.

The HTATOT salt of ANIT (**6**) crystallizes in the monoclinic space group $P2_1/c$ in the form of colorless blocks and a density of 1.803 g cm^{-3} at 298 K which is slightly higher than the density of the parent compound **1**. All possible interaction sites of a HTATOT unit are saturated by four $ANIT^-$ anions and two $HTATOT^+$ cations. Hydrogen bridges with d(H···A) with distances in the region of 1.95(2)–2.31(2) Å are formed. The molecules arrange in slightly distorted sheets along the c axis, forming alternating crosses as shown in Figure S4 B) to obtain the ideal complexation and shorter hydrogen bridges.

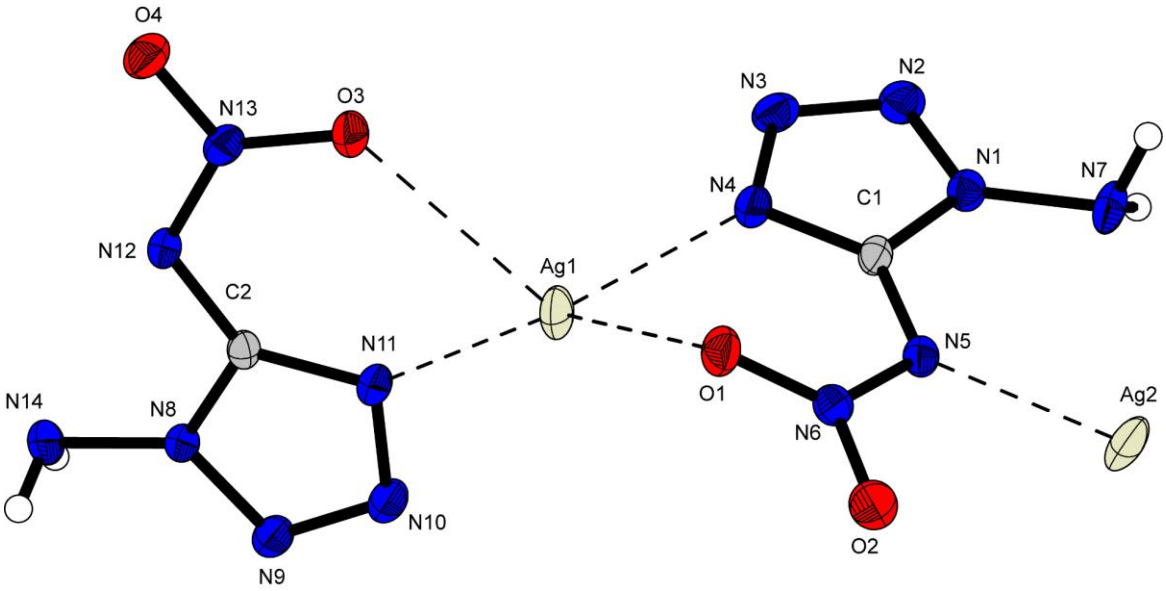

Figure S5. A) Molecular unit of **7** with thermal ellipsoids drawn at the 50% probability level. Selected bond and intermolecular distances (Å) and angles [°]: Ag1-Ag2 3.831(1), Ag1-N4 2.217(4), Ag1-N11 2.199(4), Ag1-O3-2.698(3), Ag1-O2-2.877(4), Ag2-N5 2.231(4), Ag2-N12 2.273(3), Ag2-N14 2.516(4), N6-N5-C1-N4 16.0(7), N7-N1-C1-N5 5.2(6), N11-C2-N12-N13 8.9(7), N12-C2-N8-N14 2.3(6).

AgANIT (**7**) crystallizes in the orthorhombic space group *Pbca* in the form of colorless blocks and a density of 2.988 g cm^{-3} at room temperature. (Figure S5) The two silver cations of the asymmetric cell are coordinated differently. One silver cation is coordinated in a distorted square planar fashion by two ANIT units each in a chelating manner. The complexation is initiated by the oxygens of the nitramine as well as by N4 and N11 of the tetrazoles. The second silver cation is irregularly complexed by three strong (originating from N5, N12 and N15) and several weaker interactions. The silver-silver distance is 3.831(1) Å, can therefore not considered as an argentophilic interaction.

Table S1. Crystallographic data and structure refinement details of **1**-**3**.

	1	**2**	**3**
Formula	$CH_3N_7O_2$	$CH_6N_8O_2$	$CH_7N_9O_2$
FW [g mol^{-1}]	145.10	162.14	177.16
Crystal system	monoclinic	orthorhombic	monoclinic
Space group	$P2_1/n$ (No. 14)	$P2_12_12_1$ (No. 19)	$P2_1$ (No. 4)
Color / Habit	colorless block	colorless block	colorless rod
Size [mm]	0.06 x 0.10 x 0.18	0.10 x 0.25 x 0.25	0.02 x 0.03 x 0.15
a [Å]	8.6883(4)	5.5868(8)	3.5756(3)
b [Å]	8.6632(4)	9.8955(17)	11.4593(9)
c [Å]	14.8335(6)	10.9316(16)	16.4406(13)
α [°]	90		90
β [°]	103.976(2)		96.238(3)
γ [°]	90		90
V [Å^3]	1083.44(8)	604.35(16)	669.65(9)
Z	8	4	4
ρcalc. [g cm^{-3}]	1.779	1.782	1.757
μ [mm^{-1}]	0.159	0.157	0.154
F(000)	592	336	368
λMoKα [Å]	0.71073	0.71073	0.71073
T [K]	173	101	173
θ Min-Max [°]	2.8, 27.6	2.8, 26.3	3.6, 27.5
Dataset	-11: 11 ; -11: 11 ; -19: 19	-6: 6 ; -12: 8 ; -13: 7	-4: 4 ; -13: 14 ; -21: 21
Reflections collected	25821	2016	8394
Independent refl.	2487	1234	2757
Rint	0.043	0.044	0.036
Observed reflections	2140	859	1953
Parameters	205	124	218
R1 (obs)[a]	0.0313	0.0586	0.0312
wR2 (all data)[b]	0.0817	0.1089	0.0785
S [c]	1.09	1.00	1.01
Resd. dens [e Å^{-3}]	-0.22, 0.21	-0.26, 0.32	-0.17, 0.19
Device type	Bruker D8 Venture TXS	Oxford Xcalibur3	Bruker D8 Venture TXS
Solution	SIR-92	SHELXT	SIR-92
Refinement	SHELXL-2018	SHELXL-2018	SHELXL-2018
Absorption correction	multi-scan	multi-scan	multi-scan
CCDC	2173497	2173499	2173496

[a]$R_1 = \Sigma||F_o|-|F_c||/\Sigma|F_o|$; [b]$wR_2 = [\Sigma[w(F_o^2-F_c^2)^2]/\Sigma[w(F_o)^2]]^{1/2}$; $w = [\sigma c^2(F_o^2)+(xP)^2+yP]^{-1}$ and $P=(F_o^2+2F_c^2)/3$; [c]$S = \{\Sigma[w(F_o^2-F_c^2)^2]/(n-p)\}^{1/2}$ (n = number of reflections; p = total number of parameters).

Table S2. Crystallographic data and structure refinement details of **4**-**7**.

	4	**5**	**6**	**7**
Formula	$CH_6N_8O_2$	$CH_4KN_7O_3$	$C_4H_9N_{15}O_2$	$C_2H_4Ag_2N_{14}O_4$
FW [g mol−1]	178.14	201.21	299.26	503.93
Crystal system	triclinic	monoclinic	monoclinic	orthorhombic
Space group	*P*-1 (No. 2)	*C*2/*c* (No. 15)	$P2_1/c$ (No. 14)	*Pbca* (No. 61)
Color / Habit	colorless block	yellow block	colorless block	colorless block
Size [mm]	0.10 x 0.12 x 0.20	0.04 x 0.06 x 0.20	0.04 x 0.08 x 0.10	0.04 x 0.04 x 0.08
a [Å]	7.3477(4)	13.4126(7)	12.0270(5)	7.9795(3)
b [Å]	7.3488(4)	11.8979(6)	6.2786(2)	12.2372(4)
c [Å]	7.4546(4)	9.8337(5)	14.6649(6)	22.9422(7)
α [°]	103.712(2)	90	90	
β [°]	110.124(2)	116.801(2)	102.224(1)	
γ [°]	111.085(2)	90	90	
V [Å^3]	321.35(3)	1400.70(13)	1082.28(7)	2240.23(13)
Z	2	8	4	8
ρcalc. [g cm^{-3}]	1.841	1.908	1.837	2.988
μ [mm^{-1}]	0.168	0.742	0.152	3.553
F(000)	184	816	616	1920
λMoKα [Å]	0.71073	0.71073	0.71073	0.71073
T [K]	173	173	173	299
θ Min-Max [°]	3.4, 26.4	3.4, 33.2	2.8, 27.5	3.1, 26.4
Dataset	-9: 9 ; -9: 9 ; -9: 9	-20: 20 ; -18: 18 ; -15: 15	-15: 15 ; -8: 8 ; -19: 18	-9: 9 ; -15: 15 ; -28: 28
Reflections collected	5393	19444	26602	34160
Independent refl.	1281	2690	2481	2284
Rint	0.023	0.035	0.034	0.029
Observed reflections	1198	2372	2198	2082
Parameters	133	125	226	207
R1 (obs)[a]	0.0318	0.0316	0.0392	0.0321
wR2 (all data)[b]	0.0822	0.0837	0.1061	0.0819
S [c]	1.06	1.06	1.10	1.13
Resd. dens [e Å^{-3}]	-0.19, 0.27	-0.50, 0.69	-0.27, 0.27	-0.96, 1.18
Device type	Bruker D8 Venture	Bruker D8 Venture	Bruker D8 Venture	Bruker D8 Venture
Solution	SIR-92	SHELXT	SIR-92	SIR-92
Refinement	SHELXL-2018	SHELXL-2018	SHELXL-2018	SHELXL-2018
Absorption correction	multi-scan	multi-scan	multi-scan	multi-scan
CCDC	2173502	2173501	2173500	2173498

[a] $R_1 = \Sigma||F_o|-|F_c||/\Sigma|F_o|$; [b] $wR_2 = [\Sigma[w(F_o^2-F_c^2)^2]/\Sigma[w(F_o)^2]]^{1/2}$; $w = [\sigma c^2(F_o^2)+(xP)^2+yP]^{-1}$ and $P=(F_o^2+2F_c^2)/3$; [c] $S = \{\Sigma[w(F_o^2-F_c^2)^2]/(n-p)\}^{1/2}$ (n = number of reflections; p = total number of parameters).

9.6.3 Computation

All quantum chemical calculations were carried out using the Gaussian G09 program package.[S8] The enthalpies (H) and free energies (G) were calculated using the complete basis set (CBS) method of Petersson and co-workers in order to obtain very accurate energies. The CBS models are using the known asymptotic convergence of pair natural orbital expressions to extrapolate from calculations using a finite basis set to the estimated CBS limit. CBS-4 starts with an HF/3-21G(d) geometry optimization; the zero-point energy is computed at the same level. It then uses a large basis set SCF calculation as a base energy, and an MP2/6- 31+G calculation with a CBS extrapolation to correct the energy through second order. A MP4(SDQ)/6-31+ (d,p) calculation is used to approximate higher order contributions. In this study, we applied the modified CBS-4M.

Heats of formation of the synthesized ionic compounds were calculated using the atomization method (equation E1) using room temperature CBS-4M enthalpies, which are summarized in Table S3.[S9-10]

$$\Delta_f H^\circ_{(g,\,M,\,298)} = H_{(Molecule,\,298)} - \sum H^\circ_{(Atoms,\,298)} + \sum \Delta_f H^\circ_{(Atoms,\,298)} \qquad (E1)$$

Table S3. CBS-4M electronic enthalpies for atoms C, H, N and O and their literature values for atomic $\Delta H^\circ_f{}^{298}$ / kJ mol^{-1}

	$-H^{298}$ [a.u.]	NIST[S11]
H	0.500991	218.2
C	37.786156	717.2
N	54.522462	473.1
O	74.991202	249.5
K	−599.187712	89.0

For neutral compounds the sublimation enthalpy, which is needed to convert the gas phase enthalpy of formation to the solid state one, was calculated by the *Trouton* rule.[S12] For ionic compounds, the lattice energy (U_L) and lattice enthalpy (ΔH_L) were calculated from the corresponding X-ray molecular volumes according to the equations provided by *Jenkins* and *Glasser*.[S13] With the calculated lattice

enthalpy the gas-phase enthalpy of formation was converted into the solid state (standard conditions) enthalpy of formation. These molar standard enthalpies of formation (ΔH_m) were used to calculate the molar solid state energies of formation (ΔU_m) according to equation E2.

$$\Delta U_m = \Delta H_m - \Delta n\, RT \qquad \text{(E2)}$$

(Δn being the change of moles of gaseous components)
The calculation results are summarized in Table S4.

Table S4. Calculation results.

M	−H^{298} [a] [a.u.]	$\Delta_f H°$(g, M) [b] [kJ mol^{-1}]	$\Delta_{sub} H°$ (M) [c] [kJ mol^{-1}]	$\Delta_f H°$(s) [d] [kJ mol^{-1}]	Δn	$\Delta_f U$(s) [e] [kJ kg^{-1}]
1	572.712468	416.1	78.6122	494.7	−6.0	2970.4
2	629.004042	922.6		377.6	−8.0	2451.8
3	684.237957	1060.7		528.9	−9.0	3111.9
4	704.070683	973.7		436.1	−8.5	2566.8
5	1171.39515	376.3		−165.5	−5.5	−1053.9
6	1127.68157	1367.3		898.1	−13.0	3109.3

[a] CBS-4M electronic enthalpy; [b] gas phase enthalpy of formation; [c] molecular volumes taken from X-ray structures and corrected to room temperature; [d] lattice energy and enthalpy (calculated using Jenkins and Glasser equations); [e] standard solid-state enthalpy of formation; [f] Δn being the change of moles of gaseous components when formed; [g] solid state energy of formation.

9.6.4 Thermal Analysis

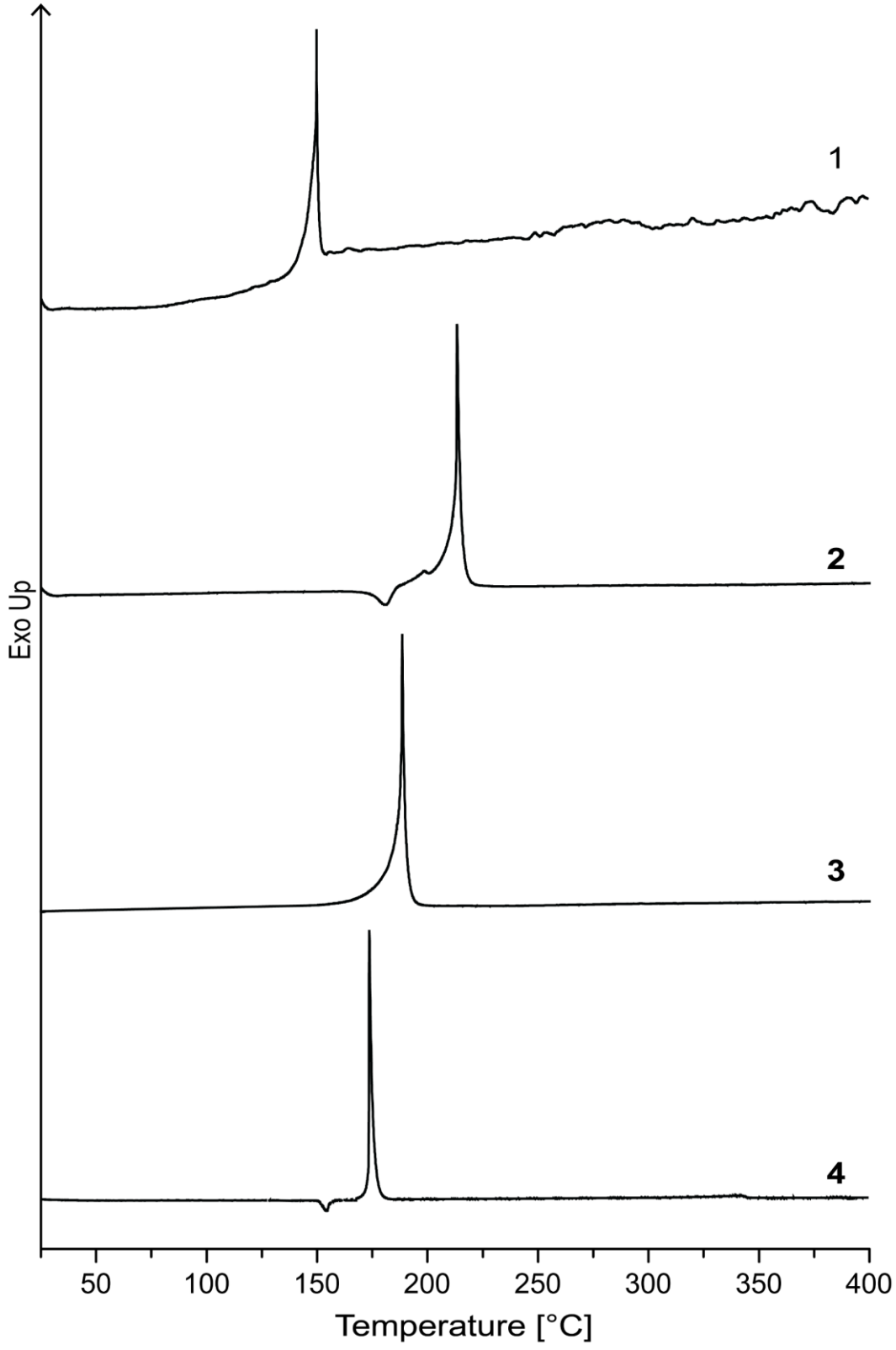

Figure S6. DTA plots of compounds **1**-**4** measured with a heating rate of 5 °C min^{-1}.

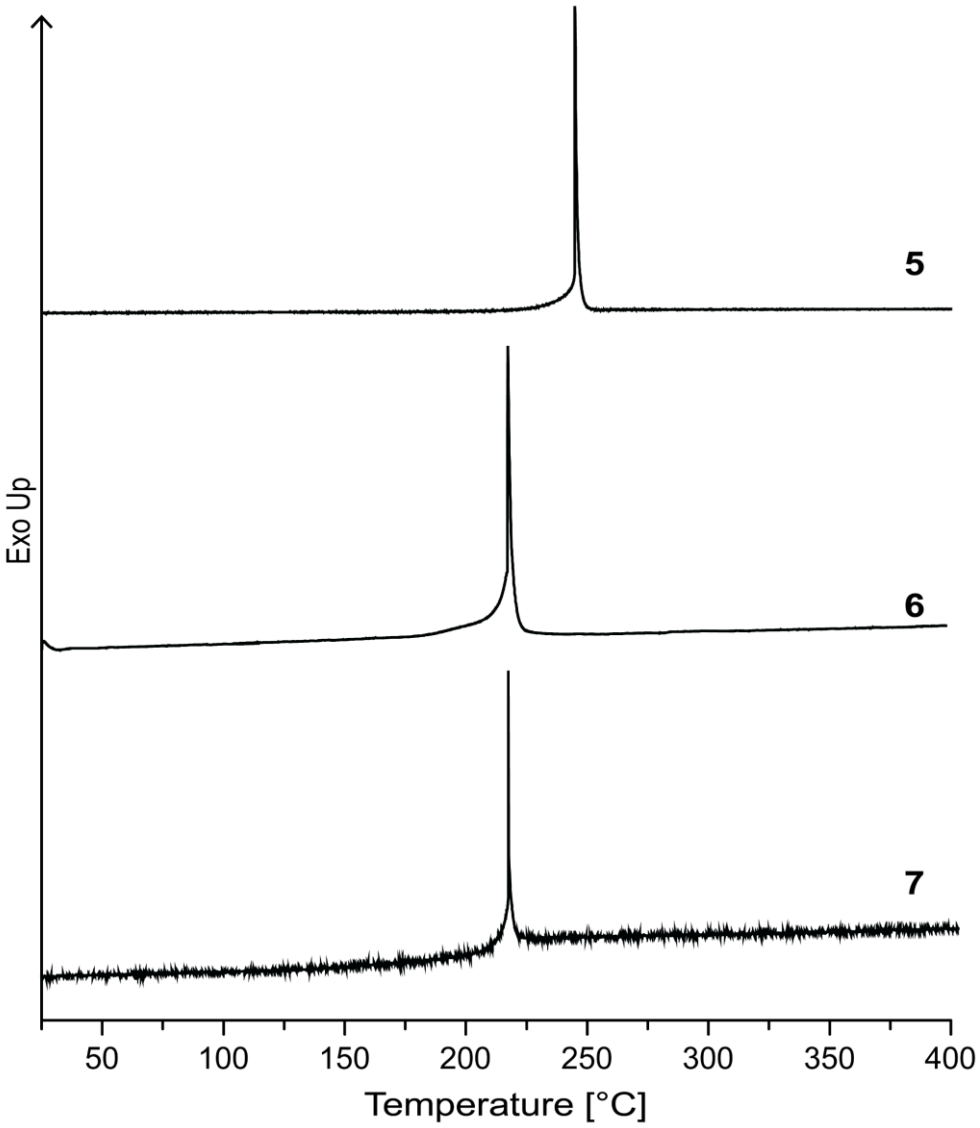

Figure S7. DTA plots of compounds **5**-**7** measured with a heating rate of 5 °C min^{-1}.

9.6.5 References

[S1] a) Test methods according to the UN Recommendations on the Transport of Dangerous Goods, *Manual of Test and Criteria*, ST/SG/AC.10/11/Rev.7, United Nations Publication, New York and Geneva, **2019**, 978-92-1-130394-0; https://unece.org/transport/dangerous-goods/rev7-files; b) Reichel & Partner GmbH, http://www.reichelt-partner.de; c) http://www.ozm.cz

[S2] M. Sućeska, EXPLO5 V6.02 program, Brodarski Institute, Zagreb, Croatia, **2014**.

[S3] *CrysAlisPro*, Oxford Diffraction Ltd. *version 171.33.41*, **2009**.

[S4] G. M. Sheldrick, *Acta Cryst.* **2015**, *A71*, 3–8.

[S5] O. V. Dolomanov, L. J Bourhis, R. J. Gildea, J. A. K. Howard, H. Puschmann, *J. Appl. Cryst.* **2009**, *42*, 339–341.

[S6] *SCALE3 ABSPACK – An Oxford Diffraction program* (1.0.4, gui: 1.0.3), Oxford Diffraction Ltd., **2005**.

[S7] *APEX3*. Bruker AXS Inc., Madison, Wisconsin, USA.

[S8] M. J. Frisch, G. W. Trucks, H. B. Schlegel, G. E. Scuseria, M. A. Robb, J. R. Cheeseman, G. Scalmani, V. Barone, B. Mennucci, G. A. Petersson, H. Nakatsuji, M. Caricato, X. Li, H.P. Hratchian, A. F. Izmaylov, J. Bloino, G. Zheng,J. L. Sonnenberg, M. Hada, M. Ehara, K. Toyota, R. Fukuda, J. Hasegawa, M. Ishida, T. Nakajima, Y. Honda, O. Kitao, H. Nakai, T. Vreven, J. A. Montgomery, Jr., J. E. Peralta, F. Ogliaro, M. Bearpark, J. J. Heyd, E. Brothers, K. N. Kudin, V. N. Staroverov, R. Kobayashi, J. Normand, K. Raghavachari, A. Rendell, J. C.Burant, S. S. Iyengar, J. Tomasi, M. Cossi, N. Rega, J. M. Millam, M. Klene, J. E. Knox, J. B. Cross, V. Bakken, C. Adamo, J. Jaramillo, R. Gomperts, R. E. Stratmann, O. Yazyev, A. J. Austin, R. Cammi, C. Pomelli, J. W. Ochterski, R. L. Martin, K. Morokuma, V. G. Zakrzewski, G. A. Voth, P. Salvador, J. J. Dannenberg, S. Dapprich, A. D. Daniels, O. Farkas, J.B. Foresman, J. V. Ortiz, J. Cioslowski, D. J. Fox, Gaussian 09 A.02, Gaussian, Inc., Wallingford, CT, USA, **2009**.

[S9] a) J. W. Ochterski, G. A. Petersson, and J. A. Montgomery Jr., *J. Chem. Phys.* **1996**, *104*, 2598–2619; b) J. A. Montgomery Jr., M. J. Frisch, J. W. Ochterski G. A. Petersson, *J. Chem. Phys.* **2000**, *112*, 6532–6542.

[S10] a) L. A. Curtiss, K. Raghavachari, P. C. Redfern, J. A. Pople, *J. Chem. Phys.* **1997**, *106*, 1063–1079; b) E. F. C. Byrd, B. M. Rice, *J. Phys. Chem*. A **2006**, *110*, 1005–1013; c) B. M. Rice, S. V. Pai, J. Hare, *Comb. Flame* **1999**, *118*, 445–458.

[S11] P. J. Lindstrom, W. G. Mallard (Editors), NIST Standard Reference Database Number 69, http://webbook.nist.gov/chemistry/ (accessed March **2022**).

[S12] M. S. Westwell, M. S. Searle, D. J. Wales, D. H. Williams, *J. Am. Chem. Soc*. **1995**, *117*, 5013–5015; b) F. Trouton, *Philos. Mag*. **1884**, *18*, 54–57.

[S13] a) H. D. B. Jenkins, H. K. Roobottom, J. Passmore, L. Glasser, *Inorg. Chem.* **1999,** *38,* 3609–3620; b) H. D. B. Jenkins, D. Tudela, L. Glasser, *Inorg. Chem.* **2002**, *41*, 2364–2367.

10. 1-Nitramino-5-aminotetrazole – A simple accessible highly energetic building block

Maximilian Benz, Thomas M. Klapötke, J. Stierstorfer

as published in *Energetic Materials Frontiers* **2022**, *3*, 161–165

DOI: 10.1016/j.enmf.2022.08.003

Keywords: nitration, primary explosives, tetrazoles, ionic derivatives, structure eludication

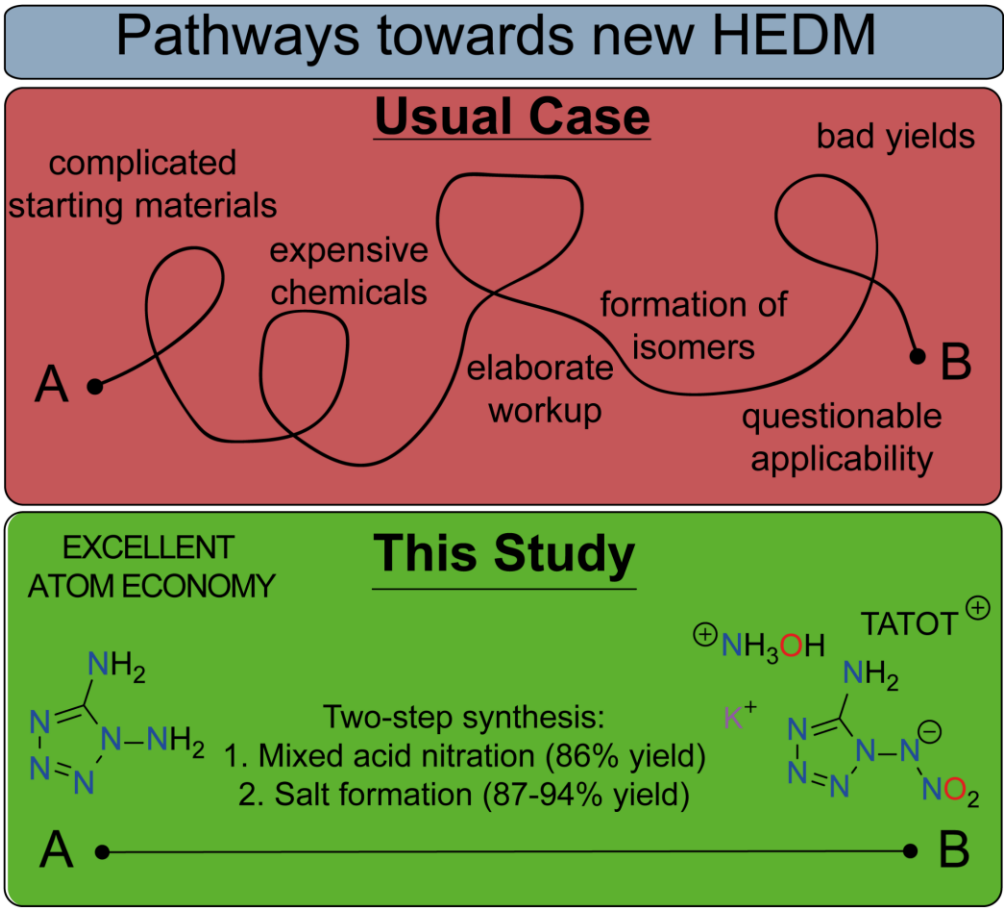

Unlike for other new energetic materials, 1-nitramino-5-aminotetrazole is obtained by mixed acid nitration of 1,5-diaminotetrazole. The three newly developed ionic derivatives show promising characteristics for use as highly energetic explosives.

Abstact: The highly energetic 1-nitrimino-5-aminotetrazole moiety can be obtained by direct nitration of 1,5-diaminotetrazole. The hydroxylammonium, 3,6,7-triamino-[1,2,4]triazolo[4,3-*b*][1,2,4]triazolium (HTATOT) and potassium derivatives were synthesized in this study through acid-base reaction because of the expected promising properties. Especially the potassium derivative shows interesting characteristics for a use as primary explosive. All new compounds were characterized through multinuclear NMR and IR spectroscopy. The purities were checked via CHNO elemental analysis and the compounds' sensitivities (IS, FS, ESD) were measured using the BAM 1 of 6 method. Based on the crystallographic densities (low-temperature X-ray diffraction experiments) and the calculated heats of formation (atomization method based on CBS-4M level of theory), the performance data were calculated using the EXPLO5 code. The potassium derivative thereby shows interesting properties for a possible use as metal free primary explosive (positive PETN initiation, T_{dec} = 180 °C). The hydroxylammonium derivative shows astonishing detonation properties (V_{det} = 9697 m s^{-1}, P_{CJ} = 38.1 GPa).

10.1 Introduction

Tetrazoles are versatile for use in all areas of energetic materials. The usually two functional sites on each tetrazole moiety (*C*-site and *N*-site) offer a great possibility for derivatization.[1-3] Through the examination of different substituents, the properties of the final compound can be varied and tuned purposefully. Next to the great adjustability, tetrazoles convince through a high heat of formation and easy synthetic accessability.[4-6] Especially as replacement for the environmentally hazardous primary explosive lead azide, advanced tetrazole chemistry faces a promising approach.[7-9]

Throughout the last years, several 1-nitraminotetrazole derivatives have been published, mainly due to the beneficial properties of their potassium derivatives as a primary explosive.[10-11] Dipotassium 1,5-di-(nitrimino)-tetrazolate (**A**), potassium 1-nitriminotetrazolate (**B**), dipotassium 1,1'-di-(nitramino)-5,5'-bistetrazolate (**C**) as well as dipotassium 1,1'-di-(nitramino)-5,5'-azobistetrazolate (**D**) can be found in Figure 1. These compounds all represented a significant improvement over the

primary explosives currently in use, especially from an environmental point of view. Nevertheless, all of them still have synthetic or peculiar drawbacks that hinder their widespread and large-scale use. For the production of all compounds **A**-**D**, fine chemicals such as N_2O_5, NO_2BF_4 or CN-N_3 must be used, which makes the production of larger quantities difficult.[12-15] In addition, $(K)_2$DNAAzT (**D**) has an extremely high sensitivity far from any measurement range to any kind of external stimuli which makes safe handling in general and especially of larger quantities problematic.[15] For another, the synthesis of $(K)_2$DNABT includes a seven steps procedure, which is also unfavorable for industrial application.[14]

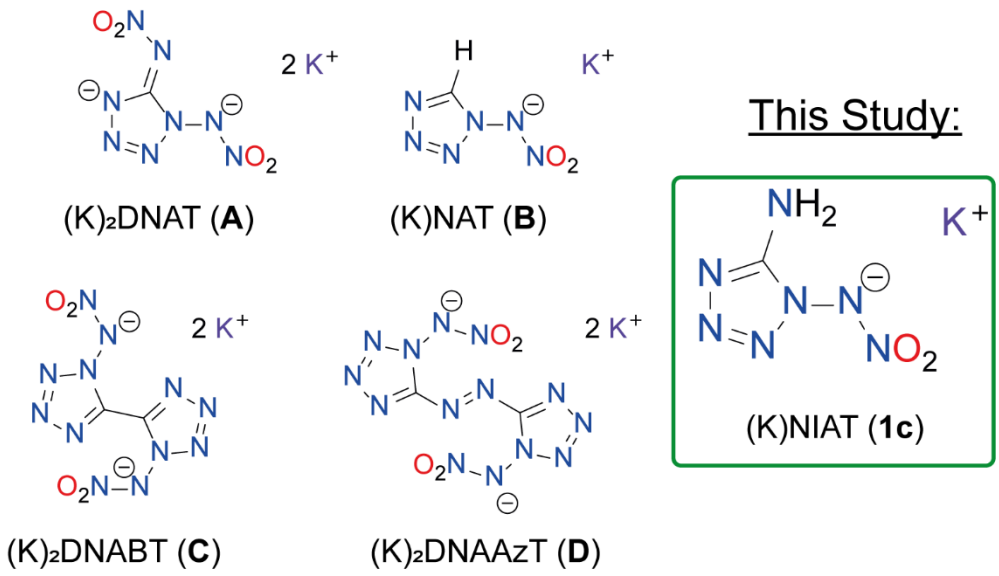

Figure 1. Literature known compounds featuring a 1-nitriminotetrazole function as the respective potassium salts.

Nevertheless, it can be stated that potassium salts of 1-nitriminotetrazoles provide a promising platform for primary explosives, but the ideal candidate has not yet been developed. In this study, we present three new ionic derivatives based on the 1-nitrimino-5-aminotetrazolate ($NIAT^-$) backbone, with the potassium salt showing extremely interesting properties in terms of use as primary explosive. The synthesis of (H)NIAT is based on an optimized prescription starting with the nitration of 1,5-diaminotetrazole using mixed acid, which makes the protocol particularly environmentally friendly due to the excellent atom economy.

10.2 Results and Discussion

The selective nitration of 1,5-diaminotetrazole is quiet challenging since the molecule consists of two differently hybridized amino moieties. The more reactive *N*-amine was already nitrated as depicted in Scheme 1. The green framed conditions were used in this study, the blue and red framed conditions are the current known literature conditions. While method C) provides unfavorable NO_2BF_4,[16] as previously mentioned, we used a protocol based on method B)[17] and were able to push the yield to 86% by lowering the temperature (−20 °C), extending the reaction time (3 h) and improving the workup. The process is an extremely economical and efficient nitration, as it provides clean product in good yield, is atomically economical as no protecting groups are used and only nitrate and sulfate salts are produced as waste, and starts from easily obtainable and insensitive 1,5-diaminotetrazole. Compound **1** was obtained elemental analysis pure and could be used for deprotonation reactions without further purifications.

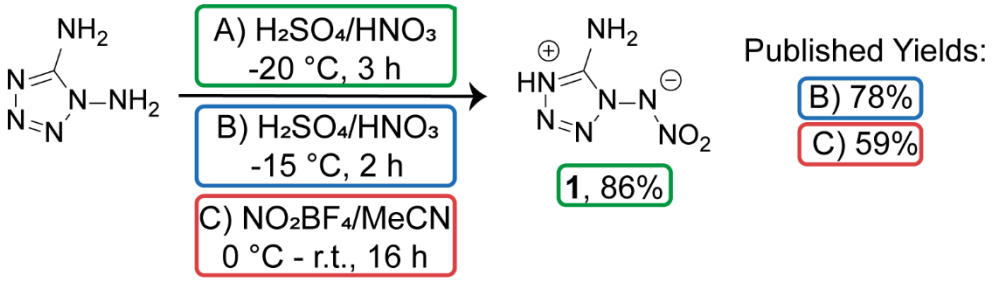

Scheme 1. Selective nitration reaction of 1,5-diaminotetrazole to 1-nitrimino-5-aminotetrazole (**1**, HNIAT).

By salination with the selected cations, we intended to optimize certain properties of our parent compound. The detonation performance could be increased by the formation of the hydroxylammonium derivative (**1a**), the thermal and mechanical resistance was increased through formation of a TATOT salt (**1b**), and a perfect imitability coupled with improved temperature resistance was achieved by the potassium derivative (**1c**).

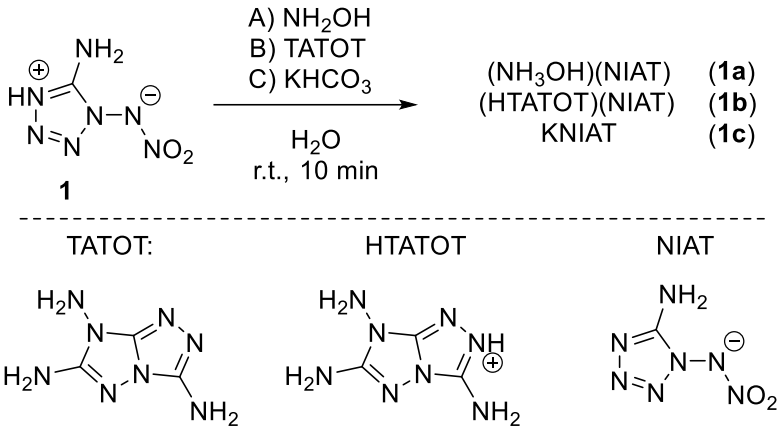

Scheme 2. Synthetic pathway toward the formation of ionic derivatives **1a**-**1c**.

All ionic derivatives were obtained by acid-base reaction in water without heating (Scheme 2) in good to excellent yields (87-94%).

All investigated compounds could be analyzed through X-ray diffraction experiments to obtain accurate densities for performance computation. Crystals were obtained by slow evaporation of common solvents. The crystal data sets were uploaded to the CSD database with the CCDC numbers 2169481 (**1a**), 2169480 (**1b**) and 2169479 (**1c**) and can be accessed free of charge.

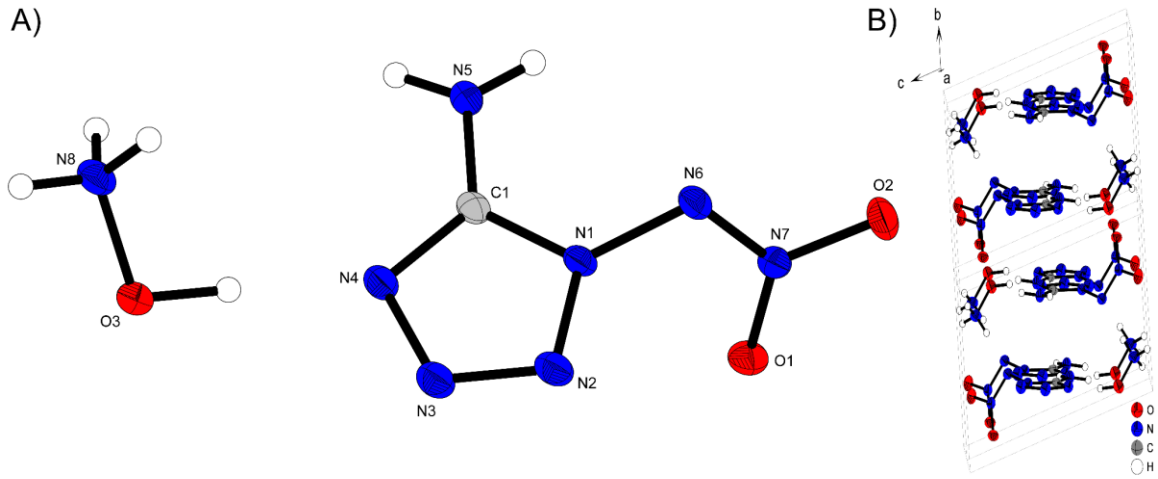

Figure 2. a) Molecular structure of **1a** as determined by low temperature X-ray diffraction with thermal ellipsoids drawn at the 50% probability level; b) Pattern of **1a** with view along the stated direction.

Hydroxylammonium derivate **1a** crystallizes in form of colorless blocks in the triclinic space group *P*−1 with a calculated density of 1.775 g cm^{-3} at 298 K. The density is only slightly lower than the one of bis(hydroxylammonium)-1,5-di(nitrimino)tetrazolate (ρ = 1.813 g cm^{-3}).[12]

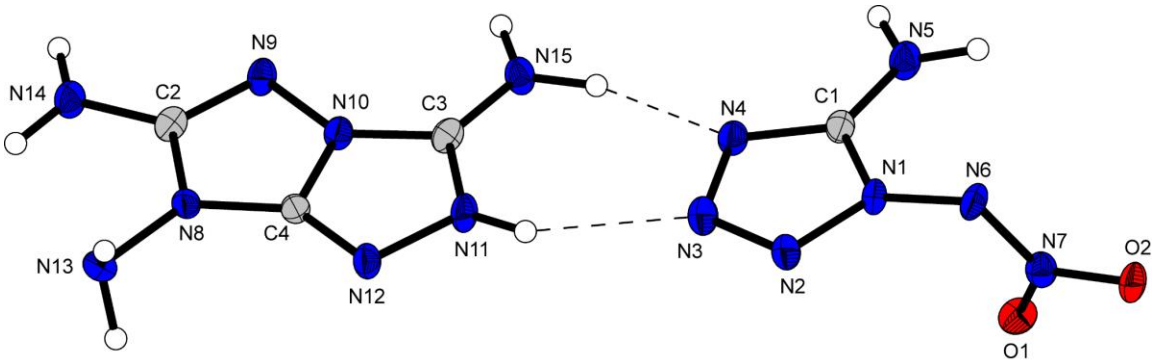

Figure 3. Molecular structure of **1b** as determined by low temperature X-ray diffraction with thermal ellipsoids drawn at the 50% probability level.

The structural motif is mainly characterized by the strong hydrogen interactions formed by the protons of the hydroxylammonium cation, which are located in the range of 1.65 Å (H1-N4) to 2.25 Å (H8C-N6) (Figure 2b).

(HTATOT)NIAT (**1b**) crystallizes anhydrously from a water/ethanol mixture in the monoclinic space group $P2_1/c$ with a density of 1.678 g cm^{-3} at 298 K. The molecular unit is shown in Figure 3. The HTATOT$^+$ and the NIAT$^-$ moieties are located in a plane. Only the nitramine function is twisted out by 92.6 ° (C1-N1-N6-N7). A complex interaction network is formed, in which all hydrogen atoms interact with neighboring units.

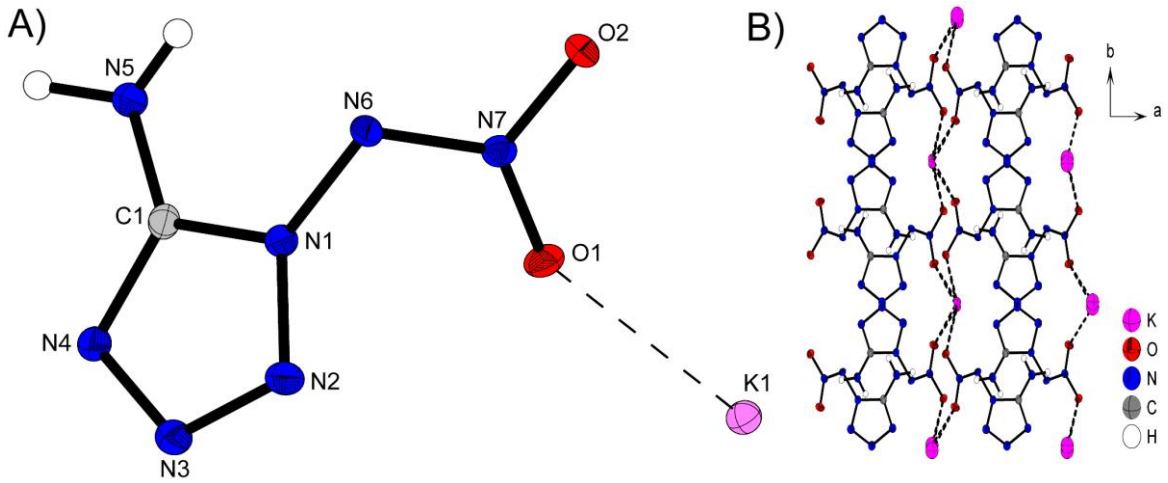

Figure 4. a) Molecular structure of **1c** as determined by low temperature X-ray diffraction with thermal ellipsoids drawn at the 50% probability level; b) Pattern of **1c** with view along *c*.

Crystals of potassium 1-nitrimino-5-aminotetrazolate (**1c**) were obtained directly from the reduced reaction solution. It crystallizes in the form of colorless plates in

the monoclinic space group $P2_1/c$ with four molecules per unit cell and features a room temperature density of 1.955 g cm^{-3}. As expected, this value is lower than for the double potassium salts **A**, **C** and **D** but approximately in the area as of potassium 1-nitriminotetrazolate (**B**, ρ = 1.928 g·cm^{-3}).[13] As observed for the other derivatives, the nitrimino moiety is twisted out of the plane formed by the tetrazole ring by 68.5 ° (N2-N1-N6-N7) (Figure 4). The potassium cations are mainly coordinated by oxygen atoms of the nitro moieties forming a section in which predominantly K-O interactions are found, which exhibit a length of approximately 2.7–2.8 Å.

Table 1. Physico-chemical properties of compounds **1**, **1a**-**1c**, RDX, (K)NAT (**B**) and LA.

	1	**1a**	**1b**	**1c**	RDX[19]	(K)NAT (**B**)[13]	$Pb(N_3)_2$ (RD-1333)[14]
Formula	$CH_3N_7O_2$	$CH_6N_8O_3$	$C_4H_9N_{15}O_2$	$KCH_2N_7O_2$	$C_3H_6N_6O_6$	$KCHN_6O_2$	PbN_6
M [g mol^{-1}]	145.08	178.12	299.23	183.18	222.12	167.98	291.24
IS /J [a]	<1	<1	1	<1	7.5	<1	4
FS /N [b]	0.5	7.5	120	2	120	<0.1	<0.1
ESD /mJ [c]	9	25	150	35	200	0.9	<5
ρ [g cm^{-3}] [d]	1.808[16]	1.775	1.678	1.955	1.806	1.926	4.8
N + O [%] [e]	89.6	89.9	81.0	71.0	81.0	69.0	28.9
Ω [%] [f]	−5.5	−9.0	−34.8	−17.5	−21.6	−6.2	−11.0
T_{dec} [°C] [g]	104	100	174	180	210	180	315
$\Delta_f H^0$ [kJ mol^{-1}] [h]	381.9	396.8	864.7	−210.5	86.3	93.4	450.1
$\Delta f U^0$ [kJ mol^{-1}] [i]	396.7	417.9	896.9	−196.9	108.6	104.4	458.7
			EXPLO5 V6.05.02				
$-\Delta_{Ex} U^0$ [kJ kg^{-1}] [j]	5590	6120	4478	2723	5740	4613	1560
T_{det} [K] [k]	3826	3792	3035	2242	3745	3326	3372
V_0 [L kg^{-1}] [l]	871	941	858	560	784	513	252
p_{CJ} [kbar] [m]	365	381	268	218	336	237	357
V_{det} [m s^{-1}] [n]	9417	9697	8606	7567	8801	7643	6187

a Impact sensitivity (BAM drophammer (1 of 6)). b Friction sensitivity (BAM friction tester (1 of 6)). c Electrostatic discharge device (OZM research). d From X-Ray diffraction analysis recalculated to 298 K. e Combined nitrogen and oxygen content. f Oxygen balance with respect to CO. g Decomposition temperature (DTA; β = 5 °C min^{-1}). h Calculated enthalpy of formation. i Calculated energy of formation. j Energy of explosion. k Detonation temperature. l Volume of detonation products (assuming only gaseous products). m Detonation pressure at Chapman-Jouguet point. n Detonation velocity.

As expected, the hydroxylammonium derivative shows the highest detonation performance with an incredible value of nearly 9700 m s^{-1} and is therefore comparable with the most powerful, non-nuclear explosives published. The sensitivities are in the range of primary explosives (IS < 1 J, FS = 7.5 N) and the thermal decomposition occurs sharply at 100 °C. To improve the thermal and mechanical sensitivity, we decided to synthesize the TATOT derivative of $NIAT^-$ since TATOT salts are known to increase the stability towards external stimuli, but at the same time reduce the performance.[18-19] TATOT derivatives are particularly suitable for combination with extremely energetic and sensitive anions to form secondary explosives. Unluckily, the density of **1b** is quiet low (1.678 g cm^{-3}) and therefore also the detonation velocity is only calculated to be 8606 m s^{-1}. However, the thermal capacity could be increased to 174 °C, and the friction sensitivity to 120 N. Nevertheless, **1b** is still extremely sensitive toward impact (IS = 1 J) making it unsuitable and too poor for a use as secondary explosive.

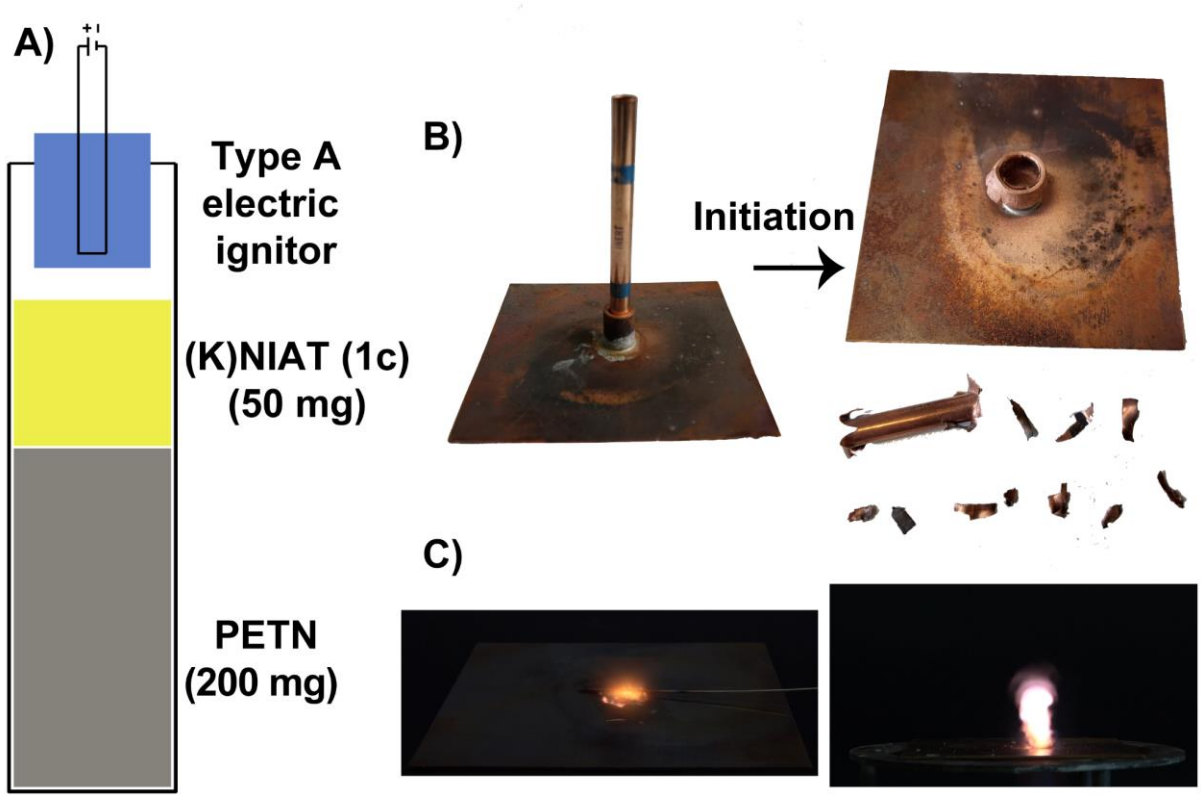

Figure 5. A) Schematic setup of the initiation test; B) Copper sleeve and plate before and after the initiation of 50 mg **1c** and 200 mg PETN; C) Moment of detonation of 15 mg **1c** during hot needle test (left) and moment of detonation of 15 mg **1c** during hot plate test (right).

The potassium derivative **1c** was prepared to provide a high performance and thermally stable primary explosive. The decomposition temperature of 180 °C is therefore in an acceptable range. Also, the friction sensitivity with FS = 2 N makes the compound still well manageable but on the other side sensitive enough for possible initiation. With a crystallographic density of 1.955 g cm^{-3} and a calculated detonation velocity of 7567 m s^{-1}, **1c** is in the same range as (K)NAT (**B**).

In order to evaluate the initiation capability, which is considered the main prerequisite for primary explosives, hot plate (15 mg of **1c** placed on a copper plate were heated rapidly with a Bunsen burner) and a hot needle (penetration of 15 mg of tamped **1c** with a red glowing needle) tests were performed. The compound undergoes DDT (deflagration to detonation transition) in both tests (Figure 5c)). Accordingly, we investigated (K)NIAT (**1c**) in a classical initiation test toward the booster explosive PETN. The setup and result are shown in Figure 5a). Therefore, 50 mg of compressed (K)NIAT (80 N) (**1c**) were placed on top of 200 mg of compressed PETN (<100 µm, 80 N) in a copper shell. The ignition and the positive observation of the DDT of **1c** was confirmed by the hole in copper plate and the fragmentation of the sleeve (Figure 5b)). To further test the compatibility of **1c** with PETN, we produced a formulation containing (K)NIAT (**1c**) and PETN (1:1). We did not obtain a premature decomposition of the formulation in a DTA measurement. Therefore, **1c** can be considered to be compatible with PETN. As demonstrated, potassium salt **1c** meets all the essential requirements for a new primary explosive in the first stage of synthesis and characterization.[14, 20-21]

10.3 Conclusion

We report the synthesis of three new ionic derivatives (hydroxylammonium (**1a**), TATOT (**1b**) and potassium (**1c**)) of the 1-nitrimino-5-aminotetrazolate anion. The parent compound ((H)NIAT (**1**)) was obtained through simple mixed acid nitration of readily available 1,5-diaminotetrazole and the yield could be pushed to 86%. The hydroxylammonium derivative **1a** shows the overall highest detonative properties within this study and competes with the most powerful non-nuclear explosives (V_{det} = 9697 m s^{-1}). The potassium derivative **1c** shows extremely promsing properties as an easy accesible and heavy metal free primary explosive.

Potassium 1-nitrimino-5-aminotetrazole (**1c**) shows positive result in an initiation test toward PETN. Combined with a thermal stability of 180 °C, a low but well handable sensitivity (IS < 1 J, FS = 2 N) and an efficient and straigthforward synthesis through a simple two step procedure, which could be easily upscaled it can be considered as next generation primary explosive.

10.4 Acknowledgement

For financial support of this work by Ludwig-Maximilian University (LMU), the Office of Naval Research (ONR) under grant no. ONR N00014-19-1-2078 and the Strategic Environmental Research and Development Program (SERDP) under contract no. W912HQ19C0033 are gratefully acknowledged.

10.5 References

[1] Y.-H. Joo, J. H. Chung, S. G. Cho, E. M. Goh, *New J. Chem.* **2013**, *37*, 1180–1188.

[2] S. R. Yocca, M. Zeller, E. F. C. Byrd, D. G. Piercey, *J. Mater. Chem. A* **2022**, *10*, 1876–1884.

[3] M. Benz, M. S. Gruhne, T. M. Klapötke, N. Krüger, T. Lenz, M. Lommel, J. Stierstorfer, *Eur. J. Org. Chem.* **2021**, *2021*, 4388–4392.

[4] P. N. Gaponik, V. P. Karavai, Y. V. Grigor'ev, *Chem. Heterocycl. Compd.* **1985**, *21*, 1255–1258.

[5] T. M. Klapötke, M. Kofen, L. Schmidt, J. Stierstorfer, M. H. H. Wurzenberger, *Chem. Asian J.* **2021**, *16*, 3001–3012.

[6] Y.-H. Joo, J. M. Shreeve, *J. Am. Chem. Soc.* **2010**, *132*, 15081–15090.

[7] T. Brinck*, Green Energetic Materials*, Wiley, Hoboken, **2014**.

[8] D. Chen, H. Yang, Z. Yi, H. Xiong, L. Zhang, S. Zhu, G. Cheng, *Angew. Chem. Int. Ed.* **2018**, *57*, 2081–2084.

[9] M. H. H. Wurzenberger, V. Braun, M. Lommel, T. M. Klapötke, J. Stierstorfer, *Inorg. Chem.* **2020**, *59*, 10938–10952.

[10] Q. Zhang, D. Chen, D. Jing, G. Fan, L. He, H. Li, W. Wang, F. Nie, *Green Chemistry* **2019**, *21*, 1947–1955.

[11] C. He, J. M. Shreeve, *Angew. Chem. Int. Ed.* **2016**, *55*, 772–775.

[12] D. Fischer, T. M. Klapötke, J. Stierstorfer, *Angew. Chem. Int. Ed.* **2015**, *54*, 10299–10302.

[13] N. Szimhardt, M. H. H. Wurzenberger, P. Spieß, T. M. Klapötke, J. Stierstorfer, *Propellants Explo. Pyrotech.* **2018**, *43*, 1203–1209.

[14] D. Fischer, T. M. Klapötke, J. Stierstorfer, *Angew. Chem. Int. Ed.* **2014**, *53*, 8172–8175.

[15] D. Fischer, T. M. Klapötke, J. Stierstorfer, N. Szimhardt, *Chem. Eur. J.* **2016**, *22*, 4966–4970.

[16] T. M. Klapötke, F. A. Martin, J. Stierstorfer, *Chem. Eur. J.* **2012**, *18*, 1487–1501.

[17] L. Liu, C. He, C. Li, Z. Li, *J. Chem. Crystallogr.* **2012**, *42*, 816–823.

[18] P. Yin, J. Zhang, D. A. Parrish, J. M. Shreeve, *J. Mater. Chem. A* **2015**, *3*, 8606–8612.

[19] T. M. Klapötke, P. C. Schmid, S. Schnell, J. Stierstorfer, *Chem. Eur. J.* **2015**, *21*, 9219–9228.

[20] M. Benz, T. M. Klapötke, J. Stierstorfer, *Org. Lett.* **2022**, *24*, 1747–1751.

[21] M. Deng, Y. Feng, W. Zhang, X. Qi, Q. Zhang, *Nat. Commun.* **2019**, *10*, 1339.

10.6 Supporting Information

10.6.1 Experimental Procedure

^{1}H, ^{13}C and ^{14}N NMR spectra were recorded on *BRUKER AMX 400* instruments. Chemical shifts are referenced with respect to tetramethylsilane (^{1}H/^{13}C) and nitromethane (^{14}N). Infrared spectra (IR) were recorded in the region 4000-400 cm^{-1} on a *PERKIN ELMER Spectrum BX-59343* instrument with a *SMITHS DETECTION DuraSamplIR II Diamond ATR* sensor. Decomposition temperatures were measured via differential thermal analysis (DTA) with an *OZM Research DTA 552-Ex* instrument at a heating rate of 5 °C/min and in a range of room temperature to 400 °C. Sensitivities toward impact (IS) and friction (FS) were determined according to the UN Recommendations on the Transport of Dangerous Goods (ST/SG/AC.10/11/Rev.7) using a BAM drop hammer and a BAM friction apparatus

by applying the 1 of 6 method.[S1] All energetic compounds were tested for sensitivity towards electrical discharge using an *Electric Spark Tester ESD 2010 EN* from OZM. Energetic properties have been calculated with the EXPLO5 6.02 computer [S2] code using the RT converted X-ray density and calculated solid state heats of formation.

CAUTION! *All investigated compounds are potentially explosive materials. Safety precautions and equipment (such as wearing leather coat, face shield, Kevlar sleeves, Kevlar gloves, earthed equipment and ear plugs) must be used during all manipulations.*

1-Nitrimino-5-aminotetrazole (**1**)

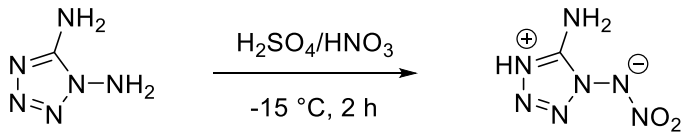

1

Nitration of 1,5-diaminotetrazole was performed according to a slightly modified literature known procedure.[S3] Fuming nitric acid (1.5 mL) was added to sulfuric acid (96%, 1.5 mL) while maintaining the temperature at around 0 °C. After stirring for 10 min, the mixture was cooled to −20 °C and 1,5-diaminotetrazole (1.00 g, 10.0 mmol, 1.0 eq) was added in portions over 30 min keeping the temperature at below −10 °C. The mixture was allowed to stir for 3 h at around −20 °C. After that time, water (7.0 mL) was added to the nitration mixture under intensive stirring and the flask was sealed and placed in the fridge at −30 °C for 4 h. The precipitated solid was carefully filtered and washed with three portions of diethyl ether (10 mL) to afford 1-nitrimino-5-aminotetrazole (1.25 g, 0.86 mmol 86%) as colorless powder.

The measured analytic data fit with the published ones.[S3-S4]

DTA (5 °C min^{-1}): 104 °C (exo); Sensitivities: BAM drophammer: <1 J; friction tester: 0.5 N; ESD: 9 mJ (at grain size 100–500 µm); Elem. Anal. ($CH_2N_7O_2$, 145.08 g mol^{-1}): calcd: C 8.28, H 2.08, N 67.58 %; found: C 7.93, H 2.31, N

66.08 %; ^{1}H NMR (DMSO-D_6, 400 MHz, ppm) δ = 8.39 (br s, 3H); ^{13}C NMR (DMSO-D_6, 101 MHz, ppm) δ = 150.3; ^{14}N NMR (DMSO-D_6, 29 MHz, ppm) δ = −8.

General Procedure for the Synthesis of Ionic Derivatives **1a**-**1c**

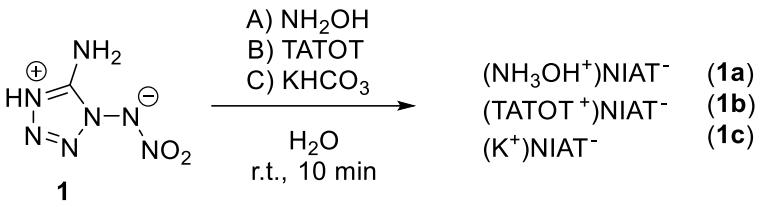

1

1-Nitrimino-5-aminotetrazole (1) (0.25 g, 1.72 mmol, 1.0 eq) was dissolved in water (10 mL) and one equivalent of the respective base (aqueous hydroxylamine (50% w/w, 0.11 mL, 1.72 mmol) for 1a, potassium hydrogen carbonate (0.18 g, 1.72 mmol) for 1b and 3,6,7-triamino-[1,2,4]triazolo[4,3-b][1,2,4]triazole (TATOT, 0.26 g, 1.72 mmol) for 1c) was added in one portion and the mixture was stirred for 10 min at room temperature. After filtration, the solvent was evaporated to obtain the respective ionic derivatives 1a-1c without further purification. It is important that the reaction mixtures are not heated. For several experiments, we obtained the loss of the nitro group and were able to detect traces of 1,5-diaminotetrazole.

Hydroxylammonium 1-nitrimino-5-aminotetrazolate (**1a**)

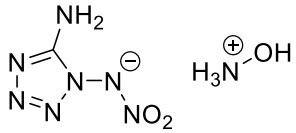

1a

Yield: 0.29 g (1.63 mmol, 94%) as colorless crystalline solid.
DTA (5 °C min^{-1}): 100 °C (exo); Sensitivities: BAM drophammer: <1 J; friction tester: 7.5 N; ESD: 25 mJ (at grain size 100–500 µm); Elem. Anal. ($CH_6N_8O_3$, 178.11 g mol^{-1}): calcd: C 6.74, H 3.40, N 62.91 %; found: C 6.54, H 3.13, N 61.90 %; IR (ATR) $\tilde{\nu}$ (cm^{-1}) = 3419(m), 3133(m), 2976(m), 2857(m), 2693(m),

2525(m), 1651(s), 1570(m), 1521(m), 1474(m), 1368(s), 1300(vs), 1174(s), 1124(s), 1062(s), 1006(vs), 994(vs), 978(s), 890(s), 821(s), 768(s), 729(s), 604(s), 535(m), 444(s), 436(vs), 428(vs), 408(vs); ^{1}H NMR (DMSO-D_6, 400 MHz, ppm) δ = 9.85 (br s, 4H), 6.08 (s, 2H); ^{13}C NMR (DMSO-D_6, 101 MHz, ppm) δ = 153.0; ^{14}N NMR (DMSO-D_6, 29 MHz, ppm) δ = −2, −358.

3,6,7-Triamino-[1,2,4]triazolo[4,3-b][1,2,4]triazolium 1-nitrimino-5-aminotetrazolate (**1b**)

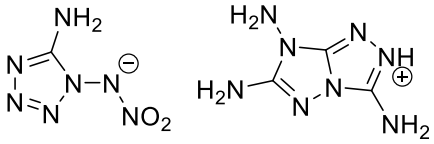

1b

Yield: 0.45 g (1.50 mmol, 87%) as yellowish solid.
DTA (5 °C min^{-1}): 174 °C (exo); Sensitivities: BAM drophammer: 1 J; friction tester: 120 N; ESD: 150 mJ (at grain size 100–500 µm); Elem. Anal. ($C_4H_9N_{15}O_2$, 299.22 g mol^{-1}): calcd: C 16.06, H 3.03, N 70.22 %; found: C 15.87, H 2.89, N 68.45 %; IR (ATR) $\tilde{\nu}$ (cm^{-1}) = 3411(m), 3307(m), 3204(s), 1705(m), 1658(s), 1651(vs), 1645(vs), 1510(m), 1446(m), 1392(s), 1291(s), 1246(s), 1121(s), 1064(s), 1030(s), 935(m), 894(m), 839(m), 781(m), 765(m), 731(m), 721(m), 696(s), 599(s), 524(s), 512(s), 508(s), 480(s), 456(s), 436(s), 424(s), 409(s); ^{1}H NMR (DMSO-D_6, 400 MHz, ppm) δ = 13.32 (br s, 1H), 8.20 (s, 2H), 7.23 (s. 2H), 6.09 (s, 2H), 5.77 (s, 2H); ^{13}C NMR (DMSO-D_6, 101 MHz, ppm) δ = 160.2, 152.5, 147.4, 141.1; ^{14}N NMR (DMSO-D_6, 29 MHz, ppm) δ = −3.

Potassium 1-nitrimino-5-aminotetrazolate (**1c**)

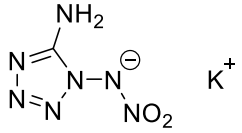

1c

Yield: 0.29 g (1.57 mmol, 91%) as slightly yellowish crystalline solid.
DTA (5 °C min^{-1}): 180 °C (exo); Sensitivities: BAM drophammer: <1 J; friction tester: 2 N; ESD: 35 mJ (at grain size 100–500 µm); Elem. Anal. ($KCH_2N_7O_2$, 183.17 g mol^{-1}): calcd: C 6.56, H 1.10, N 53.53 %; found: C 6.22, H 1.45, N 51.99 %; IR (ATR) $\tilde{\nu}$ (cm^{-1}) = 3303(m), 3193(m), 1651(m), 1645(s), 1580(m), 1394(s), 1312(s), 1107(vs), 1075(vs), 1022(s), 992(m), 984(m), 877(m), 737(m), 611(vs), 500(m); ^{1}H NMR (DMSO-D_6, 400 MHz, ppm) δ = 6.09 (s, 2H); ^{13}C NMR (DMSO-D_6, 101 MHz, ppm) δ = 153.0; ^{14}N NMR (DMSO-D_6, 29 MHz, ppm) δ = −3.

10.6.2 Crystallography

Crystal structure data were obtained from an Oxford Xcalibur3 diffractometer with a Spellman generator (voltage 50 kV, current 40 mA) and a Kappa CCD area for data collection using Mo-*Kα* radiation (*λ* = 0.71073 Å) or a Bruker D8 Venture TXS diffractometer equipped with a multilayer monochromator, a Photon 2 detector and a rotation-anode generator (Mo-K_α radiation). The data collection was performed using the CRYSTALIS RED software.[S5] The solution of the structure was performed by direct methods and refined by full-matrix least-squares on F2 (SHELXT)[S6] implemented in the OLEX2[S7] software suite. The non-hydrogen atoms were refined anisotropically and the hydrogen atoms were located and freely refined. The absorption correction was carried out by a SCALE3 ABSPACK multiscan method.[S8] The DIAMOND2 plots shown with thermal ellipsoids at the 50% probability level and hydrogen atoms are shown as small spheres of arbitrary radius. The SADABS program embedded in the Bruker APEX3 software was used for multi-scan absorption corrections in all structures.[S9]

Table S1. Crystallographic data of ionic derivatives **1a**-**1c**.

	1a	**1b**	**1c**
Formula	$CH_2N_7O_2$, H_4NO	$CH_2N_7O_2$, K	$CH_2N_7O_2$, $C_3H_7N_8$
FW [g mol^{-1}]	178.14	183.20	299.26
Crystal system	triclinic	monoclinic	monoclinic
Space group	*P*−1 (No. 2)	$P2_1/c$ (No. 14)	$P2_1/c$ (No. 14)
Color / Habit	colorless block	colorless plate	yellow plate
Size [mm]	0.50 x 0.50 x 0.50	0.05 x 0.25 x 0.25	0.10 x 0.10 x 0.25
a [Å]	5.9544(6)	7.3099(5)	13.2887(18)
b [Å]	6.2796(7)	11.4133(6)	6.8787(9)
c [Å]	8.9546(9)	7.4648(4)	13.4634(16)
α [°]	104.461(9)	90	90
β [°]	91.345(8)	103.847(6)	110.814(14)
γ [°]	92.421(8)	90	90
V [Å^3]	323.73(6)	604.69(6)	1150.4(3)
Z	2	4	4
$\rho_{calc.}$ [g cm^{-3}]	1.827	2.012	1.728
μ [mm^{-1}]	0.167	0.837	0.143
F(000)	184	368	616
$\lambda_{MoK\alpha}$ [Å]	0.71073	0.71073	0.71073
T [K]	99	102	100
θ Min-Max [°]	2.3, 28.3	2.9, 32.6	3.1, 26.4
Dataset	-7: 7 ; -8: 7 ; -11: 11	-10: 11 ; -16: 16 ; -11: 11	-16: 16 ; -8: 8 ; -16: 16
Reflections collected	2960	6558	5037
Independent refl.	1602	2054	2354
R_{int}	0.030	0.032	0.057
Observed reflections	1300	1714	1388
Parameters	133	108	226
R_1 (obs)[a]	0.0471	0.0342	0.0578
wR_2 (all data)[b]	0.1337	0.0850	0.1164
S [c]	1.07	1.08	0.98
Resd. dens [e Å^{-3}]	-0.29, 0.36	-0.32, 0.52	-0.27, 0.29
Device type	Xcalibur Sapphire3	Xcalibur Sapphire3	Xcalibur Sapphire3
Solution	SIR-92	SIR-92	SIR-92
Refinement	SHELXL-2013	SHELXL-2013	SHELXL-2013
Absorption correction	multi-scan	multi-scan	multi-scan
CCDC	2169481	2169480	2169479

[a]$R_1 = \Sigma||F_0|-|F_c||/\Sigma|F_0|$; [b]$wR_2 = [\Sigma[w(F_0^2-F_c^2)^2]/\Sigma[w(F_0)^2]]^{1/2}$; $w = [\sigma c^2(F_0^2)+(xP)^2+yP]^{-1}$ and $P=(F_0^2+2F_c^2)/3$; [c]$S = \{\Sigma[w(F_0^2-F_c^2)^2]/(n-p)\}^{1/2}$ (n = number of reflections; p = total number of parameters).

10.6.3 Thermal Analysis

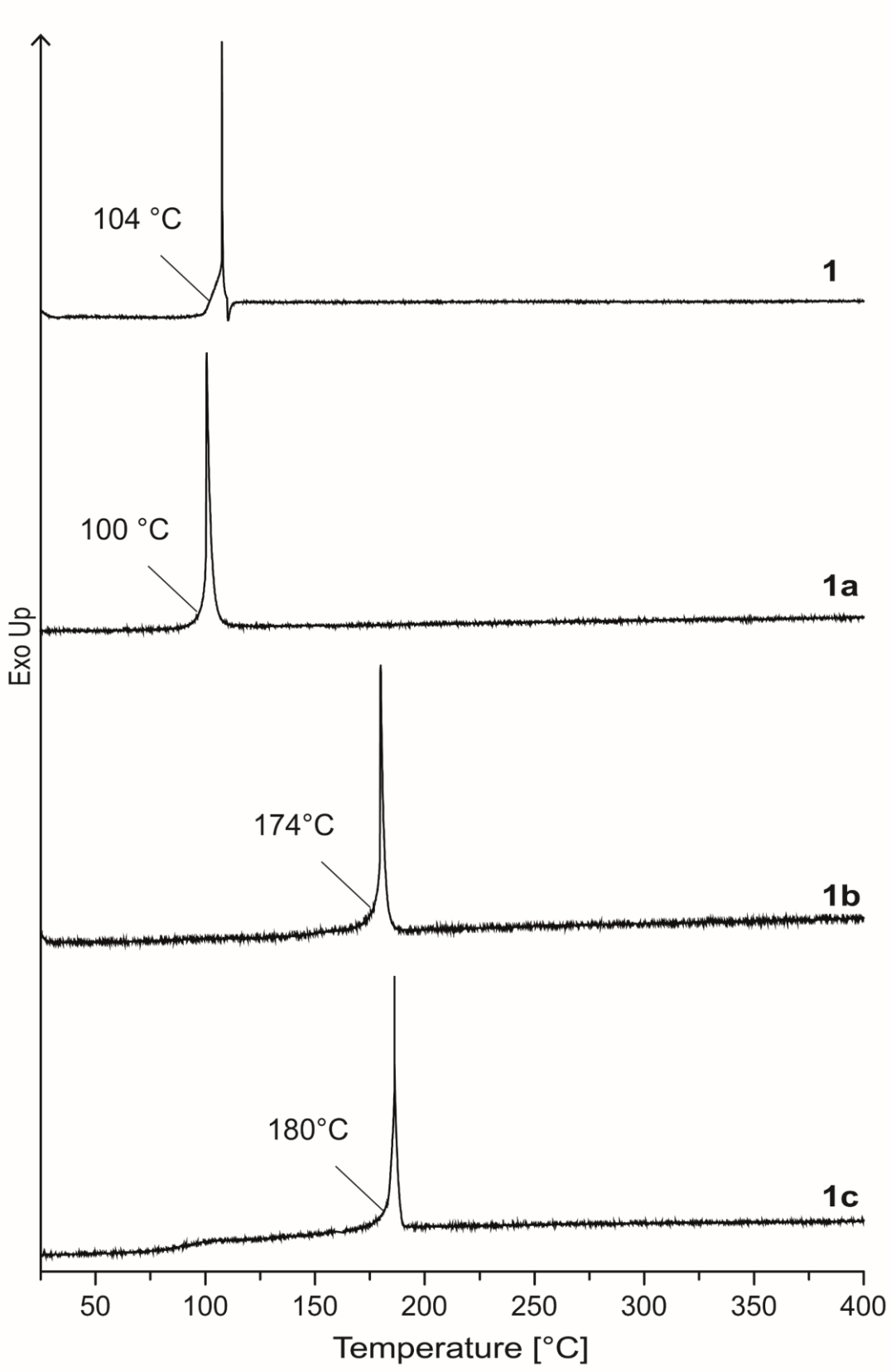

Figure S1. DTA plots of compounds **1** and **1a**-**1c** measured with a heating rate of 5 °C min^{-1}.

10.6.4 Computation

All quantum chemical calculations were carried out using the Gaussian G09 program package.[S10] The enthalpies (H) and free energies (G) were calculated using the complete basis set (CBS) method of Petersson and co-workers in order to obtain very accurate energies. The CBS models are using the known asymptotic convergence of pair natural orbital expressions to extrapolate from calculations using a finite basis set to the estimated CBS limit. CBS-4 starts with an HF/3-21G(d) geometry optimization; the zero-point energy is computed at the same level. It then uses a large basis set SCF calculation as a base energy, and an MP2/6- 31+G calculation with a CBS extrapolation to correct the energy through second order. A MP4(SDQ)/6-31+ (d,p) calculation is used to approximate higher order contributions. In this study, we applied the modified CBS-4M.
Heats of formation of the synthesized ionic compounds were calculated using the atomization method (equation E1) using room temperature CBS-4M enthalpies, which are summarized in Table S2.[S11, S12]

$$\Delta_f H^\circ_{(g,\,M,\,298)} = H_{(Molecule,\,298)} - \sum H^\circ_{(Atoms,\,298)} + \sum \Delta_f H^\circ_{(Atoms,\,298)} \qquad (E1)$$

Table S2. CBS-4M electronic enthalpies for atoms C, H, N and O and their literature values for atomic $\Delta H^\circ_f{}^{298}$ / kJ mol^{-1}

	$-H^{298}$ [a.u.]	NIST[S13]
H	0.500991	218.2
C	37.786156	717.2
N	54.522462	473.1
O	74.991202	249.5

For neutral compounds the sublimation enthalpy, which is needed to convert the gas phase enthalpy of formation to the solid state one, was calculated by the *Trouton* rule.[S14] For ionic compounds, the lattice energy (U_L) and lattice enthalpy (ΔH_L) were calculated from the corresponding X-ray molecular volumes according to the equations provided by *Jenkins* and *Glasser*.[S15] With the calculated lattice enthalpy the gas-phase enthalpy of formation was converted into the solid state

(standard conditions) enthalpy of formation. These molar standard enthalpies of formation (ΔH_m) were used to calculate the molar solid state energies of formation (ΔU_m) according to equation E2.

$$\Delta U_m = \Delta H_m - \Delta n\, RT \qquad \text{(E2)}$$

(Δn being the change of moles of gaseous components)
The calculation results are summarized in Table S3.

Table S3. Calculation results for compounds **1a**-**1c.**

	$-H^{298}$ [a] [a.u.]	$\Delta_f H°(g,M)$ [kJ mol^{-1}] [b]	V_M [Å^3] [c]	ΔU_L; ΔH_L [d] [kJ mol^{-1}]	$\Delta_f H°(s)$ [e] [kJ mol^{-1}]	Δn [f]	$\Delta_f U(s)$ [g] [kJ kg^{-1}]
(H)NIAT	572.728437	452.8	-	-	381.9	−6.0	2734.6
NIAT$^-$	572.223403	245.4					
NH_3OH^+	131.863229	686.5					
TATOT$^+$	555.474133	1080.0					
K^+	599.187712	89.0					
1a	-	931.8	167	530.1; 535.0	396.8	−8.5	2346.0
1b	-	1325.4	296	455.8; 460.7	864.7	−13.0	2997.6
1c	-	234.4	156	539.9; 544.9	−210.5	−5.5	−1366.6

[a] CBS-4M electronic enthalpy; [b] gas phase enthalpy of formation; [c] molecular volumes taken from X-ray structures and corrected to room temperature; [d] lattice energy and enthalpy (calculated using Jenkins and Glasser equations); [e] standard solid state enthalpy of formation; [f] Δn being the change of moles of gaseous components when formed; [g] solid state energy of formation.

10.6.5 NMR Spectroscopy

^{1}H-NMR (400 MHz, DMSO-D$_6$, ppm)

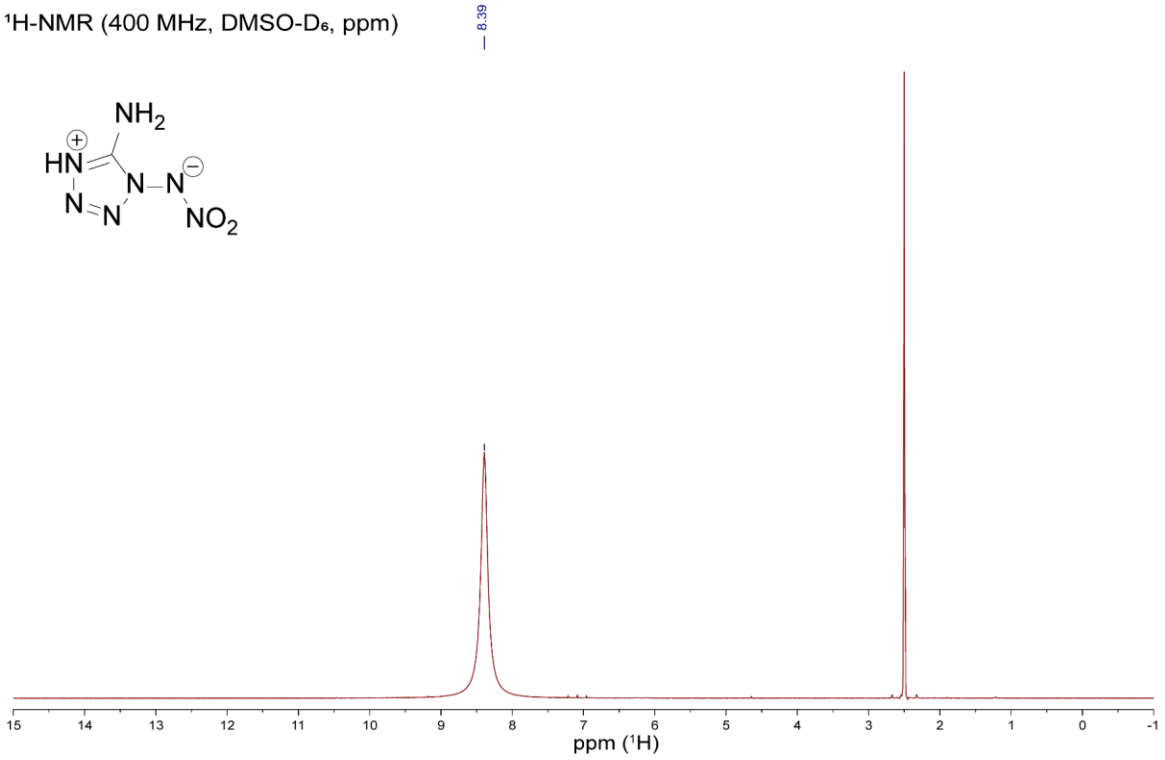

^{13}C-NMR (101 MHz, DMSO-D$_6$, ppm)

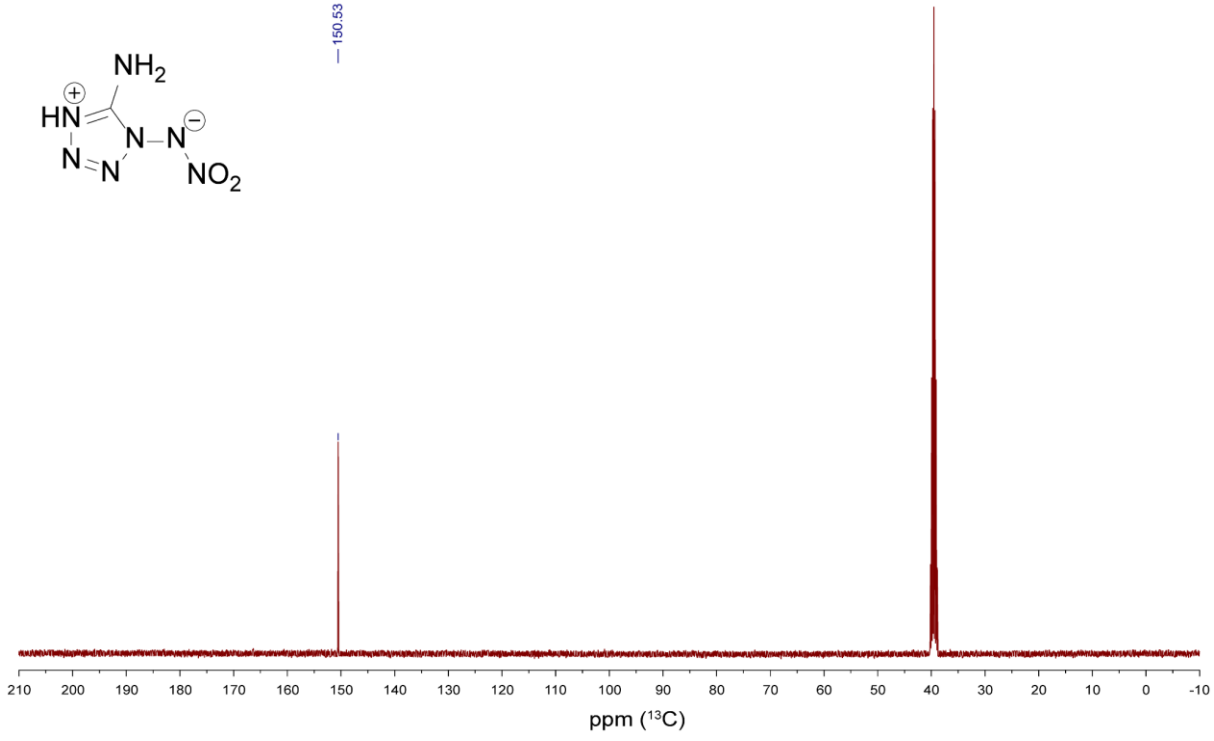

^{14}N-NMR (29 MHz, DMSO-D$_6$, ppm)

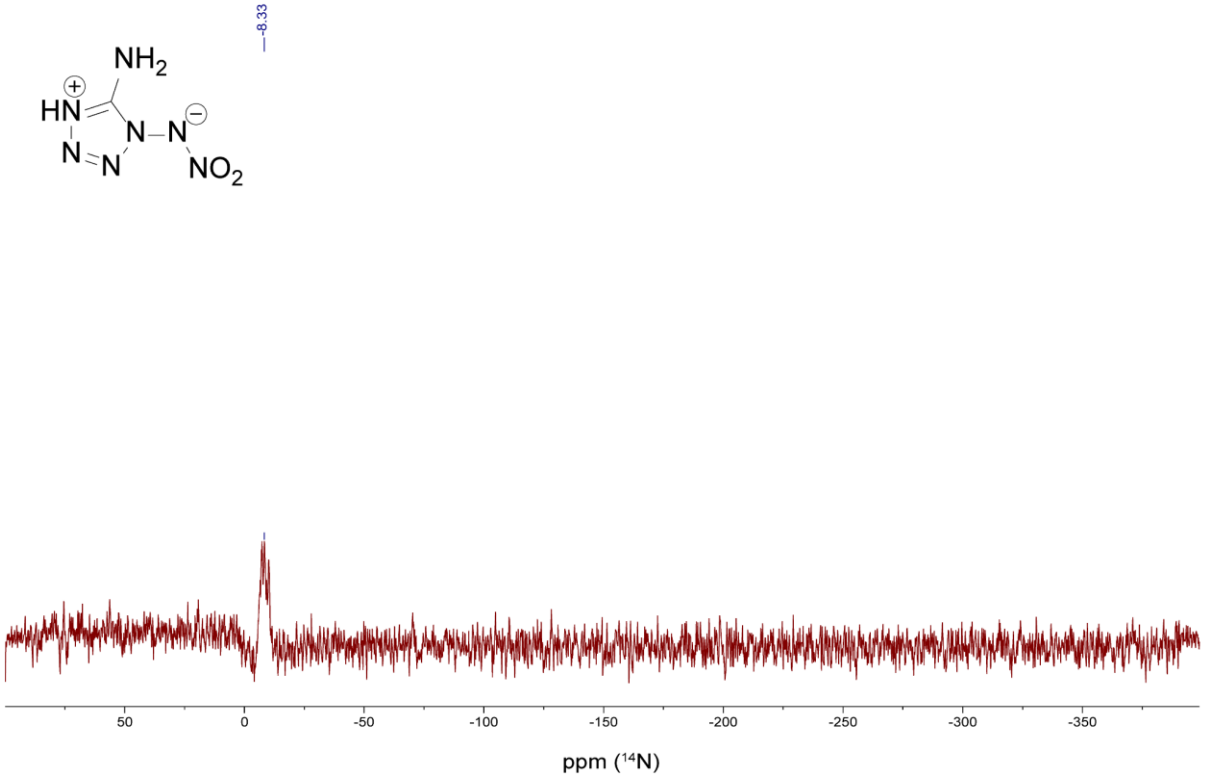

^{1}H-NMR (400 MHz, DMSO-D$_6$, ppm)

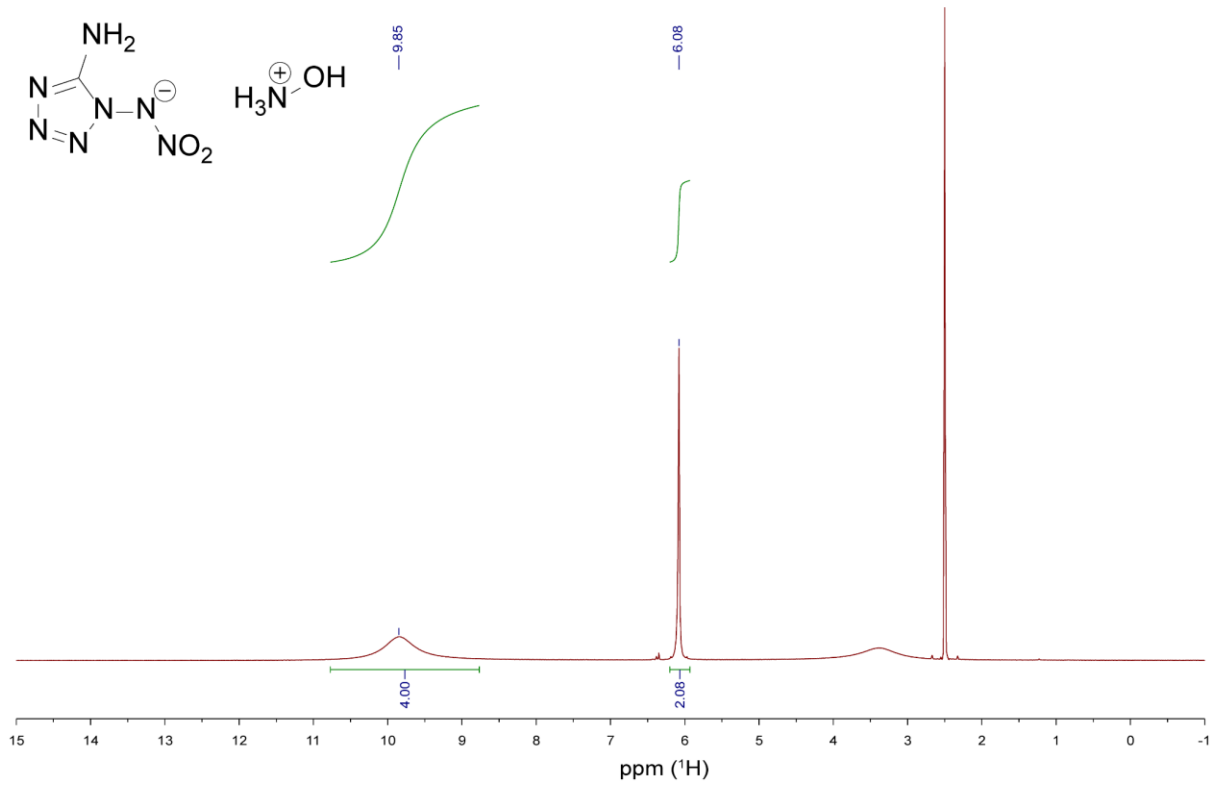

^{13}C-NMR (101 MHz, DMSO-D$_6$, ppm)

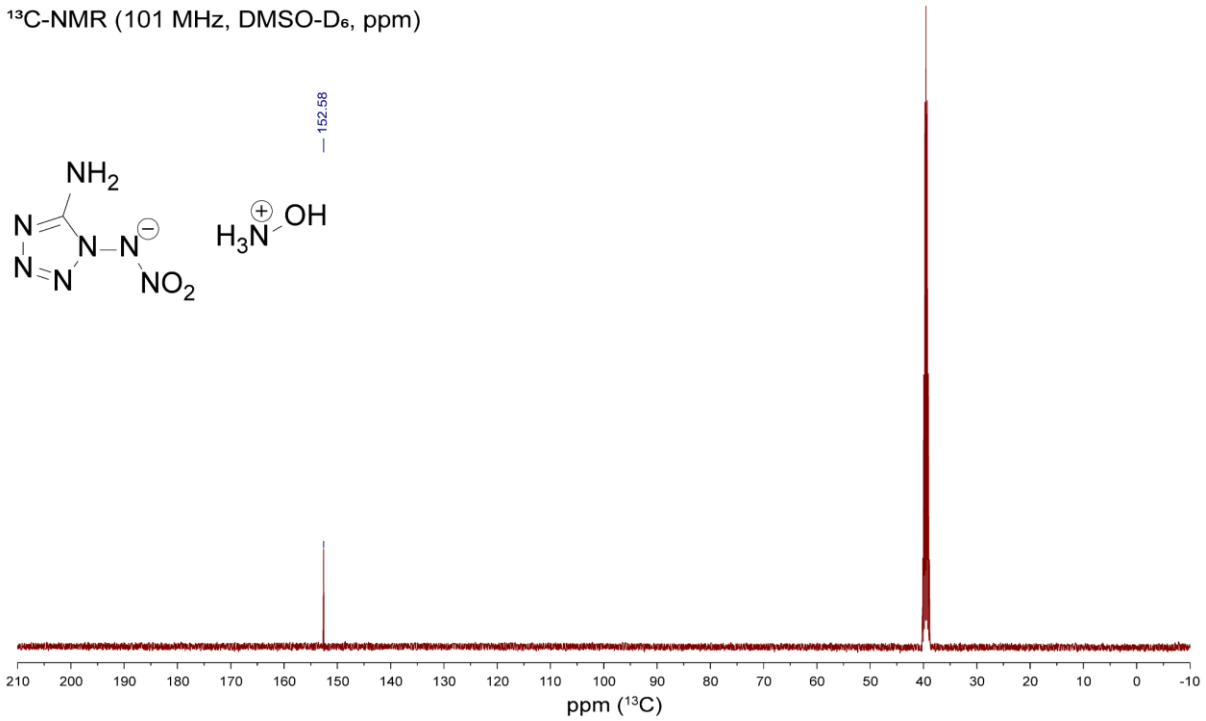

^{14}N-NMR (29 MHz, DMSO-D$_6$, ppm)

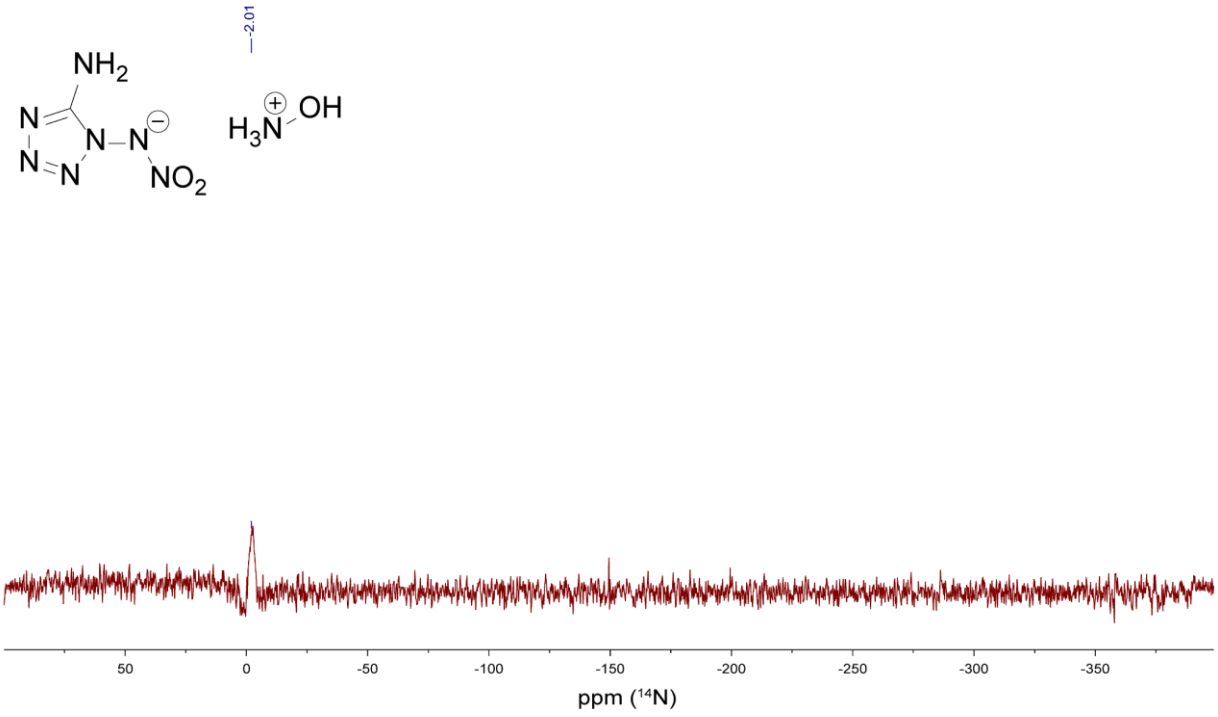

¹H-NMR (400 MHz, DMSO-D₆, ppm)

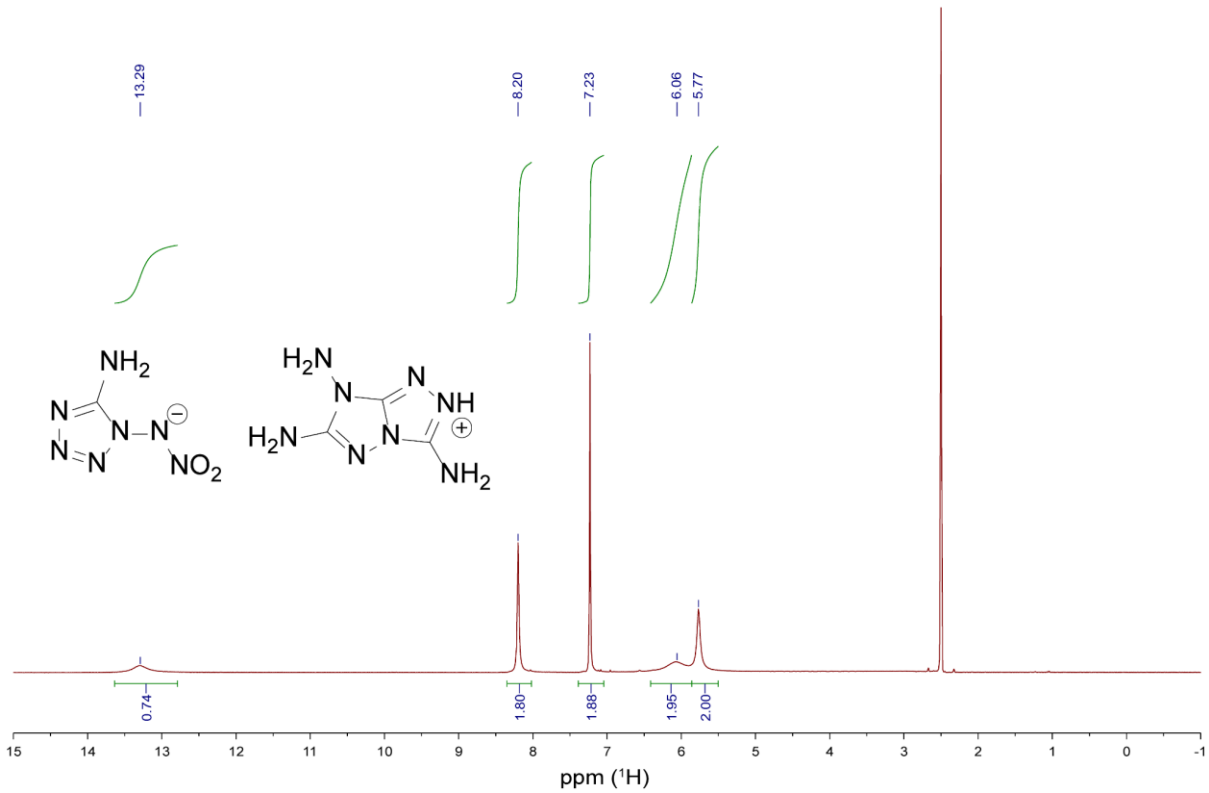

¹³C-NMR (101 MHz, DMSO-D₆, ppm)

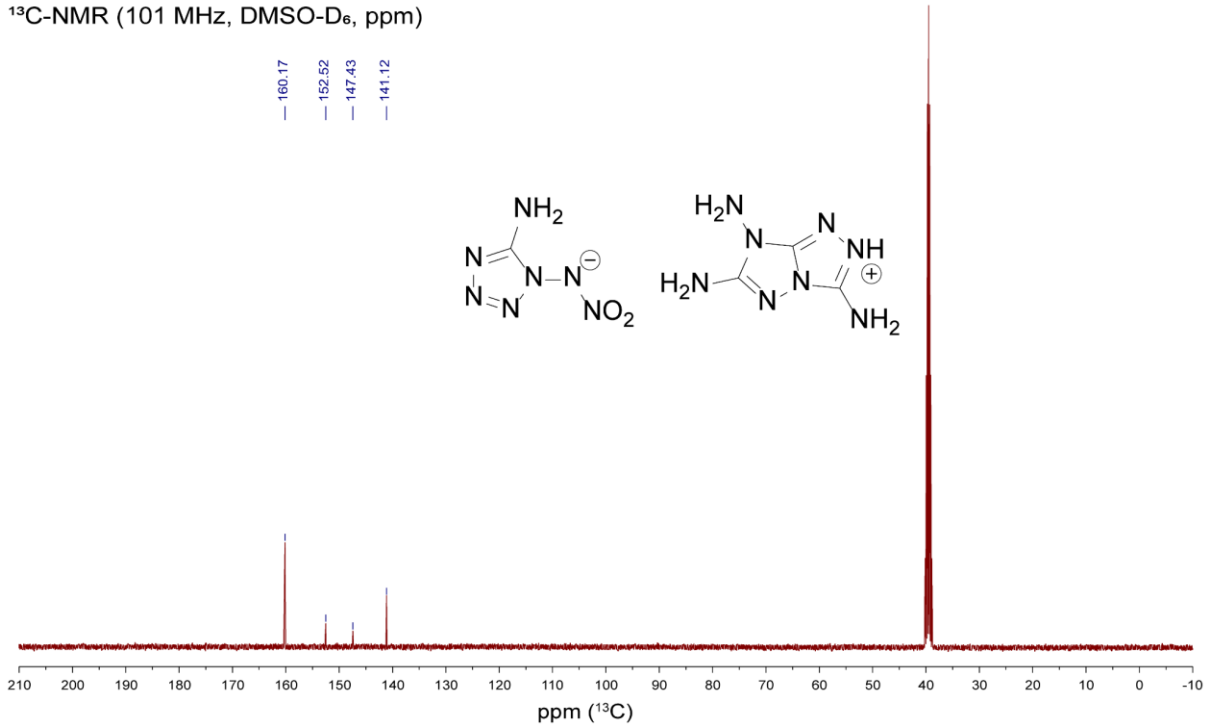

^{14}N-NMR (29 MHz, DMSO-D$_6$, ppm)

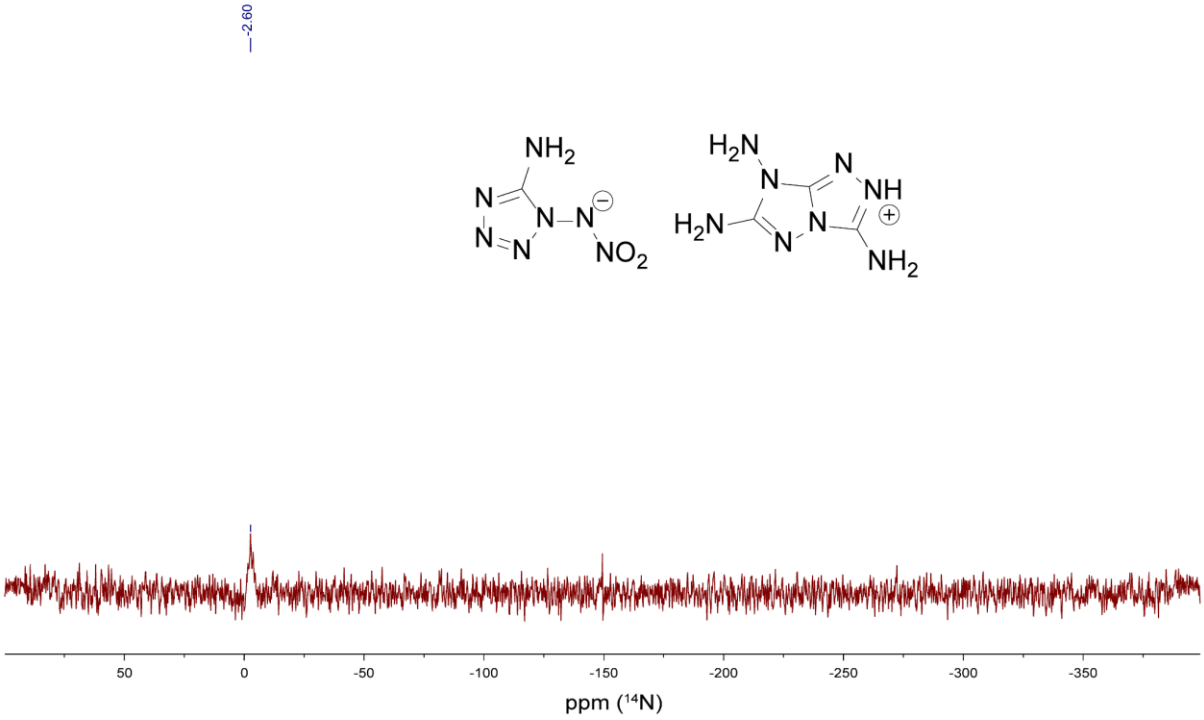

^{1}H-NMR (400 MHz, DMSO-D$_6$, ppm)

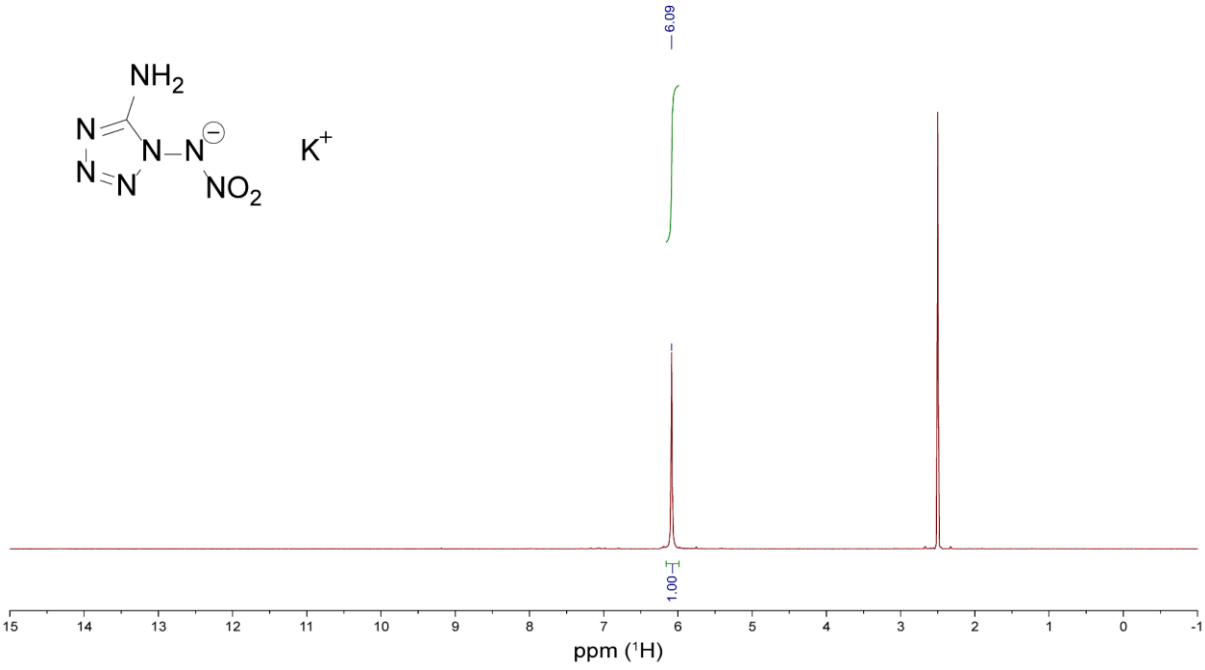

^{13}C-NMR (101 MHz, DMSO-D$_6$, ppm)

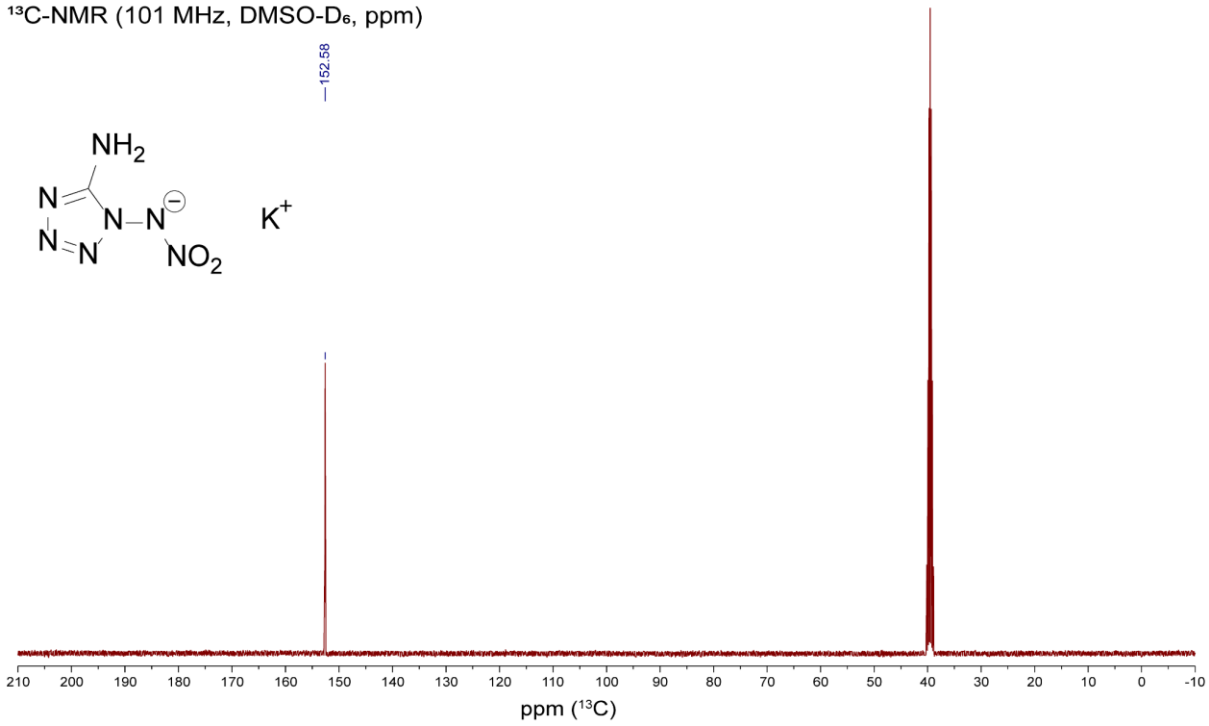

^{14}N-NMR (29 MHz, DMSO-D$_6$, ppm)

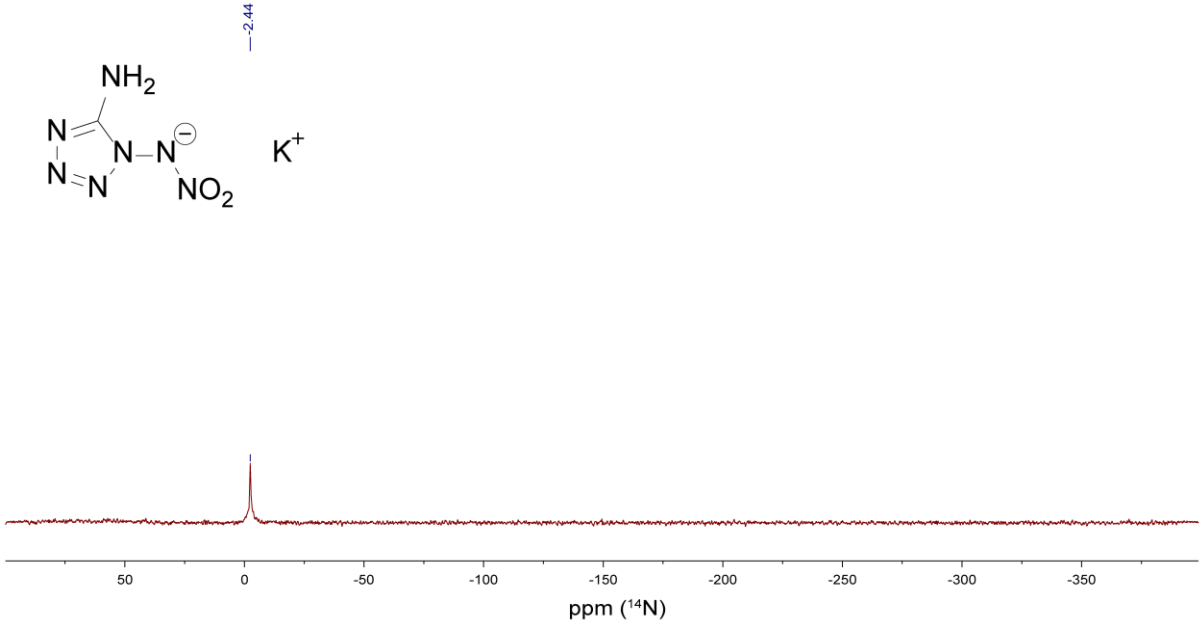

10.6.6 References

[S1] a) Test methods according to the UN Recommendations on the Transport of Dangerous Goods, *Manual of Test and Criteria*, ST/SG/AC.10/11/Rev.7, United Nations Publication, New York and Geneva, **2019**, 978-92-1-130394-0; https://unece.org/transport/dangerous-goods/rev7-files; b) Reichel & Partner GmbH, http://www.reichelt-partner.de; c) http://www.ozm.cz

[S2] M. Sućeska, EXPLO5 V6.02 program, Brodarski Institute, Zagreb, Croatia, **2014**.

[S3] L. Liu, C. He, C. Li, Z. Li, *J. Chem. Crystallogr.* **2012**, *42*, 816–823.

[S4] T. M. Klapötke, F. A. Martin, J. Stierstorfer, *Chem. Eur. J.* **2012**, *18*, 1487–1501.

[S5] *CrysAlisPro*, Oxford Diffraction Ltd. *version 171.33.41*, **2009**.

[S6] G. M. Sheldrick, *Acta Cryst.* **2015**, *A71*, 3–8.

[S7] O. V. Dolomanov, L. J Bourhis, R. J. Gildea, J. A. K. Howard, H. Puschmann, *J. Appl. Cryst.* **2009**, 42, 339–341.

[S8] *SCALE3 ABSPACK – An Oxford Diffraction program* (1.0.4, gui: 1.0.3), Oxford Diffraction Ltd., **2005**.

[S9] *APEX3*. Bruker AXS Inc., Madison, Wisconsin, USA.

[S10] M. J. Frisch, G. W. Trucks, H. B. Schlegel, G. E. Scuseria, M. A. Robb, J. R. Cheeseman, G. Scalmani, V. Barone, B. Mennucci, G. A. Petersson, H. Nakatsuji, M. Caricato, X. Li, H.P. Hratchian, A. F. Izmaylov, J. Bloino, G. Zheng, J. L. Sonnenberg, M. Hada, M. Ehara, K. Toyota, R. Fukuda, J. Hasegawa, M. Ishida, T. Nakajima, Y. Honda, O. Kitao, H. Nakai, T. Vreven, J. A. Montgomery, Jr., J. E. Peralta, F. Ogliaro, M. Bearpark, J. J. Heyd, E. Brothers, K. N. Kudin, V. N. Staroverov, R. Kobayashi, J. Normand, K. Raghavachari, A. Rendell, J. C. Burant, S. S. Iyengar, J. Tomasi, M. Cossi, N. Rega, J. M. Millam, M. Klene, J. E. Knox, J. B. Cross, V. Bakken, C. Adamo, J. Jaramillo, R. Gomperts, R. E.Stratmann, O. Yazyev, A. J. Austin, R. Cammi, C. Pomelli, J. W. Ochterski, R. L. Martin, K. Morokuma, V. G. Zakrzewski, G. A. Voth, P. Salvador, J. J. Dannenberg, S. Dapprich, A. D. Daniels, O. Farkas, J.B. Foresman, J. V. Ortiz, J. Cioslowski, D. J. Fox, Gaussian 09 A.02, Gaussian, Inc., Wallingford, CT, USA, **2009**.

[S11] a) J. W. Ochterski, G. A. Petersson, and J. A. Montgomery Jr., *J. Chem. Phys.* **1996**, *104*, 2598–2619; b) J. A. Montgomery Jr., M. J. Frisch, J. W. Ochterski G. A. Petersson, *J. Chem. Phys.* **2000**, *112*, 6532–6542.

[S12] a) L. A. Curtiss, K. Raghavachari, P. C. Redfern, J. A. Pople, *J. Chem. Phys.* **1997**, *106*, 1063–1079; b) E. F. C. Byrd, B. M. Rice, *J. Phys. Chem*. A **2006**, *110*, 1005–1013; c) B. M. Rice, S. V. Pai, J. Hare, *Comb. Flame* **1999**, *118*, 445–458.

[S13] P. J. Lindstrom, W. G. Mallard (Editors), NIST Standard Reference Database Number 69, http://webbook.nist.gov/chemistry/ (accessed June **2020**).

[S14] M. S. Westwell, M. S. Searle, D. J. Wales, D. H. Williams, *J. Am. Chem. Soc*. **1995**, *117*, 5013–5015; b) F. Trouton, *Philos. Mag*. **1884**, *18*, 54–57.

[S15] a) H. D. B. Jenkins, H. K. Roobottom, J. Passmore, L. Glasser, *Inorg. Chem.* **1999,** *38,* 3609–3620; b) H. D. B. Jenkins, D. Tudela, L. Glasser, *Inorg. Chem.* **2002**, *41*, 2364–2367.

11. 1-Nitrimino-5-azidotetrazole: Extending Energetic Tetrazole Chemistry

Maximilian Benz, Thomas M. Klapötke, J. Stierstorfer

as published in *ChemPlusChem* **2022**, e202200186

DOI: 10.1002/cplu.202200186

Keywords: azides, energetic materials, heterocycles, nitration, tetrazoles

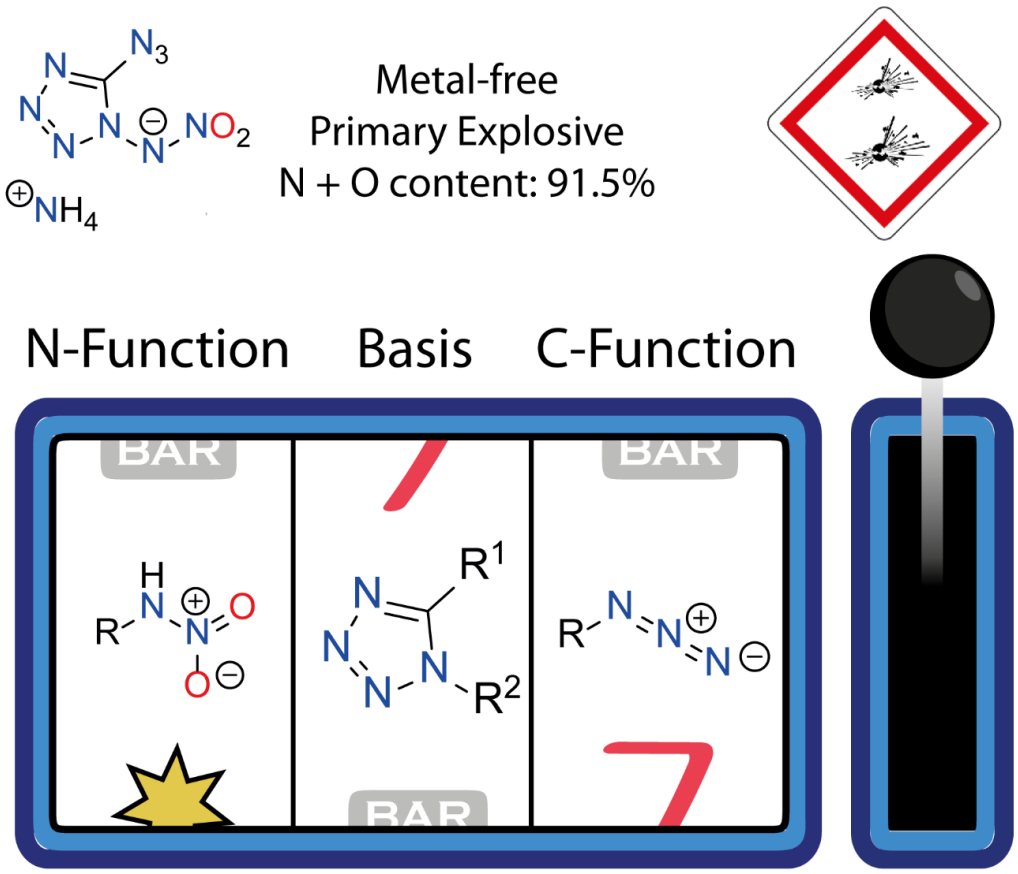

The combination of a nitrimine and an azide function on a monotetrazole creates one of the most powerful heterocyclic explosives, namely 1-nitrimino-5-azidotetrazole. Even the ammonium derivative is able to initiate PETN, which is unusual for metal-free salts. From an energetic point of view, the generation of this unit was somewhat overshooting the target, since the taming of this high-energy unit seems almost impossible.

Abstract: Azide and nitrimino functions are among the most energetic substituents that can be introduced to the skeleton to enhance the energetic properties of a compound. In this study, we report the successful synthesis of a compound that combines both, azide and nitrimino substituents directly attached to one tetrazole scaffold. 1-Nitrimino-5-azidotetrazole is prepared by nitration of 1-amino-5-azidotetrazole. Subsequent salination with ammonia and guanidinium carbonate yields two highly energetic derivatives. All energetic compounds, as well as the intermediate steps of an alternatively developed synthesis strategy, were analysed and characterized in detail. In addition to multinuclear NMR and IR spectroscopy, crystal structures of all key compounds were measured. The sensitivities (friction, impact, electrostatic discharge and thermal) were determined accordingly. In addition, the detonation parameters of all energetic substances were calculated with the EXPLO5 code, which was fed with the enthalpy of formation (atomization method based on CBS-4M) and the crystallographic densities.

11.1 Introduction

Alongside ever greater efforts to develop more powerful explosives, the environmental aspect in particular is a central factor for the development of new energetic materials.[1-3] For this, some basic properties should be fulfilled, whereby newly developed substances should be free of heavy metals and perchlorates. Compounds containing these components are demonstrably harmful to the environment and hazardous to humans' health.[4-5] Similarly, nitroaromatics, which despite being discovered and researched 150 years ago, still have an enormously wide range of applications.[6-7] In order to find possible substitutes, research has been conducted on nitrogen-rich heterocycles as basic building blocks the past years.[1, 8] These have several advantages over other structural units. Firstly, the high nitrogen content of the compounds, which leads to the fact that after decomposition, most of the nitrogen is converted into elemental dinitrogen. In addition, unlike benzene, which serves as the basic building block for TNT, these heterocycles already have a considerable enthalpy of formation, which leads to improved explosion properties. In addition, many heterocycles are easily synthetically accessible.[9-11]

In principle, it should be noted that a clever increase of the nitrogen and oxygen content of explosives, often results in higher density but also higher amount of gaseous and mainly non-hazardous decomposition products (N_2, CO, CO_2). Not only therefore, from an environmental point of view, an all nitrogen compounds such as pentazole or its N-oxides would be the best possible energetic compound.[12-15] Research has focused for many years on the development of new tetrazole derivatives. Even unsubstituted 1H-tetrazole has a nitrogen content of almost 80% and an enthalpy of formation of 4732 kJ kg^{-1}.[16-17] By introducing suitable substituents to the tetrazole base, not only the nitrogen content but also the enthalpy of formation can be further tuned. However, the same applies for the substituents: the more nitrogen and oxygen, the better the impact on the environment and the resulting explosion parameters.[18]

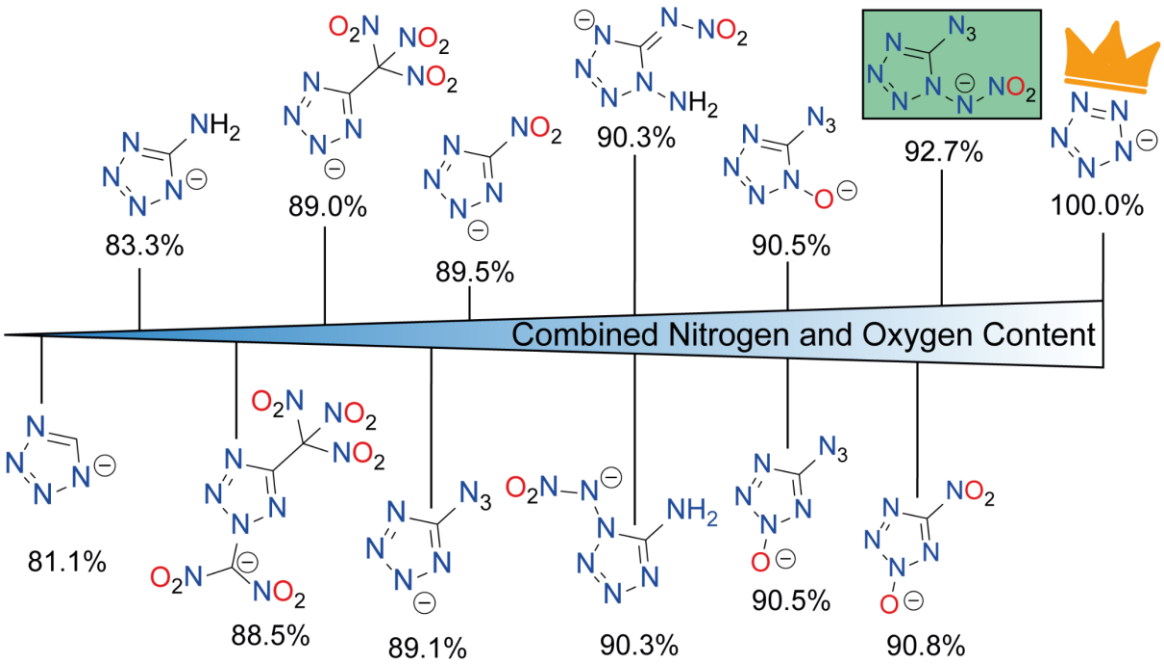

Figure 1. Single deprotonated monotetrazolates sorted by increasing combined nitrogen and oxygen content.

Using this tactic: Combining tetrazole-based explosives with suitable (high N and O content), energy contributing substituents, major research successes have already been achieved (Figure 1).[19-21] Groups composed exclusively of nitrogen and oxygen have proved to be particularly attractive for use as substituents. Particularly suitable in this context are covalently bonded azides (only possible as C-substituents at tetrazoles), which, in addition to an energy contribution of

256 kJ mol^{-1}, also increase explosion properties and normally adjust sensitivities. In addition, azides are easy to install and their composition makes them particularly environmentally compatible, since they formally consist only of nitrogen.

In addition to azides, nitramines (or nitrimines) possess a favorable functionality, which in most cases can be introduced simply by nitration of amines.[22-23] The two oxygens contained in the nitramino not only increase the oxygen balance of the compound but also the density, since oxygen is heavier than the other components (mostly hydrogen, carbon and nitrogen). In addition, primary nitramines have another advantage. Although free nitramines (−N(*H*)NO_2) are often only stable to a limited extent, they can be functionalized by the formation of salts. The acidity of the proton is usually sufficient to deprotonate nitramines even with mild bases. The properties of the resulting compound can be further adjusted and adapted by the appropriate choice of cation.

In accordance with the modular principle, a various number of target compounds have already been successfully synthesized and investigated. In this study, we were focusing on the synthesis and characterization of 1-nitrimino-5-azidotetrazole (CHN_9O_2) and several ionic derivatives thereof. The parent compound (HNAAT, **2**) and the derivatives are high-energy explosives with a combined nitrogen and oxygen content of up to 91.5% and outstanding energetic parameters.

11.2 Results and Discussion

11.2.1 Synthesis

In general, tetrazoles with substitution at N1 are difficult to synthesize as soon as an electron-withdrawing group is located at position C1. Direct reactions of C-electron-withdrawing tetrazolates (e. g. 5-azidotetrazolate, 5-nitrotetrazolate or 5-cyanotetrazolate) with electrophiles always give the derivatives substituted at N2, as has been shown, for amination,[24-25] N-oxidation[21, 26-27] or methylation[28-29] reactions. Consequently, two possible synthesis strategies arise for substitutions for particular tetrazolates at position N1. On the one hand, the functionality at position N1 can be introduced first, followed by the electron-withdrawing carbon function, or by reaction pathways that proceed via a selective mechanism, in which case rearrangement or selected ring closures automatically result in a substitution

at position N1.[30] In the literature, the synthesis of 1-amino-5-azidotetrazole (**1**) is performed through double diazotization of triaminoguanidinium chloride (Scheme 1) with two equivalents of HNO_2.[31] By rapid quench with a base (Na_2CO_3), 1-amino-5-azidotetrazole (**1**) is obtained as the main product. We modified the published procedure and were able to push the yield to 26 %. Despite the poor yield, only small quantities of starting materials (4 mmol) were reacted in one batch because of the formation of extremely sensitive byproducts (C_2N_{14} and 1-(aminoazidocarbamoyl)-5-azidotetrazole). The side species were removed using column chromatography.

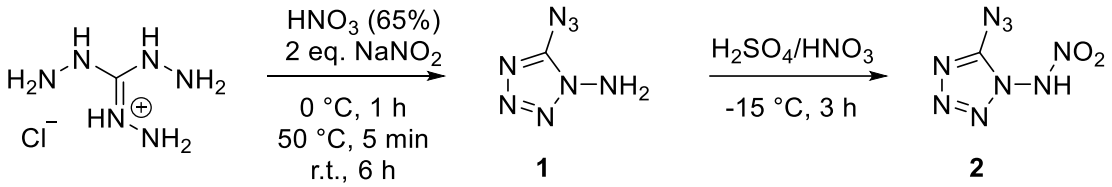

Scheme 1. Synthesis of 1-amino-5-azidotetrazole (**1**) through diazotization of triaminoguanidinium chloride and nitration using mixed acid to 1-nitrimino-5-azidotetrazole (**2**).

We had to do try several different nitration methods to obtain the desired 1-nitrimino-5-azidotetrazole (**2**). We did not obtain any reaction with nitric acid at different temperatures (−30–60 °C). Even aprotic nitration using NO_2BF_4 or N_2O_5 as nitrating agent in acetonitrile only yielded starting material. Finally, we applied a method that runs successfully for the N-nitration of 1,5-diaminotetrazole. In this process, nitration is performed with a sulfuric acid/nitric acid (1 : 1) mixture at −15 °C.[32] In our case, 1-amino-5-azidotetrazole (**1**) was added to the nitration mixture pre-dissolved in a small amount of concentrated sulfuric acid (Scheme 1). This method provided 1-nitrimino-5-azidotetrazole (**2**) in 54 % yield in the form of a viscous oil. The nitration of the recently published isomeric 2-amino-5-azidotetrazole[24] through various methods (N_2O_5, NO_2BF_4 or mixed acid as for **1**) was not successful since only decomposition products were obtained.

Since the literature known synthesis of **1** includes, as above mentioned, the formation of several extremely sensitive 5-azidotetrazole derivatives and therefore has to be worked up through column chromatography, we tried to find another synthetic pathway toward **1**. The procedure should start from simple starting materials, involve as few synthesis steps as possible, deliver good yields, as well

as not contain any extremely energetic or unstable intermediates. In addition, easy scalability should be achieved in order to be able to produce larger quantities of the compound. The sequence starts with ethyl carbazate (**3**), which can be easily synthesized by equimolar reaction of hydrazine hydrate with diethyl carbonate. Carbazate **3** undergoes condensation reaction with glyoxalic acid to precipitate hydrazone **4**. This reaction step was performed in a scale of up to 80 g. Bromine indicated decarboxylation of **4** under basic conditions results in the dibromo hydrazone **5**. We were also able to perform this step by replacing Br_2 by NBS, however, the yield is declining as a result.

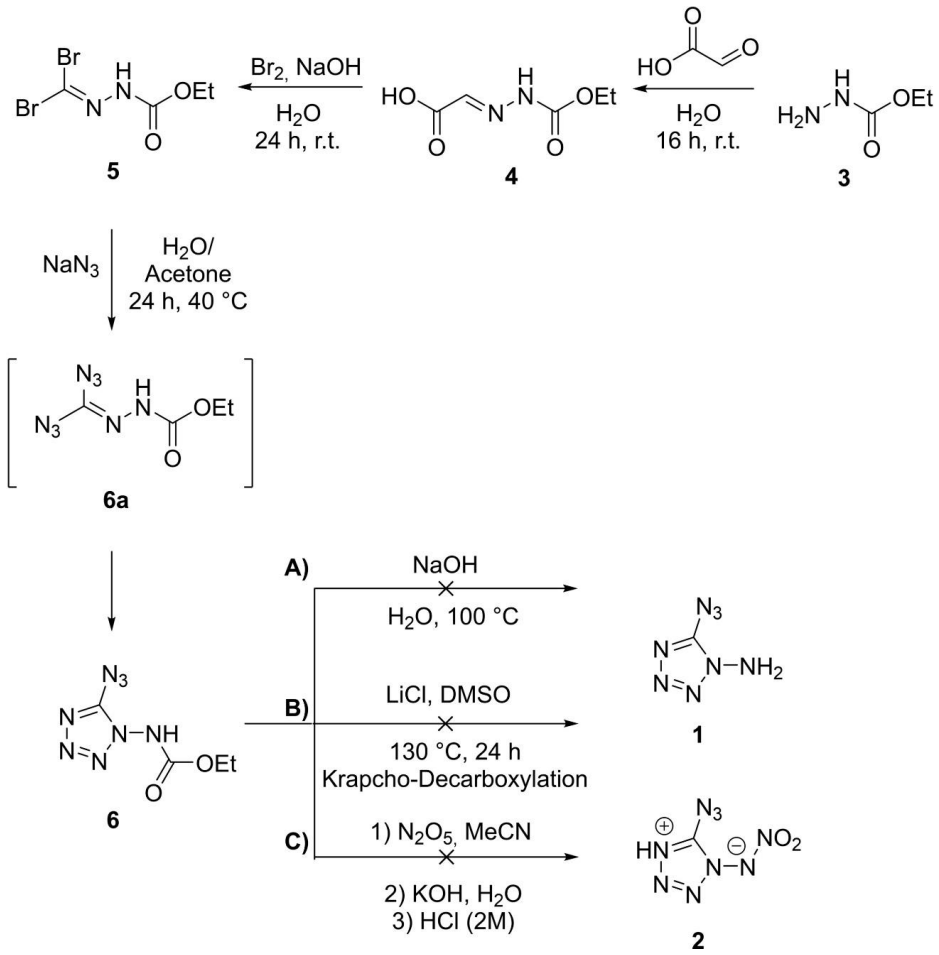

Scheme 2. Failed reaction attempts with 5-azidotetrazole carbamate **6**.

The subsequent bromo-azide exchange was carried out in a mixture of water and acetone and required a slight heating of the reaction solution to 40 °C (Scheme 2). The cyclization of the diazido hydrazone (**6 a**) to the 5-azidotetrazole derivative **6** proceeded directly in solution. As the bromo-azide exchange was carried out at

room temperature, only one bromine was substituted and after the in situ cyclization, the 5-bromotetrazole derivative was obtained, which was not studied in more detail. Similar observations were made recently for the reaction of dibromoformaldoxime with sodium azide.[20]

The main goal in the synthesis of 1-ethoxycarbamate-5-azidotetrazole was the better and easier accessibility of **1** and **2**, respectively. However, we were not successful with the deprotection of **6**. Our main synthetic approaches are shown in Scheme 2. Normally, ethyl carbamates can be cleaved in water under the exposure of a base at elevated temperature or of a strong acid.[33-34] However, our system was only deprotonated under basic conditions and the carbamate protecting group could not be removed. Acidic cleavage using TFA did yield starting material. Likewise, it could not be eliminated by Krapcho reaction, as was the case with recently published 1,1'-(diethoxycarbonyl)-diaminotetrazole.[35] Nor could the protecting group be removed by previous nitration and basic work-up, as is successfully performed for K_2DNABT.[36]

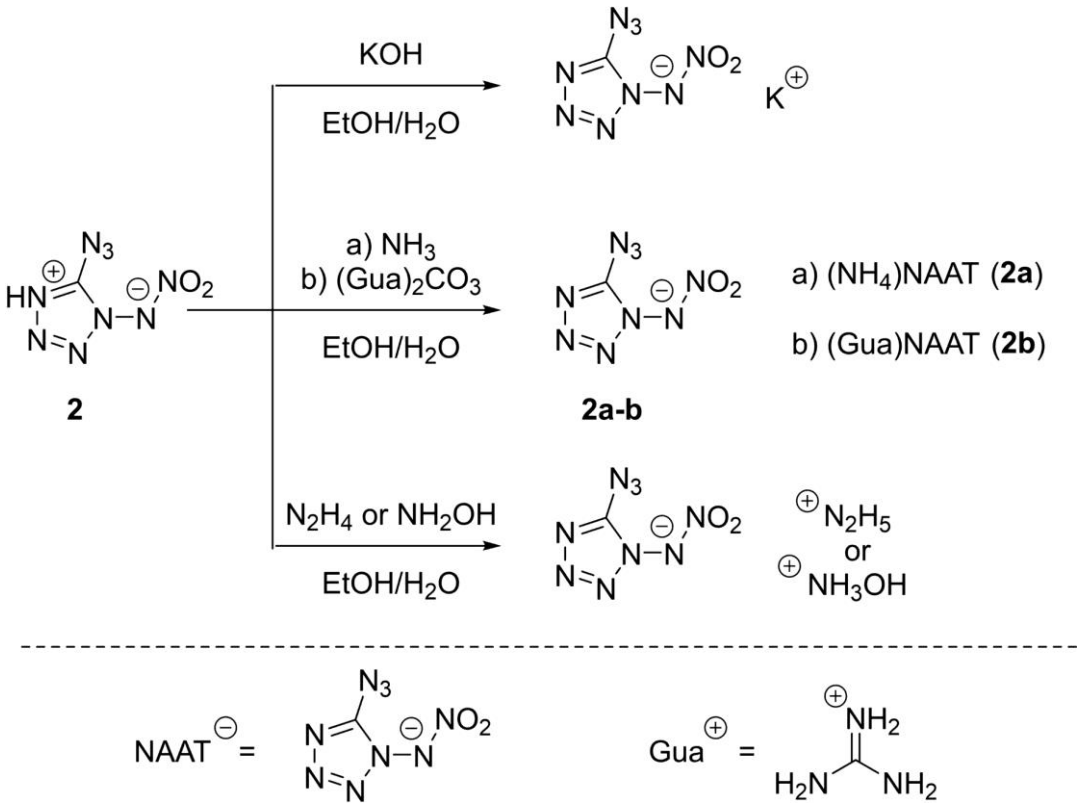

Scheme 3. Synthetic pathway toward the formation of ionic derivatives **2a** and **2b**.

Despite the small amounts of 1-nitrimino-5-azidotetrazole (**2**), we were able to synthesize some new ionic nitrogen-rich derivatives. Sadly, we were only able to characterize the ammonium (**2a**) and the guanidinium (**2b**) derivative in more detail. Therefore, the oily free acid **2** was dissolved in ethanol and the respective bases were added. For the ammonium derivative **2a**, gaseous ammonia was bubbled through the solution, for the guanidinium derivative, $(Gua)_2CO_3$ dissolved in water was added equimolar (Scheme 3). For the hydroxylammonium and hydrazinium derivatives, which are considered to exhibit the highest calculated detonation performance, it was only possible to isolate extremely hygroscopic salts, which could not be further characterized. In addition, we made some attempts to isolate the potassium derivative. However, after complete evaporation of the reaction solution, spontaneous detonation of the solidified potassium 1-nitrimino-5-azidotetrazolate occurred. Therefore, no more detailed analytical data on the potassium derivative are given in this paper. We also strongly recommend not to synthesize this compound, since detonative decomposition occurs even at the weakest external influences. The ionic derivatives **2a** and **2b** were obtained elemental analysis pure from the reduced reaction solution (**2a**) or after recrystallization from hot methanol (**2b**) in good to excellent yields.

11.2.2 X-Ray Diffraction

Crystallographic investigations could be performed for all energetic solid derivatives (**2**, **2a**, **2b** and **6**). The crystal structures of **3** and **5** can be found in the Supporting Information. Deposition Numbers 2170430 (for **1**), 2170433 (for **2a**), 2170432 (for **2b**) and 2170434 (for **6**) contain the supplementary crystallographic data for this paper. These data are provided free of charge by the joint Cambridge Crystallographic Data Centre.

1-Amino-5-azidotetrazole (**1**) crystallizes in the orthorhombic space group $Pna2_1$ in the form of colorless plates. It shows a room temperature density of 1.636 g cm^{-3}. Therefore, it is 0.1 g cm^{-3} lower than for its isomer 2-amino-5-azidotetrazole (ρ = 1.736 g cm^{-3} @298 K)[24] and is also below the estimated value.[31]

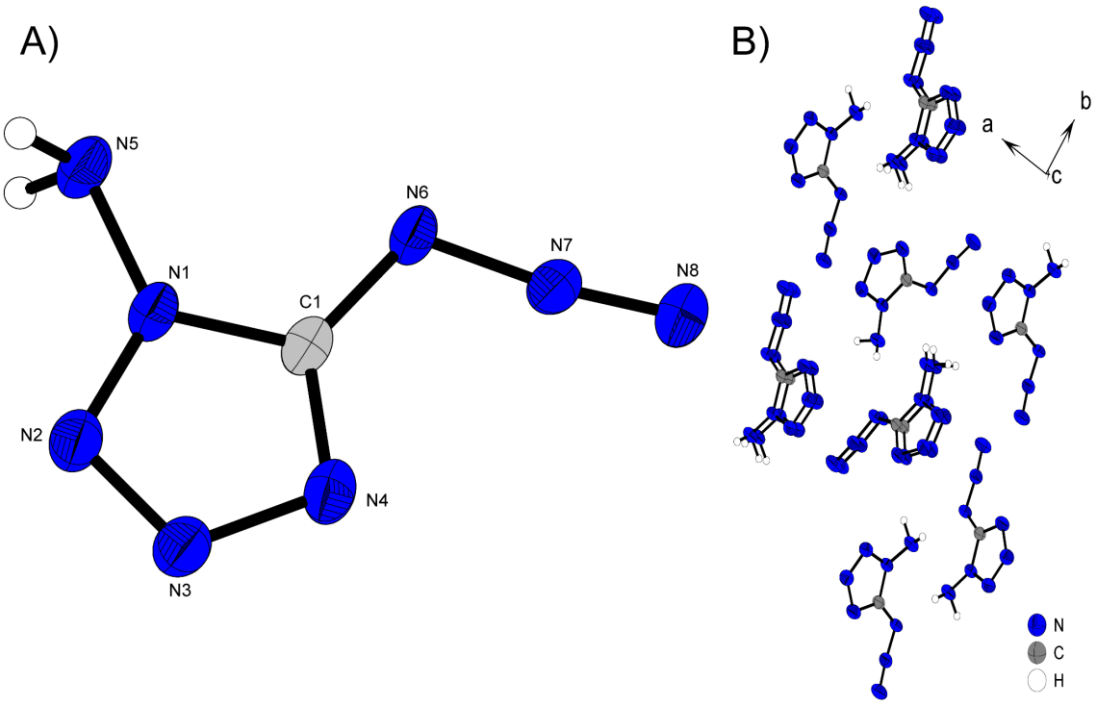

Figure 2. A) Molecular unit of **1** with thermal ellipsoids drawn at the 50 % probability level. Selected bond distances (Å) and angles [°]: N1−N5 1.394(5), C1−N6 1.379(6), N6−N7 1.271(5), N7−N8 1.109(5), N2−N1−N5 125.4(3), C1−N1−N5 1.121(8), N6−N7−N8 172.1(5), N4−C1−N6−N7 0.6(7); B) layer structure of **1** with view along the *c* axis.

The molecule itself is planar. As expected for covalent azides, the N_3 is slightly bent by N6−N7−N8=172.1(5) ° The bond length of the amine bound to N1 (N1−N5 1.394(5) Å) is in between the bond length of a N−N single and double bond, suggesting an electron-donating effect of the N-amine. Due to the resulting three-dimensional structure, hydrogen bonds are formed with the two most electron-rich nitrogen atoms of the respective neighboring molecules (Figure 2). These are medium strength interactions in the range of *d*(H···A)=2.27–2.37 Å, which are formed by both protons of the amino groups to N4 of the tetrazole ring and N_α of the azide function.

Ammonium 1-nitrimino-5-azidotetrazolate (**2a**) crystallizes in the monoclinic space group $P2_1/n$ with four molecular units per cell. The density is calculated to be 1.727 g cm^{-3} at 298 K (Figure 3). Through the introduction of the nitrimino function, the density could be raised about 0.14 g cm^{-3} compared with the density of ammonium 5-azidotetrazolate (ρ = 1.585 g cm^{-3} @298 K).[16]

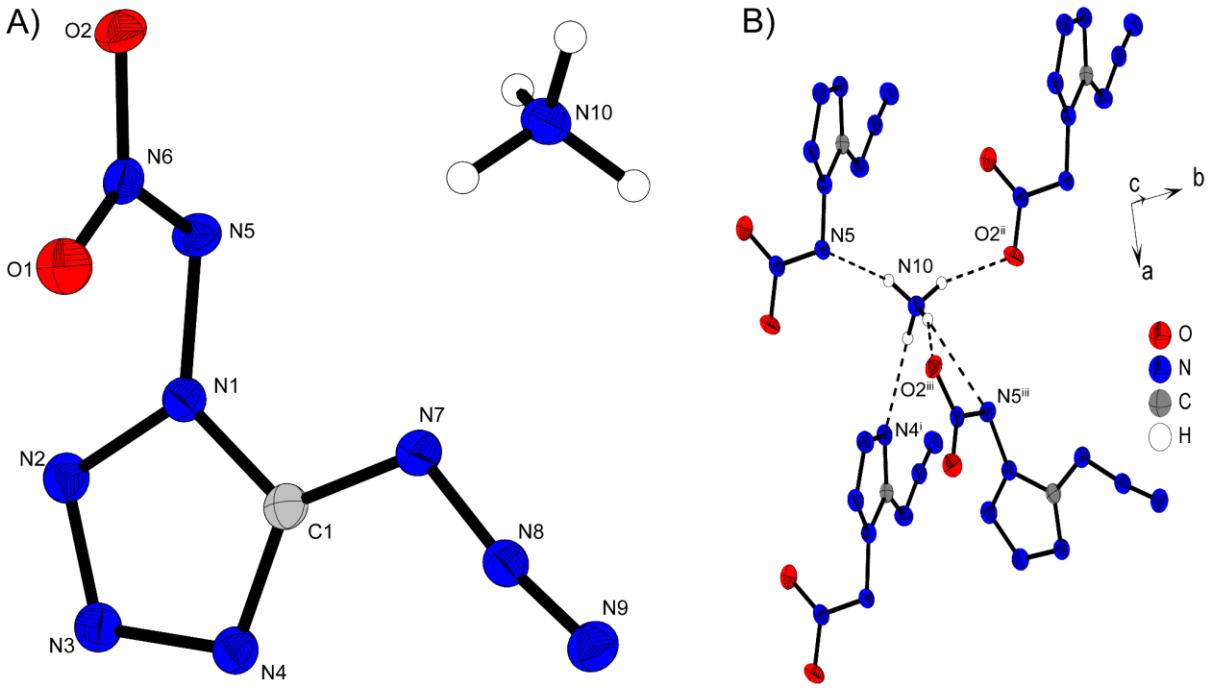

Figure 3. A) Molecular unit of **2a** with thermal ellipsoids drawn at the 50 % probability level. Selected bond and intermolecular bond distances (Å) and angles [°]: N1−N5 1.394(2), N5−N6 1.345(2), C1−N7 1.383(2), N5···H10D−N10 2.30(2), $N4^{i}$···H10C−N10 2.16(2), $O2^{ii}$···H10B−N10 2.05(2), $O2^{iii}$···H10A−N10 2.03(2), N5−H10D−N10 148.9(2), $N4^{i}$−H10C−N10 148.5(2), $O2^{ii}$−H10B−N10 157.7(2), $O2^{iii}$−H10A−N10 163.0(2), N6−N5−N1−N2 93.3(2); B) Representation of the surrounding of a ammonium moiety within the crystal packing; Symmetry codes: (i) 1+x,+y,+z, (ii)+x, 1+y,+z, (iii) 1.5 – x, 0.5+y, 1.5 – z.

Despite nitration, the bond length N1-N5 is unchanged compared to **1** and, in addition, the nitro group of the nitrimine is orthogonal to the tetrazole ring (N6−N5−N1−N2 93.3(2) °), which indicates a still strong electron-donating effect of N5 toward the tetrazole. Each ammonium cation is coordinated by four anionic sites. Strong interactions are formed between the protons of NH_4^+ and N4, O1 and O2 of the anion with lengths *d*(H···A) of about 2.0 Å and somewhat weaker ones originating from N5 (N5···H10D−N10). Due to the introduction of the nitrimino group, the azide function no longer participates in intermolecular interactions and is rotated off the ammonium units in the crystal lattice.

The guanidinium derivative of 1-nitrimino-5-azidotetrazole crystallizes in the triclinic space group *P*−1 in the form of colorless needles. The density at room temperature is 1.656 g cm^{-3}. Therefore, its density is about 0.05 g cm^{-3} higher than for guanidinium 5-azidotetrazolate (ρ = 1.610 g cm^{-3} @298 K).[20]

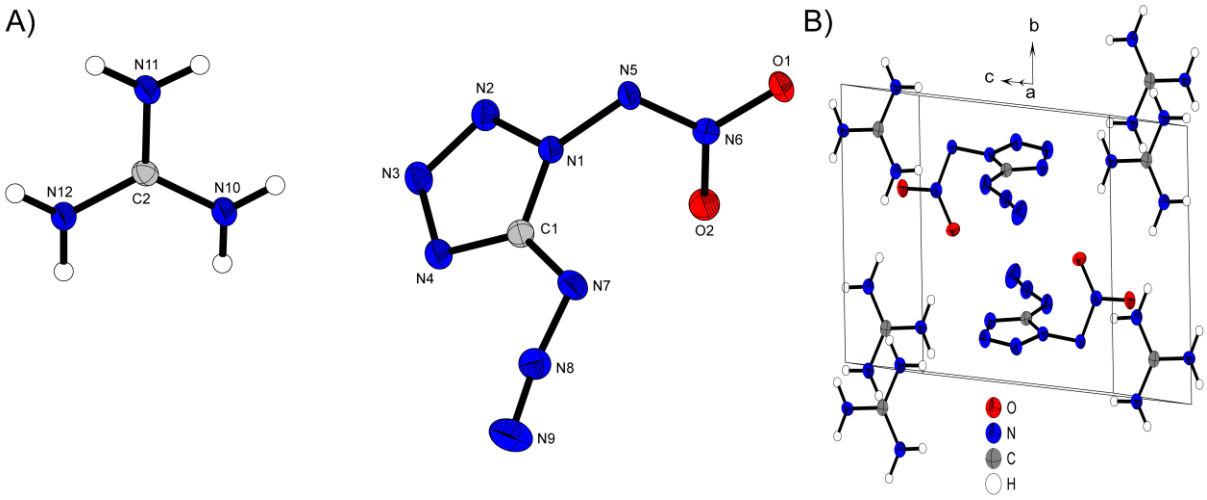

Figure 4. A) Molecular unit of **2 b** with thermal ellipsoids drawn at the 50 % probability level. Selected bond and intermolecular bond distances (Å) and angles [°]: N1−N5 1.398(2), N5−N6 1.332(2), C1−N7 1.390(2), N5···H12B−N12 2.20(3), O1···H11A−N11 2.10(3), N6−N7−N8 171.2(3), N5−H12B−N12 174.0(2), O1−H11A−N11 177.0(3), N10−C2−N12 120.2(2), N6−N5−N1−N2 107.7(2); B) layer structure of **2 b** with view along the stated direction.

The nitro units of the nitramine groups are offset parallel to the planar guanidinium cations. Each guanidinium cation is saturated by four $NAAT^-$ anions, which follows a clear pattern. O1 and O2 or O2 and N5 of an anion unit coordinate in a pincer-like manner to one hydrogen atom each of two different amines of the same guanidinium cation. Thus, four hydrogens are already coated, which are found with distances of *d*(H···A)=2.10–2.22 Å (Figure 4). The remaining two hydrogens of the guanidinium form moderate hydrogen bonds to N4 and N_α of the third and fourth coordinating anion units.

Compound **6** crystallizes in the monoclinic space group $P2_1/c$ in the form of colorless blocks. The density is 1.441 g cm^{-3} at 298 K, which is the lowest one included in this study. The structure is mainly characterized by one strong hydrogen bridge $O1^{i}$···H5−N5 (1.98 Å) (Figure 5). This results in the formation of chain-like molecular arrangements, which are arranged around this characteristic interaction. The respective neighboring molecules are twisted against each other, but form both regions where the azidotetrazole units overlap and the ester residues intersect.

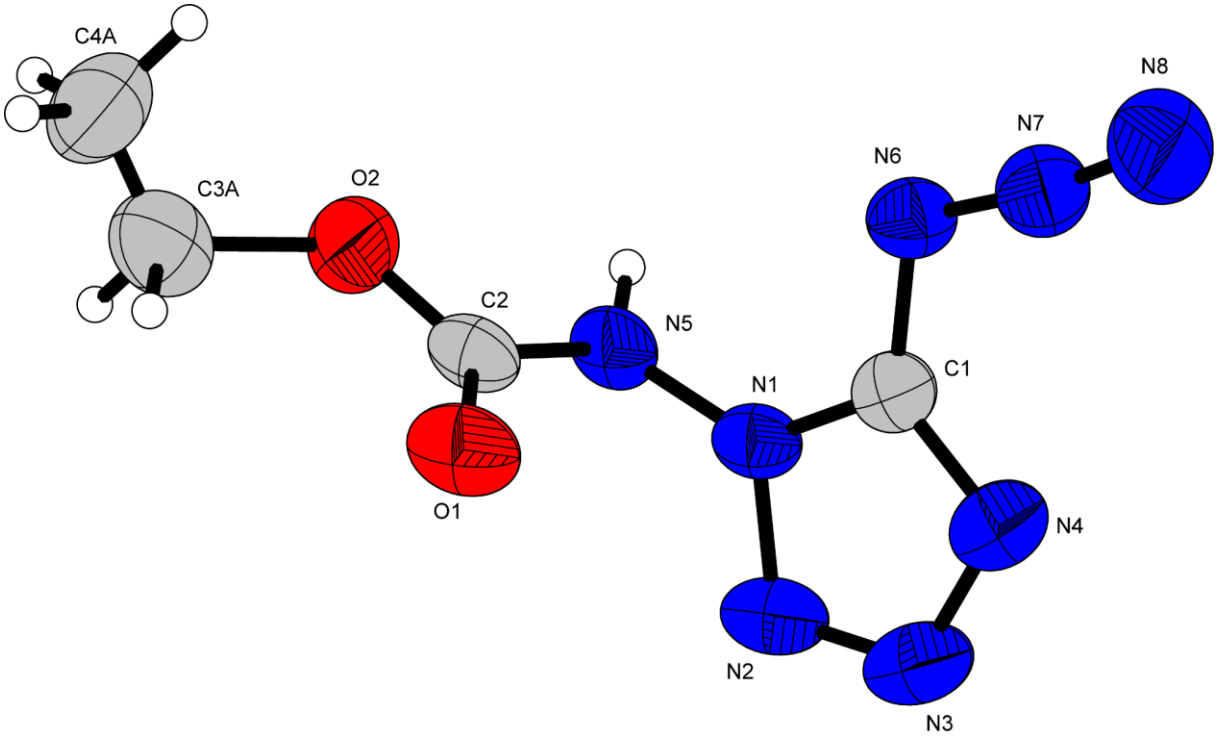

Figure 5. A) Molecular unit of **6** with thermal ellipsoids drawn at the 50 % probability level. Selected bond distances (Å) and angles [°]: N1−N5 1.356(3), N5−C2 1.359(3), C1−N6 1.387(4), N6−N7−N8 172.4(4), C2−N5−N1 117.3(2), N2−N1−N5−C2 85.8(3), N7−N6−C1−N4 2.1(5).

11.2.3 Physico-chemical Properties

We measured the sensitivities of all 5-azidotetrazole derivatives and calculated the performance parameters based on the crystallographic density and the CBS-4M heat of formation for **1**, **2**, **2a** and **2b** using the EXPLO5 code. Since **2** is a liquid, the density was measured using a gas pycnometer. For **6**, the calculations were omitted, since the compound is a precursor to the essential compounds of this study. Nevertheless, **6** is a high energetic material, which has been confirmed by the measurement of its sensitivities toward friction and impact (FS=1.5 N, IS <1 J). Further information about the thermal and mechanical sensitivity for **6** can be found in the Supporting Information and are not further discussed in here.

The combined nitrogen and oxygen content feature an impressive value for all investigated compounds, with the ammonium **2a** derivative even clearly exceeding 90 % (91.5 % for **2a**). Similarly, the N+O content of the guanidinium NAAT with 83.9% is one of the highest values for a mono-guanidinium derivative.

Table 1. Physico-chemical properties of compounds **1**, **2**, **2a** and **2b** as well as lead azide.

	1	**2**	**2a**	**2b**	LA
IS [J][a]	1	<1	1	2	4
FS [N][b]	4	>360	1	30	<0.1
ESD [mJ][c]	75	-	20	125	<5
P [g cm^{-3}][d]	1.636	1.78*	1.727	1.656	4.8
N + O [%][e]	88.9	92.4	91.5	83.9	28.9
Ω [%][f]	−25.4	4.7	−8.5	−20.9	−11.0
T_{dec} [°C][g]	165	85	145	149	315
$\Delta_f H°$ [kJ mol^{-1}][h]	726.8	934.2	708.5	678.4	450.1
		EXPLO5 V6.05.02			
T_{det} [K][i]	5830	5625	6126	4974	3372
P_{CJ} [kbar][j]	302	410	347	284	357
V_{det} [m s^{-1}][k]	9027	9829	9337	8723	6187
Hot Plate	det.	det.	det.	def.	det.
Hot Needle	def.	det.	def/det.	dec.	det.
PETN Initiation	neg.	n.d.	pos.	neg.	pos.

[a] Impact sensitivity (BAM drophammer (1 of 6)). [b] Friction sensitivity (BAM friction tester (1 of 6)). [c] Electrostatic discharge device (OZM research). [d] From X-Ray diffraction analysis recalculated to 298 K (* pycnometric measurement). [e] Combined nitrogen and oxygen content. [f] Oxygen balance with respect to CO [g] Decomposition temperature (DTA; β=5 °C min^{-1}). [h] Calculated enthalpy of formation. [i] Detonation temperature. [j] Detonation pressure at Chapman-Jouguet point. [k] Detonation velocity; det.: detonation, def: deflagration, dec.: decomposition; neg.: negative; pos.: positive.

The impact sensitivities for all compounds are clearly in the range of primary explosives (1–2 J). Due to its liquid nature, **2** has an impact sensitivity of <1 J, but a friction sensitivity of >360 N, similar to nitroglycerin. **1** and **2a** show equally extremely high friction sensitivities (4 N for **1** and 1 N for **2a**). All compounds are therefore more sensitive toward impact but less sensitive toward friction compared to lead azide (Table 1). In the case of guanidinium derivative **2b**, it could be increased to 30 N. **1** decomposes sharply at 165 °C. Due to the nitration and the salination with the selected cations, which are known from empirical experience to increase the decomposition temperature, we expected a similar if not even higher decomposition points then for **1**. Unfortunately, both ionic derivatives decompose shortly before 150 °C, whereby **2a** even decomposes denotatively. 1-Amino-5-azidotetrazole (**1**) has a higher positive enthalpy of formation than its two-substituted isomer (726.8 kJ mol^{-1} vs. 703.7 kJ mol^{-1}), but the latter has a

calculated detonation velocity almost 400 m s^{-1} more than **1** (V_{det} = 9027 m s^{-1}), which is mainly due to the large difference in density. The free acid **2** features impressive detonation properties (P_{CJ} = 410 kbar; V_{det} = 9829 m s^{-1}) and competes with most powerful non-nuclear explosives. Ammonium derivative **2a** has a detonation velocity of 9337 m s^{-1} and is therefore in the same range as HMX, guanidinium derivative **2b** possesses a calculated detonation velocity of 8723 m s^{-1}, which is in the range of RDX and outstanding for a derivative like this. Hot plate and hot needle tests were performed to find out whether the substances undergo a deflagration to detonation transition (DDT). Both tests allow an initial assessment of whether the compounds could be used as primary explosives.

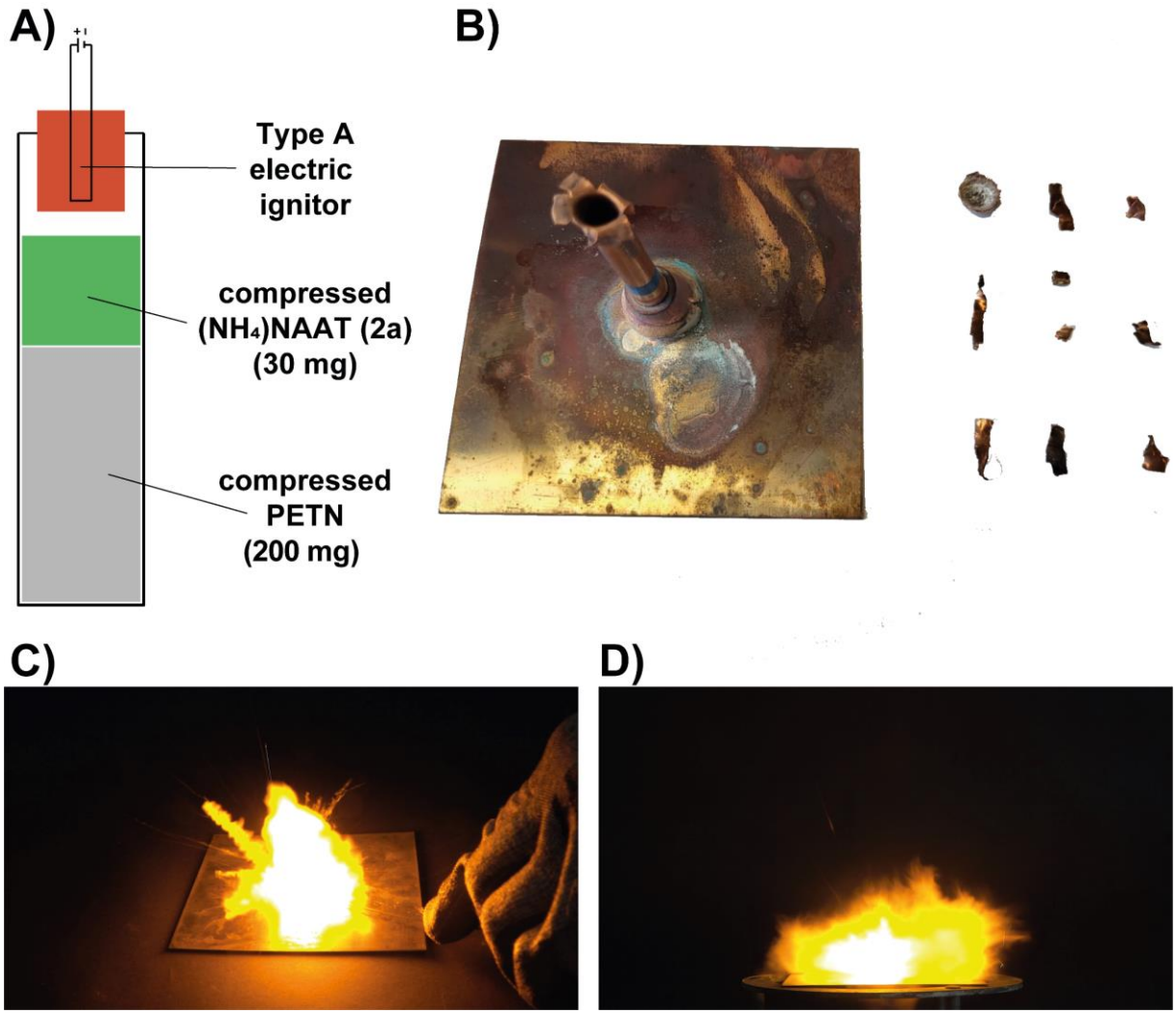

Figure 6. A) Schematic setup of the performed initiation test. B) Result of the initiation test with the shredded copper shell as well as the perforated copper plate. C) Hot Needle Test: Moment of detonation of 10 mg (NH_4)NAAT (**2 a**) during hot needle test D) Hot Plate Test: Moment of detonation of 10 mg (NH_4)NAAT (**2 a**) during hot plate test.

1-Amino-5-azidotetrazole (**1**) detonates in the hot plate test and deflagrates sharply in the hot-needle test. Ammonium 1-nitrimino-5-azidotetrazole (**2a**) behaved similarly to **1**, with the compound already decomposing close to detonation in the hot needle test (Figure 6C)–D)). As expected, **2b** deflagrated during the HP test and decomposed without the formation of a flame in the HN test. Due to the promising properties of **1** and **2 a** during the heating tests, both compounds were subjected to a classical initiation test toward PETN. The schematic setup and the result are shown in Figure 6A)–B). PETN (200 mg, <100 µm) was therefore pressed into a copper shell (80 N) and the respective primary explosive (50 mg of **1** or 30 mg **2a**) was filled on top and compressed as well (80 N). After initiation of the primary explosive charge using an electrical ignitor, a negative test result occurred only for **1** but a positive one for **2a**. This was determined by fragmentation of the copper shell and the hole in the copper witness plate. 30 mg of the ammonium derivative **2a** are thus capable of igniting the booster explosive PETN. To the best of our knowledge, **2a** is the first highly energetic ammonium salt, which was successfully tested as a primary explosive. 30 mg of **2a** were used for the PETN initiation, which demonstrates also its high initiation efficiency. This property is usually possessed mainly by metal salts of energetic azoles, but in very few cases by nitrogen-rich derivatives.

11.3 Conclusion

In this study, we described the synthesis and characterization of 1-nitrimino-5-azidotetrazole (**2**) through mixed acid nitration of 1-amino-5-azidotetrazole (**1**). A reaction toward **2** through a selective reaction procedure was not possible. Especially, the ammonium salt **2a**, with a combined nitrogen and oxygen content of 91.5 % shows promising properties with a calculated detonation velocity of 9337 m s^{-1}. With the friction sensitivity of 1 N and impact sensitivity of 1 J and the positive hot plate and hot needle test, we considered **2a** as possible primary explosive. The initiation of PETN was positive and therefore our compound is one of the only ammonium derivatives being able to act as primary explosive. Once again, we have been able to demonstrate the potential of energetically substituted tetrazole systems and hope that our contribution will encourage researchers to

intensify their studies in this research area. Nevertheless, it must be noted here that 1-nitrimino-5-azidotetrazole is one of the most energetic mono-heterocycles. Although the taming through the formation of guanidinium or ammonium salt resulted in a significant reduction of the sensitivities, still the compounds are overpowered by the used anion.

11.4 Acknowledgement

For financial support of this work by Ludwig-Maximilian University (LMU), the Office of Naval Research (ONR) under grant no. ONR N00014-19-1-2078 and the Strategic Environmental Research and Development Program (SERDP) under contract no. W912HQ19C0033 are gratefully acknowledged. Open Access funding enabled and organized by Projekt DEAL.

11.5 References

[1] H. Gao, J. M. Shreeve, *Chem. Rev.* **2011**, *111*, 7377–7436.

[2] W. Cao, W. Dong, Z. Lu, Y. Bi, Y. Hu, T. Wang, C. Zhang, Z. Li, Q. Yu, J. Zhang, *Chem. Eur. J.* **2021**, *27*, 13807–13818.

[3] Z. Cong, C. Xiang, H. Yongpeng, B. Yang, G. Zhaoqi, F. Daidi, M. Haixia, *RSC Adv.* **2020**, *10*, 36287–36294.

[4] M. A. S. Laidlaw, G. Filippelli, H. Mielke, B. Gulson, A. S. Ball, *Environ. Health* **2017**, *16*, 34.

[5] M. S. Gruhne, T. Lenz, M. Rösch, M. Lommel, M. H. H. Wurzenberger, T. M. Klapötke, J. Stierstorfer, *Dalton Trans.* **2021**, *50*, 10811–10825.

[6] Q. Sun, N. Ding, C. Zhao, Q. Zhang, S. Zhang, S. Li, S. Pang, *Sci. Adv.* **2022**, *8*, eabn3176.

[7] M. Reichel, D. Dosch, T. Klapötke, K. Karaghiosoff, *J. Am. Chem. Soc.* **2019**, *141*, 19911–19916.

[8] O. T. O'Sullivan, M. J. Zdilla, *Chem. Rev.* **2020**, *120*, 5682–5744.

[9] Y.-H. Joo, J. M. Shreeve, *Org. Lett.* **2008**, *10*, 4665–4667.

[10] A. A. Larin, A. V. Shaferov, M. A. Epishina, I. N. Melnikov, N. V. Muravyev, I. V. Ananyev, L. L. Fershtat, N. N. Makhova, *ACS Appl. Energy Mater.* **2020**, *3*, 7764–7771.

[11] N. Fischer, D. Fischer, T. M. Klapötke, D. G. Piercey, J. Stierstorfer, *J. Mater. Chem.* **2012**, *22*, 20418–20422.

[12] M. I. Eremets, A. G. Gavriliuk, I. A. Trojan, D. A. Dzivenko, R. Boehler, *Nat. Mater.* **2004**, *3*, 558–563.

[13] K. O. Christe, W. W. Wilson, J. A. Sheehy, J. A. Boatz, *Angew. Chem. Int. Ed.* **1999**, *38*, 2004–2009.

[14] C. Zhang, C. Sun, B. Hu, C. Yu, M. Lu, *Science* **2017**, *355*, 374–376.

[15] Y. Xu, Q. Wang, C. Shen, Q. Lin, P. Wang, M. Lu, *Nature* **2017**, *549*, 78–81.

[16] T. M. Klapötke, J. Stierstorfer, *J. Am. Chem. Soc.* **2009**, *131*, 1122–1134.

[17] J. Stierstorfer, T. M. Klapötke, A. Hammerl, R. D. Chapman, *Z. Anorg. Allg. Chem.* **2008**, *634*, 1051–1057.

[18] T. M. Klapötke, F. A. Martin, J. Stierstorfer, *Chem. Eur. J.* **2012**, *18*, 1487–1501.

[19] R. Haiges, K. O. Christe, *Inorg. Chem.* **2013**, *52*, 7249–7260.

[20] Y. Hu, X.-J. Wang, W.-S. Dong, Y.-F. Bi, Z.-J. Lu, W.-L. Cao, J.-G. Zhang, Q. Zhang, D. Chen, *Organic Chemistry Frontiers* **2021**, *8*, 2420–2428.

[21] M. Göbel, K. Karaghiosoff, T. M. Klapötke, D. G. Piercey, J. Stierstorfer, *J. Am. Chem. Soc.* **2010**, *132*, 17216–17226.

[22] G. Zhao, C. He, P. Yin, G. H. Imler, D. A. Parrish, J. M. Shreeve, *J. Am. Chem. Soc.* **2018**, *140*, 3560–3563.

[23] P. Yin, D. A. Parrish, J. M. Shreeve, *J. Am. Chem. Soc.* **2015**, *137*, 4778–4786.

[24] M. Benz, T. M. Klapötke, J. Stierstorfer, M. Voggenreiter, *J. Am. Chem. Soc.* **2022**, *144*, 6143–6147.

[25] T. M. Klapötke, D. G. Piercey, J. Stierstorfer, *Dalton Trans.* **2012**, *41*, 9451–9459.

[26] T. M. Klapötke, D. G. Piercey, J. Stierstorfer, *Chem. Eur. J.* **2011**, *17*, 13068–13077.

[27] F. Boneberg, A. Kirchner, T. M. Klapötke, D. G. Piercey, M. J. Poller, J. Stierstorfer, *Chem. Asian J.* **2013**, *8*, 148–159.

[28] M. Benz, T. M. Klapötke, T. Lenz, J. Stierstorfer, *Chem. Eur. J.* **2022**, *28*, e202200772.

[29] J. Stierstorfer, *Dissertation,* Ludwig-Maximilians-Universität München, **2009**.

[30] D. Fischer, T. M. Klapötke, D. G. Piercey, J. Stierstorfer, *Chem. Eur. J.* **2013**, *19*, 4602–4613.

[31] T. M. Klapötke, B. Krumm, F. A. Martin, J. Stierstorfer, *Chem. Asian J.* **2012**, *7*, 214–224.

[32] L. Liu, C. He, C. Li, Z. Li, *J. Chem. Crystallogr.* **2012**, *42*, 816–823.

[33] R. Da Silva Rodrigues, E. T. Luis, D. L. Marshall, J. C. McMurtrie, K. M. Mullen, *New J. Chem.* **2021**, *45*, 4414–4421.

[34] D. A. Mundal, J. J. Lee, R. J. Thomson, *J. Am. Chem. Soc.* **2008**, *130*, 1148–1149.

[35] M. Benz, T. M. Klapötke, J. Stierstorfer, *Org. Lett.* **2022**, *24*, 1747–1751.

[36] D. Fischer, T. M. Klapötke, J. Stierstorfer, *Angew. Chem. Int. Ed.* **2014**, *53*, 8172–8175.

11.6 Supporting Information

11.6.1 Experimental Procedure

^{1}H, ^{13}C and ^{14}N NMR spectra were recorded on *BRUKER AMX 400* instruments. Chemical shifts are referenced with respect to tetramethylsilane (^{1}H/^{13}C) and nitromethane (^{14}N). Infrared spectra (IR) were recorded in the region 4000-400 cm^{-1} on a *PERKIN ELMER Spectrum BX-59343* instrument with a *SMITHS DETECTION DuraSamplIR II Diamond ATR* sensor. The absorption bands are reported in wavenumbers (cm^{-1}). Decomposition temperatures were measured via differential thermal analysis (DTA) with an *OZM Research DTA 552-Ex* instrument at a heating rate of 5 °C/min and in a range of room temperature to 400 °C. All sensitivities toward impact (IS) and friction (FS) were determined according to BAM (Bundesanstalt für Materialforschung und Prüfung) standards using a BAM drop hammer and a BAM friction apparatus by applying the 1 of 6 method.[S1] All energetic compounds were tested for sensitivity towards electrical discharge using an *Electric Spark Tester ESD 2010 EN* from OZM. Energetic properties have been

calculated with the EXPLO5 6.02 computer [S2] code using the RT converted X-ray density and calculated solid state heats of formation.

CAUTION! *All investigated compounds are potentially very powerful explosive materials. Safety precautions and equipment (such as wearing leather coat, face shield, Kevlar sleeves, Kevlar gloves, earthed equipment and ear plugs) must be used during all manipulations.*

1-Amino-5-azidotetrazole (**1**)

Compound **1** was obtained by a modified literature known procedure.[S3]

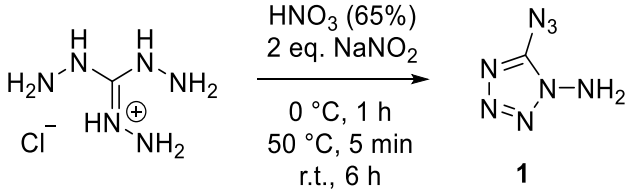

Triaminoguanidinium hydrochloride (564 mg, 4.00 mmol, 1.0 eq) was dissolved in water (50 mL) and nitric acid (65%, 0.60 mL). The solution was cooled to 0 °C and sodium nitrite (556 mg, 8.00 mmol, 2.0 eq) dissolved in water (30 mL) was added dropwise over 20 min. The solution was stirred at 0 °C for 1 h and afterwards heated to 50 °C. Sodium bicarbonate (0.60 g, 5.66 mmol, 2.8 eq) was added in one portion and the solution was stirred at room temperature for 6 h. The solution was extracted with ethyl acetate (3 x 100 mL), dried over anhydrous sodium sulfate and the solvent was evaporated. The yellow residue was purified by column chromatography (*i*Hex/EtOAc: 3:1; R_f = 0.22) to obtain **1** as yellow oil (0.13 g, 1.03 mmol, 26%) which solidifies after few days in the fume hood. The NMR shifts fit with the published values.

^{1}H NMR (CD_3CN, 400 MHz, ppm) δ = 5.88 (s, 2H); ^{13}C NMR (CD_3CN, 101 MHz, ppm) δ = 151.9.

1-Nitrimino-5-azidotetrazole (**2**)

Nitration of compound **1** was performed according to a modified nitration protocol of other N-aminotetrazoles.[S4]

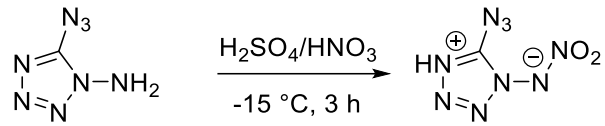

1 **2**

Sulfuric acid (96%, 2.0 mL) was cooled to 0 °C and nitric acid (100%, 1.5 mL) was added over 10 min. The mixture was stirred for 10 min and then cooled to −20 °C. 1-Amino-5-azidotetrazole (**1**) (0.20 g, 1.59 mmol, 1.0 eq) dissolved in sulfuric acid (96%, 1.0 mL) was added dropwise keeping the temperature below −15 °C. The mixture was then stirred for 3 h at this temperature and quenched on 50 mL ice water. The mixture was extracted with ethyl acetate (3 x 50 mL) and the combined organic phases were washed with brine (50 mL). The organic phases were dried over anhydrous sodium sulfate and the solvent was evaporated to yield 1-nitrimino-5-azidotetrazole (**2**) (0.15 g, 0.86 mmol, 54%) as slightly yellowish hygroscopic oil. DTA (5 °C min^{-1}): 85 °C (exo); Sensitivities (liquid): BAM drop hammer: <1 J, friction tester: 360 N, ESD: -; IR (ATR) $\tilde{\nu}$ (cm^{-1}) = 3155(w), 3059(w), 2917(w), 2851(w), 2761(w), 2633(w), 2146(s), 1790(w), 1555(s), 1509(m), 1493(m), 1346(vs), 1194(vs), 1157(vs), 1043(s), 1013(s), 834(vs), 784(s), 742(s), 726(s), 602(s), 529(s), 448(m), 436(m), 419(s), 414(m), 404(s); Elem. Anal. (CHN_9O_2, 171.08 g mol^{-1}) calcd.: C 7.02, H 0.59, N 73.69%. Found: C 6.88, H 0.88, N 72.78%; ^{1}H NMR (DMSO-D_6, 400 MHz, ppm) δ = 12.63 (br s, 1H); ^{13}C NMR (DMSO-D_6, 101 MHz, ppm) δ = 150.0; ^{14}N NMR (DMSO-D_6, 29 MHz, ppm) δ = −3, −11, −146; HRMS (ESI) *m/z*: [M−] Calcd for CN_9O_2 170.0180, found: 170.0181.

Ammonium 1-nitrimino-5-azidotetrazolate (**2a**)

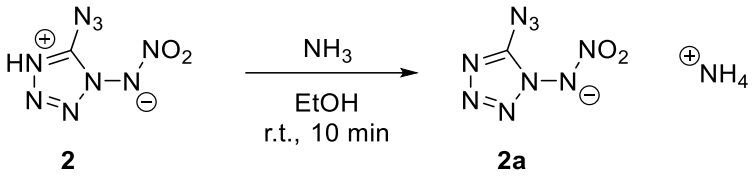

2 **2a**

1-Nitrimino-5-azidotetrazole (**2**) (151 mg, 0.86 mmol, 1.0 eq) was dissolved in ethanol (10 mL) and gaseous ammonia was bubbled through. The solution turns its color to yellow-orange and the solvent was evaporated. After one day, orange crystalline **2a** was obtained (147 mg, 0.78 mmol, 91%).

DTA (5 °C min^{-1}): 145 °C (exo); Sensitivities: BAM drop hammer: 1 J, friction tester: 1 N, ESD: 20 mJ; IR (ATR) $\tilde{\nu}$ (cm^{-1}) = 3174(m), 3056(m), 2166(s), 1556(m), 1539(s), 1393(vs), 1387(s), 1305(s), 1283(vs), 1246(vs), 1185(s), 1117(s), 1075(s), 995(m), 966(m), 899(s), 834(m), 792(s), 781(s), 716(m), 682(m), 594(m), 527(s), 510(m), 479(m), 456(m), 449(m), 421(s), 403(m); Elem. Anal. ($CH_4N_{10}O_2$, 188.11 g mol^{-1}) calcd.: C 6.39, H 2.14, N 74.46%. Found: C 5.98, H 2.13, N 72.32%; ^{1}H NMR (DMSO-D_6, 400 MHz, ppm) δ = 7.14 (br s, 4H); ^{13}C NMR (DMSO-D_6, 101 MHz, ppm) δ = 149.6; ^{14}N NMR (DMSO-D_6, 29 MHz, ppm) δ = −3, −145, −359.

Guanidinium 1-nitrimino-5-azidotetrazolate (**2b**)

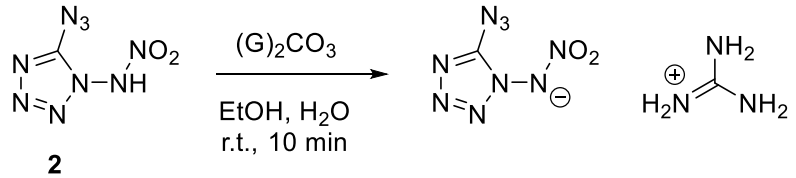

2 **2b**

1-Nitramino-5-azidotetrazole (**2**) (237 mg, 1.39 mmol, 1.0 eq) was dissolved in ethanol (10 mL) and guanidinium carbonate (126 mg, 0.70 mmol, 0.5 eq) dissolved in water (5 mL) was added. The solvent was evaporated and the mixture was recrystallized from hot methanol (20 mL). After one day, orange crystalline **2b** was obtained (278 mg, 1.21 mmol, 87%).

DTA (5 °C min^{-1}): 149 °C (exo); Sensitivities: BAM drop hammer: 2 J, friction tester: 30 N, ESD: 125 mJ; IR (ATR) $\tilde{\nu}$ (cm^{-1}) = 3469(w), 3350(m), 3276(m),

3201(m), 2147(s), 1652(s), 1573(m), 1529(s), 1467(m), 1404(s), 1299(s), 1246(s), 1179(s), 1116(m), 1083(s), 1009(m), 896(m), 772(m), 737(m), 726(m), 682(m), 509(s), 488(vs), 446(s), 407(vs); Elem. Anal. ($C_2H_6N_{12}O_2$, 230.07 g mol^{-1}) calcd.: C 10.44, H 2.63, N 73.03%. Found: C 10.20, H 2.77, N 71.98%; ^{1}H NMR (DMSO-D_6, 400 MHz, ppm) δ = 6.97 (br s, 6H); ^{13}C NMR (DMSO-D_6, 101 MHz, ppm) δ = 157.9, 149.5; ^{14}N NMR (DMSO-D_6, 29 MHz, ppm) δ = −3, −138, −146.

Failed alternative route toward **2**

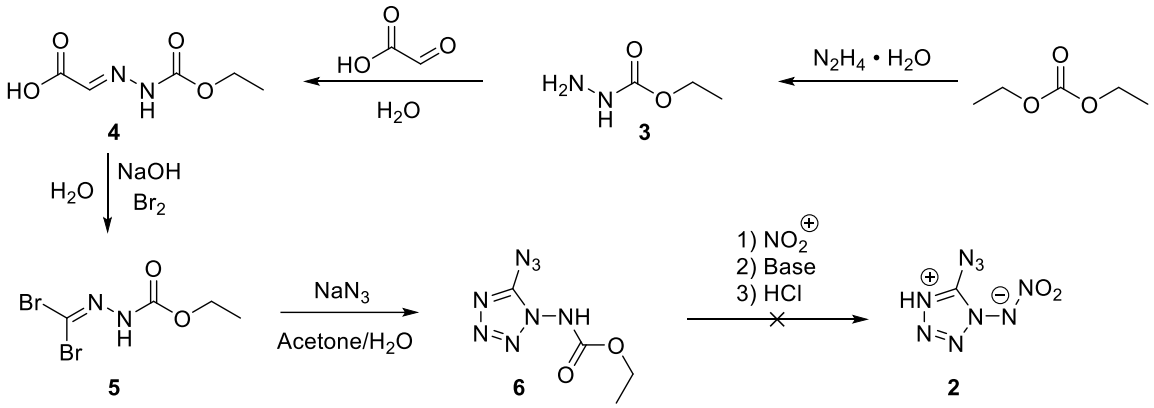

Ethylcarbazate (**3**)

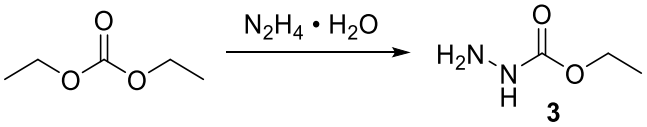

Diethyl carbonate (100 mL, 0.83 mol, 0.96 eq) was placed in a 250 mL round-bottom flask and hydrazine hydrate (41.7 mL, 0.86 mol, 1.0 eq) was added in one portion. The mixture was stirred vigorously to obtain a intermixing of the two phases. After stirring overnight, the solvent was removed under reduced pressure and **3** was solidified to colorless crystals by means of high vacuum (78.0 g, 0.75 mol, 91%). The measured NMR shifts fit with the published ones.

^{1}H NMR (DMSO-D_6, 400 MHz, ppm) δ = 8.05 (br s, 1H), 3.99 (q, ^3J = 6.9 Hz, 2H), 1.15 (t, ^3J = 7.0 Hz, 3H); ^{13}C NMR (DMSO-D_6, 101 MHz, ppm) δ = 158.4, 59.9, 14.7.

Ethylcarbazate acetic acid (**4**)

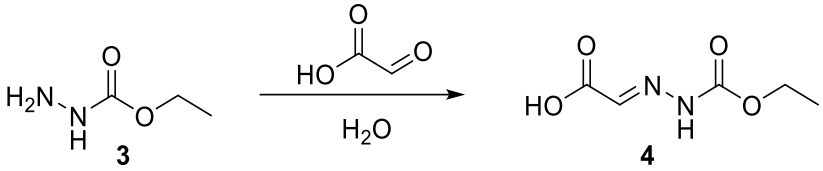

Ethylcarbazate (**3**) (60.0 g, 0.58 mol, 1.05 eq) was dissolved in water (100 mL) and glyoxalic acid (50% w/w in water, 66.8 mL, 0.55 mol, 1.00 eq) was added dropwise. The mixture was stirred overnight, cooled to 0 °C, filtered and washed with a small amount of cold water to yield **4** as beige solid powder (82.4 g, 0.51 mol, 89%). The measured NMR shifts fit with the published ones.

^{1}H NMR (DMSO-D_6, 400 MHz, ppm) δ = 11.21 (s, 1H), 7.90 (s, 1H), 4.68 (q, ^{3}J = 7.0 Hz, 2H), 1.71 (t, ^{3}J = 7.0 Hz, 3H); ^{13}C NMR (DMSO-D_6, 101 MHz, ppm) δ = 164.6, 153.3, 135.1, 61.5, 14.5.

Ethyl 2-(dibromomethylene)hydrazinecarboxylate (**5**)

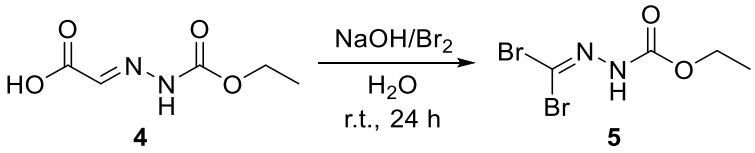

Ethoxycarbonylhydrazono-acetic acid (10.0 g, 62.7 mmol, 1.0 eq.) was dissolved in water (150 mL). NaOH (5.00 g, 0.13 mol, 2.0 eq.) was added and the mixture was cooled with an ice bath to 0 °C. At this temperature, bromine (8.10 mL, 0.16 mol, 2.5 eq) was added slowly while stirring. The stirring was continued at ambient temperature for 24 h. Sulfuric acid (70 mL, 1 M) was added and the reaction mixture was extracted with DCM (3 x 30 mL). The combined organic phases were dried over anhydrous sodium sulfate. Evaporation of the solvent yields compound **8** as a reddish-brown solid (4.74 g, 17.3 mmol, 28%).

IR (ATR) $\tilde{\nu}$ (cm^{-1}) = 3305(m), 2994(w), 1758(vs), 1584(w), 1496(s), 1479(s), 1457(m), 1447(m), 1384(m), 1324(w), 1208(vs), 1163(s), 1058(s), 1013(s), 888(s), 867(vs), 761(s), 749(s), 661(w), 589(w), 543(m), 510(m), 496(s), 459(vs); Elem. Anal. ($C_4H_6N_2O_2Br_2$, 273.91 g mol^{-1}) calcd.: C 17.54, H 2.21, N 10.23%. Found: C 18.12, H 2.44, N 10.55%; ^{1}H NMR (Acetone-D_6, 400 MHz, ppm) δ = 9.38 (s, 1H),

4.20 (q, ^{3}J = 7.1 Hz, 2H), 1.26 (t, ^{3}J = 7.1 Hz, 3H); ^{13}C NMR (Acetone-D_6, 101 MHz, ppm) δ = 152.9, 84.3, 62.9, 14.7; HRMS (ESI) *m/z*: [M−] Calcd for $C_4H_7N_2O_2Br_2$ 272.8869, found: 272.8873.

5-Azidotetrazole-1-ethylcarbamate (**9**)

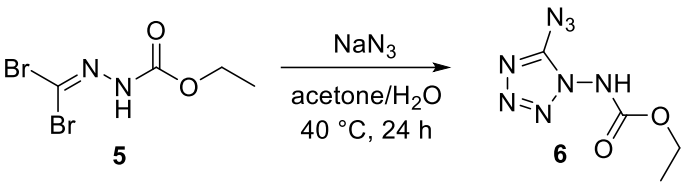

Compound **8** (1.00 g, 3.70 mmol, 1.0 eq.) was dissolved in water (8 mL) and acetone (8 mL). Sodium azide (0.60 g, 9.25 mmol, 2.5 eq.) was added in portions while stirring. The reaction mixture was stirred at 40 °C for 24 h. Afterwards, sulfuric acid (30 mL, 1 M) was added, the mixture was extracted with DCM (3 x 30 mL) and the combined organic phases were dried over anhydrous sodium sulfate. After evaporation of the solvent, the product was obtained as a brown, viscous oil (0.59 g, 1.89 mmol, 51%). Purification via column chromatography (*i*Hex/EtOAc: 3:1; R_f = 0.25) resulted in the formation of **9** as a colorless oil, which solified after a few days to colorless crystals.

DTA (5 °C min^{-1}): 160 °C (exo); Sensitivities: BAM drop hammer: ≤1 J, friction tester: 1.5 N, ESD: 45 mJ; IR (ATR) $\tilde{\nu}$ (cm^{-1}) = 3190 (vw), 2985(w), 2157(s), 1736(s), 1550(vs), 1479(s), 1372(m), 1313(s), 1242(vs), 1198(s), 1111(m), 1051(s), 960(m), 918(m), 838(m), 768(m), 722(m), 676(m), 527(m), 484(m), 451(m); Elem. Anal. ($C_4H_6N_8O_2$, 188.11 g mol^{-1}) calcd.: C 24.25, H 3.05, N 56.55%. Found: C 23.89, H 3.00, N 55.94%; ^{1}H NMR (Acetone-D_6, 400 MHz, ppm) δ = 10.86 (s, 1H), 4.28 (q, ^{3}J = 7.1 Hz, 2H), 1.28 (t, ^{3}J = 7.1 Hz, 3H); ^{13}C NMR (Acetone-D_6, 101 MHz, ppm) δ = 154.3, 152.9, 63.4, 14.6; ^{14}N NMR (Acetone-D_6, 29 MHz, ppm) δ = −147; HRMS (ESI) *m/z*: [M−] Calcd for $C_4H_5N_8O_2$ 197.0541, found: 197.0540.

11.6.2 Thermal Analysis

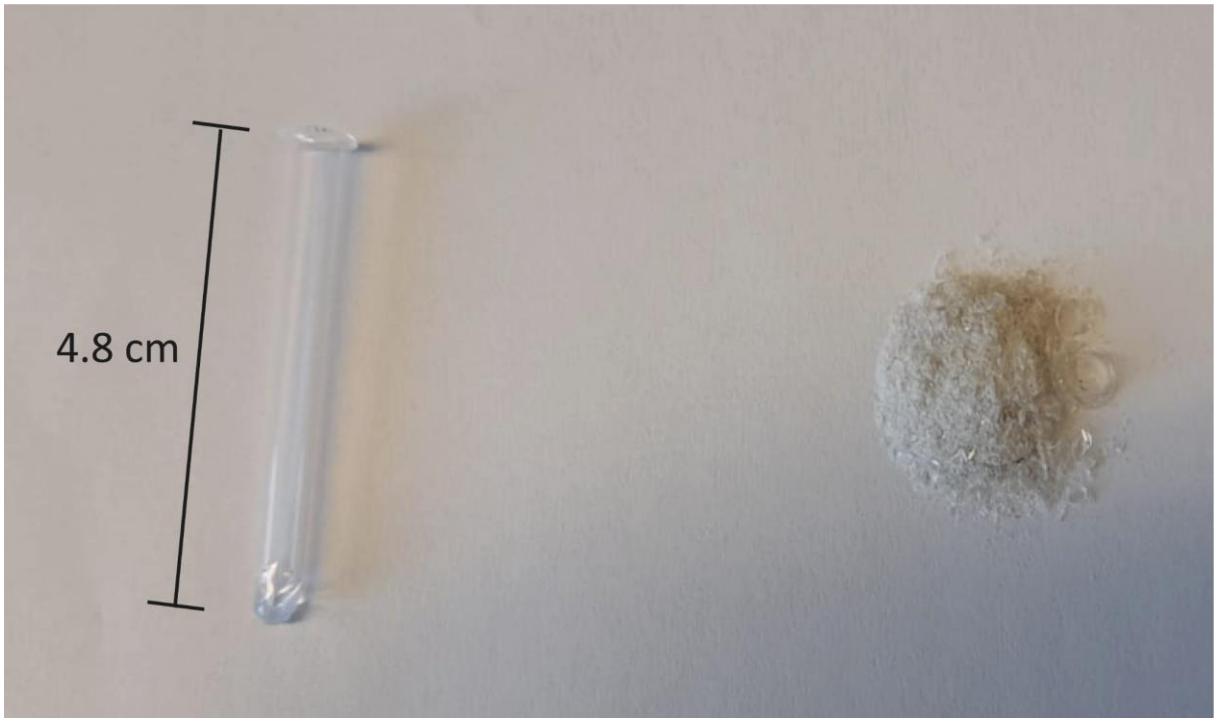

Figure S1. DTA test tube (left) and destructed one (right) after DTA measurement of approx. 5 mg **2a**. Similar results were obtained for all 5-azidotetrazole derivatives.

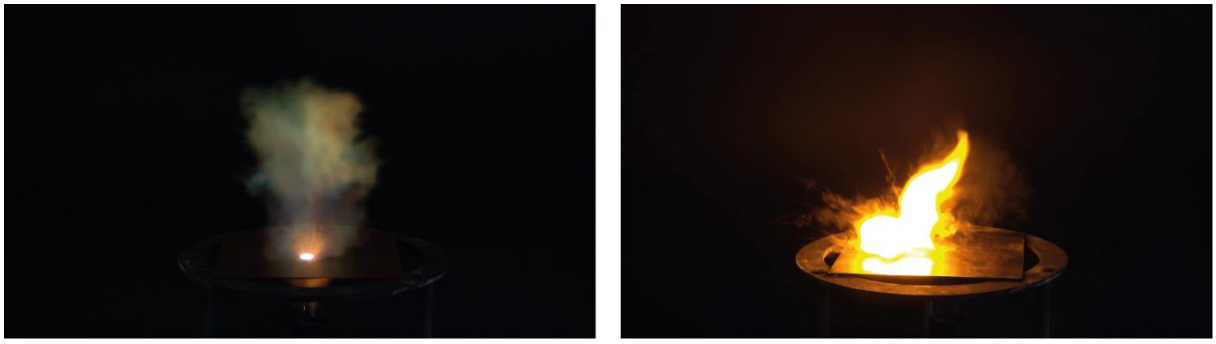

Figure S2. Moment of detonation of 15 mg of 1-amino-5-azidotetrazole (**1**) (left) and moment of deflagration of 20 mg of guanidinium 1-nitrimino-5-azidotetrazolate (**2b**) (right) during hot plate test.

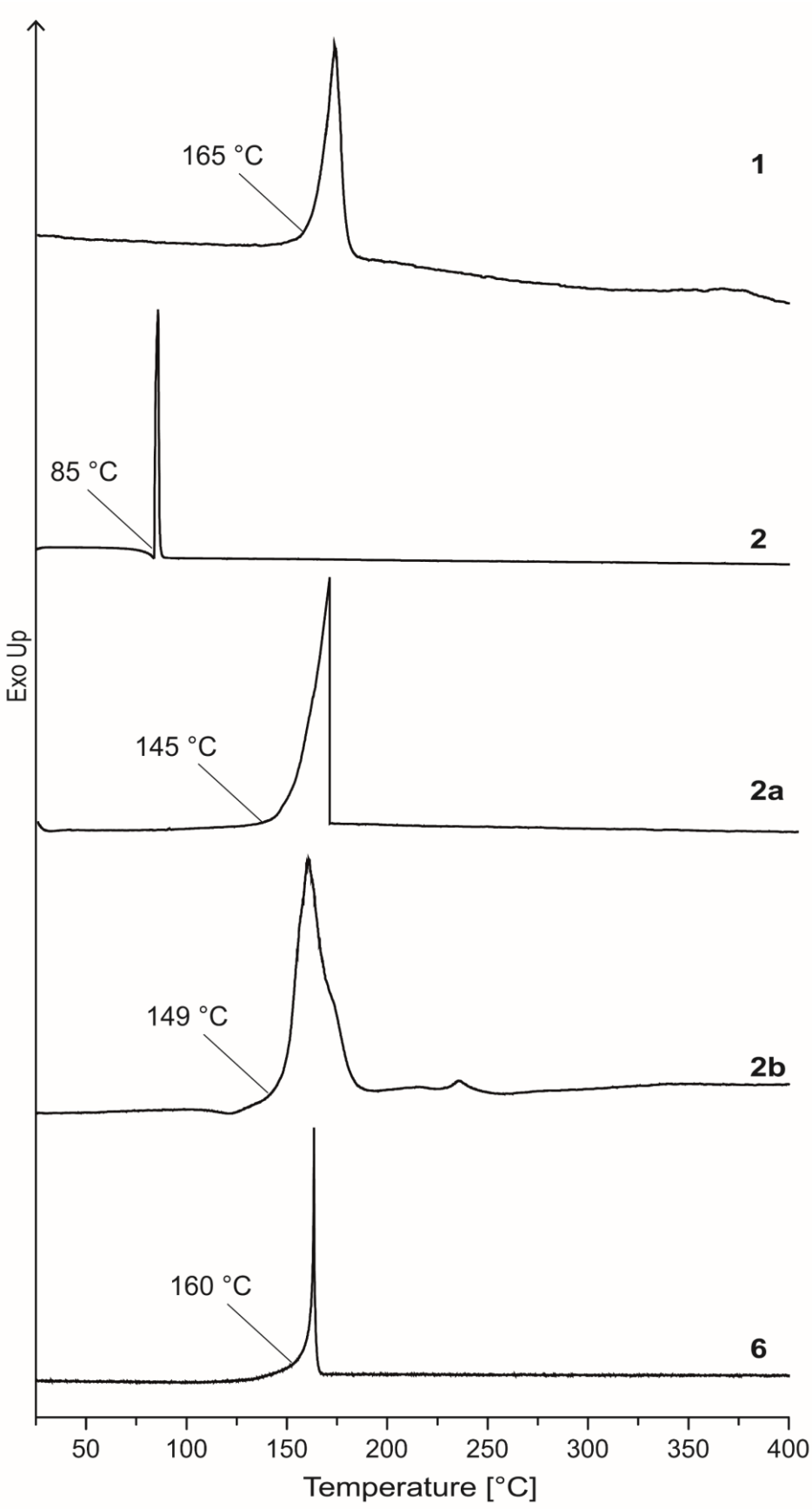

Figure S3. DTA plots of compounds **1**, **2**, **2a**, **2b** and **6**. All measurements were obtained with a heating rate of 5 °C min^{-1}.

11.6.3 Crystallogrpahy

Table S1. Crystallographic data of compounds **1** and **2a**-**2b**.

	1	**2a**	**2b**
Formula	CH_2N_8	CN_9O_2, NH_4	CN_9O_2, CH_6N_3
FW [g mol^{-1}]	126.11	188.14	230.19
Crystal system	orthorhombic	monoclinic	triclinic
Space group	*Pna*2$_1$ (No. 33)	*P*2$_1$/*n* (No. 14)	*P*−1 (No. 2)
Color / Habit	colorless plate	colorless plate	colorless needle
Size [mm]	0.02 x 0.25 x 0.50	0.01 x 0.20 x 0.40	0.02 x 0.03 x 0.15
a [Å]	9.863(2)	7.7654(10)	6.4859(6)
b [Å]	11.0361(17)	6.8237(7)	7.6119(7)
c [Å]	4.5703(10)	14.0285(17)	9.7795(10)
α [°]	90	90	83.710(3)
β [°]	90	105.915(14)	70.831(4)
γ [°]	90	90	88.410(4)
V [Å^3]	497.47(17)	714.86(15)	453.28(8)
Z	4	4	2
$\rho_{calc.}$ [g cm^{-3}]	1.684	1.748	1.687
μ [mm^{-1}]	0.136	0.154	0.144
F(000)	256	384	236
$\lambda_{MoK\alpha}$ [Å]	0.71073	0.71073	0.71073
T [K]	101	123	173
θ Min-Max [°]	2.8, 26.4	2.7, 29.1	2.7, 26.4
Dataset	-12: 7 ; -8: 13 ; -5: 5	-10: 10 ; -9: 9 ; -18: 19	-8: 8 ; -9: 9 ; -12: 12
Reflections collected	1709	10223	7474
Independent refl.	985	1782	1851
R_{int}	0.038	0.047	0.039
Observed reflections	811	1362	1517
Parameters	91	134	169
R_1 (obs)[a]	0.0526	0.0402	0.0460
wR_2 (all data)[b]	0.1356	0.0973	0.1036
S [c]	1.06	1.07	1.12
Resd. dens [e Å^{-3}]	-0.28, 0.23	-0.22, 0.25	-0.26, 0.22
Device type	Xcalibur Sapphire3	Xcalibur Sapphire3	Bruker D8 Venture
Solution	SIR-92	SIR-92	SIR-92
Refinement	SHELXL-2013	SHELXL-2013	SHELXL-2013
Absorption correction	multi-scan	multi-scan	multi-scan
CCDC	2170430	2170433	2170432

[a]$R_1 = \Sigma||F_o|-|F_c||/\Sigma|F_o|$; [b]$wR_2 = [\Sigma[w(F_o^2-F_c^2)^2]/\Sigma[w(F_o)^2]]^{1/2}$; $w = [\sigma c^2(F_o^2)+(xP)^2+yP]^{-1}$ and $P=(F_o^2+2F_c^2)/3$; [c]$S = (\Sigma[w(F_o^2-F_c^2)^2]/(n-p))^{1/2}$ (n = number of reflections; p = total number of parameters).

Table S2. Crystallographic data of compounds **3** and **5**-**6**.

	3	**5**	**6**
Formula	$C_3H_8N_2O_2$	$C_4H_6Br_2N_2O_2$	$C_4H_6N_8O_2$
FW [g mol^{-1}]	104.11	273.93	198.17
Crystal system	orthorhombic	monoclinic	monoclinic
Space group	$P2_12_12_1$ (No. 19)	$P2_1/n$ (No. 14)	$P2_1/c$ (No. 14)
Color / Habit	colorless block	yellow block	colorless block
Size [mm]	0.15 x 0.25 x 0.30	0.10 x 0.15 x 0.20	0.05 x 0.08 x 0.16
a [Å]	5.0464(4)	4.0260(5)	9.7013(5)
b [Å]	7.6524(6)	10.6390(8)	10.0865(5)
c [Å]	13.3101(16)	18.490(2)	9.4333(4)
α [°]	90	90	90
β [°]	90	91.223(11)	98.394(2)
γ [°]	90	90	90
V [Å^3]	514.00(8)	791.80(14)	913.18(8)
Z	4	4	4
$\rho_{calc.}$ [g cm^{-3}]	1.345	2.298	1.441
μ [mm^{-1}]	0.112	10.181	0.119
F(000)	224	520	408
$\lambda_{MoK\alpha}$ [Å]	0.71073	0.71073	0.71073
T [K]	100	103	298
θ Min-Max [°]	3.1, 26.3	2.2, 26.4	2.9, 26.4
Dataset	-6: 6 ; -9: 9 ; -16: 16	-5: 4 ; -13: 10 ; -23: 11	-12: 12 ; -12: 12 ; -11: 11
Reflections collected	6003	3908	16501
Independent refl.	1050	1603	1857
R_{int}	0.069	0.040	0.031
Observed reflections	825	1192	1346
Parameters	96	91	152
R_1 (obs)[a]	0.0425	0.0785	0.0584
wR_2 (all data)[b]	0.0789	0.1996	0.1883
S [c]	1.06	1.08	1.06
Resd. dens [e Å^{-3}]	-0.17, 0.17	-0.90, 5.46	-0.18, 0.26
Device type	Xcalibur Sapphire3	Xcalibur Sapphire3	Bruker D8 Venture
Solution	SIR-92	SIR-92	SIR-92
Refinement	SHELXL-2013	SHELXL-2013	SHELXL-2013
Absorption correction	multi-scan	multi-scan	multi-scan
CCDC	2170431	2170435	2170434

[a]$R_1 = \Sigma||F_0|-|F_c||/\Sigma|F_0|$; [b]$wR_2 = [\Sigma[w(F_0^2-F_c^2)^2]/\Sigma[w(F_0)^2]]^{1/2}$; $w = [\sigma c^2(F_0^2)+(xP)^2+yP]^{-1}$ and $P=(F_0^2+2F_c^2)/3$; [c]$S = (\Sigma[w(F_o^2-F_c^2)^2]/(n-p))^{1/2}$ (n = number of reflections; p = total number of parameters).

Crystal structure data were obtained from an Oxford Xcalibur3 diffractometer with a Spellman generator (voltage 50 kV, current 40 mA) and a Kappa CCD area for data collection using Mo-*Kα* radiation (λ = 0.71073 Å) or a Bruker D8 Venture TXS diffractometer equipped with a multilayer monochromator, a Photon 2 detector and a rotation-anode generator (Mo-K_α radiation). The data collection was performed using the CRYSTALIS RED software.[S5] The solution of the structure was performed by direct methods and refined by full-matrix least-squares on F2 (SHELXT)[S6] implemented in the OLEX2[S7] software suite. The non-hydrogen atoms were refined anisotropically and the hydrogen atoms were located and freely refined. The absorption correction was carried out by a SCALE3 ABSPACK multiscan method.[S8] The DIAMOND2 plots shown with thermal ellipsoids at the 50% probability level and hydrogen atoms are shown as small spheres of arbitrary radius. The SADABS program embedded in the Bruker APEX3 software was used for multi-scan absorption corrections in all structures. [S9]

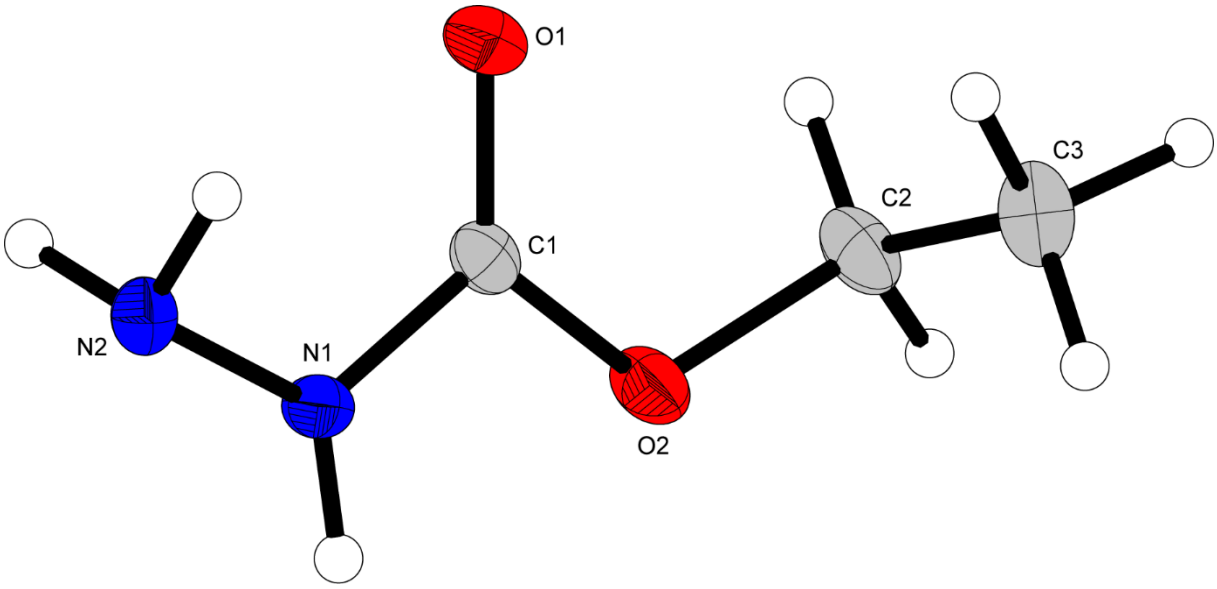

Figure S4. Representation of the molecular unit **3**, showing the atom-labeling scheme. Thermal ellipsoids represent the 50% probability level and hydrogen atoms are shown as small spheres of arbitrary radius.

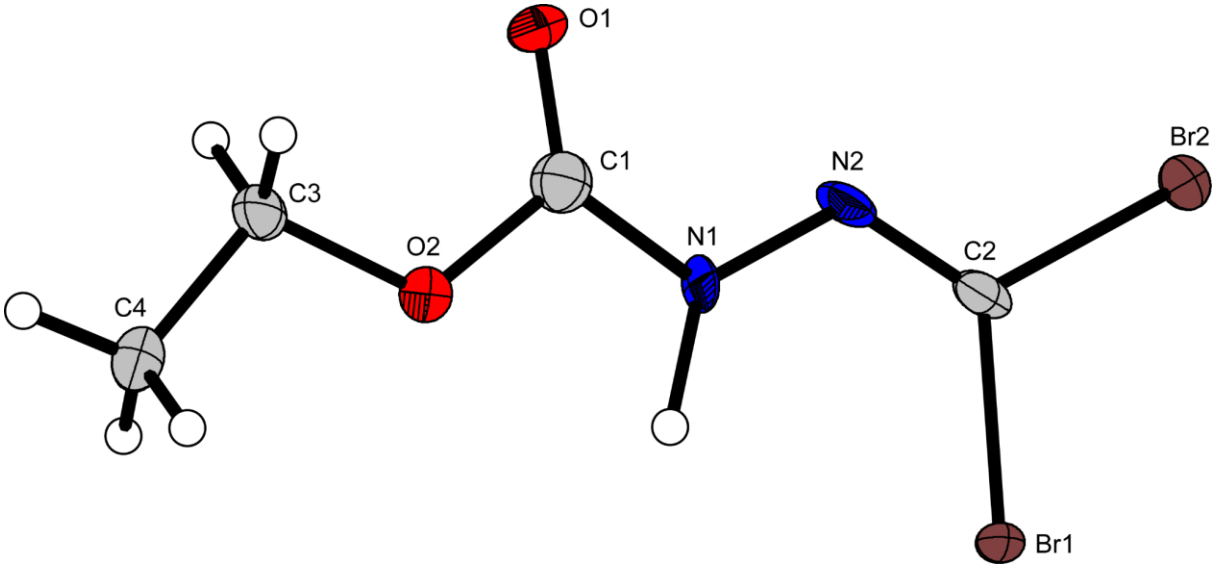

Figure S5. Representation of the molecular unit **4**, showing the atom-labeling scheme. Thermal ellipsoids represent the 50% probability level and hydrogen atoms are shown as small spheres of arbitrary radius.

11.6.4 Computation

All quantum chemical calculations were carried out using the Gaussian G09 program package.[S10] The enthalpies (H) and free energies (G) were calculated using the complete basis set (CBS) method of Petersson and co-workers in order to obtain very accurate energies. The CBS models are using the known asymptotic convergence of pair natural orbital expressions to extrapolate from calculations using a finite basis set to the estimated CBS limit. CBS-4 starts with an HF/3-21G(d) geometry optimization; the zero-point energy is computed at the same level. It then uses a large basis set SCF calculation as a base energy, and an MP2/6- 31+G calculation with a CBS extrapolation to correct the energy through second order. A MP4(SDQ)/6-31+ (d,p) calculation is used to approximate higher order contributions. In this study, we applied the modified CBS-4M.

Heats of formation of the synthesized ionic compounds were calculated using the atomization method (equation E1) using room temperature CBS-4M enthalpies, which are summarized in Table S3.[S11, S12]

$$\Delta_f H^\circ_{(g,\,M,\,298)} = H_{(Molecule,\,298)} - \sum H^\circ_{(Atoms,\,298)} + \sum \Delta_f H^\circ_{(Atoms,\,298)} \qquad (E1)$$

Table S3. CBS-4M electronic enthalpies for atoms C, H, N and O and their literature values for atomic $\Delta H°_f^{298}$ / kJ mol^{-1}

	$-H^{298}$ [a.u.]	NIST[S13]
H	0.500991	218.2
C	37.786156	717.2
N	54.522462	473.1
O	74.991202	249.5

For neutral compounds the sublimation enthalpy, which is needed to convert the gas phase enthalpy of formation to the solid state one, was calculated by the *Trouton* rule.[S14] For ionic compounds, the lattice energy (U_L) and lattice enthalpy (ΔH_L) were calculated from the corresponding X-ray molecular volumes according to the equations provided by *Jenkins* and *Glasser*.[S15] With the calculated lattice enthalpy the gas-phase enthalpy of formation was converted into the solid state (standard conditions) enthalpy of formation. These molar standard enthalpies of formation (ΔH_m) were used to calculate the molar solid state energies of formation (ΔU_m) according to equation E2.

$$\Delta U_m = \Delta H_m - \Delta n\, RT \qquad \text{(E2)}$$

(Δn being the change of moles of gaseous components)
The calculation results are summarized in Table S4.

Table S4. Calculation results.

	$-H^{298}$ [a] [a.u.]	$\Delta_f H°$(g,M) [kJ mol^{-1}] [b]	V_M [Å^3] [c]	ΔU_L; ΔH_L [d] [kJ mol^{-1}]	$\Delta_f H°$(s) [e] [kJ mol^{-1}]	Δn [f]	$\Delta_f U$(s) [g] [kJ kg^{-1}]
A^-	680.325907	598.4					
NH_4^+	56.796608	635.3					
Gua^+	205.453192	571.2					
2	680.769743	966.4			934.2	−6.0	5547.6
2a		1233.7	179	520.3; 525.2	708.5	−8.0	3871.6
2b		1169.6	231	486.2; 491.2	678.4	−10.0	3055.3
1	476.547661	786.3			726.8	−5.0	5863.3

[a] CBS-4M electronic enthalpy; [b] gas phase enthalpy of formation; [c] molecular volumes taken from X-ray structures and corrected to room temperature; [d] lattice energy and enthalpy (calculated using Jenkins and Glasser equations); [e] standard solid state enthalpy of formation; [f] Δn being the change of moles of gaseous components when formed; [g] solid state energy of formation.

11.6.5 NMR Spectroscopy

^{1}H-NMR (400 MHz, CD_3CN, ppm)

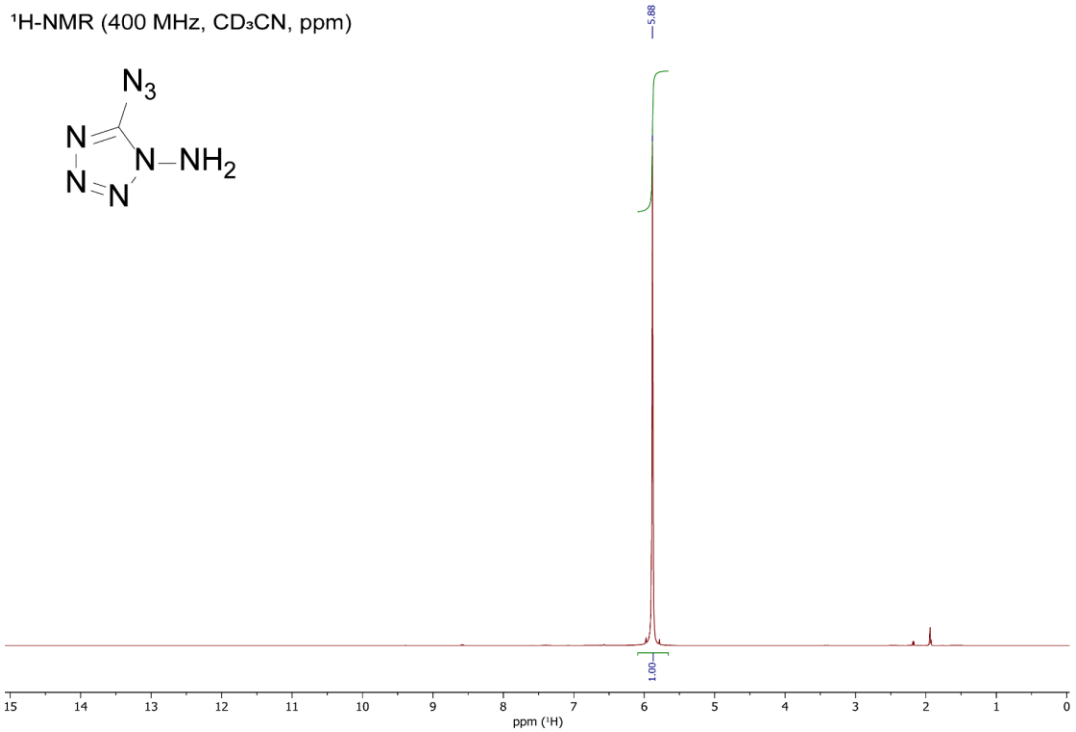

^{13}C-NMR (101 MHz, CD_3CN, ppm)

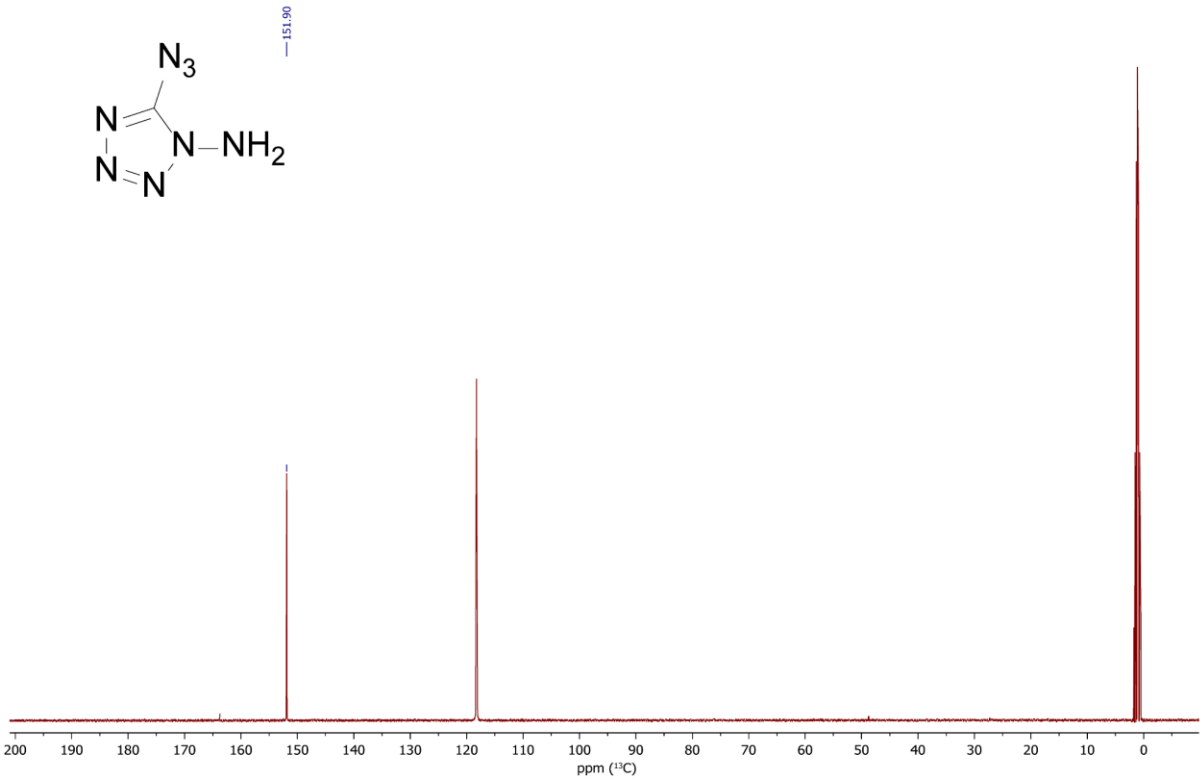

^{1}H-NMR (400 MHz, DMSO-D$_6$, ppm)

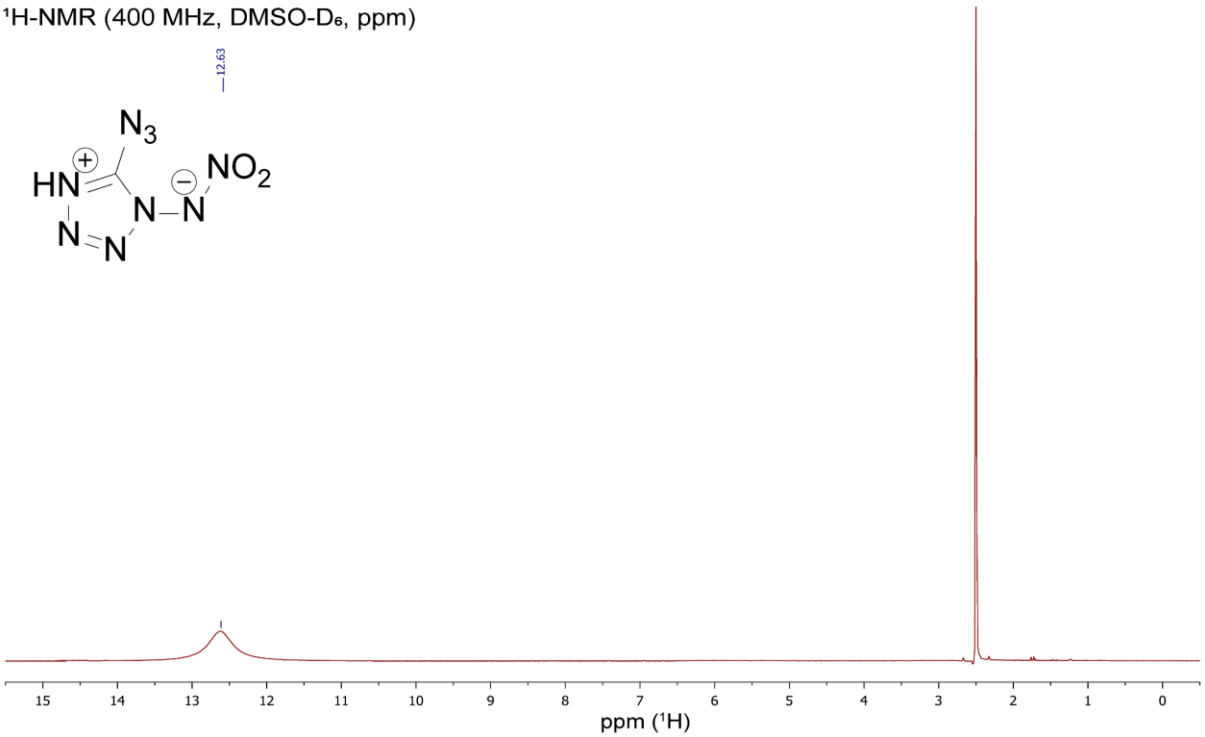

^{13}C-NMR (101 MHz, DMSO-D$_6$, ppm)

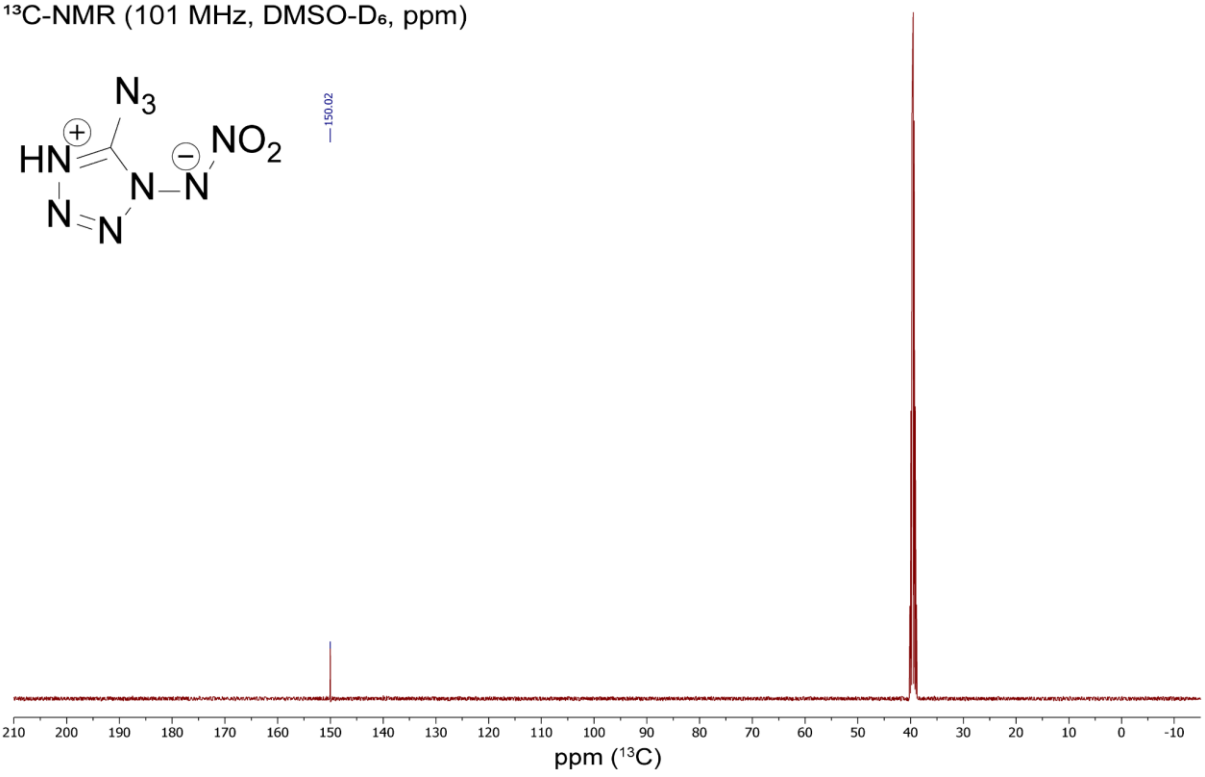

^{14}N-NMR (29 MHz, DMSO-D$_6$, ppm)

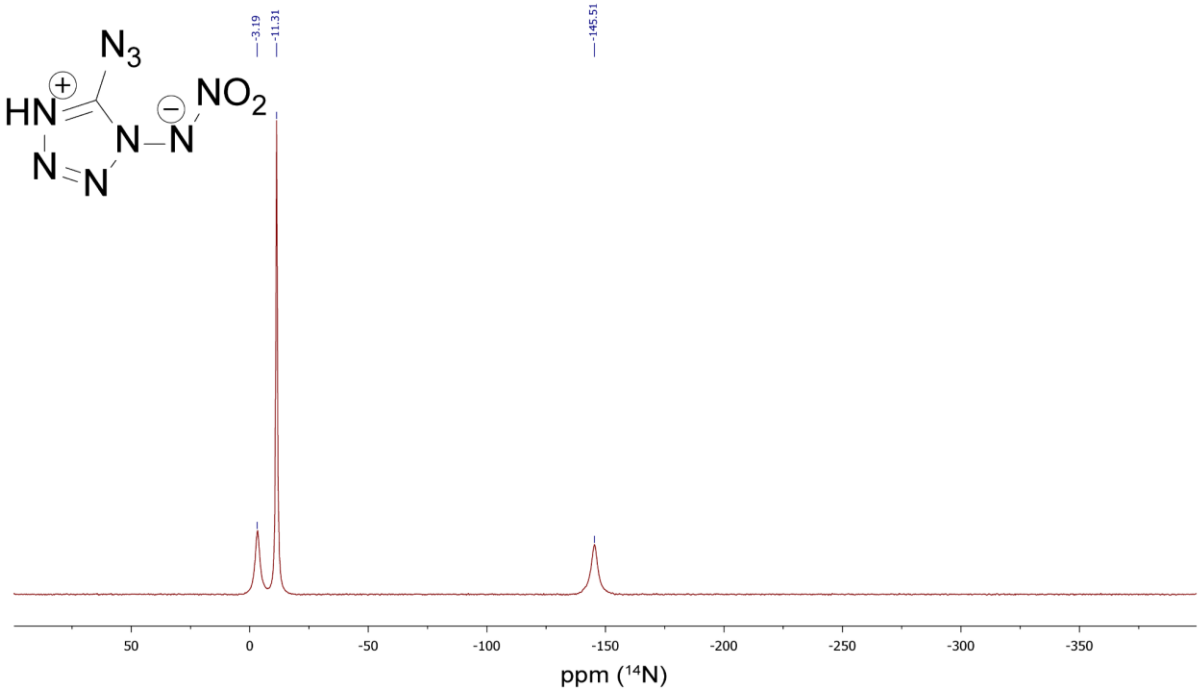

^{1}H-NMR (400 MHz, DMSO-D$_6$, ppm)

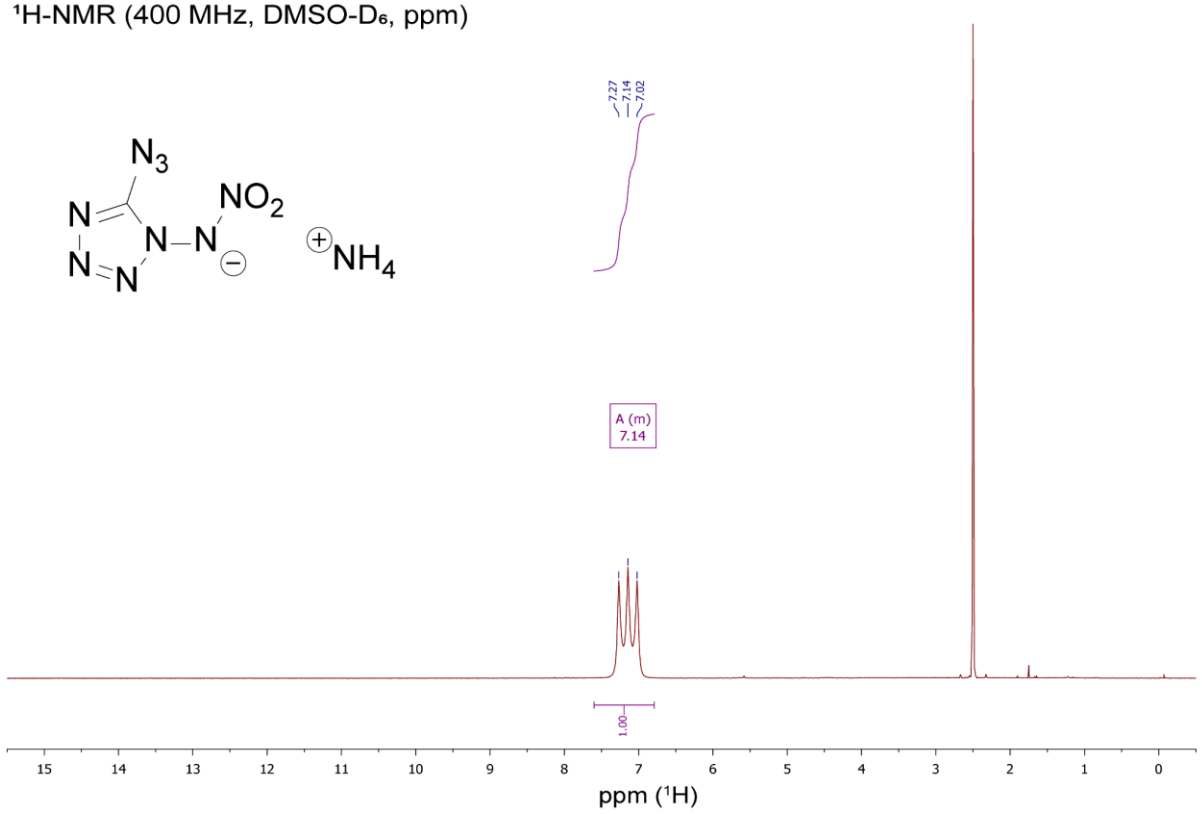

^{13}C-NMR (101 MHz, DMSO-D$_6$, ppm)

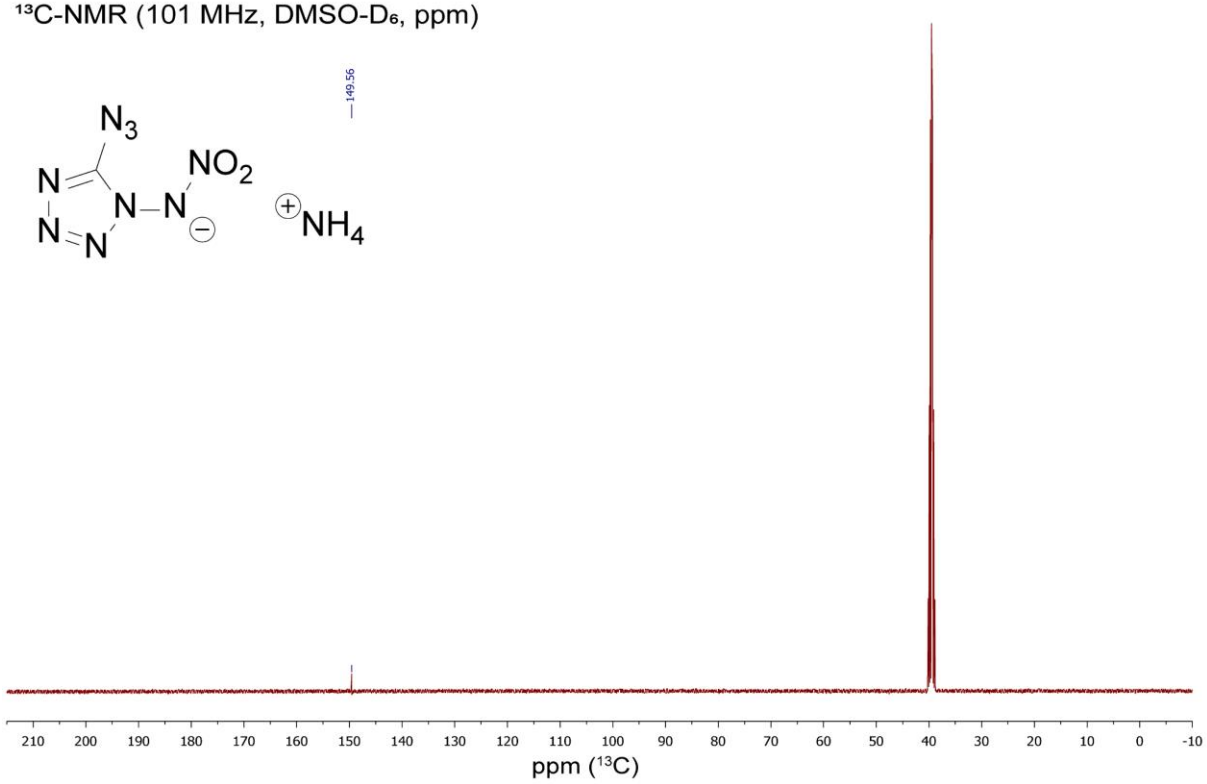

^{14}N-NMR (29 MHz, DMSO-D$_6$, ppm)

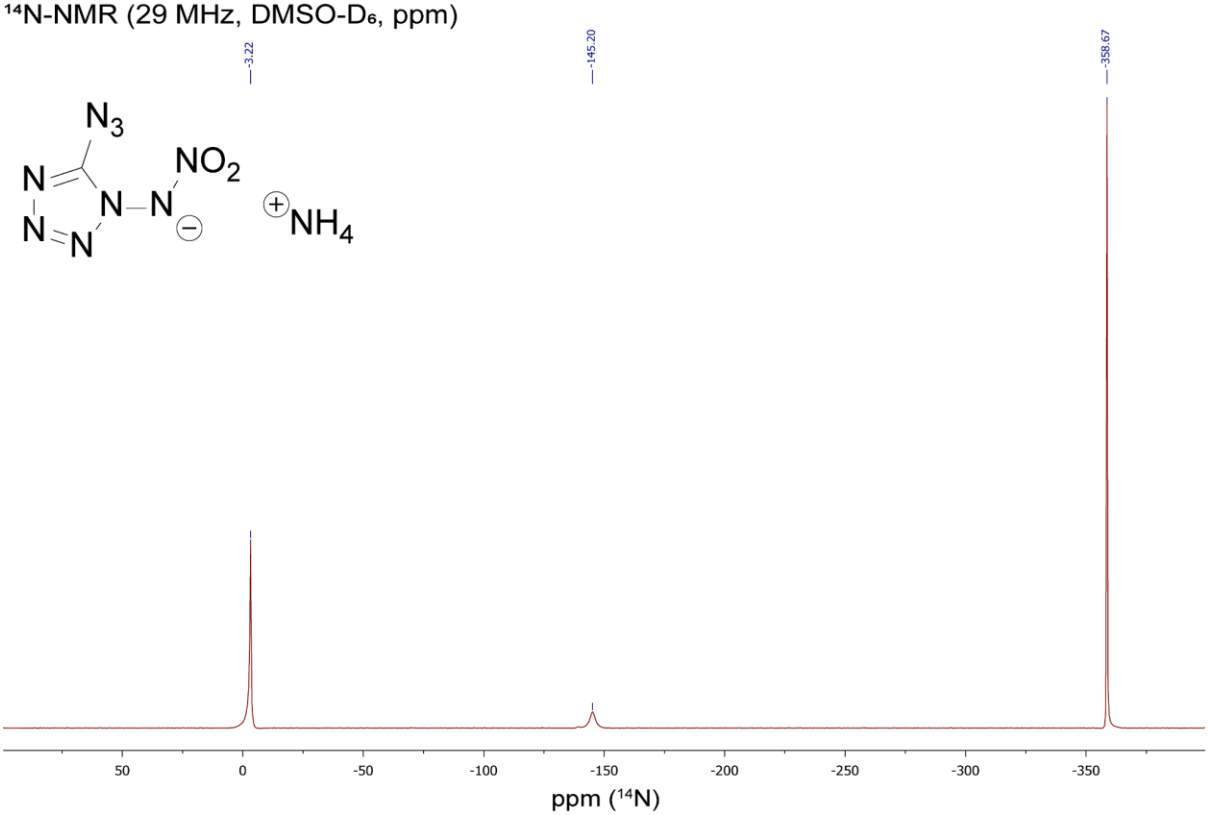

¹H-NMR (400 MHz, DMSO-D₆, ppm)

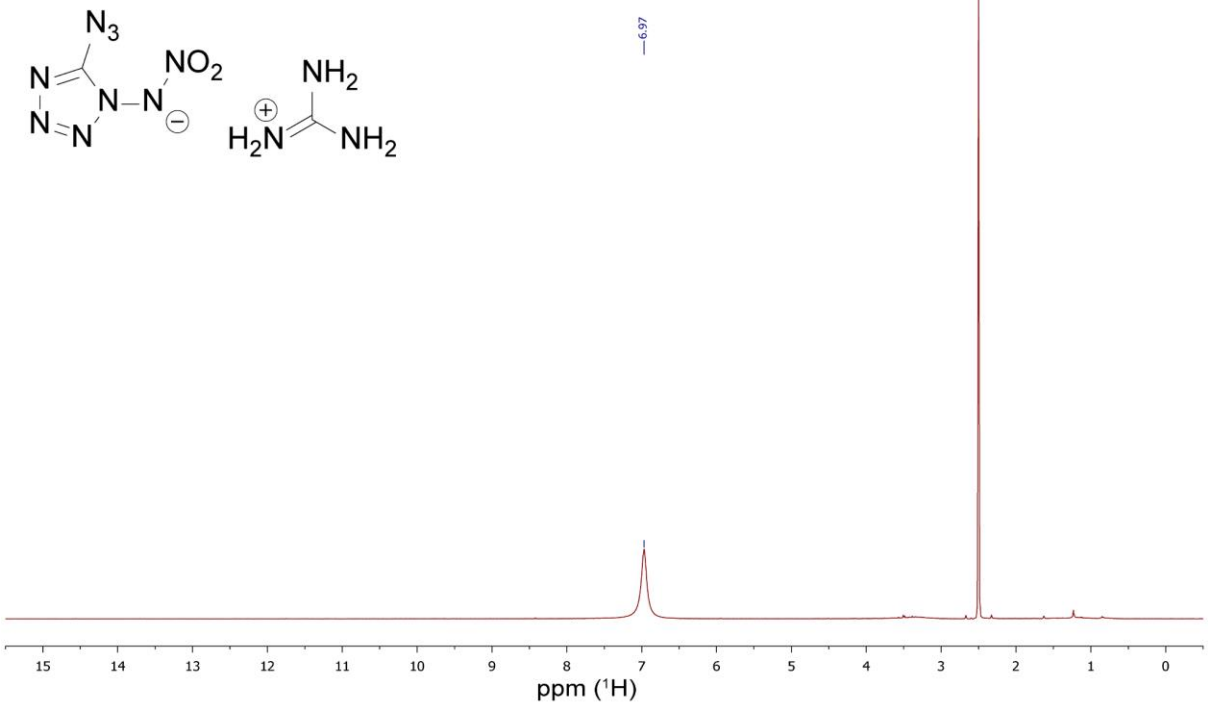

¹³C-NMR (101 MHz, DMSO-D₆, ppm)

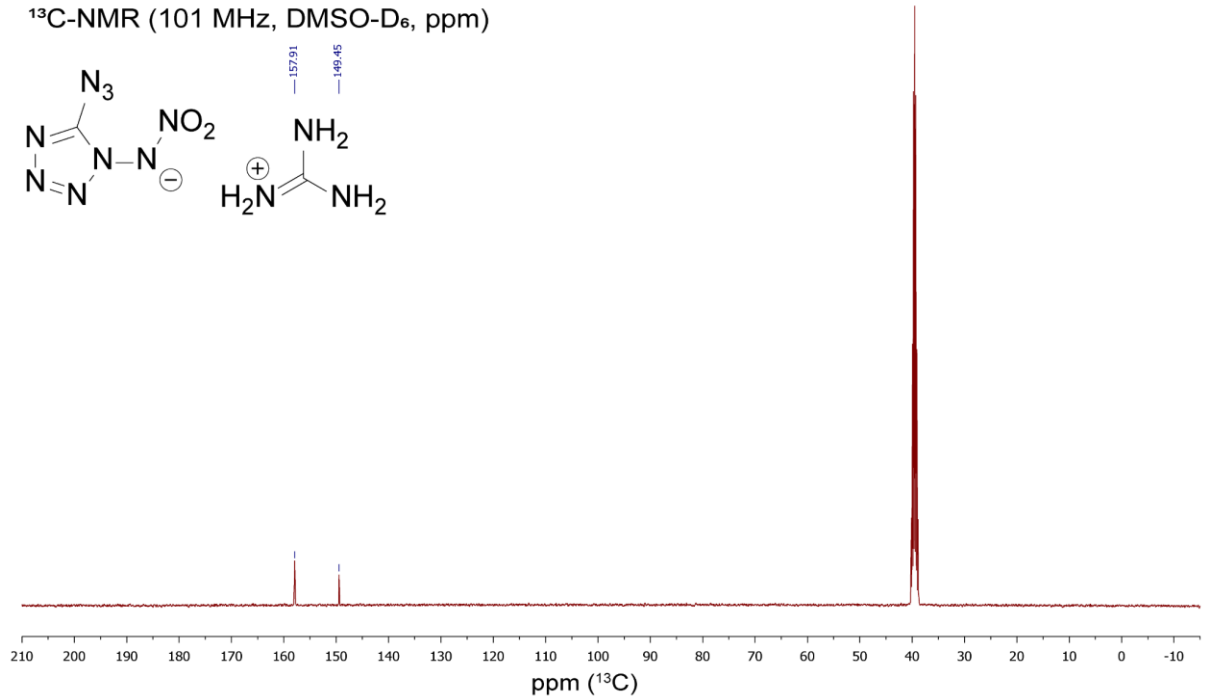

^{14}N-NMR (29 MHz, DMSO-D$_6$, ppm)

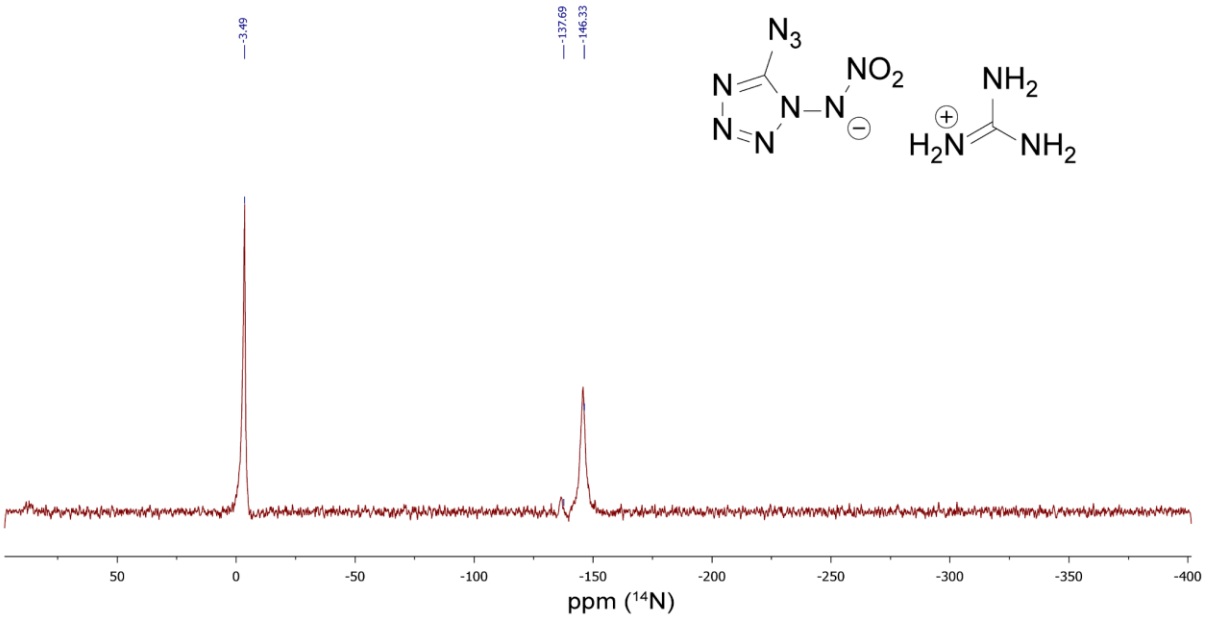

^{1}H-NMR (400 MHz, DMSO-D$_6$, ppm)

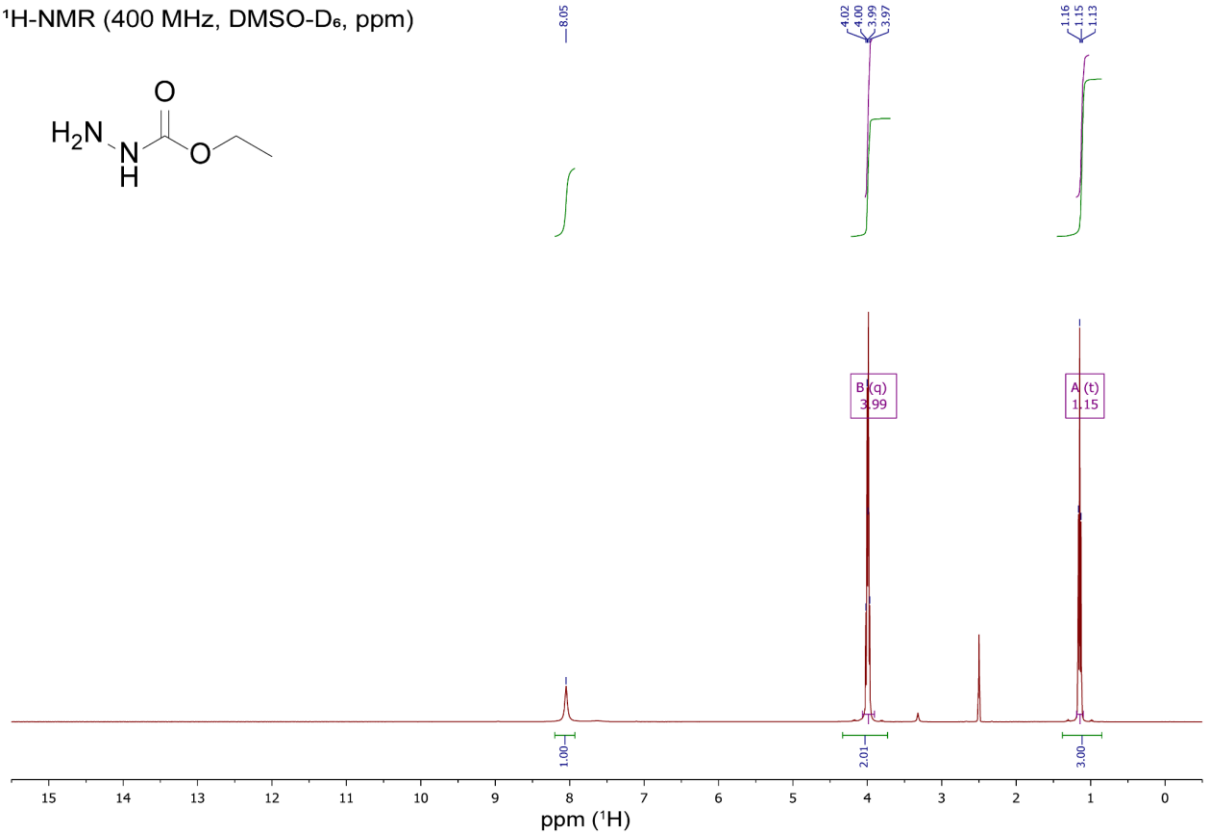

^{13}C-NMR (101 MHz, DMSO-D$_6$, ppm)

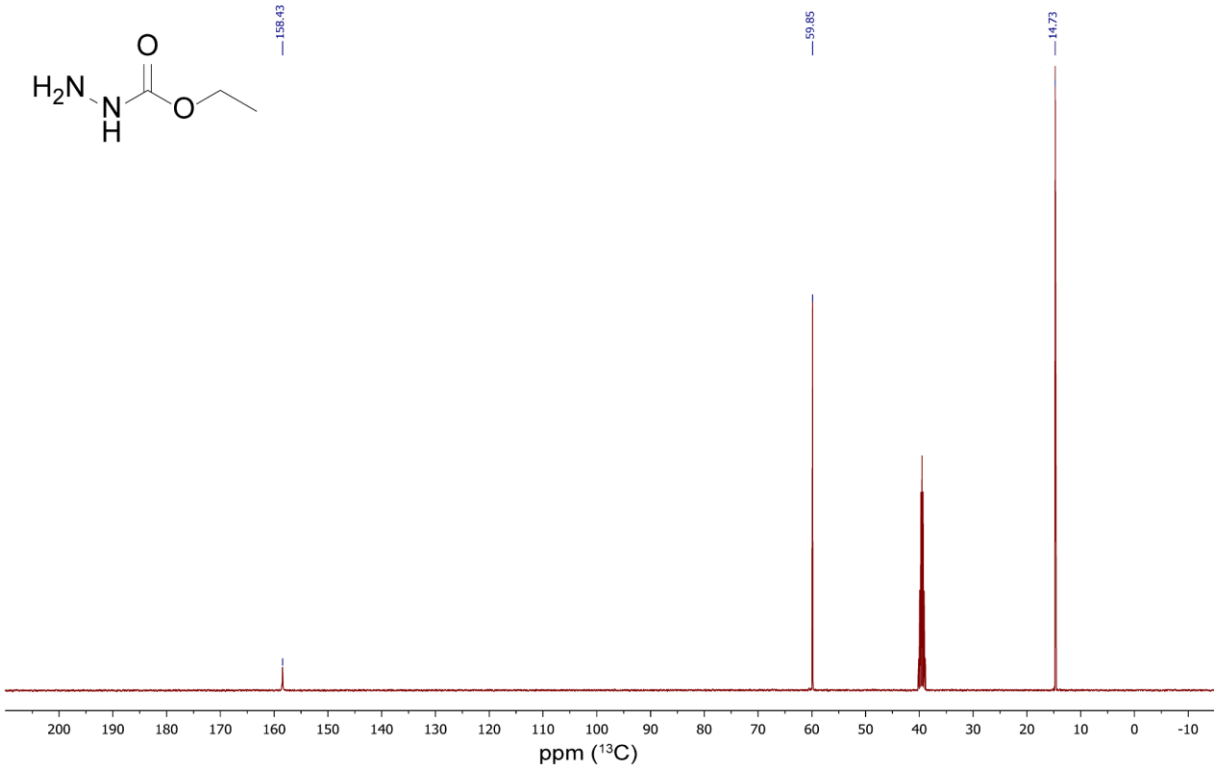

^{1}H-NMR (400 MHz, DMSO-D$_6$, ppm)

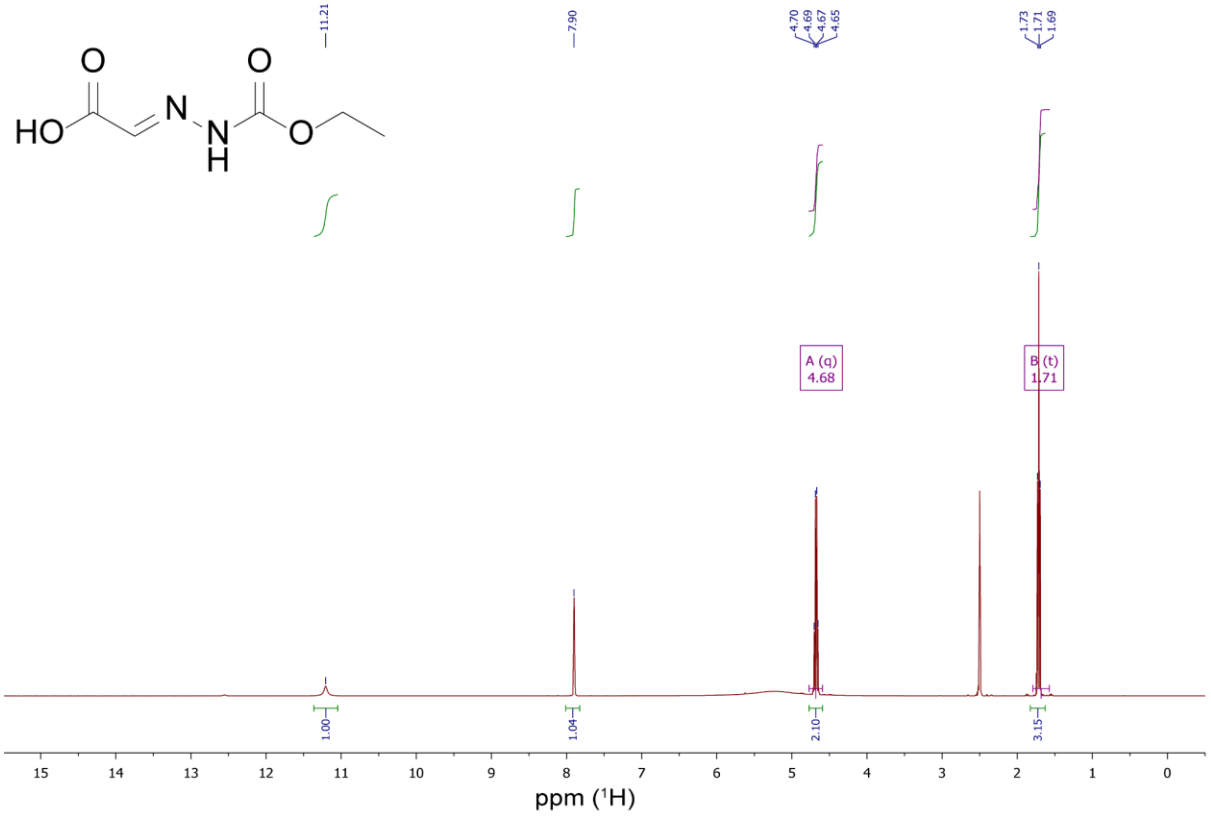

^{13}C-NMR (101 MHz, DMSO-D$_6$, ppm)

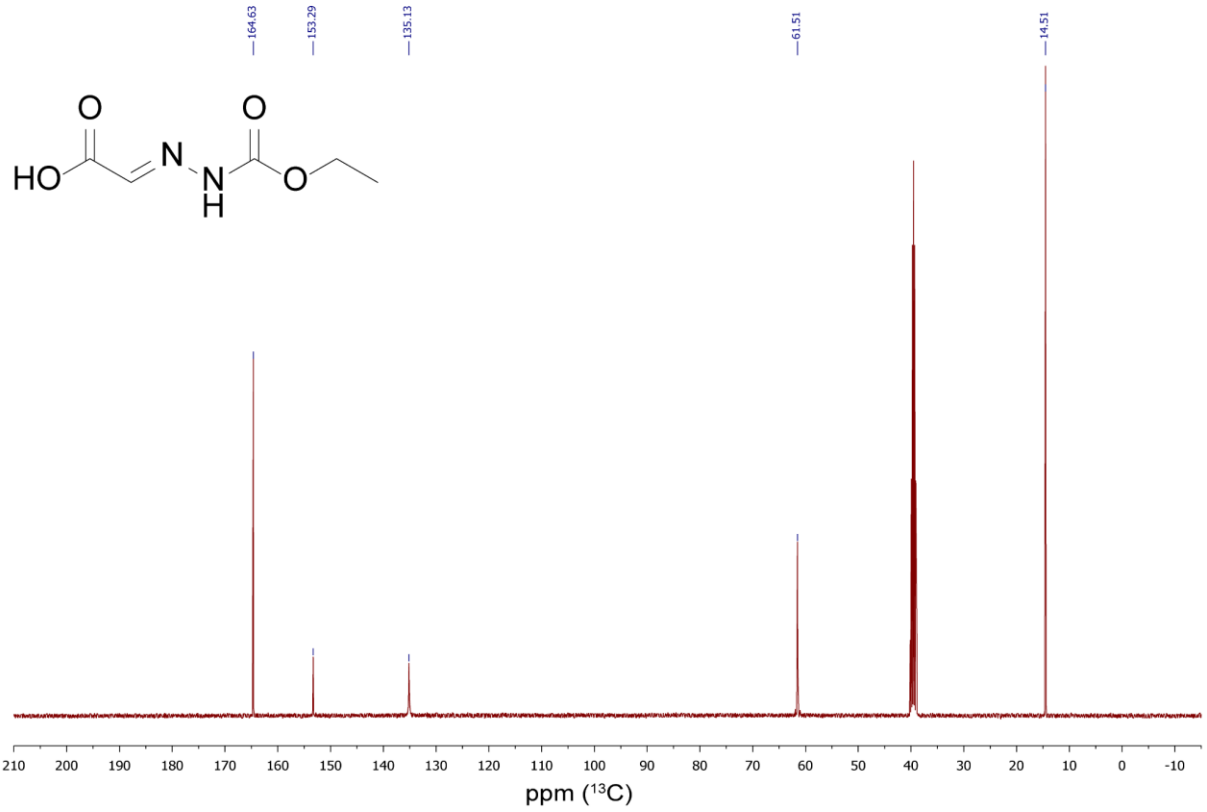

^{1}H-NMR (400 MHz, Acetone-D$_6$, ppm)

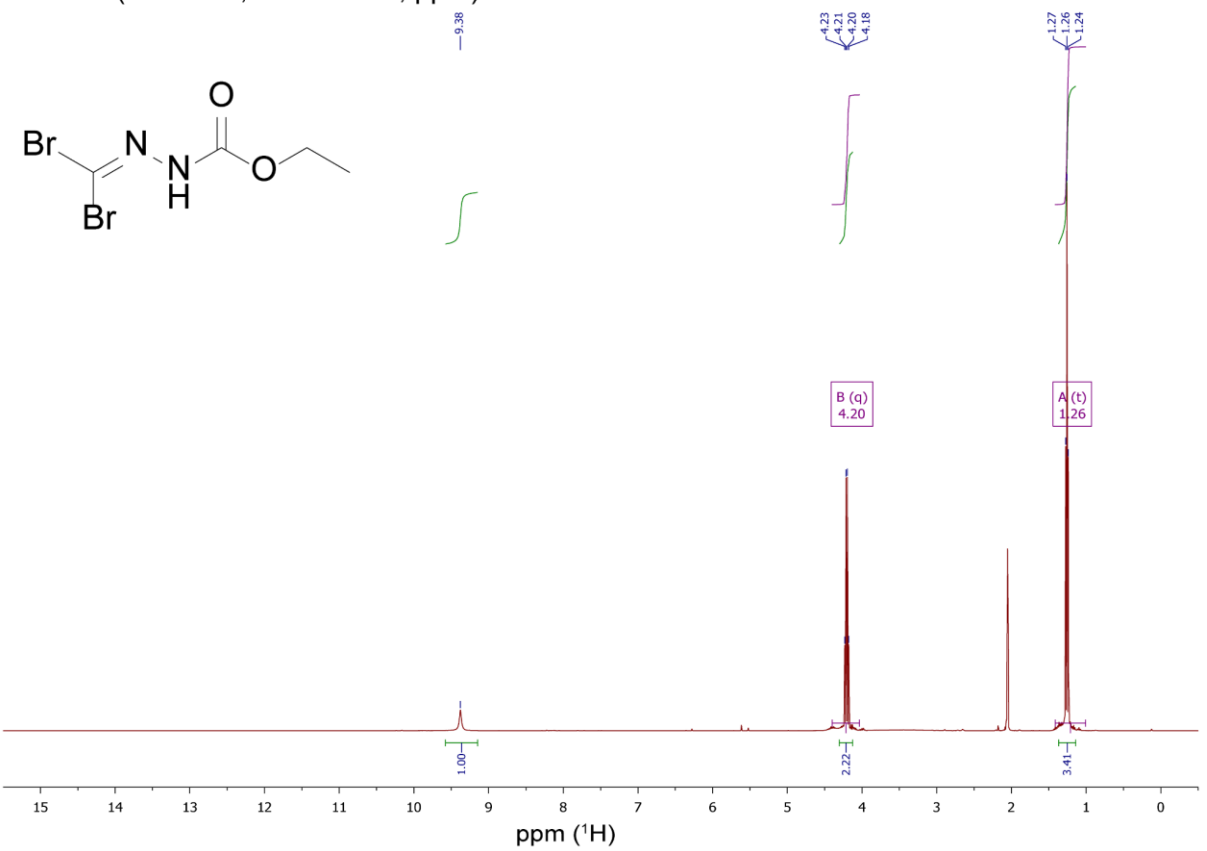

^{13}C-NMR (101 MHz, Acetone-D$_6$, ppm)

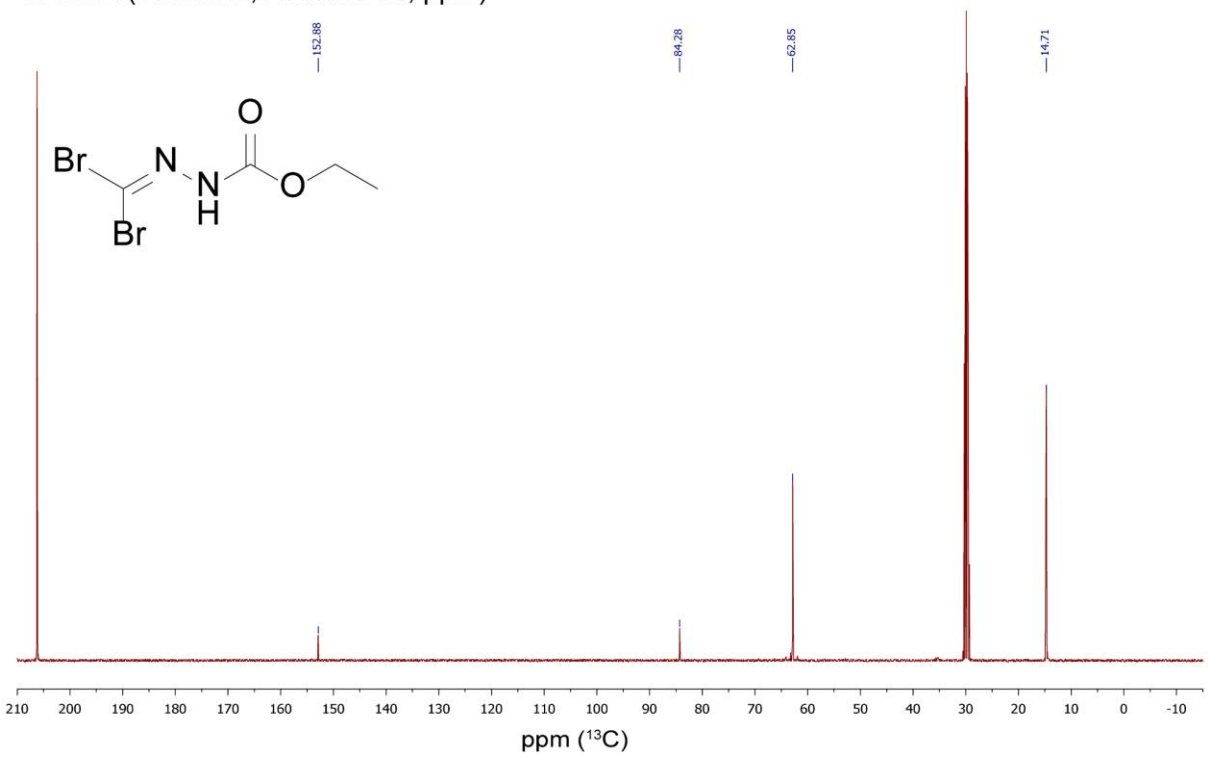

^{1}H-NMR (400 MHz, Acetone-D$_6$, ppm)

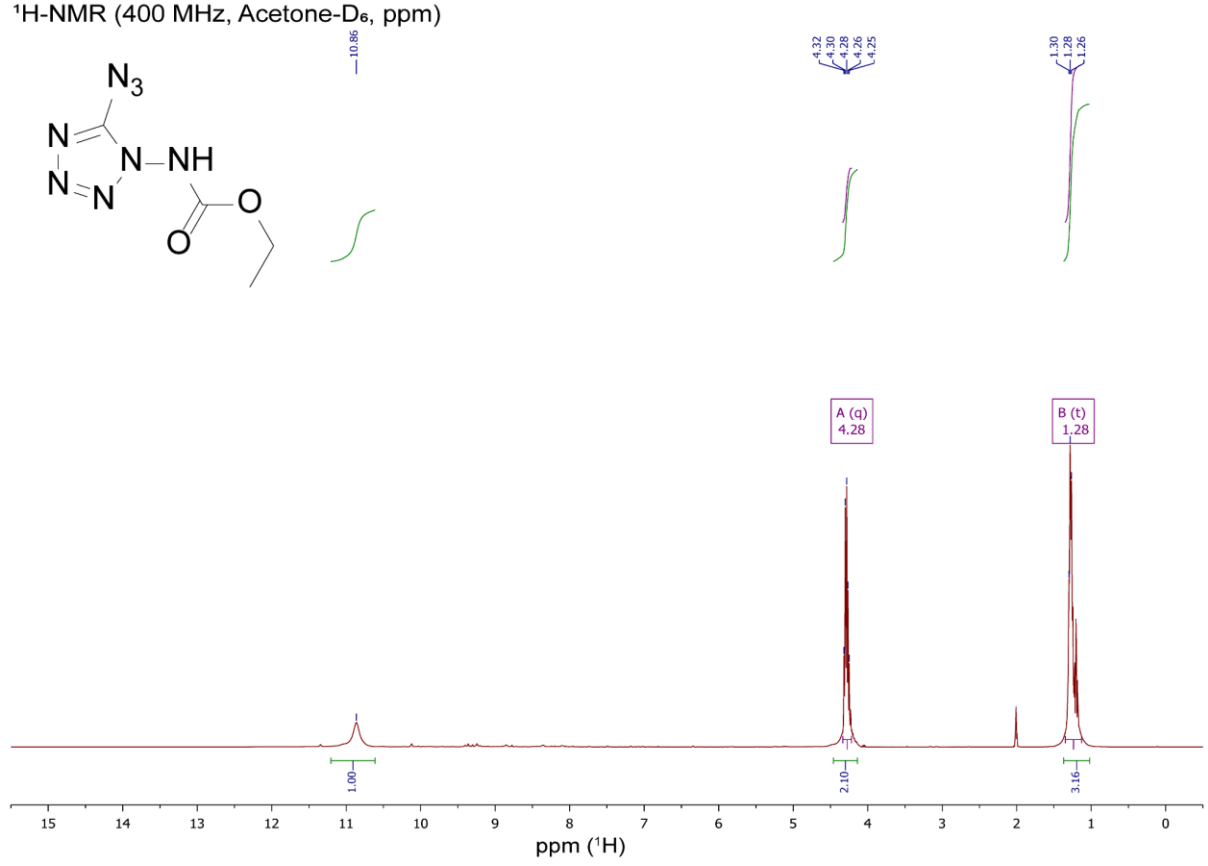

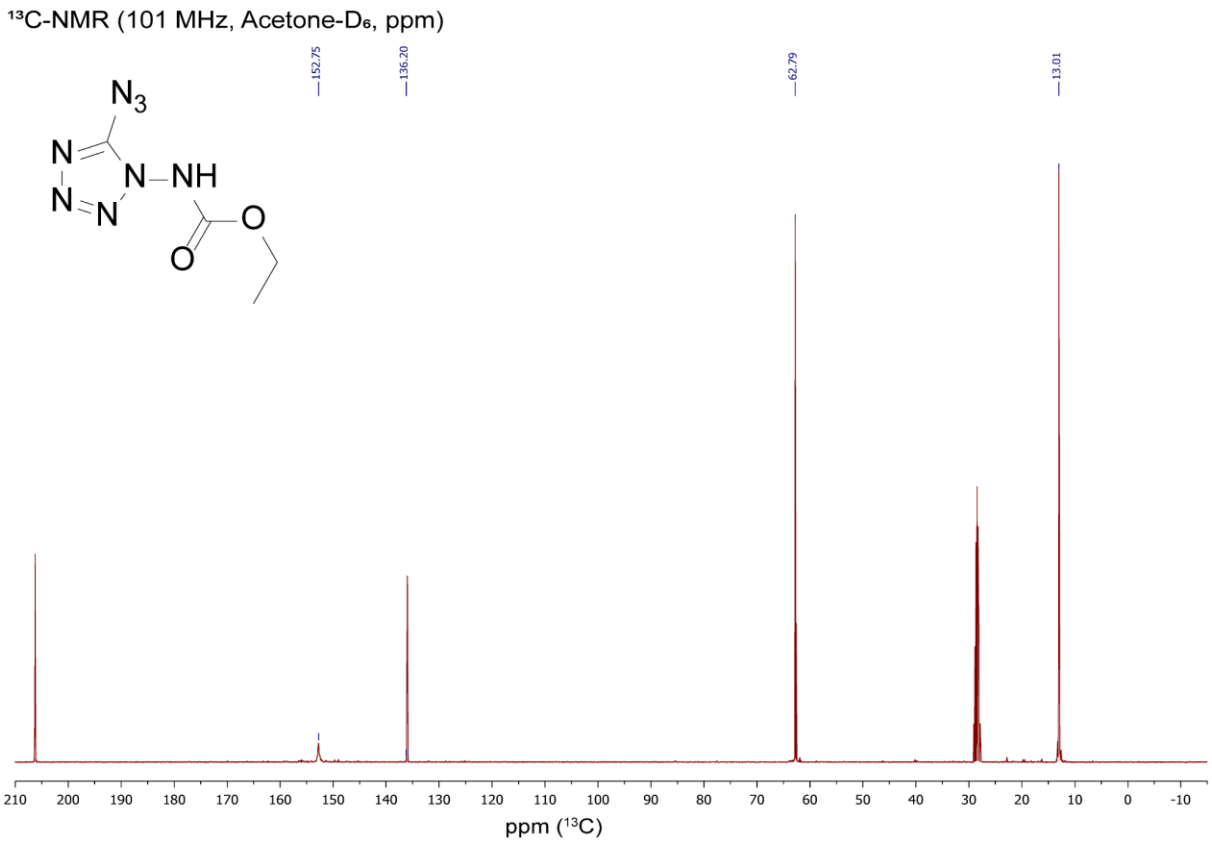

11.6.6 References

[S1] a) Test methods according to the UN Recommendations on the Transport of Dangerous Goods, *Manual of Test and Criteria*, ST/SG/AC.10/11/Rev.7, United Nations Publication, New York and Geneva, **2019**, 978-92-1-130394-0; https://unece.org/transport/dangerous-goods/rev7-files; b) Reichel & Partner GmbH, http://www.reichelt-partner.de; c) http://www.ozm.cz

[S2] M. Sućeska, EXPLO5 V6.02 program, Brodarski Institute, Zagreb, Croatia, **2014**.

[S3] T. M. Klapötke, F. A. Martin, J. Stierstorfer, *Chem. Eur. J.* **2012**, *18*, 1487–1501.

[S4] L. Liu, C. He, C. Li, Z. Li, *J. Chem. Crystallogr.* **2012**, *42*, 816–823.

[S5] *CrysAlisPro*, Oxford Diffraction Ltd. *version 171.33.41*, **2009**.

[S6] G. M. Sheldrick, *Acta Cryst.* **2015**, *A71*, 3–8.

[S7] O. V. Dolomanov, L. J Bourhis, R. J. Gildea, J. A. K. Howard, H. Puschmann, *J. Appl. Cryst.* **2009**, *42*, 339–341.

[S8] *SCALE3 ABSPACK – An Oxford Diffraction program* (1.0.4, gui: 1.0.3), Oxford Diffraction Ltd., **2005**.

[S9] APEX3. Bruker AXS Inc., Madison, Wisconsin, USA.

[S10] M. J. Frisch, G. W. Trucks, H. B. Schlegel, G. E. Scuseria, M. A. Robb, J. R. Cheeseman, G. Scalmani, V. Barone, B. Mennucci, G. A. Petersson, H. Nakatsuji, M. Caricato, X. Li, H.P. Hratchian, A. F. Izmaylov, J. Bloino, G. Zheng, J. L. Sonnenberg, M. Hada, M. Ehara, K. Toyota, R. Fukuda, J. Hasegawa, M. Ishida, T. Nakajima, Y. Honda, O. Kitao, H. Nakai, T. Vreven, J. A. Montgomery, Jr., J. E. Peralta, F. Ogliaro, M. Bearpark, J. J. Heyd, E. Brothers, K. N. Kudin, V. N. Staroverov, R. Kobayashi, J. Normand, K. Raghavachari, A. Rendell, J. C. Burant, S. S. Iyengar, J. Tomasi, M. Cossi, N. Rega, J. M. Millam, M. Klene, J. E. Knox, J. B. Cross, V. Bakken, C. Adamo, J. Jaramillo, R. Gomperts, R. E. Stratmann, O. Yazyev, A. J. Austin, R. Cammi, C. Pomelli, J. W. Ochterski, R. L. Martin, K. Morokuma, V. G. Zakrzewski, G. A. Voth, P. Salvador, J. J. Dannenberg, S. Dapprich, A. D. Daniels, O. Farkas, J.B. Foresman, J. V. Ortiz, J. Cioslowski, D. J. Fox, Gaussian 09 A.02, Gaussian, Inc., Wallingford, CT, USA, **2009**.

[S11] a) J. W. Ochterski, G. A. Petersson, and J. A. Montgomery Jr., *J. Chem. Phys.* **1996**, *104*, 2598–2619; b) J. A. Montgomery Jr., M. J. Frisch, J. W. Ochterski G. A. Petersson, *J. Chem. Phys.* **2000**, *112*, 6532–6542.

[S12] a) L. A. Curtiss, K. Raghavachari, P. C. Redfern, J. A. Pople, *J. Chem. Phys.* **1997**, *106*, 1063–1079; b) E. F. C. Byrd, B. M. Rice, *J. Phys. Chem*. A **2006**, *110*, 1005–1013; c) B. M. Rice, S. V. Pai, J. Hare, *Comb. Flame* **1999**, *118*, 445–458.

[S13] P. J. Lindstrom, W. G. Mallard (Editors), NIST Standard Reference Database Number 69, http://webbook.nist.gov/chemistry/ (accessed June **2021**).

[S14] M. S. Westwell, M. S. Searle, D. J. Wales, D. H. Williams, *J. Am. Chem. Soc*. **1995**, *117*, 5013–5015; b) F. Trouton, *Philos. Mag*. **1884**, *18*, 54–57.

[S15] a) H. D. B. Jenkins, H. K. Roobottom, J. Passmore, L. Glasser, *Inorg. Chem.* **1999,** *38,* 3609–3620; b) H. D. B. Jenkins, D. Tudela, L. Glasser, *Inorg. Chem.* **2002**, *41*, 2364–2367.

12. Tuning the Properties of 5-Azido and 5-Nitramino-tetrazoles by Diverse Functionalization – General Concepts for Future Energetic Materials

Maximilian Benz‡, Thomas M. Klapötke, Tobias Lenz‡, Jörg Stierstorfer

as published in *Chemistry – A European Journal* **2022**, *28*, e202200772

DOI: 10.1002/chem.202200772

Keywords: azides, energetic materials, NMR spectroscopy, tetrazoles, X-ray diffraction

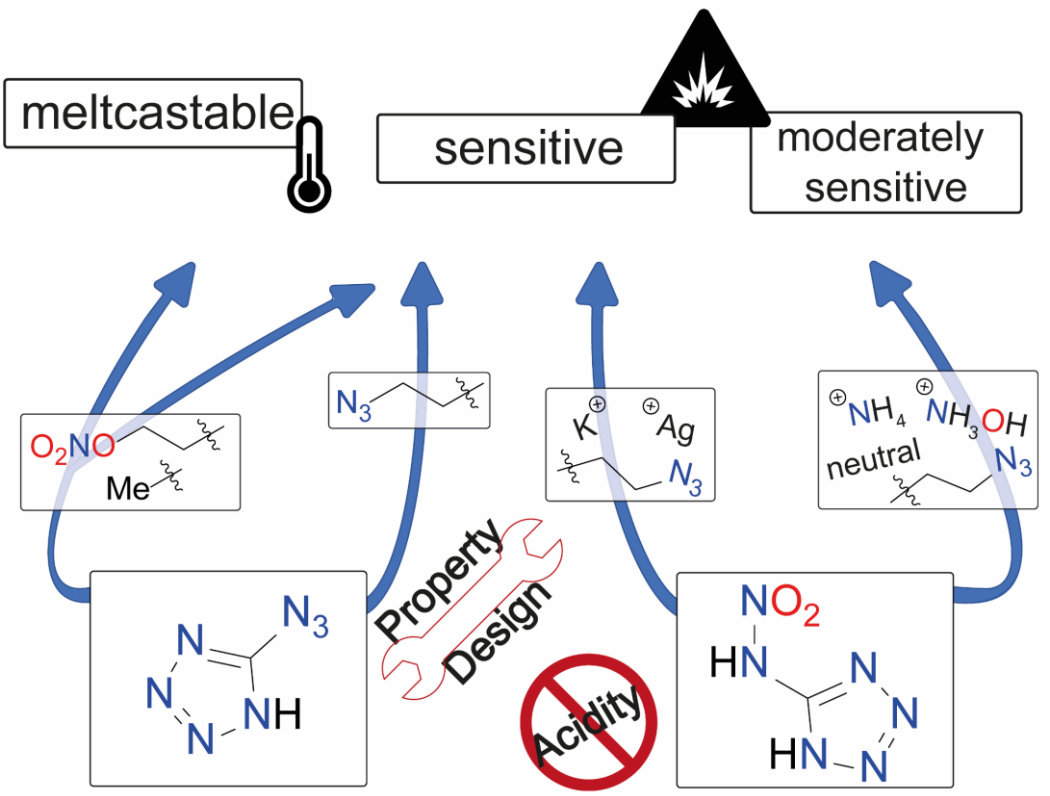

Derivatization of 5-azido and 5-nitraminotetrazole with an azidoethyl, nitratoethyl or methyl group gives access to less acidic high explosives with versatile properties. Salt formation of the nitraminotetrazoles with nitrogen-rich and metal cations was performed to achieve less acidity, lower vapor pressure and higher thermal stability.

Abstract: 5-Azido and 5-nitraminotetrazole backbones are established heterocyclic motifs in the research field of energetic materials synthesis. Despite the high energy content of the compounds, the problem with many derivatives is that their sensitivities are far too high. Functionalization of one of the ring nitrogen atoms is the aim of this study to adjust the sensitivity by inserting nitratoethyl, azidoethyl and methyl groups. In this context, derivatives of 2-(2-azidoethyl)-5-nitraminotetrazoles (**2**, **2a**–**2d**), as well as 1-nitrato and 1-azidoethyl substituted 5-azidotetrazole (**7** and **10**) and the methylation products of 5-azidotetrazole (5-azido-1-methyl-tetrazole, **11** and 5-azido-2-methyl-tetrazole, **12**) were prepared. The obtained nitrogen-rich compounds were extensively characterized through multinuclear NMR spectroscopy and IR spectroscopy. The structural confinement was checked by X-ray diffraction experiments. The pure samples (verified by elemental analysis) were investigated regarding their behavior toward friction, impact (BAM methods) and electrostatic discharge as well as heating (DTA and DSC). For all metal-free compounds the detonation properties were computed with the EXPLO5 code using their density and heat of formation, calculated based on CBS-4 M level of theory.

12.1 Introduction

The application of energetic materials is spread over various fields and thus a material must fulfill suitable criteria.[1] Explosives are divided into three main categories. A) Sensitive explosives, such as sensitizers, igniters or detonants; B) less sensitive but powerful explosives, secondary explosives; and C) insensitive, tertiary explosives. Many of the materials used were developed before or at the beginning of the 20th century, with only a little focus on sustainability or environmental impact.[2] The common primary explosives are often heavy metal based, as there are lead azide or styphnate. Their use is found to contaminate training grounds and application sites.[3] The secondary explosive trinitrotoluene, which is widely used due to its advantageous melt castable properties, shows to have disadvantageous environmental impact and is a possible carcinogenic, as stated by the U.S. Environmental Protection Agency.[4a]

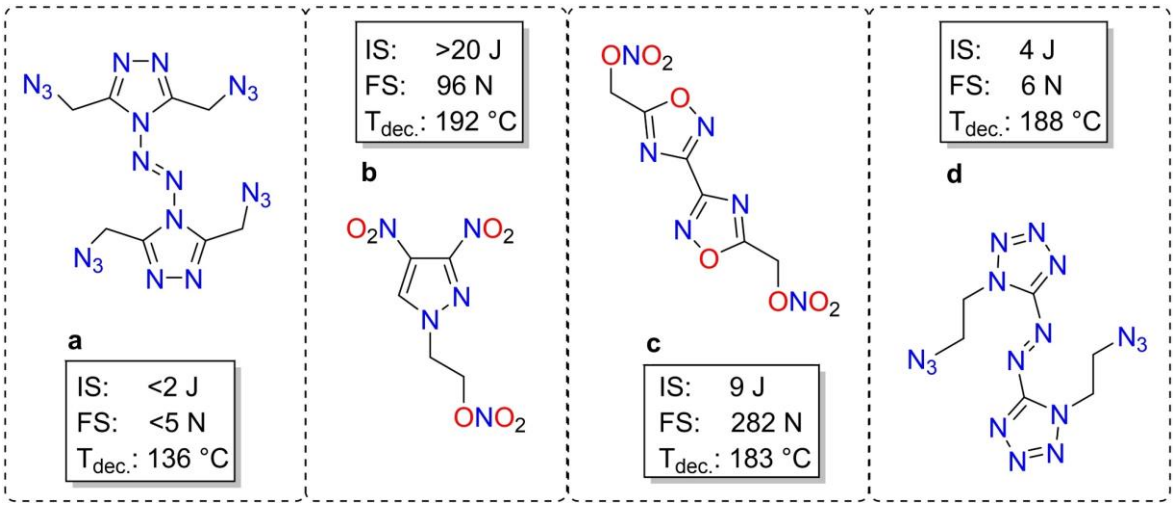

Figure 1. Representatives of energetic N-alkyl substituted azoles. 3,3',5,5'-Tetra(azidomethyl)-4,4'-azo-1,2,4-triazole (a), 1(2-nitratoethyl)-3,4-dinitropyrazole (b), bis(1,2,4-oxadiazole)bis(methylene) dinitrate (c) and 1,1'-bis(2-azidoethyl)-azotetrazole (d).

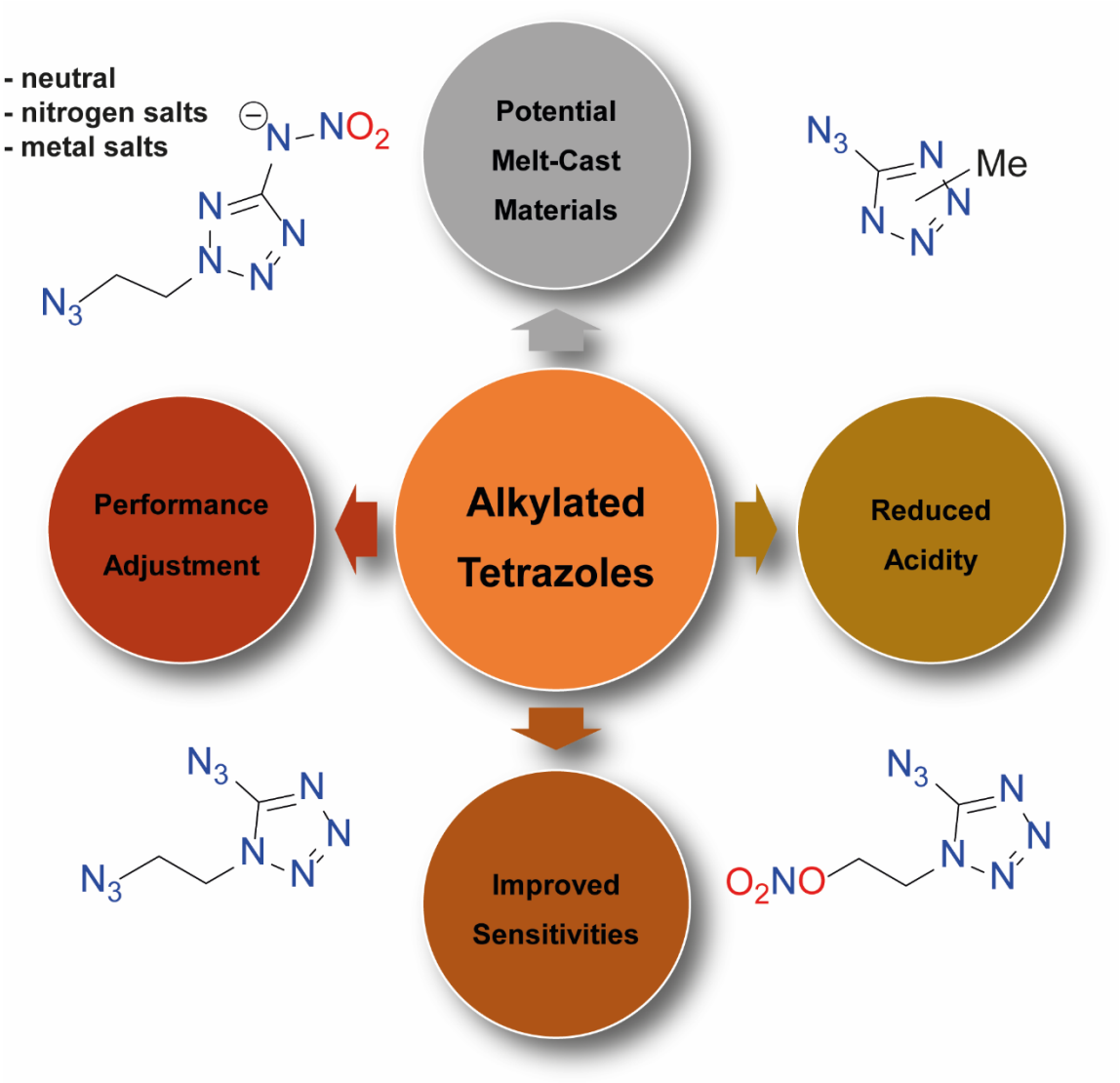

Figure 2. Derivatization of 5-azido- and 5-nitraminotetrazole reveals new applications.

The urgent need for sustainable and environmentally friendly replacements poses major challenges for the energetic materials community.[4b] A state-of-the-art synthetic approach consists of derivatization of known oxygen- and nitrogen-rich azoles in combination with short alkyl, azidoalkyl or nitratoalkyl chains.

Sabatini et al. found that bis-5-(nitratomethyl)bis(1,2,4-oxadiazole) (c) is suitable to replace trinitrotoluene while showing significantly higher performance data.[5] Furthermore furazanes[6], 1,2,3-triazoles[7], 1,2,4-triazoles[8], tetrazoles[9] and pyrazoles[10] were functionalized by energetic azido or nitratoalkyl side chains (Figure 1).

In the search for ever higher nitrogen and energy contents, the energetic compounds, 5-nitramino-[11] and 5-azidotetrazole[12], arouse attention. Both molecules are intensively studied as free acids[13] or salinized,[14] and are promising building blocks due to their straight forward accessibility. Here we report different approaches to reduce the acidity of those high energy and nitrogen-rich tetrazole building blocks. Insights into the changes of the sensitivity are gained. For the 5-nitraminotetrazole replacement of the acidic tetrazole proton by an azidoethyl function led to a monobasic acid (**2**) that was further salinized (**2a**–**d**) to reduce the acidity, lower the vapor pressure and increase the thermal stability. Also melt-castable primary explosives would be of great interest. Therefore, the acidic proton of 5-azidotetrazole was exchanged by an azidoethyl (**7**), nitratoethyl (**10**) or methyl (**11**, **12**) functionality. Functionalization reveals compounds that are suitable for various applications (Figure 2).

12.2 Results and Discussion

12.2.1 Synthesis

With the synthetic protocol for 2-(2-azidoethyl)-5-aminotetrazole (**1**) in hand, which was recently published by our group[9a], we were investigating suitable conditions to perform the nitration of the amino function to the respective nitraminotetrazole **2**. We found a pre-cooled mixture of sulfuric acid and fuming nitric acid (ratio 8 : 3) to work best and this yields pure **2** without further purification in 86 % yield (Scheme 1).

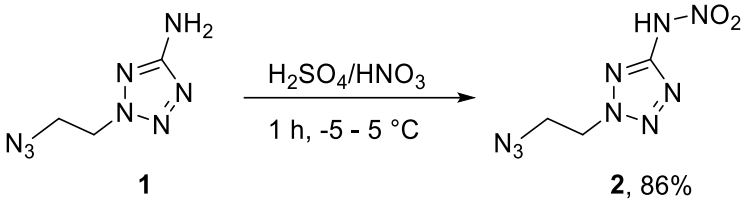

Scheme 1. Nitration of **1** to form the nitramino derivative **2** using mixed acid at low temperatures.

The nitrogen-rich salts **2a** and **2b** as well as the metal salts **2c** and **2d** were obtained by simple acid-base reactions of the free nitramine **2** and the respective base, or in the case of **2d** with $AgNO_3$ solution (Scheme 2). All compounds were obtained elemental analysis pure and could be analyzed without further purification. In attempting to prepare the hydrazinium salt of **2**, pure **1** was isolated. As has already occurred for other aromatic nitramines[9b], the reaction with aqueous hydrazine leads to a reduction of the nitramine function to the amine.

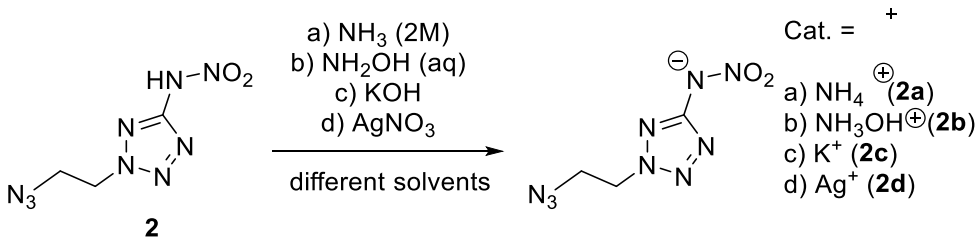

Scheme 2. Preparation of ionic derivatives **2a**–**2d** starting from the free nitramino derivative **2** through reaction with the respective cation containing reagents.

To achieve functionalized 5-azidotetrazoles classic bromination of 5*H*-tetrazoles was performed for three days at reflux (Scheme 3). The 1-(2-azidoethyl)-tetrazole (**3a**) was reacted to 1-(2-azidoethyl)-5-bromotetrazole (**4a**) in very good yields. The bromination of 1-(2-acetoxyethyl)-tetrazole (**3b**) was performed similar to the literature,[15] and 5-bromo-1-(2-acetoxyethyl)-tetrazole (**4b**) was yielded in excellent yields (Scheme 3).

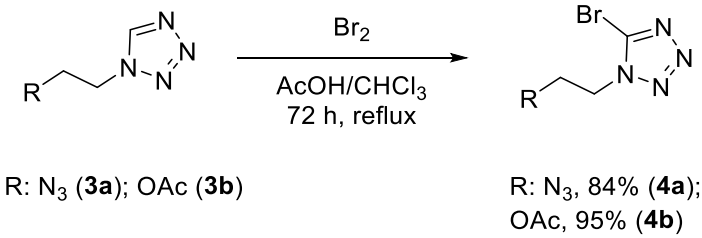

Scheme 3. Bromination of 1-functionalized 5*H*-tetrazoles.

Substitution at the 5-bromo position was then performed by hydrazine. The strong nucleophilicity of hydrazine and the low solubility of the resulting hydrazinium bromide in isopropanol makes bromine-hydrazine exchange possible, even at room temperature. The reaction was performed either at room temperature for three days or at elevated temperature for shorter periods of time. Compound **4a** can be reacted at 60 °C for 2 h to synthesize 1-(2-azidoethyl)-5-hydrazineyltetrazole (**5**). However slow decomposition at room temperature complicated the purification and therefore only a crystal structure and ^{1}H and ^{13}C NMR were measured. To stabilize and purify compound **5** it was precipitated as hydrochloride salt, 1-(2-azidoethyl)-5-hydraziniumtetrazol chloride (**6**), from a concentrated isopropanol solution. The overall reaction from compound **4a** to compound **6** proceeds in acceptable yields. Finally, 1-(2-azidoethyl)-5-azidotetrazole (**7**) was synthesized through reaction of **6** with sodium nitrite under acidic conditions in excellent yields after column chromatography (Scheme 4).

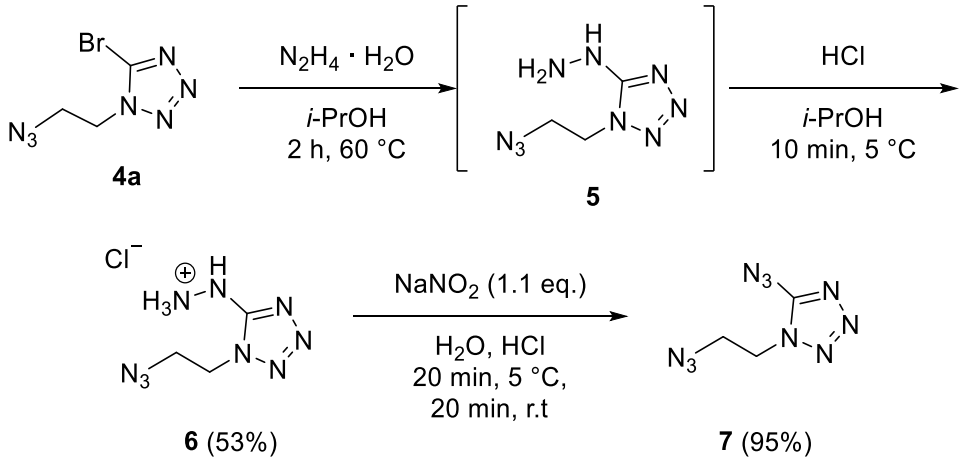

Scheme 4. Reaction pathway towards 1-(2-azidoethyl)-5-azidotetrazole (**7**) by reacting the 5-position of the tetrazole from bromine to hydrazine to azide.

Reaction of compound **4b** with hydrazine over three days at ambient temperature lead to 5-hydrazineyl-1-(2-hydroxyethyl)-tetrazole (**8**). The acetoxy moiety of **4b** reacts with hydrazine to acetohydrazide. Several attempts to purify compound (**8**) failed, only a crystal structure and ^{1}H and ^{13}C NMR were measured. Also, a crystal structure of the hydrochloride was observed by a similar procedure than for **6** (can be found in the Supporting Information). The crude of **5** was reacted with sodium nitrite under acidic conditions to give 5-azido-1-(2-hydroxyethyl)-tetrazole (**9**). After

column chromatography the overall yield from **4b** to **9** is 40 %. In the last step of the synthesis towards 5-azido-1-(2-nitratoethyl)-tetrazole (**10**), compound **9** was nitrated using white fuming nitric acid in very good yields (Scheme 5).

For the synthesis of the two isomers of 5-azido-methyltetrazole, various synthetic pathways had to be pursued as depicted in Scheme 6. Methylation of in situ generated 5-azidotetrazole with dimethyl sulfate produces only the 5-azido-2-methyltetrazole (**12**) isomer due to the two-position directing effect of the azido group. Therefore, an alternative route toward the 5-azido-1-methyltetrazole (**11**) had to be established starting with a 1-methyl substituted tetrazole derivative and subsequent generation of the azide function at position 5.

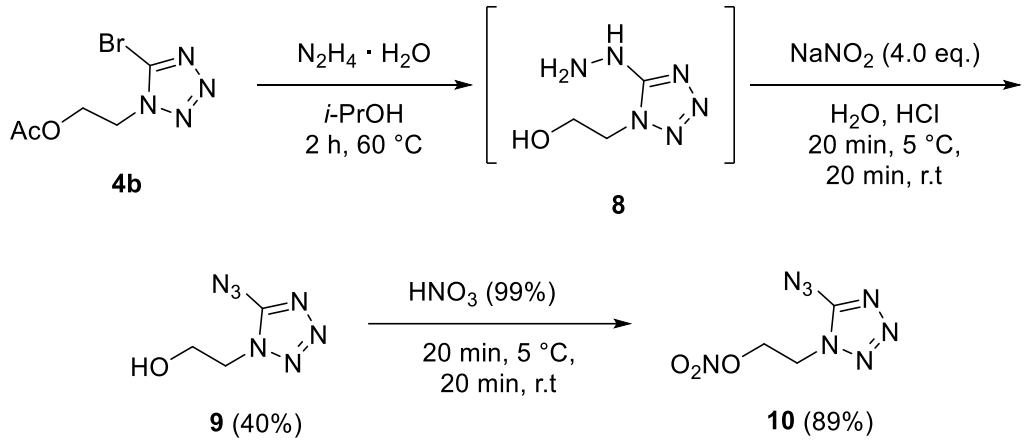

Scheme 5. Reaction pathway towards 5-azido-1-(2-nitratoethyl)-tetrazole (**10**) by bromine-hydrazine exchange followed by reaction with sodium nitrite and the nitration of the hydroxy group to its organic nitrate.

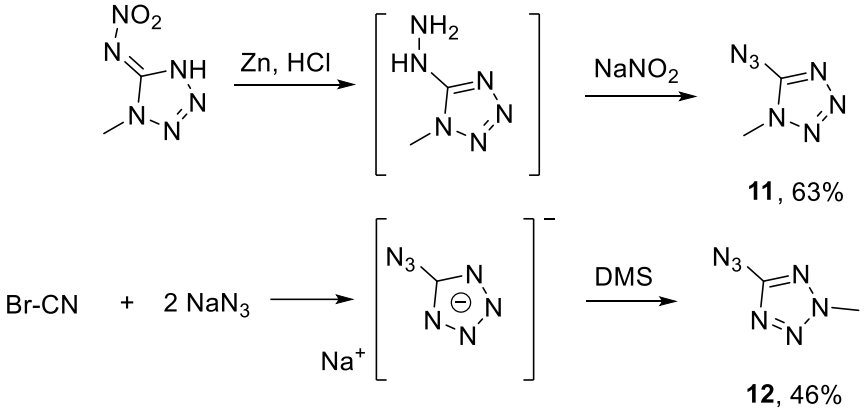

Scheme 6. Pathway for selective synthesis of 5-azido-1-methyltetrazole (**11**) through diazotization of 5-hydrazino-1-methyltetrazole and 5-azido-2-methyltetrazole (**12**) through methylation of 5-azidotetrazole.

Thus, we started with 1-methyl-5-nitrimino-4*H*-tetrazole,[16] and were able to reduce the nitrimino function with zinc dust under acidic conditions to the respective 5-hydrazino-1-methyltetrazole, which was directly converted to 5-azido-1-methyltetrazole (**11**) through diazotization using one equivalent of sodium nitrite.

12.2.2 X-Ray Diffraction

Crystals suitable for X-ray diffraction experiments could be obtained by recrystallization from different common solvents for **2a**, **2b**, **2d** and **10**–**12**. Deposition Numbers 2157201 (for **2a**), 2157198 (for **2b**), 2157203 (for **2 d**), 2157204 (for **5**), 2157196 (for **6**), 2157199 (for **7**), 2157197 (for **8** · HCl), 2157202 (for **9**), 2157200 (for **10**), 707542 (for **11**) and 707543 (for **12**) contain(s) the supplementary crystallographic data for this paper. These data are provided free of charge by the joint Cambridge Crystallographic Data Centre and Fachinformationszentrum Karlsruhe Access Structures service. Crystalline diazido derivative **7** could be generated and picked by cooling of a saturated solution of **7** in Et_2O at −30 °C since it is a liquid at room temperature.

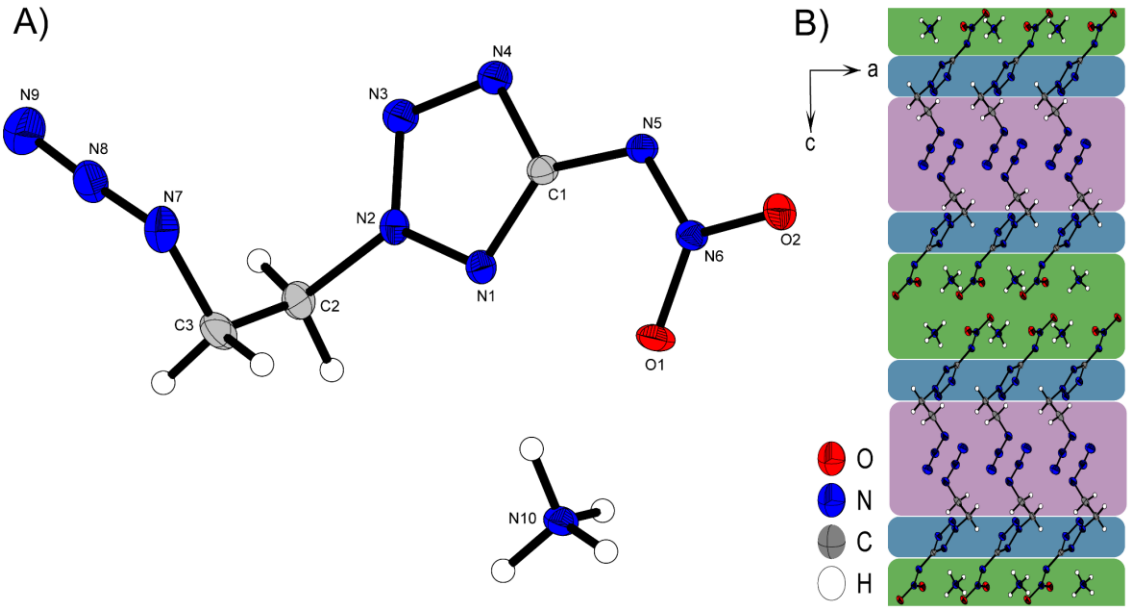

Figure 3. A) Molecular unit of **2a** with thermal ellipsoids drawn at the 50 % probability level. Selected bond distances (Å) and angles [°]: C1-N5 1.382(2), C2-N2 1.467(2), N7-N8 1.241(2), N8-N9 1.128(2), N10-H10A···O1 2.10(2), N10-H10B···O2 2.02(2), N10-H10C···N1 2.12(2), N10-H10D···N5 2.05(2), N7-N8-N9 173.6(2), N7-C3-C2-N2 62.08(2), O1-N6-N5-C1 1.7(2); B) Layer structure of **2a** with view along the *b* axis. Green, blue and red regions are labeled based on their different components for intermolecular bond formation.

Additional information about the depicted crystal structures and the measuring and computation methods as well as further crystal structures for various precursor compounds (**5**, **6**, **8**, **9**) can be found in the Supporting Information. Ammonium and hydroxylammonium salts **2a** and **2b** crystallize both in the triclinic space group *P*−1. As expected, the hydroxylammonium derivative has a slightly higher room temperature density (1.624 g cm^{-3} for **2b**) then the respective ammonium salt (1.575 g cm^{-3} for **2a**). The densities are in a range that was expected, when comparing them with related crystal structure densities. As shown in detail in previous studies[9a-9b, 9d] the densities of *N*-azidoethyl substituted tetrazoles are always well below those of *N*-nitratoethyl substituted ones. Compared with the room temperature densities of the hydroxylammonium salts of 1-and 2-nitratoethyl-5-nitraminotetrazole (density for both is 1.720 g cm^{-3})[9e], the density of **2b** is about 0.1 g cm^{-3} lower, which was to be expected due to the substitution at position two.

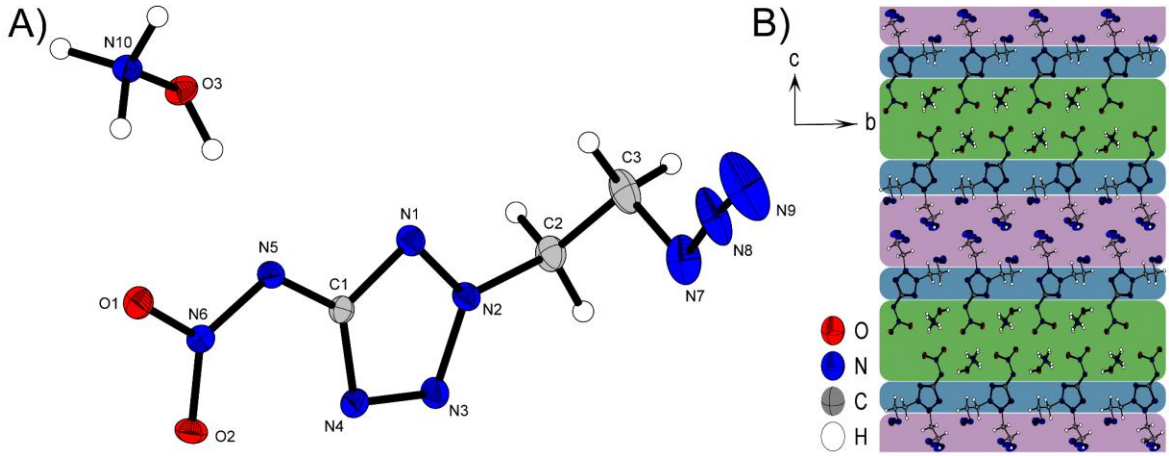

Figure 4. A) Asymmetric unit of **2b** with thermal ellipsoids drawn at the 50 % probability level. Selected bond distances (Å) and angles [°]: C1-N5 1.392(3), C2-N2 1.472(3), N7-N8 1.256(3), N8-N9 1.128(4), N10-H10A···O4 2.22(3), N10-H10B···O2 2.08(3), N10-H10C···N11 2.13(3), N10-H10C···O5 2.15(3), O3-H3···N5 1.80(4), N7-N8-N9 173.5(4), N7-C3-C2-N2 69.9(3), O1-N6-N5-C1 0.2(2); B) Layer structure of **2b** with view along the *a* axis. Green, blue and red regions are labeled based on their different components for intermolecular bond formation.

The three-dimensional configuration of the two salts **2a** and **2b** behave very similarly and can be schematically divided into three different parts depicted in Figure 3B) Figure 4B). The interactions in the red areas are exclusively weak van der Waals interactions between the C-H protons of the ethyl groups and the azide functions. The shortest ones can be found in **2b** (C2-H2A···N19 2.65 Å) and are therefore negligible for stability discussion due to their weak character. In the blue

region are mainly the tetrazole rings, which also loosely interact with each other through π–π-interactions. But mainly this layer forms both, linking and buffer layer between non-polar, weakly interacting azidoethyl sites and the strongly stabilizing, polar sites consisting of the respective cations and nitramine functions, highlighted in green. In this region of the two crystal structures of **2a** and **2b**, dominated by strong polar interactions, the overall strongest intermolecular, ionic interactions are found. These are formed through all protons of the cations with the respective nitrogen and oxygen atoms of the nitramine function (O1, O2 and N6) as well as with N1 of the tetrazole moiety. The average bond length *d*(D−H···A) is 2.06 Å with O3-H3···N5 1.80(4) Å being the shortest hydrogen bridge and therefore clearly below the van der Waals radius for a strong interaction.

Compound **2d** crystalizes in the orthorhombic space group *Pbca* with a density of 2.362 g cm^{-3} at 298 K and 16 molecular moieties per unit cell. The structure is mainly characterized by the formation of a close silver-silver contact. The neighboring anions arrange themselves around this structural motif in such manner that the formed argentophilic interaction can be interactively stabilized in the best possible way as depicted in Figure 5B). Argentophilic interactions are van der Waals contract below a bond distance of 3.44 Å and can be observed in several Ag containing structures.[17]

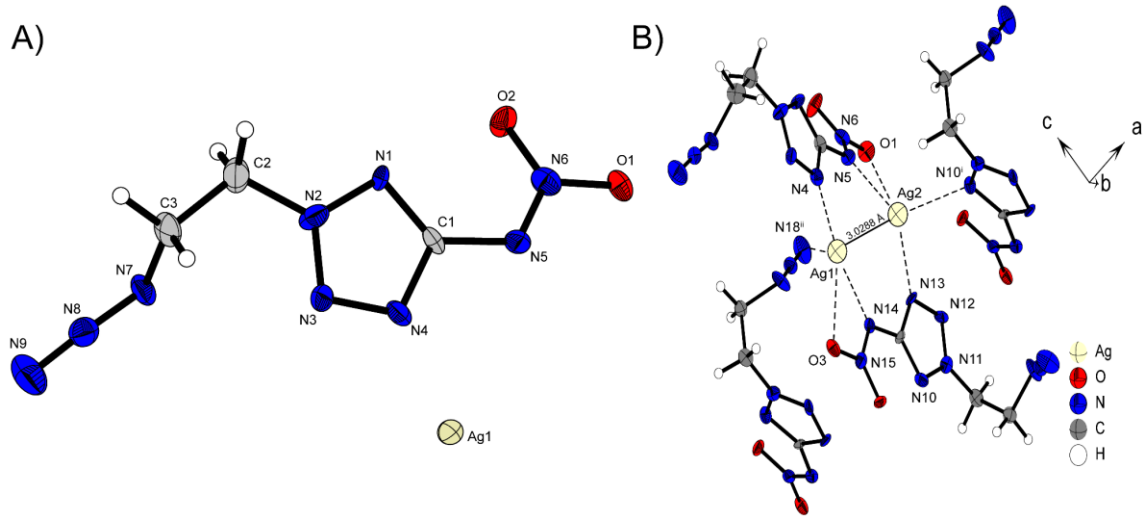

Figure 5. A) Asymmetric unit of **2d** with thermal ellipsoids drawn at the 50 % probability level. Selected bond distances (Å) and angles [°]: Ag1-Ag2 3.0288(11), Ag1-N14 2.126(7), Ag1-O3 2.877(6), Ag1-N4 2.137(7), Ag1-N18^{ii} 3.154(10), Ag2-N13 2.216(7), Ag2-N5 2.201(7), Ag2-O1 2.822(7), Ag2-N10^{i} 2.489(7), N14-Ag1-N4 167.3(3), N13-Ag2-N5 144.8(3), N15-N14-C4-N10 8.4(1), N6-N5-C1-N1 29.3(1); B) Representation of the argenophilic interaction between Ag1 and Ag2 with anionic moieties involved in the stabilization; Symmetry codes: (i) 0.5+x, 0.5−y, 1−z, (ii) 1−x, 1−y, 1−z.

Compared to the shortest ever measured Ag−Ag contact (2.7599(3) Å)[18] the silver-silver distance is with a length of 3.0288(11) Å clearly above, but can still be considered as argentophilic interaction.[19]

The Ag−Ag building block is stabilized by four anionic moieties forming several close contacts. These interactions originate from one nitrogen and one oxygen of the nitramine function, the tetrazole nitrogen atoms N1 and N4 as well as from the γ-nitrogen of the azide functionality. These electron donating interactions of the complexing N and O atoms are observed in the range of 2.126(7) Å for Ag1-N14 to 3.154(10) Å for Ag1-N18^{ii}. In order to optimize the assembly around the silver dimer, some unusual arrangements occur within the anion. For example, one nitramino group is clearly twisted out of the plane formed by the tetrazole (N6-N5-C1-N1 29.3(1)°). However, this rotation improves the complexation of the silver. Nevertheless, this arrangement is unusual for 5-nitraminotetrazoles, which normally bear 5-substituted nitramino groups planar with the tetrazole ring.

Ethyl substituted 5-azidotetrazole derivatives crystallize in the orthorhombic space group *Fdd*2 (for **7**) and in the monoclinic space group $P2_1/n$ (for **10**). The molecular moieties are depicted in Figure 6 and Figure 7. The room temperature density of nitratoethyl compound **10** is clearly superior to that of the azidoethyl derivative (1.519 g cm^{-3} for **7**, 1.638 g cm^{-3} for **10**).

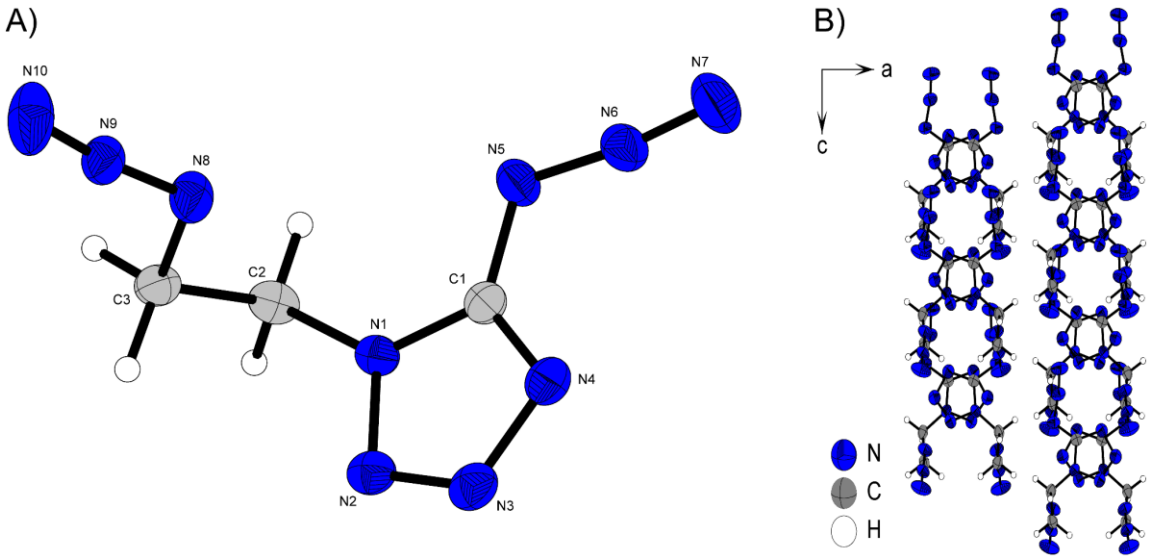

Figure 6. A) Molecular unit of **7** with thermal ellipsoids drawn at the 50 % probability level. Selected bond distances (Å) and angles [°]: C1-N5 1.386(4), C2-N1 1.458(4), N5-N6 1.251(4), N6-N7 1.114(4), N8-N9 1.221(4), 1.127(4), N5-N6-N7 171.4(3), N8-N9-N10 172.9(3), N9-N8-C3-C2 171.1(3); B) Layer structure of **9** with view along the *b* axis.

This trend has also been observed in previous studies[20], since the nitratoethyl unit offers more possibilities for intermolecular interactions on the one hand and contains more and heavier atoms on the other, which also arrange themselves better in space. Since there are no good opportunities for intermolecular interactions for the present nonpolar residues, the three-dimensional structure of **7** is mainly based on the fact that the azido and azidoethyl substituents avoid each other with a as large spatial distance as possible in order to counteract possible destabilizing interaction (Figure 6B)).

The three-dimensional pattern of **10** in Figure 7B) shows the assembly of two molecular units resulting in a linear chain structure of those pairs along *b*. Schematically, a molecular unit of **10** consists of two molecular planes that diverge from each other at an angle of about 112 °. One plane is formed by the azidotetrazole backbone and the second by the ethyl group, in the linear direction of which the nitrate ester is connected (O3-N8-O1-C3 179.5(3)°; N8-O1-C3-C2 175.1(2)°). The molecular units within a pair always arrange themselves in an alternating manner, i. e. they are rotated 180 ° to each other and thus a nitratoethyl rest is always superimposed with the azido function of its partner molecule.

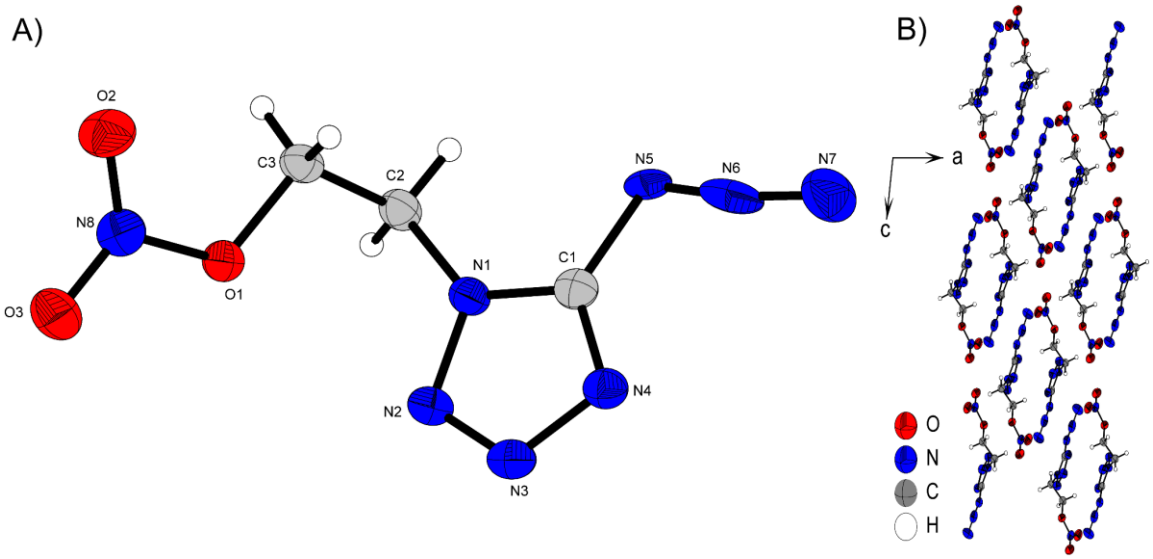

Figure 7. A) Molecular unit of **10** with thermal ellipsoids drawn at the 50 % probability level. Selected bond distances (Å) and angles [°]: C1-N5 1.463(4), C2-N1 1.458(4), N5-N6 1.074(4), N6-N7 1.207(4), C3-O1 1.449(4), O1-N8 1.388(3), N5-N6-N7 171.5(3), N1-C2-C3 112.6(2), N6-N5-C1-N1 1.7(3); B) Layer structure of **10** with view along the *b* axis.

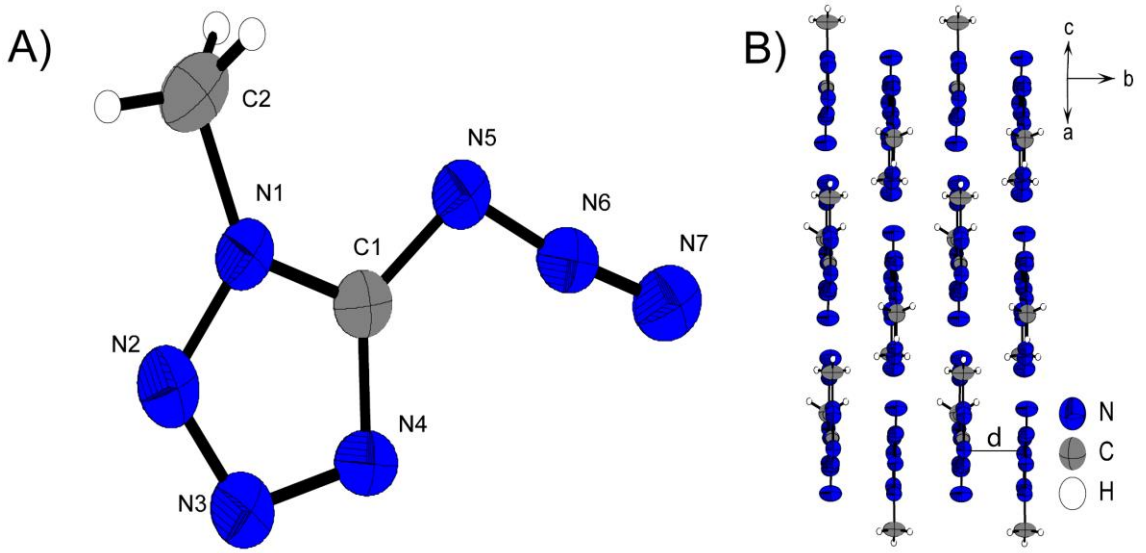

Figure 8. A) Molecular unit of **11** with thermal ellipsoids drawn at the 50 % probability level. Selected bond distances (Å) and angles [°]: C1-N5 1.392(3), N5-N6 1.253(2), N6-N7 1.113(3), N1-C2 1.455(3), N2-N1-C2 121.2(2), C1-N1-C2 131.4(2), N5-N6-N7 172.5(2), N6-N5-C1-N4 0.0(2); B) Layer structure of **11**.

The 1- and 2-methyl substituted 5-azidotetrazoles both crystalize in monoclinic systems, $P2_1/m$ for **11** and $P2_1/c$ for **12**. This also results in similar three-dimensional arrangements for both compounds. As shown in Figure 8B) and Figure 9B), layers are formed in the illustrated orientations. The alignment to layers is preferred firstly due to the planar character of **11** and **12**, and secondly as a result of the two hydrophobic azide and methyl substituents that do not form a good docking site for pronounced intermolecular interactions. The distances between the respective layers of the two 5-azido-methyltetrazoles are in the same range (d(**11**)=3.12 Å, d(**12**)=3.31 Å).

Despite the high structural conformity, the ordering of the molecular moieties within one layer changes as a result of the different substitution positions. **12** forms linear chains along the orientation depicted in Figure 9B), with the azide group facing the methyl group with its γ-nitrogen (N7), and is therefore tightly embraced by these protons. Since this configuration of molecular units in **12** is more space saving then in the molecular pattern of **11**, significant differences arise in the density of the isomers. **11** comes up with a density of 1.459 g cm^{-3} at 298 K whereas, **12** is about 0.08 g cm^{-3} denser than its respective one substituted isomer (ρ(**12**)=1.542 g cm^{-3}).

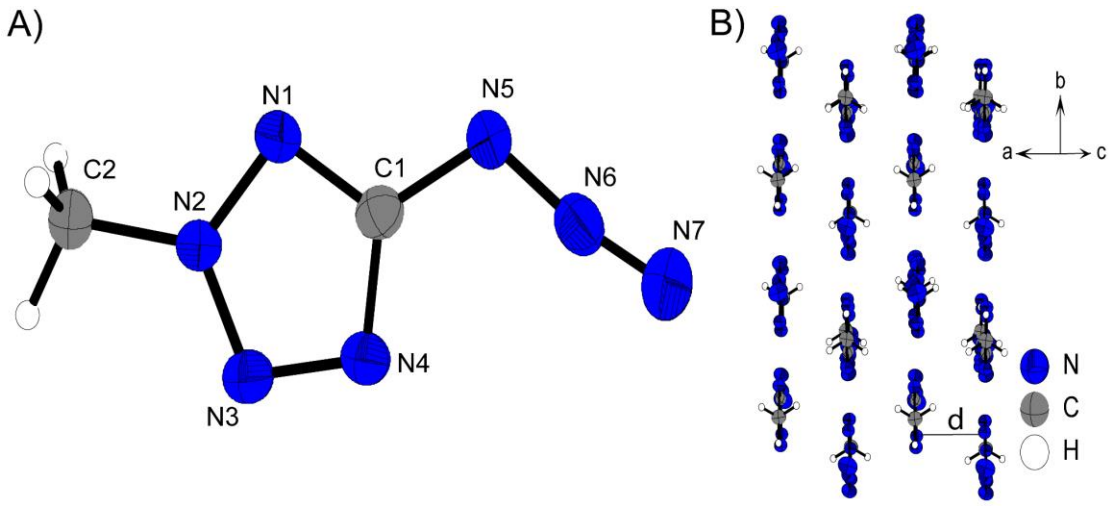

Figure 9. A) Molecular unit of **12** with thermal ellipsoids drawn at the 50 % probability level. Selected bond distances (Å) and angles [°]:C1-N5 1.394(2), N5-N6 1.259(2), N6-N7 1.113(2), N2-C2 1.448(2), N1-N2-C2 123.0(1), C2-N2-N3 123.1(1), N5-N6-N7 171.5(2), N6-N5-C1-N4 1.6(2); B) Layer structure of **12**.

12.2.3 NMR Spectroscopy

All compounds were characterized through ^{1}H and $^{13}C\{^{1}H\}$ NMR spectroscopy and the respective resonances are listed in Table 1. Resonances for the azidoethyl function at position 2 in compounds **2** and **2a**–**2d** can be found in the range of 4.69-4.94 ppm as multiplets (^{1}H) and 51.6-53.0 ppm (^{13}C) representing the CH_2-group linked to the tetrazole ring and at 3.86-3.97 ppm as multiplets (^{1}H) and 48.9–49.6 ppm (^{13}C) representing the CH_2 protons bonded to N_α. Additional proton signals for these compounds can be found for **2** (nitramine proton) as broad peak at *δ*=9.69 ppm and the cationic moieties for **2a** and **2b** at *δ*=7.17 and 10.03 ppm, respectively. The deprotonation of **2** results in a shift to deeper fields of the tetrazole carbon from 157.3 ppm for **2** by about 10 ppm for all ionic derivatives. For compounds **7** and **10** the tetrazole resonance is detected at 153 ppm in the ^{13}C NMR. For the nitratoethyl function of **10** the resonance of the CH_2 lined to the organic nitrate assigns at 5.02 ppm and the CH_2 unit bonded to N1 at 4.68 ppm. The ethylene unit of **7** shows signals at 4.20 and 3.74 ppm.

For the methyl group signals of **11** (*δ*=3.77 ppm) and **12** (*δ*=4.28 ppm), the signal for the 2-substitution is shifted to higher fields compared to the 1-substituted one. The ^{13}C shifts for **11** ($\delta(CN_4)$=152.9 ppm; $\delta(CH_3)$=33.1 ppm) and **12** ($\delta(CN_4)$=161.9 ppm; $\delta(CH_3)$=40.7 ppm) are in good accordance with other alkyl substituted 5-azidotetrazoles.[21]

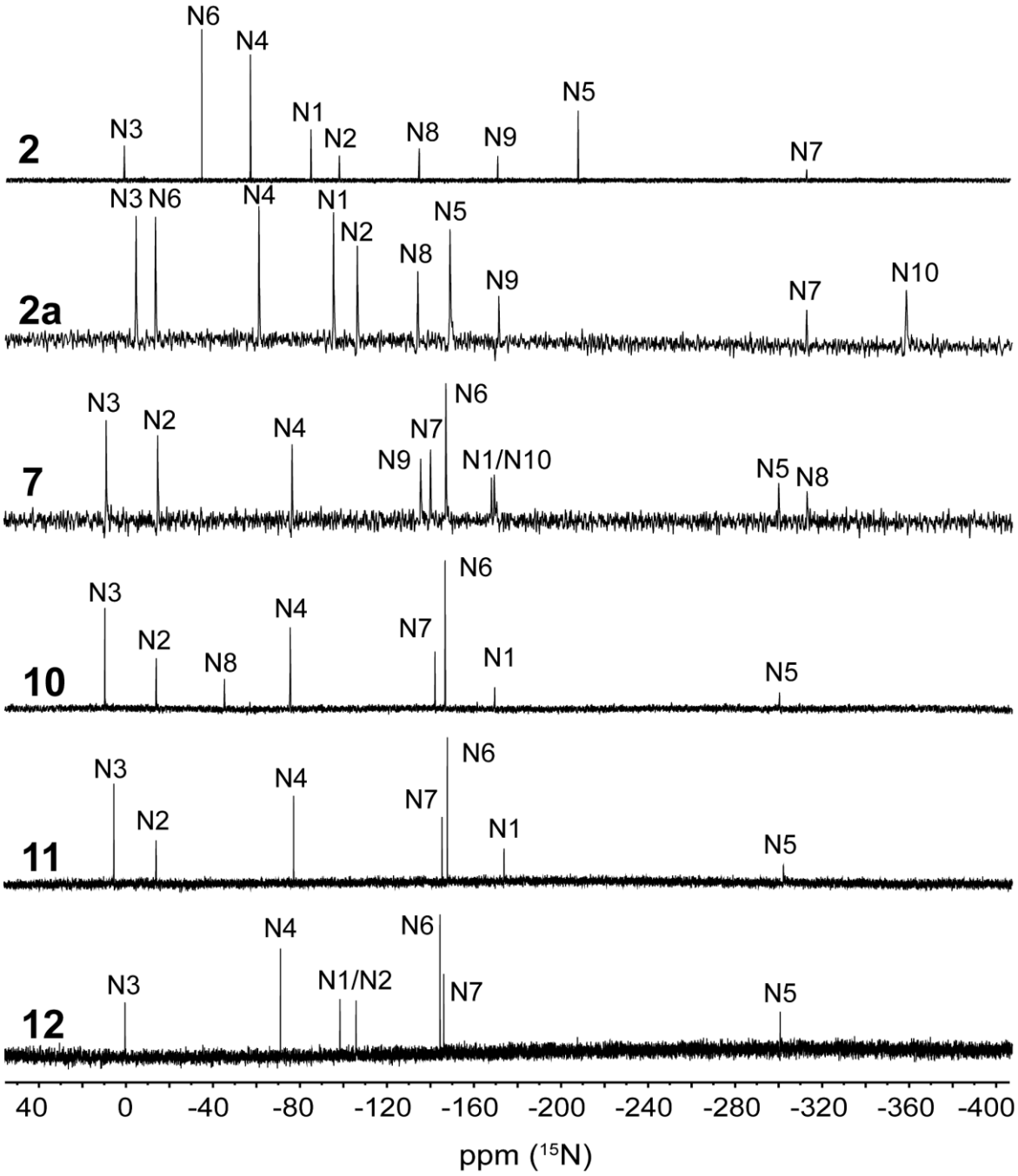

Figure 10. ^{15}N NMR spectra of compounds **2**, **2a**, **7** and **10–12**. Chemical shifts are reported in ppm with respect to $MeNO_2$. Measurements of **2**, **2a** and **11**–**12** were performed in DMSO-D_6, for **7** and **10** in $CDCl_3$ and in acetone-D_6, respectively.

Additionally, compounds **2**, **2a** (as representative for the 2-(2-azidoethyl)-5-nitraminotetrazolate anion), **7** and **10**–**12** were analyzed through proton coupled ^{15}N spectroscopy. The spectra are illustrated in Figure 10.

Table 1. ^{1}H and ^{13}C-NMR resonances for compounds **2**, **2a**-**2d**, **7** and **10**-**12** measured in DMSO-D6, chemical shifts are reported in ppm with respect to TMS ($Si(CH_3)_4$).

Compound	*δ*/ppm	
	^{1}H	^{13}C
2	9.69, 4.94, 3.97	157.3, 53.0, 48.9
2a	7.17, 4.69, 3.86	168.3, 51.6, 49.2
2b	10.03, 4.70, 3.87	168.0, 51.7, 49.2
2c	4.69, 3.87	169.0, 51.9, 49.6
2d	4.81, 3.93	166.5, 52.3, 49.0
7	4.20, 3.74	152.8, 49.1, 45.6
10	5.02, 4.68	152.9, 69.8, 43.8
11	3.77	152.9, 33.1
12	4.28	161.9, 40.7

The nitrogen atoms are named as in the corresponding crystal structures. For the tetrazole moieties, signals for all four nitrogen atoms can be found in very similar ranges, depending on the substitution site (1- and 2-substituted). For 1-substituted tetrazoles **7**, **10** and **11** signals appear at around 0 ppm for N3, −13 ppm for N2, −75 ppm for N4 and −170 ppm for N1. For two substituted isomers **2**, **2a** and **12**, the chemical shifts for N3 and N4 do not differ hardly compared with 1-substituted isomers. Values for N1 and N2 can be found around −90 ppm and −102 ppm, respectively.

The same applies to the azide functionalities. Here, however, a distinction must be made between aromatic and alkyl azides. Resonances for aromatic azides can be found in the spectra of compounds **7** and **10**–**12** in typical ranges of around −300 ppm for N_α, −145 ppm for N_β and −143 ppm for N_γ, whereas N_β having the highest intensity, followed by N_γ and N_α being the less intensive signal. Compared to the aromatic azides, alkyl azide resonances appear high-field shifted at around −315 ppm for N_α, −171 ppm for N_β and −135 ppm for N_γ with equal intensities. These signals are detectable for compounds **2**, **2a** and **7**. In the case of aromatic azides, the signals of N_β and N_γ appear relatively close together, whereas for alkyl

azides, there is a clear gap of around 35 ppm between the two signals. N_γ always emerges at higher fields than N_β.

Additional signals can be found in the spectra of **2**, **2a** and **10**. These are the nitro group of the protonated nitramine function (N6) of **2** at −34.7 ppm, the nitro group of the deprotonated nitramine function (N6) in **2a** at −13.9 ppm and the organic nitrate (N8) of **10** at −13.3 ppm.

12.2.4 Physico-chemical Properties

Compounds **2**, **2a**–**2d**, **7** and **10**–**12** were tested toward the behavior on certain external stimuli as there are impact, friction, electrostatic discharge and temperature (DTA or DSC). The resulting values are listed in Table 2. All investigated compounds can be declined as energetic materials, since they are more or less sensitive facing those external stimuli, according to UN Recommendations on the Transport of Dangerous Goods.[22] The free acid of 2-azidoethyl-5-nitraminotetrazole **2** is insensitive toward friction and shows an impact sensitivity of 10 J. The two nitrogen-rich salts (**2a** and **2b**) are moderately sensitive, whereas the two metal-containing salts (**2c** and **2d**) are already classified as extremely sensitive with **2d** being the most sensitive compound of the 2-azidoethyl-5-nitramino derivatives (IS < 1 J, FS = 15 N). All 5-azidotetrazole derivatives (**7**, **10**–**12**) show impact sensitivities less or equal to 1 J and friction sensitivities of 5 N (for **10**) or below for **7**, **11** and **12** and are therefore classified as sensitive explosives. Metal containing ionic derivatives **2c** and **2d** are the thermally most stable compounds in this study decomposing at 180 °C and 181 °C, respectively. Nitrogen-rich derivatives **2a** and **2b** decompose around 170 °C, whereby **2a** shows a smooth melting point at 113 °C. The free nitramine **2** is even liquid after long time storage −30 °C and explodes violently at 93 °C. 5-Azidotetrazole derivatives **7** and **10**–**12** all undergo decomposition between 160 °C and 167 °C and possess a melting point in advance. Compound **7** is liquid at room temperature and melts at about −20 °C, **10**, **11** and **12** are solids at ambient temperatures and melt at 45 °C, 20 °C and 62 °C, respectively. Based on the densities and the calculated enthalpies of formation, the detonation parameters for all metal-free were calculated using the EXPLO5 code.

Table 2. Energetic properties and detonation parameters of **2**, **2a**-**2d**, **7** and **10**-**12**.

	2	**2a**	**2b**	**2c**	**2d**	**7***	**10**	**11**	**12**
Formula	$C_3H_5N_9O_2$	$C_3H_8N_{10}O_2$	$C_3H_8N_{10}O_3$	$C_3H_4N_9O_2K$	$C_3H_4N_9O_2Ag$	$C_3H_4N_{10}$	$C_3H_4N_8O_3$	$C_2H_3N_7$	$C_2H_3N_7$
M [g mol^{-1}]	199.1	216.2	232.2	237.2	306.0	180.1	200.1	125.1	125.1
IS [J][a]	10	30	9	1	<1	<1	1	<1	<1
FS [N][b]	360	120	40	30	15	<0.1	5	<5	<5
ESD [mJ][c]	-	100	100	25	13	-	10	50	80
ρ [g cm^{-3}][d]	1.60*	1.575	1.624	1.93*	2.362	1.519	1.638	1.459	1.542
N [%][e]	62.4	64.8	60.3	53.1	41.2	77.8	56.0	78.4	78.4
Ω [%][f]	−28.1/ −52.2	−37.0/ −59.2	−27.6 /−48.2	−20.2/ −40.5	−15.7/ −31.4	−44.4/ −71.1	−16.0/ −40.0	−44.8/ −70.3	−44.8 /−70.3
T_{melt}/T_{dec} [°C][g]	n.d./ 93	113/ 172	-/ 171	126/ 180	-/ 181	−20/ 167	45/ 166	20/ 160	62/ 162
Δ_fH^0 [kJ mol^{-1}][h]	647.1	649.1	705.5	-	-	932.7	514.5	594.5	566.9
Δ_fU^0 [kJ mol^{-1}][i]	666.9	673.9	731.5	-	-	950.1	533.1	606.9	579.3
				EXPLO5 V6.05.02					
$-\Delta_{Ex}U^0$ [kJ kg^{-1}][j]	5282	5199	6281	-	-	5123	5409	4769	4563
T_{det} [K][k]	3650	3321	3845	-	-	3535	3872	3383	3199
V_0 [L kg^{-1}][l]	833	889	889	-	-	802	809	817	810
P_{CJ} [kbar][m]	248	256	295	-	-	215	261	202	216
V_{det} [m s^{-1}][n]	8138	8430	8796	-	-	7898	8165	7616	7916

[a] Impact sensitivity (BAM drophammer (1 of 6)). [b] Friction sensitivity (BAM friction tester (1 of 6)). [c] Electrostatic discharge device (OZM research). [d] From X-Ray diffraction analysis recalculated to 298 K; *pycnometric measurement. [e] Nitrogen content. [f] Oxygen balance with respect to CO/CO2 [g] Decomposition temperature (DTA/DSC; β = 5 °C min−1). [h] Calculated enthalpy of formation. [i] Calculated energy of formation. [j] Energy of explosion. [k] Detonation temperature. [l] Volume of detonation products (assuming only gaseous products). [m] Detonation pressure at Chapman-Jouguet point. [n] Detonation velocity. *Explo5 V6.05.02 calculation for the theoretical solid state at room temperature.

All investigated compounds show highly positive values for their heat of formation, with **9**, containing two azido moieties showing the overall highest heat of formation of Δ_fH^0 = 932.7 kJ mol^{-1}. The calculated detonation velocity for **2b** is 8796 m s^{-1} and therefore in the range of RDX (V_{det} = 8801 m s^{-1}). The performance parameters of the corresponding ammonium derivative as well as of the neutral compound are significantly lower, since they have both lower density and enthalpy of formation. Ethyl substituted 5-azidotetrazoles **7** and **10** differ about 270 m s^{-1} is their detonation velocity, whereas nitratoethyl derivative **10** has the higher value with 8165 m s^{-1}. This trend is in accordance with recently published ethyl substituted 5,5'-azobistetrazoles.[9a] In terms of detonation parameters, two methyl

substituted 5-azidotetrazole (**12**) is clearly superior to its one substituted isomer **11**. The detonation velocities are 7616 m s^{-1} for **11** and 7916 m s^{-1} for **12** and thus exactly 300 m s^{-1} apart, which is mainly attributed to the different densities. Unfortunately, the calculated detonation parameters fell short of expectations due to the low densities of the compounds. Both 5-azidotetrazole backbones and azidoethyl substitutions yield enormous increases in the calculated formation detonation parameters, but the nonpolar properties of the substituents offer only limited opportunities for attractive interactions.

12.3 Conclusion

By introducing azidoethyl, nitratoethyl and methyl groups to 5-azidotetrazoles, the physico-chemical properties could be specifically modified. Nitratoethyl shows a lower sensitivity and a higher melting point (45 °C) with better performance (8165 m s^{-1}) then the respective azidoethyl homologue. Furthermore, the methyl functionalization at N2 not only outperforms its N1-isomer in terms of physico-chemical properties but also shows a much easier synthesis. The melting points of the isomers differ by 40 °C with the 2-isomer melting at 62 °C. The decomposition temperatures of the 5-azides are not altered by functionalization. The sensitivities are all in the area of primary explosives with 1-(2-azidoethyl)-5-azidotetrazole (**7**) being the most sensitive compound which is unusual because this compound is a liquid.

With the synthesis of 2-(2-azidoethyl)-5-nitraminotetrazole (**2**) and its nitrogen rich ionic derivatives (**2a**, **b**) new highly energetic secondary explosives were discovered. The hydroxylammonium salt **2b** owns the best explosive performance in this study with a detonation velocity of about 8800 m s^{-1}. The metal salts (**2c**, **d**) are more sensitive explosives and as all ionic derivatives in this work stable up to 180 °C.

12.4 Acknowledgement

For financial support of this work by Ludwig-Maximilian University (LMU), the Office of Naval Research (ONR) under grant no. ONR N00014-19-1-2078 and the

Strategic Environmental Research and Development Program (SERDP) under contract no. W912HQ19C0033 are gratefully acknowledged. We thank Prof. Dr. Konstantin Karaghiosoff for the measurement of the ^{15}N NMR spectra. Open Access funding enabled and organized by Projekt DEAL.

12.5 References

[1] a) J. P. Agrawal, R. D. Hodgson, *Organic Chemistry of Explosives*, 1 ed., John Wiley & Sons Inc., Chichester, **2006**; b) J. Köhler, R. Meyer, A. Homburg, *Explosivstoffe*, 10 ed., Wiley-VCH Weinheim, **2008**.

[2] T. M. Klapötke, *Chemistry of High-Energy Materials,* 5 ed*.,* De Gruyter, **2019**.

[3] M. A. S. Laidlaw, G. Filippelli, H. Mielke, B. Gulson, A. S. Ball, *Environ. Health* **2017**, *16*, 34.

[4] a) U. S. E. P. Agency, "Technical Fact Sheet - 2,4,6-Trinitrotoluene (TNT)" can be found under https://www.epa.gov/fedfac/technical-fact-sheet-246-trinitrotoluene-tnt, **2022**; b) M. L. Gettings, M. T. Thoenen, E. F. C. Byrd, J. J. Sabatini, M. Zeller, D. G. Piercey, *Chem. Eur. J.* **2020**, *26*, 14530.

[5] E. C. Johnson, J. J. Sabatini, D. E. Chavez, R. C. Sausa, E. F. C. Byrd, L. A. Wingard, P. E. Guzmàn, *Org. Process Res. Dev.* **2018**, *22*, 736–740.

[6] A. B. Sheremetev, S. F. Mel'nikova, E. S. Kokareva, R. E. Nekrutenko, K. V. Strizhenko, K. Y. Suponitsky, T. D. Pham, A. N. Pivkina, V. P. Sinditskii, *Def. Technol.* **2021**.

[7] P. Gaur, S. Dev, S. Kumar, M. Kumar, A. A. Vargeese, P. Soni, P. F. Siril, S. Ghosh, *ACS Omega* **2017**, *2*, 8227–8233.

[8] Y. Tang, J. M. Shreeve, *Chem. - Eur. J.* **2015**, *21*, 7285–7291.

[9] a) M. Benz, M. S. Gruhne, T. M. Klapötke, N. Krüger, T. Lenz, M. Lommel, J. Stierstorfer, *Eur. J. Org. Chem.* **2021**, *2021*, 4388–4392; b) N. Fischer, T. M. Klapötke, J. Stierstorfer, C. Wiedemann, *Polyhedron* **2011**, *30*, 2374–2386; c) Y.-H. Joo, J. M. Shreeve, *Angew. Chem.* **2009**, *48*, 564–567; d) J. Stierstorfer, K. R. Tarantik, T. M. Klapötke, *Chem. - Eur. J.* **2009**, *15*, 5775–5792; e) R. Yang, Z. Dong, Z. Ye, *ChemistrySelect* **2019**, *4*, 14208–14213.

[10] S. Song, F. Chen, Y. Wang, K. Wang, M. Yan, Q. Zhang, *J. Mater. Chem. A* **2021**, *9*, 21723–21731.

[11] R. M. Herbst, J. A. Garrison, *J. Org. Chem.* **1953**, *18*, 941–945.

[12] E. Lieber, D. R. Levering, *J. Am. Chem. Soc.* **1951**, *73*, 1313–1317.

[13] a) J. Stierstorfer, T. M. Klapötke, A. Hammerl, R. D. Chapman, *Z. Anorg. Allg. Chem.* **2008**, *634*, 1051–1057; b) N. Fischer, T. M. Klapötke, J. Stierstorfer, *Z. Anorg. Allg. Chem.* **2009**, *635*, 271–281.

[14] a) T. M. Klapötke, J. Stierstorfer, *J. Am. Chem. Soc.* **2009**, *131*, 1122–1134; b) T. Fendt, N. Fischer, T. M. Klapötke, J. Stierstorfer, *Inorg. Chem.* **2011**, *50*, 1447–1458.

[15] D. E. Bayes (Glaxo Group Limited), EP0117368A1, **1982**.

[16] a) J. A. Garrison, R. M. Herbst, . *Org. Chem.* **1957**, *22*, 278–283; b)T. M. Klapötke, J. Stierstorfer, *Helv. Chim. Acta* **2007**, *90*, 2132–2150.

[17] a) M. H. H. Wurzenberger, M. S. Gruhne, M. Lommel, V. Braun, N. Szimhardt, J. Stierstorfer, *Inorg. Chem.* **2020**, *59*, 17875–17879; b) G.-G. Gao, P.-S. Cheng, T. C. W. Mak, *J. Am. Chem. Soc.* **2009**, *131*, 18257–18259; c) Q.-Y. Wang, J. Wang, S. Wang, Z.-Y. Wang, M. Cao, C.-L. He, J.-Q. Yang, S.-Q. Zang, T. C. W. Mak, *J. Am. Chem. Soc.* **2020**, *142*, 12010–12014.

[18] P. Ai, A. A. Danopoulos, P. Braunstein, K. Y. Monakhov, *Chem. Commun.* **2014**, *50*, 103–105.

[19] a) H. Schmidbaur, A. Schier, *Angew. Chem.* **2015**, *54*, 746–784; b) L. Mistry, O. El-Zubir, G. Dura, W. Clegg, P. G. Waddell, T. Pope, W. A. Hofer, N. G. Wright, B. R. Horrocks, A. Houlton, *Chem. Sci.* **2019**, *10*, 3186–3195.

[20] M. S. Gruhne, T. Lenz, M. Rösch, M. Lommel, M. H. H. Wurzenberger, T. M. Klapötke, J. Stierstorfer, *Dalton Trans.* **2021**, *50*, 10811–10825.

[21] T. M. Klapötke, S. M. Sproll, *Eur. J. Org. Chem.* **2009**, *2009*, 4284–4289.

[22] U. Nations, in *Manual of Tests and Criteria, Vol. ST/SG/AC.10/11/Rev.6* New York and Geneva, **2015**.

12.6 Supporting Information

12.6.1 Experimental Procedure

^{1}H, ^{13}C, ^{14}N and ^{15}N NMR spectra were recorded on *BRUKER AMX 400* instruments. Chemical shifts are referenced with respect to tetramethylsilane ($^{1}H/^{13}C$) and nitromethane ($^{14}N/^{15}N$). Infrared spectra (IR) were recorded in the region 4000-400 cm^{-1} on a *PERKIN ELMER Spectrum BX-59343* instrument with a *SMITHS DETECTION DuraSamplIR II Diamond ATR* sensor. The absorption bands are reported in wavenumbers (cm^{-1}). Decomposition temperatures were measured via differential thermal analysis (DTA) with an *OZM Research DTA 552-Ex* instrument at a heating rate of 5 °C/min and in a range of room temperature to 400 °C. All sensitivities toward impact (IS) and friction (FS) were determined according to BAM (Bundesanstalt für Materialforschung und Prüfung) standards using a BAM drop hammer and a BAM friction apparatus by applying the 1 of 6 method.[S1] All energetic compounds were tested for sensitivity towards electrical discharge using an *Electric Spark Tester ESD 2010 EN* from OZM. Energetic properties have been calculated with the EXPLO5 6.02 computer [S2] code using the RT converted X-ray density or the densities measured with a gas pycnometer at 298 K and calculated solid state heats of formation.

CAUTION! *All investigated compounds are potentially explosive materials. In particular compound **7**, 1-(2-azidoethyl)-5-azidotetrazole, is extremely sensitive and tends to explode during solidification. Safety precautions and equipment (such as wearing leather coat, face shield, Kevlar sleeves, Kevlar gloves, earthed equipment and ear plugs) must be used during all manipulations.*

2-(2-Azidoethyl)-5-nitraminotetrazole (**2**)[S3]

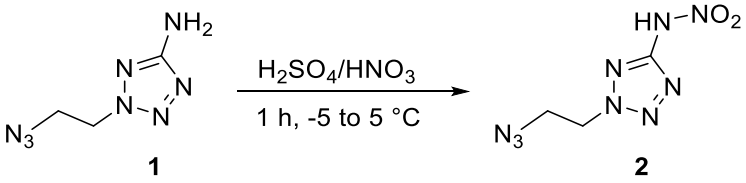

1 **2**

2-(2-Azidoethyl)-5-aminotetrazole (**1**) (1.00 g, 6.50 mmol, 1.0 eq) was dropwise added to a mixture of sulfuric acid (96%, 8.00 mL) and nitric acid (100%, 3.00 mL) keeping the temperature below 5 °C (*CAUTION!* By rising the temperature above 5 °C, the reaction mixture decomposes exothermically including the formation of large amount of nitrous gases, heat and flames in the reaction flask). The mixture was stirred for 1 h and was allowed to heat to 5 °C. The mixture was poured on ice water (150 mL) and extracted with diethyl ether (3 x 50 mL). After drying over anhydrous sodium sulfate, the organic solvent was evaporated, the title compound **2** was obtained as slightly brownish liquid (1.16 g, 5.60 mmol, 86%).

DTA (5 °C min^{-1}): 93 °C (dec); Sensitivities: BAM drop hammer: 10 J (liquid), friction tester: 360 N (liquid), ESD: -; IR (ATR) $\tilde{\nu}$ (cm^{-1}) = 3023(w), 2102(s), 1700(w), 1610(s), 1488(m), 1440(m), 1299(vs), 1227(s), 1097(m), 1029(m), 893(m), 827(m), 758(m), 632(m), 554(m), 493(s), 445(m), 435(m), 428(m), 419(m), 412(m); Elem. Anal. ($C_3H_5N_9O_2$, 199.13 g mol^{-1}) calcd.: C 18.09, H 2.53, N 63.31 %. Found: C 17.94, H 2.82, N 62.37 %; ^{1}H NMR (DMSO-D_6, 400 MHz, ppm) δ = 9.69 (br s, 1H), 4.94 (m, 2H), 3.97 (m, 2H); ^{13}C NMR (DMSO-D_6, 101 MHz, ppm) δ = 157.3, 53.0, 48.9; ^{15}N NMR (DMSO-D_6, 41 MHz, ppm) δ = 1.0, −34.7, −57.1, −85.0, −98.1, −134.9, −171.2, −208.2, −313.5 ; HRMS (ESI) *m/z*: [M – H^+] Calcd for $C_3H_4N_9O_2$ 198.0493; Found: 198.0492.

Ammonium 2-(2-azidoethyl)-5-nitraminotetrazolate (**2a**)

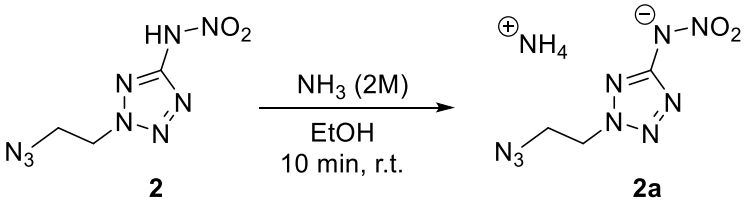

2 **2a**

2-(2-Azidoethyl)-5-nitraminotetrazole (**2**) (0.69 g, 3.47 mmol, 1.0 eq) was dissolved in ethanol (25 mL) and ammonia (2M dissolved in ethanol, 1.75 mL, 3.50 mmol, 1.0 eq) was added dropwise. The solvent was reduced and the precipitate was filtered to yield pure ammonium 2-(2-azidoethyl)-5-nitraminotetrazolate (**2a**) (0.66 g, 3.06 mmol, 88%) as brown solid.

DTA (5 °C min^{-1}): 113 °C (melt), 172 °C (dec); Sensitivities: BAM drop hammer: 30 J (≤ 500 µm), friction tester: 120 N (≤ 500 µm), ESD: 0.1 J (≤ 500 µm). IR (ATR) $\tilde{\nu}$ (cm^{-1}) = 3194(s), 2120(s), 1480(s), 1463(s), 1452(s), 1434(s), 1397(s), 1367(s), 1343(s), 1294(vs), 1240(s), 1204(s), 1168(s), 1097(s), 1059(m), 1036(s), 1013(s), 974(s), 953(m), 888(s), 833(s), 771(s), 757(s), 742(m), 699(s), 675(m), 646(m), 560(m), 512(s), 467(s), 448(m); Elem. Anal. ($C_3H_8N_{10}O_2$, 216.17 g mol^{-1}) calcd.: C 16.67, H 3.73, N 64.80 %. Found: C 16.75, H 3.80, N 63.48 %; ^{1}H NMR (DMSO-D_6, 400 MHz, ppm) δ = 7.17 (s, 4H), 4.69 (m, 2H), 3.86 (m, 2H); ^{13}C NMR (DMSO-D_6, 101 MHz, ppm) δ = 168.3, 51.6, 49.2; ^{15}N NMR (DMSO-D_6, 41 MHz, ppm) δ = −5.0, −13.9, −61.4, −95.6, −106.5, −134.3, −149.0, −171.4, −312.7, −358.4.

Hydroxylammonium 2-(2-azidoethyl)-5-nitraminotetrazolate (**2b**)

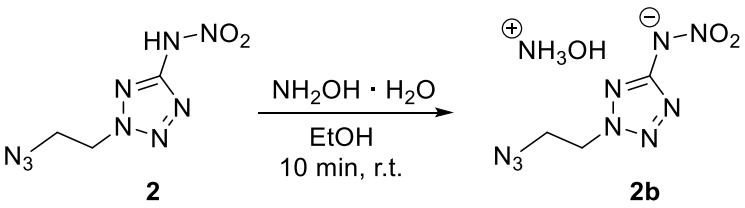

2 **2b**

2-(2-Azidoethyl)-5-nitraminotetrazole (**2**) (0.87 g, 4.47 mmol, 1.0 eq) was dissolved in ethanol (18 mL) and aqueous hydroxylamine solution (50% w/w, 0.28 mL, 4.70 mmol, 1.05 eq) was added dropwise. The solvent was reduced and the precipitate was filtered to yield pure hydroxylammonium 2-(2-azidoethyl)-5-nitraminotetrazolate (**2b**) (0.85 g, 3.66 mmol, 82%) as yellow solid.

DTA (5 °C min^{-1}): 171 °C (dec); Sensitivities: BAM drop hammer: 9 J (≤ 500 µm), friction tester: 40 N (≤ 500 µm), ESD: 0.1 J (≤ 500 µm). IR (ATR) $\tilde{\nu}$ (cm^{-1}) = 3112(m), 2691(m), 2141(s), 2102(s), 1485(s), 1437(s), 1406(s), 1358(s), 1341(vs), 1290(vs), 1238(s), 1213(s), 1169(vs), 1119(s), 1101(s), 1038(s), 1009(s), 953(m), 897(m), 884(m), 839(m), 775(s), 751(s), 695(m), 688(m), 669(s),

626(s), 555(s), 502(s), 456(s), 441(s); Elem. Anal. ($C_3H_8N_{10}O_3$, 232.16 g mol^{-1}) calcd.: C 15.52, H 3.47, N 60.33 %. Found: C 14.90, H 3.63, N 59.85 %; ^{1}H NMR (DMSO-D_6, 400 MHz, ppm) δ = 10.03 (br s, 4H), 4.70 (m, 2H), 3.87 (m, 2H); ^{13}C NMR (DMSO-D_6, 101 MHz, ppm) δ = 168.0, 51.7, 49.2; ^{14}N NMR (DMSO-D_6, 29 MHz, ppm) δ = −3, −13, −134, −173, −359.

Potassium 2-(2-azidoethyl)-5-nitraminotetrazolate (**2c**)

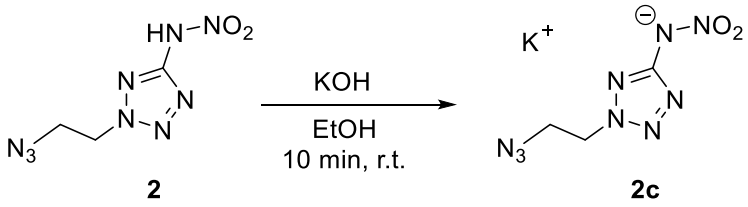

2 **2c**

2-(2-Azidoethyl)-5-nitraminotetrazole (**2**) (0.85 g, 4.24 mmol, 1.0 eq) was dissolved in ethanol (18 mL) and potassium hydroxide (0.24 g, 4.24 mmol, 1.0 eq) dissolved in ethanol (8 mL) was added in one portion. The immediately formed solid was filtered and washed with little amount of cold ethanol to yield potassium 2-(2-azidoethyl)-5-nitraminotetrazolate (**2c**) (0.90 g, 3.80 mmol, 90%) as brownish solid.

DTA (5 °C min^{-1}): 126 °C (melt), 180 °C (dec); Sensitivities: BAM drop hammer: 1 J (≤ 500 µm), friction tester: 30 N (≤ 500 µm), ESD: 25 mJ (≤ 500 µm). IR (ATR) $\tilde{\nu}$ (cm^{-1}) = 2118(s), 2080(m), 1486(s), 1417(s), 1407(s), 1383(s), 1320(vs), 1299(vs), 1261(s), 1208(s), 1099(s), 1041(s), 1006(s), 971(m), 944(m), 883(m), 828(s), 777(s), 760(s), 696(m), 647(m), 557(m), 507(m), 463(m); Elem. Anal. ($C_3H_4N_8O_2K$, 237.22 g mol^{-1}) calcd.: C 15.19, H 1.70, N 53.14 %. Found: C 15.49, H 1.80, N 52.10 %; ^{1}H NMR (DMSO-D_6, 400 MHz, ppm) δ = 4.69 (m, 2H), 3.87 (m, 2H); ^{13}C NMR (DMSO-D_6, 101 MHz, ppm) δ = 169.0, 51.9, 49.6; ^{14}N NMR (DMSO-D_6, 29 MHz, ppm) δ = −12, −135, −173.

Silver 2-(2-azidoethyl)-5-nitraminotetrazolate (**2d**)

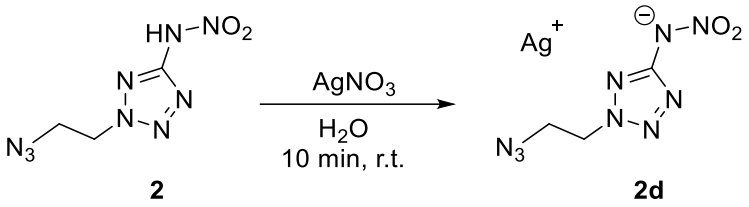

2 **2d**

2-(2-Azidoethyl)-5-nitraminotetrazole (**2**) (0.29 g, 1.43 mmol, 1.0 eq) was dissolved in ethanol (5 mL) and silver nitrate (0.25 g, 1.45 mmol, 1.0 eq) dissolved in water (5 mL) was added in one portion. The immediately formed solid was filtered and washed with little amount of cold water to obtain silver 2-(2-azidoethyl)-5-nitraminotetrazolate (**2d**) (0.43 g, 1.40 mmol, 98%) in quantitative yield as beige powder.

DTA (5 °C min^{-1}): 181 °C (dec); Sensitivities: BAM drop hammer: <1 J (≤ 500 µm), friction tester: 15 N (≤ 500 µm), ESD: 13 mJ (≤ 500 µm). IR (ATR) $\tilde{\nu}$ (cm^{-1}) = 2138(s), 2101(s), 1509(s), 1438(s), 1406(s), 1357(s), 1343(s), 1286(vs), 1213(s), 1170(s), 1120(m), 1101(m), 1038(s), 1010(s), 952(m), 884(m), 752(m), 743(m), 694(m), 689(m), 670(s), 626(m), 555(m), 503(m), 456(m), 441(m); Elem. Anal. ($C_3H_4N_8O_2Ag$, 305.99 g mol^{-1}) calcd.: C 11.78, H 1.32, N 41.20 %. Found: C 11.77, H 1.51 N 40.29 %; ^{1}H NMR (DMSO-D_6, 400 MHz, ppm) δ = 4.81 (m, 2H), 3.93 (m, 2H); ^{13}C NMR (DMSO-D_6, 101 MHz, ppm) δ = 166.5, 52.3, 49.0; ^{14}N NMR (DMSO-D_6, 29 MHz, ppm) δ = −16, −135.

1-(2-Azidoethyl)-5-bromotetrazole (**4a**)

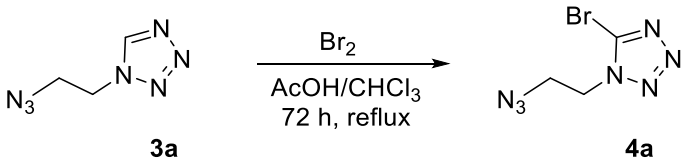

3a **4a**

To a solution of 1-(2-azidoethyl)-tetrazole (**3a**) (5.00 g, 35.9 mmol, 1.0 eq) in acetic acid (35 mL) and chloroform (70 mL) was added bromine (11.5 g, 71.8 mmol, 2.0 eq) in chloroform (15 mL). After 72 h at reflux the solvent was evaporated and excess saturated sodium bicarbonate solution was added to the residue. The

mixture was extracted with ethyl acetate (3 x 100 mL), the solvent was dried over sodium sulfate and removed to yield 1-(2-azidoethyl)-5-bromotetrazole (**4a**) (6.60 g, 30.3 mmol, 84%) as yellow liquid.

Sensitivities: BAM drop hammer: 40 J (liquid), friction tester: >360 N (liquid); IR (ATR) $\tilde{\nu}$ (cm^{-1}) = 2099(vs), 1455(m), 1429(s), 1414(s), 1398(s), 1352(m), 1286(m), 1248(m), 1228(m), 1180(s), 1123(m), 981(w), 826(w), 663(m), 647(m), 631(m), 494(m); Elem. Anal. ($C_3H_4N_7Br$, 218.02 g mol^{-1}) calcd.: C 16.53, N 44.97, H 1.85%. Found: C 16.40, N 43.27, H 2.00%; ^{1}H NMR (DMSO-D_6, 400 MHz, ppm) δ = 4.63 – 4.59 (m, 2H), 3.93 – 3.86 (m, 2H).^{13}C NMR (DMSO-D_6, 101 MHz, ppm) δ = 135.0, 49.1, 42.5; HR-MS (ESI, 70 eV): [$C_3H_5N_7Br_2$] calcd.: 297.8879 [M – Br^-], found: 297.8882.

5-Bromo-1-(2-acetoxyethyl)-tetrazole (**4b**)[S4]

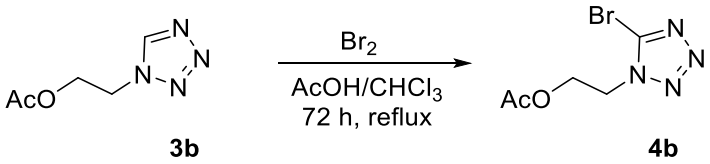

3b **4b**

To a solution of 1-(2-acetoxyethyl)-tetrazole (**3b**) (4.1 g, 26 mmol, 1.0 eq) in acetic acid (25 mL) and chloroform (50 mL) was added bromine (2.7 ml, 8.4 g, 52 mmol, 2.0 eq) in chloroform (10 mL). After 72 h at reflux the solvent was evaporated and excess saturated sodium bicarbonate solution was added to the residue. The mixture was extracted with ethyl acetate (3 x 50 mL), the solvent was dried over sodium sulfate and removed to yield 5-bromo-1-(2-chloroethyl)-tetrazole (**4b**) (5.8 g, 25 mmol, 95%) as yellow liquid.

^{1}H NMR (DMSO-D_6, 400 MHz, ppm) δ = 4.69 (m, 2H), 4.44 (m, 2H), 1.96 (s, 3H); ^{13}C NMR (DMSO-D_6, 101 MHz, ppm) δ = 170.0, 135.0, 61.2, 47.4, 20.4.

1-(2-Azidoethyl)-5-hydraziniumtetrazole chloride (**6**)

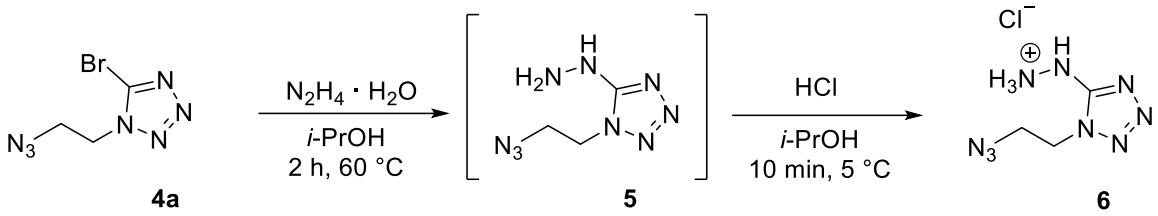

To a solution of 1-(2-azidoethyl)-5-bromotetrazole (**4a**) (1.00 g, 4.57 mmol, 1.0 eq.) in 2-propanole (20 mL) was added hydrazine hydrate (100%, 0.66 ml, 13.70 mmol, 3.0 eq.). After 2 h at 60 °C the solvent was removed and the residue was dissolved in water (50 mL) and extracted with ethyl acetate (3 x 50 mL). The organic phase was dried over sodium sulfate and evaporated to yield a crude oil of 1-(2-azidoethyl)-5-hydrazineyltetrazole (**5**) that forms colorless crystals over time. (^{1}H NMR (DMSO-D_6, 400 MHz, ppm) δ = 8.14 (s, 1H), 4.48 (s, 2H), 4.44 – 4.37 (m, 2H), 3.78 – 3.68 (m, 2H). ^{13}C NMR (DMSO-D_6, 101 MHz, ppm) δ = 158.3, 48.9, 44.9; HR-MS (ESI, 70 eV): [$C_3H_8N_9$] calcd.: 170.0898 [M – H^+], found: 170.0899. The residue was then dissolved in 2-propanol (10 mL) and an excess of a solution of HCl in 2-propanol (4-6 N, 3 mL) was added. After full precipitation and crystallization at 5 °C over night the product was filtered and washed with ether to yield white solid 1-(2-azidoethyl)-5-hydraziniumtetrazol chloride (**6**) (498 mg, 2.42 mmol, 53%).

Sensitivities: BAM drop hammer: >40 J (≤ 500 µm), friction tester: >360 N (≤ 500 µm); IR (ATR) $\tilde{\nu}$ (cm^{-1}) = 3204(m), 2788(s), 2646(s), 2593(s), 2138(s), 2096(vs), 1599(s), 1570(vs), 1548(s), 1494(s), 1444(s), 1421(s), 1370(m), 1343(s), 1331(m), 1300(s), 1278(s), 1253(m), 1184(m), 1125(m), 1102(s), 1063(m), 1009(s), 971(m), 827(s), 732(s), 667(m), 607(s), 534(s), 486(s); Elem. Anal. ($C_3H_8N_9Cl$, 205.61 g mol^{-1}) calcd.: C 17.52, H 3.92, N 61.31 %. Found: C 18.01, H 4.09, N 60.24 %; ^{1}H NMR (D_2O, 400 MHz, ppm) δ = 4.52 – 4.26 (m, 2H), 3.98–3.54 (m, 2H).^{13}C NMR (DMSO-D_6, 101 MHz, ppm) δ = 154.6, 48.9, 46.1.; ^{14}N NMR (DMSO-D_6, 29 MHz, ppm) δ = −135.4, −168.6; HR-MS (ESI, 70 eV): [$C_3H_7N_9Cl$] calcd.: 204.0518 [M – Cl^-], found: 204.05179.

1-(2-Azidoethyl)-5-azidotetrazole (**7**)

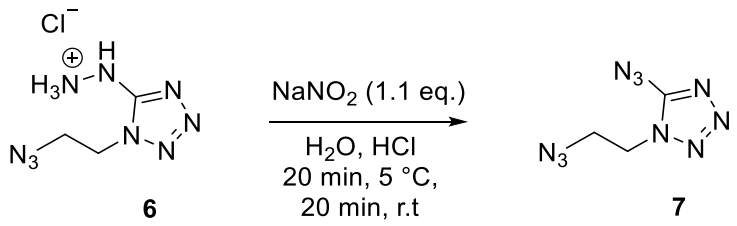

To a solution of 1-(2-azidoethyl)-5-hydraziniumtetrazol chloride (**6**) (200 mg, 0.97 mmol, 1.0 eq) in water (10 mL) and aqueous hydrochloric acid (2N, 2 mL) was added slowly sodium nitrite (74 mg, 1.07 mmol, 1.1 eq.) at 5 °C. After 20 min at 5 °C the solution was stirred at room temperature for further 20 min. Then the reaction was extracted with ether (3 x 20 mL) (using a plastic separation funnel and plastic vessels!). The organic layer was washed with water, dried over sodium sulfate and evaporated under a nitrogen stream to yield a yellowish oil of 5-azido-1-(2-azidoethyl)-tetrazole (**7**). The oil was purified by column chromatography (EtOAc/Ihex; 8/2; Rf: 0.35) to yield white **7** (265 mg, 1.71 mmol, 40%) (166 mg, 0.92 mmol, 95%) as highly sensitive colorless oil.

(**CAUTION!** *The reaction and workup have to be performed very carefully with personal protection and blast shield as the product is highly sensitive. A violent detonation occurred while handling the azido tetrazole with a glass pipette. Therefore, plastic equipment is recommended.)*

DTA (5 °C min^{-1}): 167 °C (dec.); Sensitivities: BAM drop hammer: <1 J (liquid), friction tester: <0.1 N (liquid). IR (ATR) $\tilde{\nu}$ (cm^{-1}) = 2156(s), 2101(s), 1531(vs), 1470(m), 1445(m), 1352(w), 1326(m), 1294(m), 1252(m),1226(m), 1181(m), 1125(w), 1089(m), 827(w), 723(m), 654(m), 636(w), 555(w), 528(m), 502(w), 436(w), 426(w); Elem. Anal. ($C_3H_4N_{10}$, 180.14 g mol^{-1}) calcd.: C 20.00, H 2.24, N 77.76 %. Found: not determinable; ^{1}H NMR (DMSO-D_6, 400 MHz, ppm) δ = 4.20 (m, 2H), 3.74 (m, 2H).^{13}C NMR (DMSO D_6, 101 MHz, ppm) δ 152.8, 49.1, 45.6; ^{15}N NMR ($CDCl_3$, 41 MHz, ppm) δ = 9.9, −13.9, −76.1, −135.7, −140.2, −147.3, −168.4, −169.7, −301.3, −314.4; HR-MS (ESI, 70 eV): [$C_3H_5N_{10}$] calcd.: 181.0694 [M – H^+], found: 181.0695.

5-Azido-1-(2-hydroxyethyl)-tetrazole (**9**)

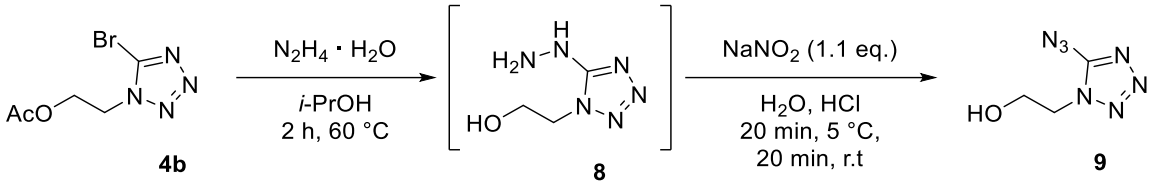

To a solution of 5-bromo-1-(2-acetoxyethyl)-tetrazole (**4b**) (1.00 g, 4.25 mmol, 1.0 eq.) in 2-propanole (25 mL) was added hydrazine hydrate (100%, 0.83 ml, 17.00 mmol, 4.0 eq.). After 72 h at ambient temperature, the precipitated crystals were removed by filtration. The solvent was evaporated to yield a crude mixture of 5-hydrazineyl-1-(2-hydroxyethyl)-tetrazole (**8**) and acetohydrazide. Without further purification the mixture was dissolved in hydrochloric acid (2M, 75 mL) and cooled to 0 – 5 °C. Slowly sodium nitrite (2.65 g, 38.2 mmol, 9.0 eq) in a little amount of water was added. After 20 min at 5 °C the solution was allowed to come to room temperature and was then extracted with ethyl acetate (3x50 mL). The organic layer was washed with water, dried over sodium sulfate and evaporated under a nitrogen stream to yield a crude oil of 5-azido-1-(2-hydroxyethyl)-tetrazole (**9**). The oil was purified by column chromatography (EtOAc/Ihex; 8/2; Rf: 0.35) to yield white crystalline **9** (265 mg, 1.71 mmol, 40%)

DTA (5 °C min^{-1}): 45 °C (melt.), 177 °C (dec.); IR (ATR) $\tilde{\nu}$ (cm^{-1}) = 2944(w), 2156(s), 2134(s), 2101(s), 1531(vs), 1470(m), 1445(m), 1352(w), 1326(m), 1252(m), 1226(m), 1181(m), 1125(w), 1089(m), 827(w), 808(w), 723(m), 654(m), 636(w), 555(w), 528(m); Elem. Anal. ($C_3H_5N_7O$, 155.12 g mol^{-1}) calcd.: C 23.23, H 3.25, N 63.21 %. Found: C 23.88, H 3.37, N 60.17 %.; ^{1}H NMR (DMSO-D_6, 400 MHz, ppm) δ = 5.05 (t, J = 5.7 Hz, 1H), 4.19 (dd, J = 5.7, 4.9 Hz, 2H), 3.74 (q, J = 5.5 Hz, 2H). ^{13}C NMR (DMSO-D_6, 101 MHz, ppm) δ = 152.6, 58.5, 49.2; ^{14}N NMR (DMSO-D_6, 29 MHz, ppm) δ = −133.8; HR-MS (EI, 70 eV): [$C_3H_5N_7O$] calcd.: 155.0556 [M^+], found: 155.0550.

5-Azido-1-(2-nitratoethyl)-tetrazole (**10**)

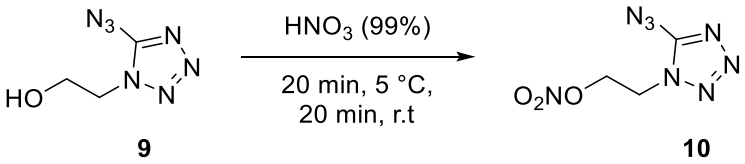

9 **10**

5-Azido-1-(2-nitratoethyl)-tetrazole (**9**) (150 mg,1.03 mmol) was added to white fuming nitric acid (99%, 2 mL) at 5°C. After 20 min the reaction was allowed to come to room temperature and after further 20 min the reaction was quenched on ice. After extraction with ethyl acetate (3x20 mL) and neutralization with saturated sodium bicarbonate solution the organic layer was washed with water, dried over sodium sulfate and evaporated under a nitrogen stream to yield a crude oil of 5-azido-1-(2-nitratoethyl)-tetrazole (**10**). For purification the oil was dissolved in a small amount of methanol (5-10% water) and left for crystallization at 5°C to yield white crystalline **10** (173 mg, 0.87 mmol, 84%)

DTA (5 °C min^{-1}): 45 °C (melt.), 166 °C (dec.); Sensitivities: BAM drop hammer: <1 J, friction tester: 5 N; IR (ATR) $\tilde{\nu}$ (cm^{-1}) = 2967(w), 2923(w), 2158(s), 1745(w), 1635(s), 1534(vs), 1471(m), 1429(m), 1331(m), 1279(vs), 1185(m), 1090(m), 1027(m), 1006(m), 885(s), 840(vs), 754(m), 724(m), 705(m), 659(m), 633(m), 528(m); Elem. Anal. ($C_3H_4N_8O_3$, 200.12 g mol^{-1}) calcd.: C 18.01, H 2.01, N 55.99 %. Found: C 18.41, H 2.36, N 54.57 %.; ^{1}H NMR (Acetone-D_6, 400 MHz, ppm) δ = 5.02 (m, 2H), 4.68 (m, 2H); ^{13}C NMR (Acetone-D_6, 101 MHz, ppm) δ = 152.9, 69.8, 43.8; ^{15}N NMR (Acetone-D_6, 41 MHz, ppm) δ = 10.5, −13.3, −44.9, −75.3, −142.3, −147.0, −169.9, −301.7; HR-MS (EI, 70 eV): [$C_3H_5N_8O_3$] calcd.: 200.0406 [M^+], found: 200.0404.

5-Azido-1-methyltetrazole (**11**)

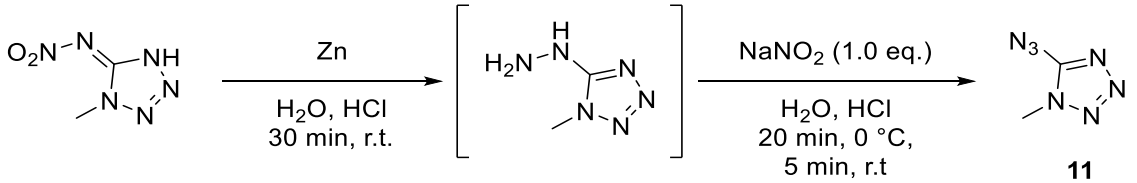

11

1-Methyl-5-nitriminotetrazole (1.44 g, 10.0 mmol, 1.0 eq) was dissolved in water (10 mL). To this, an excess of zinc powder (2.00 g) was added and the mixture was cooled using an ice bath. Hydrochloric acid (30 mL, 2 M) was added in drops and the mixture was stirred for 30 min at room temperature. After the remained zinc powder was removed by filtration a solution of sodium nitrite (0.65 g, 10.0 mmol, 1.0 eq) in water (10 mL) was added dropwise at temperatures below 0 °C until a clear formation of NO_2 was observed. After stirring the solution for further 5 min, the product was extracted DCM (3 x 20 mL). The organic phases were combined, washed once with hydrochloric acid (2 M) and two times with a concentrated solution of Na_2CO_3. The organic phase was dried using sodium sulfate and evaporated. Liquid **11** (0.78 g, 6.30 mmol, 63%) was remained which could be solidified by cooling in a freezer.

DSC (5 °C min^{-1}): 20 °C (melt.), 160 ° (dec.); Sensitivities: BAM drop hammer: <1 J; friction tester: <5 N; ESD: 50 mJ; EA ($C_2H_3N_7$, 125.11) calcd.: C 19.20, H 2.42, N 78.38 %; Found: C 19.30, H 2.81, N 78.00; IR (ATR) $\tilde{\nu}$ (cm^{-1}) = 2962 (w), 2160 (vs), 1630 (w), 1547 (s), 1476 (s), 1447 (m), 1413 (m), 1377 (w), 1304 (s), 1259 (s), 1221 (s), 1166 (w), 1092 (m), 1036 (w), 971 (w), 816 (w), 723 (m), 693 (w), 673 (s), 528 (w); ^{1}H NMR (DMSO-D_6, 400 MHz, ppm) δ = 3.77 (CH_3); ^{13}C NMR (DMSO-D_6, 101 MHz, ppm) δ = 152.9, 33.1; ^{15}N NMR (DMSO-D_6, 41 MHz, ppm) δ = 7.2 (N3), –12.2 (N2, q, $^3J_{NH}$ = 1.6 Hz), –75.6 (N4), –144.0 (N7), –146.5 (N6), –172.6 (N1, q, $^2J_{NH}$ = 2.0 Hz), –301.6 (N5); *m/z* (DEI): 83 (1), 58 (13), 53 (8), 43 (42), 42 (3), 40 (4), 32 (2), 28 (13), 15 (10).

5-Azido-2-methyltetrazole (**12**)

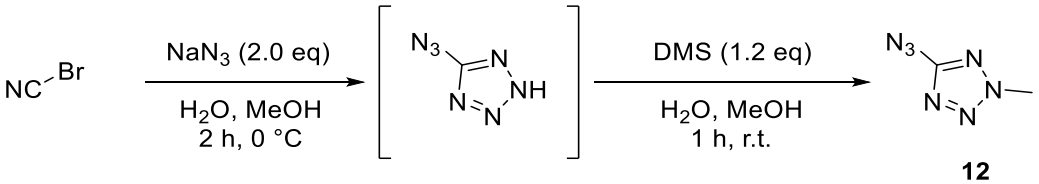

12

Cyanogen bromide (0.53 g, 5.00 mmol, 1.0 eq) was dissolved in a mixture of cold water (16 mL) and MeOH (4 mL). To this, a solution of sodium azide (0.65 g, 10.0 mmol, 2.0 eq) was added drop wise while cooling in an ice bath. After 2 h,

dimethyl sulfate (0.28 mL, 3.0 mmol, 1.2 eq) was added slowly and the solution was allowed to come to room temperature. After one hour, the precipitate formed was filtered off and washed with a small amount of cold water. The analytically pure **12** (0.29 g, 2.30 mmol, 46%) can be recrystallized from hot water.

DSC (5 °C min^{-1}): 62 °C (melt), 162 °C (dec); Sensitivities: BAM drop hammer: <1 J friction sensitivity: <5 N; ESD: 80 mJ; EA ($C_2H_3N_7$, 125.11) calcd.: C 19.20, H 2.42, N 78.38 %; Found: C 19.19, H 2.21, N 77.41; IR (ATR) $\tilde{\nu}$ (cm^{-1}) = 3038 (w), 2956 (w), 2417 (w), 2285 (w), 2160 (vs), 1725 (w), 1588 (m), 1550 (s), 1506 (s), 1476 (s), 1421 (m), 1396 (m), 1305 (m), 1259 (w), 1218 (m), 1182 (m), 1091 (w), 1050 (w), 1026 (w), 794 (m), 739 (m), 721 (w), 674 (m), 527 (m); ^{1}H NMR (DMSO-D_6, 400 MHz, ppm): δ = 4.28 (CH_3); ^{13}C NMR (DMSO-D_6, 101 MHz, ppm): δ = 161.9, 40.7; ^{15}N NMR (DMSO-D_6, 41 MHz, ppm): δ = 0.4 (N1, q, $^{3}J_{NH}$ = 2.0 Hz), –71.0 (N4), –98.3 (N1, q, $^{3}J_{NH}$ = 1.9 Hz), –105.7 (N2, q, $^{2}J_{NH}$ = 2.3 Hz), –144.2 (N6), –146.0 (N7), –300.5 (N5); *m/z* (DEI): 125 (43), 83 (1), 69 (12), 57 (1), 55 (3), 54 (23), 53 (12), 43 (100), 40 (11), 29 (11), 28 (29), 27 (12), 26 (14), 31 (8), 28(29), 18 (14), 15 (48).

Thermal Analysis

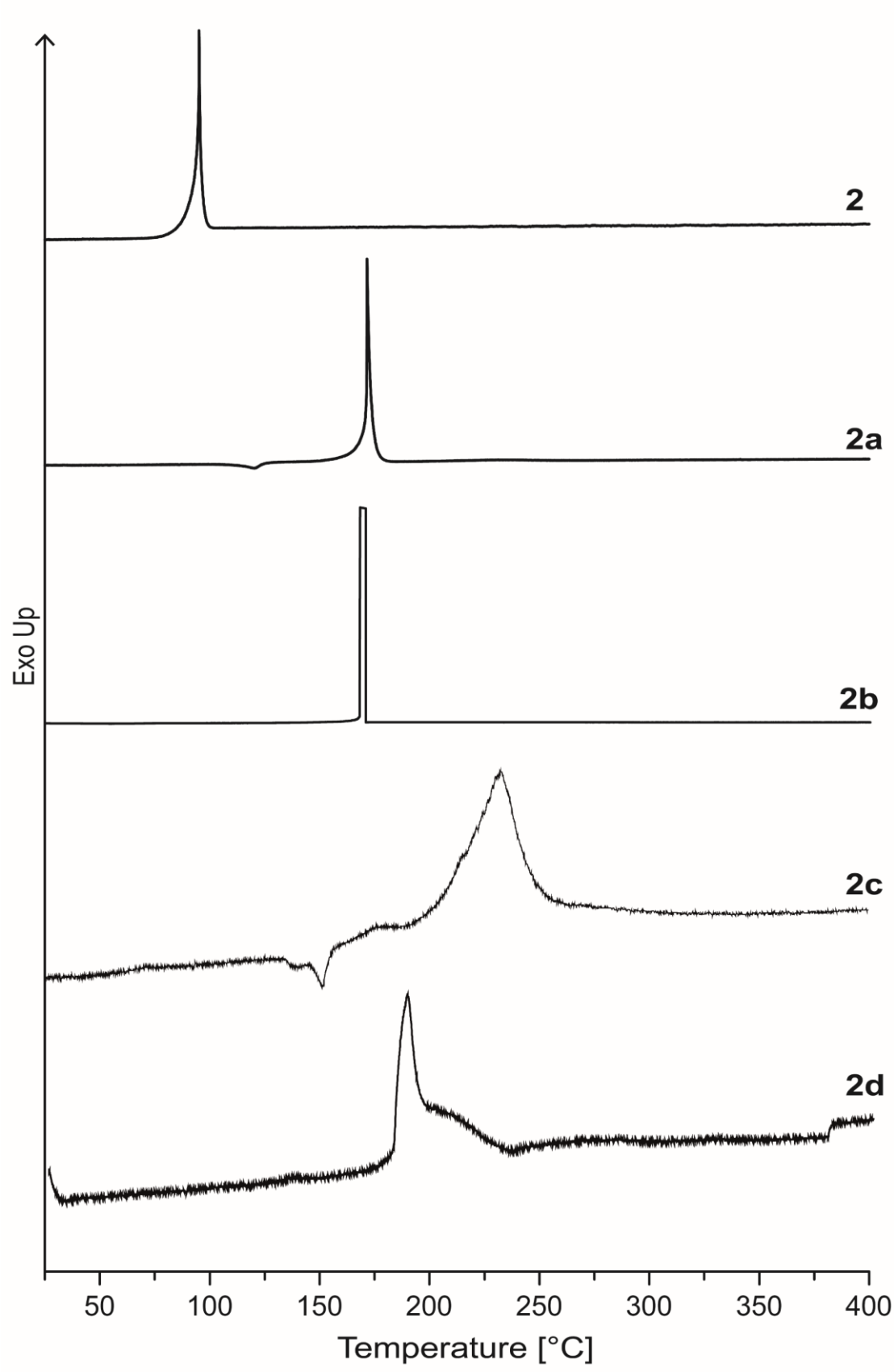

Figure S1. Thermal analysis through DTA of compounds **2** and **2a**-**2d**.

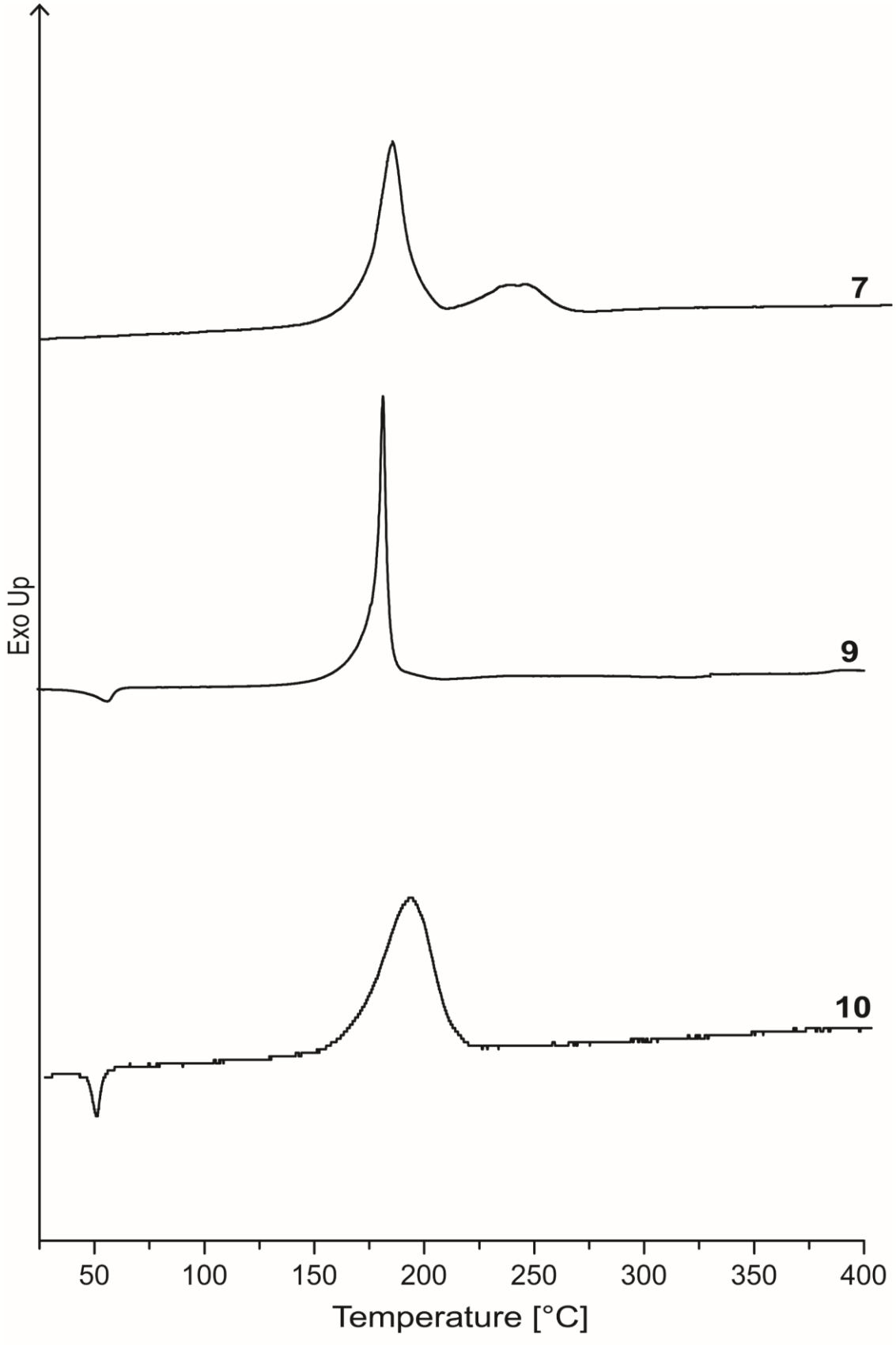

Figure S2. Thermal analysis through DTA of compounds **7** and **9**-**10**.

12.6.2 Crystallography

Crystal structure data were obtained from an Oxford Xcalibur3 diffractometer with a Spellman generator (voltage 50 kV, current 40 mA) and a Kappa CCD area for data collection using Mo-*Kα* radiation (*λ* = 0.71073 Å). The data collection was performed using the CRYSTALIS RED software.[S5] The solution of the structure was performed by direct methods and refined by full-matrix least-squares on F2 (SHELXT)[S6] implemented in the OLEX2[S7] software suite. The non-hydrogen atoms were refined anisotropically and the hydrogen atoms were located and freely refined. The absorption correction was carried out by a SCALE3 ABSPACK multiscan method.[S8] The DIAMOND2 plots shown with thermal ellipsoids at the 50% probability level and hydrogen atoms are shown as small spheres of arbitrary radius. The SADABS program embedded in the Bruker APEX3 software was used for multi-scan absorption corrections in all structures.[S9]

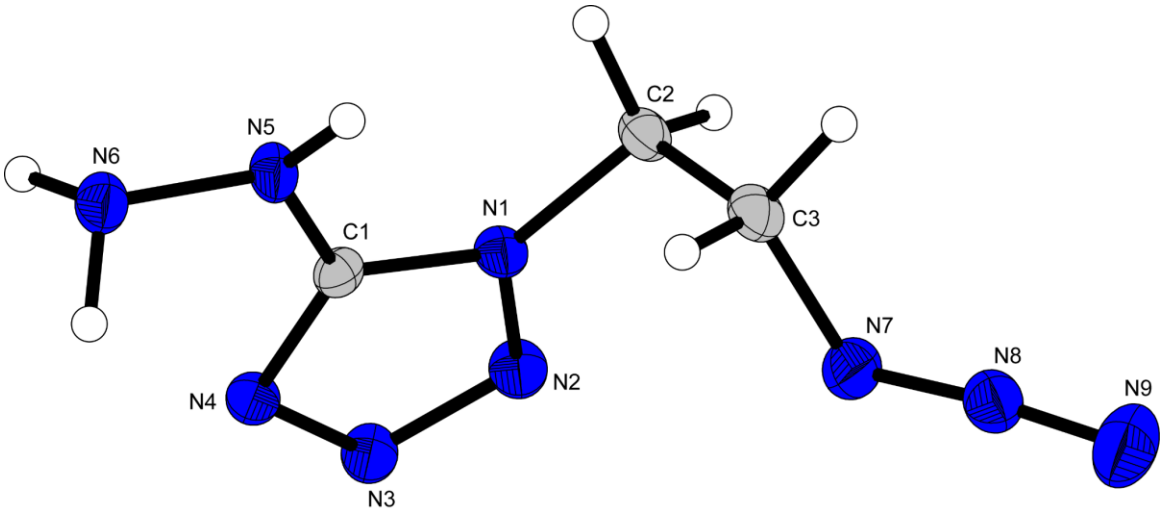

Figure S3. Representation of the molecular unit of **5**, showing the atom-labeling scheme. Thermal ellipsoids represent the 50% probability level and hydrogen atoms are shown as small spheres of arbitrary radius.

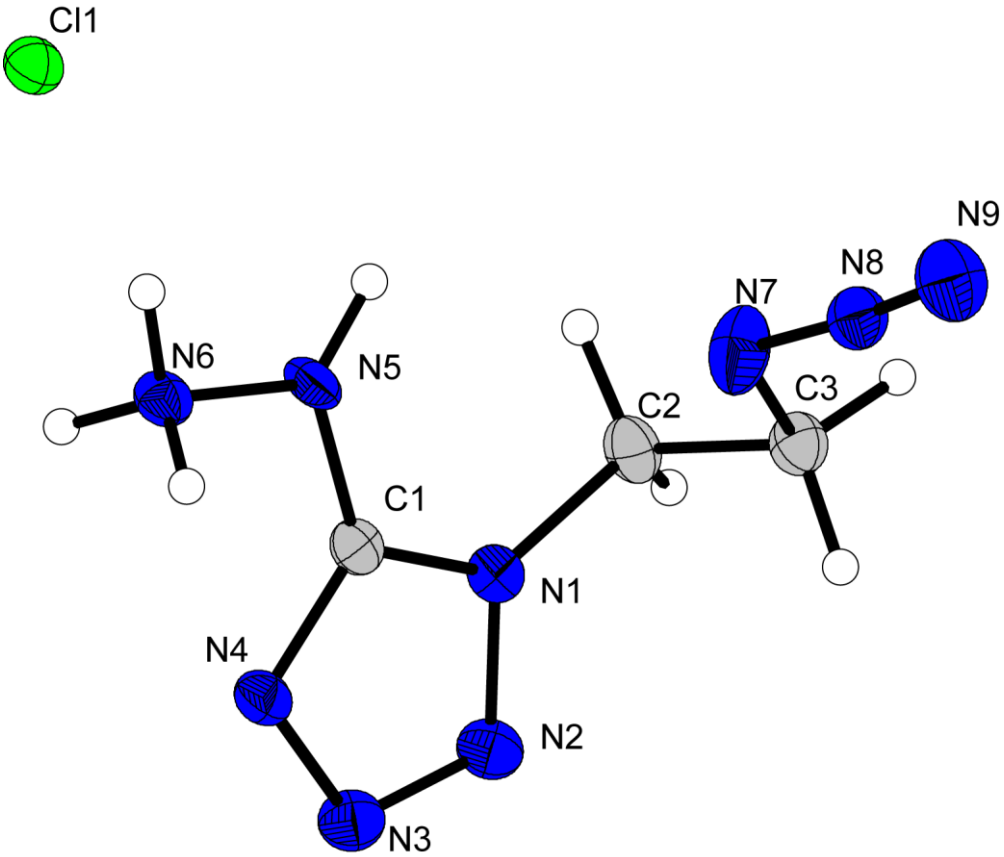

Figure S4. Representation of the molecular unit of **6**, showing the atom-labeling scheme. Thermal ellipsoids represent the 50% probability level and hydrogen atoms are shown as small spheres of arbitrary radius.

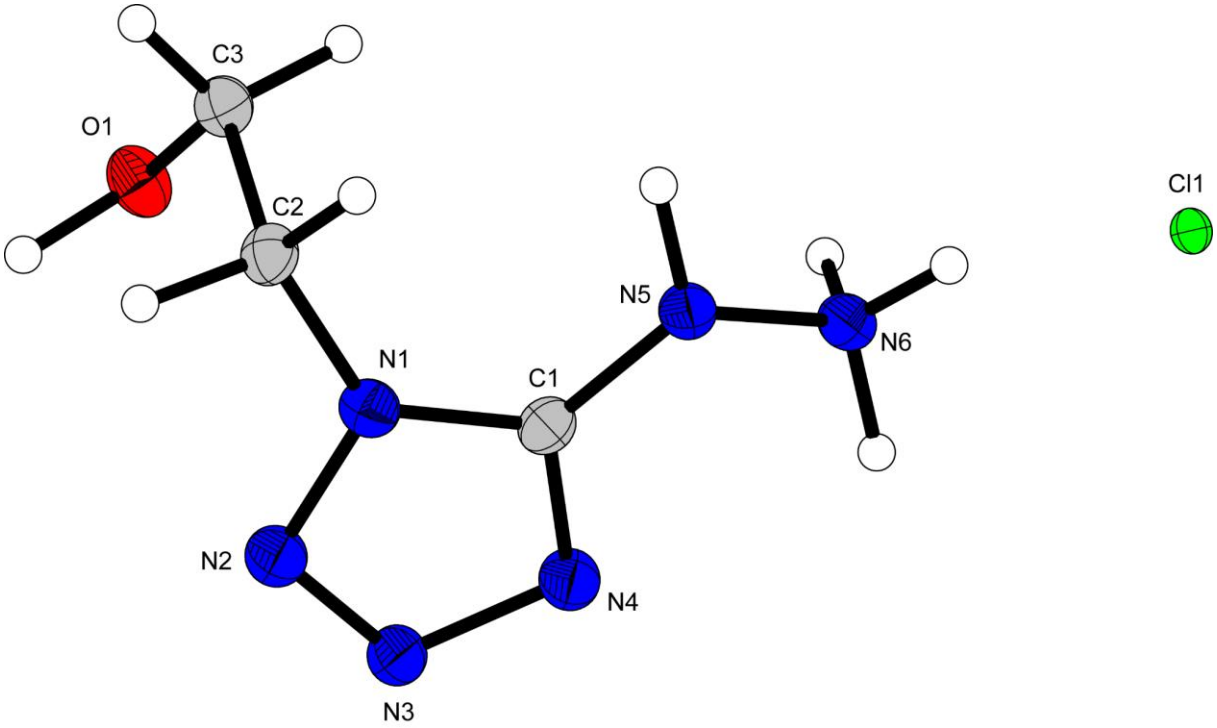

Figure S5. Representation of the molecular unit of **8** · HCl, showing the atom-labeling scheme. Thermal ellipsoids represent the 50% probability level and hydrogen atoms are shown as small spheres of arbitrary radius.

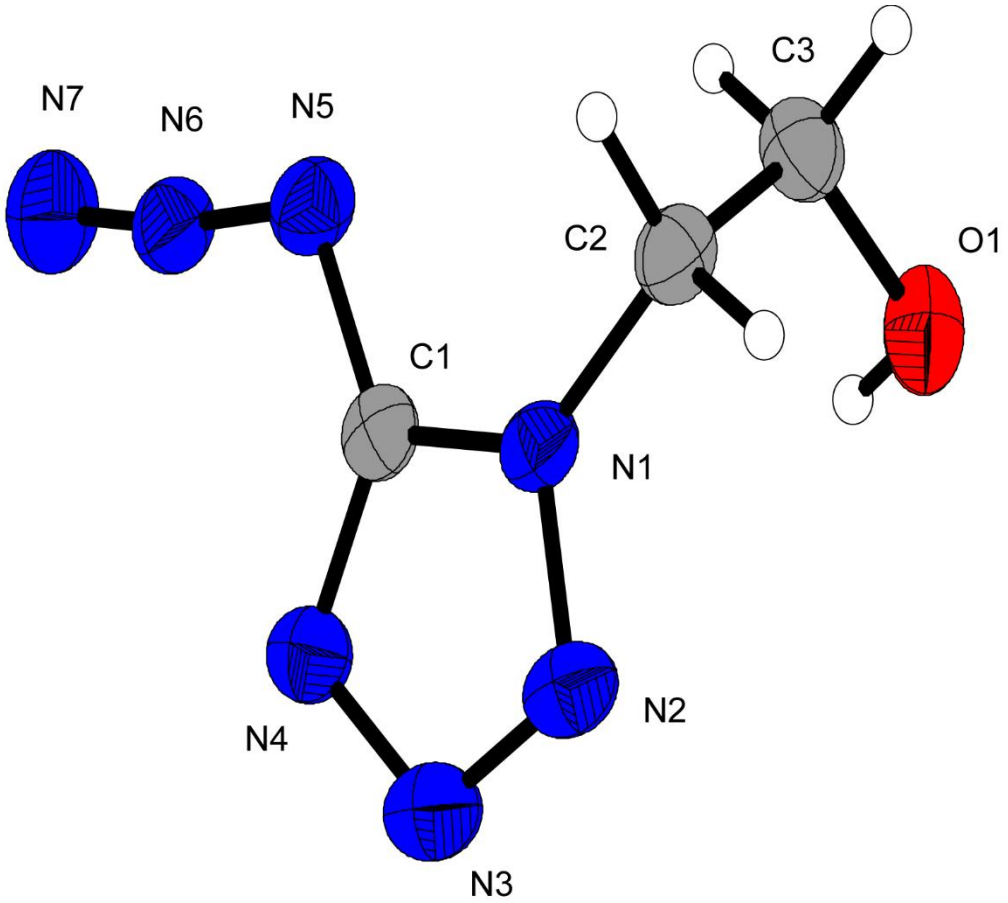

Figure S6. Representation of the molecular unit of **9**, showing the atom-labeling scheme. Thermal ellipsoids represent the 50% probability level and hydrogen atoms are shown as small spheres of arbitrary radius.

Table S1. Crystallographic data and structure refinement details for the prepared compounds **2a**, **2b** and **2d**.

	2a	**2b**	**2d**
Formula	$C_3H_4N_9O_2$, NH_4	$C_3H_4N_9O_2$, NH_3OH	$Ag_2C_6H_8N_{18}O_4$
FW [g mol^{-1}]	216.19	232.19	612.04
Crystal system	triclinic	triclinic	orthorhombic
Space group	*P*−1 (No. 2)	*P*−1 (No. 2)	*Pbca* (No. 61)
Color / Habit	colorless plate	colorless block	colorless platelet
Size [mm]	0.01 x 0.30 x 0.30	0.30 x 0.30 x 0.50	0.10 x 0.15 x 0.25
a [Å]	4.3043(3)	7.2416(6)	8.9776(6)
b [Å]	6.2716(5)	7.3297(8)	11.1520(12)
c [Å]	16.6686(13)	18.1018(18)	33.395(3)
α [°]	83.082(6)	89.358(9)	
β [°]	88.293(6)	79.717(8)	
γ [°]	84.288(6)	77.681(8)	
V [Å^3]	444.40(6)	923.26(16)	3343.5(5)
Z	2	4	8
$\rho_{calc.}$ [g cm^{-3}]	1.616	1.671	2.432
μ [mm^{-1}]	0.135	0.144	2.411
F(000)	224	480	2368
$\lambda_{MoK\alpha}$ [Å]	0.71073	0.71073	0.71073
T [K]	123	105	293
θ Min-Max [°]	2.5, 26.4	2.3, 26.4	2.4, 26.4
Dataset	-5: 5 ; -7: 7 ; -20: 20	-9: 9 ; -9: 7 ; -20: 22	-11: 11 ; -13: 13 ; -41: 41
Reflections collected	6814	7565	28293
Independent refl.	1812	3765	3406
R_{int}	0.035	0.032	0.166
Observed reflections	1427	2433	2254
Parameters	168	353	271
R_1 (obs)[a]	0.0363	0.0485	0.0650
wR_2 (all data)[b]	0.0869	0.1216	0.1368
S [c]	1.02	1.03	1.09
Resd. dens [e Å^{-3}]	-0.19, 0.21	-0.24, 0.30	-0.85, 1.58
Device type	Xcalibur Sapphire3	Xcalibur Sapphire3	Xcalibur Sapphire3
Solution	SIR-92	SIR-92	SIR-92
Refinement	SHELXL-2013	SHELXL-2013	SHELXL-2013
Absorption correction	multi-scan	multi-scan	multi-scan
CCDC	2157201	2157198	2157203

[a] $R_1 = \Sigma||F_0|-|F_c||/\Sigma|F_0|$; [b] $wR_2 = [\Sigma[w(F_0^2-F_c^2)^2]/\Sigma[w(F_0)^2]]^{1/2}$; $w = [\sigma c^2(F_0^2)+(xP)^2+yP]^{-1}$ and $P=(F_0^2+2F_c^2)/3$; [c] $S = (\Sigma[w(F_o^2-F_c^2)^2]/(n-p))^{1/2}$ (n = number of reflections; p = total number of parameters).

Table S2. Crystallographic data and structure refinement details for the prepared compounds **5**-**7**.

	5	**6**	**7**
Formula	$C_3H_7N_9$	$C_3H_8N_9Cl$	$C_3H_4N_{10}$
FW [g mol^{-1}]	169.18	205.63	180.16
Crystal system	monoclinic	monoclinic	orthorhombic
Space group	*P*2$_1$/*c* (No. 14)	*P*2$_1$/*c* (No. 14)	*Fdd*2 (No. 43)
Color / Habit	colorless block	colourless block	colorless block
Size [mm]	0.50 x 0.50 x 0.50	0.10 x 0.50 x 0.50	0.05 x 0.25 x 0.50
a [Å]	6.0070(5)	12.7917(11)	25.526(2)
b [Å]	10.9792(10)	7.7802(6)	12.6485(10)
c [Å]	10.9160(11)	8.8236(6)	9.4801(9)
α [°]	90	90	
β [°]	95.467(7)	101.731(6)	
γ [°]	90	90	
V [Å^3]	716.66(11)	859.80(12)	3060.8(4)
Z	4	4	16
$\rho_{calc.}$ [g cm^{-3}]	1.568	1.589	1.564
μ [mm^{-1}]	0.120	0.416	0.122
F(000)	352	424	1472
$\lambda_{MoK\alpha}$ [Å]	0.71073	0.71073	0.71073
T [K]	101	101	102
θ Min-Max [°]	2.6, 29.2	3.1, 26.4	2.8, 26.4
Dataset	-7: 7 ; -13: 5 ; -14: 12	-12: 15 ; -7: 9 ; -10: 11	-31: 31 ; -15: 15 ; -11: 11
Reflections collected	3304	6302	11967
Independent refl.	1627	1755	1568
R_{int}	0.022	0.042	0.062
Observed reflections	1285	1369	1343
Parameters	137	119	135
R_1 (obs)[a]	0.0420	0.0438	0.0366
wR_2 (all data)[b]	0.0985	0.1159	0.0758
S [c]	1.04	1.06	1.05
Resd. dens [e Å^{-3}]	-0.19, 0.24	-0.67, 0.62	-0.12, 0.17
Device type	Xcalibur Sapphire3	Xcalibur Sapphire3	Xcalibur Sapphire3
Solution	SIR-92	SIR-92	SIR-92
Refinement	SHELXL-2013	SHELXL-2013	SHELXL-2013
Absorption correction	multi-scan	multi-scan	multi-scan
CCDC	2157204	2157196	2157199

[a] $R_1 = \Sigma||F_o|-|F_c||/\Sigma|F_o|$; [b] $wR_2 = [\Sigma[w(F_o^2-F_c^2)^2]/\Sigma[w(F_o)^2]]^{1/2}$; $w = [\sigma c^2(F_o^2)+(xP)^2+yP]^{-1}$ and $P=(F_o^2+2F_c^2)/3$; [c] $S = (\Sigma[w(F_o^2-F_c^2)^2]/(n-p))^{1/2}$ (n = number of reflections; p = total number of parameters).

Table S3. Crystallographic data and structure refinement details for the prepared compounds **8**·HCl-**10.**

	8 · HCl	**9**	**10**
Formula	$C_3H_9N_6OCl$	$C_3H_5N_7O$	$C_3H_4N_8O_3$
FW [g mol^{-1}]	180.61	155.14	200.14
Crystal system	monoclinic	monoclinic	monoclinic
Space group	*P*2$_1$/*c* (No. 14)	*P*2$_1$/*n* (No. 14)	*P*2$_1$/*n* (No. 14)
Color / Habit	colorless block	colorless block	colorless rod
Size [mm]	0.20 x 0.50 x 0.50	0.08 x 0.12 x 0.15	0.10 x 0.20 x 0.50
a [Å]	10.738(3)	8.3335(6)	9.5705(13)
b [Å]	6.5212(11)	8.3390(6)	6.7210(7)
c [Å]	11.244(2)	9.5255(7)	12.3677(16)
α [°]	90	90	90
β [°]	100.26(2)	98.792(7)	97.633(12)
γ [°]	90	90	90
V [Å^3]	774.8(3)	654.18(8)	788.48(17)
Z	4	4	4
$\rho_{calc.}$ [g cm^{-3}]	1.548	1.575	1.686
μ [mm^{-1}]	0.448	0.127	0.148
F(000)	376	320	408
$\lambda_{MoK\alpha}$ [Å]	0.71073	0.71073	0.71073
T [K]	104	200	101
θ Min-Max [°]	3.6, 26.4	4.3, 26.0	2.5, 25.7
Dataset	-13: 12 ; -8: 8 ; -14: 14	-10: 10 ; -10: 10 ; -11: 11	-9: 11 ; -8: 8 ; -15: 13
Reflections collected	5599	3070	5590
Independent refl.	1577	1284	1494
R_{int}	0.039	0.022	0.033
Observed reflections	1309	924	1215
Parameters	136	120	143
R_1 (obs)[a]	0.0492	0.0302	0.0595
wR_2 (all data)[b]	0.1418	0.0691	0.1736
S [c]	1.09	0.91	1.12
Resd. dens [e Å^{-3}]	-0.42, 0.91	-0.18, 0.15	-0.37, 0.60
Device type	Xcalibur Sapphire3	Xcalibur Sapphire3	Xcalibur Sapphire3
Solution	SIR-92	SIR-92	SIR-92
Refinement	SHELXL-2013	SHELXL-2013	SHELXL-2013
Absorption correction	multi-scan	multi-scan	multi-scan
CCDC	2157197	2157202	2157200

[a]$R_1 = \Sigma||F_0|-|F_c||/\Sigma|F_0|$; [b]$wR_2 = [\Sigma[w(F_0^2-F_c^2)^2]/\Sigma[w(F_0)^2]]^{1/2}$; $w = [\sigma c^2(F_0^2)+(xP)^2+yP]^{-1}$ and $P=(F_0^2+2F_c^2)/3$; [c]$S = (\Sigma[w(F_o^2-F_c^2)^2]/(n-p))^{1/2}$ (n = number of reflections; p = total number of parameters).

Table S4. Crystallographic data and structure refinement details for the prepared compounds **11** and **12**.

	11	**12**
Formula	$C_2H_3N_7$	$C_2H_3N_7$
FW [g mol^{-1}]	125.11	125.11
Crystal system	monoclinic	monoclinic
Space group	*P*2$_1$/*m* (No. 11)	*P*2$_1$/*c* (No. 14)
Color / Habit	colorless needle	colorless block
Size [mm]	0.06 x 0.10 x 0.26	0.10 x 0.12 x 0.13
a [Å]	8.7382(4)	6.6219(5)
b [Å]	6.2408(4)	8.7588(7)
c [Å]	10.2986(6)	9.6392(8)
α [°]	90	90
β [°]	90.722(4)	108.858(7)
γ [°]	90	90
V [Å^3]	561.57(6)	529.06(8)
Z	4	4
$\rho_{calc.}$ [g cm^{-3}]	1.480	1.571
μ [mm^{-1}]	0.115	0.123
F(000)	256	256
$\lambda_{MoK\alpha}$ [Å]	0.71073	0.71073
T [K]	200	173
θ Min-Max [°]	3.8, 26.0	4.0, 26.0
Dataset	-10: 8 ; -7: 7 ; -12: 8	-5: 8 ; -10: 8 ; -10: 11
Reflections collected	2919	2662
Independent refl.	1206	1037
R_{int}	0.037	0.036
Observed reflections	729	674
Parameters	112	94
R_1 (obs)[a]	0.0320	0.0331
wR_2 (all data)[b]	0.0926	0.0854
S [c]	0.97	0.90
Resd. dens [e Å^{-3}]	-0.18, 0.16	-0.16, 0.18
Device type	Xcalibur Sapphire3	Xcalibur Sapphire3
Solution	SIR-92	SIR-92
Refinement	SHELXL-2013	SHELXL-2013
Absorption correction	multi-scan	multi-scan
CCDC	707542	707543

[a] $R_1 = \Sigma||F_o|-|F_c||/\Sigma|F_o|$; [b] $wR_2 = [\Sigma[w(F_o^2-F_c^2)^2]/\Sigma[w(F_o)^2]]^{1/2}$; $w = [\sigma c^2(F_o^2)+(xP)^2+yP]^{-1}$ and $P=(F_o^2+2F_c^2)/3$; [c] $S = (\Sigma[w(F_o^2-F_c^2)^2]/(n-p))^{1/2}$ (n = number of reflections; p = total number of parameters).

12.6.3 Computation

All quantum chemical calculations were carried out using the Gaussian G09 program package.[S10] The enthalpies (H) and free energies (G) were calculated using the complete basis set (CBS) method of Petersson and co-workers in order to obtain very accurate energies. The CBS models are using the known asymptotic convergence of pair natural orbital expressions to extrapolate from calculations using a finite basis set to the estimated CBS limit. CBS-4 starts with an HF/3-21G(d) geometry optimization; the zero-point energy is computed at the same level. It then uses a large basis set SCF calculation as a base energy, and an MP2/6- 31+G calculation with a CBS extrapolation to correct the energy through second order. A MP4(SDQ)/6-31+ (d,p) calculation is used to approximate higher order contributions. In this study, we applied the modified CBS-4M.
Heats of formation of the synthesized ionic compounds were calculated using the atomization method (equation E1) using room temperature CBS-4M enthalpies, which are summarized in Table S5.[S11, S12]

$$\Delta_f H^\circ_{(g,\,M,\,298)} = H_{(Molecule,\,298)} - \sum H^\circ_{(Atoms,\,298)} + \sum \Delta_f H^\circ_{(Atoms,\,298)} \qquad (E1)$$

Table S5. CBS-4M electronic enthalpies for atoms C, H, N and O and their literature values for atomic $\Delta H^\circ_f{}^{298}$ / kJ mol^{-1}.

	$-H^{298}$ [a.u.]	NIST[S13]
H	0.500991	218.2
C	37.786156	717.2
N	54.522462	473.1
O	74.991202	249.5

For neutral compounds the sublimation enthalpy, which is needed to convert the gas phase enthalpy of formation to the solid state one, was calculated by the *Trouton* rule.[S14] For ionic compounds, the lattice energy (U_L) and lattice enthalpy (ΔH_L) were calculated from the corresponding X-ray molecular volumes according to the equations provided by *Jenkins* and *Glasser*.[S15] With the calculated lattice enthalpy the gas-phase enthalpy of formation was converted into the solid state

(standard conditions) enthalpy of formation. These molar standard enthalpies of formation (ΔH_m) were used to calculate the molar solid state energies of formation (ΔU_m) according to equation E2.

$$\Delta U_m = \Delta H_m - \Delta n\, RT \qquad \text{(E2)}$$

(Δn being the change of moles of gaseous components)
The calculation results are summarized in Table S6.

Table S6. Calculation results.

	$-H^{298}$ [a] [a.u.]	$\Delta_f H°(g,M)$ [kJ mol^{-1}] [b]	V_M [Å^3] [c]	ΔU_L; ΔH_L [d]	$\Delta_f H°(s)$ [e] [kJ mol^{-1}]	Δn [f]	$\Delta_f U(s)$ [g] [kJ mol^{-1}]
A^- (2)	758.815212	506.6					
NH_4^+	56.796608	635.3					
NH_3OH^+	112.630523	773.4					
2	759.333150	680.1	-	-	647.1	−8.0	666.9
2a	-	-	228.0	487.8; 492.8	649.1	−10.0	673.9
2b	-	-	238.0	482.6; 487.6	705.5	−10.5	731.5
7	663.165046	980.3	-	-	932.7	−7.0	950.1
10	779.173027	574.3	-	-	514.5	−7.5	533.1
11	460.540365	649.6	-	-	594.5	−5.0	606.9
12	460.547855	630.0	-	-	566.9	−5.0	579.3

[a] CBS-4M electronic enthalpy; [b] gas phase enthalpy of formation; [c] molecular volumes taken from X-ray structures and corrected to room temperature; [d] lattice energy and enthalpy (calculated using Jenkins and Glasser equations); [e] standard solid state enthalpy of formation; [f] Δn being the change of moles of gaseous components when formed; [g] solid state energy of formation.

12.6.4 NMR Spectroscopy

^{1}H-NMR (400 MHz, DMSO-D$_6$, ppm)

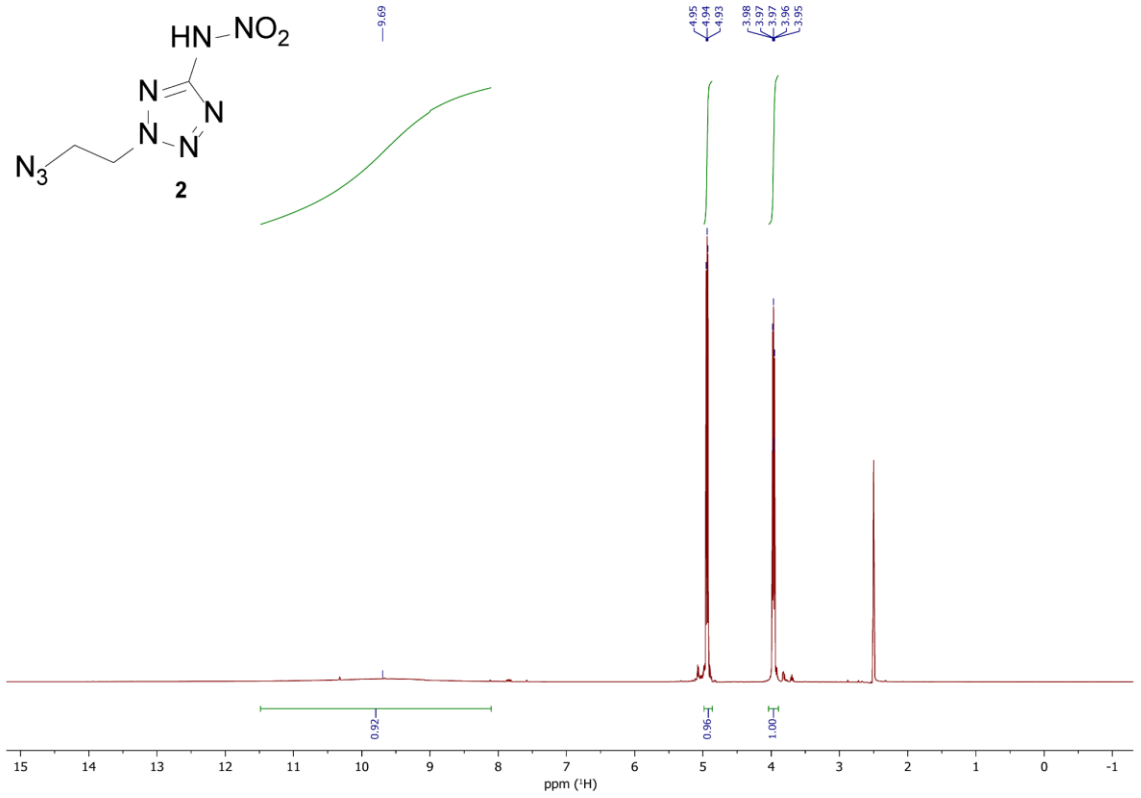

^{13}C-NMR (101 MHz, DMSO-D$_6$, ppm)

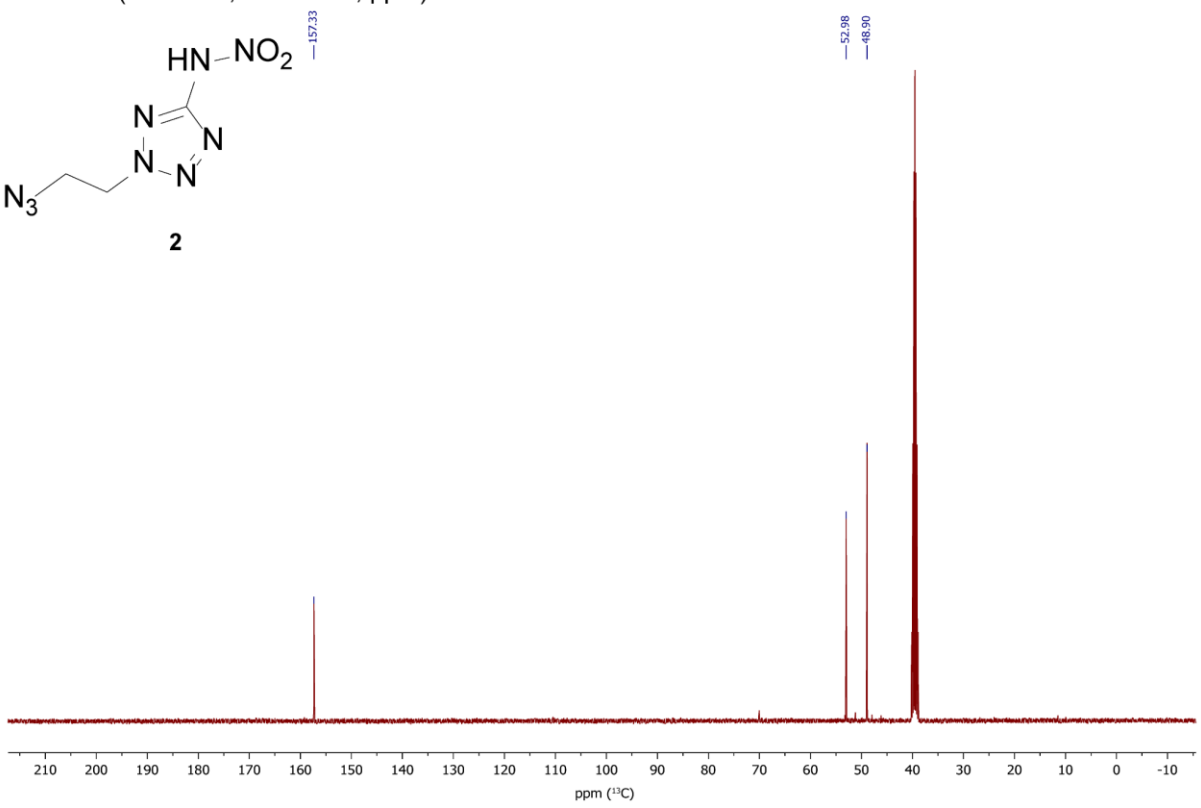

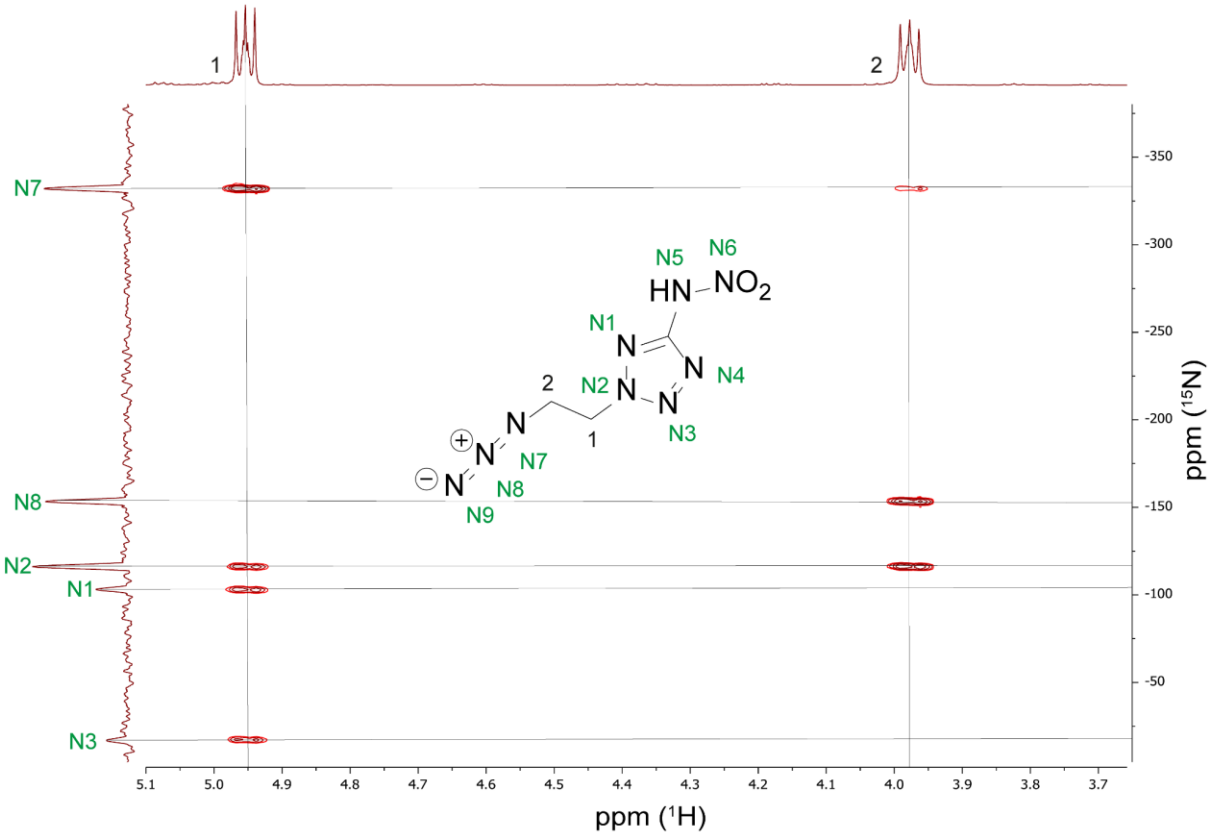
1
2
N7
N8
N2
N1
N3
N5
N6
HN
NO2
N1
N
N
N4
2
N2
N
N
N3
1
N
N7
N8
N9
-350
-300
-250
-200
-150
-100
-50
ppm (15N)
5.1
5.0
4.9
4.8
4.7
4.6
4.5
4.4
4.3
4.2
4.1
4.0
3.9
3.8
3.7
ppm (1H)

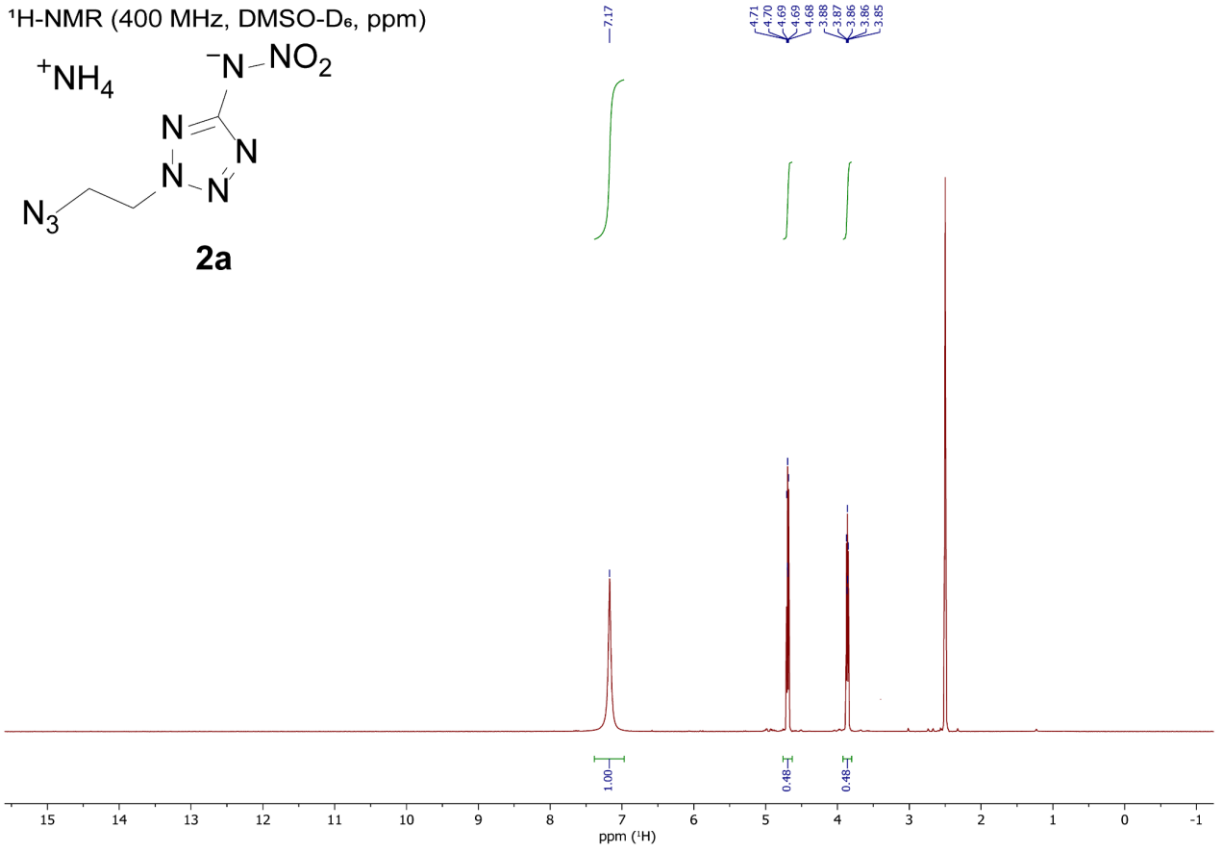
1H-NMR (400 MHz, DMSO-D6, ppm)
+NH4
−N
NO2
N
N
N
N
N3
2a
7.17
4.71
4.70
4.69
4.69
4.68
3.88
3.87
3.86
3.86
3.85
1.00
0.48
0.48
15
14
13
12
11
10
9
8
7
6
5
4
3
2
1
0
-1
ppm (1H)

^{13}C-NMR (101 MHz, DMSO-D$_6$, ppm)

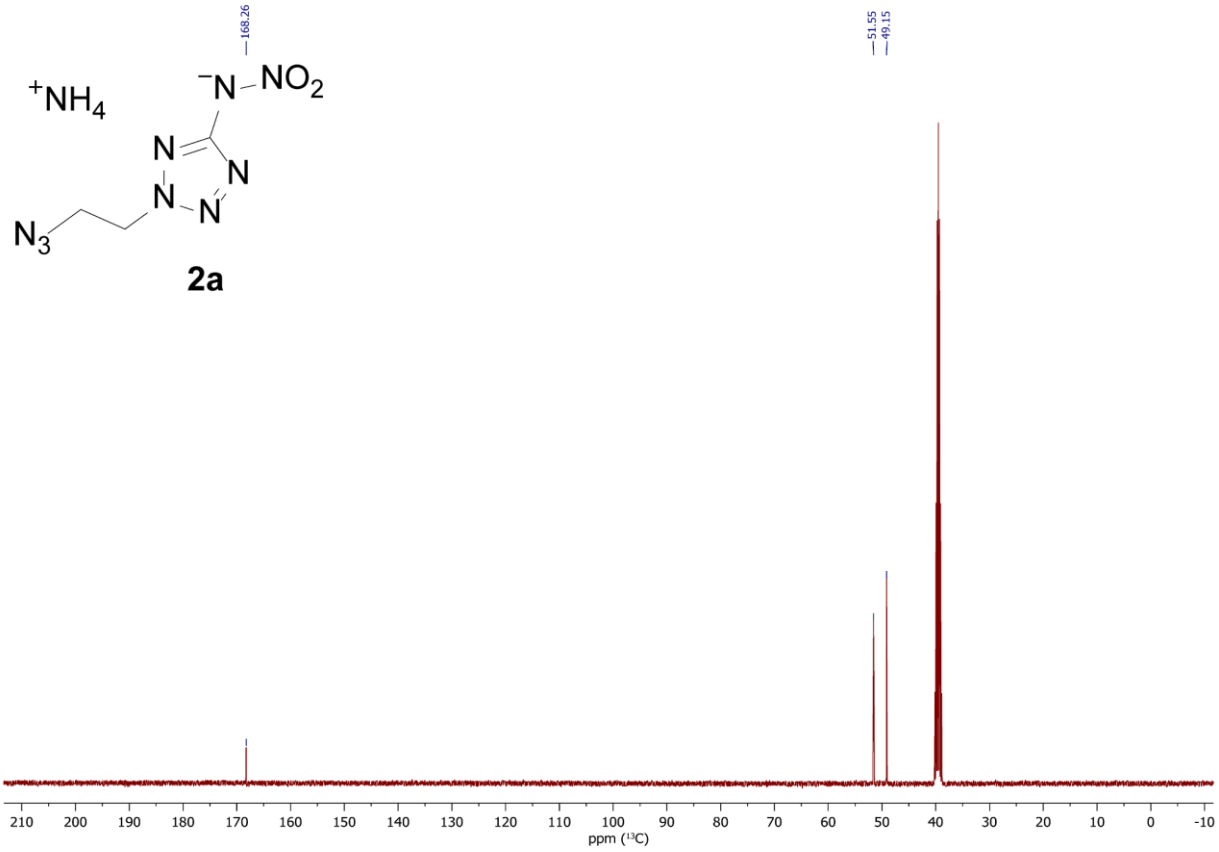

2a

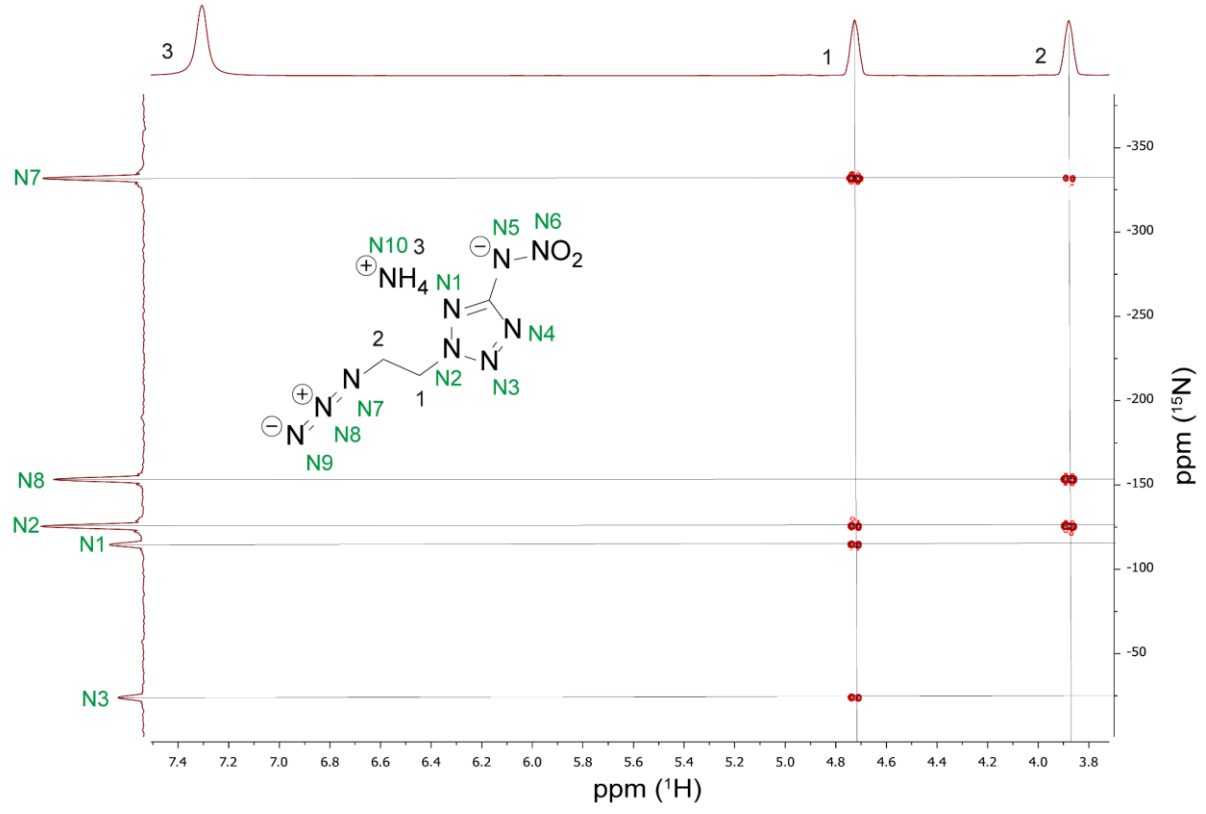

¹H-NMR (400 MHz, DMSO-D₆, ppm)

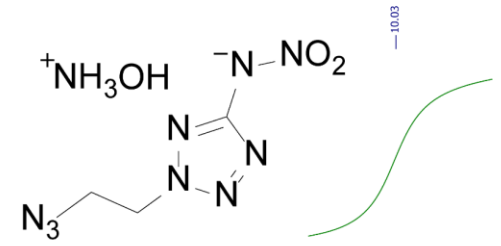

2c

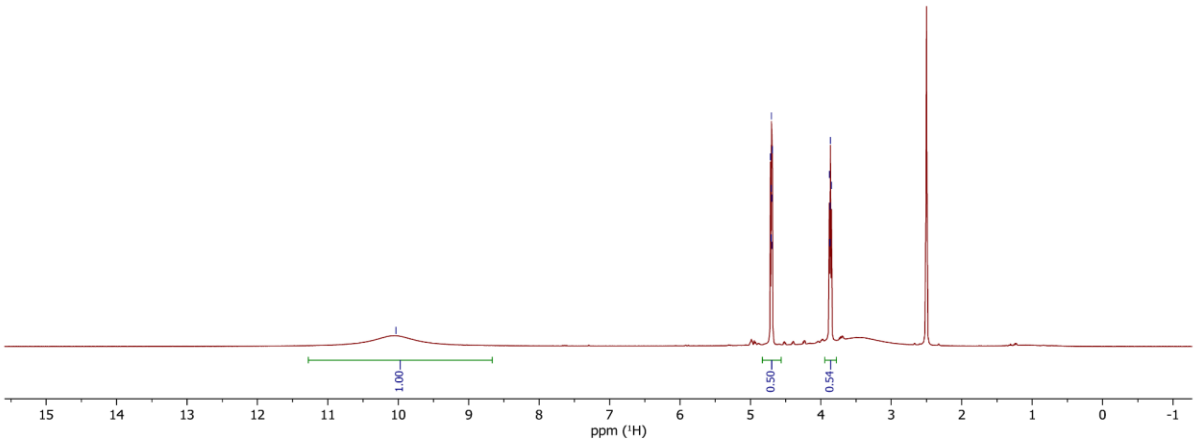

¹³C-NMR (101 MHz, DMSO-D₆, ppm)

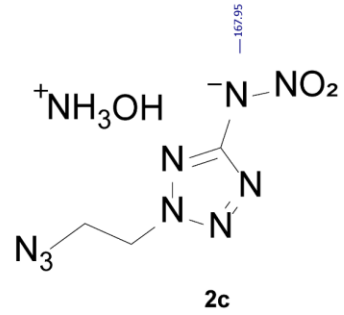

2c

¹H-NMR (400 MHz, DMSO-D₆, ppm)

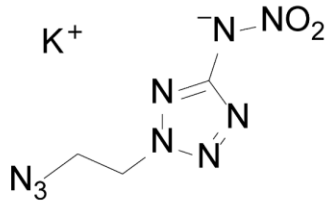

2d

¹³C-NMR (101 MHz, DMSO-D₆, ppm)

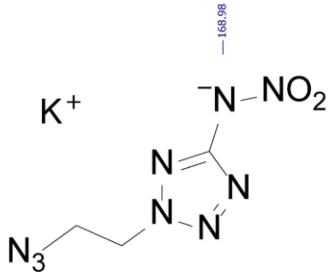

2d

¹H-NMR (400 MHz, DMSO-D₆, ppm)

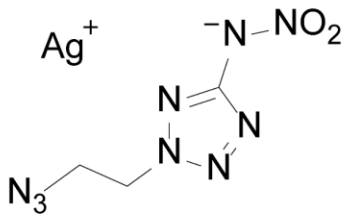

2e

¹³C-NMR (101 MHz, DMSO-D₆, ppm)

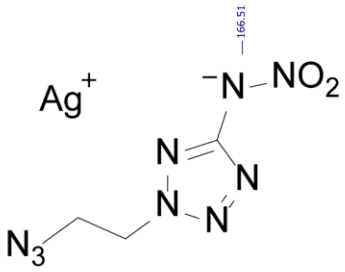

2e

^{1}H NMR (400 MHz, DMSO-D$_6$, ppm)

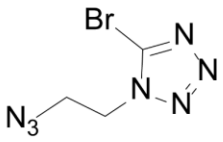

4a

^{13}C NMR (101 MHz, DMSO-D$_6$, ppm)

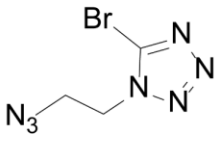

4a

^{1}H NMR (400 MHz, DMSO-D$_6$, ppm)

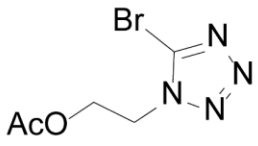

4b

^{13}C NMR (101 MHz, DMSO-D$_6$, ppm)

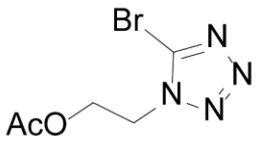

4b

^{1}H NMR (400 MHz, DMSO-D$_6$, ppm)

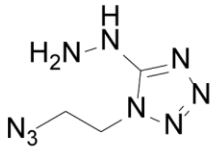

5

^{13}C NMR (101 MHz, DMSO-D$_6$, ppm)

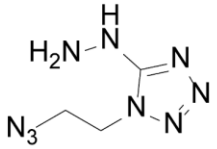

5

^{1}H NMR (400 MHz, D_2O, ppm)

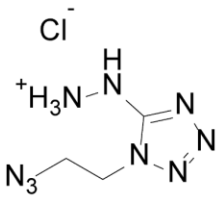

6

^{13}C NMR (101 MHz, D_2O, ppm)

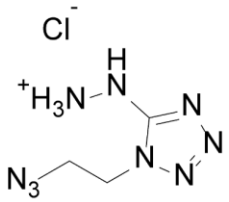

6

^{1}H NMR (400 MHz, DMSO-D$_6$, ppm)

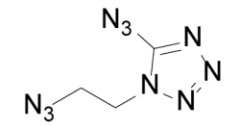

7

^{13}C NMR (101 MHz, DMSO-D$_6$, ppm)

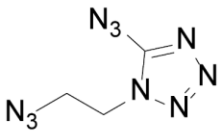

7

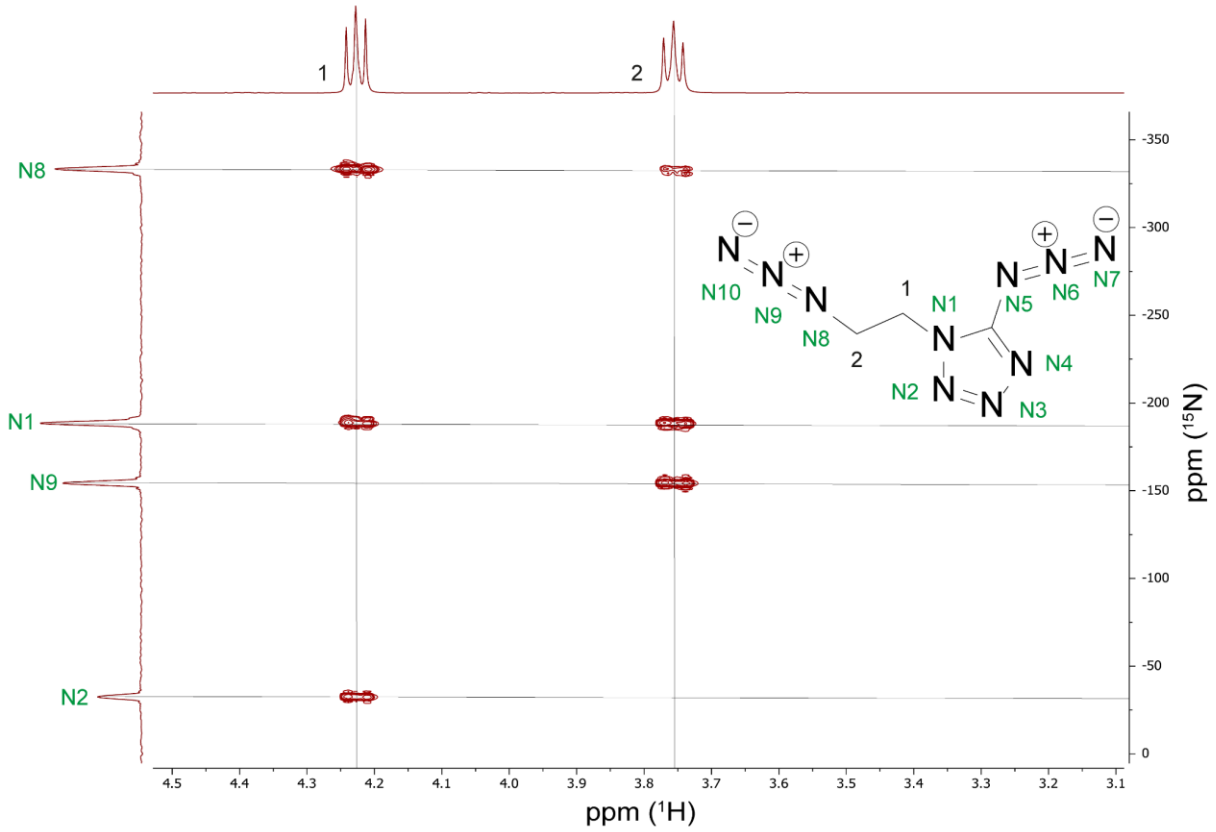

¹H NMR (400 MHz, DMSO-D₆, ppm)

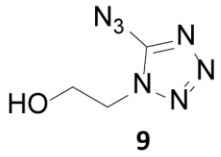

9

^{13}C NMR (101 MHz, DMSO-D$_6$, ppm)

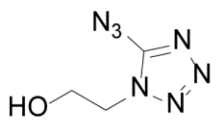

9

^{1}H NMR (400 MHz, Acetone-D$_6$, ppm)

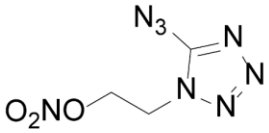

10

^{13}C NMR (101 MHz, Acetone-D$_6$, ppm)

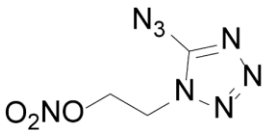

10

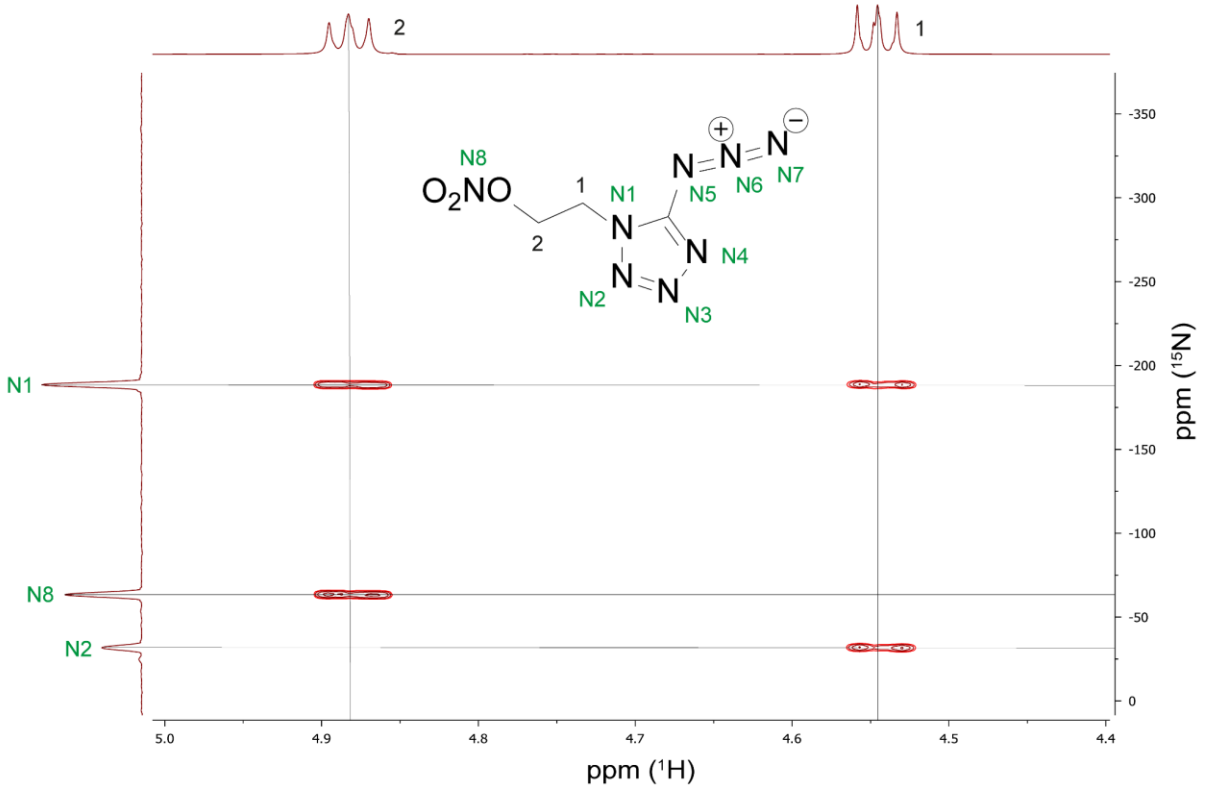

12.6.5 References

[S1] a) Reichel & Partner GmbH, http://www.reichelt-partner.de; b) Test methods according to the UN Recommendations on the Transport of Dangerous Goods, *Manual of Test and Criteria*, fourth revised edition, United Nations Publication, New York and Geneva, **2003**, ISBN 92–1-139087–7, Sales No. E.03.VIII.2; 13.4.2 Test 3 a (ii) BAM Fallhammer.

[S2] M. Sućeska, EXPLO5 V6.02 program, Brodarski Institute, Zagreb, Croatia, **2014**.

[S3] R. Yang, Z. Dong, Z. Ye, *ChemistrySelect* **2019**, *4*, 14208–14213.

[S4] D. E. Bayes (Glaxo Group Limited), EP0117368A1, **1982**.

[S5] *CrysAlisPro*, Oxford Diffraction Ltd. *version 171.33.41*, **2009**.

[S6] G. M. Sheldrick, *Acta Cryst.* **2015**, *A71*, 3–8.

[S7] O. V. Dolomanov, L. J Bourhis, R. J. Gildea, J. A. K. Howard, H. Puschmann, *J. Appl. Cryst.* **2009**, *42*, 339–341.

[S8] *SCALE3 ABSPACK – An Oxford Diffraction program* (1.0.4, gui: 1.0.3), Oxford Diffraction Ltd., **2005**.

[S9] *APEX3*. Bruker AXS Inc., Madison, Wisconsin, USA.

[S10] M. J. Frisch, G. W. Trucks, H. B. Schlegel, G. E. Scuseria, M. A. Robb, J. R. Cheeseman, G. Scalmani, V. Barone, B. Mennucci, G. A. Petersson, H. Nakatsuji, M. Caricato, X. Li, H.P. Hratchian, A. F. Izmaylov, J. Bloino, G. Zheng, J. L. Sonnenberg, M. Hada, M. Ehara, K. Toyota, R. Fukuda, J. Hasegawa, M. Ishida, T. Nakajima, Y. Honda, O. Kitao, H. Nakai, T. Vreven, J. A. Montgomery, Jr., J. E. Peralta, F. Ogliaro, M. Bearpark, J. J. Heyd, E. Brothers, K. N. Kudin, V. N. Staroverov, R. Kobayashi, J. Normand, K. Raghavachari, A. Rendell, J. C. Burant, S. S. Iyengar, J. Tomasi, M. Cossi, N. Rega, J. M. Millam, M. Klene, J. E. Knox, J. B. Cross, V. Bakken, C. Adamo, J. Jaramillo, R. Gomperts, R. E. Stratmann, O. Yazyev, A. J. Austin, R. Cammi, C. Pomelli, J. W. Ochterski, R. L. Martin, K. Morokuma, V. G. Zakrzewski, G. A. Voth, P. Salvador, J. J. Dannenberg, S. Dapprich, A. D. Daniels, O. Farkas, J.B. Foresman, J. V. Ortiz, J. Cioslowski, D. J. Fox, Gaussian 09 A.02, Gaussian, Inc., Wallingford, CT, USA, **2009**.

[S11] a) J. W. Ochterski, G. A. Petersson, and J. A. Montgomery Jr., *J. Chem. Phys.* **1996**, *104*, 2598–2619; b) J. A. Montgomery Jr., M. J. Frisch, J. W. Ochterski G. A. Petersson, *J. Chem. Phys.* **2000**, *112*, 6532–6542.

[S12] a) L. A. Curtiss, K. Raghavachari, P. C. Redfern, J. A. Pople, *J. Chem. Phys.* **1997**, *106*, 1063–1079; b) E. F. C. Byrd, B. M. Rice, *J. Phys. Chem*. A **2006**, *110*, 1005–1013; c) B. M. Rice, S. V. Pai, J. Hare, *Comb. Flame* **1999**, *118*, 445–458.

[S13] P. J. Lindstrom, W. G. Mallard (Editors), NIST Standard Reference Database Number 69, http://webbook.nist.gov/chemistry/ (accessed June **2020**).

[S14] M. S. Westwell, M. S. Searle, D. J. Wales, D. H. Williams, *J. Am. Chem. Soc*. **1995**, *117*, 5013–5015; b) F. Trouton, *Philos. Mag*. **1884**, *18*, 54–57.

[S15] a) H. D. B. Jenkins, H. K. Roobottom, J. Passmore, L. Glasser, *Inorg. Chem.* **1999,** *38,* 3609–3620; b) H. D. B. Jenkins, D. Tudela, L. Glasser, *Inorg. Chem.* **2002**, *41*, 2364–2367.

13. Evolving the Scope of 5,5'-Azobistetrazoles in the Search for High Performing Green Energetic Materials

Maximilian Benz, Michael S. Gruhne, Thomas M. Klapötke, Nina Krüger, Tobias Lenz, Marcus Lommel, Jörg Stierstorfer

as published in *European Journal of Organic Chemistry* **2021**, 4388–4392.

DOI: 10.1002/ejoc.202100747

Keywords: Azo compounds, crystallography, energetic materials, NMR spectroscopy, tetrazoles

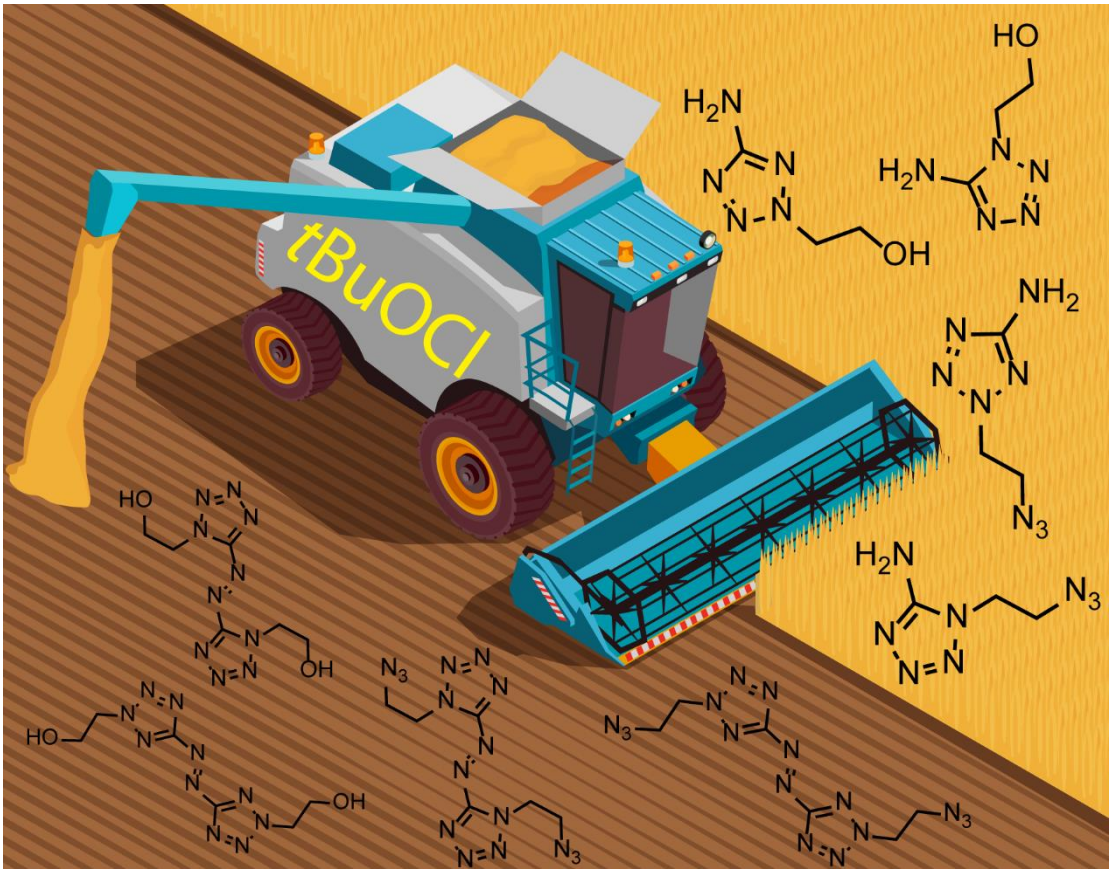

Tert-butyl hypochlorite is a powerful, cheap and handy reagent for performing oxidative azo coupling of amines. By the formation of differently substituted azotetrazoles, new energetic molecules were created through an elegant synthetic route.

Abstract: The azotetrazole moiety represents a great platform for energetic materials, it offers a planar and nitrogen-rich backbone, combined with a high heat of formation, which easily can be functionalized and tuned. Herein, we start from sodium 5-aminotetrazolate and obtain two isomers by substitution reaction with 2-chloroethanol. Azidoethyl and nitratoethyl substituted azo- tetrazoles were finally synthesized by oxidative azo coupling of the respective *N*-ethyl functionalized 5-aminotetrazole precursors using *tert*-butyl hypochlorite as reagent. All compounds were analyzed through multicore NMR and IR spectroscopy as well as mass spectrometry. All solid compounds were further investigated using low-temperature X-ray crystallography. The purity was verified by CHNO elemental analysis and the decomposition temperature (DTA) and sensitivities toward impact, friction and electrostatic discharged were determined. Based on the CBS-4M calculation results, the energetic properties were calculated using the EXPLO5 code.

13.1 Introduction

In the field of energetic materials, the most common approaches for the synthesis of new molecules are the introduction of cage or ring strain, the oxidation of the carbon backbone, or a raise of the molecule's nitrogen content.[1] Widely used examples of merging these models are mainly 2,4,6-trinitrotoluene (TNT), cyclotrimethylenetrinitramine (RDX), or hexanitrohexaaza-isowurtzitane (CL-20).[2-3] However, since TNT in particular, as well as the decomposition products of RDX, turned out to be toxic, an intensive search for a substitute is underway.[4-5] Suitable substitutes should not only surpass the performance of their predecessors, but also exhibit high thermal stability with low sensitivity.[6-7] Furthermore, the synthesis should be carried out in a few steps with simple processing while being inexpensive and environmentally friendly. However, the opportunities available here are looking increasingly exhausted. CL-20 for example is currently part of many studies, trying to compensate the high sensitivity by co-crystallization of insensitive molecules.[8-9]

In addition to trying to improve known molecules, increasing the nitrogen content also provides a good starting point.[5] The building blocks represented in this area are primarily azoles. The most nitrogen-rich azole, pentazole, is currently only used

as a salt and is extremely difficult to access.[10-11] The first 5-aminopentazole derivative was only recently detected by NMR spectroscopy by Banert *et al*.[12] However, tetrazoles represent a more stable alternative. Currently, these are not considered toxic and are even used in various medicines.[1, 13] Tetrazoles have already found their way into the field of energetic materials, with the best-known representatives in this field probably being TKX-50 or DBX-1.[14-15] Furthermore, their use as ligands in nitrogen-rich complexes as lead azide or lead styphnate substitutes is being investigated.[16-17]

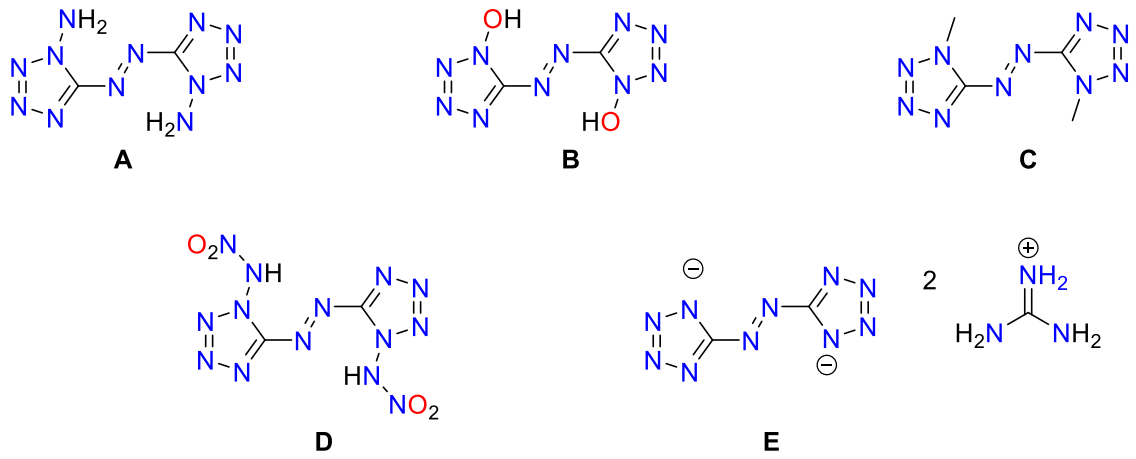

Figure 1. A) 1,1'-Diaminoazotetrazole, B) 1,1'-dihydroxyazotetrazole, C) 1,1'-dimethylazotetrazole, D) 1,1'-dinitraminoazotetrazole, E) bisguanidinium azotetrazolate.

A particularly interesting moiety because of its detonation parameters improving character, is the azo bridge. In pyrazoles and triazoles, this building block is already widely used.[18-19] However, since tetrazoles are more limited with respect to their derivatizability, this unit is hardly found so far. Substituents are usually introduced before the azo coupling, and the neutral 5,5'-azobistetrazole (often called simply azotetrazole) is primarily used for the preparation of nitrogen-rich salts. Therefore, only methyl, amino, hydroxy or nitramino derivatives have been prepared by azo coupling of the respective 5-aminotetrazoles (Figure 1) yet.[20-24]

13.2 Results and Discussion

In this work, we present the synthesis of four new symmetric energetic azotetrazoles, containing azidoethyl or nitratoethyl functionalities. The main access

to this substance class was generated through a well-known reaction of sodium 5-aminotetrazolate with 2-chloroethanol resulting in the formation of the two isomers **1a** and **1b** (Scheme 1 and Scheme 2).[25] For **1a** and **2a** an additional selective route is the reaction of cyanogen azide with 2-aminoethanol and 2-chloroethylamine hydrochloride, respectively.[26] Straightforward chlorination of **1a** and subsequent chlorine-azide exchange formed the azidoethyl unit of **3a**.[27] In order to introduce energetic groups only in the last synthesis step, **2a** was azo-coupled to the corresponding 1,1′-chloroethyl-azotetrazole (**7**, for more information see the SI), but the compound decomposed during the attempt of a chloro-azide exchange. With **1a** and **3a** in hands undergoing oxidative azo coupling with *tert*-butyl hypochlorite (*t*-BuOCl)[28] in acetonitrile, 1,1'-bishydroxyethyl-azotetrazole (**4a**) and 1,1'-bisazidoethyl-azotetrazole (**6a**) could be synthesized in good yields. Compound **4a** was further nitrated in 100 % nitric acid to yield the bis-nitratoethyl compound **5a**. The complete synthetic protocol presented is featuring the use of only industrially accessible chemicals as there are 5-aminotetrazole, chloroethanol, thionyl chloride, sodium azide, *t*-BuOCl and nitric acid, making all products easily available.

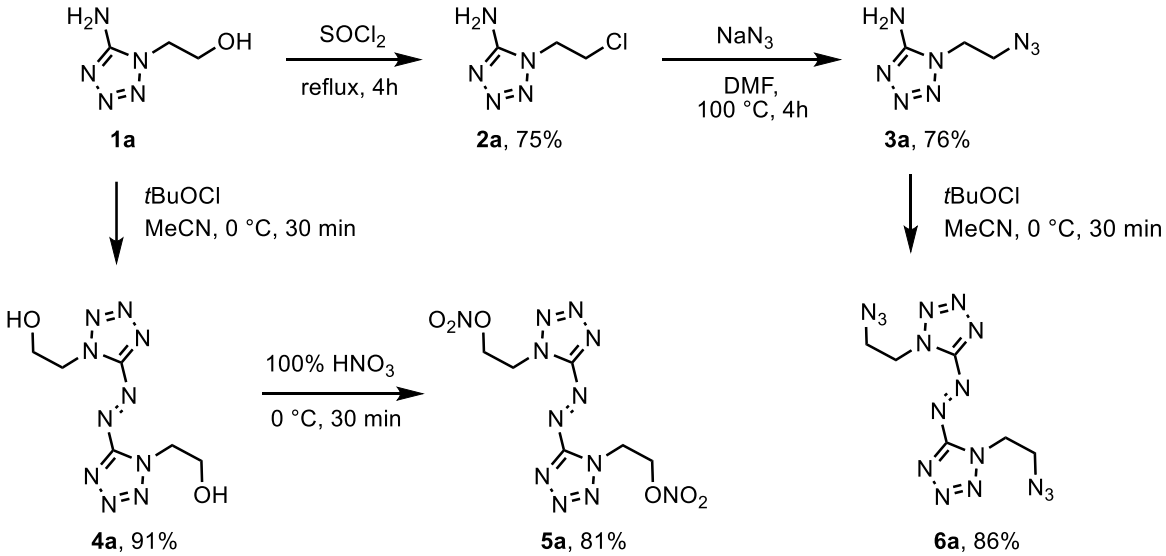

Scheme 1. Synthetic pathway for the synthesis of 1-substituted isomers starting from 1-(2-hydroxyethyl)-5-aminotetrazole (**1a**).

Despite the long knowledge of hydroxyethyl-5-aminotetrazoles, hardly any reactions are known about 2-(1-hydroxyethyl)-5-aminotetrazole (**1b**), whereas there are plenty of references about the corresponding 1-isomer **1a** and its

derivatives.[25] Nonetheless, chloromethyl (**2b**) and azidoethyl (**3b**) derivatives could be synthesized in the same manner as for the other isomer (**2a** and **3a**). Oxidation of **1b** followed by nitration results in the formation of **5b**, which was purified by recrystallization (Scheme 2). To avoid recrystallization, **1b** was protected with a TBS group to prevent the formation of by-products during azo formation or nitration (for more information see the SI compound **8**). However, the above-mentioned reactions led to the cleavage of the protective group. Following the procedure for the preparation of compound **6a**, bis(2,2'-(2,2'-azidoethyl)-azotetrazole (**6b**) was prepared in an identical manner by oxidative dimerization of **3b** using *t*-BuOCl as reagent.

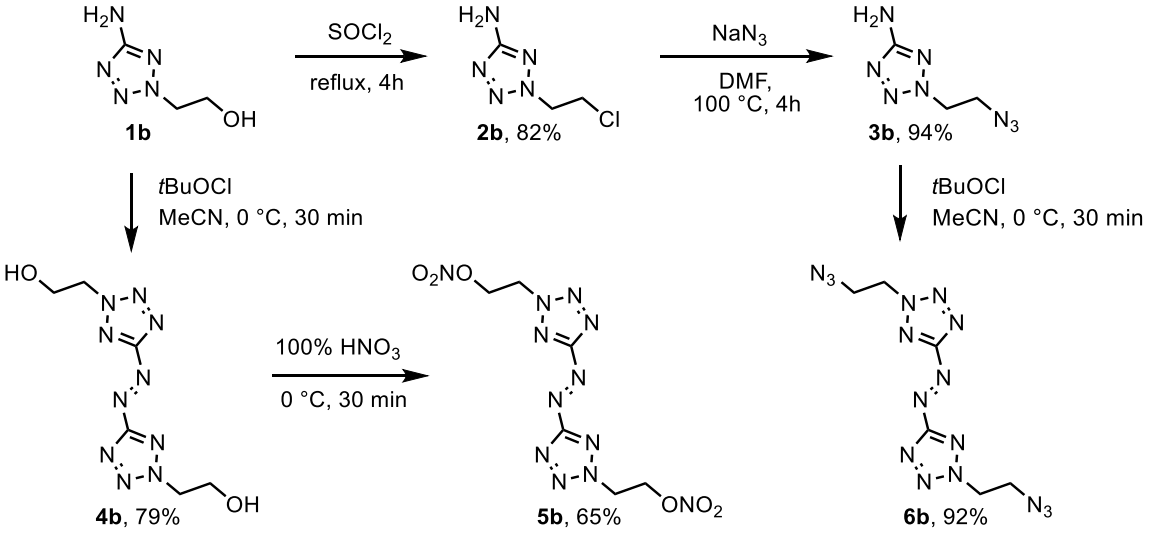

Scheme 2. Synthetic pathway for the synthesis of 2-substituted isomers starting from 2-(2-hydroxyethyl)-5-aminotetrazole (**1b**).

Single crystals suitable for low temperature X-ray diffraction were obtained directly from the reaction mixture (**4a**, **6a**, **6b**) or after recrystallization from dichloromethane (**5a**) or a mixture of acetonitrile and water (**5b**). Details on the structures of the compounds **4a** (CCDC no. 2090053) together with measurement and refinement data of all crystallographically investigated compounds can be found in the Supporting Information (Figures S1–2, Table S1). The datasets were uploaded to the CSD database under the CCDC nos. 2090058 (**5a**), 2090057 (**6a**), 2090056 (**5b**) and 2090054 (**6b**) and can be obtained free of charge. The bond lengths and angles in the 5,5'-azobistetrazole moieties, as well as in the nitratoethyl and azidoethyl groups as substituents on tetrazoles are in accordance with similar

structures already described in the literature and are therefore not part of the discussion.[20-21]

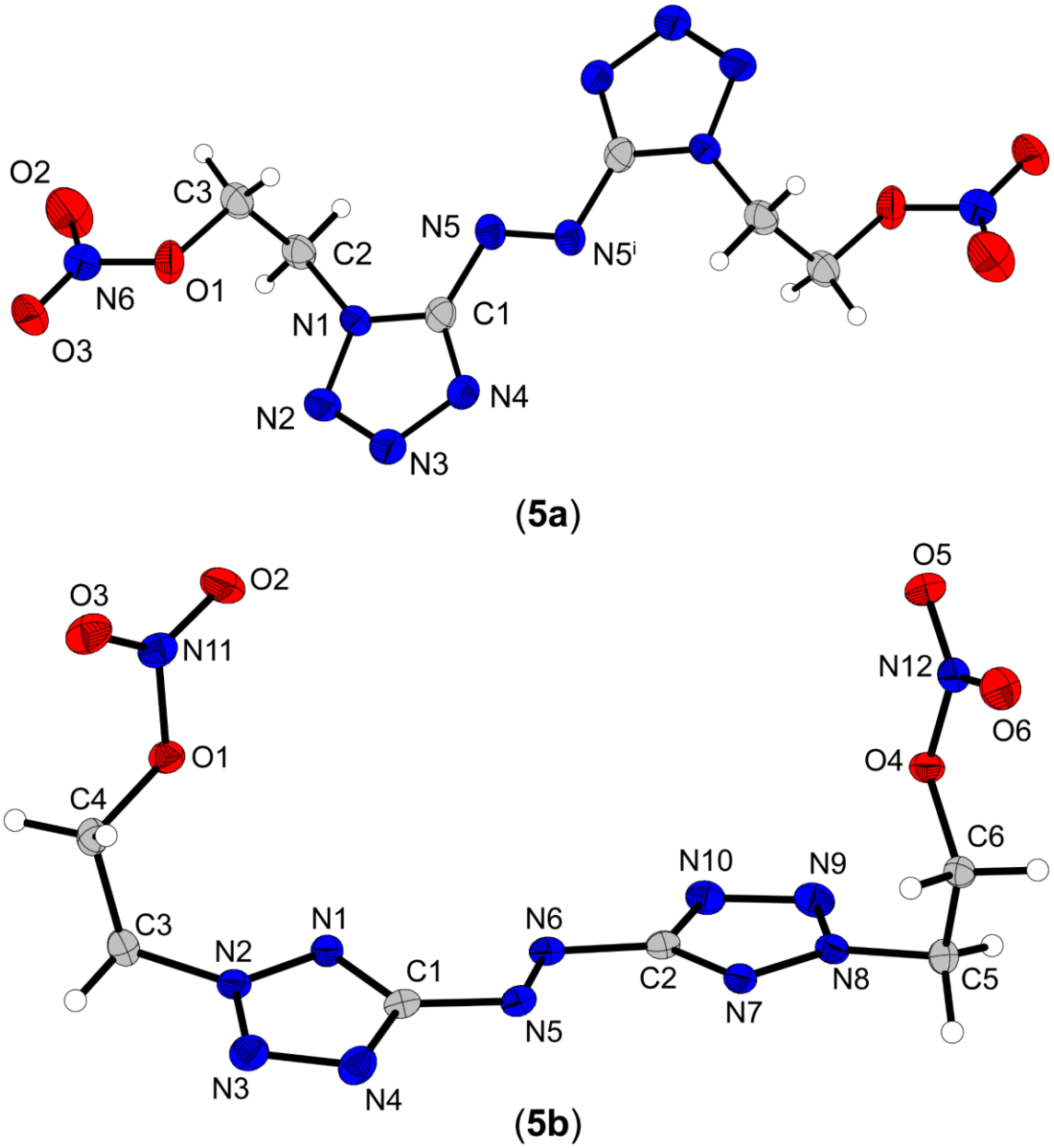

Figure 2. Low temperature crystal structures of the compounds **5a** and **5b**. Selected bond lengths (Å) of **5a**: N5−N5^{i} 1.259(3), N1−C2 1.460(3), O1−C3 1.456(3). Selected bond lengths (Å) of **5b**: N5−N6 1.258(2), N2−C3 1.461(2), C4−O1 1.453(2). Selected bond angles (°) of **5a**: N5^{i}−N5−C1 111.7(2), C1−N1−C2 130.69(18), C3−N6−N7 115.66(19). Selected bond angles (°) of **5b**: N6−N5−C1 112.20(15), N1−N2−C2 123.19(15), C4−O1−N11 113.20(14).

Both nitratoethyl derivatives crystalize in the monoclinic space group $P2_1/c$ with respectively two (**5a**) or four (**5b**) formula units per unit cell. In both structures, the ethyl groups are rotated out of the plane at approximately the same angle (**5a**: C1−N1−C2−C3=92.4(3) °; **5b**: N1−N2−C3−C4=83.21(18) °). The inversion

symmetry in **5a** results in an opposite position of the two ethyl groups, whereas in **5b**, due to the lack of symmetry, both residues stand away in roughly the same direction (Figure 2).

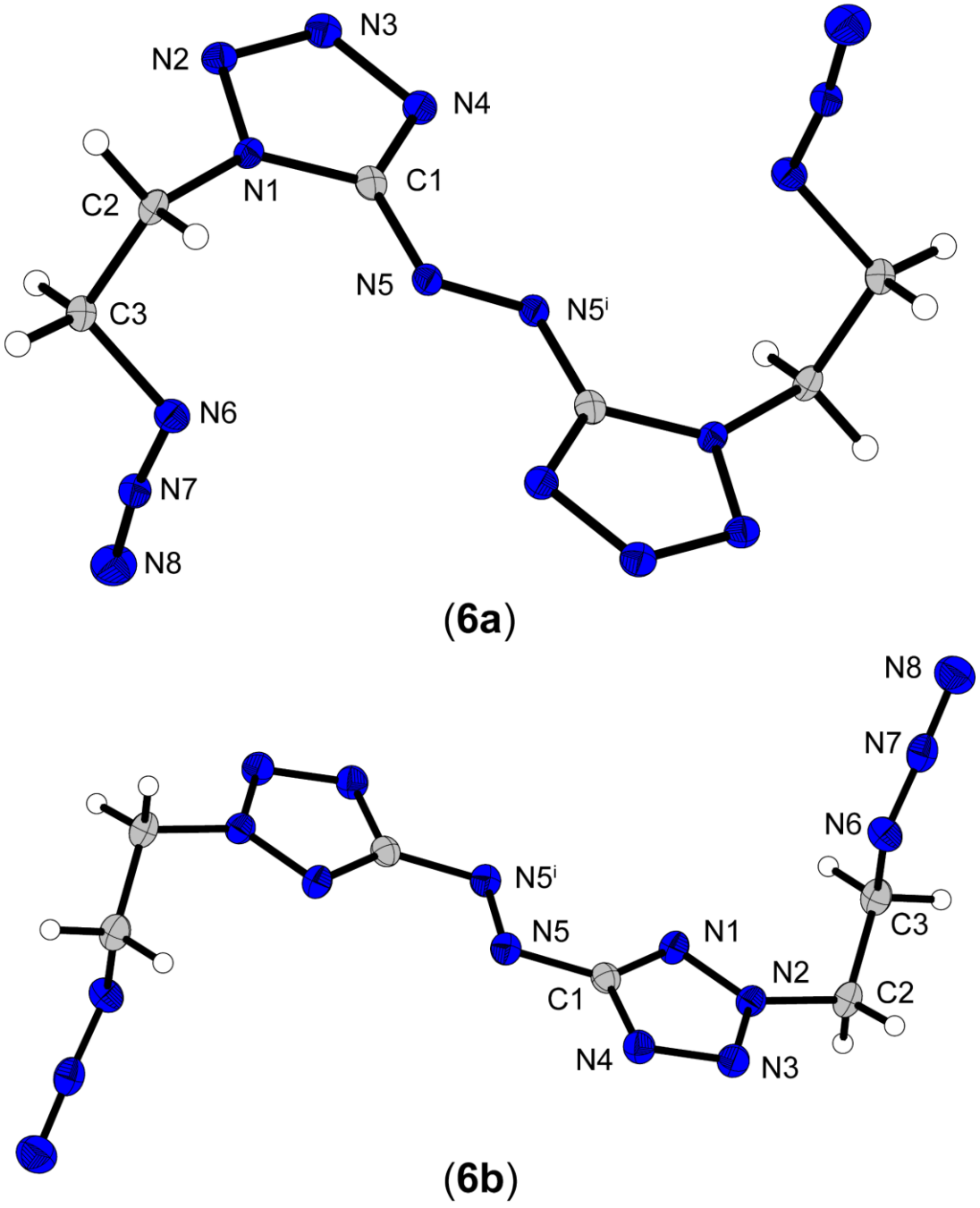

Figure 3. Low temperature crystal structures of the compounds **6a** and **6b**. Selected bond lengths (Å) of **6a**: N5−N5^{i} 1.263(4), N1−C2 1.469(3), N6−C3 1.480(3). Selected bond lengths (Å) of **6b**: N5−N5^{i} 1.2536(2), N2−C2 1.46606(17), C3−N6 1.4870(2). Selected bond angles (°) of **6a**: N5^{i}−N5−C1 111.4(3), C1−N1−C2 131.0(2), C3−N6−N7 114.3(2). Selected bond angles (°) of **6b**: N5^{i}−N5−C1 112.452(8), N1−N2−C2 123.753(10), C3−N6−N7 115.139(11).

The azidoethyl derivatives crystallize in a monoclinic space group (**6b**: $P2_1/n$) and a triclinic space group (**6a**: $P\bar{1}$). As already observed for compounds **5a** and **5b**,

the arrangement of the side chains of the molecule is represented by the torsion angle created by the tetrazole and ethyl groups. Since in this case both molecules possess an inversion symmetry, the azidoethyl moieties are located in opposite directions. The torsion angles, however, differ more clearly for **6a** (C1−N1−C2−C3=90.4(3) °) and **6b** (N1−N2−C2−C3=39.959(7)°) compared to **5a** and **5b** (Figure 3).

All compounds were investigated using ^{1}H and ^{13}C NMR spectroscopy. The C*H*$_2$ signals in the proton spectra for the respective ethyl functions, splitting up to doublet of doublet (dd) or multiplet (m) signals, appear, depending on the functional group (−Cl, −OH, −ONO_2, −N_3), in a region of 3.76–5.29 ppm.

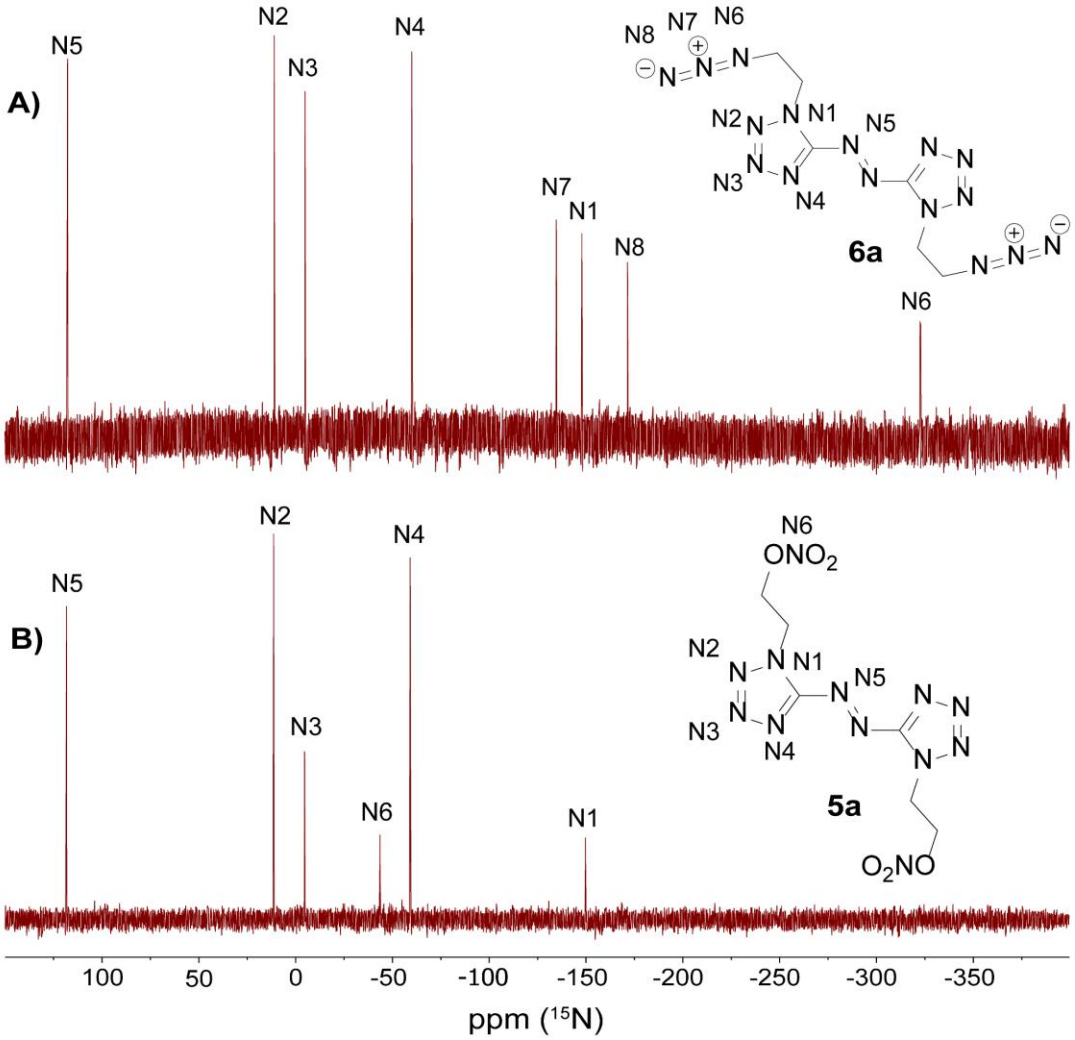

Figure 4. Proton coupled ^{15}N NMR spectra of **6a** (A) and **5a** (B) measured in DMSO-D_6.

Depending on the molecule, additional resonances for the respective O*H* or N*H*$_2$ function are detectable. Successful azo coupling is easily detectable by the

disappearance of the NH_2 singlet signal. All investigated compounds show three signals in the ^{13}C spectrum. The signals for the tetrazole carbon of the monomers occurs at around 156 ppm for the 1-substituted tetrazoles **1a**–**3a** and 167 ppm for 2-substituted derivatives (**1b**–**3b**) while the respective azo coupled products show a slight downfield shift for this signal. Furthermore, two signals for the ethyl rest are detectable, depending on the particular substitution thereof. As a result of inversion symmetry, for azo coupled compounds **4a**, **b**–**6a**, **b** only the half of the expected number of different resonances is obtained.

Due to poor solubility, ^{15}N NMR spectra were only measured for **5a** and **6a** (Figure 4). Assignments were only measured for performed on basis of spectra of several azotetrazoles[21] derivatives and 2D ^{1}H, ^{15}N HMBC spectra (for more details see the Supporting Information). Azotetrazole resonances N1−N5 appear homogenously for both compounds with the nitrogen N5, involved in the azo bridge, as the most downfield shifted signal (117.7 ppm for **6a** and 118.3 ppm for **5a**). Signals N1−N4 arise in the regular range as expected for 1-alkyl-5-aminotetrazoles. In addition, **5a** shows a signal at −43.6 ppm representing the organic nitrate N6. Nitrogen resonances of the azido function can be detected at −134.8 ppm (N_β), −171.6 ppm (N_γ) and −322.6 ppm (N_α) in the spectrum of **6a**.

Generally, compounds **5a**, **5b**, **6a** and **6b** can be classified[29] as sensitive to very sensitive energetic materials with high heats of formation (Table 1). The crystallographically determined room temperature densities range from 1.702 g cm^{-3} (**5a**) to 1.539 g cm^{-3} (**6b**), with the 2-substituted isomers each being less dense than the 1-substituted ones. The same applies to the comparison of nitrates and corresponding azides within the same substitution position. The calculated detonation parameters, which are closely linked to the respective density and heat of formation, respond analogously. Organic nitrates **5a** (8179 m s^{-1}) and **5b** (8060 m s^{-1}) both show higher values for detonation velocity then the respective azidoethyl derivatives. Azido compound **6a** (8148 m s^{-1}) is just slightly below the value of **5a**, whereas **6b** (7801 m s^{-1}) differs about 250 m s^{-1} from the nitrate **5b** due to a higher difference in density. The 1-isomeres also achieve higher decomposition temperatures than the 2-isomers. **5a** and **6a** decompose at around 180 °C, whereas **5b** already decomposes shortly below 100 °C. Sensitivity values toward impact and friction for **5a** (IS = 2 J, FS = 60 N) are comparable with those of PETN. As a trend for both, the respective azides and

the 2-substituted isomers are more sensitive compared to the 1-substituted homologs. Azide **6b** is the most sensitive compound in this study with IS < 1 J and FS = 0.2 N, which is in the range for primary explosives.

Table 1. Energetic properties and detonation parameters of azo compounds **5a**, **5b**, **6a** and **6b**.

	5a	**5b**	**6a**	**6b**	TNT
Formula	$C_6H_8N_{12}O_6$	$C_6H_8N_{12}O_6$	$C_6H_8N_{16}$	$C_6H_8N_{16}$	$C_7H_5N_3O_6$
M [g mol^{-1}]	344.21	344.21	304.24	304.24	227.13
IS [J][a]	2	< 1	4	< 1	15
FS [N][b]	60	20	6	0.2	353
ESD [J][c]	0.1	1.5	0.25	0.75	-
ρ [g cm^{-3}][d]	1.702	1.676	1.605	1.539	1.648
N [%][e]	48.8	48.8	73.7	73.7	18.5
Ω [%][f]	−18.6/−46.5	−18.6/−46.5	−52.6/−84.1	−52.6/−84.1	−24.7/−74.0
T_{melt}/T_{dec} [°C][g]	167/179	-/97	147/188	72/140	290
$\Delta_f H°$ [kJ mol^{-1}][h]	630.1	613.0	1456.2	1439.2	−55.5
$\Delta_f U°$[kJ mol^{-1}][i]	662.3	645.3	1486.0	1468.9	−168.0
		EXPLO5 V6.05.02			
$-\Delta_{Ex}U$ [kJ kg^{-1}][j]	5195	5135	4759	4702	4427
T_{det} [K][k]	3608	3598	3175	3181	3222
V_0 [L kg^{-1}][l]	782	785	777	782	633
P_{CJ} [kbar][m]	266	256	233	207	194
V_{det} [m s^{-1}][n]	8179	8060	8148	7801	6824

[a] Impact sensitivity (BAM drophammer (1 of 6)). [b] Friction sensitivity (BAM friction tester (1 of 6)). [c] Electrostatic discharge device (OZM research). [d] From X-ray diffraction analysis recalculated to 298 K. [e] Nitrogen content. [f] Oxygen balance with respect to CO/CO_2 [g] Melting/Decomposition temperature (DTA; β = 5 °C min^{-1}). [h] Calculated enthalpy of formation. [i] Calculated energy of formation. [j] Energy of explosion. [k] Detonation temperature. [l] Volume of detonation products (assuming only gaseous products). [m] Detonation pressure at Chapman-Jouguet point. [n] Detonation velocity.

13.3 Conclusion

Summarized, we report the synthesis by oxidative azo coupling of several 1- and 2-substituted 5-aminotetrazoles using *tert*-butyl hypochlorite as oxidation agent and characterization (XRD, NMR etc.) of 1- and 2-substituted nitratoethyl and azidoethyl substituted 5,5'-azotetrazoles and the examination of the utility as energetic materials. The 1-substituted isomers showed more promising results in term of detonation properties and thermal stabilities compared with the respective

2-substituted derivatives. In terms of sensitivity toward external stimuli and the respective calculated energetic parameters azidoethyl derivative **6a** and **6b** could be further investigated for potential application as primary explosives. Organic nitrate **5a** shows the most promising characteristics as it outperforms TNT with a detonation velocity of about 8200 m s^{-1} and a thermal stability as well as sensitivity values in the same range then PETN. Due to the simple and cheap synthesis, further applications in the field of sensitizers in rocket propellant mixtures are conceivable.

13.4 Acknowledgement

For financial support of this work by Ludwig-Maximilian University (LMU), the Office of Naval Research (ONR) under grant no. ONR N00014-19-1-2078 and the Strategic Environmental Research and Development Program (SERDP) under contract no. W912HQ19C0033 are gratefully acknowledged. We thank Prof. Konstantin Karaghiosoff for NMR measurements. Open access funding enabled and organized by Projekt DEAL.

13.5 References

[1] H. Gao, J. M. Shreeve, *Chem. Rev.* **2011**, *111*, 7377–7436.

[2] P. Pagoria, *Propellants, Explos., Pyrotech.* **2016**, *41*, 452–469.

[3] J. Ma, A. K. Chinnam, G. Cheng, H. Yang, J. Zhang, J. M. Shreeve, *Angew. Chem. Int. Ed.* **2021**, *60*, 5497–5504.

[4] T. M. Klapötke, *Chemistry of High-Energy Materials*, De Gruyter, Boston, Berlin, **2017**.

[5] O. T. O'Sullivan, M. J. Zdilla, *Chem. Rev.* **2020**, *120*, 5682–5744.

[6] T. M. Klapötke, T. G. Witkowski, *ChemPlusChem* **2016**, *81*, 357–360.

[7] W.-J. Geng, Q. Ma, Y. Chen, W. Yang, Y.-F. Jia, J.-S. Li, Z.-Q. Zhang, G.-J. Fan, S.-M. Wang, *Cryst. Growth Des.* **2020**, *20*, 2106–2114.

[8] S.-F. Zhu, Q. Gan, C. Feng, *ACS Omega* **2019**, *4*, 13408–13417.

[9] Z. Yang, H. Wang, Y. Ma, Q. Huang, J. Zhang, F. Nie, J. Zhang, H. Li, *Cryst. Growth Des.* **2018**, *18*, 6399–6403.

[10] P. Yin, J. M. Shreeve, in *Advances in Heterocyclic Chemistry, Vol. 121*, Academic Press, **2017**, 89–131.

[11] H. Huang, J. Zhong, L. Ma, L. Lv, J. S. Francisco, X. C. Zeng, *J. Am. Chem. Soc.* **2019**, *141*, 2984–2989.

[12] K. Banert, T. Pester, *Angew. Chem. Int. Ed.* **2020**, *59*, 12315–12320.

[13] S. Shaaban, A. Negm, A. M. Ashmawy, D. M. Ahmed, L. A. Wessjohann, *Eur. J. Med. Chem.* **2016**, *122*, 55–71.

[14] N. Fischer, D. Fischer, T. M. Klapötke, D. G. Piercey, J. Stierstorfer, *J. Mater. Chem.* **2012**, *22*, 20418–20422.

[15] J. W. Fronabarger, M. D. Williams, W. B. Sanborn, J. G. Bragg, D. A. Parrish, M. Bichay, *Propellants, Explos., Pyrotech.* **2011**, *36*, 541–550.

[16] M. H. H. Wurzenberger, M. Lommel, M. S. Gruhne, N. Szimhardt, J. Stierstorfer, *Angew. Chem. Int. Ed.* **2020**, *59*, 12367–12370.

[17] Q. Sun, X. Li, Q. Lin, M. Lu, *J. Mater. Chem. A* **2019**, *7*, 4611–4618.

[18] M. Zhang, W. Fu, C. Li, H. Gao, L. Tang, Z. Zhou, *Eur. J. Inorg. Chem.* **2017**, *2017*, 2883–2891.

[19] Y. Tang, J. M. Shreeve, *Chem. Eur. J.* **2015**, *21*, 7285–7291.

[20] F. Li, X. Cong, Z. Du, C. He, L. Zhao, L. Meng, *New J. Chem.* **2012**, *36*, 1953–1956.

[21] D. Fischer, T. M. Klapötke, D. G. Piercey, J. Stierstorfer, *Chem. Eur. J.* **2013**, *19*, 4602–4613.

[22] A. Hammerl, G. Holl, Thomas M. Klapötke, P. Mayer, H. Nöth, H. Piotrowski, M. Warchhold, *Eur. J. Inorg. Chem.* **2002**, *2002*, 834–845.

[23] D. Fischer, T. M. Klapötke, J. Stierstorfer, N. Szimhardt, *Chem. Eur. J.* **2016**, *22*, 4966–4970.

[24] T. Küblböck, G. Angé, G. Bikelytė, J. Pokorná, R. Skácel, T. M. Klapötke, *Angew. Chem. Int. Ed.* **2020**, *59*, 12326–12330.

[25] R. A. Henry, W. G. Finnegan, *J. Am. Chem. Soc.* **1954**, *76*, 923–926.

[26] Y.-H. Joo, J. M. Shreeve, *Org. Lett.* **2008**, *10*, 4665–4667.

[27] J. Stierstorfer, K. R. Tarantik, T. M. Klapötke, *Chem. Eur. J.* **2009**, *15*, 5775–5792.

[28] D. E. Chavez, J. C. Bottaro, M. Petrie, D. A. Parrish, *Angew. Chem. Int. Ed.* **2015**, *54*, 12973–12975.

[29] Impact: Insensitive > 40 J, less sensitive ≥ 35 J, sensitive ≥ 4 J, very sensitive ≥ 3 J; friction: Insensitive > 360 N, less sensitive = 360 N, sensitive < 360 N, > 80 N, very sensitive ≥ 80 N, extreme sensitive ≥ 10 N; according to the UN recommendations on the transport of dangerous goods.

13.6 Supporting Information

13.6.1 Experimental Procedure

^{1}H, ^{13}C, ^{14}N and ^{15}N NMR spectra were recorded on *BRUKER AMX 400* instruments. Chemical shifts are referenced with respect to tetramethylsilane ($^{1}H/^{13}C$) and nitromethane ($^{14}N/^{15}N$). Infrared spectra (IR) were recorded in the region 4000-400 cm^{-1} on a *PERKIN ELMER Spectrum BX-59343* instrument with a *SMITHS DETECTION DuraSamplIR II Diamond ATR* sensor. Raman spectra were recorded with a Bruker MultiRAM. The absorption bands are reported in wavenumbers (cm^{-1}). Decomposition temperatures were measured via differential thermal analysis (DTA) with an *OZM Research DTA 552-Ex* instrument at a heating rate of 5 °C/min and in a range of room temperature to 400 °C. All sensitivities toward impact (IS) and friction (FS) were determined according to BAM (Bundesanstalt für Materialforschung und Prüfung) standards using a BAM drop hammer and a BAM friction apparatus by applying the 1 of 6 method.[S1] All energetic compounds were tested for sensitivity towards electrical discharge using an *Electric Spark Tester ESD 2010 EN* from OZM. Energetic properties have been calculated with the EXPLO5 6.02 computer [S2] code using the RT converted X-ray density and calculated solid state heats of formation.

CAUTION! *All investigated compounds are potentially explosive materials. Safety precautions and equipment (such as wearing leather coat, face shield, Kevlar sleeves, Kevlar gloves, earthed equipment and ear plugs) must be used during all manipulations.*

The synthesis of compounds **1a** and **1b** was prepared according to literature known methods by Finnegan et al.[S3] Compounds **2a** and **3a** were synthesized following

the described procedures in the literature.[S4] These procedures, excluding the work-ups, were used in the same manner for the synthesis of **2b** and **3b**.[S4]

Bis(1,1'-(2,2'-hydroxyethyl))azotetrazole (**4a**)

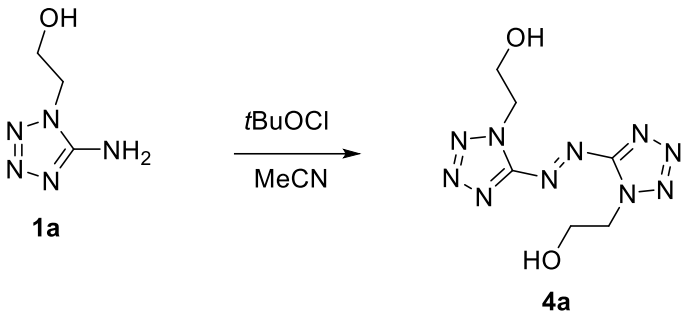

1-(2-Hydroxyethyl)-5-aminotetrazole (**1a**) (1.00 g, 7.75 mmol, 1.0 eq) was dissolved in MeCN (50 mL) and cooled to 0 °C with an ice bath. *t*BuOCl (2.19 mL, 19.3 mmol, 2.5 eq) was added dropwise and the mixture was stirred for 30 min 0 °C. After further stirring at room temperature for 1 h sodium carbonate (3.00 g) was added to quench the reaction. The solid was filtered off and the filtrate was evaporated to yield bis(1,1'-(2,2'-hydroxyethyl))azotetrazole (**4a**) as orange microcrystalline powder (0.90 g, 3.53 mmol, 91%).

DTA (5 ° min^{-1}): 164 °C (melt), 183 °C (dec); IR (ATR) $\tilde{\nu}$ (cm^{-1}) = 3467(s), 2955(w), 1615(w), 1517(m), 1483(w), 1457(s), 1428(m), 1378(m), 1352(w), 1326(w), 1255(m), 1146(m), 1058(vs), 1032(s), 1005(m), 947(m), 867(m), 760(s), 745(s), 717(w), 680(s), 549(s), 499(vs), 424(vs).; Elem. Anal. ($C_6H_{10}N_{10}O_2$, 254.21 g mol^{-1}) calcd.: C 28.35, N 55.10, H 3.97%. Found: C 28.22, N 55.22, H 3.89%; ^{1}H NMR (DMSO-D_6, 400 MHz, ppm) δ = 4.84 (dd, *J* = 5.7, 4.8 Hz, 4H), 3.90 (dd, *J* = 5.7, 4.7 Hz, 4H); ^{13}C NMR (DMSO-D_6, 101 MHz, ppm) δ = 159.9, 59.2, 51.3; HR-MS (ESI, 70 eV): [$C_6H_{10}N_{10}O_2$] calcd.: 255.1061 (M + H+) , found: 255.1062.

Bis(1,1'-(2,2'-nitratoethyl))azotetrazole (**5a**)

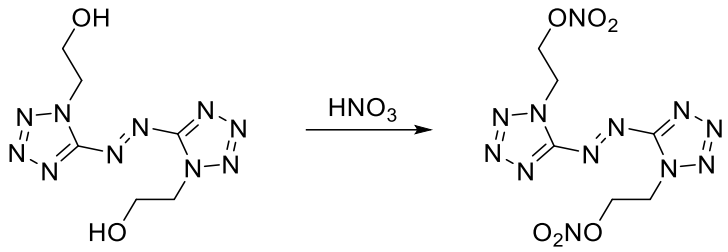

4a **5a**

Bis(1,1'-(2,2'-hydroxyethyl))azotetrazole (**4a**) (0.70 g, 2.76 mmol, 1.0 eq) was added in portions to HNO_3 (6 mL, 100%) at 0 °C. The mixture was stirred at this temperature for 30 min. The cooling-bath was removed and the mixture was quenched on ice-water (60 mL). The formed precipitate was filtered and washed with little amount of cold water to yield bis(1,1'-(2,2'-nitratoethyl))azotetrazole (**5a**) (0.77 g, 2.23 mmol, 81%) as orange solid.

Sensitivities: BAM drop hammer: 2 J (<100 µm), friction tester: 60 N (<100 µm), ESD: 100 mJ (<100 µm); DTA (5 ° min^{-1}): 167 °C (melt), 179 °C (dec); IR (ATR) ṽ (cm^{-1}) = 1630(s), 1452(m), 1427(m), 1280(vs), 1244(w), 1156(m), 1066(m), 1009(w), 987(m), 918(w), 893(vs), 846(s), 751(m), 741(m), 718(w), 710(w), 679(s), 641(m), 572(w), 552(w), 542(w), 496(m), 420(m); Elem. Anal. ($C_6H_8N_{12}O_6$, 344.21 g mol^{-1}) calcd.: C 20.94, N 48.83, H 2.34%. Found: C 21.02, N 48.65, H 2.39%; ^{1}H NMR (DMSO-D_6, 400 MHz, ppm) δ = 5.19 (dd, *J* = 5.5, 4.1 Hz, 4H), 5.09 (dd, *J* = 5.5, 4.0 Hz, 4H); ^{13}C NMR (DMSO-D_6, 101 MHz, ppm) δ = 159.4, 70.2, 46.3; ^{15}N NMR (DMSO-D_6, 41 MHz, ppm) δ = 118.3, 11.4, −4.6, −43.6, −59.1, −149.8; HR-MS (ESI, 70 eV): [$C_6H_8N_{12}O_6$] calcd.: 343.0617 (M − H+) , found: 343.0621.

Bis(1,1'-(2,2'-azidoethyl))azotetrazole (**6a**)

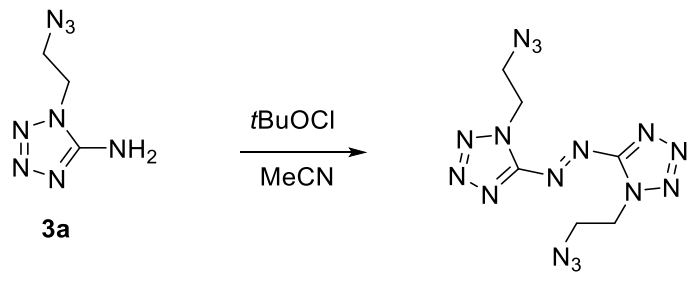

3a **6a**

1-(2-Azidoethyl)-5-aminotetrazole (**3a**) (1.00 g, 6.49 mmol, 1.0 eq) was dissolved in MeCN (50 mL) and cooled to 0 °C with an ice bath. *t*BuOCl (1.83 mL, 16.2 mmol, 2.5 eq) was added dropwise and the mixture was stirred for 30 min 0 °C. After further stirring at room temperature for 1 h sodium carbonate (3.00 g) was added to quench the reaction. The solid was filtered off and the filtrate was evaporated to yield bis(1,1'-(2,2'-azidoethyl))azotetrazole (**6a**) as pale orange crystals (0.85 g, 2.79 mmol, 86%).

Sensitivities: BAM drop hammer: 4 J (<100 µm), friction tester: 6 N (<100 µm), ESD: 250 mJ (<100 µm); DTA (5 ° min^{-1}): 147 °C (melt), 188 °C (dec); IR (ATR) $\tilde{\nu}$ (cm^{-1}) = 2142(vs), 2106(vs), 1500(m), 1444(s), 1425(s), 1372(m), 1342(s), 1291(vs), 1255(m), 1245(s), 1230(s), 1200(m), 1144(s), 1049(m), 1011(m), 949(s), 837(m), 760(s), 738(s), 662(s), 631(vs), 563(vs), 551(s), 489(vs), 422(vs); Elem. Anal. ($C_6H_8N_{16}$, 304.24 g mol^{-1}) calcd.: C 23.69, N 73.66, H 2.65%. Found: C 24.27, N 73.10, H 2.74%; ^{1}H NMR (DMSO-D_6, 400 MHz, ppm) δ = 5.03 – 4.91 (m, 4H), 4.08 – 3.95 (m, 4H); ^{13}C NMR (DMSO-D_6, 101 MHz, ppm) δ = 159.5, 49.1, 48.2; ^{15}N NMR (DMSO-D_6, 41 MHz, ppm) δ = 117.7, 11.0, −5.0, −60.1, −134.8, −148.0, −171.6, −322.6; HR-MS (ESI, 70 eV): [$C_6H_8N_{16}$] calcd.: 304.1118 (M) , found: 304.1126.

2-(2-Chloroethyl)-5-aminotetrazole (**2b**)[S4]

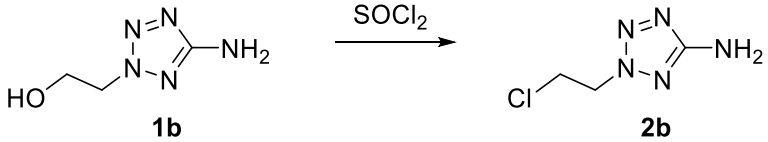

1b **2b**

2-(2-Hydroxyethyl)-5-aminotetrazole (**1b**) (2.00 g, 15.5 mmol, 1.0 eq) was added to $SOCl_2$ (6.6 mL) keeping the temperature below 20 °C. After the addition was complete the mixture was refluxed at 80 °C for 4 h. The solvent was removed under reduced pressure and the remaining thionyl chloride was quenched by adding cold ethanol (20 mL) and cold water (20 mL). The solvent was removed under reduced pressure and the crude product was recrystallized from hot benzene to separate 2-(2-chloroethyl)-5-aminotetrazole (**2b**) (1.87 g, 12.7 mmol, 82%) as a slightly brownish oil.

DTA (5 ° min^{-1}) = 201 °C (dec); IR (ATR) ṽ (cm^{-1}) = 3335(m), 3230(w), 1622(s), 1543(vs), 1434(m), 1373(m), 1290(m), 1198(s), 1147(m), 1081(m), 1011(m), 956(m), 908(m), 788(m), 756(s), 668(s), 624(s), 452(s), 436(s), 419(s), 404(s); Elem. Anal. ($C_3H_6N_5Cl$, 147.57 g mol^{-1}) calcd.: C 24.42, N 47.46, H 4.10%. Found: C 24.64, N 47.10, H 4.31%; ^{1}H NMR (DMSO-D_6, 400 MHz, ppm) δ = 5.85 (s, 2H), 4.75 (dd, *J* = 6.0, 5.0 Hz, 2H), 4.07 (dd, *J* = 6.0, 5.0 Hz, 2H); ^{13}C NMR (DMSO-D_6, 101 MHz, ppm) δ = 167.2, 53.5, 42.1; HR-MS (ESI, 70 eV): [$C_3H_6N_5Cl$] calcd.: 148.0384 (M + H+), found: 148.0385.

2-(2-Azidoethyl)-5-aminotetrazole (**3b**)[S4]

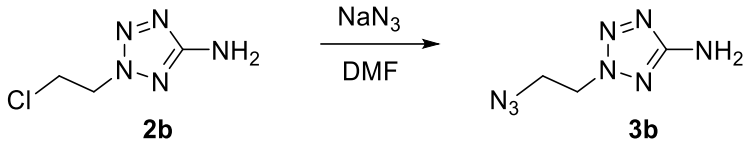

2-(2-Chloroethyl)-5-aminotetrazole (**2b**) (1.87 g, 12.7 mmol, 1.0 eq) was solved in DMF (25 mL) and sodium azide (0.91 g, 140.0 mmol, 1.1 eq) was added. The mixture was stirred for 4 h at 100 °C. The solvent was removed under reduced pressure and water (50 mL) was added. The mixture was extracted with EtOAc (3 x 50 mL), the organic phases were dried over anhydrous sodium sulfate and the solvent removed under reduced pressure to yield 2-(2-azidoethyl)-5-aminotetrazole (**3b**) (1.83 g, 11.9 mmol, 94%) as brownish oil.
DTA (5 ° min^{-1}) = 209 °C (dec); IR (ATR) ṽ (cm^{-1}) = 3336(m), 2101(vs), 1622(s), 1542(vs), 1440(m), 1365(m), 1280(m), 1199(s), 1081(m), 1011(m), 790(m), 757(m), 625(s), 553(s), 497(s), 443(s), 416(s), 407(s); Elem. Anal. ($C_3H_6N_5Cl$, 154.14 g mol^{-1}) calcd.: C 23.38, N 72.70, H 4.26%. Found: C 23.61, N 72.13, H 4.26%; ^{1}H NMR (DMSO-D_6, 400 MHz, ppm) δ = 6.07 (s, 2H), 4.66 – 4.54 (m, 2H), 3.86 – 3.76 (m, 2H); ^{13}C NMR (DMSO-D_6, 101 MHz, ppm) δ = 167.8, 51.8, 49.5; HR-MS (ESI, 70 eV): [$C_3H_6N_8$] calcd.: 155.0788 (M + H+), found: 155.0794.

Bis(2,2'-(2,2'-hydroxyethyl))azotetrazole (**4b**)

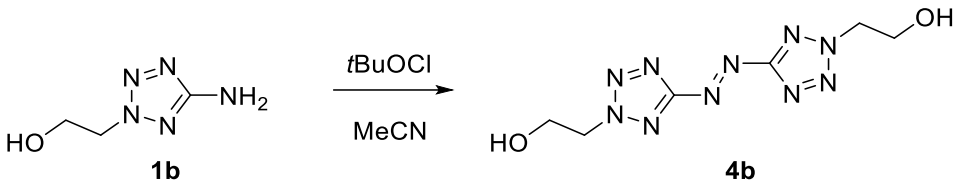

2-(2-Hydroxyethyl)-5-aminotetrazole (**1b**) (1.00 g, 7.75 mmol, 1.0 eq) was dissolved in MeCN (50 mL). *t*BuOCl (2.19 mL, 19.3 mmol, 2.5 eq) was added dropwise and the mixture was stirred for 30 min at ambient temperature. Afterwards, sodium carbonate (3.00 g) was added to quench the reaction. The solid was filtered off and the filtrate was evaporated to yield bis(2,2'-(2,2'-hydroxyethyl))azotetrazole (**4a**) as a yellowish oil (0.78 g, 3.06 mmol, 79%).
DTA (5 ° min^{-1}) = 101 °C (dec); IR (ATR) $\tilde{\nu}$ (cm^{-1}) = 3361(m), 3224(w), 2950(w), 1739(w), 1633(w), 1524(m), 1469(s), 1397(m), 1363(m), 1195(m), 1066(vs), 1030(s), 956(m), 868(s), 827(m), 764(s), 741(s), 660(s), 601(s), 507(vs), 452(s), 442(s), 415(s), 405(s); Elem. Anal. ($C_6H_{10}N_{10}O_2$, 254.21 g mol^{-1}) calcd.: C 28.35, N 55.10, H 3.97%. Found: C 27.91, N 54.02, H 4.61%; ^{1}H NMR (Acetone-D_6, 400 MHz, ppm) δ = 4.84 – 4.75 (m, 4H), 4.30 (t, *J* = 5.9 Hz, 2H), 4.13 (q, *J* = 5.4 Hz, 4H); ^{13}C NMR (Acetone-D_6, 101 MHz, ppm) δ = 167.4, 57.7, 55.9; HR-MS (ESI, 70 eV): [$C_6H_{10}N_{10}O_2$] calcd.: 255.1061 (M + H+), found: 255.1059.

Bis(2,2'-(2,2'-nitratoethyl))azotetrazole (**5b**)

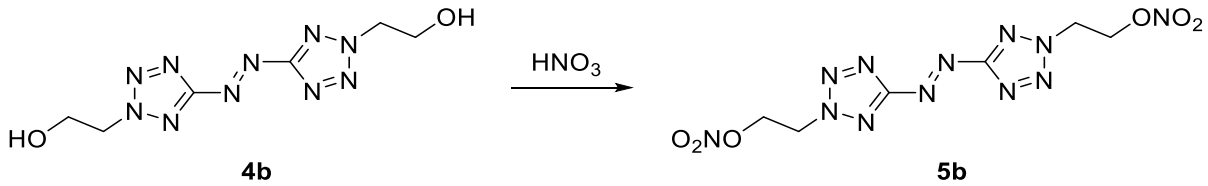

Bis(2,2'-(2,2'-hydroxyethyl))azotetrazole (**4b**) (0.56 g, 2.20 mmol, 1.0 eq) was added dropwise to HNO_3 (4 mL, 100%) at 0 °C. The mixture was stirred at this temperature for 30 min. The cooling-bath was removed and the mixture was stirred for further 30 min at ambient temperature. Afterwards, the solution was quenched on ice-water (60 mL). The solution was extracted with ethyl acetate (3 x 50 mL).

The combined organic phases were dried over anhydrous sodium sulfate and the solvent was reduced to yield bis(2,2'-(2,2'-nitratoethyl))azotetrazole (**5b**) (0.49 g, 1.43 mmol, 65%) as yellowish solid.

Sensitivities: BAM drop hammer: <1 J (<100 µm), friction tester: 20 N (<100 µm), ESD: 1.5 J (<100 µm); DTA (5 ° min^{-1}): 97 °C (dec); IR (ATR) ṽ (cm^{-1}) = 1631(s), 1611(s), 1519(w), 1430(m), 1361(m), 1279(vs), 1213(m), 1158(w), 1095(w), 1061(w), 1036(m), 1020(m), 889(vs), 848(s), 772(m), 755(s), 714(s), 706(s), 679(m), 646(m), 637(m), 575(m), 565(m), 508(m), 492(m), 438(m); Elem. Anal. ($C_6H_8N_{12}O_6$, 344.21 g mol^{-1}) calcd.: C 20.94, N 48.83, H 2.34%. Found: C 20.19, N 47.99, H 2.27%; ^{1}H NMR (Acetone-D_6, 400 MHz, ppm) δ = 5.41 – 5.38 (m, 4H), 5.31 – 5.29(m, 4H); ^{13}C NMR (Acetone-D_6, 101 MHz, ppm) δ = 172.7, 70.8, 52.5; ^{14}N NMR (Acetone-D_6, 29 MHz, ppm) δ = −44; HR-MS (ESI, 70 eV): [$C_6H_8N_{12}O_6$] calcd.: 379.0384 (M + Cl−) , found: 379.0389.

Bis(2,2'-(2,2'-azidoethyl))azotetrazole (**6b**)

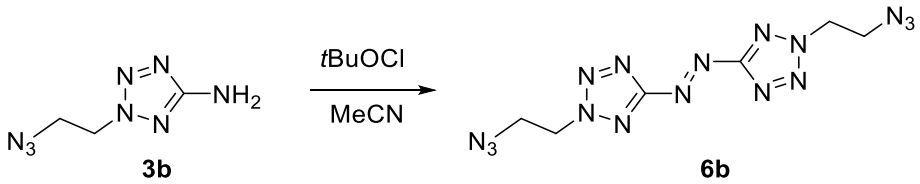

3b **6b**

2-(2-Azidoethyl)-5-aminotetrazole (**3b**) (0.50 g, 3.25 mmol, 1.0 eq) was dissolved in MeCN (50 mL) and cooled to 0 °C with an ice bath. *t*BuOCl (0.92 mL, 8.1 mmol, 2.5 eq) was added dropwise and the mixture was stirred for 30 min at 0 °C. After further stirring at room temperature for 1 h sodium carbonate (1.50 g) was added to quench the reaction. The solid was filtered off and the filtrate was evaporated to yield bis(2,2'-(2,2'-azidoethyl))azotetrazole (**6b**) as low melting orange crystals (0.46 g, 1.50 mmol, 92%).

Sensitivities: BAM drop hammer: <1 J (<100 µm), friction tester: 0.2 N (<100 µm), ESD: 750 mJ (<100 µm); DTA (5 ° min^{-1}): 72 °C (melt), 140 °C (dec); IR (ATR) ṽ (cm^{-1}) = 1631(s), 1611(s), 1519(w), 1430(m), 1361(m), 1279(vs), 1213(m), 1158(w), 1095(w), 1061(w), 1036(m), 1020(m), 889(vs), 848(s), 772(m), 755(s), 714(s), 706(s), 679(m), 646(m), 637(m), 575(m), 565(m), 508(m), 492(m), 438(m); Elem. Anal. ($C_6H_8N_{16}$, 304.24 g mol^{-1}) calcd.: C 23.69, N 73.66, H 2.65%. Found: C 24.05, N 71.02, H 2.67%; ^{1}H NMR (Acetone-D_6, 400 MHz, ppm) δ = 5.15 – 5.08

(m, 4H), 4.20 – 4.17 (m, 4H); ^{13}C NMR (Acetone-D_6, 101 MHz, ppm) δ = 172.8, 54.3, 50.3; ^{14}N NMR (Acetone-D_6, 29 MHz, ppm) δ = −90, −135, −170, −315; HR-MS (ESI, 70 eV): [$C_6H_8N_{16}$] calcd.: 304.1118 (M) , found: 304.1124.

Bis(1,1'-(2,2'-chloroethyl))azotetrazole (**7**)

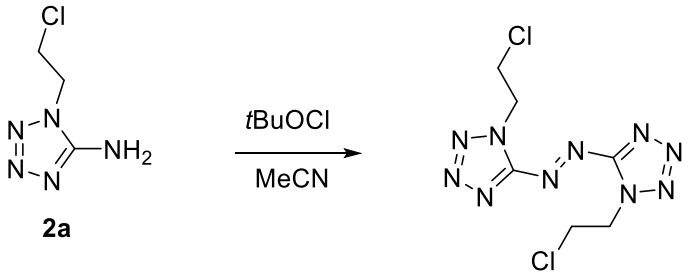

Bis(1,1'-(2,2'-chloroethyl))azotetrazole (**7**) was synthesized through oxidative azo coupling starting from 1-(2-chloroethyl)-5-aminotetrazole (**2a**). The subsequent chlorine-azide exchange failed and ended up with decomposition products.

1-(2-Chloroethyl)-5-aminotetrazole (**2a**) (1.00 g, 6.80 mmol, 1.0 eq) was dissolved in MeCN (50 mL) and cooled to 0 °C with an ice bath. *t*BuOCl (1.92 mL, 17.0 mmol, 2.5 eq) was added dropwise and the mixture was stirred for 30 min 0 °C. After further stirring at room temperature for 1 h sodium carbonate (3.00 g) was added to quench the reaction. The solid was filtered off and the filtrate was evaporated to yield bis(1,1'-(2,2'-chloroethyl))azotetrazole (**7**) as orange crystals (0.87 g, 2.99 mmol, 88%).

DTA (5 ° min^{-1}) = 119 °C (melt), 181 °C (dec); IR (ATR) ṽ (cm^{-1}) = 3334(m), 3150(m), 1647(s), 1590(s), 1479(m), 1442(m), 1428(m), 1303(s), 1132(s), 1103(s), 991(m), 944(s), 908(m), 744(m), 681(s), 651(vs), 563(s), 484(s), 451(vs), 436(s), 424(s), 414(s), 406(m); Elem. Anal. ($C_6H_8N_{10}Cl_2$, 291.10 g mol^{-1}) calcd.: C 24.76, N 48.12, H 2.77%. Found: C 24.80, N 47.29, H 3.11%; ^{1}H NMR (Acetone-D_6, 400 MHz, ppm) δ = 5.32 (dd, *J* = 6.0, 5.4 Hz, 4H), 4.31 (dd, *J* = 6.0, 5.4 Hz, 4H); ^{13}C NMR (Acetone-D_6, 101 MHz, ppm) δ = 161.1, 51.1, 43.0; HR-MS (ESI, 70 eV): [$C_6H_8N_{10}Cl_2$] calcd.: 290.0310 (M), found: 290.0317.

1-(2-((*Tert*-butyldimethylsilyl)oxy)ethyl)-5-aminotetrazole (**8**)

1-(2-((*Tert*-butyldimethylsilyl)oxy)ethyl)-5-aminotetrazole (**8**) was prepared using a classic procedure for the TBS protection of alkylic hydroxy groups. **8** should be further reacted to the azo compound but this reaction failed and ended up with decomposition products.

2-(2-Hydroxyethyl)-5-aminotetrazole (**1b**) (1.00 g, 7.75 mmol, 1.0 eq) was dissolved in DMF (10 mL) and imidazole (1.27 g, 18.6 mmol, 2.4 eq) was added. After 10 min, TBSCl (1.52 g, 10.1 mmol, 1.3 eq) was added in one portion and the mixture was stirred overnight. The solvent was evaporated under reduced pressure and water (20 mL) was added. After extraction with EtOAc (3 x 50 mL), the combined organic phases were dried over sodium sulfate and the solvent was evaporated. **8** was obtained after purification using flash column chromatography (*i*Hex/EtOAc: 3:1) as transparent crystals (1.39 g, 5.72 mmol, 74%).
IR (ATR) $\tilde{\nu}$ (cm^{-1}) = 3365(m), 3226(w), 2928(m), 2880(w), 2856(m), 1647(m), 1551(s), 1471(m), 1459(m), 1431(w), 1388(m), 1373(w), 1360(w), 1260(m), 1250(m), 1192(s), 1114(s), 1088(m), 1066(w), 1018(m), 1007(m), 971(w), 935(vs), 840(s), 827(s), 810(s), 797(s), 777(vs), 759(s), 727(s), 682(m), 664(s), 630(s), 574(m), 498(m), 475(m), 442(m), 402(m); Elem. Anal. ($C_9H_{21}N_5OSi$, 243.39 g mol^{-1}) calcd.: C 44.41, N 28.78, H 8.70%. Found: C 44.32, N 28.45, H 8.75%; ^{1}H NMR (DMSO-D_6, 400 MHz, ppm) δ = 5.95 (s, 2H), 4.44 (dd, *J* = 5.6, 4.7 Hz, 2H), 3.99 (dd, *J* = 5.6, 4.7 Hz, 2H), 0.77 (s, 9H), -0.07 (s, 6H); ^{13}C NMR (DMSO-D_6, 101 MHz, ppm) δ = 167.0, 60.6, 54.5, 25.6, 17.8, −5.6; HR-MS (ESI, 70 eV): [$C_9H_{21}N_5OSi$] calcd.: 244.1588 (M + H+), found: 244.1589.

13.6.2 Crystallography

Crystal structure data were obtained from an Oxford Xcalibur3 diffractometer with a Spellman generator (voltage 50 kV, current 40 mA) and a Kappa CCD area for data collection using Mo-*Kα* radiation (*λ* = 0.71073 Å) or a Bruker D8 Venture TXS diffractometer equipped with a multilayer monochromator, a Photon 2 detector and a rotation-anode generator (Mo-K_α radiation). The data collection was performed using the CRYSTALIS RED software.[S5] The solution of the structure was performed by direct methods and refined by full-matrix least-squares on F2 (SHELXT)[S6] implemented in the OLEX2[S7] software suite. The non-hydrogen atoms were refined anisotropically and the hydrogen atoms were located and freely refined. The absorption correction was carried out by a SCALE3 ABSPACK multiscan method.[S8] The DIAMOND2 plots shown with thermal ellipsoids at the 50% probability level and hydrogen atoms are shown as small spheres of arbitrary radius. The SADABS program embedded in the Bruker APEX3 software was used for multi-scan absorption corrections in all structures.[S9]

Deposition Numbers 2090058 (for **5a**), 2090057 (for **6a**), 2090056 (for **5b**), and 2090054 (for **6b**) contain the supplementary crystallographic data for this paper.

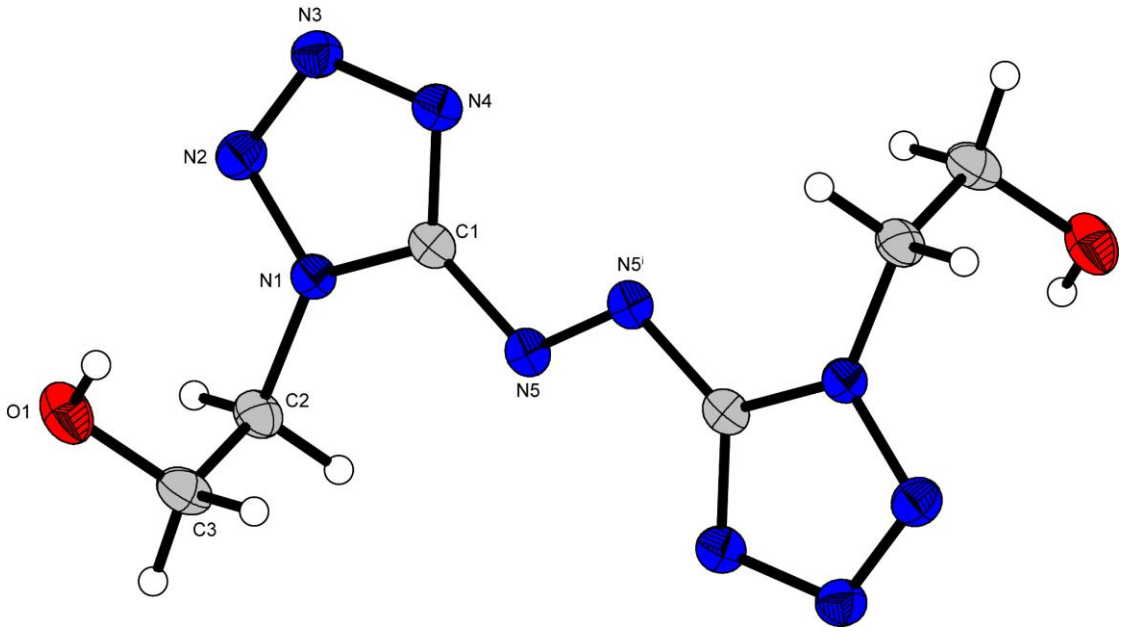

Figure S1. Representation of the molecular unit of bis(1,1'-(2,2'-hydroxyethyl))azotetrazole (**4a**), showing the atom-labeling scheme. Thermal ellipsoids represent the 50% probability level and hydrogen atoms are shown as small spheres of arbitrary radius. Symmetry code: (i) 1−x, −y, 1−z.

Table S1. Crystallographic data of **4a**–**6a**.

	4a	**5a**	**6a**
Formula	$C_6H_{10}N_{10}O_2$	$C_6H_8N_{12}O_6$	$C_6H_8N_{16}$
FW [g mol^{-1}]	254.24	344.24	304.28
Crystal system	monoclinic	monoclinic	triclinic
Space group	*P*2$_1$/*c* (No. 14)	*P*2$_1$/*c* (No. 14)	*P*-1 (No. 2)
Color / Habit	yellow plate	yellow plate	yellow block
Size [mm]	0.17 x 0.28 x 0.56	0.04 x 0.23 x 0.44	0.08 x 0.15 x 0.25
a [Å]	7.9346(6)	10.6870(19)	5.7863(6)
b [Å]	5.3456(3)	6.3382(7)	6.7887(9)
c [Å]	13.1451(10)	9.7961(11)	8.6292(13)
α [°]	90	90	107.343(13)
β [°]	99.932(7)	99.437(14)	96.706(11)
γ [°]	90	90	104.792(10)
V [Å^3]	549.20(7)	654.57(16)	305.93(8)
Z	2	2	1
$\rho_{calc.}$ [g cm^{-3}]	1.537	1.747	1.652
μ [mm^{-1}]	0.122	0.154	0.127
F(000)	264	352	156
$\lambda_{MoK\alpha}$ [Å]	0.71073	0.71073	0.71073
T [K]	101	123	101
θ Min-Max [°]	2.6, 29.1	3.8, 26.4	2.5, 26.4
Dataset	-6: 10 ; -6: 7 ; -17: 16	-11: 13 ; -7: 7 ; -12: 12	-7: 7 ; -8: 8 ; -10: 9
Reflections collected	3398	4795	2265
Independent refl.	1278	1331	2265
R_{int}	0.021	0.056	0.056
Observed reflections	1036	853	1490
Parameters	102	125	117
R_1 (obs)[a]	0.0362	0.0471	0.0390
wR_2 (all data)[b]	0.0863	0.0825	0.1108
S [c]	1.07	0.99	0.94
Resd. dens [e Å^{-3}]	-0.23, 0.23	-0.21, 0.20	-0.24, 0.29
Device type	Xcalibur Sapphire3	Xcalibur Sapphire3	Xcalibur Sapphire3
Solution	SIR-92	SIR-92	SIR-92
Refinement	SHELXL-2013	SHELXL-2013	SHELXL-2013
Absorption correction	multi-scan	multi-scan	multi-scan
CCDC	2090053	2090058	2090057

[a] $R_1 = \Sigma||F_o|-|F_c||/\Sigma|F_o|$; [b] $wR_2 = [\Sigma[w(F_o^2-F_c^2)^2]/\Sigma[w(F_o)^2]]^{1/2}$; $w = [\sigma c^2(F_o^2)+(xP)^2+yP]^{-1}$ and $P=(F_o^2+2F_c^2)/3$; [c] $S = (\Sigma[w(F_o^2-F_c^2)^2]/(n-p))^{1/2}$ (n = number of reflections; p = total number of parameters).

Table S2. Crystallographic data of **5b** and **6b**.

	5b	**6b**
Formula	$C_6H_8N_{12}O_6$	$C_6H_8N_{16}$
FW [g mol^{-1}]	344.24	304.28
Crystal system	monoclinic	monoclinic
Space group	$P2_1/c$ (No. 14)	$P2_1/n$ (No. 14)
Color / Habit	yellow plate	yellow block
Size [mm]	0.11 x 0.36 x 0.50	0.20 x 0.50 x 0.50
a [Å]	7.4267(7)	5.1580(7)
b [Å]	16.8712(17)	10.7193(15)
c [Å]	11.037(1)	11.548(2)
α [°]	90	90
β [°]	106.561(10)	91.751(12)
γ [°]	90	90
V [Å^3]	1325.5(2)	638.19(17)
Z	4	2
$\rho_{calc.}$ [g cm^{-3}]	1.725	1.584
μ [mm^{-1}]	0.152	0.121
F(000)	704	312
$\lambda_{MoK\alpha}$ [Å]	0.71073	0.71073
T [K]	103	101
θ Min-Max [°]	2.3, 29.3	2.6, 29.3
Dataset	-9: 9 ; -21: 21 ; -14: 11	-6: 7 ; -13: 14 ; -14: 15
Reflections collected	9249	5104
Independent refl.	3126	1502
R_{int}	0.032	0.035
Observed reflections	2216	1043
Parameters	249	116
R_1 (obs)[a]	0.0437	0.0444
wR_2 (all data)[b]	0.0949	0.1074
S [c]	1.05	1.08
Resd. dens [e Å^{-3}]	-0.31, 0.25	-0.26, 0.20
Device type	Xcalibur Sapphire3	Xcalibur Sapphire3
Solution	SIR-92	SIR-92
Refinement	SHELXL-2013	SHELXL-2013
Absorption correction	multi-scan	multi-scan
CCDC	2090056	2090054

[a] $R_1 = \Sigma||F_o|-|F_c||/\Sigma|F_o|$; [b] $wR_2 = [\Sigma[w(F_o^2-F_c^2)^2]/\Sigma[w(F_o)^2]]^{1/2}$; $w = [\sigma c^2(F_o^2)+(xP)^2+yP]^{-1}$ and $P=(F_o^2+2F_c^2)/3$; [c] $S = (\Sigma[w(F_o^2-F_c^2)^2]/(n-p))^{1/2}$ (n = number of reflections; p = total number of parameters).

Table S2. Crystallographic data of **7** and **8**.

	7	**8**
Formula	$C_6H_8Cl_2N_{10}$	$C_9H_{21}N_5OSi$
FW [g mol^{-1}]	291.12	243.40
Crystal system	monoclinic	monoclinic
Space group	$P2_1/n$ (No. 14)	$P2_1/c$ (No. 14)
Color / Habit	yellow block	colorless platelet
Size [mm]	0.18 x 0.38 x 0.69	0.01 x 0.35 x 0.40
a [Å]	6.9577(5)	16.3221(14)
b [Å]	10.1969(6)	7.0344(7)
c [Å]	8.6636(7)	12.1424(11)
α [°]	90	90
β [°]	109.474(8)	92.685(8)
γ [°]	90	90
V [Å^3]	579.49(8)	1392.6(2)
Z	2	4
$\rho_{calc.}$ [g cm^{-3}]	1.668	1.161
μ [mm^{-1}]	0.561	0.160
F(000)	296	528
$\lambda_{MoK\alpha}$ [Å]	0.71073	0.71073
T [K]	135	123
θ Min-Max [°]	3.2, 26.4	2.5, 26.4
Dataset	-8: 8 ; -12: 12 ; -10: 10	-19: 20 ; -8: 8 ; -15: 15
Reflections collected	4250	10764
Independent refl.	1187	2855
R_{int}	0.025	0.057
Observed reflections	1096	1904
Parameters	82	229
R_1 (obs)[a]	0.0340	0.0519
wR_2 (all data)[b]	0.0901	0.1165
S [c]	1.14	1.03
Resd. dens [e Å^{-3}]	-0.24, 0.41	-0.24, 0.34
Device type	Xcalibur Sapphire3	Xcalibur Sapphire3
Solution	SIR-92	SIR-92
Refinement	SHELXL-2013	SHELXL-2013
Absorption correction	multi-scan	multi-scan
CCDC	2090055	2091285

[a]R1 = Σ||F0|−|Fc||/Σ|F0|; [b]wR2 = [Σ[w(F02−Fc2)2]/Σ[w(F0)2]]1/2; w = [σc2(F02)+(xP)2+yP]−1 and P=(F02+2Fc2)/3; [c]S = (Σ[w(Fo2−Fc2)2]/(n−p))1/2 (n = number of reflections; p = total number of parameters).

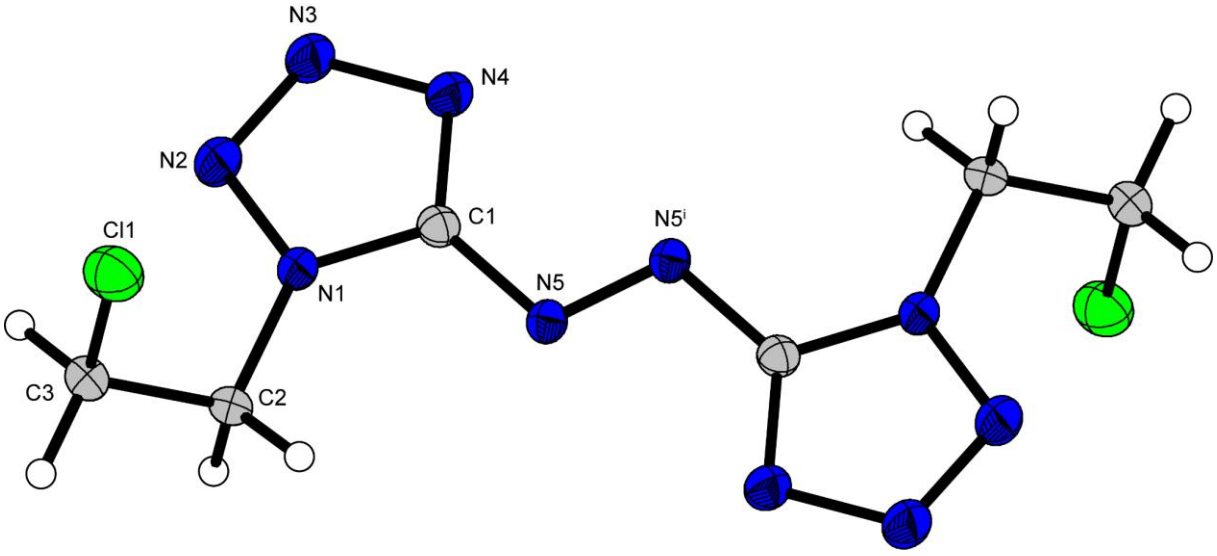

Figure S2. Representation of the molecular unit of bis(1,1'-(2,2'-chloroethyl))azotetrazole (**7**), showing the atom-labeling scheme. Thermal ellipsoids represent the 50% probability level and hydrogen atoms are shown as small spheres of arbitrary radius. Symmetry code: (i) 1−x, −y, 1−z.

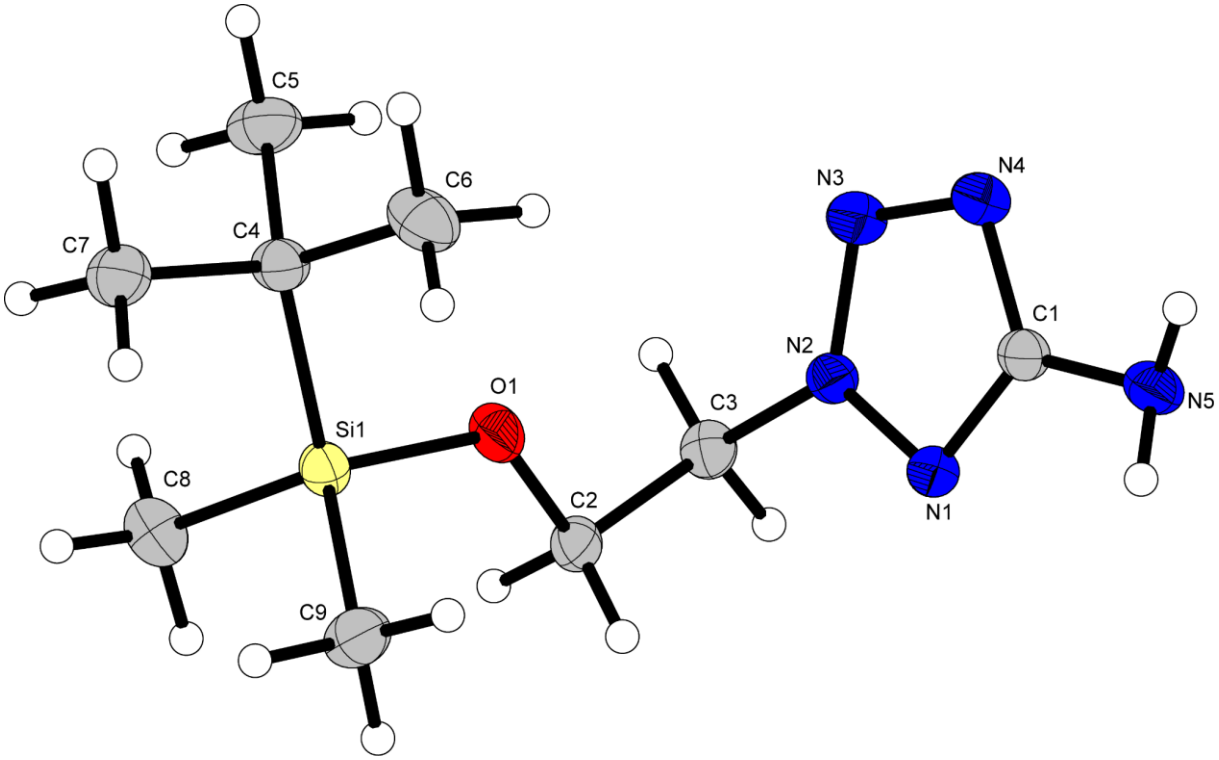

Figure S3. Representation of the molecular unit of 1-(2-((tert-butyldimethylsilyl)oxy)ethyl)-5-aminotetrazole (**8**), showing the atom-labeling scheme. Thermal ellipsoids represent the 50% probability level and hydrogen atoms are shown as small spheres of arbitrary radius.

13.6.3 Computation

All quantum chemical calculations were carried out using the Gaussian G09 program package.[S10] The enthalpies (H) and free energies (G) were calculated using the complete basis set (CBS) method of Petersson and co-workers in order to obtain very accurate energies. The CBS models are using the known asymptotic convergence of pair natural orbital expressions to extrapolate from calculations using a finite basis set to the estimated CBS limit. CBS-4 starts with an HF/3-21G(d) geometry optimization; the zero-point energy is computed at the same level. It then uses a large basis set SCF calculation as a base energy, and an MP2/6- 31+G calculation with a CBS extrapolation to correct the energy through second order. A MP4(SDQ)/6-31+ (d,p) calculation is used to approximate higher order contributions. In this study, we applied the modified CBS-4M.

Heats of formation of the synthesized ionic compounds were calculated using the atomization method (equation E1) using room temperature CBS-4M enthalpies, which are summarized in Table S4.[S11, S12]

$$\Delta_f H^\circ_{(g,\,M,\,298)} = H_{(Molecule,\,298)} - \sum H^\circ_{(Atoms,\,298)} + \sum \Delta_f H^\circ_{(Atoms,\,298)} \qquad (E1)$$

Table S4. CBS-4M electronic enthalpies for atoms C, H, N and O and their literature values for atomic $\Delta H^\circ_f{}^{298}$ / kJ mol^{-1}

	$-H^{298}$ [a.u.]	NIST[S13]
H	0.500991	218.2
C	37.786156	717.2
N	54.522462	473.1
O	74.991202	249.5

For neutral compounds the sublimation enthalpy, which is needed to convert the gas phase enthalpy of formation to the solid state one, was calculated by the *Trouton* rule.[S14] For ionic compounds, the lattice energy (U_L) and lattice enthalpy (ΔH_L) were calculated from the corresponding X-ray molecular volumes according to the equations provided by *Jenkins* and *Glasser*.[S15] With the calculated lattice enthalpy the gas-phase enthalpy of formation was converted into the solid state (standard conditions) enthalpy of formation. These molar standard enthalpies of

formation (ΔH_m) were used to calculate the molar solid state energies of formation (ΔU_m) according to equation E2.

$$\Delta U_m = \Delta H_m - \Delta n\, RT \qquad \text{(E2)}$$

(Δn being the change of moles of gaseous components)

The calculation results are summarized in Table S5.

Table S5. Calculation results.

	$-H^{298}$ [a] [a.u.]	$\Delta_f H°$(g,M) [kJ mol^{-1}] [b]	V_M [Å^3] [c]	ΔU_L; ΔH_L [d] [kJ mol^{-1}]	$\Delta_f H°$(s) [e] [kJ mol^{-1}]	Δn [f]	$\Delta_f U$(s) [g] [kJ kg^{-1}]
5a	1339.702032	712.9	-	-	630.1	13	1924.2
5b	1339.713477	682.8	-	-	613.0	13	1874.6
6a	1107.682135	1535.2	-	-	1456.2	12	4884.3
6b	1107.693998	1504.1	-	-	1439.2	12	4828.3

[a] CBS-4M electronic enthalpy; [b] gas phase enthalpy of formation; [c] molecular volumes taken from X-ray structures and corrected to room temperature; [d] lattice energy and enthalpy (calculated using Jenkins and Glasser equations); [e] standard solid state enthalpy of formation; [f] Δn being the change of moles of gaseous components when formed; [g] solid state energy of formation.

13.6.4 Thermal Analysis

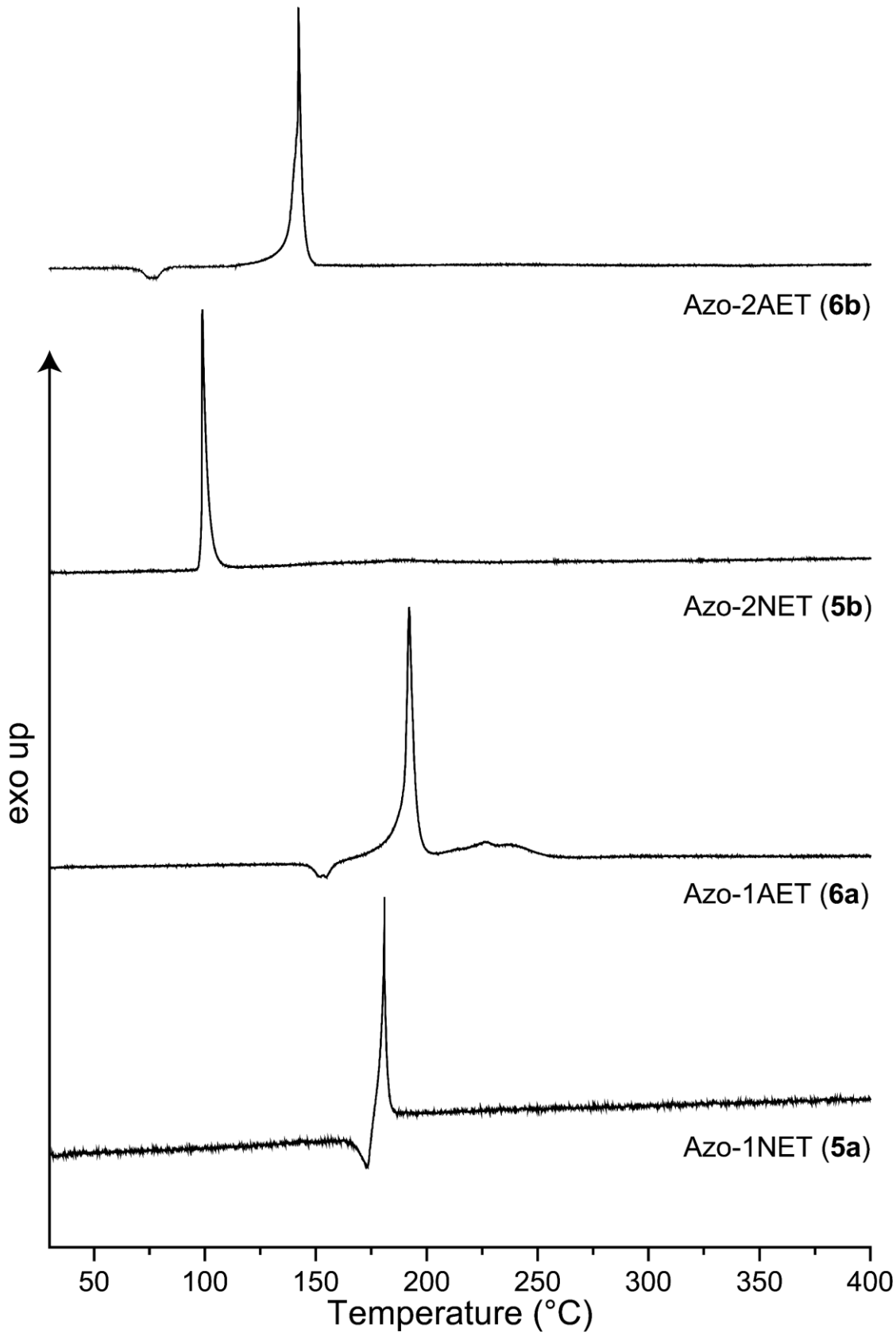

Figure S4. DTA plots of compounds **5a**, **5b**, **6a** and **6b**.

13.6.5 Scanning Electron Microscopy (SEM)

To show the microscopic differences of the gained compounds **5a**, **5b**, **6a** and **6b** scanning electron microscopy (SEM) was performed. In each case, images were taken at low magnification to show the entirety of the crystals and to assess the morphology. Close-up images of the crystals show the surface texture.
Bis(1,1'-(2,2'-nitratoethyl))azotetrazole (**5a**) crystallizes in very thin plates that tend to form stacks (Figure S5). The crystal surface is very smooth and there is hardly any intergrowth between the crystals.

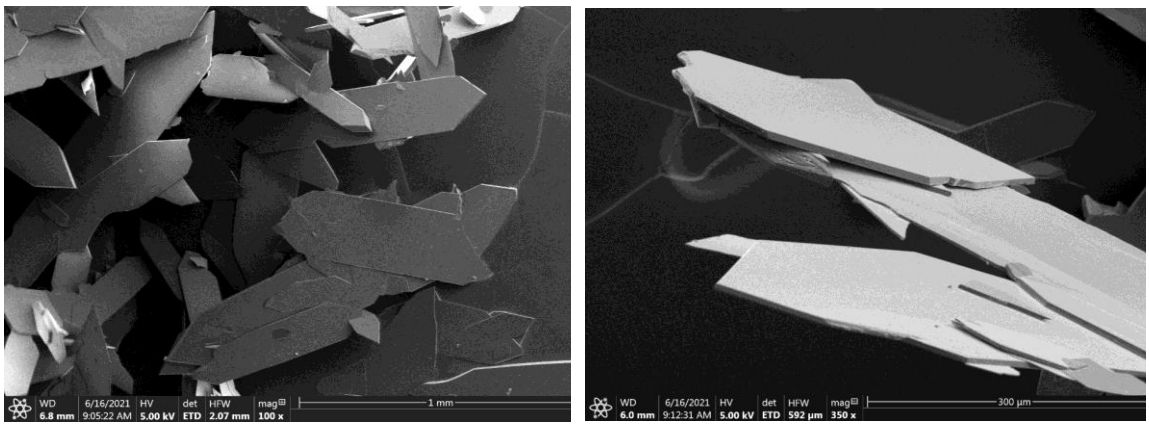

Figure S5. SEM images with 100x magnitude (left) and 350x magnitude (right) of **5a**.

The 2-substituted isomer bis(2,2'-(2,2'-nitratoethyl))azotetrazole (**5b**) consists of mostly long elongated blocks (Figure S6). The surface of the crystal is rougher than for **5a** and some crystals are intergrown.

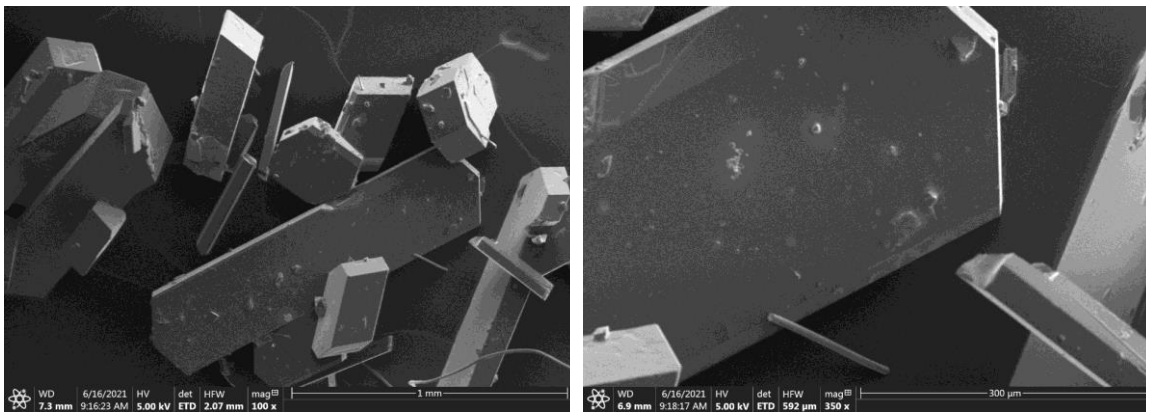

Figure S6. SEM images with 100x magnitude (left) and 350x magnitude (right) of **5b**.

The crystals of bis(1,1'-(2,2'-azidoethyl))azotetrazole (**6a**) form agglomerates of rods and blocks (Figure S7). They are strongly intergrown and exhibit also microcrystalline areas on the surface.

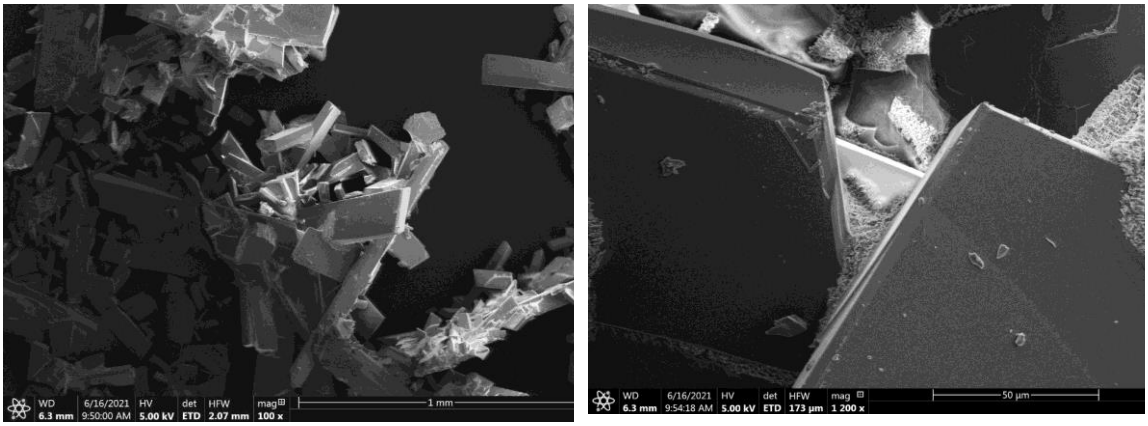

Figure S7. SEM images with 100x magnitude (left) and 1200x magnitude (right) of **6a**.

Bis(1,1'-(2,2'-azidoethyl))azotetrazole (**6b**) shows a different habit than the compounds above (Figure S8). During crystallization large agglomerates are formed with a rigid and pours surface.

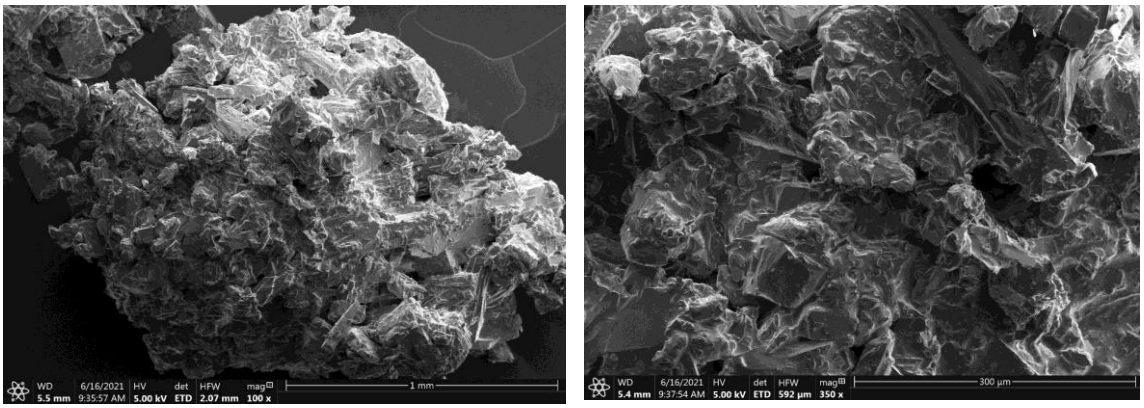

Figure S8. SEM images with 100x magnitude (left) and 350x magnitude (right) of **6b**.

13.6.6 NMR Spectroscopy

^{1}H-NMR (400 MHz, DMSO-D$_6$, ppm)

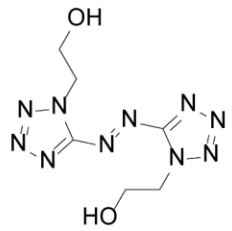

4a

^{13}C-NMR (101 MHz, DMSO-D$_6$, ppm)

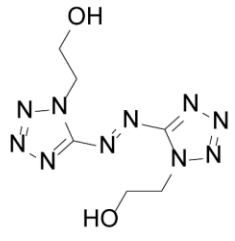

4a

¹H-NMR (400 MHz, DMSO-D₆, ppm)

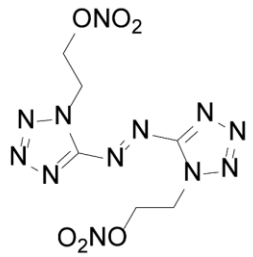

5a

¹³C-NMR (101 MHz, DMSO-D₆, ppm)

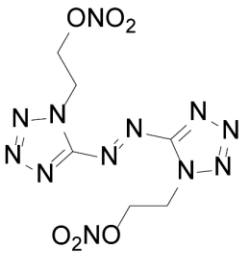

5a

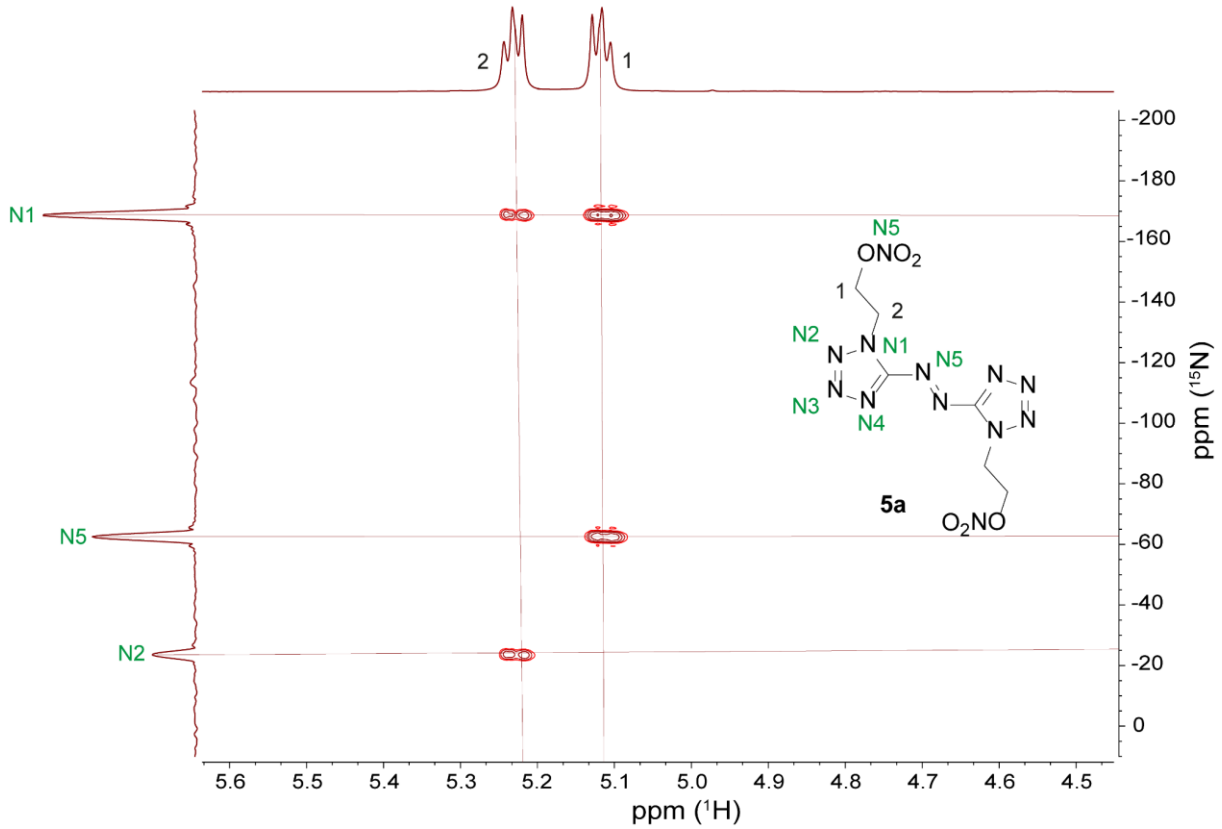
2
1
N1
N5
N2
-200
-180
-160
-140
-120
-100
-80
-60
-40
-20
0
ppm (15N)
5.6
5.5
5.4
5.3
5.2
5.1
5.0
4.9
4.8
4.7
4.6
4.5
ppm (1H)
N5
ONO2
1
2
N2
N1
N5
N3
N4
5a
O2NO

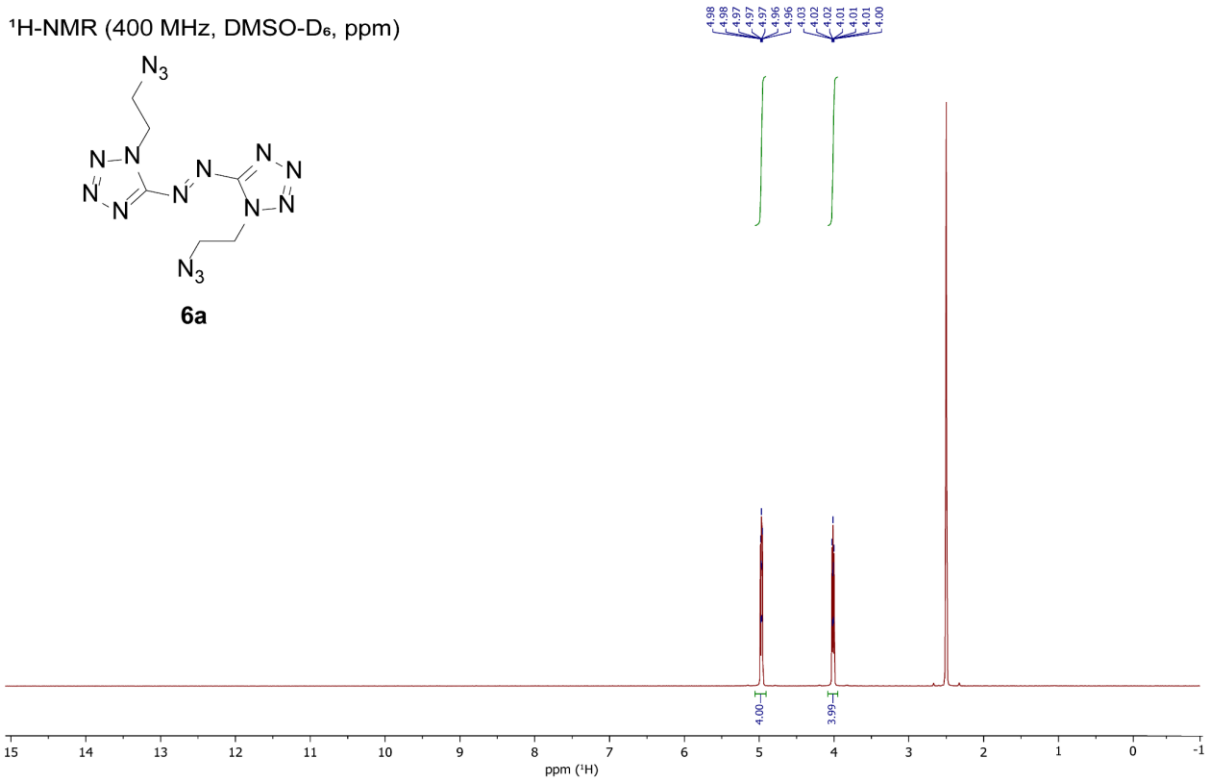
1H-NMR (400 MHz, DMSO-D6, ppm)
N3
N3
6a
4.98
4.98
4.97
4.97
4.97
4.96
4.96
4.03
4.02
4.02
4.01
4.01
4.01
4.00
4.00
3.99
15
14
13
12
11
10
9
8
7
6
5
4
3
2
1
0
-1
ppm (1H)

^{13}C-NMR (101 MHz, DMSO-D$_6$, ppm)

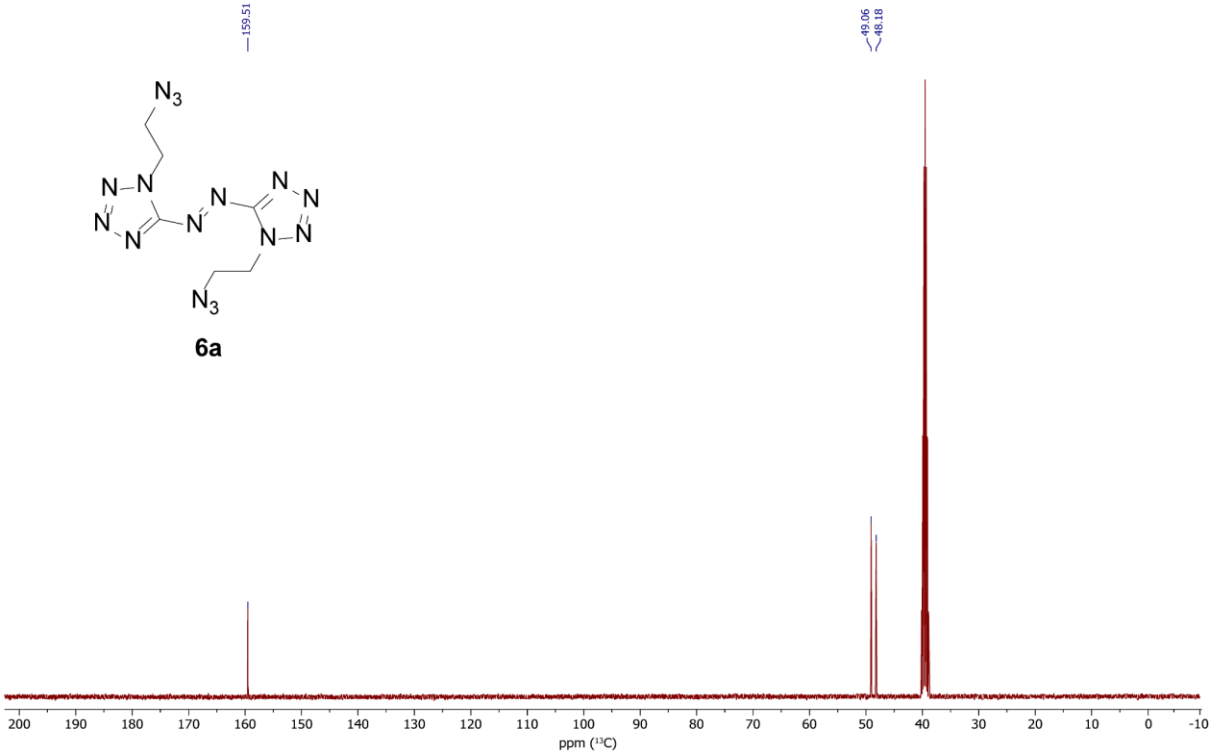

6a

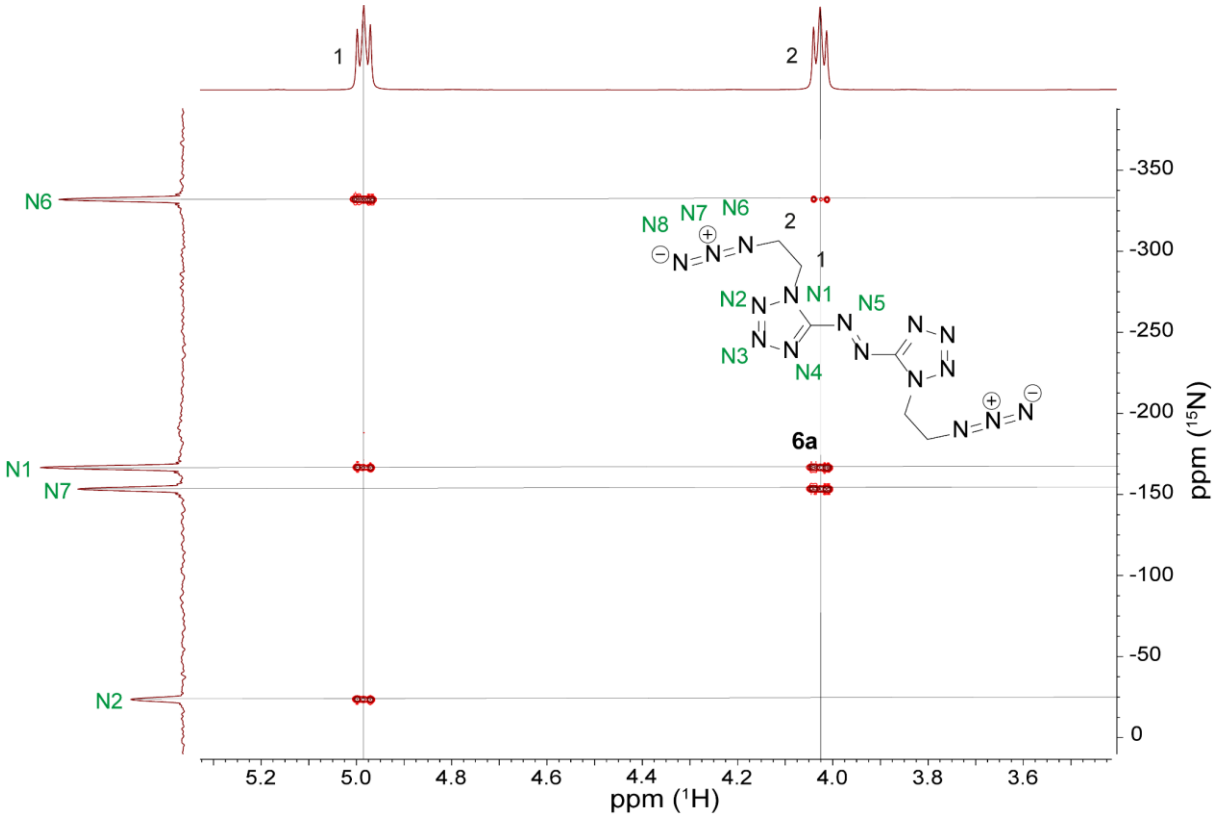

¹H-NMR (400 MHz, DMSO-D₆, ppm)

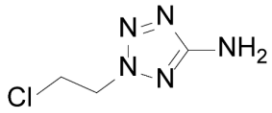

2b

¹³C-NMR (101 MHz, DMSO-D₆, ppm)

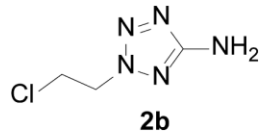

2b

¹H-NMR (400 MHz, DMSO-D₆, ppm)

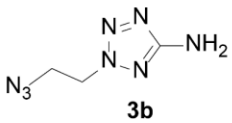

3b

¹³C-NMR (101 MHz, DMSO-D₆, ppm)

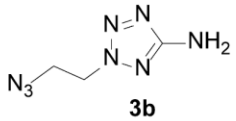

3b

¹H-NMR (400 MHz, Acetone-D₆, ppm)

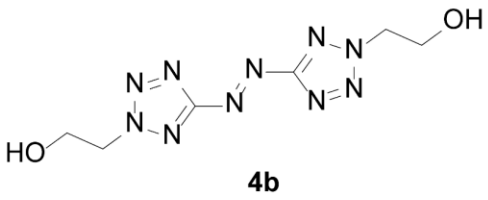

4b

¹³C-NMR (101 MHz, Acetone-D₆, ppm)

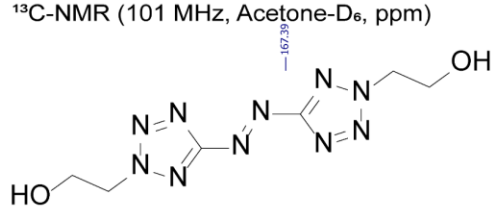

4b

¹H-NMR (400 MHz, Acetone-D₆, ppm)

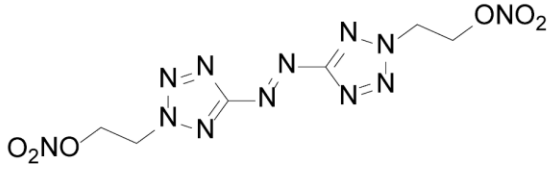

5b

¹³C-NMR (101 MHz, Acetone-D₆, ppm)

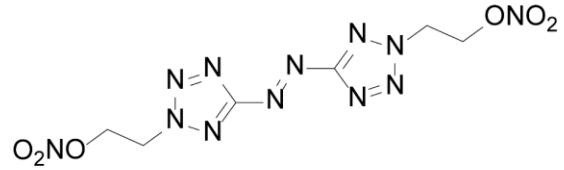

5b

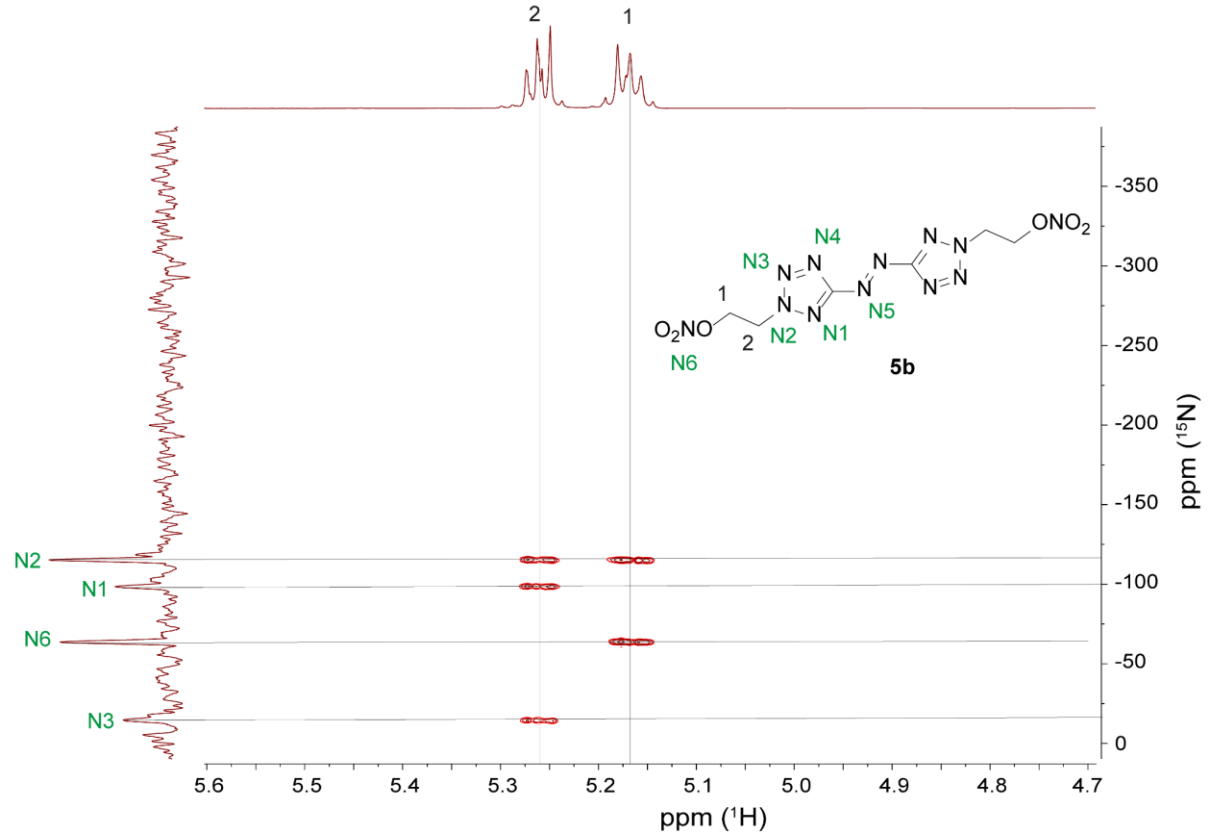

^{1}H-NMR (400 MHz, Acetone-D$_6$, ppm)

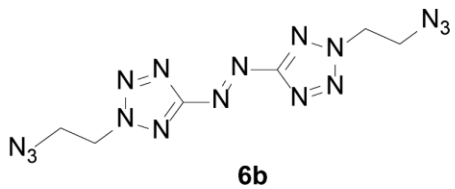

6b

^{13}C-NMR (101 MHz, Acetone-D$_6$, ppm)

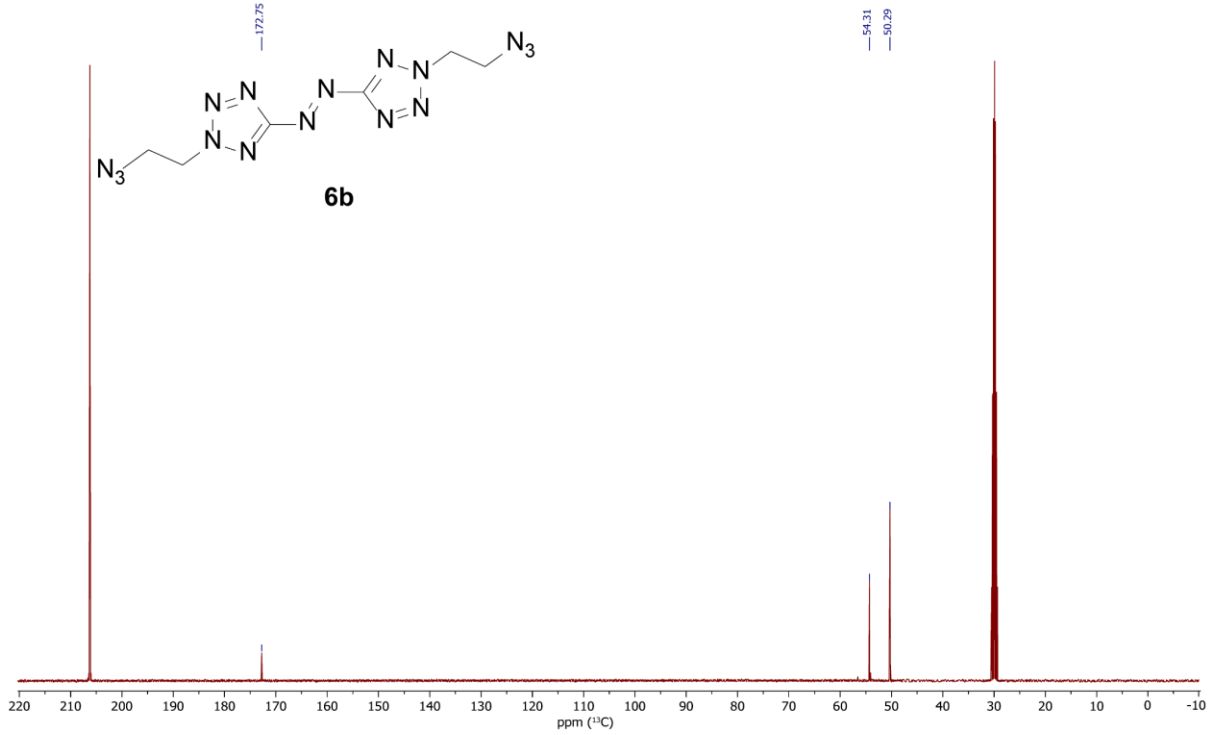

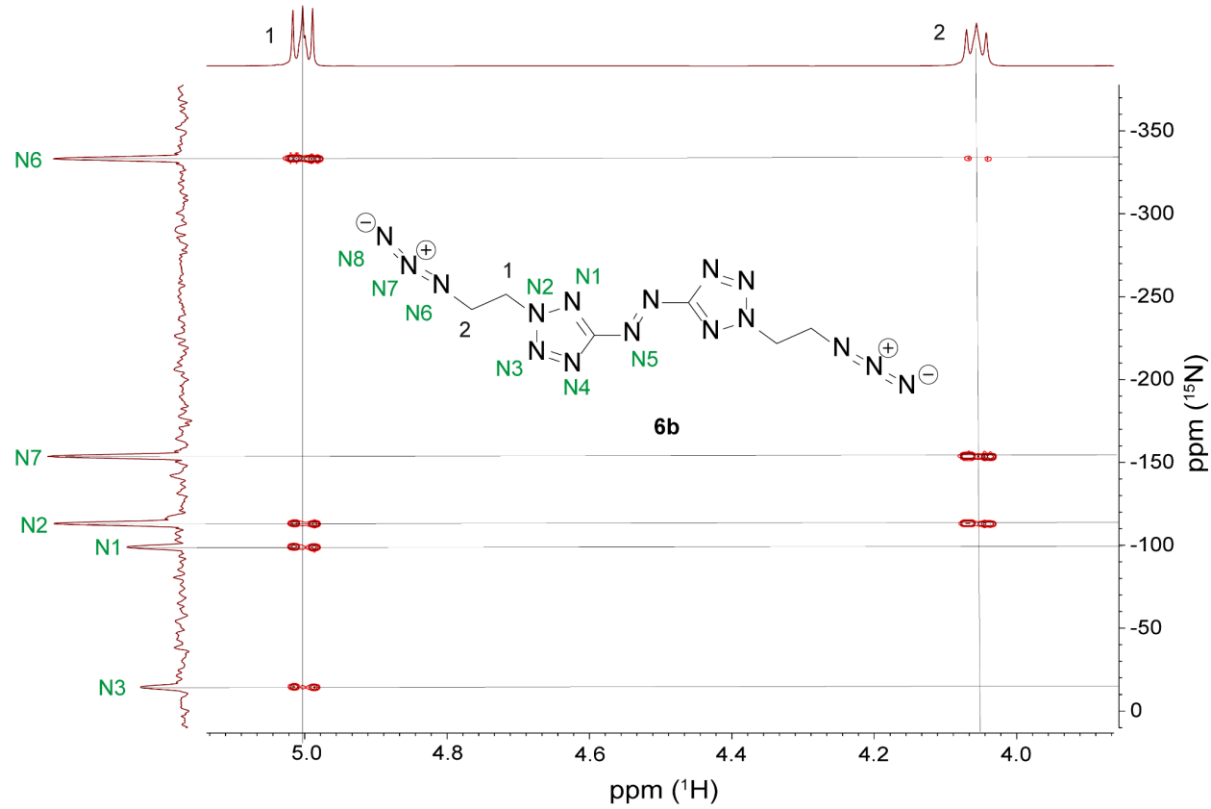

¹H-NMR (400 MHz, Acetone-D₆, ppm)

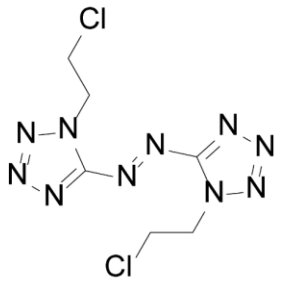

7

¹³C-NMR (101 MHz, Acetone-D₆, ppm)

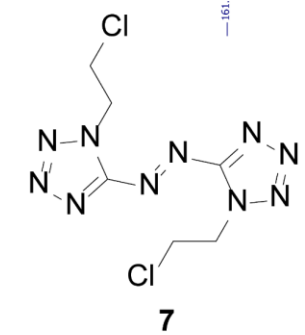

7

¹H-NMR (400 MHz, DMSO-D₆, ppm)

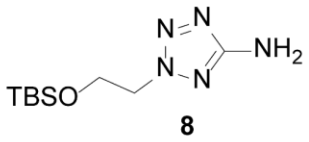

8

¹³C-NMR (101 MHz, DMSO-D₆, ppm)

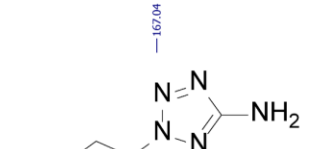

8

13.6.7 References

[S1] a) Reichel & Partner GmbH, http://www.reichelt-partner.de; b) Test methods according to the UN Recommendations on the Transport of Dangerous Goods, *Manual of Test and Criteria*, fourth revised edition, United Nations Publication, New York and Geneva, **2003**, ISBN 92–1-139087–7, Sales No. E.03.VIII.2; 13.4.2 Test 3 a (ii) BAM Fallhammer.

[S2] M. Sućeska, EXPLO5 V6.02 program, Brodarski Institute, Zagreb, Croatia, **2014**.

[S3] R. Yang, Z. Dong, Z. Ye, *ChemistrySelect* **2019**, *4*, 14208–14213.

[S4] D. E. Bayes (Glaxo Group Limited), EP0117368A1, **1982**.

[S5] *CrysAlisPro*, Oxford Diffraction Ltd. *version 171.33.41*, **2009**.

[S6] G. M. Sheldrick, *Acta Cryst.* **2015**, *A71*, 3–8.

[S7] O. V. Dolomanov, L. J Bourhis, R. J. Gildea, J. A. K. Howard, H. Puschmann, *J. Appl. Cryst.* **2009**, *42*, 339–341.

[S8] *SCALE3 ABSPACK – An Oxford Diffraction program* (1.0.4, gui: 1.0.3), Oxford Diffraction Ltd., **2005**.

[S9] *APEX3*. Bruker AXS Inc., Madison, Wisconsin, USA.

[S10] M. J. Frisch, G. W. Trucks, H. B. Schlegel, G. E. Scuseria, M. A. Robb, J. R. Cheeseman, G. Scalmani, V. Barone, B. Mennucci, G. A. Petersson, H. Nakatsuji, M. Caricato, X. Li, H.P. Hratchian, A. F. Izmaylov, J. Bloino, G. Zheng, J. L. Sonnenberg, M. Hada, M. Ehara, K. Toyota, R. Fukuda, J. Hasegawa, M. Ishida, T. Nakajima, Y. Honda, O. Kitao, H. Nakai, T. Vreven, J. A. Montgomery, Jr., J. E. Peralta, F. Ogliaro, M. Bearpark, J. J. Heyd, E. Brothers, K. N. Kudin, V. N. Staroverov, R. Kobayashi, J. Normand, K. Raghavachari, A. Rendell, J. C. Burant, S. S. Iyengar, J. Tomasi, M. Cossi, N. Rega, J. M. Millam, M. Klene, J. E. Knox, J. B. Cross, V. Bakken, C. Adamo, J. Jaramillo, R. Gomperts, R. E. Stratmann, O. Yazyev, A. J. Austin, R. Cammi, C. Pomelli, J. W. Ochterski, R. L. Martin, K. Morokuma, V. G. Zakrzewski, G. A. Voth, P. Salvador, J. J. Dannenberg, S. Dapprich, A. D. Daniels, O. Farkas, J.B. Foresman, J. V. Ortiz, J. Cioslowski, D. J. Fox, Gaussian 09 A.02, Gaussian, Inc., Wallingford, CT, USA, **2009**.

[S11] a) J. W. Ochterski, G. A. Petersson, and J. A. Montgomery Jr., *J. Chem. Phys.* **1996**, *104*, 2598–2619; b) J. A. Montgomery Jr., M. J. Frisch, J. W. Ochterski G. A. Petersson, *J. Chem. Phys.* **2000**, *112*, 6532–6542.

[S12] a) L. A. Curtiss, K. Raghavachari, P. C. Redfern, J. A. Pople, *J. Chem. Phys.* **1997**, *106*, 1063–1079; b) E. F. C. Byrd, B. M. Rice, *J. Phys. Chem*. A **2006**, *110*, 1005–1013; c) B. M. Rice, S. V. Pai, J. Hare, *Comb. Flame* **1999**, *118*, 445–458.

[S13] P. J. Lindstrom, W. G. Mallard (Editors), NIST Standard Reference Database Number 69, http://webbook.nist.gov/chemistry/ (accessed June **2020**).

[S14] M. S. Westwell, M. S. Searle, D. J. Wales, D. H. Williams, *J. Am. Chem. Soc*. **1995**, *117*, 5013–5015; b) F. Trouton, *Philos. Mag*. **1884**, *18*, 54–57.

[S15] a) H. D. B. Jenkins, H. K. Roobottom, J. Passmore, L. Glasser, *Inorg. Chem.***1999,** *38,* 3609–3620; b) H. D. B. Jenkins, D. Tudela, L. Glasser, *Inorg. Chem.* **2002**, *41*, 2364–2367.

14. Synthesis and Characterization of Binary, Highly Endothermic, and Extremely Sensitive 2,2′-Azobis(5-azidotetrazole)

Maximilian Benz, Thomas M. Klapötke, Jörg Stierstorfer, Michael Voggenreiter

as published in *Journal of the American Chemical Society* **2022**, *144*, 6143–6147

DOI: 10.1021/jacs.2c00995

Keywords: azides, azo compounds, binary CN compounds, heterocycles, nitrogen

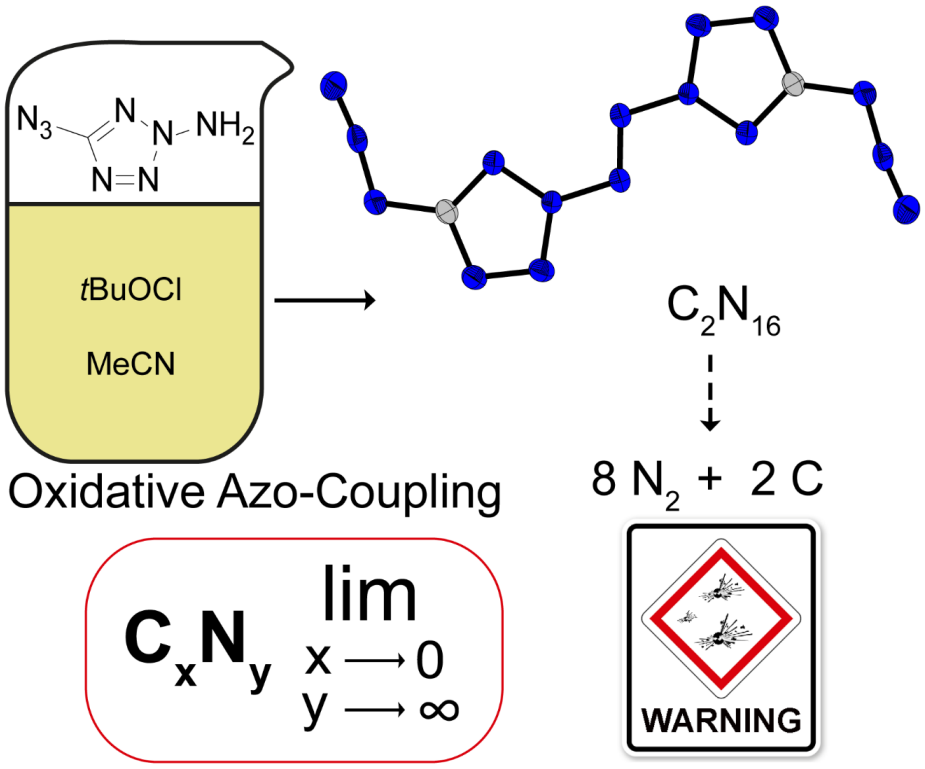

16 Nitrogen atoms held together by only two carbon atoms in one molecule. 2,2'-Azobis-5-azidotetrazole, which is produced by oxidative azo coupling of 2-amino-5-azidotetrazole, was synthesized and characterized including X-ray diffraction and sets new standards with regard to the nitrogen content of heterocyclic binary CN compounds.

Abstract: 2,2′-Azobis(5-azidotetrazole) (C_2N_{16}, **3**), a highly energetic nitrogen-rich binary CN compound was obtained in a three-step synthesis through the formation of 5-azidotetrazole (**1**), subsequent amination using *O*-tosylhydroxylamine to give 2-amino-5-azidotetrazole (**2**), and oxidative azo coupling of **2** using *t*BuOCl as an oxidant in MeCN. A nitrogen:carbon ratio of 8:1, eight nitrogen atoms in a row, and a nitrogen content of over 90% was unknown for a binary heterocyclic compound until now. The successful isolation was confirmed through X-ray diffraction as well as by vibrational and ^{13}C NMR spectroscopy. C_2N_{16} can explode instantly and shows mechanical sensitivities far higher than quantitatively measurable. Nevertheless, it features interesting energetic performances, which were calculated using different quantum-chemical methods.

14.1 Introduction

Binary CN compounds aroused enormous interest even in the early days of chemistry. Generations of chemists have paid great attention to this class of substances because of the complexity of their synthesis. This is mainly due to the fact that with an increase in the nitrogen content, the sensitivity of the compounds is drastically increased.[1] With the improvement of the nitrogen content, other properties relevant for energetic materials research are evoked similarly, including mainly the high energy of formation and the formation of almost exclusively gaseous reaction products.[2] Ideal improvement of these energetic parameters would be obtained with compounds that are composed exclusively of nitrogen (e.g., cubic gauche nitrogen (cg-N),[3] (N_5^+)(N_3^-),[4-5] and N_5^- derivatives[6]). However, because of their elaborate synthesis and partial instability, research on new CN substances is just as promising, since these compounds can fulfill the above-mentioned properties comparably well. Some examples of nitrogen-rich CN compounds are listed in Figure 1.

While cyanogen ($(CN)_2$) is a stable gas,[7-8] γ-C_3N_4 is a solid that is predicted to have extreme hardness properties,[9] and the valuable synthetic building block cyanogen azide (N_3CN, with a N:C ratio of 4:1), first described by Darzens in 1912, tends to detonate spontaneously in the dry state. Other examples of high-nitrogen CN compounds are based on azide-substituted heterocycles, especially

triazines,[10-11] tetrazines,[12-14] and tetrazoles.[1] In 2007, Banert et al. succeeded in preparing and fully characterizing the binary CN derivative tetraazidomethane ($C(N_3)_4$).[15] It is to date the compound with the highest N:C ratio and at the same time one of the formally simplest CN derivatives. However, tetraazidomethane is a highly sensitive liquid and has not been structurally characterized except by detection of consecutive reaction or decomposition products.

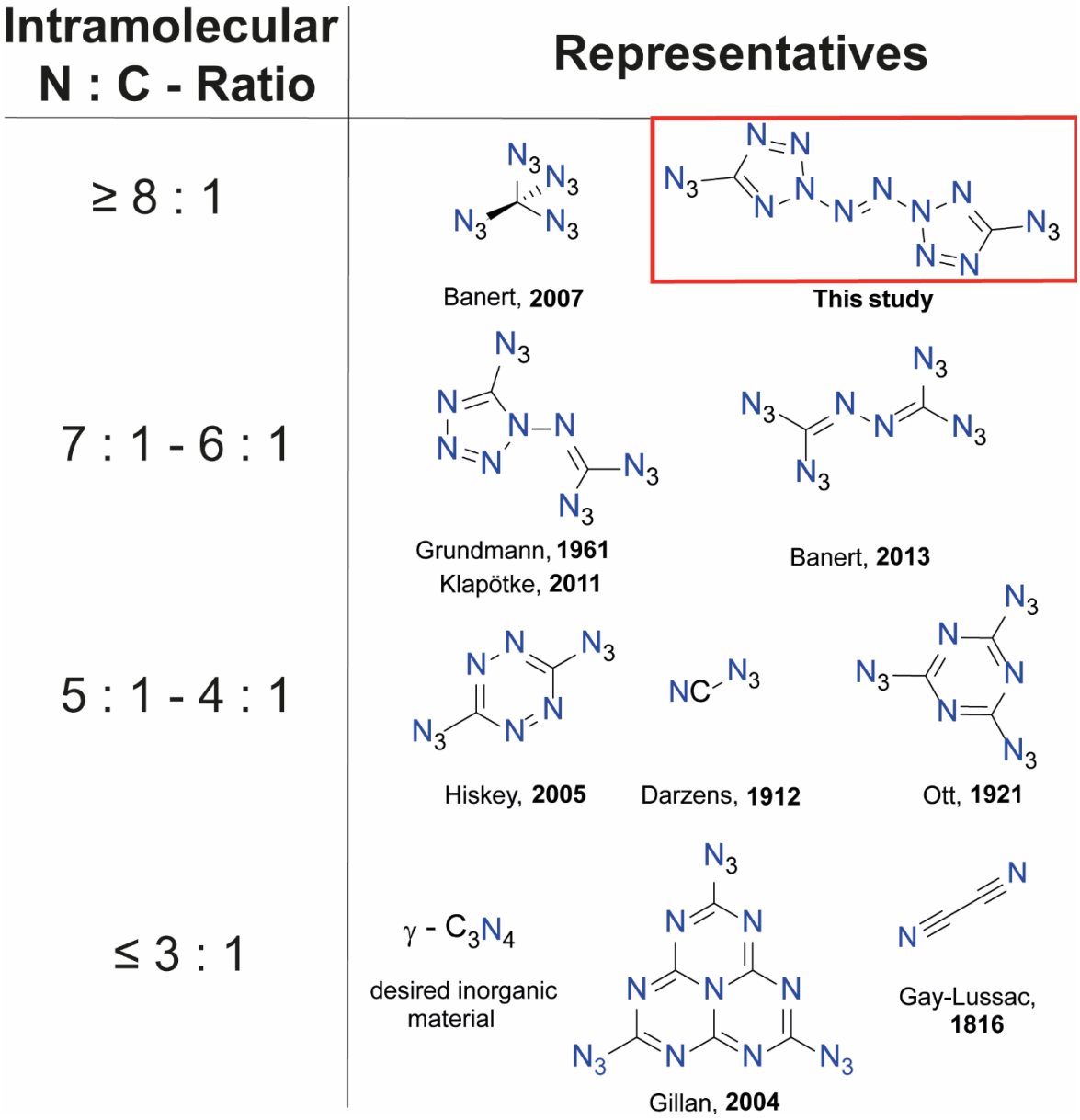

Figure 1. Structures of binary CN compounds, ranked according to increasing N:C ratio.

More recently, work on C_2N_{14}, among others, has caused great interest throughout the scientific community. This research revealed the existence of C_2N_{14} in “open-

chain" form as liquid isocyanogen tetraazide[16] and in "closed" form as solid 1-diazidocarbamoyl-5-azidotetrazole[1, 17] and showed that the open form can be isomerized into the closed form at elevated temperatures.[16] However, what they have in common is their extreme sensitivity to external influences. On the basis of the insights gained from the study of C_2N_{14}, we succeeded in increasing the N:C ratio again by applying the use of a tetrazole backbone with azide functions and additionally introducing an azo bridge.[18-19]

2,2′-Azobis(5-azidotetrazole) (C_2N_{16}, **3**) presented in this study not only has the highest N:C ratio for binary heterocyclic molecules but also features a chain of eight catenated nitrogen atoms, setting a new benchmark for CN compounds.

14.2 Results and Discussion

Our synthetic procedure starts with the formation of 5-azidotetrazole (**1**) from sodium azide and cyanogen bromide using a literature procedure.[20-21] The subsequent *N*-amination of **1** was carried out in acetonitrile with 1 equivalent of base (DBU) and *O*-tosylhydroxylamine (THA) as the amination agent. This reaction yielded **2** as the only product. Electron-withdrawing groups on the tetrazole carbon atom usually direct electrophilic substituents toward the 2-position (Scheme 1).[22-23]

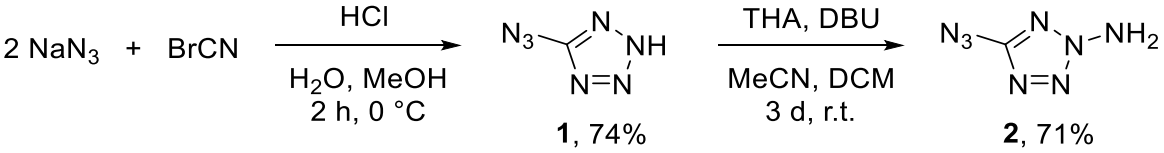

Scheme 1. Synthesis of 5-azidotetrazole (**1**) from sodium azide and cyanogen bromide and subsequent amination using THA to give 2-amino-5-azidotetrazole (**2**).

Since compound **2** is a new compound and also a potential starting material for further energetic derivatizations, it was characterized as well. Crystalline **2**, which was obtained from slow evaporation of MeOH, crystallized in the orthorhombic space group $P2_12_12_1$ with four molecular units per unit cell (Figure 2A). The density is 1.769 g cm^{-3} at 173 K, which is higher than that for 1-amino-5-azidotetrazole.[24] As depicted in Figure 2B, **2** forms a chainlike motif along *c* that is mainly stabilized through moderately strong hydrogen bonds between the protons and the ring or N_γ

of the azide function. The NMR data for **2** display a broad signal at 6.65 ppm for the amino protons and a ^{13}C resonance at 160.6 ppm. In differential thermal analysis (DTA) experiments, **2** showed smooth melting at 62 °C followed by a sharp decomposition at 142 °C.

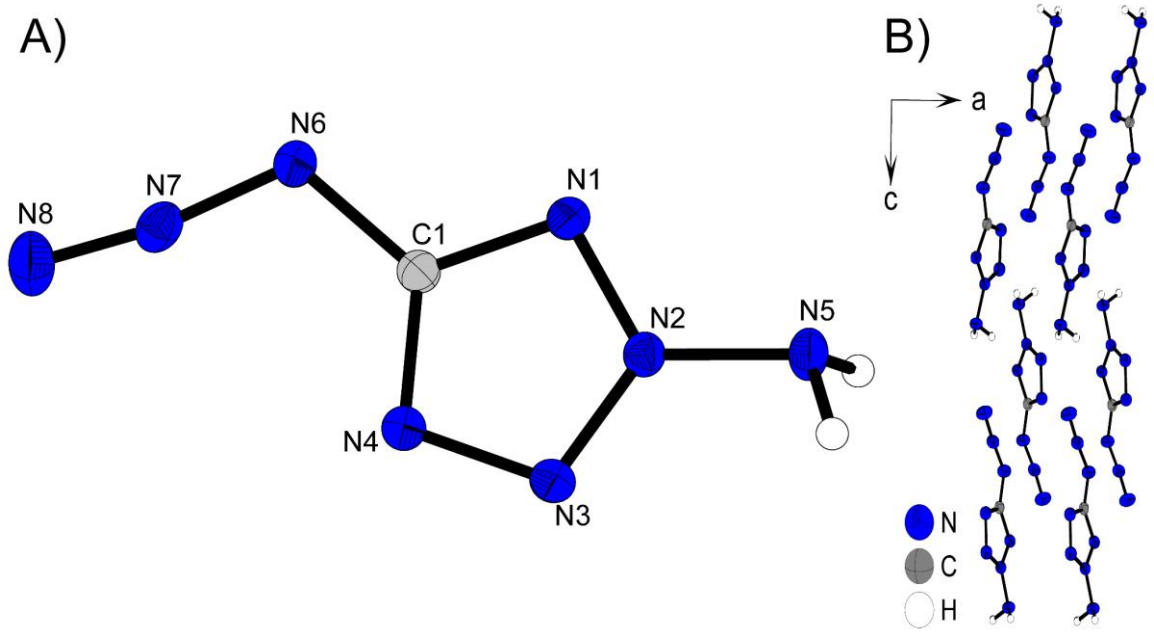

Figure 2. (A) Molecular structure of **2** as determined by low-temperature X-ray diffraction with thermal ellipsoids drawn at the 50% probability level. (B) View of the packing of **2** along the *b* axis. Selected bond lengths [Å]: N2–N5 1.393(2); C1–N6 1.395(2). Selected hydrogen bonds: N5–H5A···N1: N5–H5A 0.88(3) Å, H5A···N1 2.42(2) Å, N5···N1 3.238(2) Å, N5–H5A–N1 156(2)°; N5–H5B···N3: N5–H5B 0.88(3) Å, H5B···N3 2.34(3) Å, N5···N3 3.201(2) Å, N5–H5B–N3 167(2)°; N5–H5A···N8: N5–H5A 0.88(3) Å, H5A···N8 2.69(2) Å, N5···N8 3.028(2) Å, N5–H5A–N8 104.8(2)°.

The key step of our study, the oxidative azo coupling of **2**, was very challenging. The established synthetic protocols for oxidative azo coupling of *N*-amines using sodium dichloroisocyanuric acid or trichloroisocyanuric acid[25-27] could also be successfully applied to our reaction. However, consequent spontaneous detonations appeared as a result of precipitation of the substance during the reaction. To avoid this, we tried to keep **3** in solution as long as possible during the reaction and to minimize the shock possibilities within the reaction vessel (no stirring bar, soft plastic reaction vessel), without success. Finally, we decided to use *t*BuOCl, which is widely used in similar oxidation reactions,[28-30] as the oxidant because of the advantageous solvent mixture during the reaction (Scheme 2). In contrast to the oxidations with derivatives of isocyanuric acid, the method we have chosen uses and produces only volatile reactants (MeCN, *t*BuOH), which can be evaporated carefully. From this mixture, **3** crystallized in the form of slightly yellow-

greenish blocks. Because of the risk of spontaneous and mechanically caused explosions during the isolation, only very small batches (50 mg of starting material) were performed. Through this method, a sufficient amount of **3** could be gathered over several batches to allow all possible analyses to be performed. In addition, **3** is not stable long-term[31-32] and decomposes slowly in solution with evolution of nitrogen.

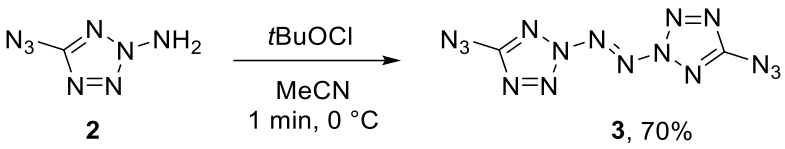

Scheme 2. Synthesis of 2,2′-azobis(5-azidotetrazole) (ABAT, **3**) through oxidation of **2** using *t*BuOCl.

During the investigation of **3**, several detonative events were observed (see Figure 4D) and plastic as well as glass fragments of different sizes (nano to macro) were obtained. It should be pointed out that **3** is one of the most sensitive materials we have ever handled.

As mentioned above, **3** was obtained in the form of slightly yellow-greenish blocks suitable for X-ray diffraction. The stated color was proven by UV–vis calculations (see the Supporting Information). It crystallizes in the triclinic space group *P*−1 with a density of 1.803 g cm^{-3} at 298 K, which is the highest one reported for a binary CN compound.

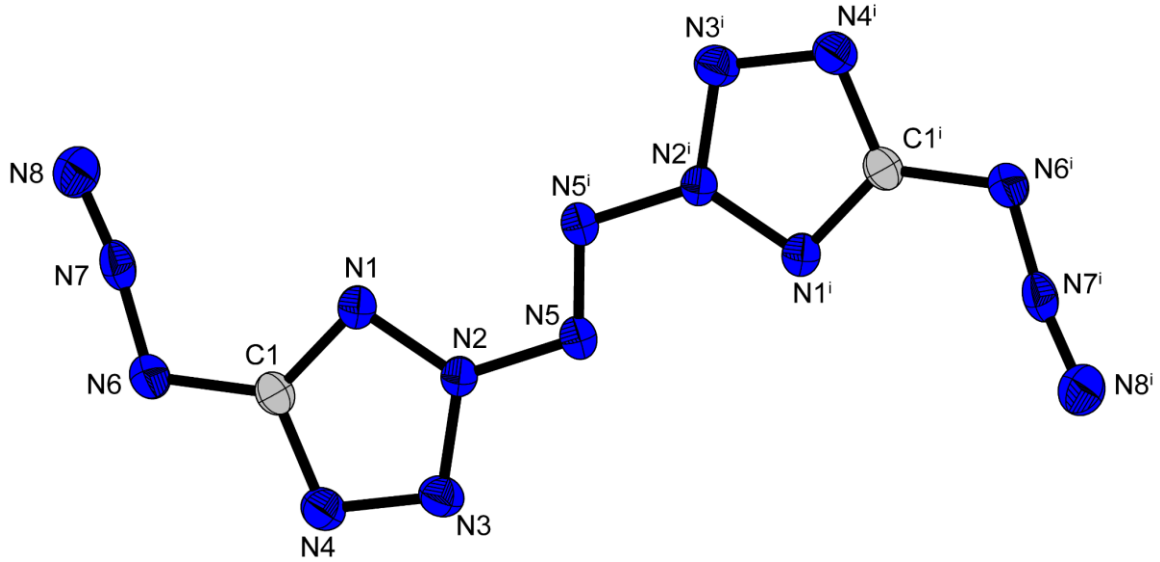

Figure 3. Molecular unit of **3** determined by low-temperature X-ray diffraction with thermal ellipsoids drawn at the 50% probability level. Selected bond distances [Å] and angles [deg]: N6–N7 1.264(3), N7–N8 1.111(3), N2–N5 1.374(2), N5–N5^{i} 1.252(3), N2–N5–N5^{i} 109.5(2), N1–C1–N6 126.7(2), N1–C1–N6–N7 3.4(2), N3–N2–N5–N5^{i} 0.1(2).

The structure features an inversion center located directly on the azo bridge (Figure 3). The molecule itself is arranged in an almost planar fashion.

The presence of a conjugated π system is one of the reasons for its very high density. The values of the bond distances (Figure 3) and angles for the *N*-azo bridge and the azide moieties show no peculiarities and are similar to those observed for known related compounds.[20, 27]

The 2D structure of **3** is almost completely determined by the formation of electrostatic interactions between nitrogen atoms due to the absence of hydrogen atoms and the resulting unavailability of hydrogen bridges. A coplanar layer of molecular units is formed in the *bc* plane; they are not arranged in a coplanar fashion but are twisted against each other. The pattern along the space diagonal appears to behave like a zigzag structure. Figure S1–S3 show the 2D structures.

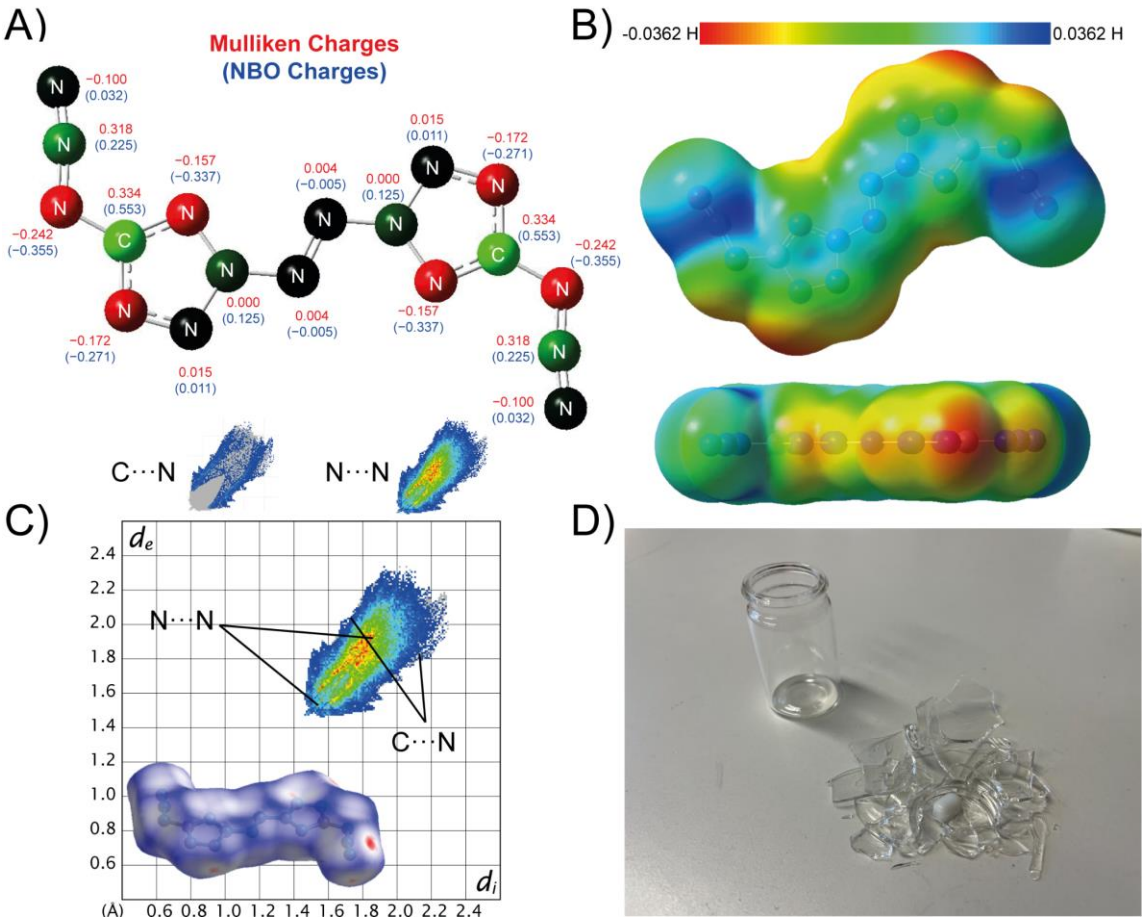

Figure 4. Additional analyses and calculations of **3** (for more details, see the Supporting Information): (A) Mulliken and NBO charges; (B) ESP; (C) Hirshfeld surface and respective fingerprint plot; (D) result of a detonation of approximately 45 mg of **3** during its synthesis in MeCN.

The shortest intramolecular contacts can be found between N_β of the azide function and nitrogen atoms N1 and N4 of the tetrazole ring (N7–N9 3.154(2) Å, N4–N15 3.100(3) Å). The observed crystal structure is formed and stabilized solely by the interactions between electron pairs and positively polarized nitrogen atoms.

The calculated Mulliken charges and the electrostatic potential (ESP) show a clear charge separation within the molecule (Figure 4). Here the strongest positively polarized atoms are C1 and N_β, and the strongest negatively polarized atoms are N_α, N1, and N4. Through the analysis of the Hirshfeld surfaces[33] (Figure 4C), an extremely high sensitivity can be assumed, since only few and very weak interactions are demonstrated. This creates an unstable crystal packing in which the molecules can easily be displaced against each other, thus leading to decomposition.[34] The closest near contacts (N···N) are in the range of 3 Å.

In addition to the crystal structure, we were able to perform only NMR and IR spectroscopy. For compound **3**, the carbon resonance was observed at 164.1 ppm, in the typical range for 2-substituted 5-azidotetrazoles.

The IR spectrum of **3**, which was hard to record because of the enormously high sensitivity of the compound, mainly shows a characteristically intense band for the azide stretching mode at 2150 cm^{-1}. Compared with the spectrum of **2**, the disappearance of the proton vibrations at around 3300 cm^{-1} is additional evidence for the formation of **3**. The theoretical vibrational frequencies were calculated at the BLYP/6-31G(d) level of theory (point group C_{2h} for the gas phase). They are in good accordance with the measured values and can be found Table S3 along with more details about the calculation.

The sensitivity values for **2** and **3** are clearly in the range for extremely sensitive compounds, but the two compounds differ significantly in their handling. **2** can be classified as a primary explosive (impact sensitivity (IS) < 1 J, friction sensitivity (FS) = 2 N) but can be handled without hesitation if all safety precautions (plastic equipment, earthed equipment, etc.) are obeyed. The scenario is entirely different for **3**. Its IS and FS are way below our devices' measuring capabilities (Table 1). **3** decomposes detonatively under any kind of stress, whether thermal or mechanical, as well as spontaneously in the absence of light and without any noticeable external influence. **3** is thermally stable up to 114 °C, which is surprisingly high since only a few intramolecular interactions result from the crystal structure.

Table 3. Physico-chemical properties of **2** and **3** as well as for C_2N_{14} (1-diazidocarbamoyl-5-azidotetrazole) and lead azide.

	2	**3**	C_2N_{14}[1]	$Pb(N_3)_2$ (RD-1333)
Formula	CH_2N_8	C_2N_{16}	C_2N_{14}	PbN_6
IS [J][a]	<1	<<<0.25	<0.25	4
FS [N][b]	2	<<<0.1	<5	<0.1
ρ [g cm^{-3}][c]	1.736	1.803	1.679	4.8
N [%][d]	88.9	90.3	89.1	28.9
T_{melt}/T_{dec}[e]	62/142	-/114	78/124	-/315
$\Delta_f H°$ [kJ mol^{-1}][f]	703.7 (668.8)	1700.7 (1664.9)	1495.0	450.1
$-\Delta_{Ex}U°$ [kJ kg^{-1}][g]	5672 (5401)	6705 (6561)	6632	1560
P_{CJ} [kbar][h]	343 (334)	366 (362)	300	357
V_{det} [ms^{-1}][i]	9472 (9384)	9515 (9476)	8853	6187

[a] Impact sensitivity (BAM drophammer (1 of 6)). [b] Friction sensitivity (BAM friction tester (1 of 6)). [c] Density from X-ray diffraction analysis recalculated to 298 K ($d_{298K} = \frac{d_T}{1+\alpha_v(298-T_0)}$; . α_v = 1.6·10^{-4} K^{-1})[35] [d] Nitrogen content. [e] Melting/Decomposition temperature (DTA; β = 5 °C min^{-1}). [f] Calculated enthalpy of formation CBS-4M (CBS-QB3). EXPLO5_V6.05.02: [g] Energy of explosion. [h] Detonation pressure at Chapman-Jouguet point. [i] Detonation velocity.

The calculated enthalpies of formation (values from CBS-4M calculations) again illustrate the enormously high endothermic character of **2** ($\Delta_f H°$ = 703.7 kJ mol^{-1}) and **3** ($\Delta_f H°$ = 1700.7 kJ mol^{-1}). Through the high crystallographic densities paired with the extremely high energies of formation, the detonation velocities are calculated to be around 9500 m s^{-1} using the EXPLO5 code.

14.3 Conclusion

In conclusion, we obtained 2,2′-azobis(5-azidotetrazole) (**3**) through straightforward synthesis involving amination of 5-azidotetrazole to obtain 2-amino-5-azidotetrazole (**2**) followed by oxidative azo coupling of **2** using *t*BuOCl. The sensitivities of **3** are far below the measurement limits of our equipment. The nitrogen contents, crystallographic densities, and calculated enthalpies of formation for **3** and its precursor **2** are remarkably high, resulting in impressive

theoretical values for the detonation velocity and energy. The synthesis of **3** sets a new benchmark for a binary heterocyclic CN compound with a nitrogen:carbon ratio of 8:1 and should inspire the community to continue the quest for all-nitrogen compounds.

14.4 Acknowledgement

Financial support of this work by Ludwig-Maximilian University (LMU), the Office of Naval Research (ONR) under Grant ONR N00014-19-1-2078, and the Strategic Environmental Research and Development Program (SERDP) under Contract W912HQ19C0033 is gratefully acknowledged. We thank Mr. Marcus Lommel (LMU Munich) for X-ray diffraction experiments and Ms. Jasmin Lechner (LMU Munich) for DSC measurements and assistance with graphical illustrations.

14.5 References

[1] T. M. Klapötke, F. A. Martin, J. Stierstorfer, *Angew. Chem. Int. Ed.* **2011**, *50*, 4227–4229.

[2] O. T. O'Sullivan, M. J. Zdilla, *Chem. Rev.* **2020**, *120*, 5682–5744.

[3] M. I. Eremets, A. G. Gavriliuk, I. A. Trojan, D. A. Dzivenko, R. Boehler, *Nat. Mater.* **2004**, *3*, 558–563.

[4] K. O. Christe, W. W. Wilson, J. A. Sheehy, J. A. Boatz, *Angew. Chem. Int. Ed.* **1999**, *38*, 2004–2009.

[5] D. A. Dixon, D. Feller, K. O. Christe, W. W. Wilson, A. Vij, V. Vij, H. D. B. Jenkins, R. M. Olson, M. S. Gordon, *J. Am. Chem. Soc.* **2004**, *126*, 834–843.

[6] C. Zhang, C. Sun, B. Hu, C. Yu, M. Lu, *Science* **2017**, *355*, 374–376.

[7] W. Kesting, *Ber. Dtsch. Chem. Ges.* **1924**, *57*, 1321–1324.

[8] J. L. Gay-Lussac, *Ann. Phys.* **1816**, *53*, 139–183.

[9] W. Schnick, *Angew. Chem. Int. Ed.* **1993**, *32*, 1580–1581.

[10] E. Ott, E. Ohse, *Ber. Dtsch. Chem. Ges.* **1921**, *54*, 179–186.

[11] D. R. Miller, D. C. Swenson, E. G. Gillan, *J. Am. Chem. Soc.* **2004**, *126*, 5372–5373.

[12] D. Chen, H. Yang, Z. Yi, H. Xiong, L. Zhang, S. Zhu, G. Cheng, *Angew. Chem. Int. Ed.* **2018**, *57*, 2081–2084.

[13] M. H. V. Huynh, M. A. Hiskey, D. E. Chavez, D. L. Naud, R. D. Gilardi, *J. Am. Chem. Soc.* **2005**, *127*, 12537–12543.

[14] M. H. V. Huynh, M. A. Hiskey, J. G. Archuleta, E. L. Roemer, R. Gilardi, *Angew. Chem. Int. Ed.* **2004**, *43*, 5658–5661.

[15] K. Banert, Y.-H. Joo, T. Rüffer, B. Walfort, H. Lang, *Angew. Chem. Int. Ed.* **2007**, *46*, 1168–1171.

[16] K. Banert, S. Richter, D. Schaarschmidt, H. Lang, *Angew. Chem. Int. Ed.* **2013**, *52*, 3499–3502.

[17] C. J. Gundmann, W. J. Schnabel (O.M.C. Corp.), US 2290412, **1961**.

[18] Q. Zhang, J. M. Shreeve, *Angew. Chem. Int. Ed.* **2013**, *52*, 8792–8794.

[19] Y. Tang, H. Yang, B. Wu, X. Ju, C. Lu, G. Cheng, *Angew. Chem. Int. Ed.* **2013**, *52*, 4875–4877.

[20] T. M. Klapötke, J. Stierstorfer, *J. Am. Chem. Soc.* **2009**, *131*, 1122–1134.

[21] J. Stierstorfer, T. M. Klapötke, A. Hammerl, R. D. Chapman, *Z. Anorg. Allg. Chem.* **2008**, *634*, 1051–1057.

[22] T. M. Klapötke, D. G. Piercey, J. Stierstorfer, *Chem. Eur. J.* **2011**, *17*, 13068–13077.

[23] T. M. Klapötke, D. G. Piercey, J. Stierstorfer, *Dalton Trans.* **2012**, *41*, 9451–9459.

[24] T. M. Klapötke, B. Krumm, F. A. Martin, J. Stierstorfer, *Chem. Asian J.* **2012**, *7*, 214–224.

[25] F. Li, X. Cong, Z. Du, C. He, L. Zhao, L. Meng, *New J. Chem.* **2012**, *36*, 1953–1956.

[26] Y. Tang, H. Yang, J. Shen, B. Wu, X. Ju, C. Lu, G. Cheng, *New J. Chem.* **2012**, *36*, 2447–2450.

[27] T. M. Klapötke, D. G. Piercey, *Inorg. Chem.* **2011**, *50*, 2732–2734.

[28] D. E. Chavez, J. C. Bottaro, M. Petrie, D. A. Parrish, *Angew. Chem. Int. Ed.* **2015**, *54*, 12973–12975.

[29] Y. Tang, D. Kumar, J. M. Shreeve, *J. Am. Chem. Soc.* **2017**, *139*, 13684–13687.

[30] Y. Tang, C. He, P. Yin, G. H. Imler, D. A. Parrish, J. M. Shreeve, *Eur. J. Org. Chem.* **2018**, *2018*, 2273–2276.

[31] M. V. Gorn, N. P. Gritsan, C. F. Goldsmith, V. G. Kiselev, *J. Phys. Chem. A* **2020**, *124*, 7665–7677.

[32] X. Zhao, C. Qi, R. Zhang, S. Zhang, S. Li, S. Pang, *J. Mol. Model.* **2015**, *21*, 223.

[33] P. R. Spackman, M. J. Turner, J. J. McKinnon, S. K. Wolff, D. J. Grimwood, D. Jayatilaka, M. A. Spackman, *J. Appl. Crystallogr.* **2021**, *54*, 1006–1011.

[34] M. Reichel, D. Dosch, T. Klapötke, K. Karaghiosoff, *J. Am. Chem. Soc.* **2019**, *141*, 19911–19916.

[35] T. M. Klapötke, *Chemistry of High-Energy Materials*, De Gruyter, Boston, Berlin, **2019**.

14.6 Supporting Information

14.6.1 Experimental Procedure

^{1}H, ^{13}C, ^{14}N and ^{15}N NMR spectra were recorded on *BRUKER AMX 400* instruments. Chemical shifts are referenced with respect to tetramethylsilane (^{1}H/^{13}C) and nitromethane (^{14}N/^{15}N). Infrared spectra (IR) were recorded in the region 4000-400 cm^{-1} on a *PERKIN ELMER Spectrum BX-59343* instrument with a *SMITHS DETECTION DuraSamplIR II Diamond ATR* sensor. The absorption bands are reported in wavenumbers (cm^{-1}). Decomposition temperatures were measured via differential thermal analysis (DTA) with an *OZM Research DTA 552-Ex* instrument or differential scanning calorimetry (DSC) using a *Linseis PT10 DSC* device at a heating rate of 5 °C/min and in a range of room temperature to 400 °C. All sensitivities toward impact (IS) and friction (FS) were determined according to BAM (Bundesanstalt für Materialforschung und Prüfung) standards using a BAM drop hammer and a BAM friction apparatus by applying the 1 of 6 method.[S1] **2** was tested for sensitivity towards electrical discharge using an *Electric Spark Tester ESD 2010 EN* from OZM. Energetic properties have been calculated with the EXPLO5 6.02 computer [S2] code using the RT converted X-ray density and calculated solid state heats of formation.

CAUTION! *All investigated compounds are potentially explosive materials. In particular the title compound, ABAT (**3**), is extremely sensitive and tends to explode*

in dry state and even spontaneously without the influence of any kind of external stimuli. Safety precautions and equipment (such as wearing leather coat, face shield, Kevlar sleeves, Kevlar gloves, earthed equipment and ear plugs) must be used during all manipulations.

Tert-butyl hypochlorite

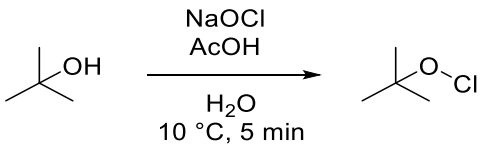

Tert-butyl hypochlorite was synthesized according to a literature known procedure.[S3]

NaOCl solution (13% active chlorine, 500 mL) was placed in a round bottom flask and cooled to below 10 °C with an ice bath. A mixture of *tert*-butanol (37.0 mL, 390 mmol) and acetic acid (24.5 mL, 430 mmol) was added in one portion and the solution was stirred vigorously for 5 min. Afterward, the aqueous layer was discarded and the yellow organic phase was washed with sodium carbonate solution (10%, 100 mL) and water (100 mL). The product can then be stored over $CaCl_2$ in the fridge at 8 °C. The yield is 80%. The purity was checked by ^1H NMR.

2-Amino-5-azidotetrazole (**2**)

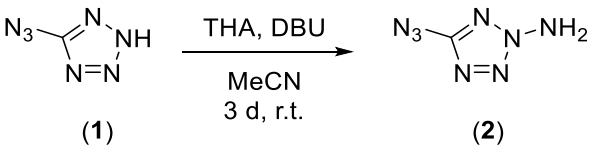

(**1**) (**2**)

Amination reaction was performed according to a literature known protocol for amination of azoles using THA.[S4]

Freshly prepared ethyl *O*-*p*-tosylsulphonylacetohydroximate (1.71 g, 6.52 mmol, 1.5 eq) was added in portions to perchloric acid (60%, 10 mL) and the mixture was stirred for 3 h. The now-free tosylhydroxylamine (THA) suspension was quenched on ice water (60 mL) and after the ice melted it was extracted with dichloromethane

(5 x 30 mL). The combined organic phases were dried over anhydrous sodium sulfate and added in one portion to an ice cooled solution of 5-azido-2*H*-tetrazole (0.48 g, 4.34 mmol, 1.0 eq) and 1,8-diazabicyclo(5.4.0)undec-7-ene (DBU) (0.66 mL, 4.34 mmol, 1.0 eq) in acetonitrile (70 mL). The solution was stirred for three days at room temperature. The slightly cloudy solution was evaporated under reduced pressure and purified using column chromatography (*i*Hex/EtOAc: 4:1; R_f = 0.18) to yield **2** as colorless crystalline solid (0.39 g, 3.08 mmol, 71%). DTA (5 °C min^{-1}): 62 °C (endo), 142 °C (exo); Sensitivities: BAM drop hammer: <1 J, friction tester: 2 N, ESD: 45 mJ; IR (ATR) $\tilde{\nu}$ (cm^{-1}) = 3325(s), 3260(m), 3197(m), 2918(w), 2178(s), 2150(vs), 1611(w), 1505(s), 1423(s), 1391(s), 1355(s), 1303(m), 1223(s), 1195(vs), 1177(s), 1046(w), 1030(s), 990(m), 906(vs), 795(m), 740(s), 725(s), 686(m), 678(m), 661(m), 542(s), 523(s), 493(m), 464(w), 457(w), 444(m), 432(m), 419(m), 412(m), 403(s); Elem. Anal. ($CH_2N_8O_6$, 126.08 g mol^{-1}) calcd.: C 9.53, H 1.60, N 88.87 %. Found: C 9.21, H 1.90, N 86.43%; ^{1}H NMR (CD_3-CN, 400 MHz, ppm) δ = 6.65(s, 2H); ^{13}C NMR (CD_3-CN, 101 MHz, ppm) δ = 160.6; ^{14}N NMR (DMSO-D_6, 29 MHz, ppm) δ = −144, −303; ^{15}N NMR (CD_3OD, 42 MHz, ppm) δ = −9.9, −79.7, −95.1, −102.5, −144.4, −145.2, −292.3, −301.4; HRMS (ESI) *m/z*: [M+] Calcd for CH_3N_8 127.0475, found: 127.0473.

2,2'-Azobis-(5-azidotetrazole) (**3**)

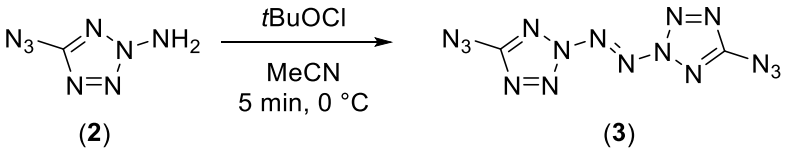

(**2**) (**3**)

2-Amino-5-azidotetrazole (46 mg, 0.36 mmol, 1.0 eq) was dissolved in MeCN (1.5 mL) in a plastic beaker and cooled to 0 °C using an ice bath. Freshly prepared *t*BuOCl (71 mg, 0.66 mmol, 1.8 eq.) was added dropwise and the mixture was allowed to stand for 60 seconds. The solution was transferred in a plastic bowl and the solvent was evaporated behind a face shield. Due to the high sensitivity of the **3** the yield could not be determined exactly but was measured to be around 70%. DSC (5 °C min^{-1}): 114 °C (exo); Sensitivities: BAM drop hammer: <<1 J, friction tester: <<0.1 N, ESD: too sensitive for measurement; IR (ATR) $\tilde{\nu}$ (cm^{-1}) = 2150

(vs), 1608 (w), 1505 (s), 1411 (w), 1377 (m), 1221 (w), 1184 (w), 1090 (w), 1024 (w), 942 (m), 883 (m), 819 (w), 798 (w), 737 (m), 682 (w), 527 (w), 496 (w); Elem. Anal. (C_2N_{16}, 248.13 g mol^{-1}) calcd.: C 9.68, N 90.32 %. Found: too sensitive for measurement; ^1H NMR (CD_3-CN, 400 MHz, ppm) δ = - ; ^{13}C NMR (CD_3-CN, 101 MHz, ppm) δ = 164.1.

14.6.2 Crystallography

Crystal structure data were obtained from a Bruker D8 Venture TXS diffractometer equipped with a multilayer monochromator, a Photon 2 detector and a rotation-anode generator (Mo-K_α radiation). The data collection was performed using the CRYSTALIS RED software.[S5] The solution of the structure was performed by direct methods and refined by full-matrix least-squares on F2 (SHELXT)[S6] implemented in the OLEX2[S7] software suite. The non-hydrogen atoms were refined anisotropically and the hydrogen atoms were located and freely refined. The absorption correction was carried out by a SCALE3 ABSPACK multiscan method.[S8] The DIAMOND2 plots shown with thermal ellipsoids at the 50% probability level and hydrogen atoms are shown as small spheres of arbitrary radius. The SADABS program embedded in the Bruker APEX3 software was used for multi-scan absorption corrections in all structures.[S9]

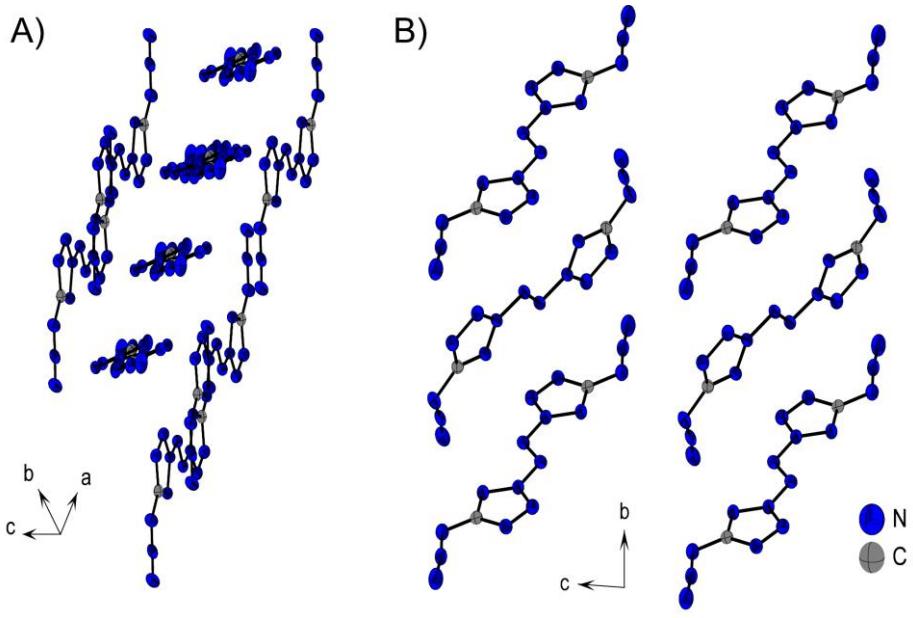

Figure S1. Illustration of the three-dimensional arrangement of **3** A) along an arbitrary viewing direction, B) along the *a* axis.

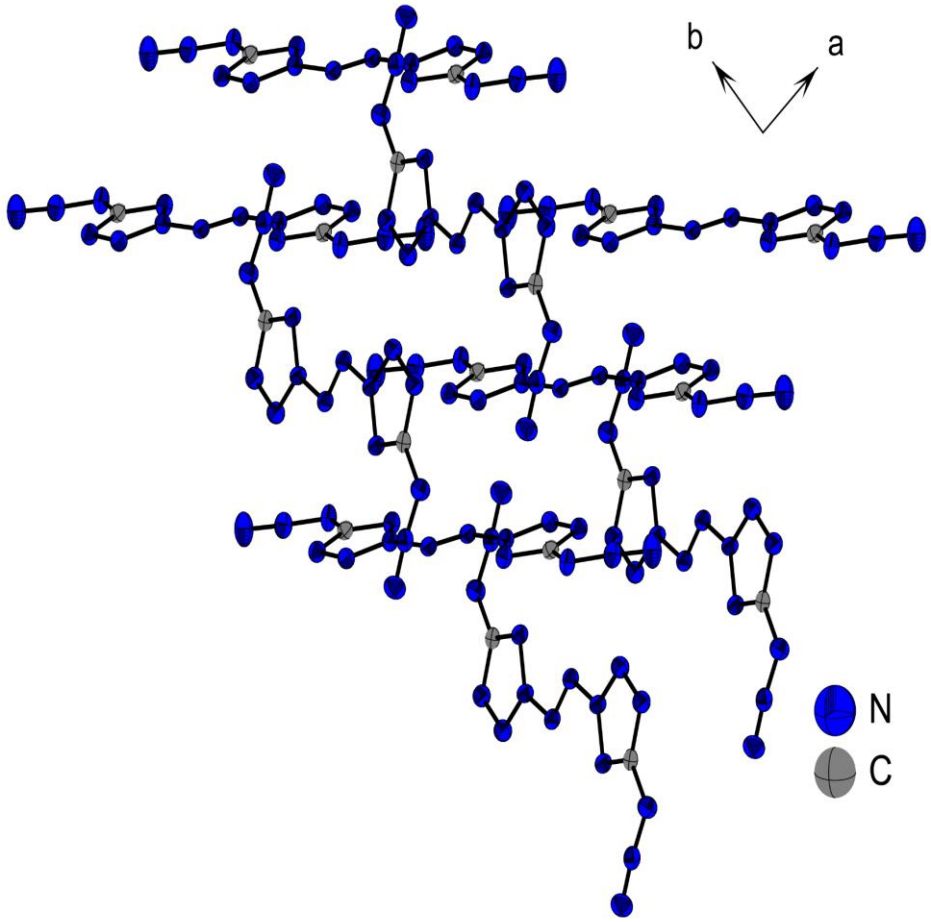

Figure S2. Representation of the pattern along c.

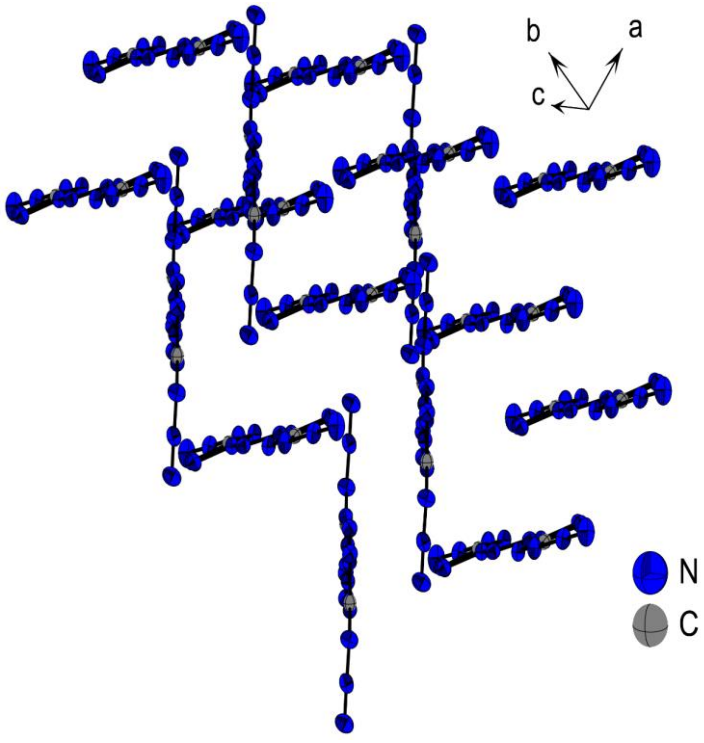

Figure S3. Representation of the zigzag pattern along the stated room direction.

Table S1. Crystallographic data and structure refinement details for **2** and **3**.

	2	**3**
Formula	CH_2N_8	C_2N_{16}
FW [g mol^{-1}]	126.11	248.18
Crystal system	orthorhombic	triclinic
Space group	$P2_12_12_1$ (No. 19)	$P\bar{1}$ (No. 2)
Color / Habit	colorless block	green block
Size [mm]	0.10 x 0.13 x 0.14	0.02 x 0.08 x 0.18
a [Å]	3.5082(2)	5.0759(3)
b [Å]	7.0952(4)	9.4232(5)
c [Å]	19.0265(9)	9.4790(5)
α [°]	90	86.025(2)
β [°]	90	83.192(2)
γ [°]	90	86.782(2)
V [Å^3]	473.60(4)	448.59(4)
Z	4	2
$\rho_{calc.}$ [g cm^{-3}]	1.769	1.837
μ [mm^{-1}]	0.143	0.150
F(000)	256	248
$\lambda_{MoK\alpha}$ [Å]	0.71073	0.71073
T [K]	173	173
θ Min-Max [°]	3.1, 28.3	2.2, 27.2
Dataset	-4: 4 ; -9: 9 ; -24: 25	-6: 6 ; -11: 12 ; -12: 12
Reflections collected	8830	7911
Independent refl.	1183	2000
R_{int}	0.026	0.038
Observed reflections	1163	1603
Parameters	91	163
R_1 (obs)[a]	0.0274	0.0491
wR_2 (all data)[b]	0.0668	0.0978
S [c]	1.17	1.14
Resd. dens [e Å^{-3}]	-0.20, 0.15	-0.24, 0.24
Device type	Bruker D8 Venture	Bruker D8 Venture
Solution	SIR-92	SIR-92
Refinement	SHELXL-2013	SHELXL-2013
Absorption correction	multi-scan	multi-scan
CCDC	2142885	2142884

[a] $R_1 = \Sigma||F_o|-|F_c||/\Sigma|F_o|$; [b] $wR_2 = [\Sigma[w(F_o^2-F_c^2)^2]/\Sigma[w(F_o)^2]]^{1/2}$; $w = [\sigma c^2(F_o^2)+(xP)^2+yP]^{-1}$ and $P=(F_o^2+2F_c^2)/3$; [c] $S = \{\Sigma[w(F_o^2-F_c^2)^2]/(n-p)\}^{1/2}$ (n = number of reflections; p = total number of parameters).

Hirshfeld Analysis

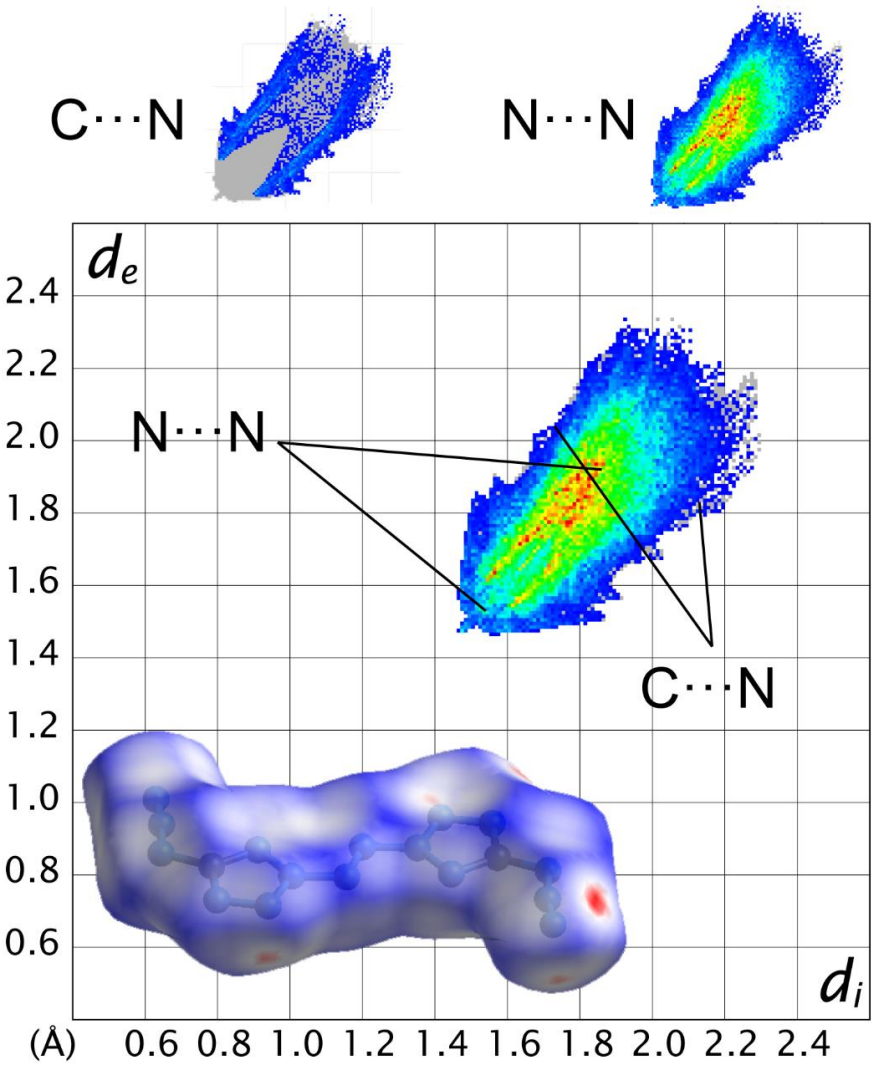

Figure S4. Representation of the Hirshfeld surface of **3** and the thereof calculated 2D fingerprint plot.

Hirshfeld surfaces are based on the respective crystal structure of the investigated compound and can therefore calculated using the respective cif file.[S10] The Hirshfeld surface shows the next close contacts (red color) within the crystal pattern. The thereof generated 2D fingerprint pot indicated the distance and type of interaction toward the surrounding atoms in the crystal layering structure (d_e: distance of the Hirshfeld surface to the nearest exterior atom, d_i: distance of the Hirshfeld surface to the nearest interior atom).[S10] The 2D fingerprint plot shows only week interactions of N···N (93.4%) in the area of $d_e + d_i > 3$ Å and C···N (6.6%) in the area of $d_e + d_i > 3.3$ Å. From the Hirshfeld analysis only a few weak repulsive interactions (N···N) and no attractive polar interactions result.

14.6.3 Computation

14.6.3.1 Heat of Formation

All quantum chemical calculations were carried out using the Gaussian G09 program package.[S11] The enthalpies (H) and free energies (G) were calculated using the complete basis set (CBS) method of Petersson and co-workers in order to obtain very accurate energies. The CBS models are using the known asymptotic convergence of pair natural orbital expressions to extrapolate from calculations using a finite basis set to the estimated CBS limit.

CBS-4 starts with an HF/3-21G(d) geometry optimization; the zero-point energy is computed at the same level. It then uses a large basis set SCF calculation as a base energy, and an MP2/6-31+G calculation with a CBS extrapolation to correct the energy through second order. A MP4(SDQ)/6-31+ (d,p) calculation is used to approximate higher order contributions. In this study, we applied the modified CBS-4M.[S12,S13]

The CBS-QB3 has been modified by the inclusion of diffuse functions in the geometry optimization step to give CBS-QB3.[S14] The five-step CBS-QB3 series of calculations starts with a geometry optimization at the B3LYP level, followed by a frequency calculation to obtain thermal corrections, zero-point vibrational energy, and entropic information. The next three computations are single-point calculations (SPCs) at the CCSD(T), MP4SDQ, and MP2 levels. The CBS extrapolation then computes the final energies.[S15]

Table S2. Heat of Formation calculation results based on CBS-4M and CBS-QB3.

	$-H^{298}$ [a] [a.u.] CBS-4M	$\Delta_f H°(g,M)$ [kJ mol^{-1}] [b]	$\Delta_f H°(s)$ [c] [kJ mol^{-1}]	$-H^{298}$ [d] [a.u.] CBS-QB3	$\Delta_f H°(g,M)$ [kJ mol^{-1}] [e]	$\Delta_f H°(s)$ [f] [kJ mol^{-1}]
2	476.555101	766.8	703.7	476.555101	766.8	703.7
3	950.682697	1773.5	1700.7	950.682697	1773.5	1700.7

[a] CBS-4M electronic enthalpy; [b] gas phase enthalpy of formation based on CBS-4M; [c] standard solid state enthalpy of formation based on CBS-4M; [d] CBS-QB3 electronic enthalpy; [e] gas phase enthalpy of formation based on CBS-QB3; [f] standard solid state enthalpy of formation based on CBS-QB3;

The standard molar enthalpy of formation of solids **2** and **3** was calculated using $\Delta_f H(g)$ subtracting the enthalpy of sublimation estimated by applying *Trouton´s* rule

[S16]. (ΔH_{sub} = 188 T_m). Since no melting point was observed for **3**, its decomposition temperature has been used. (**2**: T_m 62 °C, ΔH_{sub} = 63.0 kJ mol^{-1}, **3**: T_{dec} 114 °C, ΔH_{sub} = 72.8 kJ mol^{-1}). The calculation results are summarized in Table S2.

14.6.3.2 IR Frequencies

Table S3. IR frequencies and intensities calculated at the BLYP/6-31G(d) level of theory. The frequencies were fitted with a scaling factor of 0.9940 according to Witek et al.[S17] Frequencies highlighted in gray with an intensity of 0 do not result in real measured frequencies due to the symmetry present in the molecule.

IR Frequencies	IR Frequencies (fitted)	IR Intensities
-	20	0.35
-	46	1.36
-	60	0.75
	77	0.00
	90	0.00
-	101	0.45
	129	0.00
-	138	1.84
	215	0.00
	248	0.00
-	277	0.09
	314	0.00
	370	0.00
-	386	3.14
-	419	1.65
	444	0.00
	495	0.00
496	496	12.88
-	502	44.57
	524	0.00
527	543	97.66
	602	0.00
-	611	3.26
682	681	56.53
	706	0.00
737	707	12.37
	746	0.00

798	790	62.52
	862	0.00
883	877	536.97
	938	0.00
	1017	0.00
1024	1019	10.73
1090	1064	112.05
	1083	0.00
1184	1173	631.61
	1188	0.00
	1191	0.00
	1199	0.00
	1253	0.00
1221	1264	96.79
	1349	0.00
1377	1360	134.60
	1400	0.00
1505	1473	1058.83
	1482	0.00
2150	2162	1251.06
	2166	0.00

14.6.3.3 Electrostatic Potential (ESP)

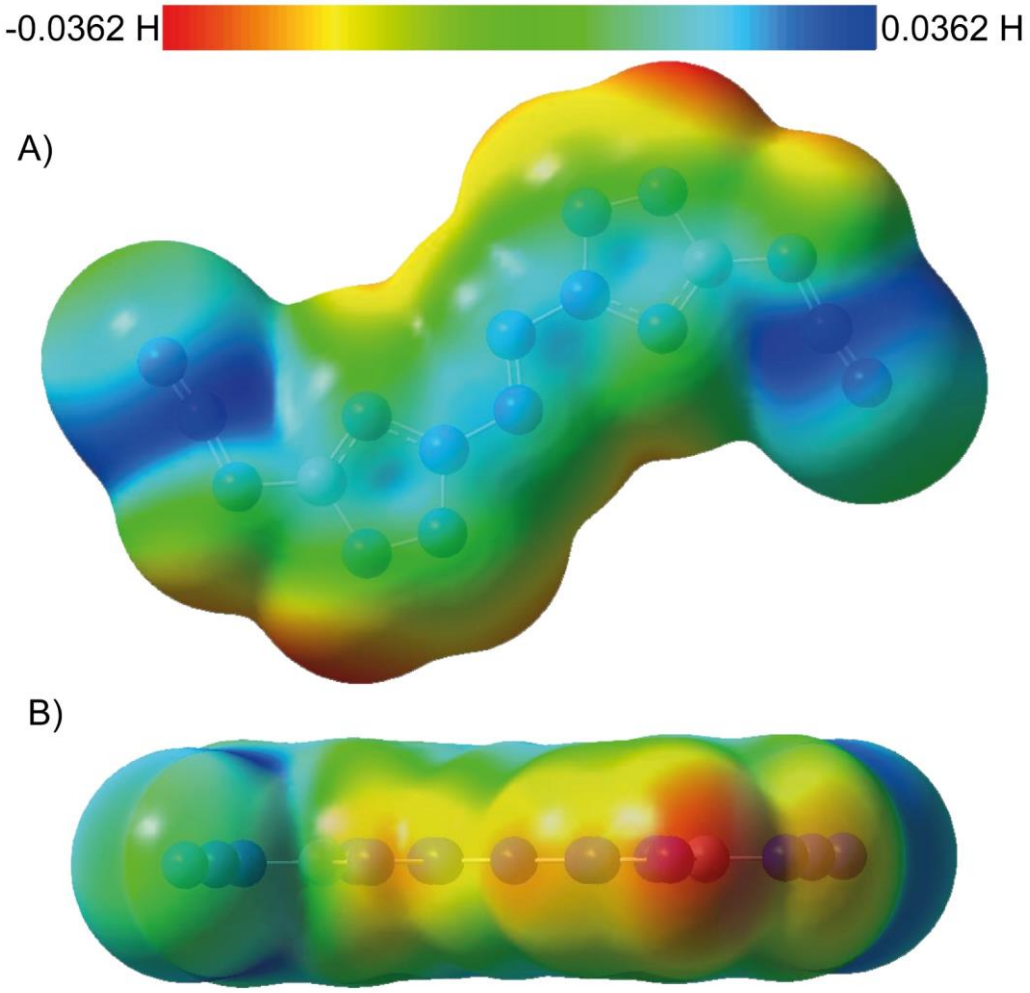

Figure S5. Representation of the molecular electrostatic potential of **3** in the 0.001 e bohr^{-3} isosurface computed at the B3LYP/6-31G(d,p) level with the color range from −0.036 to 0.036 H. Red color represent electron-rich and blue color electron-deficient regions. A) top view, B) side view.

To get a better insight of the electronic situation of **3** its electrostatic potential (ESP) was calculated at the B3LYP/6-21G(d,p) level of theory in the gas phase structure (C2h). The output of the calculation of the ESP can be found in Figure S4. There, the highest electron density can be detected to be on the double-bonded nitrogen atoms N1, N3 and N4 of the tetrazole. A lack of electrons is determined at the N_β of the azide function as well as for the planar 2,2'-azobistetrazole system.

The consideration of the electrostatic potential of **3** results in the observable bond characteristics in the crystal, which occur between positively and negatively polarized regions.

14.6.3.4 Neutral Bond Orbital (NBO) and Mulliken Charges

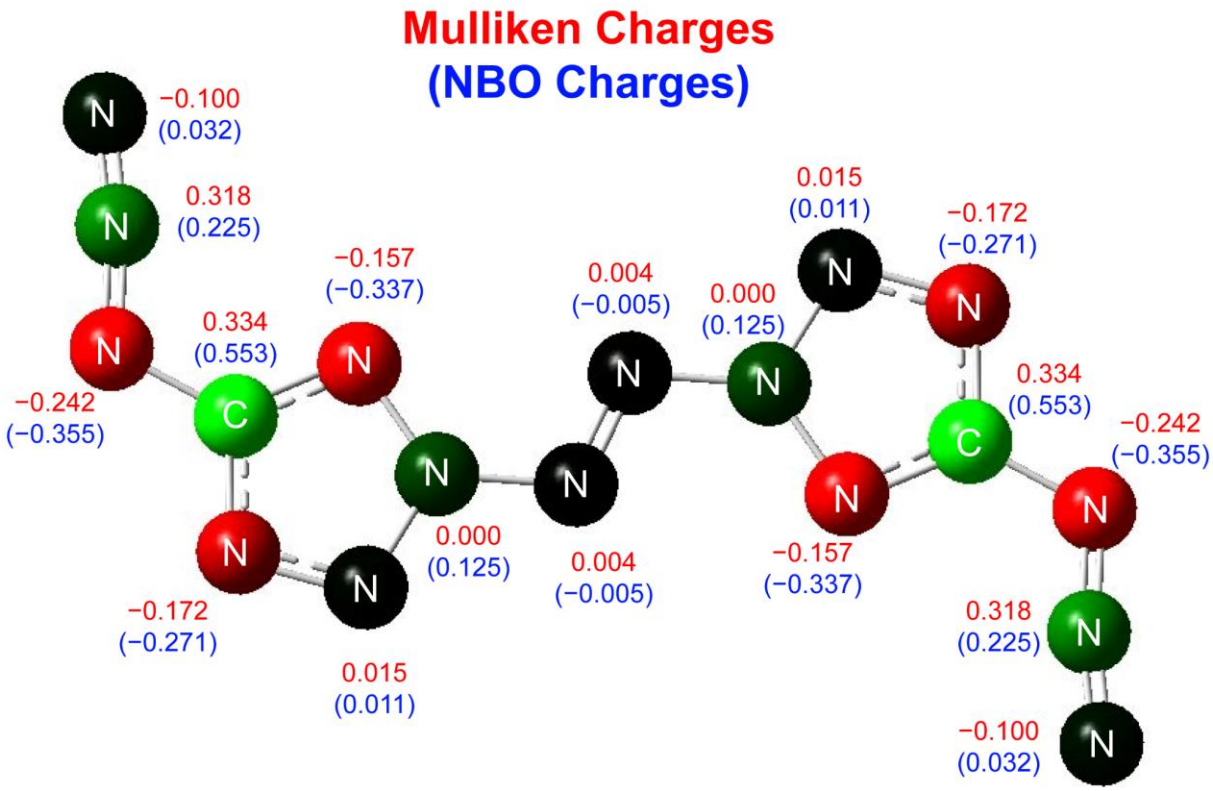

Figure S6. Representation of the natural bond orbital (NBO) and Mulliken charges of **3** calculated based on the B3Lyp/cc-pVDZ level of theory.

Since we assumed kind of a charge separation within the molecule, NBOs (natural bond orbitals) as well as Mulliken charges of 2,2'-azobis-(5-azidotetrazole) (**3**) were calculated on the B3LYP/cc-pVDZ level of theory using the gas phase structure (C_{2h}). The values for the NBO and Mulliken calculation differ slightly but show the same trend. For both methods, the highest positively charged atom is the carbon, consisting of three neighbor atoms with a higher electronegativity. Moreover, N_β is also positively polarized, which is illustrated by the Lewis structure of covalent azides, in which it is always partially positively charged. N_α, N1 and N4 are strongly negatively polarized, with N_α having the highest negative polarization for both calculation methods. The azo bridge does not show any polarization and, as already shown in the ESP and the crystal structure, does not participate in intermolecular interactions.

14.6.3.5 UV/Vis

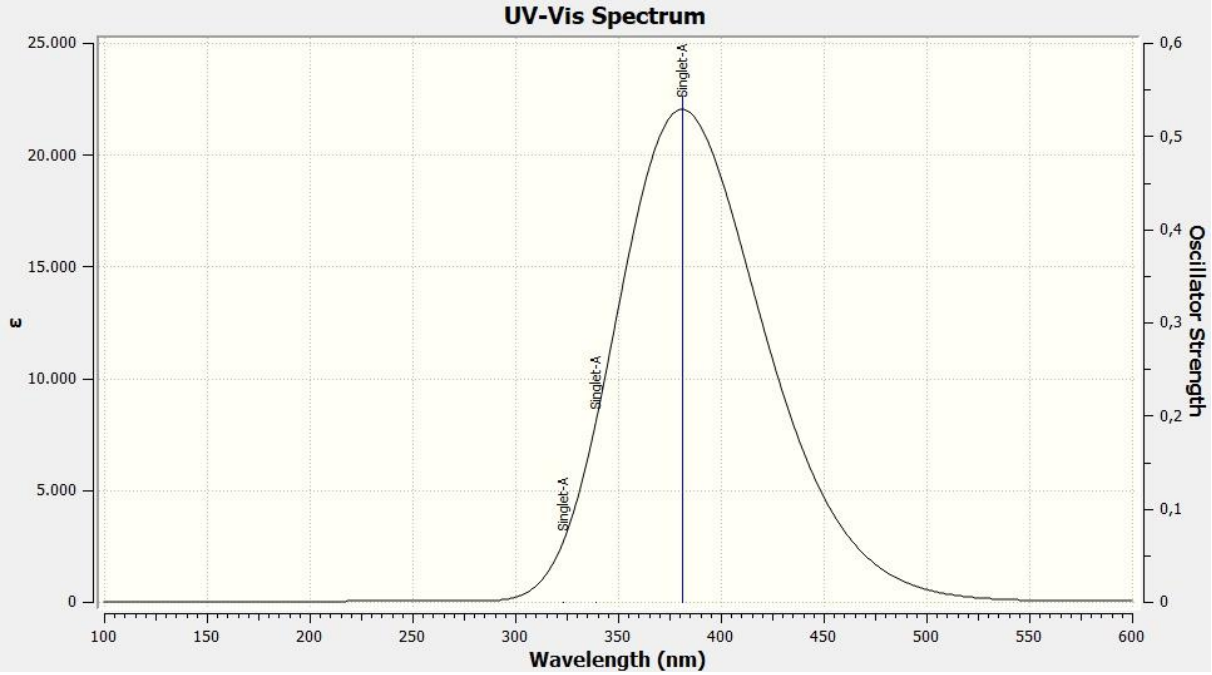

Figure S7. Calculated UV/Vis spectrum of compound **3**.

The calculation was performed using TD-SCF DFT calculations applying method B3LYP with a basis set of 6-311G. The result of the calculation is depicted in Figure S7. For compound **3**, an absorption maximum at 381 nm is observed. Therefore, the compound should appear in a yellowish color.

14.6.4 Spectroscopy

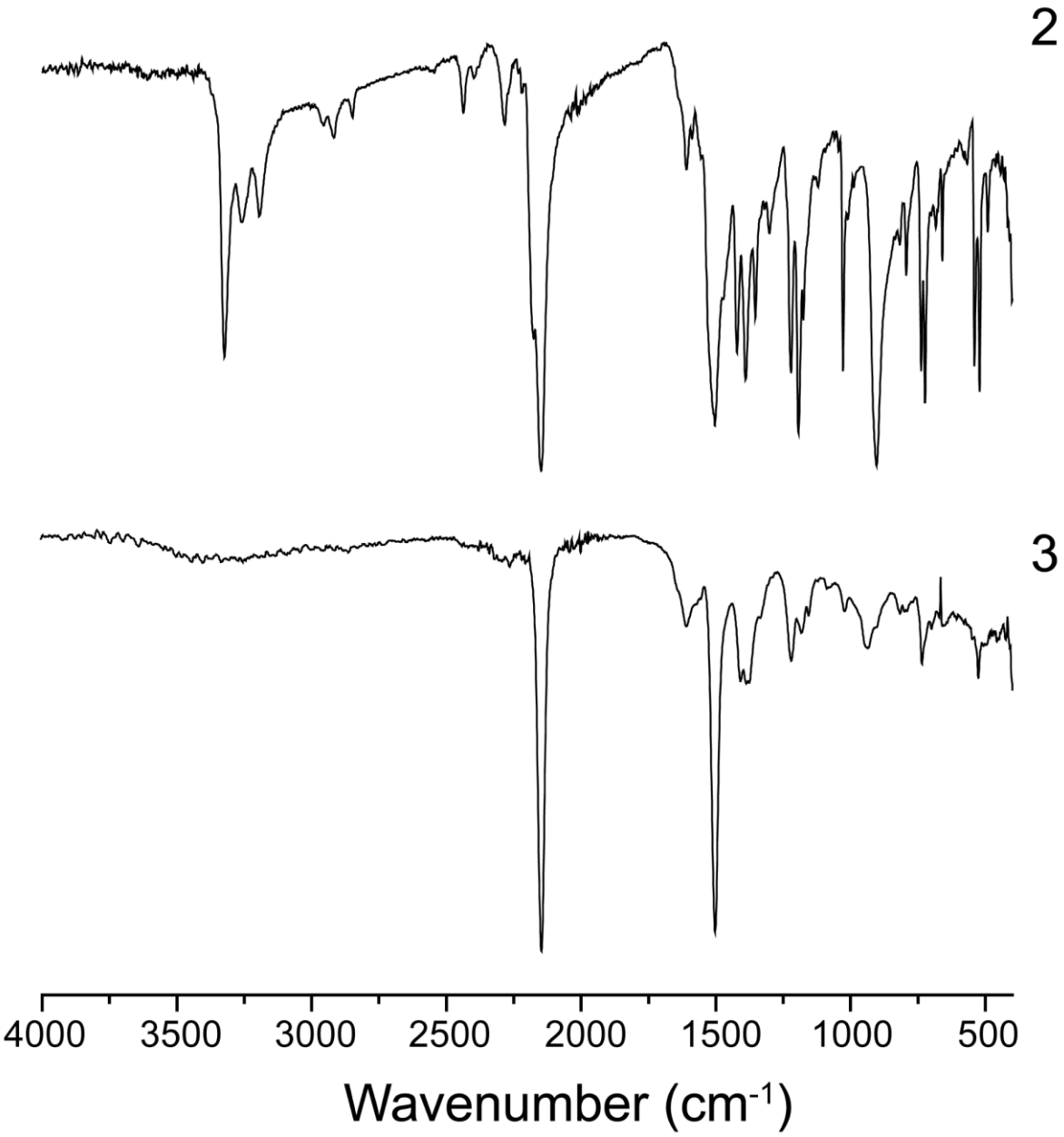

Figure S8. IR spectra of compounds **2** and **3**.

^{1}H-NMR (400 MHz, CD_3CN, ppm)

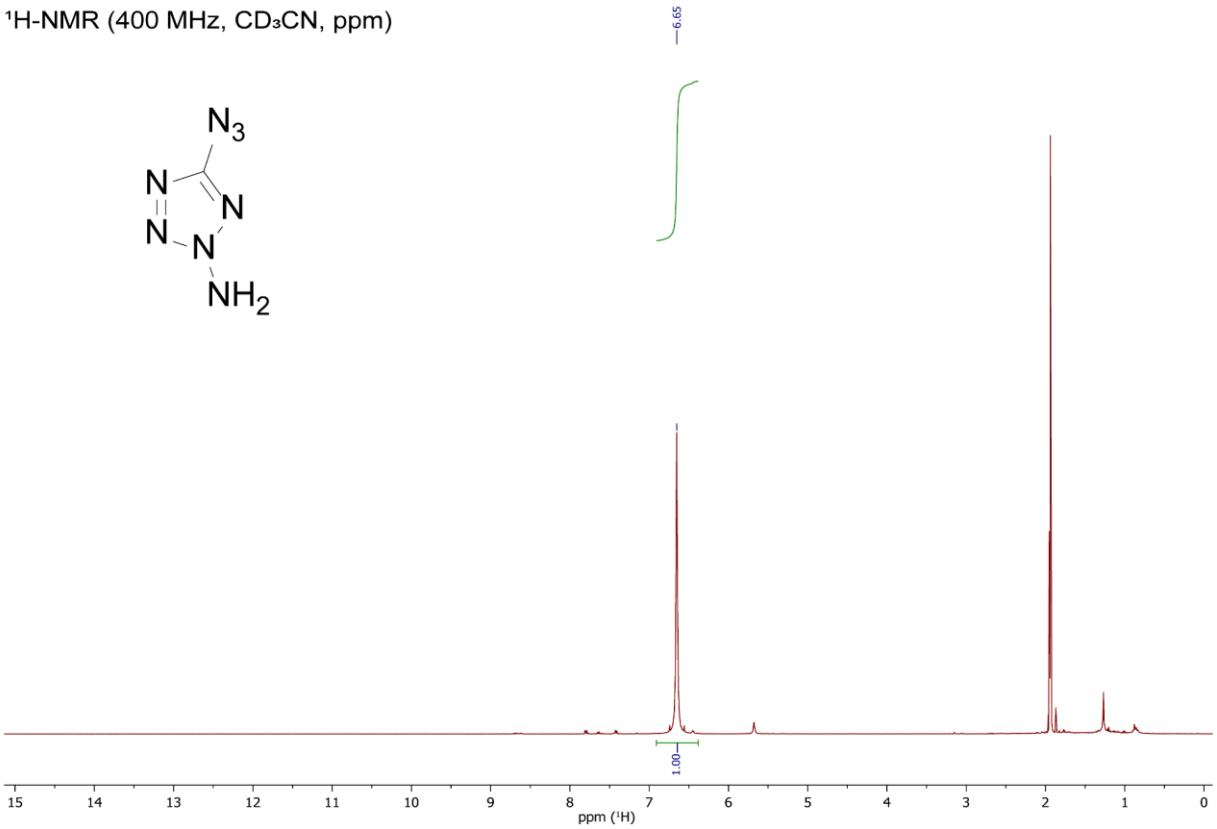

^{13}C-NMR (101 MHz, CD_3CN, ppm)

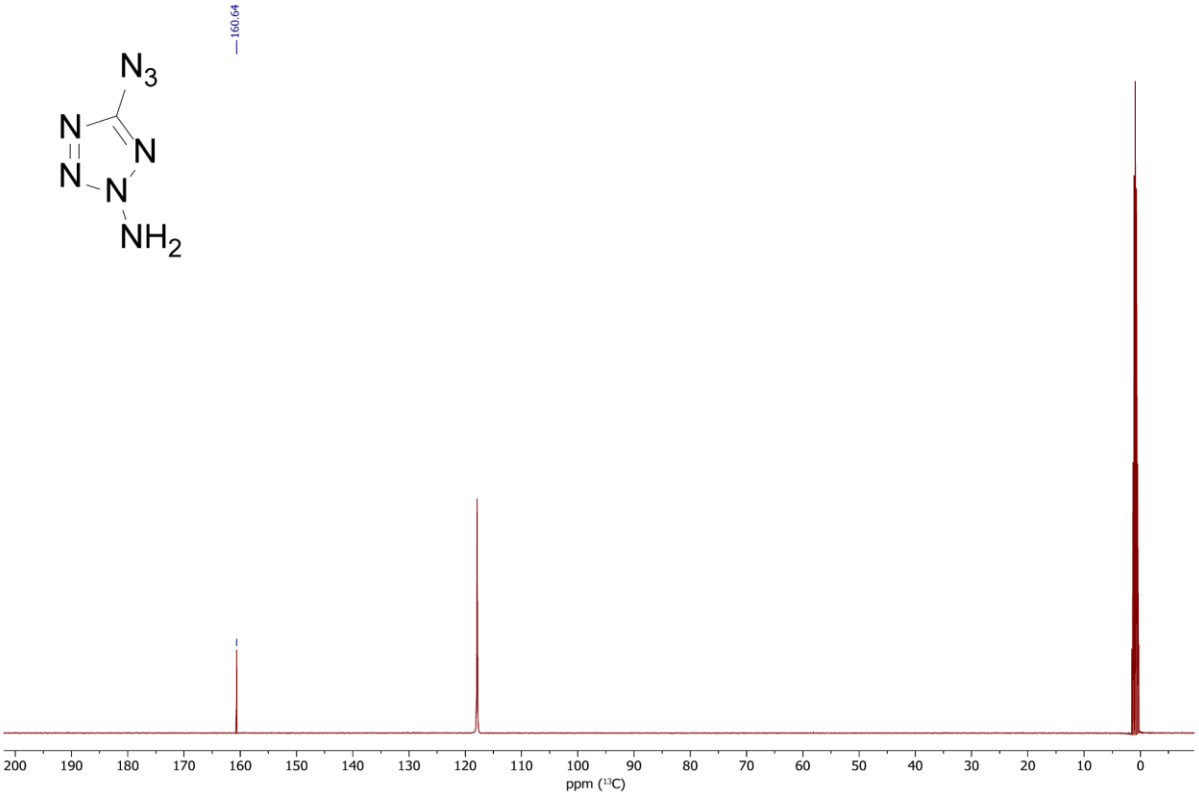

^{15}N-NMR (41 MHz, CD_3OD, ppm)

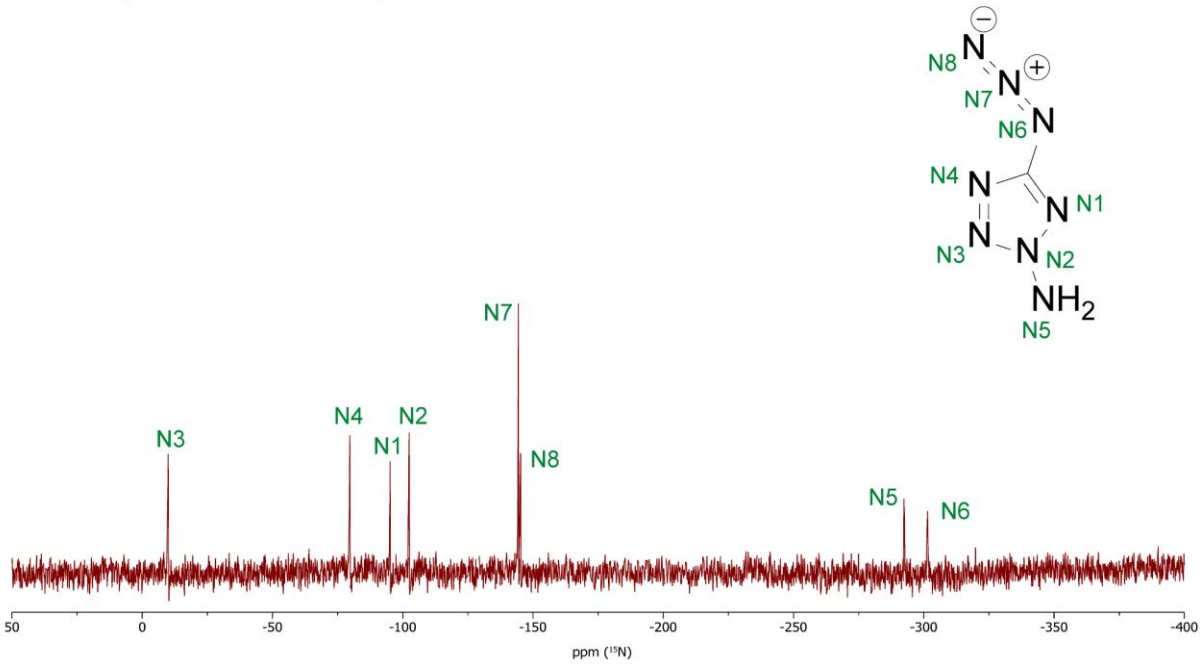

^{13}C-NMR (101 MHz, CD_3CN, ppm)

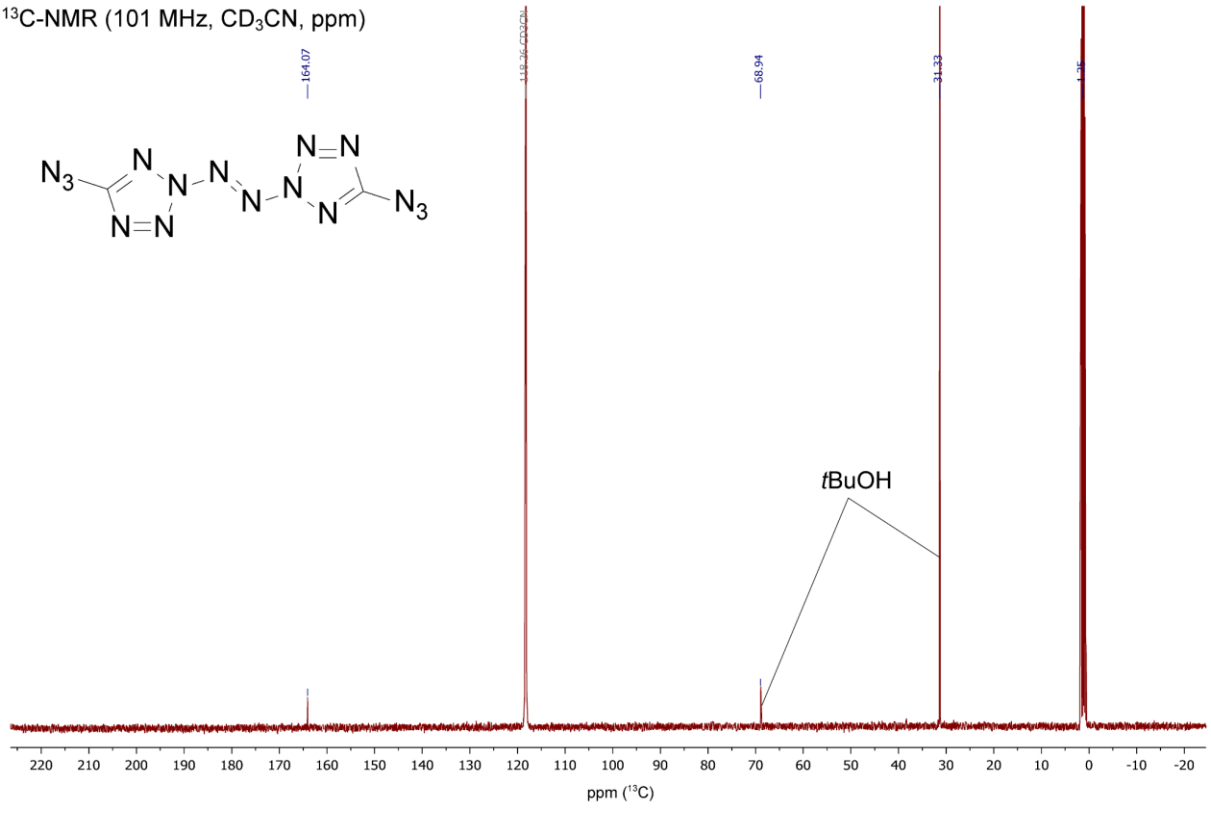

14.6.5 Thermal Analysis

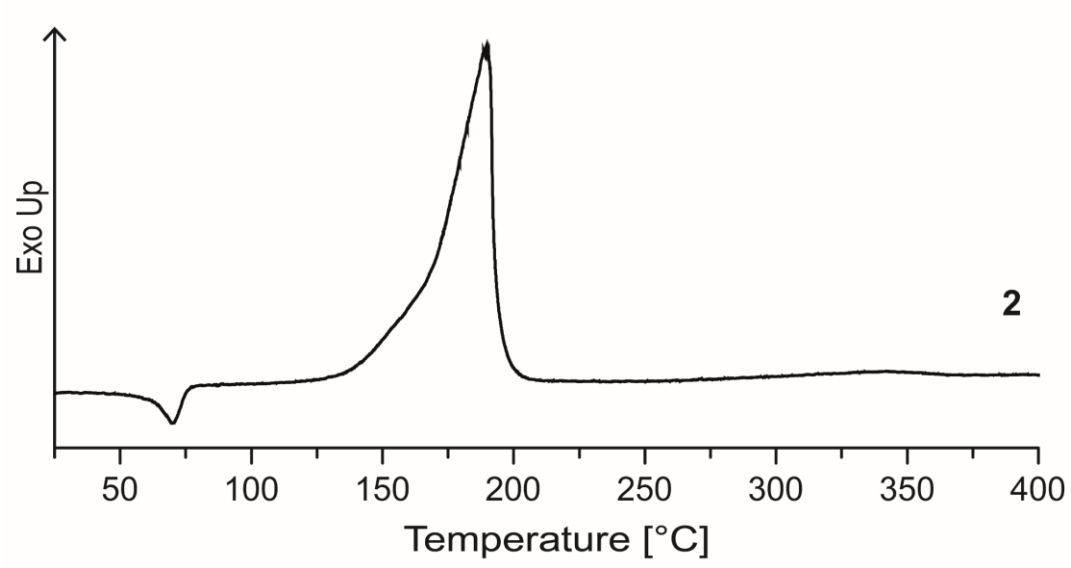

Figure S9. DTA plot of compound **2** with a heating rate of 5 °C min^{-1}.

14.6.6 References

[S1] a) Reichel & Partner GmbH, http://www.reichelt-partner.de; b) Test methods according to the UN Recommendations on the Transport of Dangerous Goods, *Manual of Test and Criteria*, fourth revised edition, United Nations Publication, New York and Geneva, **2003**, ISBN 92–1-139087–7, Sales No. E.03.VIII.2; 13.4.2 Test 3 a (ii) BAM Fallhammer.

[S2] M. Sućeska, EXPLO5 V6.02 program, Brodarski Institute, Zagreb, Croatia, **2014**.

[S3] M. J. Mintz, C. Walling, *Org. Synth.* **2003**, *49*, 9.

[S4] a) T. M. Klapötke, D. G. Piercey, J. Stierstorfer, *Dalton Trans.* **2012**, *41*, 9451–9459, b) E. E. Glover, K. T. Rowbottom *J. Chem. Soc., Perkin Trans.* **1976**, *1*, 367–371

[S5] *CrysAlisPro*, Oxford Diffraction Ltd. *version 171.33.41*, **2009**.

[S6] G. M. Sheldrick, *Acta Cryst.* **2015**, *A71*, 3–8.

[S7] O. V. Dolomanov, L. J Bourhis, R. J. Gildea, J. A. K. Howard, H. Puschmann, *J. Appl. Cryst.* **2009**, *42*, 339–341.

[S8] *SCALE3 ABSPACK – An Oxford Diffraction program* (1.0.4, gui: 1.0.3), Oxford Diffraction Ltd., **2005**.

[S9] *APEX3*. Bruker AXS Inc., Madison, Wisconsin, USA.

[S10] a) P. R. Spackman, M. J. Turner, J. J. McKinnon, S. K. Wolff, D. J. Grimwood, D. Jayatilaka, M. A. Spackman, *J. Appl. Crystallogr.,* **2021**, *54* (3), 1006–1011, b) L. Bauer, M. Benz, T. M. Klapötke, T. Lenz, J. Stierstorfer, *J. Org. Chem.,* **2021**, *86*, 9, 6371–6380.

[S11] M. J. Frisch, G. W. Trucks, H. B. Schlegel, G. E. Scuseria, M. A. Robb, J. R. Cheeseman, G. Scalmani, V. Barone, B. Mennucci, G. A. Petersson, H. Nakatsuji, M. Caricato, X. Li, H.P. Hratchian, A. F. Izmaylov, J. Bloino, G. Zheng, J. L. Sonnenberg, M. Hada, M. Ehara, K. Toyota, R. Fukuda, J. Hasegawa, M. Ishida, T. Nakajima, Y. Honda, O. Kitao, H. Nakai, T. Vreven, J. A. Montgomery, Jr., J. E. Peralta, F. Ogliaro, M. Bearpark, J. J. Heyd, E. Brothers, K. N. Kudin, V. N. Staroverov, R. Kobayashi, J. Normand, K. Raghavachari, A. Rendell, J. C. Burant, S. S. Iyengar, J. Tomasi, M. Cossi, N. Rega, J. M. Millam, M. Klene, J. E. Knox, J. B. Cross, V. Bakken, C. Adamo, J. Jaramillo, R. Gomperts, R. E. Stratmann, O. Yazyev, A. J. Austin, R. Cammi, C. Pomelli, J. W. Ochterski, R. L. Martin, K. Morokuma, V. G. Zakrzewski, G. A. Voth, P. Salvador, J. J. Dannenberg, S. Dapprich, A. D. Daniels, O. Farkas, J.B. Foresman, J. V. Ortiz, J. Cioslowski, D. J. Fox, Gaussian 09 A.02, Gaussian, Inc., Wallingford, CT, USA, **2009**.

[S12] a) J. W. Ochterski, G. A. Petersson, and J. A. Montgomery Jr., *J. Chem. Phys.* **1996**, *104*, 2598–2619; b) J. A. Montgomery Jr., M. J. Frisch, J. W. Ochterski G. A. Petersson, *J. Chem. Phys.* **2000**, *112*, 6532–6542.

[S13] a) L. A. Curtiss, K. Raghavachari, P. C. Redfern, J. A. Pople, *J. Chem. Phys.* **1997**, *106*, 1063–1079; b) E. F. C. Byrd, B. M. Rice, *J. Phys. Chem*. A **2006**, *110*, 1005–1013; c) B. M. Rice, S. V. Pai, J. Hare, *Comb. Flame* **1999**, *118*, 445–458.

[S14] J. A. Montgromery, M. J. Firsch, J. W. Ochterski, G. A. A. Petersson, *J. Chem. Phys.,* **2000**, *112*, 6532–6542.

[S15] F. C. Pickard, E. K. Pokon, M. D. Liptak, G. C. Shields, *J. Chem. Phys.,* **2005**, *122*, 24302–24307.

[S16] M. S. Westwell, M. S. Searle, D. J. Wales, D. H. Williams, *J. Am. Chem. Soc*. **1995**, *117*, 5013–5015; b) F. Trouton, *Philos. Mag*. **1884**, *18*, 54–57.

[S17] H. A. Witek, M. Keiji, *J. Comp. Chem. THEOCHEM* **2004**, *25*, 1858–1864.

15. Linear Correlation between Confined Explosive Quantity and Dent Volume of an Underlying Aluminium Block Using the SSRT Setup

Lukas Bauer‡, Maximilian Benz‡, Thomas M. Klapötke

as published in *Propellants Explosives Pyrotechnics* **2022**, *47*, e202100332

DOI: 10.1002/prep.202100332

Keywords: correlation, detonation properties, explosives, PETN, SSRT

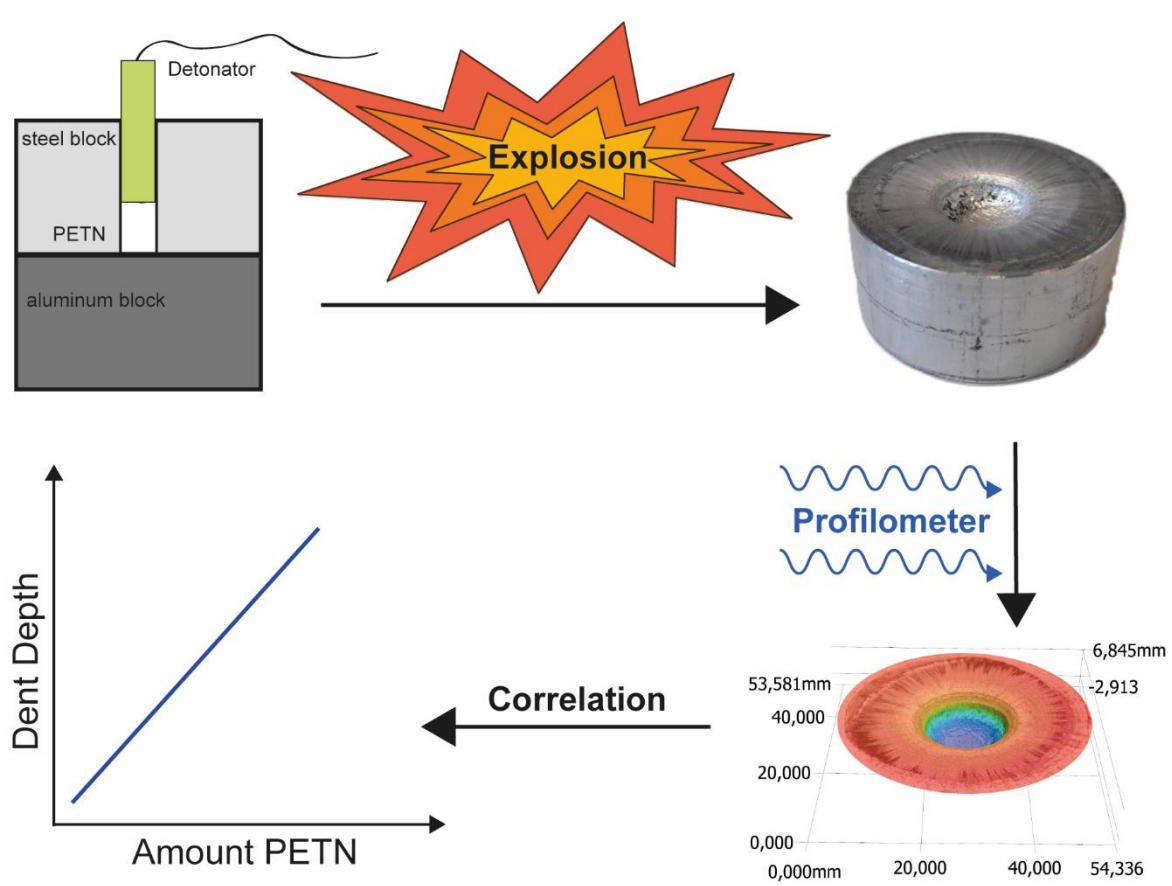

Testing the correlation of a defined amount of explosive and the respective dent of an aluminum block underneath using the SSRT setup. This study gives insights in the behavior of an explosive output by steady increase of the explosive quantity.

Abstract: The SSRT setup gives smart access to test various properties of explosive materials and requires only little substance quantities. Unlike the standardized SSRT, we studied the bulge development from the blast of different amounts of PETN (200–1300 mg). The bulge of the corresponding aluminum blocks was evaluated with the help of a profilometer (Keyence VR-5200). This device, which measures the volume of the dents using the offset of structured light projected on the object, has allowed us to analyze the differences precisely. Despite the experimental limitations and the resulting undirected explosion direction, a throughout linear correlation between the respective amounts of PETN and the resulting dent depth could be determined. Our study thus forms an illustrative development of how the explosion behavior, represented by the dent of an aluminum block, of compressed energetic materials behaves in with increasing filling quantity, which is transferable to larger experimental setups as well as to other explosives.

15.1 Introduction

Initiating explosives in the Small Scale Shock Reactivity Test (SSRT)is a method, which can be used to investigate how explosivea substance is, and provides an initial estimate of the detonation behavior of the substance – even if the test is carried out below the critical diameter.[1] This test was developed to combine the advantages of the classic lead block and gap tests.[2-3] The SSRT test uses a similar procedure as the plate dent test.[4-5] In this test, the explosive under investigation is initiated by a commercial detonator and the depth (volume) of the dent formed in a solid aluminum block after initiation of the explosive materialis measured using appro-priate methods. The volume of the dent correlates with the power of the explosive. The volume of a crater (massive dent) formed by the detonation of an explosive charge lying freely on the ground does not scale linearly with the mass of the explosive.[6-9] However,it has remained unclear how the dent volume in a SSRT test scales with the mass of explosive. To answer this question, we carried out the study presented in this paper.

15.2 Experimental Procedure

CAUTION! *Despite the large quantities that were handled, PETN is classified as a primary explosive and therefore extremely sensitive toward any kind of external stimuli and can detonate as a result of improper handling. Safety precautions and equipment (such as wearing a leather coat, face shield, Kevlar sleeves, Kevlar gloves, earthed equipment, and earplugs) must be used during all manipulations.*

A 100 mL double jacked vessel, connected to a circulating cooler and equipped with a mechanical stirrer, was loaded with white fuming nitric acid (99%, 50 mL, 75 g, 5 Parts). At 15±3 °C 2,2-bis(hydroxymethyl)propane-1,3-diol (15.0 g, 110 mmol, 1 Part) was added portion-wise over 25 min. Then the reaction was left for completion at 5 °C for 30 min. The suspension was filtrated over a PTFE membrane filter (10 µm). The solid was transferred into diluted nitric acid (11%, 150 mL) stirred for 15 min, and filtrated again. The acidic PETN was dissolved in acetone and ammonia was bubbled through the solution until neutralization was achieved. An excess of water was added slowly to yield PETN after filtration as a fine powder (33.5 g, 106 mmol, 96%, grain size: 100–200 µm (85 %)).
DTA (5 °C min^{-1}, onset): 143 °C (melt) followed by decomposition; Sensitivities: BAM drop hammer: 3.5 J, friction tester: 54 N; IR (ATR) $\tilde{\upsilon}$(cm^{-1}) = 2986 (w), 2904 (w), 1638 (s), 1630 (s), 1473 (m), 1396 (w), 1305 (m), 1283 (s), 1266 (s), 1036 (m), 998 (s), 939 (m), 833 (s), 752 (s), 701 (s), 619 (s), 458 (m); Elem. Anal. ($C_5H_8N_4O_{12}$, 316.15 g mol^{-1}) calcd.: C 19.00, H 2.55, N 17.72 %. Found: C 19.01, H 2.28, N 17.47 %; ^{1}H NMR (DMSO-D_6, 400 MHz, ppm) δ = 4.70 (s, 8H); ^{13}C NMR (DMSO-D_6, 101 MHz, ppm) δ = 70.3, 40.8; ^{14}N NMR (DMSO-D_6, 29 MHz, ppm) δ = −45.

15.3 Results and Discussion

15.3.1 Sample Preparation

For our experimental determinations, we used a classic setup as described for SSRT (small-scale shock reactivity test) experiments.[1b] The experimental setup consists of a cylindrical aluminum block (height: 25.0 mm, diameter: 50.0 mm, EN AW-2007) with a matching steel block (height: 25.0 mm, diameter: 50.0 mm, hot-

rolled mild steel) placed on top of the aluminum block. The steel block is provided with a 7.5 mm wide hole in the center, into which the substance to be tested is later filled. For easier handling, both blocks are temporarily tied together with the help of a crepe tape (Figure 1). Subsequently, the appropriate amounts of PETN were poured into the hole of the steel block with a funnel.

Figure 1. Experimental setup consisting of an aluminum block and steel block with hole connected by crepe tape (left), test setup during the pressing process (right).

Particularly with filling quantities of 1000 mg or more, the material had to be pre-compacted manually by tapping to accommodate the entire quantity. A suitable steel pin (diameter: 7.45 mm) was then placed in the hole on top of the PETN and pressed with the aid of a hydraulic press at a pressure of 3 tons. This was repeated twice in order to obtain the maximum possible compression. After removal of the steel pin, a thin PETN layer remained on the inner wall of the steel block bore. This was removed with the aid of a pipe cleaner to ensure a maximum insertion length of the detonator later on.

The blocks with the compressed PETN were then placed in a steel plate with a matching recess at the bottom. A corresponding steel lid with an opening around the steel hole was then placed on top of the blocks. The two steel plates are each provided with four holes, allowing matching threaded rods to be used for fixation. The respective screws for fastening were hand-tightened (Figure 2–3). This setup was designed to prevent the blocks from slipping and counteract the force of the

explosion and project the maximum of the released energy onto the aluminum block.

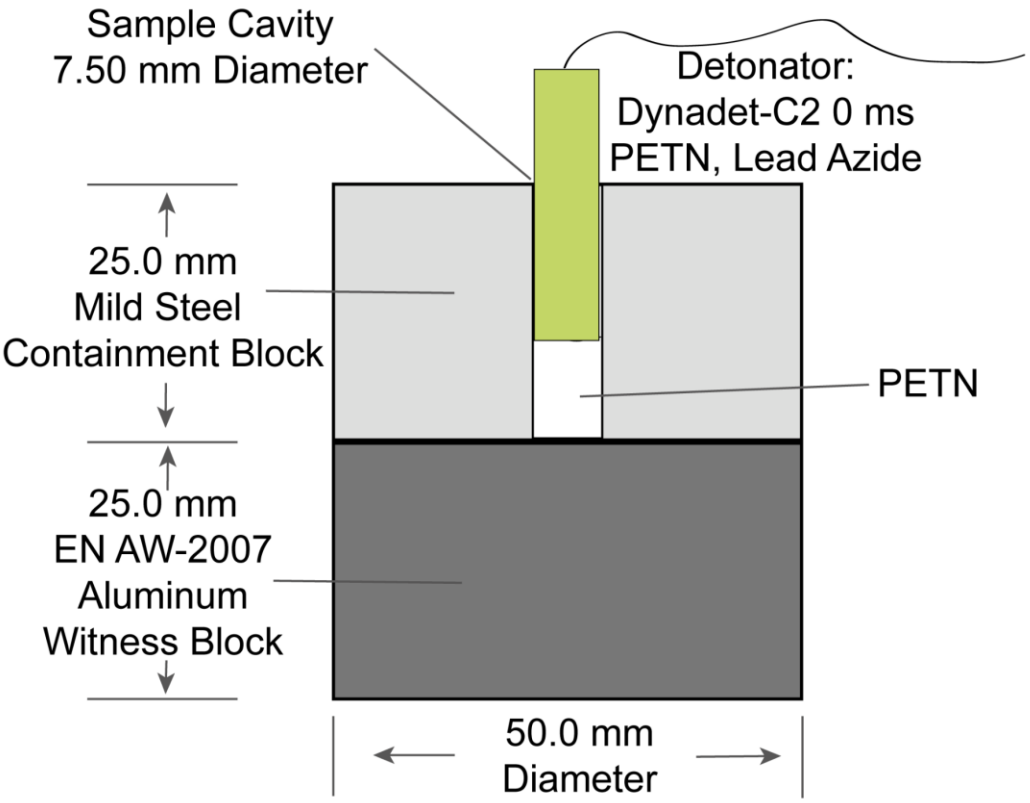

Figure 2. Schematic setup of the experiment as displayed in Figure 3 (left).

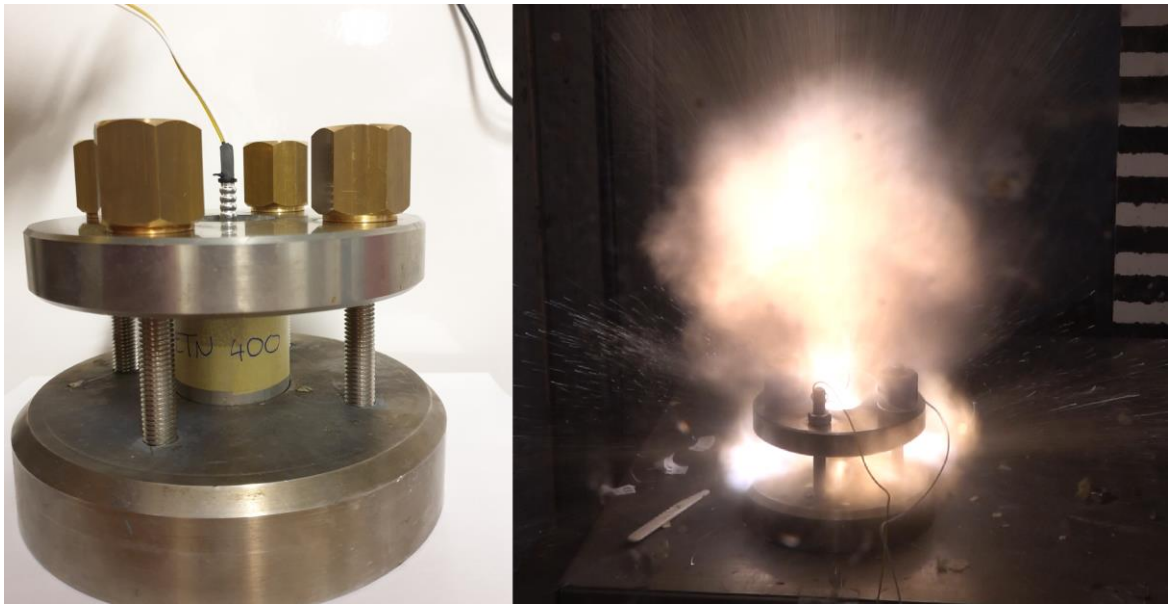

Figure 3. Test blocks in fixing device with detonator inserted in the steel block hole (left), Moment of detonation of 400 mg PETN (right).

The detonator (Dynadet-C2) was then inserted into the bore of the steel block and placed as close as possible to the compressed PETN with the appropriate force. After initiation, the screws of the fastening device were loosened and the aluminum block was removed. In the case of smaller quantities of PETN, it happened that parts of the aluminum sleeve of the detonator were blasted into the block. These could be easily removed with pliers. The block was cleaned of any soot present by washing it with water and acetone.

15.3.2 Analysis

The obtained aluminum blocks were analyzed through non-contact measurements with the XYZ-axis motorized 3D profilometer VR-5200, produced by Keyence (Osaka, Japan; Figure 4). The measuring range is 200 mm×100 mm×50 mm with a resolution of up to 1 µm.[10] Structured light is emitted by two angled telecentric transmitter lenses and projected on the surface of the aluminum block. The offset of the structured light is detected by the receiver lens and appears banded and bent based on the changes of topography on the surface of the block.[11] The offset of the structured light is then used to calculate the dimensions of the block and the dent depth using the light sectioning method and triangulation.[10, 12]

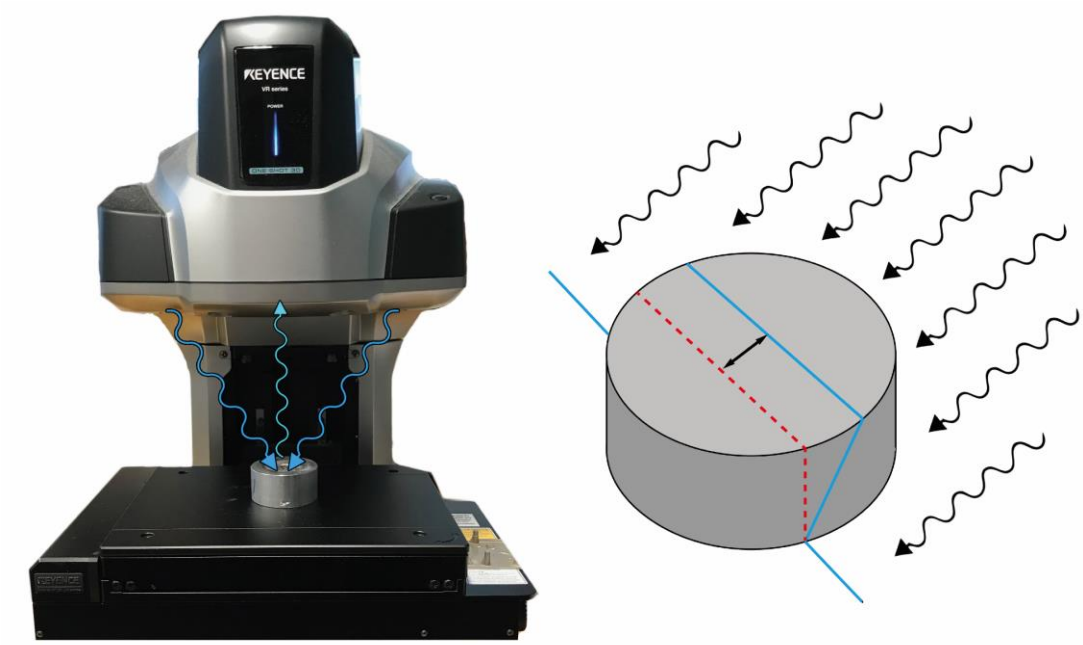

Figure 4. Profilometer with indicated light emitting from the angled lenses and detected by the receiver lens in the middle (left); Illustration of the light sectioning method and triangulation (right).

No anti-reflective spray was needed for these measurements. Up to six blocks were measured in one pass, then turned by 90 ° and measured again to avoid blind spots in the measurement. The volume of the dent was determined as follows: In the analysis software, a ring of 1 mm thickness and an average diameter of 47 mm was placed on the block. The resulting area was used as a reference area to determine the reference height of the block (Figure 5).

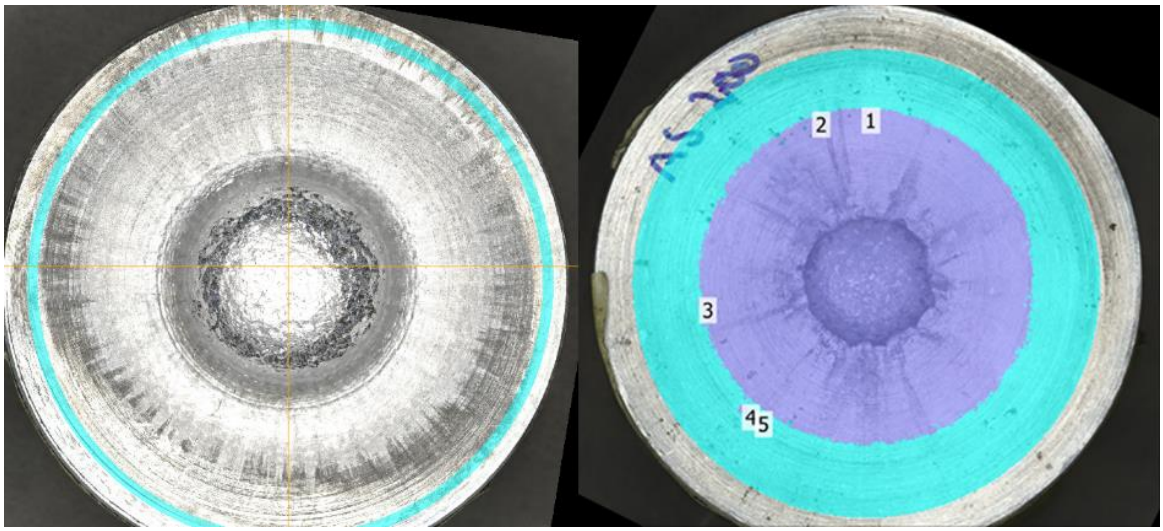

Figure 5. Reference area indicated in cyan (left); measured area indicated in cyan and detected indentations indicated in violet and numbered.

The blocks were then aligned and the depth of the dent inside the area of the ring was determined. Finally, the two values for the first second measurement were averaged.

15.3.3 Method and Evaluation

For our test series, we decided on quantities of PETN starting from 200 mg (minimum compressible quantity) in 100 mg intervals progressively up to 1300 mg (maximum filling quantity of the borehole). The tests with the respective PETN quantities were performed twice to be able to form an average value of the dent volumes and thus minimize the error and deviation. Since the detonator used contains a considerable amount of explosive material and thus has an effect on the depth of the dent, this effect was investigated separately. A blank test, containing

$(NH_4)_2SO_4$ instead of PETN was carried out for each filling quantity and thus for each filling height since it was to be expected that the influence of the detonator decreases with increasing distance to the aluminum block.

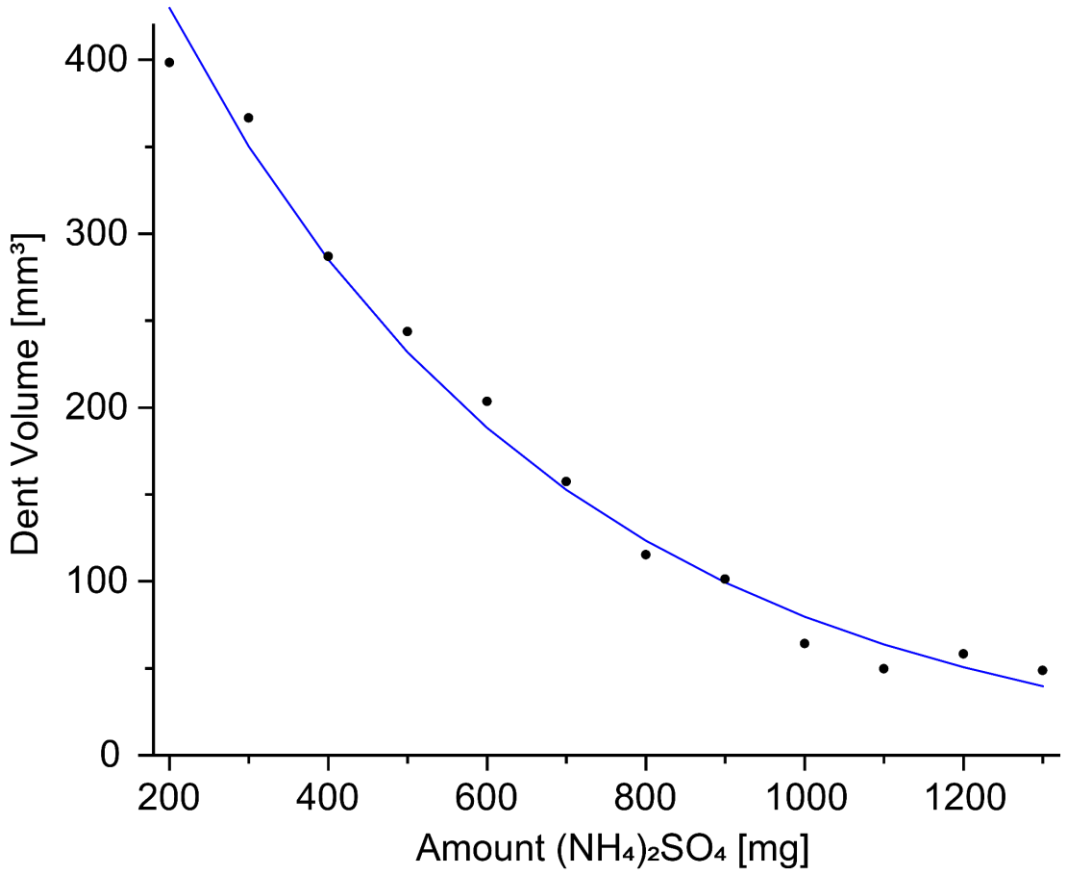

Figure 6. Dent depth caused by the detonator depending on the distance from aluminum block ensured by different amounts of ammonium sulfate as filler material. The blue line corresponds to an exponential regressive fit with the equation $y = 658.21 \cdot e^{-0.002x}$.

Finely ground ammonium sulfate was used as filler material for the blank samples, as it has the same ideal crystal density as PETN (1.77 g cm^{-3}), is not particularly moisture sensitive or hygroscopic, not ignitable, thermally stable, and can be readily compacted in fine powder form. The respective samples were then prepared and ignited as described in section 14.3.1.

As expected, the dent depth decreases with increasing filling level of unreactive material. The blue fitting line included in Figure 6 illustrates an exponential regression of the dent depth. It is nevertheless remarkable that a filling quantity of 1300 mg of ammonium sulfate still results in a similarly strong bulge as with 1000 mg since the detonator was only a few millimeters inside the steel block and

thus the explosion energy was able to escape uncentered and distributed in all directions.

The values obtained were identified as zero points for the experiments with PETN to illustrate only the corresponding influence of the explosive force of PETN on the dent depth. The values, as well as the graph for the absolute blast depth, can be found in the Supporting Information.

The blocks were measured twice and rotated by 90 ° in-between measurements to capture any unexposed areas. The volumes obtained were averaged for the values of blast 1 and blast 2. To obtain the adjusted volumes, the dent depth values caused by the detonator obtained by the fitted exponential regression curve were subtracted from the absolute averaged volumes displayed in Table 1.

Table 1. Values obtained for the dent depth of the two blasts with respective PETN charges, deviation of the values from each other, averaged absolute volume of blast 1 and 2, and adjusted blast volume of the PETN charges calculated as average volume minus the dent volume generated by the detonator.

Amount PETN [mg]	Blast 1 [mm^3]	Blast 2 [mm^3]	Deviation [%]	Average Volume [mm^3]	Adjusted Volume [mm^3]
200	874,25	937,21	3,48	905,73	497,95
300	1072,27	1010,01	2,99	1041,14	617,18
400	1074,13	1137,51	2,87	1105,82	736,41
500	1151,01	1238,23	3,65	1194,62	855,64
600	1262,35	1233,94	1,14	1248,15	974,87
700	1263,54	1244,03	0,78	1253,79	1094,1
800	1260,68	1343,54	3,18	1302,11	1213,33
900	1377,05	1333,14	1,62	1355,10	1332,56
1000	1543,19	1519,20	0,78	1531,19	1451,79
1100	1624,01	1688,12	1,94	1656,06	1571,02
1200	1694,67	1776,06	2,35	1735,37	1690,25
1300	1807,79	1909,65	2,74	1858,72	1809,48

The values obtained from the PETN measurements, corrected by the ammonium sulfate experiments, result in the graph shown in Figure 7 with a linear fit added as a blue line. Considering some errors, there is a linear relationship between the

amount of explosive and the dent depths, for the chosen amounts of explosive. We did not expect a linear dependence but rather a sloping curve. We arrived at this assumption because, as the quantity of PETN filled in increased, we reached the capacity limit of the steel block and the explosive contained in it could no longer just emit a targeted pressure wave in the direction of the aluminum block, but could also increasingly decay upwards.

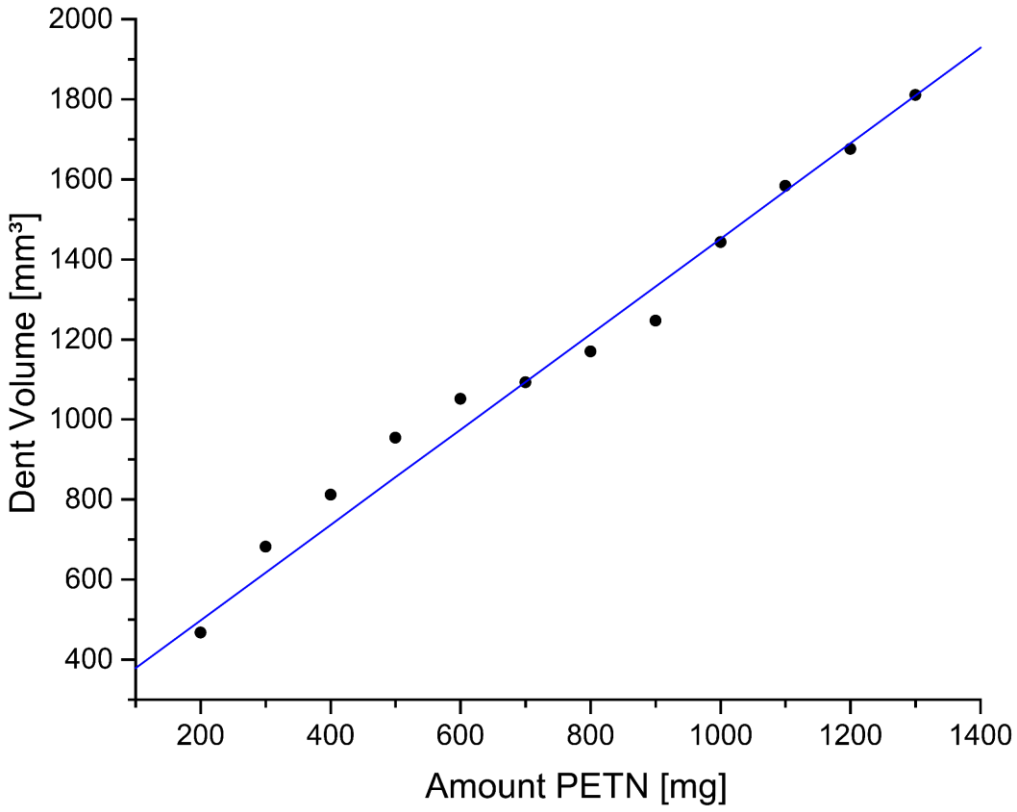

Figure 7. Aluminum block buckling caused by PETN subtracting the pre-determined fitted base buckling caused by the detonator. The blue line corresponds to a linear fit with the equation y = 1.1923x+259.49.

We consider several factors to be responsible for the deviation of some of the values from the ideal blue line. First, each set of PETN amounts was shot only twice, which gives a useful tendency but cannot be called statistically exact. The material used was weighed, filled, and pressed manually, whereby inaccuracies and deviations in the quantity may occur. In addition, despite the compression method used, there is no guarantee that the PETN used has compacted ideally. Should this not have been the case in a batch, this may have led to an increase in porosity and thereby the addition of small cavities. This, in turn, would reduce the resulting dent volume, as not all energy is transferred to the witness block but is

also used for the compression of the sample and gases in the cavities. Despite the chosen SSRT setup, the detonation also releases some of the energy into the deformation of the steel block. Figure 8 shows a steel block before detonation and below a steel block after the detonation of 1300 mg PETN. The force of the detonation caused the borehole to widen from 7.5 mm to 11.7 mm. We assume that with an increase of the amount of explosive proportionally more energy is released in other directions. Larger explosive quantities will likely result in a flattening of the curve.

Figure 8. Steel block (left) and aluminum block (right) before (top) and after (bottom) the detonation of 1300 mg PETN.

15.3.4 Conclusion

In summary, we investigated the correlation between the amount of PETN (200 mg–1300 mg) filled in a SSRT setup and the resulting dell depth of the associated aluminum block after the ignition of the explosive. The evaluation of the respective depths of the aluminum blocks after the explosion was carried out with the aid of a profilometer. The resulting extremely precise measurement data made it possible to compare the blocks with each other and to work out a trend. Taking into account some experimental errors and the influence caused by the detonator,

a linear relationship could be drawn. The results of this study could be applied to other energetic materials as well and serve as an experimental basis for future theoretical calculations or possible larger test quantities.

15.4 Acknowledgement

For financial support of this work by Ludwig-Maximilian University (LMU), the Office of Naval Research (ONR) under grant no. ONR N00014-19-1-2078 and the Strategic Environmental Research and Development Program (SERDP) under contract no. W912HQ19C0033 are gratefully acknowledged. The authors are indebted to thank Tobias Lenz for the synthesis of PETN. Open Access funding enabled and organized by Projekt DEAL.

15.5 References

[1] a) J. E. Felts, H. W. Sandusky and R. H. Granholm, Development of the smallscale shock sensitivity test (SSST), *AIP Conf. Proc.* **2009**, *1195*, 233; b) H. W. Sandusky, R. H. Granholm, D. G. Bohl, "Small-Scale Shock Reactivity Test (SSRT)," IHTR 2701, Naval Surface Warfare Center, Indian Head, MD, 12 Aug **2005**. c) R. H. Granholm and H. W. Sandusky, SMALL-SCALE SHOCK REACTIVITY AND INTERNAL BLAST TEST, IP Conference Proceedings 845, 1257, **2006**.

[2] T. M. Klapötke, T. G. Witkowski, *ChemPlusChem* **2016**, *81*, 357–360.

[3] K. V. Domasevitch, I. Gospodinov, H. Krautscheid, T. M. Klapötke, J. Stierstorfer, *New J. Chem.* **2019**, *43*, 1305–1312.

[4] N. Dhawan, B. D. Majumdar, B. Abraham, A. G. Rajendran, Comments on the dent test vs. metal acceleration, 9th Intl. High Energy Materials Conf. and Exhibits, HEMCE-363, SVVC, Trivandrum, India, Feb. 13–15, **2014**.

[5] B. T. Neyer, Use of VISAR to replace detonator dent tests, 31st AIAA/ASME/SAE/ASEE Joint Propulsion Conference and Exhibit, San Diego, CA, **1995**.

[6] I. D. Bjelovuk, S. Jaramaz, P. Elek, D. Micković, L. Kričak, *Tehnički vjesnik* **2015**, *22*, 227–232.

[7] D. Ambrosini, B. Luccioni, R. Danesi, , *Mecanica Computacional* **2003**, XXII, 678–692.

[8] T. M. Klapötke, Chemistry of High Energy Materials, 6th edn., chapter 1.3, Walter de Gruyter, Berlin/Boston, **2022**.

[9] R. Mayer, J. Köhler, A. Homburg, Explosives, 5th edn., Wiley-VCH, Weinheim, **2002**, 148.

[10] Keyence, https://www.keyence.de/ landing/lpc/vrprofilometer.jsp (accessed November 2021).

[11] M. A. A. Neil, R. Juškaitis, T. Wilson, *Opt. Lett.* **1997**, *22*, 1905–1907.

[12] T. Takatsuji, A. Kirita, T. Kurosawa, *Meas. Sci. Technol.* **1997**, *8*, 782–786.

15.6 Supporting Information

15.6.1 General Experimental Methods

^{1}H, ^{13}C and ^{14}N NMR spectra were recorded on *JEOL 270* and *BRUKER AMX 400* instruments. The samples were measured at room temperature in standard NMR tubes (Ø 5 mm). Chemical shifts are reported as d values in ppm relative to the residual solvent peaks of DMSO-D_6 (δ H: 2.50, δ C: 39.5). Solvent residual signals and chemical shifts for NMR solvents were referenced against tetramethylsilane (TMS, δ = 0 ppm) and nitromethane. Unless stated otherwise, coupling constants were reported in Hertz (Hz) and for the characterization of the observed signal multiplicities the following abbreviations were used: s (singlet), m (multiplet) and br (broad). Infrared spectra (IR) were recorded from 4000 cm^{-1} to 400 cm^{-1} on a *PERKIN ELMER Spectrum BX- 59343* instrument with a *SMITHS DETECTION DuraSamplIR II Diamond ATR* sensor. The absorption bands are reported in wave-numbers (cm^{-1}). Decomposition temperatures were measured via differential thermal analysis (DTA) with an *OZM Research DTA 552-Ex instrument* at a heating rate of 5 $K \cdot min^{-1}$ and in a range of room temperature to 400 °C. All sensitivities toward impact (IS) and friction (FS) were determined according to BAM (German: Bundesanstalt für Materialforschung und Prüfung) standards using a BAM drop hammer and a BAM friction apparatus by applying the 1 of 6 method.[S1]

CAUTION! *PETN is a potentially explosive material, although no hazards were observed during preparation and handling. Nevertheless, safety precautions (such as wearing leather coat, face shield, Kevlar sleeves, Kevlar gloves, earthed equipment and ear plugs) should be drawn especially when manipulating dry material.*

15.6.2 Profilometer Measurements

In the following pages the pictures, generated by a Keyence 3D profilometer VR-5200[S2], and analysis data for the measurements of PETN as well as $(NH_4)_2SO_4$ are given as follows: Top left: Picture of the aluminum block with the measured area indicated in cyan and the indentations in violet. Top right: Color coded height measurements with red for the reference area and blue for the deepest indentation. Bottom left: Cross sections of the height profiles of the aluminum block at a 90 ° angle to each other.

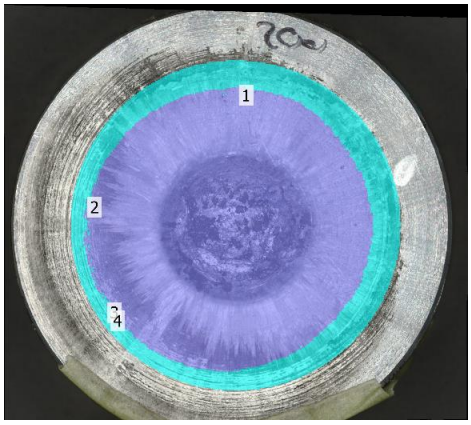

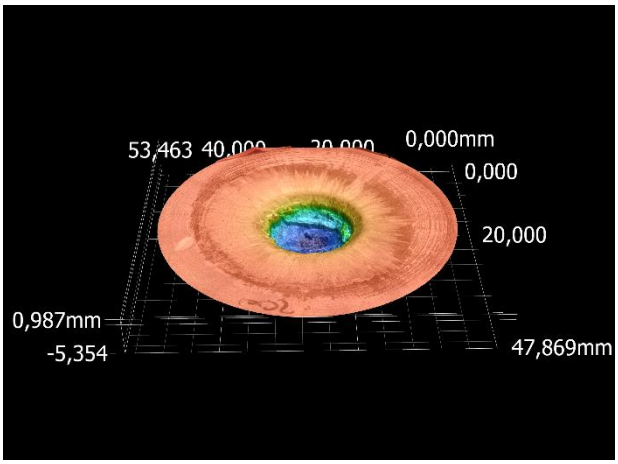

200 mg PETN Blast 1	
Measurement 1 [mm³]	875,16
Measurement 2 [mm³]	873,35
Average Volume [mm³]	874,25

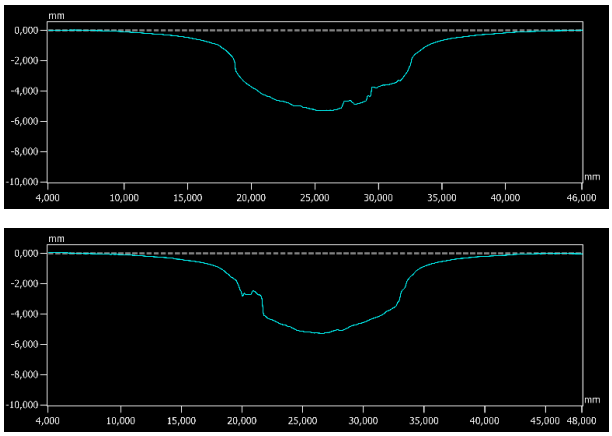

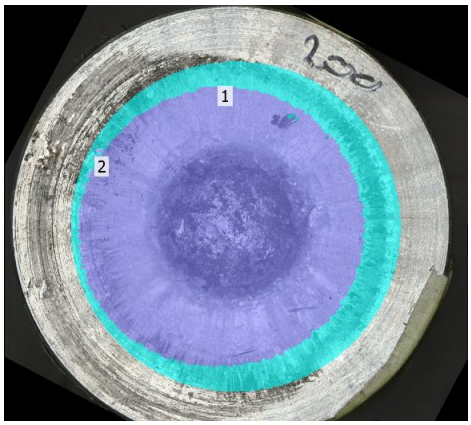

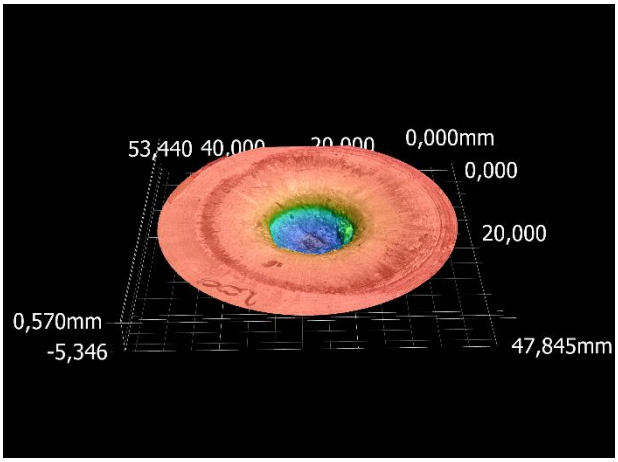

200 mg PETN Blast 2	
Measurement 1 [mm³]	932,47
Measurement 2 [mm³]	941,94
Average Volume [mm³]	937,21

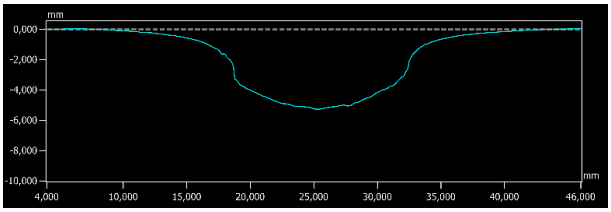

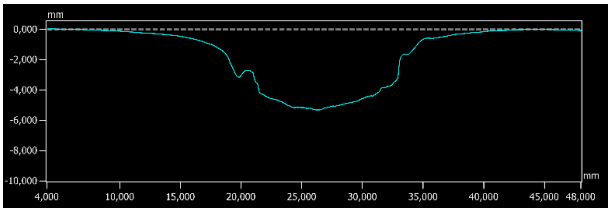

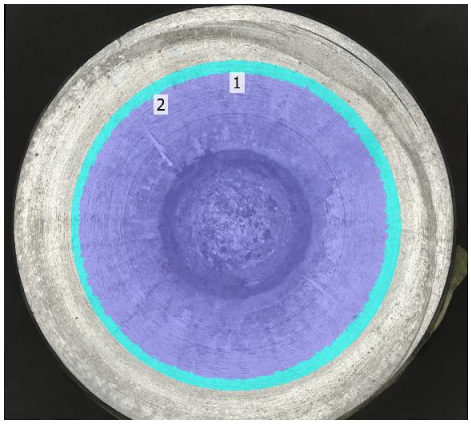

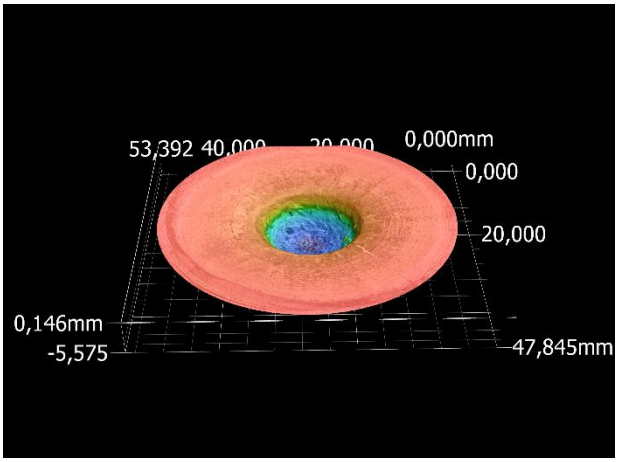

300 mg PETN Blast 1	
Measurement 1 [mm³]	1071,75
Measurement 2 [mm³]	1072,80
Average Volume [mm³]	1072,27

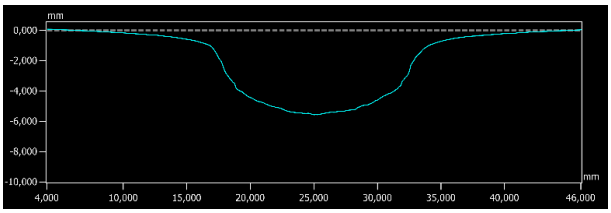

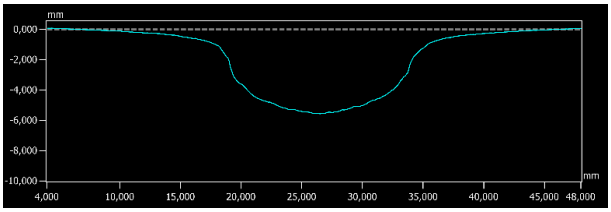

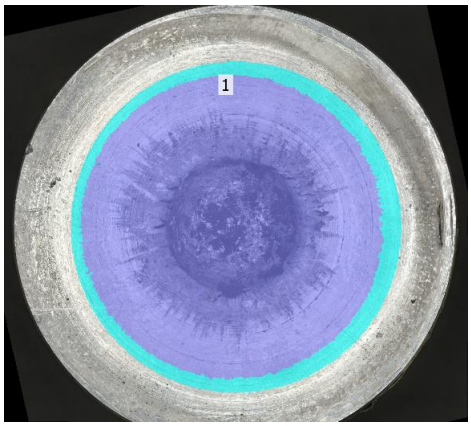

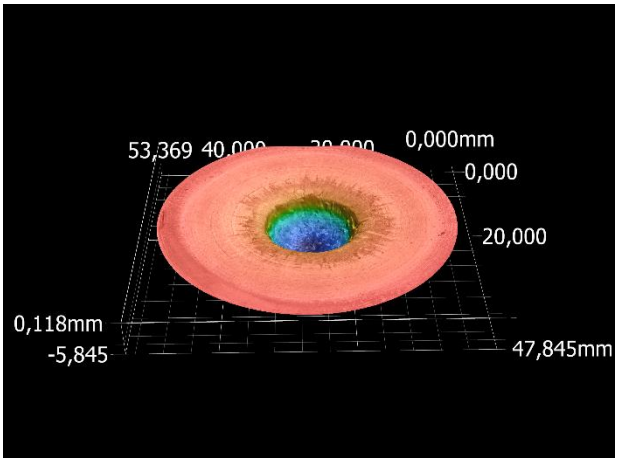

300 mg PETN Blast 2	
Measurement 1 [mm³]	1009,65
Measurement 2 [mm³]	1010,37
Average Volume [mm³]	1010,01

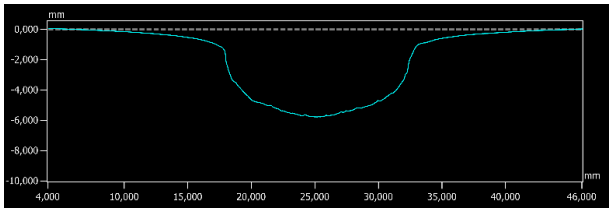

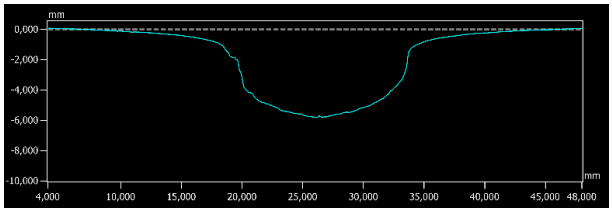

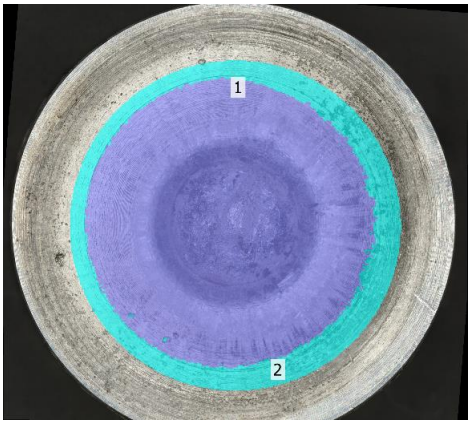

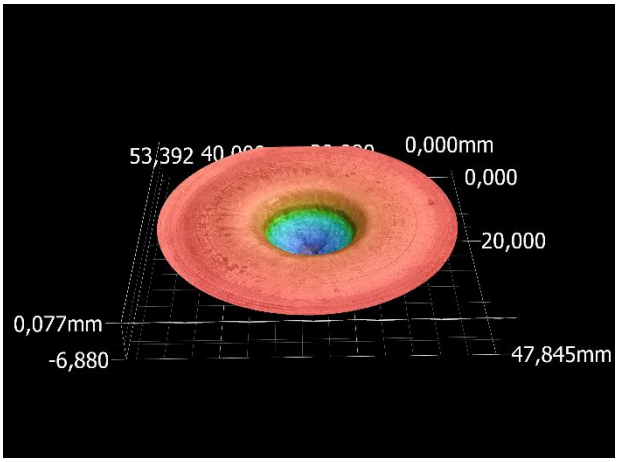

400 mg PETN Blast 1	
Measurement 1 [mm³]	1073,32
Measurement 2 [mm³]	1074,94
Average Volume [mm³]	1074,13

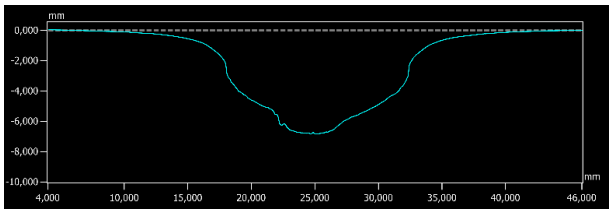

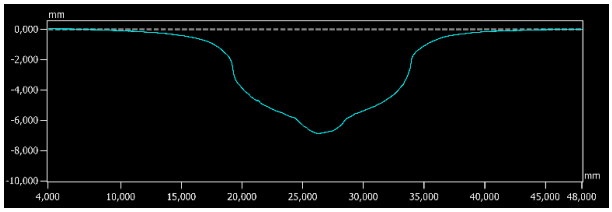

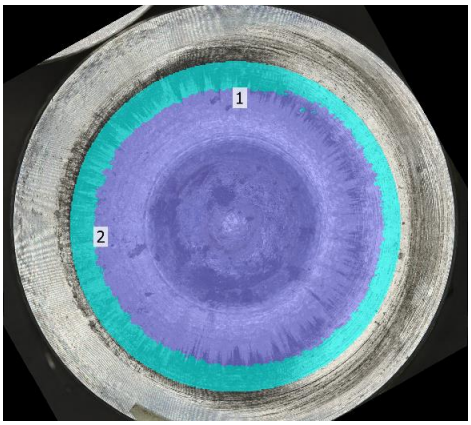

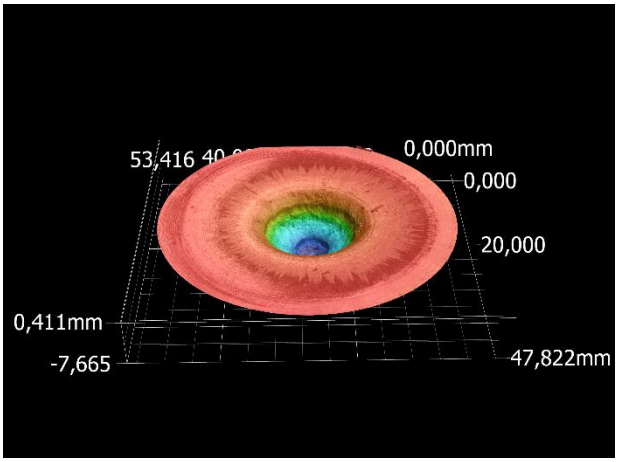

400 mg PETN Blast 2	
Measurement 1 [mm³]	1147,42
Measurement 2 [mm³]	1127,59
Average Volume [mm³]	1137,51

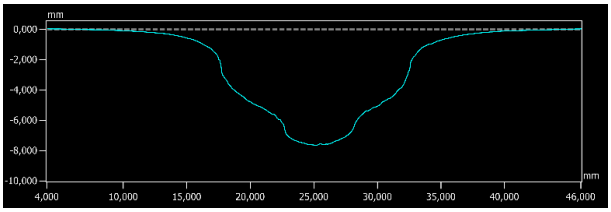

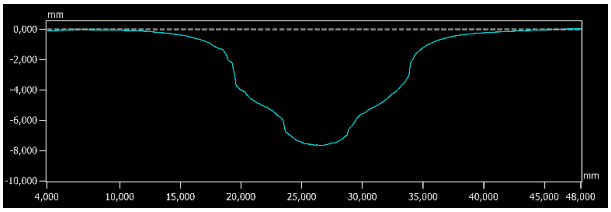

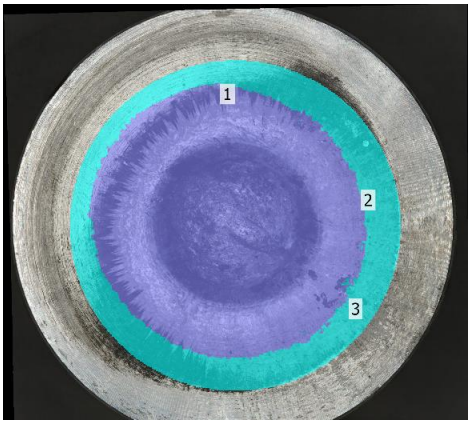

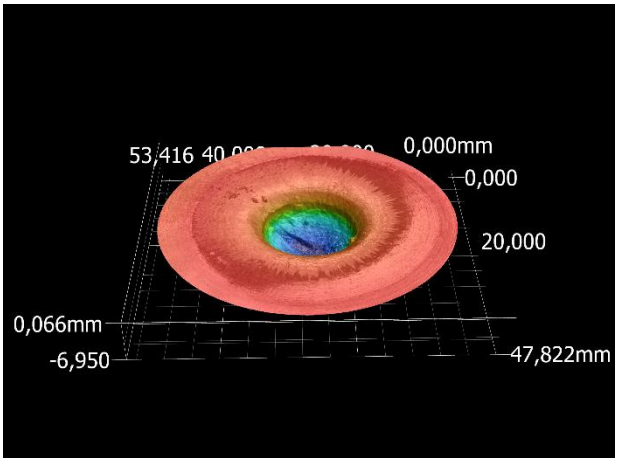

500 mg PETN Blast 1	
Measurement 1 [mm³]	1147,43
Measurement 2 [mm³]	1154,59
Average Volume [mm³]	1151,01

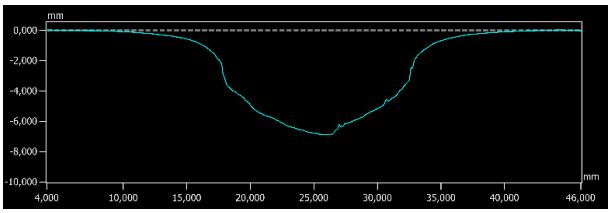

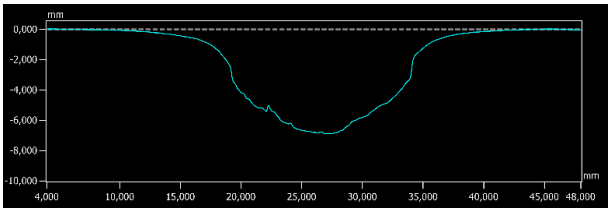

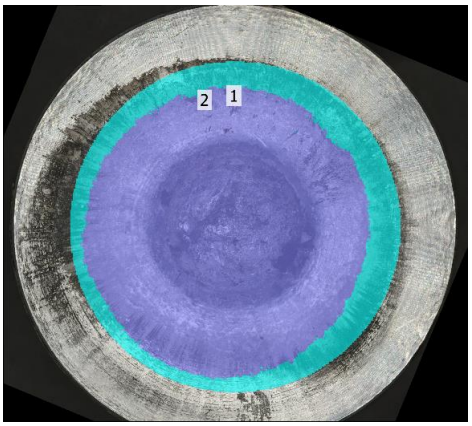

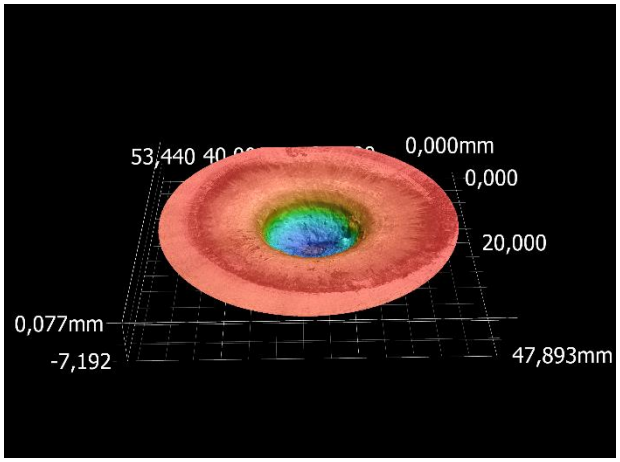

500 mg PETN Blast 2	
Measurement 1 [mm³]	1236,45
Measurement 2 [mm³]	1240,01
Average Volume [mm³]	1238,23

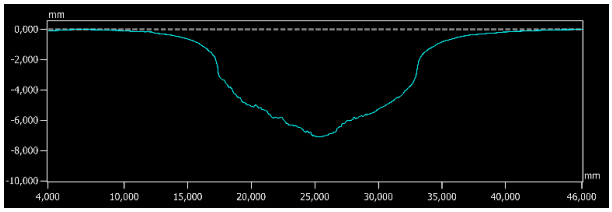

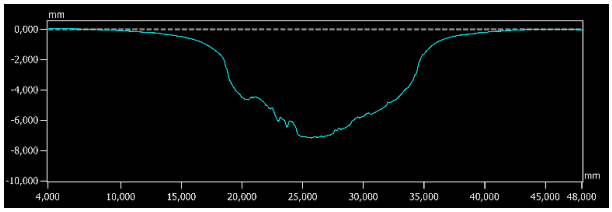

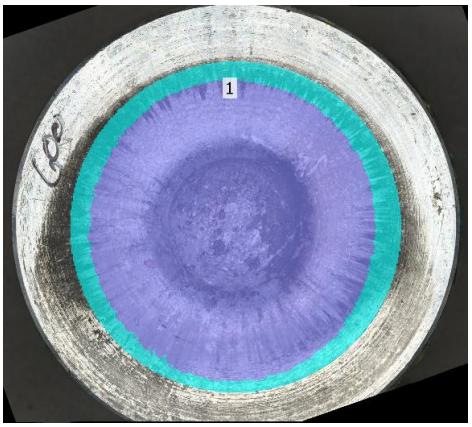

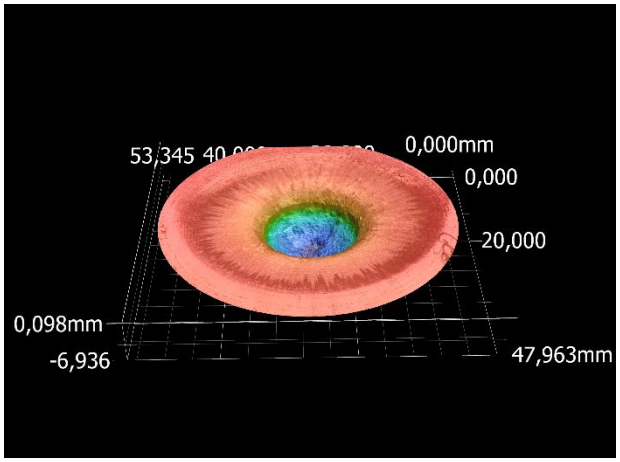

600 mg PETN Blast 1	
Measurement 1 [mm³]	1242,72
Measurement 2 [mm³]	1281,98
Average Volume [mm³]	1262,35

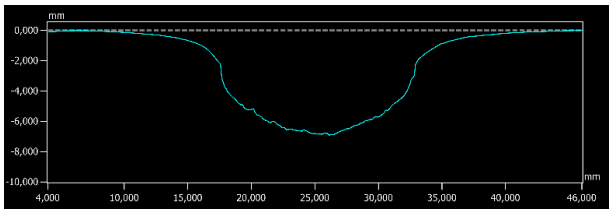

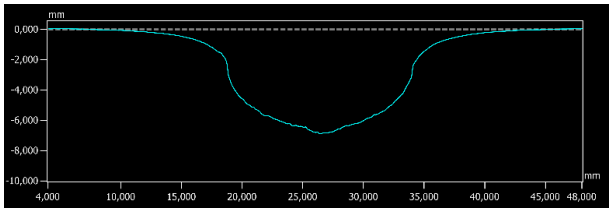

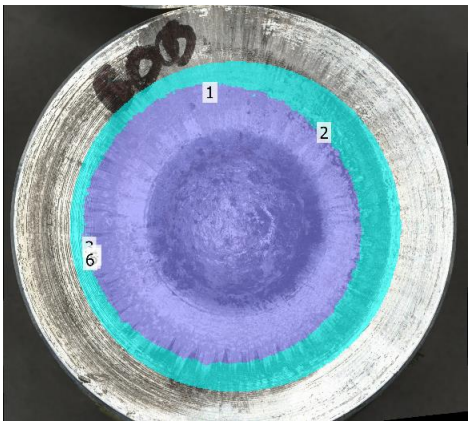

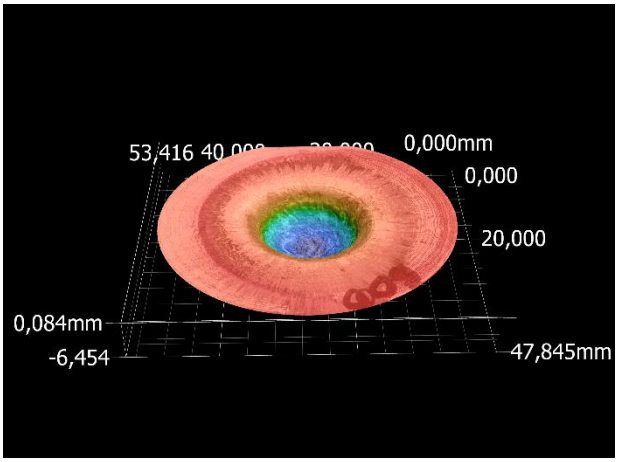

600 mg PETN Blast 2	
Measurement 1 [mm³]	1223,68
Measurement 2 [mm³]	1244,21
Average Volume [mm³]	1233,94

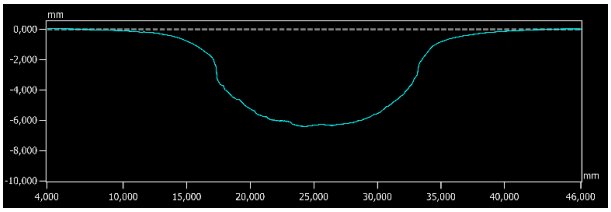

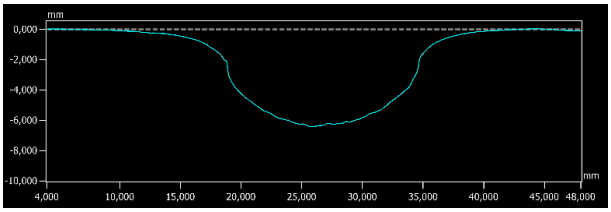

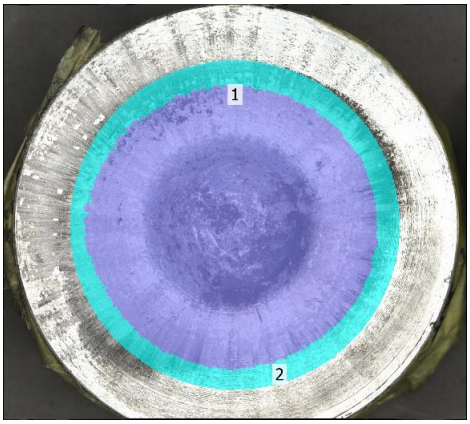

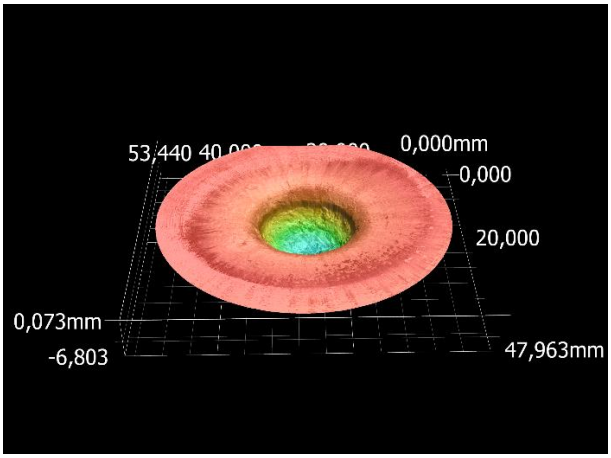

700 mg PETN Blast 1	
Measurement 1 [mm³]	1240,62
Measurement 2 [mm³]	1286,46
Average Volume [mm³]	1263,54

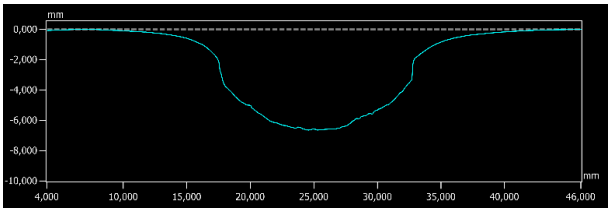

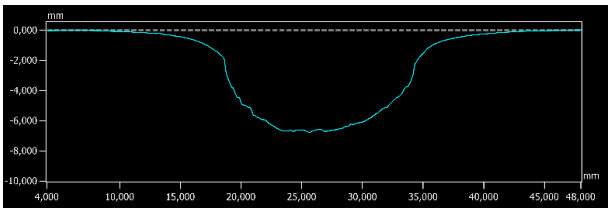

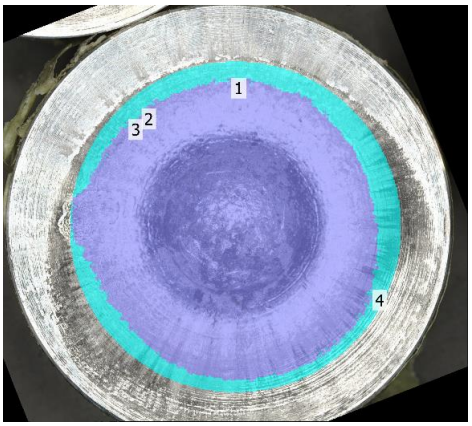

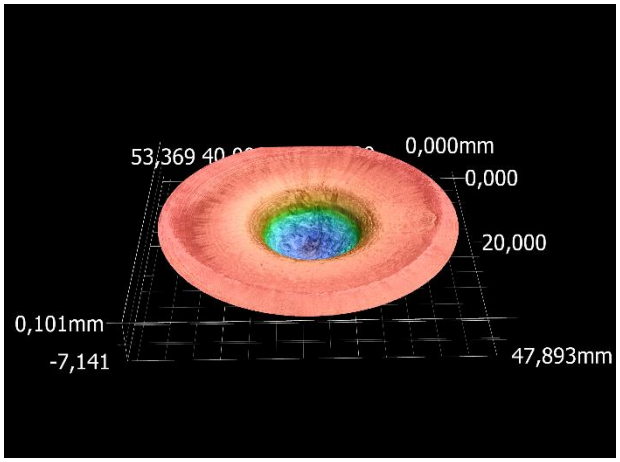

700 mg PETN Blast 2	
Measurement 1 [mm³]	1243,24
Measurement 2 [mm³]	1244,63
Average Volume [mm³]	1244,02

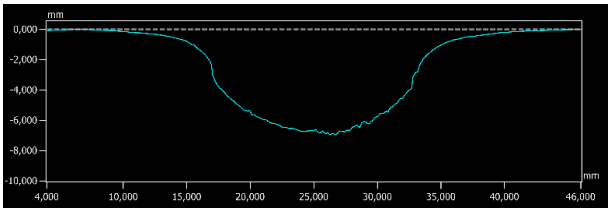

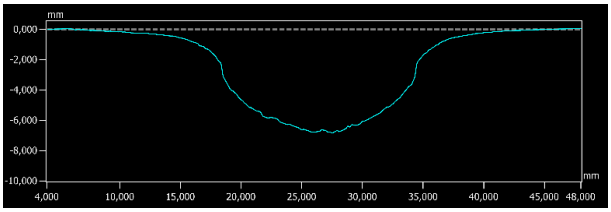

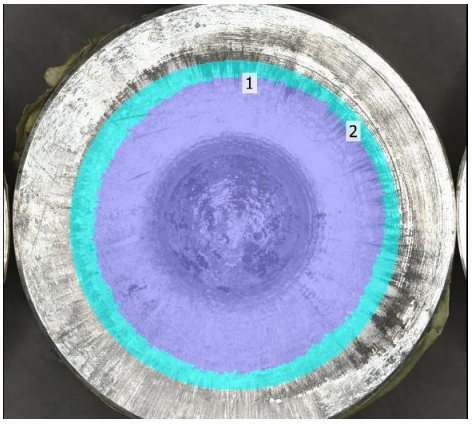

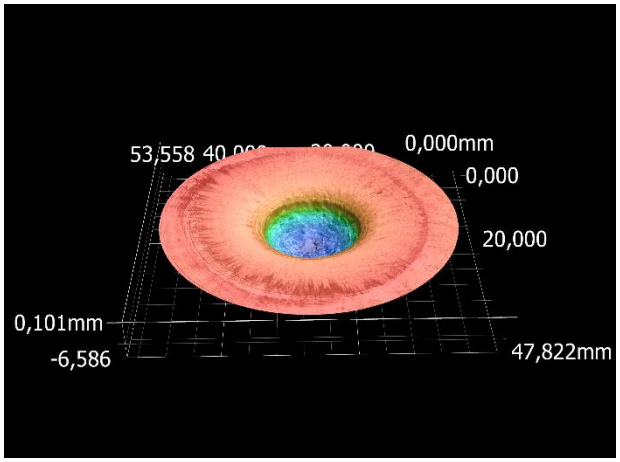

800 mg PETN Blast 1	
Measurement 1 [mm³]	1260,77
Measurement 2 [mm³]	1260,59
Average Volume [mm³]	1260,68

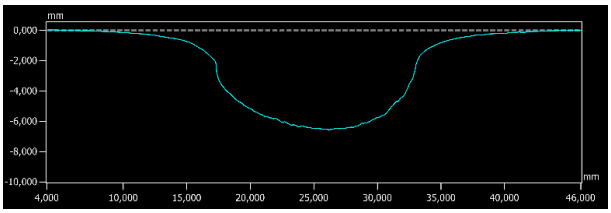

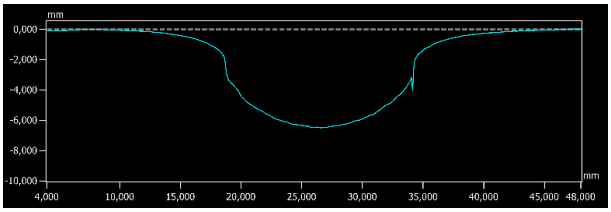

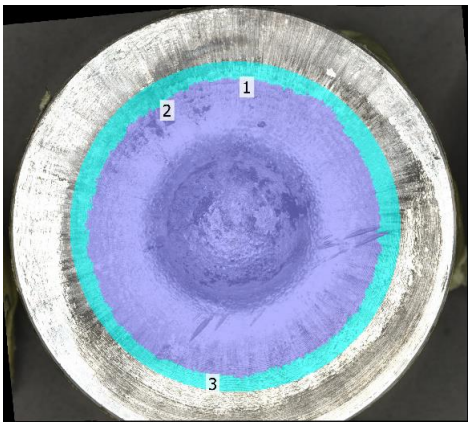

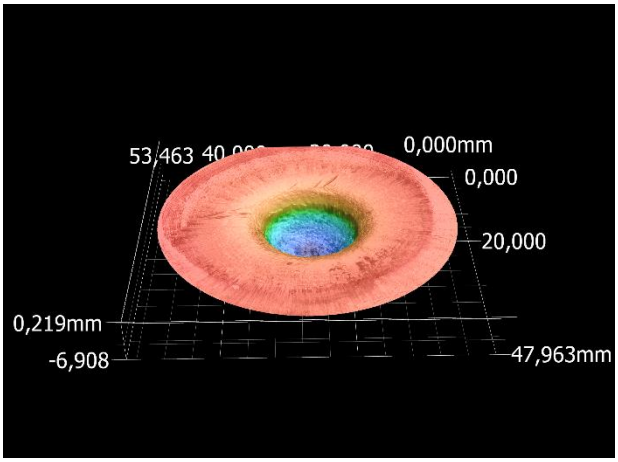

800 mg PETN Blast 2	
Measurement 1 [mm³]	1342,82
Measurement 2 [mm³]	1344,26
Average Volume [mm³]	1343,54

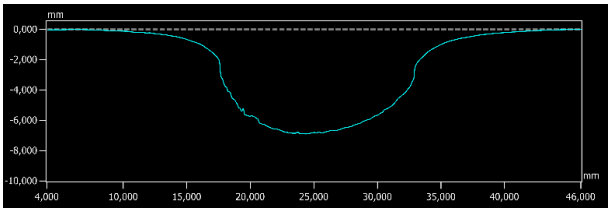

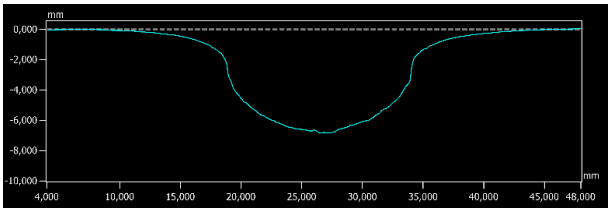

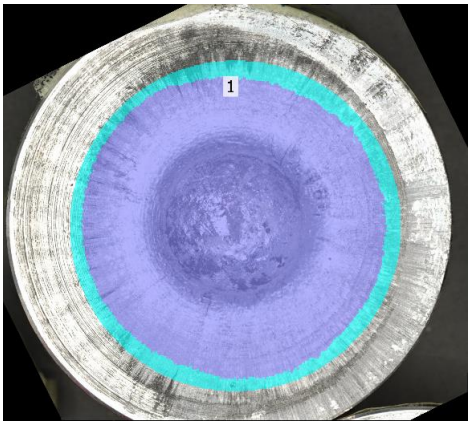

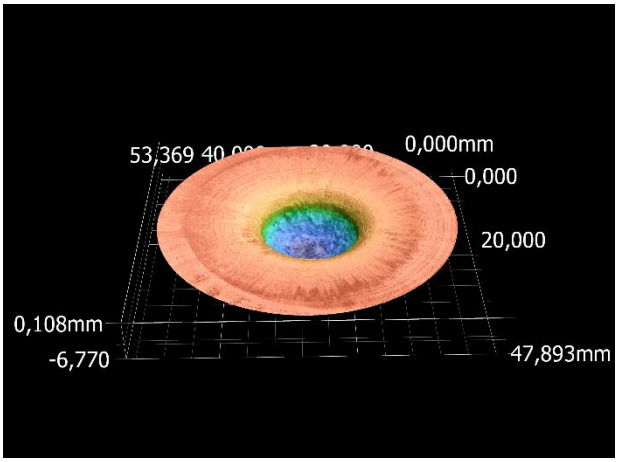

900 mg PETN Blast 1	
Measurement 1 [mm³]	1375,24
Measurement 2 [mm³]	1378,87
Average Volume [mm³]	1377,05

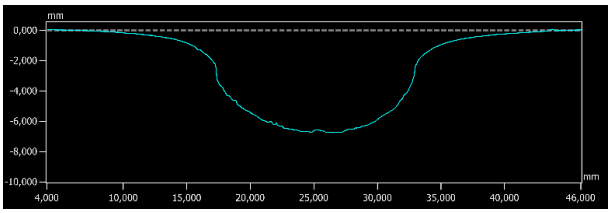

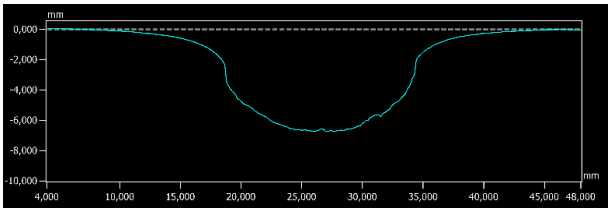

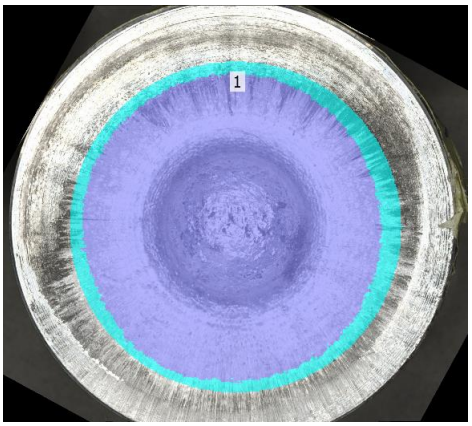

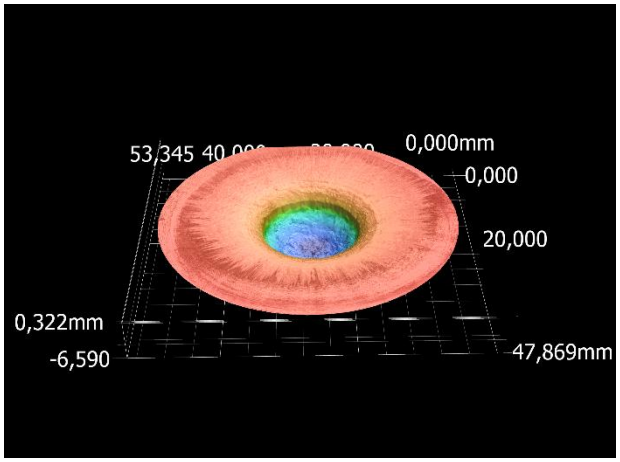

900 mg PETN Blast 2	
Measurement 1 [mm³]	1330,89
Measurement 2 [mm³]	1335,39
Average Volume [mm³]	1333,14

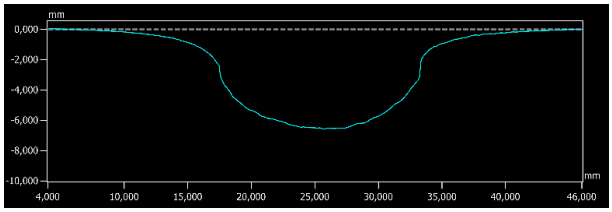

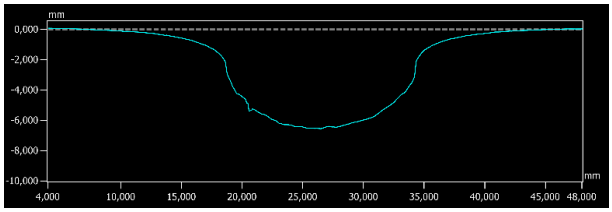

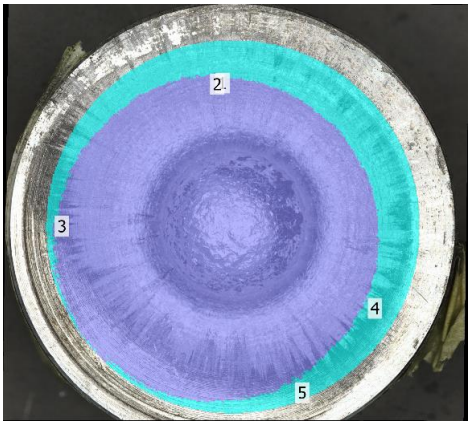

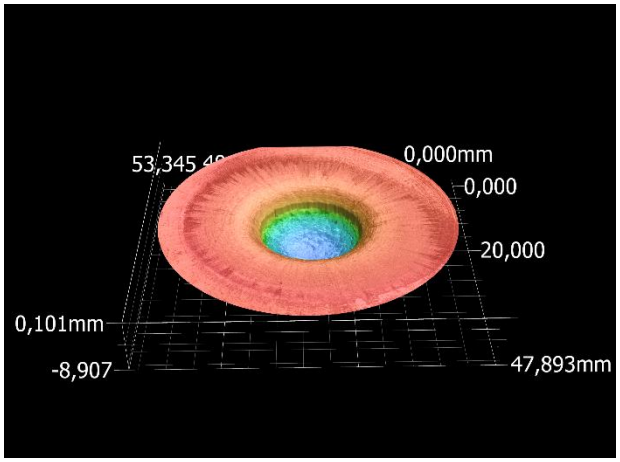

1000 mg PETN Blast 1	
Measurement 1 [mm³]	1544,67
Measurement 2 [mm³]	1541,70
Average Volume [mm³]	1543,19

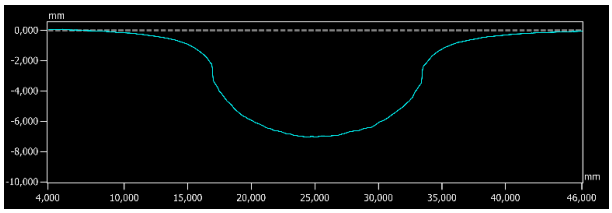

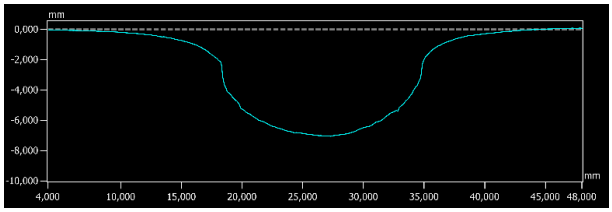

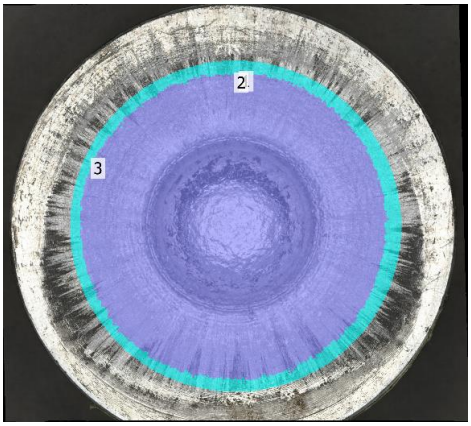

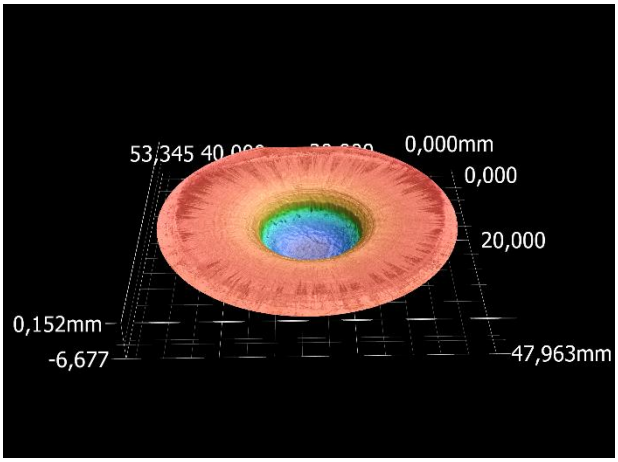

1000 mg PETN Blast 2	
Measurement 1 [mm³]	1517,85
Measurement 2 [mm³]	1520,55
Average Volume [mm³]	1519,20

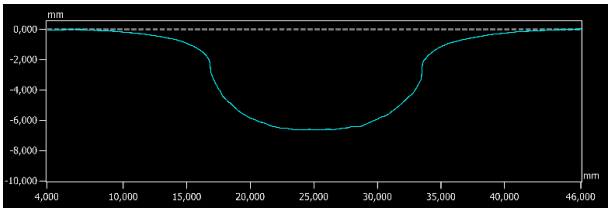

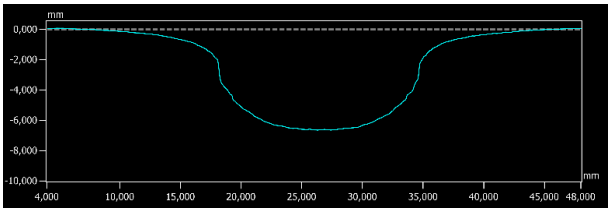

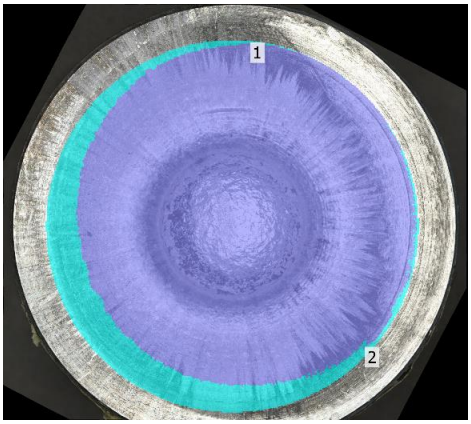

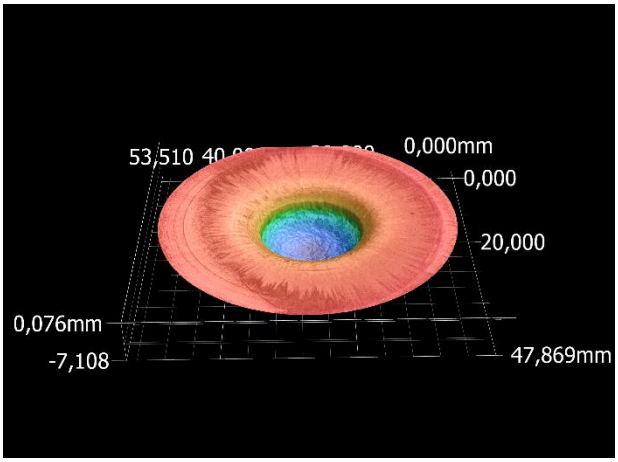

1100 mg PETN Blast 1	
Measurement 1 [mm³]	1622,22
Measurement 2 [mm³]	1625,79
Average Volume [mm³]	1624,01

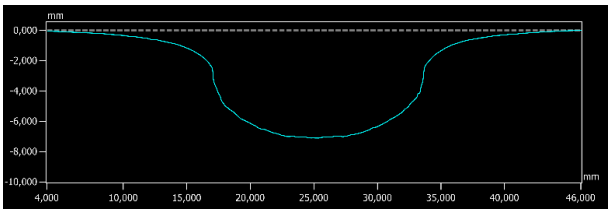

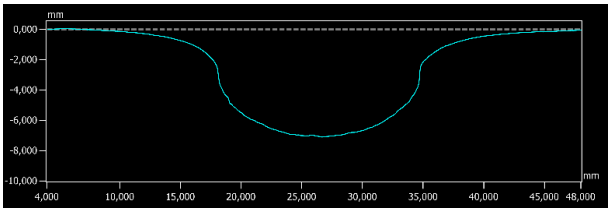

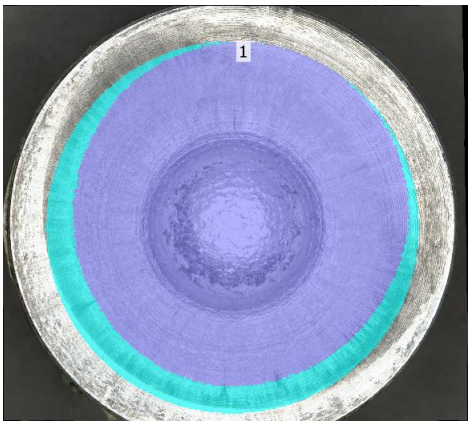

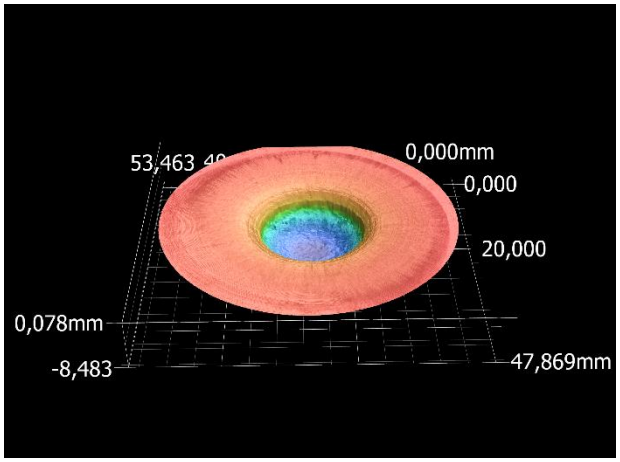

1100 mg PETN Blast 2	
Measurement 1 [mm³]	1688,06
Measurement 2 [mm³]	1688,16
Average Volume [mm³]	1688,12

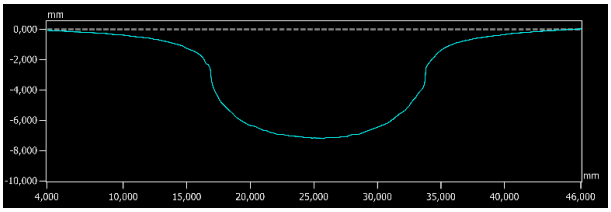

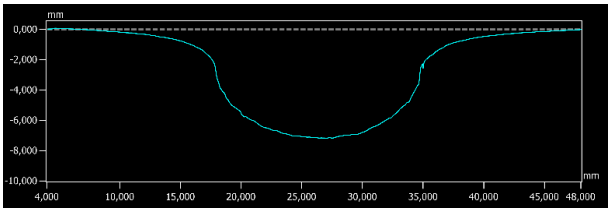

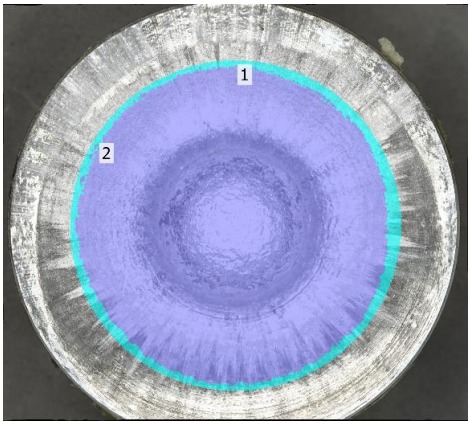

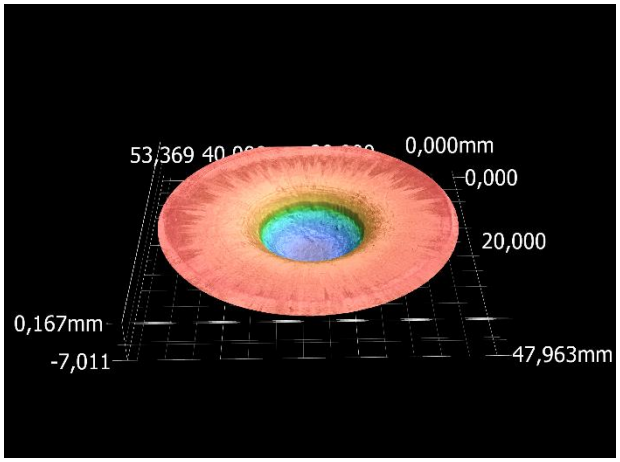

1200 mg PETN Blast 1	
Measurement 1 [mm³]	1694,70
Measurement 2 [mm³]	1694,64
Average Volume [mm³]	1694,67

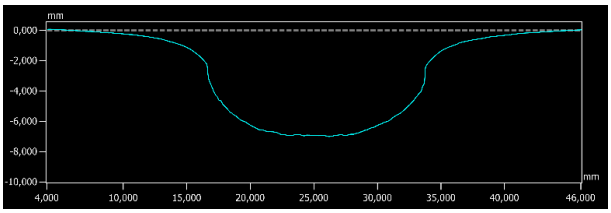

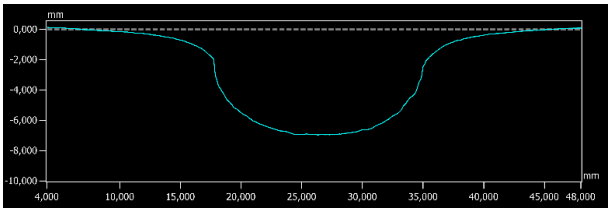

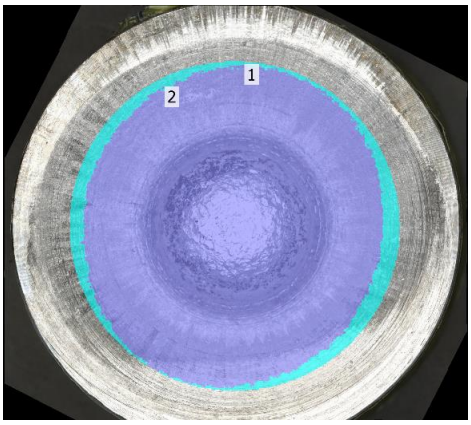

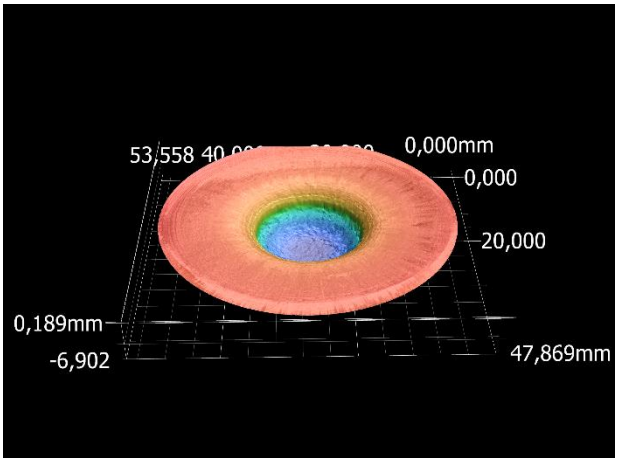

1200 mg PETN Blast 2	
Measurement 1 [mm³]	1776,52
Measurement 2 [mm³]	1775,60
Average Volume [mm³]	1776,06

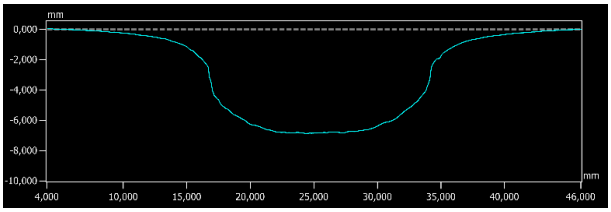

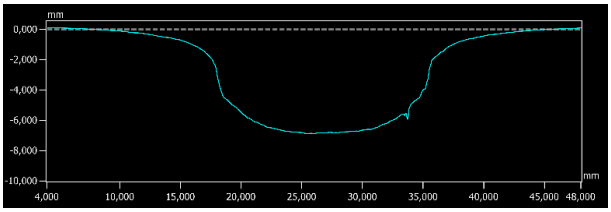

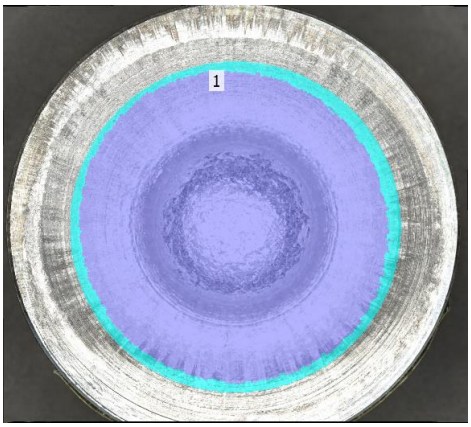

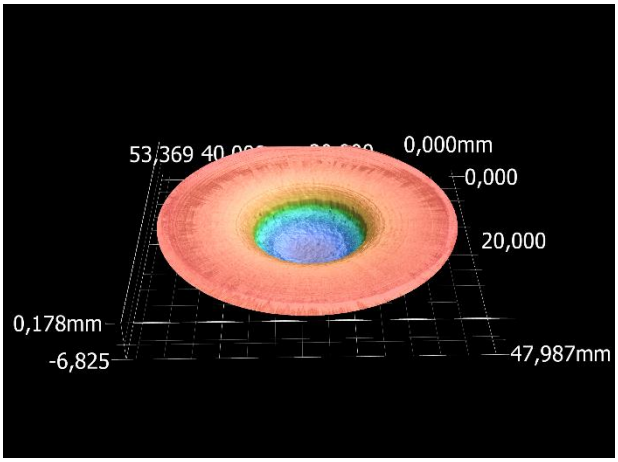

1300 mg PETN Blast 1	
Measurement 1 [mm³]	1808,34
Measurement 2 [mm³]	1807,25
Average Volume [mm³]	1807,79

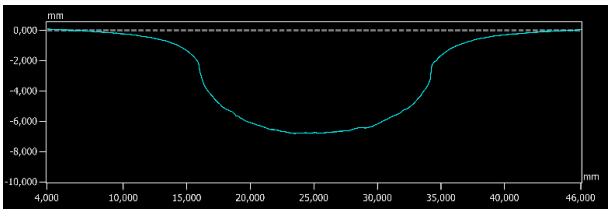

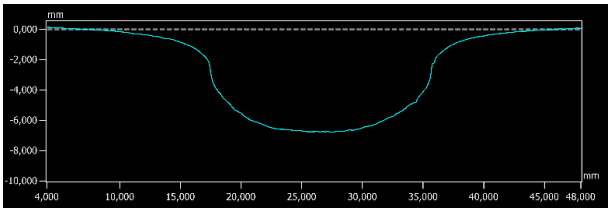

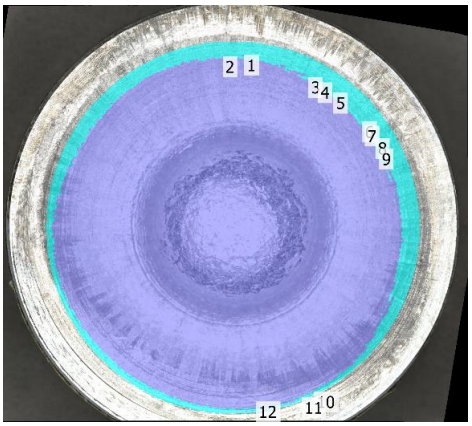

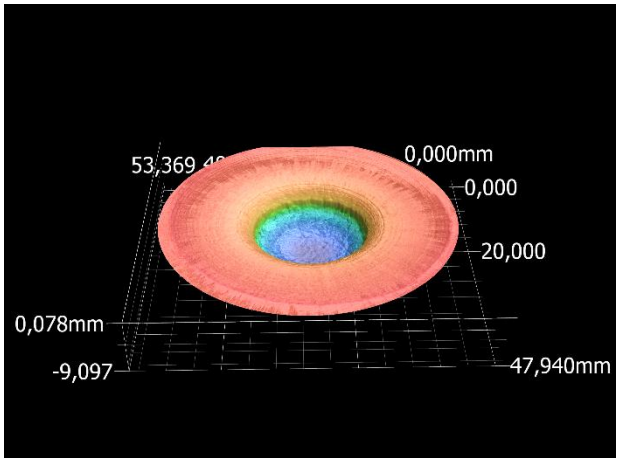

1300 mg PETN Blast 2	
Measurement 1 [mm³]	1909,94
Measurement 2 [mm³]	1909,36
Average Volume [mm³]	1909,65

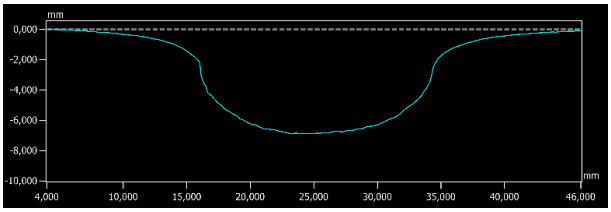

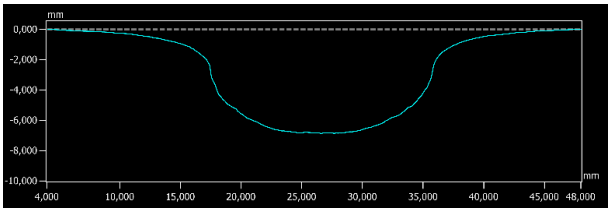

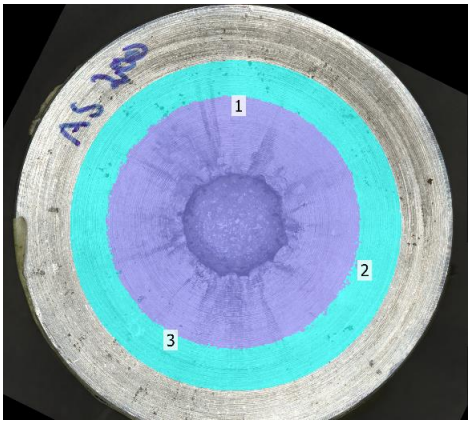

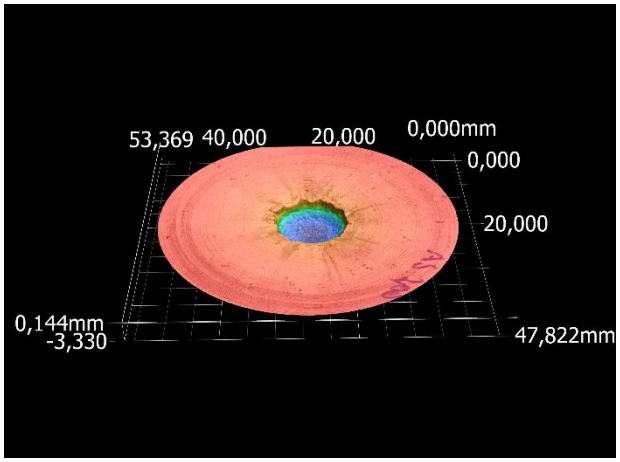

200 mg $(NH_4)_2SO_4$	
Volume [mm³]	398,48

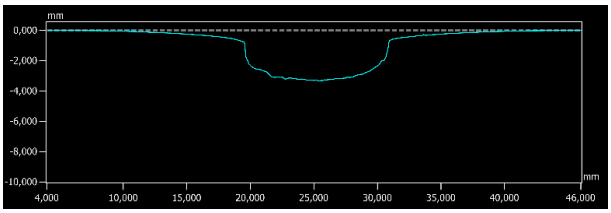

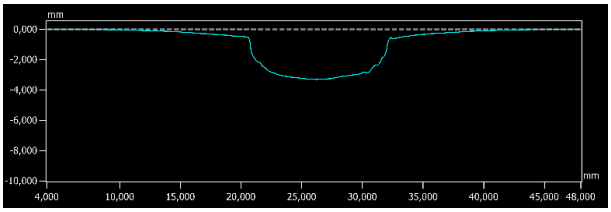

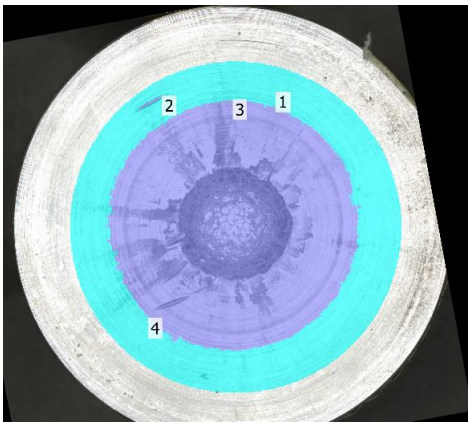

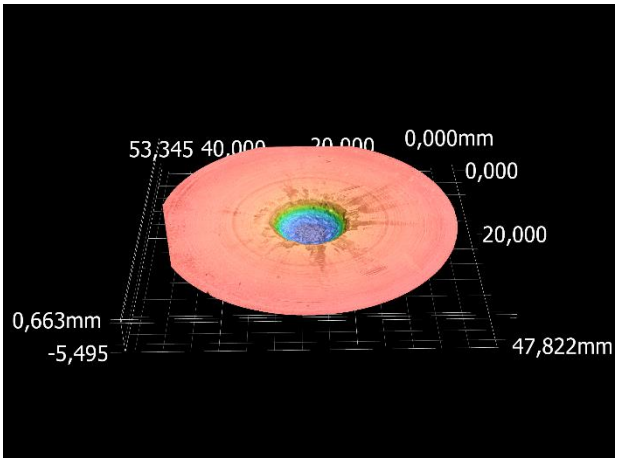

300 mg $(NH_4)_2SO_4$	
Volume [mm³]	366,42

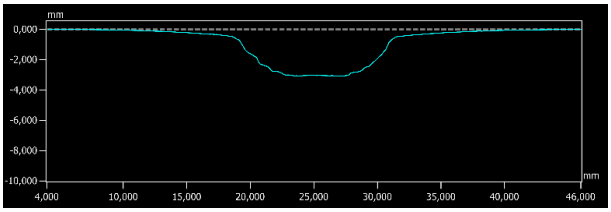

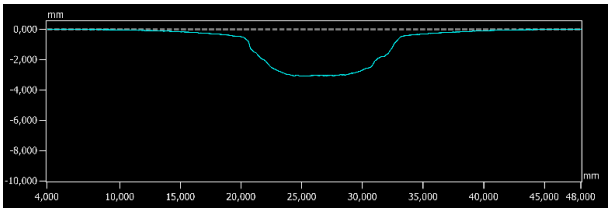

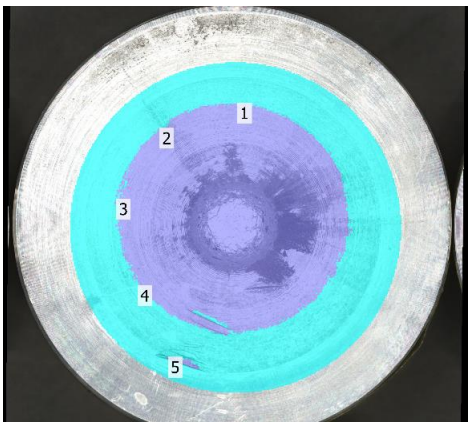

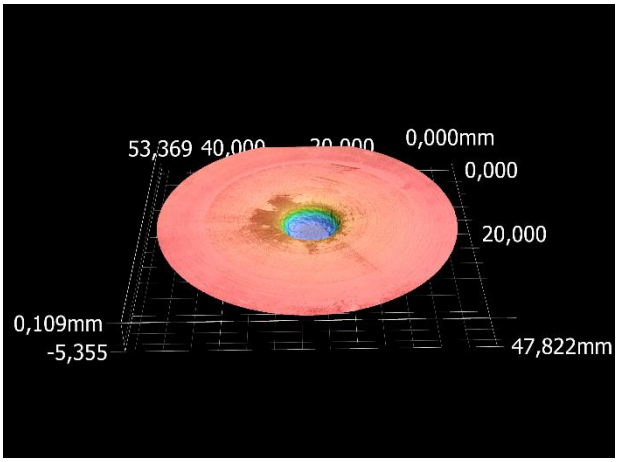

400 mg $(NH_4)_2SO_4$	
Volume [mm³]	286,99

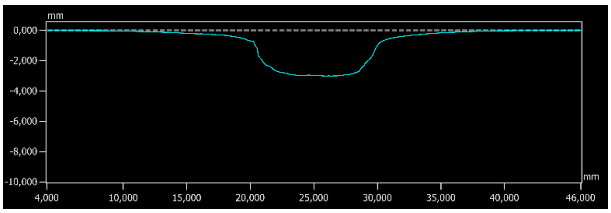

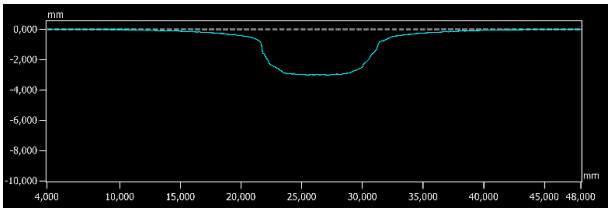

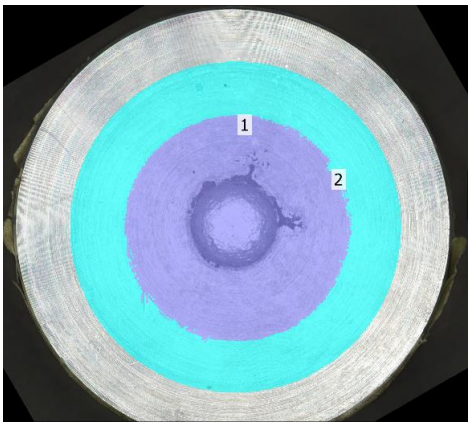

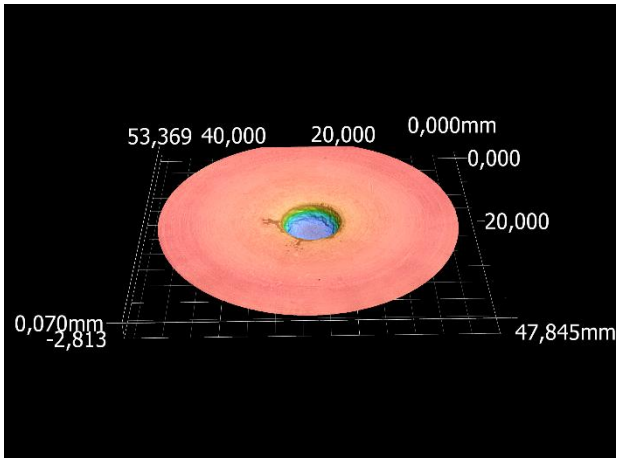

500 mg $(NH_4)_2SO_4$	
Volume [mm³]	243,66

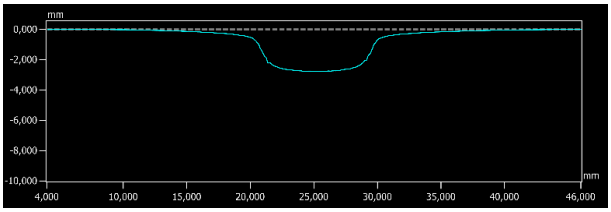

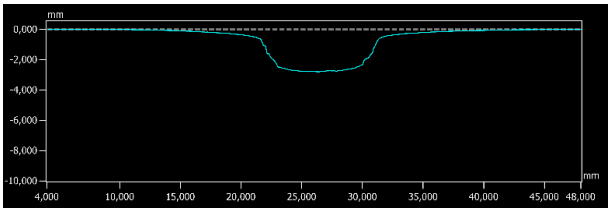

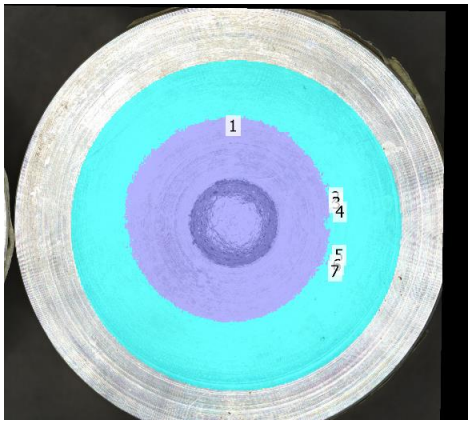

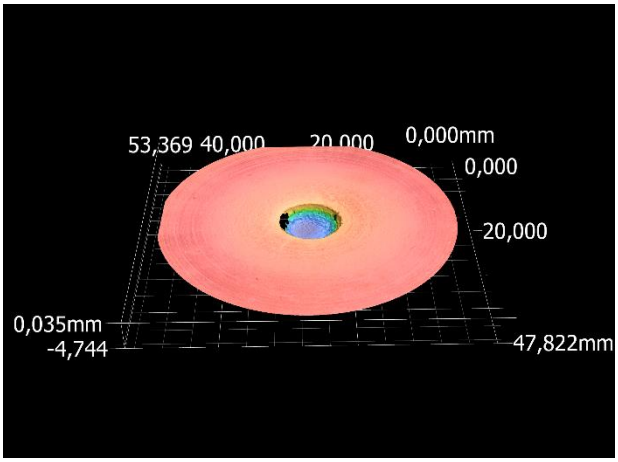

600 mg $(NH_4)_2SO_4$	
Volume [mm³]	203,47

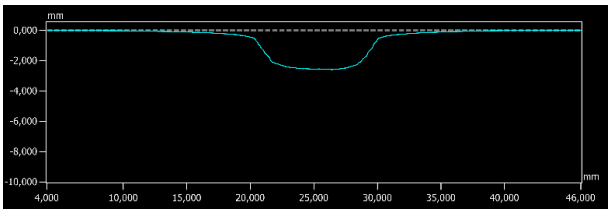

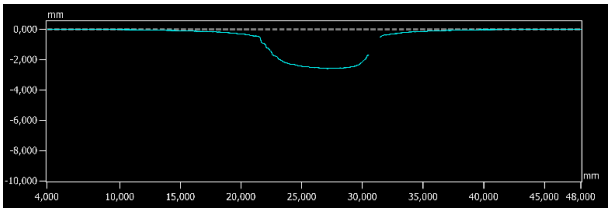

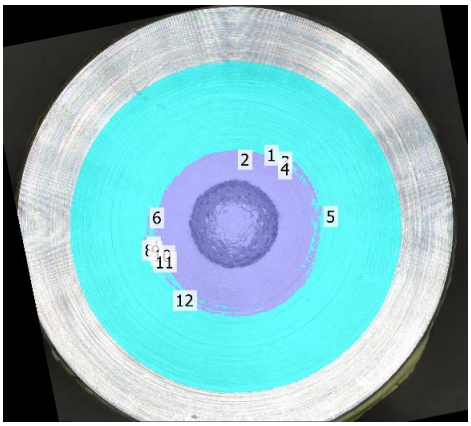

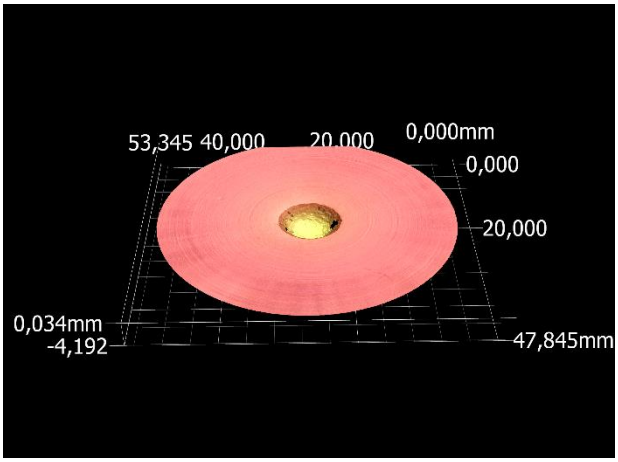

700 mg $(NH_4)_2SO_4$	
Volume [mm³]	157,31

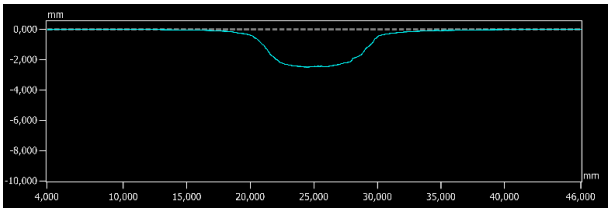

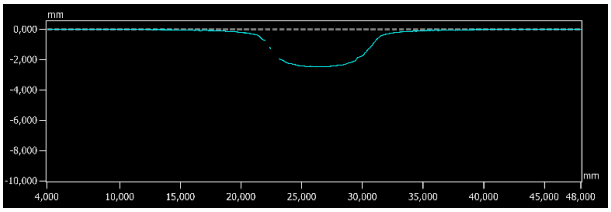

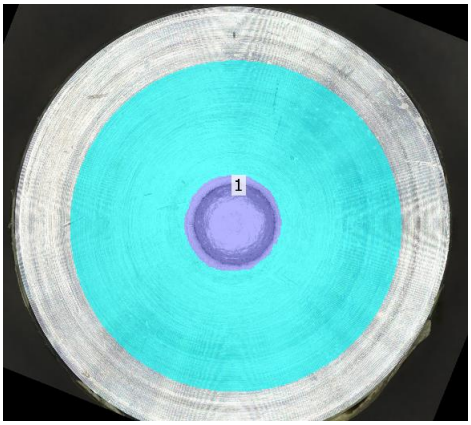

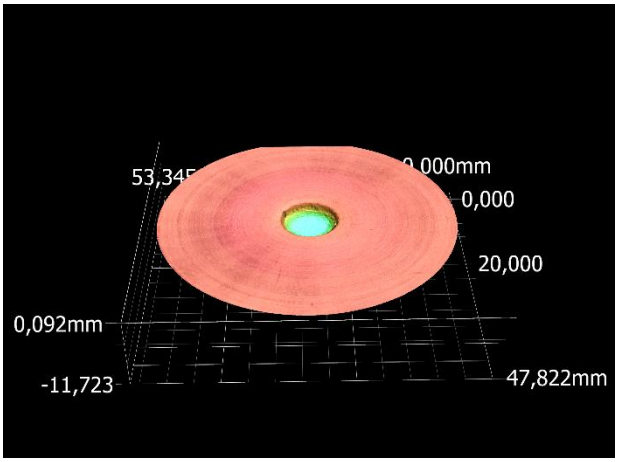

800 mg $(NH_4)_2SO_4$	
Volume [mm³]	115,38

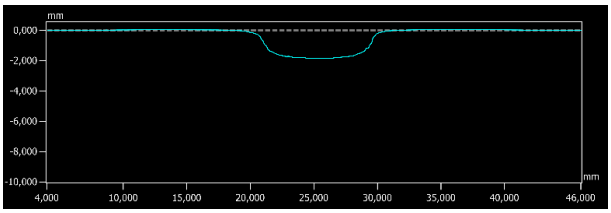

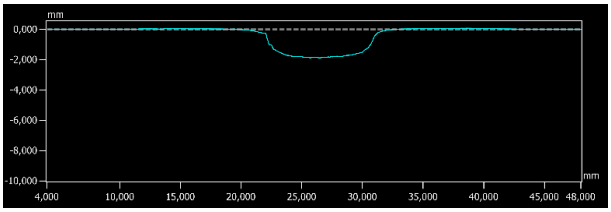

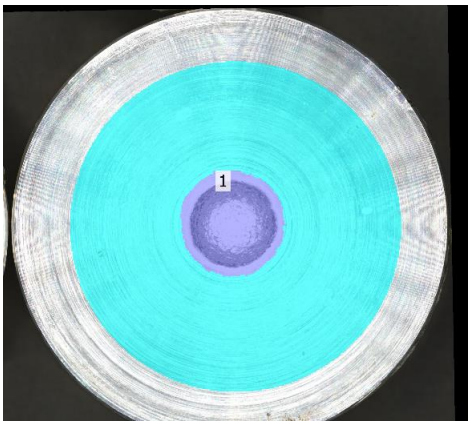

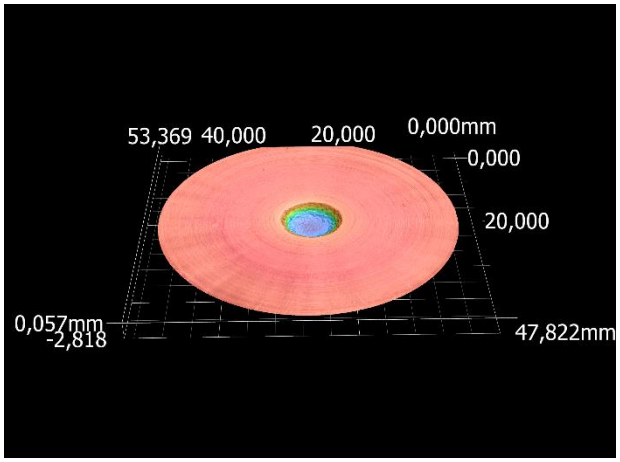

900 mg $(NH_4)_2SO_4$	
Volume [mm³]	101,23

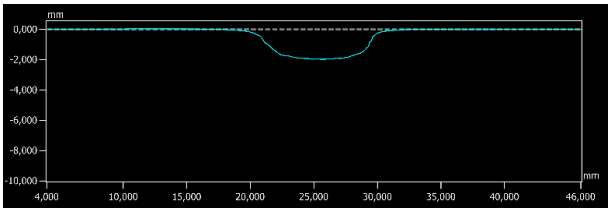

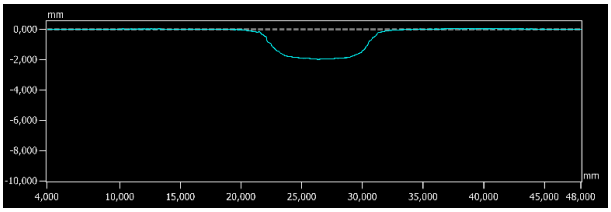

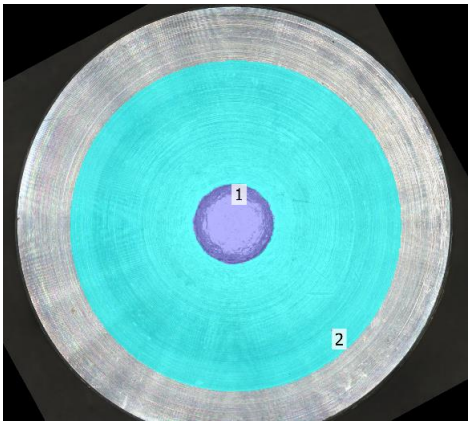

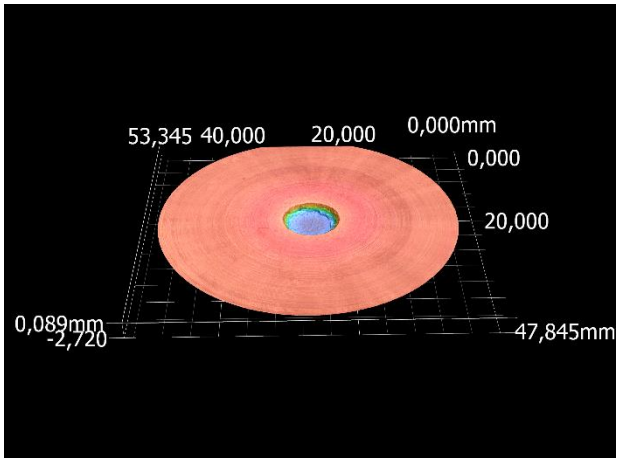

1000 mg $(NH_4)_2SO_4$	
Volume [mm³]	64,21

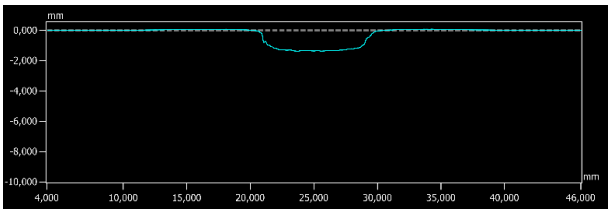

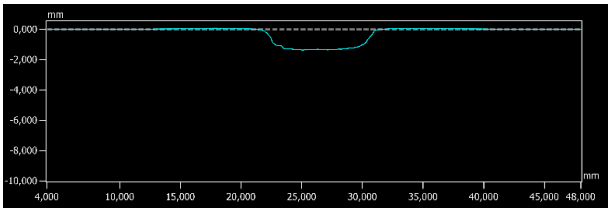

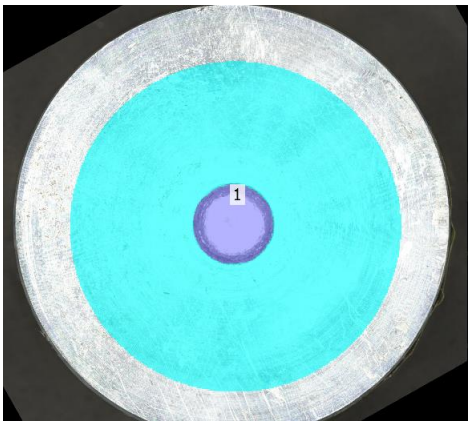

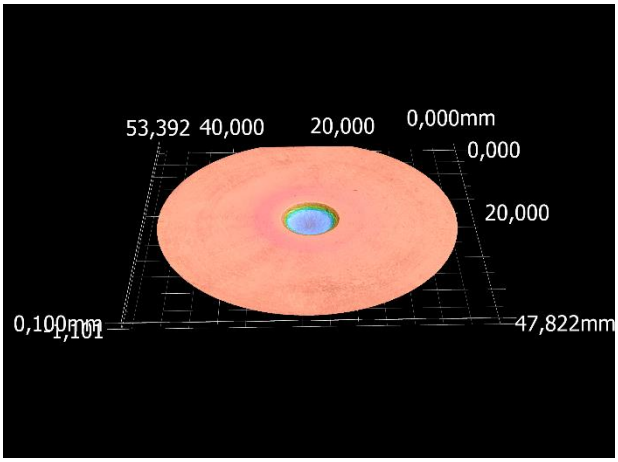

1100 mg $(NH_4)_2SO_4$	
Volume [mm³]	49,62

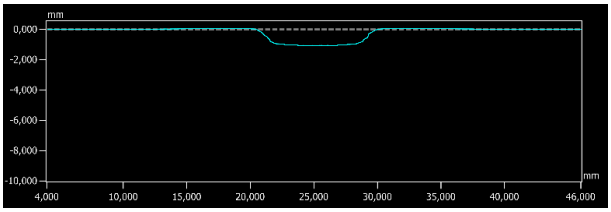

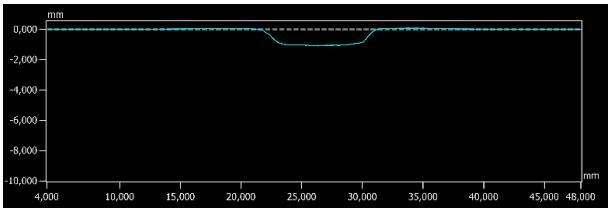

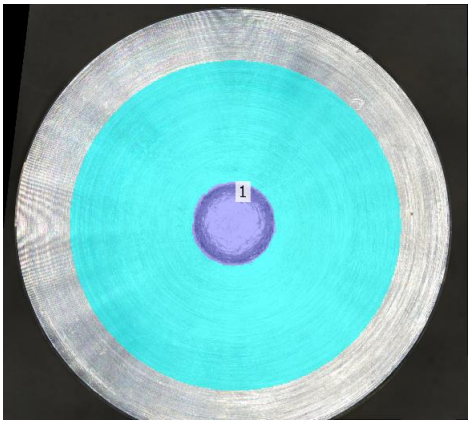

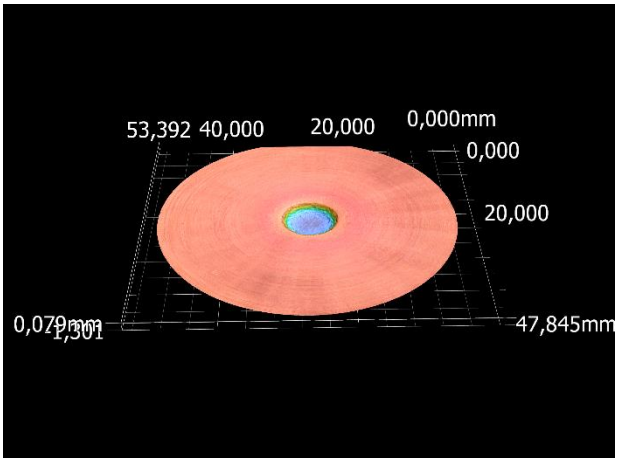

1200 mg $(NH_4)_2SO_4$	
Volume [mm³]	58,24

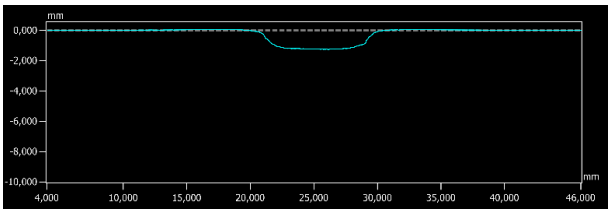

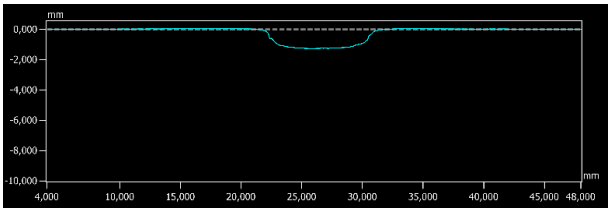

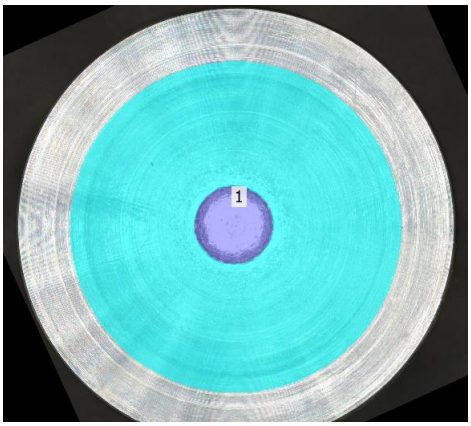

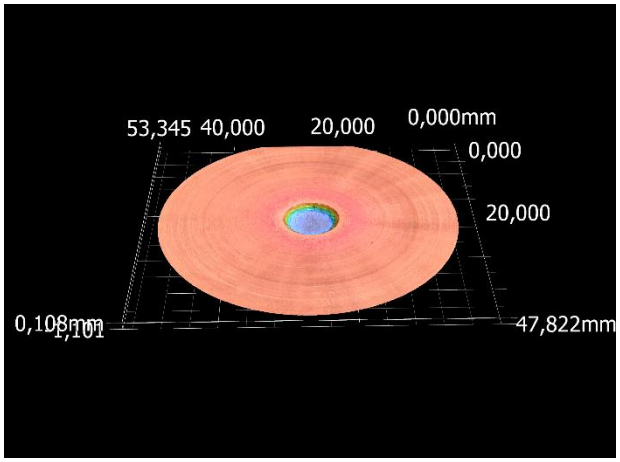

1300 mg $(NH_4)_2SO_4$	
Volume [mm³]	48,84

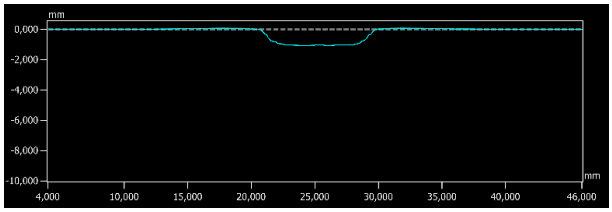

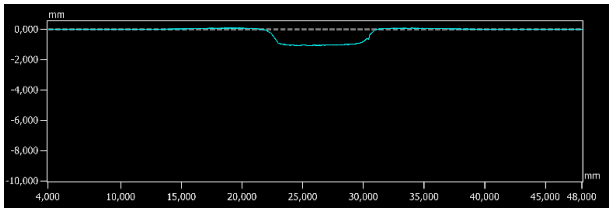

15.6.3 Graphical Evaluation

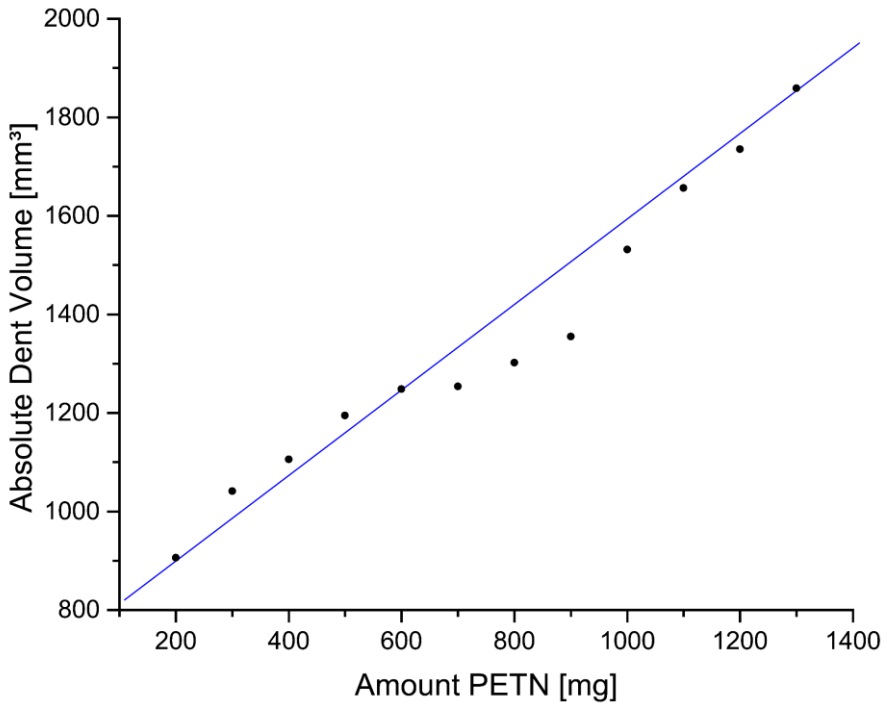

Figure S1. Aluminum block buckling (absolute value) caused by PETN.

The figure below shows the absolute dent depth (PETN and detonator) as a function of the PETN filling quantity. Figure 7 in the manuscript is therefore based on these values minus the absolute values for the explosive force of the bare detonator (Figure 5). Again, a linear fit was fitted (blue line y = 0.8116x + 736.63). Compared to the relative values in the manuscript, the fitted curve does not fit that well.

15.6.4 References

[S1] a) Reichel & Partner GmbH, http://www.reichelt-partner.de (accessed November 2021); b) Test methods according to the UN Recommendations on the Transport of Dangerous Goods, *Manual of Test and Criteria*, fourth revised edition, United Nations Publication, New York and Geneva, **2003**, ISBN 92–1-139087–7, Sales No. E.03.VIII.2; 13.4.2 Test 3 a (ii) BAM Fallhammer.

[S2] Keyence, https://www.keyence.de/landing/lpc/vrprofilometer.jsp (accessed November 2021).

16. Evaluation of SSRT-Test by Classical Gravimetric Analysis and Optical Topographic Measurement: A Comparative Study

Lukas Bauer‡, Maximilian Benz‡, Thomas M. Klapötke, Andreas Selmeier

as published in *Propellants Explosives Pyrotechnics* **2022**, e202200113

DOI: doi.org/10.1002/prep.202200113

Keywords: detonation properties, evaluation, explosives, high explosives, SSRT

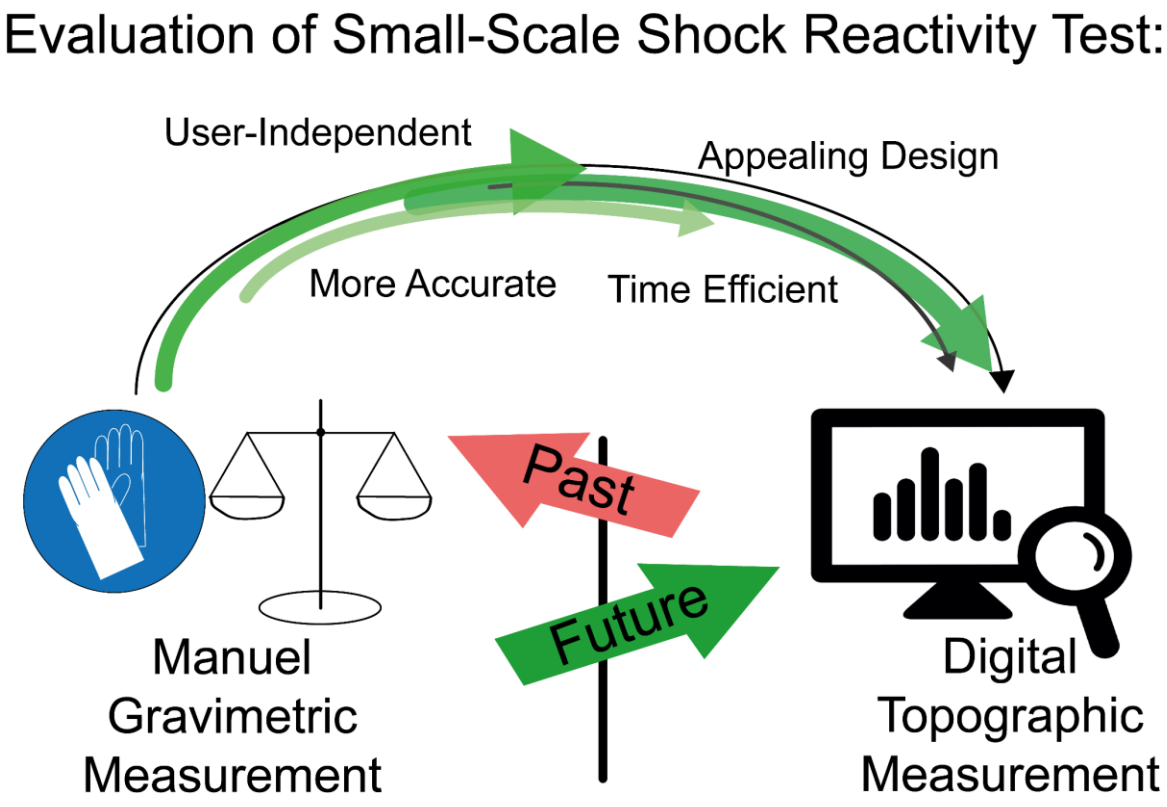

The SSRT (small-scale shock reactivity test) gives a nice insight in compounds' explosiveness, while only small quantities (approx. 0.5 g) are used per shot. But the evaluation is still a problem, since it originally uses a gravimetric measurement method. Therefore, we established a digital, topographic method utilizing a profilometer.

Abstract: To establish a database of performance values in the SSRT test, common secondary explosives based on organic nitrates (e.g. PETN) and nitramines (e.g. RDX and HMX) as well as aromatic (e.g. TNT), heteroaromatic (e.g. TKX-50 and MAD-X1) and open chain systems (e.g. FOX-7) were investigated. The evaluation of the test results was carried out by two different methods. On the one hand, manually by weighing out the resulting dents with sand, and on the other hand, optically with the aid of a profilometer. The two analysis methods were compared and evaluated with respect to their absolute results and absolute as well as relative standard deviations.

16.1 Introduction

The small-scale shock reactivity test (SSRT) was developed in 2005 by Bohl et al.[1] and gives experimental insights for the explosiveness of secondary explosives, which can be transferred to the compounds' behavior in application below their critical diameter. The test setup, which consists of a steel block with a bore and an aluminum block underneath, allows to measure the explosiveness of energetic materials in a practical way (Figure 1).

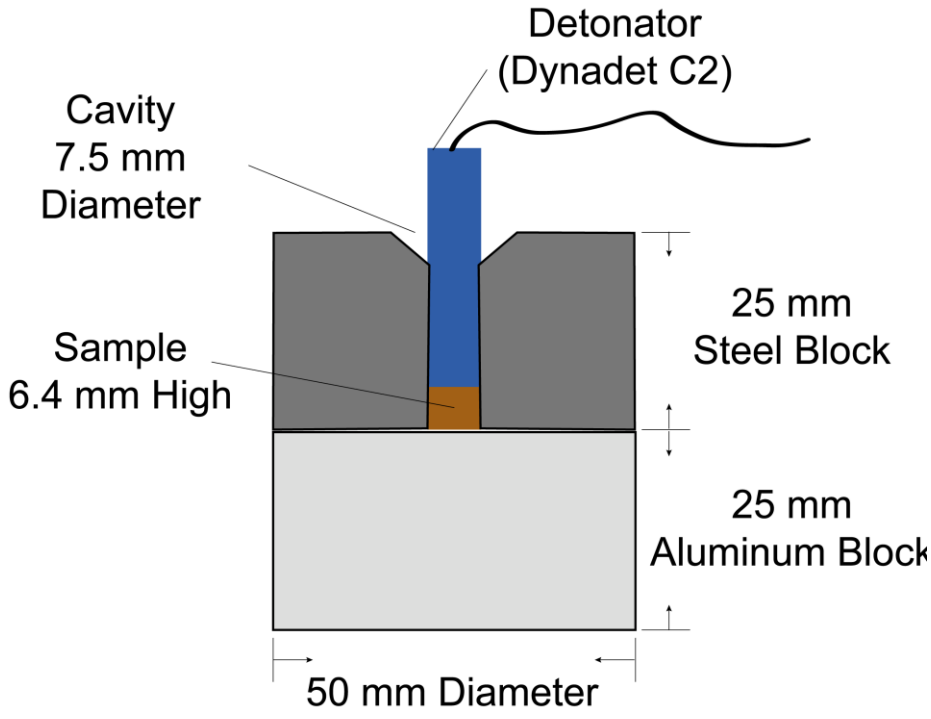

Figure 1. Schematic setup of a SSRT.

It therefore shows advantages over the Trauzl lead block test, which requires a significantly higher quantity of testing substance. An equal volume of sample substance is always filled into the test device, by using the maximum density of the compounds. This method makes the results comparable with each other, referring to the filling level which is relevant for energetic materials research.
The small scale shock reactivity test is a proven means for initial characterization of secondary explosives. The evaluation of this test is classically performed by filling the cavity in the aluminum block with sand and subsequent weighing. Since this evaluation is extremely dependent on the operator and the selected sand (density, grain size, bulk density), it is difficult to compare the obtained data between different working groups. The approach we follow in this study deals with the optical topographic determination of the dent volume with the help of a profilometer. This method offers the advantage of an easy transferability, since the dent volume is determined independently of additional auxiliary substances. In addition, the measurements are extremely precise and can be carried out in a short time. Furthermore, we compare the results of the small-scale shock reactivity tests, evaluated by the gravimetric sand method and by the optical profilometer measurement, and thus create a small database for SSRT results, which can be used as a reference for further research.

16.2 Experimental Section

CAUTION! *All of the compounds which were investigated in this study are potentially explosive energetic materials, showing sensitivities to various types of external stimuli (heat, friction, impact, electrostatic discharge). Therefore, respective safety precautions such as safety glasses, earthed equipment and shoes, leather jacket, ear plugs, Kevlar sleeves, Kevlar gloves and face shield should be used or worn throughout the entire handling.*
The compounds to be tested were used from the same reaction batch for all three test blasts in order to be able to avoid the differences in purity/composition. We did not include the grain size of the respective samples in the evaluation as these were pressed anyway. All samples for the SSRT tests were used as they were obtained from the reaction.

Nitration of pentaerithritol (PE) using fuming nitric acid and neutralization with sodium bicarbonate solution yields PETN (**1**).[2] FOX-7 (**2**) is obtained by nitration (mixed acid) of 2-methylpyrimidine-4,6-diol and a subsequent hydrolization of the nitration mixture in ice water.[3] NTO (**3**) was obtained by nitration of 1,2,4-triazol-5-on using concentrated nitric acid.[4] Potassium imidazo[4,5-d]imidazole-1,3,4,6-tetrasulfonate was prepared through condensation reaction of potassium sulfamate, formaldehyde and glyoxal. This respective tetrakis-potassiumsulfamat derivative was reacted to BCHMX (**4**) using fuming nitric acid.[5]

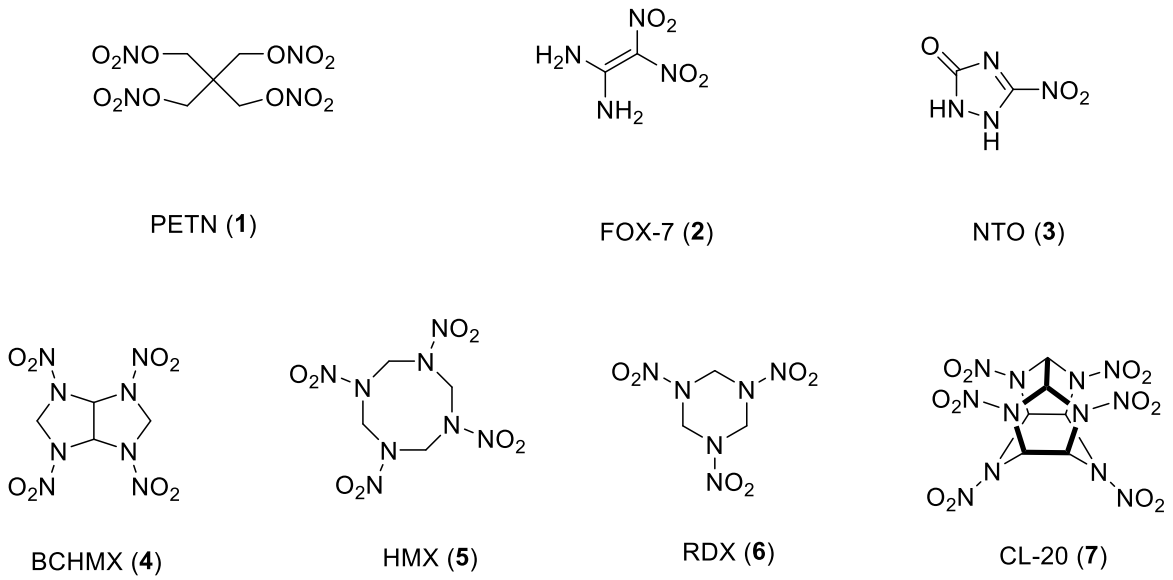

Scheme 1. Prepared non-aromatic high explosives **1**-**7**.

HMX (**5**) and RDX (**6**) were synthesized by nitration of hexamine following the Bachmann process.[6-7] CL-20 was prepared following a procedure of *Nielsen et al.* The protected hexaazaisowurtzitan backbone was obtained through condensation of benzyl amine and glyoxal solution under acidic catalysis followed by partial deprotection using H_2 and Pd/C. Subsequent anhydrous oxidation and nitration ($NOBF_4/NO_2BF_4$) yields CL-20 (**7**).[8]

TNT (**8**) and PA (**9**) were obtained by nitration of the respective benzolic parent compound (toluene for TNT and phenol for PA).[9-10] HNS (**10**) was obtained by oxidation of TNT using NaOCl.[11] 5*H*-tetrazole (**11**) was obtained by reaction of sodium azide, ammonium chloride and triethyl orthoformate in acetic acid.[12]

BODN (**12**) was prepared by a procedure of *Sabatini et al* starting from diaminoglyoxime.[13] 3,4-DN-1-NMP (**13**) was produced via a five step procedure

starting from 1*H*-pyrazole including *N*-nitration, nitro-rearrangement, *C*-nitration, *N*-hydroxymethylation and *O*-nitration.[14] BTNPM (**14**) was obtained through a five step reaction sequence starting from 1*H*-pyrazole.[15] MAD-X1 (**15**) and TKX-50 (**16**) were synthesized following literature known procedures starting from oxalic acid/aminoguanidinium carbonate and aqueous glyoxal solution, respectively.[16-17] The purity of all compounds was checked through ^{1}H NMR spectroscopy and CHNO elemental analysis.

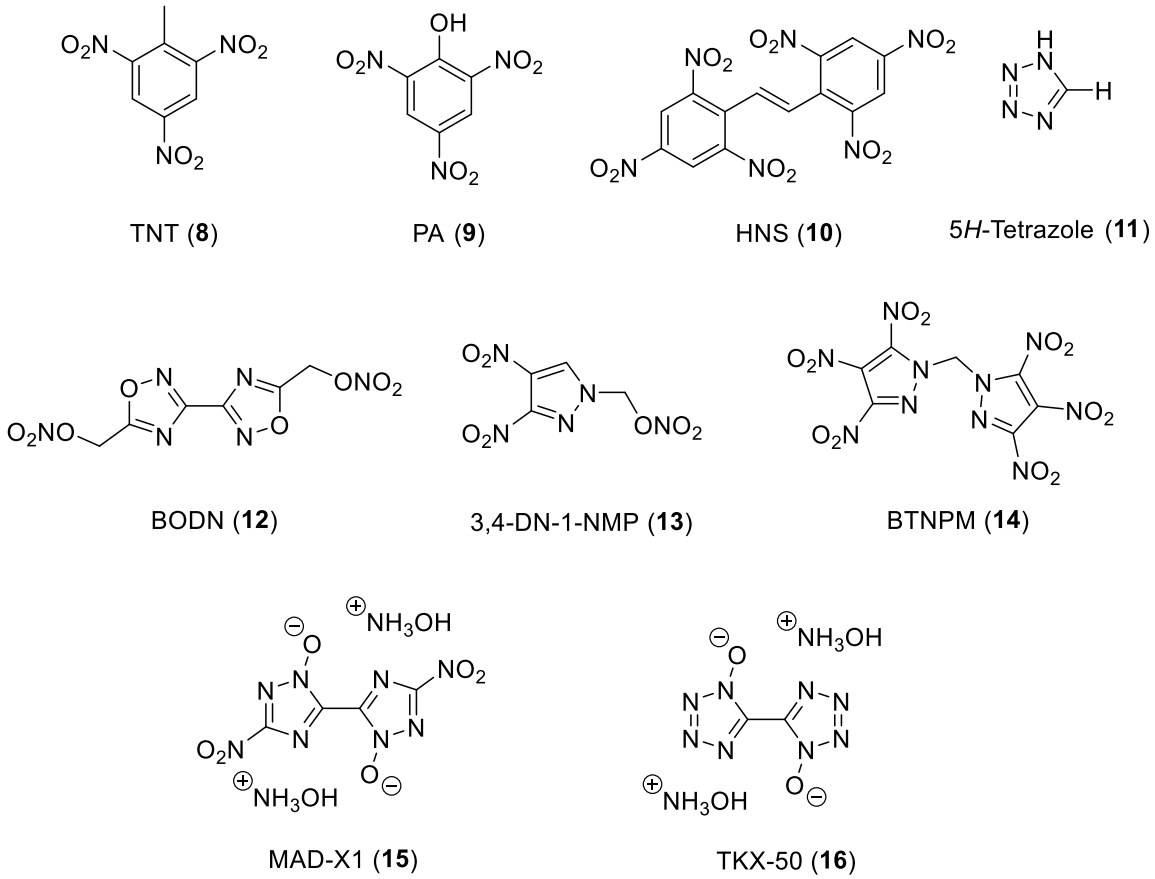

Scheme 2. Prepared aromatic high explosives **8**-**16**.

16.3 Results and Discussion

To perform the test series, the synthesized compounds **1**–**16** were weighed and prepared for detonation in the SSRT setup as recently described.[ii] For the SSRT method, a constant volume of explosive is needed to be comparable within the other tested substances. The sample volume V_s is recommended to be 283 mm^3, which corresponds to a filling height of 6.4 mm for the required 7.5 mm of diameter

of the drill hole in the steel block. The used sample weight m_s was calculated according to the formula given in Equation 1.

$$m_s = 0.95 \times V_s \times \rho_{Xray} \qquad (E1)$$

This ensured that the identical fill level was used for all compounds investigated, whereby we always assumed the ideal crystallographic density of the substances. The calculated quantities of the respective substances can be found in the Supporting Information. Each substance was tested with three blasts in order to to obtain a reliable average value and to minimize the effect of outliers.

After the test was carried out and the aluminum block cleaned, all the blocks were evaluated using two different methods. On the one hand, an optical topographic measurement of the generated dents was performed using a Keyence profilometer. The exact implementation of this measurement method can be found in detail in a recently published study.[18] On the other hand, a gravimetric method was used as originally proposed for the evaluation of the SSRT.[1]

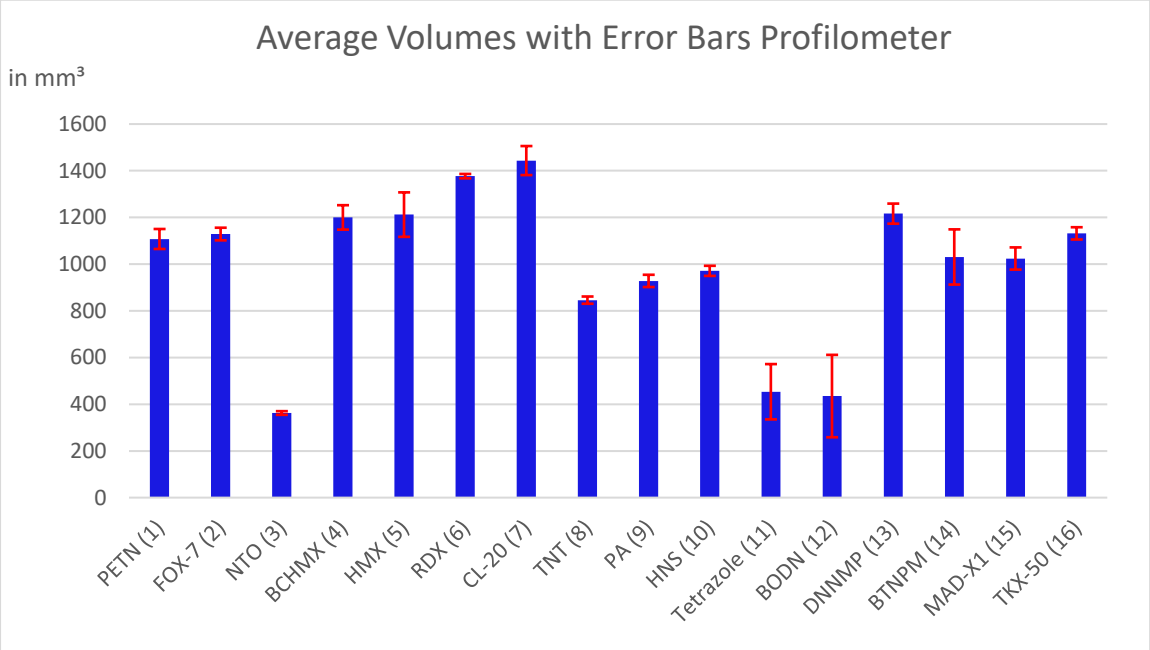

Figure 2. Average dent volumes in mm³ for compounds **1**–**16** with error bars, measured by the profilometer. Error bars are calculated using the averaged values for each blast.

Commercially available, unground sand was used as the filler, which was poured into the dent of the corresponding aluminum block and smoothed with an object

carrier to remove the excess sand. Using the empty aluminum block as reference, the mass of the poured sand was determined by weighing it out. This measurement was repeated ten times per block to obtain a good average with a reasonable standard deviation. The results of the various measurements are outlined in the graphs below.

The largest dent volumes were obtained with CL-20 and RDX, while PETN, HMX, BCHMX, DNNMP and TKX-50 show similarly high volumes (Figure 2). TNT, PA and HNS show lower volumes than the aforementioned, as could be expected from their performance parameters. Due to the high calculated performances, larger bulges were expected for numerous compounds (especially for TKX-50). However, this test setup aims to produce detonations below many compounds' critical diameter. Since this critical diameter is often not achieved (diameter of the cavity is 7.5 mm), the detonations cannot spread ideally and the test results are lower than expected. NTO, tetrazole and BODN show distinctly low dent volumes and tetrazole as well as BODN large error bars. This is due to the fact, that full initiation was not achieved for all blasts as can be seen in Figure 3. There are several possible reasons but, above all, the lower explosiveness and consequently, more difficult initiation of the two substances is noteworthy. All other compounds were initiated successfully with the used setup.

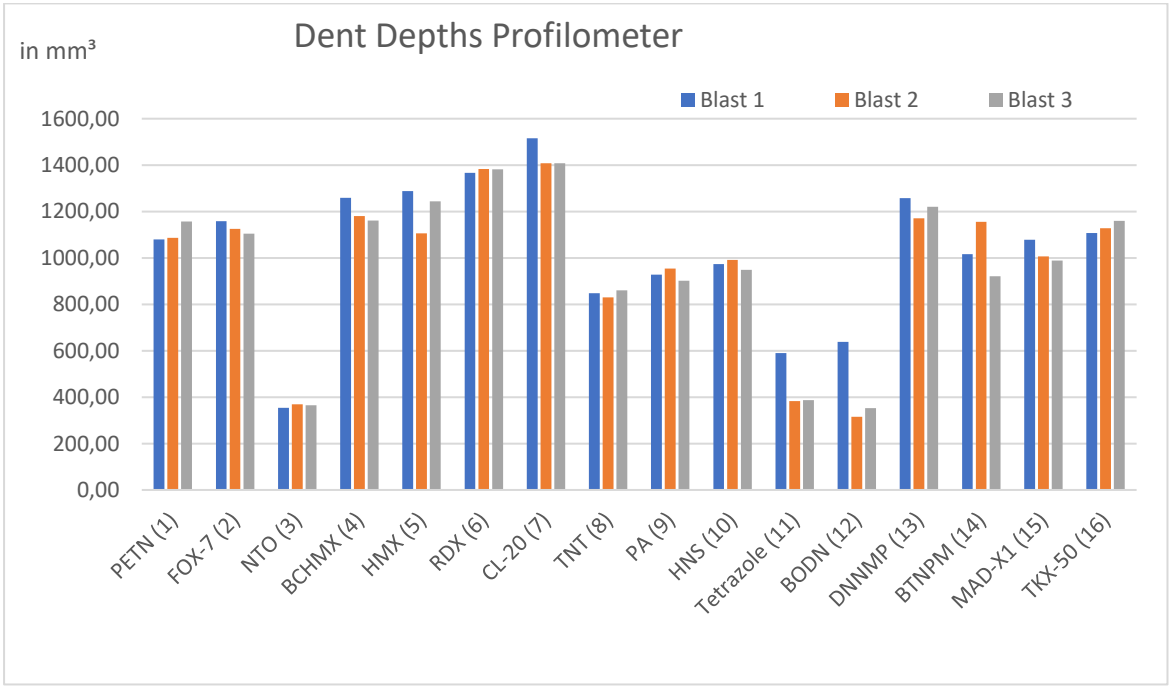

Figure 3. Dent volumes in mm³ for each blast performed for compounds **1**–**16**, measured by the profilometer.

In comparison to each other, the three blasts show generally very similar data (Figure 3) except when initiation is not achieved like for tetrazole and BODN.

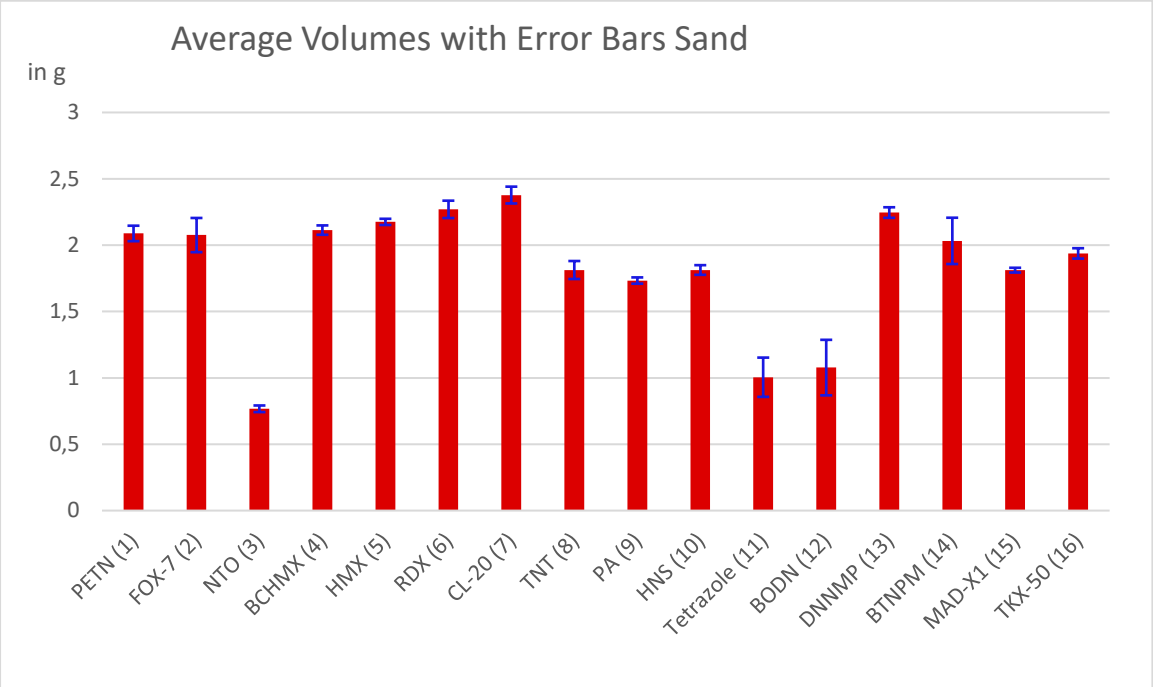

Figure 4. Average sand weight in grams needed for filling the dent in the aluminum block for compounds **1**–**16**, with error bars.

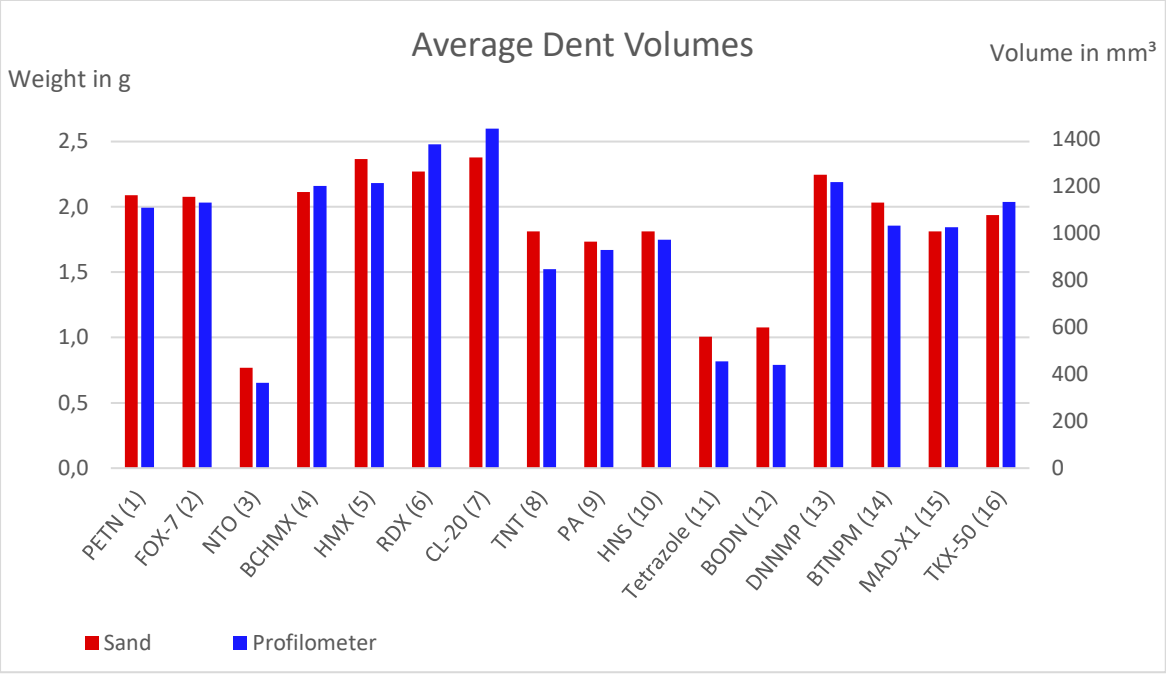

Figure 5. Average dent volumes for both measurement methods compared. Gravimetric method in red, profilometric method in blue.

Deviations between the blasts can result from small errors in the weighing and filling process e.g. from imperfect pressing of the compounds into the steel block cavity. The values obtained by the gravimetric method agree with the values obtained by the optical topographic measurement and show a comparable error bar distribution. The results are depicted in Figure 4.

When comparing the values side by side (Figure 5) it can be seen, that especially low or high values can differ from one testing method to another. The gravimetric method shows a smaller difference between the highest (CL-20) and lowest (NTO) values than the topographic method. The dent depth of NTO compared to CL-20 is 32% for the gravimetric method and only 25% for the topographic method. To assess the quality of the obtained data for both methods, the relative standard deviation is a valuable tool, as it helps to visualize the size of the minimum measurement error for a given test setup.

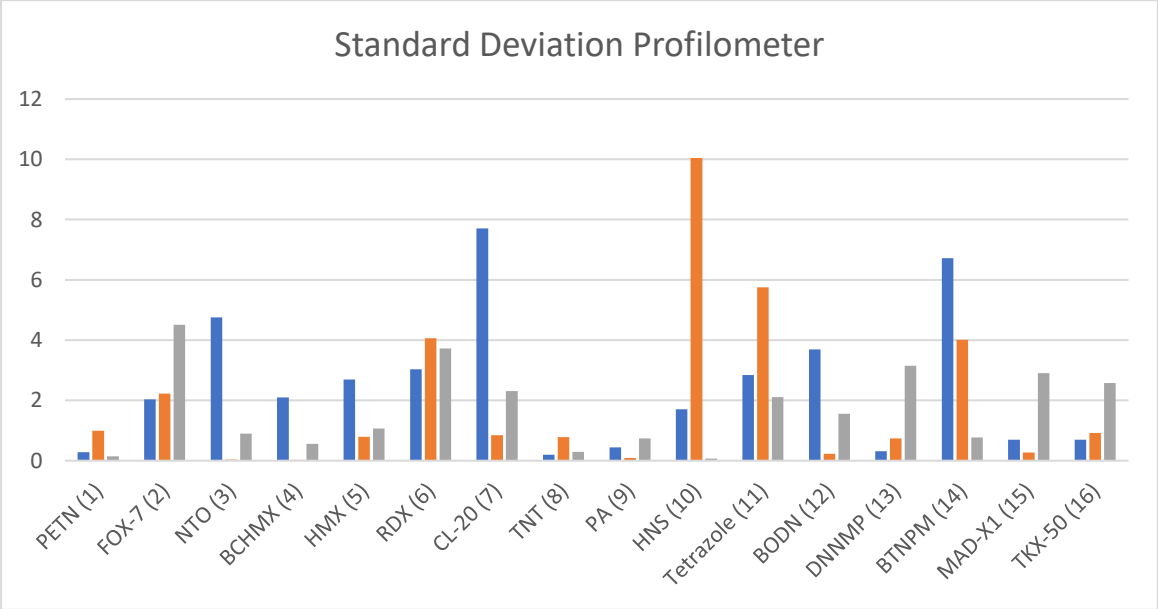

Figure 6. Relative deviation in % of the two profilometer measurements for each compound.

The profilometer measurements were performed two times per blast to offset the impact of formed concavities or convexities in the overall dent profile of the witness block. The blocks were rotated by 90° in-between measurements to minimize the problem, but more measurements per block would give data with even higher accuracy. Nevertheless, the relative standard deviation is in the range of 0% – 1.5% with most measurements below 0.5%. Up to six blocks can be

measured in succession without further user interaction, reducing the actively spent time massively.

Figure 7 shows the result of the two topographic measurements with irregular dent shapes of HNS blast 1 (top) and PETN blast 1 (bottom). The measurement method with the profilometer, which is based on triangulation of polarized light, can lead to blind spots in certain areas of the block and thus to a serious error in the resulting volume values. This means that an increased number of measurements would have to be taken at different angles for each block in order to avoid this source of error. However, in the blocks investigated, there are only a few samples with extreme bulges (concavities or convexities), which we have already been able to average well with two measurements, which represents the volume with high accuracy.

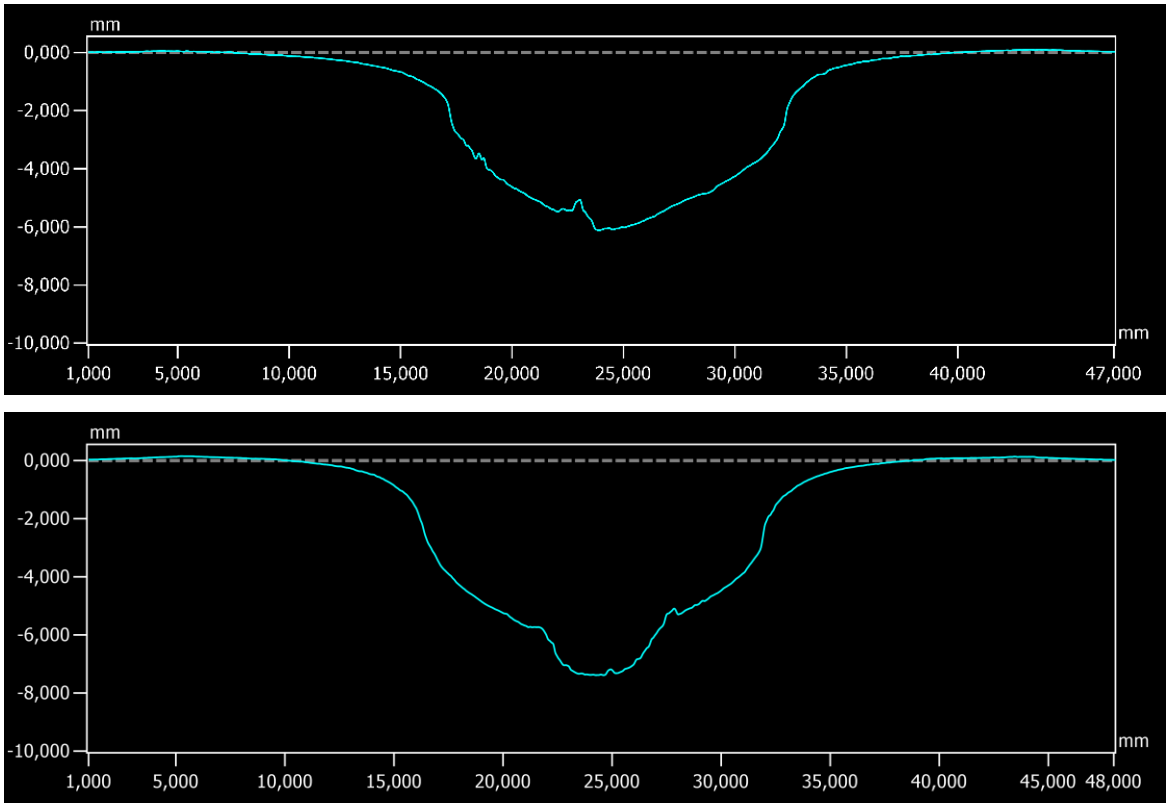

Figure 7. 2D profile measurements. a) HNS blast 1 with a convex tip in the profile; b) PETN blast 1 with concave hole in the profile.

The relative standard deviation graph (Figure 8) for the gravimetric method exposes a significant problem: operator-dependency. TNT and BTNPM show the highest deviations of up to 2.5%, while the other compounds show a very similar

deviation spread with values of around 0.25%-0.5%. TNT was the first and BTNPM the second compound to be measured by the operator. When a large amount of experiments is to be conducted, this flaw can be easily bypassed by refining the measuring process first. However, most SSRT experiments only compare a few selected compounds like RDX or PETN to the respective new compounds.

In addition to the measurement inaccuracy that occurs with an unestablished methodology, the measurement time is another disadvantage of the gravimetric method. Although the measurement duration is not as important for a few isolated samples, such as the analysis of a single compound, as it is for the preparation of a large collection of data, as in this study, it is nevertheless a factor that cannot be neglected. In our series of measurements, the time required to determine the mass of the sand for one compound (three tested blocks with ten dent measurements each) was approximately one hour. Compared with the 6 min for the profilometeric measurement of three blocks, there is a clear advantage for the digital measurement method.

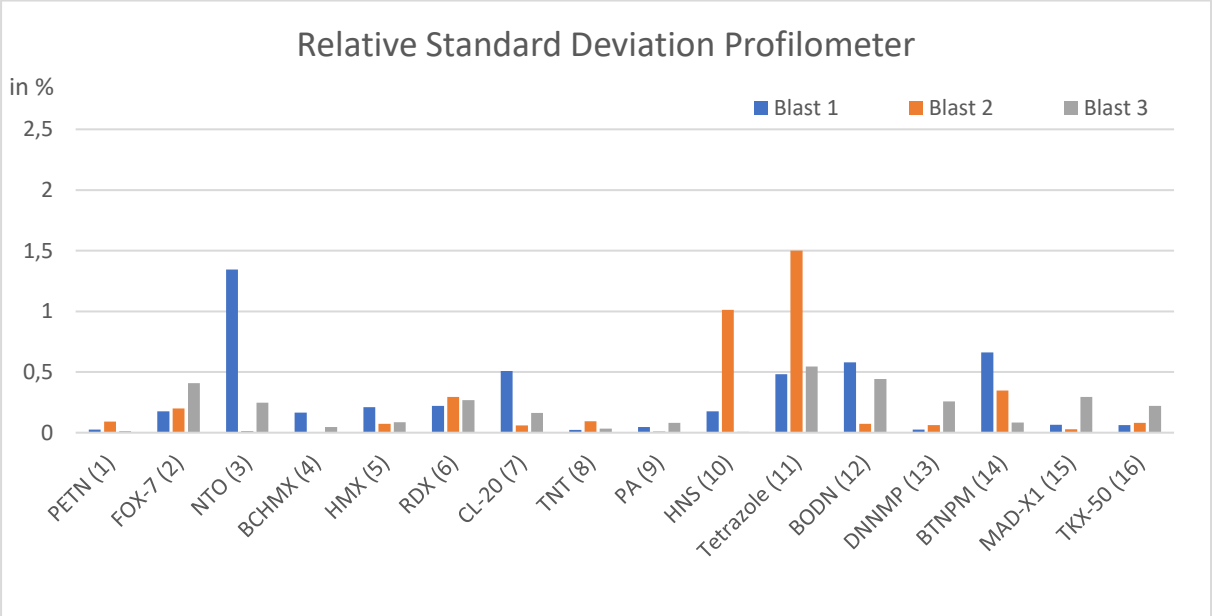

Figure 8. Relative deviation in % of the gravimetric measurements for each compound.

16.4 Conclusion

In the present study, two evaluation methods for SSRT experiments were compared; the classical gravimetric analysis, which uses sand as a filling material,

and an optical topographic measurement method, which generates its results through digital profilometer measurements. Basically, our two series of measurements yield similar results and trends. Nevertheless, we were able to gain some advantages from the measurement method with the profilometer. Among other things, the digital measurements are less time-consuming, more accurate, graphically better representable and reproducible independent of the operator. In addition, when evaluating with the profilometer, volumes are obtained as measurement results, which can be more easily compared with other measurement series than sand masses, which are the output of the gravimetric measurement method and are therefore dependent on the type and properties of the used sand. In addition, we present in our study the results of SSRT experiments for 16 common explosives, which can be used as reference value in the future.

16.5 Acknowledgement

For financial support of this work by Ludwig-Maximilian University (LMU), the Office of Naval Research (ONR) under grant no. ONR N00014-19-1-2078 and the Strategic Environmental Research and Development Program (SERDP) under contract no. W912HQ19C0033 are gratefully acknowledged. The authors are indebt to thank Jasmin Lechner, Elena Reinhardt, Alexander Harter and Tobias Lenz (all LMU Munich) for the synthesis of several high explosives.

16.6 References

[1] H. W. Sandusky, R. H. Granholm, D. G. Bohl, Small-Scale Shock Reactivity Test (SSRT), IHTR 2071, Naval Surfave Warfare Center, Indian Head, MD, **2005**.

[2] E. Berlow, R.H. Barth, J.E. Snow, The Pentaerythritols, Reinhold Publishing Corporation, New York **1958**.

[3] B. A. Czeskis, *J. Label. Compd. Rad.* **2004**, *47* (10), 699–704.

[4] W. Manchot, R. Noll, *Liebigs Ann*. **1905**, *343*, 1–27.

[5] D. Klasovity, S. Zeman, *Improved process for preparation of cis-1,3,4,6-tetranitrooctahydroimidazo[4,5-d]imidazole propellant and explosive by nitration of metal sulfonate salt*, CZ302068-B6, Czech Republic, **2010**.

[6] W. E. Bachmann, E. L. Jenner, *J. Am. Chem. Soc.* **1949**, *71*, 1842–1845.

[7] W. E. Bachmann, J. C. Sheehan, *J. Am. Chem. Soc.* **1951**, *73*, 2773–2775.

[8] A. T. Nielsen, A. P. Chafin, S. L. Christian, D. W. Moore, M. P. Nadler, R. A. Nissan, D. J. Vanderah, R. D. Gilardi, C. F. Geroge, J. L. Flippen-Anderson, *Tetrahedron*, **1998**, *54* (39), 11793–11812.

[9] R. C. Dorey, W. R. Carper, *J. Chem. Eng. Data*, **1984**, *29* (1), 93–97.

[10] F. Olsen, J. C. Goldstein, *Ind. Eng. Chem.* **1924**, *16* (1), 66–71.

[11] K.G. Shipp, L. A. Kaplan, *J. Org. Chem*, **1966**, *31* (3), 857–861.

[12] J. Stierstorfer, *PhD thesis*, Ludwig-Maximilians-Universität München, **2009**.

[13] E. C. Johnson, J. J. Sabatini, D. E. Chavez, R. C Sausa, E. F. C. Byrd, L. A. Wingard, P. E. Guzman, *Org. Process Res. Dev.* **2018**, *22*, 736–740.

[14] S. Song, F. Chen, Y. Wang, K. Wang, M. Yan, Q. Zhang, *J. Mater. Chem. A,* **2021**, *9*, 21723–21732.

[15] D. Fischer, J. L. Gottfried, T. M. Klapötke, K. Karaghiosoff, J. Stierstorfer, T. G. Witkowski, *Angew. Chem. Int. Ed.* **2016**, *55*, 16132–16135.

[16] A. A. Dippold, T. M. Klapötke, *J. Am. Chem. Soc.* **2013**, *135*, 9931–9938.

[17] N. Fischer, D. Fischer, T. M. Klapötke, D. G. Piercey, J. Stierstorfer, *J. Mater. Chem.* **2012**, *22*, 20418–20422.

[18] L. Bauer, M. Benz, T. M. Klapötke, *Propellants Explo. Pyrotech.* **2022**, e202100332.

16.7 Supporting Information

16.7.1 General Experimental Methods

^{1}H and ^{13}C NMR spectra were recorded on *JEOL 270* and *BRUKER AMX 400* instruments. The samples were measured at room temperature in standard NMR tubes (Ø 5 mm). Chemical shifts are reported as d values in ppm relative to the residual solvent peaks of DMSO-D_6 (δ H: 2.50, δ C: 39.5). Solvent residual signals and chemical shifts for NMR solvents were referenced against tetramethylsilane (TMS, δ = 0 ppm). Unless stated otherwise, coupling constants were reported in

Hertz (Hz) and for the characterization of the observed signal multiplicities the following abbreviations were used: s (singlet), m (multiplet) and br (broad). **CAUTION!** *All investigated substances are potentially explosive materials, although no hazards were observed during preparation and handling. Nevertheless, safety precautions (such as wearing leather coat, face shield, Kevlar sleeves, Kevlar gloves, earthed equipment and ear plugs) should be drawn especially when manipulating dry material.*

16.7.2 Compound Quantities

Table S1. Quantities of tested explosives **1**–**16** calculated accordring to equotation E1.

	Compound	Chemical Formula	Molar Mass	Density at 298K	Weight [mg]	Mol [mmol]
1	PETN	$C_5H_8N_4O_{12}$	316,15	1,778	477,57	1,51
2	FOX-7	$C_2H_4N_4O_4$	148,08	1,893	508,46	3,43
3	NTO	$C_2H_2N_4O_3$	130,06	1,910	513,02	3,94
4	BCHMX	$C_4H_6N_8O_8$	294,14	1,861	499,86	1,70
5	HMX	$C_4H_8N_8O_8$	296,18	1,904	511,41	1,73
6	RDX	$C_3H_6N_6O_6$	222,14	1,806	485,09	2,18
7	CL-20	$C_6H_6N_{12}O_{12}$	438,19	2,035	546,60	1,25
8	TNT	$C_7H_6N_3O_6$	227,13	1,648	442,65	1,95
9	PA	$C_6H_3N_3O_7$	229,11	1,763	473,54	2,07
10	HNS	$C_{14}H_6N_6O_{12}$	450,23	1,740	467,36	1,04
11	Tetrazole	CH_2N_4	70,06	1,632	438,35	6,26
12	BODN	$C_6H_4N_6O_8$	288,13	1,830	491,53	1,71
13	DNNMP	$C_4H_3N_5O_7$	233,10	1,848	496,37	2,13
14	BTNPM	$C_7H_2N_{10}O_{12}$	418,19	1,934	519,47	1,24
15	MAD-X1	$C_4H_8N_{10}O_8$	324,17	1,900	510,34	1,57
16	TKX-50	$C_2H_8N_{10}O_4$	236,15	1,877	504,16	2,13

16.7.3 Profilometer Measurements

In the following pages the pictures, generated by a Keyence 3D profilometer VR-5200, and analysis data for the measurements of compounds are given as follows: Top left: Picture of the aluminum block with the measured area indicated in cyan and the indentations in violet. Top right: Color coded height measurements with red for the reference area and blue for the deepest indentation. Bottom right: Cross sections of the height profiles of the aluminum block at a 90 ° angle to each other.

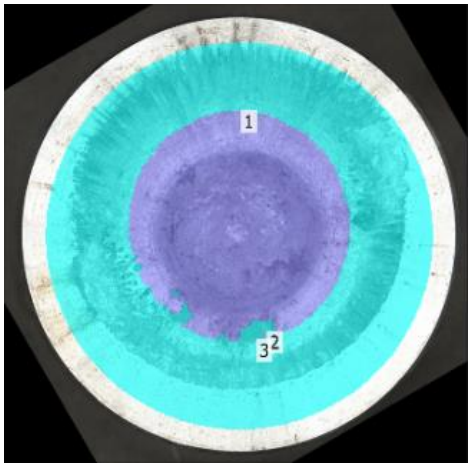

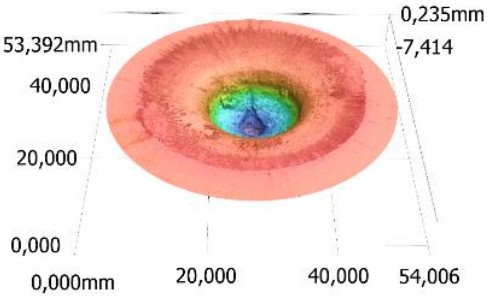

PETN Blast 1	
Measurement 1 [mm³]	1079,29
Measurement 2 [mm³]	1079,69
Average Volume [mm³]	1079,49

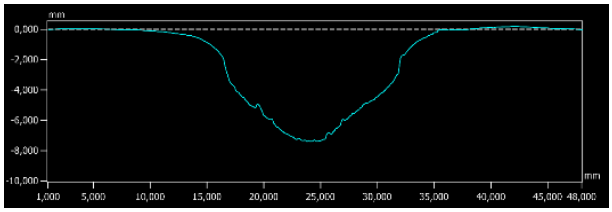

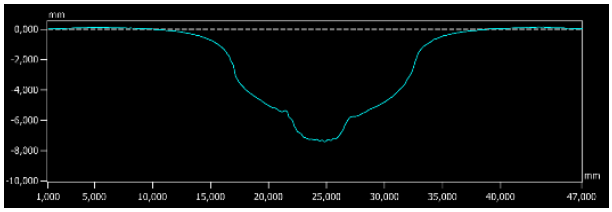

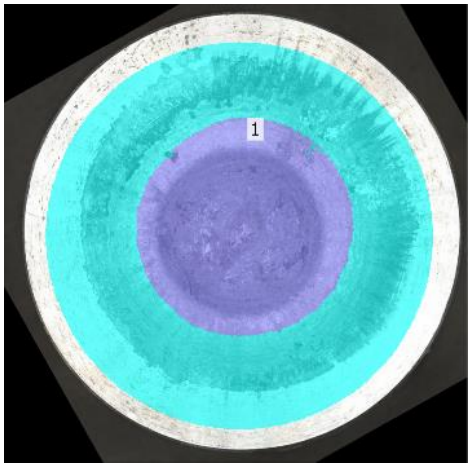

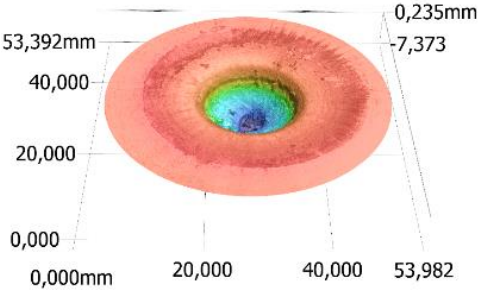

PETN Blast 2	
Measurement 1 [mm³]	1086,28
Measurement 2 [mm³]	1087,68
Average Volume [mm³]	1086,98

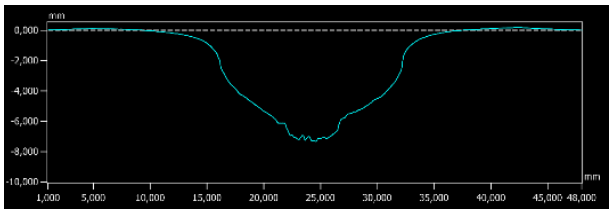

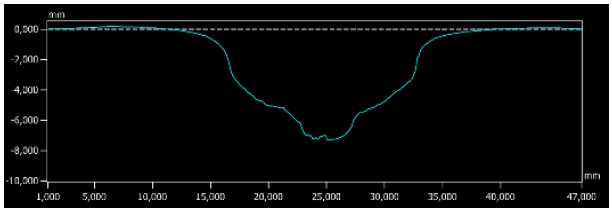

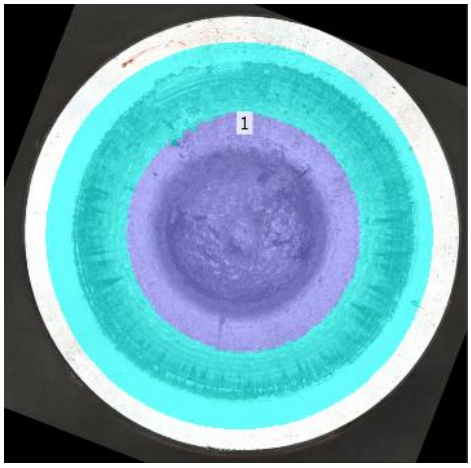

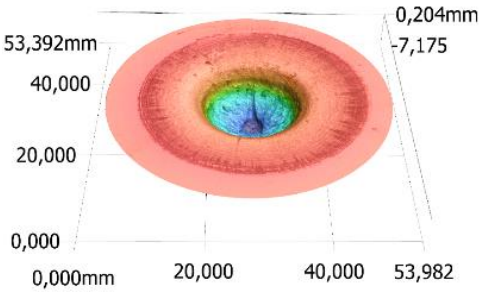

PETN Blast 3	
Measurement 1 [mm³]	1157,09
Measurement 2 [mm³]	1156,89
Average Volume [mm³]	1156,99

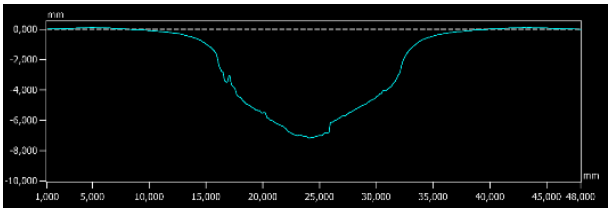

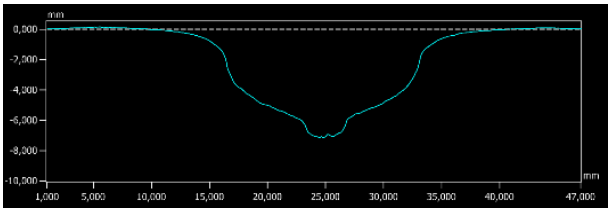

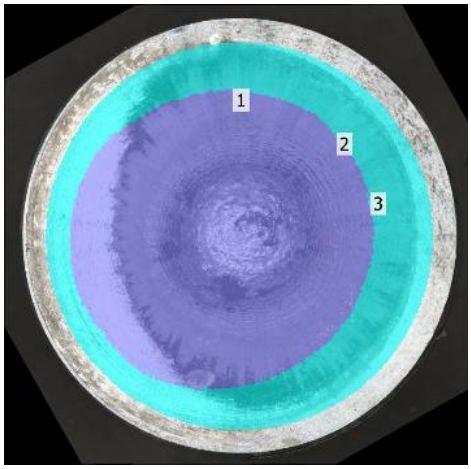

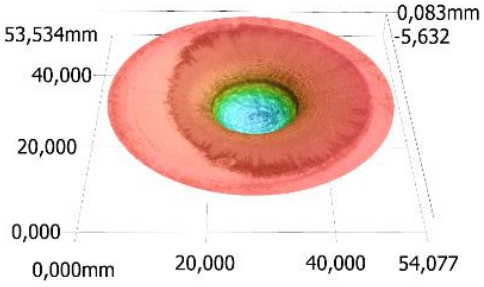

8

FOX-7 Blast 1	
Measurement 1 [mm³]	1159,34
Measurement 2 [mm³]	1156,45
Average Volume [mm³]	1157,90

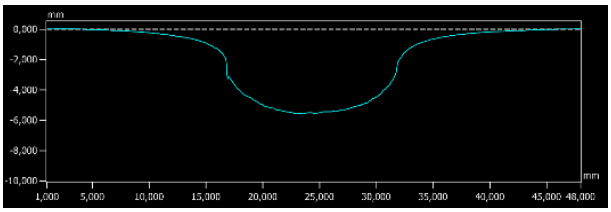

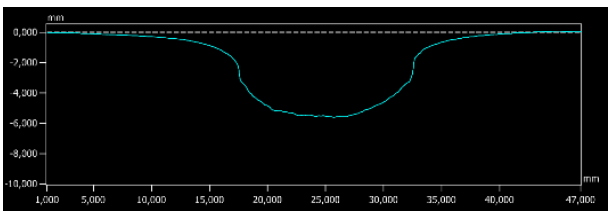

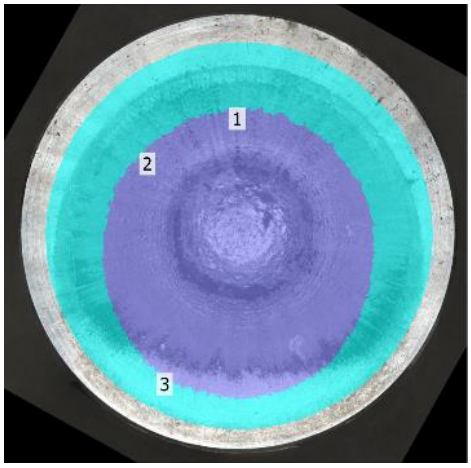

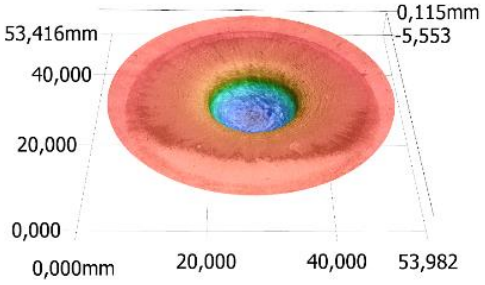

FOX-7 Blast 2	
Measurement 1 [mm³]	1126,66
Measurement 2 [mm³]	1123,51
Average Volume [mm³]	1125,09

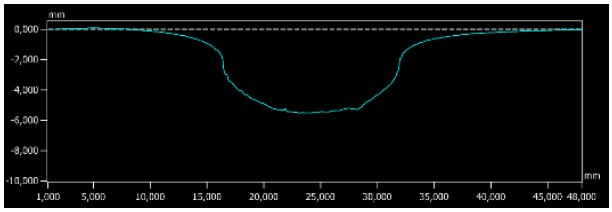

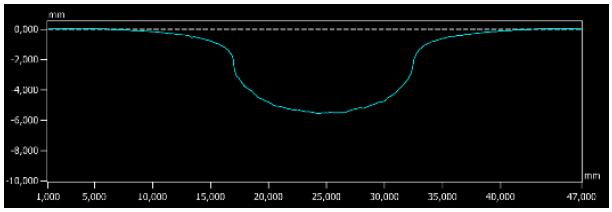

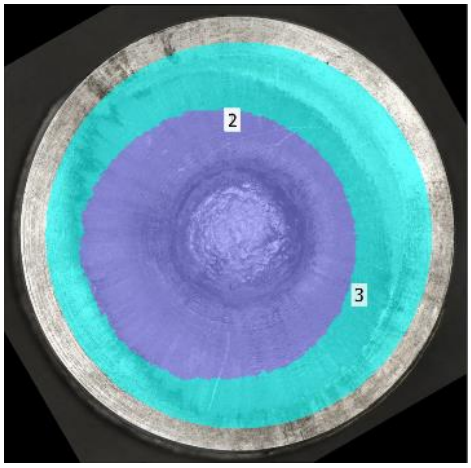

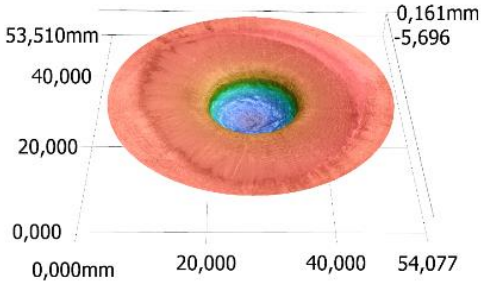

FOX-7 Blast 3	
Measurement 1 [mm³]	1107,40
Measurement 2 [mm³]	1101,03
Average Volume [mm³]	1104,22

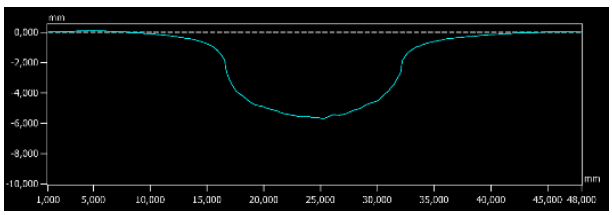

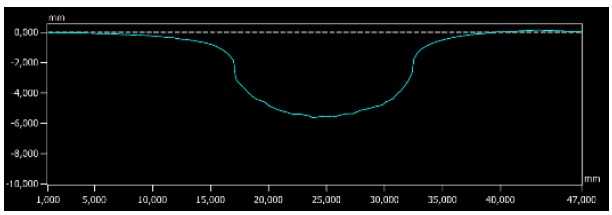

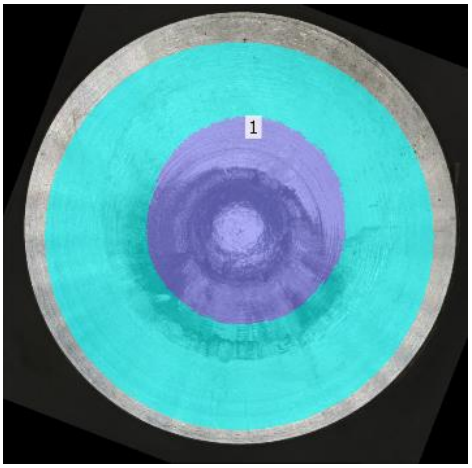

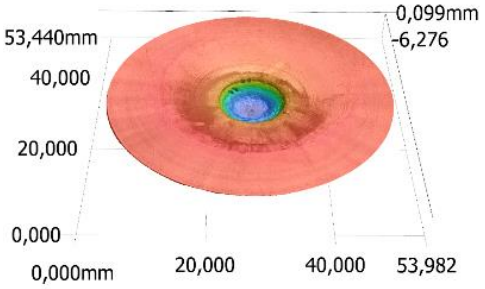

NTO Blast 1	
Measurement 1 [mm³]	350,40
Measurement 2 [mm³]	357,12
Average Volume [mm³]	353,76

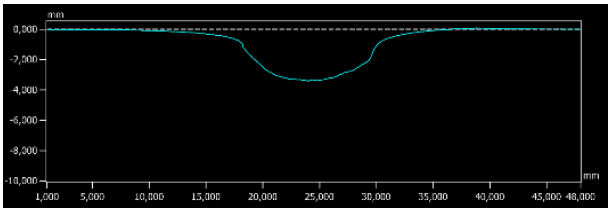

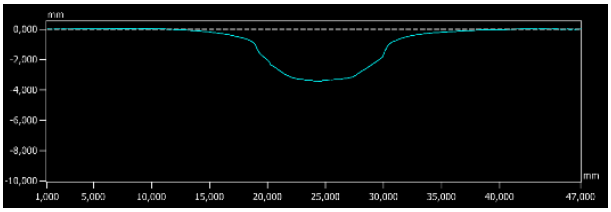

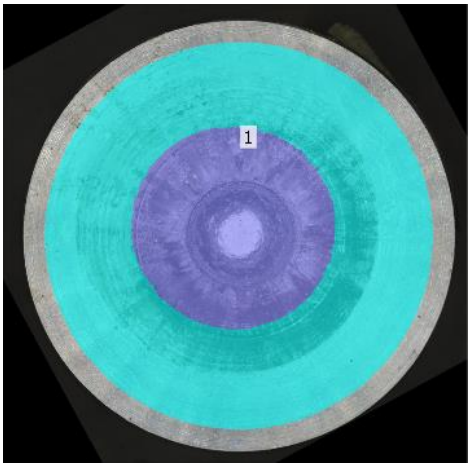

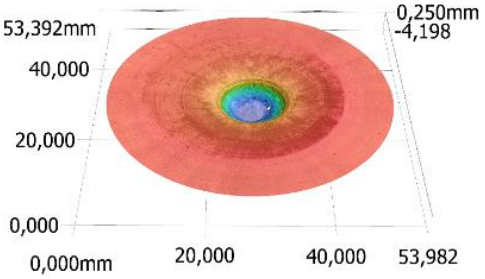

NTO Blast 2	
Measurement 1 [mm³]	369,02
Measurement 2 [mm³]	369,08
Average Volume [mm³]	369,05

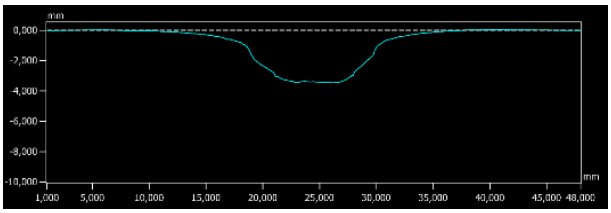

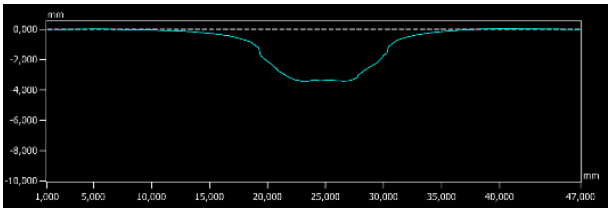

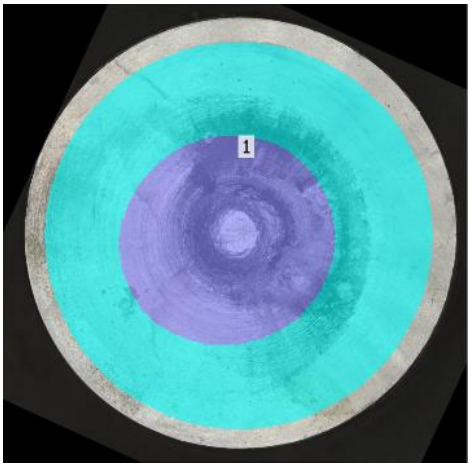

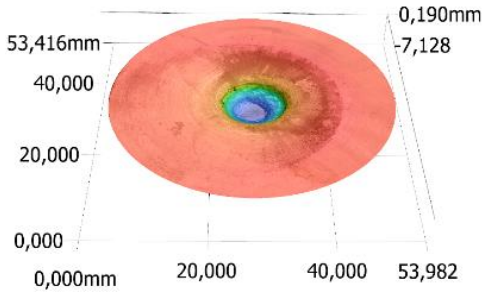

NTO Blast 3	
Measurement 1 [mm³]	365,05
Measurement 2 [mm³]	363,77
Average Volume [mm³]	364,41

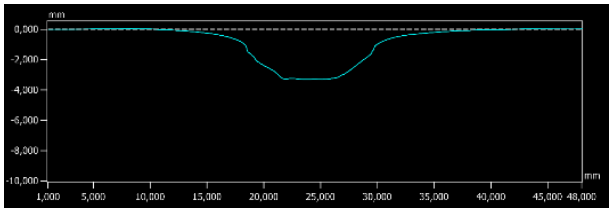

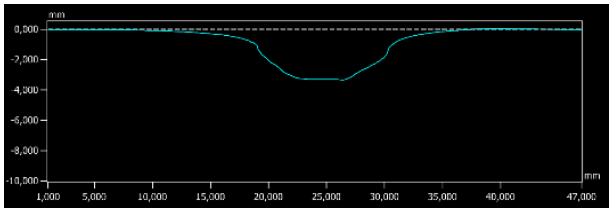

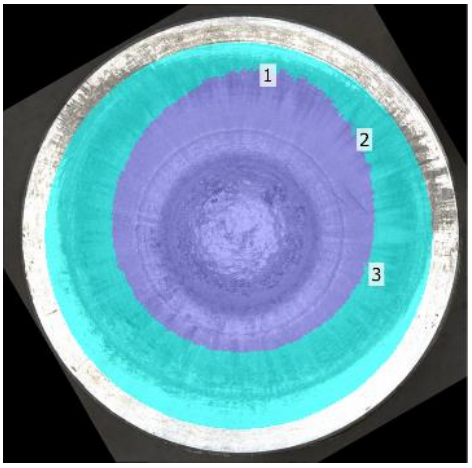

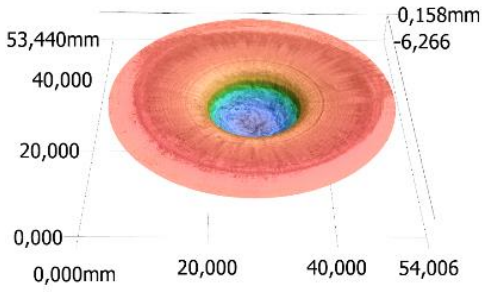

BCHMX Blast 1	
Measurement 1 [mm³]	1258,21
Measurement 2 [mm³]	1261,18
Average Volume [mm³]	1259,69

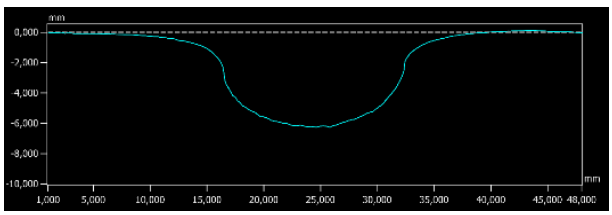

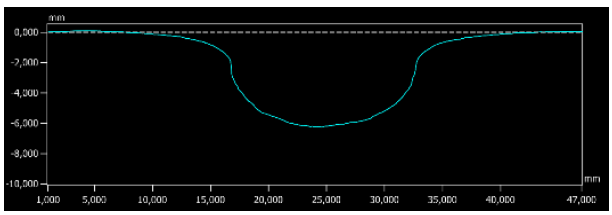

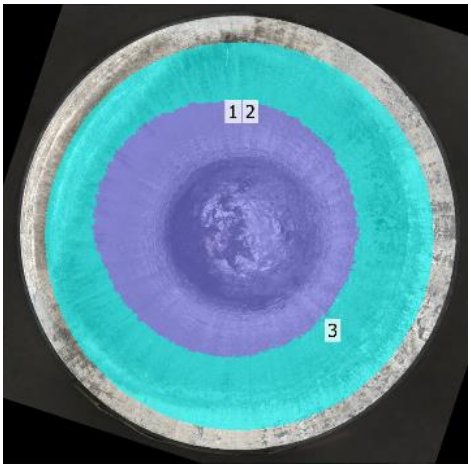

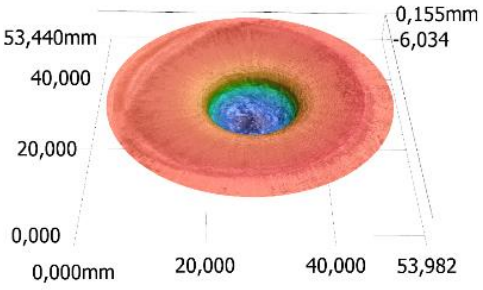

BCHMX Blast 2	
Measurement 1 [mm³]	1179,98
Measurement 2 [mm³]	1179,94
Average Volume [mm³]	1179,96

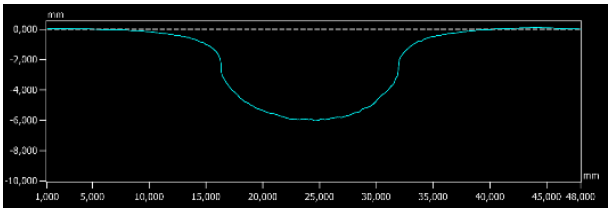

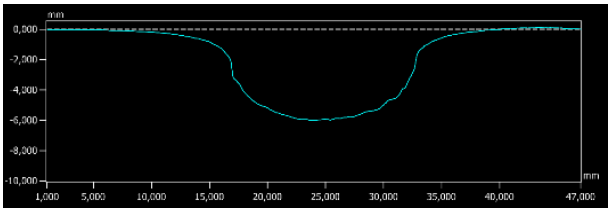

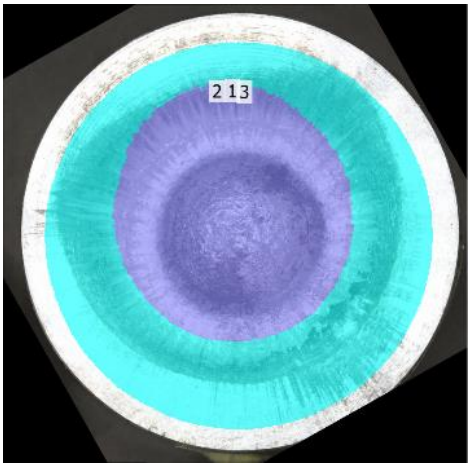

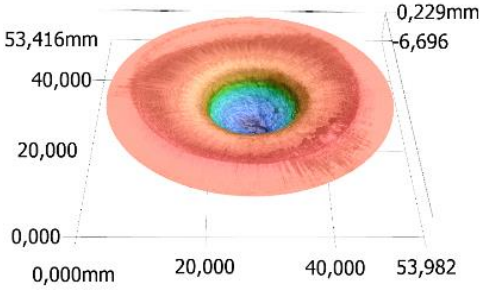

BCHMX Blast 3	
Measurement 1 [mm³]	1160,82
Measurement 2 [mm³]	1161,61
Average Volume [mm³]	1161,22

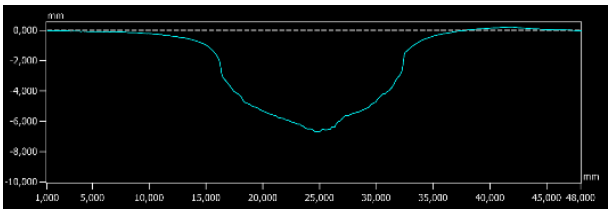

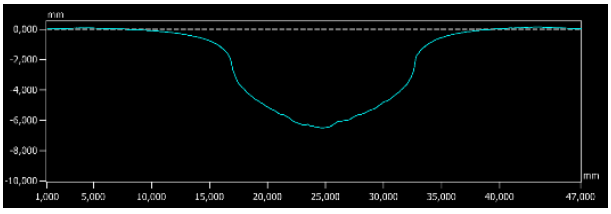

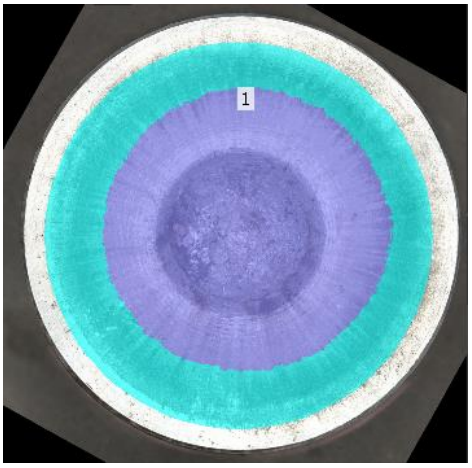

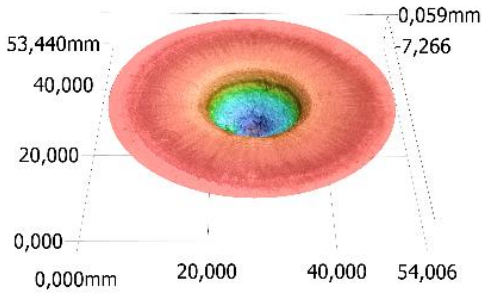

HMX Blast 1	
Measurement 1 [mm³]	1286,21
Measurement 2 [mm³]	1290,02
Average Volume [mm³]	1288,12

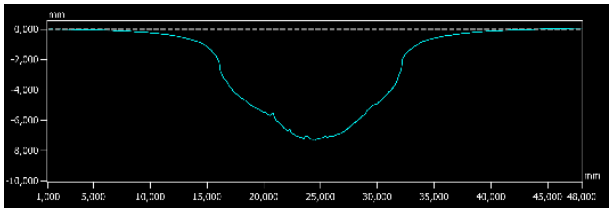

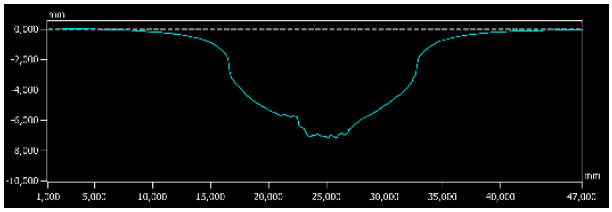

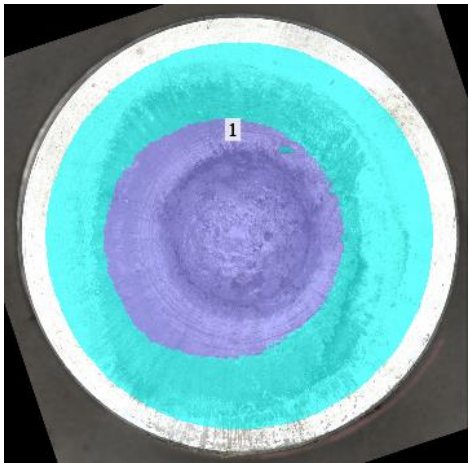

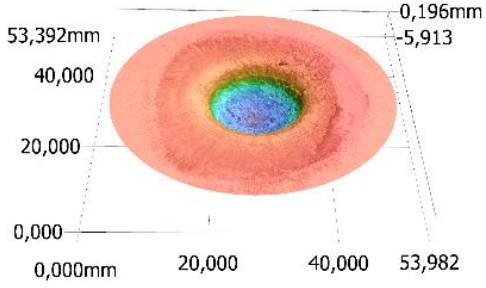

HMX Blast 2	
Measurement 1 [mm³]	1105,94
Measurement 2 [mm³]	1104,81
Average Volume [mm³]	1105,38

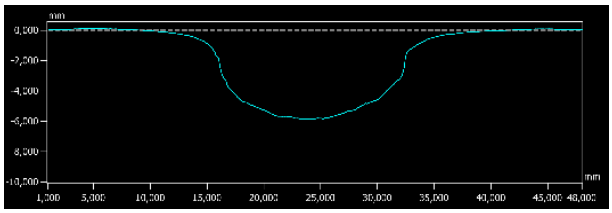

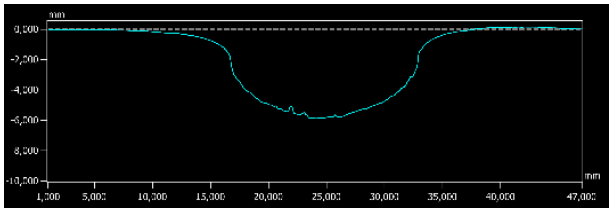

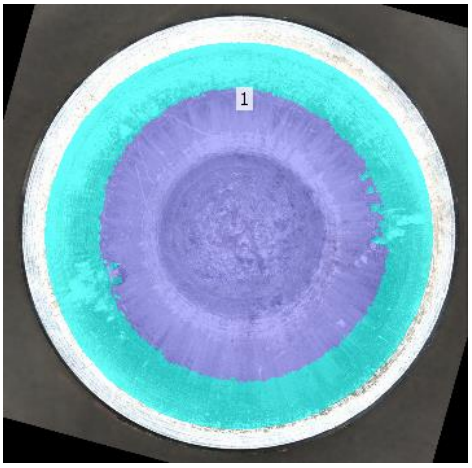

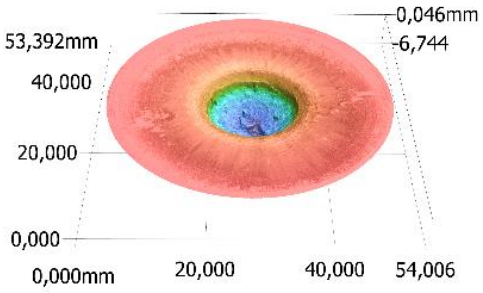

HMX Blast 3	
Measurement 1 [mm³]	1242,43
Measurement 2 [mm³]	1243,95
Average Volume [mm³]	1243,19

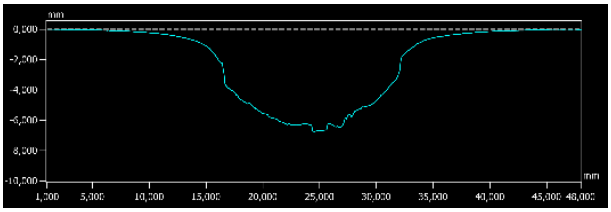

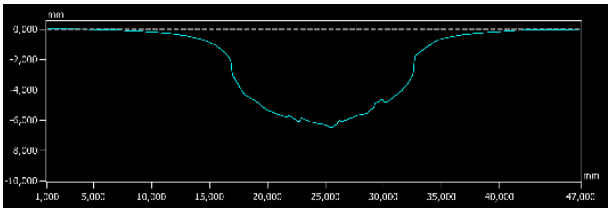

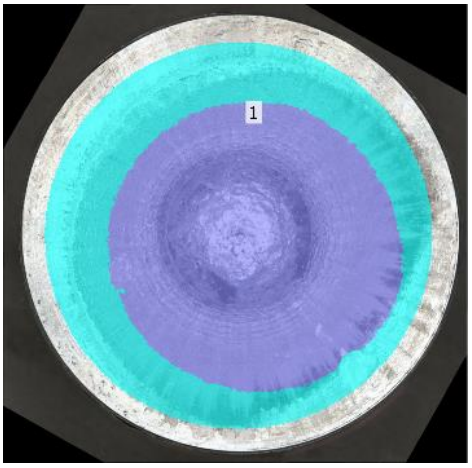

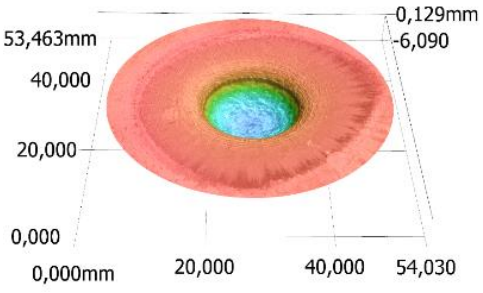

RDX Blast 1	
Measurement 1 [mm³]	1364,01
Measurement 2 [mm³]	1368,30
Average Volume [mm³]	1366,16

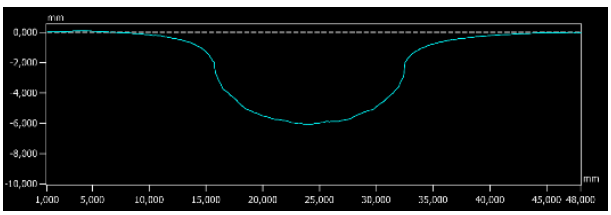

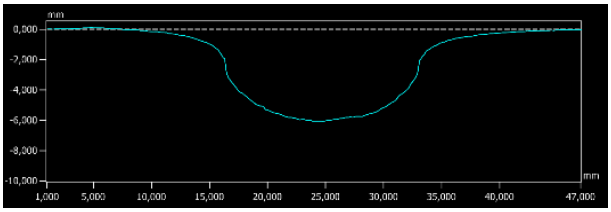

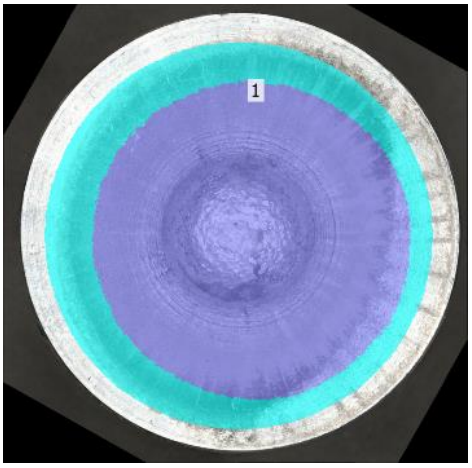

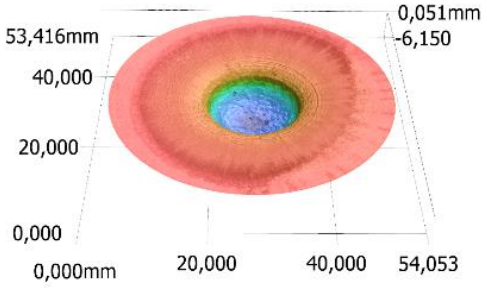

RDX Blast 2	
Measurement 1 [mm³]	1380,13
Measurement 2 [mm³]	1385,88
Average Volume [mm³]	1383,01

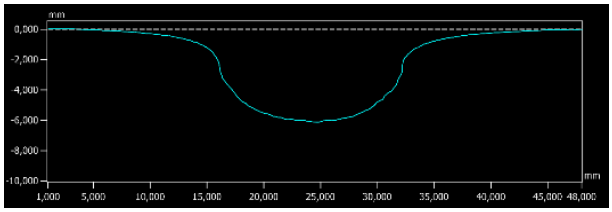

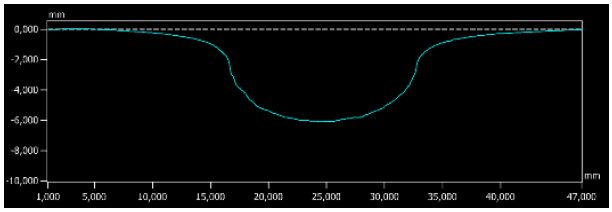

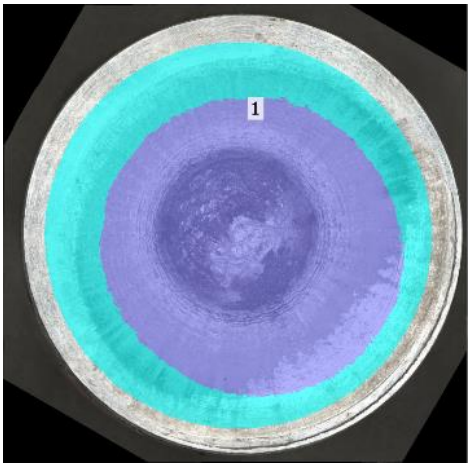

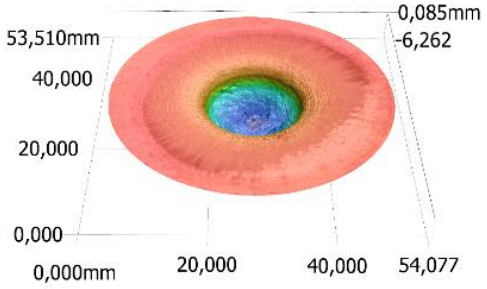

RDX Blast 3	
Measurement 1 [mm³]	1379,36
Measurement 2 [mm³]	1384,62
Average Volume [mm³]	1381,99

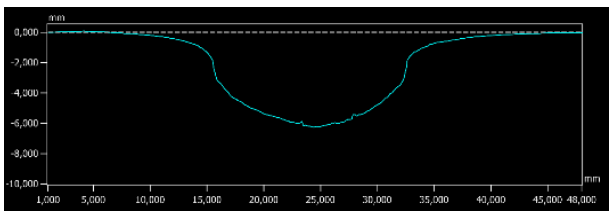

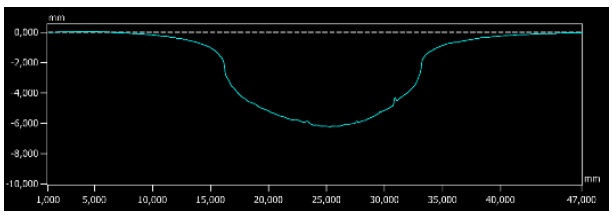

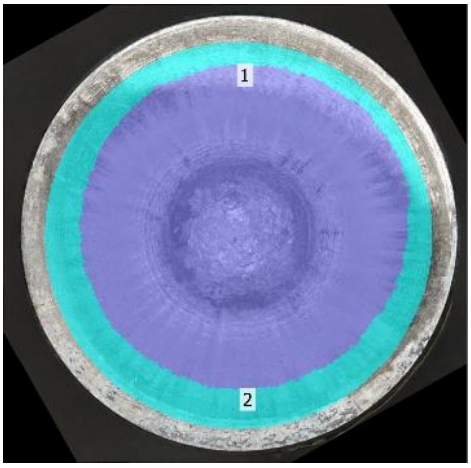

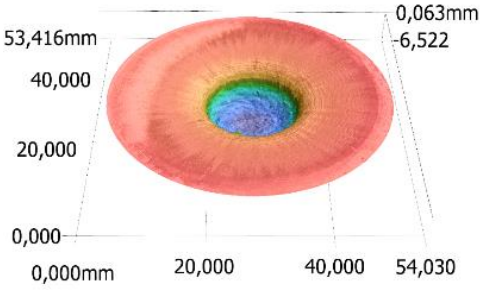

CL-20 Blast 1	
Measurement 1 [mm³]	1510,05
Measurement 2 [mm³]	1520,95
Average Volume [mm³]	1515,50

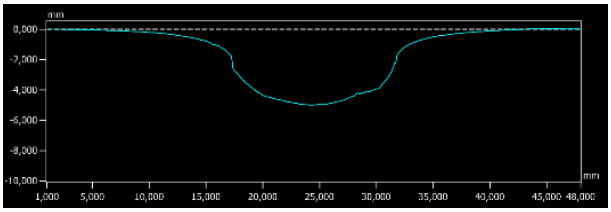

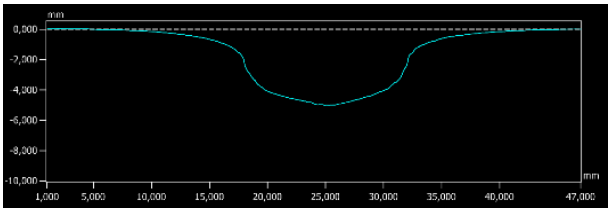

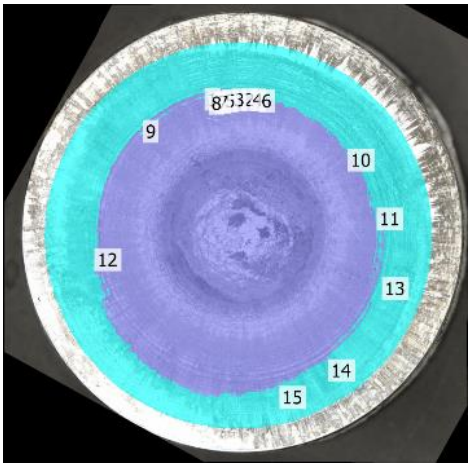

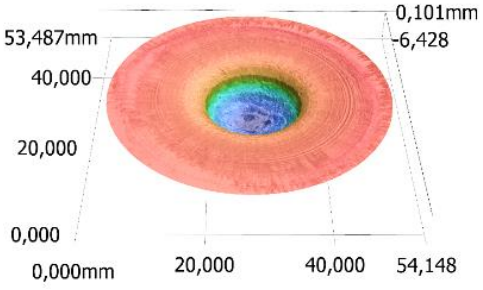

CL-20 Blast 2	
Measurement 1 [mm³]	1407,47
Measurement 2 [mm³]	1408,67
Average Volume [mm³]	1408,07

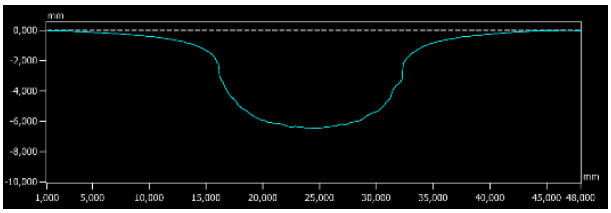

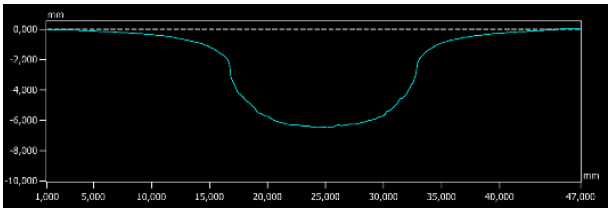

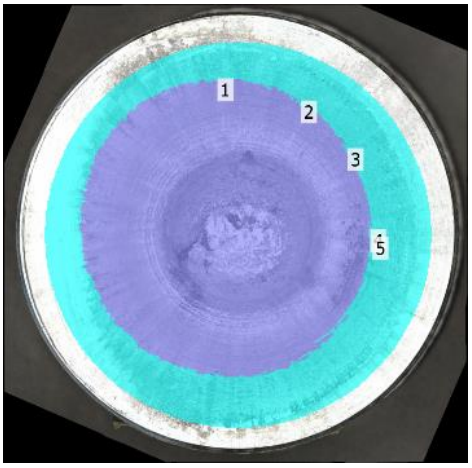

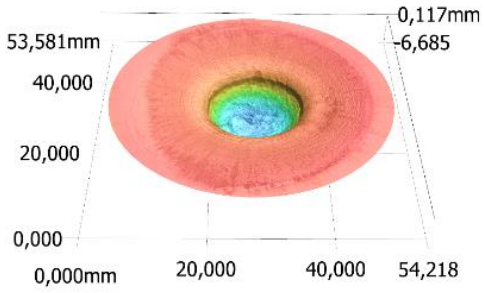

CL-20 Blast 3	
Measurement 1 [mm³]	1409,16
Measurement 2 [mm³]	1405,90
Average Volume [mm³]	1407,53

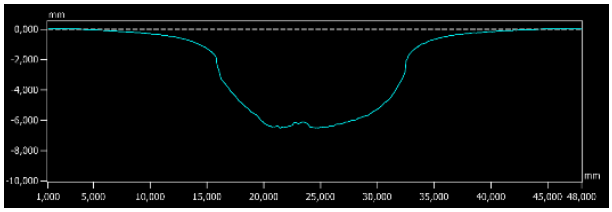

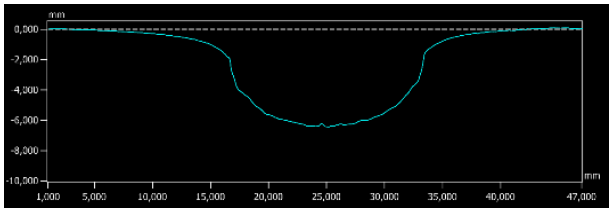

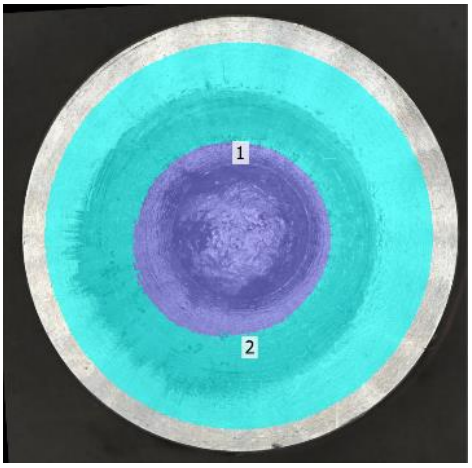

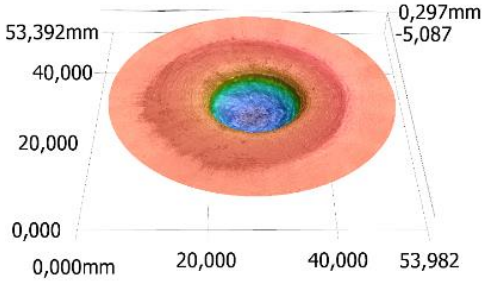

TNT Blast 1	
Measurement 1 [mm³]	848,07
Measurement 2 [mm³]	847,79
Average Volume [mm³]	847,93

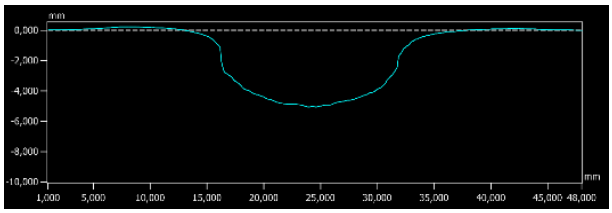

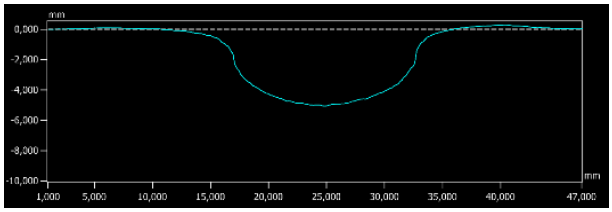

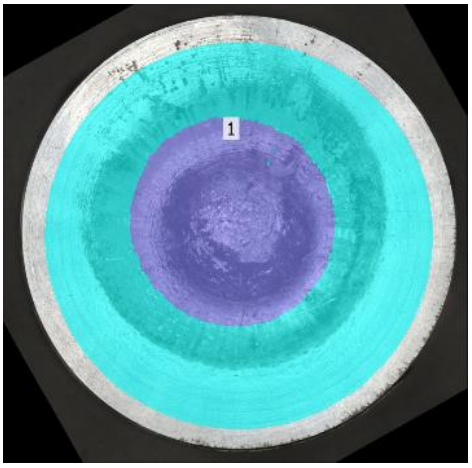

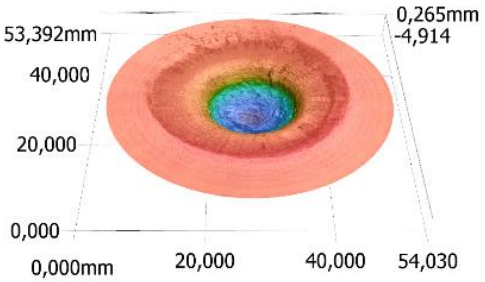

TNT Blast 2	
Measurement 1 [mm³]	828,94
Measurement 2 [mm³]	830,05
Average Volume [mm³]	829,49

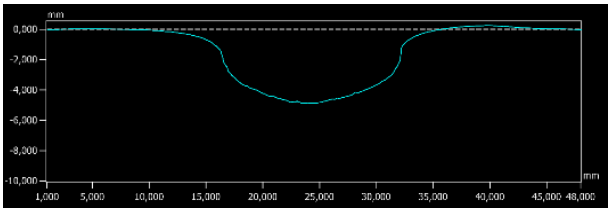

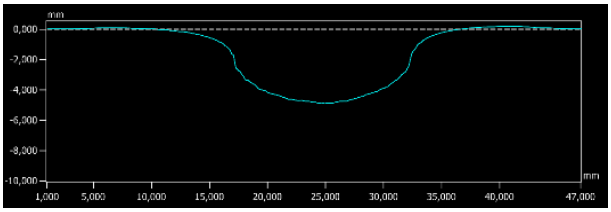

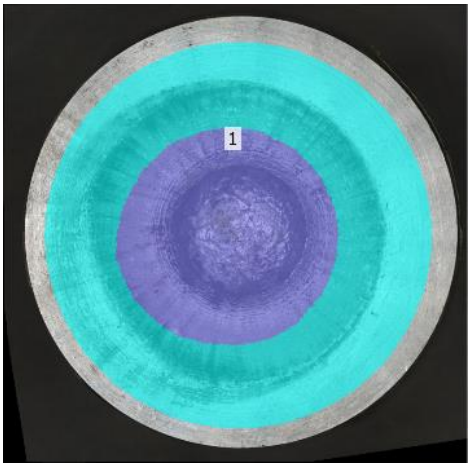

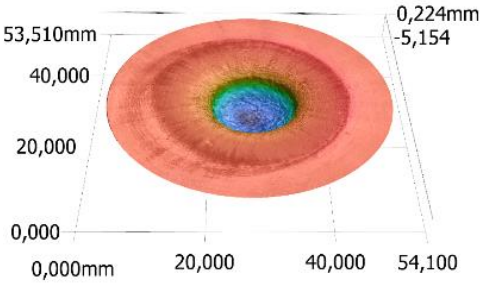

TNT Blast 3	
Measurement 1 [mm³]	860,02
Measurement 2 [mm³]	860,44
Average Volume [mm³]	860,23

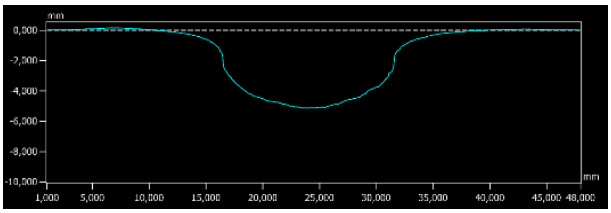

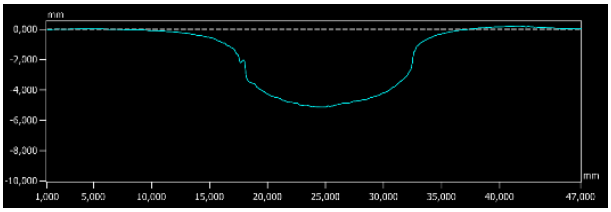

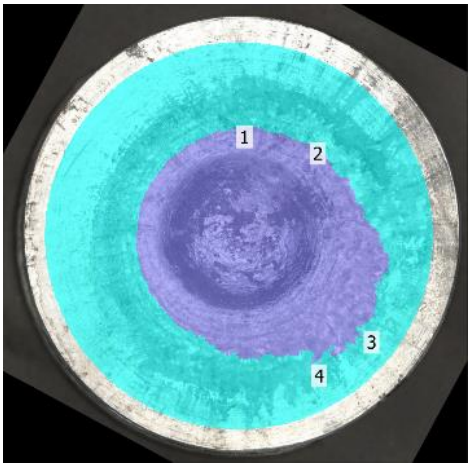

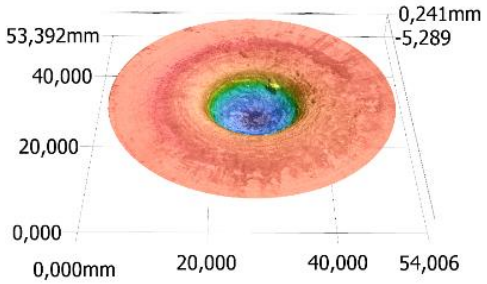

PA Blast 1	
Measurement 1 [mm³]	928,57
Measurement 2 [mm³]	927,95
Average Volume [mm³]	928,26

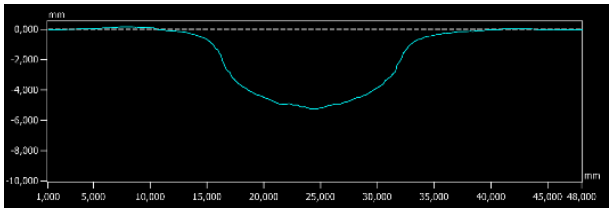

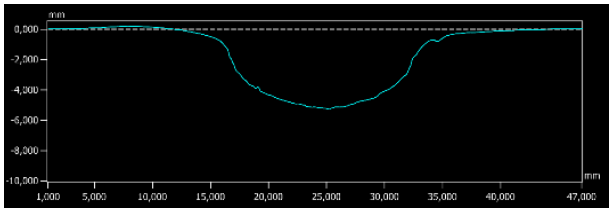

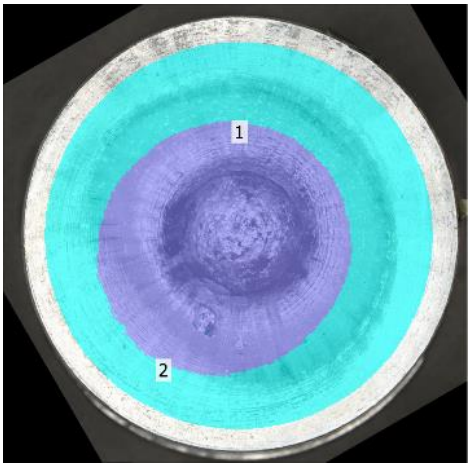

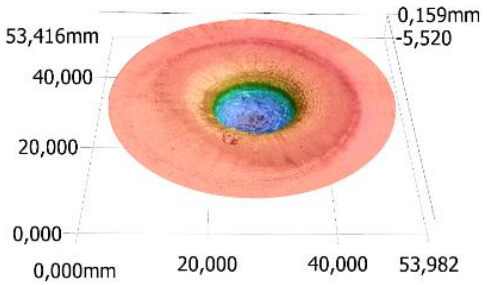

PA Blast 2	
Measurement 1 [mm³]	954,40
Measurement 2 [mm³]	954,53
Average Volume [mm³]	954,47

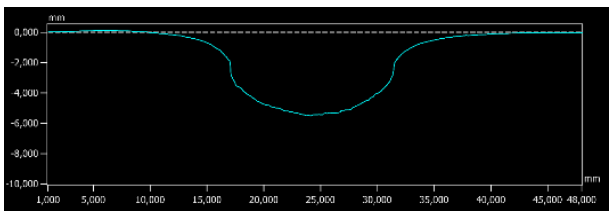

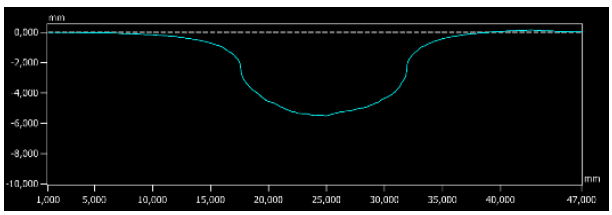

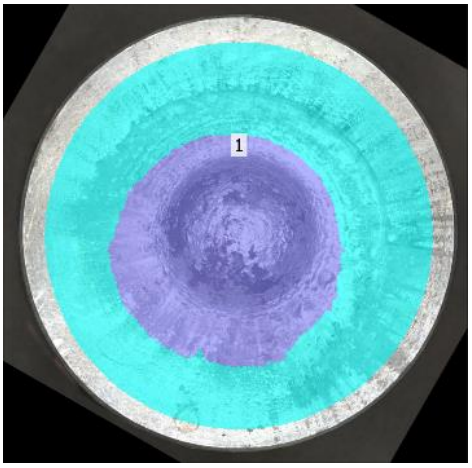

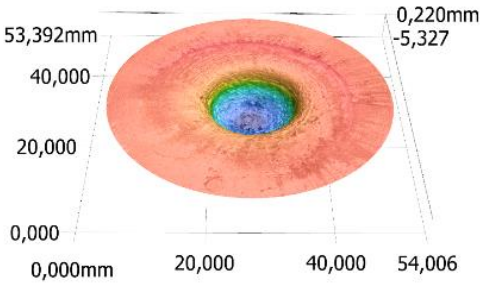

PA Blast 3	
Measurement 1 [mm³]	902,45
Measurement 2 [mm³]	901,41
Average Volume [mm³]	901,93

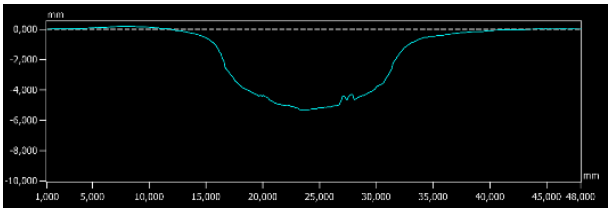

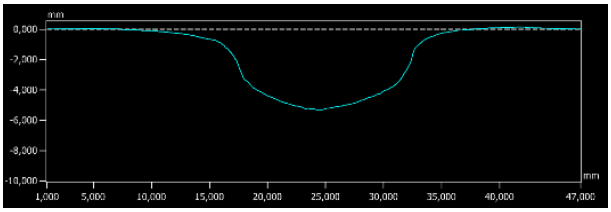

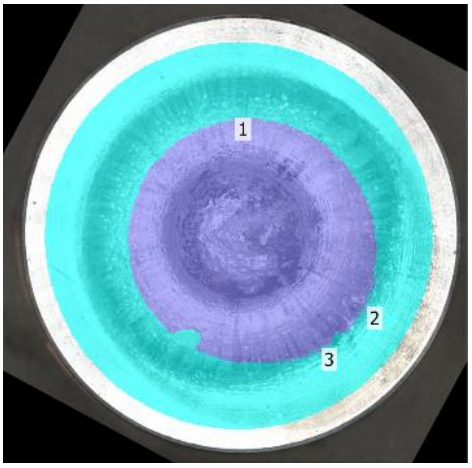

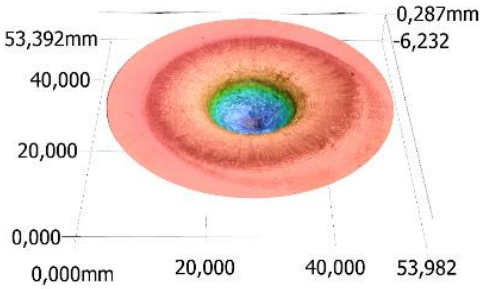

HNS Blast 1	
Measurement 1 [mm³]	974,48
Measurement 2 [mm³]	972,07
Average Volume [mm³]	973,27

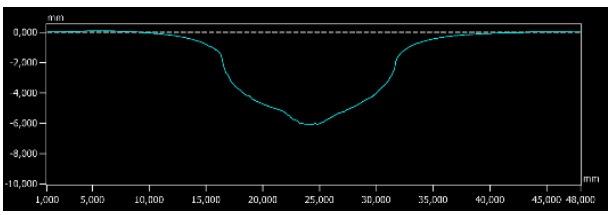

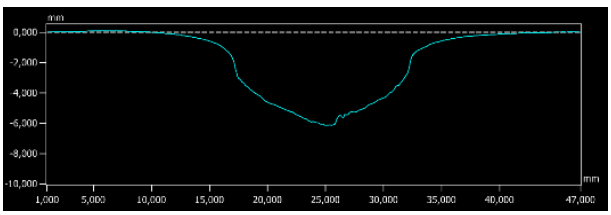

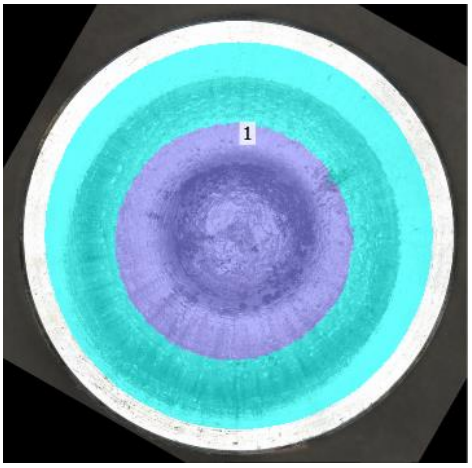

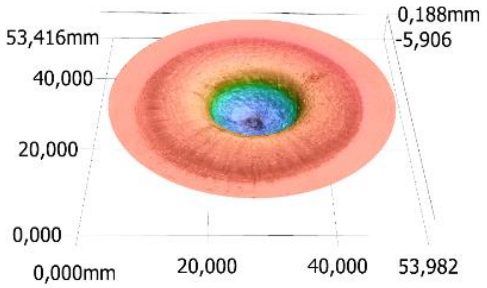

HNS Blast 2	
Measurement 1 [mm³]	999,16
Measurement 2 [mm³]	984,96
Average Volume [mm³]	992,06

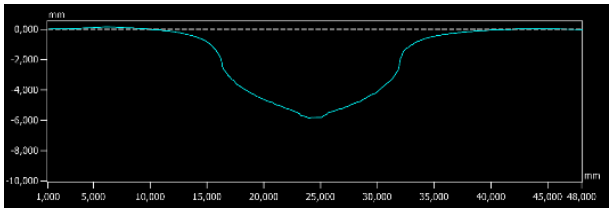

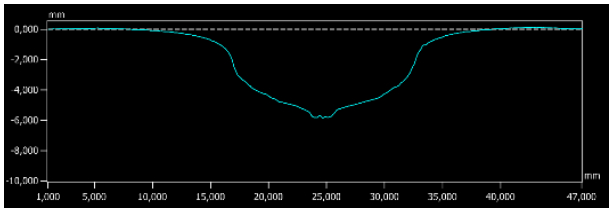

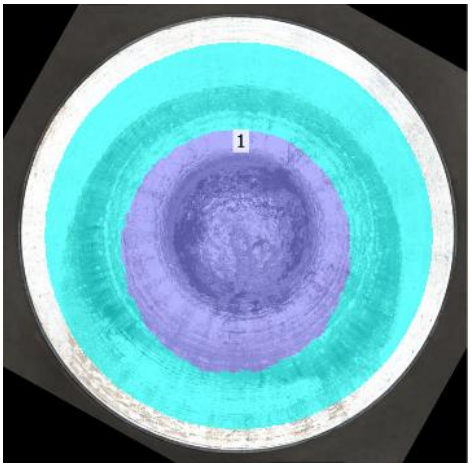

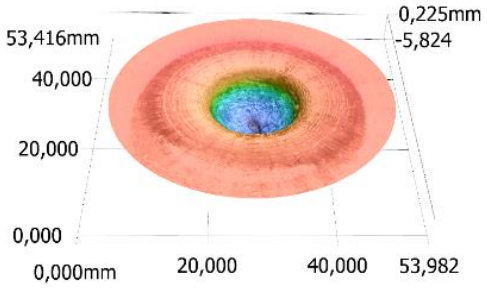

HNS Blast 3	
Measurement 1 [mm³]	948,85
Measurement 2 [mm³]	948,76
Average Volume [mm³]	948,80

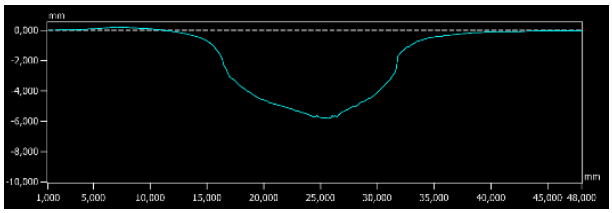

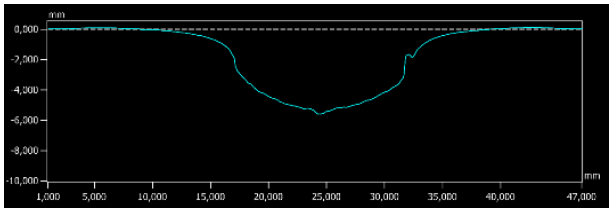

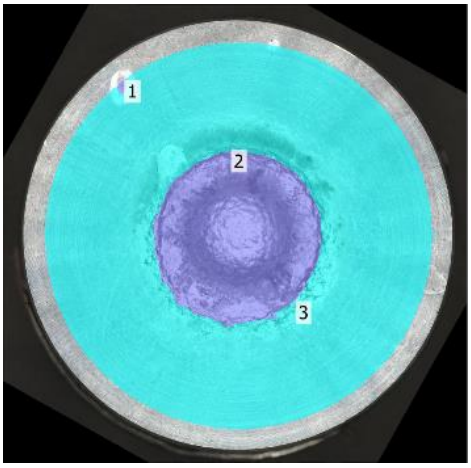

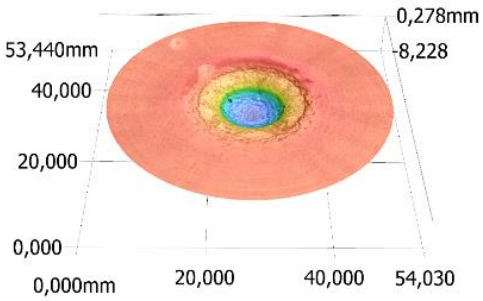

Tetrazole Blast 1	
Measurement 1 [mm³]	588,23
Measurement 2 [mm³]	592,25
Average Volume [mm³]	590,24

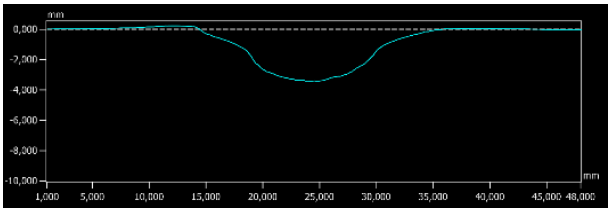

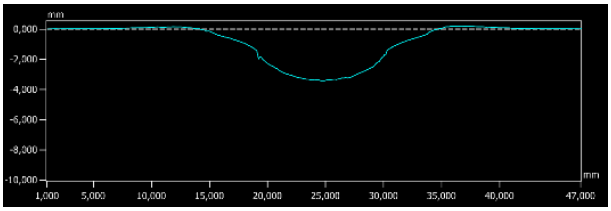

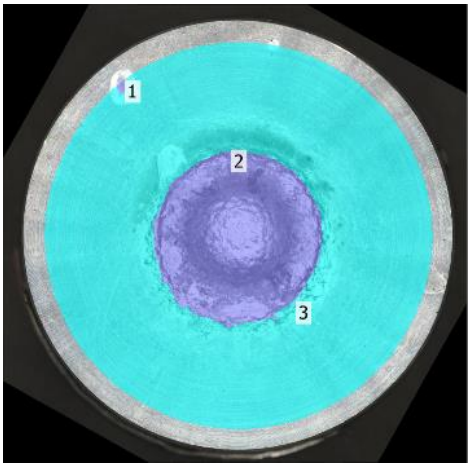

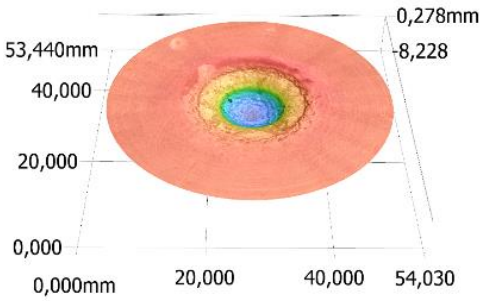

Tetrazole Blast 2	
Measurement 1 [mm³]	387,45
Measurement 2 [mm³]	379,32
Average Volume [mm³]	383,38

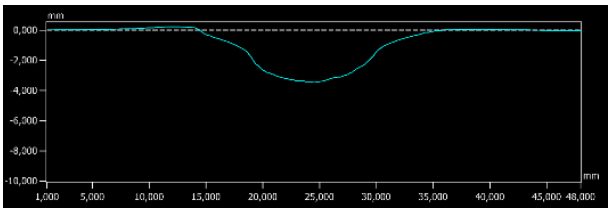

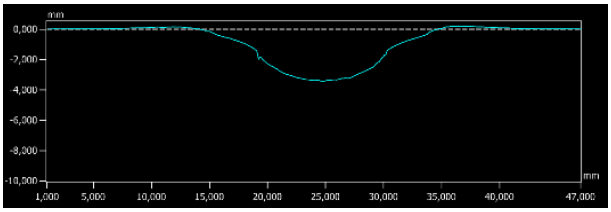

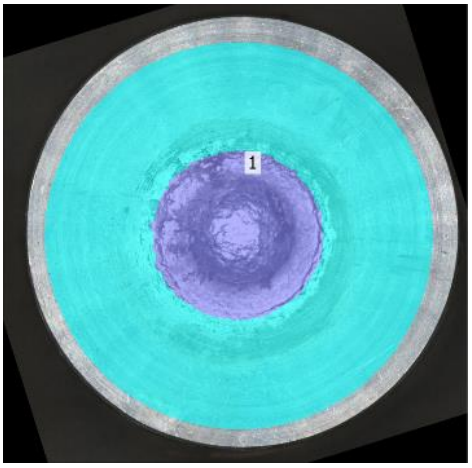

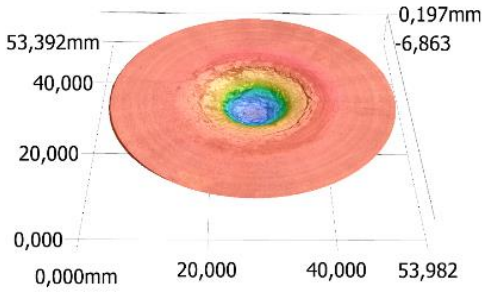

Tetrazole Blast 3	
Measurement 1 [mm³]	385,31
Measurement 2 [mm³]	388,29
Average Volume [mm³]	386,80

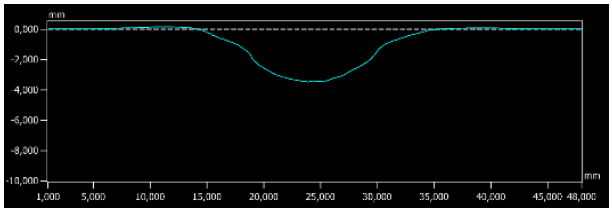

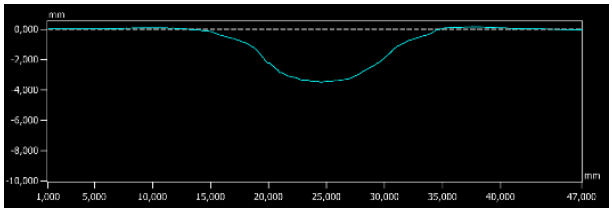

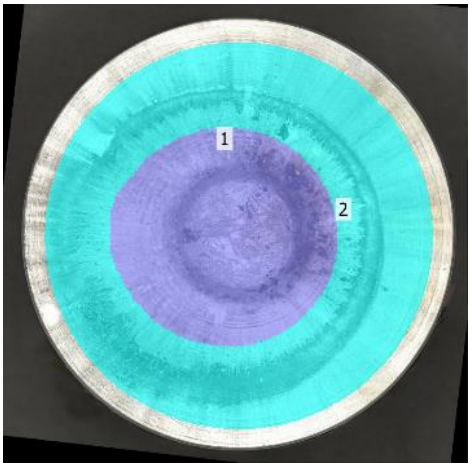

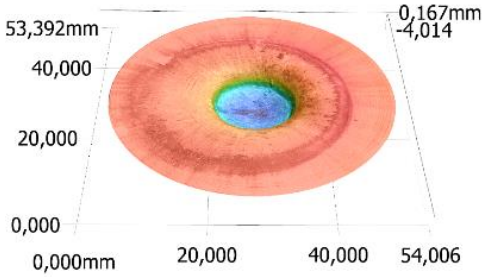

BODN Blast 1	
Measurement 1 [mm³]	640,19
Measurement 2 [mm³]	634,97
Average Volume [mm³]	637,58

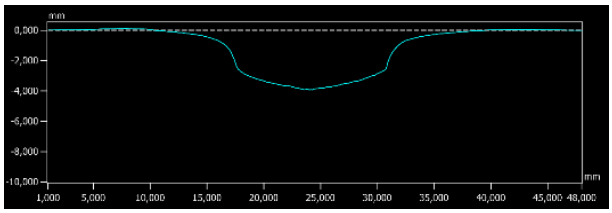

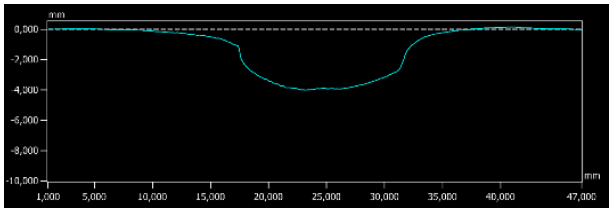

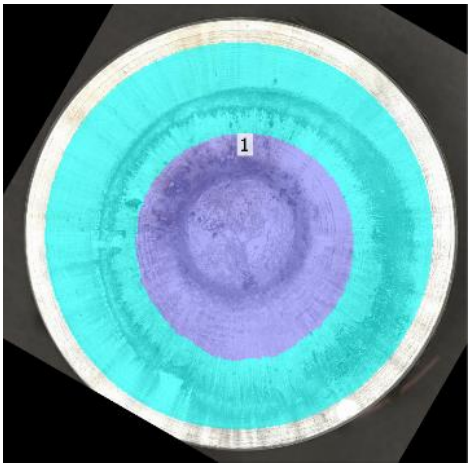

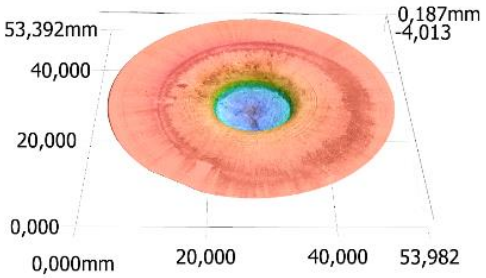

BODN Blast 2	
Measurement 1 [mm³]	315,13
Measurement 2 [mm³]	314,80
Average Volume [mm³]	314,97

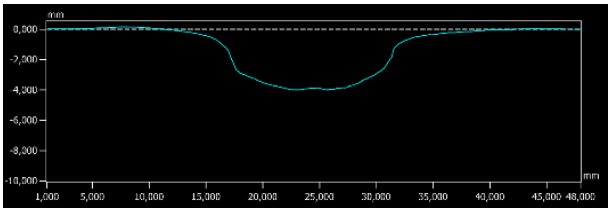

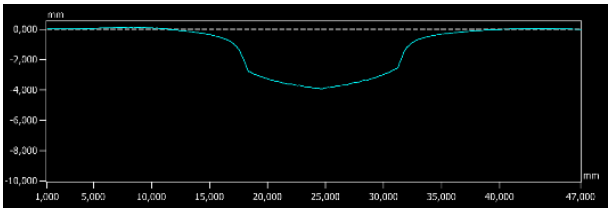

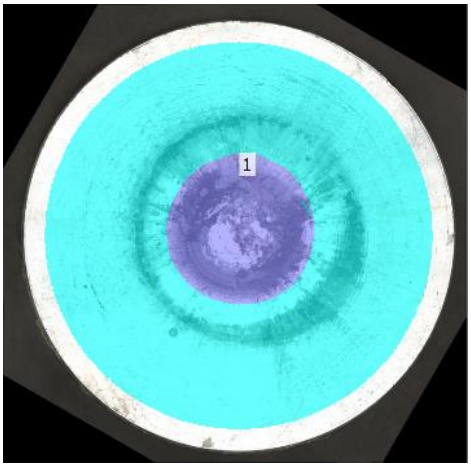

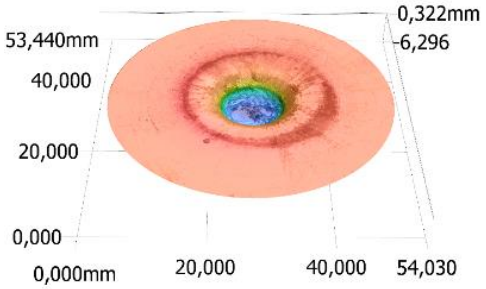

BODN Blast 3	
Measurement 1 [mm³]	353,49
Measurement 2 [mm³]	351,29
Average Volume [mm³]	352,39

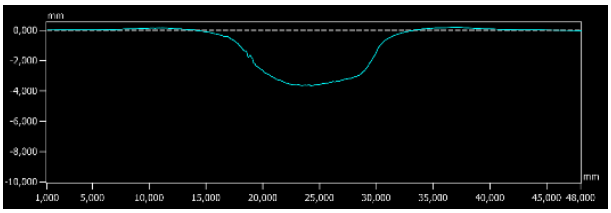

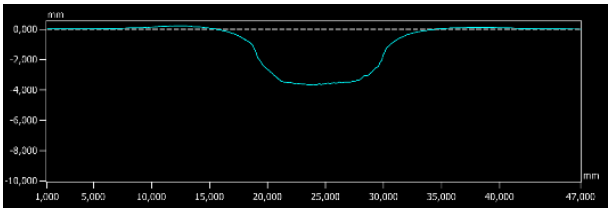

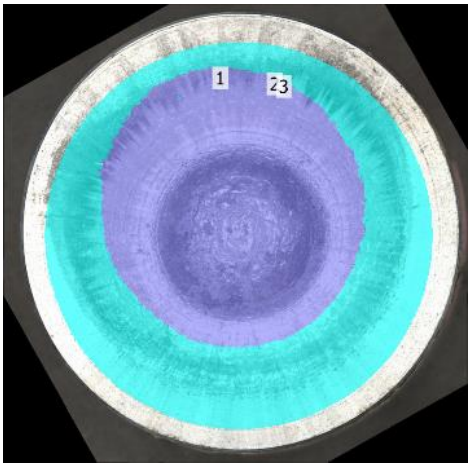

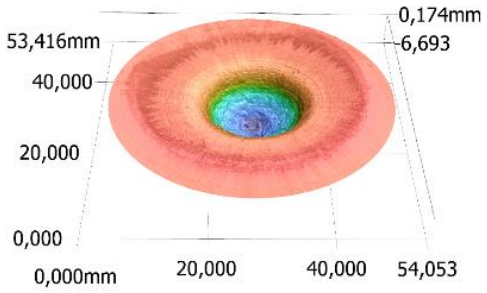

3,4-DN-1-NMP Blast 1	
Measurement 1 [mm³]	1256,76
Measurement 2 [mm³]	1257,21
Average Volume [mm³]	1256,98

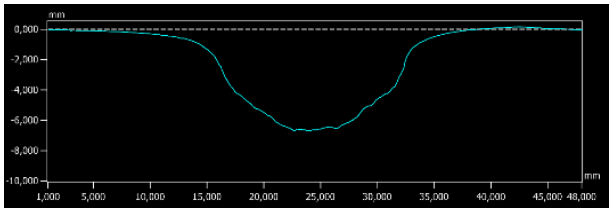

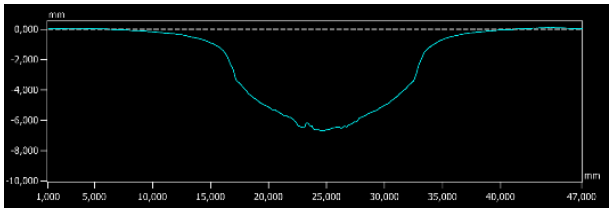

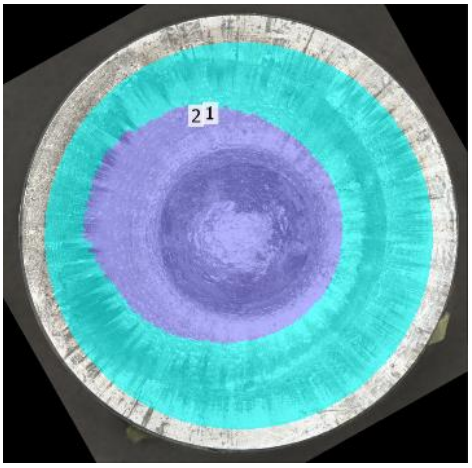

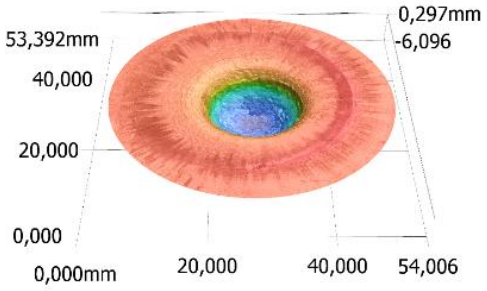

3,4-DN-1-NMP Blast 2	
Measurement 1 [mm³]	1171,79
Measurement 2 [mm³]	1170,75
Average Volume [mm³]	1171,27

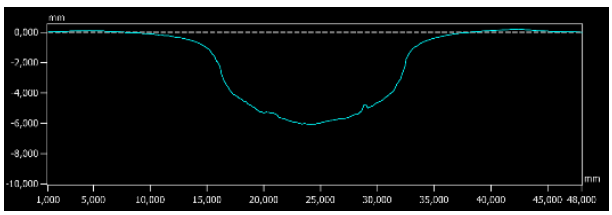

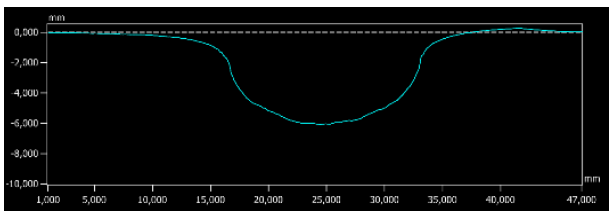

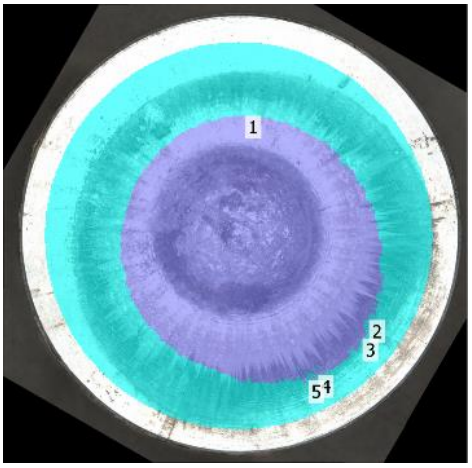

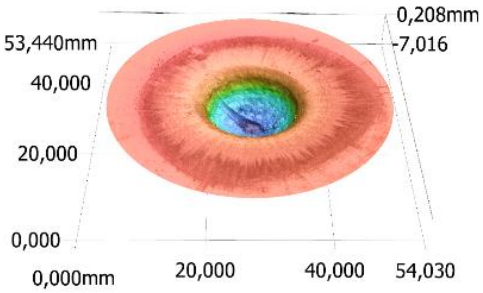

3,4-DN-1-NMP Blast 3	
Measurement 1 [mm³]	1218,68
Measurement 2 [mm³]	1223,13
Average Volume [mm³]	1220,90

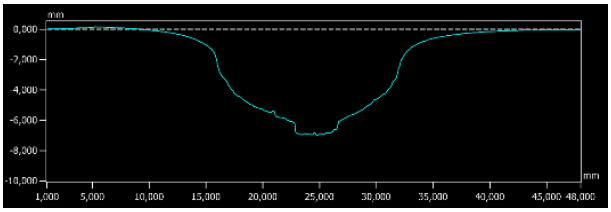

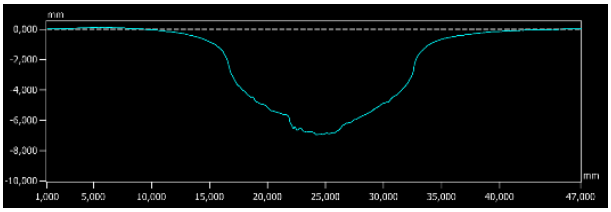

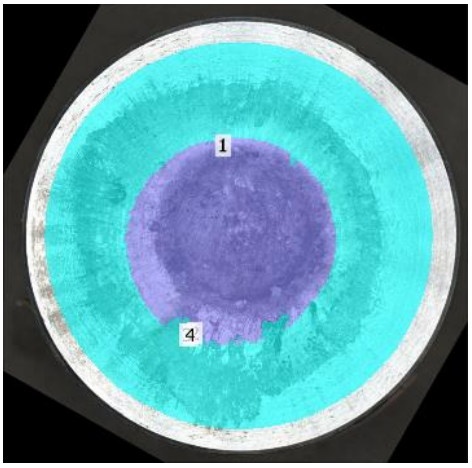

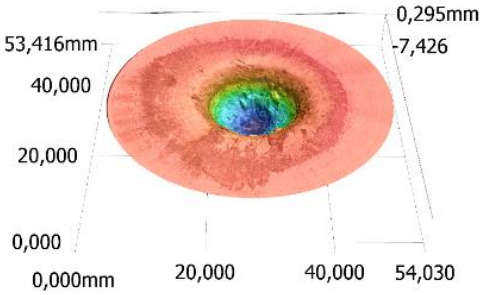

BTNPM Blast 1	
Measurement 1 [mm³]	1020,68
Measurement 2 [mm³]	1011,18
Average Volume [mm³]	1015,93

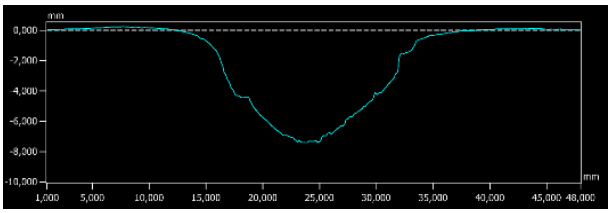

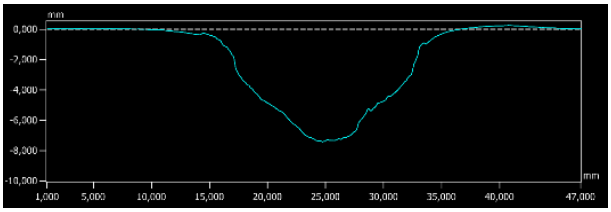

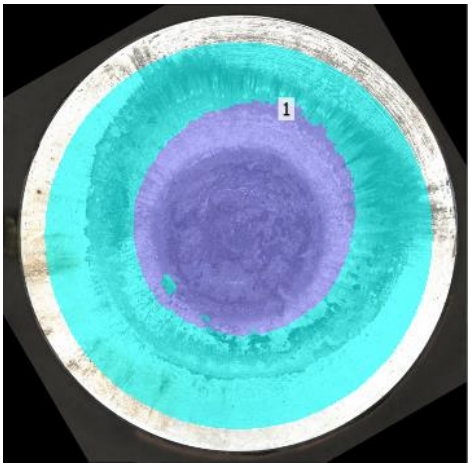

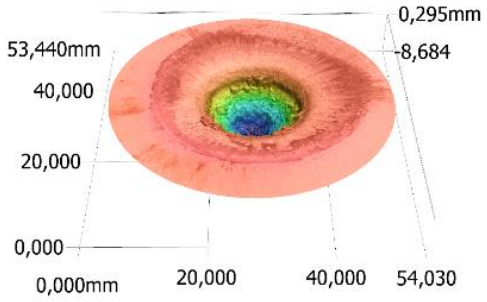

BTNPM Blast 2	
Measurement 1 [mm³]	1152,95
Measurement 2 [mm³]	1158,62
Average Volume [mm³]	1155,79

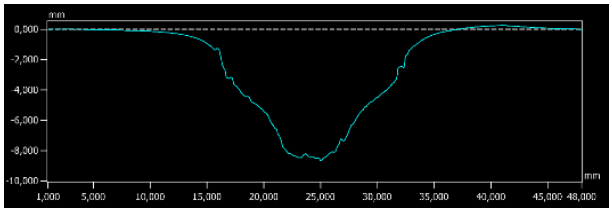

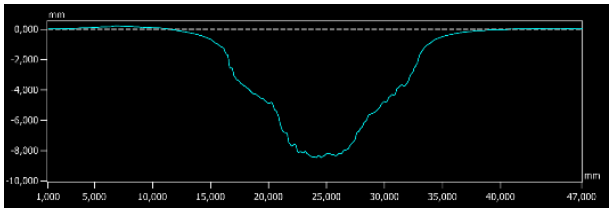

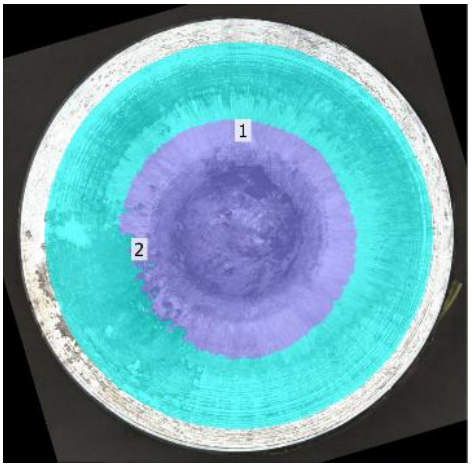

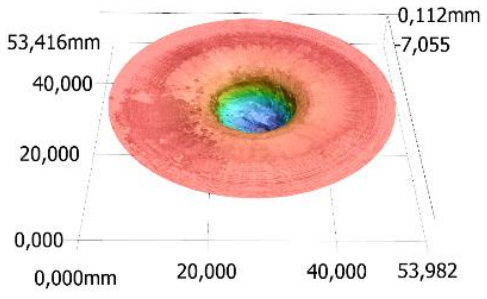

BTNPM Blast 3	
Measurement 1 [mm³]	921,21
Measurement 2 [mm³]	920,12
Average Volume [mm³]	920,67

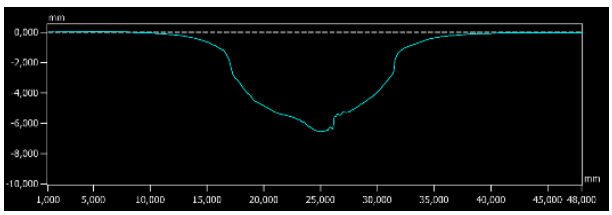

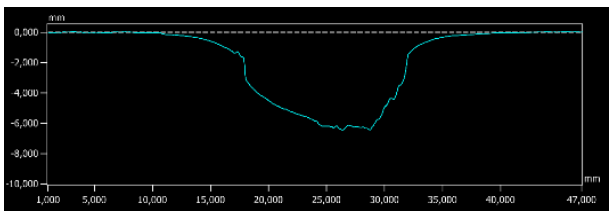

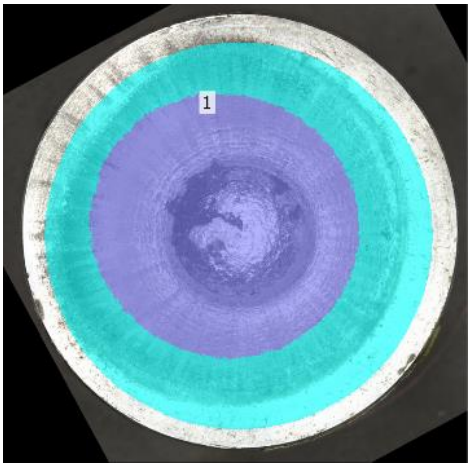

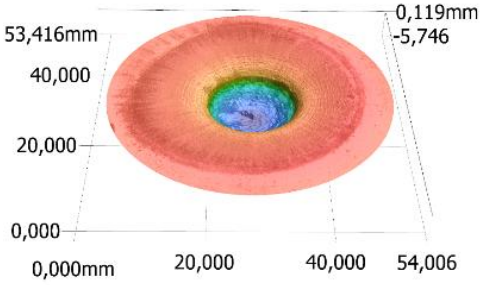

MAD-X1 Blast 1	
Measurement 1 [mm³]	1078,53
Measurement 2 [mm³]	1077,55
Average Volume [mm³]	1078,04

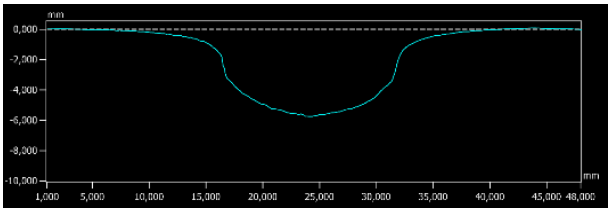

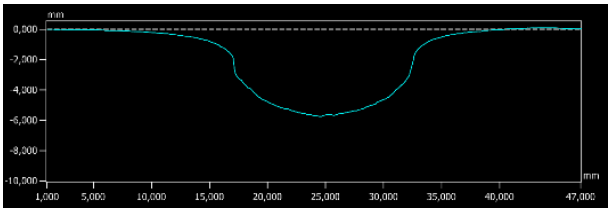

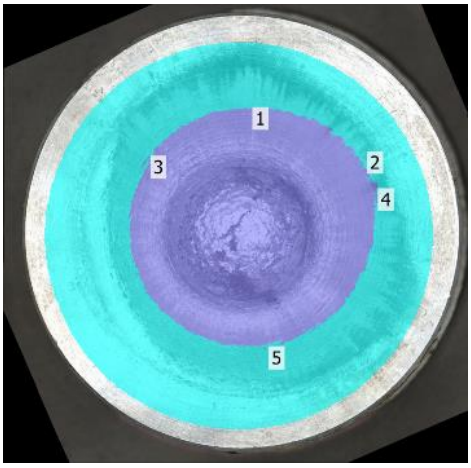

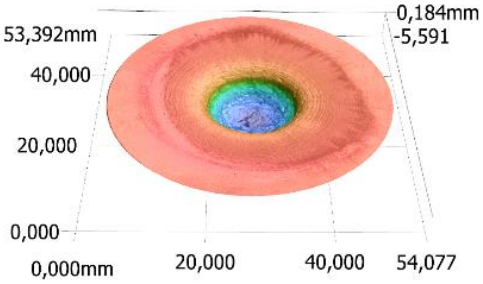

MAD-X1 Blast 2	
Measurement 1 [mm³]	1006,67
Measurement 2 [mm³]	1006,28
Average Volume [mm³]	1006,48

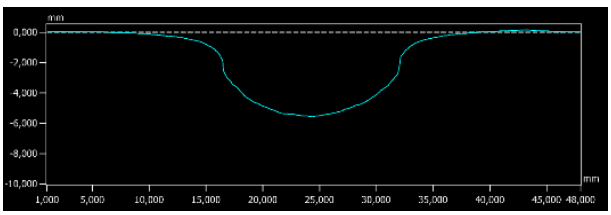

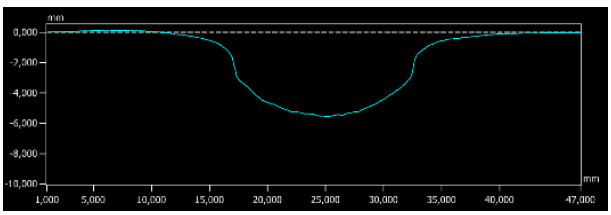

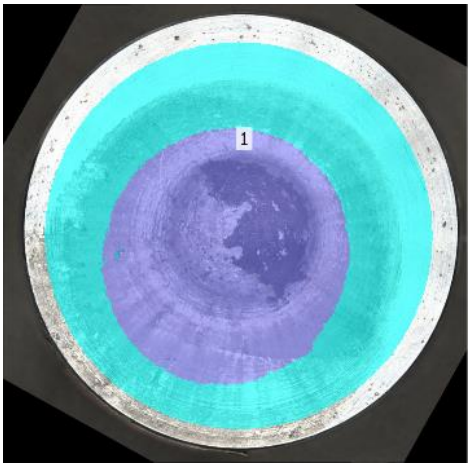

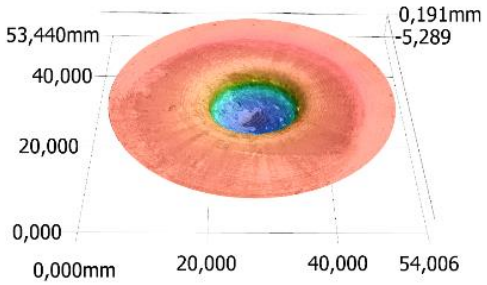

MAD-X1 Blast 3	
Measurement 1 [mm³]	990,21
Measurement 2 [mm³]	986,10
Average Volume [mm³]	988,15

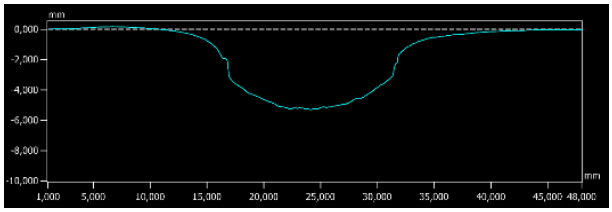

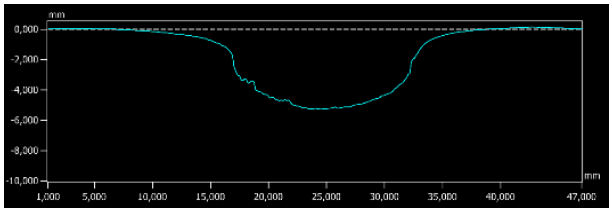

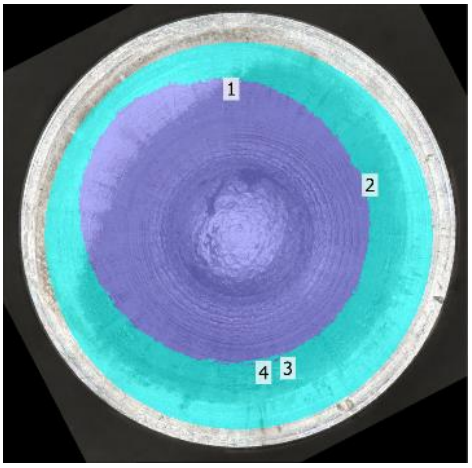

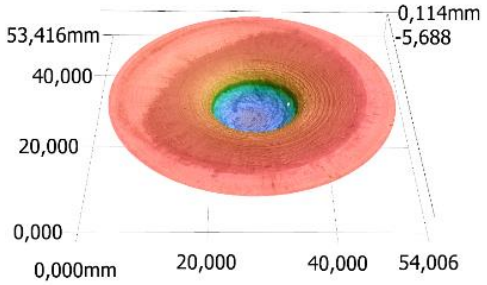

TKX-50 Blast 1	
Measurement 1 [mm³]	1108,27
Measurement 2 [mm³]	1107,29
Average Volume [mm³]	1107,78

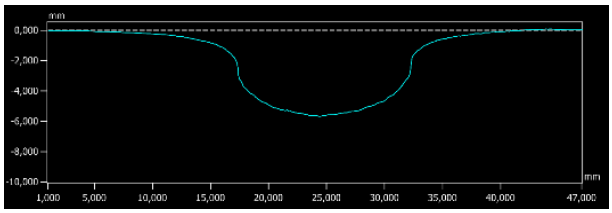

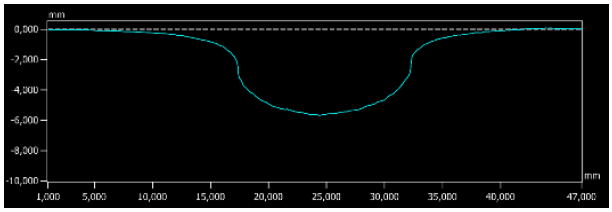

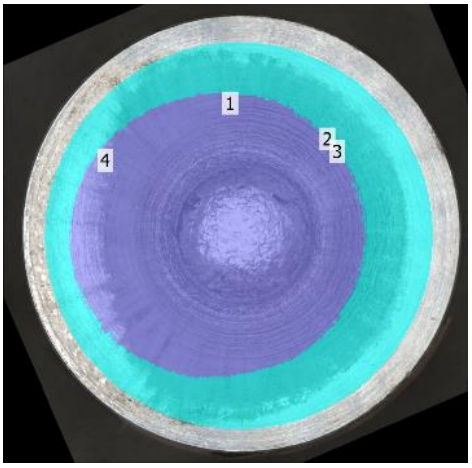

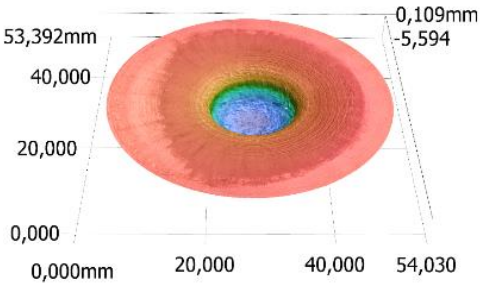

TKX-50 Blast 2	
Measurement 1 [mm³]	1128,52
Measurement 2 [mm³]	1127,22
Average Volume [mm³]	1127,87

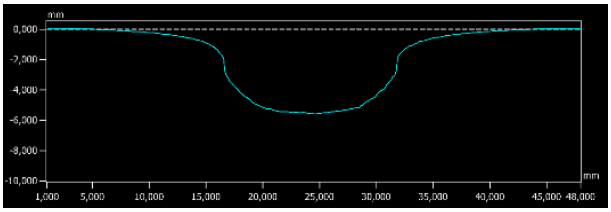

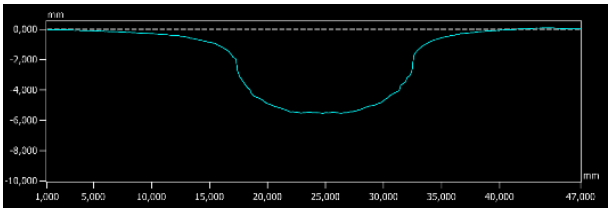

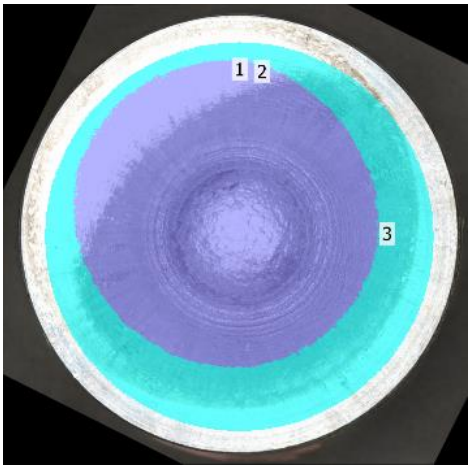

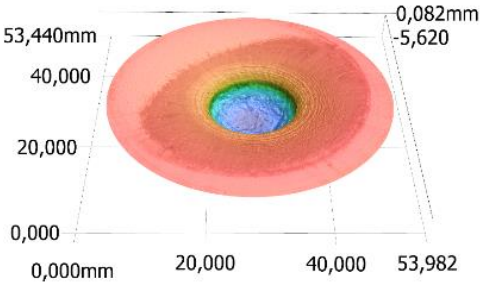

TKX-50 Blast 3	
Measurement 1 [mm³]	1158,13
Measurement 2 [mm³]	1161,77
Average Volume [mm³]	1159,95

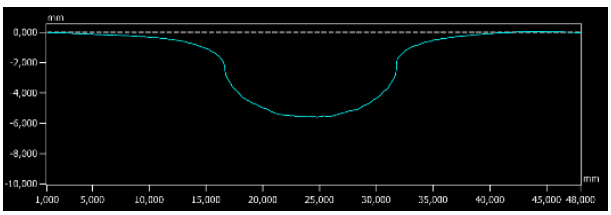

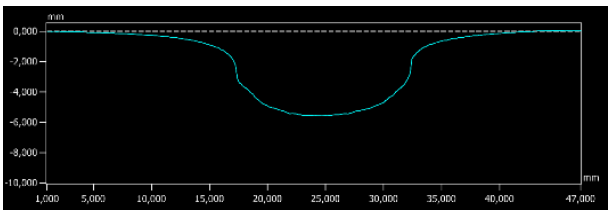

17. Summary and Conclusion

In context of this thesis, it was possible to complete 15 publications as first author or shared first author. All scientific chapters (2–16) of this work have been published or are at least accepted or in the review process in peer-reviewed journals, which are listed below:

- Journal of the American Chemical Society (2x) (*J. Am. Chem. Soc.*)
- Organic Letters (*Org. Lett.*)
- Chemistry – A European Journal (*Chem. Eur. J.*)
- Dalton Transaction (*Dalton Trans.*)
- Journal of Organic Chemistry (*J. Org. Chem.*)
- ACS Applied Engeneering Materials (*ACS Appl. Eng. Mater.)*
- Crystal Growth and Design (*Cryst. Growth Des.*)
- Materials Advances (*Mater. Adv.*)
- ChemPlusChem (*ChemPlusChem*)
- European Journal of Organic Chemistry (*Eur. J. Org. Chem.*)
- Energetic Materials Frontiers
- Propellants Explosives and Pyrotechnics (2x) (*Propellants Explos. Pyrotech.*)
- Zeitschrift für Allgemeine und Anorganische Chemie (*Z. anorg. Allg. Chem.*)

As indicated in the motivation of the thesis, new explosives were synthesized through the extended use of tetrazole and azide building blocks. The results of these synthetic projects are described in chapters 2–14 and will be extensively summarized in the following. For the analysis of the new compounds, a variety of analytical and spectroscopic methods were used to verify both purity and cleanliness. In addition, all energetic compounds were analyzed by means of various mechanical and physicochemical tests, which provide conclusions for their safe use as well as for their suitability as explosive materials. This involves:

- multinuclear NMR spectroscopy (mainly ^{1}H, ^{13}C, ^{14}N, ^{15}N),
- infrared spectroscopy (IR),

- Raman spectroscopy,
- elemental analysis (CHNO),
- mass spectrometry (ESI and EI),
- scanning electron microscopy,
- thermal gravimetric analysis (TGA),
- differential scanning calorimetry (DSC),
- differential thermal analysis (DTA),
- X-ray diffraction,
- sensitivity measurements (BAM drophammer, BAM friction tester, ESD tester),
- hot needle test,
- hot plate test,
- small-scale shock reactivity test (SSRT),
- initiation test toward PETN.

One of the most important analytical methods was the X-ray structural analysis of crystals. Besides the absolute certainty of a successful reaction, it provided precise densities, which were essential for the calculation of detonation properties. A total of 82 new crystal structures were measured and published. Most of the obtained crystal structures were assigned to triclinic, monoclinic or orthorhombic crystal systems, with just over half of the compounds crystallizing in $P2_1/n$ or $P2_1/c$ (Figure 1).

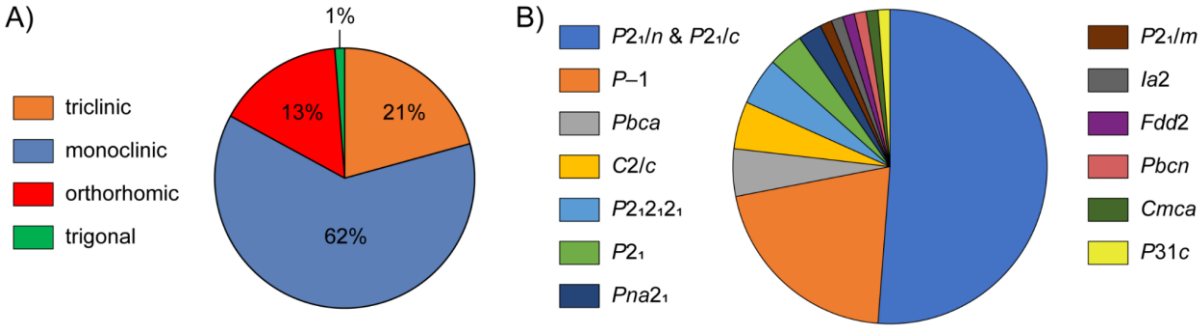

Figure 1. A) subdivision of the measured crystal structures into the respective crystal systems; B) subdivision of the measured crystal structures into the respective space groups.

In addition to the main synthetic part, intensive studies were carried out on the SSR test (small-scale shock reactivity test), which can be classified as another standard test for the early-stage energetic characterization of secondary explosives. As the name

suggests, the SSR test uses a relatively small amount of substance (approximately 500 mg per shot) to measure an initial level of shock sensitivity of the tested substance, which is an indication of the particular explosiveness and the critical diameter. The results of these studies are summarized in chapters 15–16.

Chapter 2 deals with the synthesis and characterization of nitrocarbamoyl azide (HNCA) as a highly energetic member of the substance class of carbonyl azides. HNCA was obtained through diazotization of nitro semicarbazide (Figure 2). Next to the neutral parent compound, which is stable in pure and dry state at room temperature, a series of salts were synthesized through reaction with the respective bases. Particularly remarkable here were the hydroxylammonium derivative, which exhibits a detonation velocity of 9460 m s^{-1} but is sensitive toward hydrolysis, and the potassium salt, which can be used as a primary explosive due to its suitable sensitivities. Next to the ionic derivatives, the decomposition pathway of HNCA in protic solvents was studied. In contrast to the typical behavior of carbonyl azides, decomposition does not occur via the Curtius rearrangement including the elimination of N_2 toward the respective isocyanate, but rather nitroisocyanate is formed by HN_3 elimination, here. Through trapping experiments using methanol and hydrazine, the respective addition products could be detected, whereby the decomposition path could be inferred.

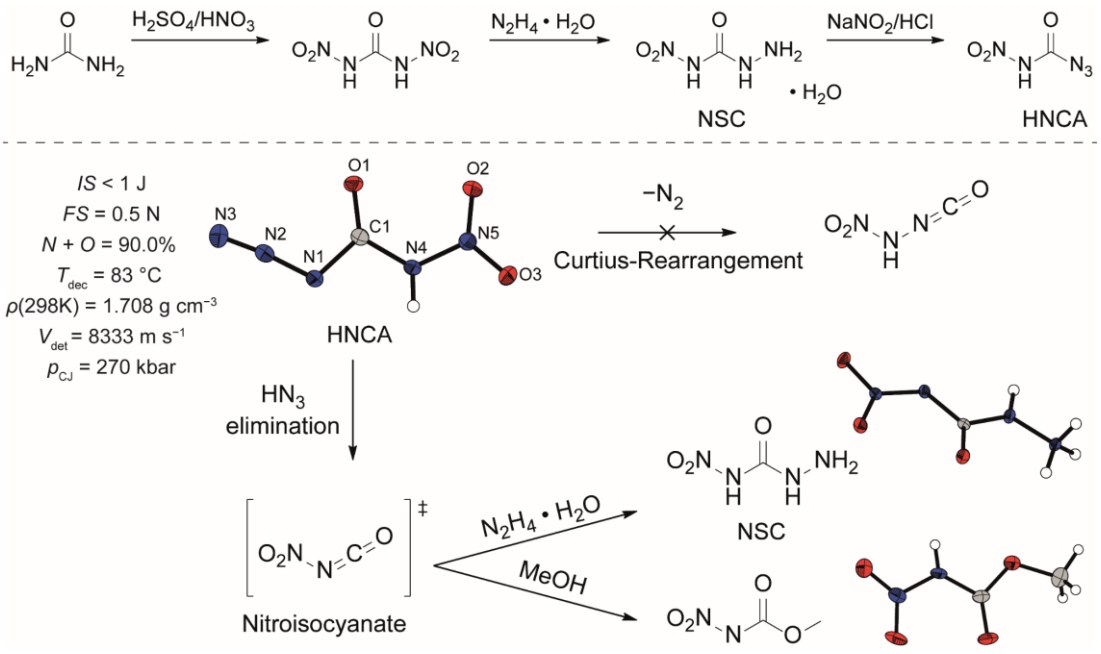

Figure 2. Top: synthetic pathway toward nitrocarbamoyl azide (HNCA); bottom: crystal structure of HNCA with key properties and decomposition pathway including trapping experiments using methanol and hydrazine.

The scope of **Chapter 3** was the synthesis of ionic derivatives as well as energetic coordination compounds (ECCs) based on the nitrocyanamide anion (NCA^-). The study was inspired by recently published work on energetic coordination compounds of dinitramide (DN^-)[1] and dicyanamide (DCA^-)[2] as anions. By following the same approach with nitrocyanamide, which is a hybrid of these two structures, it was intended to combine the advantages and exclude the drawbacks of DN^- and DCA^-, respectively. Nitrocyanamide is precipitated as its silver salt through alkaline promoted diazomethane cleavage of N-methyl-N′-nitro-N-nitrosoguanidine (Figure 3). The metathesis reactions with corresponding nitrogen-rich hydrochlorides yielded the ionic derivatives. All nitrogen-rich salts can be characterized as moderate sensitive to insensitive compounds with decomposition temperatures not exceeding 177 °C and detonation velocities ranging from 7956 m s^{-1} to 8915 m s^{-1}. The complexes are based on $Cu(NCA)_2$, which was generated by reaction of AgNCA with $CuCl_2$. Similar to complexes of DCA^-, NCA^- occurs as a coordinating (via *N*≡C) but not as bridging anion. The sensitivities of all ECCs are not suitable for use as primary explosives, which results in the negative initiation tests toward PETN.

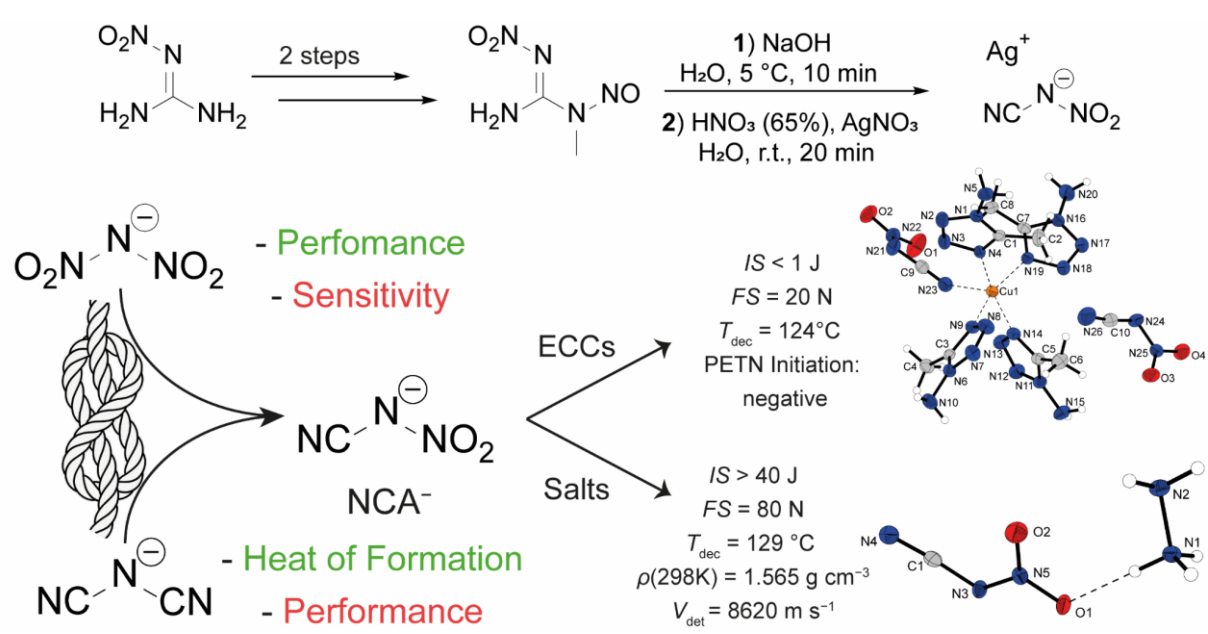

Figure 3. Top: synthetic pathway toward silver nitrocyanamide (AgNCA); bottom left: schematic illustration of the motivation for the investigation of NCA^- as hybrid molecule of dicyanamide and dinitramide; bottom right: representation of crystal structure and key parameters of $[Cu(AMT)_4(NCA](NCA)$ and $(N_2H_5)NCA$.

Chapter 4 covers the chemistry of azidomethyl units linked to selected bi- or tri-heterocycles. The target was to develop energetic compounds with a suitable melting

point for use as melt-castable explosives. This concept was recently realized with some of the utilized heterocyclic scaffolds in combination with nitratomethyl groups.[3-4] The synthesis of the respective compounds was performed via the respective chloromethyl precursors and subsequent chlorine azide exchange in acetonitrile or water (Figure 4). The bis-azidomethyl derivatives of 3,4-bis-(1,2,4-oxadiazol-3-yl)-fuazan and 3,4-bis-(1,2,4-oxadiazol-3-yl)-furoxan were obtained as liquids and 4,4′,5,5′-tetrakis(azidomethyl)-3,3′-bisisoxazole was obtained in the form of a low-melting and extremely sensitive solid. But for 3,3′-bis(azidomethyl)-5,5′-bis(1,2,4-oxadiazole) (DAMBO) the exactly right melting range desired for new melt-cast explosives was hit. DAMBO melts at 70 °C while decomposing at 209 °C. It is available starting from diaminoglyoxime, chloroacetyl chloride and sodium azide in easy and good yielding two step synthesis. In terms of performance, it is superior to TNT while possessing nearly the same crystallographic density. Remarkably is the insensitivity of DAMBO toward impact and friction (IS > 40 J, FS > 360 N).

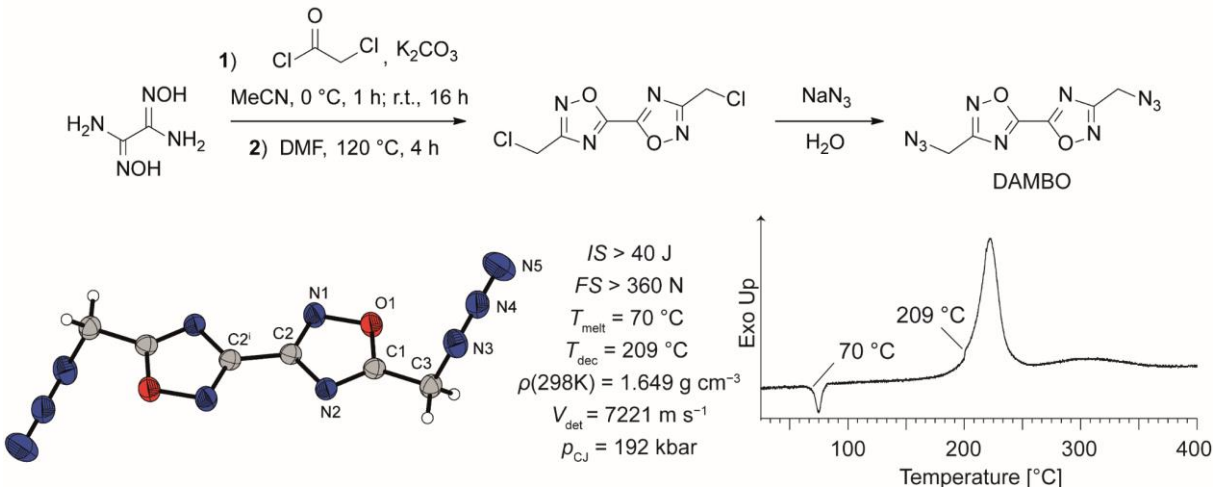

Figure 4. Top: synthetic pathway toward DAMBO; bottom left: crystal structure and key properties of DAMBO; bottom right: DTA plot of DAMBO with a heating rate of 5 °C min^{-1}.

Chapter 5 deals with the synthesis of the asymmetric bis-heterocycle 5-(3,5-dinitropyrazo-4-yl)-tetrazole. The aim was to combine the high heat of formation, which tetrazoles moieties contribute to compounds, with the oxidative, highly dense and thermally stable 3,5-dinitropyrazole building block. The key step of the synthesis was the Sandmeyer reaction of 4-amino-3,5-dinitropyrazole, which was obtained by a three-step protocol starting from pyrazole, toward sodium 4-cyano-3,5-

dinitropyrazolate (NaDCNP), using CuCN as cyanide source. NaCDNP was finally reacted to desired 5-(3,5-dinitropyrazo-4-yl)-tetrazole (H_2DNPT) using sodium azide and zinc chloride in a [2+3]-cycloaddition (Figure 5). In order to obtain better performance and sensitivities compared to H_2DNPT (IS = 2 J, FS = 120 N, V_{det} = 8062 m s^{-1}), several mono salts by deprotonation of the more acidic pyrazole position were synthesized. Through the synthesis of the 1,5-diaminotetrazolium derivative, the performance could be raised about 400 m s^{-1}. Increased thermal stabilities were reached by the salination with ammonia or aminoguanidine, respectively.

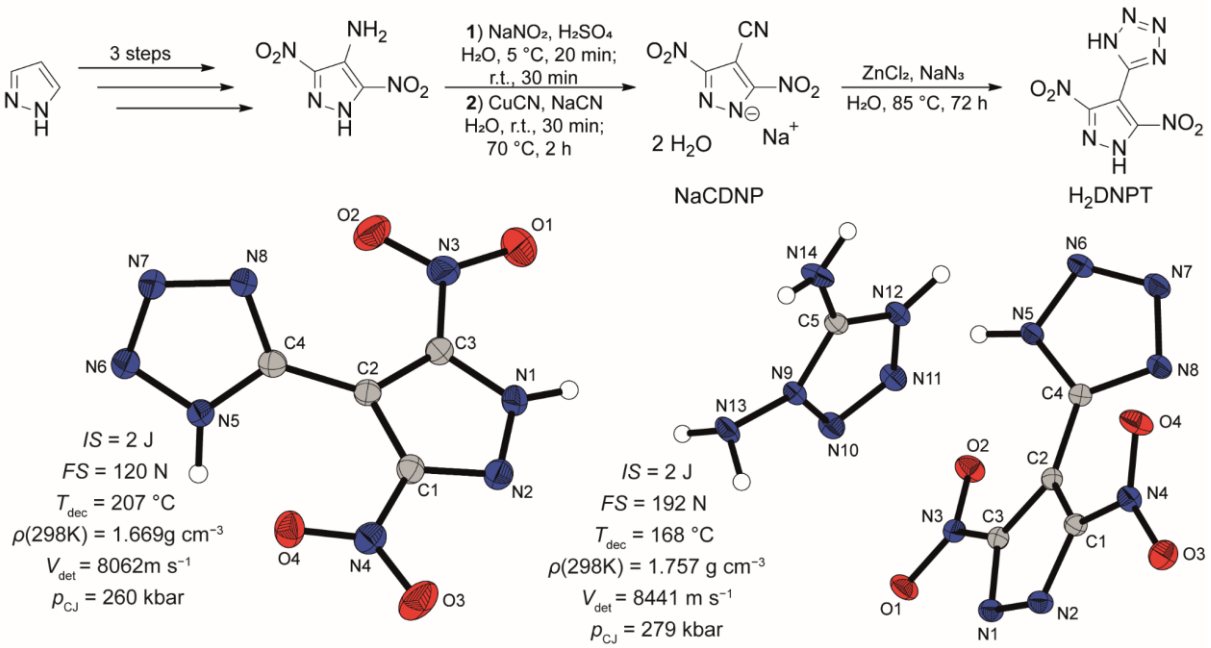

Figure 5. Top: Synthetic pathway toward H_2DNPT; bottom: crystal structures and key properties of H_2DNPT and 1,5-diaminotetrazolium 3,5-dinitro-4-(tetrazol-5-yl)-pyrazolate.

In **Chapter 6**, 5-(1-hydroxy-3-nitro-1,2,4-triazol-5-yl)-1-hydroxy-tetrazole and selected nitrogen-rich salts were synthesized. The procedure starts from 3-amino-5-cyano-1,2,4-triazole, which is transformed to 5-(3-nitro-1,2,4-triazol-5-yl)-1-hydroxy-tetrazole within five steps (Figure 6).[5] The final reaction sequence includes the selective oxidation of the triazole at position 5 using Oxone in buffered aqueous solution. The title compound was afterwards derivatized by the reaction with selected nitrogen-rich bases. The best ionic derivative turned out to be the bis-hydroxylammonium salt, which is the hybrid molecule of TKX-50 and MAD-X1, two promising next-generation

secondary explosives. The double hydroxylammonium derivative is moderately sensitive toward impact (IS = 20 J) and nearly insensitive toward friction (FS = 324 N). The decomposition occurs sharply at 205 °C. Despite the low sensitivities and the substantial thermal stability, a detonation velocity of 9490 m s^{-1} was achieved, which is significantly higher than the commonly used secondary explosives RDX and HMX. In addition, the change in the energetic properties in comparison with the bis-hydroxylammonium derivatives of 5-(3-nitro-1,2,4-triazol-5-yl)-tetrazole and 5-(3-nitro-1,2,4-triazol-5-yl)-1-hydroxy-tetrazole, i.e. the homologs with no and one N-oxide, respectively, was investigated. Towards the bis-hydroxylammonium 5-(3-nitro-1,2,4-triazol-1-olate-5-yl)-tetrazol-1-olate, a steady increase in density and in the decomposition temperature can be detected. The growing density results in a clear tendency for the detonation velocity to increase with an associated elevation in the number of N-oxides.

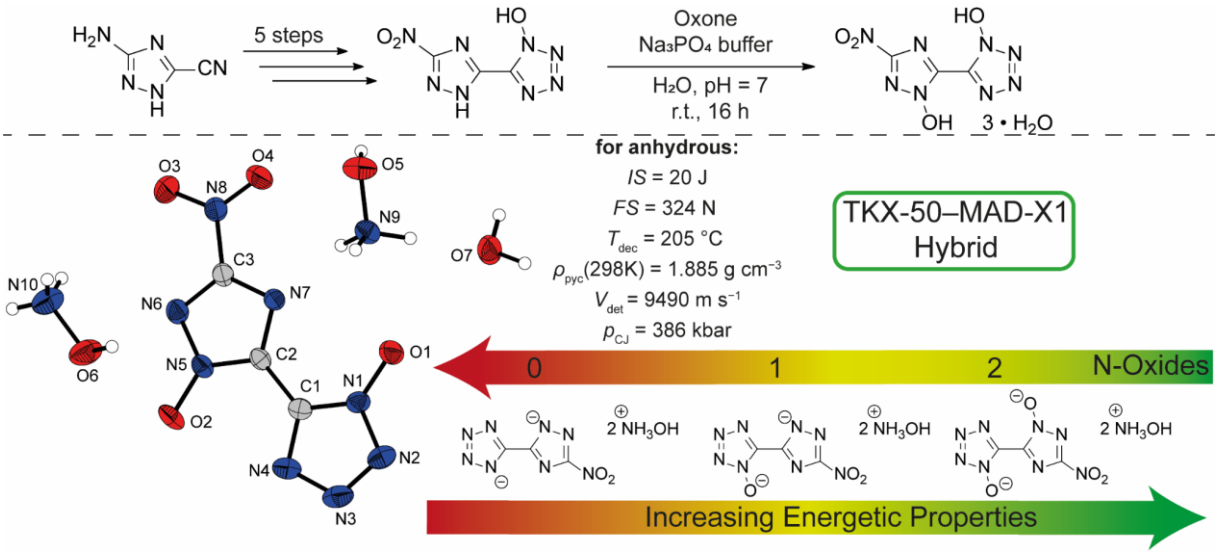

Figure 6. Top: Synthesis toward 5-(1-hydroxy-3-nitro-1,2,4-triazol-5-yl)-1-hydroxy-tetrazole; left: crystal structure and key properties of bis-hydroxylammonium 5-(3-nitro-1,2,4-triazol-1-olate-5-yl)-tetrazol-1-olate; bottom right: illustration of the effect on the energetic properties of the 3-nitrotriazol-5-yl-tetrazole backbone with increasing numbers of N-oxides.

Chapter 7 includes a new synthetic strategy toward 1,1'-diamino-5,5'bistetrazole (1,1'-DABT) and its utilization as metal-free primary explosive. Diamino-5,5'-bistetrazoles (1,1' and 1,2 isomer) were reported to be synthesized using THA amination of 5,5'-bistetrazolate, with poor yields as isomeric mixture.[6] Based on the insights gained from dihydroxy-5,5'-bistetrazole chemistry,[7] the 1,1' isomer (1,1'-DABT) was assumed

to be the most interesting isomer in terms of energetic properties. The synthetic approach started with readily available diethoxy carbonyl 1,1'-diamino-5,5'-bistetrazole, which can easily be produced in high quantities. Several methods for the deprotection of the amine were applied. Using Krapcho decarboxylation (Figure 7), a method in organic chemistry for deprotection of esters with an electron-withdrawing group in *β*-position, was successful and permitted the production of 1,1'-DABT on a multi-gram scale. Unlike the literature known method, the new protocol does not require any complex purification. In addition, the synthesis is isomer-specific. 1,1'-DABT was characterized as a metal-free, CHN-based, and high-performing primary explosive, which is stable up to 200 °C. The handling is particularly appropriate because of the friction sensitivity (3 N) and sensitivity toward electrostatic discharge (20 mJ).

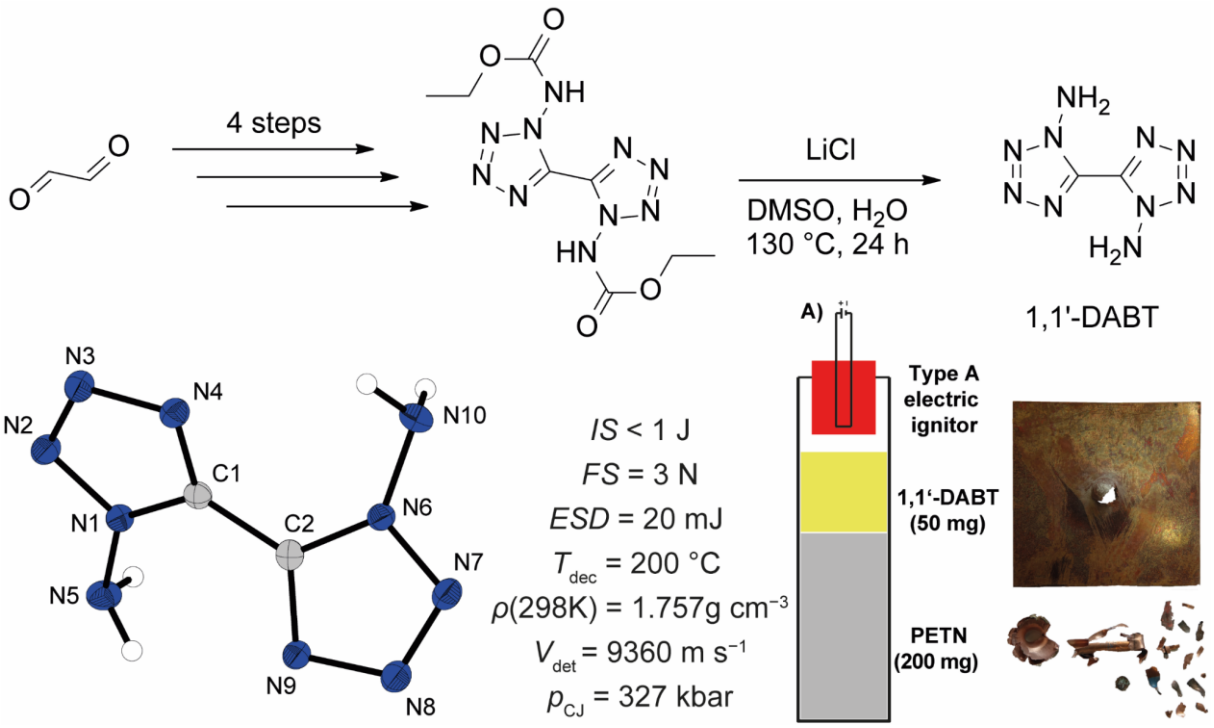

Figure 7. Top: synthetic pathway toward 1,1'-diamino-5-5'-bistetrazole (1,1'-DABT); bottom left: crystal structure of 1,1'-DABT and key properties; bottom right: schematic setup for PETN initiation test and result of the test including perforated copper plate and fragmented copper sleeve.

Focus in **Chapter 8** is placed on the investigation of 2,5-diaminotetrazole (2,5-DAT) and the derivatization thereof. The synthesis was achieved by amination (HOSA) of sodium 5-aminotetrazolate, followed by an elaborate workup to separate the isomers (1,5-DAT and 2,5-DAT) through several recrystallization steps and a final column

chromatography. Even if 2,5-DAT was already described more than 50 years ago, it has not been properly analyzed and characterized. Therefore, a protocol for the gram-scale synthesis was developed. To further push the energetic properties of 2,5-DAT modification in form of addition reactions and salination of the respective tetrazolium cation were performed (Figure 8). For the protonation, 2,5-diaminotetrazolium was obtained as nitrate and perchlorate salt. Both compounds showed increased performance compared to 2,5-DAT but were only stable up to 115 °C. To counteract this trend, the insertion of a methyl group through reaction with methyl iodide was evolved. The 2,5-diamino-4-methyltetrazolium iodide was converted to more energetic salts by metathesis reaction with silver nitrate, perchlorate and azide. Methylated compounds were thermally more stable than the protonated ones but lacked in their performance with the 2,5-diamino-4-methyltetrazolium nitrate giving the best value (V_{det} = 8714 m s^{-1}).

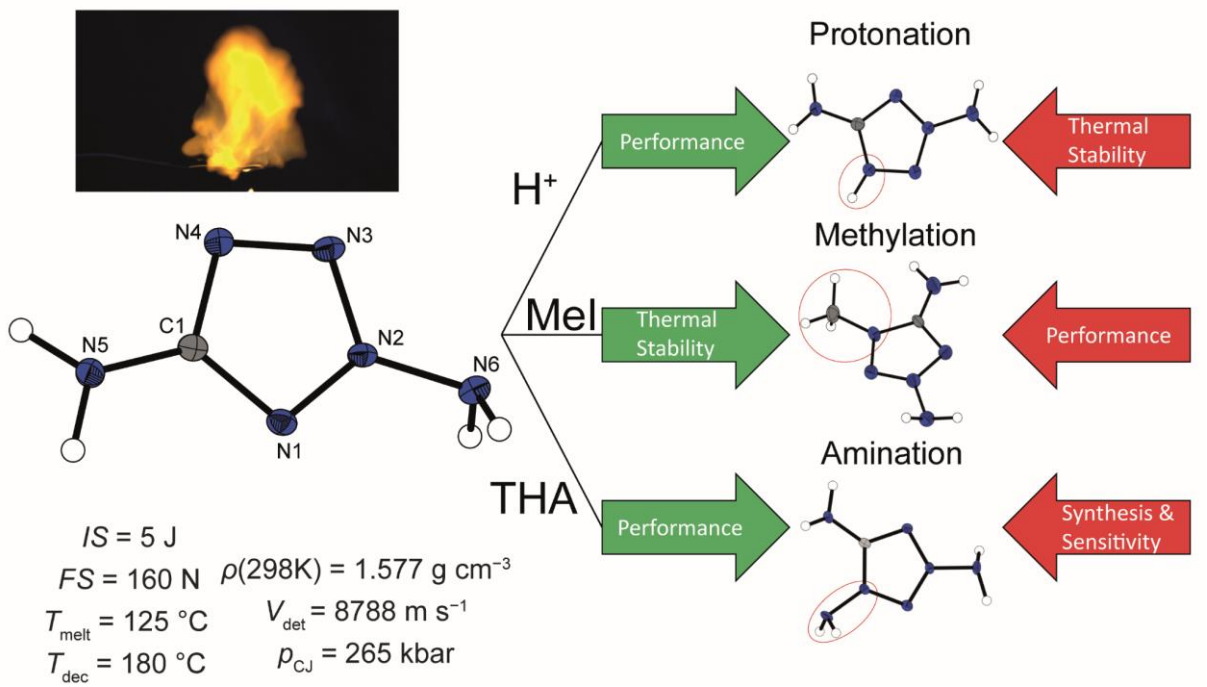

Figure 8. Left: flame test, crystal structure and key parameters of 2,5-diaminotetrazole (2,5-DAT); right: schematic illustration of functionalizations performed on the 2,5-DAT backbone.

Additionally, amination toward the 1,3,5-triaminotetrazolium (TAT) cation was performed, which was analyzed as tosylate, bromide and 5,5'-bistetrazole-1,1'-diolate (BTO) double salt. $(TAT)_2BTO$ exhibits a detonation velocity of 9416 m s^{-1} and

decomposes sharply at 170 °C. Nonetheless, it shows sensitivities in the range of a primary explosive (IS = 2 J, FS = 30 N).

Chapter 9 and **10** face the investigation of the two isomers of amino-nitrimino-tetrazoles. 1-Amino-5-nitriminotetrazole (HANIT) is obtained through N_2O_5 nitration of 5-amino-1-(propan-2-ylideneamino)-tetrazole and in situ deprotection of the amine upon quenching on water whereas 1-nitrimino-5-aminotetrazole (HNIAT) is directly synthesized from 1,5-diaminotetrazole using mixed acid at −20 °C (Figure 9).

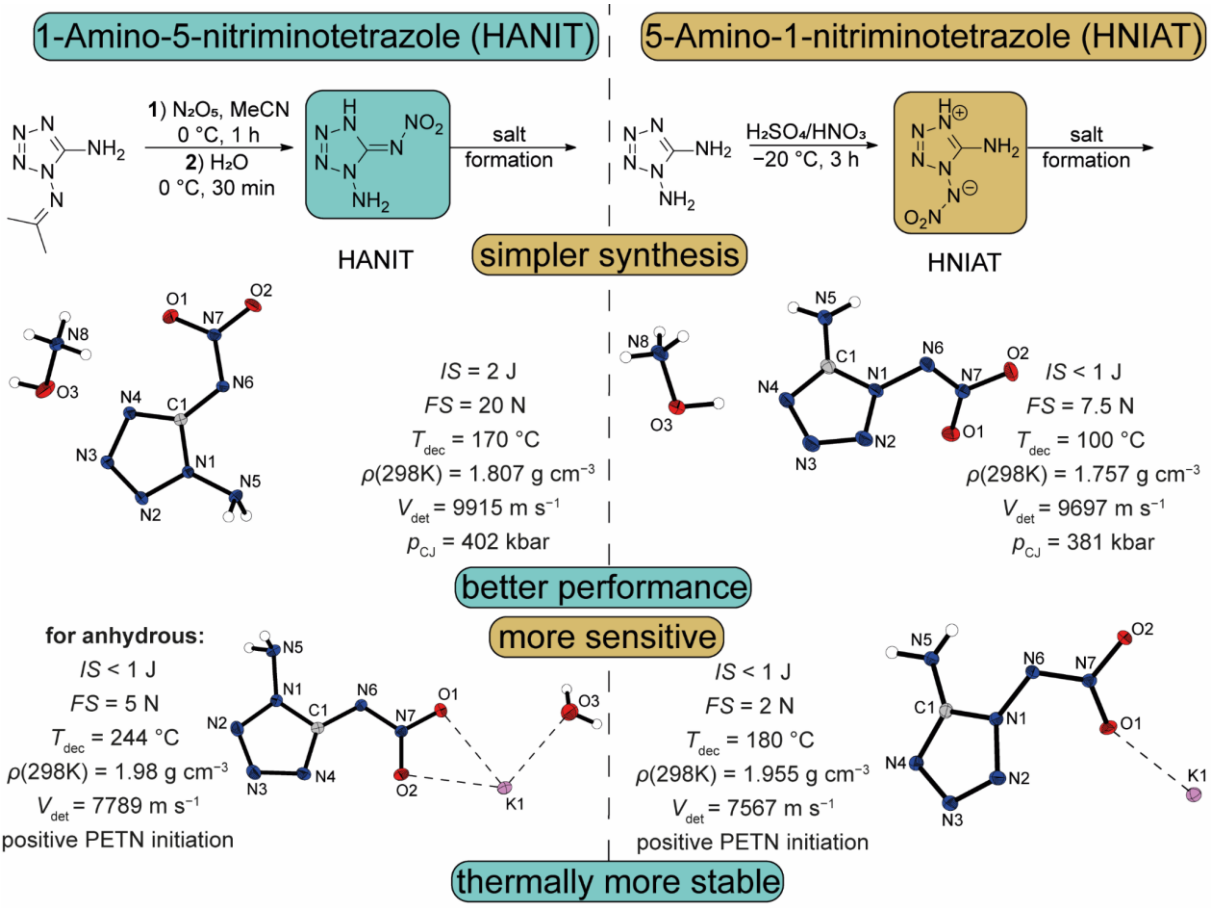

Figure 9. Left: synthetic scheme toward 1-amino-5-nitriminotetrazole (HANIT) and crystal structures and key properties of (Hx)ANIT and (K)ANIT; right: synthetic scheme toward 5-amino-1-nitriminotetrazole (HNIAT) and crystal structures and key properties of (Hx)NIAT and (K)NIAT.

For both isomers, a series of ionic derivatives were synthesized by metathesis reaction with the respective nitrogen-rich or metal bases. In terms of performance, the best ones turned out to be the hydroxylammonium derivatives (V_{det}((Hx)ANIT) = 9915 m s^{-1}, V_{det}((Hx)NIAT) = 9697 m s^{-1}). Potassium derivatives of ANIT$^-$ as well as NIAT$^-$ proofed to be powerful heavy-metal free primary explosives.

They are both capable of initiating PETN. Furthermore, the synthesis of the TATOT derivatives ((HTATOT)ANIT and (HTATOT)NIAT) gave the best values for both thermal stability (215 °C and 174 °C, respectively) and sensitivities (e.g. FS = 240 N and FS = 120 N, respectively) for CHNO-based compounds. Overall, trends can also be distinguished within the ionic compounds of the isomers. Accordingly, the $ANIT^-$ derivatives always give better calculated performances compared to the $NIAT^-$ salts. This is mainly due to the higher density of the N-amines ($ANIT^-$) compared with the C-amines ($NIAT^-$), from which the better properties can be directly inferred. The direct comparison of salts with the same cation shows that $ANIT^-$ derivatives are thermally more stable then $NIAT^-$ derivatives, whereas 1-nitrimino-5-aminotetrazolate compounds generally show higher sensitivities.

In **Chapter 11** the chemistry of 1-nitrimino-5-azidotetrazole (1-HNAAT) and selected salts thereof is evaluated. The precursor molecule, 1-amino-5-azidotetrazole (1-AAT) is accessible by double diazotization of triaminoguanidinium chloride, after separation from various other azotetrazoles by column chromatography. Nitration of 1-AAT toward 1-HNAAT was performed in mixed acid at −15 °C. In order to realize a selective route without the formation of by-products, a new reaction pathway toward 5-azidotetrazole-1-ethylcarbamate was established. However, both the deprotection to 1-amino-5-azidotetrazole (1-AAT) or the nitration and subsequent deprotection of the protected nitramine failed. Since the free acid 1-HNAAT is liquid, several ionic derivatives were synthesized to preserve solids (Figure 10). This included the hydrazinium and hydroxylammonium, which, as the parent compound appeared as pure but oily and hygroscopic substances and were therefore not further characterized. Next to the potassium salt, which immediately detonated upon crystallization and could therefore not properly investigated, only the ammonium ((NH_4)NAAT) and guanidinium ((Gua)NAAT) derivate could be realized as solids and were analyzed intensively. The detonation velocities of those salts are in the range of RDX for (Gua)NAAT (V_{det} = 8723 m s^{-1}) and even in the range of HMX for (NH_4)NAAT (V_{det} = 9337 m s^{-1}).

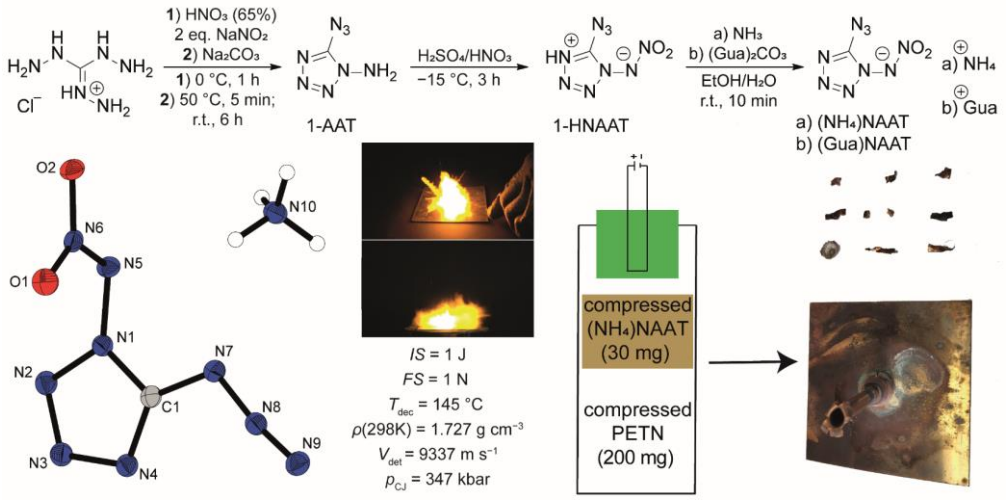

Figure 10. Top: synthetic pathway toward 1-nitrimino-5-azidotetrazole (1-HNAAT) and the respective ammonium ((NH4)NAAT) and guanidinium ((Gua)NAAT) derivative; bottom: crystal structure and key properties of (NH4)NAAT; results of hot needle and hot plate test of 10 mg (NH4)NAAT, respectively; schematic setup for the initiation test and result of the test.

Both compounds are capable up to a decomposition temperature of around 150 °C and have sensitivities in the range of primary explosives, with the ammonium derivative being more sensitive (IS = 1 J, FS = 1 N). Based on the detonative results from the hot plate and hot needle test combined with the measured sensitivities, (NH4)NAAT was evolved as possible primary explosive. The initiation test toward PETN was performed successfully, making (NH4)NAAT a rare representative of ammonium salts capable to initiate PETN.

Chapter 12 deals with the synthesis and characterization of selected alkyl-substituted 5-azido and 5-nitriminotetrazoles. The main goal was to reduce the acidity and adjust the performance and the sensitivities (Figure 11 top). Three different systems were examined for this purpose. 2-Azidoethyl-5-nitriminotetrazole was obtained through mixed acid nitration of the respective amine and was further derivatized through salt formation with nitrogen-rich and metal bases. 1-Nitratoethyl and 1-azidoethyl-5-azidotetrazoles were synthesized starting from 1-azidoethyltetrazole and 1-acetoxyethyltetrazole, respectively, following the same procedure for both compounds. This includes bromination of the tetrazole CH position, bromo-hydrazine exchange through reaction with aqueous hydrazine and diazotization to the respective 5-azidotetrazole. For 1-acetoxyethyltetrazole, the acetoxy group was removed upon

contact with hydrazine yielding hydroxyethyl-5-hydrazineyltetrazole, which had to be nitrated at the end of the sequence using fuming HNO_3.

Isomerically pure methyl substituted 5-azidotetrazoles were obtained by direct methylation of sodium 5-azidotetrazolate (for 2-methyl-5-azidotetrazole) and zinc induced reduction of 1-methyl-5-nitriminotetrazole and subsequent diazotization (for 1-methyl-5-azidotetrazole). Especially all 5-azidotetrazole derivatives show high sensitivities (IS ≤ 1 J, FS ≤ 5 N) which means that none of the selected groups is suitable to tame the 5-azidotetrazole moiety to moderate sensitivities. The decomposition temperature could be adjusted to 180 °C for the metal-containing 2-azidoethyl-5-nitriminotetrazole derivatives, to 170 °C for the nitrogen-rich 2-azidoethyl-5-nitriminotetrazoles and to approx. 160 °C for all 5-azidotetrazole derivatives. The crystallographic densities do not exceed the value of 1.638 g cm^{-3} (1-nitratoethyl-5-azidotetrazole) for all CHNO-based compounds, which is due to the poor packing properties of azides in general. The detonation velocities are all in the range RDX or below with hydroxylammonium 2-azidoethyl-5-nitriminotetrazolate (V_{det} = 8796 m s^{-1}) giving the highest value.

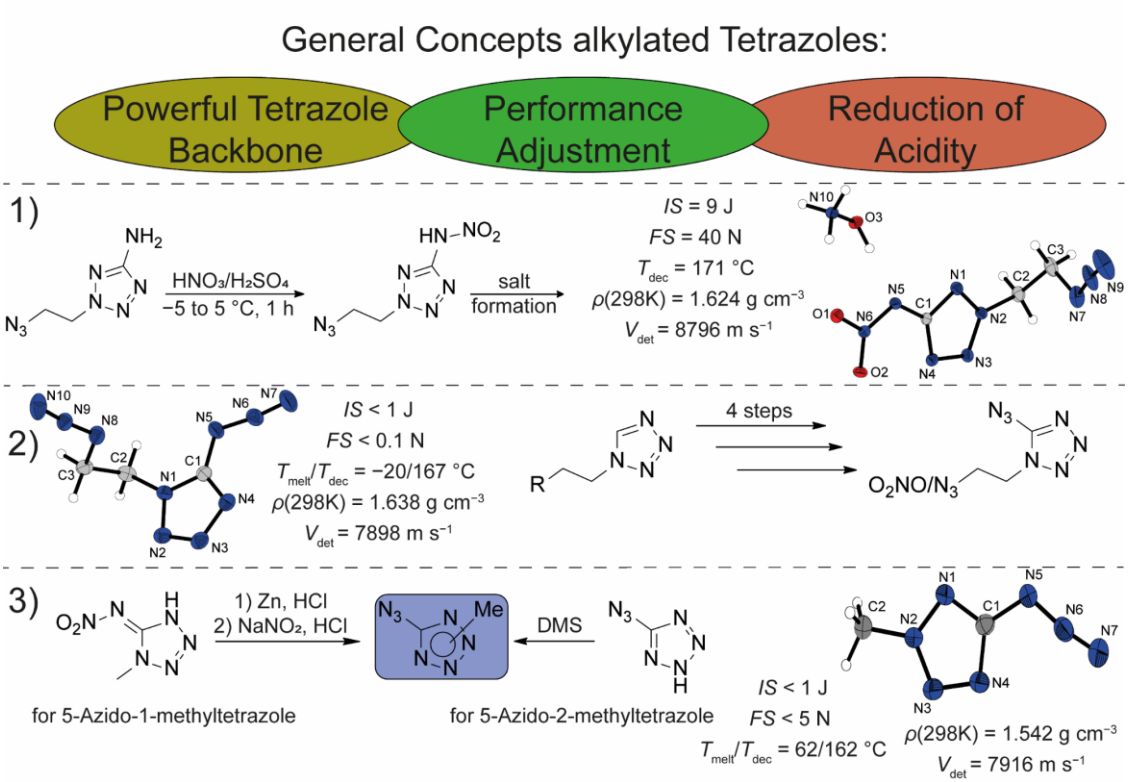

Figure 11. Synthetic approaches and selected crystal structures with key properties for the three different molecular moieties within this project: 1) 2-azidoethyl-5-nitriminotetrazole; 2) 1-nitrato/azidoethyl-5-azidotetrazoles and 3) methyl-5-azidotetrazoles.

Chapter 13 features the synthesis and characterization of bis-azido (1-/2-BAEAzT) and nitroatoethyl (1-/2-BNEAzT) substituted 5,5'-azotetrazoles. Substitution occurred at positions N1 and N2, yielding a total of four new 5,5'-azotetrazole derivatives. 1- and 2- hydroxyethyl-5-aminotetrazole, which were obtained by substitution reaction of chloroethanol with sodium 5-aminotetrazolate, served as starting material (Figure 12). The isomers were separated using column chromatography. The key step here included the oxidative azo coupling of the hydroxyethyl or azidomethyl derivatives, using tert-butyl hypochlorite (*t*BuOCl) as oxidant. The azidoethyl-5-aminotetrazole derivatives were synthesized by chlorination of the hydroxyethyl-5-aminotetrazoles using $SOCl_2$ and subsequent chlorine-azide exchange. For the nitroatoethyl derivatives, the azo coupled bis-hydroxyethyl-azotetrazoles were nitrated to the respective organic nitrates using HNO_3. For the various substitution sites and substitutes, clear trends are discernible. N1-substituted compounds are significantly more thermally stable than their respective N2-substituted isomers (T_{dec}(1-BNEAzT) = 179 °C vs. T_{dec}(2-BNEAzT) = 97 °C; T_{dec}(1-BAEAzT) = 188 °C vs. T_{dec}(2-BAEAzT) = 140 °C).

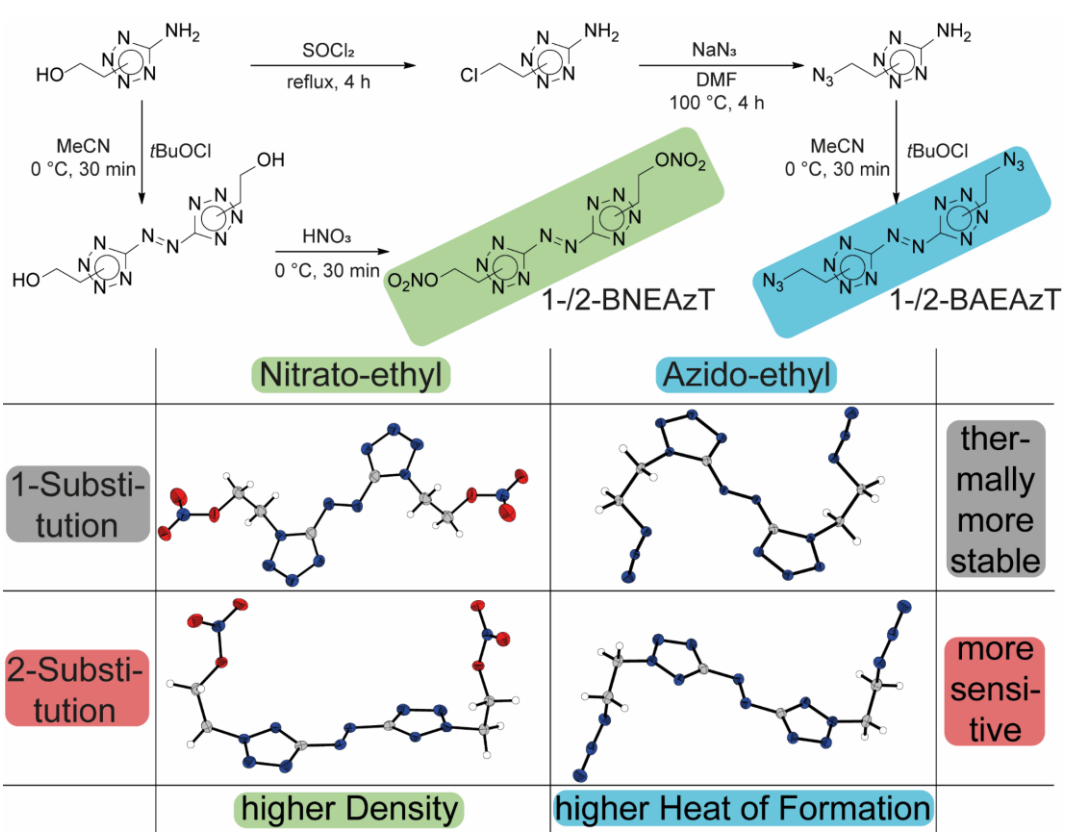

Figure 12. Top: synthetic pathway toward the synthesis of azido and nitroatoethyl substituted 5,5'-azotetrazoles; bottom: crystal structures and comparison of the most remarkable properties of all four compounds.

In contrast, the N2-substituted derivatives are significantly more sensitive to friction and impact than the N1-substituted azotetrazoles. In addition, as expected, higher densities are obtained for the nitratoethyl compounds, with 1-BNEAzT having among the highest (ρ = 1.702 g cm^{-3}), but higher enthalpies of formation for the azidoethyl derivatives ($\Delta_f H°$(1-BAEAzT) = 1456.2 kJ mol^{-1}).

Chapter 14 is about the distinctive molecule C_2N_{16} (2,2'-azobis(5-azidotetrazole), a highly endothermic, binary CN compound. The isolation and characterization of C_2N_{16} is an important step toward all-nitrogen compounds which are environmentally and energetically desired.

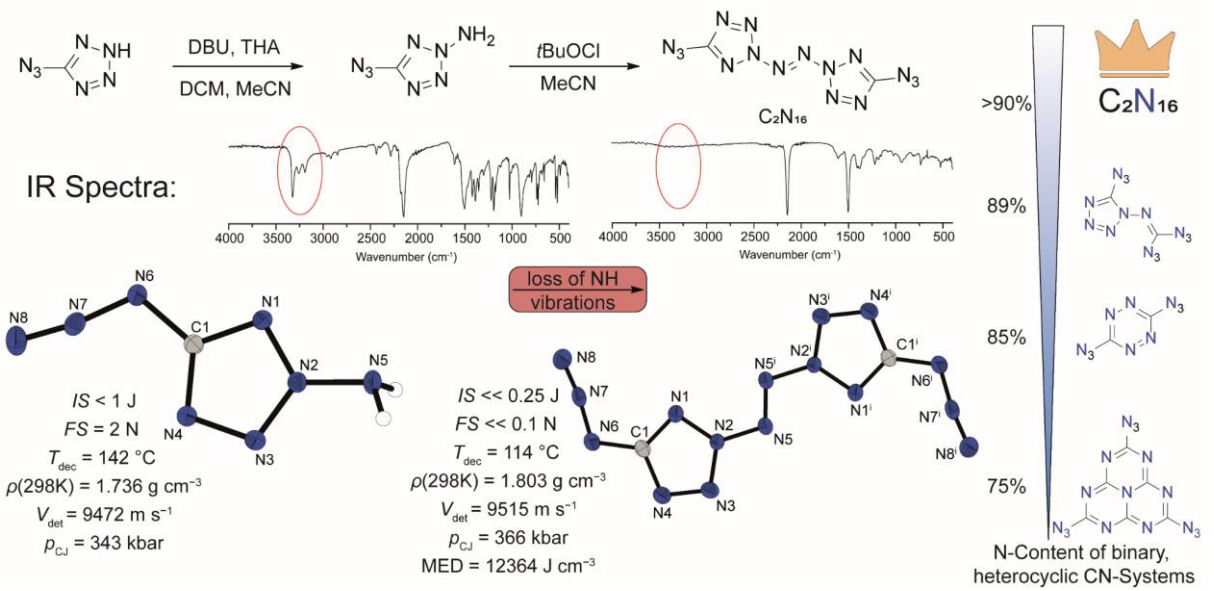

Figure 13. Left: reaction scheme toward C_2N_{16}; IR spectra of 2-amino-5-azidotetrazole and C_2N_{16}; crystal structures and key properties of 2-amino-5-azidotetrazole and C_2N_{16}; right: ranking of binary, heterocyclic CN-systems according to their nitrogen content.

The synthesis starts with the amination of 5-azidotetrazolate, using *O*-tosylhydroxylamine (THA) (Figure 13). Due to the electron withdrawing effect of the C-substituted azide, the reaction yields selectively the 2-amino-5-azidotetrazole isomer. Subsequent oxidative azo coupling using *t*BuOCl as oxidant, results in the formation of C_2N_{16}. With a nitrogen content of 90.3%, it is the only heterocyclic and solid compound in the class of binary CN compounds with a value of this magnitude. The high nitrogen content also results in an enormously high energy content of the substance, which is reflected in the values of the maximum energy density and the

detonation velocity. However, the high N-content is also accompanied by extreme sensitivity. C_2N_{16} shows sensitivities, which are beyond our device's capability of measurement. The extreme sensitivity also made the handling extremely difficult, since only very small quantities could be produced per portion.

Chapter 15 and **16** give a closer look on the small-scale shock reactivity test (SSRT). As the name suggests, the test investigates shock reactivities of secondary explosives, often below their critical diameter. The setup consists of a ductile aluminum block, on which a precision-fit steel block with a bore hole is placed (Figure 14). The test substance is filled into the cavity, pressed and then initiated with a detonator. The dent created in the aluminum block allows initial practical conclusions to be drawn about the explosiveness of the substances.

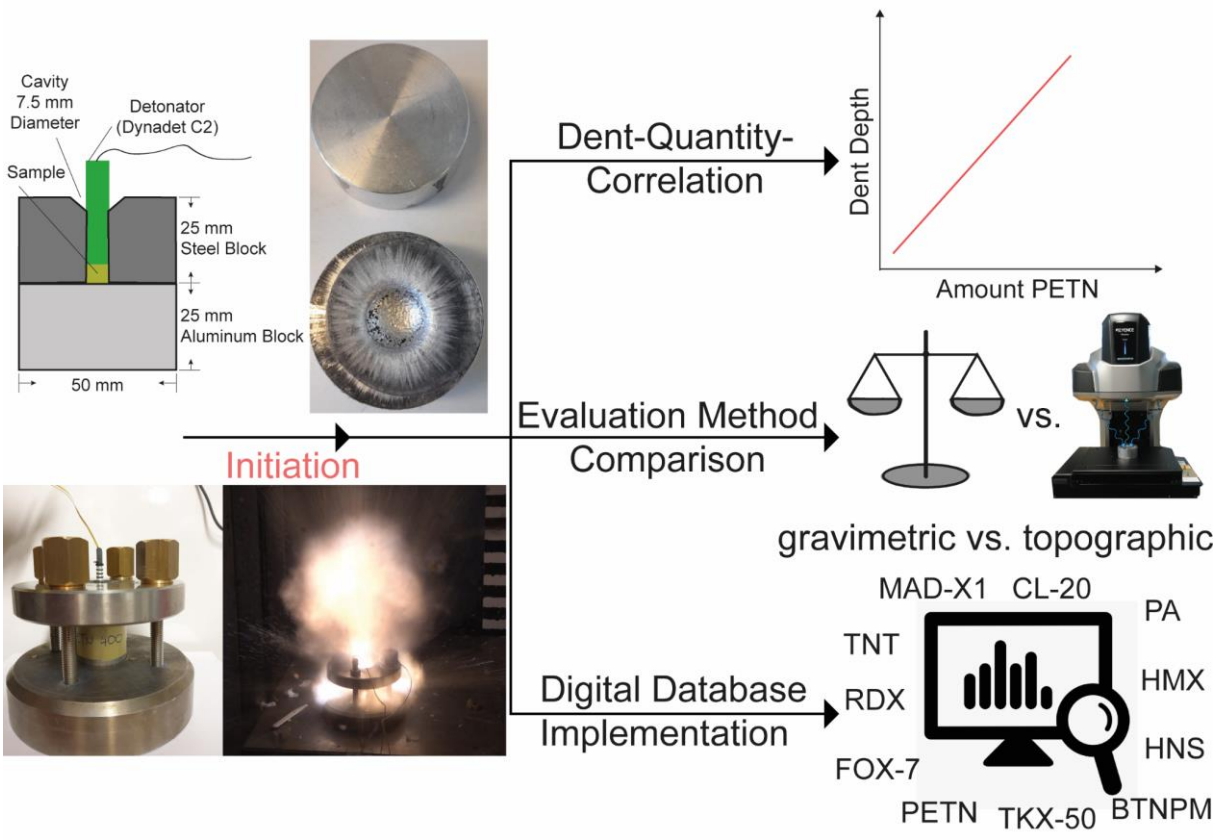

Figure 14. Left) schematic and life test setup, moment of initiation and comparison of the aluminum block before and after detonation; right) schematic illustration of the three main goals of the SSRT project.

Concerning this test setup, three different questions were discussed in particular. First, the correlation between the filling quantity of the explosive (for this study, PETN was used) and the dent depth of the aluminum block was investigated. Here a linear

relationship, at least for the limits of our experimental setup could be verified. In addition, two evaluation methods of the test were compared. For this purpose, the current manual gravimetric method, which uses sand for weighing, was compared with the new digital topographic method, which determines the dent depth optically with the aid of a profilometer. In addition to the greater precision of the digital measurements, the time savings and user-independence were identified as the main advantages for the profilometer methodology. Based on the measurement data obtained from the topographic measurements, the foundation for a digital database for the respective results for SSRT measurements, which can independently use the dent volumes as comparative values for measurements of new substances was laid.

Among the numerous newly developed compounds, some are particularly noteworthy. This is due to their properties, which have been determined so far, rendering them as possible replacements for currently used explosives. 3,3′-Bis(azidomethyl)-5,5′-bis(1,2,4-oxadiazole) (DAMBO) shows promising characteristics for a possible TNT substituent. The main criteria for a new melt-cast explosive, the appropriate range for the melting and decomposition temperature, is clearly fulfilled, since DAMBO melts at 70 °C and decomposes about 140 °C later at 209 °C (Figure 15). The calculated detonation velocity of 7221 m s^{-1} exceeds that of TNT by 400 m s^{-1}. In addition, DAMBO is completely insensitive toward impact and friction and can be prepared by a simple and easily scalable synthesis using diaminoglyoxime, chloroacetyl chloride and sodium azide.

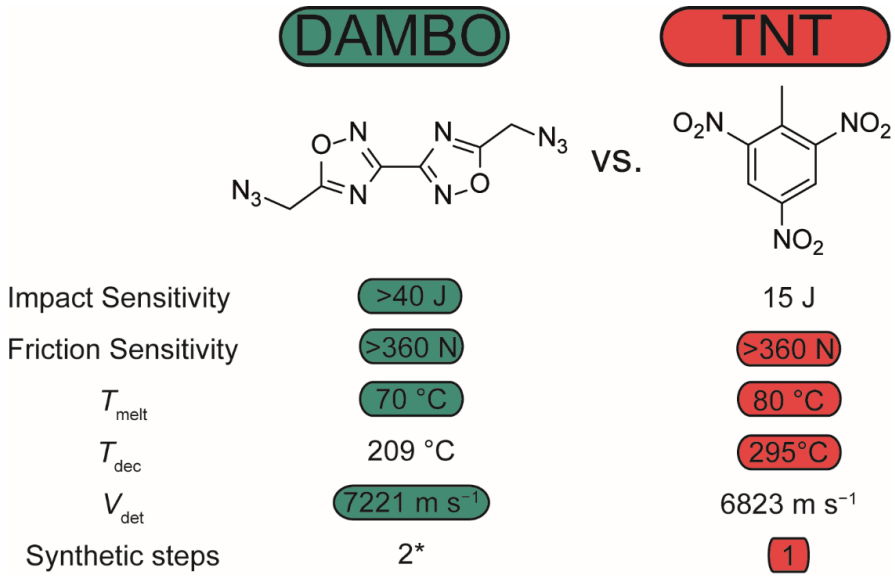

Figure 15. Comparison of the key properties of DAMBO and TNT. *: Synthesis starting from diaminoglyoxime.

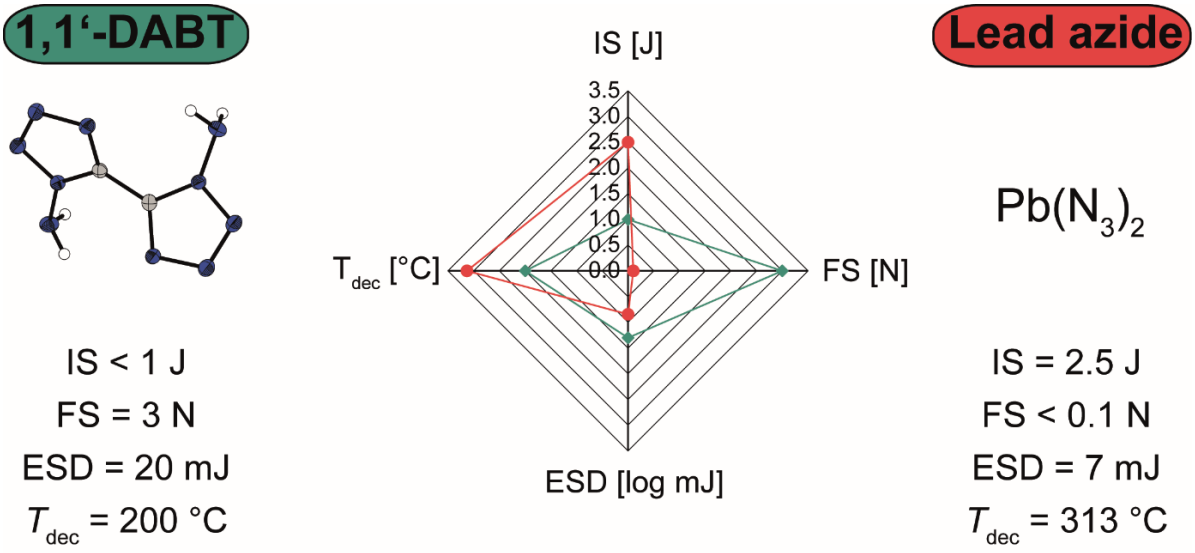

Figure 16. Comparison of the sensitivities and decomposition temperature of 1,1’-DABT and lead azide (LA).

1,1’-DABT complies all required criteria for a possible lead azide replacement (Figure 16). Next to the environmental advantageous and metal-free composition of only C, H and N, 1,1’-DABT shows beneficial sensitivities, which facilitate the handling (FS = 3 N, ESD = 20 mJ). The compound is stable up to a temperature of 200 °C and is capable of initiating PETN in the compressed state (50 mg, 80 N). The synthesis route starting from glyoxal comprises five steps and offers potential for optimization including the reduction of reaction steps.

(HTATOT)ANIT shows encouraging properties for potential application as RDX substitute (Figure 17). The compound is prepared by three synthetic steps (protection, nitration, salt formation) starting from 1,5-DAT. (HTATOT)ANIT is significantly less sensitive than RDX (IS = 20 J, FS = 240 N), while exhibiting similar thermal stability. Likewise, the detonation pressure is in a similar region to that of RDX, but the detonation velocity of 9312 m s^{-1} significantly exceeds that of RDX.

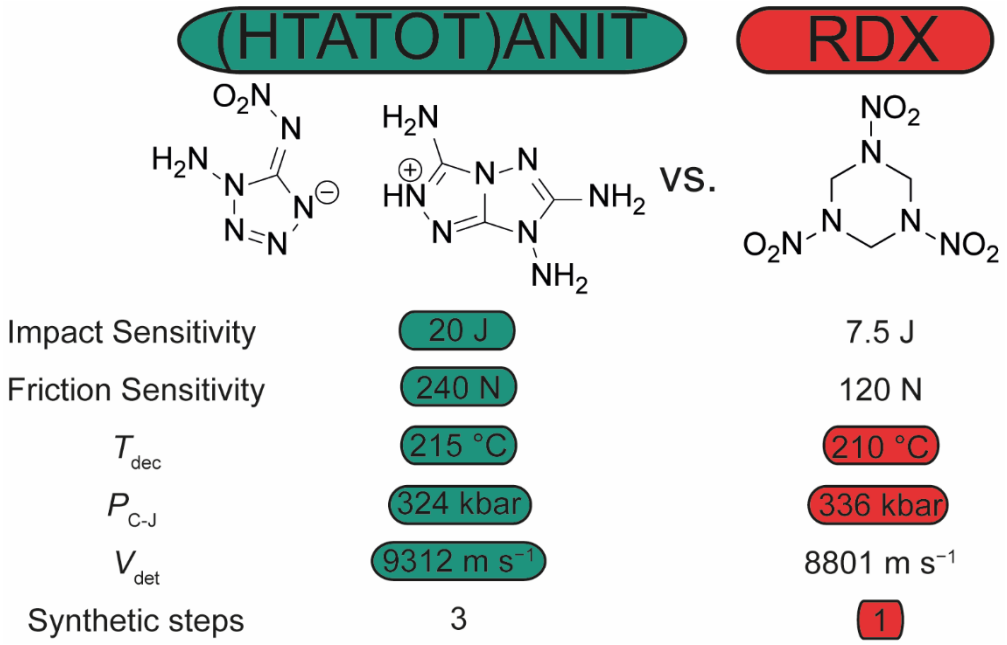

Figure 17. Comparison of the key properties of (HTATOT)ANIT and RDX.

In addition to the principal substitutes, the synthesis and investigation of academically interesting molecules was another target. In this context, C_2N_{16} is particularly worth mentioning (Figure 18). 2,2′-Azobis(5-azidotetrazole) (C_2N_{16}) is one of the few representatives of the class of binary CN compounds, which are characterized above all by the high heat of formation of its members. C_2N_{16} is on a frontier of possible existence, which is characterized by an extremely high sensitivity to all kind of extern stimuli.

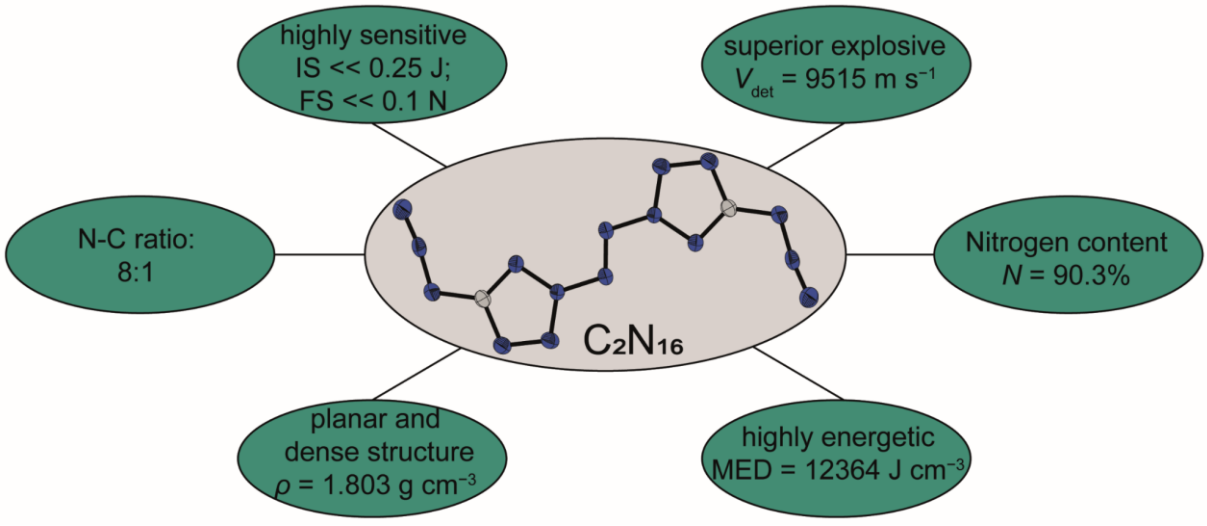

Figure 18. Crystal structure of C_2N_{16} and key characteristics.

The through crystallography determined density (ρ_{298K} = 1.803 g cm^{-3}) and calculated enthalpy of formation ($\Delta_f H°$ = 1700.7 kJ mol^{-1}) are unique for a binary CN compound and result in an astonishing value of 12364 J cm^{-3} for the maximum energy density. The synthesis and characterization of C_2N_{16} provided another link to all-nitrogen compounds, which could be of great importance not only from an energetic point of view. Besides the particularly potent compounds mentioned recently, a large number of compounds could be newly synthesized based on covalent azides, multi-substituted tetrazoles or combinations thereof. Thereby, representatives for almost every category of explosives were obtained. This work thus demonstrated the potency of the structural motifs used. Often, the compounds were on a fine line between too high sensitivity and stability and sufficiently high performance. Nevertheless, the stated concept has been reconfirmed and further evaluated to synthesize new and auspicious molecules.

References

[1] M. S. Gruhne, M. H. H. Wurzenberger, M. Lommel, J. Stierstorfer, *Chem. Eur. J.* **2021**, *27*, 9112–9123.

[2] M. H. H. Wurzenberger, J. T. Lechner, J. Stierstorfer, *ChemPlusChem* **2020**, *85*, 769–775.

[3] E. C. Johnson, J. J. Sabatini, D. E. Chavez, R. C. Sausa, E. F. C. Byrd, L. A. Wingard, P. E. Guzmàn, *Org. Process Res. Dev.* **2018**, *22*, 736–740.

[4] L. A. Wingard, E. C. Johnson, P. E. Guzmán, J. J. Sabatini, G. W. Drake, E. F. C. Byrd, R. C. Sausa, *Eur. J. Org. Chem.* **2017**, *13*, 1765–1768.

[5] A. A. Dippold, D. Izsák, T. M. Klapötke, *Chem. Eur. J.* **2013**, *19*, 12042–12051.

[6] T. M. Klapötke, D. G. Piercey, J. Stierstorfer, *Dalton Trans.* **2012**, *41*, 9451–9459.

[7] K. Hafner, T. M. Klapötke, P. C. Schmid, J. Stierstorfer, *Eur. J. Inorg. Chem.* **2015**, *2015*, 2794–2803.